JEAN H. FUTRELL

Fourteenth Annual Conference on Mass Spectrometry and Allied Topics

May 22-27, 1966
Dallas, Texas

Arranged by the Officers of
ASTM Committee E-14

Fourteenth Annual Conference on Mass Spectrometry and Allied Topics

May 22-27, 1966
Dallas, Texas

Arranged by the Officers of
ASTM Committee E-14

Preface

This volume is a collection of papers presented at the Fourteenth Annual Conference on Mass Spectrometry and Allied Topics*, held in Dallas, Texas, May 22-27, 1966. It is intended that this volume be distributed only to registrants of the conference and, therefore, should not be considered as a publication.

It is suggested that where necessary individual reports be cited in the form: author(s), presented at the Fourteenth Annual Conference on Mass Spectrometry and Allied Topics, Dallas, May 22-27, 1966.

H.M. Rosenstock, Program Chairman

*Arranged by the officers of the ASTM Committee E-14

N.D. Coggeshall, Chairman
H.M. Rosenstock, Vice-Chairman
M.K. Testerman, Vice-Chairman
G.L. Cook, Secretary
H.I. Schiff, Member-at-Large
W.M. Hickam, Member-at-Large

TABLE OF CONTENTS

FOURTEENTH ANNUAL CONFERENCE ON MASS SPECTROMETRY AND ALLIED TOPICS

DALLAS, TEXAS, May, 1966

Page No.

SYMPOSIUM ON SOLIDS STUDIES

1. * Photoionization of Vapors of Inorganic Elements and Compounds
J. Berkowitz and W.A. Chupka, Argonne National Laboratory Argonne, Illinois..... 1

2. * Studies of Partial Molar Quantities at High Temperatures Using a Mass Spectrometer
E.K. Storms, Los Alamos Scientific Laboratory, Los Alamos, New Mexico..... 2

3. * The Determination of Activities at High Temperatures by Mass Spectroscopy
G.R. Belton, R. Fruehan, M. Ginsberg, and R. Svedberg, University of Pennsylvania, Philadelphia, Pennsylvania..... 3

4. * The Vaporization of Some Simple Inorganic Compounds
Alfred Buchler and James L. Stauffer, Arthur D. Little, Inc., Cambridge, Massachusetts..... 4

5. Inhomogeneous Field Deflection for Determination of Electronic and Geometric Structure of High Temperature Molecules Observed with a Mass Spectrometer
Gary D. Blue, University of California, Santa Barbara, California, and David J. Meschi, Lawrence Radiation Laboratory, University of California, Berkeley, California..... 5

6. Knudsen Cell Measurements to Determine the Stability of Gaseous Cesium and Rubidium Oxides
J. H. Norman and H. G. Staley, General Dynamics/General Atomics San Diego, California..... 6

7. Mass Spectrometric Determination of the Dissociation Energy of $Na_2(g)$. The Ionization Cross Section of Na(g)
R.F. Pottie, National Research Council, Ottawa, Canada..... 14

* Invited Paper

FUNDAMENTAL ASPECTS

Page No.

8. The Photoionization of H_2, HD, D_2 and N_2 at 584Å
D.C. Frost, C.A. McDowell, and D.A. Vroom, University of British Columbia, Vancouver, British Columbia..... 18

9. Mass Spectrometric Study of the Photoionization of Hydrogen Chloride and Methyl Halides
V. H. Dibeler, J.A. Walker, and M. Jruss, National Bureau of Standards, Washington, D.C..... 24

10. Photoionization of Lower Aliphatic Alcohols
W.A. Chupka and K. M. Refaey, Argonne National Laboratory, Argonne, Illinois..... 25

11. Mass Spectrometric Study of the Photoionization of Ammonia, Water, Ethylene, and 1,2-Ethylene-d_2
R. Botter, V. H. Dibeler, J.A. Walker, and H.M. Rosenstock, National Bureau of Standards, Washington, D.C..... 32

12. Non-Exponential Decay in Uni-Molecular Reactions
F. Mies and M. Krauss, National Bureau of Standards, Washington, D.C..... 36

13. Isotope Effect in the Dissociative Attachement of Electrons in Methane
T.E. Sharp, Lockheed Missiles and Space Company, Palo Alto, California..... 37

14. On the Relationship of H_2^+ to H_2^*
D. J. Keenan and E.M. Clarke, St. Francis Xavier University, Antigonish, Nova Scotia..... 42

15. Double Ionization of Molecular Hydrogen by Electron Impact
K.E. McCulloh and H.M. Rosenstock, National Bureau of Standards, Washington, D.C..... 43

16. Field Ionization Mass Spectrometry: I. Saturated Hydrocarbons.II. Monochloro-Substituted Alkanes
Morris J. Weiss, Louis G. Pobo, and Dwight A. Hutchison, Argonne National Laboratory, Argonne ,Illinois..... 46

17. Correlation of Ionization Probabilities with Charge Cross-Section
A. Bruce King, Gulf Research and Development Company, Pittsburgh, Pennsylvania..... 49

FUNDAMENTAL ASPECTS-Continued

Page No.

18. The Mass Spectrum of Silylarsine
Fred E. Saalfeld,
U.S. Naval Research Laboratory,
Washington, D.C..... 50

SOLIDS MASS SPECTROMETRY AND RELATED TOPICS

19. Simple Two Filament Ion Source for Single Filament Instruments
W.E. Duffy and R.E. Carr,
General Electric Company,
Pleasanton, California..... 54

20. High Abundance Sensitivity Mass Spectrometry in Neutron Cross Section and Effective Neutron Temperature Measurements
L. Forman and F.A. White,
Rensselaer Polytechnic Institute,
Troy, New York..... 57

21. Determination of Electron Affinity Differences by Surface Ionization
C.S. Harden, D. Stelman, and
E.E. Muschlitz, Jr.,
University of Florida,
Gainesville, Florida..... 61

22. High Efficiency Surface Ionization Sources
Otto K. Husmann,
Hughes Research Laboratories,
Malibu, California..... 66

23. Vacuum Lock Surface Ionization Sources
E.J. Michael and E.G. Kerfoot,
Nuclide Corporation,
State College, Pennsylvania..... 72

24. The Production of Vapor Species in a Mass Spectrometer Ionization Chamber by Laser Heating
F. J. Vastola, A. J. Pirone, and
B.E. Knox,
Pennsylvania State University,
University Park, Pennsylvania..... 78

25. Application of Laser to Mass Spectrometry
N.C. Fenner, R. G. Ridley, R. W. D. Hardy,
and N. R. Daly,
Atomic Weapons Research Establishment,
Aldermaston, Berkshire,
England..... 83

26. Cryogenic Mass Spectrometry
H.A. McGee, Jr., D. B. Bivens,
T. J. Malone, and J. H. Wilson,
Georgia Institute of Technology,
Atlanta, Georgia..... 88

Page No.

27. Ion Sampling from Hydrocarbon Combustion Plasmas
William J. Miller,
AeroChem Research Laboratories, Inc.,
Princeton, New Jersey..... 89

28. Mass Spectrometry Without Ions
B.R. F. Kendall,
Pennsylvania State University,
University Park, Pennsylvania..... 96

29. Mass Spectrometric Studies of Diffusion and Permeability in Polymeric Films
R. L. Bredeweg and V. J. Caldecourt,
The Dow Chemical Company,
Midland, Michigan..... 102

SYMPOSIUM ON IONIC COLLISION PROCESSES

30. * Chemical Ionization Mass Spectrometry. I. General Introduction
M. S. B. Munson and F. H. Field,
Esso Research and Engineering Company,
Baytown, Texas..... 108

31. * Negative Ion Identification from Attachments-Detachment Equilibrium Studies in O_2 and Mixtures of O_2 and CO_2
A. V. Phelps, J.L. Pack and
J. L. Moruzzi,
Westinghouse Research Laboratories,
Pittsburgh, Pennsylvania..... 109

32. * Reaction Studies Using Low Energy Ion Beams
Ben T. Turner,
General Dynamics/General Atomic,
San Diego, California..... 110

33. * Thermal Energy Ion-Molecule Reactions
Fred C. Fehsenfeld,
Institute for Telecommunication Sciences and Aeronomy,
ESSA, Boulder, Colorado..... 119

34. * Low Energy Collisions Between Atomic Ions and Atoms
Felix T. Smith,
Stanford Research Institute
Menlo Park, California..... 120

35. Photoionization Study of Diatomic-Ion Formation in Argon, Krypton, and Xenon
R. E. Huffman and D. H. Katayama
Air Force Cambridge Research Laboratories,
Bedford, Massachusetts..... 121

* Invited Papers

ANALYSIS OF SOLIDS

Page No.

36. Operation of a Thermal Ionization Source on a Double Focusing Mass Spectrometer
K. J. Dickens, J.M. Holmes, A. J. Monks, P. Powers, and A. Riddoch, Scientific Apparatus Department, Associated Electrical Industries, LTD., Manchester, England..... 123

37. Minimizing the Contribution of Residual Gases to the Mass Spectrum of a Spark Source Mass Spectrometer
A. J. Socha and R. K. Willardson, Bell and Howell Research Center, Pasadena, California..... 127

38. Atom Clusters and Molecule Ions Observed in Spark Source Mass Spectra
H. D. Cook, Westinghouse Electric Corporation, West Mifflin, Pennsylvania..... 133

39. A Mass Spectrographic Technique for the Analysis of Molybdenum Additive in Tantalum Oxide Capacitor Films
D. L. Malm, Bell-Telephone Laboratories, Inc., Murray Hill, New Jersey..... 138

40. A Comparison of Mass Spectrographic, Photometric and Electrical Measurements of Impurities in Gallium Phosphide
A. J. Ahearn, F. A. Trumbore, C. J. Frosch, C. L. Luke, and D. L. Malm, Bell-Telephone Laboratories, Incorporated, Murray Hill, New Jersey..... 143

41. Spark Source Mass Spectrographic Assay of Rare Earth Metals and Oxides
R. J. Conzemius, J. Capellen, and H.J. Svec, Iowa State University, Ames, Iowa..... 149

42. Analysis of Plutonium Metal by Spark Sources Mass Spectroscopy
A. J. Johnson, A. Kozy, and R. N. Morris, Dow Chemical Company, Golden, Colorado..... 154

43. Analysis of Organic Thin Layers Using the Spinning Electrode Spark Source Mass Spectrograph
L.C. Scala, G.G. Sweeney, and W. M. Hickam, Westinghouse Research Laboratories, Pittsburgh, Pennsylvania..... 160

Page No.

44. Spinning Electrode Spark Source Mass Spectrographic Study of PVC Containing TiO_2
G.G. Sweeney and W.M. Hickam
Westinghouse Research Laboratories,
Pittsburgh, Pennsylvania, and
L. B. Crider,
B. F. Goodrich Chemical Company,
Avon Lake, Ohio..... 165

45. Solid Propellant Investigation With Spark Ion Mass Spectrography
B. Goshgarian,
Air Force Rocket Propulsion Laboratory,
(AFSC) Edwards, California..... 170

46. Pyrolytic Investigation of Silica-Phenolic Ablative Resins
S.N. Cohz,
Rocketdyne Corporation,
Canoga Park, California..... 180

COLLISIONS AND ION MOLECULE REACTIONS

47. On a Semi-Classical Model for the Collision-Induved Dissociation of Fast Ions
J. Durup,
Laboratoire de Chimie Physique,
Orsay, France..... 190

48. Studies of Collision-Induced Dissociation and Endothermic Ion-Molecule Reactions
K.M. Refaey and W.A. Chupka,
Argonne National Laboratory,
Argonne, Illinois..... 197

49. On Obtaining Microscopic Cross Sections for Ion-Molecule Reactions
G. Gioumousis, D.D. Briglia, and
T. E. Sharp,
Lockheed Missiles and Space Company,
Palo Alto, California..... 203

50. Isotope Effects in the Dissociation Reactions of Rare Gas Hydride Ions
R. W. Rozett and W.S. Koski,
The Johns Hopkins University,
Baltimore, Maryland..... 210

51. A Tandem Mass Spectrometer for the Study of Ion-Molecule Reactions
H. Futrell, C.D. Miller and
Fred P. Abramson,
Aerospace Research Laboratories,
Wright-Patterson Air Force Base, Ohio..... 215

Page No.

52. Mass Spectrometric Investigation of H^- and H_2^-, H and H_2 Transfer Reactions in C_3- C_4 Hydrocarbons
L. Wayne Sieck, Fred P. Abramson, and Jean H. Futrell, Aerospace Research Laboratories, Wright-Patterson Air Force Base, Ohio..... 223

53. Reaction Rate Studies Using Pulsed Ion Cyclotron Resonance
R. A. Fluegge and Darold Wobschall, Cornell Aeronautical Laboratory, Inc. Buffalo, New York..... 231

54. Competition Between Charge Transfer and Ion-Molecule Mechanisms in an Endothermic Negative Ion-Neutral Reaction
J. F. Paulson, L.G. Hanscom Field, Bedford, Massachusetts, and F. Dale, Control Equipment Corporation, Needham Heights, Massachusetts..... 238

55. Ion-Molecule Reactions in Acetonitrile and Propionitrile
J. L. Franklin, Yasuo Wada, P. Natalis and P.M. Hierl, Rice University, Houston, Texas..... 246

56. Ion-Molecule Reactions in Methane, Ethane, and Propane
Fred P. Abramson, Larry I. Bone, and Jean H. Futrell, Aerospace Research Laboratories, Wright-Patterson Air Force Base, Ohio..... 247

57. Ion-Molecular Reactions in Ethanol and Methanol
L. Wayne Sieck, Fred P. Abramson, and Jean H. Futrell, Aerospace Research Laboratories, Wright-Patterson Air Force Base, Ohio..... 257

DETECTION AND DATA PROCESSING

58. The Evaporated Silver Bromide Film as an Ion Detector
Maynard H. Hunt, Air Force Cambridge Research Laboratories, Bedford, Massachusetts..... 267

59. Photographic Versus Electric Recording
K. Habfast and K. H. Maurer, Fried, Krupp Mess-Und Analysentechnik, Bremen, Germany..... 271

Page No.

60. Automatic Evaluation of Photographically Registered Mass Spectrogrammes. Instrumentation, Physical and Technological Limitations
Klaus Heinecke,
Ernst Lietz GMBH,
Wetzlar, Germany..... 277

61. A System for the Quantitative Evaluation of Mass Spectrograph Plates
P.R. Kennicott,
General Electronic Research and Development Center,
Schenectady, New York..... 278

62. Propagation of Error from Densitometer Data to Spectrographic Results
J.M. McCrea,
Applied Research Laboratory,
U.S. Steel Corporation,
Monreville, Pennsylvania..... 282

63. Electronic Analog Computer for Measuring Intensity Areas on Mass Spectrographic Plates
P.J. Paulsen and P.E. Branch,
Spectrochemical Analysis Section,
National Bureau of Standards,
Washington, D.C..... 290

64. Computer Techniques for Fast Scanning High Resolution Mass Spectrometers
W. J. McMurray and S.R. Lipsky,
Yale University School of Medicine,
New Haven, Connecticut..... 297

65. Scintillation Detection Coincidence System
W. E. Duffy and C. P. Puiz,
General Electric Company,
Pleasanton, California..... 302

66. A Flexible Digital Data System for Sector Field Instruments
G.H. Riley and D. L. Bacon,
Graduate Research Center of the Southwest,
Dallas, Texas..... 305

67. Semi-Automatic Data Collection Systems for Mass Spectrometer
C.M. Stevens, D.B. Walling and
P. E. Moreland, Jr.,
Argonne National Laboratory,
Argonne, Illinois..... 312

68. A Programmed Voltage Scanner and Data Collection System for High Speed Ion Pulse Couting
W.E. Duffy,
General Electronic Company,
Pleasanton, California..... 318

Page No.

69. * Computer-Aided Interpretation of High Resolution Mass Spectra
K. Biemann and P.V. Fennessey,
Massachusetts Institute of Technology,
Cambridge, Massachusetts 322

70. * Current Status of Type Analysis by Mass Spectrometry
W. C. Ferguson,
Union Oil Company of California
Brea, California..... 327

71. * Use of Labeled Molecules in Mass Spectral Studies of Organic Molecules
L.C. Leitch,
National Research Council,
Ottawa, Canada..... 328

72. * Supplemental Measurements in Probing Electron Impact-Induced Decomposition VIA Mass Spectra of Labeled Compounds
Seymour Meyerson,
American Oil Company,
Whiting, Indiana..... 329

73. * Mass Spectrometric Identification of Gaseous Products from Thermal Analysis
R.S. Gohlke,
Dow Corning Corporation,
Midland, Michigan, and
H.G. Langer,
The Dow Chemical Company,
Wayland, Massachusetts..... 334

74. * The Use of Photoionization in Analytical Mass Spectrometry
C.E. Brion,
University of British Columbia,
Vancouver, British Columbia..... 338

75. * Simplified Mass Spectra II - by Means of a Dual Field Ionization/Electron Bombardment Source
Graham G. Wanless and George A. Glock,Jr.,
Esso Research and Engineering Company,
Linden, New Jersey..... 345

INSTRUMENTATION I

76. A Mass Spectrograph With Very Large Dispersion
H. Matsuda, S. Fukumoto and
Y. Kuroda
Osaka University,
Toyonaka, Osaka, Japan, and
M. Nojiri,
Japan Electron Optics Laboratory,
1418, Nakagamicho, Akishimashi, Japan..... 356

* Invited Paper

Page No.

77. A New Commerical Double Focusing Mass Spectrometer/Spectrograph with a Mattaush-Herzog Optics Design
S. Guibourg, J.C. Merlivat, Ph. Dard, and B. Swiners, Thomson-Houston, Cie, Paris, France..... 361

78. Mass Spectrograph with Spherical Condenser
L.A. Cambey, R. J. Hessler, and L.E. Snurr, Nuclide Corporation, State College, Pennsylvania..... 364

79. Constant Momentum Mass Spectrometer for Ionospheric Investigations
H.M. Luther and B.R.F.Kendall, Ionosphere Research Laboratory, Pennsylvania State University, University Park, Pennsylvania..... 369

80. A New Universal Single Focusing 12" -15,000 Volt Mass Spectrometer of High Performances
S. Guibourg, J.C. Merlivat, G. Bernard, Ph. Dard, and B. Swiners, Thomson-Houston, Cie, Paris, France..... 373

81. Mass Spectrometer for Routine Works on Radioactive Products
C. Nief, P. Lonez, and M. Lucas, Commissariat a l'Energie Atomique, Saclay, France..... 381

82. The Small Mass Spectrometer - A New Approach to Analysis
D. Allenden, Associated Electrical Industries,Limited, Urmston, Manchester..... 387

83. New Performance Results for the 12-90G Mass Spectrometer System
D.J. Marshall and T. J. Eskew, Nuclide Corporation, Medford, Massachusetts..... 388

84. Performance Characteristics of a New Time-Of-Flight Mass Spectrometer
R. W. Bonham and D.C. Damoth, Bendix Corporation, Cincinnati, Ohio..... 395

85. A Solid State Digitizer of Peak Height and Mass Number for Mass Spectrometers
S. Guibourg, J.C. Merlivat, R. Sigelle, and B. Swiners, Thomson-Houston Cie, Paris, France..... 400

Page No.

86. Mass Spectra of Organic Compounds Demonstrating a New Vacuum Lock Direct Introduction System and Automatic Mass Marking
H.W. Major, Jr., and A.H. Struck,
Perkin-Elmer Corporation,
Norwalk, Connecticut..... 405

MASS SPECTRA OF ORGANIC MOLECULES

87. Thermal Decomposition and Electron Impact Fragmentation of Some Typical Organic Molecules
C. Brunnee, K. Habfast, and
K. Kronenberger,
Fried.Krupp Mess-Und Analysentechnik,
Bremen, Germany..... 410

88. Temperature Effect Upon Ketone Mass Spectra
R.A. Meyer, and M. Cher,
North American Avaition Science Center,
Thousand Oaks, California..... 416

89. Mass Spectrometry and Radiation Chemistry of Gases Studies on Acetone and Other Light Ketones
J.H. Green and B.C. DeSouza,
The University of New South Wales,
Sydney, Australia..... 421

90. A Computerized Mass Spectral Correlation Study on Cyclic Ketones
Mynard C. Hamming and E. J. Eisenbraun,
Continental Oil Company,
Ponca City, Oklanoma, and
Oklahoma State University,
Stillwater, Oklahoma..... 427

91. A Generalized Mechanism for Mass Spectral Reactions
F.W. McLafferty,
Purdue University,
Lafayette, Indiana..... 435

92. Structures of Gaseous Ions: Utilization of Metastable Ion Transitions
T. W. Shannon and F.W. McLafferty
Purdue University,
Lafayette, Indiana..... 436

93. Some Aspects of the Production of Metastables
R.I. Reed and (Miss) M-T. Robert-Lopez,
The University of Glasgow,
Glasgow, W.2, England..... 442

Page No.

94. Appearance Potential Studies of Some Polyphenyls Using an Automatic Voltage Scanner
E.J. Gallegos and R.F. Klaver, Chevron Research Company, Richmond, California..... 446

95. The Decomposition of Tropylium and Substituted Tropylium Ions
K.R.Jennings and J.H. Futrell, Aerospace Research Laboratories, Wright-Patterson Air Force Base, Ohio..... 455

96. Mass Spectra of Substituted Phenyl Esters
John G. Larson and A. Bruce King, Gulf Research and Development Company, Pittsburgh, Pennsylvania..... 462

97. Mass Spectrometric Studies of Selected Ions in Deuterated Alkythiophenes
Norman G. Foster and Robert W. Higgins, Texas Woman's University, Denton, Texas..... 463

SYMPOSIUM ON INSTRUMENTATION DEVELOPMENT

98. * The Response of Ion-Sensitive Plates as a Function of Ion Energy
J.R. Woolston, R.E. Honig, and E.M. Botnick, RCA Laboratories, Princeton, New Jersey..... 471

99. * Gelatine-Free Ion-Sensitive Plates for Mass Spectrography
R.E. Honig, J.R. Woolston, and D.A. Kramer, RCA Laboratories, Princeton, New Jersey..... 481

100. * The Use of Negative Thermal Ions for the Determination of the Isotopic Composition of Boron, Etc.
S. J. van Rensburg, South African Atomic Energy Board, Pelindaba, Union of South Africa..... 492

101. * A Six Inch Radius Mass Spectrometer Which Simultaneously Collects Positive and Negative Ions
Harry J. Svec and Geral D. Flesch, Iowa State University, Ames, Iowa..... 499

102. * Present Status of the Princeton RF Spectrometer
L.G. Smith, Princeton University, Princeton, New Jersey..... 506

* Invited Paper

Page No.

103. Magnet Design of a Multi-Trajectory Ion Beam Analyzer
F.A. White,
Rensselaer Polytechnic Institute,
Troy, New York..... 514

104. Use of a Time-Of-Flight Mass Spectrometer as a Modulated Molecular Beam Detector
F. T. Green and T.A. Milne,
Midwest Research Institute,
Kansas City, Missouri..... 516

105. An Information Retrieval System for Organic Mass Spectrometry
Sixten Abrahamsson, Gunnar Haggstrom, and Einar Stenhagen,
Institute of Medical Biochemistry,
University of Goteborg, Sweden..... 522

INSTRUMENTATION II

106. Simplified Units and Equations Appropriate for Use with Mass Spectrometer Calculations
Wilson M. Brubaker,
Bell and Howell Research Center,
Pasadena, California..... 528

107. Theoretical Aspects of a Momentum Focusing Ion Optic System
W.S. Updegrove,
Automatic Welding Company,
Tulsa, Oklahoma..... 532

108. Mattauch-Herzog Type Mass Spectrograph with Two-Stage Electrostatic Field
Isoa Takeshita,
Matsushita Electric Industrial Company,
Kadoma, Osaka, Japan..... 533

109. Precise Mass Determination with a Medium Resolution Mass Spectrometer
Harmon W. Brown and Robert C. Jones,
Varian Associates,
Palo Alto, California..... 539

110. The Effects of Inhomogeneous Fields in a Cycloidal Mass Spectrometer
Hanspeter Benz, Harmon W. Brown, and John Pavkovich,
Varian Associates,
Palo Alto, California..... 545

111. Measurement of Translational Energy in a Time-Of-Fligth Mass Spectrometer
J.L. Franklin, Peter M. Hierl, and David A. Whan,
Rice University,
Houston, Texas..... 550

Page No.

112. Structure of Gaseous Ions: Utilization of Substitutent Effects
Maurice M. Bursey and F.W. McLafferty, Purdue University, Lafayette, Indiana 558

113. A Comparison of Mass-Spectrometric and Solvolytic Behavior of Certain Organic Molecules
Don C. S. Jongh and Stephen R. Shrader, Wayne State University, Detroit, Michigan 564

114. Spectra of Derivatives of Some Aromatic Compounds
Nobuhide Wasada and Toshikazu Tsuchiya, Government Chemical Industrial Research Institute, Tokyo, Japan 567

115. Mass Spectrometric Fragmentation of Substituted Propionic and Butyric Acids
R.D. Grigsby, M.C. Hamming, E. J. Eisenbraun, D.V. Hertzler, and N. Bradley, Continental Oil Company, Ponca City, Olkahoma; Oklahoma State University, Stillwater, Oklahoma; and Panhandle A and M College, Goodwell, Oklahoma 574

116. Mass Spectrometric Analysis of Some 8-Quinolinols
Robert L. Stevenson and Morton E. Wacks, University of Arizona, Tucson, Arizona 581

117. Electron Impact Studies I: Skeletal Rearrangements of Semi-Carbazones and Thiosemicarbazones
K.G. Das and P.S. Kulkarni, National Chemical Laboratory, Poona 8, India 588

118. Fragmentation of Some β-Lactams
M.S. Manhas, B.N. Ghosh-Mazumdar and Ajay K. Bose, Stevens Institute of Technology, Hoboken, New Jersey 591

Page No.

119. High Resolution Mass Spectrometry in Fragmentation Studies of Sesquiterpenes and Related Compounds
Catherine Fenselau, W.J. Richter, and A.L. Burlingame, University of California, Berkeley, California..... 593

120. High Resolution Mass Spectrometry in Molecular Structure and Stereochemical Studies: Effect of Stereochemistry on the Fragmentation of Epimeric Derivatives of Azabicyclo-Alkanes
D.H. Smith, H.K. Schnoes, and A. L. Burlingame, University of California, Berkeley, California..... 599

121. The Use of Fragmentation Patters of 1,4 Benzodiazepines for the Structure Determination of their Metabolites by High Resolution Mass Spectrometry
P. Bommer and F.M. Vane, Hoffmann-Laroche, Inc., Nutley, New Jersey..... 606

122. The High Resolution Mass Spectra of Primary Aliphatic Alcohols
P.A. Wadsworth, Shell Development Company, Emeryville, California..... 610

123. Analysis of Complex Mixtures of Aromatic Compounds by High Resolution Mass Spectrometry
B.H. Johnson and Thomas Aczel, Esso Research and Engineering Company, Baytown, Texas..... 611

124. Interpretation of High Resolution Mass Spectra
M. Barber, P. Powers, and W.A. Wolstenholme, Associated Electrical Industries Limited, Manchester, England..... 618

125. Long-Range Peak Matching Techniques Using the MS-9
H.M. Fales, R. Binks, M. Elliot, and R. Freeman, National Institutes of Health, Bethesda, Maryland..... 625

126. Automatic Reduction of High-Resolution Mass Spectral Data
R. Venkataraghavan, F.W. McLafferty, and J.W. Amy, Purdue University, Lafayette, Indiana..... 627

Page No.

127. The Mass Spectra of Some Organo Phosphorus Pesticidal Compounds
Joseph N. Damico, Department of Health, Education, and Welfare, Washington, D.C. 633

128. Mass Spectrometry of Biosynthetically Labeled Ricinine
George Waller and Ragnar Rynage, The Karolinska Institutet, Stockholm, Sweden, and Seymour Meyerson, American Oil Company, Whiting, Indiana 643

129. Rearrangements in the Mass Spectrum of Methyl Isobutyrate
D. R. Black, W. H. McFadden, and L. Boggs, Western Regional Research Laboratory, Albany, California 650

ELECTRON IMPACT PROBLEMS; DATA PROCESSING

130. A More Efficient Electron Gun for Sector Mass Spectrometers
G. D. Flesch and H.J. Svec, Iowa State University, Ames, Iowa 651

131. Some Characteristics of Electron-Impact Ion Sources
R. Clampitt, The University, Bristol, England 658

132. Multiple-Impact Ionization in Neon and Argon Using a Trapped-Ion Source
P.A. Redhead, National Research Council, Ottawa, Canada 661

133. Electron Monochromator Ion Source System
A.L. Yergy, D. J. Marshall, and T. J. Eskew, Nuclide Corporation, State College, Pennsylvania 668

134. A Two-Stage Double-Hemispherical Electron-Energy Selector
Kogoro Maeda and F.P. Lossing, National Research Council, Ottawa, Canada 669

Page No.

135. Resolution of Fine Structure in Ionization Efficiency Curves
Robert E. Winters, Jerome H. Collins, and William L. Courchene, The Procter and Gamble Company, Cincinnati, Ohio..... 677

136. Fine Structure in Appearance Potential Curves by Instrumental and Analytical Techniques
Dwight A. Hutchison, Argonne National Laboratory, Argonne, Illinois..... 687

137. Techniques for Improving the CRT Display of Rapid Scanning Magnetic Deflection Mass Spectrometers
George E. Salser, New York University, Bronx, New York..... 688

138. Computer Data Processing for Time Resolved Mass Spectrometry
R.T. Meyer, C.E. Olsen, and R.R. Berlint, Sandia Laboratory, Albuquerque, New Mexico..... 693

139. Search of the Mass Spectroscopy Literature by Means of a Computer Program
J. Capellen, H.J. Svec, and C. R. Sage, Iowa State University, Ames, Iowa..... 700

140. The NBS Mass Spectrometry Data Center
F.N. Harllee, J.T. Herron, and H.M. Rosenstock, National Bureau of Standards, Washington, D.C..... 707

140A Mass Spectrometry Data Center-Aldermaston
R.G. Ridley, Atomic Weapons Research Establishment, Aldermaston, Berks, England..... 710

ANALYTICAL TECHNIQUES

141. A Combined Electron Impact/Field Ion Source for High Molecular Weight Samples of Low Volatility
C. Brunnee, Fried.Krupp Mess-Und Analysentechnick, Bremen, Germany..... 712

Page No.

142. A General Method for Collection and Mass Spectrometer Analysis of Submicrogram Samples
E.M. Chait, J.W. Amy, and F.W. McLafferty, Purdue University, Lafayette, Indiana..... 719

143. Analysis of Natural Products by the Direct Combination of Gas Chromatography and Mass Spectrometry
A.H. Struck and W. Averill, Perkin-Elmer Corporation, Norwalk, Connecticut..... 721

144. Mass Spectrometric Determination of Trace Impurities in Oxygen
John Roboz, Air Reduction Company, Murray Hill, New Jersey..... 728

145. A Cold Cathode-Quadrupole Mass Spectrometer
F.L. Torney and P. Blum, National Research Corporation, Cambridge, Massachusetts..... 734

146. Equilibrium in the Isotopic Disproportionation Reaction Between Light and Heavy Water
James W. Pyper, Ray S. Newbury, and George W. Barton, Jr., Lawrence Radiation Laboratory, University of California, Livermore, California..... 746

147. Evolution of Sampling Techniques for Mass Spectrometric Analysis of Sealed Devices
B.I. Grady, Jr., General Electric Company, Owensboro, Kentucky..... 751

148. Evaluation of Incandescent Lamps with the Mass Spectrometer
H.R. Schoenfeldt, General Electric Company, Cleveland, Ohio..... 758

149. Ghost Peaks from Quadrupole Field Mass Spectrometers
N.E. Hamilton, Lennecott Copper Corporation, Lexington, Massachusetts..... 762

Bibliography - Fundamental and Theoretical Aspects of Mass Spectrometry..... 763

Bibliography - High Mass Spectrometry Literature..... 799

Bibliography - Mass Spectrometry of Solids..... 817

Photoionization of Vapors of Inorganic Elements and Compounds*

J. Berkowitz and W.A. Chupka
Argonne National Laboratory
Argonne, Illinois

Abstract

A vacuum ultraviolet monochromator has been combined with a very-high-transmission magnetic mass spectrometer to make possible photoionization studies of vapor species of low concentrations, such as occur in molecular beams formed by effusion from high-temperature Knudsen cells. Photoionization cross sections as a function of photon energy have been measured for a number of molecules of several elements and metal halides. Very accurate ionization potentials and dissociation energies have been determined in favorable cases.

* Work performed under the auspices of the U.S. Atomic Energy Commission.

Studies of Partial Molar Quantities at High Temperatures
Using A Mass Spectrometer

E. K. Storms
University of California
Los Alamos Scientific Laboratory
Los Alamos, New Mexico

Abstract

A number of carbides, including the Zr-C and U-C systems, have been studied as a function of composition. From the measured pressures, the partial molar free energy and partial molar heat of vaporization were obtained. The techniques used to obtain the data and the significance of the results are discussed.

The Determination of Activities at High Temperatures By Mass Spectroscopy

G.R. Belton, R. Fruehan, M. Ginsberg, and R. Svedberg
University of Pennsylvania
Philadelphia, Pennsylvania

Abstract

In this paper, the conditions necessary for the determination of activities are presented and discussed. Experimental work from time-of-flight mass spectroscopy is presented for both metallic and salt solutions using three techniques: (a) internal standardization by means of a congruently vaporizing inert substance, (b) the measurement and comparison of monomer/dimer ratios, and (c) the measurement of the ratio of the ion currents of the solution components and subsequent Gibbs-Duhem integration.

The Vaporization of Some Simple Inorganic Compounds

Alfred Buchler and James L. Stauffer
Arthur D. Little, Inc.,
Cambridge, Massachusetts

Abstract

An electric quadrupole deflecting field has been used together with a magnetic deflection mass spectrometer to study the vaporization of alkali oxides, hydroxides, metaborates, and sulfates. The quadrupole lens is placed between the Knudsen effusion sample cell and the ion source of the mass spectrometer. It permits discrimination between the polar and non-polar components of the effusing vapor and thus provides data concerning the molecular structure of the species involved. Use of the quadrupole lens as a filter to eliminate the non-polar polymeric components of such vapors as those of the hydroxides and metaborates permits the determination of the fragmentation patterns and ionization efficiency curves of the polar monomers.

Inhomogeneous Field Deflection for Determination of Electronic And Geometric Structure of High Temperature Molecules Observed with a Mass Spectrometer

Gary D. Blue
University of Califronia
Santa Barbara, California

and

David J. Meschi
Lawrence Radiation Laboratory
University of California
Berkeley, California

Abstract

Inhomogeneous magnetic and electric field devices may be used in conjunction with a hign temperature oven as a molecular beam source and a mass spectrometer as a detector, thus utilizing the deflecting or focussing properties of these devices for the elucidation of the electronic and geometric structures of high temperature molecules by means of the measurement of their magnetic and electric moments. In addition, these devices may often be used to aid in the identification of the neutral precursors of the ions observed with the mass spectrometer.

An inhomogeneous field deflecting magnet of improved design has been constructed at the Lawrence Radiation Laboratory and tested with beams of paramagnetic atoms. The application to the identification of the electronic states of molecules will be discussed with special emphasis given to the possible existence and importance of multiplet states of the alkaline earth chalcogenides. The simply calculated and experimentally measured values of the field gradient in a Rabi-type magnet differ by as much as 50% and this fact must be considered in certain types of molecular beam experiments. A computer program, TRIM (IBM 7090), has been used to determine the location and shape of magnetic equipotentials for the Rabi pole pieces and is presently being applied to the improvement of the pole tip shapes in order to achieve greater fields and gradients.

Inhomogeneous electric fields have been used by other investigators to identify molecules which have permanent dipole moments and also to differentiate between Σ and π states of certain molecules. Such investigations showed the more ionic molecules of the alkaline earth dihalides to be bent. An improved ionic model has been formulated which successfully reproduces the observed trends in the shapes of these molecules and which may be used to predict the geometry of others.

The importance of the determination of the aforementioned structural parameters to a correct thermodynamic characterization of high temperature vapor molecules will be presented.

KNUDSEN CELL MEASUREMENTS TO DETERMINE THE STABILITIES OF GASEOUS CESIUM AND RUBIDIUM OXIDES*

J. H. Norman and H. G. Staley

General Atomic Division of General Dynamics Corporation
John Jay Hopkins Laboratory for Pure and Applied Science
San Diego, California

INTRODUCTION

Gaseous oxides of the alkali metals other than lithium have been considered to be rather unstable. Brewer and Mastick[1] expressed this opinion as a result of Born-Haber cycle calculations on gaseous linear $M^+—O^=—M^+$. Recently, Klemm and Scharf[2] have expressed doubt as to the validity of these conclusions and have experimentally searched for clues suggesting the presence of alkali metal oxide vapors. They suggest that a search for these species ought to be made by mass spectrometric means. More recently, Borisov, Gusarov, and Gorokhov[3] have investigated the vapors effusing from a cell containing CsO_2, apparently finding both Cs_2O and Cs_2O_4 vapor species. A considerable amount of work has been done on the lithium-oxygen system. Brewer and Margrave[4] and Nesmeyanov and Belykh[5] used Knudsen cell effusion measurements to demonstrate vaporization thermodynamic properties of lithium oxide. Berkowitz, et al., [6] used a mass spectrometric technique to study a lithium oxide-Knudsen cell effusate. They measured the heat of sublimation of $Li_2O(g)$. Hildenbrand, Hall, and Potter[7] made torsion cell measurements on this system. Büchler, et al., [8] have demonstrated Li_2O to be nonpolar, that is, linear or nearly so, and White, et al., [9] determined the matrix isolation spectra of Li_2O and analyzed these data. The latter authors also observed the species $Li_2O_2(g)$ mass spectrometrically. It is apparent then that while lithium oxide has been studied at length and is quite well defined, very little is known concerning other alkali metal oxide vapors.

GASEOUS IONIC MODEL CALCULATIONS

Brewer and Mastick's[1] Born-Haber cycle calculations on a linear ionic model for the alkali metal MOM species are reproduced in Table 1. In obtaining their values these authors estimated the Born repulsion factors for the individual oxides and developed a scheme for estimating the M-O bond distances. Also, they used an electron affinity for the process $O \rightarrow O^=$ of -168 kcal/mole. The resulting M-O bond energies are given in the last column of Table 1. One can see the trend toward lower bond energies with the heavier alkali metals. A check on these estimates is available only for Li_2O, which has been measured to be about 20 kcal/mole lower than Brewer's estimate.

After considering Brewer and Mastick's calculations, Klemm and Scharf[2] concluded that there was considerable question about the bond energies obtained by the earlier authors. They argue that polarization of the higher atomic number alkali metal ions by their surroundings would considerably increase the stability of the higher molecular weight oxides. They also used -155 kcal/mole for the electron affinity of an O atom for two electrons. Table 2 gives the bond energies obtained using the linear ionic model with the polarizabilities back-calculated from Klemm and Scharf's results. The calculated polarization energies per bond-mole for the alkali metal oxides are also presented. The Klemm and Scharf calculations indicate a significantly higher stability of the gaseous oxides and they certainly do create considerable interest in whether these oxides might have sufficient stability to be worth investigating.

These arguments, in addition to Borisov, Gusarov, and Gorokhov's[3] observations of the molecular ions, $Cs_2O_4^+$ and Cs_2O^+, have led us into a thermodynamic study of the alkali metal oxides.

*This work was supported by the Office of Civil Defense through U. S. Naval Radiological Defense Laboratory under contract N0022866C0403, Work Unit OCD No. 3111A, T.O. No. 65-200 (18).

EXPERIMENTAL

The systems $CsO_x(s)$ and $RbO_x(s)$ were studied by investigating the effusate of a platinum Knudsen cell containing the oxides. A 0.008 cm^2 area orifice was used for the cesium studies, while an ~0.0008 cm^2 area orifice was used for the rubidium studies. Cesium was oxidized in place in the mass spectrometer or cesium oxide obtained from Penn Rare Metals Inc. was placed in the cell. Rubidium oxide obtained from Chemicals Procurement Laboratories was found to be suitable for these studies. The cell was fitted with an oxygen feed system. The furnace, cell, and oxygen feed system as installed in a 21-703 CEC mass spectrometer are shown in Fig. 1. In these studies the cell was radiatively heated and the cell temperature was measured using a Pt–Pt-10%-Rh thermocouple attached to the base of the cell. A sample of $CsO_x \cdot (SiO_2)_y$ was also put in the cell and investigated as a portion of this study. In this case, electron bombardment heating was employed, as used in similar studies,[10] and cell temperatures were measured optically.

RESULTS

Four types of data were obtained in these studies:

1. electron impact appearance potentials of the observable ions,
2. oxygen pressure dependence of the ion intensities at constant temperature,
3. temperature dependence of these intensities, and
4. comparative ion intensity measurements where the cell pressure of a particular effusing substance is well known.

All of these studies were made after hydroxide species had been reduced to negligible quantities by evaporative processes.

Appearance potential measurements provided reasonable values for the observed oxide ions, as demonstrated in Table 3. The cesium study values and the species observed, however, were not in good agreement with the results of Borisov.[3] First, the ion $Cs_2O_4^+$ was not observed. If Borisov's experiment was performed under Knudsen conditions, he could not have had much higher oxygen activity in his system than was extant in this study. That is, the oxygen feed system was used for this work to bring the oxygen cell pressure near the Knudsen limit (~10^{-3} atm) at temperatures similar to those reportedly used by Borisov. In contrast, the species $Cs_2CO_3^+$ was observed in this study. Second, no agreement is seen in the other reported values. Borisov gives a value for the appearance potential of Cs_2O^+ which is about three volts higher than was found in this study. Also, Borisov did not observe $Cs_2O_2^+$, and his reported value for Cs^+ certainly indicates that this ion was from a fragmentation process. The ionizing voltage scale he reports seems somewhat unusual. The values obtained here were derived from linear extrapolation of ion currents calibrated against a similar mercury determination of 10.4 volts. Generally reliable values have been obtained in this laboratory using this method. The studies of Cs_2O evaporation did not provide an appearance potential for Cs^+ from Cs(g) since there was not an appreciable amount of cesium metal vapor effusing from the cell.

Rubidium appearance potentials obtained by similar methods were reasonable and do include a value of the Rb^+ appearance potential which is in good agreement with values reported in Kiser's compilation.[11] The value for the $Rb_2CO_3^+$ appearance potential seems to be about what might have been anticipated.

As a guide to whether fragmentation or kinetics could cause problems in the thermodynamic analysis, studies were made of the oxygen pressure dependence of the observed ion signals under isothermal conditions. Two bits of information could be obtained from these data: one, did the data indicate the anticipated thermodynamic behavior, and two, what was the condensed state like? If the ratios

$$P_M^2 \, P_{O_2}^{\frac{1}{2}} / P_{M_2O}$$

and where applicable

$$P_{M_2O} \, P_{O_2}^{\frac{1}{2}} / P_{M_2O_2}$$

TABLE I

GASEOUS ALKALI METAL OXIDE STABILITY

BREWER AND MASTICK'S[1] IONIZED LINEAR MODEL

	R CRYST (Å)	R_g (CALC) Å	REPULSION CORRECTION (1-1/n)	CRYSTAL ENERGY (KCAL/MOLE)	D(M-O) (KCAL/BOND MOLE)
Li_2O	2.00	1.52	0.834	633	108.0
Na_2O	2.40	1.94	0.857	510	52.0
K_2O	2.79	2.27	0.875	446	39.0
Rb_2O	2.92	2.37	0.883	424	32.0
Cs_2O	3.09	2.78	0.895	372	12.0

TABLE 2

POLARIZATION EFFECTS ACCORDING TO KLEMM AND SCHARF[2]

	α_{Me^+} (Å^3)	P(KCAL/BOND MOLE)	D(M-O) (KCAL/BOND MOLE)
Li_2O	0.076	6.0	121
Na_2O	0.209	6.4	65
K_2O	0.876	16.8	62
Rb_2O	1.82	25.8	64
Cs_2O	2.80	21.3	40

TABLE 3

APPEARANCE POTENTIALS (eV) OF CESIUM AND RUBIDIUM OXIDES

	Cs(B.G.G.)[3]	Cs	Rb
M^+	~6.5	(4.0)	4.3
M_2O^+ I	7.4	4.6	4.9
M_2O^+ II	10.4		
$M_2O_2^+$		4.9	
$M_2CO_3^+$		P	6.3
$M_2O_4^+$	P?		

were constant with varying oxygen pressures, it was believed that fragmentation was not causing a problem and that probably gas-phase equilibrium essentially existed in the cell. This condition was attained in both the cesium and rubidium studies.

The results of the oxygen dependence experiments are illustrated in Fig. 2. In these studies, data pertaining to the condensed phase were also obtained. The $Cs_2O_2^+$ ion intensity increased with increasing oxygen to a degree similar to the degree that the Cs_2O^+ intensity decreased. This would suggest that the solid-phase composition was between Cs_2O and Cs_2O_2 over the oxygen pressure range studied. One might suggest that it was not very near either end composition. The Rb_2O^+ ion intensity had the same type of oxygen pressure dependence as Cs_2O^+, indicating that the condensed phase present in these studies was $Rb_2O_{(1+x)}$ similarly.

To study the thermodynamics associated with the observed gaseous oxides, ion intensity ratios measured at a nominal 20 eV were studied over the condensed oxides as a function of cell temperature T. The temperature dependence of

$$\frac{I_{Cs_2O}\, T^{\frac{1}{4}}}{I_{Cs_2O_2}}$$

was studied and is reported in Fig. 3. Four separate determinations of this quantity between 960° and $770^\circ K$ lead to 21.5 ± 1.7 kcal/mole for the heat of the reaction

$$Cs_2O_2(g) \longleftrightarrow Cs_2O(g) + \tfrac{1}{2}O_2 \quad . \tag{1}$$

These experiments were carried out with a constant high oxygen flux into and out of the cell. For this reason, the cell pressure of oxygen was assumed proportional to $T^{\frac{1}{2}}$.

The temperature dependence of the ion ratio

$$\frac{I^2_{Cs}\, T^{\frac{5}{4}}}{I_{Cs_2O}}$$

which governs the reaction

$$Cs_2O(g) \longleftrightarrow 2Cs(g) + \tfrac{1}{2}O_2 \tag{2}$$

where a high oxygen flux is passed through the Knudsen cell is shown in Fig. 4. The data shown are typical of the three determinations of this temperature coefficient. These effusion studies were made on a cesium silicate melt. The degree of dissociation of $Cs_2O(g)$ from this melt was greatly increased because of the higher temperatures and/or lower pressures employed with this sample. These data exhibited somewhat more scatter than desirable. In this study it was necessary to contend with time dependence of the ion intensities since the cesium activity was changing in the silicate melt. The measured heat for reaction (2) was 77.1 ± 6.3 kcal/mole in the temperature range 1600° to $1320^\circ K$.

Rubidium oxide data were measured without excess oxygen flux over the oxide sample. The temperature dependence for the reaction

$$Rb_2O(g) \longleftrightarrow 2Rb(g) + \tfrac{1}{2}O_2 \tag{3}$$

was thus determined by following the ion intensity ratio

$$\frac{I^2_{Rb}\, I^{\frac{1}{2}}_{O_2}\, T^{\frac{3}{2}}}{I_{Rb_2O}}$$

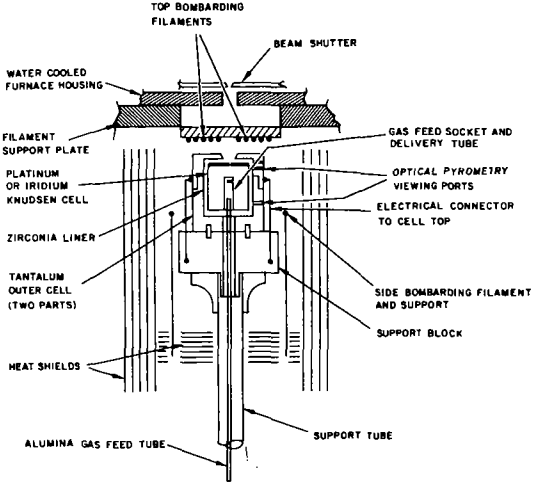

FIG. 1 IRIDIUM KNUDSEN CELL AND FURNACE

FIGURE 2
OXYGEN DEPENDENCE OF ALKALI METAL SIGNALS

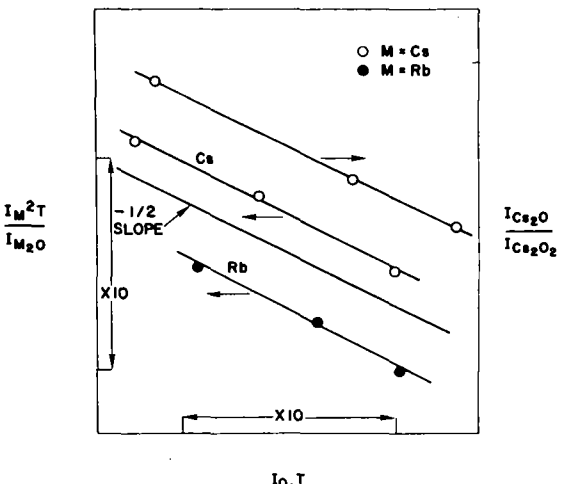

as the temperature was varied. This study gave a heat of reaction (3) of 51.4 ± 1.7 kcal/mole between 1160° and 1010°K. One of three measurements is shown in Fig. 5. A search for Rb_2O_2 did not reveal this species; however, a severe background problem made this search insensitive.

Vapor pressure calibrations were made for these systems by co-effusing some element whose vapor pressure is reasonably well known and comparing ion intensities of this species with that of the unknown species. This comparison was made using Otvos and Stevenson's[12] cross sections and employing ionizing voltages and multiplier gains according to the method described by Inghram and Drowart.[13] Multiplier gains inversely proportional to molecular weight were employed.

The vapor pressures of Cs(l), before conversion of this material in situ to $Cs_2O_{(l+x)}$, was used to calibrate reaction (1) pressures. Reaction (2) and (3) pressures were calibrated using silver vapor pressures. The silver was held in a platinum cup inside the Knudsen cell. Since the apparatus employs a cell with an orifice in the bottom (the oxygen feed system) as well as in the top, vapor pressures of the pure substance had to be employed, that is, total evaporation experiments could not be used. Entropies measured in the same temperature regions as the heats of reactions (1), (2), and (3) were determined, respectively, to be 18.9 ± 2, 34.7 ± 4, and 30.5 ± 2 e.u. The uncertainties presented here are such that these last two entropies may be considered to be essentially the same statistically.

DISCUSSION

Dissociation energies calculated from the heats of reactions (2) and (3) most certainly lead one to strongly question the calculation system presented by Brewer and Mastick[1] for estimating the stability of the oxides. From the data of this study one would calculate a Cs-O bond energy in Cs_2O as 69 kcal/mole at 1460°K. This is indeed in excess of the 12 kcal/mole calculated by Brewer. The Rb-O bond energy similarly is 56 kcal/mole, while Brewer calculates 32 kcal/mole. Klemm and Scharf's[2] calculations, although they were presented as indicating tendencies only, are closer but do not seem to give a proper rubidium-cesium trend. The polarizabilities they selected have been questioned,[14] but the differences are not critical. Polarization energies of rubidium and cesium, then, probably do not totally solve the bond energy calculational problem. The solution must be elsewhere. For instance, both White[9] and Büchler[8] report $Li_2O(g)$ as being a linear molecule, while Büchler[15] has suggested that $Cs_2O(g)$ is quite polar and, hence, nonlinear.

Further studies of the alkali metal oxides are planned. It is hoped that the results of these studies will help to clarify the calculational problem and certainly to demonstrate the thermodynamics associated with the formation of $M_2O(g)$ molecules for the alkali metals.

REFERENCES

1. Brewer, L., and D. F. Mastick, J. Am. Chem. Soc., 73, 2045 (1951).
2. Klemm, V. W., and H. J. Scharf, Z. Anorg. Allg. Chem., 303, 236 (1960).
3. Borisov, Y. A., A. V. Gusarov, and L. N. Gorokhov, Teplofizika Vysokikh Temperatur, 2, 487 (1964).
4. Brewer, L., and J. L. Margrave, J. Phys. Chem., 59, 421 (1955).
5. Nesmeyanov, A. N., and L. P. Belykh, Zh. Fiz. Khim., 34, 841 (1960).
6. Berkowitz, J., W. A. Chupka, G. D. Blue, and J. L. Margrave, J. Phys. Chem., 63, 644 (1959).
7. Hildenbrand, D. L., W. F. Hall, and N. D. Potter, J. Chem. Phys., 39, 296 (1963).
8. Büchler, A., J. L. Stauffer, W. Klemperer, and L. Wharton, J. Chem. Phys., 39, 2299 (1963).

FIGURE 3
DISSOCIATION OF Cs_2O_2 (g)

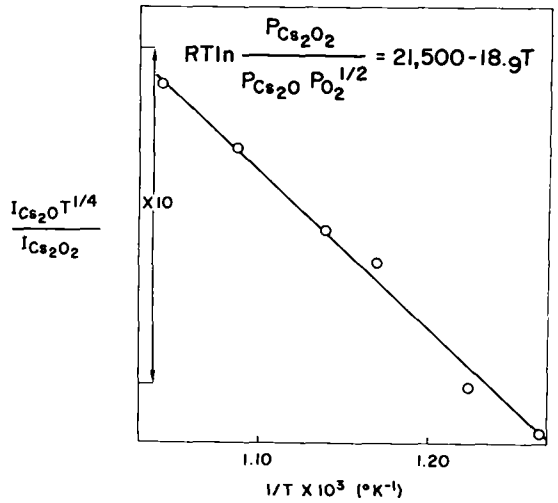

FIGURE 4
DISSOCIATION OF Cs_2O (g)

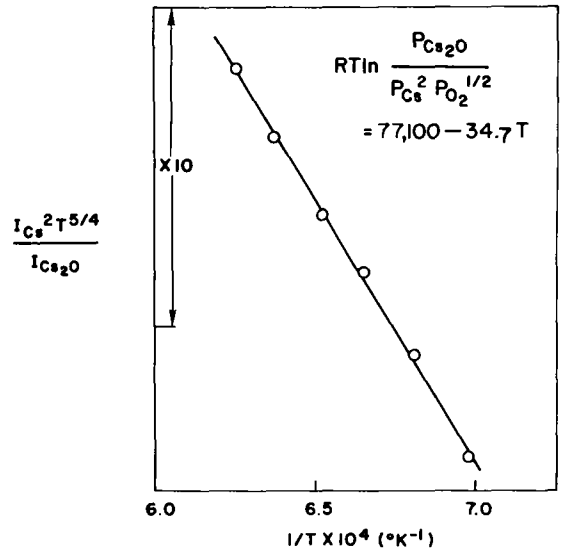

9. White, D., K. S. Seshadri, D. F. Dever, D. E. Mann, and M. J. Linevsky, J. Chem. Phys., 39, 2463 (1963).

10. Norman, J. H., H. G. Staley, and W. E. Bell, J. Phys. Chem., 69, 1373 (1965).

11. Kiser, R. W., Tables of Ionization Potentials, USAEC Report TID-6142, 1960.

12. Otvos, J. W., and D. P. Stevenson, J. Am. Chem. Soc., 78, 546 (1956).

13. Inghram, M. G., and J. Drowart, in Proceedings of the International Symposium on High Temperature Technology, held at Asilomar Conference Grounds, California, October 1959.

14. Tessman, J. R., A. H. Kahn, and W. Shockley, Phys. Rev., 92, 890 (1953).

15. Büchler, A., and J. L. Stauffer, in Fourteenth Annual Conference on Mass Spectrometry and Allied Topics, held at Dallas, Texas, May 1966.

FIGURE 5
DISSOCIATION OF $Rb_2O(g)$

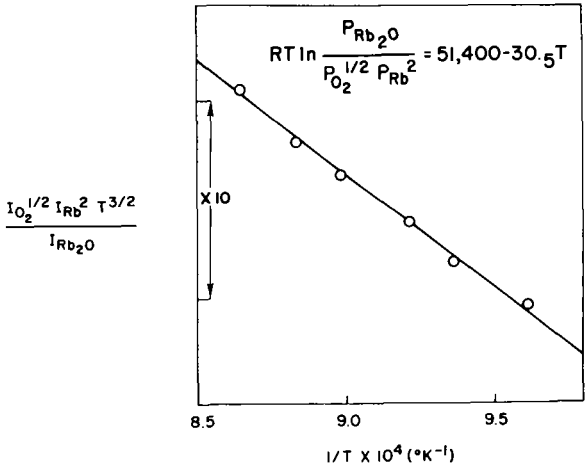

Mass Spectrometric Determination of the Dissociation Energy of $Na_2(g)$. The Ionization Cross Section of Na(g).

R.F. Pottie, Division of Applied Chemistry,
National Research Council, Ottawa, Canada.

Summary

The ion source of a mass spectrometer was modified for use as the reaction chamber in the determination of the equilibrium constant for the reaction: $Na_2(g) \rightleftharpoons 2\ Na\ (g)$.

Measurements in the temperature range: 150-200°C lead to ΔH_0^0 = 16.36 ± 0.48 Kcal/mole. The vapor pressures of Na_2 were significantly lower than those derived from previous measurements.

The cross section for ionization of Na(g) by 50 ev electrons was found to be 1.7 ± 0.2 x 10^{-16} cm^2.

Introduction

Experimental studies of the dissociation of diatomic sodium have been made by means of flame[1], molecular beam[2], and spectroscopic[3] techniques. A very thorough evaluation[4] of the vapor pressure and vapor density data for sodium has resulted in a value of the dissociation energy, D_0^0, which does not agree with that derived from the molecular beam or spectroscopic measurements. It was felt that direct study of this reaction by mass spectrometry could perhaps resolve the difficulty. The addition of an ion-collection electrode to the ion source of the mass spectrometer should also permit measurement of the ionization cross section of atomic sodium.

Experimental

The modified ion source that was employed for this study is shown in Figure 1. Details of the operation of this source have been published elsewhere[5]. Using an electron beam energy of 50 ev., ion currents were collected for m/e 23 (Na^+) and m/e 46 (Na_2^+). The vapor pressures of Na were taken from the tabulation of Nesmeyanov[6]. The following equations were used to determine the equilibrium constant for the reaction:

$$Na_2(g) \rightleftharpoons 2Na(g) \qquad \ldots. \quad (1)$$

$$P_{Na_2} = \frac{i^+Na_2}{i^+Na} \times \frac{\sigma_i(Na)}{\sigma_i(Na_2)} \times P_{Na} \qquad \ldots. \quad (2)$$

$$K_P = \frac{(P_{Na})^2}{(P_{Na_2})} = \frac{\sigma_i(Na_2)}{\sigma_i(Na)} \times \frac{i^+Na}{i^+Na_2} \times P_{Na} \qquad \ldots. \quad (3)$$

A value of 1.5 was assumed for the ratio of ionization cross sections, $\sigma_i\ (Na_2)\ /\sigma_i\ (Na)$.

Because of electrical difficulties in the ion source, it was not possible to obtain the ionization cross section of sodium by measuring the saturation current with the ion-collection electrode. Instead, ion currents were measured for m/e 23 and for a reference rare gas (argon or neon) that was introduced through the cell-inlet. Previously, relationships had been established between gas pressures in the inlet system and in the ion source by collection of saturation ion currents. The following equation relates the ion intensities to ionization cross sections:

$$\sigma_i\ (Na) = \frac{i^+Na}{i^+Ref.} \times \frac{T_{Na}}{273} \times \frac{P_{Ref,273°}}{P_{Na}} \times \sigma_i\ (Ref) \qquad \ldots. \quad (4)$$

The pressure of the reference gas is corrected for differences in temperature between the ion source and the gas reservoir.

Results and Discussion

A. The Ionization Cross Section of Atomic Sodium.

Following introduction of the sample, the ion sensitivity of sodium gradually increased over a two week period, after which it became constant and remained so for better than two months. Ion currents were measured during this latter period for source temperatures of 120-200°C, with the result: $\sigma_i(Na) = 1.7 \pm 0.2 \times 10^{-16}$ cm^2 for 50 ev electrons. The maximum yield of ions occurs at an ionizing voltage of 14 ev, and from the ionization efficiency curve we obtain σ_i max. = 3.6×10^{-16} cm^2. The value of $\sigma_i(Na)$ for 75 ev electrons is 1.33×10^{-16} cm^2.

In previous studies, Tate and Smith[7] employed the saturation current method to obtain σ_i max. = 1.05×10^{-16} cm^2, and Brink[8], using a modulated molecular beam with ionization detector, found σ_i max. = 8.6×10^{-16} cm^2. In the earlier work, no details of temperature regulation of the ion source are given, and in the later work, possible errors in assignment of beam density, efficiency of detection, and the relatively low sensitivity of the method could perhaps introduce an error of as much as a factor of two into the result.

The relative ionization cross section calculated by Otvos and Stevenson[9], when converted to an absolute scale[5], lead to $\sigma_i(Na) = 4.75 \times 10^{-16}$ cm^2 for 75 ev electrons, but by analogy to other atoms, this value should better approximate σ_i max. Application of the polarizability vs. ionization cross section relation of Lampe, Franklin and Field[10] combined with an atomic polarizability[11] of 22×10^{-24} cm^3 results in $\sigma_i(Na) = 2.7 \times 10^{-16}$ cm^2. This presumably is also a maximum yield.

We therefore conclude that the most probable value for $\sigma_i(Na)$ max. = $3 \pm 1 \times 10^{-16}$ cm^2.

B. The Dissociation Energy of $Na_2(g)$.

The results of the third law calculation of ΔH°_{298} for the dissociation of $Na_2(g)$ are given in Table I. The values for the free energy functions necessary for these calculations were obtained from the JANAF tables. The error listed is the standard deviation and the temperature is the average temperature of the ion source. From these results we obtain $\Delta H^\circ_{298} = 16.84 \pm 0.16$ kcal/mole, and $D^\circ_0 = 16.36$ kcal/mole. The limits of error are increased somewhat if we assign a reasonable uncertainty to the ratio of ionization cross sections in equation (2). *If this ratio is in the range* 1.5 ± 0.5, *then we have:* $D^\circ_0 = 16.36 \pm 0.48$ kcal/mole. The high value would obtain for $\sigma_i(Na_2) = \sigma_i(Na)$, a rather unlikely occurrence in view of the nature of the ionization efficiency curves for Na^+ and Na_2^+.

In Table II we have a summary of the various experimental values of D°_0. The result that is accepted by most critical compilations is that of Loomis, 17.2 ± 0.6 kcal/mole. It was obtained by a Birge-Sponer extrapolation of spectra taken by the magnetic rotation method. This value does not agree with that calculated by Thomson and Garelis from vapor pressure and density data.

A possible source of error in the mass spectrometric method is fragmentation of Na_2^+ induced by electron impact. This would reduce the calculated vapor pressures of Na_2 and would therefore result in a lower limit for D°_0. In table III the effect of D°_0 on the vapor pressure of Na_2 is presented via the third law method. It is seen that a relatively large uncertainty in vapor pressure produces little change in D°_0, whereas a small error in D°_0 would result in a large change in the calculated vapor pressures of Na_2. Thus for agreement with Thomson and Garelis, we must raise our D°_0 by 1.8 kcal/mole, or equivalently, the vapor pressures of Na_2 would have to be almost ten times those obtained in this investigation. It is most improbable that fragmentation of Na_2^+ in the mass spectrometer could account for such a discrepancy.

The conflict remains unresolved by this study, although the results reported here do give some support to the spectroscopic value of $D^\circ_0(Na_2)$ rather than to that which is based on the density and pressure data of sodium vapor.

TABLE 1. DISSOCIATION ENERGY OF DIATOMIC SODIUM

$Na_2(g) \rightleftharpoons 2Na(g)$, $\Delta H^\circ_{298} = 16.84 \pm .16$ Kcal/mole

T°k	PNa Atm x 10^8	PNa_2 Atm x 10^{11}	-Log k_p	ΔH°_{298} Kcal/mole
460	5.26	1.80	3.8133	16.54
464	6.49	2.57	3.7854	16.63
455	4.93	2.30	3.9759	16.70
450	3.59	1.38	4.0297	16.63
447	1.68	0.387	4.1371	16.73
456	4.93	1.89	3.8907	16.56
466	6.49	2.45	3.7648	16.66
453	3.68	1.20	3.9574	16.59
457	3.22	0.832	3.9045	16.62
457	3.03	0.812	3.9465	16.71
471	8.95	4.63	3.7620	16.83
472	9.41	5.09	3.7595	16.86
472	9.41	5.05	3.7563	16.85
460	3.82	1.20	3.9151	16.76
454	2.34	0.672	4.0890	16.90
452	2.05	0.624	4.1717	16.99
450	1.82	0.463	4.1455	16.86
441	1.17	0.263	4.2836	16.80
473	10.39	6.09	3.7513	16.88
474	10.66	6.26	3.7411	16.89
463	4.79	2.07	3.9556	16.95
462	4.49	1.89	3.9718	16.95
454	2.34	0.688	4.0991	16.92
447	1.58	0.492	4.2947	17.06
464	5.07	2.18	3.9284	16.93
463	5.26	2.42	3.9420	16.92
457	3.12	1.21	4.0944	17.03
456	3.03	1.12	4.0963	16.99
474	11.32	8.16	3.8041	17.03
473	10.33	6.64	3.7941	16.97
470	8.75	5.35	3.8435	16.97
445	1.36	0.299	4.2086	16.80
457	2.41	0.721	4.0939	17.02
472	5.39	2.13	3.8655	17.09

TABLE 11

D°_0 Values For $Na_2(g) \rightleftharpoons 2Na(g)$

D°_0 Kcal/mole	Reference and Method	
18.6 ± 1.0	H. Ootuka (1930)	$Na_2 + B_r$ Flames.
17.2 ± 0.6	F.W. Loomis (1932)	Magnetic Rot.Spectrum.
16.8 +	F.W. Loomis (1932)	Includes Van der waals forces (lower limit).
16.80 ± 0.20	L.C. Lewis (1931)	Magnetic separation of molecular beam.
18.20	Thomson & Garelis (1956)	Value selected for best agreement of V.P. data.
16.36 ± 0.48	This research	Mass spectrometric

REFERENCES

1. H. Ootuka, Z. Physik Chem. B7, 407 (1930).
2. L.C. Lewis, Z. Physik 69, 786 (1931).
3. F.W. Loomis and R.E. Nusbaum, Phys. Rev. 40, 380 (1932).
4. G.W. Thomson and E. Garelis, Chapter 3 in "Sodium, its manufacture, properties and uses", edited by M. Sittig (Reinhold Publishing Co., Inc., New York, 1956).
5. R.F. Pottie, J. Chem. Phys. 44, 916 (1966).
6. A.N. Nesmeyanov, "Vapor Pressures of the Chemical Elements", edited by R. Gary (Elsevier Publishing Co., Inc., New York 1963).
7. J.T. Tate and P.T. Smith, Phys. Rev. 46, 773 (1934).
8. G.O. Brink, Phys. Rev. A134, 345 (1964).
9. J.W. Otvos and D.P. Stevenson, J. Am. Chem. Soc. 78, 546 (1956).
10. B. Bederson and E.J. Robinson, Chapter on "Beam Measurements of Atomic Polarizabilities" in "Molecular Beams" edited by John Ross (Interscience Publishers, New York, 1966).

FIGURE 1

Mass-spectrometer ion source:
A, ion-collection electrode; B, ion-source furnace; C, sample furnace; D, sample holder with metal sample; E, gas-inlet tube; G, mounting plate; F, filament; T, electron trap; TC_1, source thermocouple; TC_2, sample thermocouple.

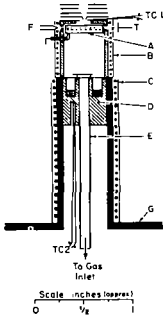

TABLE 111

Effect of D_0^0 on Vapor Pressure of Na_2

D_0^0 Kcal/mole	Vapor Pressure Na_2 - Atm 425°K	450°K	475°K	500°K
16.00	3.02×10^{-12}	2.64×10^{-11}	1.85×10^{-10}	1.03×10^{-9}
17.00	9.95×10^{-12}	8.08×10^{-11}	5.32×10^{-10}	2.80×10^{-9}
18.00	3.23×10^{-11}	2.47×10^{-10}	1.54×10^{-9}	7.67×10^{-9}
19.00	1.05×10^{-10}	7.57×10^{-10}	4.43×10^{-9}	2.10×10^{-8}

The Photoionization of H_2, HD, D_2 and N_2 at 584 Å

by D. C. Frost, C. A. McDowell and D. A. Vroom
Chemistry Department, University of British Columbia,
Vancouver, Canada

In the reaction

$$h\nu + AB \rightarrow AB^+ + \text{photoelectron}$$

conservation of momentum predicts that the photoelectron is endowed with virtually all the energy over and above that used to ionize AB. If $h\nu$ is known and the photoelectron kinetic energy measured, the ionization potential of AB may be deduced.

There is often the possibility that AB^+ may be formed in one of several vibrational states, and in these cases we expect to find groups of photoelectrons whose kinetic energies differ by the vibrational energy spacing in the ion. The relative intensities of the groups should reflect the populations of the vibrational states.

The apparatus is shown in Figure 1. Helium at a pressure of several microns passes through a 2450 mc/s microwave discharge tube. The gas is removed by rapid pumping, and the almost exclusively 584 Å radiation passed to an ionization region at the spheres' center. Photoelectrons and any energetic ions proceed outwards, the ions to be repelled by a suitable intergrid field and the electrons to be energy analyzed by a variable retarding field between outergrid and collector. A digital voltmeter is used to measure the photoelectron retarding voltage.

Our spherical grid apparatus, briefly reported on previously (1), has an advantage over the cylindrical designs hitherto employed (2) in that the photoelectrons are retarded by a field normal to their trajectories. This results in a much 'cleaner' photoelectron spectrum.

H_2, HD and D_2

A direct recorder trace of the photoelectron stopping curve for hydrogen is shown in Figure 2. The lower curve is the background obtained with no sample present. The first threshold, labelled 0-0, arises from photoelectrons ejected through transitions to the zero ionic vibrational level, and the steps at lower retarding voltages indicate photoelectron groups associated with transitions to successively higher levels. In all, nine levels are resolved.

The vibrational spacings and relative transition probabilities are measured directly from the stopping curve, the latter by extending the steps parallel to the background as indicated in Figure 2.

Table I compares our results for the H_2^+ vibrational spacings with other experimental and calculated values. The overall agreement is quite good. Our results are the average of at least 10 runs, and the quoted errors are standard deviations.

The relative transition probabilities to the various vibrational states of H_2^+ are given in Table II together with the appropriate Franck-Condon factors. The experimental 584 Å probabilities clearly differ from the calculated threshold values, the higher vibrational levels being relatively more highly populated at the higher energy.

The discrepancies may, of course, arise through invalid assumptions in the Franck-Condon factor calculations. In particular the variation of the electronic transition moment is assumed to be small and the Franck-Condon factors q are found through evaluation of

Table I

Ionization data for H_2

$E_{(v^1)} - E_{(v^1-1)}$ eV

v^1	Calc.(a)	Electron (b) Impact	This work
0	-	-	-
1	0.269	0.268 ± 0.01	0.27 ± 0.01
2	0.254	0.266	0.25 ± 0.01
3	0.239	0.235	0.24 ± 0.01
4	0.223	0.245	0.23 ± 0.01
5	0.208	0.20	0.21 ± 0.01
6	0.193	-	0.20 ± 0.01
7	0.177	-	0.19 ± 0.01
8	0.161	-	0.17 ± 0.01
9	0.146	-	0.16 ± 0.01

(a) See ref. 3
(b) See ref. 4

Table II

Ionization data for H_2

Transition Probabilities

v^1	Calculated (a)	Calculated (c)	Electron (b) Impact	This work
0	0.4706	0.47038	0.53	0.48 ± 0.04
1	0.8938	0.89375	0.91	0.90 ± 0.03
2	1.0000	1.00000	1.00	1.00
3	0.8678	0.86776	0.35	0.91 ± 0.03
4	0.6508	0.65051	0.35	0.74 ± 0.05
5	0.4461	0.44573	-	0.58 ± 0.03
6	0.2889	0.28877	-	0.44 ± 0.04
7	0.1812	0.190135	-	0.28 ± 0.03
8	0.1118	0.11697	-	0.15 ± 0.05
9	0.0684	0.06805	-	-

(a) See ref. 3
(b) See ref. 4
(c) See ref. 5

$$q = \left|\int \psi_{v^1}\psi_{v11}dr\right|^2$$

We might also expect deviations from the threshold probabilities at higher energies for the following reason. The optical photoionization coefficient for hydrogen is known to fall off between 18 and 21 ev., and so the probability of ionization to each H_2^+ vibrational level is expected to fall off as well. At our incident photon energy of 21.21 ev. the higher the vibrational quantum number of the final state the less will the ionization to that state have fallen off from its threshold value. As a consequence the relative

PHOTOELECTRON SPECTROMETER

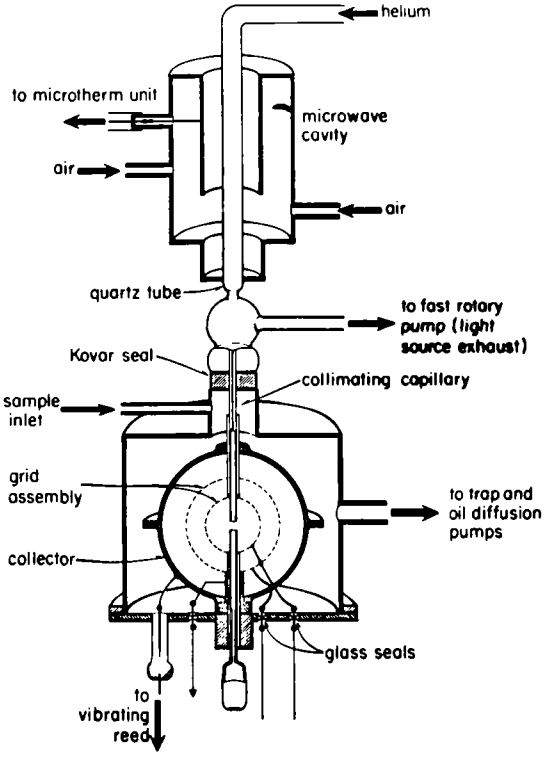

Figure 1.

ionization probabilities for the various vibrational states are almost certainly energy dependent with the higher levels relatively more populated at higher energies.

Tables III and IV give the experimental (584 Å) and calculated vibrational spacings, and the relative transition probabilities for HD and D_2.

Table III

Ionization data for HD

	$E_{v^1} - E_{(v^1-1)}$		Transition Probabilities	
v^1	Spec.*	This work	Calc.*	This work
0			0.3619	0.37
1	0.2350	0.23	0.7919	0.84
2	0.2235	0.23	1.0000	1.00
3	0.2120	0.22	0.9625	0.96
4	0.2005	0.20	0.7875	0.84
5	0.1889	0.20	0.5780	0.71
6	0.1775	0.19	0.3982	0.60
7	0.1658	0.17	0.2611	0.45
8	0.1544	0.16	0.1667	0.32
9	0.1428	0.15		

* See ref. 6

Table IV

Ionization data for D_2

	$E_{v^1} - E_{(v^1-1)}$		Transition Probabilities	
v^1	Spec.*	This work	Calc.*	This work
0			0.2197	0.19
1	0.1937	0.20	0.5897	0.56
2	0.1861	0.19	0.8901	0.86
3	0.1784	0.18	1.0000	1.00
4	0.1706	0.17	0.9354	0.94
5	0.1630	0.17	0.7728	0.87
6	0.1554	0.16	0.5798	0.77
7	0.1476	0.15	0.4165	0.66
8	0.1399	0.15	0.2831	0.55
9	0.1323	0.14	0.1862	0.39
10	0.1246	0.13		

* See ref. 6

Nitrogen

The photoelectron stopping curve for nitrogen is shown in Figure 3, and the ionization data is given in Tables V and VI. The new results we present are mainly concerned with the location of several vibrational levels of the $N_2^+ \, ^2\pi_u$ electronic state and the relative transition probabilities to them.

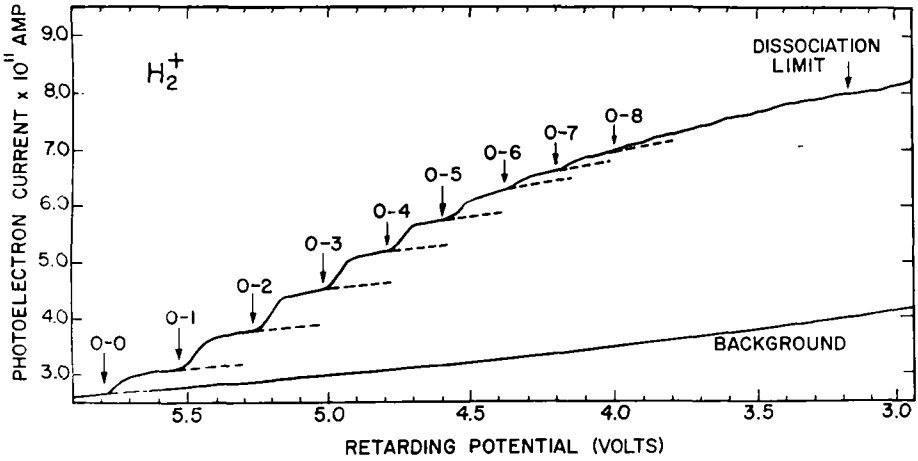

Figure 2.

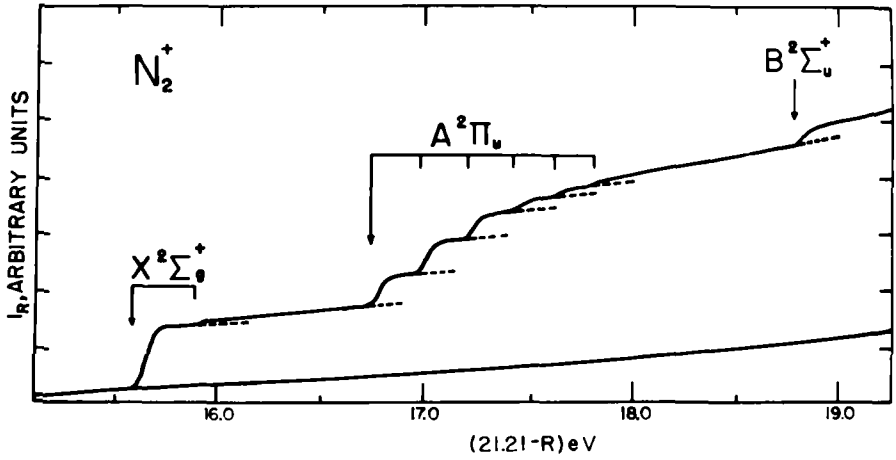

Figure 3.

Table V

Ionization data for $N_2(X^1\Sigma_g^+) \rightarrow N_2^+(X^2\Sigma_g^+)$

	$E_{(v^1)} - E_{(v^1-1)}$ eV		Transition Probabilities	
v^1	Calculated[a]	This work	Calculated[b]	This work
0	-	-	1.0000	1.00
1	0.29	0.33 ± 0.01	0.1004	0.054 ± 0.01

(a) See ref. 7
(b) See ref. 5

Table VI

Ionization data for $N_2(X^1\Sigma_g^+) \rightarrow N_2^+(A^2\pi_u)$

	Transition Probabilities		$E_{(v^1)} - E_{(v^1-1)}$ eV	
v^1	Spectroscopic[a]	This work	Spectroscopic[b]	This work
0	0.7875	0.85 ± 0.02	-	-
1	1.0000	1.00	0.24	0.23 ± 0.01
2	0.7251	0.71 ± 0.03	0.23	0.23 ± 0.01
3	0.3978	0.46 ± 0.03	0.23	0.22 ± 0.01
4	0.1846	0.21 ± 0.03	-	0.21 ± 0.01
5	0.0769	0.14 ± 0.03	-	0.20 ± 0.01
6	0.0298	0.08 ± 0.05	-	0.19 ± 0.01

(a) See ref. 5
(b) See ref. 8

Again we find only fair agreement between Franck-Condon factors and 584 Å probabilities at the higher levels. The reasons are likely to be similar to those discussed above in the case of hydrogen.

We gratefully acknowledge generous financial support from the National Research Council of Canada.

References

1. Frost, D. C., McDowell, C. A. and Vroom, D. A. Phys. Rev. Letters 15, 612, 1965.
2. (a) Al-Joboury, M. I. and Turner, D. W. J. Chem. Soc. 5141, 1963.
   (b) Schoen, R. I., J. Chem. Phys. 40, 1830, 1963.
3. Wacks, M. E. J. of Research N.B.S. 68a, 631, 1964.
4. Kerwin, L., Marmet, P. and Clarke, E. M. "Advances in Mass Spectrometry II" 1963. London: Pergamon Press, p. 522.
5. Halmann, M. and Laulicht, I. J. Chem. Phys. 43, 1503, 1965.
6. Wacks, M. E. J. Chem. Phys. 41, 930, 1964.
7. Herzberg, G. "Spectra of Diatomic Molecules" 1950. New York: D. Van Nostrand Co. Inc.
8. Worley, R. E. Phys. Rev. 89, 863, 1953.

Mass Spectrometric Study of the Photoionization of the Methyl Halides and HCl

V. H. Dibeler, M. Krauss, and J. Walker
Physical Chemistry Division
National Bureau of Standards
Washington, D.C. 20234

The photoionization efficiency curves of HCl, CH_3F, CH_3Cl, CH_2DCl, CHD_2Cl, CD_3Cl, and CH_3Br have been measured from their thresholds to 600 Å. All observable ions in this energy range are reported. In particular, ion-pair processes were observed for CH_3F, CH_3Cl, CH_2DCl, and CHD_2Cl.

Analysis of such a series is usually undertaken in the expectation of the similarities that are revealed. In this instance the differences are more striking. Ion-pair processes are observed only for the methyl fluoride and chlorides but not the bromide or iodide. The qualitative behavior of the efficiency curves for both the ion-pair and all other positive ions is different from halide to halide. These differences can be correlated with the electronic structure in an approximate manner. What is most evident is the need for complementary information from other experiments or theory. The photoionization efficiency curves by themselves cannot be interpreted in an unambiguous manner. In particular the spin-orbit doublet in CH_3Cl is not clearly seen in the PE curves. However, a table of bond energies can be deduced from the appearance potentials. These are attached.

In addition, the isotope effect of the ion-pair process in methyl chloride favors the recently proposed crossing probability expressions with v^{-2} dependence in the exponent.

$D(H\text{-}Cl) = 4.33$ eV

$D(H\text{-}Cl^+) = 4.63$ eV

$D(CH_3\text{-}F) = 6.30$ eV $= A(CH_3^+)-I(CH_3)$

$= 6.17$ eV $= A(F^-)$ or $A(CH_3^+)-I(CH_3)+EA(F)$

$D(CH_3^+\text{-}F) = 3.75$ eV

$D(CH_2F^+\text{-}H) = 0.87$ eV

$D(CH_3\text{-}Cl) = 4.03$ eV $= A(CH_3^+)-I(CH_3)$

$= 3.84$ eV $= A(Cl^-)$ or $A(CH_3^+)-I(CH_3)+EA(Cl)$

$D(CH_3^+\text{-}Cl) = 2.59$ eV

$D(CH_3\text{-}Br) = 2.93$ eV

$D(CH_3^+\text{-}Br) = 2.24$ eV

PHOTOIONIZATION OF THE LOWER ALIPHATIC ALCOHOLS*

W. A. Chupka and K. M. Refaey†

Argonne National Laboratory, Argonne, Illinois

The photoionization of methanol, ethanol, n-propanol, and isopropanol has been studied with monochromatic photons from threshold to 13.5 eV with mass analysis of the ionic products. The data have been treated to yield breakdown curves for the parent ions, as well as appearance potentials of the major fragments. The results are compared with those obtained earlier by workers who used electron impact and charge exchange and also with the predictions of the statistical theory of mass spectra.

This paper describes studies of photoionization and subsequent dissociation of the lower aliphatic alcohols (methanol, ethanol, n-propanol, and iso-propanol) as a function of photon energy. The studies include data on the major processes that occur below a photon energy of 14.5 eV. The results were obtained by use of the photoionization machine described in an earlier paper.[1]

The photoionization technique has been employed by several authors[2-4] for the investigation of polyatomic molecules such as alkanes. In a more recent application, it has been employed for the investigation of high-temperature vapors.[1] An important reason for applying the photoionization technique to polyatomic molecules is to test the statistical theory. Since its inception, this theory has been used[5-7] to predict breakdown curves of various molecules, among which are the lower aliphatic alcohols.[6] Although the predicted breakdown curves of some of these alcohols have been compared with experimental ones obtained by the charge-exchange technique, curves obtained by photoionization offer not only valuable confirmation by an independent method but also additional fine details. It is to be mentioned that the theoretically predicted breakdown curves were obtained by employing dissociation schemes extracted from electron-impact spectra. Some of these schemes were found to be in error as will be pointed out later.

The direct experimental results of this investigation are in the form of parent, fragment, and metastable ionization-efficiency curves. Some of these curves are shown in Figs. 1-5. In these curves, the ion intensity was multiplied by the factor indicated next to each curve in order to plot several curves in one figure as well as to indicate their relative intensities. In some cases the measurements started at an energy higher than the appearance potential of the ion, and hence the appearance potentials associated with these ions are only best estimates. However, for most fragments the measurements started well below the threshold. The ionization potentials as well as the appearance potentials of the parent and fragment ions from alcohols are given in Table I. The values obtained earlier by other investigators are also listed in the table. The appearance potentials designated by ‡ were obtained from the corresponding metastable ions. Since the measurements were obtained at room temperature and the parent molecules have significant amounts of internal thermal energy, the use of the metastables in determining these values eliminates much of the ambiguity that arises from this effect. The production of the metastable ion in the absence of thermal energy should follow very nearly a step function at the threshold appearance potential of the fragment. The thermal energy then will produce a tail in its ionization-efficiency curve, but the energy at which the curve levels off is the appearance potential of the corresponding fragment from molecules with no internal thermal energy.

---

*Work performed under the auspices of the U. S. Atomic Energy Commission.

† Permanent address, U.A.R. Atomic Energy Establishment, Cairo, U.A.R.

TABLE I. Ionization potential (IP) and appearance potential (AP) of ions from alcohols and ethylene

Molecule	Ion	IP or AP (eV)	
		This Investigation	Other Work
CH_3OH	CH_3OH^+ (m=32)	10.84 ± 0.02	10.85 ± 0.02[a], 10.8 ± 0.2[b], 10.9[c]
	CH_2OH^+ (m=31)	11.67 ± 0.03	11.8 ± 0.1[b], 12.15[c]
	CH_2O^+ (m=30)	12.45*	12.4 ± 0.1[b], 12.7[c]
C_2H_5OH	$C_2H_5OH^+$ (m=46)	10.47 ± 0.02	10.48 ± 0.05[a], 11.3 ± 0.2[b], 10.7[c]
	$C_2H_4OH^+$ (m=45)	10.78 ± 0.02‡	11.0 ± 0.1[b], 11.35[c]
	CH_2OH^+ (m=31)	11.25*	11.3 ± 0.2[b], 11.6[c]
	CH_2O^+ (m=30)	11.80*	12.8 ± 0.2[b], 12.7[c]
	$C_2H_5^+$ (m=29)	12.90*	14.2 ± 0.2[b], 12.65[c]
	$C_2H_4^+$ (m=28)	12.00*	11.3 ± 0.3[b], 11.1[c]
n-C_3H_7OH	$C_3H_7OH^+$ (m=60)	10.21 ± 0.04	10.20[a], 10.7[c]
	$C_3H_6^+$ (m=42)	10.65 ± 0.02‡	10.9[c]
	$C_3H_6OH^+$ (m=59)	10.74*	11.35[c]
	$C_2H_4OH^+$ (m=45)	10.42(?), 11.20*	11.1[c]
	CH_2OH^+ (m=31)	11.43*	11.65[c]
	$C_3H_7^+$ (m=43)	10.65*, 11.5*	11.9[c]
	$C_2H_4^+$ (m=28)	11.92*	
	$C_2H_5^+$ (m=29)	12.40*	12.1[b]
	$C_3H_5^+$ (m=41)	12.80*	12.5[b]
iso-C_3H_7OH	$C_3H_7OH^+$ (m=60)	10.12 ± 0.02	10.16[a], 10.7[c]
	$C_2H_4O^+$ (m=44)	10.27 ± 0.02‡	
	$C_2H_4OH^+$ (m=45)	10.40*	10.9[c]
	$C_3H_6OH^+$ (m=59)	10.55*, 11.35*	11.30[c]
	$C_3H_7^+$ (m=43)	11.70*, 12.45*	11.9[c]

(a) Watanabe et al.[8] (b) Cummings and Bleakney[9] (c) Friedman et al.[6]

One should subtract from this the band width of the photon beam. This was used only in obtaining the appearance potentials of the first fragments since those usually lead to the production of metastable ions. For higher order fragments, the effect of thermal energy was taken into account approximately and the values designated * were obtained. Although these values are uncertain, they can be considered good to within ± 0.07 eV.

The direct experimental results (Figs. 3-5) obtained on iso-propanol are given as the photoionization-efficiency curves of the parent (m=60), metastable (m=32.3), and fragment ions. The ionization potential of iso-propanol and the appearance potentials of the fragments are given in Table I. Two values are reported for the appearance potential of $C_3H_6OH^+$ (m=59). The low value of 10.55 eV could be due to the production of $C_3H_6OH^+$ via a mechanism of ion-pair formation according to the scheme

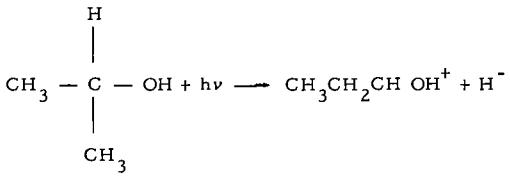

while the higher value of 11.35 eV is due to the production of $C_2H_4OH^+$ by the dissociation of $C_3H_2OH^+$. The difference (0.80 eV) between these two values should then be the value of the electron affinity of the hydrogen atom. The agreement with the known value of this quantity (0.754 eV) is within experimental error. This supports the mechanism of ion-pair formation.

Two values are also reported for the appearance potential of $C_3H_7^+$ (m=43). The low value (11.70 eV) could be due to ion-pair formation, while the higher one (12.45 eV) may then be due to the dissociation of $C_3H_7OH^+$. This interpretation would imply that the electron affinity of OH is about 0.75 eV. Thus since the known value of this quantity is 1.78 eV, it seems unlikely that this is the correct explanation. Another possible interpretation is that the $C_3H_7^+$ ion may exist with two structures, for instance a ring and a chain, and hence two processes producing an ion with the same mass could be observed. A small amount of n-propanol impurity would not account for the observed lower energy process.

The ionization potential of iso-propanol obtained in this investigation is in good agreement with that obtained by Watanabe et al. A proposed mechanism for the decomposition of iso-propanol ion is

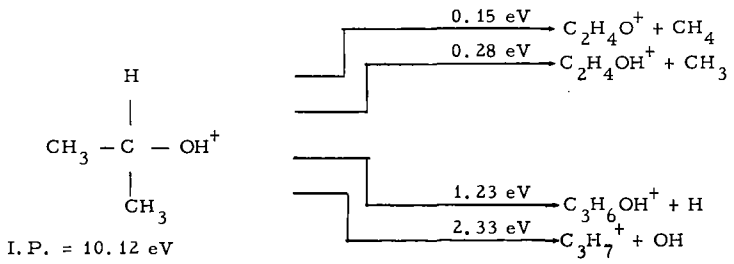

where the numbers above the arrows give the energies in eV necessary to produce the fragment ions from the parent ion. Those numbers are entirely different from those obtained by Friedman et al.[6] The two decomposition mechanisms are very different. In this investigation, the acetaldhyde ion $C_2H_4O^+$ (m=44) was found to be the first fragment. Strong evidence in support of this conclusion is the production of the metastable ion (m=32.3) which could only be due to the production of $C_2H_4O^+$ from $C_3H_7OH^+$.

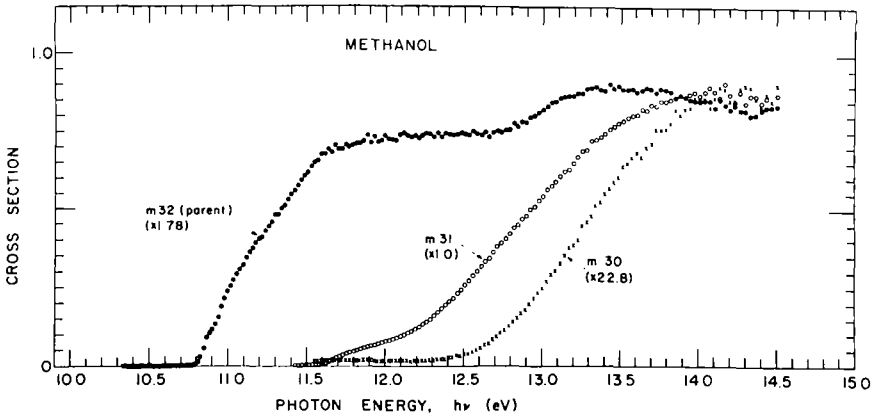

Fig. 1. Ionization-efficiency curves of ions from methanol (•-parent ion m=32; o-fragment ion m=31; x-fragment ion m=30).

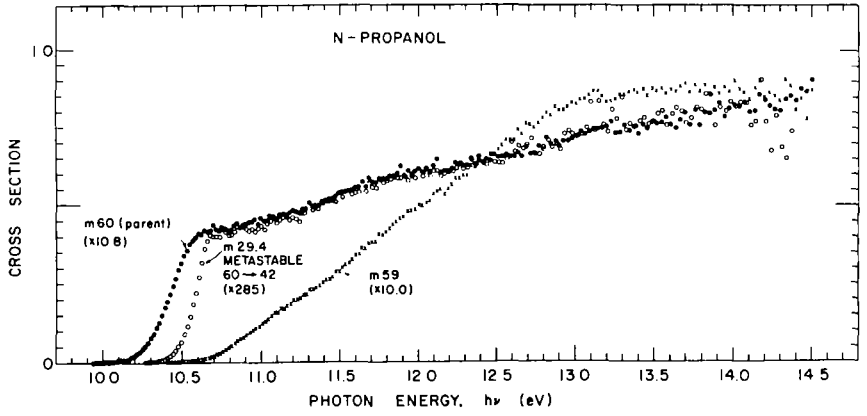

Fig. 2. Ionization-efficiency curves of ions from n-propanol (•-parent ion m=60; o-metastable ion m=29.4; x-fragment ion m=59).

In the mechanism proposed by Friedman et al.[6] $C_3H_6^+$ (m=42) is assumed to be the first fragment. Although it has been searched for, there was no evidence that it even existed in any appreciable abundance. Friedman et al. also propose that the decomposition of iso-$C_3H_7OH^+$ into $C_3H_6^+$ proceeds with zero energy. This would mean that every parent ion formed would decompose into $C_3H_6^+$ or other fragments and that the breakdown curve of the parent ion should fall practically to zero at the ionization threshold. This was not found to be the case.

Breakdown curves were obtained by use of a computer and smoothed out so as to present the most probable dissociation pattern. The breakdown curves of n-propanol as obtained by the computer are shown in Fig. 6.

The breakdown curves of iso-propanol as obtained in this investigation are shown in Fig. 7. Those obtained by Friedman et al.[6] are shown in Fig. 8. There is a marked difference between the two sets of curves. In this investigation, although the parent ion decomposes at lower energies than the other alcohols studied, appreciable amounts remain undecomposed—contrary to the suggestion of Friedman et al. The first fragment observed in this investigation is $C_2H_4O^+$ (m=44) while the one proposed by Friedman et al. is $C_3H_6^+$ (m=42). The second fragment in each case is the same. The third fragment ion process observed in this investigation is the production of $C_3H_6OH^+$ (m=59). However, this process has low probability and was not even reported by Friedman et al. This molecule was not investigated by use of the charge-exchange technique, and hence no supporting evidence for any of these two mechanisms can be obtained.

For other molecules, the breakdown curves obtained in this investigation were in general agreement with those obtained by Lindholm and co-workers[10-12] who use the charge-exchange technique.

Friedman et al[6] calculated the breakdown curves of the lower aliphatic alcohols by use of the statistical theory. Those authors used decomposition schemes extracted from electron-impact data. Most of these data were found to be in error and hence some of the proposed decomposition mechanisms were also in error. Moreover, the use of the classical approximation in the theory caused the rate constant to vary more slowly with energy than observed. This fact was observed by Friedman et al. and others. The use of recently improved approximations and the correct decomposition mechanisms in the theory should yield breakdown curves in at least semi-quantitative agreement with those obtained in this investigation.

It should be noticed that the cross-section for production of the parent ion in some cases (especially methanol) exhibits a second rise above the onset of dissociation. This feature can be attributed either to (a) autoionization which yields many parent ions with internal energies below the dissociation threshold or (b) production of an electronically excited state of the parent ion which does not make a rapid radiationless transition to the ground electronic state. The shape of the feature favors explanation (a).

REFERENCES

1. J. Berkowitz and W. A. Chupka, Submitted to the J. Chem. Phys.
2. B. Steiner, C. F. Giese and M. Inghram, J. Chem. Phys. 34, 189 (1961).
3. H. Hurzeler, M. G. Inghram and J. D. Morrison, J. Chem. Phys. 28, 76, (1958).
4. W. A. Chupka and J. Berkowitz, to be published in J. Chem. Phys.
5. H. M. Rosenstock, M. B. Wallenstein, A. L. Wahrhaftig and H. E. Eyring, Proc. Nat. Academy of Science, U.S. 38, 667 (1952).
6. L. Friedman, F. A. Long and M. Wolfsberg, J. Chem. Phys. 27, 613 (1957).
7. L. Friedman, F. A. Long and M. Wolfsberg, J. Chem. Phys. 30, 1605 (1959).
8. K. Watanabe, T. Nakayama and J. Mottle, Final Report on Ionization Potential of Molecules by a Photoionization Method, Dept. of Physics, University of Hawaii (Dec. 1959).
9. C. S. Cummings and W. Bleakney, Phys. Rev. 58, 787 (1940).
10. P. Wilmenius and E. Lindholm, Arkiv Fysik 21, 97 (1962).
11. H. Von Koch and E. Lindholm, Arkiv Fysik 19, 123 (1961).
12. E. Pettersson, Arkiv Fysik 25, 181 (1963).

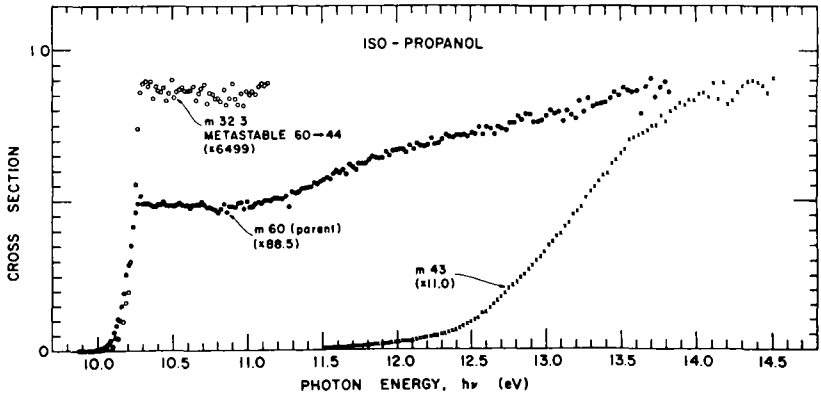

Fig. 3. Ionization-efficiency curves of ions from iso-propanol (•-parent ion m=60; o-metastable ion m=32.3; x-fragment ion m=43).

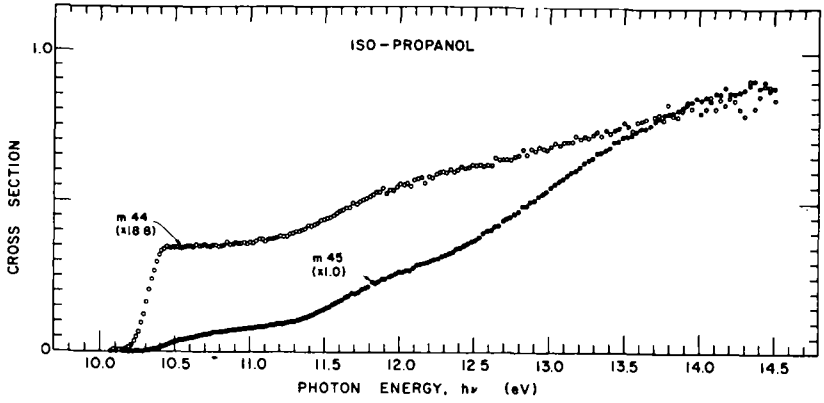

Fig. 4. Ionization-efficiency curves of ions from iso-propanol (•-fragment ion m=44; o-fragment ion m=45).

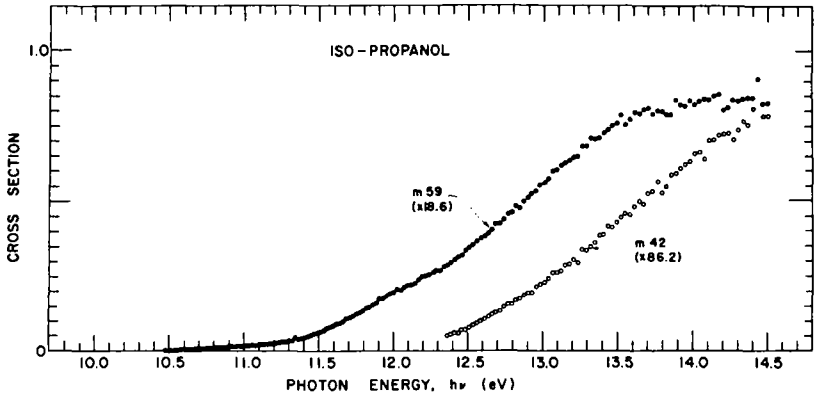

Fig. 5. Ionization-efficiency curves of ions from iso-propanol (•-fragment ion m=59; o-fragment ion m=42).

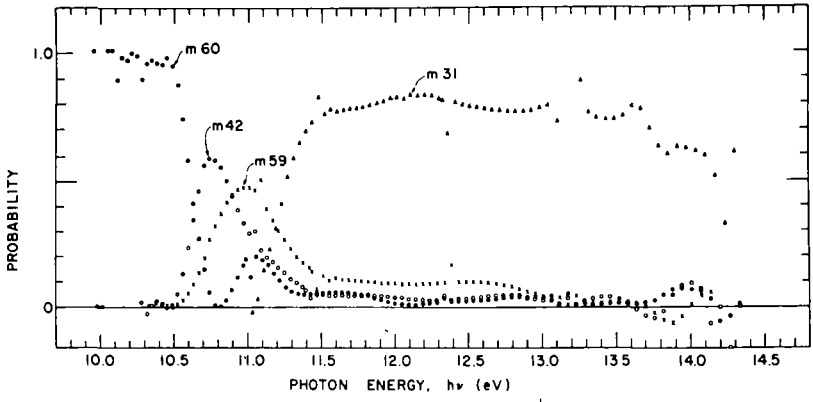

Fig. 6. Breakdown diagram for n-$C_3H_7OH^+$, as displayed by the computer.

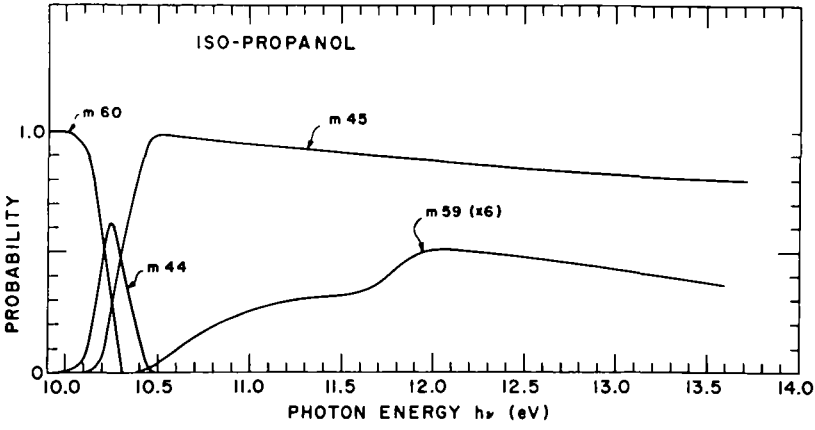

Fig. 7. Breakdown diagram for iso-$C_3H_7OH^+$

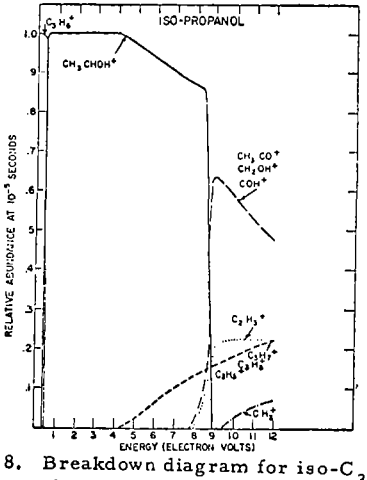

Fig. 8. Breakdown diagram for iso-$C_3H_7OH^+$ obtained by Friedman et al. (Ref. 6).

Mass Spectrometric Study of the Photoionization of Ammonia, Water, Ethylene and 1,2-Ethylene-d_2

R.Botter*, V. H. Dibeler, J.A. Walker, and H.M. Rosenstock
Mass Spectrometry Section
National Bureau of Standards
Washington, D.C. 20234

This is a brief report on recent studies of the photoionization of molecules made as part of a continuing program. A more detailed account of the measurement on ethylene will appear in the Journal of Chemical Physics whereas those of water and ammonia will appear in the Journal of Research of the National Bureau of Standards.

The apparatus has been described in previous publications[1,2]. Briefly, the vacuum ultraviolet radiation is dispersed by a 1-m Seya-Namioka monochromator employing a gold coated grating having 1200/mm grooves and blazed at 800Å. The photon flux is measured by the photoelectron emission from a clean tungsten sheet. The argon continuum, the hydrogen many-line spectrum, and the helium continuum were used to cover the wavelength region from onset of ionization to 600Å. Mass analysis of the photoions was by means of a conventional 6-inch radius of curvature, sector-field mass spectrometer attached directly to the exit arm of the monochromator.

The compounds used were the best grade of research material commercially available and were used without further purification.

A. $C_2H_4^+$ and $CHDCHD^+$

The photoionization efficiency curves for $C_2H_4^+$ and $CHDCHD^+$, and associated fragments are shown in Figs.1 and 2, respectively. Wavelength regions shorter than 750Å are not shown but are essentially flat and featureless to 600Å. The minimum onset occurs at 10.50±0.01 eV for both species and some staircase structure is shown corresponding to various combinations of even overtones of the twisting vibration (440 cm^{-1}) and C-C stretching (1400 cm^{-1}). Above the initial Franck-Condon region both curves are fairly flat with deviations at about 11.7, 12.88 eV and 14.10 for $C_2H_4^+$. These are not necessarily related directly to higher ionization thresholds because of autoionization.

B. $C_2H_2^+$, C_2HD^+, and $C_2D_2^+$

The fragmentation process producing $C_2H_2^+$ involves only well-known thermochemical and spectroscopic information and the threshold value of 13.12 eV. Assuming the acetylenic structure, bounds on the thermochemical heat of reaction may be computed from the adiabatic ionization energy 11.406±0.01 eV[3] and the heats of formation[4] of ethylene and acetylene. This results in the vaule 13.132±0.01 eV. This is in excellent agreement with the observed value of 13.12±0.03 eV.

Studies on the 1,2-dideuteroethylene were made in an attempt to find some supporting evidence for the structure of the $C_2H_2^+$ ion in addition to that suggested by the above-mentioned excellent agreement between calculated and observed reactions energies. However, it is very probable that rearrangement occurs.

---

*Guest Worker, Present Address: Centre d'Etude Nucleaire de Saclay, Service des Isotopes Stables, Saclay, France.

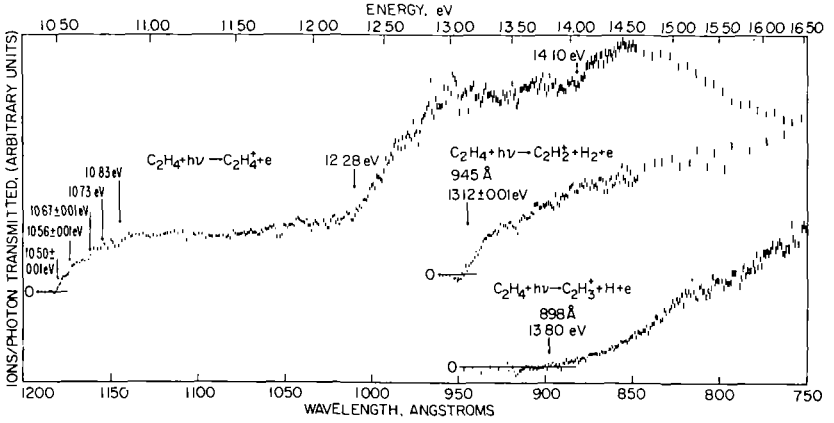

Fig. 1

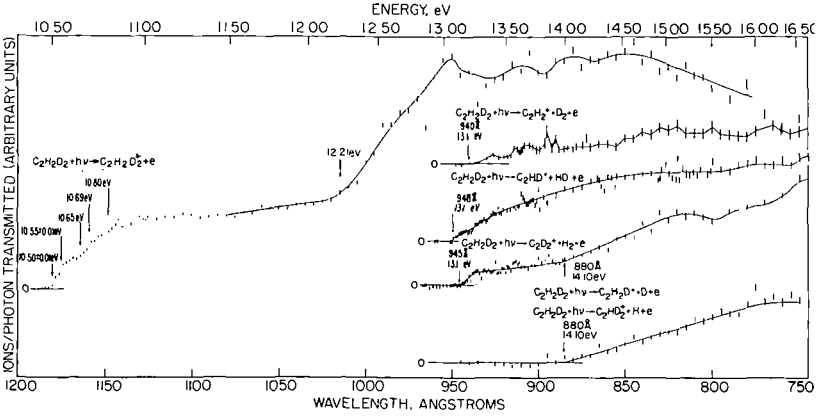

Fig. 2

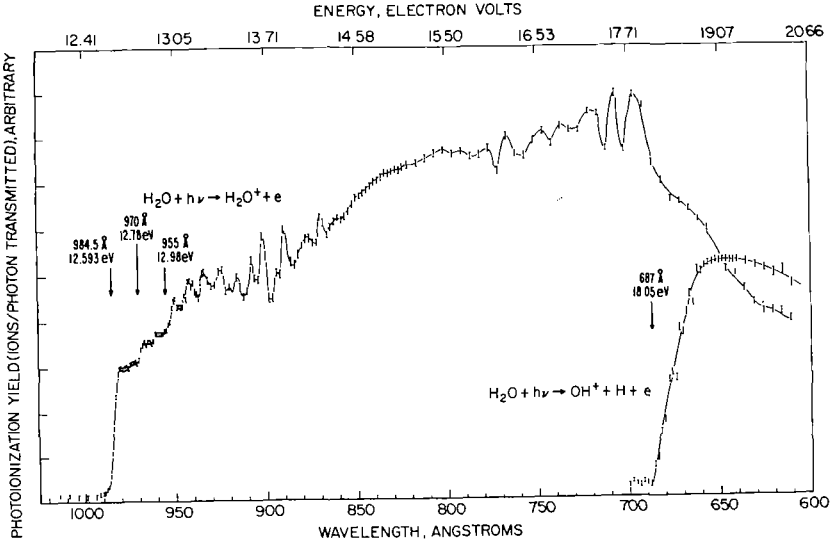

Fig. 3

C. $C_2H_3^+$, $C_2H_2D^+$, and $C_2HD_2^+$

The onset of the $C_2H_3^+$ is most clearly defined. Recent electron impact values [5] for $I(C_2H_3)$ lead to a $D(C_2H_3\text{-}H)$ bond energy of ~100 kcal.

D. H_2O^+ and OH^+

Figure 3 shows the photoionization efficiency curves for the H_2O^+ and OH^+ ions of water. The first onset of the H_2O^+ ion (12.593 eV) is in excellent agreement with both photoionization[6] and electron impact[7] data. This is followed by two pronounced steps with intervals of about 1500 cm^{-1} suggesting the bending overtone. Using the method of Sharp and Rosenstock[8] and force constants given by Bell[9], we calculate intensities of bending and sym. stretching overtones relative to the (000-000) transition for various values of bond length and angle for both D_2O and H_2O. These are plotted in Fig. 4. Our photoionization data indicate an H_2O^+ bond angle of about 112° in close agreement with spectroscopic results[9].

The observed value for dissociative ionization is considerably below previously reported thresholds. From our value and the appropriate heats of formation[4], we obtain I(OH)=12.88 eV (297.0 kcal).

E. NH_3^+ and NH_2^+

The photoionization efficiency curves for the NH_3^+ and NH_2^+ ions of ammonia are given in Fig. 5. There is no clear evidence for autoionization in the present study. However, it may very well be present in the region 900 to 800Å. The general shape of the onset region is quite unlike that of the H_2O^+ ion and indicates and important structural change upon ionization. The onset at 10.16 eV is ascribed to the 0-0 transition. Intervals of the steps following onset are about 920 cm^{-1} corresponding to the out-of-plane vibration.

The NH_2^+ ion shows a sharp onset at 15.73 eV; about the same wavelength at which the ionization of the NH_3^+ ion decreases markedly. From the threshold value we calculate a $\Delta Hf(NH_2^+)$=299.6 kcal. Using $H_3N\text{-}H$ given by Altshuller[10] we calculate $I(NH_2)$=11.22 eV (258.7 kcal).

We gladly acknowledge the assistance of Ituro Omura in obtaining some of the photionization data.

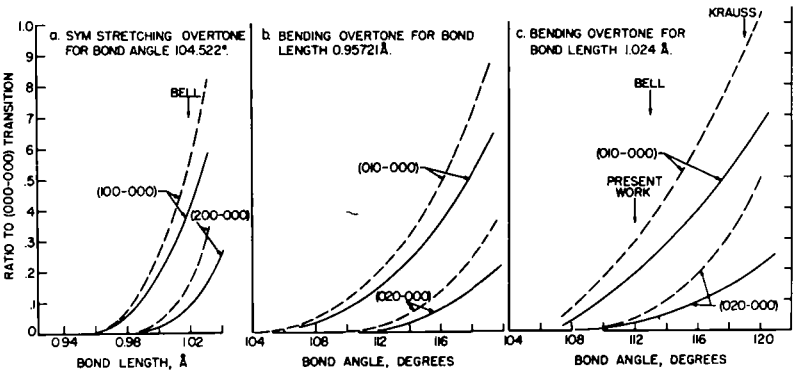

Fig. 4

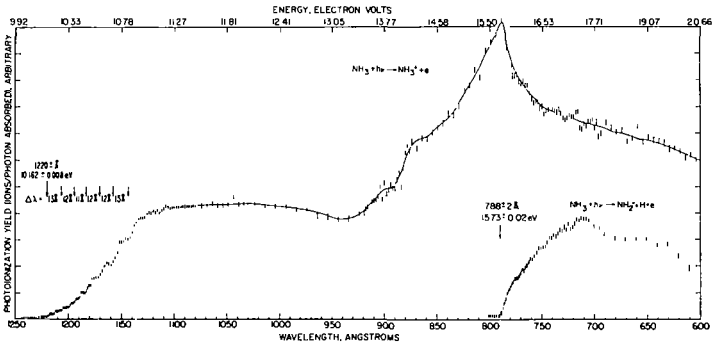

Fig. 5

Figure Captions

Fig. 1. Photoionization efficiency curves for the $C_2H_4^+$, $C_2H_3^+$, and $C_2H_2^+$, ions of ethylene.

Fig. 2. Photoionization efficiency curves for the $C_2H_2D_2^+$, $C_2H_2D^+$, $C_2H_2^+$, C_2HD^+, $C_2D_2^+$, and $C_2HD_2^+$ ions of 1.2-dideuteroethylene.

Fig. 3. Photoionization efficiency curves for the H_2O^+ and OH^+ ions of water.

Fig. 4. Calculated bending and sym. stretching overtone for various bond angles and length of the H_2O^+ and D_2O^+ ions. Solid lines are for H_2O^+ and broken lines are for D_2O^+.

Fig. 5. Photoionization efficiency curves for the NH_3^+ and NH_2^+ ions of ammonia.

Reference

1. V.H. Dibeler and R.M. Reese, J.Res. Natl. Bur. Std. (U.S.) A68, 409 (1964).

2. R. Botter, V.H. Dibeler, J.A. Walker, and H.M. Rosenstock, J. Chem. Phys. 44, 1271 (1966).

3. V.H. Dibeler and R.M. Reese, J. Chem. Phys. 40, 2034 (1964).

4. F.D. Rossini, D.D. Wagman, W.H. Evans, S. Levine, and I. Jaffe, Natl. Bur. Std. Circ. No. 500 (1952)

5. A.G. Harrison and F.P. Lossing, J. Am. Chem. Soc. 82, 519 (1960).

6. K. Watanabe, T. Nakayama, and J. Mottl, J. Quant. Spectry. Radiative Transfer 2, 369 (1962).

7. D.C. Frost and C.A.McDowell, Can. J. Chem. 36, 39 (1958).

8. T.E. Sharp and H.M. Rosenstock, J.Chem. Phys. 41, 3453 (1964).

9. S. Bell, J.Mol. Spectry. 16, 205 (1965).

10. A.P. Altshuller, J. Chem. Phys. 22, 1947 (1954)

Time Dependent Behavior of Activated Molecules. High Pressure Unimolecular Rate Constant and Mass Spectra

F. H. Mies and M. Krauss
National Bureau of Standards
Washington, D.C. 20234

Abstract

A quantum mechanical theory of the unimolecular decay of metastable, or activated, molecules is developed using Fano's treatment of resonance scattering. A resonance state is synonymous with the so-called activated molecule in unimolecular kinetics, and a set of widths is associated with each state which is a measure of the coupling to the various dissociation continuum channels (each channel designates and "activated complex"). If the widths are small compared to the spacings between those neighboring states which are coupled to the same continua, then an ensemble of molecules prepared in a given activated state will decay exponentially in time, as a radiating or autoionizing excited atomic state does. However, unimolecular decay is fundamentally a problem in "overlapping" resonances widths, and is best considered using Fano's theory, which incorporates proper treatment of the overlap. This paper is particularly concerned with the implications of overlapping widths on the high pressure rate constant, and on mass spectra.

There are two effects of overlapping which are most striking. First, the time decay of an ensemble of metastable molecules is no longer a pure exponential, but for the special cases considered is represented by a sum of exponential, oscillatory, and/or linear terms; this can affect the interpretation of mass spectra. Second, the high pressure rate constant is related to the initial rate of decay of a canonical ensemble of activated molecules, and proper consideration of overlap imposes an upper bound on the rate of dissociation without any artifically imposed restrictions on the widths. This bound yields the "universal rate constant" kT/h times a transmission coefficient which is a function of the widths and spacings of the activated molecules, and has an upper limit of one.

Isotope Effects in Dissociative Attachment
of Electrons in Methane

T. E. Sharp and J. T. Dowell
Lockheed Palo Alto Research Laboratory
Palo Alto, California 94304

Introduction

In dissociative attachment, (DA), an electron strikes a molecule, dissociates it, and remains attached to one of the fragments. The products are a negative ion and neutral fragment(s). Another mode of negative ion formation, which occurs at higher energies, is ion-pair production. The products are a positive ion, a negative ion, and an electron. These types of processes are shown in Fig. 1 for CH_4.

In a molecule containing hydrogen atoms, substitution of deuterium atoms can result in an isotope effect. Previous experimental studies of isotope effects in dissociative attachment were confined to hydrogen, where large isotope effects have been found[1,2]. The value of studying the isotope effect is that it may lead to a greater understanding of the dissociative attachment process and of the formation and decay of temporary negative ion states. The similarity of the C-H bond energy in methane[3] (4.41± 0.02 eV) to that of the H-H bond in hydrogen[4] (4.48 eV) suggested the possibility of an isotope effect in DA in methane.

Two previous studies of negative ion formation in methane have been made, although neither used isotopic substitution. In 1937 L. Smith[5], using a mass spectrometer, identified the principal negative ions formed in DA as H^- and CH_2^-; smaller amounts of CH^- and C^- were also observed. (The CH_3^- ion was observed as a product in ion-pair formation, but not in DA.) A recent investigation by von Trepka and Neuert[6], also using a mass spectrometer, confirmed the earlier identification of the ions and measured the relative peak heights for the negative ions. These experiments were subject to the well known discrimination effects in the collection efficiency of mass spectrometers - an especially serious effect for energetic fragment ions as diverse in mass as H^- and CH_2^-. To the extent that these effects are operative, the ratios between the peak heights are inaccurate. A much smaller error is expected in the ratio of CH^- and C^- to CH_2^-. Because of the preponderance of CH_2^- among the carbon-containing fragment ions, the contributions of the C^- and CH^- ions to DA are assumed to be negligible in the remainder of this paper.

Apparatus

The apparatus, a total ionization tube similar to the device of Tate and Smith[7], has been described previously[8]. The electron beam was obtained from an indirectly heated, oxide-coated cathode and collimated by an axial magnetic field of 550 gauss. The beam current was 0.5μA with an energy spread of 0.4 eV full width at half height. The gas pressure in the ionization region for most runs was 5×10^{-5} Torr. Complete collection of all ions formed in a fixed path length of the electron beam was achieved by increasing the ion draw-out field until there was no further increase in current to the ion collector plate. The field required to saturate the ion current ranged from 13 V/cm for CD_4 to 20 V/cm for CH_4. Other consistency checks are described in Ref. 8. The energy scale was determined in two independent ways which checked to within ± 0.05 eV. Electron beam retardation measurements were used to determine the contact potential. As a check, the appearance potential of the parent (positive) ion was measured and compared with published electron impact data[9]. Cross sections were determined by comparing the negative ion peak with the maximum of the total positive ionization cross section at 85 eV. The ratio of positive to negative ions was in the range 4×10^3, and was measured with a precision of ± 2%. The maximum cross section for positive ionization has been measured[8] as 3.70 A^{o2} for CH_4 at 85 eV. Values for the deuterated methanes are unavailable; we arbitrarily set their cross sections equal to that for CH_4. (This should be a very good approximation for total positive ionization as evidenced by sensitivity measurements for analytical purposes in mass spectrometers[10]. The accuracy of the cross sections is estimated to be within ± 10%.)

A limited mass analysis capability has been incorporated into the apparatus. By reversing the polarity of the ion draw-out field, the ions are caused to travel through a slit into a one-inch radius, 180° mass-spectrometer. The magnetic field used to collimate the electron beam also serves for the mass analysis. The resolution of the instrument is insufficient to separate mass 13 from mass 14, but H^-, D^-, and carbon-containing negative ions are easily resolved.

Results

The cross section for negative ion formation in DA in CH_4 is shown by the open circles in Fig. 2. Two peaks are present in the total cross section, although they are not clearly resolved. The mass analyzed currents are shown in Fig. 3. The lower energy peak, due to H^-, overlaps the higher energy peak due to CH_2^-. (Note that the peaks are arbitrarily adjusted to be about the same height).

The cross section curves for CH_3D, CH_2D_2, and CHD_3 are shown in Figs. 4, 5, and 6, respectively. Each of these curves exhibits two partially resolved peaks. Mass analysis confirms the presence of H^-, D^-, and methylene negative ion in each case. Examination of the figures shows that the higher energy peak (methylene negative ion) becomes smaller upon increasing the deuteration of the methane.

The cross section for CD_4, shown by the closed circles in Fig. 2, contains only a single peak, due to D^-. A search for CD_2^- at higher gas pressure and larger electron beam current sets an upper limit for the cross section for CD_2^- production of 3.6×10^{-22} cm^2. This value is 260 times smaller than the maximum of the total cross section for negative ion formation.

The disappearance of the methylene negative ion peak is clearly shown in the comparison of CH_4 and CD_4 in Fig. 2. The data also show that the cross section for D^- production from CD_4 exceeds that for H^- production from CH_4. This behavior is opposite to that observed in hydrogen[1,2], where the cross sections for all DA peaks decrease upon deuteration.

Discussion

To interpret the observed effects it is convenient to arbitrarily divide the DA process into two steps. In the first step, the incoming electron causes an electronic transition to a temporary negative ion state of the parent molecule. This step may be followed by a number of competing reactions: a) Elastic scattering, in which the electron is re-emitted with its original energy and the molecule returns to its ground state. b) Inelastic scattering, in which the electron is ejected with less than its original energy. The balance of the energy goes into excitation of dissociation of the parent molecule. c) Dissociative attachment, in which the electron is not re-emitted, but remains attached to a fragment of the dissociated molecule. The isotope effect may arise in either or both steps.

In Fig. 7 are shown hypothetical potential energy curves which will be used in discussing this process. The vertical positions of the upper curves are arbitrary. The Franck-Condon region is shown by pairs of vertical lines; the inner, cross-hatched area refers to the heavier isotope, the outer area to the lighter isotope.

A transition to the purely repulsive curve (at center of Fig. 7) would result in populating the negative ion state as shown to the left of the diagram. The areas under the two curves will be equal for equal transition probabilities for both isotopes. The peak of the heavier isotope will be higher and narrower than that for the lighter isotope. This is a consequence of the smaller spread in distance of the vibrational wave function for the heavier isotope. Once the negative parent ion has been formed, if the probability of re-ejecting an electron were the same for each isotope, (or higher for the lighter isotope), a cross section with a higher peak for the heavier isotope negative ion fragment would result. Such a model might explain D^- and H^- production in methanes. However, this last assumption of equal probabilities for ejection of the electron appears to be very poor both from the viewpoint of theory[11-15] and by analogy to the experimental observations in hydrogen. Some other mechanism to account for the depletion of H^- relative to D^- is probably required.

Table 1 shows the energetics of the possible reactions leading to dissociative attachment. The onset for production of H^- appears to occur below 8.5 eV (even allowing for energy spread), and consequently the only energetically allowed reaction at threshold is $CH_4 + e^- \rightarrow H^- + CH_3$. This mechanism implies that the H^- is formed with more than 4 eV of kinetic energy, which is consistent with the large draw-out field needed to completely collect the H^- current. It also implies that the initial transition is made to a highly repulsive portion of the potential energy curve, consistent with the middle curve of Fig. 7. At higher energies, other processes become possible yielding H^- with lower kinetic energy as shown in Table 1.

A simple mechanism, which must be examined as a possible explanation of the large isotope effect in methylene negative ion formation, is transition to an attractive negative ion curve[16] (upper curve, Fig. 7). If the transition is made to the attractive portion of the curve, there is insufficient energy to form a negative fragment ion. Only

elastic or inelastic scattering will occur. DA can take place only for transitions to the repulsive portion of the potential curve lying above the product energy. If the intersection of the product energy and the repulsive portion of the curve lies at a distance which is within the Franck-Condon region for the lighter isotope, a negative fragment ion can be formed. If this intersection lies to the left of the narrower Franck-Condon region for the heavier isotope, very few negative fragment ions of the heavier isotope can be formed. This mechanism predicts a vertical onset in the cross section for DA at the product energy and a decreasing amount of methylene negative ion formation with increasing deuteration of the methane used. The sizable energy spread of our electron beam makes it difficult to detect a vertical onset. In the analogous case of O^- formation from CO^{17}, a vertical onset at 9.65 eV was considerably broadened by energy spread. From the observations in that experiment, if there is a vertical onset in CH_2^- formation, then it should occur about halfway up the rising portion of the peak, at about 9.9 eV. This is considerably higher than predicted for onset at either of the calculated product energy levels (Table 1). Thus, the simple mechanism does not completely account for the experimental observations in methane. (The proposed mechanism does appear to be in accord with all the experimental observations in the large isotope effect reported by Schulz and Asundi[2] near 3.7 eV in hydrogen. They found convincing evidence of a vertical onset of H^- production at the product energy for formation of H and H^-. The corresponding peak for D^- from D_2 was at least 200 times smaller.)

Neither of the isotope effects observed in methane is completely explained in terms of the simple mechanisms considered. Before proceeding to more complicated explanations, one should obtain a more detailed experimental picture of the processes. Three steps in this direction are a reduction in the energy spread of the electron beam, better resolution in the mass analysis, and determination of the absolute cross sections for positive ion production in the deuterated species. Reduction in the electron energy spread would result in better values for the onset energies for negative ion formation and would reveal any structure which might be present. Better resolution in the mass analysis would permit separation of the low-abundance CH^- and C^- processes from the CH_2^- formation. In addition, the isotopic composition of the methylene negative ions from methane-d_1, -d_2, and -d_3 could be determined. Finally, the determination of absolute cross sections for positive ionization of the deuterated methanes would establish better numerical values for the isotope effect. With this detailed knowledge, one could proceed with more confidence to devise satisfactory mechanisms for the isotope effects.

Acknowledgements

We are indebted to Mr. Vincent Galea for his valuable assistance in restoring the apparatus to health after its many maladies. We also thank Dr. Donald Rapp for useful discussions. This work was carried out under the Lockheed Independent Research Program.

TABLE I. Energetics of DA Processes

PROCESS	ENERGY (eV)
$CH_4 + e^- \rightarrow H^- + CH_3$	3.66
$H^- + CH_2 + H$	8.53
$H^- + CH + H_2$	9.43
$H^- + CH + 2H$	13.91
$CH_4 + e^- \rightarrow CH_2^- + H_2$	4.80 - EA(CH_2)
$CH_2^- + 2H$	9.28 - EA(CH_2)

References

1. D. Rapp, T. E. Sharp, and D. D. Briglia, Phys. Rev. Letters 14, 533 (1965).

2. G. J. Schulz and R. K. Asundi, Phys. Rev. Letters 15, 946 (1965).

3. V. H. Diebler, M. Krauss, R. M. Reese and F. N. Harllee, J. Chem. Phys. 42, 3791 (1965).

4. G. Herzberg, "Spectra of Diatomic Molecules", 2d. ed., Van Nostrand, New York (1950), p. 530.

5. L. G. Smith, Phys. Rev. 51, 263 (1937).

6. L. v. Trepka and H. Neuert, Z. Naturforsch, 18a, 1295 (1963).

7. J. T. Tate and P. T. Smith, Phys. Rev. 39, 270 (1932).

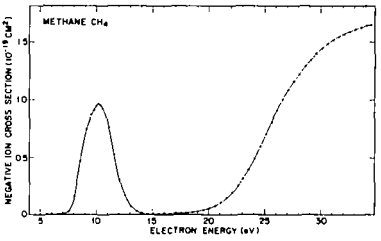

Fig. 1

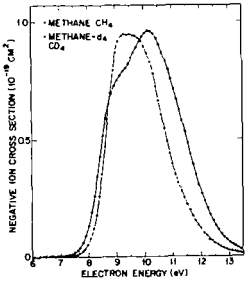

Fig. 2

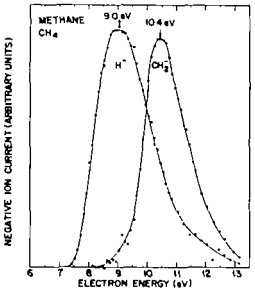

Fig. 3

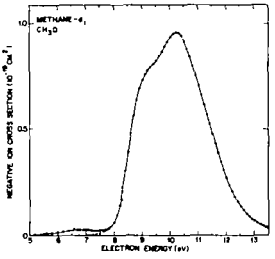

Fig. 4

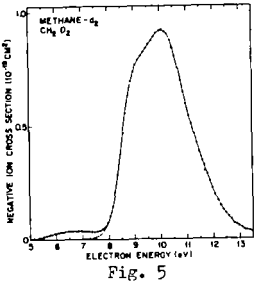

Fig. 5

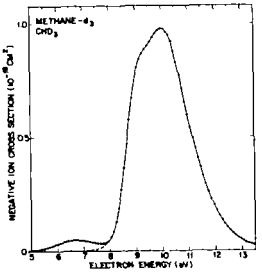

Fig. 6

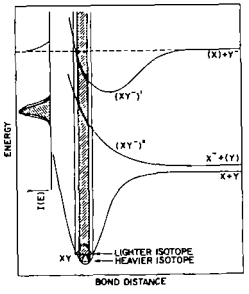

Fig. 7

8. D. Rapp and P. Englander-Golden, J. Chem. Phys. 43, 1464 (1965); D. D. Briglia and D. Rapp, J. Chem. Phys. 42, 3021 (1965).

9. F. H. Field and J. L. Franklin, "Electron Impact Phenomena," Academic Press, New York (1957). p. 251.

10. A. S. Newton, Private Communication.

10a. D. D. Briglia and D. Rapp, Bull. Am. Phys. Soc. 11, 69 (1966).

11. Y. N. Demkov, Phys. Letters 15, 235 (1965).

12. J. N. Bardsley, A. Herzenberg, and F. Mandl, Atomic Collision Processes (M.R.C. McDowell, Ed.) North Holland, Amsterdam (1964), p. 415; J. N. Bardsley, A. Herzenberg and F. Mandl, IVth International Conference on the Physics of Electronic and Atomic Collisions, Science Bookcrafters, Inc., Hastings, N. Y. (1965), p. 359.

13. T. F. O'Malley, "Theory of Dissociative Attachment", Defense Research Corp. Tech Memo 344 (1966). Submitted to Phys. Rev.

14. H. S. Taylor, G. V. Nazaroff, and A. Golebiewski, "Qualitative Aspects of Resonances in Electron-Atom and Electron-Molecule Scattering, Excitation, and Reactions" (1966). Submitted to J. Chem. Phys.

15. J.C.Y.Chen, Phys. Rev. 148, 40 (1966) (to be published).

16. A similar explanation is offered by O'Malley to explain certain isotope effects. Cf. Ref. 13, pp. 44, 47.

17. D. Rapp and D. D. Briglia, J. Chem. Phys. 43, 1480 (1965).

18. The basic values used were $D(CH_3 - H) = 4.41$ eV, $D(CH_2 - H) = 4.87$ eV, (Ref. 3); $D(H-H) = 4.48$ eV, (Ref. 4); $D(CH-H) = 5.38$ eV, (Cottrell, "Strengths of Chemical Bonds," 2d. ed., Butterworths, London (1958). p. 270).

Figure Captions

Fig. 1. Negative ion formation in methane. The process below 15 eV is dissociative attachment. The higher energy process is ion-pair production.

Fig. 2. Dissociative attachment in methane (open circles) and methane-d_4 (full circles). Two unresolved peaks are present in methane. Only a single peak due to D^- is present in methane-d_4.

Fig. 3. Mass analysis of negative ions from methane. The two peaks have been arbitrarily adjusted to be about the same height.

Fig. 4. Dissociative attachment in methane-d_1. Two overlapping peaks are formed. Mass analysis (not illustrated) shows the presence of H^- and D^-, and methylene negative ion of undetermined isotopic composition is present at higher energies. The peak at low energies is caused by an impurity.

Fig. 5. Dissociative attachment in methane-d_2. Cf. remarks on Fig. 4.

Fig. 6. Dissociative attachment in methane-d_3. Cf. remarks on Fig. 4.

Fig. 7. Hypothetical potential energy curves. The vertical location of the upper curves is arbitrary. The vertical lines define the Franck-Condon regions. The cross-hatched area is the Franck-Condon region for the heavier isotope. To the left is shown the negative ion current as a function of electron energy for the postulated processes.

On the Relationship of H_3^+ to H_2^*

D.J. Keenan and E.M. Clarke
St. Francis Xavier University
Antigonish, Nova Scotia

Abstract

Production of H_3^+ by monoenergetic electron bombardment of H_2 has been related to intermediate excited states of H_2. These experiments indicate that the process is predominantly of the type.

$$e + H_2 \rightarrow H_2^* + e$$
$$H_2^* + H_2 \rightarrow H_3^+ + H + e$$

rather than of the type

$$e + H_2 \rightarrow H_2^+ + 2e$$
$$H_2^+ + H_2 \rightarrow H_3^+ + H$$

Double Ionization of Molecular Hydrogen by Electron Impact

K.E. McCulloh and H.M. Rosenstock
Physical Chemistry Division
National Bureau of Standards
Washington, D.C. 20234

Introduction

Although the Franck-Condon principle has been invoked in attempts to explain observed kinetic energy distributions for fragment ions resulting from dissociative ionization of simple molecules, such attempts have not met with unqualified success. It may be necessary to consider the variation of electronic transition moment with internuclear separation, as well as the possibility that more than one process may contribute to the observations. Discrepancies between calculated and observed distributions remain unexplained in the case of protons resulting from dissociative single ionization of H_2 by electron impact[1].

Modification of recently developed coincidence techniques for observing decomposition of doubly charged ions[2] has made the double ionization of H_2 accessible to experiment. This process is particularly attractive for kinetic energy measurements, not only because the potential energy curves required for Franck-Condon calculations are well known, but also because it is likely that only direct double ionization contributes significantly to the observations.

Experimental

The double ionization of H_2 was studied by coincidence techniques involving simultaneous detection of both protons. The energy of the ionizing electrons could be varied within the range 0.5-1 keV. The electron beam was directed nominally perpendicular to a uniform electrostatic field which accelerated the protons. A simplified schematic is shown in Figure 1. Two rectangular apertures in a plane 3 cm from the electron beam transmitted only those pairs of protons that satisfied certain initial conditions of position and momentum (initial kinetic energy within the apparatus resolution, and the decomposition axis oriented within a limited solid angle about the direction normal to both the electron beam and the field). This selection of proton pairs provided the basis for kinetic energy measurements. Beyond the aperture plane the protons were accelerated to 4 kV and detected by a pair of ion-electron multipliers. Multiplier output pulses, after amplification and shaping by discriminators, were fed to a coincidence circuit. A scaler driven by the coincidence circuit counted proton pairs. Counts were corrected for background (accidentally-coincident pairs of single ionization events, impurity pulse pairs, and spurious pulse pairs which may have been an artifact of the detection system).

The kinetic energy distribution of the protons resulting from double ionization was observed at a number of nominal kinetic energies, E_{nom}. The nominal kinetic energy setting of the apparatus was selected by adjusting the ion-accelerating field. Because of the limited kinetic energy resolution of the system it was necessary to account for smearing of the kinetic energy distribution by the apparatus. The apparatus function, proton pair collection efficiency as of function of E, the kinetic energy imparted to each proton by decomposition, was computed at several fixed E_{nom} values. Calculations were performed on a computer by a Monte Carlo method, which in a number of respects represented a direct simulation of the experiment. Factors taken into account included electron beam thickness, displacement of the electron beam by the ion-accelerating field, aperture geometry, thermal velocity of the molecules, and an assumed isotropic ionization cross section. Since the results,

Fig. 1.

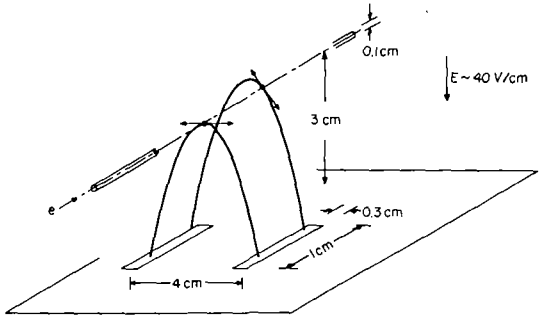

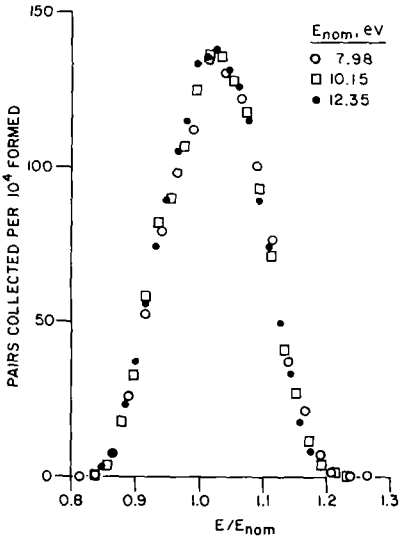

Fig. 2.

Fig. 3.

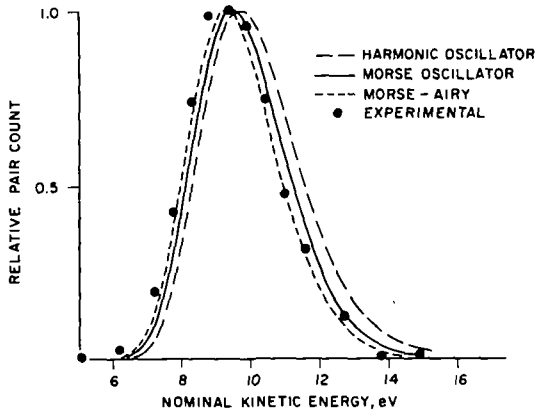

Figure 2, were similar for a sufficient range of E_{nom}, it was possible to treat instrumental smearing of the true kinetic energy distribution in the form of a convolution integral.

Results

Observed proton pair count data are compared in Figure 3 with theoretical predictions based on the Franck-Condon principle. Successive stages of theoretical refinement led to improved agreement with observation. The curves marked "harmonic oscillator" and "Morse oscillator" are based on the simple reflection approximation for estimating Franck-Condon factors. The curve designated "Morse-Airy" is based on an asymptotic treatment in which Airy functions replace the Coulomb wave functions for motion of the mutually-repelling protons. It should be pointed out that the simple reflection approximation is an intuitive approach with no sound mathematical basis, while the more accurate "Morse-Airy" curve is in fact based on a derived reflection approximation. The variation of electronic transition moment with internuclear separation was neglected in these calculations, since it was found that calculated kinetic energy distributions were quite insensitive to assumed variations within reasonable bounds.

Since the multipliers and the pressure gage were not calibrated, absolute cross sections could not be determined. It was possible, however, to study the variation of double ionization cross section with electron energy, since only relative measurements were required. Within the accuracy of the measurements this cross section is inversely proportional to electron energy in the range 0.5-1 keV, while the proton kinetic energy distribution is independent of electron energy.

Concluding Remarks

The agreement between observed and predicted kinetic energy distributions is excellent, lying within the limits of experimental error (±0.2 eV on the energy scale, with relative count rates typically uncertain to ± 5 percent of the maximum). A more detailed account of this study will be published in an appropriate journal.

1. G.H. Dunn and L.J. Kieffer, Phys. Rev. 132, 2109 (1963). Dr. Dunn and Dr. Kieffer have generously made their most recent results available to the authors prior to publication.
2. K.E. McCulloh, T.E. Sharp and H.M. Rosenstock, J. Chem. Phys. 42, 3501 (1965).
3. A.S. Coolidge, H.M. James, and R.S. Present, J. Chem. Phys. 4, 193 (1936).

Figure Captions

Fig. 1. Schematic of ion source (not to scale) with apertures for selecting proton pairs according to their initial momenta. Sample trajectories illustrate how selection occurs.

Fig. 2. The apparatus function, proton pair collection efficiency vs. reduced kinetic energy, E/E_{nom}.

Fig. 3. Observed and calculated relative proton pair counts vs. nominal kinetic energy setting of the apparatus.

Field Ionization Mass Spectrometry: I Saturated Hydrocarbons

II Monochloro-substituted Alkanes.*

Morris J. Weiss,† Louis G. Pobo, and Dwight A. Hutchison

Argonne National Laboratory, Argonne, Illinois

The field ionization mass spectra of a number of branched and unbranched organic molecules have been examined. Electric fields causing the ionization of these molecules were produced near the surface of fine platinum wires having a diameter of 2.5μ.

A schematic illustration of the field ionization source used in these studies is shown in Fig. 1. It essentially consists of a fine wire W situated 2 mm. below the plane cathode C. The wire is normally operated at a potential of 4 Kv above ground while the cathode potentials range from 6 to 7 Kv below ground. Field gradients in the neighborhood of 1×10^7 V/cm are obtained. Ions are produced in the vicinity of the wire from gases introduced into the ionization region through the pinhole leak L. Ions passing through the slit S in the cathode are partially focused by the beam focusing plates BF_1, BF_2 which also serve to direct the ion beam on the mass analyzer entrance slit shown in the schematic. A maximum potential of 150 volts could be applied across BF_1, BF_2.

Ions having nominally 4 kev of kinetic energy enter the field free region of a 9-inch radius 60° magnetic sector direction-focusing mass spectrometer, designed by and constructed under the direction of one of us (D.A.H.). Those ions which have been mass selected are collected on the first dynode of a nine stage silver-magnesium electron multiplier. Ion currents at the first dynode of the multiplier ranged from 10^{-15} to 10^{-16} amperes for a source pressure of approximately 10^{-5} mm.

The field ionization mass spectrum of n-hexane is shown in Fig. 2. The spectrum, typical of unbranched molecules essentially consists of the parent ion plus small contributions of ions formed from the loss of H or H_2 from the parent molecule. The non-integral mass peak at 36.5 is due to the decomposition of an excited parent ('metastable') ion in the field free region of the mass spectrometer.

Shown in Fig. 3 is the mass spectrum of 2,3-dimethylbutane which is seen to undergo a considerable amount of fragmentation about the central C-C bond in the molecule. Fragmentation always occurs preferably at branched positions in a molecule such as 2,3-dimethylbutane rather than at unbranched positions.

The effect of an electric field on a molecule containing a quaternary carbon atom is illustrated in Fig. 4 for 2,2-dimethylbutane. The most intense peak ($C_4H_9^+$) results from the fragmentation of the bond adjacent to the most highly substituted (quaternary) carbon atom. Significant amounts of $C_5H_{11}^+$, $C_4H_8^+$ and $C_2H_5^+$ ions are also observed in addition to that of the parent ion. The ion at mass 43 is $C_3H_7^+$, probably formed by a rearrangement mechanism since two C-C bonds would have to be simultaneously broken to form this ion. A metastable peak is also shown at m/e = 36.5.

---

*Based on work performed under the auspices of the U. S. Atomic Energy Commission.

†Argonne Postdoctoral Research Fellow for 1965-1966.

Mass spectra of organic molecules containing one Cl atom were also determined for branched and unbranched species. A mass spectrum for n-amyl chloride taken at 11 Kv is shown in Fig. 5. There is a large amount of $C_5H_{10}Cl^+$ ions formed from the parent molecule by the loss of H however, the only other peak of any significance is that at m/e = 45.4, 46.3 corresponding to a metastable process involving the loss of HCl^{35} and HCl^{37} from the corresponding isotopic parent ions.

The spectrum for a field ionized isoamyl chloride molecule is shown in Fig. 6. It is evident that fragmentation takes place easily at the point of branching. Both $C_3H_7^+$ and $C_2H_4Cl^+$ ions, formed from ionization of both halves of the fragmented bond, are detected.

Analgous to 2,2-dimethylbutane the mass spectral behavior of 1-chloro-2,2-dimethyl propane (Fig. 7) indicates that it undergoes considerable fragmentation at the bond adjacent to the quaternary carbon atom. No parent ion could be detected for this molecule.

As mentioned earlier the field ionization of these molecules often results in the appearance of non-integral mass peaks corresponding to long-lived states of the parent ions which decompose in the field free region of the mass spectrometer. A summary of some of these so called metastable processes is given in the following table. Column one lists the parent ion which eventually dissociates, column two gives the dissociative process, e.g. p-HCl represents the metastable decomposition corresponding to the loss of an HCl molecule from the parent ion. Columns 3 and 4 list the effective mass and relative abundances respectively of the metastable peaks.

Table 1

Some Metastable Processes Resulting from Field Ionization

Molecule-Ion	Process	$m^* = m^2/M$	Rel. Abundance‡
n-Hexane	$P-C_2H_6$	36.6	0.88
	$P-C_2H_5$	37.8	2.1
2-3-Dimethylbutane	$P-CH_4$	57.0	1.9
	$P-CH_3$	58.6	1.4
n-Amyl Chloride	P-HCl	46.3†	8.9
Isoamyl Chloride	P-HCl	46.3†	14.9

†m* given for most abundant isotope of chlorine

‡Parent ion intensity ≡ 100

The wide range in intensity for such transitions from n-hexane to isoamyl chloride is noteworthy. The behavior of the metastable peak intensity with pressure behind a molecular leak has been studied for only two metastable transitions, in 3-methylpentane and isobutyl chloride. The conclusion reached was that for these molecules the process resulted from a unimolecular dissociation of the parent ion in the field free region of the mass spectrometer.

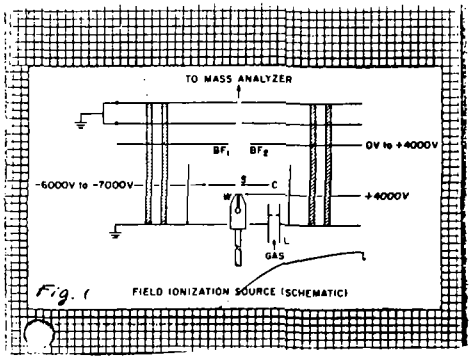

Fig. 1 FIELD IONIZATION SOURCE (SCHEMATIC)

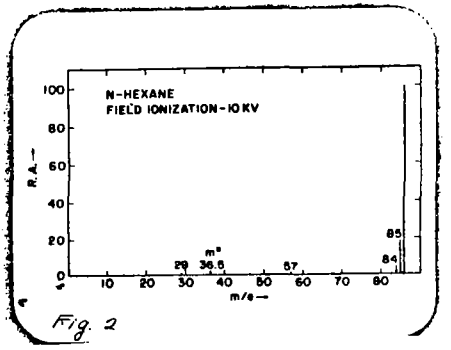

Fig. 2

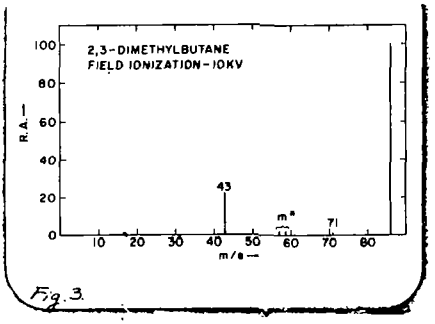

Fig. 3.

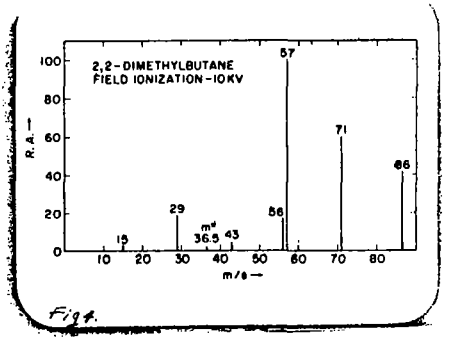

Fig. 4.

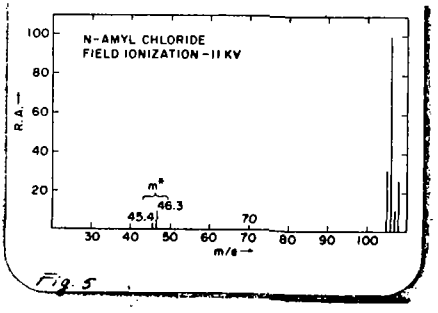

Fig. 5

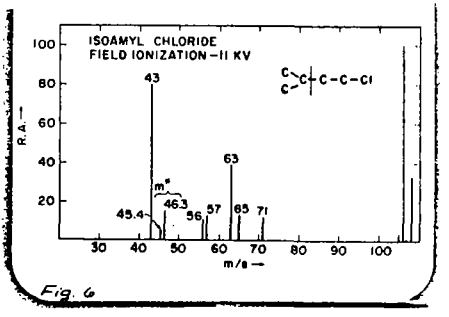

Fig. 6

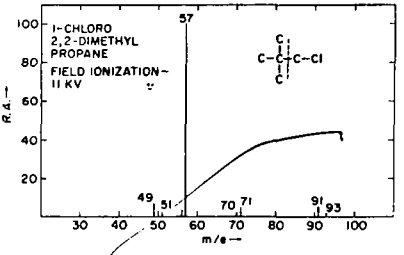

Fig. 7

CORRELATION OF IONIZATION PROBABILITIES WITH GEOMETRIC CHARGE CROSS-SECTIONS

by

A. Bruce King
Gulf Research & Development Company
Pittsburgh, Pennsylvania 15230

SUMMARY

The previous study[1] of the ionization probabilities has been extended to include additional high molecular weight unsubstituted polynuclear aromatic hydrocarbons. The charge distributions for these ions were calculated using Hückel molecular orbitals. These charge distributions were used to calculate a geometric charge cross-section by an impact parameter approach assuming a simple classical collision model. The geometric charge cross-sections were found to correlate with the molecular ionization probabilities for the unsubstituted compounds, suggesting that the relative ionization probabilities for these compounds result from purely geometric considerations.

The polymethyl benzene series was studied to determine whether the marked effect of substituent groups is purely geometric or whether additional group effects exist. It was found that a threefold greater group efficiency of methyl groups relative to the ring was necessary to explain these data. Studies with several nitrogen heterocyclics showed a significant reduction of the ionization probability with nitrogen substitution. These results did not agree with the HMO calculations suggesting that ionization of the π-electron system does not play a dominant role in the threshold ionization probability.

---

1. Deverse, F. T. and A. B. King, J. Chem. Phys. 41, 3833 (1964)

The Mass Spectrum of Silylarsine

F. E. Saalfeld
U. S. Naval Research Laboratory
Washington, D. C. 20390

ABSTRACT

The mass spectrum of silylarsine, $AsSiH_5$, has been studied. From the appearance potential data the $H_2As-SiH_3$ bond dissociation energy (39.2 Kcal/mole) and the heat of formation of silylarsine (28.7 Kcal/mole) have been calculated. The measurements were first made on silylarsine containing silicon of normal isotopic abundance and the results were then corroborated using silylarsine prepared with monoisotopic silicon, ^{28}Si.

INTRODUCTION

Silylarsine has been prepared by several investigators,[1,2] and while a mass spectrometer was employed in one of the studies[1] for the identification of this mixed hydride, neither the fragmentation pattern nor any appearance potential measurements were reported. It is the purpose of this paper to furnish these data and then use the appearance potential measurements with data obtained from arsine, silane, and disilane to calculate the bond dissociation energy and standard heat of formation of silylarsine.

EXPERIMENTAL

Preparation

Silylarsine was prepared by the method of Drake and Jolly[1] in a vacuum system which used no greased stopcocks or joints. Equimolar amounts of silane and arsine were circulated by an automatic Toepler pump through a silent electric discharge, operated at 6 kv AC, and a U-trap cooled with an ethanol slush (-125°C) for six hours. At one-hour intervals, the discharge reaction was stopped, the U-trap cooled with liquid nitrogen and any volatiles remaining in the system were quickly evacuated. The products produced in the discharge reaction were separated by fractional distillation using conventional vacuum techniques.[3] By this method, it was impossible to completely separate silylarsine from tetrasilane Si_4H_{10}. Indeed, even gas chromatography did not afford a complete separation of these two compounds. Thus, the data reported below was observed for a mixture of these two hydrides and, for this reason, none of the SiH_x^+ (x = 0 to 3) fragment ions are reported. Tetrasilane fragment ions do not interfere with any of the ions arising from silylarsine except in the mass-to-charge range of 28 to 33. This mixture therefore was not detrimental to the appearance potential measurements.

Several times during the course of this investigation, an explosion occurred in the sample bulb; at first, it was thought that air had leaked into the bulb and caused the tetrasilane to detonate. However, mass spectral analysis of the volatile compounds remaining in the sample bulb after the explosion showed only the silylarsine had been decomposed; the amount of tetrasilane was the same before and after the explosion. Further, no arsine or air was observed in the analysis and the metallic mirror formed on the bulb in the explosion gave a positive spot test for arsenic. It was found that the explosion could be prevented if the sample was shielded from light; thus, all the sample bulbs were painted black and stored in a light-tight photographic sleeve, and the experiments conducted in a darkened room.

Mass Spectral Data

The data reported here was obtained on a 12-107 Bendix Time-of-Flight mass spectrometer, operated in the pulsed ion mode, which has been modified[4] for appearance potential measurements. This modification, which takes advantage of the multiple analog output systems of the Bendix instrument, permits the chart drive of a number of two-pen recorders to be synchronized with the continuously decreasing voltage of the linear electron energy control. A start-stop time energizes simultaneously the chart drive and the electron energy control drive motor. The electron energy control potentiometer is rotated by a synchronous 60-cycle motor, mechanically coupled to the potentiometer through a gear rack. Thus it was possible to measure the appearance potentials of two ions (an ion from the hydride and argon, the internal standard used to calibrate the voltage scale) simultaneously in less than two minutes. The fragmentation pattern was obtained using 70-V electrons and an ionizing current of 0.125 μa. Mass spectral data for silylarsine, prepared using the separated isotope of silicon, ^{28}Si, are shown in Table 1.

TABLE 1

Mass Spectral Properties of $As^{28}SiH_5$*					
Ion	Relative Abundance	Appearance Potential** e.v.	Appearance Potential** Kcal/mole***	Postulated Neutral Species	$\Delta H_f^\circ(+)$ Kcal/mole
$As^{28}SiH_5^+$	59.0	10.1	232.8	none	261.5
$As^{28}SiH_4^+$	18.1	11.0	253.6	H	230.2
$As^{28}SiH_3^+$	100	9.7	223.6	H_2	252.3
$As^{28}SiH_2^+$	22.5	13.7	315.8	H_2 + H	292.4
$As^{28}SiH^+$	90.1	13.4	308.9	$2H_2$	285.5
$As^{28}Si^+$	41.6	16.8	387.3	$2H_2$ + H	363.9
AsH_3^+	0.1	11.4	262.8	SiH_2	-
AsH_2^+	42.6	12.4	285.8	SiH_3	-
AsH^+	42.3	-	-	-	-
As^+	56.1	-	-	-	-

* All measurements are the average of seven determinations.
** Warren's method[3] of extrapolated difference was employed to obtain the appearance potential value.
***1 ev = 23.053 Kcal/mole.

In order to calculate the dissociation energy and standard heat of formation for silylarsine from the data given in Table 1, the ancillary data in Table 2 and the mass spectral data of arsine delineated in Table 3 are required. A comment on the data cited in Table 3 is in order; while the relative abundances of all the arsine ions and the appearance potentials for the As^+ and AsH^+ agree well with the data previously published,[9] the appearance potentials for the AsH_2^+ and AsH_3^+ in the two studies are in discord. It has been pointed out by Svec[10] that the appearance potentials for AsH_3^+ and AsH_2^+ cited in the earlier work[9] may have been for an excited state. This seems to be the case, as the value for the ionization potential of AsH_3 reported here agrees well with the value of 10.6 e.v. cited by Kiser.[11]

TABLE 2

Ancillary Data Used in Silylarsine Calculations		
Compound or Radical	ΔH_f°(Kcal/mole)	Reference
AsH_3	15.9	6
Si_2H_6	17.1	6
SiH_4	7.3	6
As_2H_4	35.2	7
SiH_3	50.4	8
AsH_2	17.8	this study

TABLE 3

Mass Spectral Properties of Arsine*					
Ion	Relative Abundance	Appearance Potential**		Postulated Neutral Species	$\Delta H_f^\circ(+)$ Kcal/mole
		e.v.	Kcal/mole***		
AsH_3^+	70.2	10.5	242.0	none	249.5
AsH_2^+	22.8	13.40	308.90	H	264.1
AsH^+	100	12.53	288.8	H_2	296.1
As^+	36.5	14.98	345.3	H_2 + H	300.5
AsH_3^{++}	0.04	-			
AsH_2^{++}	0.3	-			
AsH^+	2.2	-			
As^{++}	1.5	-			

* All values cited are averages of twelve determinations.
** Warren's method[5] of extrapolated differences was employed to find the a.p.
***1 ev = 25.053 Kcal/mole.

DISCUSSION

The relationship between appearance potentials and heats of formation and bond energies is well known, as are the errors in this type of measurement.[9,12] In using the data presented in Tables 1, 2 and 3 to calculate the heat of formation and bond dissociation, it has been assumed that the measured appearance potentials do not contain excess kinetic or excitation energy. Since this assumption could not be tested experimentally, the values cited here should be taken as a lower limit for the heat of formation and an upper limit for the bond dissociation energy. These values are 28.7 and 39.2 Kcal/mole, respectively. The former value agrees, within experimental error, with the heat of formation of 26.15 Kcal/mole calculated using Franklin's method[13] and the data cited in Table 2. The agreements between the calculated heat of formation and the experimentally measured value suggests that there is little dative $(p \rightarrow d)\pi$ bonding in silylarsine because the calculated method assumes that there is no interaction between the silicon and arsenic atoms in the molecule. It would be interesting to measure the silicon-arsenic bond distance in silylarsine to ascertain if the bond length is the same as the sum of the covalent radii of silicon and arsenic. This value could also be compared with the silicon-phosphorus or silicon-germanium bond distances in silylphosphine and silylgermane, where dative bonding has been postulated.[14]

ACKNOWLEDGEMENT

The author wishes to thank M. V. McDowell for his aid in obtaining a portion of the data used in this report.

REFERENCES

1. J. E. Drake and W. L. Jolly, Chem. and Ind. 1962, 1470 (1962)
2. B. J. Aylett, H. J. Emeleus and A. G. Maddock, J. Inorg. and Nucl. Chem. 1, 187 (1955)
3. R. T. Sanderson, "Vacuum Manipulation of Volatile Compounds," John Wiley and Sons, New York, N. Y. (1948)
4. R. S. Olfky and F. E. Saalfeld, Report of NRL Progress, June 1965, p. 56
5. J. W. Warren, Nature 165, 811 (1950)
6. S. R. Gunn and L. G. Green, J. Phys. Chem. 65, 779 (1961)
7. F. E. Saalfeld and H. J. Svec, Inorg. Chem. 2, 50 (1963)
8. F. E. Saalfeld and H. J. Svec, ibid 3, 1442 (1964)
9. F. E. Saalfeld and H. J. Svec, ibid 2, 46 (1963)
10. H. J. Svec in "Mass Spectrometry," R. I. Reed, ed., Academic Press, New York, N. Y., p. 245
11. R. W. Kiser, "Introduction to Mass Spectrometry and its Applications," Prentice-Hall, Inc., Englewood Cliffs, N. J., 1965, p. 308
12. F. H. Field and J. L. Franklin, "Electron Impact Phenomena and the Properties of Gaseous Ions," Academic Press, Inc., New York, N. Y.
13. J. L. Franklin, Ind. Eng. Chem. 41, 1070 (1949)
14. F. E. Saalfeld and H. J. Svec, to be published in J. Phys. Chem.

SIMPLE TWO FILAMENT ION SOURCE FOR SINGLE FILAMENT INSTRUMENTS

by

W. E. Duffy and R. E. Carr

General Electric Company
Nuclear Technology Department
Vallecitos Atomic Laboratory
Pleasanton, California

Ion sources used in mass spectrometry for the isotopic analysis of inorganic elements generally employ a single filament, a triple filament or a crucible bombarded by electrons. In the first case the sample to be analyzed is loaded upon the single filament. This is then heated electrically until thermal ions are formed. Before the ionization temperature is reached many unionized molecules of the sample are lost by simple evaporation. In the second case three filaments are located side by side in the source. One side filament is loaded with the sample, the middle filament is heated very hot ($\approx 2500^{\circ}C$) and the sample filament heated slowly to evaporate molecules, some of which strike the hot middle filament and ionize. The other side filament is used only to provide electrical symmetry. Each of the filaments is supplied from a separate power supply and is isolated electrically from the others. This second arrangement permits careful control of sample evaporation and often allows analysis of elements which cannot be analyzed with a single filament design. The arrangement is inherently more complicated both electrically and mechanically. Contamination of parts becomes a serious problem in some cases.

In the third arrangement the sample is placed in a crucible and bombarded with a stream of electrons to produce the ions of interest. This method is used when the first two methods do not provide sufficient ion intensity. It is generally awkward and tedious and not a method amenable to rapid analysis. Detailed descriptions of these techniques are found in the literature of mass spectrometry and the standard texts.

The system described hereafter is suggested as a useful compromise between the first and second methods containing some of the advantages of each. Furthermore, it provides the possesser of a mass spectrometer with a single filament source with the means to analyze materials previously not practicable.

In this system a sample containing filament and a hotter, ionizing filament are heated in parallel with a single filament current power supply. Since the same voltage is applied to each branch the current through each is a function of its resistance. The resistance will vary directly with length and temperature and inversely with cross sectional area. Thus the temperatures of the sample and ionizing filaments are controlled by adjusting length, cross-section and nature of each. The ionizing filament is placed very near and directly above the sample containing filament. The sample containing filament may be flat or V-shaped. The ionizing filament may be ribbon or wire. Typical assemblies employed in this laboratory are shown in Figure I. The V-filament holds the sample in each case. The round wire or flat ribbon ionizes the evaporating sample. The selection of different ribbon and wire sizes easily provides a temperature differential of several hundred degrees centigrade between the sample filament and the ionizing filament. Figure II shows the respective temperature curves of a typical double filament assembly. Here the ionizing wire is 0.004" diameter tungsten-rhenium alloy (3% Rh). It is 0.25" long and spot-welded to 0.040" diameter Kovar insulated leads. The sample filament is a dimpled rhenium ribbon 0.001" x 0.030" x 0.6" in dimension. Normally the distance between the wire and the ribbon is approximately 0.005"-0.010". The dimple in the ribbon is 0.012"-0.015" wide at the top, 0.010"-0.012" deep and 0.10" long.

After the filament assembly is completed the sample filament may be pushed to one side for loading. Thus the ionizing filament does not become contaminated. The use of one type of material (rhenium, tungsten, tantalum, etc.) for the sample filament and another type (rhenium, tungsten, tantalum, etc.) for the ionizing filament often permits a wider variety of filament temperatures to be used. Choice of the various tungsten rhenium alloys for the ionizing wire has been quite useful.

Figure III shows a list of the elements most commonly analyzed at this laboratory and the type of filament (single or double) which is used for the analysis. The column labeled (HT) signifies that the filament has been cleaned prior to loading by heating to 2200°C for approximately one hour in vacuum. The column labeled (Butene) signifies that after the high temperature treatment the filament is heated to 1400°C and exposed to 200 μ Torr of butene gas for 30 minutes. The decomposition of the butene releases

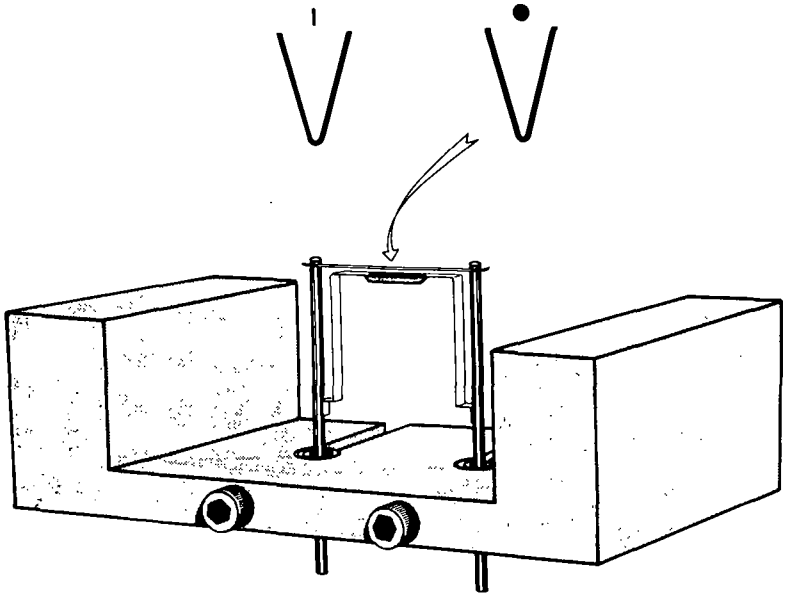

FIGURE 1.

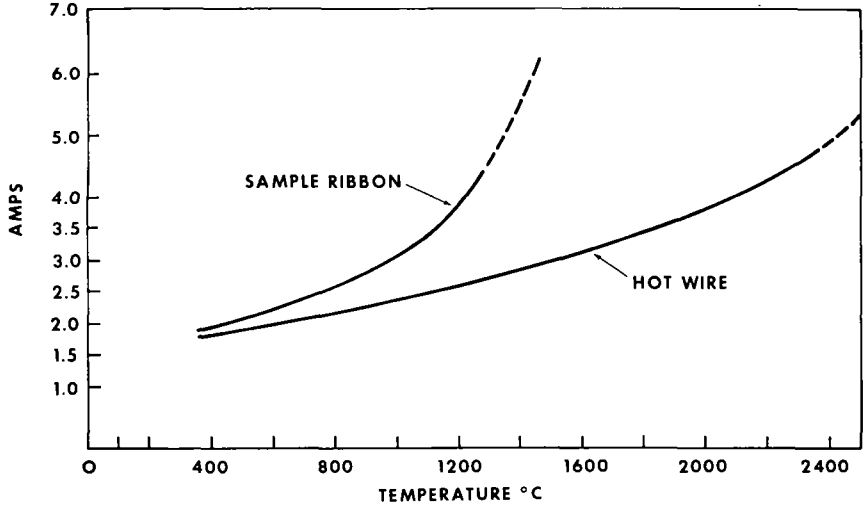

FIGURE 2.

carbon which is then dissolved in the filament (i.e. rhenium). The column labeled (Sucrose) is a further extension of the butene treatment and signifies that the sample is either loaded from a 0.05M solution of sucrose or that a drop of this solution is added after the loading. This technique is discussed in Reference 1.

The physical configuration of the double filament assembly may be modified to suit the user and to adapt to his particular instrument. For example, it may be practicable and preferable to use a different filament holder and employ different insulated leads for each filament while still connecting them in parallel to a common power supply. The possible variations and combinations may be left to the user.

Reference

1. M. H. Studier, et al, ASTM E-14 Committee Proceedings, March, 1961, pp. 245-247.

FILAMENT PREPARATION FOR MASS ANALYSIS

ELEMENT	FILAMENT MATERIAL			FILAMENT TYPE		PRETREATMENT			COMPOUND LOADED	ION ANALYZED
	Re	Ta	W	SINGLE	DOUBLE	HT	BUTENE	SUCROSE		
AMERICIUM	X			X		X	X		$AmCl_3$	Am^+
BARIUM		X		X		X			$BaCl_2$	Ba^+
BORON	X			X		X			$Na_2B_4O_7$	$Na_2BO_2^+$
CADMIUM	X				X	X	X	X	$CdSO_4$	Cd^+
CERIUM		X		X		X			$CeCl_3$	CeO^+
CESIUM	X			X		X	X	X	CsCl	Cs^+
COPPER	X				X	X	X	X	$CuSO_4$	Cu^+
CURIUM	X			X		X	X		$CmCl_3$	Cm^+
ERBIUM		X		X		X			$ErCl_3$	Er^+
EUROPIUM	X			X		X	X	X	$EuCl_3$	Eu^+
HAFNIUM	X			X		X			$Hf(NO_3)_4$	Hf^+
INDIUM	X			X		X	X		$InCl_3$	In^+
LANTHANUM	X			X		X	X		$LaCl_3$	La^+
LITHIUM	X				X	X	X		LiI	Li_2I^+
MOLYBDENUM	X			X		X	X	X	$MoCl_6$	Mo^+
NEODYMIUM	X			X		X	X	X	$NdCl_3$	Nd^+
PLUTONIUM	X			X		X	X	X	$PuCl_4$	Pu^+
RUBIDIUM	X			X		X	X	X	RbCl	Rb^+
RUTHENIUM	X			X		X	X	X	$RuCl_3$	Ru^+
SAMARIUM	X			X		X	X	X	$SmCl_3$	Sm^+
TELLURIUM	X				X	X	X	X	$TeSO_3$	Te^+
THORIUM	X			X		X	X	X	$ThCl_4$	Th^+
TIN	X				X	X	X	X	$Sn(SO_4)_2$	Sn^+
URANIUM	X			X		X	X	X	UCl_4	U^+
ZINC	X				X	X	X	X	$ZnSO_4$	Zn^+

FIGURE 3.

HIGH ABUNDANCE SENSITIVITY MASS SPECTROMETRY IN NEUTRON CROSS SECTION AND EFFECTIVE NEUTRON TEMPERATURE MEASUREMENTS

L. Forman[+] and F. A. White

Department of Nuclear Engineering and Science
Rensselaer Polytechnic Institute
Troy, New York

ABSTRACT

The thermal neutron cross section of Sm-147 has been measured by the mass spectrometric determination of the number of SM-148 atoms formed by neutron capture.

Small samples ($\sim 10^{12}$ atoms) of high isotopic purity were separated at the final focal point of a large radius four-stage mass spectrometer. The isotope collectors were rhenium ribbons which were subsequently irradiated in a well thermalized neutron spectrum. After the irradiation, each ion-impregnated rhenium ribbon served as a sample filament in a double-filament surface ionization source. Since the pre-irradiation Sm-148/Sm-147 was less than 10^{-6}, it was possible to compute a cross section value directly from a post irradiation Sm-148/Sm-147 ratio of 0.00025 = 8%. Normalization of the data to neutron spectrum parameters, time integrated neutron flux and effective neutron temperature, was accomplished by means of the simultaneous irradiation of minute quantities of other rare-earth isotopes (Sm-149 and Gd-157) whose neutron cross sections as a function of effective neutron temperature are known.

INTRODUCTION

The basis of a mass spectrometric determination of a thermal neutron capture cross section is the change in isotopic ratio that is caused by neutron absorption. The first observation of this kind was reported by Dempster[1] in 1947. By comparing the isotopic abundances of neutron irradiated cadmium with those of natural cadmium, he demonstrated that the isotope responsible for the high neutron capture was Cd^{113}. Since that time, most experiments have been based on neutron induced changes in the higher purity isotopes that are commercially available. In this experiment, by applying high abundance sensitivity mass spectrometry for both sample separation and analysis, we were able to measure the thermal neutron capture cross section of Sm-147 based on a change in isotopic ratio of 250 parts per million. Since commercially available isotopic purities in this mass region are typically characterized by an (A + 1)/A ratio of 0.01, the increase in sensitivity achieved in observing neutron induced isotopic ratio changes is substantial using the high purity approach.

The instrument employed in this experiment was the large radius four-stage mass spectrometer located at Rensselaer Polytechnic Institute. When used as an isotope separator, isotopic purities of better than one part per million were achieved in the mass 150 region. An abundance sensitivity of better than $10^8/1$ insured analysis free of spectral interference. Details of this instrument were reported at the 1964 Mass Spectrometer Conference.[2]

[+] Present address: U. S. Army Ballistics Research Laboratory,

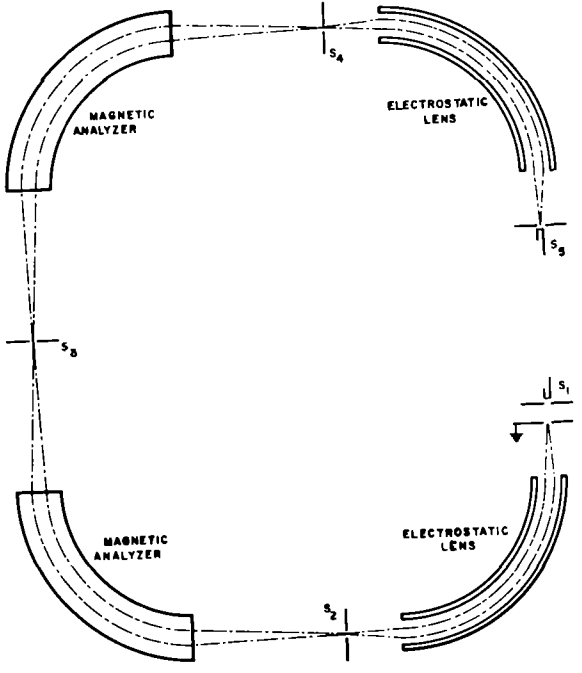

Fig. 1

Schematic of Four-Stage Mass Spectrometer

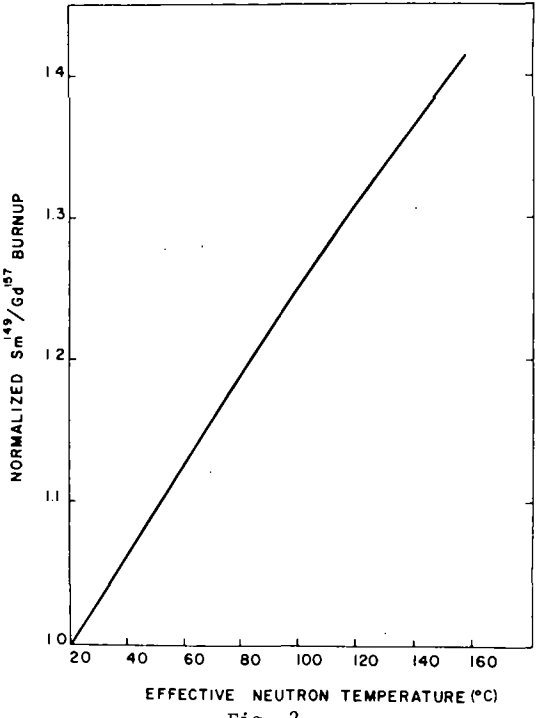

Fig. 2

Normalized Sm^{149}/Gd^{157} Burnup for Determining Effective Neutron Temperature

THEORY

The isotopic ratio is related to the thermal neutron capture cross section in the following manner:

$$e^{\sigma_A \phi t} = \frac{1 + R}{1 + R_o} \qquad (1)$$

Where σ_A is the thermal neutron capture cross section of an isotope of atomic mass A, ϕt represents the time integrated neutron flux, and R_o and R are the pre-irradiation and post irradiation (A + 1)/A ratios respectively. This equation assumes that the (A + 1) daughter nuclide is stable, and that there is negligible depletion of the daughter during the irradiation. It is clear from Equation (1) that in order to calculate a cross section from the isotopic ratio data, it is necessary to determine the magnitude of the time integrated neutron flux. We should first, however, consider the energy distribution of neutrons in a reactor since this may also affect the absorption.

The energy distribution of thermal neutrons, in many instances, in a reactor is a Maxwellian distribution which has been distorted by the preferential absorption of the lower velocity neutrons. If the distortion is not large, the resultant spectrum may be approximated by a Maxwellian distribution of higher temperature than that of the host medium. This temperature is referred to as the effective neutron temperature.

Westcott[3] has demonstrated, that materials whose energy dependent cross sections are known exhibit calculable absorption as a function of effective neutron temperature, and, this absorption may be used as a monitor for effective neutron temperature. Figure 1 shows the sensitivity of the absorption in SM-149 and Gd-157 to effective neutron temperature. This curve was generated from Westcott's Sm-149 data, and calculations performed on some recent Gd-157 energy dependent cross section data.

Once the effective neutron temperature has been established, Equation (1) may be used with the proper cross section value, with either the Sm-149 absorption or the Gd-157 absorption. to obtain the time integrated neutron flux. The magnitudes of these cross sections are quite large (254,000 barns for Gd-157) so that the method is quite sensitive.

EXPERIMENTAL

The sample material was separated onto a rhenium ribbon at the final focal point of the mass spectrometer by ion beam implantation. The ion source was a surface ionization source with a canoe-type filament. The amount of material separated was determined by integrating the ion beam current as measured at the collector. Typical samples of approximately 2×10^{12} atoms were obtained in this manner.

The collectors were irradiated in the graphite reflector region of the Argonne CP-5 reactor. The absorption in this region is quite small so that the concept of effective neutron temperature is appropriate. Gold cadmium ratio data indicated that the proportion of absorption due to neutrons of energy higher than thermal was less than 1% in all cases.

After the irradiation, the collectors served as sample filaments in a double filament surface ionization source. A 19-stage Allen type multiplier was used in the pulsed counting mode for the spectrometer detector. Less than 2×10^9 atoms of Sm-148 were produced during the irradiation.

RESULT AND CONCLUSIONS

The result of this experiment indicates a thermal neutron capture cross section of Sm-147 of 75 ± 11 barns at an effective neutron temperature of 127°C. This result lies well within the 87 ± 60 barn measurement of Jowitt et al. The value of the time integrated neutron flux obtained with the Sm-149 and Gd-157 was 3.41 ± 3% x 10^{18} neutrons/cm^2, to be compared to 3.42 ± 20% x 10^{18} neutrons/cm^2 indicated by the reactor staff.

The techniques used in this experiment have a number of advantages over conventional methods using commercially available separated isotopes:

1. Increased sensitivity to change of isotopic ratio caused by neutron capture is achieved by using very high purity isotopes.
2. Self depression factors are negligible where minute amounts of material are used.
3. No sample chemistry is required.

Additional cross section measurements are in progress at Rensselaer and the techniques are being refined. It is expected that other nuclear parameters will be investigated in a similar manner.

REFERENCES

1. A. J. Dempster, Phys. Rev. 73, 829 (1947).
2. F. A. White and L. Forman, "A Tandem Double Focusing Mass Analyzer of Large Radius", (Thirteenth Annual Conference on Mass Spectrometry and Allied Topics; St. Louis, May 1965).
3. C. H. Westcott, "Effective Cross Section Values for Well-Moderated Reactor Spectra", AECL-1101 (July 1962).

Determination of Electron Affinity Differences by Surface Ionization*

C. S. Harden, D. Stelman, and E. E. Muschlitz, Jr.
Department of Chemistry, University of Florida

INTRODUCTION

Determination of electron affinities by surface ionization has long been a field of great interest. Several factors make experimental negative ion current measurements difficult. Relatively high temperatures are required for negative ion emission, hence, thermionic electrons are also emitted and contribute to the negative ion current. The electrons may also form negative ions in gas phase collisions and thereby tend to obscure the effects of the surface ionization. Various methods, such as keeping the surface temperature low so the electron emission is small[1] and supressing the electrons with a magnetic field parallel to the cathode,[2] have been used to separate the effect of thermoelectrons from ion emission. The former method allows excessive contamination of the surface by gas atoms leading to erroneous results. Both methods require the assumption that the negative ion current is due to a single species. Mass spectrometric methods prove far superior to either of the above techniques since not only are the electron and ion beams separated but identification of the emitted ions is made possible.

Several papers involving determinations of electron affinity differences of the halogens utilizing mass analysis of the product ions have been published.[3,4] These experiments were largely limited to filaments surrounded by dilute atmospheres of diatomic interhalogen compounds or double beams of alkali halides directed upon a hot filament. In this work a well collimated molecular beam is incident upon a small portion of a tungsten ribbon filament so that there should be a negligible temperature gradient across the beam-surface interface. The purpose of these experiments is to explore the feasibility of using polyatomic molecules containing two electronegative species for the determination of electron affinity differences, and to examine the extent of dissociation of such molecules on a hot tungsten surface as a function of surface temperature.

THEORY

The electron affinity, E(X), of an atom X is defined as the energy at 0°K of the electron attachment reaction.

$$X + e \rightarrow X^- \tag{1}$$

This quantity may be obtained from a measurement of the equilibrium constant, K_p, for the reaction. For (1),

$$\ln K_p = \ln(P_{X^-}/P_X P_e) = -\Delta F^{(o)}/RT \tag{2}$$

or,

$$RT \ln K_p = -E(X) + F_e^{(o)} + F_X^{(o)} - F_{X^-}^{(o)} \tag{3}$$

where $F_i^{(o)}$ are the free energies of the reactants and products chosen so that they are zero at 0°K and P_i equal to one atmosphere. The partial pressures, P_i, may be calculated from the numbers, Z_i, of species i being emitted from a hot surface at temperature T from the relation

$$P_i = Z_i(2\pi m_i kT)^{1/2} \tag{4}$$

The method of electron affinity differences used in this work involves the measurement of negative ion currents of X^- and Y^- emitted from a hot tungsten surface upon which impinges a beam of molecules of the type CX_mY_n, where X=F and Y=Cl. The ratio of these currents then gives the difference in the electron affinities of the two halogens.

If a CX_mY_n molecule dissociates on a hot surface according to

$$CX_mY_n \rightarrow C + mX + nY \tag{5}$$

*Supported by the National Aeronautics and Space Administration

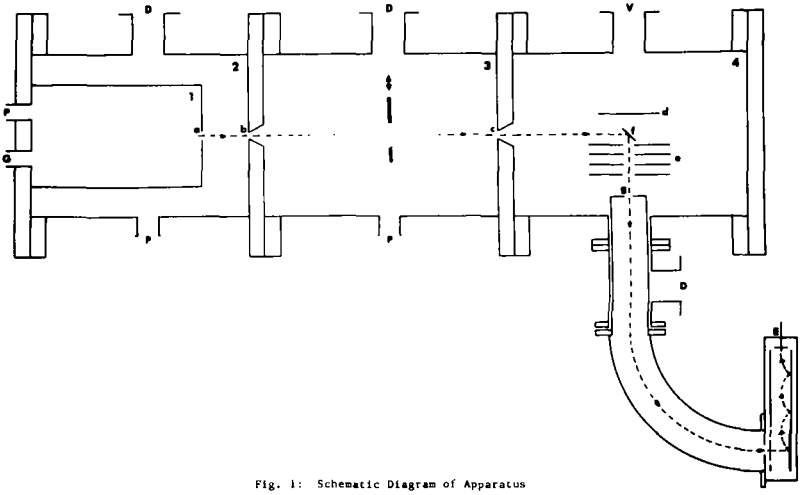

Fig. 1: Schematic Diagram of Apparatus

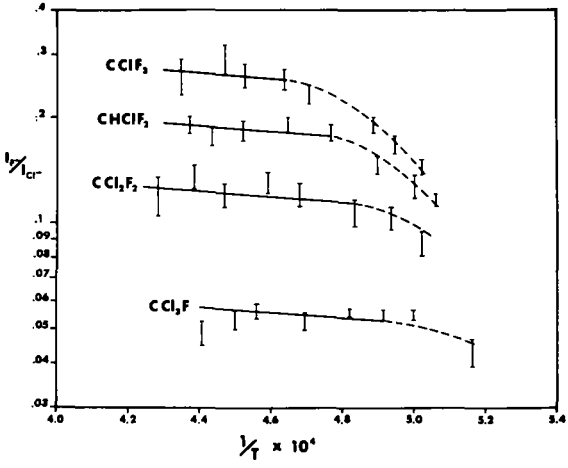

Fig. 2: I_X^-/I_{Cl^-} vs 1/T

equilibrium between the two halogens emitted from the surface will exist as

$$X + Y^- \rightleftarrows X^- + Y \tag{6}$$

For (6),

$$-\Delta F^{(o)}/RT = \ln K_p = \ln[(Z_{X^-}/Z_{Y^-})(Z_Y/Z_X)] \tag{7}$$

and,

$$-\Delta F^{(o)} = E(X) - E(Y) + (F_X^{(o)} - F_{X^-}^{(o)}) - (F_Y^{(o)} - F_{Y^-}^{(o)}) \tag{8}$$

The $F_i^{(o)}$ may be evaluated in terms of Q_i, the internal partition functions of species i. Substituting this with (8) into (7) gives the difference between the electron affinities of X and Y:

$$E(X)-E(Y) = RT \ln[(Z_{X^-}/Z_{Y^-})(Z_Y/Z_X)(Q_{Y^-}/Q_{X^-})(Q_X/Q_Y)] \tag{9}$$

Z_{X^-}/Z_{Y^-} is simply the ratio of the emitted ion currents. Z_Y/Z_X is the ratio of the numbers of Y and X atoms leaving the surface or the ratio of their concentrations on the surface and is equal to n/m since $Z_{X^-} << Z_X$ and $Z_{Y^-} << Z_Y$. Hence

$$\ln[(I_{X^-}/I_{Y^-})(Q_{Y^-}/Q_{X^-})(Q_X/Q_Y)] = \{[E(X)-E(Y)]/RT\} + \ln m/n \tag{10}$$

Therefore the slope of a plot of the left hand side of (10) vs 1/T gives the electron affinity difference and the intercept at 1/T=0 gives m/n, if the dissociation on the surface is complete.

The electronic partition function of the X and Y atoms is given by

$$Q = g_o + \sum g_j \exp(-E_j/kT) \tag{11}$$

where g_o and g_j are the degeneracies of the ground and j^{th} excited states respectively and E_j is the difference in the energies of the two states. Fluorine and chlorine each have a low-lying $^2P_{1/2}$ excited state of energies above the $^2P_{3/2}$ ground state corresponding to 404 and 881 cm^{-1} respectively. The ions in the ground states possess $^1S_0$ configurations and presumably have no low-lying excited states. Hence the ratio of fluorine to chlorine partition functions is

$$Q_F/Q_{Cl} = [4 + 2 \exp(-404 \times 1.439/T)]/[4 + 2 \exp(-881 \times 1.439/T)] \tag{12}$$

If the assumptions made above are correct the ratio of the ion currents is independent of the work function of the surface and the beam flux incident upon the surface. Also, it must be assumed that the accomodation coefficients for electron exchange between the surface and X and Y atoms on the surface are unity.

APPARATUS

The apparatus is shown schematically in Fig. 1. The gas is introduced into chamber 1 where it effuses out of a 1/2 mm orifice at (a) and is collimated by orifices (b) and (c). The beam then impinges upon a polycrystalline tungsten filament (f) and the ions are extracted and accelerated by a series of electrodes at (e) and (g). The ion beam enters a 3 inch radius-of-curvature 90° magnetic deflection mass spectrometer and strikes the cathode of a Bendix magnetic electron multiplier. The output currents of the multiplier are measured with a Keithley electrometer amplifier. The lower limit of measurement of ion currents is approximately 2×10^{-16} amp. Chambers 2, 3, and 4 and the analyzer tube of the mass spectrometer are all separately pumped resulting in background pressures of about 10^{-7} torr in the reaction chamber (#4). A beam shutter located in chamber 3 allows interuption of the molecular beam so that the background ion current due to both surface ionization and electron bombardment of the residual gas may be measured.

MEASUREMENTS

The pressure of the reactant gas is raised in the beam source (Chamber #1, Fig. 1) and a beam is formed which strikes the target filament. The ions are extracted from the filament and focused on the entrance slit of the mass spectrometer. The ion energy upon entrance to the mass spectrometer is 1000 volts. The mass spectrum is swept and peaks are observed at m/e of 16, 19, 35, and 37. Mass 16 (O^-) is assumed to arise from electron bombardment of background gas and oxides on the filament. Masses 19, 35, and 37 are F^-, $(Cl^{35})^-$, and $(Cl^{37})^-$. The $(Cl^{37})^-$ to $(Cl^{35})^-$ ratio is 1/3 in all cases. Peaks 19 and 35 were swept successively and their ratio, corrected for $(Cl^{37})^-$, taken as a function of the filament temperature. The temperature measurements were made by sighting on the filament with an optical pyrometer of the dissappearing filament type.

RESULTS

Figure 2 shows a plot of $\log[(I_F-/I_{Cl}-)]$ vs 1/T for CF_3Cl, CHF_2Cl, CF_2Cl_2, and $CFCl_3$. The straight lines are assigned a slope corresponding to E(Cl) - E(F) equal to 0.20 eV as reported by Bailey[3] and are fitted to the experimental points at high temperatures by the method of least squares. The plots indicate the correct trend of the intercepts to higher values of m/n as the F to Cl atom ratio increases in each molecule. However, the intercepts are far below the values expected if the molecules are completely dissociated on the surface. Table 1 gives the theoretical and observed values of m/n.

Table 1.

CF_mCl_n	$(m/n)_{theory}$	$(m/n)_{obs.}$
CF_3Cl	3	0.56
CHF_2Cl	2	0.35
CF_2Cl_2	1	0.23
$CFCl_3$	1/3	0.12

Over a portion of the temperature range covered the straight line fits the experimental points fairly well. This combined with the low values of the intercepts suggests that the molecules are incompletely dissociated on the surface and that the degree of dissociation, although not unity, is at least constant over some temperature interval. The change in slope at lower temperatures indicates that the degree of dissociation is changing in this temperature range. It should be noted that the straight line portion of the plots extends over a greater range of temperatures and that the fall off is less steep as the F to Cl atom ratio decreases.

No peaks correponding to undissociated fragments of the molecules (e.g. CF^-) were observed. A search for ions of the type WF_x^- was also made without success. If such ions are emitted from the surface then the electron affinities of the radicals must be $\lesssim$ 3 eV.

CONCLUSIONS

It is not evident why the degree of dissociation should be constant at the higher temperatures when it is still less than unity. The increasing degree of dissociation at lower temperatures may be explained by considering the C-F and the C-Cl bond strengths. The average C-F bond strength is about 4.4 eV and the average C-Cl bond strength is about 3.3 eV. As the temperature increases the relative probability of breaking a C-F bond to that of breaking a C-Cl bond increases.

These results indicate that polyatomic molecules can be used at sufficiently high temperatures for determining electron affinity differences, although the results are not completely satisfying because of the incomplete dissociation observed.

A degree of dissociation for each molecule may be calculated from the value of the intercept of the plot in Fig. 2. If no assumptions are made as to the nature of the dissociation, then $\alpha = [(m/n)_{obs}/(m/n)_{theory}]$ gives a relative degree of dissociation in the temperature interval of its constancy. A reasonable assumption to make, however, is that the C-Cl bonds are completely broken. Then α equals the degree of dissociation of the C-F bonds. Table 2 gives the results of calculating the degree of dissociation.

Table 2.

CF_mCl_n	α
CF_3Cl	0.18
CHF_2Cl	0.18
CF_2Cl_2	0.23
$CFCl_3$	0.36

BIBLIOGRAPHY

1. Jagudajew, M.D. and Shuppe, G.N., Akad. Nauk Uzbek S.S.R. (Bulletin) 3, 3(1946).

2. Sutton, P.P. and Mayer, J.E., J. Chem. Phys. 3, 20(1935).

3. Bailey, T.L., J. Chem. Phys. 28, 792(1958).

4. Bakulina, I.N. and Ionov, N.I., Doklady Akad. Nauk S.S.S.R. 105, 680(1955).

High Efficiency Surface Ionization Sources*

by
O. K. Husmann**
Hughes Research Laboratories, Malibu, California

Abstract

For ion source neutral efflux reduction high work function refractory metals and alloys have been investigated with regard to their electron work function and threshold temperature for surface ionization up to 10 mA/cm^2 cesium ion current density. Included here are filaments of tungsten, four tungsten-rhenium alloys with max. 25 weight percent rhenium, rhenium and iridium. The data have been measured in a guard ring diode with directly heated filament under clean surface conditions. The electron work functions and threshold temperatures show a continuous nonlinear increase from those of tungsten toward the rhenium data.

The minimum work functions of the cesiated W-25% Re, Re and Ir filaments are 1.3 eV, 1.1 eV, and 1.3 eV respectively.

One porous tungsten-25% rhenium pellet and two porous tungsten substrates, chemically coated with a thin layer of rhenium and iridium have been evaluated with regard to their neutral efflux and threshold temperatures. The electron work functions of these three pellets were below those measured with the corresponding filaments. However, even so the neutral efflux data show an improvement over porous tungsten with the same pore density. With 2×10^6 pores per cm^2 and 10 mA/cm^2 cesium ion current density, the neutral efflux from the rhenium coated pellet (ϕ = 4.69 eV) is 1% $\pm$ 0.1%. Extrapolated to clean rhenium surface conditions, the minimum neutral efflux is 0.3% at above pore and ion current densities.

Introduction

High efficiency ion sources combine high power efficiency with high ionization efficiency, i.e., low neutral efflux. Here high efficiency is the product of both. High efficiency insures long term continuous operation. In particular, long term continuous operation is only feasible in connection with low neutral efflux. Under optimal conditions (with only charge exchange sputtering) increases the deterioration of the critical structural high perveance ion gun dimensions slowly.

At 10 mA/cm^2 ion current density becomes the power efficiency of the electron impact and the surface ionization ion sources comparable and is better than 80%. It asymtotically approaches 100% with further increasing ion current density. In addition, surface ionization sources allow control of the neutral efflux over the whole emitter area. With present day technology this neutral efflux can be maintained at 1% of the total cesium flow rate.

* * * *

The ionization efficiency β follows from the Saha equation. The neutral efflux F complements β and is

$$F = \left[1 - (g_i/g_a) \exp (\phi - I)\, 11600/T \right]^{-1}$$

g_i and g_a are the statistical weights of the ion and atom states. (For alkalies is $g_i/g_a = \frac{1}{2}$). ϕ and I are the emitter work function and the ionization potential. The high ionization efficiency considerations impose $(\phi - I) \geq 0.6$ eV to above equation. In connection with this limitation govern on poly-crystalline surfaces the same patches electron and ion emission. The electron emission from a patchy surface has to be weighted exponentially with the patch work function.[1] Under this consideration the Richardson equation is

$$\nu_e = \frac{T^2}{e} \sum_k A_k F_k \exp - \frac{\phi_k}{kT} \ \mathrm{Sec}^{-1}$$

* The work reported herein was supported by the National Aeronautics and Space Administration under contract NAS-3-6270

** Now with Nortronics, A Division of Northrop Corporation, Applied Research Department, Newbury Park, California.

with ν_e the number of electrons emitted per second, T the emitter temperature in ^oK and F_k the surface area of the kth patch with the Richardson constant A_k. The number of ions ν_i emitted from the patchy surface is

$$\nu_i = \frac{\sigma_o}{\tau_o} \sum_k \theta_k F_k \exp - \frac{Q_k}{kT} \sec^{-1}$$

This equation is derived at by using $\tau = \tau_o \exp Q/kT$ and the relation

$$\nu_i = \frac{\sigma_o \theta F}{\tau}$$

Q is the ion desorption energy with[2]

$$Q = 0.722\,\phi - 1.34 \text{ eV}$$

measured for cesium ions on refractory metals. From these equations follows at 1300^oK,

$$\Delta \nu_i = \frac{\sigma_o \theta}{\tau_o} \exp - \frac{Q}{kT} \left[F_i - F_k \exp - \frac{0.722\,\Delta\phi}{kT}\right]$$

$$\Delta \nu_e = \frac{T^2}{e} \exp - \frac{\phi}{kT} \left[A_i F_i - A_k F_k \exp - \frac{\Delta\phi}{kT}\right]$$

$$\Delta \nu_i \propto \exp - 6.44\,\Delta\phi$$

and

$$\Delta \nu_e \propto \exp - 8.9\,\Delta\phi\,.$$

In both cases, ion as well as electron emission, the work function change is in the exponent of the weighting factor. The weighting functions emphasize the emission contributions from the same work function patches.

In connection with the increased mean ion life time on high work function patches, the surface coverage there increase relative to the low work function patches and therefore migration to the low work function patches is probable. In case of $(\phi e - I) = 0.2$ eV, on polycrystalline tungsten a Saha equation work function of 4.7eV has been measured, indicating, that in such case the higher work function patches take over.[3]

The power efficiency is expressed by[4]

$$\eta = [1 + 3\,\epsilon\,\sigma\,T^4 / \tfrac{1}{2}\, j^{5/3}\, p^{-2/3}]^{-1}$$

Here it is assumed, that one-third of the heater power input is radiated from the emitter surface.* ϵ is the total emissivity, j the ion current density in amps/cm^2 and p the ion gun perveance in amps/volt$^{3/2}$. T is in ^oK.

The threshold temperature for surface ionization increases with the emitter work function and is related to the ion desorption energy by

$$Q = \frac{k}{e} \frac{T_2 \times T_1}{T_2 - T_1} \left[\ln \frac{j_2}{j_1} - \ln \frac{\theta_2}{\theta_1}\right]$$

T_1 and T_2 are threshold temperatures. j_1 and j_2 are the corresponding ion current densities and θ_1 and θ_2 the relative surface coverages for these current densities. The threshold temperature for surface ionization is

$$T_L = 1.16 \times 10^4\, Q/[(1.16 \times 10^4\, Q/T_1) - \ln(j_2/j_1) + \ln(\theta_2/\theta_1)]$$

* Higher efficiency heater-emitter systems are feasible.

If the surface coverage term is disregarded, the threshold temperature equation has the form $T = A / (B - \log j)$.

A) Filament Investigation

For work function and threshold temperature studies a number of refractory metal and alloy filaments have been investigated. For these experiments a guard ring diode was employed. To avoid temperature gradients, the entire tube is made of stainless steel and its outside is copper clad, with a window for pyrometer readings. The tube is sealed with a copper gasket. All electrodes as well as the filament are supported by Al_2O_3 ceramic bushings, based on a stainless steel flange. During the experiments in cesium atmosphere, the 4-in. flange (including the bushings, ion pump, and the cesium reservoir) is maintained at temperatures more than 100° C higher than those of the tube in order to avoid excessive cesium deposition on the insulator surfaces. Insulator bypass currents under this condition were below any critical level. Ultra high vacuum conditions were maintained with a o.2 liter/sec ion pump, with the final pressure in the 10^{-9} Torr range. To establish a fixed vapor pressure, the tube was submerged in a water thermostat with the temperature controlled within o.o2° C. The maximum bath temperature did not exceed 84° C.

Filament temperatures were calibrated with a micropyrometer. The spectral emissivities of W-25% Re and iridium were measured in the range between 1000°K and 2000°K by comparison with black body radiation. At1500°K, the spectral emissivity of iridium is o.33 and is o.49 at 1300°K for the W-25% Re alloy.

The filament bulk clean up usually took more than four days, connected with a work function change toward its final stabilization.

Electron and ion currents were measured with a calibrated Keithley 600 A electrometer amplifier instrument. - No curvature of the Richardson plots has been observed, even though a patchy surface such as that investigated here may produce an upward concave slope.[5] - Microscope studies of all filaments showed a practically flat surface, confirming that the current densities are not overestimated. Table I combines the work function data of the investigated filaments.

TABLE I
Work functions and Richardson Constants

Filament	ϕ, eV	A, A/deg^2cm^2
Tungsten	4.54	120
W-5% Re	4.55	120
W-7% Re	4.56	120
W-15% Re	4.59	120
W-25% Re	4.695	146
Rhenium	4.88	164
Iridium	5.4	140

For W-25% Re, Re and Ir the Richardson work functions ϕ_R are reported. For Tungsten and the remaining alloys the effective work functions ϕ_E are given.

When alkali from the vapor phase (in contrast to diffusion) is deposited on the ionizer surface, hysteresis of the ion current in the threshold region is observed. The hysteresis width increases with (ϕ - I) and also with the applied electric field; it decreases with increasing ion current density.[6] In connection with the hysteresis we differentiate between lower T_L and upper threshold temperature T_U. The high perveance guard ring diode permits use of relative low extraction potentials. The corresponding low E-fields reduce the Schottky effect. At 10 KV/cm, the threshold temperature is reduced by 11°K. $dQ = e(eE)^{1/2}$ and

$$dT = \{[1/2\,(T_1 + T_2)]^2 - (dQ/Q)\,(T_1 \times T_2)\}^{1/2} - 1/2\,(T_1 + T_2)$$

At ion energies above the sputtering threshold the filament becomes contaminated with Ni from the outer electrode.[7] The Ni sputtering threshold energy is about 2o eV. Therefore, with a Cs - ion perveance of 4.74 x $1o^{-8}$ amps/$V^{3/2}$, ion current densities up to 0.2 mA/cm^2 can be measured without sputtering. Table II provides the upper threshold temperature equation constants.

TABLE II
Upper Threshold Temperature Constants

Filament	A	B
tungsten	14.0×10^3	8.764
tungsten - 5% Re	13.8×10^3	8.52
tungsten - 7% Re	13.9×10^3	8.53
tungsten - 15% Re	13.81×10^3	8.30
tungsten - 25% Re	14.0×10^3	8.32
rhenium	14.91×10^3	8.59
iridium	16.81×10^3	9.1

The tungsten-rhenium alloys show a continuous nonlinear increase in both, work function and threshold temperature. (Fig. 1)

The minimum electron work functions of the cesiated W-25% Re alloy, rhenium and iridium (with ϕ = 5.2 eV) are 1.3, 1.1, and 1.3 eV, respectively.

B) Porous Pellet Evaluation

For evaluation of porous pellets, the ion beam deflection technique has been employed, as described earlier.[3] Besides other advantages, this technique prevents metal sputter deposition onto the ion emitter. The neutral efflux is measured opposite the emitter. Previous investigations indicated the pore density as the parameter, governing the neutral efflux[4] (in addition to the Saha equation neutral efflux, which is governed by the work function ionization potential difference). Structure stable pellets presently are limited[10] to about 3 x $1o^6$ pores per cm^2 (traverse counting technique.[8]) The optimum pore density depends on the alkali distribution around the pore exit. Ionization only takes place, if the surface coverage is below about 4% of one monolayer. The dilution approximately follows 1/r, with r the distance from the pore exit. Quantitative thermal emission ion microscope studies showed for tungsten ion emission center radii in the two micron range. They are fairly independent of the flow rate per pore and the emitter temperature.

The pellet transmission coefficient was measured with He in the temperature range between 3oo and 16oo°K and ξ * is proportional to $T^{-\frac{1}{2}}$. The pellet electron work functions, measured under ultra high vacuum conditions, did not yield those, measured with the corresponding filaments, but lower ones.

Surface roughness may lead to an over estimation of the ion current density and to a somewhat lower work function, if not considered. In case of an average 1 micron pore radius and one micron pore depth, the increase in surface area on 20% porous material corresponds to a work function increase in the order of o.o3 eV.

The emitter work function, measured per neutral efflux (Saha equation) is in agreement with the Richardson work function at ion current densities below o.1 mA/cm^2 and decreases with increasing flow rate per pore. In case of 2 x 10^6 pores per cm^2 and 1o mA/cm^2 cesium ion current density, the neutral efflux work function is o.18 eV below the electron work function, as measured on porous tungsten. Because of the dominant 1/r dilution of the surface coverage, such work function reduction is typical for all porous ion emitters.

* ξ is the flow rate.

All investigators agree to cosine neutral efflux distribution in case of no ion extraction. However, cosine neutral efflux distribution in case of ion extraction is questioned by some workers in this field.[9] Our neutral efflux measurements yield a constant geometry factor that closely agrees with that computed for cosine distribution, also in case of ion extraction. The neutral efflux, multiplied by the geometry factor, complements the ion current. This is of particular importance in the threshold region. Both facts, agreement of the Saha equation work function with the electron work function in the low ion current density range and agreement of the neutral detector geometry factor with that computed for cosine distribution also in case of ion extraction confirm cosine distribution of the neutrals under all conditions.

Cesium evaporation from structures oppositely located to the emitter contributes to ion emission in case of ion extraction and to the neutral efflux in case of no ion extraction. Consequently this fact leads to an underestimation of the actual neutral efflux. Charge exchange neutrals slightly increase the neutral detector reading, as has been shown earlier.[10]

None of the here investigated pellets showed the work function of the W-25% Re, Re and Ir filaments. Two porous tungsten substrates were coated with thin layers of rhenium and iridium by chem. deposition. The third pellet was fabricated from prealloyed and spheroidized W-25% Re powder of narrow size distribution. Table III presents the pellet data.

TABLE III
Pellet Data

	ϕ, eV	transmission coefficient	pore density pores per cm^2
W 25% Re	4.64	7.19×10^{-5}	1.7×10^{6}
W - iridium coat	4.70	4.5×10^{-5}	1.9×10^{6}
W - rhenium coat	4.69	9.78×10^{-5}	2.27×10^{5}

Fig. 2 shows the neutral efflux from these pellets in the cesium ion current density range between 1 and 10 mA/cm^2, and for 2×10^6 pores per cm^2. The rhenium coat considerably improves the neutral efflux, compared to tungsten, with 1% (± 0.1%) at 10 mA/cm^2. If we assume for rhenium the same decrease in work function with increasing ion current density, i.e. 0.18 eV as measured on porous tungsten at 10 mA/cm^2 cesium ion current density and 2×10^6 pores per cm^2, then extrapolation yields 0.3% neutral efflux (with ϕ = 4.88 eV). Optimum pore densities are in the 10^7 pores per cm^2 range. Under consideration of the porous structure time stability[11], rhenium presently seems to be the best choice as emitter material.

Conclusion:

The ion source power efficiencies increase with increasing ion current density and are between 80% and 90% at 10 mA/cm^2 cesium ion current density,[4] approaching asymtotically 100%. Ionization efficiencies better than 99% are in reach with rhenium ionizers. This leads to a total efficiency between 79% and 89%. Further improvement will be achieved with increasing ion current densities and improved emitter heater systems. A limit may be the long term stability of the porous structure, i.e., deterioration of the pore density.[11]

References

1) O.K. Husmann, AIAA preprint 66-223 (1966)
2) O.K. Husmann, Phys. Rev. 140. A 546. 1965.
3) O.K. Husmann, Progress in Astronautics and Aeronautics (Academic Press Inc., New York, 1963), vol 9. 195. (1963)
4) O.K. Husmann, AIAA J. 1. 2607. (1963)
5) G.F. Smith, Phys. Rev. 94. 295. (1954)
6) E.F. Chaikovskii and G.M. Pyatigorskii, Soviet Phys. -Tech. Phys. 9. 847. (1964)
7) R.V. Stuart and G.N. Wehner, J. Appl. Phys. 33. 2845. (1962)
8) H. Muenzer and P. Schneiderhoehn, Heidelberger Beitr.Mineral.Petrog. 3. 456. (1953)
9) D.F. Hall, A.Y. Cho, and H. Shelton, AIAA Preprint 66-218 (1966); also B. Thompson, G. Kuskevics and M. LaChance, AIAA preprint 66-219 (1966)
10) O.K. Husmann and R. Turk, AIAA J. 3. 1653. (1965)
11) R. Turk, "Tungsten Ionizers with Controlled Porosity for Cesium Ion Engines," preprint no. 418., International Powder Metallurgy Conference, New York 1965; also A. R. Porter, J. Less Common Metals, 4.2 (1962)

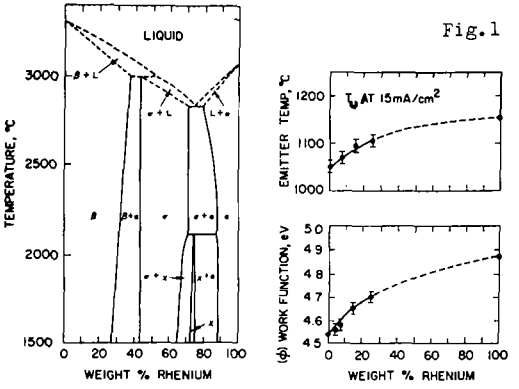

Fig.1 Work functions and threshold temperatures of the tungsten-rhenium alloys. The dashed lines are interpolations.

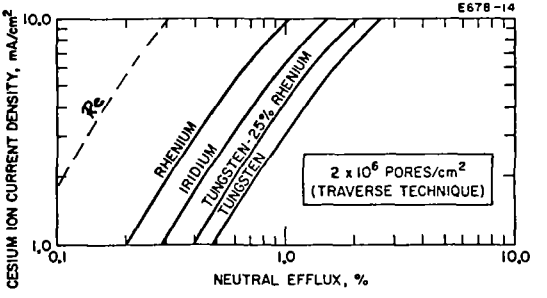

Fig. 2 Neutral efflux at cesium ion current density in the range between 1 mA/cm^2 and 10 mA/cm^2 on porous rhenium, iridium, and W-25% Re. The pore density is 2 x 10^6 pores/cm, measured by the traverse technique. It should be noted that the thermionic work functions for the iridium and rhenium coats used here are 4.7 and 4.69 eV. The work function for the W-25% Re alloy is 4.64 eV. In relation to the Saha equation it is assumed that under clean surface conditions the neutral efflux from iridium, rhenium, and W-25% Re is below that indicated here. The dashed line is an extrapolation to clean rhenium surface.

VACUUM LOCK SURFACE IONIZATION SOURCES

By E. J. Michael and E. G. Kerfoot

Nuclide Corporation
State College, Pennsylvania

A vacuum lock is a device which permits the interchange of some piece of equipment into or out of a vacuum chamber without loss of vacuum. In the field of mass spectroscopy, the use of a vacuum lock device to interchange samples for ionization by the thermal emission method has proven to be very helpful, particularly to those investigators whose needs require a high quantity of routine analyses to be performed.

Two main types of vacuum locks are in common use for introducing sample holders-these are the sliding bar type of lock and the sliding bar with a gate valve type. Some characteristics and performance details are herein described for each type used with mass spectrometers.

Generally, the smaller in diameter one constructs a sliding bar vacuum lock, the more readily a low conductance seal can be maintained around it; therefore, many vacuum locks have been made with a working diameter from one to one and a half inches. Two considerations favor the use of a size significantly larger than this, however; to enable use of accelerating potentials up to fifteen kilovolts and to permit the interchange not only of the sample "hat", but of the other high voltage source electrodes as well.

A sliding-bar vacuum lock with a three inch diameter allows a carriage size sufficient to contain a multi-pin ceramic header capable of sustaining pin-to-shell voltage differences up to eighteen kilovolts. In this case, the carriage includes a demountable source section comprised of four high voltage plates, each two inches in diameter, and a triple filament hat. The filament hat is separately removable from the source section.

The sliding-bar lock depends on one or more stages of differential pumping to successfully accomplish the transition from atmosphere to 10^{-7} Torr. Three stages of pumping are used on the gasketless lock, since each stage can tolerate about a (5×10^2) pressure difference across the metal-to-metal sealing regions. When the interstage seal consists of a teflon gasket instead of a close metal fit, the pressure differential tolerance is increased to (2×10^3), so the number of stages can be reduced to two.

Figure 1 schematically shows the pumping arrangement for the gasketless lock. Note that similar pump stages on each side of the lock are connected for common pumping. This lock can be loaded from either end, and thus is symmetrical about the source chamber. For the same reason, the blank carriage also spans the entire width of the lock housing. Figure 2 shows a sample carriage partially inserted into the gasketless lock. Inserting the carriage into the lock is initially a manual operation, but once it has been inserted sufficiently to achieve vacuum at the first stage, further motion is controlled by alternate roughing and venting of the manifold can, in reality a vacuum cylinder, which surrounds the blank carriage at the right of the figure.

Typical pressures maintained by the various stages of the gasketless vacuum lock under steady state conditions are:

First stage: 50 microns with a 250 liter-per-minute forepump
Second stage: 1 micron with a 70 liter-per-minute forepump
Third stage: 5×10^{-8} Torr with a 20 liter-per-second Hg. diffusion pump
Source Region: 2×10^{-8} Torr with a 20 liter-per-second Hg. diff. pump

A typical operating cycle for the gasketless lock would be as follows:

Insert carriage to First stage: Pump 1-1/2 minutes to 100 microns
Advance carriage to Second stage: Pump 1-1/2 minutes to 5 microns
Advance carriage to Third stage: Pump 3 minutes to 5×10^{-8} Torr
Advance carriage to Source: Pump 4 minutes to 5×10^{-8} Torr

With the gasketless lock there is a slight interaction between stages, e.g., a 50 micron pressure rise in the second stage may cause a .05 micron pressure rise in the third stage, but the interaction does not normally carry over more than one stage.

Figure 3 shows the gasketless lock in its operating configuration. In this position, the sample carriage alignment can be adjusted, rotationally and axially, to optimize ion intensity and peak shape. Once adjusted, the alignment can be "locked in", so that the sample carriage can be removed and reinserted with a reproducible effect.

The gasketed cross-loading vacuum lock is very similar to the gasketless lock described above except that, having only two stages of differential pumping, it is somewhat more compact. Also, since no close metal-to-metal fits are involved, this lock is usually motorized, resulting in considerably greater ease of operation. Figure 4 schematically shows the gasketed lock in the ready to load configuation. Note that the second stage pump is connected to the shaft packing on the dummy side of the lock. One stage of differential pumping is sufficient at the shaft since its diameter is only 3/4 inch.

The lock is shown in Figure 5 in its operating configuration. Again, the initial positioning of the sample carriage is a manual operation, but the inward travel of the carriage is self-sustaining once a pressure differential is established across it. Adjustment of the final position of the sample carriage is provided in the same manner as described for the gasketless lock.

Typical pressures maintained by the several stages of the gasketed lock under steady state conditions are:

First stage: 25 microns with a 140 liter-per-minute forepump
Second stage: 10^{-5} Torr with a 10 liter-per-second oil diffusion pump
Source: 5×10^{-8} Torr with a 20 liter-per-second Hg. diffusion pump,
5×10^{-9} Torr with a 100 liter-per-second ion pump

A typical operating cycle for this lock is as follows:

Insert carriage to First stage: Pump 30 to 60 seconds to 30-40 microns
Advance carriage to Second: Pump 1 minute to 3×10^{-5} Torr
Advance carriage to Source: Pump momentarily to 10^{-8} range

(Usually the source pressure will not deviate from its previous value for more than 10 seconds after the carriage has been inserted, provided the sample loaded is not more than a few micrograms.)

Although it is possible to start filament outgassing while the carriage is in the second stage of the lock, it is actually faster to do the outgassing after the carriage is in the source region, since the pumping speed there is considerably greater. The ideal preparation, of course, is to bake or outgas the loaded filaments in a separate chamber prior to loading them into the vacuum lock. In this way, it is possible to routinely start running the sample within five minutes after first introducing it into the lock.

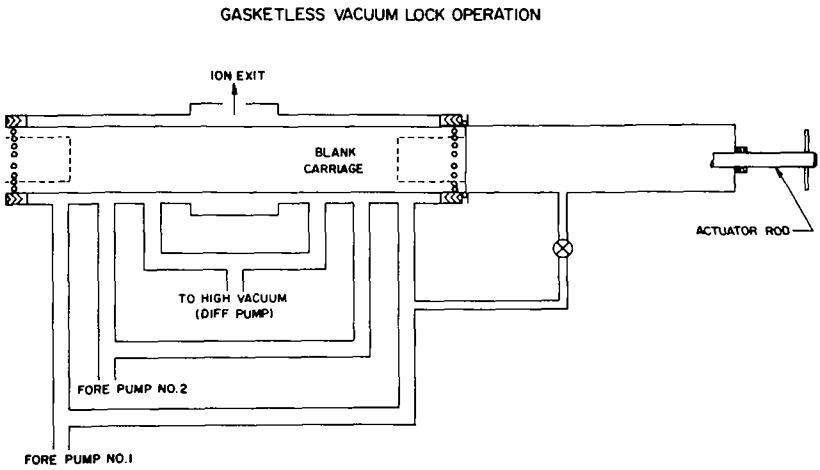

Figure 1: Vacuum Lock ready to load

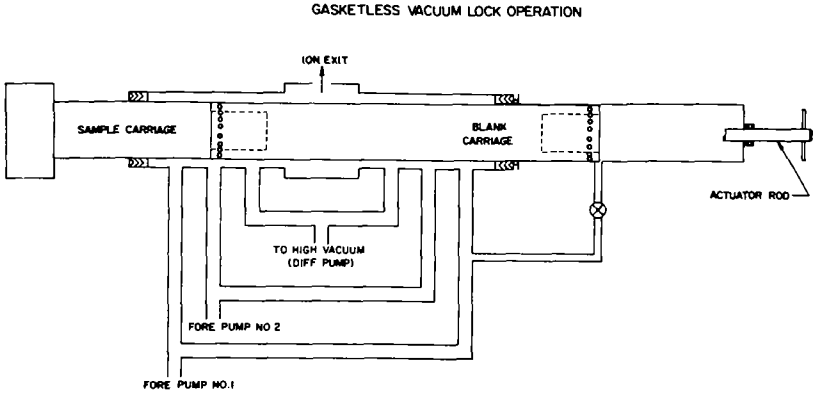

Figure 2: Vacuum Lock in roughing configuration

The other principal type of vacuum lock combines the features of the sliding-bar type with an isolation gate valve interposed between the differential pumping chamber and the ion source. This type of arrangement could be used with cross-loading locks described earlier, but it is almost mandatory to use it when one requires an end-loading lock, where the axis of loading is coincident with the axis of the ion beam.

The arrangement used is shown schematically in Figure 6. When unloaded, the ion source is exposed only to the gate valve, but the differential pumping chamber is open to atmosphere. With the pump port valves closed as shown here, the following pressures are maintained under static conditions:

First stage: 10 microns with a 140 liter-per-minute forepump
Second stage: 5×10^{-6} Torr with a 150 liter-per-second oil diff. pump
Source: 10^{-7} Torr with 20 liter-per-second Hg. diffusion pump

A typical operating cycle for this vacuum lock is outlined below:

Insert carriage to First stage: Pump 1-1/2 minutes to 50 microns
Advance carriage to Second stage: Pump 3 minutes to 2×10^{-5} Torr
Advance carriage to Source: Pump 4 minutes to 10^{-7} Torr range

The operating cycle for the end-loading lock is somewhat longer than for the cross-loading lock because the vented volume which must be re-evacuated is about three times greater, and the vented surface area to be outgassed again is also somewhat larger. Due mostly to the longer operating cycle of the end-loading lock, the insertion sequence is controlled automatically by two separate vacuum measuring circuits and a series of micro-switches operated at various positions of the sample carriage travel.

Briefly, the system operates as follows:

1. The carriage insertion is started by an operator-controlled switch.
2. The carriage is stopped by a travel limit switch and the rough valve opens.
3. A thermocouple gage circuit monitors the first stage pressure, until the preset level from 100 microns to 10 microns is reached, when the carriage travel begins again.
4. The carriage is stopped by a travel limit switch (after first sealing on the interstage differential seal ring), and the fine vacuum valve then opens.
5. A special ion gage circuit monitors the fine vacuum, and operates a trigger control when the preset level from 10^{-4} to 10^{-7} Torr is attained, at which time the carriage advances toward the source. If the filament outgas control has been actuated, outgassing will commence two minutes after the fine vacuum valve opens, and the pumpdown will be commensurately slower.
6. After the carriage seals on the last teflon seal ring, a limit switch actuates the gate valve and the carriage advances to the source region. Safety interlocks prevent accidental closing of the gate valve with the carriage inserted and prevent accidental ramming of the closed gate valve by the carriage.

Obviously, a vacuum controlled insertion cycle could be used on the previously described cross-loading locks as well as on the end-loading lock, but it would hardly be worthwhile on the gasketed version, since the loading cycle is so short. One instance where it would be useful to use a vacuum-controlled sequence would be where one wished to include filament outgassing during the loading cycle.

GASKETLESS VACUUM LOCK OPERATION

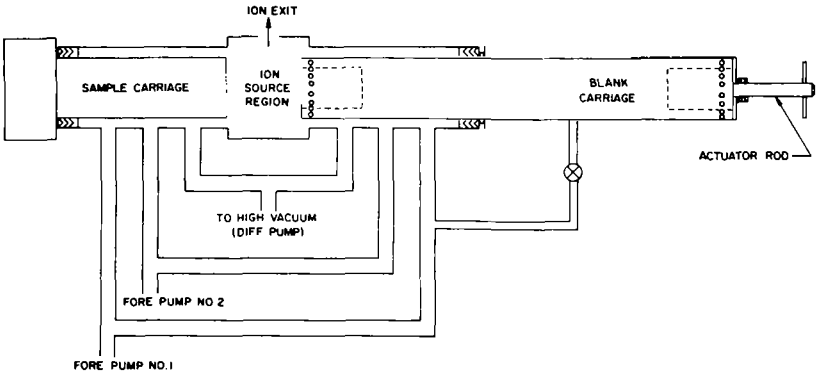

Figure 3: Vacuum Lock ready to operate

GASKETED VACUUM LOCK OPERATION

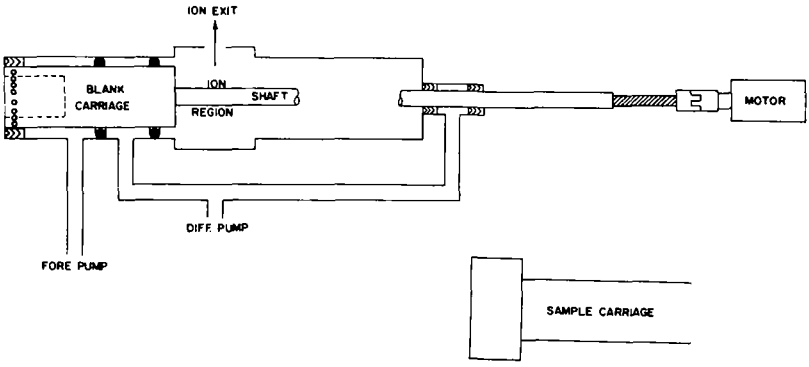

Figure 4: Vacuum Lock ready to load

A comparision, then, of loading cycle times for the three sliding-bar vacuum locks is:

Metal-to-metal lock: 6 minutes insertion time to the source region.
Gasketed lock: 1 to 2 minutes to the source region.
End-loading lock: 4-1/2 minutes to the source region.

Any of the vacuum lock systems described would be an appropriate lock for a given application, but it would seem that the gasketed cross-loading vacuum lock is the most versatile and useful for the majority of cases where a vacuum lock is being considered.

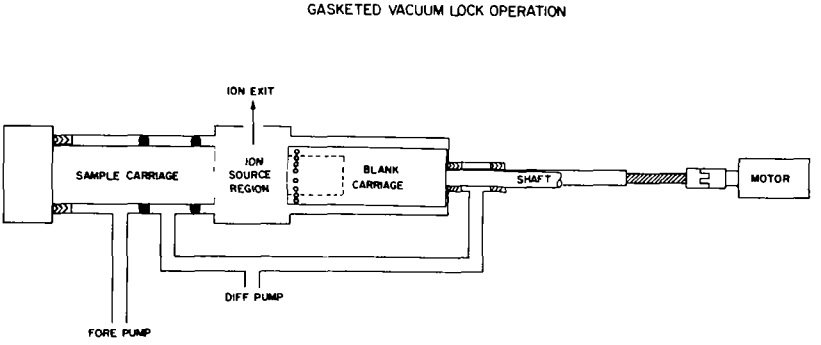

Figure 5: Vaccum Lock ready to operate

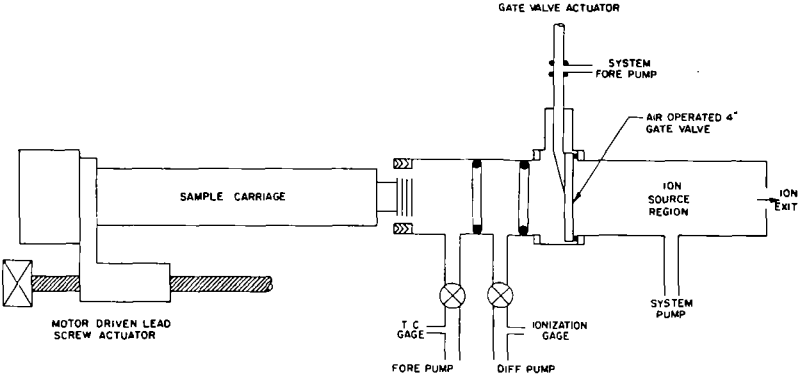

Figure 6: End loading vacuum lock in ready to load configuration

The Production of Vapor Species in a Mass Spectrometer Ionization Chamber

F. J. Vastola, A. J. Pirone, and B. E. Knox

The Pennsylvania State University
University Park, Pa.

Abstract

The light output of a small, pulsed ruby laser is focused on a target situated just below the electron beam in the ionization chamber of a time-of-flight mass spectrometer. Oscilloscopic recording with adjustable delay times allows one to obtain spectra of the vaporized species at various times during and after the laser pulse. This laser heating technique produces rapid surface heating of areas as small as 100 square microns. By viewing the target through the laser optical system, the area to be vaporized can be selected, thus enabling heterogeneous samples to be analyzed. Spectra of organic and inorganic materials are presented.

Introduction

One of the problems encountered in the mass spectrometric study of solids is that of converting the solid material to its vapor phase. The introduction of a furnace into a mass spectrometer has been the conventional method of solving the problem. However, there are many other problems which arise when this technique is used. The development of the laser has made available a compact source of energy which can provide controlled heating fluxes of 10^8 watts/cm^2. The 'marriage' of the laser and the mass spectrometer is a natural development utilizing good features of both instruments.

Focused lasers previously have been used to vaporize solids in mass spectrometers (1,2) as well as to produce ionic species (3,4,5). When a solid material is heated by a focused laser beam, the energy can be controlled so that only a few nanograms are vaporized; this is a sufficient quantity for analysis if the vapor species are produced within the ionization chamber of a mass spectrometer. Since the heating time is short (ca. 0.4 milliseconds), only a time-of-flight mass spectrometer can be used to produce a complete spectrum from a single flash. Since the ion pulse width is of the order of 5 microseconds, many spectra can be recorded during and after a single energy pulse from the laser. If the sample is viewed through the same optical system that is used to focus the laser output, the area to be vaporized can be selected before pulsing and examined afterwards. By utilizing micromovement in the laser mounting system, one can construct a microprobe of high sensitivity and high spacial resolution, useful for the analysis of inorganic, organic and biological solid materials.

Experimental

The laser and its associated optical system are shown in Figure 1. The function of the optical system is to focus the coherent light output of the laser on a small target area within the ionization chamber of the mass spectrometer. For the convenience of placing the laser and optical system outside the vacuum system, an objective lens of long working distance is needed: however, there is the conflicting requirement, that in order to obtain maximum light concentration, a lens of short focal length is needed. A compromise is made by using a 2X objective lens (Leitz VO) which has a working distance of 75 mm.

The laser head consists of a T.R.G., Inc. Model 103 Minilaser and Model 153 microscope coupling. The laser is a 6.35 mm. x 38 mm. ruby rod pumped by a helical gas discharge lamp. When the laser is pumped by a 230 joule discharge its output is 100 millijoules. The output pulse length is 0.3 to 0.4 milliseconds in duration; the wavelength of the laser light is 6943Å. The laser concentration and viewing system is constructed around a Leitz binocular-monocular FS microscope head.

The 25X eyepieces (Leitz periplanatic wide field) in conjunction with the 1.25X tube factor and the 2X objective give a total magnification of 62.5X. The high power eyepiece in conjunction with the low

power objective degrades image resolution, but this solution is necessary due to the problem of the working distance mentioned above. However, image quality is sufficient to locate the desired target areas. The target is illuminated for viewing by a vertical illuminator: the reflecting surface of the illuminator is a microscope slide mounted permanently in the optical path at an angle of 45 degrees. In order to minimize clearance problems the objective lense is mounted at the end of a 86 mm. x 12 mm. extension tube. The entire optical system is mounted outside of the vacuum system. The flange above the ion source in the Bendix Model 12-107 TOF mass spectrometer has a 25 mm. x 100 mm. well with an optically flat window at its lower surface. The objective lens can be lowered down into this well to reach its proper working distance. With this configuration craters as small as 10 microns in diameter can easily be produced.

The sample (12 mm. x 3 mm. surface) is mounted in a positioning clamp and inserted into the mass spectrometer through a modified Bendix Model 843A direct inlet port. In position, the sample is located just underneath the electron beam in the mass spectrometer ionization chamber.

Figure 2 is a block diagram showing the electrical interconnection of the various units of the spectrometer system. The various delays, gates, and ramp signal are derived from two Tektronix Model RM 45B oscilloscopes with type CA amplifiers. The output can be presented on the oscilloscope in several modes: single sweep at a preset time after the laser-fire signal; multiple sweep (ramp used to displace spectra) which enables up to eight spectra to be recorded; or a raster display with Z-axis modulation which enables about 100 spectra to be recorded (6). In all of these displays each sweep can be adjusted to give a complete mass scan (1-2000 A.M.U.) or a magnified presentation of a limited mass range. The spectra are recorded on Polaroid Polascope Type 410 film (10,000 ASA).

Figure 3 shows the timing of the operation sequence. The master clock (Tektronix Model 180-S1) provides 10KHz synchronizing pulses as well as 200 and 1000 KHz reference time markers. The TOF spectrometer is set to run synchronously with the 10KHz master clock. When the laser-fire switch is activated, the first 10KHz pulse to arrive fires the flash tube in the laser head and starts the delay timer in the oscilloscope, which in turn starts the selected display.

Applications

It is possible to obtain spectra of both the ion and neutral species produced by laser heating. Figure 4 shows spectra for selenium obtained by several techniques. Spectrum (a) was obtained with zero ionizing current (ionization chamber filament off) and shows the ions produced by laser heating. The resolution was not high enough on this sweep (m/e 50-800) to resolve the selenium isotopes. Although molecular ions up to Se_5^+ were detected, no Se_1^+ was found. The major ion produced was Se_5^+. Using the multiple sweep presentation it was found that these ions were produced for a period of about 100 microseconds during the laser burst. Spectrum (b) was obtained in the same manner as (a) but with an ionizing current of 0.15 μa. at a potential of 15 volts. The fact that Se_1^+ ions were not produced by laser heating but were produced by the impact of 15 volt electrons with the laser-generated vapor species indicated that the energies of electrons in the laser-induced plasma were probably less than 15 eV. Neutral species were produced for periods of several milliseconds after the laser discharge. As the sample cooled, the spectra became more equivalent to those obtained by direct heating. Spectrum (c) was produced by electron impact ionization (15 eV, 0.15 μa.) of vapor species formed by the direct heating of selenium in an open crucible to a temperature of 1475°K.

Laser-produced spectra of organic materials are more complex than those obtained from inorganic materials. Both ionic and neutral species are produced. The laser heating technique is particularly suited for the study of heterogeneous materials such as coal. Table 1 shows species produced in the C_2 to C_3 range by laser heating of a vitrain component of a bituminous coal.

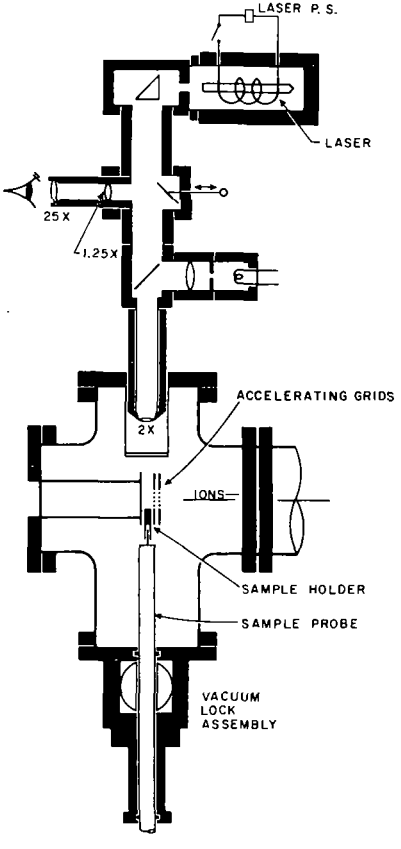

SCHEMATIC OF SYSTEM
FIGURE 1

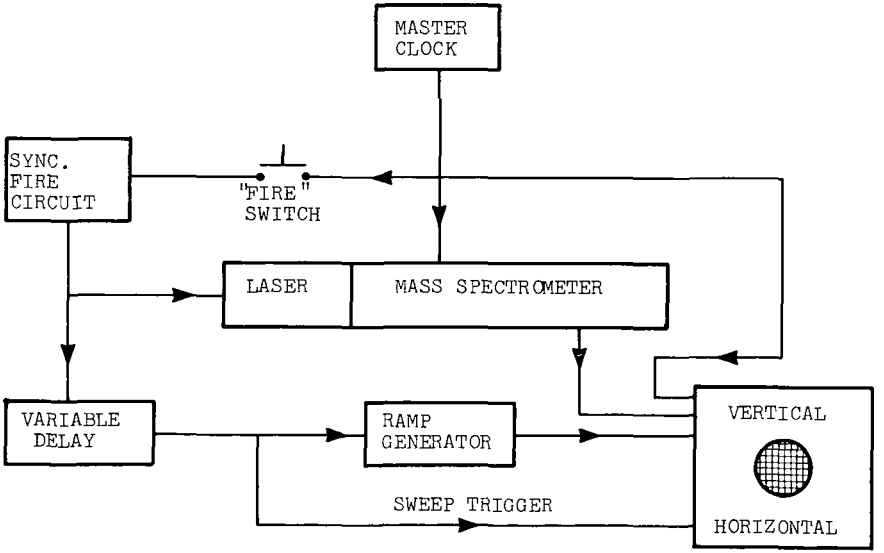

FIGURE 2. BLOCK DIAGRAM

Table 1

m/e	Assignment	Relative Intensity 25 eV	0 eV
24	C_2	1	3
25	C_2H	1	
26	C_2H_2	3	1
27	C_2H_3	3	
28	C_2H_4, CO, N_2	3	1
29	C_2H_5	2	
30	C_2H_6	2	
32	O_2, S	2	
33	HS	2	
34	H_2S	3	

Evolution of ions generated by laser heating of the coal lasts for periods of several hundred microseconds after the laser discharge, while the evolution of molecular species continues for periods of several milliseconds. The major ions produced are C_2 and C_5; no C_1, C_3 or C_5 ions are detected. The fragmentation patterns of the neutral spiecies are indicative of high free radical concentrations.

Acknowledgement

This research was supported by National Science Foundation Grant Numbers GP-3232 and GP-3687.

References

1. Honig, R. E. and Woolston, J. R., Appl. Phys. Letters 2, 138 (1963).
2. Berkowitz, J. and Chupka, W. A., J. Chem. Phys. 40, 2735 (1964).
3. Lichtman, D. and Ready, J. F., Phys. Rev. Letters 10, 342 (1963).
4. Isenor, N. R., Appl. Phys. Letters 4, 152 (1964).
5. Levine, L. P., Ready, J. F. and Bernal, E., Research/Development, Dec. 1965, p. 56.
6. Lincoln, K. A., Rev. Sci. Instr. 35, 1688 (1964).

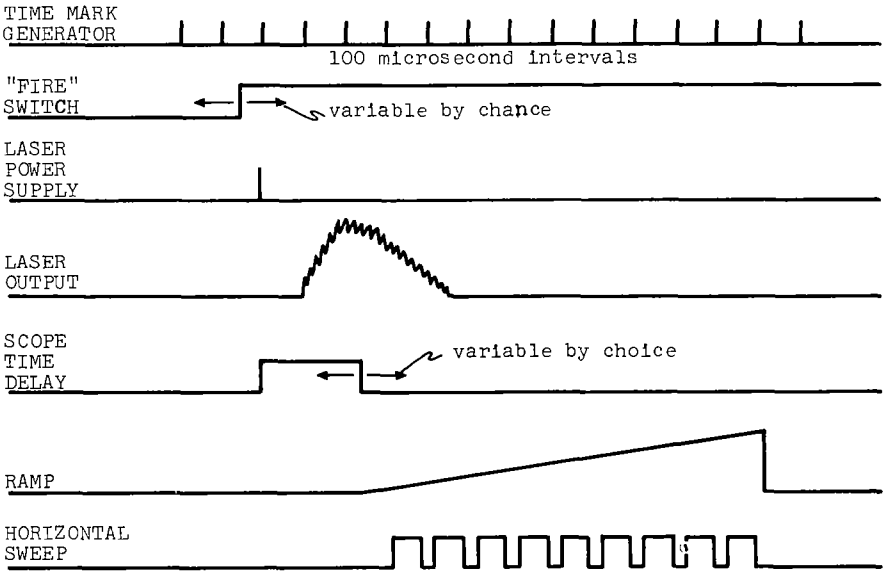

FIGURE 3. OPERATIONS SEQUENCE

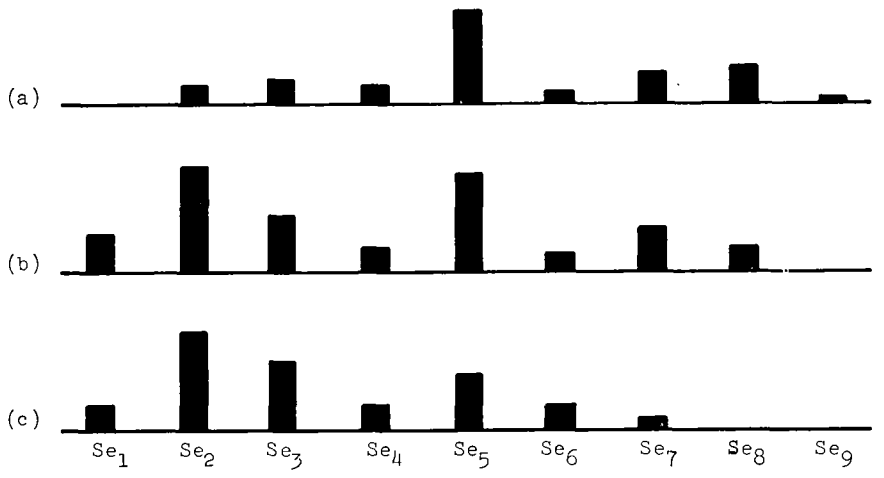

FIGURE 4. SELENIUM SPECTRA

APPLICATION OF LASER TO MASS SPECTROMETRY

N.C. Fenner, R.G. Ridley, R.W.D. Hardy, N.R. Daly

Atomic Weapons Research Establishment, Aldermaston

Abstract

A ruby laser can be used to concentrate an intense beam of radiation on to a small area. This high energy density was shown by several workers to be capable of evaporating material from a surface and also ionising some of the vapour. This method of ionisation was investigated at AWRE with the purpose of providing a source of ions for a mass spectrometer.

Two approaches to the problem were made: a 180° magnetic deflection spectrometer and a time of flight spectrometer. In both experiments the sample was in the form of a thin foil, either self supporting or held on a thin glass disc. In the time of flight apparatus a giant pulse laser was used to give a short, i.e. 100 ns, burst of ions and a resolution of 30 was achieved. The magnetic deflection spectrometer uses a conventional 1 joule laser and ionisation efficiency is improved by forming a plasma in the source region.

Both systems when fully developed will be capable of making a complete elemental analysis of a solid sample of 10^{-8} gm. At present high accuracy and high ratio measurements are not possible but improvement in these features may be expected as the work develops.

Introduction

Since the development of the laser as a high intensity source of light there have been several investigations (1,2,3) of the evaporation and ionisation of solid material by focussed laser light. There have also been a number of papers giving theoretical explanations (4,5,6) of the ionisation of solids and gases by the high optical power densities produced by giant pulse lasers. These papers give a general picture of many electrons and ions with large energies being released from solids and produced in gases at the focus of a laser beam.

The first application of this method of ionisation to mass spectrometry was by Honig and Woolston (7). A hole 150 μ diameter and 125 μ deep was produced in a bulk target when 2×10^{17} atoms were evaporated and 2×10^{14} ions were produced in a pulse lasting 50 secs. The ions were analysed on an MS 7, a double focussing mass spectrometer, but the high ion currents gave rise to space charge broadening of the peaks of the larger components.

Experiments in this work were undertaken with the object of producing a mass spectrometer with an ion source that could be used on small samples.

Experimental

In all our early work thin metal foils were used and these have some advantages over a sample of bulk material. Normally a smaller amount of material is ionised and hence the space charge effects experienced by Honig (7) are reduced. The variation of the power of a laser beam is considerable from pulse to pulse, depending on the temperature of the ruby and the age of the flash tube. The number of ions from a foil is relatively insensitive to laser power and control of the sample size is possible by variation of the foil thickness. Another advantage is that when samples in the form of a solution are put onto a thin foil they give a higher signal to background ratio than would be obtained from a solution layed on a thick backing. Finally it is very simple geometrically to arrange to fire the laser onto one side of the foil and take the ions from the other.

At Aldermaston we have two laser source experiments; one employs a 1 joule laser with 180° magnetic analysis and photographic detection, the other a giant pulse laser with time of flight analyser. Fig. 1 shows the magnetic system, the laser, the lens system, the foil, ion path, and photographic plate.

Magnetic Spectrometer

A foil of the sample material about 3000 Å thick is evaporated on to a thin glass disc - 1/10 mm thick and 25 mm in diameter. The beam from a 1 joule ruby laser is

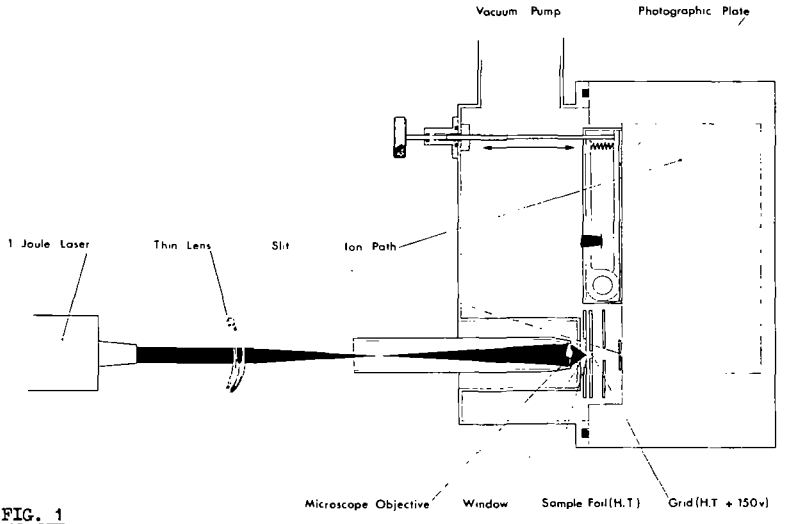

FIG. 1

180° MAGNETIC ANALYSER WITH LASER SOURCE

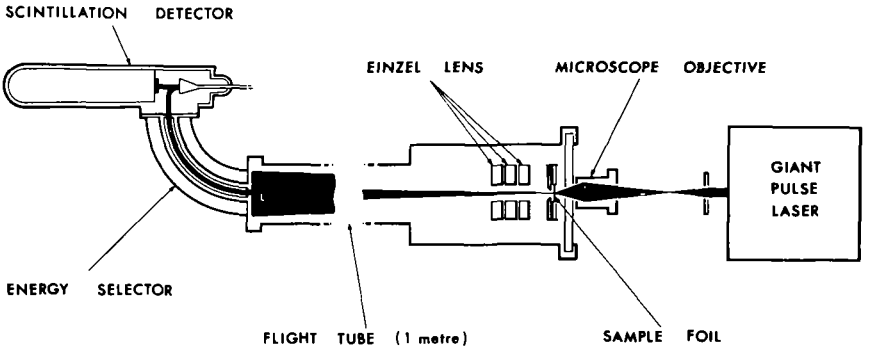

FIG. 2

LASER TIME OF FLIGHT SPECTROMETER

focussed by a lens system through a window in the casing of the apparatus, through the glass disc and on to the foil. A fine copper grid is placed beyond the foil at a distance of 1 mm and is maintained at a potential of 500 - 800 volts +ve with respect to it. This grid is followed by the entrance slit to the magnet; the grid is held at a potential of $\sim 2\frac{1}{2}$ kV with respect to the slit which is at earth potential and is about 3/10 mm wide. The magnet allows a 180° trajectory, with a maximum reading of 9 cms; the pole pieces which form the boundary of the vacuum region are separated by a gap of 7 mm; the working field is 12,600 g. The ion beam is analysed, and focussed by the magnet on to a photographic plate which is in the same plane as the entrance slit. The emulsion on the plate is Ilford Q2. Spectra have been obtained from the following foil materials: Al, Ni, Cu, Sn, Au, Pb and Al/Au composite foil. The ratio of the intensity of the lines due to aluminium and gold obtained from the composite foil was measured by counting the silver grains under the microscope. The value of the ratio thus obtained was in fair agreement with the known ratios of the quantity of the two elements in the foil. A measure of the efficiency of the whole system was obtained by measuring the area of foil removed, estimating the number of atoms contained therein and dividing the number into that obtained from counting grains. This gave an average figure of 10^{-7} ions collected per atom of sample.

One of us has recently undertaken a theoretical study of the mechanism of ionisation in the foil-grid region. The results of this give some promise of providing an explanation of one of the central problems in this work.

Time of Flight Spectrometer

The combination of a Q switched laser and time of flight analysis has been used [8,9,10] to measure the properties of ions leaving a surface. We have used this system as the basis for a time of flight spectrometer.

The laser light is focussed onto a sample, vaporising a small part of it and ionising some of the vapour. The ions are accelerated by a high positive potential and allowed to drift down a one metre tube to the collector at the far end. This system gives rise to time resolved spectra that are displayed on an oscilloscope and photographed. Fig. 2 shows a diagram of the apparatus used in this work, the laser, focussing system, sample foil, flight tube, and collector system.

The laser, which gave a photon pulse of up to 30 millijoules in .03 microseconds, was switched by a Kerr cell from which a monitor pulse was used to trigger the oscilloscope displaying the trace. The light beam was focussed onto an area 3×10^{-5} cm^2 by a long working distance microscope objective. It was possible to view the target foil through this lens using a subsidiary eye piece and so focus the laser beam onto the foil. The position of the laser was adjusted so that the focal spot of the beam coincided with the intersection of the cross wires and so a particular point on the foil could be selected for analysis. Material was found to evaporate from a rather larger area than the laser focal spot due to conductive and radiative heating.

Ions from the foil were found to have a high energy spread and this gave rise to poor resolution when a simple plate collector was used, e.g. the resolution was only 6 with an HT of 2 kV. To overcome this a 90° deflection electrostatic filter with a resolution of 100 was built onto the end of the flight tube. However, the instrument resolution was only 30 at mass 60 due to the finite time spread (2×10^{-7} sec) of the ions. This is probably a space charge effect in the source or the flight tube. The filter cut down the ions collected by a factor of 10^4 and so a scintillation detector[11] was added to give the required amplification

The large energy spread also makes it very difficult to focus the ions. A shaped source electrode and a higher HT (5 kV) have had some effect, but an Einzel lens and deflector plates after acceleration have proved virtually ineffective. The overall transmission of the tube was 10^{-8} and statistics on the number of ions collected set the limit to the accuracy of measurement with the present apparatus.

Ionisation of Sample by Q Switched Laser

At the focus of the laser beam the power on the foil is $\sim 10^{10}$ watt/cm^2. This vaporises and ionises the material and gives the ions a velocity of up to 6×10^6 cm/sec using a foil of 6×10^{18} atoms/cm^2 of carbon. Recent experiments show that from a given foil the velocity distribution is almost the same for all the ions and not such that all ions have the same energy. It is not well established by what mechanism the ions receive this energy but it seems likely that thermionic electrons, released when the laser heats the solid, pick up energy from photons by a reverse bremsstrahlung effect. Ionisation of the vaporised sample takes place in a small plasma region. The plasma rapidly expands into the vacuum tending to plume in the forward direction. The plasma temperature is $\sim$ 20 eV giving single, double and a small fraction of triple ionised atoms. This agrees with the description of Ehler[8]. Further work has shown that using foils with equal

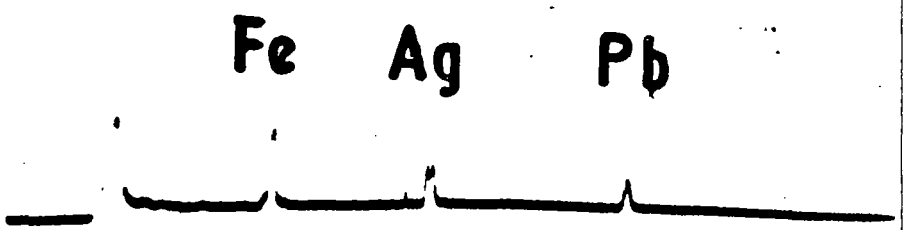

FIG. 3

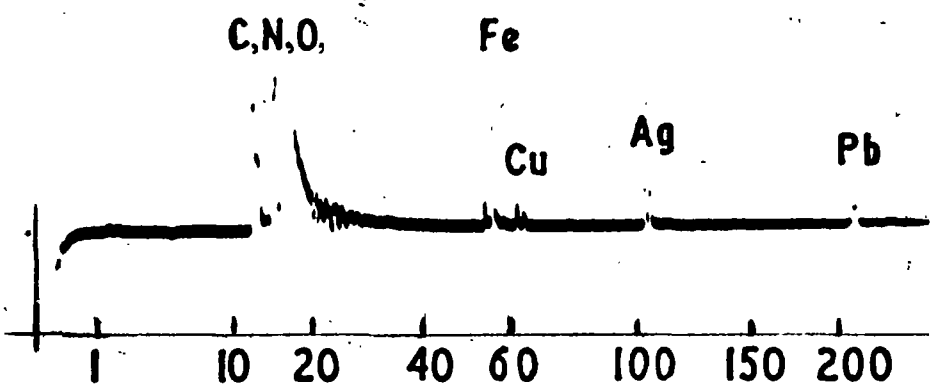

FIG. 4

atom/cm^2 of only one element the energy is such that the energy is similar for all ions, agreeing with the work of Lindor (2), Isenor (1).

Results

The laser produced 6 x 10^{12} ions when 4 x 10^{13} atoms (2 x 10^{-9} gm) of copper were evaporated, i.e. an ionisation efficiency of 3 x 10^{-2} ions per atom. Most metal foils used to date, e.g. Li, Be, B, C, Al, Fe, Cu, Ag, Sn, Pb, Au, gave efficiencies within an order of magnitude of this figure. Na and K evaporated as metal on to glass backing crystallised (presumably to the hydroxide) on transfer to the source and gave a rather high efficiency. These two metals also often appear as background peaks in the spectrum of a sample.

Fig. 3 shows the mass spectrum produced by equal layers (3 x 10^{17} atoms/cm^2) of Fe, Ag, Pb deposited on a microscope cover slide.

The peaks from the metals are easily identified and show comparable ionisation efficiency. One disadvantage of the glass backed foil as seen in Fig. 3 was that a number of peaks were found in the mass range 23-30, presumably due to sodium and silicon from the glass. These peaks were always smaller when ions of 100 eV or higher were selected for the analysis but they were always present. To overcome this problem self supporting foils were investigated and found to give cleaner spectra. However, at high laser powers (> 5 millijoules) peaks are observed at masses 1, 12, 14, 16, 18, 28 and 32. These are presumably due in the main to gases adsorbed on the foils.

It is unlikely that many unknown samples will be in the form of metal foils and so other more likely forms of material were investigated. Solutions of various compounds, e.g. metallic nitrates, hydroxides and chlorides were put on self supporting copper and aluminium foils. In the spectra obtained the molecules were completely dissociated and only atomic ions were observed. The ionisation efficiency of the different metal elements was comparable in this type of sample but up to two orders of magnitude difference in efficiency was found for the various other components of the sample, e.g. H, N, O, Cl.

Many solutions put on the thin Cu or Al 'dissolve' it and so VYNS (a PVC copolymer) has been used as the backing for some solutions.

Fig. 4 shows the spectrum obtained when the solution of equal weights of Fe, Ag and Pb nitrates, crystallised on a VYNS backing, was analysed. This figure is the analysis of a point where the sample appeared homogeneous in the microscope, but by firing the laser at a particular crystal the metal peak corresponding to it was found to predominate in the spectrum and so the crystal could be identified.

It can be seen in Fig. 4 that the isotopes of Ag are nearly resolved, indicating that in the case of small signals, in which the space charge effects will be small, the resolution is higher than that quoted earlier.

Higher laser powers (e.g. 1 MW) have been used in an attempt to increase the ionisation efficiency and get equal efficiency for all elements. The efficiency is increased but so is the velocity of the expanding plasma, aggravating the problem of ions having a wide energy range. It is hoped to improve the situation by steadily reducing the voltage during acceleration and so the high mass ions will receive less energy, or by using higher accelerating voltage.

Acknowledgements

We wish to thank Mr. S. H. Terry and Mr. S. Pocock for their help in these experiments; and Mr. R. H. Christie for the loan of the laser system. We also wish to thank the Director of the Atomic Weapons Research Establishment for permission to present this paper.

References

1. N. R. Isenor, Can. Jnl. Phys., 42, 1413, (1964).
2. W. I. Lindor, Phys. Rev. Letters, 12, 383, (1964).
3. J. F. Ready, Jnl. Appl. Phys., 36, 462, (1965).
4. J. M. Dawson, Phys. of Fluids, 7, 981, (1964).
5. P. Nelson, P. Vegrie, M. Berry, Y. Durand, Phys. Letters, 13, 226, (1964).
6. D. A. Tozer, Phys. Rev., 137, A1665, (1965).
7. R. E. Honig, Appl. Phys. Letters, 2, 138, (1963).
8. A. W. Ehler, Hughes Research Labs. Report No. 336.
9. E. Bernal, J. F. Ready, L. P. Levine, Phys. Letters, 19, 645, (1966).
10. H. Opower, W. Press, Zeits. f. Naturf., 21A, 344, (1966).
11. N. R. Daly, Rev. Sci. Instr., 31, 264, (1960).

Cryogenic Mass Spectrometry

H.A. McGee, Jr., D.B. Bivens, T.J. Malone and J.H. Wilson
Georgia Institute of Technology
Atlanta, Georgia

Abstract

There is an interesting class of molecules which exist as chemical reagents only at very low temperatures, that is, the activation energies for the loss processes of these substances are very low. Typical members of this family are H_2O_4, O_2F_2, O_3F_2, N_2H_2 and BH_3. A cryogenically cooled inlet arrangement has been constructed which permits positive identification of such species, and the development of their molecular energetics from ionization efficiency studies. This paper will summarize the essential design features and operation of the unusual apparatus, the synthesis and elementary properties of several of these cryochemicals, and will be principally concerned with the structure and energetic arguments that have been developed from the mass spectra data.

ION SAMPLING FROM HYDROCARBON COMBUSTION PLASMA*

by

William J. Miller

AeroChem Research Laboratories, Inc.
Princeton, New Jersey
a subsidiary of Ritter Pfaudler Corporation

INTRODUCTION

Research programs on the nature of ionic processes in flames have been actively pursued at AeroChem for the past ten years. Much of the work since 1961 has employed a mass spectrometer for the sampling and identification of flame ions, a schematic of which is given in Fig. 1. Details of the system have been presented in a previous publication,[1] and pertinent aspects of the instrumentation were discussed at the Ninth Annual E-14 Conference.[2]

Initially, the mass spectrometer was used only to identify the ions present in hydrocarbon combustion plasma, while other diagnostic techniques--notably the Langmuir probe--were applied to obtain absolute ion concentrations. As the research progressed, however, and the need arose for more detailed information, the mass spectrometer ion profiles examined with the goal of yielding such quantities as recombination coefficients, charge-transfer reaction rate constants, and ambipolar diffusivities. It therefore became imperative that quantitative relationships between mass spectrometer ion currents and actual ambient ion concentrations be established. Data taken previous to this analysis have since been re-examined and the results quantitatively confirmed.

The behavior of the ion beam in the focusing and analyzer sections of the instrument is that common to all mass spectrometric analysis. It is in the flame sampling process that the greatest uncertainties exist. The problems encountered are essentially the same as those discussed by Milne and Greene[3] in their free radical sampling experiments and by Spokes and Evans[4] in their ion studies. The objective of sampling system design in either radical or ion studies is to provide a probe which will not materially disturb the ambient reacting gas mixture but through which gas samples may be continuously withdrawn without change in composition into a low-pressure vessel where their compositions may somehow be determined.[7] The pressure downstream of the sampling orifice must be low enough to assure (1) freezing of chemical composition in the expansion and (2) very low subsequent collision frequency.

In many respects, the sampling of ions is a simpler process than the sampling of free radicals. Ions may be accelerated by electrostatic lens components inside the sampling system to decrease their residence time in the region of necessarily higher pressure just inside the orifice. This is an especially important consideration in view of the large reaction rate coefficients that exist for many ion-molecule reactions.

The sampling system, then, should be of a configuration that effects a compromise between the requirements of high vacuum downstream of the orifice and minimum disturbance of ambient conditions by the physical presence of the probe. So far, a truncated cone with the sampling orifice in the tip has proven to be the most satisfactory geometry. This paper describes a series of experiments in which the effects of sampling system configuration and electrostatic field have been empirically determined in an attempt to optimize the sampling process with respect to the above requirements.

---

* AeroChem TP-138

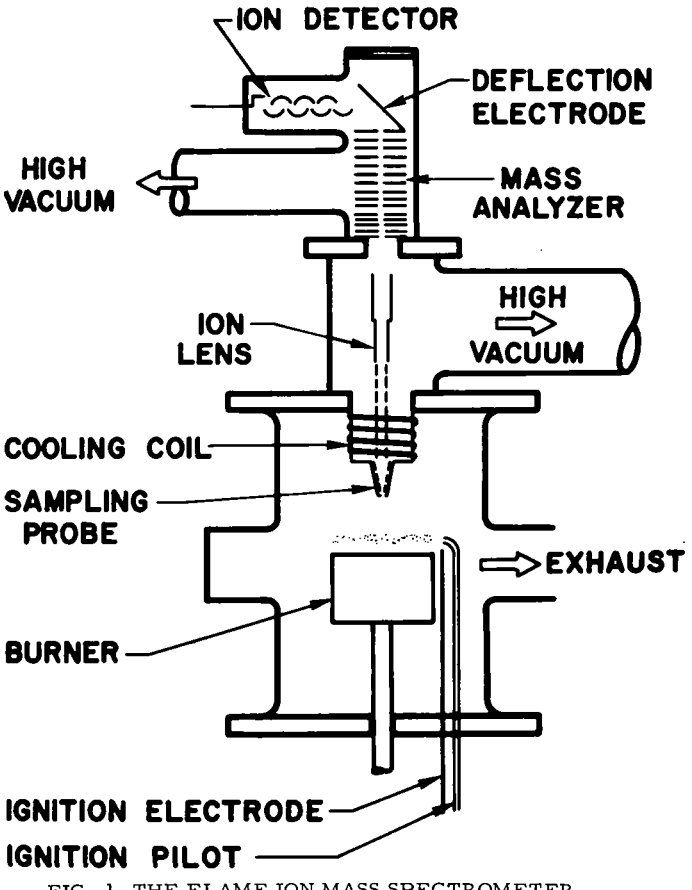

FIG. 1 THE FLAME ION MASS SPECTROMETER

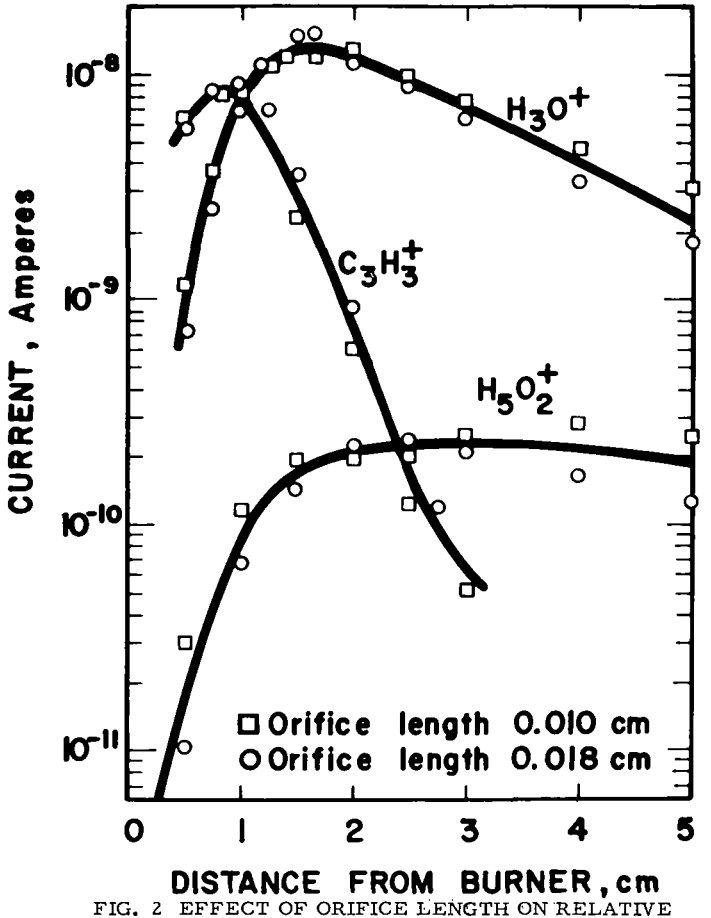

FIG. 2 EFFECT OF ORIFICE LENGTH ON RELATIVE INDIVIDUAL ION CURRENT

0.018 cm data multiplied by 6.6

RESULTS AND DISCUSSION

The first set of experiments was designed to test the effect of orifice length on relative ion currents; the results are given in Fig. 2. Three ions, H_3O^+, $C_3H_3^+$, and $H_5O_2^+$, were examined with a truncated conical probe and a sampling orifice of 0.010 cm diam and two different orifice lengths--0.010 and 0.018 cm. The only significant effect observed is a reduction in ion current using the longer orifice. After normalizing the currents by multiplying the lower numbers by a factor of 6.6, the profiles fall very nearly on top of one another, as shown in Fig. 2. Further thinning of the plate in which the orifice is drilled increased the currents only slightly. The fact that individual currents retain their original relationships indicates that reactions which may occur in the boundary layers around the input system are apparently not enhanced by lengthening the orifice--at least not at the low pressures (e.g., 2 Torr) employed in this program. However, it will be seen that boundary layer effects are important for certain cone configurations.

Figures 3 and 4 show the effect of changing the surface area of the plate in which the orifice is placed. All curves were taken in the same flame--C_2H_4/O_2--at 2 Torr. In the case denoted by the solid lines the hole was in a truncated cone tip. The diameter of the flattened portion was 0.6 cm and orifice diameter was 0.025 cm. The broken lines are profiles taken using a flat plate 8 cm in diameter and the same size hole employed to take the data represented by the solid lines. All curves are shifted considerably downstream and, with the exception of $H_5O_2^+$ (monohydrated H_3O^+), all decrease slightly in magnitude. The $H_5O_2^+$ profile, on the other hand, was observed to increase, perhaps due to the enhancement of hydration in the passage of H_3O^+ through a much thicker cool boundary layer outside the orifice. Comparison of these data with those in Fig. 2, in which the cone tip is only some 0.3 cm across, reveals strange behavior on the part of $H_5O_2^+$: The maximum H_3O^+: $H_5O_2^+$ ratio in Fig. 2 is approximately 60:1; in Fig. 3 using the truncated cone the ratio is about 13:1; and the flat plate gives a ratio of 0.7. The variation in the relative amount of $H_5O_2^+$ observed is apparently a function of the area about the orifice--larger areas giving higher concentrations. The lesson here is that to minimize hydration effects in the boundary layer outside the orifice, and for good spatial resolution one should use as pointed a cone as possible. However, it has been found that a pointed cone terminating in a 0.025-cm-diam hole yields ion currents lower by an order magnitude but with profiles very similar to the solid lines in Fig. 3 and 4; i.e., the H_3O^+:$H_5O_2^+$ ratio is again about 13:1. The hydration of H_3O^+ in this case probably occurs inside the cone where the extension to pointed geometry reduces pumping efficiency and increases local pressure. The formation of large quantities of $H_5O_2^+$ in either case is a strong indication of poor sampling system performance.

We have also examined the effect of imposing a potential across the flame front between burner top and sampling cone or plate. The ion currents at a fixed position in the flame are given in Figs. 5 and 6. These data show that a negative burner potential has little effect on positive ions. In normal operation the burner and cone are at the same potential. A negative burner potential would therefore be expected to have a retarding effect on positive ions. If the ions are all influenced to the same extent by an electrostatic charge, primary ions should be inhibited in their path to the sampling orifice, and the result should be an enhancement of secondary ions. The effect, if operative, is too small to be seen from the data. The converse--preferential sampling of primary ions at positive (accelerating) burner potentials--is observed to the extent that at least the ion most commonly cited as the primary ion, CHO^+, undergoes the largest increase upon imposing a positive potential. The same experiment when performed using a flat plate resulted in much smaller departures from normal response. This may simply be a reflection of the drastic differences in the electrostatic fields surrounding the two bodies, i.e., one would normally expect much steeper gradients in the fields about a cone as compared with those about a flat plate oriented normal to the flow. It must be emphasized that all these data were taken with the burner fixed relative to the sampling system, but this distance was different for the flat plate and cone experiments. In each case, the point at which the burner was fixed was determined by the position at which the $C_3H_3^+$ and H_3O^+ ion currents were approximately equal. These distances coincide closely with the

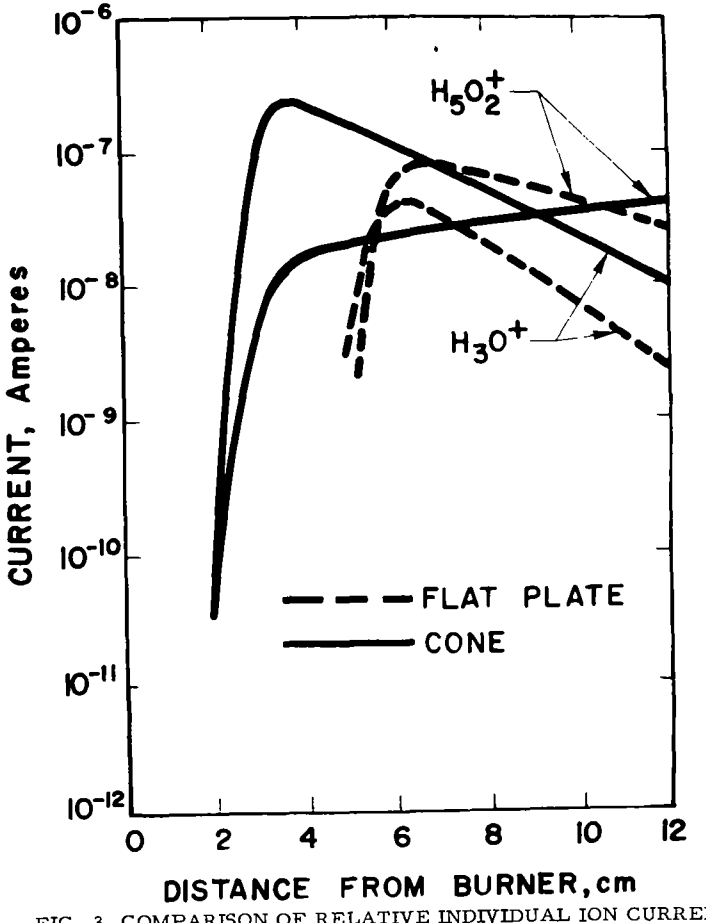

FIG. 3 COMPARISON OF RELATIVE INDIVIDUAL ION CURRENTS SAMPLED THROUGH A CONE AND A FLAT PLATE

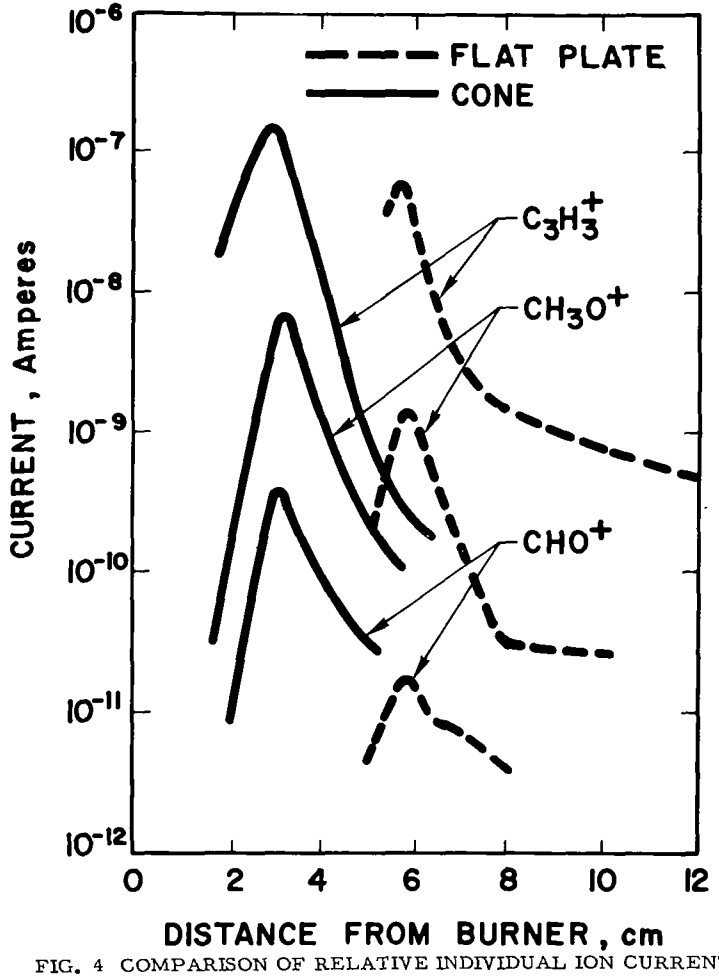

FIG. 4 COMPARISON OF RELATIVE INDIVIDUAL ION CURRENTS SAMPLED THROUGH A CONE AND A FLAT PLATE

positions of the maxima in Fig. 4. When taken in their entirety, the profiles substantiate the trends established in Figs. 5 and 6 and individual ion currents are observed to vary with distance from the flame front in the manner depicted in Figs. 3 and 4.

The effect of imposing a potential on the burner has also been studied for the case of negative ion sampling. The system examined in this case was a C_2H_2/O_2 diffusion flame of the Polanyi type. The bulk of the negative charge carriers in this flame are electrons; negative ion concentrations are approximately 1% of the total positive ion concentration. Negative ions are formed by electron attachment to hydrocarbon and hydroxycarbon species.[5] Electrons diffuse rapidly to the surfaces outside the flame creating a net positive charge in the flame which must be overcome to efficiently sample negative ions. No negative ions are apparently sampled when the burner is charged more than about 0.25 V positive with respect to the cone due to space charge effects around the cone surface. As shown in Fig. 7, changing the burner potential from +0.25 to -0.25 V results in a 100-fold increase in resultant negative ion currents. The relative individual negative ion currents and their spatial distributions are unchanged over the entire range of potential studied. This result may be contrasted with the positive ion data in Fig. 5. If the interpretation of preferential response to primary ions upon the imposition of an accelerating field is invoked as in positive ion sampling, the negative ion results lead one to conclude that ion-molecule reactions involving negative ions are unimportant in this flame and each negative ion is the result of an independent electron attachment process. This hypothesis will be checked in future experiments.

CONCLUSIONS

Sampling systems which present large obstructions to flow in a low-pressure flame apparently give rise to boundary layers in which hydration reactions and/or ion-molecule reactions may occur. These reactions also occur downstream of orifices in sampling systems in which the geometry does not provide adequately for efficient reduction of pressure immediately inside the sampling aperture. Truncated cones have been found to constitute a suitable probe geometry, provided a compromise can be effected between these flow obstruction requirements and the maintenance of suitably high vacuum immediately downstream of the orifice. The degree of cone truncation for optimum sampling will depend on the temperature and flow velocity of the system under investigation, as well as the pumping capacity in the vacuum chamber. If the sampling system presents a large obstruction to flow, spatial resolution will be lost and changes in apparent relative ion concentrations will result. Inadequate vacuum downstream of the sampling orifice causes a reduction in sensitivity and again leads to ion-molecule reactions which produce relative individual ion currents which are not an accurate representation of ambient conditions.

Electric field effects have been found to be much more significant when the sampling system geometry is a cone rather than a flat plate. In both of these cases, sensitivity and response to individual ions are essentially unchanged when the probe is biased 0 to +60 volts with respect to the plasma and its surroundings. Negative ions, on the other hand, can only be sampled when the probe is biased positive.

ACKNOWLEDGEMENTS

The author gratefully acknowledges financial support of the Office of Naval Research for this study under Contract Nonr-3809(00) and the assistance of J. J. Houghton with the execution of experiments.

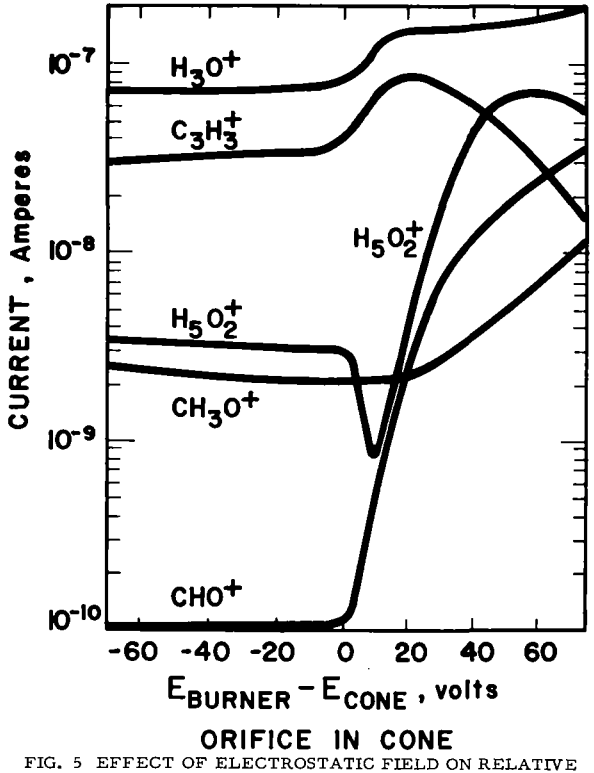

FIG. 5 EFFECT OF ELECTROSTATIC FIELD ON RELATIVE INDIVIDUAL ION CURRENTS SAMPLED WITH A CONE

data taken at a fixed position of 3.2 cm downstream of the burner

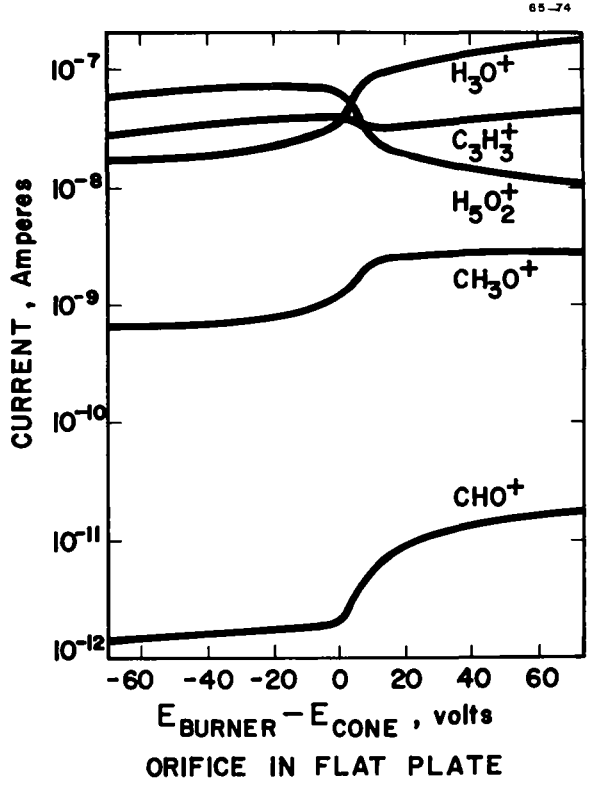

FIG. 6 EFFECT OF ELECTROSTATIC FIELD ON RELATIVE INDIVIDUAL ION CURRENT SAMPLED THROUGH A FLAT PLATE

data taken at a fixed position of 6.0 cm downstream of the burner

REFERENCES

1. Calcote, H.F. and Reuter, J. Chem. Phys. 38, 310 (1963).
2. Calcote, H.F., "Mass Spectrometric Studies of Ion Profiles in Low-Pressure Flames," Proceedings of the ASTM Committee E-14 on Mass Spectrometry, Chicago, Illinois, June 4-9, 1961.
3. Milne, T. A. and Greene, F. T., J. Chem. Phys. 44, 2444 (1966).
4. Spokes, G.N. and Evans, B.G., Tenth Symposium (International) on Combustion, (The Combustion Institute, Pittsburgh), 1965, p. 639.
5. Calcote, H.F., Kurzius, S.C. and Miller, W. J., Tenth Symposium (International) on Combustion, (The Combustion Institute, Pittsburgh), 1965, p. 605.

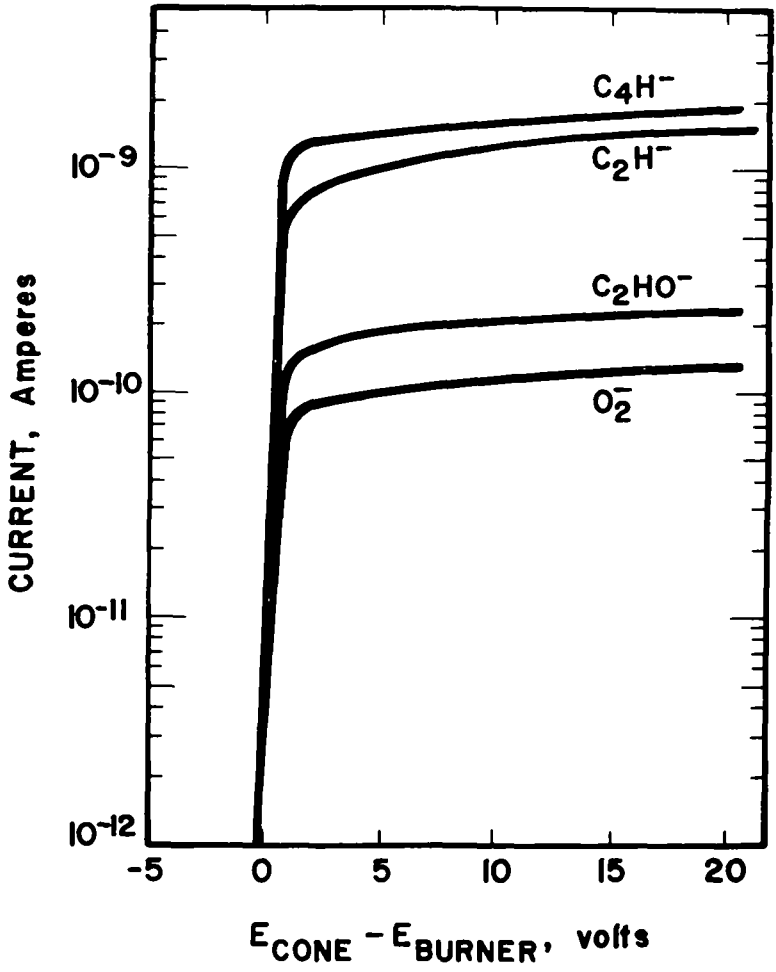

FIG. 7 EFFECT OF ELECTROSTATIC FIELD ON RELATIVE INDIVIDUAL NEGATIVE ION CURRENTS SAMPLED WITH A CONE

Mass Spectrometry Without Ions

by

B. R. F. Kendall

Ionosphere Research Laboratory
and
Department of Physics
The Pennsylvania State University
University Park, Pennsylvania

Abstract

A new method is proposed for analyzing gas mixtures. It is based on differences in the molecular-flow conductances of porous metal membranes for gases of different molecular weights. The membranes are components of a vacuum "filter circuit" analogous to an electrical filter circuit. The output data can be processed into a form similar to a conventional mass spectrum, except that there are no fragment peaks. Preliminary results obtained with an experimental system are discussed.

Introduction

Equations similar to those used to describe electrical circuits can be used to describe the flow of gases if pure molecular-flow conditions exist. This similarity has been noted and used by Dushman,[1] Teubner,[2] Barnes[3] and others for solving various problems in vacuum physics.

Molecular-flow circuits

Systems can be constructed which consist of volumes connected by small orifices. When operated so that molecular-flow conditions exist at the orifices, such systems can be regarded as molecular-flow circuits.

Figure 1 shows the equivalence of expressions which apply to an electrical circuit and to a molecular-flow circuit containing an isotopically pure gas. The pressure difference P across an orifice corresponds to the potential difference across a resistor. The flow rate F corresponds to an electrical current and the reciprocal of the pumping speed S corresponds to a resistance. For an enclosed volume, the internal pressure corresponds to the potential across a capacitor with one side grounded, and the magnitude of the volume corresponds to a capacitance. There are apparently no naturally-occurring molecular-flow inductances. Kirchhoff's laws apply for pressure differences P and flow rates F in the same way as for the corresponding electrical quantities.

When a mixture of gases with different molecular weights is flowing in a molecular-flow circuit the situation becomes more complicated. Figure 2 summarizes the equations which must be used to describe the behavior of orifices, enclosed volumes and combinations of these when a gas mixture is used. A given orifice now has a different conductance for each gas. Under molecular-flow conditions, the effective impedance for the jth gas of a mixture is given by a quantity $(Km_j^{\frac{1}{2}})$, where K is a constant which will be called the unit-mass impedance and m_j is numerically equal to the molecular weight of the gas in atomic mass units. An enclosed volume exhibits the same capacitance V for all gases. The closed-path and junction equations corresponding to Kirchhoff's Laws hold separately for each gas.

The mass-dependent impedance of an orifice has an effect analogous to the frequency-dependent impedance of a capacitor in an electrical circuit. Mass discrimination appears in the form of differences in gas composition in different parts of the circuit, and in different time scales for the propagation of pressure disturbances through the circuit. A familiar example is the mass discrimination which can occur as a result of effusion through a molecular leak in a mass spectrometer inlet system. This effect has been used by Eden[4] for approximate mass measurements with gases of high molecular weight.

Obviously a molecular-flow circuit has some of the fundamental properties of a mass spectrometer. Although the resolving power of the circuit itself may be very low there exists a possibility of extracting the desired mass spectral information by suitable data-processing techniques.[5]

Theoretical analyses of molecular-flow circuits

The simplest possible molecular-flow circuit is an analog of an RC electrical circuit (Figure 3). Consider its operation when a gas mixture is entering an initially empty enclosed volume. The pressure as a function of time is given by a summation of the form shown, where V and K can be determined by appropriate calibrations. It can be shown that, if the pressure-time curve is recorded with sufficient accuracy, the constants P_j and m_j can be determined. These constants represent partial pressures and molecular weights, respectively. If the possible values of m_j are known, the problem reduces to one of solving a set of simultaneous equations.

More complicated molecular-flow circuits have also been analyzed. These are basically mass filter circuits, designed to give maximum mass discrimination in the same way that electrical RC filter circuits can be designed for maximum frequency discrimination. For a step-function input, some of these devices appear capable of giving output waveforms which can be roughly interpreted by eye even before data processing is carried out on them.

Inherent characteristics of molecular-flow mass analyzers

A mass spectrometer based on molecular-flow circuits would have certain unique advantages combined with some very obvious disadvantages. It would be simple and rugged. Simple spectra would be obtained because there would be no fragment peaks. Samples could be re-used indefinitely. There would be no hot filaments to cause changes in sample gas composition. Moreover, such a device could operate at quite high pressures. The limitation is that molecular-flow conditions must exist at each orifice. In practice it is probably more convenient to use a porous membrane or plug, instead of a simple orifice. Modern membranes and other porous materials give molecular-flow conditions at pressures as high as 50-100 torr.[6, 7]

Disadvantages of a molecular-flow mass analyzer include the need for a pressure-measuring device with a very linear response, the need for data processing to extract the mass spectral information, the need for maintaining uniform temperatures and complete gas mixing within each enclosed volume, and the possibility of polymerization of some gases during expansion through membranes at high operating pressures. It nevertheless seems possible that in some circumstances the advantages may outweigh the disadvantages.

An example of one possible application is given in Figure 4, which shows a design study of a molecular-flow mass spectrometer for analyzing planetary atmospheres. In its simplest form it could consist merely of a small evacuated chamber, a valve to start external gases flowing through a membrane into the chamber, and a pressure-sensing device to produce a record of the internal pressure increase as a function of time. This function would be telemetered to earth and subsequently processed with a digital computer to give the molecular weights and concentrations of the gases present. Repeated analyses would be possible by repeatedly producing small pressure differentials across the membrane, and again recording the pressure-time functions. The pressure-time functions would be of the same form as those given in Figure 3. After equilibrium was reached at the end of an operating cycle the pressure-measuring device would indicate the total external pressure.

Experimental molecular-flow mass spectrometer

Tests of an experimental molecular-flow mass spectrometer have recently begun. Figure 5 shows the circuit of this device in its present form and the equivalent electrical circuit. The movable membrane corresponds to a vibrating grounded plate in a symmetrical electrical capacitor and is used to produce repeated step-function volume changes in the two sections of the divided chamber. These in turn give rise to pressure transients. This rather unusual layout is used because, to a first-order approximation, it gives the same time constant for both increasing and decreasing pressures in either section of the chamber.

The membrane is of porous silver containing 0.2 micron holes. It has an area of 0.3 cm^2 and a unit-mass impedance of 16 sec/li.

The first results obtained are shown in Figure 6. Responses to step-function volume changes are given for pure helium, air and carbon dioxide at total pressures in the range 0.8-4 torr. The helium and carbon dioxide curves are close to pure exponentials, and can easily be identified by their time constants. The air curve indicates a predominant constituent at mass 28, but noise, drift and other defects of the capacitance manometer have so far prevented resolution of the two components. Although the eye is quite insensitive to the presence of multiple exponentials, there

Electrical	Molecular Flow - one gas
<u>Ohm's Laws for</u>	
Resistor: $v = IR$	Orifice or porous membrane: $P = F(\frac{1}{S})$
Capacitor: $v = \frac{\int_0^T I dt}{C}$	Enclosed Volume: $P = \frac{\int_0^T F dt}{V}$
Inductor: $v = L\frac{dI}{dt}$	--------
<u>Kirchhoff's Laws</u>	
$\sum v = 0$ (closed path)	$\sum P = 0$ (closed path)
$\sum I = 0$ (junction)	$\sum F = 0$ (ideal junction)

FIGURE 1 - Corresponding expressions for electrical and molecular-flow circuits. P = pressure difference, F = flow rate, S = conductance, V = volume. The enclosed volume is assumed empty at t = 0. The internal pressure is measured at time T.

<u>Orifice or porous membrane:</u>

$$P_{tot} = \sum_{j=1}^{n} P_j = \sum_{j=1}^{n} F_j(\frac{1}{S_j}) = \sum_{j=1}^{n} F_j(Km_j^{\frac{1}{2}})$$

where K is unit-mass impedance, m_j is molecular weight of jth gas.

<u>Closed Volume:</u>

$$P_{tot} = \sum_{j=1}^{n} P_j = \sum_{j=1}^{n} \left[\frac{\int_0^T F_j dt}{V} \right] = \frac{\int_0^T F_{tot} dt}{V}$$

<u>Closed path:</u> $\sum P_j = 0$ for all j

<u>Ideal junction:</u> $\sum F_j = 0$ for all j

FIGURE 2 - Equations describing molecular-flow circuit carrying mixture of n different gases.

exist both digital and analog methods for resolving the components under suitable conditions.

Experiments with various versions of this apparatus and a self-contained data processing unit designed for it are continuing. The difficulty of obtaining sufficiently noise- and drift-free pressure records does not appear to be a fundamental problem, and should be overcome when a capacitance manometer capable of meeting its manufacturer's specifications is obtained.

Particular attention is being paid to the possibility of obtaining low-impedance membranes with holes an order of magnitude smaller than those now in use, so that molecular-flow conditions can be obtained at even higher pressures. It may eventually be possible to obtain molecular flow at atmospheric pressure. It would then be possible to have a mass spectrometer which would operate without a vacuum as well as without ions.

Acknowledgments

The assistance of Donald R. David, Robert E. Pulfrey and John A. Kreher in the construction and testing of the apparatus is gratefully acknowledged. The project was supported by NASA Sustaining Grant No. NGR-39-009-015.

References

1. Dushman, S., "Scientific Foundations of Vacuum Technique", 2nd Ed., J. Wiley and Sons, N.Y., 1962.

2. Teubner, W., Exper. Tech. der Phys. 10, 278 (1962).

3. Barnes, C. B., Vacuum 14, 429 (1964).

4. Eden, M. et al, Anal. Chem. 23, 1735 (1951).

5. Kendall, B. R. F., J. Sci. Instr. 39, 267 (1962).

6. Owens, C. L., J. Vac. Sci. and Tech. 2, 104 (1965).

7. Christian, R. G. and Leck, J. H., J. Sci. Instr. 43, 229 (1966).

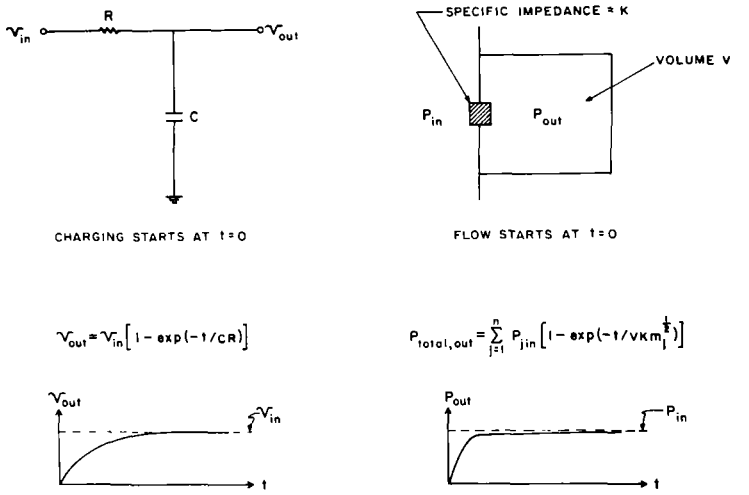

FIGURE 3. MOLECULAR FLOW INTO ENCLOSED VOLUME

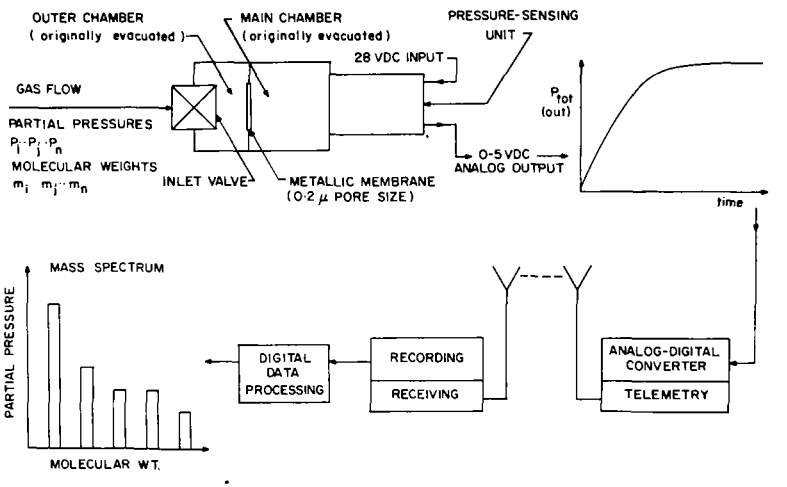

FIGURE 4
MOLECULAR-FLOW MASS SPECTROMETER FOR PLANETARY ATMOSPHERE ANALYSIS

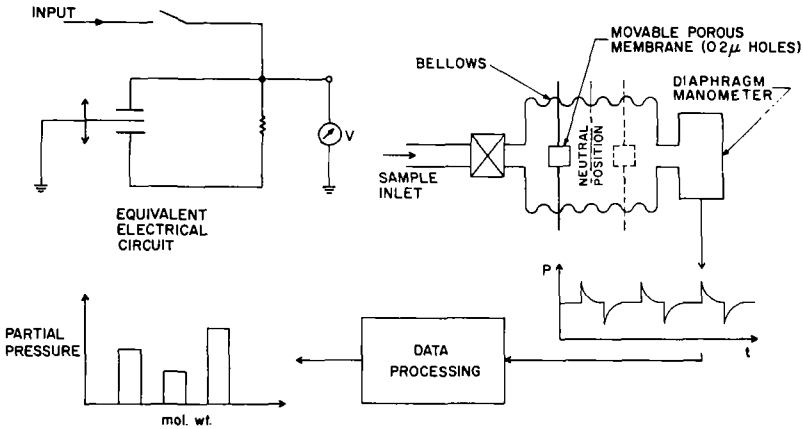

FIGURE 5. CIRCUIT OF EXPERIMENTAL MOLECULAR-FLOW DEVICE

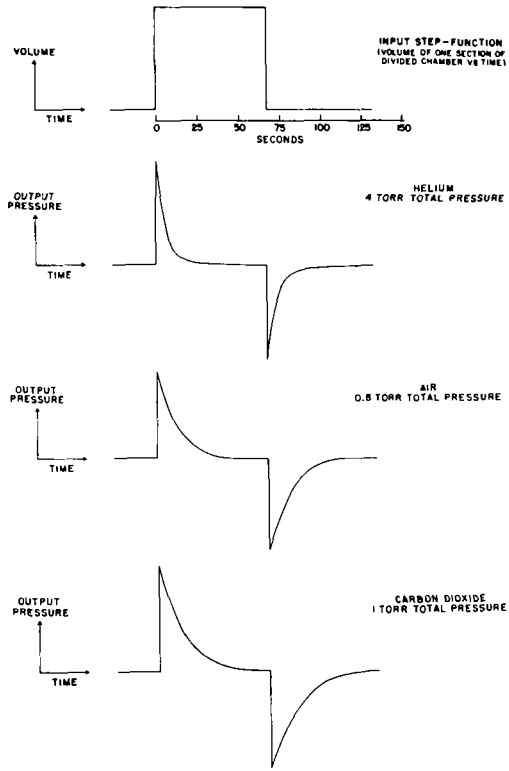

FIGURE 6. RESPONSE OF MOLECULAR-FLOW CIRCUIT TO STEP-FUNCTION INPUT

Mass Spectrometric Studies of Diffusion and Permeability in Polymeric Films

R. L. Bredeweg and V. J. Caldecourt
Chemical Physics Research Laboratory
The Dow Chemical Company
Midland, Michigan

Abstract

A technique using a low resolution mass spectrometer to measure the diffusion and permeability of gases, liquids and vapors through polymeric films has been developed. The low pressure side of the film is directly exposed to the "ion source", hence, there is very little time lag between permeation and detection. The high sensitivity of the mass spectrometer allows one to rapidly measure the gas permeability of films of low permeability. The specificity of the mass spectrometer allows one to identify air leaks and to run mixtures of gases and vapors.

Introduction

The ability of a material to transmit gas, liquids and vapors, called the permeability of a material, is an important property to know in the packaging industry, paint industry and in other allied fields. The type of polymeric film used to package certain foods depends very much on the desired end result. For example, fresh red meats require films with high oxygen permeability, whereas cooked meats, sausages and many cheeses require films with low oxygen permeability. The packages for vegetables must have high permeability so the vegetables can breathe and maintain their freshness. In desalination of sea water, the polymeric film must be able to pass water and not the salt. Preservation of frozen foods requires films of low permeability. So one can see that the permeability of a polymeric film is very important if one is to select the right film for the application.

One very common method used to measure the permeability of thin films is with the ASTM (D 1434-58) gas transmission cell as shown in Figure 1. This cell is referred to as the Dow Cell (1). It is a volumetric method. The film specimen to be tested is first placed in position and the top of the cell clamped down. Both sides of the film are initially evacuated. Gas is then applied to the top side of the film and the capillary tube connected to the low pressure side of the film is filled with mercury. The rate at which the mercury is displaced in the capillary tube can be calibrated to give the permeability. This volumetric method is a good, simple and easy method for most permeability determinations.

The mass spectrometer has been used very successfully to measure the permeability of plastic films and it has advantages over the volumetric method for certain applications and situations. Before these advantages are pointed out, I would first like to show you the mass spectrometer apparatus used to make such permeability measurements.

Experimental Apparatus

The mass spectrometer used in this permeability work is a low resolution instrument, with resolution of 25 and a mass range of 10-100. The analyzer is a Diatron machine from CEC. The associated electronics and vacuum equipment were built in our laboratory. Polyphenylether (Convalex 10) was used as the diffusion pump oil and it gave no detectable background even without a cold trap. Approximately two inches of copper mesh at room temperature was used as a baffle to stop back streaming of the diffusion pump oil.

Figure 2 shows a flow diagram for the permeability work. As you can see, there are three sections, the calibration section, the gas transmission cell and the mass spectrometer section. To make permeability measurements, it is essential that the mass spectrometer be calibrated accurately. To accomplish this, a one mil hole is drilled in a small disk

of platinum foil which serves as a molecular leak. Argon gas at a pressure of 0.1 torr. in the calibration chamber provides a known throughput with which to calibrate the mass spectrometer. A calibrated thermocouple pressure gauge is used to measure the pressure in the chamber.

A two sq. in. film to be tested is placed in the gas transmission cell and then both sides of the film are evacuated. The test gas is then applied to the top side of the film and the pressure in the cell is measured by a mercury manometer. The gas that permeates the film goes directly into the mass spectrometer by a short section of $\frac{1}{4}$" stainless steel tubing. A strip chart recorder, is used to record the results.

Figure 3 shows a detailed description of the gas transmission cell. A thin disk of sintered metal serves as a good support for the film specimen, which is necessary when there is one to five atmospheres of pressure across the film. The sintered metal also allows the transmitted gas to exit to the mass spectrometer very rapidly. The upper O-ring compresses the film specimen against the metal base to make a seal between the film and the metal.

The guard vacuum serves two purposes. First of all, the guard vacuum places a quick and uniform force on the compression O-ring, thus eliminating the need for mechanical clamps to hold the cell together. Secondly with the guard vacuum, there is a very small pressure differential between the low pressure side of the film and the guard vacuum area, thus minimizing the gas that leaks past the film-metal seal into the mass spectrometer. The gas that permeates through the film goes directly into the ion source of the mass spectrometer.

As mentioned previously, the use of the mass spectrometer to measure permeability has some advantages over the Dow Cell for certain applications. The volumetric method cannot be used to measure the permeability of one gas when a mixture of gases or vapors are applied to the high pressure side of the film. Such a cell does not identify the type of gas but only measures the total permeated gas pressure including air leakage. The mass spectrometer method has the advantage of specificity and thus can be used in the case of mixtures of gases.

With permanent gases the presence of one gas has no effect on the permeation of other gases through polymeric films (2). The permeation of each gas depends only on its partial pressure. Thus a good deal of time can be saved with the mass spectrometer by simultaneously measuring the permeability of several gases through the same sample simply by applying a mixture of gases at known partial pressures. This I have done with N_2, O_2 and CO_2.

There are some situations for non-permanent gases where the presence of one gas or vapor affects the permeability to another gas or vapor by causing the film to swell. For example, the percent relative humidity will affect the permeation of O_2 and CO_2 through cellophane (3). Another example is organic vapors such as n-hexane and CCl_4 which will affect the permeability of N_2 and O_2 through polyethylene (4).

Another advantage of the mass spectrometer is its sensitivity. Since the mass spectrometer can detect very small quantities of gases, permeability measurements can be made on films with permeabilities several orders of magnitude lower than can be measured with the volumetric method. Also, the mass spectrometer can detect and identify small leaks which could give erroneous permeability results.

Results

Figure 4 shows a typical mass spectrometer response curve of N_2 through 1.9 mil polystyrene. The mass spectrometer response (strip chart recorder reading) is plotted along the ordinate and the elapsed time along the abscissa. At t=o, the N_2 was applied to the top side of the film. At the time t_1, the N_2 is just beginning to come through the film. At time t_2, the N_2 is increasing at a steady rate and at t_3, the N_2 is going through at a steady rate. It is from that flat part of the curve the permeability is determined. The actual calculation of the permeability involves the calibration factor of the mass spectrometer, the area of

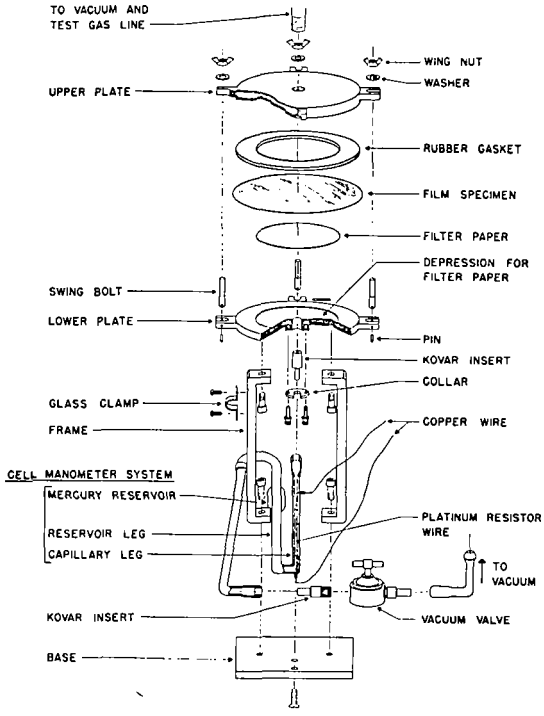

EXPLODED VIEW SHOWING DETAILED CONSTRUCTION OF THE CELL

FIG. 1

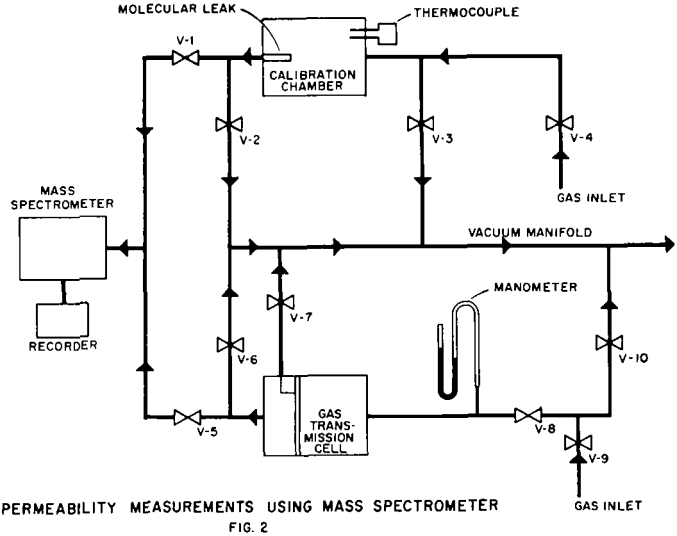

PERMEABILITY MEASUREMENTS USING MASS SPECTROMETER

FIG. 2

the film used, thickness of film, pressure differential across the film and the number of chart divisions at the flat portion of the permeability curve. The actual permeability value for this curve as shown in Figure 5 is $\frac{53.3\ CC(STP)\text{-}mil}{100\ in^2\text{-}atm\text{-}day}$. This reads as 53.3 CC(STP) for one mil thick film for one hundred square inches, per atm. pressure differential, per day. The following table shows typical data from the two methods on the same film specimen.

Specimen	Mass Spectrometer	Volumetric
#1	51.0	60
#2	52.2	51

Another important factor to consider in gas transmission through polymeric films is the diffusion coefficient D which is defined by Ficks law as shown in Figure 6. This differential equation governs the transport of gases through polymeric films (as you recognize this is also the equation for heat conduction). The diffusion coefficient is related to the speed with which the gas molecules diffuse from one side of the film to the other side. D can be found from the permeability curve as shown in Figure 7 using the following equations,

$$D = \ell^2/6\theta$$

D = Diffusion Coefficient
ℓ = Thickness of Film

$$\theta = -\frac{A_1}{A_2}(t_2 - t_1) + t_1$$

θ = Induction Time
A = Area

As seen in this slide, A_1 is the area under the curve from t=o to t_1 and A_2 the area under the curve from t_1 to t_2. So θ can be calculated and thus D can also be calculated. As a general rule of thumb, it takes about 3 times the induction time "θ" for the gas to permeate the film at a steady rate.

Once the permeability and diffusion of a gas in a film specimen has been determined, the solubility can be calculated. The solubility equals the permeability divided by the diffusion coefficient $S = P/D\ \frac{CC(STP)\ gas}{CC\ polymer}$. So the solubility, diffusion coefficient, and permeability can be determined from the permeability curve.

In summary the mass spectrometer method is a good technique for measuring the permeability of polymeric films. The high sensitivity of the mass spectrometer allows one to rapidly measure the gas permeability of films of low permeability. The specificity of the mass spectrometer allows one to identify air leaks and to run mixtures of gases and vapors.

Bibliography

1. Brown, W. E. and Sauber, W. J.
   Gas Transmission by Plastic Films.
   Modern Plastics 111 (Aug., 1959).

2. Meyer, J. A., Rogers, C. E., Stannett, V. and Szware, M.
   Permeation of Mixed Gases and Vapors.
   TAPPI 40, 142 (1957).

3. Fricke, H. L.
   Gas Chromatograph Measures Film Permeability.
   Package Engineering 51 (Dec., 1962).

4. Pilar, F. L.
   The Flow of Gases Through High Polymer Films in Equilibrium with Sorbed Vapors.
   J. Polymer Sci. 45, 205 (1960).

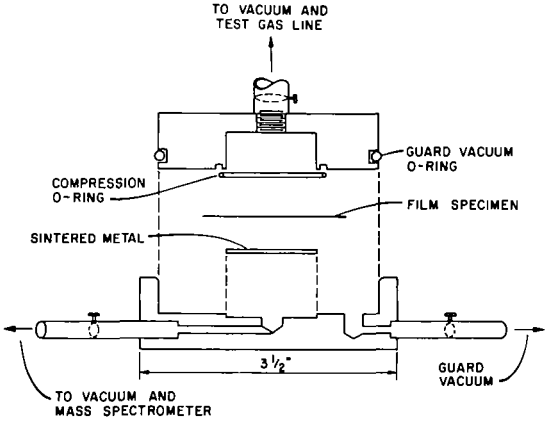

GAS TRANSMISSION CELL

FIG. 3

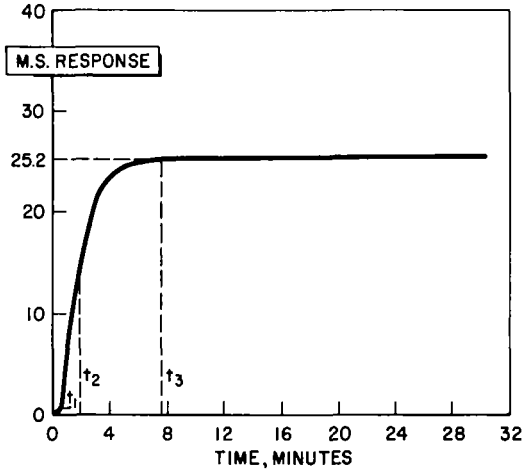

DATA:

GAS - NITROGEN
FILM - POLYSTYRENE
THICKNESS - 1.9 MIL
TEMPERATURE - 23°C

AREA - 1.51 SQ. IN.
RANGE - x 10

PERMEABILITY OF N_2 THROUGH POLYSTYRENE

FIG. 4

$$\text{PERMEABILITY} = \frac{53.3\ \text{CC(STP)-MIL}}{100\ \text{SQ. IN.-ATM.-DAY}}$$

PERMEABILITY OF N_2 IN POLYSTYRENE

FIG. 5

$$\frac{\partial C}{\partial t} = D \frac{\partial^2 C}{\partial x^2}$$

C - CONCENTRATION

D - DIFFUSION COEFFICIENT

t - TIME

x - DISTANCE IN FILM

FICKS LAW

FIG. 6

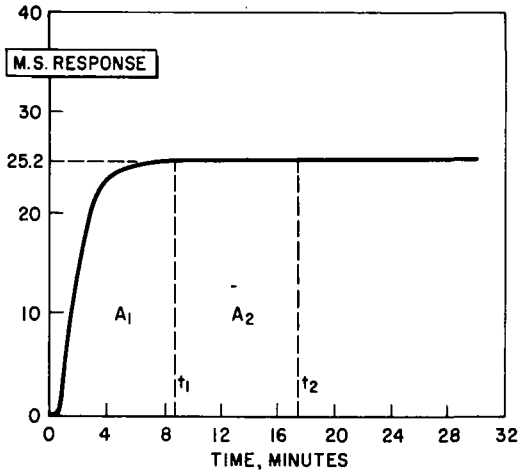

$D = l^2/6\theta$

D-DIFFUSION COEFFICIENT
l-FILM THICKNESS
θ-INDUCTION TIME

$$\theta = \frac{-A_1}{A_2}(t_2 - t_1) + t_1$$

A-AREA
t-TIME

$\theta = 2.4$ MINUTES

DIFFUSION OF N_2 IN 1.9 MIL POLYSTYRENE

FIG. 7

Chemical Ionization Mass Spectrometry.
I. General Introduction

M.S.B. Munson and F.H. Field
Esso Research and Engineering Company
Baytown, Texas

Abstract

The purpose of this paper is to present a new technique in mass spectrometry, chemical ionization mass spectrometry, which is based on the formation of the ions of an unknown material by chemical reactions in the gas phase. A reaction gas is introduced into the ionization chamber of a mass spectrometer at pressures of one Torr. This reaction gas is ionized and a set of ions is produced which does not react further with the reaction gas. If a small amount of another material is present in the mixture at these high pressures, the stable ions of the reaction gas will react with this second material to produce a spectrum of ions characteristic of the second material. The spectra which are produced by chemical reactions are frequently different from those spectra produced by conventional electron impact methods and are often more useful for determining the structure of compounds and identifying compounds and mixtures than electron impact spectra. The fragmentation patterns of chemical ionization mass spectrometry correspond closely to the structures of the molecules and appear to result from localized attack at reactive centers in the molecule. Reasonable hypotheses are offered for the reactions forming the major product ions of several types of molecules.

NEGATIVE ION IDENTIFICATION FROM ATTACHMENT-DETACHMENT EQUILIBRIUM STUDIES IN O_2 AND MIXTURES OF O_2 AND CO_2*

by

A. V. Phelps, J. L. Pack and J. L. Moruzzi

Westinghouse Research Laboratories, Pittsburgh, Pennsylvania

Abstract

A drift tube technique has been developed for the study of the equilibrium between electrons and negative ions which results from collisional attachment and detachment processes at high gas densities. If only a single negative ion is present in significant concentrations and if attachment and detachment collisions are sufficiently rapid, the identity of the negative ion can be determined by studies of the effect of variations in the gas density on the equilibrium. The electron affinity and some information regarding the structure of the negative ion can be obtained by varying the gas temperature. This technique has been successfully applied to pure O_2 and O_2-CO_2 mixtures where the negative ions are found to be O_2^- and CO_4^-, respectively, with electron affinities of 0.43 ± 0.02 eV and 1.2 ± 0.1 eV, respectively. Recent mass spectrometer studies confirming the identity of these ions will be presented.

* This work was supported in part by the Air Force Weapons Laboratory.

Reaction Studies Using Low Energy Ion Beams*

Ben R. Turner
General Atomic Division of General Dynamics Corporation
John Jay Hopkins Laboratory for Pure and Applied Science
San Diego, California

ABSTRACT

Charge exchange and ion-atom interchange processes have been studied by crossing a magnetically analyzed ion beam with a neutral stable molecular beam. Emphasis was placed on collisions involving diatomic molecules and both atomic and molecular ions of atmospheric interest. Ion energies ranged from about 2 eV to several hundred eV. The product ions were 1) extracted and momentum analyzed, or 2) scanned as a function of angle with a quadrupole mass filter, or 3) collected on a total slow ion collector. It was possible to demonstrate the importance of excited reactant ions in these reactions by measuring the change in the cross sections, at constant interaction energy, as the energy of the ionizing electrons in the ion source was varied. A general method to determine the fractional concentration of excited and ground-state ions in an ion beam was developed and applied. Specific results were obtained for the case of O_2^+ ions produced in an electron bombardment ion source. The fractional composition of ground state ions in the beam was determined as a function of source electron energy.

INTRODUCTION

At General Atomic, we have been studying ion-molecule reactions primarily because of their role in determining the composition of the upper atmosphere. It is recognized that the ion composition, and therefore the electron concentration, is regulated to some degree by several ion-molecule reactions. Because of the potentially crucial part played by these reactions, it is of considerable importance that these reactions be systematically examined.

There are several ways to study ion-atom interchange processes, and two methods will be described which we have used. Then a study of excited ions produced by electron bombardment is described, a study which was a natural extension of the ion-molecule reaction work.

The first method used to examine an ion-atom interchange process was the measurement of the angular distribution of the products.[1,2] This is one of the best ways to get information on the details of a collision. From such measurements, it should be possible to distinguish whether or not the reaction results from a "sticky" collision, that is, one involving the formation of an intermediate complex. In addition, an estimate of the amount of the reacting system's internal energy transformed into kinetic energy (or vice versa) could be made. From an energy analysis at fixed scattering angles of a product, the exchange of energy between internal modes and translational would again be determinable. Angular distribution studies have already been conducted using a crossed beam experiment for neutral-neutral reactions,[3,4,5] and many of the aspects of reactive collisions have been examined. The total reactive cross sections can be calculated by integration of the differential cross sections.

The second method we used involved the total collection of secondary ions.[1,6] This gave more reliable data for the total cross section.

APPARATUS FOR ANGULAR DISTRIBUTION STUDIES

A schematic diagram of the experimental apparatus is shown in Fig. 1. With this apparatus, the reaction $N_2^+ + D_2 \rightarrow N_2D^+ + D$ was studied. This reaction was particularly suitable, from the point of view of large signal, because the product ions are confined to a fairly narrow forward cone in the laboratory system. The primary N_2^+ ions were formed in a Heil-type source, mass-analyzed at 1 keV in a magnetic mass spectrometer, and then retarded to the desired energy by a multi-element exponential lens. Pusher plates immediately before the reaction zone were used to provide final alignment of the ion beam before it passed through the neutral beam. The ion beam was then collected in a Faraday cage mounted in front of the movable product-ion detector. Typical primary-ion beam currents were about 5×10^{-9}A.

The neutral D_2 beam issued at room temperature from a small aperture in the source and traveled through a source chamber, a buffer chamber (not shown), and then into the experimental chamber. By telescoping the chambers one into another, the total beam path from the source aperture to the center of the interaction zone was about 8 cm. The neutral beam was mechanically chopped and then crossed the dc ion beam above the pivot point of the carriage supporting the secondary-ion detector. Typical neutral-beam densities at the interaction region were calculated to be $\sim 1 \times 10^{11}$ molecules cm^{-3}. The distance from the pivot point to the entrance aperture of the detector was about 6 cm.

The secondary-ion detector could be rotated from about 15 deg on one side of the primary-ion beam to almost 90 deg on the other side, in the plane containing the neutral beam and the primary ion beam.

The quadrupole mass filter was the ideal detector for this experiment since the energy and momentum of a product ion depended on the scattering angle. In fact, for this reaction, two different scattering angles in the center-of-mass coordinates corresponded to the same laboratory scattering angle, and the N_2D^+ ions possessed two distinct energies at a given scattering angle in the laboratory system.

Noise originating from either fast neutral molecules or by photons was eliminated by mounting the multiplier perpendicular to the axis of the quadrupole filter. The mass-analyzed ions were swept into the multiplier by means of an electrostatic velocity selector. Narrow-band amplification and phase-sensitive detection were used to reduce the background noise.

To obtain absolute differential cross sections, the secondary-ion current scattered into the detector was determined. The ion-current detection system was calibrated by modulating the primary-ion beam electrically at the chopping frequency of the neutral beam, measuring the ion current entering the detector, and then measuring the deflection it produced in the recorder.

The pressure in the chamber was always $\sim 10^{-6}$ torr, and the number density of D_2 in the beam was, therefore, comparable to that of the background gas.

RESULTS AND DISCUSSION

Figure 2 is a typical plot of the differential cross section as a function of the scattering angle in the laboratory system. Included in the figure is the angular distribution of the primary N_2^+ ions. In this case, the angular width at half maximum for the primary ions was 2.0 deg. The distribution of the secondary ions (N_2D^+) extended a little over 8 deg on either side of its maximum and showed a slight skewness toward positive angles due to the thermal motion of the neutral D_2.

To determine the dynamics of the reaction, the observed angular distribution of the N_2D^+ ions was compared with those distributions which may be computed for different collision models. Accordingly, calculations have been carried out for what we called glory scattering and Hard-sphere scattering. Account was taken in these calculations of the finite detector aperture.

For Glory Scattering, that is, the differential cross section in the c.m. system is proportional to

$$\frac{1}{\sin\chi}$$

where χ is the scattering angle in the center-of-mass system, the result was a single maximum with some enhancement at the wings of the distribution. For Hard-sphere Reactive Scattering, that is, the differential cross section in the c.m. system is a constant, it was found that two maxima occurred close to the cutoff angle.

The experimentally determined curves most closely resembled the curves derived on the basis of glory scattering and were clearly at variance with the Hard-sphere model. The results were consistent with the formation of complex as discussed by Gioumousis and Stevenson,[7] although other collision models were not excluded - particularly stripping models.

The total cross sections for reaction have been obtained from the observed differential cross sections, and from measurements in which total collection of the secondary ions was made. The calculation of the total reactive cross section from observed differential cross sections would be quite complex to do rigorously when neither of the reactants is at rest in the laboratory system. The relationship of solid angles in the center of mass system to corresponding ones in the laboratory system is exceeding complex at best if, indeed, it has ever been worked out. Briefly, our data was treated ignoring this complication of finite D_2 velocity and then a small correction was applied to our total cross section according to a treatment given by Colwell and Fineman.[2]

APPARATUS FOR TOTAL SECONDARY ION COLLECTION

A second method to investigate further the magnitude and energy variation of the total cross section for the reaction under study was carried out with the apparatus shown in Fig. 3. Positive ions, extracted from an electron-bombardment ion source, were accelerated to 100 eV and analyzed in a 180-deg-sector mass spectrometer. The selected N_2^+ beam was retarded to the required collision energy before being collimated in a

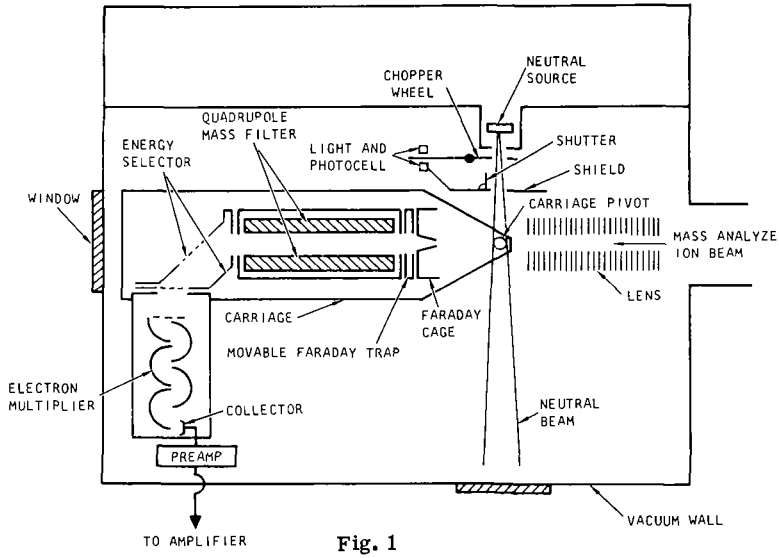
NEUTRAL SOURCE
CHOPPER WHEEL
QUADRUPOLE MASS FILTER
ENERGY SELECTOR
LIGHT AND PHOTOCELL
SHUTTER
SHIELD
WINDOW
CARRIAGE PIVOT
MASS ANALYZED ION BEAM
LENS
CARRIAGE
FARADAY CAGE
MOVABLE FARADAY TRAP
ELECTRON MULTIPLIER
COLLECTOR
NEUTRAL BEAM
PREAMP
TO AMPLIFIER
VACUUM WALL

Fig. 1

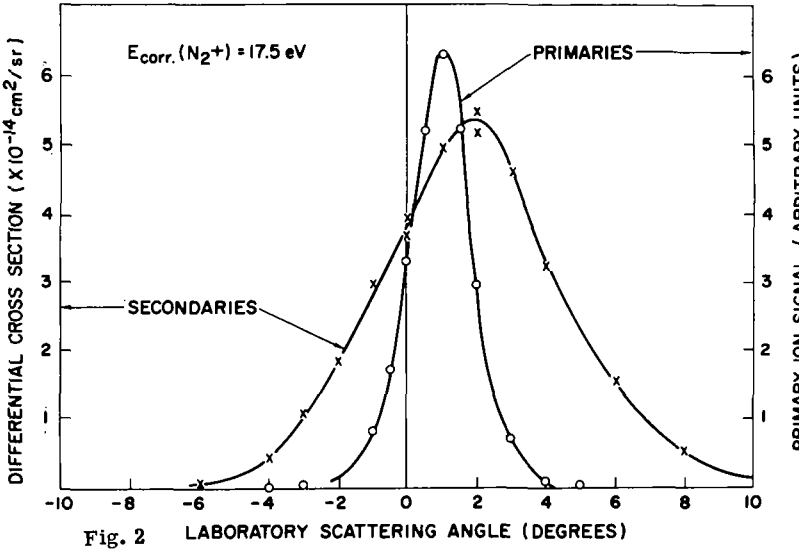
$E_{corr.}(N_2^+) = 17.5$ eV
PRIMARIES
SECONDARIES
DIFFERENTIAL CROSS SECTION (X 10^{-14} cm^2/sr)
PRIMARY ION SIGNAL (ARBITRARY UNITS)
LABORATORY SCATTERING ANGLE (DEGREES)
-10
-8
-6
-4
-2
0
2
4
6
8
10
1
2
3
4
5
6

Fig. 2

field-free region and then intersected the modulated neutral beam. Both primary and secondary ions left the interaction region through two highly transparent grids and were accelerated to 2 keV in a nearly uniform field. A quadrupole lens focussed the ions into another magnetic mass spectrometer and the selected ions impinged on the first dynode of an electron multiplier. The signals of N_2D^+ ions were measured using a slit large enough to permit total collection of the N_2D^+ ions. In order to derive absolute cross sections from these measurements, these signals were related to the corresponding ion currents at the interaction region in a manner similar to that used on the angular distribution studies.

RESULTS AND DISCUSSION

The total cross sections obtained from the angular distribution data lay consistently lower than those obtained using total collection although when account was taken of the estimated accidental errors the results of the two measurements could be reconciled. Nonetheless, we felt that this second approach was inherently more reliable and less subject to systematic errors and consequently only these results were plotted. Figure 4 shows that they lie above the theoretical curve of Gioumousis and Stevenson whose calculations were based upon an ion-induced dipole interaction.[7]

The total cross sections for the ion-molecule reaction between N_2^+ and D_2 to form N_2D^+ and D have been measured by a number of workers including Stevenson and Schissler,[8] Hutchinson and co-workers,[9] and Giese and Maier.[10] The first two studies were carried out by looking at the ions produced in an N_2 -D_2 mixture in the ion source of a mass spectrometer. Giese and Maier, however, bombarded a stationary gas target of D_2 with a mass-analyzed N_2^+ ion beam.

The apparatus, shown in Fig. 3, the two tandem mass spectrometers with the modulated neutral beam intersecting the ion beam between the mass spectrometers has been used for a series of experiments involving atmospheric ions and neutrals.[6,11,12] Positive ion and negative ion charge transfer, ion-atom interchange, collision induced dissociation, and to some extent dissociative charge transfer were studied. Because interest extended down to small collisions energies, it was necessary that only weak fields be used to the collision region. Two types of data were obtained: (1) the cross section as a function of the ion energy at the interaction region, and (2) the cross section as a function of the source electron energy with the ion energy kept constant. The latter data tells something of the effect of excited states present in the ion beam.

A number of charge transfer reactions for which values of cross sections were available in the literature were investigated with this machine using standard extraction potentials. The collection efficiencies were deduced from measurements of the beam and signal strengths. The mean value of the collection efficiency (75%) was used to evaluate the charge transfer cross sections. The collection efficiency for ion-atom interchange processes was calculated using an assumed reaction model.

In Fig. 5, the square roots of the cross sections for O_2^+ and NO^+ production in N^+ -O_2 collisions are plotted as a function of the collision velocity and energy together with the results of afterglow measurements of Fite and co-workers[13] and Ferguson and his co-workers.[14] In the present measurements, the N^+ ions were obtained from N_2 by impact of 50 eV electrons. At 10 eV the Gioumousis and Stevenson[7] complex formation cross section is about 3 on this square root scale. The agreement with their model is good, especially since two competing reactions were occurring.

The cross sections for NO^+ production in O^+ -N_2 collisions for the case in which the O^+ ions were produced from O_2 by impact of 50 eV electrons deviates strongly from the past examples shown. This cross section has a maximum for O^+ energies of about 15 eV. Giese and Paulson have also measured this cross section and are in agreement with this result. Wolf has used Light's phase space theory to rationalize this result, but with limited success

An example of the dependence of a charge exchange cross section upon the source electron energy is given in Fig. 6 where the cross section for the process $O_2^+ + N_2 \rightarrow O_2 + N_2^+$ is plotted versus source electron energy. It may be seen that for these energies ground state ions essentially do not charge exchange with N_2. A consideration of the ionization potentials makes this reasonable. The combination of the abundance of excited ions in the beam and their large cross section creates the composite cross section shown. This result led to a rather simple experimental method for studying the composition of ions beams.

APPARATUS FOR THE STUDY OF THE CONCENTRATION OF EXCITED IONS IN ION BEAMS

The apparatus for this study is shown in Fig. 7. This apparatus has a source which is quite similar to the previous apparatus. The ions are produced in one chamber

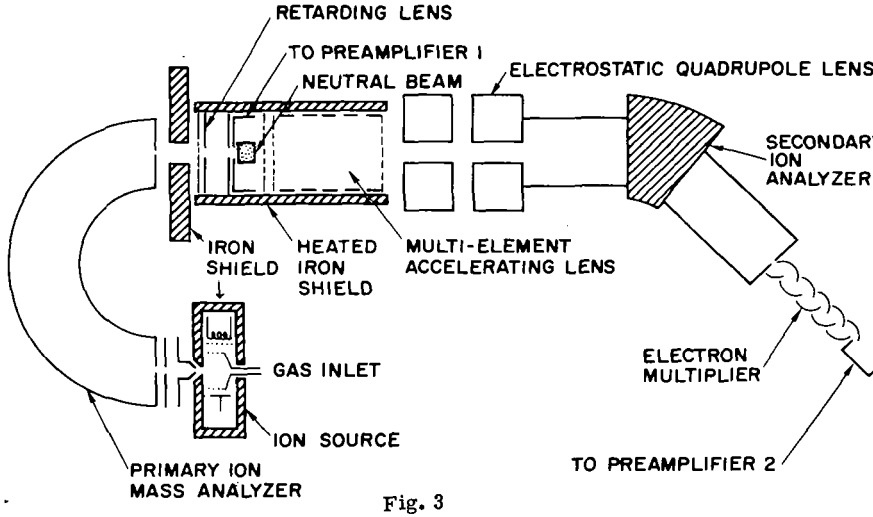
RETARDING LENS
TO PREAMPLIFIER 1
NEUTRAL BEAM
ELECTROSTATIC QUADRUPOLE LENS
SECONDARY ION ANALYZER
IRON SHIELD
HEATED IRON SHIELD
MULTI-ELEMENT ACCELERATING LENS
GAS INLET
ELECTRON MULTIPLIER
ION SOURCE
PRIMARY ION MASS ANALYZER
TO PREAMPLIFIER 2

Fig. 3

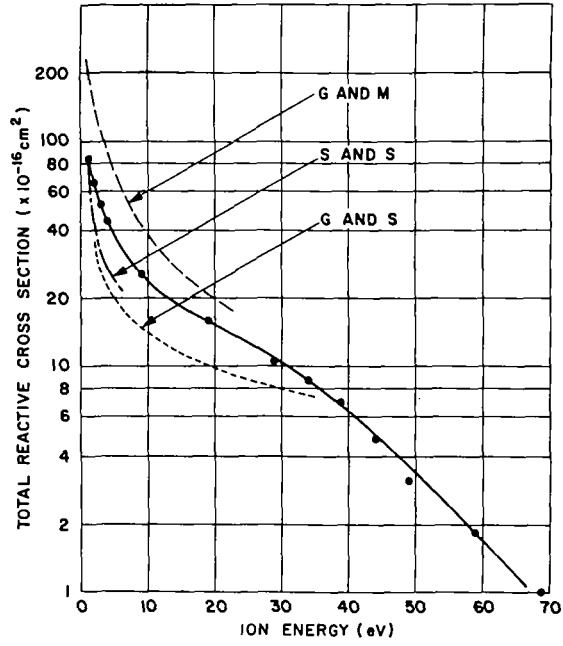
TOTAL REACTIVE CROSS SECTION (x 10^-16 cm^2)
200
100
80
60
40
20
10
8
6
4
2
1
0
10
20
30
40
50
60
70
ION ENERGY (eV)
G AND M
S AND S
G AND S

Fig. 4

and pass through a separately pumped chamber before entering a gas filled attenuation chamber. The loss of ions from the ion beam is measured as the beam passes through the gas at low pressure. A beam composed entirely of ground-state ions, passing through a fixed pathlength of gas at a pressure p, will be attenuated due to various processes. The fraction of ions reaching a collector at the end of the path will decrease exponentially with increasing gas pressure. For a single state of the ions, a semi-logarithmic plot of the fraction of ions reaching the collector versus gas pressure should then be a straight line. Ions in an excited state will have a different, typically larger, reaction cross section and would thus give a line with a different slope. An ion beam containing ground-state ions together with ions in an excited state would give a sum of two lines. By extrapolation to zero pressure the fraction of ions in the excited state can be determined.

The method was applied to a beam of O_2^+, using N_2 as the reactant gas. O_2^+ was produced in an ion source, using electrons whose energy could be varied. The results, shown in Fig. 8, were not quite ideal but it was still possible to interpret that data. When 16 eV electrons bombard O_2 to give O_2^+, the ions must all be in the ground electronic state and these ions decayed as shown. We think the initial curvature was due to a non-linearity in the pressure measurement and the final fall-off due to multiple elastic scattering. When electrons of greater energy were used, excited ions were present in the beam and the attenuation was as shown. An analysis of these curves gave the result that 12% of the ions were excited when 25 eV electrons were used to form the O_2^+, 31% when 50 eV electrons were used, and 26% when 100 eV electrons were used. These percentages referred to the ion composition about 20 μsec after ion formation. Subtracting out the decay of the ground state ions in the beam left the decay of only the excited ions. While this was not a very sensitive test, the presence of only one excited state was indicated by the linear decay.

It may be that there are excited states in O_2^+ which did not react any more strongly with N_2 than did the ground state. To check this possibility the O_2^+ beam was attenuated in Argon. Only the attenuation of ground state ions and those formed with 50 eV electrons were measured. The result was that 30% of the ions were excited when 50 eV electrons were used. Again the excited ions showed a linear decay indicating the presence of only one state.

To check further, O_2^+ ion were attenuated in hydrogen. Although the attenuation was quite different, the result was nearly the same: 28.5% of the ions were excited when 50 eV electrons produce O_2^+. Again the linear decay of the excited ions was present.

This concludes the three topics to be covered: the angular distribution study of an ion-atom interchange process, the total secondary ion collection apparatus, and the fractional concentration of excited ions present in ion beams.

ACKNOWLEDGMENTS

It is my pleasure to express appreciation to Dr. M. A. Fineman, Professor R. F. Stebbings, and Mr. J. A. Rutherford for their contributions to this research.

*This work was sponsored by the Defense Atomic Support Agency under Contract DA-49-146-XZ-354.

REFERENCES

1. B. R. Turner, M. A. Fineman, and R. F. Stebbings, Crossed-Beam Investigation of N_2D^+ Production in N_2^+-D_2 Collisions, J. Chem. Phys. 42, 4088-4096, 15 June 1965.

2. J. Colwell and M. A. Fineman, Calculation of the Total Cross Section from Angular Measurements in Crossed-Beam Experiments, J. Chem. Phys. 42, 4097 (1965).

3. E. H. Taylor and S. Datz, J. Chem. Phys. 23, 1711 (1955).

4. D. Beck, E. F. Greene, and J. Ross, J. Chem. Phys. 37, 2895 (1962).

5. D. R. Herschbach, Discussions Faraday Soc. 33, 149 (1962).

6. R. F. Stebbings, B. R. Turner, and J. A. Rutherford, Low-Energy Collisions between Some Atmospheric Ions and Neutral Particles, J. Geophys. Res. 71, No. 3, 771 (1966).

7. G. Gioumousis and D. P. Stevenson, J. Chem. Phys. 29, 294 (1958).

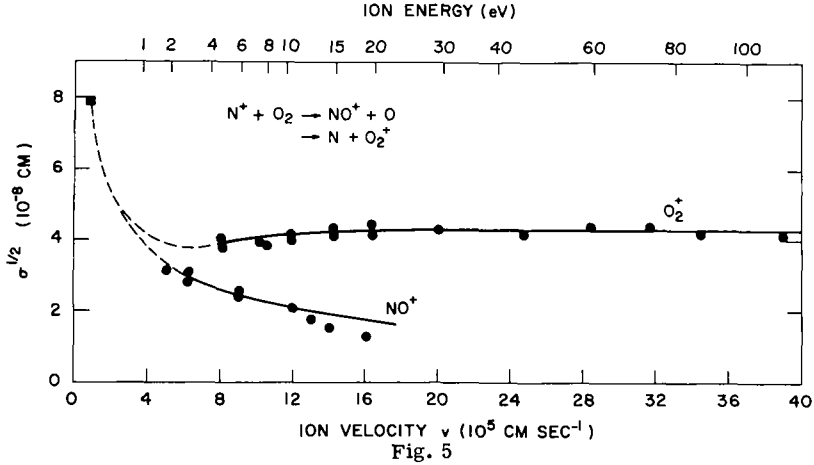
ION ENERGY (eV)
1 2 4 6 8 10 15 20 30 40 60 80 100
$N^+ + O_2 \rightarrow NO^+ + O$
$\rightarrow N + O_2^+$
O_2^+
NO^+
$\sigma^{1/2}$ (10^{-8} CM)
0 2 4 6 8
0 4 8 12 16 20 24 28 32 36 40
ION VELOCITY v (10^5 CM SEC^{-1})
Fig. 5

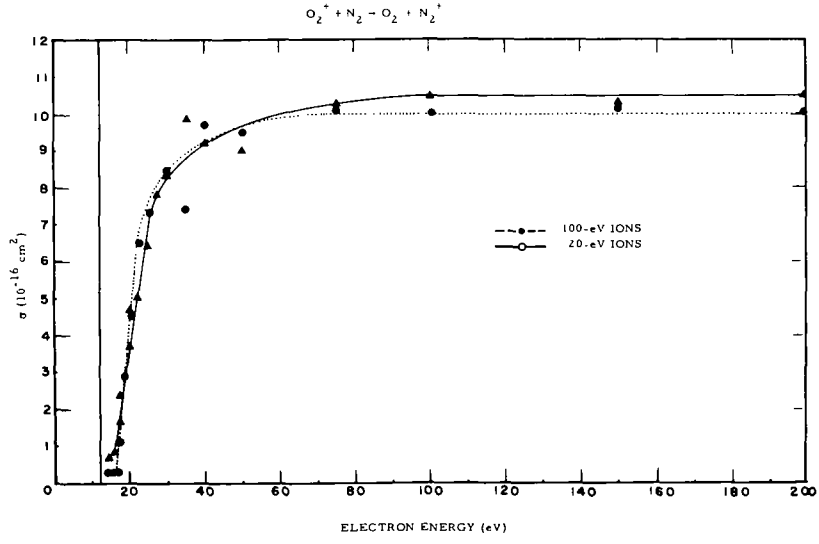
$O_2^+ + N_2 \rightarrow O_2 + N_2^+$
100-eV IONS
20-eV IONS
σ (10^{-16} cm^2)
0 1 2 3 4 5 6 7 8 9 10 11 12
0 20 40 60 80 100 120 140 160 180 200
ELECTRON ENERGY (eV)
Fig. 6

8. D. P. Stevenson and D. O. Schissler, J. Chem. Phys. 29, 282 (1958)

9. D. Hutchison, A. Kuppermann, and L. Pobo, 9th Annual Mass Spectrometry Conference, ASTM Committee E-14 1961, p. 75.

10. C. F. Giese and W. B. Maier II, J. Chem. Phys. 39, 739 (1963).

11. R. F. Stebbings, J. A. Rutherford, and B. R. Turner, Loss of He^+ Ions in the Upper Atmosphere, Planetary Space Sci. 13, 1125-1129 (1965).

12. B. R. Turner, J. A. Rutherford, and R. F. Stebbings, Charge Transfer Reactions of Nitric Oxide with Atomic and Molecular Ions of Oxygen and Nitrogen, To be published in J. Geophys. Res.

13. W. L. Fite, J. A. Rutherford, W. R. Snow and V. A. J. van Lint, Ion-Neutral Collisions in Afterglows, Discussions Faraday Soc. 33, 264-272, 1963.

14. E. E. Ferguson, F. C. Fehsenfeld, P. D. Goldan, and A. L. Schmeltekopf, Positive ion-neutral reactions in the ionosphere, J. Chem. Res., 70, 4323-4329, 1965.

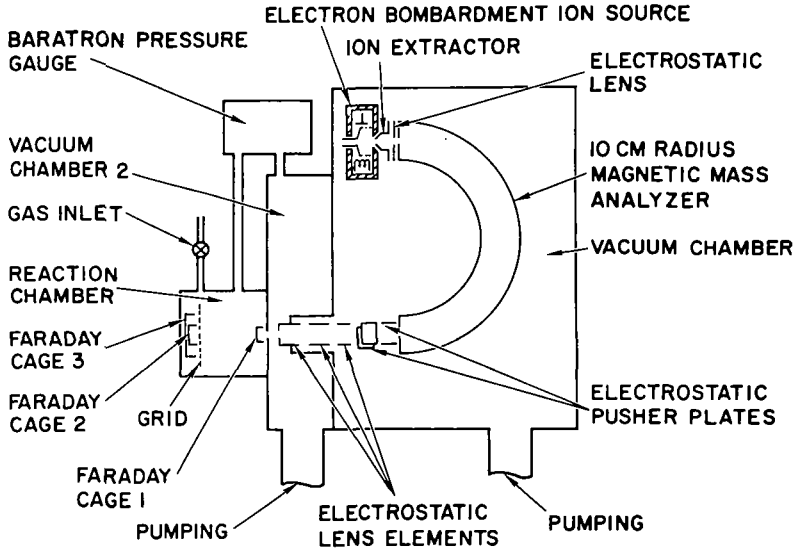
ELECTRON BOMBARDMENT ION SOURCE
BARATRON PRESSURE GAUGE
ION EXTRACTOR
ELECTROSTATIC LENS
VACUUM CHAMBER 2
10 CM RADIUS MAGNETIC MASS ANALYZER
GAS INLET
VACUUM CHAMBER 1
REACTION CHAMBER
FARADAY CAGE 3
FARADAY CAGE 2
GRID
ELECTROSTATIC PUSHER PLATES
FARADAY CAGE 1
PUMPING
ELECTROSTATIC LENS ELEMENTS
PUMPING

Fig. 7

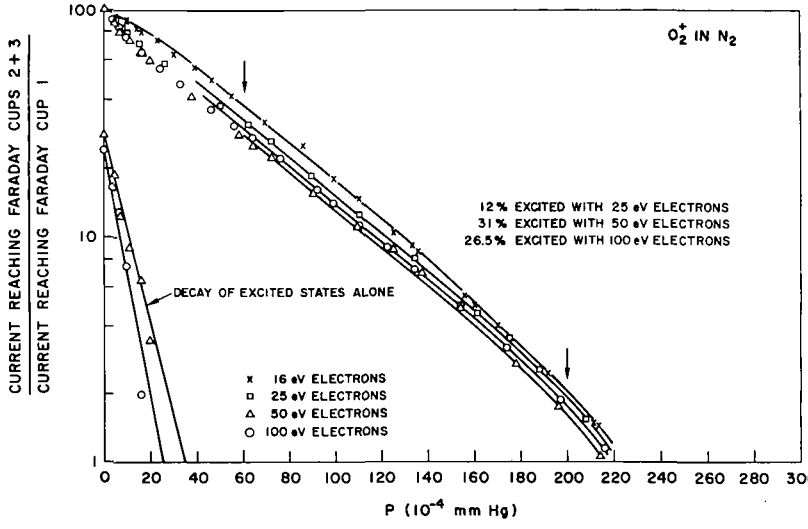
CURRENT REACHING FARADAY CUPS 2+3 / CURRENT REACHING FARADAY CUP 1
100
10
1
O_2^+ IN N_2
12% EXCITED WITH 25 eV ELECTRONS
31% EXCITED WITH 50 eV ELECTRONS
26.5% EXCITED WITH 100 eV ELECTRONS
DECAY OF EXCITED STATES ALONE
x 16 eV ELECTRONS
□ 25 eV ELECTRONS
△ 50 eV ELECTRONS
○ 100 eV ELECTRONS
0 20 40 60 80 100 120 140 160 180 200 220 240 260 280 300
P (10^{-4} mm Hg)

Fig. 8

Thermal Energy Ion-Molecule Reactions

Fred C. Fehsenfeld
Institute for Telecommunication
ESSA, Boulder, Colorado

Abstract

A flowing afterglow technique utilizing a quadrupole mass spectrometer for ion detection has been developed for the study of thermal energy ion molecule reactions. This technique has several advantages:

1. There is considerable versatility in the selection of ionic and neutral species to be reacted. Reaction rates have been measured involving unstable species such as atomic oxygen, atomic nitrogen and vibrationally excited molecular nitrogen as the neutral species.

2. The conditions of the experiment allow the atomic ions to decay to their ground electronic state before reaction.

3. The ambiguity of concurrent reactions does not arise since the neutral reactant species does not pass through the ionization region.

Many reaction rate constants involving both positive and negative ion reactions have been measured. The rate constant for the reaction.

$$O^+ + N_2 \rightarrow NO^+ + N$$

has been measured as a function of the vibrational quantum number of N_2 and will be reported.

The correlations between a number of measured rate constants and some available theoretical models will be discussed.

A number of the reactions to be reported have important implications for the ion chemistry of planetary atmospheres.

Low Energy Collisions Between Atomic Ions and Atoms

Felex T. Smith
Stanford Research Institute
Menlo Park, California

Abstract

Careful study of the angular dependence of elastic and inelastic scattering in simple ion-atom systems at energies above a few eV reveals a wealth of detail of spectroscopic quality providing much information on the potential curves for the electronic states of the diatomic ions and on the interactions between states. A survey of some scattering spectra from such systems as Li^+ + He, He^+ + He, Ne and Ar will illustrate a number of specific features of elastic scattering such as rainbow scattering, charge-exchange and nuclear-symmetry interference oscillations in symmetric systems, and structure due to crossings of potential curves; the strong angular dependence of inelastic scattering into specific excited states will also be illustrated. By comparison with the potential energy curves for the ion-atom systems in question, the interactions responsible for these scattering phenomena will be pointed out. Some of the parameters that can be measured from the scattering data- parameters of the potentials, location of crossing points, energies of interaction between states-will be discussed.

Photoionization Study of Diatomic-Ion Formation in Argon, Krypton, and Xenon

Robert E. Huffman and Daniel H. Katayama

Air Force Cambridge Research Laboratories, Bedford, Massachusetts

Ionization current at wavelengths of discrete absorption lines of five resonance series of argon, krypton, and xenon has been observed in the vacuum ultraviolet. This ionization is due to a collision process between electronically excited and ground state atoms resulting in formation of a diatomic ion and an electron.[1, 2] Using the helium and argon continuum light sources, it was possible to identify over twenty reacting states for each gas, and to observe that the ionization is found at every absorption line of shorter wavelength than a definite ionization threshold. For these experiments, a parallel-plate ionization cell designed for photoionization cross-section measurements was used. An example of the data is shown in Fig. 1 for argon. Analagous energy levels were found for krypton and xenon.

Ionization thresholds and lower limits of $D(X_2^+)$ are shown in Table 1. The thresholds are in good agreement with some electron impact appearance potentials.[3]

The mechanism which explains the pressure variation of the ionization yield at argon absorption lines is the following:

(1)	$Ar + h\upsilon \rightarrow Ar^*$	excitation
(2)	$Ar^* + Ar \rightarrow Ar_2^+ + e$	k_2, ionization
(3)	$Ar^* \rightarrow Ar' + h\upsilon'$	$1/\tau$, radiative deexcitation
(4)	$Ar^* + Ar \rightarrow Ar'' + Ar$	k_4, collisional deexcitation

For 15 argon ionization peaks, it was found that k_4/k_2 varied from 2.5 to 0.13 and τk_2 varied from 3.6×10^{-18} to 1.28×10^{-16} $cm^3 atom^{-1}$. Values of τk_2 are in fair agreement with electron impact results.

The primary significance of these results to recent mass spectrometer results is that many more excited states may be involved than previously observed.[4]

A detailed paper is scheduled for the 15 June 1966 issue of Journal of Chemical Physics. This research was supported in part by the Defense Atomic Support Agency through the Reaction Rates Program.

REFERENCES

1. F. Mohler and C. Boeckner, J. Res. Natl. Bur. Stds. 5 51, 399 (1930).

2. J. A. Hornbeck and J. P. Molnar, Phys. Rev. 84 621 (1951).

3. M. B. S. Munson, J. L. Franklin, and F. H. Field, J. Phys. Chem. 67 1542 (1963).

4. P. M. Becker and F. W. Lampe, J. Chem. Phys. 42 3857 (1965).

TABLE I

Observed Ionization Thresholds

Gas	Threshold (Å)	Energy Level	Threshold Energy (eV)	Electron Impact Appearance Potential (eV)	$D(X_2^+)$ Lower Limit(eV)
Ar	842.81	$4d[1/2]_1^o$	14.710 ± .009	14.7 ± .1[a]	1.049
				15.1[d]	
				15.1[c]	
				14.94 ± .02[e]	
Kr	953.40	$4d^1[1\ 1/2]_1^o$	13.004 ± .007	13.0 ± .1[a]	0.995
				13.2[b]	
				13.2[c]	
				13.20 ± .02[e]	
Xe	1110.71	$6d[1\ 1/2]_1^o$	11.162 ± .005	11.2 ± .1[a]	0.967
				11.6[b]	

[a] M. B. S. Munson, J. L. Franklin, and F. H. Field, J. Phys. Chem. 67 1542 (1963).

[b] W. Kaul and R. Taubert, Z. Naturforsch, 17a, 88 (1962).

[c] J. A. Hornbeck and J. P. Molnar, Phys. Rev. 84, 621 (1951).

[d] W. Kaul and R. Fuchs, Z. Naturforsch, 15a, 326 (1960).

[e] C. E. Melton and W. H. Hamill, J. Chem. Phys. 41, 1469 (1964).

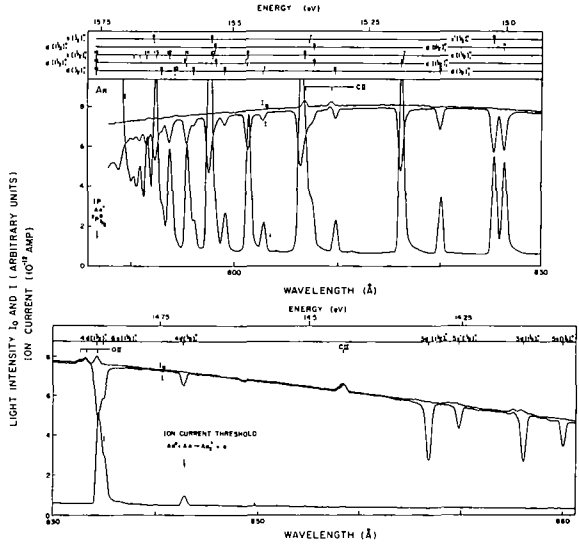

Fig. 1

OPERATION OF A THERMAL IONIZATION SOURCE ON A DOUBLE FOCUSING MASS SPECTROMETER

K. J. Dickens, J. M. Holmes, A. J. Monks, P. Powers, A. Riddoch
Scientific Apparatus Department
Associated Electrical Industries Limited
Manchester, England

ABSTRACT

The arrangement and performance of a triple filament thermal ionization source fitted to a double focusing mass spectrometer is described and the suitability of such a system for small sample analysis using ion counting techniques is discussed.

INTRODUCTION

Accurate isotopic analysis using conventional single focusing mass spectrometers is frequently hampered by the fact that these instruments have a low abundance sensitivity. Elaborate corrections for background can be necessary if ion counting methods are used.

For this reason it was decided to investigate the suitability of a thermal ionization source on a double focusing mass spectrometer and, in particular, on the Mattauch Herzog geometry of the AEI MS702.

INSTRUMENTATION

The mass spectrometer is designed so that either photoplate or electrical detection methods may be employed. The vacuum system is pumped by triode ion pumps giving analyser pressures of the order of 5×10^{-9} torr. Additional oil diffusion pumps, zeolite and cold traps are retained for occasional use as required, e.g. for prepumping photoplates or for outgassing sample filaments, etc. The instrument is fully bakeable to temperatures of 250°C for the analysers and in excess of 300°C for the source although the usual high vacua can be maintained by using much lower temperatures than these. The excellent source analyser differential pumping and source isolation facilities of the MS702 are, of course, retained.

The thermal ionization source uses the triple filament bead and is of Craig geometry so enabling a high sensitivity to be obtained. Micrometer adjustment of source slit down to 0.1 mils is provided and access to the source is such that, when cold, bead changes can be made within minutes, including repumping time.

Electrical detection, which may be used simultaneously with photoplate detection if required, is by both plate and multiplier collectors. The multiplier is of the Allen type and uses 20 activated beryllium copper stages.

PERFORMANCE

Sensitivity

As a consequence of its high ion accelerating potential (up to 20kV) and short ion path length, the instrument has an absolute sensitivity which is greater than 20% of that commonly obtained with single focusing spectrometers.

An accuracy of isotope ratio measurement of 1% standard deviation is obtained on a $^{235}U/^{234}U$ ratio of about 100:1 with a natural uranium 10^{-6} gm sample. The detection limit is such that 10^{-12} gm or less of ^{233}U can be detected in one microgram of natural uranium.

Abundance Sensitivity

The abundance sensitivity is comparable with most double magnetic (tandem) machines. Figure 1 shows the abundance sensitivity of the instrument at a 10% valley resolving power of 1,630. The shaded area indicates the overall limits on the experimental determination.

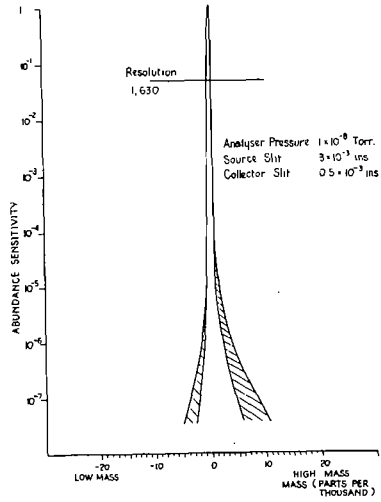

SCI 0166

MS 703 ABUNDANCE SENSITIVITY

Fig. 1

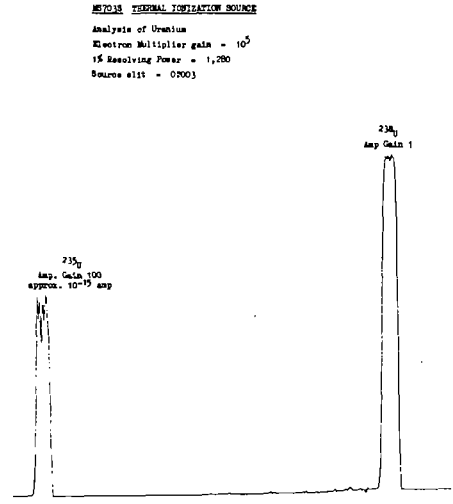

Fig. 2

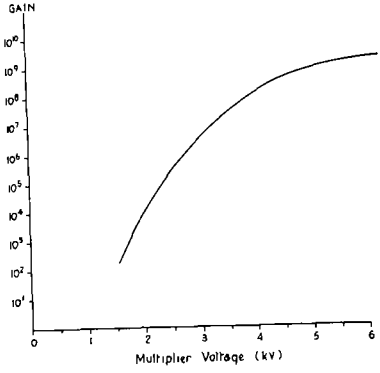

Fig. 3 MS.703 20-STAGE MULTIPLIER
TYPICAL GAIN CURVE.

SCI 0165

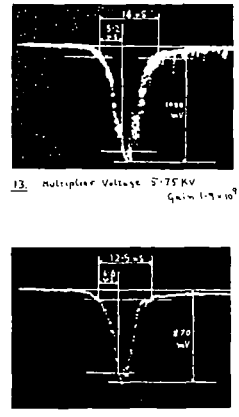

13. Multiplier Voltage 5·75 KV
Gain 1·9 x 10^9

14. Multiplier Voltage 5·75 KV
Incident ions 450 A.M.U.
Gain 1·37 x 10^9

OUTPUT PULSE OF 20-STAGE MULTIPLIER

Fig. 4 **Electron Multiplier Pulse Shape**

Examination of Figure 1 shows, for example, that at a position in the mass scale one mass unit removed from $^{m}/e$ 238 (i.e. 4.2 parts per thousand in mass) the abundance sensitivity is of the order of 10^{-7}. At a position two mass units away the abundance sensitivity is of the order of a few parts x 10^{-8}. These values have been obtained under normal instrumental operating conditions.

Resolving Power

At full transmission the 1% intensity resolving power is better than 1,000 (or 1,600 using the photoplate. This corresponds to a 50% density or visual resolving power of greater than 4,000). The flat topped peak shape is indicated in Figure 2 which shows a scan of two uranium peaks.

One of the particular advantages of a double focusing instrument is that this resolving power can be achieved on a day to day basis since energy effects due to source contamination, etc. do not affect performance.

Much higher resolving powers can be achieved at the expense of transmission, but usually are not actually required for this type of application. However, this inherent capability is useful in that it ensures good ion beam stability during counting experiments.

USE OF ION COUNTING TECHNIQUES

Three of the requirements which are either necessary or very desirable when ion counting is envisaged are:

(1) Suitable Electron Multiplier

(2) Rapid Peak Switching

(3) Facilities for Automatic Print Out

The electron multiplier response is very important if high counting rates are to be used without serious statistical corrections being required. The multiplier has a gain in excess of 10^8, see Figure 3. The pulse output exceeds 600mV per ion at low counting rates and still exceeds 100mV per ion at rates in excess of 10^6 counts per second. The pulse rise time is about 5nS. This, and the previous characteristics, are shown in Figure 4. The upper pulse display shows the shape of pulses from ions of mass 40 and the lower display that of ions of mass 450. It can be seen that there is no significant difference.

Rapid peak switching has been made possible by the provision of very fast response supplies for the ion accelerating potential and for the electrostatic analyser supply; these permit peak switching times of the order of a millisecond. A control unit is available which permits up to 6 peaks in the spectrum to be preselected and then counted in turn. This technique ensures that the fullest use is made of the available sample. On one or more of the 6 channels a preset delay can be introduced so that the instrument sensitivity may be automatically adjusted before counting commences on that peak. This means that a very intense peak may still be counted to an accuracy comparable with the less intense ones, and it ensures that extremely fast and expensive counting equipment is not required. An extra control unit can be added so that up to 12 peaks can be counted in turn.

Automatic print out facilities can be used so that results may be fed together with their channel identification into a computer.

A calculated assessment of detection limits with this type of counting system suggests the possibility of routine assessments of ^{234}U abundance in samples of natural uranium of around two nanograms.

CONCLUSIONS

The double focusing MS702 mass spectrometer which has been fitted with a triple filament thermal ionization source can be arranged to have a sensitivity very little removed from that of a conventional single focusing instrument. The abundance sensitivity, constant resolving power, and low detection limits make the spectrometer comparable with most tandem instruments.

The use of ion counting facilities further increases the scope of the instrument in the field of small sample analysis.

ACKNOWLEDGMENT

The authors wish to thank AEI Electronics Group for permission to publish this paper.

MINIMIZING THE CONTRIBUTION OF RESIDUAL GASES TO THE MASS SPECTRUM OF A SPARK SOURCE MASS SPECTROMETER*

A. J. Socha and R. K. Willardson
Bell & Howell Research Center
Pasadena, California

ABSTRACT

Ionized residual gases (including those released from the samples) in the source of a spark source mass spectrometer contribute ions to the analysis. Studies were made using samples with gas contents ranging from 10 parts per billion to 1%, source pressures ranging from 1×10^{-5} Torr to 1×10^{-8} Torr, and pumping speeds ranging from 1 to 100 liters per second (at the source). Partial pressures were monitored using a second mass spectrometer. Results show that partial pressures in the source must not only be in the 10^{-9} Torr region before sparking, but these pressures must be maintained during sparking for accurate trace analysis for gases.

* * * * * * * *

Analyses for hydrogen, carbon, nitrogen, and oxygen in solid samples utilizing a spark source mass spectrometer are seriously affected by residual gases in the source due to their contribution of ions to the mass spectrum. In analyzing samples for their particular impurities, the mass spectroscopist has invariably found when analyzing "blank" samples that quantitative results were usually higher than established or certified values, and often variable. This is especially so for oxygen and carbon. The question to be answered is what may be done to stabilize and minimize the contribution of residual gases to the mass spectrum.

The following experiments were designed to investigate the effects of source pressure, vacuum pumping speed, and gases in the sample, on the apparent gas and carbon contents found in analyses.

APPARATUS

Two types of pumping systems were used for these studies. The first was a large ion pumping system composed of a 350 liters/second Consolidated Vacuum Corporation triode ion pump. The pump was connected to the source with a 5" manifold and a 5" valve. These provide a system which has an effective pumping speed at the source of 60 liters/second (for air).

A second pump was used to obtain an additional 40 liters/second pumping speed in the source for water vapor and hydrocarbons only. This is a cold finger which is chilled with liquid nitrogen.

A three-inch quadrupole mass spectrometer was attached to the source and was used to monitor the partial pressure of gases in the source before and after the analysis of each sample. The increase in pressure during sparking was estimated by the current in the triode ion pump.

Two types of samples were investigated. The first type were samples containing large quantities of oxygen, hydrogen, carbon, and nitrogen. These samples were used to determine the effect of pumping speeds at various starting source pressures, and effects on the analysis of the liberation of large quantities of a gaseous species from the sample during sparking. The samples selected for these "high-gas" sample studies were nickel and titanium. The other type of samples investigated were materials containing very small concentrations of gases. Ultrahigh purity gallium arsenide was selected for these experiments. The low-gas samples were used to determine the effects of both the partial pressure of various source gases and the pumping speeds on analyses for carbon and the gases.

* Supported in part by Aerospace Research Laboratories, United States Air Force Contract No. AF 33(615)-2761.

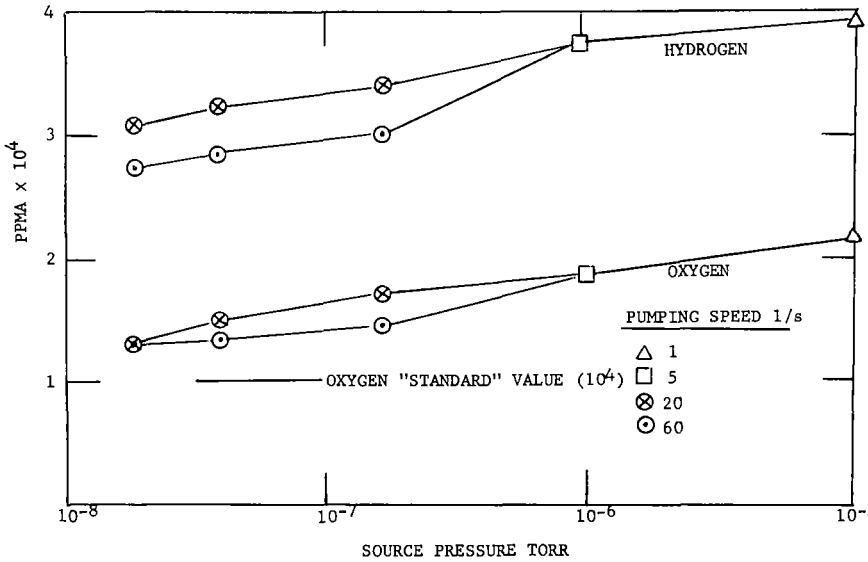

Figure 1. Apparent Hydrogen and Oxygen Concentration in Titanium as a Function of Source Pressure and Pumping Speed.

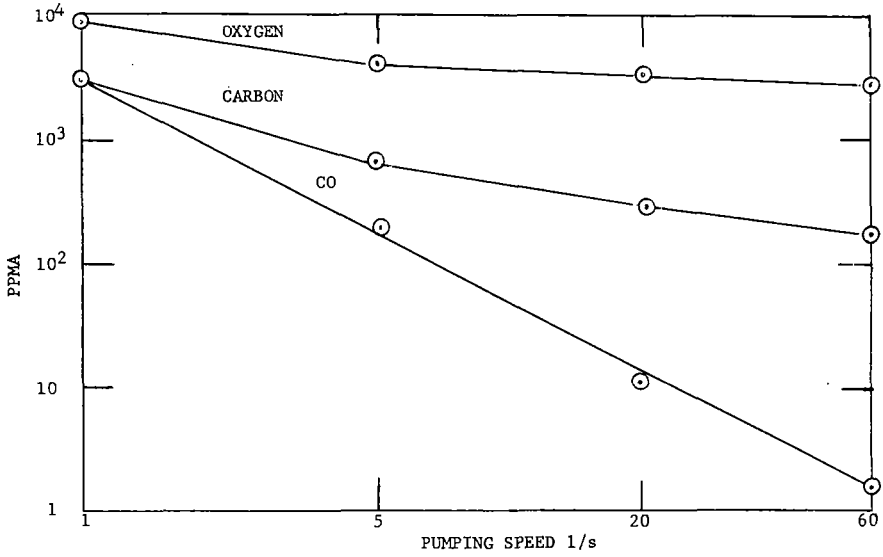

Figure 2. Apparent Concentrations of O, C, and CO in Nickel with Respect to Pumping Speed.

ANALYTICAL TECHNIQUES

For the high-gas samples, exposures were made from 1×10^{-11} to 1×10^{-9} coulomb. The exposures were made at pumping speeds of 1 and 5 liters/second with corresponding source pressures of 1×10^{-5} and 1×10^{-6} Torr, and, at both 20 and 60 liters/second at source pressures of 2×10^{-7}, 4×10^{-8}, and 2×10^{-8} Torr. Exposures were also made at 2×10^{-8} Torr utilizing the cryogenic 100 liters/second pumping speed. The partial pressure of each of the source gases was determined at each source pressure with the quadrupole mass spectrometer. The partial pressures of N, O, OH, H_2O, CO, and O_2 were found to vary directly with that of the source pressure except when using the liquid nitrogen cold finger. Utilizing the cold finger reduces the source pressures by a factor of two since approximately half of the total source pressure is due to H_2O.

All partial pressures were determined before the sample was sparked since a measurement of the source pressures during sparking proved to have a great deal of uncertainty. The extent of the usual rise in pressure from the 10^{-8} level during sparking then becomes a function of pumping speed. With the 60 liters/second pumping speed the high-gas samples with low pumping speeds experienced pressure rises of approximately 15-20 times that of the starting pressure. The low-gas samples experienced pressure increases of only a factor of 5.

RESULTS

The Effects of Pumping Speed on High-Gas Samples

A titanium "standard" sample was selected because it was calibrated for oxygen at a concentration of 1×10^4 parts per million atomic (ppma). The hydrogen content, however, was not calibrated but was known to be large. Figure 1 shows the effect of pumping speed on oxygen and hydrogen in the titanium "standard" at source pressure ranging from 1×10^{-5} to 2×10^{-8} Torr, and at pumping speeds ranging from 1 to 60 liters/second. Notice that both the pumping speed and the starting source pressure affect the apparent concentration of both the oxygen and hydrogen. The apparent oxygen concentration even at a source pressure of 2×10^{-7} Torr with a 20 liters/second pumping speed is approximately 1.7 times the accepted oxygen value. At 2×10^{-8} Torr the difference between the 20 and 60 liters/second is negligible, but the apparent oxygen concentration is still slightly higher than the accepted value of 1×10^4 ppma. In the case of the hydrogen, however, the actual hydrogen concentration in the sample cannot be determined without higher pumping speeds and lower source pressures.

Effects of Sample Gas Content

Figure 2 shows the apparent concentrations of oxygen, carbon, and CO in a nickel sample plotted with respect to pumping speed only. The sample contains large concentrations of oxygen and carbon. The apparent CO value at a pumping speed of 1 liter/second is 3×10^3 ppma. At 60 liters/second the apparent concentration is only 2 ppma. This would indicate that the CO as found on the photographic plate is a result of oxygen and carbon in the sample, and varies almost linearly with pumping speed. It also indicates that with the actual carbon value near 200 ppma the carbon concentration determined at the lower pumping speed was primarily due to the CO formed from the carbon and oxygen contained in the sample.

Effect of Source Pressure on Low-Gas Content Gallium Arsenide

H and H_2O. Figure 3 shows the apparent hydrogen and H_2O concentrations in low-gas gallium arsenide as a function of the H_2O partial pressure and pumping speed. For this particular experiment, the liquid nitrogen cold finger was used which, together with the ion pump, provided a pumping speed for H_2O of 100 liters/second. Notice that the slope of the H_2O concentration line is unity at the higher pumping speeds. This would indicate that as expected there is no H_2O in gallium arsenide. However, with a lower pumping speed, 100 parts per billion (atomic) (ppba) is found even at a partial pressure of 1.5×10^{-9} Torr. For the hydrogen, it is evident that the real hydrogen concentration is being approached as contribution to the hydrogen analysis due to the H_2O partial pressure is nil at the 100 liters/second pumping speed. Also notice that the apparent concentrations of both hydrogen and H_2O are apparently greatly affected by pumping speed.

CO and Carbon. The apparent CO and carbon concentrations in the gallium arsenide are plotted as a function of pumping speed and CO partial pressure and are given in Figure 4. In this case, the carbon in the sample must be larger than the carbon contribution from the CO in the source as the slope of the carbon line is not unity. The real value for carbon in the sample is evidently near the 100 ppba level. Notice

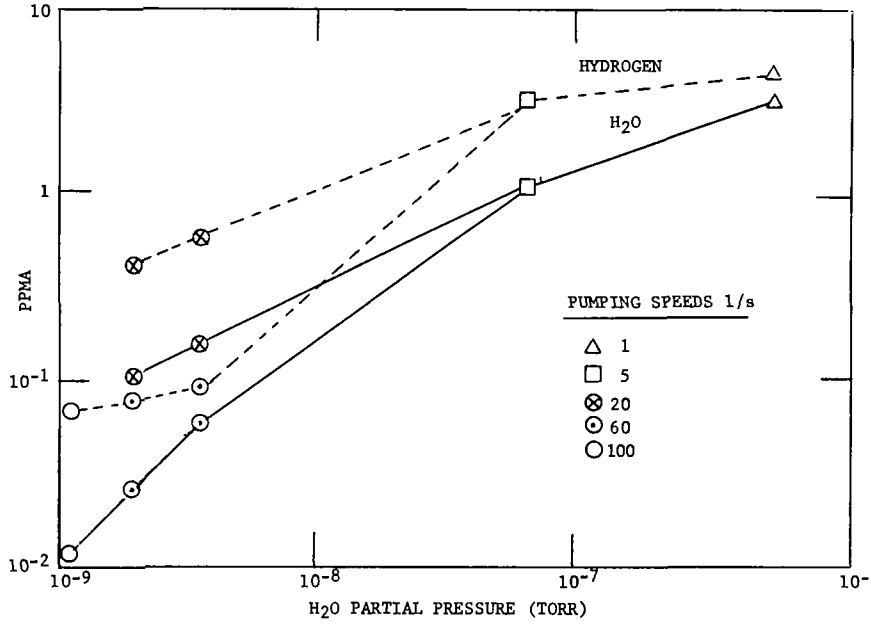

Figure 3. Apparent Hydrogen and H_2O Concentrations in GaAs as a Function of H_2O Partial Pressure and Pumping Speeds.

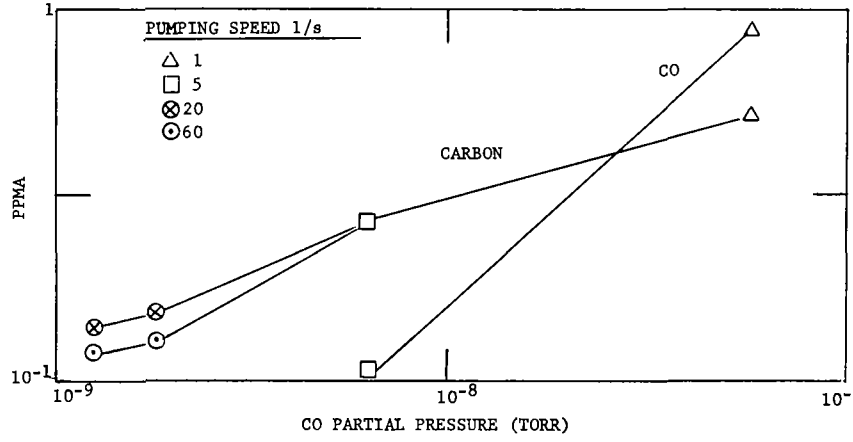

Figure 4. Apparent CO and C Concentrations in GaAs as a Function of Pumping Speed and CO Partial Pressure.

that the CO line has a slope of unity. This, as expected, is directly proportional to the CO partial pressure in the source.

Oxygen and Nitrogen. Figure 5 shows the apparent oxygen and nitrogen concentration in gallium arsenide as a function of their partial pressures and pumping speeds. The apparent nitrogen value is approaching the real sample concentration which is some value lower than 150 ppba. The oxygen concentration, however, remains unknown in that it appears to have not approached the real oxygen content in gallium arsenide. Notice in both cases that at the same partial pressure there are slight differences in the apparent concentration for oxygen and nitrogen when different pumping speeds are used, even at the same nominal starting pressures for nitrogen and oxygen.

SUMMARY

To summarize results of the low-gas sample experiments, the contribution of ions to the mass spectrum from various source gases at a partial pressure of 1×10^{-9} Torr and a pumping speed of 60 liters/second are given in Table I. Note that the oxygen is considerably higher than any of the other ions detected for the same partial pressure. Also, note that the hydrogen ion abundance is somewhat higher than that of the H_2O ion. This is probably due to other sources of hydrogen in the source, such as free hydrogen which could not be determined with the particular quadrupole arrangement used.

TABLE I

Contribution of Source Gases to the Mass Spectrum at a Partial Pressure of 1×10^{-9} Torr

Source Gas	Ion	Contribution in ppma
O	$^{16}O^+$	2
N	$^{14}N^+$	0.3
CO	$^{12}C^+$	0.01*
CO	$^{28}CO^+$	0.02
H_2O	$^{1}H^+$	0.02**
H_2O	$^{18}H_2O^+$	0.01

* Estimated.

** Includes contribution from H_2.

Table II shows the lowest detectable values for oxygen, nitrogen, carbon, and hydrogen at a total source pressure of approximately 5×10^{-8} Torr during sparking. Here again, the lowest detectable value of oxygen was 0.4 ppma. These values were obtained from hundreds of analyses of ultrahigh purity gallium arsenide and cadmium sulfide and agree closely with values extrapolated from Table I.

TABLE II

Lowest Detectable Value at a Source Pressure of 1×10^{-8} Torr ($\sim 5 \times 10^{-8}$ Torr During Sparking)

Element	ppma
O	0.4
N	0.01
C	0.01*
H	0.01

* Estimated.

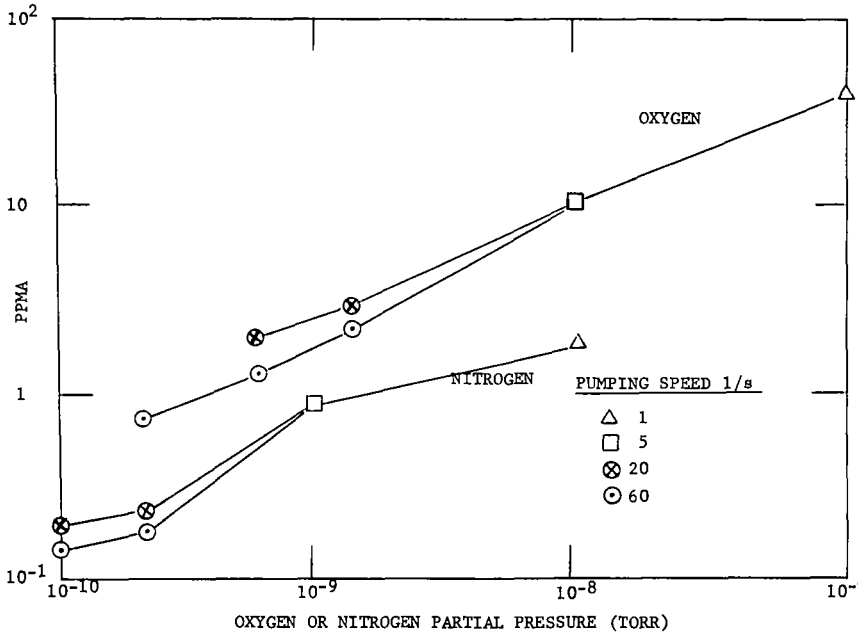

Figure 5. Apparent Oxygen or Nitrogen Concentrations in GaAs as a Function of their partial pressures and pumping speeds.

CONCLUSION

In analyses of samples with high-gas contents such as oxygen at the 10^4 ppma level in titanium, pumping speed and the quantity of gas in the sample are the important factors affecting quantitative results. Pumping speeds greater than 20 liters/second at the source and an initial source pressure less than 2×10^{-8} Torr were necessary for accurate quantitative results. Similarly, analyses of nickel which contained about 3×10^3 ppma oxygen and 200 ppma carbon indicated that pumping speeds of a few liters/second at the source were inadequate and apparent concentrations of the order of 10^3 ppma were found for CO when the actual CO in the sample was shown to be less than 3 ppma

Initial partial pressures as well as pumping speed affect the apparent gas content of low-gas samples. The apparent concentrations of nitrogen, carbon, and hydrogen are reduced to the true level or to a 0.01 ppma detection limit by utilizing a large pumping system such as the one used in these experiments. For the case of oxygen in gallium arsenide however, pumping speeds at the source on the order of several hundred liters/second and starting source pressures of better than 1×10^{-9} Torr would be required for oxygen to be detected at less than 50 ppba.

ATOM CLUSTER AND MOLECULE IONS OBSERVED IN SPARK SOURCE MASS SPECTRA

H. D. Cook

The determination of trace impurities in concentrations as low as a few parts per billion requires positive identification of the ion species producing each spectral line to ensure that the line arises from an impurity rather than a polyatomic ion of the matrix element. For example, a convenient method of exciting high purity refractory materials such as uranium oxides, thoria, zirconia and rare earth oxides is the use of pellets formed from an intimate mixture of graphite and refractory. However, the interpretation of the mass spectra produced from the graphite-refractory pellets is complicated due to the formation of polyatomic ions. This paper is a report of a study performed of spectra of various reactor materials to identify polyatomic ions and their spectral patterns to facilitate interpretation of spark source mass spectra.

Polyatomic ions observed in the mass spectra of refractory-graphite pellets are of the following forms: C_x^{+n}, $M_yC_x^{+n}$, $M_yN_x^{+1}$, $M_yO_x^{+n}$ and $M_yO_x^{+n}$.

C_x^{+1} and C_x^{+2} are polyatomic singly and doubly ionized carbon atom clusters. The singly ionized species, from C_2^{+1} thru C_{23}^{+1} were reported by Dornenburg and Hintenberger,(1) and by Hodgson, Desjardins and Baun.(2) The intensity pattern is shown in Figure 1 for reference. The pattern shown was measured in Bettis Atomic Power Laboratories for spectrographic grade graphite pellets and shows the characteristic intensity peaking at values of X equal to 5, 7, 10, 14, 18 and 22. The intensity pattern was found to be quite independent of excitation conditions. Figure 2 represents the measurable intensity pattern for doubly ionized carbon atom cluster ions. Doubly ionized clusters were not detected for values of X greater than 13. Also they could not be detected at m/e values equal to that of a singly charged carbon cluster unless the $^{13}C^{12}C_{x-1}^{+2}$ species was sufficiently intense.

Atom clusters and molecule ions of the form $M_yC_x^{+n}$, $M_yN_x^{+n}$ and $M_yO_x^{+n}$ have been identified in spectra obtained from pellets of graphite mixed with UO_2, UO_3, U_3O_8, ThO_2, Y_2O_3, ZrO_2 and rare earth oxides. The $M_yC_x^{+1}$, $M_yN_x^{+1}$, and $M_yO_x^{+1}$ species are not of concern in the identification of impurities in uranium and thorium oxides because of their relative positions in the mass spectra. The multiply charged species, however, can lead to erroneous analyses if not identified. Some of the multiply charged polyatomic ions identified in thorium oxide-graphite pellet spectra are ThC_2^{+2}, ThC_2^{+3}, ThC_2^{+4}, ThO^{+2}, ThO_2^{+2}, ThO^{+3}, ThO^{+4}, ThF^{+2}, ThN^{+2}. The polyatomic ions that fall at integral m/e values are resolved from M^{-1} ions of elements between 60 and 140 if the mass spectrograph has a resolution of 1200. Similar polyatomic ions have been identified in the spectra of uranium oxides. The spectra is complicated, when the uranium is other than natural uranium, by the presence of other isotopes. The interpretation is less difficult however since uranium isotopic patterns can be readily identified.

Spectra of yttria or zirconia-graphite pellets are not as easily interpreted. Both oxides produce polyatomic ions $M_yC_x^{+n}$ and M_y^{+1}. Some of the singly charged ions identified in the yttria spectra are YC^{+1} thru YC_{11}^{+1} and $Y_2C_2^{+1}$. The intensity patterns of YC_x^{+1} and YC_x^{+2} ions are shown in Figure 2. It is interesting to note that the only similarity of the YC_x^{+1} intensity pattern to the C_x^{+1} intensity pattern is that there are intensity peaks. The x values for the intensity peaks do not correspond with those of the carbon spectra indicating that the formation of YC_x^{+1} ions is not a simple attachment of an yttrium atom to a previously formed C_x^{+1} ion. The intensity of the $Y_2C_2^{+1}$ observed is approximately 0.01 of the YC^{+1} intensity. The YC_x^{+2} intensity pattern is also shown on Figure 3. Although there are no intensity peaks in the pattern, there are inflections at the even number carbon atoms in the polyatomic ion.

Zirconia-graphite pellets produce somewhat similar polyatomic ion spectra to that of yttria. The mass differences between these ions and ions of the lanthanides are small and corrections must be made to compensate for resulting interferences. The ZrC_x^{+n} intensity pattern is shown in Figure 4.

Polyatomic ions have been identified in spectra of metallic samples. Ions of the type $FeSi_x^{+n}$ have been observed in spectra obtained from iron and nickel base alloys that contain greater than 0.04% silicon. The intensity pattern of $FeSi_x^{+n}$ ions

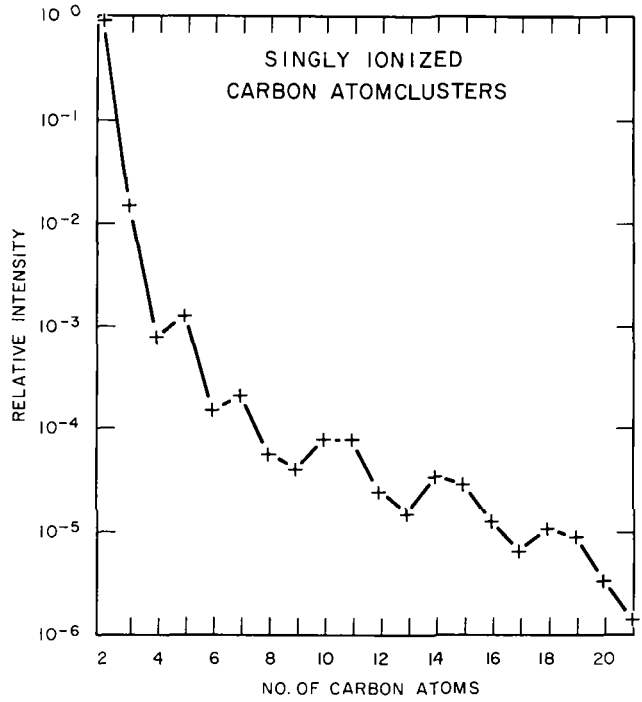

FIGURE 1

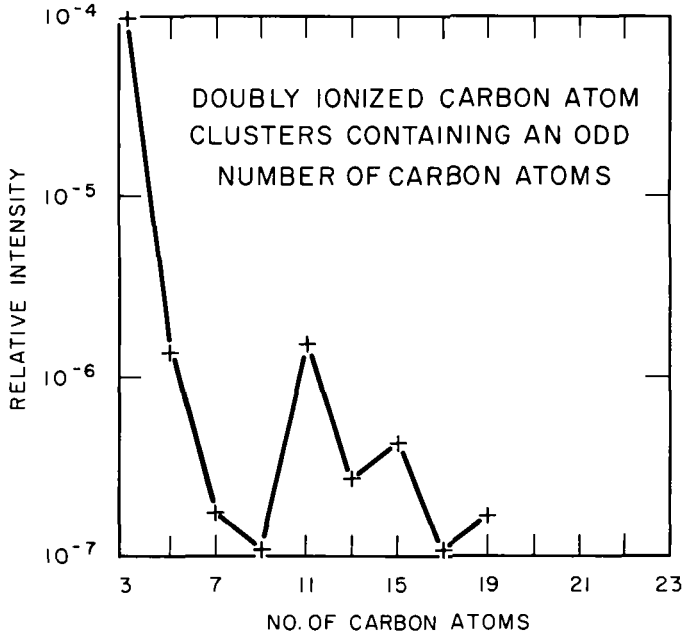

FIGURE 2

is represented in Figure 5. The spectra were produced by sparking a high purity silicon wafer against a high purity iron wire. Polyatomic $FeSi_x^{+1}$ ions for values of from 1 through 5 were identified.

Polyatomic ions in the spectra of Zircaloy have been identified as $ZrSn^{+1}$ and $ZrFe^{+1}$. These ions are produced in low abundances and are observed in spectra obtained to determine impurities in the ppb range.

Spectra of an alloy of aluminum and 1% lithium contain polyatomic ions of lithium and aluminum as well as atom clusters of aluminum up to Al_6^{+1}. Some of the polyatomic ions identified are $AlLi^{+1}$, $AlLi_2^{+1}$ and $Al_2Li_2^{+1}$. The intensity pattern of the aluminum atomcluster ions is plotted in Figure 6.

Conclusions:

Polyatomic ions and atom clusters are produced in the spark gap during rf excitation of oxide-graphite pellets or metallic specimens. The intensity patterns are quite independent of rf spark parameters. The total intensity however is very dependent on the thickness of the spark gap (the dimension parallel to the instrument ion optics); the greater this dimension the more polyatomic ions produced.

Identification of a polyatomic ion of uranium in the presence of an impurity having the same nominal m/e value can be readily made if the spectra are obtained on an instrument having a resolution of 1500 or better(3) in the mass region 60 through 140. Mass determinations to 10 mμ are required to identify the ion if either the polyatomic or impurity ion are not present.

Atom clusters of yttrium or zirconium with oxygen or carbon cause interferences with metal ions of the lanthanides but corrections can be made for these interferences to provide accurate analyses.

Acknowledgements:

The author wishes to express his appreciation to L. T. Beeles for obtaining some of the data included in the paper.

References:

1. V. E. Dornenburg and H. Hintenberger, Z. Naturforsch, 14a, 765 (1959).

2. F. N. Hodgson, M. Desjardins and W. Baun, Proceedings Eleventh Annual Conference on Mass Spectrometry and Allied Topics, 444 (1965).

3. Type 21-110 Mass Spectrometer (Spark Source Model) Operation and Maintenance Manual, Consolidated Electrodynamics Corporation, Pasadena, California (1963).

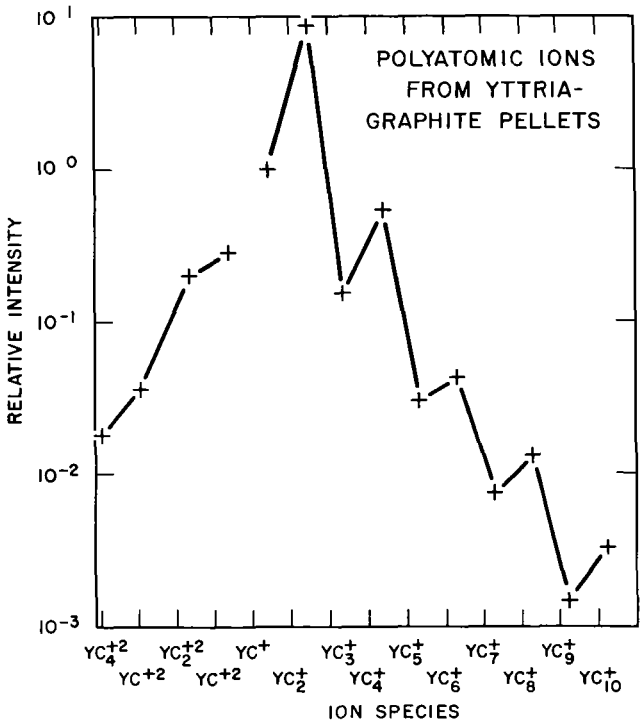

FIGURE 3

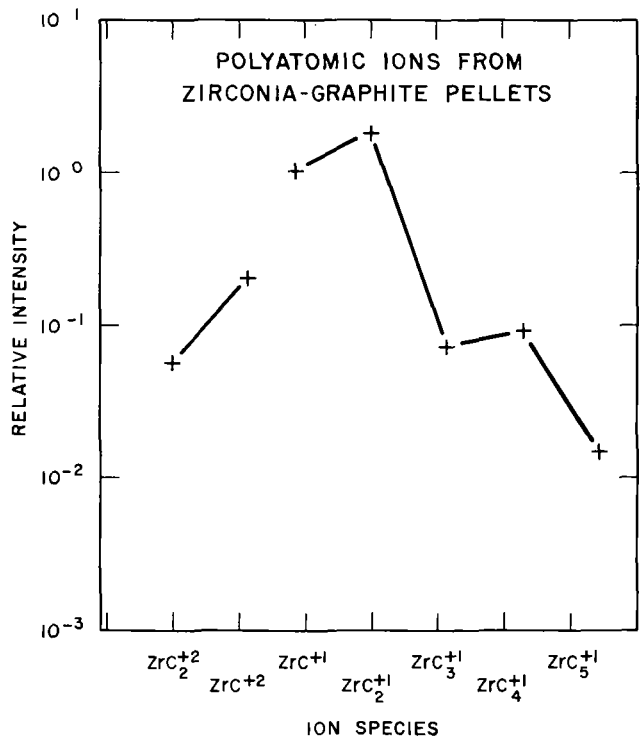

FIGURE 4

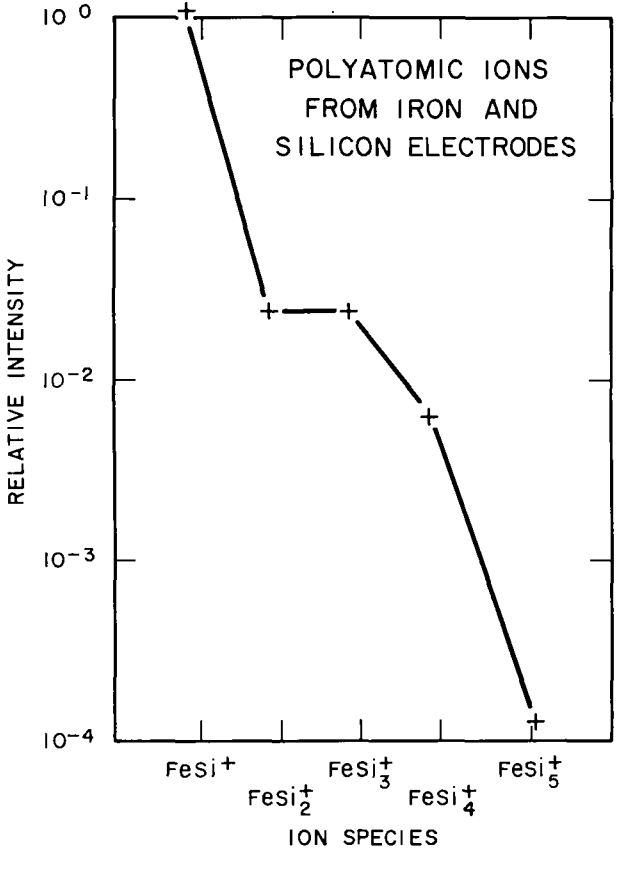

FIGURE 5

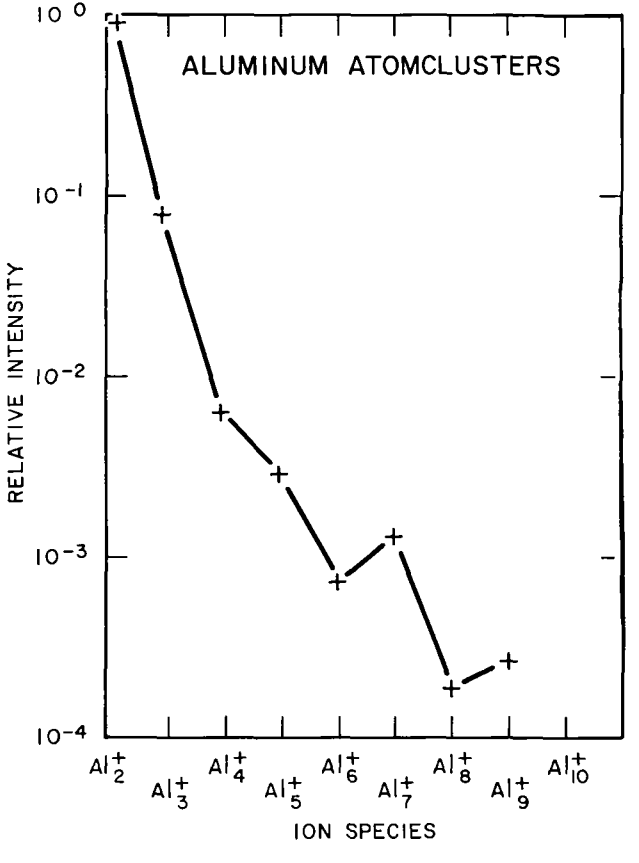

FIGURE 6

A MASS SPECTROGRAPHIC TECHNIQUE FOR THE ANALYSIS OF MOLYBDENUM ADDITIVE IN TANTALUM OXIDE CAPACITOR FILMS

by

D. L. Malm
Bell Telephone Laboratories, Inc
Murray Hill, New Jersey

ABSTRACT

Recent analytical demands in thin film technology require a means for quantitative measurements of intentionally added impurities in sputtered tantalum capacitor films. The inherent high sensitivity and surface sensing ability of the RF vacuum spark source mass spectrograph suggest its usefulness for this study.(1) It has been demonstrated that with the aid of an internal standard and a sample scanning technique which samples the film on the substrate thus eliminating any chemical separations, quantitative estimates of molybdenum additive in films 4000 Å thick can be made with an average deviation of ±23 percent.

A concentration range of 0.02 percent to 3.1 percent atomic fraction of molybdenum in tantalum films was studied. Because adequate sensitivity is attained without consuming the entire available sample, it is reasonable to predict that sensitivities of 10 ppm atomic or less may be reached.

Results show a linear increase in the molybdenum concentration as the molybdenum concentration as the molybdenum to tantalum sputtering surface ratio increases. Once this relationship has been established, films with the desired molybdenum concentration can be produced without the need for further chemical analysis.

Mass spectrographic results also indicate that the molybdenum additive is homogeneously distributed in the tantalum film.

INTRODUCTION

Eight groups of tantalum films 4000 Å thick were sputtered onto spectrographically pure carbon blocks with a surface area of about 40 mm^2. Increasing amounts of molybdenum were simultaneously sputtered with the tantalum in each group.

The method used to add the molybdenum to the film consists of simply affixing wires of the additive to the tantalum cathode. The control is achieved by varying the ratio of the area of the additive wire to that of the tantalum cathode by changing the number and diameter of the molybdenum wires.(2) In this study, increasing numbers of 0.010" molybdenum wires were added with the exception of two groups which utilized one 0.005" and one 0.001" wire respectively. However, with this method only a limited estimate can be made on the additive concentration in the film. Therefore further mass spectrographic study was necessary.

The surface sampling ability of the RF vacuum spark source mass spectrograph and its high sensitivity indicate its applicability to this study.

METHOD

The analyses were made with an MS-7 mass spectrograph. The positive ion source is a pulsed vacuum spark between a probe electrode and the sample surface. The spark voltage was ≈20 kv, the pulse length 25 microseconds and the repetition rate 10 pulses per second. These conditions were maintained throughout the analyses. The vacuum conditions with the spark off were ≈3 to 5×10^{-9} torr in the source and analyzer of the instrument.

A sample scanning technique is used for the study of the tantalum films on the substrate thus eliminating the need for a chemical separation. This method also produces a constant ion contribution from the film to the spec-

trum during sparking and allows a graded series of photographic exposures to be made in which the ion intensity measured from the photoplate is directly proportional to the ion exposure measured at the monitor. The exposures used ranged from 0.003×10^{-9} coulombs to 10×10^{-9} coulombs depending on the amount of molybdenum in the film. The optical transmission of the lines in question were measured with a microphotometer and converted to ion intensity by means of a photographic plate calibration. From the plots in Fig. 2 of the molybdenum ion intensity and that of the niobium internal standard as a function of the exposure, the concentration of the molybdenum can be derived from the ratio to the niobium exposures for a given ion intensity.

The sample configuration when mounted in the source is shown in Fig. 1. The probe is a 0.020" gold wire and the substrate on which the film is deposited is a 0.1"×0.5"×0.05" thick spectrographically pure carbon block. The probe and substrate were previously analyzed and were found free from the additive, internal standard and interfering lines. The spark is formed between the stationary gold probe and the surface on which the film has been deposited. It penetrates to a depth of about three microns into the sample surface which is enough to consume the film and part of the substrate. In order to obtain a constant ion contribution from the film, the necessary sensitivity and a graded series of exposures, a fresh sample surface must be continuously presented for sparking.

This is attained by providing a continuous motion of the sample beneath the gold probe while constantly maintaining the spark. The uniform motion of the sample across the short axis is provided by a slow speed motor which is connected to the sample manipulator from outside the source. After each traverse, the spark is stopped and a fresh surface made available by manually shifting the sample in the long axis direction. This routine is repeated until the desired exposures have been completed.

RESULTS AND DISCUSSION

The mass spectrographic results for the molybdenum concentration in the tantalum film are shown in Table I. The results shown are average values obtained from duplicate samples. Cross checks were obtained in two cases with a photometric method by C. L. Luke and are included for comparison.

TABLE I

MOLYBDENUM ADDITIVE IN TANTALUM FILM

Number of 0.010" Mo Wires Added	MS-7 WT.% Mo	Photometric Value (WT.% Mo)
8	1.62	1.79
6	1.3	--
4	0.72	0.8
3	0.63	--
2	0.35	--
1	0.18	--
0.5	0.098	--
0.1	0.015	--

Note: The designation "number of Mo wires added" refers to the number of 0.010" Mo wires that were affixed to the tantalum sputtering cathode. The 0.5 and 0.1 designate a 0.005" and 0.001" wire.

Normally, an isotope line from the matrix material is selected as the internal standard. However, in this case the ^{181}Ta (99.988 percent) line is not suitable because at exposure levels of less than 0.001×10^{-9} coulombs which are necessary for the plate calibration, the ion exposure measured at the monitor and the ion intensity measured on the photoplate are no longer proportional. It is suspected that this is partially due to inaccurate exposure measurements at these levels.

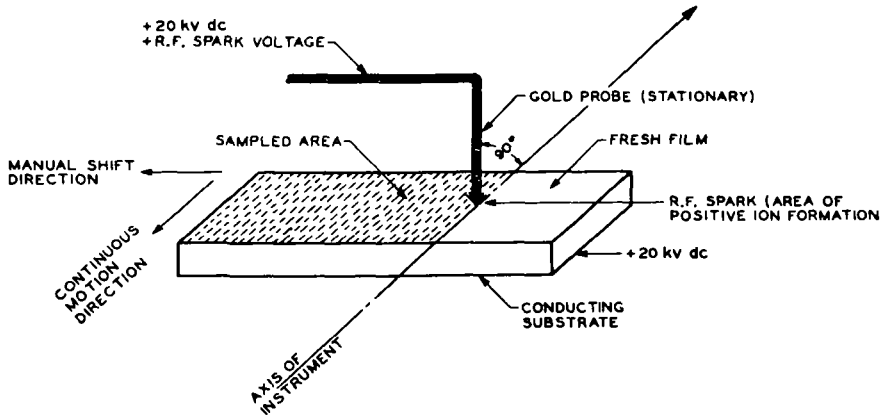

FIG. 1 ELECTRODE CONFIGURATION FOR SAMPLE SCANNING TECHNIQUE-SURFACE FILM STUDY

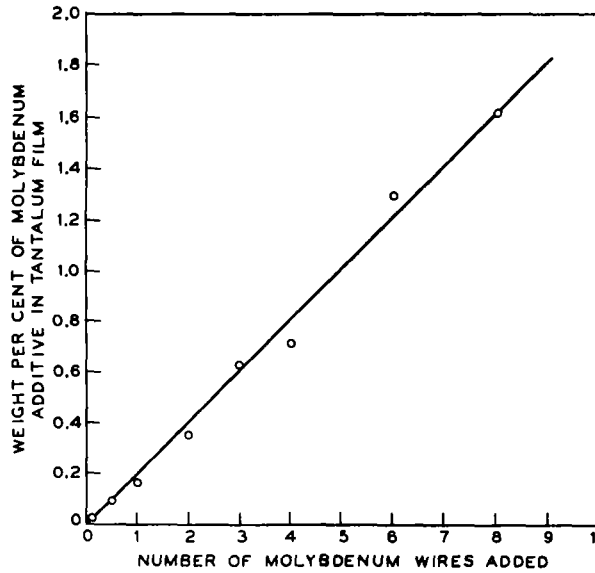

FIG. 3 LINEAR PLOT OF MOLYBDENUM CONCENTRATION VS NUMBER OF MOLYBDENUM WIRES ADDED TO TANTALUM SPUTTERING CATHODE FOR FILM DEPOSITION

The ^{180}Ta (0.012 percent) is inadequate in the longer uniform exposures because of serious line broadening and plate fogging in the area adjacent to the line. Therefore the niobium impurity in the tantalum cathode was chosen as the internal standard. The niobium value was predetermined in the tantalum cathode to be 144 ppm atomic. This value was obtained with a photometric method by C. L. Luke and is accepted in this experiment as a standard value. The mass spectrographic value for niobium in the same sample was determined as 305 ppm atomic without the aid of prepared standards. A relative sensitivity coefficient* of ≈2.1 is therefore assumed and all mass spectrographic values for niobium are adjusted to conform with the standard value.

The data plotted in Fig. 2 showing the mass spectrographic value of the niobium intensity to be directly proportional to the exposure indicates that the internal standard niobium and therefore the tantalum contribute a constant fraction of ions being analyzed, and that the molybdenum is homogeneously distributed when compared to the niobium and therefore to the tantalum film.

The straight line curve of Fig. 3 made from the data in Table I indicates that under the sputtering conditions used the rate of deposition of the molybdenum is proportional to the molybdenum area of the sputtering surface. Also, with this information, if the number, diameter and position of the molybdenum wires on the tantalum cathode is duplicated in subsequent film sputtering, satisfactory concentration values can be obtained directly from the curve, thus eliminating the need for further chemical analysis.

The possibility that there may be interference caused by a $^{92}Mo^{1}H$ (m/e 93) with ^{93}Nb is minimized as there is no evidence for the $^{98}Mo^{1}H$ (m/e 99) in the clear mass position on the photographic plate.

The photometric results for molybdenum in the tantalum film when compared with the mass spectrographic result indicate an RSC value of slightly greater than one. Considering the analytical error, no correction was made.

CONCLUSIONS

The analysis of molybdenum additive in tantalum films can be accomplished with a mass spectrograph and the sample scanning technique. There are good indications that other additives in tantalum films can be studied if the sampling probe and substrate material are carefully selected so that their contribution to the spectrum does not interfere with the additive or standard isotope lines.

ACKNOWLEDGMENTS

The writer wishes to acknowledge the collaboration with D. J. Harrington in the production of the films and A. J. Ahearn and T. C. Loomis for their suggestions and advice in various phases of the work.

REFERENCES

1. A. J. Ahearn, "Sixth National Symposium on Vacuum Technology Transaction," Pergamon Press, 1960.

2. N. N. Axelrod, B. H. Vromen, H. D. Guberman, D. J. Harrington, and N. Schwartz, "Asymmetric Conduction in Anodic Oxides Formed from Sputtered Tantalum Alloy Films," Electrochemical Society Meeting, Cleveland, Ohio, May 1-5, 1966.

$$*RSC = \frac{\text{Mass Spectrographic Value}}{\text{Standard Value}}$$

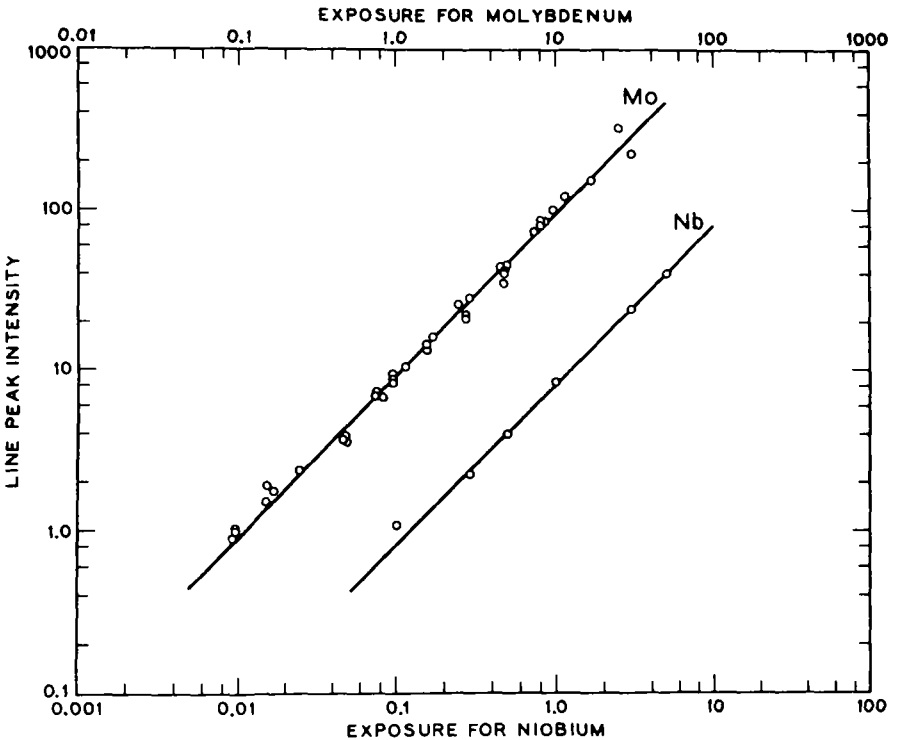

FIG. 2 LOG/LOG PLOT OF PEAK INTENSITY VS ION EXPOSURE

A COMPARISON OF SPARK SOURCE MASS SPECTROGRAPHIC, SPECTROPHOTOMETRIC AND ELECTRICAL MEASUREMENTS OF IMPURITIES IN GALLIUM PHOSPHIDE

by

A. J. Ahearn, F. A. Trumbore,
C. J. Frosch, C. L. Luke, and D. L. Malm
Bell Telephone Laboratories, Incorporated
Murray Hill, New Jersey

INTRODUCTION

The luminescent properties of gallium phosphide are strongly influenced by the presence of small amounts of various impurities often unintentionally added.[1] In order to study and control this luminescence there is an obvious need for methods of detection and quantitative determination of these impurities at levels below 10^{18} atoms/cm^3.

To see if the spark source mass spectrograph could meet this need, a comparison of this technique with spectrophotometric analyses and with impurity concentrations derived from electrical measurements was undertaken. Specifically, 15 samples of GaP containing zinc, silicon, germanium, tin, selenium, tellurium, magnesium, and sulfur were each analyzed by at least two of these three techniques. Included among the mass spectrographic analyses is one of a gallium arsenide crystal doped with copper, the level of which was determined by a radio tracer method.[2]

METHOD

The mass spectrographic analyses were made with an MS7 instrument.* The spark source was operated at an rf voltage of 25 to 75 percent (variac setting), a 25 microsecond pulse length and repetition rates from 10 to 1000 per second.

The vacuum conditions maintained during the tests were comparable with the optimum of which the MS7 is capable. The entire instrument was occasionally baked at 200°C and the source chamber was frequently baked at 250°C. Analyzer and source chamber pressures in the low 10^{-8} or high 10^{-9} Torr range were achieved. With the spark running, the source pressure increased by a factor of ten or more depending on the spark conditions.

The mass spectra were recorded in the usual graded series of exposures. From these the impurity concentration could be related to that of an isotope of the major component used as an internal standard. This was done with the aid of a photographic plate calibration relating microphotometric measurements of mass line peak optical transmission to peak ion intensity. An adequate measure of the ion intensity is obtained from these peak values by correcting the latter for background, for variations in line width and for the dependence of the photographic plate sensitivity on the chemical element in question. This sensitivity is assumed to depend only on the element mass[3] according to the relation $M^{-0.5}$.

Electrical resistivity measurements were made using the 4-point probe technique, from which the free electron or hole concentrations were derived. Some surface barrier capacitance measurements were also made to obtain values of $|N_D-N_A|$ the excess donor or acceptor concentrations.[4] These data are in Table I which also includes the mass spectrographic and spectrophotometric analyses.

In the spectrophotometric analyses, the following specific techniques were employed. Selenium was determined by the direct photometric 3, 3' diaminobenzidine method.[5] Tellurium was determined by solvent extraction and photometric determination with a chloroform solution of carbamate.[5] Zinc was determined by solvent extraction and photometric measurement with a chloroform solution of dithizone. Germanium or tin was assessed by the photometric phenylfluorone method after first isolating the metals as sulfide

*Associated Electrical Industries Ltd., Manchester, England.

TABLE I

COMPARISON OF MASS SPECTROGRAPHIC, PHOTOMETRIC AND ELECTRICAL MEASUREMENTS OF IMPURITY CONCENTRATIONS (ATOMS/CM^3) in GaP

Technique	Dopant	Spectrograph	Photometry	4 Point Probe Resistivity	Capacitance	Resistivity Type
FZ	Mg	9.1×10^{17}		1.4×10^{18}	1.5×10^{18}	p
FZ	Mg	1.8×10^{18}		$0.5\text{-}2.0\times10^{18}$		p
TG	Zn	2.2×10^{17}	4.5×10^{17}		3.3×10^{17}	p
TG	Zn	5.3×10^{17} X	"			p
TG	Zn	3.1×10^{17} X	"			p
TG	Zn	2.0×10^{17} X	"			p
TG	Zn	2.7×10^{17} X	"			p
TG	Zn	5.8×10^{18}	4.6×10^{18}		$> 2.3\times10^{18}$	p
TG	Zn	4.9×10^{18} X	"			p
TG	Zn	$3.3\text{-}7.4\times10^{18}$ X	"			p
TG	Si	4.7×10^{20}	7.2×10^{20}		1.0×10^{19}	n
FZ	Si	3.9×10^{18}		$1.7\text{-}2.7\times10^{18}$	3.8×10^{18}	n
TG	Ge	$1.8\text{-}7.0\times10^{18}$	8.5×10^{18}		2.2×10^{17}	n
FZ	S	1.0×10^{18}	1.8×10^{18}			n
FZ	S	$\leq 1.4\text{-}6.6\times10^{18}$	5.4×10^{18}	1.4×10^{18}	5.0×10^{18}	n
FZ	S	1.5×10^{18}		$2.5\text{-}4.0\times10^{18}$		n
TG	Se	3.7×10^{17}	5.2×10^{17}		$3\text{-}10\times10^{17}$	n
TG	Se	3.6×10^{18}	4.1×10^{18}		4.2×10^{18}	n
TG	Se	3.2×10^{19}	4.7×10^{19}			n
TG	Se	2.5×10^{16}			$\sim8\times10^{16}$	n
TG	Sn	5.4×10^{16}	1.3×10^{17}		1.5×10^{17}	n
TG	Te	1.5×10^{18}	2.1×10^{18}		1.5×10^{18}	n
TG	Te	3.0×10^{19}	1.4×10^{19}		5.9×10^{18}	n
TG	Te	2.2×10^{16}			$0.6\text{-}2.0\times10^{17}$	n
TG	Te	2.4×10^{17}			$1.5\text{-}4.0\times10^{17}$	n
B G GaAs	Cu	3.1×10^{16}	(2.3×10^{16} R.T.A.)			p

FZ Float Zone[13]

TG Thermal Gradient[10,12]

BG Bridgman Grown

X Not corrected for line width

R.T.A. Radio Tracer Analysis

using copper as co-precipitant.[6] Silicon was determined by the photometric molybdenum blue method after first removing phosphate on an anion exchange resin column.[7] Sulfur was determined by the photometric lead sulfide method after reducing sulfate to sulfide with HI-H_3PO_2 mixture.[8]

RESULTS - MASS SPECTROGRAPHIC vs. SPECTROPHOTOMETRIC MEASUREMENTS

In Fig. 1, the mass spectrographic concentrations are plotted against the spectrophotometric values which are in general thought to be accurate to within ±10-20 percent of the total impurity concentration.

In weighing the reliability of the points of Fig. 1, it should be pointed out that the thermal gradient samples principally used in this comparison were rods cut from large-grained polycrystalline ingots. In selecting the samples for the mass spectrographic analyses, care was taken to use samples of the best available optical quality in order to minimize the possibility of gallium inclusions containing the impurity in question. Even so, the elimination of such inclusions is difficult especially for the more heavily doped samples which are too dark to see through visually. Such inclusions would lead to mass spectrographic concentrations higher than the spectrophotometric values since in the latter case the samples were crushed and digested in suitable solvents to remove included material. Thus, more reliance should be placed on the lower values in Fig. 1, especially where there is considerable scatter as in the case of tellurium and zinc.

The solid straight line of Fig. 1 corresponds to the idealized case of exact agreement between the mass spectrographic and the spectrophotometric analyses. It is seen that with the exception of a few points, these two techniques give quantities that agree to within a factor of 2 or 3, - the large majority of the mass spectrographic values falling below the spectrophotometric ones.

Exact agreement between the mass spectrographic results and the impurity concentrations standardized by the spectrophotometric data is not necessarily expected. This would involve the assumption that the ion sample presented to the detector perfectly represents the solid sample itself. Work with standard samples shows that in general this assumption is not justified and that the disagreement[9] may be by a factor as high as ±3.

It is customary to introduce a Relative Sensitivity Coefficient (RSC) - an empirical factor which corrects for this lack of fidelity and which is obtained from data such as that plotted in Fig. 1. In this case the numbers established by the spectrophotometric technique are accepted as the absolute values of the concentrations. In addition to the solid line in Fig. 1 corresponding to an RSC value of unity, dashed lines corresponding to RSC Values of 0.5 and 1.5 are included.

The selenium data are particularly interesting; two decades in concentration are represented and the scatter is small. In addition, the spectrophotometric analysis for selenium in GaP is particularly straightforward with a minimum of chemical separations, etc. Figure 1 indicates that an RSC value of 0.7-0.8 fits the selenium values very well. Consequently, the mass spectrographic data corrected by this factor should yield absolute values of selenium in GaP accurate to better than ±50 percent.

The data of Fig. 1 strongly suggest that the RSC values for zinc, silicon, germanium, tin, sulfur and tellurium fall between 1.5 and 0.5, the lower values being favored where the data is scattered. An RSC of about 1.3 is indicated for copper in the GaAs crystal. This should also be a particularly well characterized sample since the copper was diffused into the GaAs and the problem of inclusions is absent.

RESULTS - MASS SPECTROGRAPHIC vs. ELECTRICAL MEASUREMENTS

In Fig. 2, the mass spectrographic data are plotted against the electrical measurements, these being either 4-point probe measurements of free carrier concentrations or surface barrier capacitance measurements of $|N_D-N_A|$. It should be noted that the 4-point probe resistivity data were interpreted assuming hole and electron mobilities of 65 and 110 cm^2/volt sec. Since these values are not known precisely and could change with doping level, the surface barrier capacitance measurements are considered more reliable.

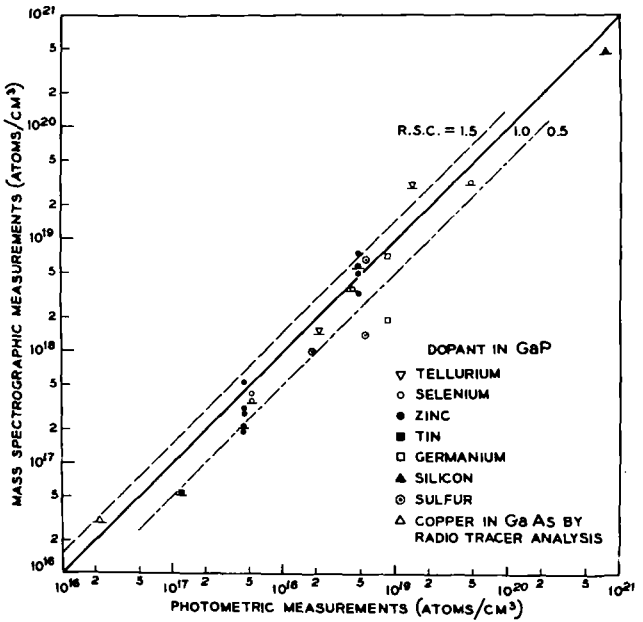
R.S.C. = 1.5
1.0
0.5
DOPANT IN GaP
TELLURIUM
SELENIUM
ZINC
TIN
GERMANIUM
SILICON
SULFUR
COPPER IN GaAs BY RADIO TRACER ANALYSIS
MASS SPECTROGRAPHIC MEASUREMENTS (ATOMS/CM³)
PHOTOMETRIC MEASUREMENTS (ATOMS/CM³)

FIG 1

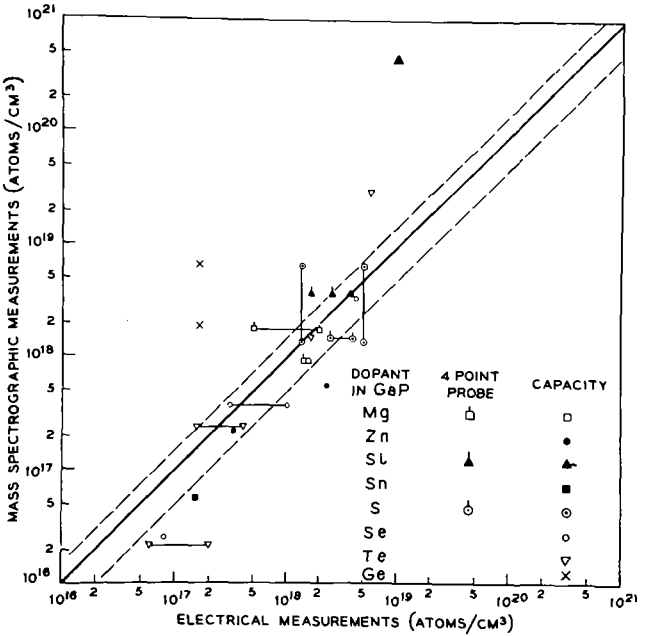
DOPANT IN GaP
4 POINT PROBE
CAPACITY
Mg
Zn
Si
Sn
S
Se
Te
Ge
MASS SPECTROGRAPHIC MEASUREMENTS (ATOMS/CM³)
ELECTRICAL MEASUREMENTS (ATOMS/CM³)

FIG 2

Just as in Fig. 1, the solid line corresponds to the idealized case of exact agreement between the mass spectrographic and the electrical data and the two dashed lines bracket the same range of mass spectrographic values as the dashed lines of Fig. 1. One immediately sees that there is more spread in the data of Fig. 2 than in Fig. 1 although most of the mass spectrographic data is common to both as shown in Table 1.

However, it should be emphasized in connection with the electrical data that, as shown previously,[10,11,12] agreement between $|N_D-N_A|$ values or free carrier concentrations and the dopant concentrations is not expected for many impurities in GaP, depending on the particular dopant and the concentrations involved. For example, germanium is highly self-compensated at all doping levels, thus explaining the large departure of the germanium data from the ideal behavior. Silicon and tin, however, become significantly self-compensated only at concentrations above 10^{18}-10^{19} atoms/cm^3. Thus for silicon, for example, the deviation is very large at the highest doping level, but at lower concentrations agreement is quite good. The sulfur, selenium and tellurium also are present to a large extent in an electrically inactive form (possibly due to neutral complexes with vacancies) at concentrations in excess of 10^{18}-10^{19} atoms/cm^3. Evidence for zinc precipitation at concentrations above 5-10×10^{17} atoms/cm^3 has also been reported.

The presence of background impurities such as silicon and sulfur at the 10^{16}-10^{17} atoms/cm^3 level also complicates the interpretation of the electrical data at the lower concentrations.

In general, agreement is good at concentrations between 10^{17} and about 5×10^{18} atoms/cm^3 where good agreement is to be expected.

CONCLUSION

The results of this comparison of mass spectrographic data with spectrophotometric analyses indicate that, for impurities magnesium, zinc, silicon, germanium, tin, sulfur, selenium and tellurium in GaP and for copper in GaAs, the spark source mass spectrograph is capable of yielding concentrations accurate to within a factor of 2 or 3 by assuming a Relative Sensitivity Coefficient of unity. More specifically, this comparison indicates an RSC of 0.7-0.8 for selenium and probably the lower end of the range 1.5-0.5 for the other elements. An RSC of 1.3 for copper in GaAs was obtained.

Since these impurities vary widely in their properties (volatility, position in periodic table, mass, etc.) it is a reasonable assumption that many other impurity elements in GaP could be measured in the same way with the same accuracy.

Furthermore, the selenium results suggest that equally homogeneous samples doped with other elements at levels high enough to be amenable to analysis by photometric or other standard techniques might be preparable. If so, a comparison of mass spectrographic data with that of these standard techniques could yield reliable RSC data. Then, mass spectrographic analyses which could be made on low concentration samples not generally amenable to analysis by other techniques could yield more accurate data than heretofore possible.

The mass spectrographic and the spectrophotometric data agree with much but not all of the concentrations derived from the electrical measurements. However, the agreement is acceptable at concentrations between 10^{17} and about 5×10^{18} atoms/cm^3 where agreement is to be expected.

REFERENCES

1. See for example M. Gershenzon, in "Semiconductors and Semimetals, Physics of the III-V Compounds", R. K. Willardson and A. C. Beer, editors, Vol. 2, Academic Press, N. Y., 1966, Chapter 13.

2. K. B. Wolfstirn, private communication.

3. E. B. Owens and N. A. Giardino, Analytical Chemistry 35, 1172-1178 (1963).

4. H. G. White and R. A. Logan, J. Appl. Phys. 34, 1990 (1963).

5. C. L. Luke, Anal. Chem. 31, 572 (1959).

6. C. L. Luke and M. E. Campbell, Anal. Chem. 28, 1273-9 (1956).

7. C. L. Luke, Anal. Chem. 25, 148 (1953).

8. C. L. Luke, Anal. Chem. 21, 1369 (1949).

9. R. Brown, R. D. Craig and R. M. Elliott, Advance in Mass Spectrometry, Vol. 2 Pergamon Press, 1962.

10. F. A. Trumbore, H. G. White, M. Kowalchik, R. A. Logan and C. L. Luke, J. Electrochem. Soc. 112, 782 (1965).

11. F. A. Trumbore, H. G. White, M. Kowalchik, C. L. Luke and D. L. Nash, J. Electrochem. Soc. 112, 1208 (1965).

12. M. Rubenstein, ibid, 112, 1010 (1965).

13. C. J. Frosch and L. Derick, J. Electrochem. Soc. 108, 251 (1961).

SPARK SOURCE MASS SPECTROGRAPHIC ASSAY OF RARE EARTH METALS AND OXIDES*

R. J. Conzemius, J. Capellen and H. J. Svec

Institute for Atomic Research and Department of Chemistry
Iowa State University, Ames, Iowa

A portion of our work with the spark source mass spectrograph during the past year has been concerned with the detection and the subsequent determination of trace impurities in rare earths. Table I shows the number of each rare earth metals and rare earth oxides for which

Table I. Rare Earth Metals and Oxides Assayed (including Y and La)

	Y	La	Ce	Pr	Nd	Sm	Eu	Gd
Metal	1	6	2	1	1	-	-	1
Oxide	1	2	1	3	1	2	4	6
	Tb	Dy	Ho	Er	Tm	Yb	Lu	Total
Metal	2	3	3	5	2	1	3	31
Oxide	2	2	3	5	9	3	3	47

Metal - rod 1 cm. long 1 sq. mm. cross section
Oxide - pelletized with graphite

we have performed a general analysis. The totals indicated in Table I are from about 3 months ago although we are continuing our work in this area. Two years ago Guthrie of Sandia described spark source analysis of some commercial rare earth metals. The present report is mainly the result of an accumulated back log of information which has been obtained while performing service analyses for various research activities in the Ames Laboratory of the Atomic Energy Commission. We have studied such things as the distribution of multiply charged ions, cluster intensities, interference problems, and reproducibility, especially for oxides. These items will be discussed in the report in the form of a progress report rather then a definitive study. These rare earth metals and oxides were extracted from the ores and purified at the Ames Laboratory. The instrument used for the work was Nuclide Corporation's Graf 2 mass spectrograph.

No special etching procedure has been used for the rare earth metals. The more reactive metals require special handling in an inert atmosphere. Presparking is used for final cleaning.

The oxide samples were prepared by pelletizing with SP-1 graphite obtained from the National Carbon Company. Our assay of the graphite used in the pellets is given in Table II. Elements not listed were below the

Table II. Graphite Analysis
ppm atomic

Element	ppm	Element	ppm
N	0.3	Cr	0.3
O	4.	Fe	1.
Na	0.03	Mn	0.01
Al	0.4	Ni	0.1
P	0.01	Cu	0.02
S	0.1	Ge	0.07
Cl	1.	Y	0.03
K	0.06	Zr	0.07
Ca	0.09	Nb	0.09
		Gd*	0.16

*Previous matrix in instrument

detection limit which was approximately 20 parts per billion atomic at mass 100. The low values for all the elements of the periodic chart, especially the common metals, was the primary reason for choosing graphite as the

* Work was performed in the Ames Laboratory of the U. S. Atomic Energy Commission.

pelletizing medium. The mixture ratio used was three parts graphite to two parts oxide by weight. This mixture was ground manually in an agate mortar and pestle and grinding was continued for about five minutes after the dry blend appeared to be uniform. Microscopic examination showed that further mixing does not appear to improve the homogeneity of the blending. The pellets were pressed in a 1/4 inch stainless steel die at approximately 40,000 pounds per square inch. No outgassing problems were observed with the pellets and although they may be delicate, handling was not unduly difficult. Normal instrumental conditions were used for sparking these samples. The ion current obtained from the pellets was about 5×10^{-10} amperes which was about five times greater than the ion current from the metals. The pressure in the source while sparking was 2 to 5×10^{-6} Torr for the metals and 2 to 9×10^{-6} Torr for the oxides. Spark source analysis of these samples is not without its esthetic features due to some rather brilliant fluorescence occuring in the RF field. Pellets of gadolinium oxide fluoresce with various colors and have an especially bright red fluorescence if small quantities of europium are present. Lanthanum oxide gives a bright green fluorescence under some conditions and yttrium oxide also fluoresces.

Photoplate detection was used for all analyses reported here. The emulsion was calibrated using the Churchill two-line method. All data manipulations, including the formation of the calibration curve, was performed on an IBM 7074 computer. The reference for each sample was a line from the matrix material where relative intensity was determined from a series of short exposures on each plate.

The mass spectra obtained from the rare earth metals are typical of spark source data. For the graphite pellets the same type of relative intensity of carbon cluster peaks were observed as has been reported by others.

Figure 1 illustrates the relative intensity of multiply charged lines. Relative intensity of the rare earth ion is on the horizontal logarithmic scale. The reference is the singly charged ion set equal to unity. Data is given for the metals and the oxides. The median value for each multiply charged ion intensity is indicated by the arrow along with maxima and minima. A point of interest is that the +2 line tends to be stronger in the oxide than in the metal. The observed oxide +2 maxima actually extends to 2.7 with a median value of 0.9 compared to the median value for the metals of 0.3. Both the oxide and the metal spectra show a decrease in intensity by approximately one order of magnitude for each additional charge starting with the +2 ions. However the higher charged ions are less abundant in the pellet spectra than in the metal spectra. The intensities do not include corrections for energy response and the calibration curve used was established with singly charged ions. Actually for an individual sample the ratios of the intensity of multiply charged lines to that of singly charged lines tend to remain relatively constant except for the +2 line which occasionally varies by as much as 100% in the short exposures. This variance of the +2 line and the fact that it provides a major contribution to the total ion intensity is a prime source of error when short exposures are used to establish the matrix material as the reference. The differences in the trends of the data between the oxides and the metals indicate a different type of discharge. These differences will natually affect relative elemental sensitivities.

Figure 2 illustrates the relative abundance of matrix ion clusters observed with the pelleted oxide samples. The horizontal scale is in parts-per-million-atomic. The median value is indicated by the arrow for each type of cluster along with maxima and minima. The ratio of clusters to one another for individual samples are relatively constant. However, the various rare earths form considerably different amounts of these clusters which accounts for the spread of the maxima and minima on the slide. The intensity of the monoxide line varies considerably for the different rare earths. Another interesting general feature in these spectra is the low intensity of the dioxide compared to the di- and tricarbides.

Table III shows an example of some rather serious interferences that can occur in the spectra and make some individual determinations

Table III. Rare Earth Clusters
Example of Serious Interference

Yb in Gd_2O_3-graphite matrix
Relative isotope distribution of species at each Yb mass

Mass	168	170	171	172	173	174	175
GdC	.20	.25	.003	.22	.002	-	-
GdO	.002	.021	.15	.20	.16	.25	.22
Yb	.0014	.030	.14	.22	.16	.32	.13
GdC_2	-	-	-	-	-	-	.002

difficult. Note the complete covering of the ytterbium isotopes by gadolinium monoxide lines as well as similar interference from the mono and dicarbides. The largest mass difference in these multiplets is 1 part in 7500. Thus the lines are completely superimposed since this mass difference is rougly an order of magnitude less than the resolution. This is one of the worst cases and actually very few elements which show this type of interference can be given lower limit values of less than ten parts per million. It often means that all significant contributions to each line must be identified.

Reproducibility of results from independent determinations were studied only in the case of the oxides. Seventy-three individual determinations were made and compared for different trace rare earths. Table IV shows how reproducible the results were. These deviations were

Table IV. Rare Earth Determinations
(73 comparisons)
(rare earths in rare earth oxide matrix)

Reproducibility

Number	Percent ave. dev.
18	0-5
21	5-20
21	20-50
12	50-75
1	96
73	

observed in separate determinations of samples taken from a particular container of each rare earth oxide. Each determination was treated as an individual analysis. The rare earth impurities in rare earth matrices gave a median value of 20 percent for the average deviation. This breakdown of the reproducibility data indicates that the determination of other rare earths in a rare earth oxide is indeed very promising. Eighteen of the comparisons showed reproducibilities of 5 percent or less.

Table V gives the concentrations of the various rare earth impurities found for the 73 determinations. There is no evidence that the degree of

Table V. Rare Earth Determinations
(73 comparisons)
(rare earths in rare earth oxide matrix)

Concentration range

Number	p.p.m. atomic
11	0.1-1.
30	1.-5.
17	5.-10.
13	10.-100
2	>100
73	

reproducibility was dependent upon the concentration level. Note that over one-half of the cases tested involved concentrations below the 5 parts per million level.

The common metal impurities in the same matrices gave a median value of 38 percent for the average deviation. This latter value however

includes the effects of nonhomogeneity, accidental contamination and the fact that many of the common metal levels found in the rare earth oxides were below the blank level of the pelletizing media.

Table VI gives the comparison for some common impurities of the spark source results and those obtained by atomic absorption measurements on solutions of the impurities concentrated from the samples by chromatographic methods. In most instances the spark source data (in which unit

Table VI. Comparison with Chromatographic Separation-Atomic Absorption Common Metal Determinations (ppm atomic)

	Mass spec.[a]/atomic absorption					
	Er_2O_3	Gd_2O_3	Dy_2O_3	Ho_2O_3	Lu_2O_3	Tb_4O_7
Ni	4./.3	.4/.4	2./<1	.4/.3	3./.3	1./.1
Cr	4./.2	-	6./<1	2./<1	3./.2	2./<1
Cu	11./.7	2./1.6	4./<1	3./.9	10./1.5	5./1.0
Ca	110/50	110/68	34/44	310/120	720/140	300/41
	100[b]	100[b]	(~100[b])	500[b]	300[b]	100[b]

a - Unit sensitivity assumed

b - Emission spectrographic results for Ca

elemental sensitivity was used) is high although the agreement is good in a few cases. The cases of chromium and nickel are at the level of these elements in the original graphite used to make the pellet. We are investigating the use of powdered metals as a pelletizing media, but thus far have found these to be less favorable than graphite from the common metal point of view. The calcium comparisons are more encouraging because of the agreement between the two methods of analysis indicated in the table. The following conclusions may be drawn from our work with the rare earths so far. First, rare earth oxides can be analyzed in a graphite pellet using a simple pelletizing technique. Reproducibility is best for trace rare earths. This fact has an advantage from a practical point of view. Rare earth impurities are difficult to determine in rare earth matrices by chemical techniques. Furthermore the detection level of present emission spectrographic methods is much higher than spark source methods. Here the spark source appears to have a distinct advantage over other techniques.

Serious interferences due to clusters such as those shown previously, are a problem, but they can be handled if all the lines in the region of interest are carefully measured and identified. This can become quite complicated. Complete computer analysis of the spectrum is very helpful in this type of work. We have developed a computer program to do this and find it very helpful.

The rare earth metals do not present serious problems due to clustering but they do present nonhomogeneity problems, especially for impurity elements whose physical properties differ greatly from those of the rare earths. Tantalum is a good example.

The following, outlines studies which we are presently working on as far as rare earths are concerned. Graphite pellets limit determinations of some common metals to the 1 ppm range due to impurities in the graphite and the limiting ratio required to produce a structurally sound pellet. A decrease in the pellet impurity blank must be achieved if common metals are to be assayed below this level. The rare earths may present a unique opportunity to study some of the mechanisms which have been proposed to be involved in the production and the ultimate detection of ions by the spark source mass spectrograph. We expect to use these materials to make closer comparisons of multiply charged ions, cluster levels, relative sensitivities, and ion energy distributions in order to test some of these proposals. An additional advantage of rare earths is the fact that they fall within a relatively narrow mass range and thus simplify the use of electrical detection methods which we believe presents a great potential for improvements on the absolute accuracy of spark source methods.

In connection with the problem of decreasing the pellet blank, a colleague at the laboratory, David Griffith, who also helped with various portions of this work, has found that structurally sound pellets can be made with weight ratios of 15 parts oxide to one part graphite and in much higher ratios with powdered metals. However the high ratio of oxide to graphite changes the thermal conductance and this may offset the advantage of the favorable high atomic ratio. We are investigating the effects of this characteristic.

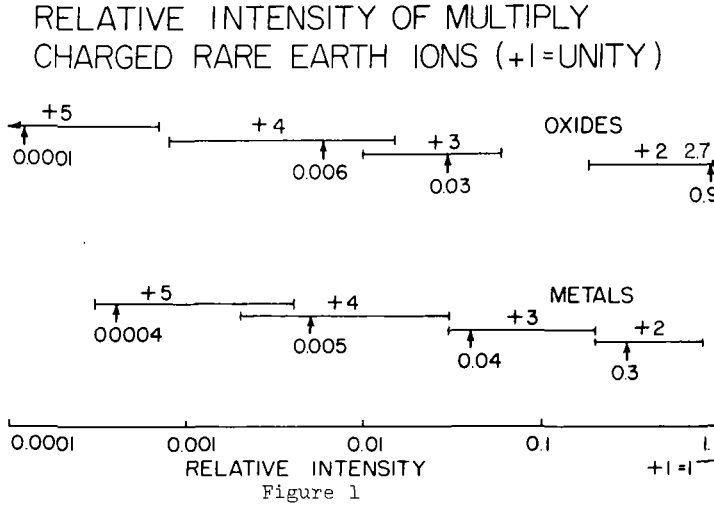

Figure 1

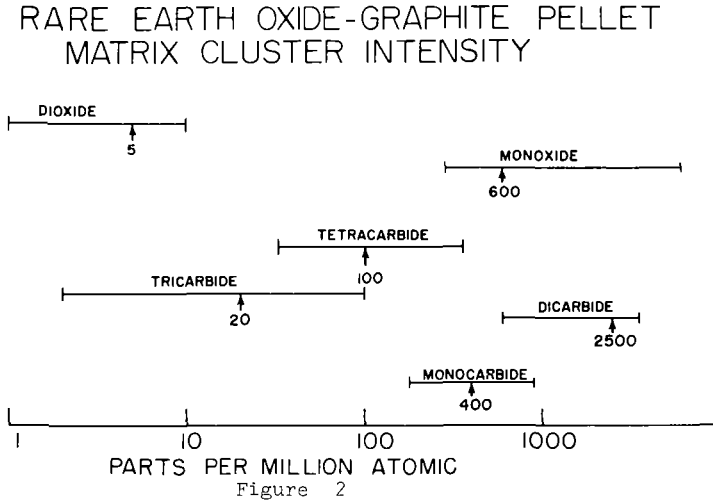

Figure 2

ANALYSIS OF PLUTONIUM METAL BY SPARK SOURCE MASS SPECTROSCOPY

A. J. Johnson
A. Kozy
R. N. Morris

THE DOW CHEMICAL COMPANY
Rocky Flats Division

U. S. Atomic Energy Commission Contract AT(29-1)-1106

ABSTRACT

A spark source mass spectrograph has been used for the determination of impurities in plutonium metal. Over 70 impurity elements are determined with one method and with similar probable accuracy. Elements which require involved procedures for their determination by wet chemical or emission spectrographic methods, such as Cl, F, S, Ta, W, and rare earths, are readily determined using the mass spectrograph. A comparison has been made between results obtained by mass spectrography and results obtained by conventional analytical methods. The operations involving the safe handling of plutonium in the mass spectrograph are also discussed.

INTRODUCTION

Improvements in purification techniques and metal production technology have resulted in the production of plutonium metal of a high degree of purity. The number of impurities and their concentration have been constantly lowered until many are now present at concentrations below the detection limits of routine spectrographic methods. Analysis of the pure metal would require separation and concentration techniques for emission spectrographic measurements. This would mean increased analysis time and higher analytical costs.

A good determination of the degree of purity of a metal requires that the concentration of elements that are not now routinely determined be measured. Formerly, a chlorine or sulfur content of 10 ppm was not very significant when there was a total of over 400 ppm of routine impurities. Now, the chlorine or sulfur might be one of the major impurities. It is, therefore, necessary to determine a greater number of elements in each sample. This again means increased time and costs.

The above considerations indicated that the use of the spark source mass spectrometer for this type of analysis would be desirable and feasible. A low level of detection limits could be attained, a large number of elements are detectable, the reported accuracy seemed acceptable, and the probable increased cost of analysis now appeared justifiable. Work was therefore initiated on a CEC 21-110 mass spectrometer to adapt it for plutonium analysis.

Safe Handling of Plutonium

The dangers from the radioactivity of plutonium are well known (1). In addition it is also a highly toxic material. Plutonium has been termed one of the most toxic elements on which large scale work is now being performed. All nonsolution work with plutonium must be handled in a closed system so that no material is freed into the room atmosphere. This can be done with a completely closed box using rubber gloves, or in an open-front box with controlled draft to keep loose material in the box.

The major plutonium contamination of the mass spectrometer was in the source section. Provisions had to be made so that the sample holders could be removed for changing samples and for containing all the resultant contamination. The electrode positioning controls are on the sample holder, so these had to be manipulated inside the enclosure. The use of a completely enclosed box to contain the source section would have necessitated performing these complex operations through heavy rubber gloves; therefore an open-front box was designed so as to contain the source and permit working in this box with surgeon's gloves. The box has proved to be satisfactory with no escaped contamination problems up to this time. Only plutonium metal samples have been handled in this box; no plutonium powders have been analyzed.

Samples are prepared for analysis in a regular closed-system glove box. In addition to the radioactive and toxic characteristics of plutonium metal, it is also pyrophoric. The cutting and filing of the metal into shapes suitable for electrodes is therefore done in an argon atmosphere. Samples are then transferred to the source box for loading into the instrument.

The source of the instrument became extremely radioactive with the first plutonium sample sparked. An average of 3-4 mg of sample is consumed during each analysis and most of this material remains in the source. It also was possible that enough plutonium was going into the instrument to constitute a hazard when the instrument was opened for necessary maintenance. After the first several weeks of operation, the instrument was opened and the inside surfaces monitored with α-counting instruments. The only areas of significant radioactivity were the slit edges back to and including the beam monitor. When the instrument is first vented, the slits may be removed and placed in a plastic bag. This practically eliminates the chance of contamination being spread. However, if the deposited plutonium is allowed to oxidize, the loose oxide will spread and be a health hazard.

The possible contamination of the photoplate was of prime interest because of handling difficulties if it were radioactive. If all of the plutonium passing the beam monitor reached the plate, the calculated amount deposited there would be about 2.5×10^{-11} grams. The radioactivity from this amount of material would be four disintegrations per minute. Actual determinations of contamination have been at the background level of the counting equipment. No contamination greater than one disintegration per minute has been detected on a developed plate, an undeveloped plate, or in the developer and fixing solutions.

Continuous sampling of the laboratory air has shown that the described method is safe for the handling of plutonium samples for spark source analysis.

EXPERIMENTAL

Instrumental Parameters

The instrument used for this work was a Consolidated Electrodynamics Corporation Model 21-110 Lot 3 double focusing mass spectrometer. One of the electrodes is at 13 KV positive to ground. A 300 cps pulse of 17 µsec duration is applied to the other electrode for the spark analysis of the metal. Source conditions which were found to be difficult to reproduce from sample to sample were sample shape, sample distance to slit, and spark gap. These varying parameters probably contributed to the experimental error. The spectra of the samples were recorded on Ilford QII photoplates.

Standardization

There are very few certified standards of any material that contain impurities at the low levels desired for spark source analysis. A few copper metal standards and an aluminum standard were obtained and used in the initial development work. There are no certified plutonium metal standards at this time. Fortunately, two samples of plutonium metal became available that had been analyzed several times by five AEC Contractors. A comparison could be made between the compiled results and the mass spectrographic results.

ANALYTICAL

The visual method of estimating impurity concentration was used for most of the analyses. In this method, as described by Craig and Wolstenholme (3), a graded series of exposures on the same sample are made and the impurity concentrations calculated using the following formula:

$$C_i = \frac{E_m}{E_i} \times \frac{C_m}{I_i} \times \frac{A.W._i}{A.W._m} \times 10^6$$

where the subscripts m and i represent matrix and impurity, respectively, E is the beam monitor reading where the line of the element is just detectable, I is the isotopic abundance of the impurity isotope in

percent, A.W. is atomic weight, and C is concentration. The concentration of the impurity will be in ppm by weight.

The plutonium samples to be analyzed presented a problem in that the isotopic ratios of the various plutonium isotopes were not constant. To remove the dependence on an additional isotopic analysis on all samples to determine C_m, an empirical E_m was used in the first calculations. The work of Brown, et al. (4), has shown that the basic ion sensitivity of a just detectable line is around 2×10^{-15} coulombs. This was verified from a few test plates, and the empirical value was used for the exposure level of the matrix in all subsequent visual calculations.

RESULTS AND DISCUSSION

The two plutonium metal samples were analyzed and the results were calculated using the visual method. Results by spark source mass spectrography are compared with emission spectrographic results (See Table I). In both samples about 80 percent of the mass spectrographic results are within a factor of two of the emission spectrographic answers; all but Mg and Zn are within a factor of three. The emission spectrographic results are the average of over 25 analyses of all elements except gallium and zinc. Only a few scattered results were available for these elements as they are not requested determinations in this cooperative analysis program. The mass spectrographic results are the average of 20 analyses.

TABLE I

Analysis of Plutonium Metal Samples Compared with Emission Spectrographic Results--Visual

All results in ppm by weight

Impurity Element	Sample A Mass Spectrography	Sample A Emission Spectrography	Sample B Mass Spectrography	Sample B Emission Spectrography
Al	28	13	65	29
Cr	3	3	54	43
Cu	1	2	22	15
Fe	29	40*	308	223*
Ga	1	3	50	25
Mg	36	8	11	7
Mn	7	5	14	10
Ni	7	7	68	54
Pb	5	3	14	5
Si	31	31	105	84
Zn	18	4	19	15
As	<0.05	--	0.2	--
Cl	2	--	4	--
F	0.2	--	0.2	--
P	1	--	8	--
S	9	--	4	--
Ta	1	--	5	--
V	<0.05	--	0.1	--

* Determined spectrophotometrically.

The second group of elements listed in Table I are some which are not routinely determined in emission spectrographic or chemical analysis. These elements, however, are determined as readily by the mass spectrographic method as such routinely determined elements as iron or magnesium. Although no values are available for comparison purposes, the degree of accuracy on these elements should be similar to that found for the other elements described.

The calculation of mass spectrographic sensitivity factors for the elements determined using the emission spectrographic results did not appear promising. Although this worked very well for steel analysis (5), where the calculations were made based on a certified standard, the plutonium metal analyzed could certainly not be considered as meeting the requirements of a basic standard. It would also be more advantageous

to have the mass spectrographic method completely independent of present methods.

Other workers (2, 4, 5) have shown that there are various factors that influence the recording of the ion on the photographic plate. Among them are plate response to mass, Z focusing, and elemental sensitivity. A single factor that would encompass all of these factors would simplify the calculation of impurity content of the samples. A program was therefore started of sparking plutonium and other pure elements and recording their spectra under the same conditions used for the sample analyses. The only difference was that the spectra were recorded at small incremental increases in the beam monitor readings. By this method the exposure of a "just detectable" line could be more accurately estimated. The sensitivities of the various elements were then calculated relative to plutonium.

Table II contains the results on some of the elemental sensitivities that have been calculated. These factors should include most of the recording variables except for matrix effect. This method can thus also be used to determine which elements exhibit significant matrix effects. A good example of a large matrix effect is shown in the case of lead. The factor calculated from the pure lead photoplate was 2.6, a value which gave extremely high comparative answers when used in the analytical calculations. The sensitivity factors calculated for lead in both a copper matrix standard and in two steel standards agreed very closely and is given in Table II; this factor was used in calculating the lead values in the plutonium samples. The gallium factor was calculated in the same manner as that of lead.

TABLE II

Relative Sensitivities by Visual Method

Element	Relative Sensitivity
Pu	1.0
U	1.6
Pt	1.9
In	5.8
Zn	6.1
Fe	7.2
Cr	5.4
Mg	11.1
C	18.5
Pb≠	18.5
Ga≠	11.1

≠ Determined in both steel and copper standards.

The results in the analyses of the two plutonium samples using these factors is shown in Table III. There is closer agreement between the mass spectrography and emission spectrography results for most of the elements. Chromium is the only element for which the analytical spread increased. The emission spectrography values for zinc are not considered as accurate as those values given for the other elements, as only a few scattered values were reported by the cooperating laboratories.

TABLE III

Analysis of Plutonium Metal Samples Using Experimentally Determined Factors--Visual

All results in ppm by weight

Impurity Element	Sample A Mass Spectrography	Sample A Emission Spectrography	Sample B Mass Spectrography	Sample B Emission Spectrography
Cr	3	3	61	43
Fe	25	40	262	223
Ga	0.4	3	27	25
Mg	20	8	6	7
Pb	2	3	5	5
Zn	18	4	19	15

Sensitivity factors and impurity concentrations were also obtained by densitometric methods. A recording microphotometer was used to obtain chart tracings on ion lines of interest on the plutonium and pure element photoplates. Absorbance values were taken from the charts, and the area of the lines were calculated using the method of Owens (6). Values from the plutonium-239 spectral recording were then used to prepare a curve relating plutonium-239 line absorbance to exposure (beam monitor reading). A similar curve was prepared for area measurement.

The exposure necessary for the plutonium-239 line to give an absorbance, or area, equal to that given by a second element line at a certain exposure was then obtained from this curve. The ratio of these exposures, corrected for isotopic abundance, was then termed the relative sensitivity of the second element. Several calculations were made for each element investigated. The average values obtained on some of these elements are shown in Table IV. The increase in the factor with decrease in atomic weight was expected, but the curve was not as smooth as hoped.

TABLE IV

Relative Sensitivities by Densitometric Methods

Element	Relative Sensitivity Absorbance	Relative Sensitivity Area
Pu	1.0	1.0
Pt	1.4	1.6
Zn	5.8	3.0
Fe	11.3	2.6
Cr	5.6	2.7
Mg	12.9	4.0
C	25.7	8.0

The corrections obtained using the experimentally obtained densitometric sensitivity factors are shown in Table V. It also shows the errors that are present if these corrections are not used. The familiar general method of ratioing matrix and impurity exposure levels at some selected line transmission reading, usually chosen at about 40% T, may give acceptable answers for impurities in some matrices such as iron, but not for impurities in plutonium. This is chiefly because of the large differences in line profiles of the plutonium line at mass 239 and the major impurities, which are below 65 on the amu scale. Although the values in the Equal Absorbance-Calculated column were corrected for the reported mass dependence of the Ilford QII emulsion (6), the values are still considerably higher than values by the area method. The method of calculating the absorbance factors included this value in the factor for each element, and this absorbance factor is applied instead of the mass dependence factor.

TABLE V

Analysis of Plutonium Metal Samples by Densitometric Methods

	Mass Spectrographic				
	Equal Absorbance		Equal Area		
Impurity Element	Mass Corrected	Sensitivity Corrected	Calculated	Sensitivity Corrected	Emission Spectrographic
Metal A					
Zn	230	82	58	20	4
Fe	105	20	68	28	24
Cr	25	10	14	5	3
Mg	120	30	97	26	8
C	585	110	755	100	95
Metal B					
Zn	116	42	78	28	15
Fe	1420	280	478	284	223
Cr	268	108	172	68	43
Mg	32	8	30	8	7
C	450	85	486	65	145

The absorbance method would be faster because of less calculations needed, but the area method yields results closer to the emission spectrographic and chemical results. The preliminary work on line intensities and intensity areas as used by Owens (6) give results very similar to those obtained by the above methods, but the precision appears to be better. More work on this is now being performed.

Results at this time indicate that most of the method requirements for analysis of pure plutonium metal have been met by the spark source mass spectrographic analysis. These results are summarized in Table VI.

TABLE VI

Analysis of Pure Plutonium Metal

Method Requirement	Attainable by Mass Spectroscopy
As many elements should be determined as is feasible.	Over 70 elements are determined by the one method.
Low levels of detectability are needed.	Most of the elements can be routinely detected at the 0.1 ppm level.
The accuracy must be adequate.	An accuracy of a factor of three is considered adequate below 10 ppm at the present time.
The cost of analysis must be justifiable.	A cost comparison of the mass spectrographic method and the other analytical methods is difficult to make, as many of the elements determined by the spark source method are not being routinely determined at this time. The total time of analysis, however, has been estimated to be about 2-1/2 times faster by use of the spark source for total trace impurity analysis. The elements F, Na, S, and Cl are included in the spark source time, but not in the other methods time.

The analysis of other actinide metals and their compounds by spark source mass spectroscopy is currently being investigated. The small sample size requirements of this method offer a decided advantage for analyzing these rare and expensive materials.

ACKNOWLEDGEMENTS

We wish to acknowledge the aid of L. A. Desantis and R. E. Schlupp in operating the instrument and in developing the photoplates.

REFERENCES

1. C. F. Metz, G. R. Waterbury, "Treatise on Analytical Chemistry, Part II" edited by I. M. Kolthoff, P. F. Elving, and E. B. Sandell, Interscience, New York, 1962, pp. 206.

2. R. M. Elliott, R. D. Craig, and G. A. Errock, Instruments and Measurements, Vol. 1, Academic Press (1961).

3. R. D. Craig and W. A. Wolstenholme, Ind. Chim. Belge, 29, (1964).

4. R. Brown, R. D. Craig, and J. D. Waldron, "Analysis of Impurities by Spark Source Mass Spectroscopy," Preparation of III-V Compounds, R. K. Willardson and H. L. Goering, editors. To be published.

5. W. L. Harrington, R. K. Skogerboc, and G. H. Morrison, Anal. Chem. 37, 1480 (1965).

6. E. B. Owens and N. A. Giardino, Anal. Chem. 35, 1173 (1963).

ANALYSIS OF ORGANIC THIN LAYERS USING THE SPINNING ELECTRODE SPARK SOURCE MASS SPECTROGRAPH

L. C. Scala, G. G. Sweeney and W. M. Hickam
Westinghouse Research Laboratories
Pittsburgh, Pennsylvania 15235

I. ABSTRACT

Very thin layers of organic compounds were investigated using the spinning electrode spark source mass spectrographic method. Analysis of multilayers of barium stearate (50-225 Å thick) indicated that extremely small quantities of barium (of the order of 2×10^{13} atoms) can be identified. The results of this type of analysis can be used to calculate the actual amount of metal-containing sample when its composition is known.

II. INTRODUCTION

The use of the spark source mass spectrograph for the elemental analysis of solids has been reported by Dempster (1), Hannay and Ahearn (2), Gorman, Jones and Hipple (3) and numerous other more recent workers in the field. The impetus for the rapid growth of this type instrumentation in recent years has been motivated by the usefulness of the instrument in supplying semi-quantitative analysis for trace impurities in high purity inorganic solids. The nearly uniform sensitivity (10^{11} atoms) exhibited throughout the periodic chart, the linear response with concentration, and the simple identification scheme associated with the mass spectra achieved are major factors responsible for this successful growth pattern.

Recently, the use of the spark source mass spectrograph as a microprobe was reported (4). In this work specified volumes as small as 25 microns in diameter and 3 microns depth were analyzed at concentrations as low as 0.1% atomic or an equivalent film thickness of 30 Å. Manually scanning larger areas allowed detection of fractional monolayer equivalent coverages. Although the technique as used exhibited the sensitivity for the detection of very thin films, it did not provide satisfactory spacial resolution to distinguish between bulk impurities and thin films.

More recently a spinning electrode technique was developed (5) in an attempt to overcome this weakness; this method provides a new analytical tool capable of supplying some of the needed compositional information associated with surfaces and reactions on surfaces.

In Figure 1 (see Fig. 1 of the next paper, No. 44) is shown a schematic of the method used in reducing the sampling depth for mass spectrographic analysis in order to provide the desired spacial resolution. The sample to be analyzed is illustrated in the form of a disc mounted on a motor and rotated at 1750 rpm. A stationary point of a noninterfering high purity metal is located near the edge of the disc and less than 25 microns removed from its surface. The linear velocity of the surface with respect to the point is 2 microns per microsecond. High voltage at 800 kc is applied between the point and moving surface to generate ions representative of the sample. The ions are mass analyzed and recorded on a photographic plate using a Mattauch double focusing mass spectrograph.

The disc, whose diameter is 7/8 inch, is usually made of high purity silicon metal, and can be used to support the material to be analyzed. Because of the fact that the spinning electrode technique distributes the energy over a large number of separated small volume increments, thus resulting in a reduction of time at temperature for the sampled volume (new material is brought to the spark at each half cycle of the spark), this method offers considerable promise in the study of organic materials (5,6). In fact, while in the use of the stationary spark technique difficulties are encountered due to the thermal and possibly catalytic degradation of the sample on prolonged exposures at elevated temperatures in contact with metallic surfaces, with further complications brought about by polymerization of smaller molecular fractions, the use of the spinning electrode system minimizes these difficulties because new undegraded material is continuously brought to the spark.

Generally the depth of sampling of this shallow sampling technique was found to be of the order of 2000 Å for inorganic samples; however, in surface and thin film studies, it is highly desirable to specify both the composition and spacial arrangement to much smaller dimensions. A promising approach seemed to be that of combining the spinning electrode spark source analysis method with the Langmuir technique for preparing compacted monomolecular layers or otherwise extremely thin films of the order of 25-100 Å thickness.

Langmuir films can be prepared by depositing on the surface of water or aqueous salt solutions a known number of molecules of amphipathic molecules (that is, containing both hydrophilic and hydrophobic groups) (7-11). These molecules orient themselves approximately perpendicularly to the aqueous surface; if lateral compression is carefully applied, the molecules can be compacted into a sheet, whose thickness is given by the length of the molecules and whose area is determined by the sum of the cross sectional areas of the molecules. In this manner films can be obtained of known uniform thickness, which can be transferred onto metallic substrates, such as silicon wafers, by the simple expedient of raising and lowering the solid substrate through the monolayer while the latter is maintained under pressure. By repeating this procedure, one can build up multilayers of known thickness. A classical example of amphipathic molecules that behave as described is stearic acid and some of its salts (soaps), such as the barium and calcium stearates. In the case of the acid, its molecules are about 25 Å long and approximately 20 $Å^2$ in cross section.

Monomolecular layers of many other types of compounds besides fatty acids have been studied. Polyvinylbenzoate (PVB) has been spread monomolecularly, as has polyvinylacetate (12-14). Albumins, proteins, sterols (especially cholesterol), digitonin, high molecular weight alcohols have all been investigated extensively (15-17). In most cases one of the most important factors in the monolayer formation and characteristics is the pH of the aqueous subphase. For example, when stearic acid molecules are spread over an aqueous subphase containing Ca or Ba ions, the extent of formation of the respective stearate salt is a function of the pH of the solution; at pH 11 the films are pure neutral soaps, while at pH below 5 the films consist of free fatty acid molecules (21).

III. EXPERIMENTAL

A. Preparation of Samples. Langmuir films were prepared according to the method and using the apparatus described by Ries and Handy and Scala (18, 19). The stearic acid used was Eastman Kodak best grade, m.p. 69-70°C, dissolved in Fisher Spectranalysed n-hexane (0.274 g of acid/100 cc of solution). The polyvinyl benzoate (14) employed in this work was dissolved in purified benzene to a concentration of 0.100 g in 50 cc of solution. The cholesterol used was also dissolved in benzene to a concentration of 9.32×10^{17} molecules per λ of solution. Buffer solutions containing barium or copper ions were used as the aqueous subphase; the pH of these buffered solutions was altered as necessary by addition of acetic acid or ammonium hydroxide as required. Polyvinyl benzoate and stearic acid thin films were layered on nearly neutral water, cholesterol films were spread on aqueous subphases containing copper ions. All these layers were transferred onto high purity silicon slices by dipping the slices vertically into the monolayers as described above, except in the case of PVB, where the slices were held horizontally under the monolayer before transfer.

Table I identifies the samples and summarizes conditions of preparation.

TABLE I

Identification and Layering Conditions of Spark Analyzed Thin Films

Sample No.	Compound	Transfer Pressure, dynes/cm	pH of Subphase	No. of Layers
1	Stearic acid	30.2	7.05	3
2	"	"	"	9
3	Ba stearate	35.8	6.9	1
4	"	"	"	2
5	"	"	"	9
6	"	30.2	5.1	9
7	"	"	7.05	9
8	"	"	8.90	9
9	Cu stearate	34.9	5.5	9
10	PVB	25.5	7.15	2
11	Cholesterol	30.2	5.0	8
12	"	"	"	10

B. Conditions for Spark Analysis. The prepared samples were placed on a metal pedestal mounted on the shaft of a motor as shown in Figure 1 (see Fig. 1 of the next paper, No. 44). The mass spectrograph was pumped with an ion getter pump to a pressure of 10^{-7} torr. Voltage of the order of 30-50 KV at 800 KC was applied between the gold point and the rotating film. The point was moved radially during the recording of the mass spectra. The scanned area approximated 1 cm^2 and corresponded to an outer diameter of 1.9 and an inner diameter of 1.5 cm. The major ions observed in the spectra on Ilford Q-2 plates were gold, silicon, carbon and oxygen. Ions associated with the monomolecular film were of the order of 1-0.1%, the intensity of the gold and silicon ions.

IV. RESULTS AND DISCUSSION

Samples 1 and 2, where 3 and 9 layers of stearic acid had been transferred, gave no spectra. This may be due to the relatively high vapor pressure of stearic acid (20) which would be responsible for the vaporization of the sample material before application of the spark. Samples 3, 4 and 5, containing 1, 2, and 9 monolayers of Ba stearate, respectively, gave interesting results. While in Sample 3 (1 Ba stearate monolayer) both the spectra of Ba and of the organic moiety were absent, the spectra of samples 4 and 5 (2 and 9 Ba stearate monolayers) showed not only the presence of increasing quantities of Ba but also, for longer exposures, the presence of hydrocarbons in the mass range of 24-27 and 36-44. This confirms the statements made by Schonhorn (20) that metallic soaps are much more stable than the corresponding fatty acid when exposed to vacuum (compare the results from the sample with 3 stearic acid monolayers with those from the sample with 2 barium stearate monolayers). In addition, the fact that the mass of the hydrocarbons detected is relatively small indicates that the 18 carbon atom chain of the stearate entity is broken into segments containing from 1 to 3 carbon atoms.

The results of the spark analysis of samples 6, 7, and 8 confirms the result of Langmuir and Schaefer (21) on the effect of pH on the formation of metallic soap. Thus, while sample 6 (pH 5.1, 9 layers) gave only questionable evidence of the presence of Ba in the multilayer, the spectra from samples 7 and 8 (9 layers, pH 7.05 and 8.9 respectively) strongly indicated not only the Ba was present but that the sample obtained at pH 8.9 contained more Ba than the sample obtained at pH 7.05. The spark method for analyzing small concentrations of material has, therefore, provided an additional proof of the pH effect on stearate monolayers. One must bear in mind, however, that the pH effect varies in magnitude according to the kind of metallic ions dissolved in the subphase. For example, sample 9 contains 9

layers of Cu stearate prepared on buffered subphase at pH 5.5, at which the salt formation is reportedly approximately 50%. Even though it was a weak exposure, the spectrum from this sample did show copper lines just above the detectable limit of the photoplate.

Polyvinylbenzoate (PVB, sample 10, 2 layers) did not give any meaningful spectra. This may have been due to the fact that 2 PVB layers are extremely thin (of the order of 5-6 Å each), as compared to monolayers of stearic salts (~25 Å) and therefore too small to be detected, or that the transfer of PVB layers to the Si slice was not successful. When one considers that a thin layer of a polymer on water does not consist of a regularly arranged array of molecules as in the case of stearic acid, but rather of a disordered conglomeration of interweaving polymeric chain, one can visualize the difficulty of transferring efficiently a portion of this material on to a solid substrate.

Finally, samples 11 and 12 (8 and 10 layers of cholesterol respectively) also failed to give spectra containing recognizable and meaningful lines. Here also the transfer technique may have been at fault. In fact, cholesterol films were transferred to Si slices held vertically; it is possible that the slices cut through the film without picking up any portion of it. The technique used in the case of PVB, namely that of positioning the slice horizontally and flat under the monolayer and then to raise it through the film might have given better results.

V. CONCLUSIONS

Most of the work described here involves Ba stearates in some form. At pH's ranging from 6 to 7, the transformation of the stearic acid to barium stearate is of the order of 50%. The area on the Si slice covered by the spark is approximately 1×10^{16} A^2; considering each molecule of stearate to have a cross sectional area of 20 A^2, and bearing in mind that the compaction pressure at which these layers were made was such that the resulting films contained about 10% voids, the area covered by the spark would contain about 4.8×10^{14} molecules of stearate, and about 1.2×10^{14} atoms of barium, if the Si slice was originally coated by the monolayer. In the case of 2 monomolecular layers, the area in depth would contain $\sim 9.6 \times 10^{14}$ molecules of stearate and correspondingly $\sim 2.4 \times 10^{14}$ atoms of barium.

In the cases where exposure to spark showed the presence of barium, the latter's 135-136 isotopes (considered to constitute between 7 and 8% of the total barium present) can be seen. This means that, on the basis of the maximum barium content of two monolayers in the sparked zone of 2.4×10^{14} atoms, about 10% or 2.4×10^{13} atoms of barium could be detected. For this reasoning to be acceptable, one must assume that the spark reaches through two, and in other cases, nine monolayers, with thicknesses ranging from 50 to 225 Å. Thus, this technique is a very sensitive one.

While its value for the determination of the structure of organic compounds has not been fully ascertained, at least in this work, possibly because of experimental difficulties, the spinning electrode spark source mass spectrographic analysis of extremely thin organic films of known composition in combination with metal additives or substitutes lends itself to surface studies in general, and to investigation of catalytic mechanisms in particular. This could be done by judicious choice of metal substrates and analysis environments.

REFERENCES

1. Dempster, A. J., Proc. Am. Phil. Soc. 75, 755 (1935).
2. Hannay, N. B., and Ahearn, A. J., Anal. Chem. 26, 1056 (1954).
3. Gorman, J. G., Jones, E. G., Hipple, J. A., Anal. Chem. 23, 438 (1951).
4. Hickam, W. M., and Sweeney, G. G., Rev. Sci. Instr. 34, No. 7, 783 (1963).
5. Hickam, W. M., and Sandler, Y. L., in "Surface Effects in Detection", J. I. Bergman and A. Dravnieks, Editors, Spartan Books, Inc., Washington, 1965, pg. 192; W. M. Hickam and G. G. Sweeney, "Mass Spectrometric Analysis of Solids", A. J. Ahearn, Editor, Elsevier (in press), Chapter V.
6. Kessler, T., Hickam, W. M., Sweeney, G. G., and Sharkey, A. G. Jr., Proc. 13th Annual Conf. on Mass Spectrometry and Allied Topics, St. Louis, May 1965, abs. 89, p. 452.
7. Langmuir, I., J. Am. Chem. Soc. 39, 1848 (1917).
8. Langmuir, I., J. Franklin Inst. 218, 143 (1934).
9. Blodgett, K. B., J. Am. Chem. Soc. 56, 495 (1934).
10. Blodgett, K. B., J. Am. Chem. Soc. 57, 1007 (1935).
11. Adam, N. K., "The Physics and Chemistry of Surfaces", Oxford University, London, 1941.
12. Ries, H. E. Jr., Beredjick, N., and Gabor, J., Nature 186, 883 (1960).
13. Ries, H. E. Jr., and Walker, D. C., J. Colloid Sci. 16, 361 (1961).
14. Scala, L. C., and Handy, R. M., J. Applied Polymer Sci. 9, 3111-3122 (Sept. 1965).
15. Langmuir, I., Schaefer, V. J., and Sobotka, H., J. Am. Chem. Soc. 59, 1406 (1937).
16. Langmuir, I., and Schaefer, V. J., J. Am. Chem. Soc. 59, 1751 (1937).
17. Deo, A. V., et al., Nature 187, 870 (1960); ibid, 191, 378 (1961).
18. Ries, H. E. Jr., Scientific American 204, 152 (1961).
19. Handy, R. M., and Scala, L. C., J. Electrochem. Soc., in press.
20. Schonhorn, H., J. Colloid Sci. 18, 445 (1963).
21. Langmuir, I., and Schaefer, V. J., J. Am. Chem. Soc. 58, 284 (1936).

SPINNING ELECTRODE SPARK SOURCE MASS SPECTROGRAPHIC STUDY OF PVC CONTAINING TiO_2

G. G. Sweeney and W. M. Hickam
Westinghouse Research Laboratories
Pittsburgh, Pennsylvania

L. B. Crider
B. F. Goodrich Chemical Company
Avon Lake, Ohio

ABSTRACT

The spinning electrode spark source mass spectrographic technique has been used to examine samples of extruded rigid polyvinyl chloride (PVC) compound containing micron and submicron particles of TiO_2. The failure to observe Ti in the mass spectra of the extruded samples suggests that all the micron and submicron particles of TiO_2 are coated or that the high voltage radio frequency spark is unable to excite Ti ions in this matrix using the spinning electrode configuration. Evidence of the presence of Ti is obtained on a freshly machined sample but at a concentration far below that at which it is present. Stationary electrode spark source mass spectrometry reveals the Ti at its expected concentration level.

I. INTRODUCTION

Early use of the stationary electrode spark source mass spectrograph for organics was reported by Hodgson, Desjardins and Baun.[1] The results revealed in the compounds examined that the parent ion molecule intensity was reduced relative to the fragment ion intensity when compared to results obtained on a gas mass spectrometer using an electron impact source. Hickam and Sweeney[2] reported on the use of the spinning electrode source for obtaining the mass spectra of some organic materials. Kessler, Hickam, Sweeney, and Sharkey[3] used the technique in the analysis of coal and coal tar products. They reported the analysis of synthetic mixtures of anthracene and chrysene based on the parent molecule ion in the mass spectra obtained with the spinning electrode configuration. The results of this work indicated that the spinning electrode configuration has considerable advantage over the stationary electrode configuration by providing a higher yield of the parent molecule ion species. This was interpreted to result from the introduction of the undegraded organic sample to the spark at a rate comparable to the running frequency of the spark. The relative velocity of the sample with respect to the point was approximately 2 microns per microsecond. This allows a sample travel distance of 1.2 microns for each half cycle firing of the 800 KC high voltage used in generating the spark.

This paper concerns the use of the spinning electrode configuration in the study of extruded sheet of PVC containing TiO_2 small particles.

II. EXPERIMENTAL PROCEDURE

The instrumentation utilized in this series of experiments was a mass spectrograph of the Mattauch-Herzog geometry using a radio frequency spark as the source of ionization. Fig. 1 represents schematically the special features of our instrument with the spinning electrode technique. A flange has been added to the source housing to allow sufficient space for the incorporation of a DC motor. The motor is driven at 1750 rpm by a battery located outside the vacuum system. Both sample and motor are connected to the high voltage supply. A sample in the form of a disc is placed on the motor platform and held in place by a retaining cap. A radio frequency spark is drawn between a counter electrode (gold) and the spinning sample. The operation of the instrument is described in the literature.[4,5] Major advantages of the spinning electrode system is the ability to restrict sampling depths to the order of a few thousand Angstroms and its potential usefulness in studying solid organics with less thermal degradation than the conventional stationary electrode system. Ilford QII plates are used for detection. The mass range covered is from 12 to 150 m/e units.

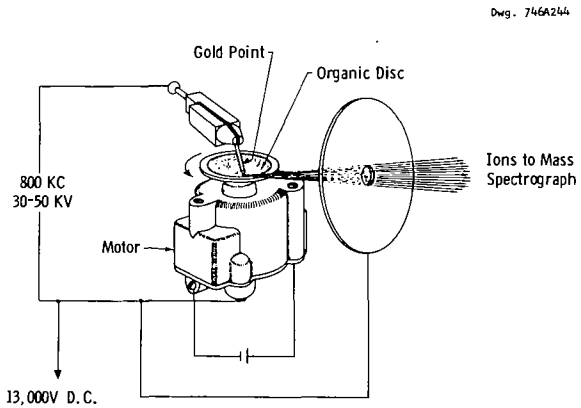

Fig. 1— Mass spectrographic rotating electrode source

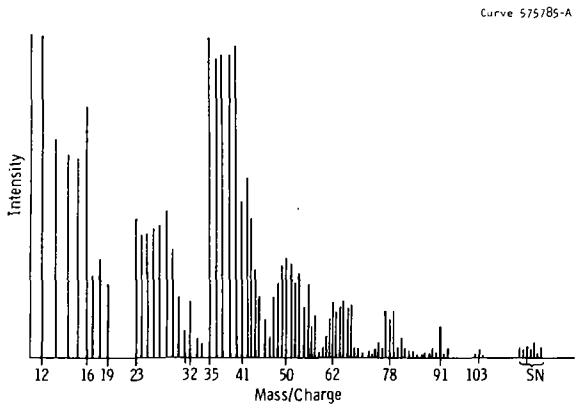

Fig. 2—Typical mass spectrum of PVC sample

III. SAMPLE IDENTIFICATION

The sample composition can be described as being a rigid PVC compound that contains about 15 wt. % TiO_2. The compound also contains a small amount of processing acid (organic salts of a fatty acid) and a thio organic tin stabilizer. The samples were cut in the form of a disc 7/8" diameter from 1/16" thick extruded sheets. The PVC containing TiO_2 is non-conducting and required a conducting film for sparking. A 500 Å film of aluminum was evaporated on most of the samples. Six of the samples were coated with gold. The film served to provide conductivity to the sample. It may act as a control to limit the depth of sampling.

IV. RESULTS

The mass spectra obtained of the samples using this technique reveals the constituent groups associated with the organic fraction of the sample, hydrogen chloride, chlorine, potassium, calcium, tin and fluorine. Although TiO_2 is present at a concentration of 15 wt. %, little or none is evident in the mass spectra. Spectra obtained from all the original samples are identical and reproducible except for minor details. Increasing the exposure brought out more lines but the ratio of adjacent lines remained in general the same. This presents a difficulty in establishing any quantitative data. A typical mass spectra is presented as a line graph in Fig. 2. The most intense group aside from carbon itself is that from 35 to 41 due to hydrogen chloride, chlorine, K and Ca. The other clusters are due to organic groups. The C_n groups decrease in intensity with increasing mass. The outstanding lines in the upper mass range are the 77-78-79 and the 91 peak. The spectra resemble that obtained in electron impact gas mass spectrometric studies of the thermal degradation products of these materials. Tin can be seen in many of the spectra. It is estimated that the total tin content of the sample is of the order of 0.5%. On certain exposures isotopes are observed which are only 5% of the total tin present. This establishes a range of .025% as a detectable limit for impurities having the same sensitivity as tin in films examined. Exposures were varied so as to bring out the most important features of the spectra.

All the samples gave a line at mass 19 which is interpreted to be fluorine. Using carbon 13 as a reference standard the fluorine concentration would be about 0.3%. The intensity of the line does not appear to go up with exposure indicating a surface impurity associated with the PVC or conducting film.

It is known that the TiO_2 concentration in the samples should be of the order of 15 wt. %. It is not clear why the Sn is observed and the Ti is not. The TiO_2 is a filler in the form of micron and sub-micron size particles. The spectra suggest that either little or no TiO_2 is present in the surface film or that the radio frequency spark is highly selective in ionizing TiO_2 in this matrix. To investigate this problem a diamond tool was used to remove .005" from the surface of the samples. A 500 Å Al coating was again evaporated and the samples re-examined. Fig. 3 shows the original spectrum of the sample. Fig. 4 is the spectrum obtained after machining, showing a marked increase in the Ti (48) line. Longer exposure on the same sample gave doubly ionized lines confirming the presence of Ti. Other machined samples were examined but gave no positive indication of Ti.

The PVC was next studied with a stationary electrode configuration. Scrapings from the interior of a sample were taken, mixed with some gold powder and packed in a silver electrode. Fig. 5, first exposure shows Ti at a concentration equivalent to that of chlorine. On the second and third exposure one can see the doubly ionized species at m/e 23.5 and 24.5 corresponding to the 47 and 49 isotopes of Ti.

V. SUMMARY AND DISCUSSION

The spinning electrode spark source mass spectrograph technique has been used to examine samples of PVC containing TiO_2 micron and sub-micron particles. The organic portion of the mass spectrum closely resembles that obtained in examining the thermal degradation products of these materials. The major ions observed correspond to C, HCl, Cl, Ca and K. Tin is present in the few tenths of a per cent level. It is estimated from the isotopes of tin that one tenth of this quantity could easily be detected. Fluorine is observed at an estimated concentration of a few tenths of one percent. Although Ti is incorporated within the sample at approximately 9 weight percent concentration in the form of powdered TiO_2, little or no evidence of Ti is found in the mass spectrum on the original sample surface.

The absence of Ti in the spectra may be indicative that few or no TiO_2 uncoated particles are present within the sampling depth or it might suggest that little or no ionization of Ti occurs in sampling with the spinning electrode technique when the Ti is incorporated as TiO_2 in the PVC matrix. In an attempt to establish which of these conditions prevailed, a diamond tool was used to machine .005" from the surface. Evidence was obtained that the Ti content of the new surface of the sample was higher than the original surface. However, the results were not entirely conclusive. Some spectra obtained on the machined surface did not show any detectable increase in Ti. Particles of the PVC removed from the interior of a sample were mixed with gold powder packed in a silver electrode and analyzed using a stationary gold counter electrode. The spectrum showed Ti of comparable intensity to the HCl and Cl, which were the most intense lines in the spectra. If the TiO_2 particles were all coated it may be that the depth of penetration in sample with the spinning electrode was insufficient to penetrate the coating. Although inconclusive, evidence has been obtained which suggests that the concentration of TiO_2 on the surface is lower than in the bulk. The failure to observe the Ti at high concentration in the bulk using the spinning electrode technique suggests that the energy of the spark is preferentially absorbed by the organic fraction of the sample. This would be consistent with the spinning electrode spark spectra obtained on anthracene, phenanthrene, and chrysene which closely resembled those obtained by electron impact at electron energies of 25 to 50 eV.

The high halogen content of the sample may alter the characteristics of the spark through the formation of negative ions. If this mechanism provides a more rapid extinction of the spark, it could be effective in decreasing both the on time and temperature achieved in a single cycle of the spark. Sulfur hexafluoride gas is used in the electrical industry for electrical discharge extinction and its functioning in this capacity is related to negative ion formation. Electron attachment leading to negative ion formation, in the spark discharge could also alter the positive ion spectra observed. The preponderance of carbon in the matrix along with the halogen may also lead to a number of carbon-chlorine negative ion species.

The fact that Ti is observed at high concentration in the stationary electrode configuration, reveals the importance of sample temperature elevation in obtaining representative mass spectra for a matrix containing materials of high electrical resistance.

It is interesting to note that a proposed advantage of the spinning electrode is to provide homogeneous ion sampling in segregated samples. The technique would therefore provide an average compositional analysis where this could not be achieved in the stationary electrode configuration. In the PVC matrix containing TiO_2 particles, the mass spectra achieved with the spinning electrode configuration reveal the enhancement of sample segregation when compared to the mass spectra obtained using the stationary electrode configuration. The failure to observe Ti in the spark source mass spectra of the PVC matrix containing 15 wt. per cent TiO_2 particles using the spinning electrode, when it was expected that concentrations of 100 ppm would be detected, is an example of non-uniform sampling with the radio-frequency spark. It suggests the possibility that the much discussed poor reproducibility of spark source mass spectrographic results should be critically reviewed and examined in light of possible compound formation in solids. The high sensitivity and wide mass range covered make it a powerful tool for investigations of this nature.

REFERENCES

(1) F. N. Hodgson, M. Desjardins, and W. L. Baun, Tech. Documentary Report No. ASD-TDR-63-383.

(2) W. M. Hickam and G. G. Sweeney, Paper 41, Annual Conference on Mass Spectrometry, Montreal (1964).

(3) T. Kessler, W. M. Hickam, G. G. Sweeney and A. G. Sharkey, Paper 90, Annual Conference on Mass Spectrometry, St. Louis (1965).

(4) W. M. Hickam and G. G. Sweeney, Chapter V, "Mass Spectrometric Analysis of Solids", A. J. Ahearn, Editor, Elsevier Publishing Co. (in press).

(5) W. M. Hickam and Y. L. Sandler, "Surface Effects in Detection", J. I. Bregman and A. Dravnieks (Editors), Spartan Books, Inc., pp. 192-196, 1965.

MASS SPECTRA OF SAMPLES

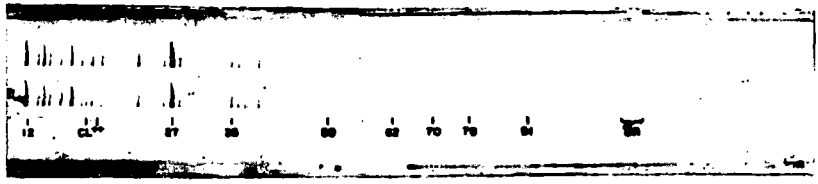

Fig. (3) Sample 107-9 AL Before Machining.

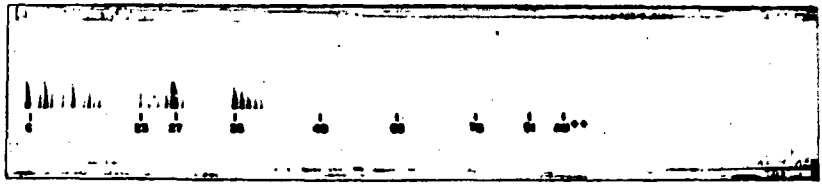

Fig. (4) Sample 107-9 AL After Machining.

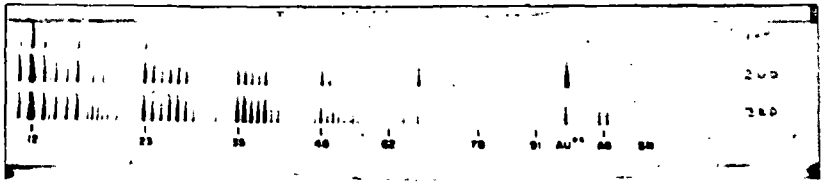

Fig. (5) Sample Packed in Silver Electrode.

SOLID PROPELLANT INVESTIGATION WITH SPARK ION MASS SPECTROGRAPHY

By

BERGE B. GOSHGARIAN

I. INTRODUCTION

Additives to solid propellants affect their burn rates, but their role in the combustion processes has not been determined.

This investigation was undertaken to show that spark ion source double-focusing mass spectrography can be useful for providing information on solid propellant combustion. The high voltage spark provides the temperature and electron bombardment necessary to combust the propellant and ionize the products. This occurs very close to the ion accelerating slit; consequently, the majority of the ions formed are accelerated and collected on the sensitive photographic plate for a complete analysis.

The double-focusing geometry resolves the many nominal mass, multi-ion peaks obtained from solid propellant combustion. Therefore, all ion species formed can be identified, and the effect of additives on them studied.

II. EXPERIMENTAL

A CEC 21-110 double-focusing mass spectrograph equipped with an RF spark ion source and photographic plate ion detection system is being used in this study. The Lot 3 instrument source housing was modified by adding another pumping station and ion gauge. This added pumping reduced source pressure during sparking from 1×10^{-5} torr to 4×10^{-6} torr. The electric sector diffusion pump was replaced with an 80 liter/sec ion getter pump, and the sector is continually heated to reduce background contamination.

Ilford Q-2 photographic plates used for ion detection were developed using the procedure described in the tentative recommended practice issued at the 1965 meeting (1).

Ion lines were reduced to normalized ion exposure values and were corrected for line width and background variations by methods similar to those presented by Hull (2) and Owens and Giardino (3). No corrections for the ion mass response of the photographic plate emulsion were made, since only relative ion concentrations were studied. Also, the radius of curvature of the ions in the magnetic sector was kept constant throughout the study.

The propellant samples were initially conditioned at 50°C in a vacuum oven for four hours, or until the pressure stabilized below 10μ. The samples were then cooled and packed in cupped silver electrodes, using the flat end of the bit used to drill the 1/16" x 1/16" cup on one end of the 1/8" diameter electrode. A sample electrode and a pointed silver probe electrode were loaded in the mass spectrograph source and pumped down overnight. Source pressure prior to sparking was approximately 2×10^{-7} torr. A 15-minute delay between sparking for a spectrum was maintained to allow the source vacuum to return to the low 10^{-7} torr region.

a. Sparking Parameters

Initial studies were conducted to determine the optimum instrument parameters for uniform sample ionization at source pressures below 1×10^{-5} torr and for optimum instrument resolution. These parameters were spark energy, pulse repetition rate and length, electrode-to-first-slit distance and electrode configuration.

Figure I shows the effect of increasing pulse amplifier power from 1 KV to 3 KV. Resolution decreased and source pressure increased. The ion peaks also broaden due to increased energy spread of ions which are formed. The source pressure at 1 KV energy rises to approximately 4×10^{-6} torr during sparking, while at 2 KV energy, the pressure rises to greater than 1×10^{-5} torr. Source pressures as high as 8×10^{-5} torr have been obtained at 3000 repetition rates and 2 KV energy. Manual pulsing of the spark must be conducted when high energies and repetition rates are used in order to maintain low source pressures. High repetition rates also tend to be more selective in sample spark position, while at repetition rates of 100 the spark travels from probe tip to the edges of the cupped sample electrode, producing more uniform spectra.

An increased concentration of polyatomic ions relative to monatomic ions occurs with increased pulse amplifier power. Figure 2 shows two plots for average polybutadiene spark spectra. A definite increase in concentation of hydrogen-containing polyatomic ions can be seen with increased pulse amplifier power. Almost no change occurs for molecules containing only carbon. Increasing the spark energy volatilizes more of the sample and reduces the sample degradation into monatomic ions which occurs more readily on the sample surface.

Another test was conducted to determine the affect of electrode-to-first-slit distances on ion yield and resolution. Figure 3 shows a strip chart recording of two sets of peaks at m/e 16 and 17, obtained at electrode slit distances of 5 mm and 3 mm.

The ion lines become much sharper as the electrode-slit distance is reduced, presumably due to better focusing on the beam-defining slit. Ion yield is reduced from an average of 4×10^{-12} amps at 5 mm to $1 \times 1 \times 10^{-12}$ amps at 3 mm.

The sparking parameters, therefore, being used in these studies are: 100 repetitions per second; 10 microsecond pulse width; 1 KV pulse amplifier power; and electrode-slit distance of 3 mm. With these parameters, source pressure is maintained below 1 x 10^{-5} torr, ion yields at the beam monitor average 1 x 10^{-12} amps, spectral non-uniformity is minimized, and optimum resolution for our instrument is obtained.

b. Computer Program

A computer program is presently being evaluated for photographic plate ion line data reduction. The system transmits the ion line density from a microphotometer through a voltage-to-frequency converter to an analog to digital converter. The signal is then fed to an SDS 910 digital computer for tape recording. An IBM 7040 is used to reduce the tape data.

A computer printout is shown in Table I. The heading consists of program input which includes the photographic plate calibration constant, and the ion masses at the beginning and end of a spectral run. Plate saturation is obtained directly from a saturated ion line transmittancy run prior to a spectral run. The program computes the ion exposure integral, which includes integrated line area and corrections for background fog variations. At present only the distance, maximum density counts, ion mass, and ion line exposure integral are printed. Future plans will include emulsion mass response corrections and selected mass summations.

The computer output for a propellant spectral run is plotted against hand calculation data for the same spectrum and is shown in Figure 4. Good correlation was obtained between the two data acquisition methods. The hand calculation method used is similar to the ones referenced earlier in this paper. Parts of this program are similar to those reported by Kennicott (4), Woolston (5), and Olsen (6) at the 1965 meeting.

III. RESULTS AND DISCUSSION

In order to study the spark spectra of solid propellants, initial studies with ammonium perchlorate are being conducted. Table 2 shows four spark spectra of ammonium perchlorate. Good spectral uniformity is obtained for this and similar compounds since sample non-uniformity is omitted. Also, all the neutral species formed during sparking are gases and are removed from the system, eliminating sample buildup on parts of the electrodes, holders, and vacuum chamber. As long as spark energy, repetition rate, and pulse width are kept constant, reproducible spectra can be obtained within $\pm$ 5% of the average exposure values.

Spectral ion exposure data (between different photographic plates) vary by as much as $\pm$ 20% of the average exposure values for the same compound, as shown in Table 3. This variation may be caused by differences in emulsion response between plates, and it can be reduced somewhat by exercising care in obtaining the plate calibration constant. Also, when comparing ammonium perchlorate against a mixture containing ammonium perchlorate, both sample data are collected on one photographic plate, thus reducing response variations.

Understanding how ammonium perchlorate decomposition is affected by low concentration of metallic additives is one phase of this study. Compilation of over 40 spark spectra each of normal and additive ammonium perchlorate indicate that the most pronounced changes occur with the OH, HCl, and ClO ion species. The OH ion concentration decreases while HCl and ClO increase with increased additive concentrations. Further studies are being conducted to clarify the proposed mechanisms involving the observed ion concentration changes.

The next phase of this study is the investigation of composite propellant combustion. A composite propellant contains a hydrocarbon binder, an oxidizer, and a metal. The composite propellant under investigation contains 16% polybutadiene, 16% aluminum (5 micron particle size) and 68% ammonium perchlorate (90% 20 micron particle size). Table 4 shows a number of spark spectra for this propellant. Pressure in the source averaged 3 x 10^{-6} torr during the sample sparking, with average ion yields of 8 x 10^{-13} amps. More ion concentration variation occurs between the individual propellant spectra than between the ammonium perchlorate spectra, because of propellant sample non-homogeneity and increase in quantity of reactions in the spark.

Subtracting spark patterns for binder and oxidizer from the propellant spark pattern shows, as in Figure 5, that 68 atomic percent of the polyatomic ion concentration remains. Combustion products, like CO, HCl, and H_2O, plus partially reacted binder and oxidizer are readily observed to remain in the subtracted pattern. The changes in relative concentrations, as in the case of NH_3 and NO, can be explained by various reaction mechanisms. One would expect the NH_3/NO ratio to increase in the propellant combustion. The more favorable reaction of oxygen from perchlorate decomposition, with hydrocarbons to form CO, reduces the quantity of oxygen available for the NH_3/NO reaction.

Additives to solid propellants affect combustion characteristics. Figure 6 shows

TABLE 1

21-110 SS MASS SPECTROMETER

Plate No. S01116 Run Date 18 January 1966 Exposure No. S-5 Sample Prop. 1-R

Plate Calib. Constant 0.850 Plate Saturation 4.0 Ref. Mass (1) 12.00000 (2) 45.99290 Distance

0 pct transmittancy = 1960. cts 100 pct transmittancy = 66. darkest line transmittancy = 1880 :TS

DISTANCE	MAX CTS	MASS	EXPOS INTEG.
1.747	1784.	12.0000	0.24557407E 04
11.629	1150.	13.0083	0.13249656E 03
16.205	1518.	13.4890	0.28846184E 03
20.987	1624.	14.0007	0.46887814E 03
30.174	1151.	15.0103	0.12769377E 03
34.430	420.	15.4900	0.15195749E 02
38.851	1740.	15.9963	0.11770941E 04
39.054	1458.	16.0197	0.25874590E 03
47.442	1473.	17.0033	0.21963911E 03
47.639	1505.	17.0268	0.24285284E 03
51.429	1304.	17.4811	0.13821643E 03
55.773	1529.	18.0092	0.28235337E 03
55.961	1124.	18.0323	0.95067791E 02
59.587	911.	18.4794	0.50949878E 02
63.882	1068.	19.0161	0.80935867E 02
101.185	737.	24.0006	0.31460194E 02
108.225	817.	25.0064	0.47876851E 02
115.125	1248.	26.0121	0.14798600E 03
121.616	1664.	26.9763	0.77269690E 03
121.891	685.	27.0176	0.45954649E 02
128.308	1255.	27.9888	0.18995724E 03
134.839	533.	28.9950	0.20573429E 02
141.147	1452.	29.9836	0.27767171E 03
141.240	603.	30.9542	0.25638969E 02
153.481	1219.	31.9645	0.16334386E 03
171.399	1662.	34.9550 - C1	0.86745524E 03
177.272	1151.	35.9643	0.13506824E 03
182.930	1395.	36.9503 - C1	0.28875454E 03
188.630	653.	37.9570	0.48399811E 02

(Continued next pg.)

TABLE 1 (Cont'd)

194.512	483.	39.0101	0.21527343E 02
221.328	523.	43.9938	0.28328918E 02
231.655	597.	45.9929	0.36099313E 02

Cl^{35} = 75.03% Comp. 75.4% Actual
Cl^{37} = 24.97% Comp. 24.6% Actual

TABLE 2

AMMONIUM PERCHLORATE RELATIVE INTENSITY PATTERN - SO 2286

	4×10^{-11}C N-2	7×10^{-11}C N-3	1×10^{-10}C N-4	6×10^{-11}C N-5	Average
N	6.61	8.48	10.0	9.22	8.58
NH	.38	.36	.32	.28	.34
O	17.3	17.6	29.1	26.2	22.5
NH_2	.50	.47	.46	.40	.46
OH	1.60	1.57	1.65	1.85	1.67
NH_3	1.00	1.00	1.00	1.00	1.00
H_2O	3.04	3.04	3.07	3.06	3.05
NH_4	.43	.49	.41	.42	.43
N_2	.21	.23	.24	.25	.24
NO	5.61	5.43	5.27	5.56	5.47
O_2	1.86	1.93	1.80	1.81	1.85
Cl^{35}	8.29	7.61	10.9	8.67	8.87
HCl^{35}	.71	.76	.83	.82	.78
Cl^{37}	2.68	2.50	3.56	2.69	2.86
NO_2	.94	.85	.67	.76	.80
$Cl^{35}O$	1.00	.78	.67	.78	.80
$Cl^{35}O_2$	.35	.28	.24	.26	.28
Cl_2^{35}	.16	.13	.14	.14	.14
Ag^{107}	.61	.52	.53	.46	.53

TABLE 3

AMMONIUM PERCHLORATE

PERCENT PATTERNS FROM VARIOUS PLATES

	S12015	S02256	S02286	S03046	S03106	Average
NH	1.82	1.68	1.50	1.50	1.39	1.58
NH_2	3.13	2.92	2.26	2.36	2.77	2.69
OH	7.79	8.68	8.20	8.28	8.89	8.37
NH_3	5.69	5.71	4.93	4.24	5.36	5.19
H_2O	10.3	12.5	15.0	11.8	11.6	12.2
NH_4	1.99	2.62	2.12	2.20	2.52	2.29
N_2	1.25	1.31	1.20	.98	1.59	1.27
NO	20.8	17.8	26.9	20.8	21.5	20.2
O_2	9.61	7.46	9.1	8.64	9.41	8.84
HCl^{35}	5.52	3.32	3.83	4.80	5.50	4.59
Cl^{37}	26.7	27.4	14.5	21.4	15.9	21.2
NO_2	1.93	2.97	3.93	3.92	4.22	3.39
$Cl^{35}O$	3.75	3.37	3.93	4.20	5.67	4.18
$Cl^{35}O_2$	.97	1.71	1.37	1.36	2.70	1.62
Cl_2^{35}	.57	.57	.69	.68	1.17	.74

curves for two average spark patterns, one for normal composite propellant and the other, the same propellant formulation with 1% additive. Definite relative ion increases are noted in the additive propellant curve. The ion species NH_3 and H_2O increase relative to NO and OH, while there is a decrease in Al and Cl ions. Interpretation of this data is presently being conducted.

Changes in ion concentrations within a spark spectrum are also of interest. In Figure 7, a number of ion species from a normal composite propellant spark analysis are plotted next to ion species from 1% additive composite propellant. Very definite trends are noted. For example, the C_2H_2, HCl, and CO all show similar curves, indicating combustion to form CO and HCl from reaction of hydrocarbon fragments with O and Cl atoms.

In the lower two graphs, ion species expected from ammonium perchlorate decomposition and reaction in the normal and additive propellant are plotted. The significant change with the 1% additive is the uniformity of the OH, NH_3, H_2O curves relative to the normal propellant curves. There is also a significant increase in NH_3 and CO, presumably caused by the 1% additive. Interpretation of this data is presently being conducted.

IV. CONCLUSION

In conclusion, the spark ion source mass spectrograph appears to be applicable as a useful technique for studying solid propellant combustion reactions. The spark spectra of solid propellants and propellant ingredients show effects caused by additives. They also show that combustion and reactions are occurring in the spark, probably in the vapor phase above the propellant surface.

This study thus far has shown that semi-quantitative data can be obtained on propellant and propellant combustion composition and reaction when constant instrument parameters are maintained.

REFERENCES:

1. "Tentative Recommended Practice for Use and Evaluation of Mass Spectrometers for Mass Spectro-Chemical Analysis of Solids", ASTM Committee E-14 on Mass Spectrometry, May 1965.

2. C. W. Hull, "Photographic Quantitative Analysis with a Solids Spark Mass Spectrograph", Tenth Annual ASTM E-14 Conference on Mass Spectrometry, June 1962.

3. E. B. Owens and N. A. Giardino, Anal. Chem., 35, No. 7, pp. 1172-1178.

4. P. R. Kennicott, "A Computer Program for the Quantitative Interpretation of Mass Spectrograph Plates", General Electric Report No. 64-RL-3766G, Research Information Section, The Knolls, Schenectady, New York.

5. J. R. Woolston, "Data Processing for the Mass Spectrographic Analysis of Solids", Thirteenth Annual ASTM E-14 Conference on Mass Spectrometry, May 1965.

6. R. W. Olsen, "Completely Automatic Data Reduction System for High Resolution Mass Spectrograms", Thirteenth Annual ASTM E-14 Conference on Mass Spectrometry, May 1965.

TABLE 4

COMPOSITE PROPELLANT SPARK PATTERNS

NORMALIZED EXPOSURE INTEGRALS - SO 3166

	6×10^{-11}C	6×10^{-11}C	6×10^{-11}C	6×10^{-11}C	8×10^{-11}C	8×10^{-11}C	8×10^{-11}C	1×10^{-11}C
m/e	N-4	N-5	N-6	N-7	N-8	N-9	N-10	N-12
CH	5.1	5.0	6.7	6.3	11.1	9.8	7.5	8.7
OH	9.7	9.3	10.9	9.2	16.8	17.1	15.9	21.6
NH_3	5.0	3.8	6.1	4.5	5.5	5.6	5.9	6.7
H_2O	6.6	8.2	10.8	10.0	19.5	16.0	19.0	20.6
NH_4	1.3	1.3	2.6	2.1	2.0	1.8	2.7	2.5
C_2	1.3	1.5	1.5	1.5	1.7	1.6	1.3	1.5
C_2H_2	5.0	6.2	3.9	5.5	4.5	4.3	4.1	3.2
Al	11.3	5.8	30.5	15.4	25.8	29.3	19.2	21.5
HCN	1.1	2.1	1.3	1.6	2.1	1.5	1.6	1.4
CO	7.9	12.2	8.3	11.9	17.2	13.6	12.4	13.0
NO	4.2	5.7	6.3	6.6	11.3	8.8	11.6	15.8
O_2	2.2	2.6	3.4	3.6	5.8	4.3	6.6	6.9
HCl^{35}	3.5	7.0	5.8	7.1	10.4	7.4	10.0	9.9
Cl^{37}	20.6	17.9	18.4	20.4	36.0	40.3	31.7	37.4
CO_2	.58	.63	.84	.92	1.2	.87	1.2	1.2
NO_2	.51	.36	.66	.62	.83	.65	.61	.81
CCl^{35}	--	.33	.46	.48	.94	.59	.86	.88
$Cl^{35}O$	.96	.96	1.6	1.4	1.9	1.6	1.9	2.2
$Cl^{35}O^2$	--	--	.66	.55	.61	.66	.67	.58
Cl_2^{35}	--	--	.31	.37	.62	.58	.47	.49
Ag^{107}	1.6	.69	3.2	3.4	5.8	3.0	4.4	4.3

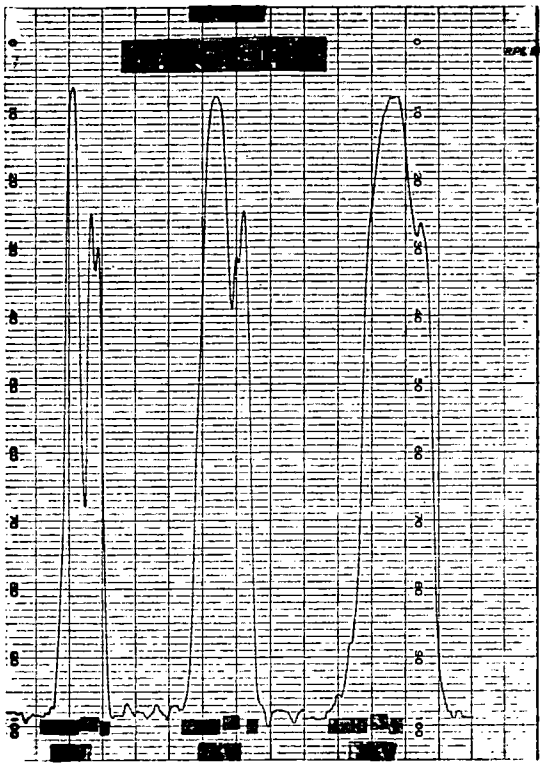

FIGURE 2
SPARK ENERGY TEST
POLYBUTADIENE

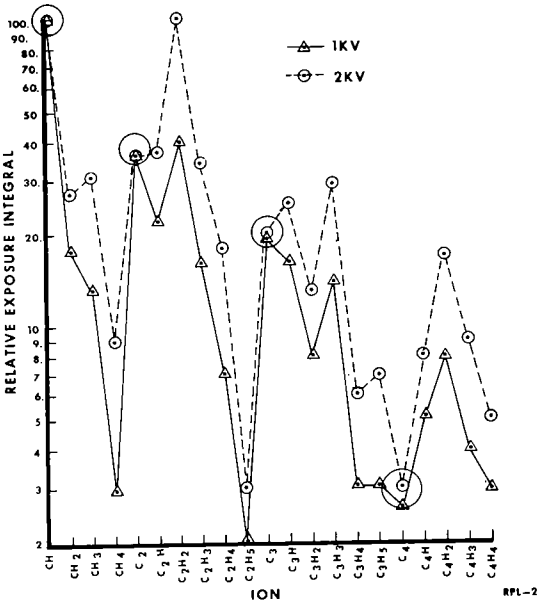

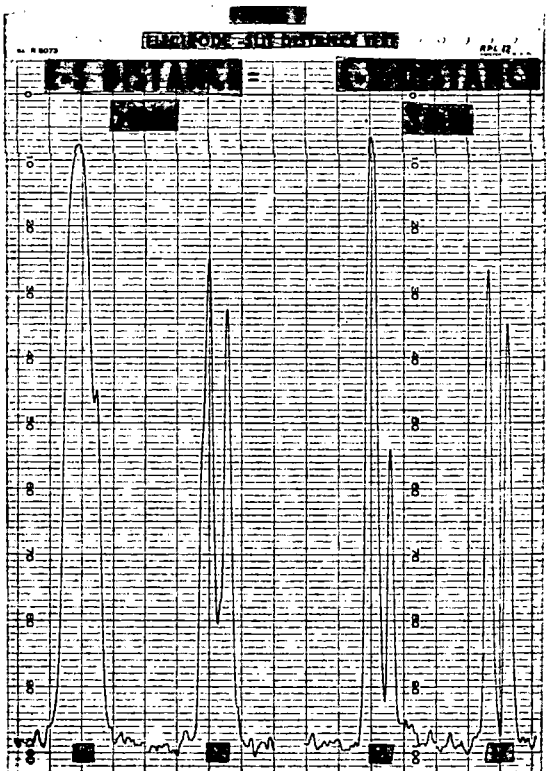

Figure 4

COMPUTER OUTPUT VS HAND CALCULATION

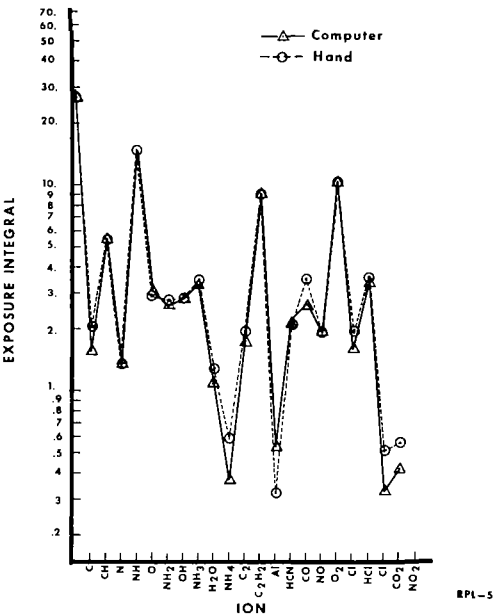

Figure 6

COMPOSITE PROPELLANT SPARK DATA BINDER & OXIDIZER CONTRIBUTION REMOVED

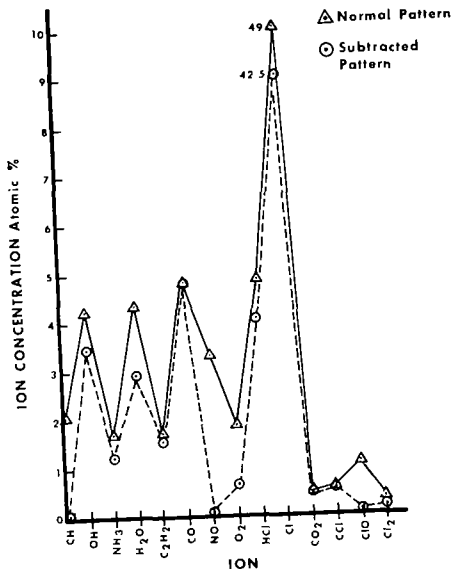

Figure 7

EFFECT OF ADDITIVE ON COMPOSITE PROPELLANT SPARK PATTERN

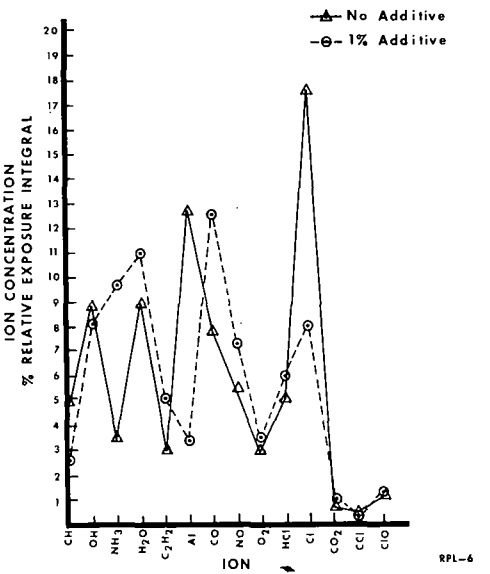

FIGURE 8

COMPOSITE PROPELLANT SPARK DATA EFFECT OF ADDITIVE ON ION CONCENTRATION

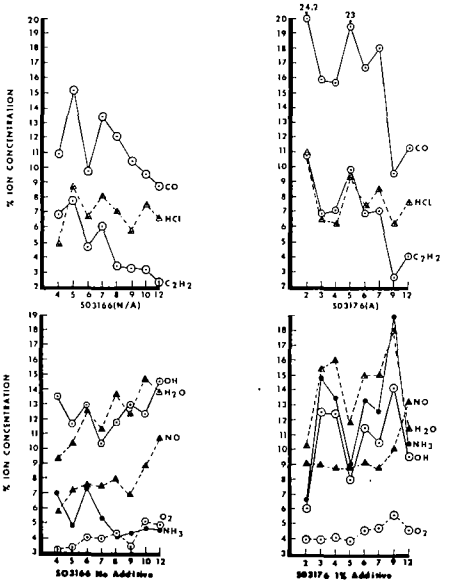

THE PYROLYTIC INVESTIGATION OF SILICA-PHENOLIC ABLATIVE RESINS

by

S. N. Cohz, M. Ladacki, and J. Hamilton

Rocketdyne
A Division of North American Aviation, Inc.,
Canoga Park, California

ABSTRACT

This paper describes the mass spectrometric determination of pyrolytic volatiles obtained from the pyrolysis of the 70/30 high silica-phenolic resin as used in the Apollo system.

A modified Zemany apparatus was used to pyrolyze samples of resin at 400, 600, and 880 C. The apparatus was connected directly to the heated inlet system of the 21-103C mass spectrometer. Up to 15 components of pyrolytic gases were identified quantitatively by mass spectrometry.

The experimental data obtained from the pyrolyses were used in conjunction with the independently determined combustion calorimetric data on virgin resins and chars, to compute the heats of pyrolysis at several temperatures.

INTRODUCTION

The pyrolysis of resin is of basic significance in the process of ablation. Not only does this pyrolysis direct the course and nature of subsequent reactions by the production of new reactants, but it also provides thermal contribution per se. The heat of pyrolysis is an important parameter in a thermal analysis of the ablation process.

The products of pyrolysis have been studied quite extensively, even in the case of such complex crosslinked systems as phenolic resins. Kinetics and mechanism of degradation of phenolics are difficult to elucidate, but even in this field some progress has been made. However, the thermochemistry of pyrolysis has not been subjected to quantitative experimental investigation. Some qualitative information is obtainable from differential thermal analysis (DTA). It is generally agreed that the process of the thermal decomposition of phenolics is endothermic. A few literature estimates of the heat of pyrolysis seem mainly based on the heat of formation of pyrolytic volatiles (which is easily computed if the nature and relative proportion of volatiles are available). A direct, calorimetric determination of the heat of pyrolysis is needed.

The heat of pyrolysis, as the heat of any chemical reaction, is the difference between the heats of formation of all the products and the heat of formation of the initial material. Therefore, in the case of a charring resin, such as phenolic, the necessary experimental determinations have to involve the heat of formation of virgin resin and the heat of formation of resin char, in addition to the average heat of formation of pyrolytic volatiles.

The present work deals with such a direct determination of the heat of pyrolysis of resin in silica-phenolic ablator. Both the pyrolytic and the calorimetric techniques are employed. Although the primary object of investigation is the phenolic resin, all the experiments are carried out on the whole composite material.

MATERIALS AND PROCEDURES

INITIAL MATERIAL

The material investigated was high silica-phenolic composite (70/30), as used in the ablative nozzle extension in the Apollo system. The sample was in the form of a billet fabricated by wrapping Refrasil cloth impregnated with Resinox SC-1008 phenolic resin; the nominal content of resin was 30 ±3 percent.

The characterization of this initial material comprised an elemental analysis, determination of the resin content, and quantitative examination of volatile matter evolved at 275 and 400 F. The elemental analysis gave average results corresponding to the molar composition $C_{100}\ H_{89.4}\ O_{17.8}\ N_8\ (SiO_2)_{64.2}$. This value forms the basis for subsequent comparisons with chars. The resin content was 29.9 ±0.8 weight percent, i.e., well within specification. The nature and amount of volatile matter evolved at prepyrolytic temperatures indicated that the resin was undergoing additional polycondensation and curing. In

general, the results were rather irreproducible from sample to sample, indicating inhomogeneity of the material. Lochte, Strauss, and Conley (Ref. 1) also find variations in properties of phenolic samples below 300 C and imply that postcuring of resins at 300 C (570 F) would "normalize" the samples. However, it is doubtful whether such modifying treatments are desirable, or even permissible, in the study of a real, specific ablative system.

PYROLYSIS OF RESIN

The pyrolysis of resin was performed by a heated-wire technique, using the modified Zemany method (Ref. 2), i.e., employing a tantalum-heated wire supported in an evacuated (10^{-6} torr) Pyrex tube attached directly to the heated inlet system of the CEC 21-103C mass spectrometer. The inlet system of the instrument was maintained at 50 C, while the ion source was constant at 250 C. The ionizing current voltage was 70 electron volts, and the ionizing current was 10.5 microamperes.

The Zemany apparatus (Fig. 1) consisted of a filament heater constructed from 2-mil tantalum sheet. The filament support rods were fabricated from 1/4-inch copper rods, which were held in place by the use of glass-to-metal seals, ensuring vacuum capabilities and rigid support.

The tantalum filament was heated by employing a step-down transformer and variac. The power supply was capable of delivering 0 to 10 amperes at voltages from 0 to 5 volts. A platinum, platinum-rhodium (90/10) thermocouple and a 10-millivolt recorder were used to measure the temperatures at which the samples were pyrolyzed. The thermocouple was kept in contact with the sample during pyrolysis.

Very small samples of the material (10 to 20 milligrams) were pyrolyzed, the time of heating being 45 seconds. The pyrolyses were carried out at 400, 600, and 880 C (750, 1110, and 1620 F, respectively), the last temperature being near the limit of the applicability of the apparatus. Prior to actual experiments, the samples were predried at 110 C (230 F) for 1 hour.

CALORIMETRIC MEASUREMENTS

The heat of formation of resin was determined by combustion method. A Parr combustion bomb and a Dickenson's design isothermal calorimeter were used. The temperature measurements were made with a platinum resistance thermometer, used in conjunction with a G-2 Mueller bridge and a high-sensitivity galvanometer. The calorimeter was standardized, using National Bureau of Standards certified benzoic acid and Parr Calorific Standard benzoic acid. After combustion, the bomb gases were bled through an absorption train consisting of a tube packed with magnesium perchlorate to absorb water, and a Nesbitt tube for the absorption of carbon dioxide. The percent combustion was determined from the analysis of the combustion gases. Several trial runs were made to ascertain conditions of complete combustion. Ignition of the powdered sample pressed into pellet gave satisfactory results. However, the technique of preparing the pellet was important if complete combustion were to be obtained.

Determinations of the heats of formation of resin chars were carried out by the same combustion method. Two difficulties have to be mentioned: (1) It was impractical to prepare by repetitions on Zemany's apparatus the large quantities of chars needed (several grams for each temperature of pyrolysis). Therefore, the chars were prepared by a simulated method: heating portions of ablative material in a Leco induction furnace (in a quartz-enclosed graphite crucible) at the temperature and to the weight loss identical with those in the Zemany run. (2) At an initial resin content of 29.9 percent and a resin volatilization of the order of 40 to 50 percent, the remaining resin char amounted only to 17 to 20 weight percent of the pyrolytic residue. Therefore, relatively large samples were required to obtain measurable and meaningful heat values, thus increasing the problem of uniformity and making a smooth, complete combustion more difficult.

EXPERIMENTAL RESULTS

HEAT OF FORMATION OF RESIN

The heat of combustion was taken as an average of four satisfactory (complete combustion) determinations. After appropriate corrections (energy equivalent of the calorimeter system, heat of combustion of fuse wire, etc.), the final value was $\Delta H_c = -2055.7$ cal/g ablative. The partial elemental analysis of the samples tested gave the average values (in weight percent): C - 21.21 percent, H - 1.68 percent. From the equation

$$\Delta H_f(\text{resin}) = \Delta H_f(CO_2) + \Delta H_f(H_2O) - H_f(O_2) - \Delta H_c \qquad (1)$$

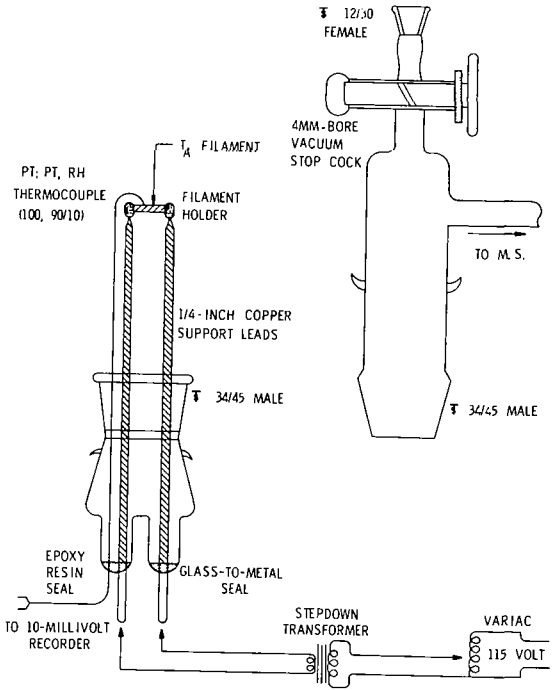

Figure 1 Modified Zemany Apparatus

Product	Mole%			Weight %		
	400°C	600°C	880°C	400°C	600°C	880°C
H_2	4.9	22.2	48.7	0.4	1.7	6.3
CO	0.4	16.5	30.0	0.4	17.8	54.4
H_2O	68.5	18.8	6.0	47.0	13.0	7.0
CH_4	3.0	15.3	5.1	1.8	9.4	5.3
C_2H_6	1.0	3.5	0.6	0.1	4.0	1.2
N_2	5.7	8.9	5.2	6.1	9.6	9.4
CO_2	6.6	2.0	1.6	11.1	3.4	4.6
O_2	0.0	3.1	1.3	0.0	3.8	2.7
Benzene	0.1	1.0	0.5	0.3	3.0	1.5
Toluene	0.1	1.5	0.4	0.3	5.3	2.4
Xylenes	0.3	0.7	0.2	1.2	2.8	1.3
Phenol	1.7	2.5	0.5	6.1	9.0	1.8
Cresols	2.9	3.0	0.5	12.1	12.5	2.1
Dimethylphenol	1.0	1.0		4.6	4.7	
2-Propanol	2.1			4.8		
Acetone	1.7			3.7		

Figure 2. Volatile Products of Pyrolysis

the heat of formation was calculated to be -174.5 cal/g ablative composite. Since the resin content in this composite was 29.9 percent, the standard (298 K) heat of formation of resin was

$$\Delta H^{o}_{f\ 298}(resin) = -583.6\ cal/g = -1050\ Btu/lb\ resin$$

Strictly, this value refers only to one particular type of resin tested. In a previous determination of the heat of formation of resin in a silica-phenolic composite (32.4 percent resin) at Rocketdyne, the value obtained was -646.4 cal/g resin. Histories of these samples, particularly extents of curing, were not the same.

PYROLYTIC VOLATILES

Mass-spectrometrically identified volatile products of pyrolyses, both in mole percent and in weight percent, are listed in Fig. 2. The values for 600 C are averages of four runs, those for 880 C of three runs, and the results for 400 C are based on one experiment. The fractions of resin volatilized (f) were: 0.107 at 400 C, 0.377 at 600 C, and 0.494 at 880 C.

On the whole, the type and relative proportions of the constituents of the pyrolytic gas agree with the results of previous investigators.

Figure 3 compares the weight losses (based on the resin) in Rocketdyne pyrolyses with the weight losses found by Madorsky (Ref. 3) in the vacuum pyrolysis of a pure phenolic resin, and with the weight losses reported by Lochte et al. (Ref. 1). From their thermogravimetric analysis (TGA) of the SC-1008 phenolic resin in an argon atmosphere. The agreement is satisfactory.

The average molecular weight (M) in g/mole of volatile products in Figure 2 is 26.2 at 400 C, 26.0 at 600 C, and 15.4 at 880 C. For a glass-phenolic resin (pyrolyzed in an arc-imaging furnace) Friedman (Ref. 4) gives M = 19.1. Tick et al. (Ref. 5) use M = 16 for a 65/35 silica-phenolic resin. No temperatures are specified. Madorsky (Ref. 3) finds M = 24/76 in the pyrolysis of a pure phenolic resin. Unlike in the present work, Madorsky's data do not show a consistent trend with the temperature of pyrolysis: M = 76 at 500 C, 24 at 800 C, and 41 at 1200 C.

CHARS (PYROLYTIC RESIDUES)

To avoid confusion, the term "char" is used here to denote the total residue (including silica), and the term "resin char" refers specifically to the portion of residue caused by the resin component.

Portions of chars (two samples for each pyrolysis temperature) were subjected to elemental analysis; the results are shown in Fig. 4. The calculated average molar compositions of these chars are given in Fig. 5; the original material is included for comparison. The molar compositions are presented in two ways: on the basis of C = 100, and on the basis of SiO_2 = 100. The first method of presentation (C = 100) shows the molar hydrogen-to-carbon ratios, and thus is convenient for direct comparison of results with those obtained on nonreinforced resins by other investigators. Recently, Lochte et al. (Ref. 1), in their TGA studies of phenolic resins, carried out an extensive analysis of pyrolytic residues. The molar hydrogen-to-carbon ratios in residues from the pyrolysis of CTL-91-LD resin were calculated from Lochte's analytical results and plotted as a function of temperature in Fig. 3, along with our results. A few results calculated from the available analytical data of Madorsky (Ref. 3) on residues from a pure phenolic resin are also included. Figure 3 shows that our resin chars were less carbonized; alternately, more carbon was lost, leaving a higher relative proportion of hydrogen. Some effect of the silica reinforcement, even at the pyrolysis level, is indicated.

The second method for expressing the molar compositions (SiO_2 = 100) in Fig. 5 simply assumes that the content of silica remains constant. It depicts general changes occurring on pyrolysis at progressively increasing temperature.

HEATS OF FORMATION OF VOLATILES AND OF RESIN CHARS

The average standard (298 K) heats of formation of volatiles for each temperature of pyrolysis were calculated from the experimental mass-spectrometric results and the known thermochemical data (mostly from the JANAF tables). The computed average molecular weights were used to convert from per mole to per gram values. The results are summarized in Fig. 6, which also lists some other results pertaining to the pyrolytic volatiles.

The heats of formation of resin chars were determined by combustion (Parr bomb) calorimetry in the analogous way to that for the resin. The percent resin char in residue, used

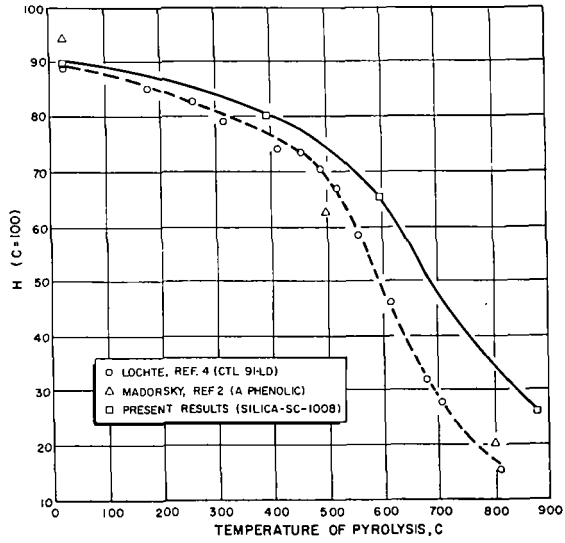

Figure 3. Molar Hydrogen Ratio in Chars (C = 100)

Sample	Weight %					
	C	H	N	O[a]	SiO_2	Ash[b]
Char, 400°C	19.58	1.27	0.04	3.23	75.30	0.58
	19.59	1.38	0.04	4.30	72.74	1.95
Char, 600°C	18.51	0.99	0.05	2.75	77.60	0.10
	18.33	1.02	(0.00)	3.02	76.90	0.73
Char, 880°C	15.55	0.32	0.04	2.09	81.54	0.46
	15.52	0.37	0.03	(3.36)	79.44	1.28

[a]Not including any O as oxides in ash

[b]Combined ash showed; by emission spectroscopy, the presence of Fe, Ca, Mg, Al, Ti, Cr, and a little Si

Figure 4. Elemental Analysis of Chars

in calculations, was obtained for each temperature from the analytical results in Fig. 4 as percent resin char = 100 percent - (percent SiO_2 + percent Ash), since the analyses were performed on portions of materials used in actual calorimetric runs. The values so obtained compared satisfactorily with the values expected from the (1 - f) fractions in Zemany runs. The average values of the heats of formation of resin chars are entered in Fig. 6.

Despite the experimental problems, the results for resin chars seem to present a coherent picture. The heat of formation of the virgin resin is -583.6 cal/g. As the resin is subjected to pyrolysis at progressively higher temperature, the heats of formation of resin chars become less and less negative. The positive heats of formation of resin chars at higher temperatures, at which the residues are more carbonized, are not really surprising. Although the heat of formation of graphite is zero by definition, various amorphous carbons are reported (Ref. 6) to have positive heats of formation (1.7 -2.6 kcal/mole). Also, the heats of formation of polynuclear aromatics (e.g., anthracene, $C_{14}H_{10}$) are positive.

HEATS OF PYROLYSIS

The thermal decomposition of resin can be represented as

$$\text{resin} \longrightarrow f \text{ volatiles} + (1 - f) \text{ resin char}$$

Hence, the heat of pyrolysis is

$$\Delta H_{py} = f\ \Delta H_f \text{ volatiles} + (1 - f)\ \Delta H_f \text{ resin char} - \Delta H_f \text{ resin} \qquad (2)$$

Substituting the obtained experimental values, the following is obtained:

$$\Delta H^o_{298} \text{ py } \underline{400\ C} = +583.6 - (0.107 \times 2217) - (0.893 \times 156.7) = +206.5 \text{ cal/g resin}$$

$$\Delta H^o_{298} \text{ py } \underline{600\ C} = +583.6 - (0.377 \times 918) + (0.623 \times 70.6) = +281.5 \text{ cal/g resin}$$

$$\Delta H^o_{298} \text{ py } \underline{880\ C} = +583.6 - (0.494 \times 948) + (0.506 \times 586) = +411.8 \text{ cal/g resin}$$

These straightforward algebraic computations are given in detail to illustrate the relative bearing of single terms on the final results.

Different heats of pyrolysis are obtained, since the pyrolytic products are different at each temperature, i.e., the reactions are not the same. It is apparent that a value of the heat of pyrolysis used alone has little meaning unless it is qualified by some specific temperature. In ablator, the pyrolysis zone is diffuse and, consequently, there is a temperature gradient. The pyrolysis occurs over a temperature range and, strictly speaking, there is no single temperature which could validly serve as the "pyrolysis temperature." For practical purpose, an arbitrary choice of a reference temperature, representing the pyrolysis, has to be made.

The best approach to this problem appears to be the familiar "half-life" concept, i.e., the choice of that temperature at which one half of the total achievable weight loss occurred. Madorsky (Ref. 3) used this criterion in the comparison of thermal stability of various polymers. Recently, Tick et al. (Ref. 5) voiced a similar approach. Inspection of Fig. 1 shows that in the Rocketdyne experiments, as in Lochte's, the 25 percent weight loss ($W/W_o \approx 0.75$) corresponds to about 520 C; if the results of Madorsky are considered, the corresponding figure is 480 C. It happens that these values are near 1000 F (538 C), a temperature which has been used (Ref. 5 and 7) as the pyrolysis temperature (T_{py}) and which is conveniently suited for computations in the English system. Had the computations been done in the metric system, the temperature of 500 C would be more convenient and also more representative. The round figures of 1000 F will be retained as an adequate and convenient approximation. The arbitrary nature of this reference temperature representing the pyrolysis, however, should be recognized.

To obtain a value of the heat of pyrolysis for the reference temperature, a somewhat unusual plot of ΔH^o_{298} py (T) vs T is drawn (Fig. 8). The values of the heats of pyrolysis refer actually to different types of reactions, as pointed out earlier. However, the linear relationship obtained indicates regularity of change and justifies interpolations. By interpolation, the heat of pyrolysis (standard states, 298 K) of resin undergoing the pyrolysis at 1000 F is

$$\Delta H^o_{298} \text{ py } \underline{1000\ F} = +477 \text{ Btu/lb resin } (= +265 \text{ cal/g})$$

Sample	Relative Proportions				
	C	H	O	N	SiO_2
		Based on C = 100			
Original Material	100	89.4	17.8	8	64.2
Char, 400°C	100	81.1	14.5	3	75.5
Char, 600°C	100	66.1	11.8	2	83.9
Char, 880°C	100	26.6	10.1	1	103.5
		Based on SiO_2 = 100			
Original material	155.9	139.3	28	12	100
Char, 400°C	132.4	107.4	19	4	100
Char, 600°C	119.1	78.8	14	2	100
Char, 880°C	96.6	25.7	10	1	100

Figure 5. Average Molar Composition (from elemental analysis)

Property	Temperature of Pyrolysis, °C		
	400	600	880
Virgin Resin			
Standard heat of formation, ΔH_f^o (298°K)			
cal/gm -583.6			
Btu/lb -1050			
Products of Pyrolysis			
Fraction of resin volatilized, f	0.107	0.377	0.494
Volatiles			
Average molecular weight (M), gm/mole	26.2	26.0	15.4
Average specific heat (C_p), cal/g-°C	0.47	0.46	0.52
Average heat of vaporization, cal/gm	290	106	46
Average standard heat of formation, $\Delta H_{f\ 298}^o$			
kcal/mole	-58.1	-23.9	-14.6
cal/g	-2217	-918	-948
Btu/lb	-3990	-1652	-1706
Resin Char			
Standard heat of formation, ΔH_f^o			
cal/g	-156.7	+70.6	+586
Btu/lb	-282	+127	+1055
Standard Heat of Pyrolysis, $\Delta H^o_{298}{}^{py}(T)$			
cal/g resin	+206	+281	+412
Btu/lb resin	+371	+506	+742

Figure 6. Thermochemistry of Pyrolysis

This value does not contain the contribution of sensible enthalpy up to the temperature of actual pyrolysis (1000 F, 811 K):

$$\Delta H^{o}_{811} = \Delta H^{o}_{298} \int_{298}^{811} (n_1 C_{p1} vol_1 + n_2 vol_2 + \ldots + n' C_p' \text{ resin char} - n'' C_p'' \text{ resin})\, dT \qquad (3)$$

Some data are unavailable. In particular, specific heats of virgin resin and resin chars, and their dependence on temperature, are unknown or uncertain. A very rough calculation, based on approximate or assumed values, indicates that the correction would be small, since the term in Eq. 3 resulting from the resin nearly offsets the other terms. In any case, the value given (standard states, 298 K) is more fundamental.

The ablation literature contains some estimates of the heat of pyrolysis of phenolic resins. Beecher and Rosenweig (Ref. 8) considered that the heat of decomposition (pyrolysis) of glass-reinforced resin amounted to only about +90 cal/g (162 Btu/lb). Tick et al. (Ref. 5) give a value of +335 Btu/lb for the heat of decomposition of 65/35 silica-phenolic resin. These and other estimates are given without reference to a temperature. It is not clear whether sensible heat effects are accommodated or not.

CONCLUDING REMARKS

The present work has provided an experimental value of the heat of pyrolysis, to supplant discordant estimates. More importantly, it showed a practical approach to the problem of complex, charring resins, in general. On the other hand, it emphasized the complexity of such systems.

In thermochemistry, where precise definitions and accurate results are essential, the heats of formation of such ill-defined systems as a crosslinked resin or a resin char, or even the heat of pyrolysis, appear somewhat artificial. Despite some objections from rigorous viewpoint, these terms are used to derive systematically a heat value of considerable practical importance. The limitations are realized; no high degree of accuracy or reproducibility is expected. The molecular weight cannot be defined; hence, the results are expressed consistently in cal/g (or Btu/lb). There is no ambiguity as far as the heat of combustion is concerned.

Different heats of pyrolysis are obtained for thermal decompositions carried out at different temperatures because different, or at least modified, reactions yielding different products are involved. Since the starting material is the same, the question arises what causes these differences. There are two distinct possibilities: (1) a change in the basic mechanism of pyrolysis, and (2) participation of secondary or "cracking" reactions.

Not enough is known of the basic mechanism alone to exclude the possibility of change. However, one criterion is useful if not entirely discriminatory: a change in mechanism would affect the nature of gases and of the residue, whereas the contribution of cracking would be reflected only in the nature of gases. The regularity of change in the composition of pyrolytic residues (e.g., Fig. 8) and the smoothness of TGA curves (e.g., Fig. 3) tell against the change in mechanism. On the other hand, a marked decrease in the concentration of some "unstable" constituents of volatiles, observed at high temperatures (Fig. 2), suggests an increasing participation of secondary or cracking reactions.

In a crosslinked phenolic system, neither the onset nor the end of pyrolysis is well defined. The process of thermal degradation is continuous and includes consecutive chemical reactions. Clear separation of some secondary reactions and of "cracking" (normally relegated to postpyrolytic processes) is not feasible, and may be merely a matter of semantics. Since the cracking reactions are normally of an endothermic nature, the endothermicity of pyrolysis is augmented at higher temperatures.

The choice of a reference temperature representing the pyrolysis, therefore, acquires, special significance. A higher reference temperature would give a higher heat of pyrolysis, but would leave less for the "heat of cracking," and vice versa. Hence, the heat of formation of resin appears actually a more basic entity than the heat of pyrolysis.

ACKNOWLEDGMENT

Information herein was prepared under the sponsorship of NASA, Houston, Texas, under Contract NAS 9-150.

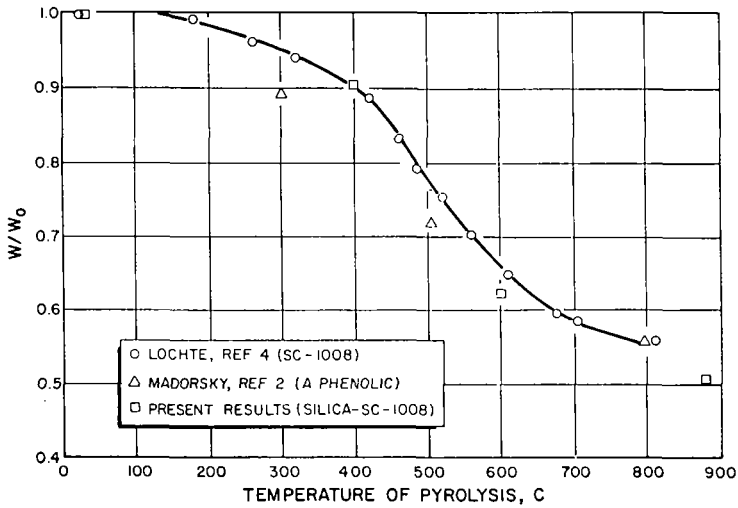

Figure 7. Pyrolysis of Phenolic Resins Weight Losses

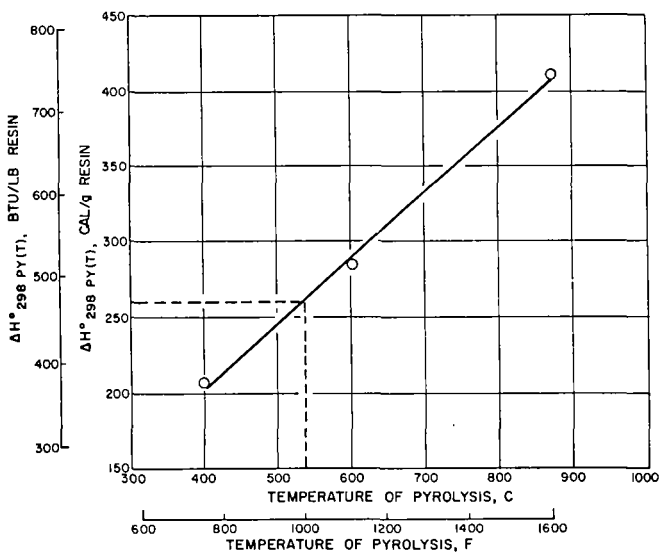

Figure 8. Standard Heat of Pyrolysis as a Function of Temperature for Silica-Phenolic Resin

REFERENCES

1. Lochte, H. W., E. L. Strauss, and R. T. Conley, "The Thermo-oxidative Degradation of Phenol-Formaldehyde Polycondensates. Thermogravimetric and Elemental Composition Studies of Char Formation," J. Applied Polymer Sci. 9, pp. 2799-2810 (1965).

2. Zemany, P. D., "Identification of Complex Organic Materials by Mass Spectroscopic Analysis of Their Pyrolysis Products," Anal. Chem. 24, pp. 1709-1713 (1952).

3. Madorsky, S. L., Thermal Degradation of Organic Polymers, Interscience Publishers, New York, Chapter XVI, pp. 288-292 (1964).

4. Friedman, H. L., "The Pyrolysis of Plastics in a High Vacuum Arc Image Furnace," General Electric Co., Missile and Space Division, TIS-R62SD57 (December 1962).

5. Tick, S. J., G. R. Huson, and R. Griese, "Design of Ablative Thrust Chambers and Their Materials," J. Spacecraft and Rockets 2, pp. 325-331 (1965).

6. Walker, P. L., F. Rusinko, and L. G. Austin, "Gas Reactions of Carbon," Advances in Catalysis, Academic Press, New York, Vol. XI, p. 133 (1959).

7. Rivers, W. J., R. Van Wyk, J. D. Seader, H. A. Friedman, and H. N. Chu, "Effect of Rocket Engine Combustion on Chamber Materials. Part I: One-Dimensional Computer Program," Rocketdyne, a Division of North American Aviation, Inc., AFRPL, TR-65-13 (January 1965).

8. Beecher, N. and R. E. Rosensweig, "Ablation Mechanism in Plastics With Inorganic Reinforcement," ARS J. 31, pp. 532-539 (1961).

ON A SEMI-CLASSICAL MODEL FOR THE COLLISION-INDUCED EXCITATION AND DISSOCIATION OF FAST IONS.,

Jean DURUP
Laboratoire de Chimie-Physique, Orsay, France

ABSTRACT

The collision-induced dissociation of fast ions is treated by a semi-classical model pertinent to the part of the phenomenon due to electronic excitation of the impinging ion. This excitation is calculated as resulting from the absorption of a virtual photon arising from the field of the induced dipole, in analogy with the FERMI-WILLIAMS method.

The cross sections thus obtained are compared for simple systems with calculations carried out by different authors using first BORN approximation. The semi-classical model is shown to give reasonable results in the kilovolt energy range.

INTRODUCTION

On might question the interest of studying semi-classical models, since any problem can be treated exactly by quantum mechanical calculations. However for some problems such calculations are lengthy as soon as one leaves simple systems such as hydrogen or helium, so that if a classical model gives an approximation even rough but valid for any species it may be of some use.

The problem we shall consider is the electronic excitation and dissociation of fast ions by collision with neutrals, in the kilovolt range. Such processes have been extensively studied by mass spectrometry (ASTON bands) and by other methods, but it is rarely possible to interpret the observed cross sections in terms of individual cross sections for incident ions in a given electronic and vibrational state. This is why the classical model we shall propose will be tested not by comparison with experiment but by comparison with quantum mechanical treatments, which are available for simple systems, particularly by the work of PEEK(1).

The model we shall use is the following : ion and neutral are considered as classical particles characterized by point charge for the ion, point induced dipole for the neutral, and by a spectrum of oscillator strenghs for the electronic transitions to be considered.

The electric field created by the induced dipole at the position of the ion varies rapidly with time during the encounter ; following an old method first developped by FERMI(2), we decompose this field into a FOURIER integral over the frequencies, so that the ion "sees" the equivalent of a spectrum of photons, one of which it may absorb, being thus excited, eventually to a dissociative state.

EXCITATION OF THE INCIDENT ION WITHOUT EXCITATION OF THE TARGET

We shall first consider the case where the ion alone becomes excited, the target atom remaining in its ground state.

The induced dipole field acting on the ion is

$$E = \frac{2\alpha Z e}{r^5} \qquad \text{with} \quad r = (b^2 + v^2 t^2)^{1/2}$$

where α is the target polarizability, $\underline{Ze}$ the charge of the ion, $\underline{b}$ the impact parameter, $\underline{v}$ the velocity of the incident ion, $\underline{t}$ the time with origin at the point of closest approach of the two particles ; the ionic trajectory is supposed to be practically linear and the target at rest.

Both components of the field are then FOURIER-decomposed :

$$E_x(t) = \int_{-\infty}^{+\infty} X(\omega) \cdot e^{-i\omega t} \, d\omega \quad ,$$

$$E_y(t) = \int_{-\infty}^{+\infty} Y(\omega)\, e^{-i\omega t}\, d\omega \quad ,$$

$X(\omega)$ and $Y(\omega)$ being given by the FOURIER integral theorem as

$$X(\omega) = \frac{1}{2\pi} \int_{-\infty}^{+\infty} E_x(t)\, e^{i\omega t}\, dt \qquad \text{,etc.}$$

leading to

$$\begin{cases} X(\omega) = -\dfrac{\alpha Z e \omega}{8 v^2 b^3}\, i \left(1 + \left|\dfrac{\omega b}{v}\right|\right) e^{-\left|\frac{\omega b}{v}\right|} \\ Y(\omega) = \dfrac{\alpha Z e}{8 v b^4} \left(3 + 3\left|\dfrac{\omega b}{v}\right| + \dfrac{\omega^2 b^2}{v^2}\right) e^{-\left|\frac{\omega b}{v}\right|} \end{cases}$$

An equivalent photon intensity for a single collision is then calculated by integration of $\frac{c}{4\pi}\left(E_x^2(t) + E_y^2(t)\right)$ from $-\infty$ to $+\infty$ (3):

$$I = \frac{c}{4\pi} \int_{-\infty}^{+\infty} dt \left(E_x^2(t) + E_y^2(t)\right)$$

$$= \frac{c}{4\pi} \int_{-\infty}^{+\infty} dt \left\{ E_x(t) \int_{-\infty}^{+\infty} X(\omega) e^{-i\omega t} d\omega + E_y(t) \int_{-\infty}^{+\infty} Y(\omega) e^{-i\omega t} d\omega \right\}$$

or, reversing the order of integrations,

$$I = \frac{c}{4\pi} \int_{-\infty}^{+\infty} d\omega \left(X(\omega)\, X^*(\omega) + Y(\omega)\, Y^*(\omega)\right)$$

indicating an equivalent differential intensity

$$J(\omega)\, d\omega = 2\, \frac{c}{4\pi}\, d\omega \left\{ \left|X(\omega)\right|^2 + \left|Y(\omega)\right|^2 \right\}$$

which may be expressed as a number of equivalent photons per unit surface and unit angular frequency by dividing by $\hbar\omega$.

This flux is then integrated over the impact parameter b to account for all the encounters which the ion may experience on a path of length l through a gas of density n atoms or molecules per unit volume :

$$\Phi_1(\omega)\, d\omega = \frac{c\, d\omega}{\hbar\omega} \int_0^{\infty} n\, l \cdot 2\pi b\, db \left\{ \left|X(\omega)\right|^2 + \left|Y(\omega)\right|^2 \right\}$$

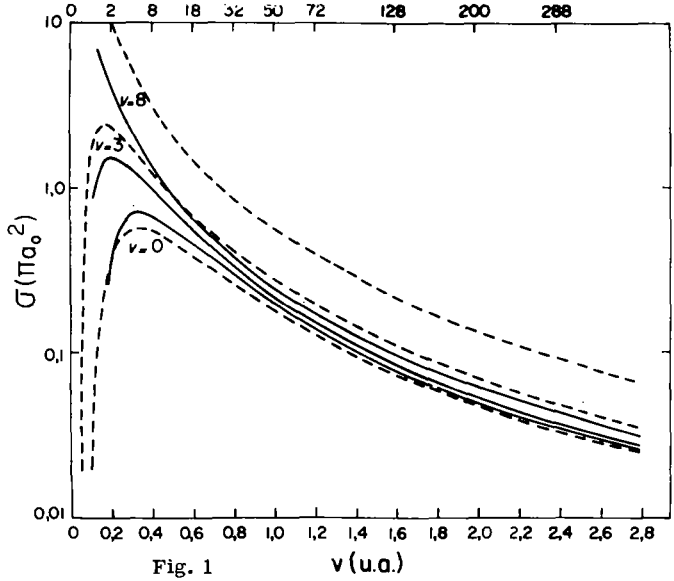
0 2 8 18 32 50 72 128 200 288
10
1,0
0,1
0,01
σ(πa₀²)
v=8
v=3
v=0
0 0,2 0,4 0,6 0,8 1,0 1,2 1,4 1,6 1,8 2,0 2,2 2,4 2,6 2,8
v (u.a.)

Fig. 1

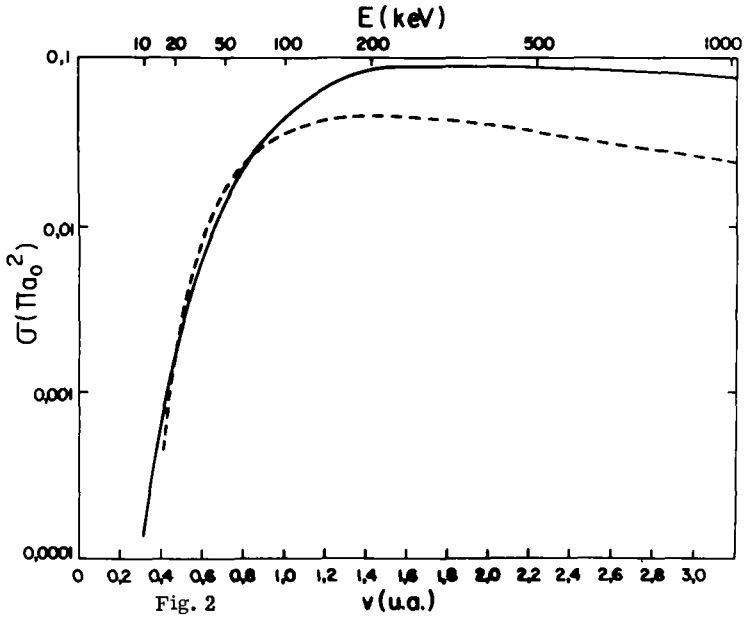
E (keV)
10 20 50 100 200 500 1000
0,1
0,01
0,001
0,0001
σ(πa₀²)
0 0,2 0,4 0,6 0,8 1,0 1,2 1,4 1,6 1,8 2,0 2,2 2,4 2,6 2,8 3,0
v (u.a.)

Fig. 2

This integral does not converge. It is necessary to introduce some minimum value b_0 of the impact parameter, under which the distance of closest approach of the two particles is assumed to decrease no more, owing to the repulsive part of the interaction potential. For this b_0 we used an averaged value of the minimum of the effective interaction potential.

We then obtain the differential cross section by introducing the absorption coefficient distribution of the ion,

$$\sigma(\omega)\,d\omega = \frac{\Phi_1(\omega)\,d\omega}{n\ell}\cdot\mu(\omega)$$

The cross section for a given transition with oscillator strength f_s, angular frequency ω_s, is then obtained by integration over the band width, yielding the final result :

$$\sigma_s = \frac{\pi^3\alpha^2 Z^2 e^4 f_s}{32\, m\hbar\, \omega_s^3 b_0^8}\; u^2(2+u)(6+9u+6u^2+2u^3)e^{-2u}\,, \qquad u = \frac{\omega_s b_0}{v}$$

This model will be first applied to the process

$$H_2^+(1s\sigma_g) + H(1s) \longrightarrow H_2^+(2p\sigma_u) + H(1s)$$

which was studied by PEEK(2) using first BORN approximation.

Fig.1 shows three pairs of curves corresponding to H_2^+ ions initially in the vibrational states v"=0,3 and 8. Curves in full line are reproduced from PEEK, dashed lines are given by the present model with b_0=1.89 atomic units, and with integration over the H_2^+ internuclear distance of the cross section multiplied by the square of the pertinent vibrational wave function.

One may see that the classical model, in spite of its simplicity, gives a reasonable account of the phenomenon. Let us then see which information it may yield regarding the variation of the cross section with velocity and kind of reactants.

The velocity dependence occurs only through the variable $u = \frac{\omega_s b_0}{v}$. Thus the decrease at high velocity is as $1/v^2$ and parallels BORN approximation. The position of the maximum corresponds to a numerical value u = 2.17, so that the velocity for the maximum cross section is given by an equation formally identical with the so-called adiabatic criterion with an adiabatic parameter $a = 0.92\,\pi\, b_0$.

The variation of the cross section with the species used as a target clearly comes essentially from the variation in b_0 ; the cross section strongly increases when b_0 decreases, that is, when the target is smaller. One may thus interpret semi-quantitatively for example the cross sections observed by MELTON and WELLS(4) for the dissociation of CO^+ induced by collision with different targets, which increase in the order :

$Kr < Ar < N_2$, $H_2 < He$.

FURTHER IONIZATION OF THE INCIDENT ION

For higher incident energies, the model is more poor, since the (ion-induced dipole) interaction should have to be replaced by a screened COULOMB potential.

Let us see however the result of the model applied to the ionization of He^+ to He^{++} by collision with H atoms, which was studied by BOYD et al.(5) using first BORN approximation.

The excitation energies involved are very high, starting from a threshold of 54eV with an important part of the oscillator strength up to energies more than one hundred eV, so that the maximum cross section occurs for high incident energies.

Because of the high velocities involved, a value of b_0 equal to 1.30 a.u., slightly lower than the equilibrium distance $He^+ - H$ (1.45 a.u.), was used in the calculation. A better approximation would be to calculate,

from the known interaction potential, the effective dependence of the distance of closest approach on impact parameter and incident velocity, but we feel that it would not change significantly the results.

Fig.2 shows the cross section obtained (dashed line) compared with BORN approximation(5) (full line). As expected, the model, correct at low energies, gives too low cross sections at high energies.

EXCITATION OF THE INCIDENT ION AND OF THE TARGET

We shall now turn to the case where the target atom does not remain in its initial state but is also excited by the collision. This case of double excitation can be treated as previously if one attributes to the target atom a complex polarizability, the imaginary part of which classically describes the absorption coefficient.

The field acting on the target is

$$\mathcal{E} = \frac{Ze}{b^2+v^2t^2}$$

and is decomposed as previously in FOURIER components, $\mathcal{X}(\omega)$ and $\mathcal{Y}(\omega)$. These induce in the target a polarization

$$\mathcal{M}_x = \int_{-\infty}^{+\infty} (\alpha + i\alpha'')\,\mathcal{X}(\omega)\,e^{-i\omega t}\,d\omega\,, \quad \mathcal{M}_y = \int_{-\infty}^{+\infty} (\alpha + i\alpha'')\,\mathcal{Y}(\omega)\,e^{-i\omega t}\,d\omega$$

where $\quad i\alpha'' = -\dfrac{i\pi e^2}{2m\,|\omega|}\dfrac{df}{d|\omega|}\,,$

the differential oscillator strength referring to the target.

The field acting on the ion is then (letting $r = (b^2+v^2t^2)^{1/2}$):

$$E_x = -\frac{r^2-3x^2}{r^5}\mathcal{M}_x - \frac{3bx}{r^5}\mathcal{M}_y\,, \qquad E_y = -\frac{3bx}{r^5}\mathcal{M}_x - \frac{r^2-3b^2}{r^5}\mathcal{M}_y$$

and the same treatment as before leads to the following expression for the equivalent photon flux :

$$\Phi_2(\omega) = \int_{b_0}^{\infty} n\ell \cdot 2\pi b\,db \cdot \frac{cZ^2e^6}{4\pi^2 m^2 \hbar\omega v^{10}} \cdot \Bigg\{ \Bigg\{ \Big(\sum_i f_i + \int \frac{df}{d\Omega}d\Omega\Big)\Big\{(\Omega+\omega)^2 \times$$

$$\times \Big(K_0\big(\tfrac{\Omega b}{v}\big)\cdot K_0\big(\tfrac{\Omega+\omega}{v}b\big) + K_1\big(\tfrac{\Omega b}{v}\big)\cdot K_1\big(\tfrac{\Omega+\omega}{v}b\big)\Big) - (\Omega-\omega)^2\cdot\Big(K_0\big(\tfrac{\Omega b}{v}\big)\times$$

$$\times K_0\big(\tfrac{|\Omega-\omega|}{v}b\big) + K_1\big(\tfrac{\Omega b}{v}\big)\cdot K_1\big(\tfrac{|\Omega-\omega|}{v}b\big)\cdot\frac{\Omega-\omega}{|\Omega-\omega|}\Big)\Big\}\Bigg\}^2 + \Bigg\{\Big(\sum_i f_i + \int\frac{df}{d\Omega}d\Omega\Big)\cdot$$

$$\cdot\Big\{(\Omega+\omega)^2\cdot\Big(K_0\big(\tfrac{\Omega b}{v}\big)\cdot K_1\big(\tfrac{\Omega+\omega}{v}b\big) + K_1\big(\tfrac{\Omega b}{v}\big)\cdot K_0\big(\tfrac{\Omega+\omega}{v}b\big) +$$

$$+ K_1\big(\tfrac{\Omega b}{v}\big)\cdot K_1\big(\tfrac{\Omega+\omega}{v}b\big)\cdot\frac{v}{(\Omega+\omega)b}\Big) + (\Omega-\omega)^2\cdot\Big(K_0\big(\tfrac{\Omega b}{v}\big)\cdot K_1\big(\tfrac{|\Omega-\omega|}{v}b\big)\cdot\frac{\Omega-\omega}{|\Omega-\omega|} +$$

$$+ K_1\big(\tfrac{\Omega b}{v}\big)\cdot K_0\big(\tfrac{|\Omega-\omega|}{v}b\big) + K_1\big(\tfrac{\Omega b}{v}\big)\cdot K_1\big(\tfrac{|\Omega-\omega|}{v}b\big)\cdot\frac{v}{|(\Omega-\omega)b|}\Big)\Big\}\Bigg\}^2\Bigg\}\,,$$

where K_0 and K_1 are modified BESSEL functions of the second kind. The calculation then goes to the cross section in the same way as in paragraph 1.

Fig.3 shows the results of this calculation(in dashed line) for the process

$$H_2^+(1s\sigma_g) + H(1s) \longrightarrow H_2^+(2p\sigma_u) + H^* \text{ (all states)}$$

again compared to PEEK's calculation by first BORN approximation[2](in full line).

One sees that the disagreement is total.

The reason is that the two calculations refer in fact to different phenomena. Indeed, if one looks at the way in which the cross section for double excitation decreases at high velocity, one finds a $1/v^4$ dependence by the classical model, $1/v^2$ by first BORN approximation. The $1/v^4$ dependence describes the probability of double excitation as a product of probabilities of two events (the excitation of the target and the excitation of the ion) which are correlated but distinct in time. The first BORN approximation, in contrast, describes a unique transition in which both particles are simultaneously excited.

Experimental evidence[6]strongly supports the behaviour found by PEEK at high energies where the cross section he finds is maximum.At lower energies however experiment is not decisive since the cross section for excitation of the ion alone without excitation of the target overwhelms the double excitation, and since in addition the unknown population of the vibrational levels of the incident ions prevent any unambiguous use of the experimental data.

It appears thus possible that both processes of double excitation, viz. in one event or two successive events, could occur independently, and that a study by the second BORN approximation would yield results representative of the sum of the phenomena described respectively by the first BORN approximation and by the semi-classical model.

In conclusion, the semi-classical model depicted appears to be helpful for the understanding of the part of collision - induced dissociations of fast ions due to electronic excitation, especially in the velocity range generally used in mass spectrometry.

(1) E. FERMI, Zts f.Phys., 29, 315 (1924).

(2) J.M. PEEK, Phys.Rev., 140, A 11 (1965).

(3) see e.g. L.D. LANDAU and E.M. LIFSHITZ, Field theory, Moscow 1962, paragraph 49.

(4) C.E. MELTON and G.F. WELLS, J. Chem. Phys., 27, 1132 (1957).

(5) T.J.M. BOYD, B.L. MOISEIWITSCH and A.L. STEWART, Proc. Phys. Soc., A 70, 110 (1957).

(6) J. GUIDINI, C.R. Acad. Sci., 253, 829 (1961) ;
G.W. Mc CLURE, Phys. Rev., 130, 1852 (1962) ;
and references quoted therein.

Figure captions.

Fig. 1 $H_2^+(1s\sigma_g, v'' = 0,3,8) + H(1s) \longrightarrow H_2^+(2p\sigma_u) + H(1s)$

- - - - This model ——— First BORN approximation[2].

Fig.2 $He^+(1s) + H(1s) \longrightarrow He^{++} + H(1s)$

- - - - This model ——— First BORN approximation[5].

Fig.3 $H_2^+(1s\sigma_g, v'' = 0) + H(1s) \longrightarrow H_2^+(2p\sigma_u) + H^*$ (all states)

- - - - This model ——— First BORN approximation[2].

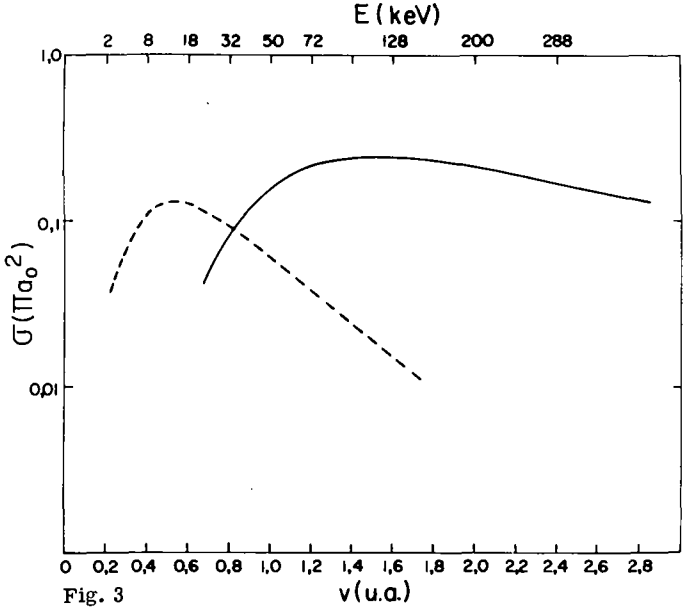

Fig. 3

STUDIES OF COLLISION-INDUCED DISSOCIATION AND ENDOTHERMIC ION-MOLECULE REACTIONS*

K. M. Refaey† and W. A. Chupka

Argonne National Laboratory, Argonne, Illinois

The cross sections for dissociation of $C_2H_4^+$ on collision with He and H_2 has been investigated over the energy range 15 — 400 eV. In the case of H_2, some ion-molecule reaction products were also investigated. The kinetic energy of fragments produced in this and other dissociations have been measured. We also have undertaken a series of collision experiments in which parent ions with varying amounts of internal energy are produced by photoionization. These experiments will be described.

This paper describes some preliminary measurements concerning the energy dependence of cross sections for collision-induced dissociation and endothermic ion-molecule reactions. An ion source with separate ionization and collision chambers was constructed for a mass spectrometer with a 60° magnetic sector of 12-in. radius. The products of collision were found to appear in the mass spectrum at the mass positions colculated by use of the relation[1]

$$m^* = \frac{(m_f)^2}{(m_p)} \frac{V_1}{V} + \left(1 - \frac{V_1}{V}\right) m_f \ , \qquad (1)$$

where m_f and m_p are the masses of the fragment and parent ions respectively, V_1 is the potential difference between the ionization chamber and the collision chamber, and V is the total accelerating potential. The investigated molecules were propane, oxygen, and ethylene. The results reported in this paper are only preliminary to experiments employing photoionization for the production of the reactant ions.

The propane ion and fragment ions produced by 70 eV electrons were accelerated through the potential difference V_1 where they collided with several species of rare gas atoms in the collision chamber leading to the dissociation into smaller fragments. Reaction mechanisms were easily identified by use of relation (1).

Peaks due to collision-induced dissociation were found to be broader than the normal peaks. This broadening was also found to increase with increasing velocity v_0 of the incident ion. This is in agreement with the fact that the broadening is due to an increase in the velocity distribution of the product ion as a result of collision. If $\pm v_1$ is the change in the speed of the product ion along the original path, then after collision, a fragment ion of mass m_1 will have an energy

$$E_1 = \tfrac{1}{2} m_1 (v_0 \pm v_1)^2 = \tfrac{1}{2} m_1 v_0^2 \pm m_1 v_1 v_0 + \tfrac{1}{2} m_1 v_1^2 \qquad (2)$$

The last term in Eq. (2) is small and can be neglected. Thus the broadening ΔE of the product peak, taken for example as the width at half height, is proportional to $2 m_1 v_1 v_0$ and hence v_0. The total internal energy released in the dissociation process can then be calculated and is given by [2]

$$T = \frac{(\Delta E)^2}{16 E_0} \frac{(m_1 + m_2)^2}{m_1 m_2} \qquad (3)$$

---

*Work performed under the auspices of the U. S. Atomic Energy Commission.

† Permanent address: U.A.R. Atomic Energy Establishment, Cairo, U. A.R.

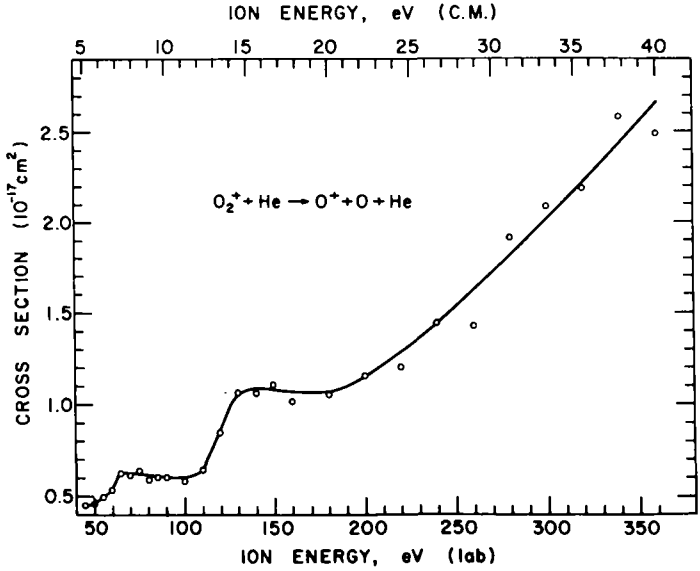

Fig. 1. Energy dependence of the cross section for the process indicated.

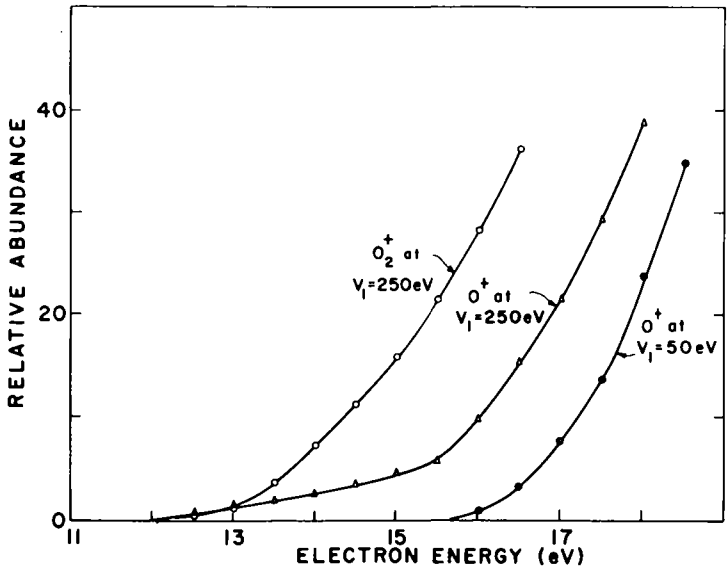

Fig. 2. Appearance potential of O_2^+ and O^+ ions produced by collision of O_2^+ on He.

where E_0 is the kinetic energy of the parent ion, m_2 is the mass of the second fragment, and ΔE as defined above can be considered as the width at half height of the product peak.

The results obtained on the propane ion and fragment ions are given in Table I

TABLE I. Total internal energy released in the dissociation of the propane ion and fragment ions as a result of collision with A and He. The standard error is given by

$$\left[\sum_{i}^{n} (\delta T_i)^2 / n\ (n-1)\right]^{\frac{1}{2}}$$

where n = 6 for He and n=5 for A. V_1 = 1510 eV and V = 3600 eV.

Collision gas	Dissociation process ($m_p \rightarrow m_f$)					
	44 → 27	43 → 27	44 → 28	44 → 29	29 → 27	28 → 26
He	0.3498* ±0.0061	0.1063 ±0.0018	0.0574 ±0.0011	0.0894 ±0.0015	0.1851 ±0.0142	0.3470 ±0.0088
A	0.3511 ±0.0069	0.1107 ±0.0031	0.0625 ±0.0021	0.1023 ±0.0045	0.2256 ±0.0234	0.3071 ±0.0082

*Calculated as if the process takes place in one step. However, this is not the case. A rigorously correct calculation cannot be made without further assumptions. Hence these values represent an upper limit.

Ottinger,[3] using this technique, was able to measure the kinetic energy of the fragments formed by the spontaneous dissociation of the metastable ions in n-heptane and n-butane. His results showed that the fragment ions were released with small kinetic energies comparable to the values obtained from Table I.

Fuch and Taubert[4] and Taubert[5] measured the average kinetic energy released in the dissociation of $C_3H_8^+$ into various fragment ions. The values obtained by those authors for the dissociation of $C_3H_8^+$ into $C_2H_5^+$ and $C_2H_4^+$ are in fair agreement with those obtained in this investigation. Hence, the evidence is very strong that the width of the collision-induced dissociation peak is due almost entirely to the kinetic energy released in the decomposition. This decomposition is mostly a result of collisions which do not impart much kinetic energy to the target gas and produce the ion with internal excitation followed by decomposition as if the ion were produced by electron or photon impact. The measurements of Taubert et al. were made on ions produced by electron impact. One can conclude that collision-induced dissociation does not occur via a mechanism which would lead to a large distribution in the kinetic energy of the product ion.

The energy dependence of the cross section for collision-induced dissociation of O_2^+ on He, Fig. 1, shows that the cross section remains to be large below the dissociation energy of the ground electronic state O_2^+ ($^2\pi_g$). The dissociation energy of ground electronic state O_2^+ ($^2\pi_g$) is 6.65 eV which in the case of collision with He should yield a threshold at 59.85 eV in the laboratory. Dissociation below this energy must then be due to excited metastable states of O_2^+ Approximate appearance-potential measurements, Fig. 2, showed them to be due to the dissociation of the excited electronic state O_2^+ ($^4\pi_u$) which is about 4 eV above

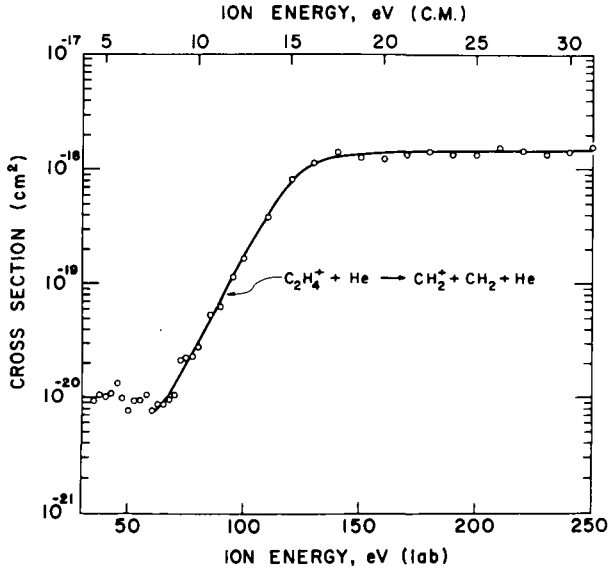

Fig. 3. Energy dependence of the cross section for the processes indicated.

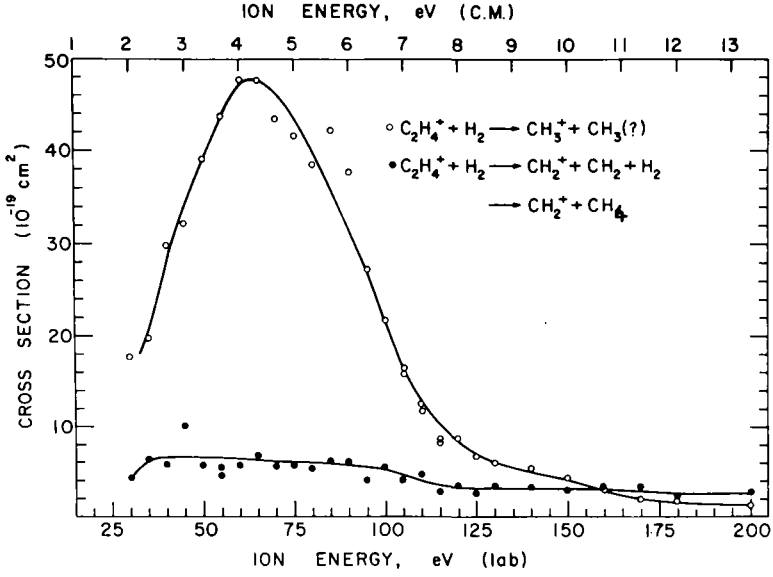

Fig. 4. Energy dependence of cross sections for the processes indicated.

the ground state. The rise in the cross section at about 60 eV may be due to the contribution of the ground electronic state.

If the rise in the cross section at about 110 eV in Fig. 1 is not an artifact of the ion optic system it might be explained as being due to the dissociation of O_2^+ ($^4\pi_u$) into the ground state of O^+ and into ^5S or ^3S excited states of O atom. These states of the O atom lie at energies 9.17 eV and 9.54 eV above the ground state. The calculated thresholds for these processes are approximately 11.71 eV and 12.08 eV, respectively. The observed value of 110 eV in the laboratory corresponds to a value of 12.2 eV.

Cross section measurements were only possible above 35 eV in the laboratory. This low energy limit was imposed by the merging of the collision-induced dissociation peak into the normal peak as V_1 in Eq. (1) becomes smaller. This led to the practice of eliminating most of the fragment ions from the mass spectrum by operating the mass spectrometer at an energy above the ionization threshold of the parent but below the appearance-potential threshold of most of the fragments. This is being done in current experiments by use of photoionization where one not only eliminates the normal fragment peaks from the spectrum but also produces the parent ion in known vibrational and electronic excited states.

Figure 3 shows the energy dependence of the cross section for collision-induced dissociation of $C_2H_4^+$ into CH_2^+ and CH_2 by collision with He. A sharp decrease in the cross section for this process indicates a threshold in the neighborhood of 62.5 eV in the laboratory. An error of about 2.5 eV can be associated with this value. This leads to an upper limit of 7.81 ± 0.31 eV for the energy of dissociation of $C_2H_4^+$ into CH_2^+ and CH_2. This value is in agreement with that obtained by Maier[6] who used dissociative charge exchange.

One might notice that the cross section did not become zero at the threshold but continues to have a finite value below it. This is only a background that could be due to collision of $C_2H_4^+$ on impurities in the He (e.g., on C_2H_4 flowing from the ionization chamber into the collision chamber).

The endothermic ion-molecule reactions (1) $C_2H_4^+ + H_2 \rightarrow CH_3^+ + CH_3$ and (2) $C_2H_4^+ + H_2 \rightarrow CH_2^+ + CH_4$ were also investigated (Fig. 4). The results did not seem to indicate thresholds at the predicted values probably due to the background difficulties mentioned above as well as the internal energy distribution in the reactant ions.

Collision of $C_2H_4^+$ on D_2 produced ions at mass 30. The method used in the investigation of this process is to make the measurements while the collision gas is in the collision chamber and to measure again without the collision gas. The difference between the two measurements gives the effect due to collision. Fig. 5 gives the energy dependence of the cross section for this process. It is seen that the cross section is decreasing below 20 eV in the laboratory. This indicates that the process is endothermic. This also led to the speculation that the reaction product must be $C_2H_4D^+$ rather than $C_2H_2D_2^+$ since in the latter case the reaction is very nearly thermoneutral.

An improved ion source which produces the reactant ions by photoionization has been constructed and measurements are now in progress. Initial experiments on the reactions of O_2^+ on H_2 and He show significant variations in cross section as a function of both vibrational and electronic states of O_2^+ for both endothermic and exothermic reactions. A typical result for the endothermic collision-induced dissociation of O_2^+ on He at 300 V shows an increase in cross section by a factor of about two for vibrationally excited O_2^+ ions produced by light of wavelength 810 Å over those produced in the ground vibrational state by 1025.5 Å radiation. Still larger cross sections were observed for O^+ in the electronically excited $^4\pi_u$ state. Further experiments are in progress.

REFERENCES

1. J. A. Hipple, R. E. Fox and E. U. Condon, Phys. Rev. 69, 347 (1946).
2. F. M. Rourke, J. C. Sheffield, W. D. David and F. A. White, J. Chem. Phys. 31, 193 (1958).
3. C. Ottinger, Phys. Letters 16, 121 (1965).
4. R. Fuchs and R. Taubert, Z. Naturforschg 19a, 494, (1964).
5. R. Taubert, Z. Naturforschg 19a, 911 (1964).
6. W. B. Maier II, J. Chem. Phys. 42, 1790 (1964).

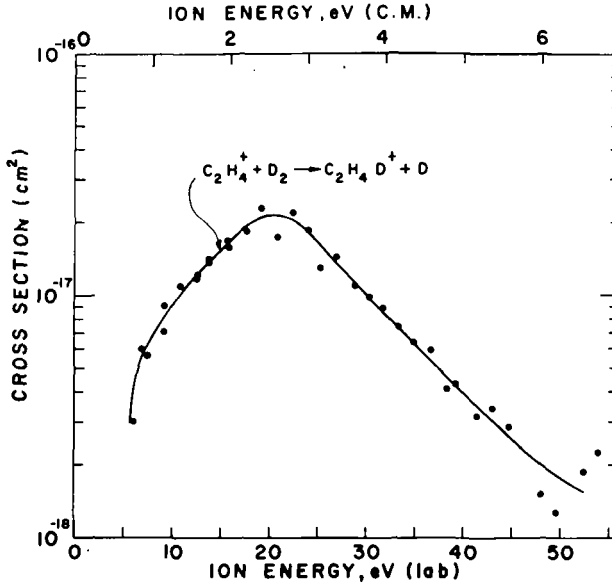

Fig. 5. Energy dependence of the cross section for the process indicated.

ON OBTAINING MICROSCOPIC CROSS SECTIONS FOR ION-MOLECULE REACTIONS

D. D. Briglia*, G. Gioumousis and T. E. Sharp
Lockheed Palo Alto Research Laboratories
Palo Alto, California

ABSTRACT

A new method is described which allows the microscopic cross section for ion-neutral collisions to be determined by use of the conventional mass spectrometer technique. The microscopic cross section is obtained by differentiation of the product of ion energy and phenomenological cross section. A numerical method is developed and applied to published data. Also, an experimental procedure is described wherein the process is performed automatically such that direct plots of the microscopic cross section versus ion energy may be obtained "on line".

New experimental data involving complex ion formation in deuterium is presented. These data indicate that at threshold a considerable amount of D_3^+ is formed by a neutral-neutral reaction,

$$D_2^* + D_2 \longrightarrow D_3^+ + (D + e^-).$$

INTRODUCTION

In this paper a procedure is suggested for obtaining the microscopic cross section for ion-molecule reactions from data obtained by the use of the conventional mass spectrometer method. To obtain the microscopic cross section a simple differentiation formula is suggested, developed into a numerical method and applied to published experimental ion-molecule data. Also, new experimental results of measurements of complex ion formation in deuterium will be presented.

DETERMINATION OF MICROSCOPIC CROSS SECTION BY NUMERICAL DIFFERENTIATION

As the pressure is raised above 10^{-5} torr in the ion source of a mass spectrometer, measurable quantities of secondary ions result from collision between neutral molecules and the primary ions formed by electron impact. In the conventional mass spectrometer method[1] in which a DC electric field is present in the reaction region, the observed secondary ions are the result of ion-molecule interactions characterized by a broad range of collision velocities. The secondary ion current, I_s, is thus proportional to an integral of the microscopic cross section, σ. As first shown by Boelrijk[2], the relationship between the secondary ion current and microscopic cross section is given in Equation (1), and is not intended to apply at very low electric fields,

$$I_s = \frac{I_p n \ell}{\varepsilon} \int_0^{\varepsilon} \sigma(\varepsilon')d\varepsilon'. \qquad (1)$$

Here I_p is the primary ion current, n is the number density of the neutral gas, ℓ is the path length, that is, the distance from the electron beam to the exit slit and ε is the relative kinetic energy of the ions at the exit slit. A phenomenological cross section Q may be defined[1] as the secondary ion current produced per unit primary ion current per molecule/cc of gas per unit path length,

$$Q = \frac{I_s}{I_p n \ell} \qquad (2)$$

Thus Q is related to the microscopic cross section by

$$Q = \frac{1}{\varepsilon} \int_0^{\varepsilon} \sigma(\varepsilon')d\varepsilon'. \qquad (3)$$

It was suggested by Boelrijk in 1961[2] and again by Light in 1964[3] that σ could be

*Present address:
ULTEK Corp., Palo Alto, California

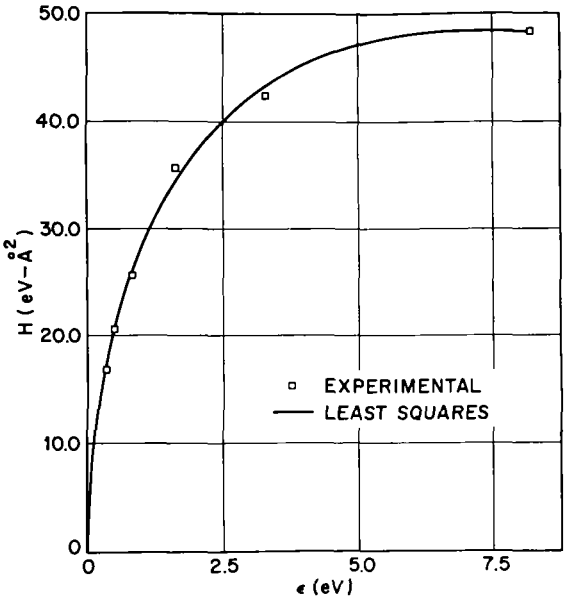
50.0
40.0
30.0
20.0
10.0
0
H (eV-Å²)
0
2.5
5.0
7.5
ε (eV)
EXPERIMENTAL
LEAST SQUARES

Fig. 1

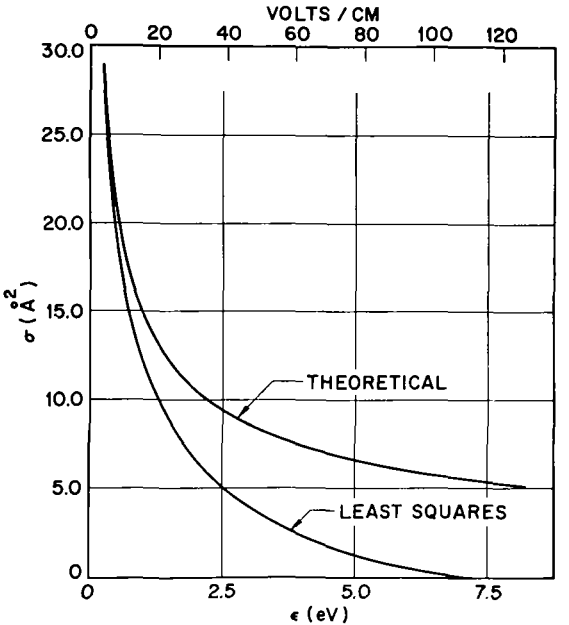
VOLTS / CM
0
20
40
60
80
100
120
30.0
25.0
20.0
15.0
10.0
5.0
0
σ (Å²)
THEORETICAL
LEAST SQUARES
0
2.5
5.0
7.5
ε (eV)

Fig. 2

obtained by differentiating Q with respect to the energy

$$\sigma(\epsilon) = Q + \epsilon \frac{dQ}{d\epsilon} . \tag{4}$$

A disadvantage is that this method involves taking the difference between two comparable quantities. An alternative method involves formation of an auxiliary function $H(\epsilon)$, which is equal to the product of kinetic energy and phenomenological cross section,

$$H(\epsilon) = \epsilon\, Q(\epsilon). \tag{5}$$

It is evident from Equations (3) and (5) that the microscopic cross section is equal to the derivative of H with respect to ϵ,

$$\sigma(\epsilon) = \frac{dH(\epsilon)}{d\epsilon} . \tag{6}$$

This relation is equivalent to that of Boerlrijk and of Light, but is simpler to apply both numerically and instrumentally. Unfortunately, the usual finite difference numerical differentiation formulas cannot be used with the scattered data points of some mass spectrometer experiments. However, we found it feasible to smooth the data by fitting a polynomial to it by a least squares Share program[4], and calculated σ by differentiating the polynomial analytically.

In Figure 1 we see the data of Reuben and Friedman[5] for the reaction between D_2^+ and D_2 leading to D_3^+, and the least squares fit of $H(\epsilon)$. The calculated cross section obtained from the data of Reuben and Friedman is shown in Figure 2, along with the theoretical prediction of Gioumousis and Stevenson for the D_3^+ reaction. The derived σ appears to go to zero at about ϵ = 7eV and becomes negative thereafter. However, because of the large spacing between the last two data points, the cross section beyond $\epsilon \approx$ 3eV cannot be trusted in detail. A better example is the data of Moran and Friedman[6] for the reaction between H_2^+ and Ne to give NeH^+ as shown in Figure 3. Here the data points are sufficiently closely spaced to allow a very good least squares fit of $H(\epsilon)$. It will be observed that $H(\epsilon)$ goes through a maximum at about ϵ = 8eV. The slope thus goes to zero here and becomes negative. This results, as shown in Figure 4, in the cross section becoming negative for the values of ϵ greater than 9eV. These results indicate that there are unexpected experimental difficulties at the higher energies. At the intermediate energies $\sigma(\epsilon)$ is about 75% of the theoretical value of Gioumousis and Stevenson[7] which is in agreement with Moran and Friedman's analysis, but there seems to be no sign of the threshold they interpreted from their data at about ϵ = 0.2eV. The exact origin of the experimental difficulty which results in an apparent negative cross section is not clear. Conceivably this is due to a mass discrimination between the primary and secondary ion which varies with the repeller voltage. It is unfortunate that the problem was not detected during the course of the experiment. In what follows a method of directly obtaining σ "on line" will be presented.

DIRECT MEASUREMENT OF σ BY AC MODULATION TECHNIQUES

By the use of AC modulation techniques the product of ϵ and $Q(\epsilon)$ can be effectively differentiated while the data are being taken. If a small sinusoidal AC voltage of amplitude δV and angular frequency ω is superimposed on the DC voltage, V, normally applied to the repeller the potential at the repeller is given by $V(t) = V + \delta V\cos\omega t$. The secondary ion current will then be modulated at the same frequency and will possess a small AC component:

$$I_s(t) = I_s + \frac{dI_s}{dV}\, \delta\, V\cos\omega t. \tag{7}$$

The ω -component of the product of the repeller voltage and secondary ion current is

$$\left[V(t)I_s(t)\right]_\omega = I_s + \frac{dI_s}{dV}\, \delta V\cos\omega t,$$

$$= \frac{d}{d\epsilon}\left[\epsilon Q(\epsilon)\right] I_p n \ell \delta\, V\cos\omega\, t \tag{8}$$

or

$$\left[V(t)I_s(t)\right]_\omega = \sigma(\epsilon)\, I_p n \ell \delta\, V\cos\omega t \tag{9}$$

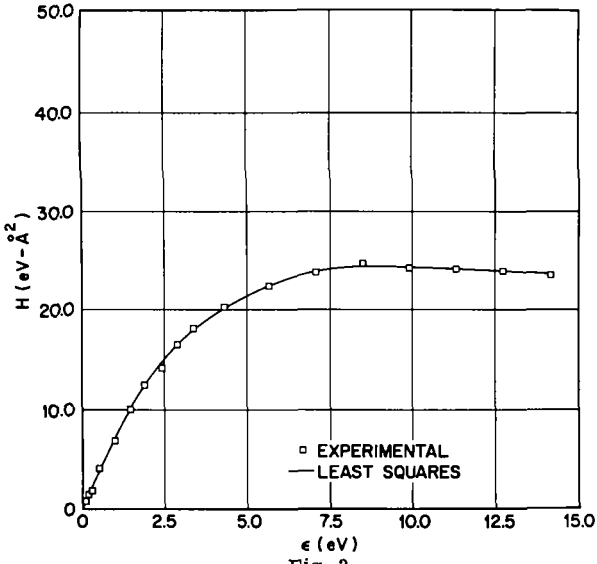
50.0
40.0
30.0
20.0
10.0
0
H (eV-Å²)
0
2.5
5.0
7.5
10.0
12.5
15.0
ε (eV)
EXPERIMENTAL
LEAST SQUARES
Fig. 3

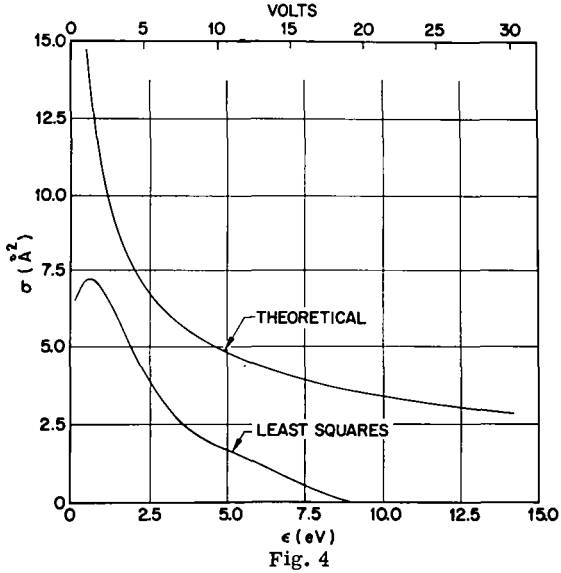
VOLTS
0
5
10
15
20
25
30
15.0
12.5
10.0
7.5
5.0
2.5
0
σ (Å²)
THEORETICAL
LEAST SQUARES
0
2.5
5.0
7.5
10.0
12.5
15.0
ε (eV)
Fig. 4

Thus the output of a detector tuned to the angular frequency ω will be directly proportional to the microscopic cross section,

$$V_{out}(\epsilon) = c\sigma(\epsilon) \tag{10}$$

All of the necessary operations can be performed by the use of commercially available electronic instrumentation. One such method is illustrated in Figure 5. The modulating voltage is obtained from the lock-in amplifier. The secondary ion current is detected by a fast electrometer or secondary emission multiplier, and fed into an analog multiplier. The DC voltage V and its AC component dV are applied to the repeller and also fed into the analog multiplier. The output of the analog multiplier is fed into the lock-in amplifier which synchronously detects the ω component. The output of the phase sensitive detector is directly proportional to σ. An AC modulation technique such as is described here will allow rapid determination of the fundamental quantity of interest, the microscopic cross section, by use of the conventional mass spectrometric method.

COMPLEX ION FORMATION IN DEUTERIUM

It is important to note, however, that there are other sources of complex ions in mass spectrometer ion sources as the data now to be presented will demonstrate. The apparatus employed, a combination of a Tate and Smith total ionization tube and a Bleakney 180° mass spectrometer, has been previously described[8] so we will only very quickly mention a few of its characteristics. As shown in Figure 3 of Reference 8, electrons emitted from an indirectly heated cathode are magnetically confined, pass through the ionization region and then are collected in an electron trap. In Figure 5 of Reference 8 the saturation characteristics of the electron trap for electrons of various energies is demonstrated. The electron current is relatively independent of electron energy due to the magnetic confinement. For studies involving mass analysis rather than total collection, the electric field is reversed and the ions are analyzed through 180° and collected on one of two collector slits.

The ionization efficiency for D_2^+ and D_3^+ has been measured in this instrument from threshold to 160 eV as shown in Figure 6. The shape of the two curves is quite similar, both passing through a maximum at $\sim$65eV. However, a detailed investigation of the region near threshold reveals an essential difference. This is shown in Figure 7. In the inset the efficiency curves near threshold for D_2^+ and D_3^+ as obtained by magnetic scanning are shown. D_3^+ is first observed when the electron energy is insufficient to form D_2^+. This is shown more strikingly by plotting the ratio of D_3^+ to D_2^+, which was obtained automatically by using two collectors, two vibrating reed electrometers and a digital ratiometer such that neither the electric field nor the magnetic field was varied. At $\sim$15.4 eV the ratio became infinite. These results indicate that a considerable portion of the D_3^+ near threshold is of non-ionic origin and suggests the existence of a Hornbeck-Molnar type process in deuterium involving long lived excited states of the neutral molecule,

$$D_2^* + D_2 \longrightarrow D_3^+ + (D + e^-).$$

Similar results were obtained in hydrogen and also in a separate experiment which used a Bleakney type ion source in conjunction with an electric quadrupole mass spectrometer. It is apparent that in using a single mass spectrometer to study ion-molecule reactions great care must be taken to ensure that contributions to the secondary ion current of non-ionic origin are not leading to incorrect values for the cross section.

CONCLUSION

In conclusion, a new method was described which allows the microscopic cross section for ion-neutral collisions to be determined by use of the conventional mass spectrometer experimental technique. The microscopic cross section is obtained by differentiation of the product of ion energy and phenomenological cross section. A numerical method was developed and applied to published data. Also an experimental procedure was described wherein the process may be performed automatically such that direct plots of the microscopic cross section versus ion energy may be obtained. Finally, new results of D_3^+ formation in D_2 were presented which indicated the existence of a Hornbeck-Molnar type process involving long lived excited states of D_2,

$$D_2^* + D_2 \longrightarrow D_3^+ + (D + e^-).$$

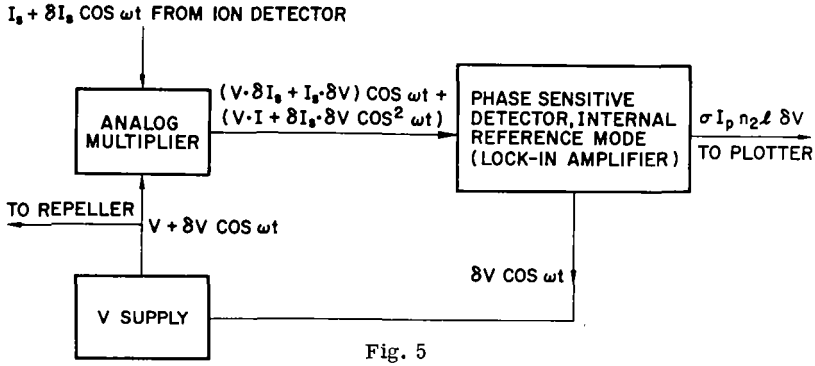

Fig. 5

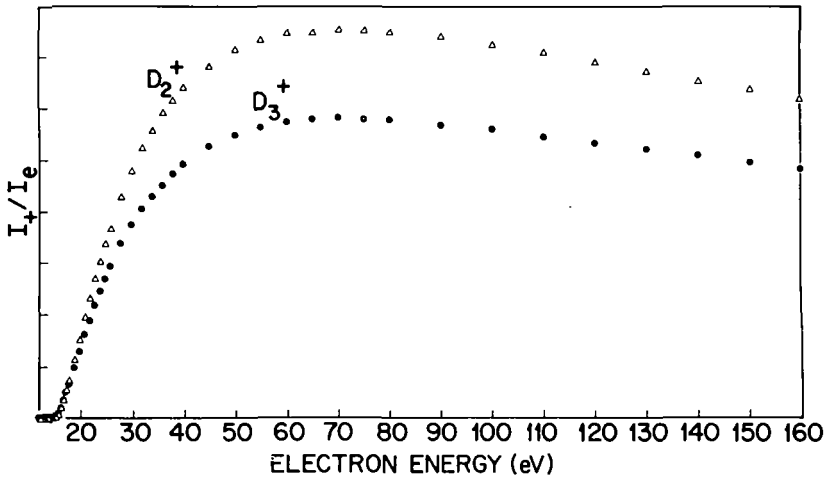

Fig. 6

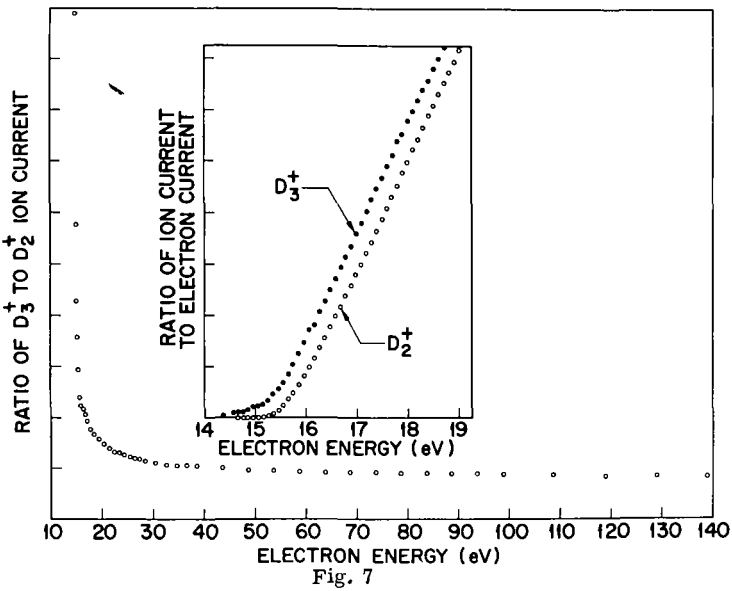

Fig. 7

REFERENCES

1. D. P. Stevenson and D. O. Schissler, J. Chem. Phys. 29, 282(1958)
2. N.A.I.M. Boelrijk, Thesis, University of Amsterdam, 1961 (Unpublished); N. Boelrijk and W. H. Hamill, J. Am. Chem. Soc. 84,732(1962)
3. J. C. Light, J. Chem. Phys. 41, 586(1964)
4. P. L. Kadakia, SHARE Program E2 SI PYFT
5. B. G. Reuben and L. Friedman, J. Chem. Phys. 37, 1636(1962)
6. T. F. Moran and L. Friedman, J. Chem. Phys. 39, 2491(1963)
7. G. Gioumousis and D. P. Stevenson, J. Chem. Phys. 29, 294(1958)
8. D. D. Briglia and D. Rapp, J. Chem. Phys. 42, 3201(1965)

FIGURE CAPTIONS

Figure 1 Least squares fit of the auxiliary function $H(\epsilon)$, using a second order polynomial, to the data of Reuben and Friedman for the reaction $D_2^+ + D_2 \rightarrow D_3^+ + D$.

Figure 2 Least square values of the microscopic cross section for D_3^+ formation obtained by differentiating the curve of Figure 1. Also shown is the theoretical prediction of Gioumousis and Stevenson for the D_3^+ formation cross section.

Figure 3 Least squares fit of the auxiliary function of $H(\epsilon)$ to the data of Moran and Friedman for the reaction $H_2^+ + Ne \rightarrow NeH^+ + H$. An eighth order polynomial was used for the points having $\epsilon < 4.75$ eV, and a fifth order polynomial for the points having $\epsilon > 4.75$eV.

Figure 4 Least squares and theoretical cross sections corresponding to the data of Figure 3 for NeH^+ formation.

Figure 5 Method for direct measurement of the microscopic cross section by use of AC modulation techniques.

Figure 6 Ionization efficiency curves for D_2^+ and D_3^+ from threshold to 160 eV.

Figure 7 D_2^+ and D_3^+ formation near threshold. The inset shows the D_2^+ and D_3^+ efficiencies as measured by use of a single slit and employing magnetic scanning. The ratio of D_3^+ to D_2^+ was obtained by simultaneously collecting the respective ion currents on each of the two slits.

ISOTOPE EFFECTS IN THE DISSOCIATION REACTIONS OF RARE GAS HYDRIDE IONS

R. W. Rozett and W. S. Koski
Department of Chemistry
The Johns Hopkins University
Baltimore, Maryland 21218

Introduction

Cross sections and isotope ratios for reactions such as:

$$X + HD^+ \rightarrow \begin{matrix} XH^+ + D \\ XD^+ + H \end{matrix} \qquad (1)$$

where X is a rare gas, have been measured as a function of energy in several tandem mass spectrometers.[1,2,3] Additional data is here supplied for the high energy form of the reaction:

$$X + HD^+ \rightarrow \begin{matrix} X + H^+ + D \\ X + D^+ + H \end{matrix} \qquad (2)$$

Together this information allows one to evaluate the adequacy of the various mechanisms proposed for ion-neutral reactions at higher energies. "High energy reactions" are defined in this context as those measured at more than several electron volts kinetic energy in the center of mass system, or those which generate large heats of reaction, or involve compounds with low dissociation energies. In such cases one expects mass transfer reactions (1) to evolve into reactions which involve the dissociation of the ionic projectile in the neutral target or the ionic products (2). Several mechanisms for such reactions will be described, evaluated and compared with experiment.

Apparatus.- The tandem mass spectrometer has been described previously.[4,5] The first stage is a modified commercial instrument, a 180° magnetic mass spectrometer with a 1 cm. radius of curvature and a constant magnetic field of 2.5 kilogauss. The second stage is a 60° magnetic sector instrument with an 8 inch radius. A gas is introduced into the ionizing chamber of the primary spectrometer where it passes through an electron beam of appropriate energy. The desired ions are mass analyzed, focused, and their energy set to any value from 2 to 200 eV. The usual primary intensities, measured in the reaction chamber, is of the order of 5×10^{-11} amps. These ions are introduced into a gas-filled collision chamber, and the product ions are extracted through a slit, focused, accelerated through 2 or 3 keV, mass analyzed, and counted by scalars with 40 megacycle resolution, working off the amplified pulse of a 17 stage electron multiplier.

I. ION-NEUTRAL REACTION MECHANISMS

1. The Complex Mechanism. The conventional interpretation of ion-molecule reactions is built around the induced polarization model introduced by Langevin. Gioumousis and Stevenson employed it to calculate rate constants from mass spectrometric data;[6] Rosenstock elaborated angular momentum considerations related to the model,[7] and others have applied it to structured ions.[8,9] Some degree of sophistication was brought to this ion-induced dipole model by the inclusion of interior degrees of freedom in a statistical-mechanical framework by Light, Tannenwald and others.[10,11]

The model envisages a projectile ion, P, approaching a polarizable target, T. Initially, at large r (inter-nuclear distance), the system is characterized by a linear kinetic energy, $E = \mu v_o^2/2$ which is gradually converted into a potential energy, $V = -\alpha e^2/2r^4$. The projectile is captured by the ion-induced dipole attraction, and spirals about the target. A rotational kinetic energy is generated which is equivalent to a repulsive potential, $E_r = L^2/2\mu r^2 = E b^2/r^2$, which limits the approach of the projectile. The cross section for such a reaction is related to the largest impact parameter, b_{max}, at which the attractive force can balance the centrifugal force. Hence the cross section decreases as the inverse square root of the incident ion energy, and inversely as the square root of the mass of the incident ion. In its simplest form, the model takes no account of permanent dipoles, the structure of the reactants, nor of the repulsive part of the interaction potential. When the cross section predicted is of the order of gas kinetic cross sections, repulsive forces become important, and the interaction no longer may be described by the Langevin potential. In the present experiments, which range as high as 30 eV in the center of mass system, one may safely assume that repulsive forces are important in the interaction potential, and that the complex mechanism no longer adequately represents the collisions.

2. The Spectator Mechanism. For higher energy reactions, Henglein and co-workers[12,13] as well as Datz,[14] have introduced the nuclear stripping model mechanism. One assumes

that the target may be treated as a swarm of independent particles, T and S. One component of the target, T, experiences an inelastic collision with the projectile P; the other component, S, is unchanged by the collision of its partner; it acquires no new momentum or kinetic energy from the collision, and is left behind as a spectator, while its partner is stripped off by the projectile.

All the relative kinetic energy of P and T, as well as the heat of reaction goes exclusively into the internal degrees of freedom of the product, PT. A simple consequence is that one may calculate the upper limit for the formation of the product ion as a function of the incident ion energy, the heat of reaction, Q, and the dissociation energy of the product ion, D. The total energy available as a source of internal energy is the sum of the initial center of mass kinetic energy, and the heat of reaction, Q. When this reaches the dissociation energy, an upper limit to product formation is reached, and the mass transfer reaction turns into a collision dissociation reaction. In the HD^+ reactions this may be formulated:

$$E^c = [(m_2+m_3)/m_3][(m_1+m_3)/m_1][D_{13}-Q]$$

E is the laboratory energy, D_{13} the dissociation energy of the product formed from masses 1 and 3, Q the heat of reaction, m_1, the monatomic target, m_2 and m_3 are the partners in the diatomic ion.

3. Rebound Mechanism.- At even higher energies than the critical limit for dissociation, mass transfer reactions are still possible by another mechanism, recently elaborated by Bates, Cook and Smith,[15] developing ideas of Thomas. Two successive binary elastic collisions are postulated, each independent of the other (impulse approximation). Compound formation is presumed if mass one is scattered from mass two, in the same direction and at the same speed as mass two is scattered from mass three. The cross section for such a process may be calculated, and expressed in simple fashion if certain mass relations hold.

1. $m_2 << m_1, m_3$

$$Q = [2\pi/3r^2][2D/m_2v_1^2]^{3/2}\sigma_{12}(60°)\sigma_{23}(60°)$$

2. $m_1 >> m_2 = m_3$

$$Q = [4\sqrt{2}\pi/3r^2][2D/m_2v_1^2]^{3/2}\sigma_{12}(90°)\sigma_{23}(90°)$$

3. $m_3 >> m_1 = m_2$

$$Q = [16\pi/3r^2][2D/m_2v_1^2]^{3/2}\sigma_{12}(90°)\sigma_{23}(90°)$$

The problem of calculating total cross sections, Q, is reduced to that of evaluating two differential elastic cross sections, $\sigma(\theta)$, and one may calculate the latter employing the classically exact expressions:[16]

$$\sigma(\theta) = b/\sin\theta \; db/d\theta$$

$$\theta = \pi - 2b\int_a^\infty r^{-2}(1-V(r)/E-b^2/r^2)^{-1/2}dr$$

One may not directly apply Bates' formulas to the HD^+ case, since the mass relationships are none of the above, but application of simple conservation laws allows one to calculate the angles at which XH^+ and XD^+ will be formed according to this mechanism. Then one may perform the above integral numerically on a computer using the Gauss-Mehler quadrature formula, first determining a, the distance of closest approach, for each incident energy and impact parameter. In our computations we employed the same set of potentials, V(r), as Bates, Cook, and Smith.

II. Isotope Ratios Predicted by the Mechanisms

1. Complex Mechanism.- The Gioumousis and Stevenson expression for the cross section predicts no isotope effect for the reactions of HD^+, since only the reactant masses appear as variables. The Rosenstock orbital angular momentum elaboration predicts a ratio = $m_{ip}m_{np}/m'_{ip}m'_{np}$ which is product dependent, but not energy dependent. (i = ion, n = neutral, p = product). The ratio XH^+/XD^+ is always greater than unity and less than two for the HD^+ reactions; for helium it is 1.67, neon 1.90, argon 1.93, krypton 1.98, and xenon 1.99.

The more elaborate theories of Light and Tannenwald are difficult to evaluate numerically, and in view of the high energy character of the reactions, this would be pointless.

2. Spectator Mechanism.- The significant advance of the spectator model is its prediction of an upper limit for cross sections. The ratios of the critical energies is given by the following formula for HD^+ reactions:

$$E^c_{XH^+}/E^c_{XD^+} = [m_2/(m_1+m_3)][(m_1+m_2)/m_3] = 2\ (m_1+2)/(m_1+1)$$

This is close to 2.0 for all the rare gases.

If we assume with Henglein that the cross sections for the isotopic reactions are the same for equal center of mass incident energy, then the hydride is always more prevalent than the deuteride in the laboratory system. Consequently, as the primary beam energy is increased, the isotope ratio XH^+/XD^+ increases from some value greater than one. When the laboratory beam energy, E, reaches $E^c_{XH^+}$, the deuteride abruptly begins to dissociate, and the isotope ratio climbs to infinity. If one observes the collision dissociation reaction which succeeds hydride and deuteride formation, then at $E^c_{XD^+}$, deuterons will appear with a D^+/H^+ ratio of infinity. As the primary beam energy is increased to $E^c_{XH^+}$, i.e. doubled, protons begin to appear, and the isotopic ratio drops to a ratio below one.

3. Rebound Mechanism.- If one applies considerations of conservation of energy and momentum to the interaction of HD^+ with a monatomic molecule, one may derive the angles at which the rebound conditions are fulfilled for the formation of the hydride and deuteride. We find in general that in the laboratory system, with ϕ the angle of deflection and θ the recoil angle; the rebound condition for compound formation is such that:[17]

$$\cos\theta = [(m_2+m_3)(m_1+m_2)/4m_1m_3]^{1/2}$$

$$\sin\phi = [(m_2^2/m_1m_3)(m_2+m_3)/(m_1+m_2)\sin^2\theta]^{1/2}$$

And in the center of mass system for the HD^+ reactions angles close to $\Theta = 75°$ and $\Theta' = 120°$ are appropriate for the rare gas reactions forming XH^+ and XD^+ respectively. The center of mass incident energy for each of the two successive collisions is the same.

An isotope ratio may then be found by computing elastic cross sections, σ, at the appropriate energy and angle:

$$\text{Ratio } XH^+/XD^+ = \frac{[\sigma_{12}(\theta,\ E/3)][\sigma_{23}(\theta,\ E/3)][M_d]^{3/2}}{[\sigma_{12}(\theta',2E/3)][\sigma_{23}(\theta',\ 2E/3)][M_h]^{3/2}}$$

If one considers the XH^+/XD^+ ratio as a product of three subratios, we find that the mass factor is a constant 2.83; each of the other ratios is always greater than one. The ratios of differential cross sections increase with incident energy; all the rare gases change in almost the same fashion with increasing energy, although xenon, krypton and argon are slightly larger than neon. Ratios from 15 to 30 have been calculated, which seem unreasonably high.

The mechanism predicts that HeD^+ cannot be formed; i.e. in this case the isotope ratio is always infinite. The deuteron cannot bounce off the proton strongly enough to fulfill the conditions for compound formation.

The cross sections predicted are quite small, varying as V^{-11}. At the same center of mass incident energy, the isotope ratio is not in general unity for HD^+ reactions.

III. Evaluation of Mechanisms.

1. Spectator Mechanism.- The stripping model has had some success in ion-molecule reactions. Henglein's work shows that the Ar^+ + HD reaction fits the calculated critical energies of 84 and 164 eV respectively, and consequently the isotope ratio approaches high values as 84 volts beam energy is reached in the laboratory system.[18] In addition, cross sections for reactions of He^+ and Ne^+ with HD are reported as small or nonexistent, and one expects no reaction from the stripping model, since D-Q is negative in each case.[19]

Moreover, in the HD^+ + Ar reactions, studied in several laboratories, evidence for a critical energy has been found, and the accompanying rise in isotope ratio as this critical upper limit is neared, which is somewhat above 20 eV.[1,2] Study of dissociation reactions in this laboratory leads to the same conclusion; at the same critical energy deuteron production becomes abundant, and at twice this energy, proton production shows a maximum. The same behavior is shown by xenon and krypton in these dissociation reactions; a proton peak appears at twice the energy of the deuteron peak.

However, this correspondence with the spectator predictions is numerically not good. The critical energies one calculates for HD^+ + X reactions are:

eV	He	Ne	Ar	Kr	Xe
$E^c_{XD^+}$	5.92	4.36	4.17	4.06	4.04
$E^c_{XH^+}$	9.85	8.35	8.15	8.05	8.0

These values scarcely fit the experimentally determined 20 eV and 40 eV. Another non-correspondence is noted in the dissociation reactions; at each of the critical energies a pair of proton and deuteron peaks appear. However, one may rationalize this doubling of peaks by assuming that a resonant charge transfer process between the D^+ and H at $E^c_{XD^+}$ and between H^+ and D at $E^c_{XH^+}$ accompanies the dissociation when the product ion and atom are still within close range of each other. Consequently, although critical energies have been observed in both the mass transfer and dissociation reactions of HD^+ with the rare gases, evidence for a pure spectator mechanism is lacking.

2. Rebound Mechanism.- The rebound mechanism does not predict an upper limit to the cross section for mass transfer, although since it varies as $E^{-5.5}$ approximately, the cross section drops to a small value very quickly. No critical upper limits are expected, though these are observed. The observation that HeD^+ cannot be formed by this mechanism shows that rebounding is not important in the measured He + HD^+ reaction. The observed isotopic ratios favor the hydride over the deuteride product in the energy range in question, as one expects from the rebound mechanism, but the calculated ratios are far greater than those measured over a wide energy range.

Consequently, the rebound mechanism seems inapplicable in the energy range of interest, or minimally, the rebound channel is relatively unimportant in the experimentally measured region.

Conclusion.- The experimental isotope ratios and cross sections for mass transfer and collision dissociation reactions of HD^+ with the rare gases bear out the assumption that a critical upper limit is of importance in the interpretation of the reactions of HD^+ with the rare gases. The complex mechanism is inadequate at the energies measured. The rebound model leads us to expect isotope ratios far higher than those observed. The spectator mechanism predicts an upper limit, which is in fact observed, but the experimental critical energy is higher than the pure spectator model leads one to expect.

Consequently, there is presently no adequate reaction mechanism for high energy ion-neutral reactions-

Acknowledgment.- This work was supported in part by the Directorate of Chemical Sciences, Air Force Office of Scientific Research, under Contract AF 49(638)-1301.

References

1. M. A. Berta and W. S. Koski, J. Am. Chem. Soc., 86, 5098 (1964).

2. J. H. Futrell, C. D. Miller and Fred P. Abramson, Proc. 14th Annual Conf. Mass Spectrometry, Dallas, Texas (1966).

3. C. F. Giese, Bull. Am. Phys. Soc. 9, 189 (1964).

4. E. R. Weiner, G. R. Hertel, and W. S. Koski, J. Am. Chem. Soc., 86, 788 (1964).

5. M. A. Berta and W. S. Koski, J. Am. Chem. Soc., 86, 5098 (1964).

6. G. Gioumousis and D. P. Stevenson, J. Chem. Phys., 29, 294 (1958).

7. H. M. Rosenstock, C. R. Mueller, M. B. Wallenstein, and M. L. Vestal, U. S. Atomic Energy Commission Report No. J.L. I.-650-3-7, UC-23 Isotopes-Industrial Technology TID-4500, 15th ed. (unpublished).

8. F. S. Klein and L. Friedman, J. Chem. Phys., 41, 1789 (1964).

9. B. Y. Ellis, M. A. Berta and W. S. Koski, Abstracts, 150th Meeting Am. Chem. Soc., Atlantic City, September, 1965.

10. J. C. Light, J. Chem. Phys., 40, 3221 (1964).

11. L. M. Tannenwald (1966).

12. A. Henglein and G. A. Muccini, J. Chem. Phys., 43, 1048 (1965).

13. A. Henglein and G. A. Muccini, Z. Naturforsch. 17a, 452 (1962).

14. R. Minturn, S. Datz and R. L. Becker, J. Chem. Phys., 44, 1149 (1966).

15. D. R. Bates, C. J. Cook, and F. J. Smith, Proc. Phys. Soc., 83, 49 (1964).

16. D. Bohm, Quantum Theory, Prentice-Hall, Englewood Cliffs, New Jersey, 1951, p. 522.

17. D. F. Munro, private communication.

18. K. Lacmann and A. Henglein, Ber. Bunsenges, physik. Chem., 69, 286 (1965).

19. L. Friedman and T. F. Moran, J. Chem. Phys., 42, 2624 (1965).

A TANDEM MASS SPECTROMETER FOR THE STUDY OF ION-MOLECULE REACTIONS

Jean H. Futrell and C. D. Miller*

Aerospace Research Laboratories
Wright-Patterson Air Force Base, Ohio

ABSTRACT

An instrument for the study of ion-neutral interactions involving momentum transfer to the product ions has been constructed. It consists of a double-focusing mass spectrometer which serves as an ion source for a collision chamber connected to a second double-focusing mass spectrometer. This instrument provides both mass and energy resolution of the impacting ion beam and the in-line configuration maximizes collection of momentum transfer products, as from ion-molecule reactions. Ion beams of experimentally useful intensity are produced over the energy range 0.2-100 eV with an energy spread of 0.3 eV.

INTRODUCTION

Early research on ion-molecule reactions used mass spectrometers which had been designed for analytical or other applications simply by increasing ion source pressures to the extent that a small number of the primary ions produced by electron impact could undergo reactive collisions with neutral molecules present in the source region. More recently efficient differential pumping techniques have been applied to permit source pressures in the millimeter range[1,2,3,4] without increasing analyzer tube pressures to unacceptably high levels. Under these conditions all primary ions suffer many collisions and are converted in successive reactions to more stable ionic products.

In favorable cases it is possible to establish from appearance potentials, ionization efficiency curves, or by isotopic labelling techniques the reactant - product relationships in a given system. This approach, however, suffers the inherent limitation that reactant ions are produced in the chamber into which the neutral reactant is introduced. Hence the neutral molecule is also exposed to electron bombardment and the many synergistic effects possible for gas mixtures undergoing electron bombardment in a heated chamber present possible complications in the interpretation of results.

An obvious solution to this problem is the physical separation of the ion source and reaction chambers by using a preliminary stage of mass analysis as an ion gun for a collision chamber into which the neutral reactant is introduced. Such instruments have been constructed previously for charge exchange studies by Weiner and Koski[5] and by Lindholm[6]. The advantages of these instruments for charge exchange studies are the same advantages they have for ion-molecule reaction studies, and they have recently been used for this purpose[7,8] also. A superior instrument for ion-molecule studies, which incorporates in-line geometry to maximize collection of momentum transfer products was constructed by Giese[9]. The instrument which we describe is conceptually very similar to the latter device and represents a substantial improvement over that instrument for certain types of experiments.

Description of Instrument

The instrument consists functionally of two double focusing mass spectrometers in tandem separated by a collision chamber with a separate gas handling system. The mass spectrometers, vacuum envelope, and basic electronic chassis were designed and constructed by the Bell and Howell Research Center under contract AF 33(657)-8249 during the period April, 1962 - October, 1964[10]. The essential features of the present instrument are described in the sections which follow and are shown schematically in Fig. 1.

---

*Visiting Research Associate, The Ohio State University Research Foundation, Columbus, Ohio.

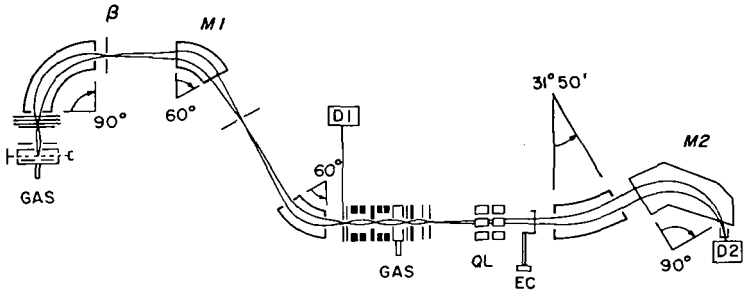

Fig. 1. Schematic of the ARL tandem mass spectrometer QL = quadrupole lens. EC = displaceable electrometer collector. M1, M2 = magnetic sectors and D1, D2 = ion detectors.

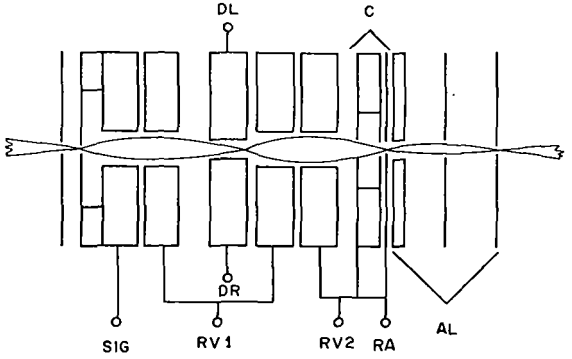

Fig. 2. Schematic of deceleration lens. Ion focal planes greatly exaggerated for clarity. SIG = source instrument ground, the reference potential for the ion gun. RV1, RV2 retarding voltage for first and second stages of deceleration. DL and DR are deflection plates for beam centering. C = collision chamber and RA = retarding analyzer for beam energy analysis. AL is the acceleration lens for the second stage spectrometer.

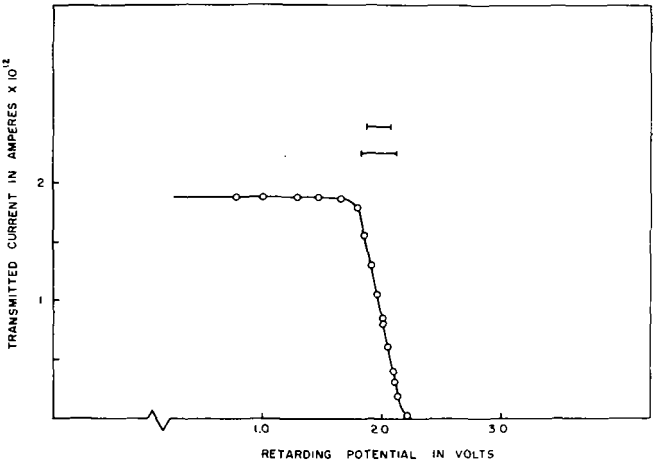

Fig. 3. Energy spread of 2 eV ion beam. Horizontal bars indicate theoretical energy spread of 0.2 eV and the experimental value of 0.3 eV deduced from this curve.

Ion Gun

The ion gun section consists of a gas handling system, an ion source, energy analyzer, mass analyzer, and various optical elements, along with the necessary electronics and vacuum components. A room temperature, glass sample handling system of conventional design with a Granville-Phillips model 203 manually variable leak is used. A modified Consolidated 21-110 gas source, model D-136900 is used. The ion exit aperture has been enlarged to 5mm x 0.62mm to increase sensitivity of the source and the focus plates have been trimmed to an aperture width of 1.1mm to make tuning less critical. At the higher ion intensities required for these studies space charge effects caused severe loss of resolution with the object slit of the source-acceleration lens system at the theoretical focal point of the electric sector. The slit was therefore moved back 0.5mm and mass resolution of the order of $M/\Delta M = 100$ for base line resolution was restored.

The mass spectrometer portion of the ion gun consists of a 90° electric sector and a 60° magnetic sector arranged geometrically so that the aberrations due to angular divergence and energy spread are corrected to second order. It corresponds to solution 9 of Table III in the treatment of Hintengerger and Konig[11] and its performance characteristics as a mass spectrometer have been described[10,12]. The electric sector has a mean optic radius of 3.396" and is terminated by Herzog shunts[13] chosen to terminate the field and to transmit an ion beam of half angle of divergence, α, of 0.0126 radians, for the object slit width of 0.0036". An energy slit, designated β in Fig. 1, with an aperture of 0.004" establishes the energy band pass of the electric sector at 0.2 eV kinetic energy and serves as an object slit for the 3" radius, 60° magnetic sector.

The electric sector has a magnification of 1.125, which when multiplied by the object slit width of 0.0036" determines the β slit width of 0.004. At the characteristic ion energy chosen for the ion gun, 169.8 eV, the energy (velocity) dispersion is thereby set at 2.77×10^{-4}, or 0.188 eV for 169.8 eV ions. The electric sector potentials required are + and - 20.00 volts on the outer and inner field plates.

The magnetic sector field is also terminated by Herzog shunts[14] and limiting stops to restrict the ion beam height to 0.150" and prevent any ions from grazing the magnetic field plates. An electromagnet is used to produce and scan the magnetic field plates, and is coupled to the field plates through a gap in the vacuum chamber which provides electrical isolation. It is obvious that the first stage mass spectrometer must float at the accelerating voltage of the second stage, so that this electrical isolation of the magnetic field plates is essential. The potential of the final acceleration slit (object slit) is the reference voltage of the ion gun assembly and is referred to as source instrument ground in subsequent discussion.

The β slit is electrically isolated from source instrument ground and is used to locate and monitor the ion beam transmitted by the electric sector. An electrometer temporarily connected to these plates is used in tuning the ion optic elements of the source and electric sector for maximum transmission. Final tuning is achieved by maximizing the dip for balanced sectors to assure that the most intense portion of the ion beam is centered. The electrometer is then disconnected and the β slit is then externally connected to source instrument ground.

Following the object slit of the ion source we have constructed as a Z-axis focusing element an Einzel lens[15] which is placed between the object slit and the electric sector as shown in Fig. 1. Assymmetric potentials are placed on the central lens element as required for steering the ion beam. Since the final optical configuration is so complicated this element is normally used only for steering in tuning the first stage. The Z-axis focusing capability is used to optimize overall ion beam transmission once a signal is obtained at the final detector.

The mass resolving slit of 0.007" is placed 4" from the exit edge of the magnetic field. The ion beam at this point theoretically has a width of ca. 0.003" and a half angle of divergence of 0.152 radius. The mass resolving slit serves as an object for the 60° turning electric sector shown in Fig. 1. This sector has an optic axis radius of 1.466", and by potentials of + and - 24.86 volts turns the beam and centers it in an aperture 0.004" wide which forms the object of the deceleration lens system. This plate also serves as a beam monitor and, when the sector voltages are unbalanced, serves as a total beam detector for the first stage mass spectrometer.

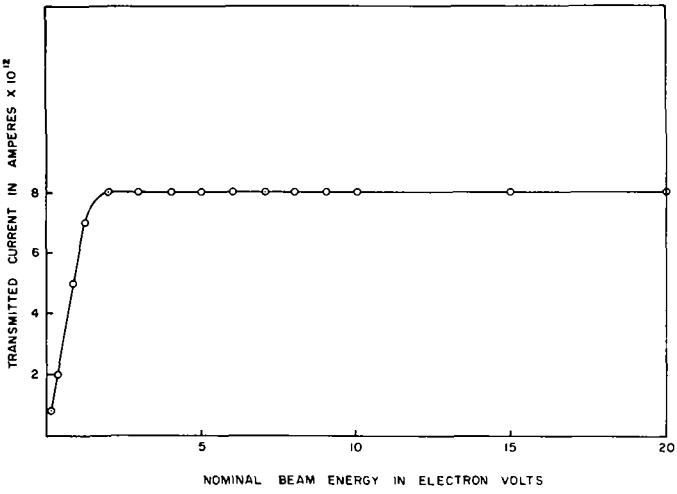

Fig. 4. Transmission curve of retarding lens.

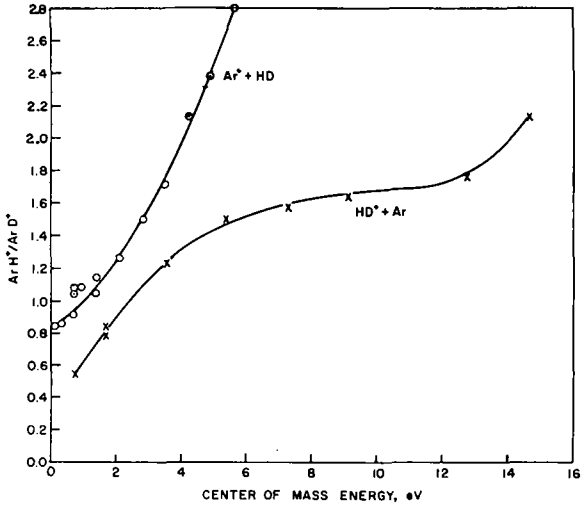

Fig. 5. Isotope effect in ion molecule reactions in the HD-argon system as a function of kinetic energy in the center of mass.

Deceleration Lens and Collision Chamber

The deceleration lens system is undoubtedly the most critical element in the application of the tandem mass spectrometer to the study of low energy ion-neutral interactions. The lens which we used was designed by Kuyatt and Simpson and is shown in Fig. 2. Nichrome V was chosen as construction material and sapphire rods and spacers were used for structural rigidity and electrical insulation.

The fixed points in the design are the location of the focal point of the turning electric sector and the object slit of the second stage mass analyzer, which in our apparatus are 2.25" apart. The design problem was therefore that of retarding ions of 169.8 eV kinetic energy to ca. 1-2 eV without defocusing the ion beam appreciably, injecting the ion beam into a collision chamber of sufficient length and accelerating and focusing product ions and unreacted primary ions on the object slit of the second spectrometer.

Achieving these objectives dictated the use of two stages for deceleration and a strong focusing system which maintains the slit geometry of the ion beam required for optimum performance of the mass spectrometers. For this purpose a "slot" lens system - i.e., thick slits which are long in the beam direction - was chosen. Since to the authors' knowledge this is the first application of slot lenses as an ion optical element, the design is presented in some detail.

The fact that slit lenses at the same voltage ratio are twice as strong focusing as circular aperture lenses is well known[16]. As a first approximation the same relationship will hold for other two dimensional lenses relative to three dimensional lenses of equivalent geometry. With this assumption the optical properties which have been worked out in detail for cylinder lenses may be used to design a slot lens system.

The design procedure may be accomplished most efficiently using P-Q curves given by Spangenberg[17]. These parametric curves present the object and image distances for a two-cylinder lens as a function of voltage ratio and magnification. The latter quantities were chosen from a consideration of acceptance angle of the second mass spectrometer with due regard for the Helmholtz-Lagrange Law[17] where α is the angle of divergence of the beam, S is beam size, and E is

$$\alpha \cdot S \cdot \sqrt{E} = \text{Constant} \qquad (1)$$

energy. From the properties of the entering ion beam and the geometrical requirements of the second stage spectrometer, an overall magnification of 4 and final energy of 2.1 eV (169.8/81 = 2.09) was chosen for the present system.

This deceleration is accomplished in two stages, so for each lens a magnification of 2 and voltage ratio of 9 pertains. Since the curves in Spangenberg[17] are drawn for an accelerated electron (or ion) beam and we are concerned with a deceleration system we interchange P and Q, the object and image distances, in the figure. Similarly a magnification of 0.5 rather than 2 is used. Finally we take into account the stronger focusing properties of the slot lens by taking the parametric curve for a voltage ratio of 18 to represent our chosen ratio of 9. The ordinate and abscissa of the M = 0.5, V_1/V_2 = 18 curves[18] yield an object distance of 1.6 slot widths and an image distance of 2.6 slot widths.

A slot width of 0.180" was used in our design, so the corresponding object and image distances are 0.288" and 0.468", respectively, as shown schematically in Fig. 2. The final image plane for the lens is the exit slit of the 0.170" long collision chamber, and a split slot for beam alignment is placed at the image plane of the first lens element. The exit slit width is 0.012", which is somewhat greater than the calculated beam width of 0.0096", and the entrance slit width is similarly somewhat larger than the beam width at that point. The exit slit of the chamber is electrically isolated from the body so that it can be used as an ion extraction slit or as a retarding potential device for measuring the kinetic energy of the impacting ion beam. For the reacceleration lens a standard lens originated by Soa[19] and described recently by Simpson[20] was selected. Both the deceleration and reacceleration lens systems are efficient, high transmission devices. Within experimental accuracy the total ion current collected by a collector placed behind the analyzer object slit was equal to the decrease in the current reading of electrometer D1 of Fig. 1 as the beam is swung into a centered position.

Since the lens system is held at the accelerating potential (1.8, 3.7, 7.5 KV) of the second mass spectrometer, it is necessary that it be carefully shielded from ground. This is accomplished by enclosing this assembly in a 90%

transparency mesh box attached to the intermediate lens. This procedure provides a good electrical shield without greatly impeding gas flow from the chamber.

A separate gas handling system connects to the collision chamber via a large diameter (12mm ID glass tube expanding to 22mm) some 3 feet in length sealed to a Granville-Phillips motor driven leak. A static pressure tube tees into this line and connects to the measuring side of a MKS Baratron model 77-M-XRD pressure sensor head of 0.1mm range. The signal generated by the Baratron is fed to a Granville-Phillips Automatic Pressure Controller which drives the leak to maintain a predetermined pressure in the chamber itself.

Contact potentials and space charge effects which alter the potential of the region from which ions are extracted from the source require occasional readjustment of repeller, focus plate, and acceleration potentials. Since the optical configuration of the ion gun transmits exactly 169.8 eV ions, however, it was possible to use a Deltron model A176 power supply and voltage divider for the retarding lens. Retarding potential analysis of the transmitted beam indicated that contact potentials in the lens and collision chamber region were negligible.

Product Ion Mass Analyzer

The second state mass spectrometer was constructed from components of a Consolidated model 21-110 mass spectrometer and has geometry identical to the commercial instrument. To make the two mass spectrometers compatible the object slit was enlarged to 0.008" and the electric sector termination slits were enlarged to 0.250". In addition the B slit which is located between the electric and magnetic sectors and which limits energy spread was removed to maximize ion transmission. A quadrupole lens scaled down by a factor of 0.8 from the design of Giese[21] was placed approximately mid-way between the object slit and the entrance slit of the electric sector. In our application the order of the potentials is approximately reversed. Giese used his lens to convert a rectangular beam into a tall, narrow beam which would match the object slit of his mass spectrometer. We use the lens to convert a tall, narrow beam to a shorter, rectangular beam which will be transmitted by the electric sector and by the rather narrow (0.100") magnet gap. In addition, assymmetric potentials are used for steering and for deflecting the beam onto electrometer collectors located in the drift spaces preceding the electric sector and between the electric and magnetic sectors.

As a detector we use an EMI model 9642B eighteen stage multiplier. The anode signal is amplified by a conventional electrometer and displayed on a Varian G14 recorder. In addition, a signal from the anode is capacitively coupled via a $27\mu_{\mu f}$ capacitor and 50 ohm cable to a Johnston Laboratories PAD-1 pulse amplifier and discriminator which drives a Computer Measurements Corporation model 706C counter. Pulse counting is the customary mode for recording secondary ion signals.

Vacuum System

In addition to the two pumping systems used for gas handling, four separate pumping systems are used in the overall instrument. The highest capacity unit is the collision chamber region consisting of a CVC (Consolidated Vacuum Corporation) PMC 1441 six inch diffusion pump, a CVC chevron ambient baffle, and a NRC (National Research Corporation) HN-6 optical baffle cold trap, backed by a Welch 1397 forepump. The trap is chilled continuously by a Tecumseh Freon-22 refrigerator. Convalex-10 polyphenyl ether pump fluid is used in all 6 diffusion pumps.

Two CVC PMC-21 4-inch pumps with chevron ambient baffles, and liquid nitrogen cold traps and backed by Welch 1400 pumps are used for the electric sector and magnetic sectors of the product analyzer. The ion gun spectrometer used a similar combination but, in addition, incorporates a CVC molecular sieve trap between the liquid nitrogen trap and the ambient baffle. This addition was found necessary because a severe problem developed in maintaining stable ion beams of moderate intensity at the low accelerating voltage used. The difficulty may be attributed to charge-up on ion bombardment of insulating films from backstreaming of pumping fluid, and the modification of the pumping system alleviated this condition. Painting of all surfaces exposed to low energy ion bombardment with colloidal graphite[22] was found to extend significantly the period of satisfactory operation before cleaning was required.

System Performance

The instrument for studying ion-molecule reactions described here performs

quite satisfactorily. The energy spread of the transmitted beam as determined by retarding potential analysis is given in Fig. 3. Similarly the transmission of the deceleration lens is quite satisfactory, as shown by a typical transmission curve is given in Fig. 4. It may be seen that the lens transmission is relatively constant over a large energy range and transmits a usable ion signal to very low energy. The curve was constructed by setting the voltage of the final lens element at the desired energy and adjusting the first lens potential for maximum signal. At higher energies than ca. 8V, this procedure resulted in only the second lens being used for deceleration.

Perhaps the most powerful characteristic of this type of instrument for ion-molecule reaction studies is the unambiguous specification of reaction partners and reaction products. It was of interest therefore to investigate one of the most often studied reaction systems, argon-hydrogen, about which considerable uncertainty as to reaction cross-sections, isotope effects, and kinetic energy effects still persist. Fig. 5 gives our experimental data for the isotope effect in this reaction as a function of center-of-mass energy of the reactants. The data show clearly that both reactions

$$Ar^+ + HD \rightarrow (ArH^+, ArD^+) + (D, H) \quad (2)$$

$$HD^+ + Ar \rightarrow (ArH^+, ArD^+) + (D, H) \quad (3)$$

occur and that isotope effects are rather different for the two reactions. This is undoubtedly related to the fact that vibrationally excited HD^+ ions are involved in reaction (3) while no initial vibrational excitation is possible in (2). More detailed considerations of new experimental data for this and other systems will be published elsewhere.

A further significant feature of the present design is the capability for operation at very low impacting ion energy. A sensitive test for low kinetic energy is the competition of H^- and H_2^- transfer reactions studied recently in this laboratory[23,24,25]. For the example

$$C_2H_4^+ + C_3H_8 \rightarrow C_3H_7^+ + C_2H_5 \quad (4)$$

$$\rightarrow C_3H_6^+ + C_2H_6 \quad (5)$$

the ratio of products from H^-/H_2^- transfer is 7/3 for low energy ions[24,26] and changes to 3.5 ± 0.5 for a terminal ion energy of 1.1 eV. Since low energy reactions predominate in conventional single-stage instruments, this variation implies a strong dependence on kinetic energy. For ca. 4 eV $C_2H_4^+$ ions, only the H^- transfer reaction is observed[27]. Our results for this ratio are 2.3 at 0.3 eV, 4 at 0.7 eV and 10 at 4 eV nominal ion energy. The correspondence with data from single-stage instruments is therefore quite good, and we take this agreement as chemical evidence that ions have the low energy indicated by physical measurements.

ACKNOWLEDGMENTS

The authors are greatly indebted to Drs. John Simpson and Chris Kuyatt of the Electron Physics Section of the National Bureau of Standards for the design of the deceleration lens system and for helpful discussion of ion optics problems. We also wish to acknowledge many helpful discussions of design and performance characteristics of double-focusing mass spectrometers with George Perkins and Dr. Charles Robinson of the Bell and Howell Research Center.

REFERENCES

1. C. E. Melton and P. S. Rudolph, J. Chem. Phys. 30, 847 (1959).

2. S. Wexler and N. Jesse, J. Am. Chem. Soc. 84, 3425 (1962).

3. F. H. Field and M. S. B. Munson, J. Am. Chem. Soc. 87, 3289 (1965).

4. P. Kebarle and A. M. Hogg, J. Chem. Phys. 42, 668 (1965).

5. E. Lindholm, Z. Naturforsch, 9a, 535 (1954).

6. E. R. Weiner, G. R. Hertel, and W. S. Koski, J. Am. Chem. Soc. 86, 788 (1964).

7. P. Wilmenius and E. Lindholm, Arkiv Fysik 21, 97 (1962).

8. M. A. Berta and W. S. Koski, J. Am. Chem. Soc. 86, 5098 (1964).

9. C. F. Geise and W. B. Maier II, J. Chem. Phys. 39, 739 (1963).

10. Inquiries regarding design and construction features of these components should be addressed to Mr. G. D. Perkins of the Bell and Howell Research Center, Pasadena, California 91107.

11. H. Hintenberger and L. A. König, in Advances in Mass Spectrometry, H. Elliott, ed, Pergamon Press, London (1959), p. 16.

12. G. Perkins, presented at the Thirteenth Annual Conference on Mass Spectrometry, Am. Soc. for Testing Materials Committee E-14, St. Louis, Missouri, May 1965.

13. R. Herzog, Zeitschrift Phys. 97, 596 (1935).

14. R. Herzog, Zeitschrift Naturforsch, 10a, 887 (1955).

15. K. R. Spangenberg, Vacuum Tubes, New York, McGraw-Hill Book Co. (1948), p. 349.

16. J. R. Pierce, Theory and Design of Electron Beams, p. 102, New York, D. Van Nostrand Co., Inc. (1949).

17. K. R. Spangenberg, ibid., p. 379.

18. The highest voltage ratio curve on the P-Q plot of reference 17 is V_1/V_2 = 11. However the curves may be calculated from the principles discussed in chapter 13 of that work. Dr. Kuyatt of the Electron Physics Section of the National Bureau of Standards, Washington, D. C. 20234, has continued the curves to V_1/V_2 = 25, and the P-Q parameters deduced here were interpolated from his curves.

19. E. A. Soa, Jenaer Jahrbuch 1959/1 (Carl Zeiss, Jena, 1959).

20. J. A. Simpson, Rev. Sci. Instr. 32, 1283 (1961).

21. C. F. Giese, Rev. Sci. Instr. 30, 260 (1959).

22. E. Lindholm, Rev. Sci. Instr. 31, 210 (1960).

23. L. W. Sieck and J. H. Futrell, J. Chem. Phys. (in press, 1966).

24. L. W. Sieck and J. H. Futrell, unpublished results.

25. L. I. Bone, F. P. Abramson, and J. H. Futrell (to be published, J. Chem. Phys., 1966).

26. M. S. B. Munson, J. L. Franklin, and F. H. Field, J. Phys. Chem. 68, 3098 (1964).

27. K. R. Ryan and J. H. Futrell, J. Chem. Phys. 42, 819 (1965).

THE REACTIONS OF $C_3H_6^+$ WITH C_3 AND C_4 PARAFFINS

L. Wayne Sieck* and J. H. Futrell

Aerospace Research Laboratories
Wright-Patterson Air Force Base, Ohio

ABSTRACT

Rate constants for H^- and H_2^- transfer from C_3 and C_4 paraffins to propylene and cyclopropane molecular ions have been determined for ions of low translational energy at the ionization threshold of $C_3H_6^+$. The results indicate that an increase in K_{H^-} is accompanied by a compensating decrease in $K_{H_2^-}$ and vice versa, such that the total reactivity of C_4 structural isomers is invariant. Using selectively labelled compounds it was possible to derive transfer probabilities for the various substituent sites on the normal butane carbon skeleton. Evidence is also presented which suggests that cyclopropane molecular ions do not assume the propylene-ion structure prior to or during reaction with C_4 paraffins. The results of the present investigation are compared with some complementary data obtained from radiolytic and photolytic systems at much higher pressures.

INTRODUCTION

In recent radiolysis and photolysis studies[1-3], the importance of H^- and H_2^- transfer reactions between hydrocarbons and unsaturated molecular ions containing fewer carbon atoms has been clearly demonstrated. The reactions are of the general type

$$C_nH_m^+ + RH_2 \rightarrow C_nH_{m+1} + RH^+ \qquad (1a)$$

$$C_nH_m^+ + RH_2 \rightarrow C_nH_{m+2} + R^+ \qquad (1b),$$

where $C_nH_m^+$ represents the olefinic ion. These processes have been observed in a number of cases in the mass spectrometer[4,5] at elevated pressures, and reactions of type (1a) have been studied in some detail for a number of systems.

Doepker and Ausloos in radiolysis and photolysis studies have been able to derive relative rate constants for (1b) for a number of hydrocarbons in the case where $C_nH_m^+$ was propylene-$C_3D_6^+$. In addition, an extensive investigation of the reverse reaction, $C_nH_m + RH_2^+ \rightarrow C_nH_{m+2} + R^+$ (2a), where RH_2^+ was the cyclohexane molecular ion has been reported by the same laboratory[6].

The present investigation was undertaken as a complementary mass spectrometric study in order to determine absolute rate constants for both processes (1a) and (1b) for the reactions of C_3 olefinic ions with C_3 and C_4 paraffins. The mass spectrometer is ideally sutied for this purpose since radiolysis studies can afford definitive information concerning only (1b) for these systems. It will be demonstrated, however, that the two techniques complement each other and that quantitative agreement concerning the mechanism of the reaction is obtained in some cases.

EXPERIMENTAL

The instrument used in this study, a modified Consolidated model 21-103C, has been described previously[7]. In order to attain the elevated source pressures required, the dimensions of the long axis of the ion exit slit and the electron beam aperature were reduced by factors of 5 and 6 respectively. These modifications resulted in an inlet system/source pressure ratio of approximately 200:1 as measured by the collected ion current technique described by Stevenson and Schissler[8].

---

*Visiting Research Associate, The Ohio State University Research Foundation. Columbus, Ohio.

Table I

Rate Constants (k's in units of 10^{-10} cc/molecule-sec.)[a]

Ion	Neutral	HD^-	H_2^-	D_2^-	H^-	D^-	$H_2^- + D^-(A)$
$C_3H_6^+$	C_3D_8			0.31		0.025	
$C_3D_6^+$	iC_4H_{10}		1.41		3.15		
	nC_4H_{10}		3.94		0.51		
$C_3H_6^+$	$CD_3CD_2CH_2CH_3$	2.15	(A)	0.71	0.20	(A)	1.03
	$CD_3CH_2CH_2CD_3$	1.30	(A)		0.36	(A)	2.69
	iC_4H_{10}	1.23			2.74		
	iC_4D_{10}			1.41		2.89	
	nC_4D_{10}[b]			2.89[b]		0.31[b]	
cyclo-$C_3H_6^+$	nC_4D_{10}[b]			0.59[b]		1.28[b]	
	iC_4D_{10}			0.05		1.46	

[a]Assuming k for $CH_4^+ + CH_4 \quad CH_5^+ + CH_3 = 1.10 \times 10^{-9}$ cc/molecule-sec.

[b]k's are lower limits (nC_4D_{10} contained significant quantities of $C_4D_8H_2$, C_4D_7H, and $C_4D_6H_4$).

Table II

Rate Constants (k's in units of 10^{-10} cc/molecule-sec.)[a]

			k
$C_3H_6^+ + C_3H_6$	→	$C_3H_7^+ + C_3H_5$	2.00
		$C_4H_8^+ + C_2H_4$	2.56
		$C_4H_7^+ + C_2H_5$	1.00
		$C_5H_9^+ + CH_3$	2.00
cyclo-$C_3H_6^+$ + cyclopropane	→	$C_3H_7^+ + C_3H_5$	0.15
		$C_4H_8^+ + C_2H_4$	0.95
$C_3D_6^+ + C_3D_6$	→	$C_3D_7^+ + C_3D_5$	1.10
		$C_4D_8^+ + C_2D_4$	2.70
		$C_4D_7^+ + C_2D_5$	0.93
		$C_5D_9^+ + CD_3$	1.55

[a]Assuming k for $CH_4^+ + CH_4 \rightarrow CH_5^+ + CH_3 = 1.10 \times 10^{-9}$ cc/molecule-sec.

In most experiments the electron energy, as defined by the filament to block voltage, was maintained at a nominal value of 8.63 eV. Because of the spread in the energy distribution and a small contribution from the repeller field this value was sufficient to cause ionization of the $C_nH_m^+$ component in the mixture without inducing significant primary ionization in the paraffin additive. This condition was necessary to eliminate possible complicating neutral transfer reactions of paraffin molecular ions (type 2a), which may concurrently generate the same secondary species as those produced by the interactions of interest in this investigation.

Electric fields in the ionization region were reduced by operating the electron trap at source potential and both ion repellers at 0.215 volts (0.86 V/cm). Some experiments were also performed at repeller fields of 10 V/cm. Space charge effects were minimized by operating at ionizing currents of 0.15 microamps and below after it was determined that somewhat higher current densities produced severe discrimination effects.

The deuterated compounds were obtained from Merck, Sharp, and Dohme. Ltd. Analysis indicated that the isotopic impurity was as follows: nC_4D_{10}-7.9% C_4D_9H, iC_4D_{10}-7.4% C_4D_9H, C_3D_8-3.91% C_3D_7H, and propylene C_3D_6-3.90% C_3D_5H. The unlabelled analogs were Phillips Research grade and all mixture componets were purified by gas chromatography. The positions of the H impurity in the perdeuterated compounds was not determined.

RESULTS

Representative samples of the raw data obtained in typical experiments are shown in Figures 1 and 2. In all experiments the data were plotted as fractions of the total ionization versus inlet pressure. The rates of formation of secondary ions were then determined relative to the rate of production of those butene molecular ions resulting from the reaction of $C_nH_m^+$ with the C_nH_m component in the mixture. This specific process occurs with a high cross section for all three reactant ions investigated in the present study ($C_3H_6^+$, $C_3D_6^+$ and cyclo-$C_3H_6^+$). For the mixture shown in Figure 1, for example, the rate constants for H^- and H_2^- transfer from n-C_4H_{10} to $C_3D_6^+$ were determined relative to that for the production of $C_4D_8^+$ resulting from $C_3D_6^+ + C_3D_6 \rightarrow C_4D_8^+ + C_2D_4$ (1). Absolute values for k_1 and for the analogous reactions of $C_3H_6^+$ and cyclo-$C_3H_6^+$ were derived in separate experiments. We have used the reaction $CH_4^+ + CH_4 \rightarrow CH_5^+ + CH_3$ as our standard for converting our relative rates to absolute values assuming $k = 1.10 \times 10^{-9}$ cc/molecule-sec at 0.86 V/cm.

The rate constants obtained by this method are listed in Table 1. Each value cited represents an average obtained from the investigation of mixtures in which the mole percentage of the RH_2 component was varied over a wide range. The error limits are estimated to be ±10% for the quoted values of k relative to the methane reaction. The relative values for R^+ and RH^+ formation for any of the *perprotonated paraffins are very reproducible, however, and can be determined* within the analytical accuracy of the instrument. Isotopic impurities in the RD_2 systems introduce a somewhat larger error into those results, and corrections for incomplete labelling could only be applied to the perdeuterated compounds. Therefore the only adjustments applied to the probabilities for H^-, D^-, H_2^-, D_2^- and HD^- transfer from CD_3CD_2- CH_2CH_3 and $CD_3CH_2CH_2CD_3$ to $C_3H_6^+$ were corrections for C_{13} contributions to adjacent ions on the mass scale.

Early in this investigation it was discovered that the combination of high current densities and low repeller fields markedly increased the extent of reaction of primary ions. The manifestation of this experimental artifact, which is probably attributable to a space-charge or ion-trapping phenomenon[9], is readily evident in Figure 3. Additional poorly reproducible source phenomena such as strange structure in ionization efficiency curves[10] and anomalous repeller curves[11] also appear under these conditions. These non-linearities in source behavior are removed by increasing repeller field strength, by decreasing gas pressure or ionizing current, or by some suitable combination of these parameters. Although this artifact is qualitatively useful for the observation of an overwhelmingly secondary ion spectrum at moderate ion source pressures, reliable kinetic data are best obtained under conditions which avoid this complication. It was most convenient in the present research to accomplish this by operating at low ionizing current (ca. 0.15 microamps). Under these conditions apparently ideal source behavior is observed. The kinetic data plotted in Figures 1 and 2 are typical of results obtained for all systems.

The rate constants for the reactions of $C_3H_6^+$ with C_3H_6, $C_3D_6^+$ with C_3D_6,

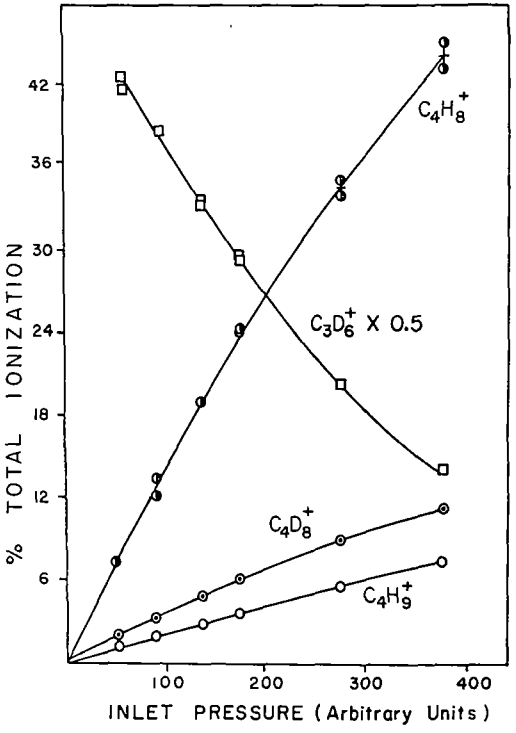

Fig. 1. Variation of Ion Distribution with Pressure for a Mixture Containing 29.7% C_3D_6 and 70.3% nC_4H_{10}.

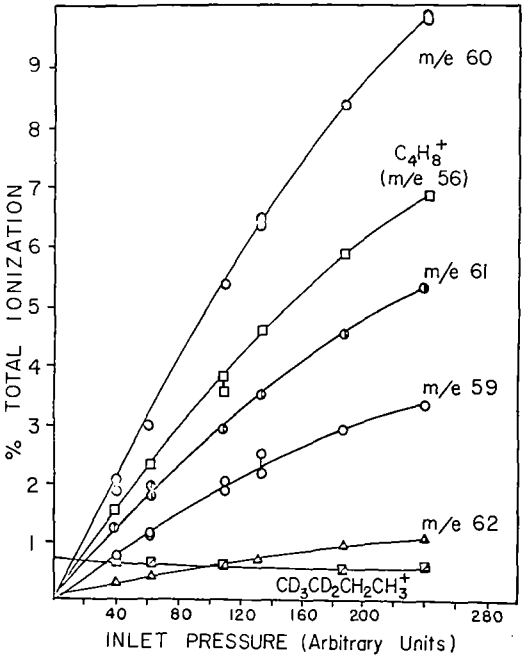

Fig. 2. Variation of Ion Distribution with Pressure for a Mixture Containing 20.1% C_3H_6 and 79.9% $nCD_3CD_2CH_2CH_3$.

and $(CH_2)_3^+$ with cyclo-C_3H_6 at field strengths of 0.86 V/cm are listed in Table II. At higher repeller fields (>10 V/cm), proton or deuteron transfer (or striping which is indistinguishable in our instrument) becomes increasingly important relative to the other alternative modes of reaction. The proton transfer reaction (or H abstraction) occurring in the $(CH_2)_3^+$ - cyclopropane system is here reported for the first time. The occurrence of this process was first postulated by Ausloos and Lias[6].

In addition to the data presented in the Tables, some other observations are of interest. In all experiments involving $C_nH_m^+$ and RH_2 mixtures, a secondary ion was noted at the mass appropriate to transfer of isotopic H· from RH_2 to $C_nH_m^+$; i.e., for a mixture of cyclo-C_3H_6 and n-C_4D_{10} the resultant species was $C_3H_6D^+$. The contribution to the total ion signal was really significant only for mixtures of C_3H_6 in C_3D_8. It was determined by appearance potential comparisons that in this particular case $C_3H_6D^+$ is produced mainly via a deuteron transfer reaction involving the propane molecular ion. The overall reaction, $C_3D_8^+ + C_3H_6 \rightarrow C_3H_6D^+ + C_3D_7$, has been reported previously. We have found this very efficient process to have a rate constant of $1.5 \pm 0.5 \times 10^9$ cc/molecule-sec. at 0.86 V/cm. The responsible precursors in the various other mixtures were not determined in the present investigation. However, by analogy with propane, proton transfer from RH_2^+ might generally be expected. If this is the case, then the cross-sections for these reactions must be quite large, for under our usual operating conditions RH_2^+ ions comprise less than 1% of the total ionization when C_nH_m is propylene. The RH_2 -cyclo-C_3H_6 system represents a different situation in this respect and will be discussed in another section. An equally plausible alternative to proton transfer is abstraction of a neutral atom by $C_nH_m^+$; viz. $C_nH_m^+ + RH_2 \rightarrow C_nH_{m+1}^+ + RH$. Recently Shannon and Harrison[12] have found both processes to occur simultaneously for a number of small molecules. Their observations suggest that in systems where one of the two alternative modes of reaction can be established, the complementary reverse reaction may also occur. This duality has been clearly demonstrated for processes of type (1b) and (2a) by Ausloos and co-workers.

The experiments involving cyclo-C_3H_6 required much more attention to detail than the analogous mixtures with propylene. Unfortunately the higher ionization potential of the cyclic structure (10.23 eV) required electron energies sufficient to produce significant ionization of the RH_2 component in the mixture. Therefore the magnitude of the contribution to the secondary spectrum initiated by RH_2^+ species had to be determined. This aspect of the problem was extremely critical since it was recognized that neutral transfer reactions involving butane molecular ions and cyclo-C_3H_6 could generate the same species as those produced by the interactions of cyclo-$C_3H_6^+$. Further complications arose because of the lower total reaction cross section of the cyclopropane molecular ion compared by propylene-$C_3H_6^+$. For this reason many more experiments were performed than with the analogous systems containing propylene and the composition of the mixtures used was varied over a considerably wider range (5 to 95 percent of each component). The data from these experiments indicated that the contributions to the secondary spectrum by the perdeutero butane molecular ions in the C_4 region were indeed negligible. Such a finding was not unexpected in view of the results of Ausloos and Lias indicating that cyclo-C_3H_6 is an order of magnitude less reactive than propylene in neutral transfer reactions[6].

DISCUSSION

The reactions of propylene ions with RH_2 additives observed in this study are of the two general types anticipated; H^- (type 1a) and H_2^- (type 1b) transfer. Although no significant variation in relative rates for the two processes were found at average ion energies below 0.2 eV, the ratio of kH^-/kH_2^- did increase for all systems at higher field strengths. From our data, however, it was not possible to determine which contributing reaction was responsible for this variation. We believe that the data listed in Tables I and II represents fairly accurately the kinetic parameters for low energy ions and that, therefore, the results may be correlated with data obtained in radiolysis and photolysis studies. In making this comparison it is only necessary to consider the relative rates of various competing processes, so that errors in the determination of absolute rate constants are not important.

In agreement with the findings of previous investigators we observe that total reactivity does not vary among structural isomers and does not depend upon the degree of isotopic substitution for the butanes studied. Furthermore, the ratio of rate constants for H_2- transfer to $C_3D_6^+$ from i-C_4H_{10} and n-C_4H_{10}

$\frac{k_{H_2^-} - (iC_4H_{10})}{k_{H_2^-} - (nC_4H_{10})}$ found in the present investigation (0.36) is in excellent agreement with the average value (0.38) for the same reactions derived from the data of Ausloos and co-workers[3]. Our results are therefore in complete accord with their prediction that an increase in k_{H^-} is accompanied by a compensating decrease in $k_{H_2^-}$, and vice versa, such that the total reactivity of structural isomers is invariant. When compared with the C_4 paraffins propane was found to exhibit a very low reactivity towards propylene ions. This finding is in accord with previous observations that the total rate of reaction generally increases with an increase in the molecular weight of RH_2. The only process occurring with a significant cross-section in this system according to our data is H_2^- transfer, the resonance exchange interaction which regenerates the reactants. The competing process, H^- transfer, is less probable by an order of magnitude, reflecting the relative inertness of primary and secondary hydrogens in this class of reactions. This trend is clearly demonstrated by the results obstained for the butane isomers, in which $\frac{k_{H^-} - (nC_4H_{10})}{k_{H^-} - (iC_4H_{10})}$ is only 0.16.

In view of the data of Ausloos and Lias[6], which suggested that cyclopropane molecular ions acquired the propylene-ion structure either prior to or during reaction with cyclohexane, we anticipated no significant differences between cyclo-$C_3H_6^+$ and propylene-C_3H_6 in their respective reactions with the perdeutero-butanes. In fact, however, the data contained in Table I indicates that marked dissimilarities exist. Even disregarding the differences in total reactivity, it is obvious that there is little or no similarity in the chemical reactions of the two types of $C_3H_6^+$ ions. For propylene ions with normal butane, an average value of $k_{H_2^-}/k_{H^-}$ of 8.6 is to be contrasted with a ratio of 0.46 for the analogous reaction of cyclo-C_3H_6 parent ion. Comparison of the isobutane mixtures yields similar differences in the mode of reaction. We must point out, however, that our data were obtained with electron energies close to the ionization threshold of cyclopropane. In a radiolysis system one might expect a spectrum of vibrationally excited molecular-ion species including a fraction which would dissociate in the much longer collision-free time available in the mass spectrometer ion source. Under these circumstances, the many cyclopropane ions may well assume the propylene structure prior to or during reaction because of a higher average excitation energy. However, our data suggest that at energies in the neighborhood of the ionization threshold cyclopropane and propylene $C_3H_6^+$ ions are readily distinguishible chemical entities.

It has been suggested (3) that only a loosely bound complex is involved in H^- and H_2^- transfer reactions. Consequently no H-D exchange occurs in the ion-molecule reaction complex lifetime. These authors also demonstrated that isomeric alkanes exhibit a constant total reactivity to $C_nH_{2n}^+$ ions. These observations are corroborated in the present research, and for the several isotopically substituted n-butanes investigated the total reactivity is essentially constant despite wide variation in relative rates of different reaction paths. Moreover, we do not observe a significant deviation in the rate constants for equivalent reactions in comparing analogous perprotonated and perdeuterated species, indicating the absence of large intramolecular isotope effects. This conclusion is also born out by our calculation of a self-consistent set of probabilities for the intramolecular transfer reactions of $CD_3CH_2CH_2CD_3$ and $CD_3CD_2CH_2CH_3$.

From these considerations it is possible to use the data of Table I to calculate which sites of the carbon skeleton participate in transfer reactions to $C_3H_6^+$. In our treatment the various probabilities are normalized to unity for all processes for a reaction pair and the customary designation of substituent position (1-4) is used. Since the data from both partially deuterated compounds is used concurrently to generate final probabilities effects of incomplete labelling are minimized. We shall first consider the H^- transfer reaction and then the more complex H_2^- transfer from various sites.

For the reaction $C_3H_6^+$ + butane → C_3H_7 + RH, the partial cross sections are readily assessed and have the values P(1) = P(4) = 0.006 and P(2) = P(#) = 0.044. The H_2^- loss from n-butane has been shown to be due in part to a stereospecific process in which the H atom in the terminal position is almost always transferred to the center carbon atom of the $C_3D_6^+$ ion (3,3a). This observation is corroborated by the magnitude of the rate constant for HD^- loss from $CD_3CH_2CH_2CH_3$ found in this investigation. In addition, reference to Table I also indicates that (1,4), (1,1), and (4,4) losses are negligible (no D_2^- loss from $CD_3CH_2CH_2$-CD_3). If we assume that (1,3) elimination is equally improbable, as implicity assumed by Gorden, then the probabilities for H_2^- loss in the process $C_3H_6^+$ + n-C_4H_{10}→products are as follows: P(2,3) = 0.53, P(3.4) = P(1,2) = 0.16, and

$P(3,3) = P(2,2) = 0.025$.

In the recent radiolysis and photolysis studies the ratio of $C_3D_7H/C_3D_6H_2$ resulting from the reaction of $C_3D_6^+$ ions with $CD_3CH_2CH_2CD_3$ was 0.80 within experimental error (3,3a). Our experimental data for this system and the positional probability calculation based on both of the partially labelled compounds would predict values of 0.50 and 0.55 respectively for this ratio. The agreement is quite satisfactory when one considers that at the much higher pressures employed by the previous workers, collisional deactivation or perturbation of the associated ion-molecule complex by surrounding molecules prior to decomposition is quite probable and may well effect the ratios obtained. On this basis (2,3) elimination would seem to require a slightly longer unimolecular half-life than the (1,2) process.

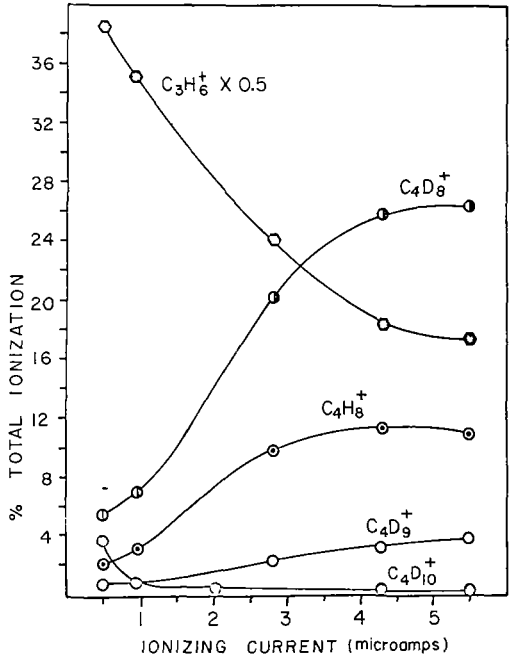

Fig. 3. Effect of Increasing Ionizing Current on Mass Spectrum of a Mixture Containing 16.6% C_3H_6 and 83.4% nC_4D_{10}.

REFERENCES

1. P. Ausloos, S. G. Lias, and I. B. Sandoval. Diss. Faraday Soc., 36, 66 (1963).

2. R. D. Doepker and P. Ausloos, presented at 148th ACS Meeting, Chicago, August-September 1964.

3. R. D. Doepker and P. Ausloos, submitted for publication.

3a. R. Gorden, Jr., R. Doepker, and P. Ausloos, submitted for publication.

4. M. S. B. Munson, J. L. Franklin, and F. H. Field, J. Phys. Chem., 68, 3098 (1964).

5. G. A. W. Derwish, A. Galli, A. Giardini-Gvidoni, and G. Volpi, J. Chem. Phys, 41, 2998 (1964).

6. P. Ausloos and S. G. Lias, J. Chem. Phys., 43, 127 (1965).

7. J. H. Futrell and T. O. Tiernan, J. Chem. Phys., 39, 2539 (1963).

8. D. O. Schissler and D. P. Stevenson, J. Chem. Phys., 24, 926 (1956).

9. M. H. Studier, Rev. Sci. Instr., 34, 1367 (1963).

10. L. Friedman, F. A. Long, and M. Wolfsberg, J. Chem. Phys., 31, 755 (1959), also R. F. Pottie and W. H. Hamill, J. Phys. Chem., 63, 877 (1959).

11. K. R. Ryan and J. H. Futrell, J. Chem. Phys., 42, 824 (1965).

12. T. W. Shannon and A. G. Harrison, J. Chem. Phys., 43, 4206 (1965).

REACTION RATE STUDIES USING PULSED ION CYCLOTRON RESONANCE

By
R. A. Fluegge and Darold Wobschall
Cornell Aeronautical Laboratory, Inc.
Buffalo, New York 14221

ABSTRACT

Recent modifications to the Ion Cyclotron Resonance Spectrometer[1] have improved its applicability to the determination of ion-molecule reaction cross sections at near thermal ion energies. A pulsed-electron beam is used for primary ionization; the number of secondary ions as well as the primary ion densities remaining in the chamber are measured as a function of reaction time. The ion concentration measurements are completed within times that are short compared to the average transit time out of the reaction chamber; hence, surface effects and apparatus parameters are negligible for reaction times in the millisecond range.

A rate constant for a charge transfer reaction in air ($N_2^+ + O_2 \longrightarrow N_2 + O_2^+$) has been determined and found to be in agreement with results of other experimenters.

* * * * *

The ion cyclotron resonance spectrometer has been under development for several years at the Cornell Aeronautical Laboratory, the work having been supported in part by the U. S. Army Research Office (Durham). The apparatus is closely related, in principle, to an omegatron type of mass spectrometer although major differences exist in its operating pressure range and in the ion detection scheme. The omegatron usually operates at pressures that minimize ion-molecule collisions, and it uses an ion collector-electrometer scheme to determine ion densities as a function of mass-to-charge ratio. In contrast, the ion cyclotron resonance spectrometer records the power absorbed by a group of ions placed in an rf electric field. To be effective, the rf field must oscillate at or near the ion's cyclotron frequency. The ICR detection scheme requires collisions that transfer momentum from ions to neutral molecules within the reaction chamber.

A simplified drawing of the steady-state ICR spectrometer is shown in Figure 1. Four circumferentially located metallic plates are used to form two sets of electrodes that surround the reaction chamber; two of the four are shown. Three longitudinally spaced electrode sets are shown; they are used in ion diffusion studies. Each pair of electrodes is used to produce an electric field which is perpendicular to the axial magnetic field of the surrounding solenoid. Ions formed by electron bombardment or through ion-molecule reactions will follow a cycloidal path about the magnetic field lines at their cyclotron frequency, eB/m, 85 KC/sec for nitrogen (N_2^+) placed in a magnetic field of 1500 gauss. Under these conditions, the radius of the ion orbit is about 0.8 mm at thermal velocities.

A block diagram of the electronics system applicable to steady-state operation is shown in Figure 2. An rf oscillator is uniformly swept in frequency between 30 and 1000 KC. This signal is fed into an rf bridge of which one arm consists of a pair of electrodes in the vacuum chamber. Power loss to the ions within the solenoid results in an unbalance of this bridge; the magnitude of the power loss is a function of the ion collision frequency. An af oscillator and phase sensitive detector are used to increase system sensitivity. A small modulation on the magnetic field within the solenoid has proved more practical than an equivalent modulation of the rf frequency. The recorder registers a signal closely approximating the differential of a Lorentzian line shape; our analysis assumes the properties of a Lorentzian line for relating the reduced collision cross section (ν_o) and the ion's mobility (μ), collision frequency (ν_c), and collision cross section (σ).

The power absorbed by an average ion as a function of the applied rf frequency can be estimated by averaging the solution to the ion's equation of motion:

$$m\dot{\underline{v}} + m\nu_o\underline{v} = e(v \times \hat{z}B + \hat{x}E_o \sin \omega t) \tag{1}$$

The velocity, $\underline{v}$, is the nonrandom velocity of an average ion cycloiding in a neutral gas. On the left side of the equation are the acceleration and momentum loss terms and on the right are the magnetic and electric force terms. The reduced collision frequency, ν_o, is related to the ion-molecule collision frequency for momentum transfer, ν_c, by

$$\nu_o = \frac{\nu_c M}{m+M} \tag{2}$$

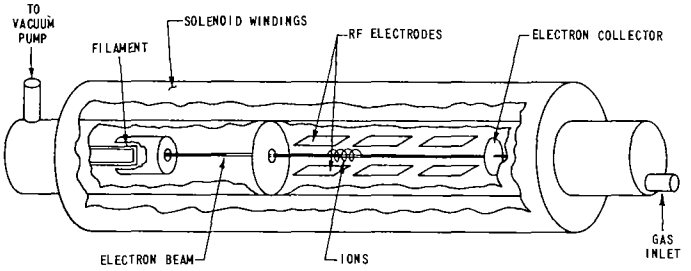

Figure 1. Ion Cyclotron Resonance Apparatus

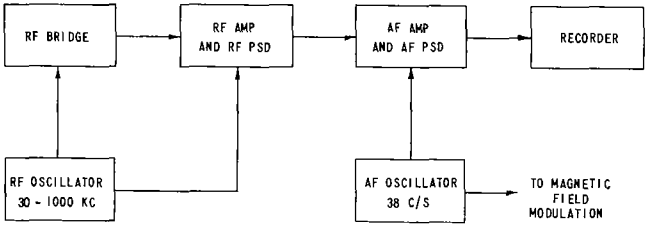

Figure 2. Steady-State ICR Spectrometer

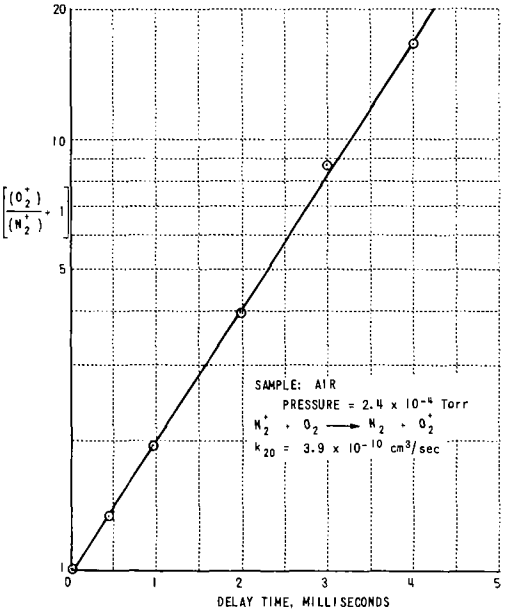

Figure 3. Effective Collision Frequency in Nitrogen

Solving equation (1) for v and time averaging the power absorption expression under the assumption of constant mean free time, one calculates that the average power, P(ω), absorbed by an average ion in an rf field is

$$P(\omega) = \frac{ne^2 E_0^2}{4m\nu_0}\left[\frac{1}{1+\left[\frac{(\omega-\omega_0)}{\nu_0}\right]^2}\right] \tag{3}$$

The power absorption is given as a function of the effective collision frequency at a given rf frequency, ω. We have shown in previous experiments that power absorption increases linearly with the number of ions in the chamber. Therefore, a term designating the particular ion density, n, has been included in equation (3). Note that maximum power absorption occurs when the rf frequency approaches the ion cyclotron frequency (ω_0). The frequency at which the peak occurs and the magnetic field strength can be related to obtain the mass-to-charge ratio of the colliding ion. The system is calibrated by putting in known gases and measuring their cyclotron frequency. Hence, the colliding ion can be identified by its mass-to-charge ratio and the number of ions in the chamber by the power absorption at resonance. Most of our experiments reported to date have been directed toward measuring the effective ion-molecule collision frequency and, hence, mobility of an ion in its parent gas. This kind of experiment results in the data shown in Figure 3. Here, the variation in the effective collision frequency for N_2^+ in N_2 as a function of pressure at a constant E/P is presented.

E/P was held constant at 5 volts/cm-Torr throughout this experiment. The ordinate intercept gives rise to a zero pressure line width approximately equal to $2\bar{c}/L$, where L is the length of the detector plates and $\bar{c}$ is the average speed of the ions. Assuming the ions are in thermal equilibrium with the molecules, the collision cross section can be estimated by:

$$\sigma = \frac{\left(1+\frac{m}{M}\right)^{1/2}}{\bar{c}}\,\frac{\nu_0}{N} \tag{4}$$

The slope of the line in Figure 3 gives rise to the ν_0/N term, and $\bar{c}$ is taken as corresponding to thermal energy. A cross section of 220 $\pm$ 25 A^2 is calculated. This cross section corresponds to a normalized mobility of 1.72 cm^2/volt-sec which is somewhat higher than the value recently reported by Keller, Martin and McDaniel[2] of 1.44 cm^2/volt-sec and about equal to the 1.70 $\pm$ 0.05 cm^2/volt-sec reported by Saporoschenko[3]. A difficulty in these measurements is the interpretation of the reduced collision frequency. The power lost by the electric field is a result of collisions that lead to ion-molecule reactions and charge transfer, as well as to elastic scattering processes. The experiments described below use a pulsed ionization and detection scheme to eliminate this problem. This new scheme only requires that power absorption be linear with ion density as given in equation (3).

A block diagram of the pulsed ICR system is shown in Figure 4. A pulse of electrons is accelerated into the cylindrically shaped measurement chamber parallel to the "Z" axis magnetic field as shown in Figure 1. The electron beam continues to flow for times adjustable between 0 and 10 milliseconds. Beam "on time" is controlled by the electron beam control grid pulse. Normally, electron beam "on time" is limited to periods on the order of 0.1 ms for slow, and on the order of 1 to 2 ms for fast, reaction rate measurements. The ions formed as a result of collisions between these electrons and gaseous molecules are constrained to the chamber axis by the intense magnetic field. A linearly polarized, rf electric field is applied at right angles to the magnetic flux; the frequency of this field is varied, and the energy absorbed by the ions is measured as a function of frequency. Maximum power absorption occurs at the ion's cyclotron frequency. The magnitude of this absorbed energy can be adjusted to be on the order of kT.

A time-delayed pulse (Pulse B Generator) is used to electronically switch the proper rf signal into the "output driver". This switching technique causes the rf phase sensitive detector to measure power absorption only during application of the time-delayed pulse. The recorder output registers a d.c. signal that is proportional to the number of ions present in the measurement chamber during the fixed time interval. The time delay between turning on the ionizing electron beam and the detection interval can be adjusted to any desired length. Ion concentrations can be measured with the electron beam still on, or after the beam is turned off and the electrons have drifted out of the measurement chamber. The system can be recycled as soon as all ions have been forced or allowed to leave the reaction chamber. Application of a "Z" axis electric field within the chamber causes a faster clearing-out process; the ions are accelerated out of the chamber, and a higher repetition rate can be used. The rf phase sensitive detector and the magnetic field intensity sweep, coupled with an af phase sensitive detector, are used to measure the ion concentrations in the chamber during fixed time intervals after their formation. The result is a measurement of ion concentrations in the reaction chamber as a function of time after creation.

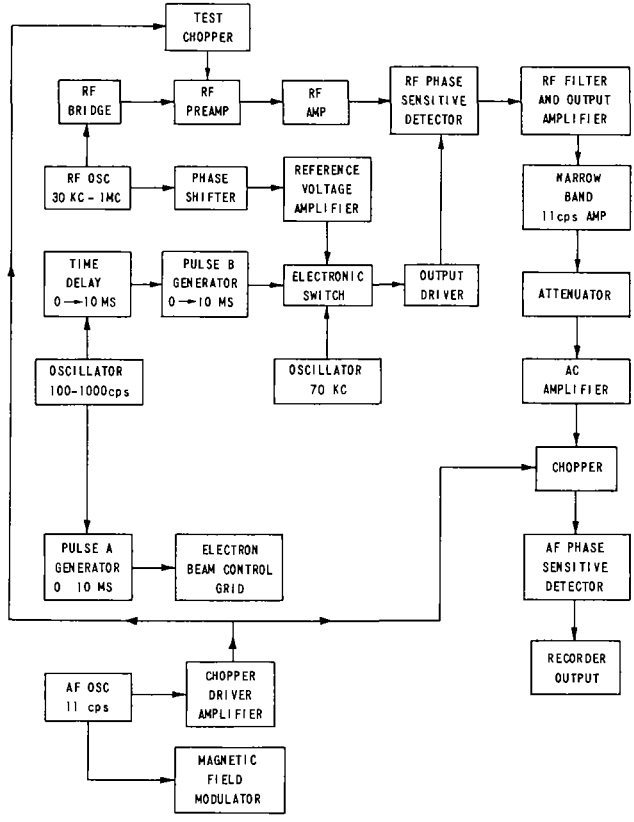

Figure 4. Pulsed ICR Spectrometer

The results of our preliminary studies in hydrogen are presented in Figure 5. The increase in the number of mass three ions as a function of time after turning on the electron beam is shown. The rate of increase can be linearly related to the ion-molecule rate constant using the following rate equations:

$$\frac{d(H_2^+)}{dt} = k_p (H_2)(e) - k_{10} (H_2^+)(H_2) \tag{5}$$

$$\frac{d(H_3^+)}{dt} = k_{10} (H_2^+)(H_2) \tag{6}$$

where:

(H_3^+) = mass 3 ion concentration

(H_2^+) = mass 2 ion concentration

(H_2) = hydrogen molecular concentration

(e) = primary electron density

k_p & k_{10} = rate constants for primary and secondary reactions, respectively.

Solutions to the above equations are:

$$(H_2^+) = \frac{k_p (H_2)(e)}{k_{10} (H_2)} \left[1 - \exp(-k_{10}(H_2)\, t)\right] \tag{7}$$

$$(H_3^+) = k_p (H_2)(e) \left[t + \frac{1}{k_{10}(H_2)} \exp(-k_{10}(H_2)\, t) - \frac{1}{k_{10}(H_2)}\right]$$

and

$$\frac{(H_3^+)}{(H_2^+)} = \frac{X}{1 - \exp(-X)} - 1 \tag{8}$$

where: $X = k_{10} (H_2)\, t.$

The conversion factors between the recorded data and a rate constant require a pressure measurement and relative ion density measurements as a function of time. The data of Figure 5 and the simultaneous measurement of the hydrogen gas density allow one to calculate a rate constant:

$$k_{10} = 1.5 \times 10^{-9}\ cm^3/sec.$$

This rate constant is between the low and high energy values of 0.6 and 2.0 x 10^{-9} cm^3/sec recently reported by Ryan and Futrell[4] and about equal to that reported by Saporoschenko[5]. We have attributed the horizontal portion of the curve in Figure 5 to ion losses at the end walls of the reaction chamber.

The results of a similar study of the reaction

$$N_2^+ + O_2 \longrightarrow O_2^+ + N_2 \tag{9}$$

are shown in Figure 6. These experimental data were obtained using different techniques than those used for the hydrogen results presented in Figure 5. The electron beam was turned on for about 0.5 ms and then turned off prior to detecting any power absorption by the N_2^+ and O_2^+ ions. The gate controlling the phase sensitive detector was turned on for fixed time intervals at several delay times after turning off the electron beam. The relative number of oxygen ions in the reaction chamber as a function of delay time after turning off the electron beam is given. The oxygen ion density increases relative to nitrogen for all times between 0 and 4 ms. The two densities are equal after a delay of 1 millisecond; beyond this time the O_2^+ ion densities increase as shown. Using rate equations similar to (5) and (6) above, a composite rate constant for charge exchange is given by:

$$k_{20} = \ln \left[\frac{(O_2^+)}{(N_2^+)} + 1\right] \Big/ (O_2)(t - t_o) \tag{10}$$

The reaction rate thus computed, 3.9 x $10^{-10} \cdot cm^3$/sec, is a composite of several reactions leading to O_2^+. Primary ions were formed by bombarding air with 65-volt electrons. N_2^+ ions as well as N^+ and perhaps some excited states of the N_2^+ ion contribute to the reaction rate reported here. Therefore, our results are probably good to

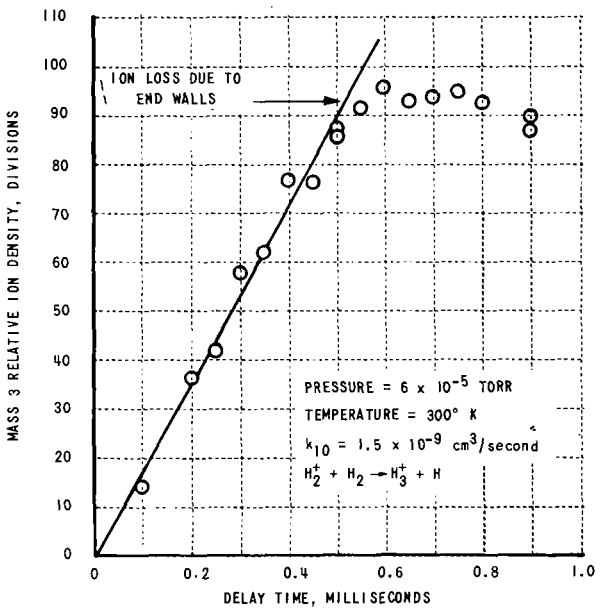

Figure 5. Ion-Molecule Reactions in Hydrogen

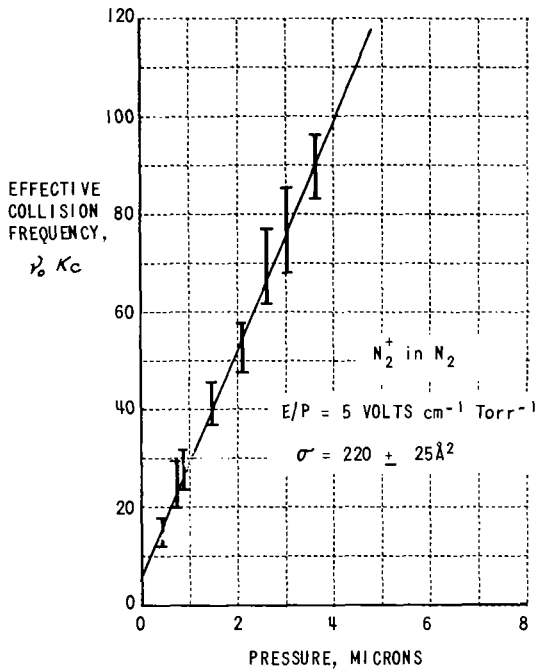

Figure 6. Ion-Molecule Reactions in Air

within a factor of 2 for the dominant $N_2^+ + O_2$ reaction occurring. This would be consistent with the recent results of Stebbings et al[6] (2×10^{-10} cm^3/sec for $N_2^+ + O_2 \longrightarrow N_2 + O_2^+$ and 5×10^{-10} cm^3/sec for $N^+ + O_2 \longrightarrow N + O_2^+$) and that of Fite et al[7] ($2 \times 10^{-10} cm^3$/sec for $N_2^+ + O_2$). These results indicate that the ICR technique can be applied to studies of low energy ion-molecule reaction rates. These rates can be calculated by relating relative ion densities to residence times in the reaction chamber. Ion densities are linearly related to power absorption; hence, most of the effects of instrumental parameters on line shape have been surmounted. We are now in a better position to obtain reliable reaction rate constants using the methods of pulsed ion cyclotron resonance.

FOOTNOTES

[1] D. Wobschall, Rev. Sci. Instr. 36, 466 (1965).

[2] Keller, G. E., Martin, D. W., and McDaniel E. W., Phys. Rev. 140 (1965) p. A1535.

[3] Saporoschenko, M., Phys. Rev. 139 (1965) p. A352.

[4] Ryan, K. R. and Futrell, J. H., J. of Chem. Phys. 42 (1965) p. 824.

[5] Saporoschenko, M., Phys. Rev. 42 (1965) p. 2760.

[6] Stebbings, R. F., Turner, B. R., and Rutherford, J. A., J. of Geo. Res. 71 (1966) p. 771.

[7] Fite, W. L., Rutherford, J. A., Snow, W. R., and Van Lint, V. A. J., Disc. Far. Soc. 33 (1962) p. 264.

[8] Warneck, P. and Poschenrieder, W. P., Paper #I2 presented at the 18th Gaseous Electronics Conference, October 1965.

[9] Fehsenfeld, F. C., Schmeltekopf, A. L., Gilman, G I., Puls, L. G., and Ferguson, E. E., Paper #I4 presented at the 18th Gaseous Electronics Conference, October 1965.

Competition Between Charge Transfer and Ion-Molecule Mechanisms in an Endothermic Negative Ion-Neutral Reaction

J. F. Paulson
Air Force Cambridge Research Laboratories
Office of Aerospace Research
Bedford, Massachusetts
and
F. Dale
Control Equipment Corporation
Needham Heights, Massachusetts

ABSTRACT

The reaction $O^- + O_2 \rightarrow O_2^- + O$ is endothermic by about 1 eV but is easily observed in a mass spectrometer ion source even at low electric field strengths because of the kinetic energy imparted to the O^- ion by the dissociative electron attachment process, $O_2 + e \rightarrow O^- + O$. The negative ion-neutral collision reaction may in principle proceed either through an electron transfer reaction or an ion-molecule reaction, i.e., ion-atom interchange, leading to formation of an unstable O_3^- ion, followed by dissociation.

Competition between charge transfer and ion-molecule mechanisms is of some theoretical interest and may be studied, in the case of the reaction considered here, by use of an isotopically labeled sample of O_2. The high pressure negative ion spectrum was obtained at repeller potentials between -4 and -12V, corresponding to field strengths from 10 to 30 V cm^{-1}. The rate constants for both reaction mechanisms increased throughout this range, reaching values of 2.2×10^{-11} $cm.^3$ $molec.^{-1}$ $sec.^{-1}$ (ion-molecule mechanism) and 6.6×10^{-11} $cm.^3$ $molec.^{-1}$ $sec.^{-1}$ (charge transfer mechanism) at the highest field strength. The ratio of these rate constants was found to be constant with field strengths between 12.5 and 30V cm^{-1}.

Introduction

Although the production of negative ions by dissociative and three-body electron attachment reactions has been extensively studied, the reactions of negative ions with neutral molecules have received little attention. Those negative ion-neutral reactions which have been observed (see e.g. references 1, 2) are estimated to have rate constants in the range of 10^{-9} to 10^{-11} $cm.^3$ $molec.^{-1}$ $sec.^{-1}$, suggesting that such processes are of possible importance in radiation chemistry and aeronomy. Competition between charge transfer and ion-atom interchange in ion-neutral reactions has also been little studied. The reaction considered here is particularly suited to an investigation of this competition because of the availability of $^{18}O^{18}O$ in high purity.

The dependence of the rate constants of ion-neutral reactions upon kinetic energy of the reactants continues to be of considerable interest. For endothermic reactions, available evidence from beam experiments (ref. 3) indicates that there is a sharp threshold in the reaction cross section at the energy in the center of mass system corresponding to the endothermicity of the reaction. The experimental system used in the present work does not permit observation of such a threshold but does show sharply increasing reaction cross sections with increasing electric field strength in the collision region.

Experimental

The reactions described were studied with a 6 inch 60 degree sector mass spectrometer. The ion source is of the Nier type, machined from a block of stainless steel and equipped with narrow electron entrance and ion exit slits so that relatively high source pressures can be maintained. The electron beam, produced by an emission regulated rhenium filament, enters the source through a 1.17 x 0.15 mm slit and is collimated by a 200 gauss magnetic field. The beam passes midway between the repeller plate and the ion exit slit and impinges on a trap maintained at the source potential. The electron current measured with a positive bias on the trap is 1×10^{-7}A. The repeller forms one side of the source chamber and is 4.0 mm from the exit slit.

Gas enters the source behind the repeller plate and must suffer many collisions with the walls before reaching the region of the electron beam. The source block is maintained at 200±10° C. Ions exit from the source through a 7.15x0.114 mm slit and are accelerated by a potential of 3500 V. The ion-accelerating region is evacuated with a two inch mercury diffusion pumping system which maintains this region at a pressure two orders of magnitude below that obtaining in the source chamber itself. The analyzer is evacuated with a six inch mercury diffusion pumping system maintaining a pressure below 1×10^{-6} torr when the pressure in the source is as high as 0.2 torr. Ion currents are measured with an electron multiplier whose gain has been calibrated with the aid of a faraday cup.

Pressure in the source is measured with a micromanometer connected to the gas inlet line following a variable leak. The micromanometer has been calibrated against molecular number densities in the source determined by collecting on the repeller all positive ions produced in each of several gases of known ionization cross section (ref. 4) with an electron beam of known energy and intensity. These calibrations agree to within 12 percent with pressure measurements made by connecting the micromanometer directly into the source chamber itself.

The mass spectrometer is equipped with an XY recorder and a motor driven potentiometer on the ionizing voltage control, giving continuous traces of ion current as a function of electron energy. Continuous traces are also obtained for ion current as a function of pressure. For the studies described here, in which low electron energies were used, it was necessary to adjust the nominal ionizing voltage as the repeller potential was varied so that the desired electron energy could be maintained. Calibration curves obtained from observation of the shift in the optimum nominal electron energy for production of O^- from CO_2 and in the half-width (full width at half maximum) of that peak are shown in Figures 1 and 2. The electron energy scale shown has been normalized at a repeller potential of 1 V to the electron energy (8.2 eV) found by Schulz (ref. 5) to be the optimum for CO_2 using a quasi-monochromatic electron beam. The normalization involved increasing the nominal electron energy, read on a differential voltmeter, by 0.2 eV. The optimum electron energy for production of the O^- peak whose onset was found by Schulz to be 3.85±0.1 eV is then 4.3 eV, compared to Schulz's value of 4.4 eV and to the value 4.3 eV obtained by Rapp and Briglia (ref. 6). The difference in optimum nominal electron energies for the two processes by which O^- is formed in CO_2 is seen from Figure 1 to be independent of repeller potential. The halfwidth increases from 1.6 eV at 1 V to 3.4 eV at 16V repeller potential. Electron energies reported in this paper are those obtained from the nominal values after correction with the aid of the calibration curves shown in Figure 1.

In this work the reacting negative ions were produced with electrons of low energy leading to resonance capture processes, rather than at higher energies where secondary electron capture and ion pair production occur. This method has the advantage that one ion species can be produced and its reactions studied largely to the exclusion of other processes possibly leading to the same product ion. In order to obtain easily measurable ion currents, however, it was necessary to use electron energies above the capture threshold, a procedure which results in the products of the dissociative resonance capture process having kinetic energies above that of the ambient gas. It is assumed in this paper that there is no spatial anisotropy in the velocity distributions of these products. Initially then, negative ions produced at any point in the electron beam have velocity vectors whose envelope is a sphere. If the repeller potential is sufficiently high, ions initially directed away from the plane of the exit slit are decelerated, their trajectories reversed, and finally accelerated toward the plane of the slit. The ion residence time and path length in the source may be estimated if it is assumed that the ion exit slit is infinitely thin and that the only ions collected are those whose initial motion is directed perpendicularly either toward or away from the plane of the slit. The average residence time, τ, for these ions is

$$\tau = \frac{d}{V_r} \left[\frac{m}{e} (2E_i + V_r) \right]^{\frac{1}{2}} \qquad (1)$$

TABLE I

RATE CONSTANTS (k) AND CROSS SECTIONS (σ) FOR $O^- + O_2 \rightarrow O_2^- + O$

Repeller Potential (V)	$10^{11} \times k$ (cm.^{3} molec.$^{-1}$ sec.$^{-1}$)	$10^{16} \times \sigma$ (cm.^{2})
4	1.7	0.51
5	2.3	0.65
6	3.0	0.80
7	4.3	1.11
8	5.6	1.37
9	6.4	1.50
10	7.6	1.71
11	8.7	1.87
12	9.3	1.93
13	10.8	2.19
14	10.9	2.14
15	12.1	2.31

TABLE II

RATE CONSTANTS FOR ION-ATOM INTERCHANGE (k_1) AND CHARGE TRANSFER(k_2)

Repeller Potential (V)	$10^{11} \times k_1$	$10^{11} \times k_2$
4	0.7	2.5
5	0.9	3.1
6	1.2	3.9
7	1.5	4.4
8	1.8	5.1
9	1.9	5.5
10	2.1	5.9
11	2.2	6.4
12	2.2	6.6

and the average path length, λ, is

$$\lambda = \frac{d}{2V_r} (2E_i + V_r) \qquad (2)$$

In equations 1 and 2, d is the distance from repeller to exit slit, V_r is the repeller potential, E_i is the initial ion kinetic energy, and m/e is the mass-to-charge ratio of the ion. Exact expressions for τ and λ for all the primary ions collected cannot be derived without information on the collection efficiencies for ions produced in the various regions of the source chamber, information not available for the type of source used here. Although data were taken over a range of repeller potentials, uncertainties in average residence times and in mass discrimination effects are more serious at low than at high V_r, and rate constants are therefore more reliable under the latter condition. It should be noted that at repeller potentials high compared to the initial kinetic energy of the reacting ions, equation 1 reduces to the usual expression for residence time of an initially thermal ion in a uniform electric field.

Results and Discussion

In Figures 3 and 4 are shown the data on O^- and O_2^- ion currents with varying electron energy and varying sample pressure. The curves in Figure 3 are seen to maximize at electron energies differing by about 1eV, probably reflecting the fact that reaction (3),

$$O^- + O_2 \rightarrow O_2^- + O \qquad (3)$$

is endothermic and that O^- ions in the high energy end of the distribution react much more rapidly than do those with lower kinetic energy. Reaction (3) was suggested by Burch and Geballe (ref. 7) to explain their data from a pulsed Townsend discharge in oxygen. The possibility that O_2^- might be formed by the three-body attachment process

$$e + O_2 + O_2 \rightarrow O_2^- + O_2 \qquad (4)$$

as suggested by Muschlitz (ref. 8), rather than by reaction (3), cannot be unequivocally eliminated, since the same second power dependence of O_2^- ion current upon sample pressure, shown in Figure 4, would be observed in either case. However, it is extremely improbable that the optimum electron energy for reaction (4) would be as high as shown in Figure 3, i.e., 6.9eV.

The initial kinetic energy of O^- ions produced by dissociative attachment in O_2 at an electron energy of 6.9eV may be determined from equation (5).

$$E_i = (1 - \beta) \left[E_e - (D-A) \right] \qquad (5)$$

In equation (5), E_i is the initial kinetic energy of the fragment ion; $\beta = m_i/M_o$ where m_i is the mass of the fragment ion and M_o the mass of the target molecule; E_e is the electron energy; D is the bond dissociation energy; and A is the electron affinity. Application of equation (5) to O^- ions from O_2, using values of 1.465 eV (ref. 9) for A(O) and 5.09 eV (ref. 10) for D(O-O), gives E_i = 1.64 eV. Rate constants and cross sections for reaction (3) from data at varying repeller potential are shown in Table I and are seen to increase sharply with increasing field strength, i.e., kinetic energy of the O^- ions, as expected for an endothermic process. The rate constants were determined by the use of the equation

$$k = \frac{i_2}{(i_1 + i_2)\, n\tau}$$

where i_1 and i_2 are the currents of primary and secondary ions, respectively, n is the number density of reactant neutral molecules, and τ is the residence time of the primary ions, given by equation (1). Cross sections were determined from

$$\sigma = \frac{i_2}{(i_1 + i_2)\, n\, \lambda}$$

where λ, the primary ion path length, is given by equation (2).

Reaction 3 might conceivably proceed through either an ion-atom interchange mechanism (reaction 6) or a charge transfer mechanism (reaction 7),

$$^{16}O^- + {}^{18}O_2 \rightarrow {}^{16}O\,{}^{18}O^- + {}^{18}O \qquad (6)$$

$$^{16}O^- + {}^{18}O_2 \rightarrow {}^{18}O\,{}^{18}O^- + {}^{16}O \qquad (7)$$

These possibilities may be investigated with an isotopically labeled sample. Using an equimolar mixture of $^{16}O_2$ and $^{18}O_2$, together with a small amount of $^{16}O\,{}^{18}O$ impurity, the following set of reactions contributing to the ion-atom interchange mechanism must be considered:

$$^{16}O^- + {}^{16}O_2 \rightarrow {}^{16}O_2^- + {}^{16}O$$

$$^{18}O^- + {}^{18}O_2 \rightarrow {}^{18}O_2^- + {}^{18}O$$

$$^{16}O^- + {}^{18}O_2 \rightarrow {}^{16}O\,{}^{18}O^- + {}^{18}O$$

$$^{18}O^- + {}^{16}O_2 \rightarrow {}^{16}O\,{}^{18}O^- + {}^{16}O$$

$$^{16}O^- + {}^{16}O\,{}^{18}O \rightarrow {}^{16}O\,{}^{18}O^- + {}^{16}O$$

$$^{16}O^- + {}^{16}O\,{}^{18}O \rightarrow {}^{16}O_2^- + {}^{18}O$$

$$^{18}O^- + {}^{16}O\,{}^{18}O \rightarrow {}^{16}O\,{}^{18}O^- + {}^{18}O$$

$$^{18}O^- + {}^{16}O\,{}^{18}O \rightarrow {}^{18}O_2^- + {}^{16}O$$

The following set contribute to the charge transfer mechanism:

$$^{16}O^- + {}^{18}O_2 \rightarrow {}^{18}O_2^- + {}^{16}O$$

$$^{16}O^- + {}^{16}O_2 \rightarrow {}^{16}O_2^- + {}^{16}O$$

$$^{18}O^- + {}^{16}O_2 \rightarrow {}^{16}O_2^- + {}^{18}O$$

$$^{18}O^- + {}^{18}O_2 \rightarrow {}^{18}O_2^- + {}^{18}O$$

$$^{16}O^- + {}^{16}O\,{}^{18}O \rightarrow {}^{16}O\,{}^{18}O^- + {}^{16}O$$

$$^{18}O^- + {}^{16}O\,{}^{18}O \rightarrow {}^{16}O\,{}^{18}O^- + {}^{18}O$$

Realizing that the last four listed reactions of the ion-atom interchange mechanism each have only one-half the statistical probability of occurring as do the first four, and assuming no isotope effect on the rate constants, we can write the following set of rate equations:

$$\frac{di_{34}}{dt} = k_1 i_{16} n_{36}\, k_1 i_{18} n_{32} + \tfrac{1}{2} k_1 i_{16} n_{34} + \tfrac{1}{2} k_1 i_{18} n_{34}\, k_2 i_{16} n_{34} + k_2 i_{18} n_{34} \qquad (8)$$

$$\frac{di_{32}}{dt} = k_1 i_{16} n_{32} + \tfrac{1}{2} k_1 i_{16} n_{34} + k_2 i_{16} n_{32} + k_2 i_{18} n_{32} \qquad (9)$$

$$\frac{di_{36}}{dt} = k_1 i_{18} n_{36} + \tfrac{1}{2} k_1 i_{18} n_{34} + k_2 i_{16} n_{36} + k_2 i_{18} n_{36} \qquad (10)$$

In equations (8), (9) and (10), i_j is the number density of the ionic species of $m/e = j$, and n_{32}, n_{34}, and n_{36} are the number densities of $^{16}O_2$, $^{16}O\ ^{18}O$, and $^{18}O_2$, respectively, in the ion source. The rate constants are k_1 and k_2 for the ion-atom interchange and charge transfer mechanisms, respectively.

Assuming equal collection efficiencies for all ionic species, it is found experimentally that $i_{16} \approx i_{18}$, $n_{32} \approx n_{36}$, and $n_{34} = 4.3 \times 10^{-2}\, n_{32}$ in the sample mixture. Realizing that at $t = 0$, $i_{32} = i_{34} = i_{36} = 0$, and that the consumption of reactant ions is negligible, we can write, from equation (8),

$$\frac{i_{34}}{i_{16}} = 2.043\, k_i\, n_{32}\, \tau + 0.086\, k_2\, n_{32} \tag{11}$$

and from equation (9)

$$\frac{i_{32}}{i_{16}} = 1.0215\, k_i\, n_{32}\, \tau + 2\, k_2\, n_{32}\, \tau \tag{12}$$

For simplicity the residence times, τ, of $^{16}O^-$ and of $^{18}O^-$ are here assumed to be equal. With equations (11) and (12) it is now possible to determine the rate constants k_1 and k_2 at different V_r. The results are shown in Table II and are in fair agreement with the rate constants obtained using ordinary oxygen. It is significant that the ratio of k_1 to k_2 is approximately independent of repeller potential in the range from about 5 to 12 V, i.e., primary ion maximum energies from 4.1 to 7.6 eV. The behavior of this ratio at still higher interaction energies would be of considerable interest to the theory of ion-neutral collision reactions.

Conclusion

It should be borne in mind that the rate constants and cross sections obtained in this work are averaged over a wide range of interaction energies and therefore can be considered only as estimates of the correct values. At low repeller potentials discrimination arising from the initial kinetic energy of the O^- ions makes their measurement uncertain. At high repeller potentials defocusing of the ion beam occurs, leading to decreased signal-to-noise ratios. However, the presence of a high electric field in the reaction region does ensure that anisotropic scattering effects are minimized and thus that primary and secondary ions are collected with approximately equal efficiency.

REFERENCES

1. R.K. Curran, Phys. Rev. 125, 910 (1962).
2. A. Henglein and G.A. Muccini, "Chemical Effects of Nuclear Transformations," pp 89-98, International Atomic Energy Agency, Vienna, 1961.
3. W.B. Maier, J. Chem. Phys. 41, 2174 (1964).
4. D. Rapp and P. Englander-Golden, J. Chem. Phys. 43, 1464 (1965).
5. G.J. Schulz, Phys. Rev. 128, 178 (1962).
6. D. Rapp and D.D. Briglia, J. Chem. Phys. 43, 1480 (1965).
7. D.S. Burch and R. Geballe, Phys. Rev. 106, 188 (1957).
8. E.E. Muschlitz, J. Appl. Phys. 28, 1414 (1957).
9. L.M. Branscomb, D.S. Burch, S.J. Smith, and S. Geltman, Phys. Rev. 111, 504 (1958).
10. B.J. McBride, S. Heimel, J.G. Ehlers, and S. Gordon, NASA Scientific Publication SP-3001, Lewis Research Center, Cleveland, 1963.

Figure Captions

Fig. 1 Optimum nominal electron accelerating voltages for production of O^- from CO_2, as a function of (negative polarity) repeller potential.

Fig. 2 Halfwidth (FWHM) of the O^- peak from CO_2 which maximizes at 8.2eV electron energy, as a function of repeller potential.

Fig. 3 Tracings of XY recordings of O^- and O_2^- ion currents as a function of electron energy. The absolute maximum amplitudes of O^- and O_2^- are in the ratio of 200 to 1. Number density of $O_2 = 3 \times 10^{14} cm^{-3}$.

Fig. 4 Ion currents of O^- and O_2^- as functions of O_2 sample number density. The slopes are 1.0 and 2.0, respectively. Measured ion currents are O^-: 6.7×10^{-14}A and O_2^-: 2.5×10^{-16}A at an O_2 number density of $10 \times 10^{14} cm^{-3}$.

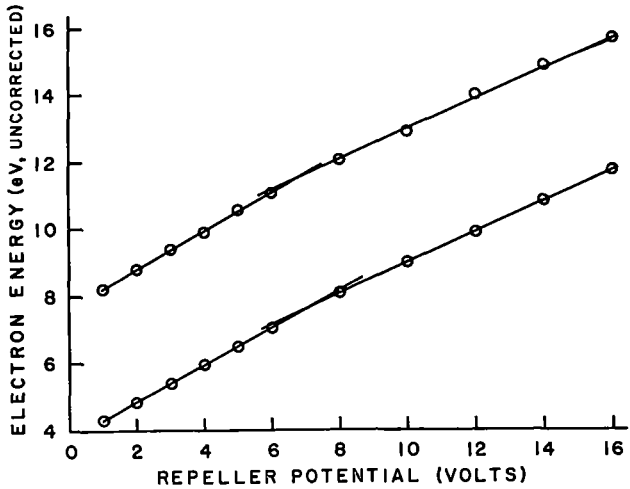

Fig. 1

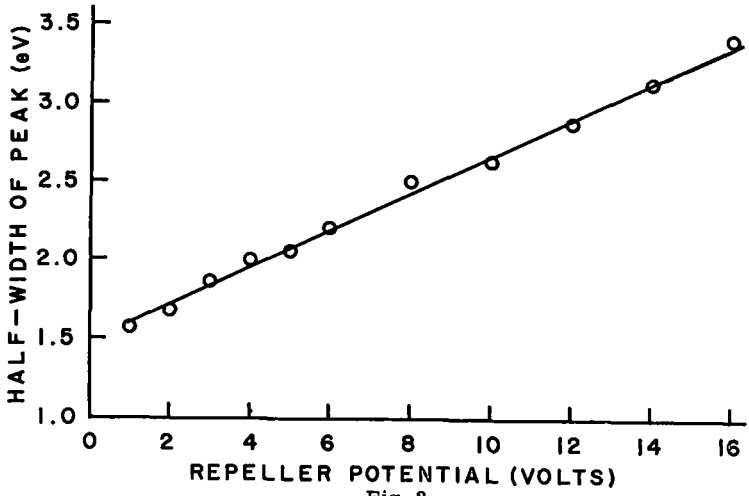

Fig. 2

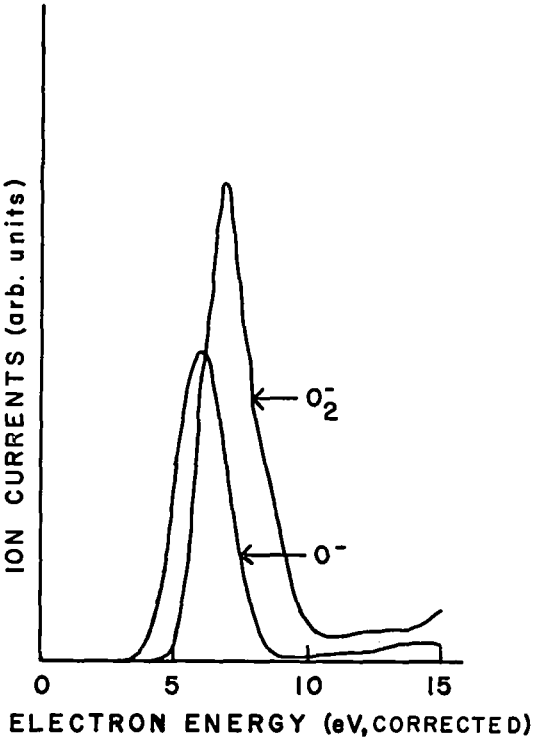
ION CURRENTS (arb. units)
O_2^-
O^-
0
5
10
15
ELECTRON ENERGY (eV, CORRECTED)
Fig. 3

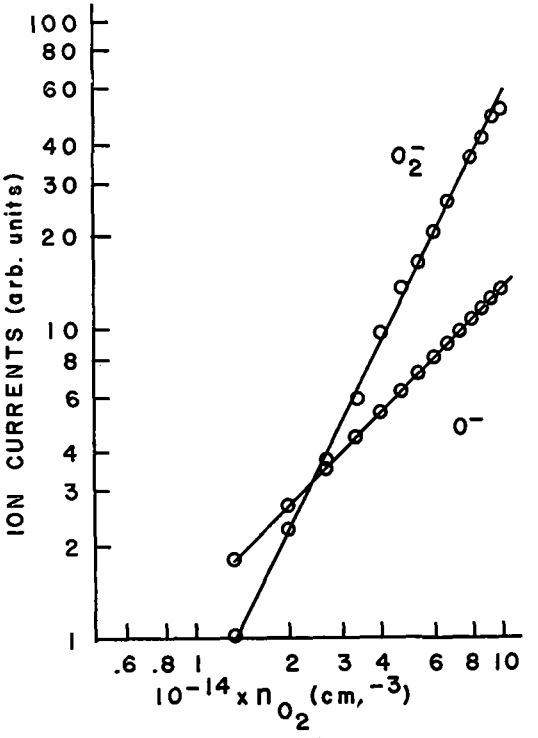
ION CURRENTS (arb. units)
100
80
60
40
30
20
10
8
6
4
3
2
1
O_2^-
O^-
.6 .8 1 2 3 4 6 8 10
$10^{-14} \times n_{O_2}$ (cm, $^{-3}$)
Fig. 4

ION-MOLECULE REACTIONS IN ACETONITRILE AND PROPIONITRILE*

J. L. Franklin, Yasuo Wada, P. Natalis** and P. M. Hierl
Department of Chemistry, Rice University, Houston, Texas

The mass spectra of acetonitrile and propionitrile have been determined as a function of pressure and time. The principal secondary ion formed with each compound is the M + 1 ion. With CH_3CN the ion $C_2H_4CN^+$ is also formed with moderate abundance and with C_2H_5CN, $C_2H_4^+$, $C_2H_6^+$, CH_3CN^+ and CH_4CN^+ are formed in moderate abundance. Both compounds exhibit a large number of secondary ions formed in small amounts. The doubly solvated proton is observed with both compounds but in intensities too small for study. In order to establish the composition of the various ions, spectra were obtained of the perdeuterated compounds also. Rate studies were made by varying both pressure and time and rate constants obtained for most of the principal reactions.

*This work was supported by a grant from the Robert A. Welch Foundation.

**Chercheur qualifie of the Belgian Fonds National de la Recherche Scientifique. On leave of absence from the University of Liege, Belgium. Present address: Institut de Chimie, Universite de Liege, 1b Quai F. D. Roosevelt, Liege, Belgium.

ION-MOLECULE REACTIONS OF METHANE

Fred P. Abramson* and Jean H. Futrell

Aerospace Research Laboratories
Wright-Patterson Air Force Base, Ohio

ABSTRACT

The ionic reactions of gaseous methane have been investigated in a tandem mass spectrometer. The reactions of each primary ion. CH_4^+, CH_3^+, CH_2^+, CH^+, C^+, have been observed at 0.3 eV and several secondary ion reactions have also been studied. An investigation of the effects of translational energy on many of these reactions demonstrated the efficient conversion of translational energy into internal energy. Evidence for randomization of the intermediate $C_2H_xD_{7-x}^+$ ion in the methyl ion-methane reaction is presented. Isotope effects in hydrogen transfer reactions have also been investigated as a function of kinetic energy. The results are interpreted in terms of a transition from a complex model of reaction to a stripping model at higher energies.

INTRODUCTION

Following the early reports of Talroze and Lyubimova[1] and of Stevenson and Schissler[2] of the formation of protonated methane via a very large cross-section ion molecule reaction of the parent ion, ionic reactions in the methane system have been extensively investigated (3-15). Despite many careful studies, however, there are only four primary ion reactions about which there is no apparent dissent. These are

$$CH_4^+ + CH_4 \rightarrow CH_5^+ + CH_3 \quad (1)$$

$$CH_3^+ + CH_4 \rightarrow C_2H_5^+ + H_2 \quad (2)$$

$$CH_2^+ + CH_4 \rightarrow C_2H_3^+ + H_2 + H \quad (3)$$

$$CH^+ + CH_4 \rightarrow C_2H_2^+ + H_2 + H \quad (4)$$

A number of additional reactions have been reported which are not as well established.

$$CH_4^+ + CH_4 \rightarrow C_2H_4^+ + 2H_2 \quad (5)$$

$$\rightarrow C_2H_6^+ + H_2 \quad (6)$$

$$CH_3^+ + CH_4 \rightarrow C_2H_3^+ + 2H_2 \quad (7)$$

$$\rightarrow C_2H_4^+ + H_2 + H \quad (8)$$

$$CH_3^+ + CD_4 \rightarrow CD_4^+ + CH_3 \quad (9)$$

$$\rightarrow CD_3^+ + CH_3D \quad (10)$$

$$CH_2^+ + CH_4 \rightarrow C_2H_4^+ + H_2 \quad (11)$$

$$\rightarrow C_2H_2^+ + 2H_2 \quad (12)$$

Because of its obvious cardinal significance to an understanding of ionic reactions of hydrocarbons, methane hase been reinvestigated in some detail. For this study we have used a tandem in-line arrangement of two mass spectrometers. the first serving as a mass and energy selector for ions injected into a collison chamber, and the second serving as a mass analyzer for product ions. This affords a direct observation of parent-daughter relationships and the opportunity to observe reaction products which are normally obscured by primary ions of the same

*National Academy of Science-National Research Council Postdoctoral Research Associate

Table I

Products From the Reaction of Low Kinetic Energy CD_4^+ with CH_4

m/e	Ionic Species	Relative Intensity, percent
21	CD_4H^+	28
19	$CH_3D_2^+$	7
18	CH_4D^+	54
17	CH_3D^+ (CD_2H^+)	3
16	CH_4^+ (CH_2D^+)	8

Table II

Reactions of $CH_nD_{4-n}^+$ with CD_4 at Low Kinetic Energy

Relative Intensity of Secondary Ions Percent

Incident Ion	Charge Transfer	Abstraction	Proton Transfer	Deuteron Transfer	k_H^+/k_D^+
CH_4^+	13	19	68		
CH_3D^+	14	21	50	15	1.1
$CH_2D_2^+$	31[a]		39	30	1.3
CHD_3^+	9	44[b]		47	

[a]Sum of charge transfer, CD_4^+, and abstraction. $CH_2D_3^+$, both of which correspond to m/e 20.
[b]Sum of abstraction and proton transfer peaks, both of which yield CD_4H^+.

Table III

Effect of Ion Translational Energy

on the Reaction of CHO^+ with CD_4

Ion Energy	Relative Intensity, counts/sec				$\frac{CD_4H^+}{CHD_2^+ + CD_3^+}$	$\frac{CHD_2^+}{CD_3^+}$
eV	CHD_2^+	CD_3^+	CD_4^+	CD_4H^+		
0.3	201	244	57	1337	3.00	0.82
1.9	219	228	61	704	1.57	0.96
4.2	242	223	79	453	0.97	1.09

nominal mass. It was anticipated that this would clarify certain of the ambiguities which have been noted. In addition we anticipated that a study of certain reactions as a function of reactant ion kinetic energy, particularly using isotopically labelled reactants, would reveal details of the reaction mechanism.

EXPERIMENTAL

All experiments were performed using the ARL tandem mass spectrometer which has been described in detail elsewhere[16]. For clarity a schematic of the pertinent features of the apparatus is given in Fig. 1. The ion gun of this apparatus is a four-inch radius double-focussing spectrometer of nominally 1/200 mass resolution which provides a mass and energy resolved beam of ca. 1-8 x 10^{-12} amps of primary ions. The energy bandwidth, or total spread in kinetic energy of the transmitted ion beam, determined by the slit aperture of the so-called β-slit of the electric sector, was set at 0.5 eV for this series of experiments. The ion beam is then decelerated by a lens system and brought to a focus inside a differentially pumped collision chamber 3.2 mm. in length. A separate gas handling system for the collision chamber incorporates a MKS Baratron pressure gauge and a Granville-Phillips automatic pressure controller to monitor and regulate the pressure in the 10^{-3} - 10^{-2}mm. pressure range.

Unreacted primary ions and secondary ions are accelerated by a Soa lens and mass analyzed by a double-focussing mass spectrometer of Mattauch-Herzog geometry. As a detector an EMI model 9642B eighteen stage electron multiplier operated in pulse counting mode is used. Each peak was counted from 1-100 sec. as desired for reliable counting statistics, and the limitation on accuracy was the long term stability of the integrated system.

Two primary ion sources of identical geometry were used in this research. One used an electrostatically collimated electron gun which operated satisfactorily only at 150 volts filament potential. The other was magnetically collimated and could be varied in electron energy; most measurements were made with 75 eV electrons as the ionizing medium. No difference in reaction products produced by primary ions from the two sources was observed. However neither source operated satisfactorily at energies near the ionization threshold of methane, and the possible participation of excited ions cannot be excluded.

Methane used in these experiments was Matheson Research Grade of stated purity of 99.95%. Deuterated methanes were obtained from Merck, Sharp, and Dohme, Ltd. and were examined mass spectrometrically for isotopic and chemical purity. Spectra were obtained with a Consolidated Model 21-103C mass spectrometer using standard low voltage techniques and 70 eV electrons.

RESULTS AND DISCUSSION

Reactions of CH_4^+. As stated in the introduction, there is general agreement that the principal product of the reaction of CH_4^+ with methane is CH_5^+. In addition, in experiments performed at elevated ion source pressures (to 400 microns) Wexler and Jesse[7] and Field, Franklin, and Munson[9] report $C_2H_6^+$ as a product. In a later paper Field and Munson[15] do not list an ion of m/e 30 in their tabulated high pressure mass spectrum of methane, although they do report a small $C_2H_7^+$ peak which they attribute to proton transfer from CH_5^+ to a small amount of ethane impurity in their sample. Similarly Fuchs[6] reports an ion at m/e 30 which is entirely accounted for as $C^{13}C^{12}H_5^+$. Wexler and Jesse[7] also suggest that $C_2H_4^+$ may be formed by reaction of excited CH_4^+ ions with methane.

We have observed very low intensities of $C_2H_4^+$, $C_2H_5^+$, and $C_2H_6^+$ when CH_4 is bombarded with CH_4^+. Those cannot be attributed to reactions of CH_4^+ with low levels of C_2H_4 and C_2H_6 impurities in the methane which was used. In any case, the cross sections for forming these ions by reaction of CH_4^+ with methane are about two orders of magnitude smaller than that for forming CH_5^+; hence these reactions are of only minor importance in the methane system.

When we bombard CH_4 with CD_4^+ ions at our lowest available energy (nominally 0.3 eV) the hydronated[17] methanes of greatest intensity are CH_4D^+ and CD_4H^+. The spectrum observed is given in Table I. The simplest interpretation of the observation that both of these ions are formed is that they represent hydron transfer and hydrogen abstraction respectively. The minor product $CH_3D_2^+$ indicates that a small number of the reaction complexes ($C_2H_4D_4^+$) have sufficient

Table IV

Isotopic Ethyl Ions Formed in the Methyl Ion-Methane Reaction

Reaction Pair	Intermediate Ion	Relative Hydrogen Elimination Observed			Calculated		
		$-H_2$	-HD	$-D_2$	$-H_2$	-HD	$-D_2$
$CH_3^+ + CD_4$	$C_2H_3D_4^+$	.47	1.00	.50	.35	1.00	.35
$CH_2D^+ + CD_3H$	$C_2H_3D_4^+$	.33	1.00	.43	.35	1.00	.35
$CHD_2^+ + CD_2H_2$	$C_2H_3D_4^+$	.33	1.00	.35	.35	1.00	.35
$CD_3^+ + CH_3D$	$C_2H_3D_4^+$	.35	1.00	.37	.35	1.00	.35
$CH_2D^+ + CH_2D_2$	$C_2H_4D_3^+$	.69	1.00	.23	.71	1.00	.18
$CHD_2^+ + CH_3D$	$C_2H_4D_3^+$	.67	1.00	.18	.71	1.00	.18
$CHD_2^+ + CD_3H$	$C_2H_2D_5^+$	.12	1.00	.70	.14	1.00	.71

Table V

Effects of Kinetic Energy on C_2 Products

Reactant Ion	Kinetic Energy	% of C_2 Secondary Ions			
		$C_2H_2^+$	$C_2H_3^+$	$C_2H_4^+$	$C_2H_5^+$
CH_3^+	0.3	0	4.1	0	96
	4.2	0	71	0	29
CH_2^+	0.3	11	25	37	27
	4.2	22	69	5	4
CH^+	0.3	13	82	5	0
	4.2	trace	a	a	0
C^+	0.3	26	74	0	0
	4.2	b	b	0	0

a. $C_2H_3^+ \simeq C_2H_4^+$

b. $C_2H_2^+ > C_2H_3^+$

lifetime for a limited amount of H-D exchange to occur. Similarly we consider the m/e 17 peak to represent a "back-reaction" of such a complex, as suggested by Wagner, Wadsworth, and Stevenson[4], while m/e 16 represents the superposition of ions formed from both a back reaction of the ion-molecule complex and from the electron-jump type of reaction which is the more customary model for simple charge-exchange. We have also indicated parenthetically in the table that these two ions could be interpreted as the products of a dissociative transfer reaction reaction

$$CX_4^+ + CX_4 \rightarrow CX_5^+ + CX_3 \quad (13a)$$

$$\rightarrow CX_3^+ + X_2 \quad (13b)$$

as suggested by von Koch[14]. However, parallel experiments with the reaction pairs CH_4^+, CH_4 and CH_4, CD_4^+, show that this reaction is unimportant for ions of low kinetic energy.

The effects of translational energy on the hydron transfer reaction

$$CH_2D_2^+ + CD_4 \rightarrow CD_4H^+ + CHD_2 \quad (14)$$

$$\rightarrow CD_5^+ + CH_2D \quad (15)$$

were investigated and the results are plotted in Fig. 2, along with data from Henglein and Muccini[8]. While quantitative agreement between the two experiments is neither expected nor observed, the results qualitatively support the same conclusion. They interpreted the large isotope effect at higher energies as the result of a stripping mechanism which is presumed operative when the effective collision time is comparable with the vibrational frequency of the molecule. Our data indicate an energy independent isotope effect below 4 eV kinetic energy and a rapidly increasing isotope effect above this energy, which may be interpreted as the transition from a "loose complex" to a "stripping" mechanism. From the rate constant for the reaction (10^{-9} cm^3-molecule^{-1} - sec^{-1}[13]) and the velocity of a 4 eV $CH_2D_2^+$ ion (6.5 x 10^5 cm/sec.) we calculate a cross section at this energy of 15 $Å^2$, corresponding to an effective diameter of 2.2 Å. The transit time of the ion in the effective range of the molecule is therefore 3.4 x 10^{-14} sec. Since the vibrational frequency for C-D stretch is ca. 2200 cm^{-1}, the period of a vibration for a C-D bond is of the order of 1.5 x 10^{-14} sec. Thus from these data it appears that the reaction mechanism can be best represented by a "stripping model" *for the activated complex when the reaction takes place in less than* two vibration cycles of the molecule.

We have also studied the effect of ion translational energy on the analogous abstraction reaction as reflected in an isotope effect in the reactions

$$CD_4^+ + CH_2D_2 \rightarrow CD_4H^+ + CHD_2 \quad (16)$$

$$\rightarrow CD_5^+ + CH_2D \quad (17)$$

The cross section for this reaction falls off much more rapidly with kinetic energy than the hydron transfer reaction so that it was not possible to extend this study beyond 4.5 eV with acceptable precision. We observed that the ratio of reactions (16)/(17) = 2.0 ± 0.3 and is independent of kinetic energy between 0.3 and 4.5 eV. Because the isotope effect in the abstraction reaction is different from that for hydron transfer, the abstraction cannot be represented as a two step process of charge transfer followed by hydron transfer.

It is of interest to speculate why there is a difference in the isotope effects for hydron transfer and for hydrogen abstraction. Naively one would not expect any difference because, although the entity being transferred is different, the bonds being broken have about the same energy and the intermediate complex should be similar in both cases. The only apparent difference is that for hydron transfer the donor molecule is charged while in the abstraction reaction the donor is neutral. The difference in appearance potentials between CH_3^+ and CH_4^+ is about 1.2 eV[18] so that methane parent ions contain a distribution of excited states with between 0 and 1.2 eV internal energy. It seems reasonable to assume that this internal excitation of the ion will appear in the intermediate complex very much as it would if the ion had been formed in an adiabatic transition from a neutral molecule at very high temperature. The limit for a primary isotope effect at high temperatures is[19] equal to the ratio of the critical vibrational frequency in the two possible complexes. If the complex is represented by the molecular parameters then the anticipated isotope effect will be 1.4 for k_H^+/k_D^+ if the frequencies of the neutral molecule apply to the ion. This is about the size of

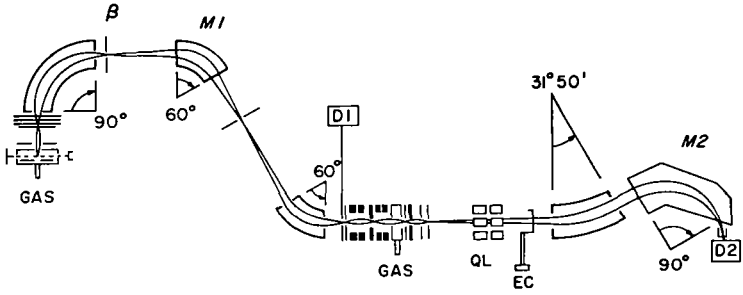

Fig. 1. Schematic of the ARL tandem mass spectrometer QL = quadrupole lens. EC = displaceable electrometer collector. M1, M2 = magnetic sectors and D1, D2 = ion detectors.

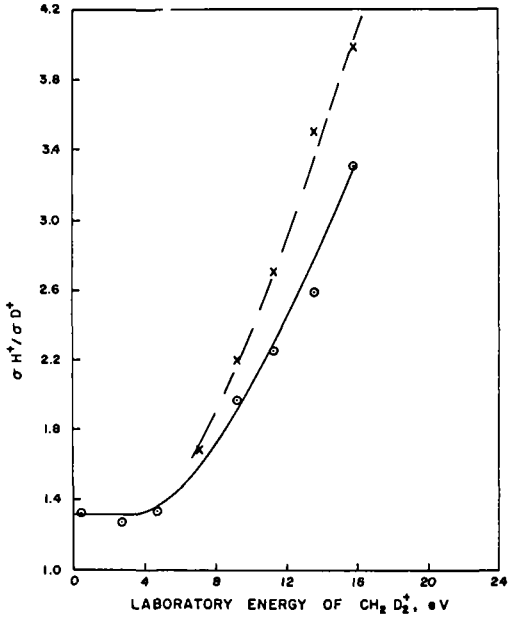

Fig. 2. Isotope effects in hydron transfer from $CH_2D_2^+$ as a function of ion kinetic energy. (X) data of Henglein and Muccini (8).

the effect which we see for hydron transfer reactions. The secondary isotope effects which cause the changes in k_H^+/k_D^+ for the individual substituted methane with kinetic energy cannot be evaluated in a simple fashion.

At moderate and low temperatures, differences in zero point energies between C-H and C-D bonds will give rise to other primary isotope effects which may cause the experimental k_H/k_D to be much larger than unity. Our observation of a $k_H/k_D = 2.0$ for the abstraction reaction indicates that such differences are operative in that reaction. It will be shown subsequently that in certain ion-molecule reactions of methane, in particular those which may be described as going via a "tight" complex, that translation energy of the impacting ion is converted rather efficiently into internal energy. Hence if a tight complex is involved in the hydrogen abstraction reaction one would expect a smooth transition from the low energy isotope effect of approximately 2 to the high temperature limit of as ion kinetic energy is increased. Within experimental error the isotope effect is independent of ion kinetic energy below 4 eV. It therefore seems that an intermediate complex $C_2H_2D_6^+$ is not a useful concept for discribing the abstraction reaction.

Isotope effects in hydron transfer reactions have been discussed previously[8,12] but both these studies involved conventional mass spectrometer sources in which the ion products from both abstraction and hydron transfer reactions are indistinguishable. Accordingly we have investigated in some detail the reactions of $CH_nD_{4-n}^+$ with CD_4. Results from this study using 0.6 eV impacting ions are summarized in Table II.

The analogous study of Shannon, Meyer, and Harrison[12] is of interest but cannot be compared strictly with our data since the isotope effect observed in their study is a superposition of those effects operative in both hydron transfer and hydrogen abstraction. It is of interest to note, however, that their value for the combined isotope effect in the reaction

$$CH_2D_2^+ + CH_2D_2 \rightarrow CH_3D_2^+ + CHD_2 \qquad (14a)$$

$$\rightarrow CH_2D_3^+ + CH_2D \qquad (15a)$$

is the same as our value for the hydron transfer reaction alone in reactions 14 and 15. Such agreement is anticipated if the abstraction reaction is of negligible importance. Our data for the only combinations of methane-molecule ion reactants for which the two reaction modes are distinguishable, however, indicate that this is not the case. In the reactions of CD_4^+ with CH_4 and of CH_4^+ with CD_4 at low energy the ratio of hydron to atom abstraction is approximately 2. It therefore seems more plausible to suggest that both types of reactions occur for CH_2D_2 as well, but that for the self reaction there may be differences in the isotope effects for the various hydrogen transfer processes such that the ratios of $\frac{14}{15}$ and $\frac{14a}{15a}$ are essentially identical for the two systems.

As we have noted, the abstraction reaction cross section appears to decrease much more rapidly with increasing kinetic energy than the hydron transfer reaction. To show this more quantitatively the reactions

$$CH_4^+ + CD_4 \rightarrow CH_4D^+ + CD_3 \qquad (18)$$

$$\rightarrow CD_4H^+ + CH_3 \qquad (19)$$

were studied at several ion kinetic energies. At 0.3 eV the ratio of m/e 21:m/e 18 was 2.3, at 1.4 eV this ratio had increased to 4.9 and at 3.5 eV was 8.3. Thus the abstraction reaction requires a longer lived complex than hydron transfer and is likely a more prominent feature of experiments in which ions of thermal energy are produced.

To gain some further insight into isotope effects in these reactions the dissociation of hydronated methane was studied briefly. For this purpose we impacted CD_4 with CHO^+ ions produced by ionizing methanol in the source of the first spectrometer. The relative amounts of protonated deuteromethane as well as decomposition products were measured at 3 energies and are reported in Table III. The reaction sequence is

$$CHO^+ + CD_4 \rightarrow CD_4H^+ + CO \qquad (20)$$

$$CD_4H^+ \rightarrow CD_3^+ + HD \qquad (20a)$$

$$\rightarrow CD_2H^+ + D_2 \qquad (20b)$$

As discussed by von Koch[14], both charge exchange and dissociative proton transfer of CHO^+ with methane are endothermic for ground state ions. At our lowest impacting ion energy the total energy of the system is insufficient to drive these reactions even if the total internal energy of the complex is available for the reaction. Hence, the beam in both our experiments and those of von Koch must contain some excited state ions CHO^{+*}. The increasing extent of dissociation with energy reported in column 6 of Table III probably indicates conversion of translational energy into internal energy.

The ratio CHD_2^+/CD_3^+ in column 7 is of interest. as it represents the relative probability of D_2/HD elimination from CD_4H^+. At 2 eV von Koch obtains a value of 0.9 for this ratio in good agreement with our results. For equivalent hydrogens and no isotope effect in CD_4H^+ we would expect 1.5 for this ratio. The slowly changing isotope effect indicated by the results may be the superposition of isotope effects resulting from the differences in zero point energies of C-H and C-D bonds and a kinetic isotope effect from the different vibrational frequencies of the two bonds. The latter effect becomes more important as the internal energy and consequently the probability of dissociation increases.

In general, we have been discussing the individual isotope effects in the neutral molecule or in the ion in an independent fashion, considering the properties of the donor species as determinative in the various cases. The actual case involves reaction between the two species such that the receptor species apparently exerts some perturbation on the donor in these reactions. That is, we cannot correctly consider the reaction of an ion with a molecule, but rather the reaction of the ion-molecule pair during the time of collision. The discussions of the magnitudes of the isotope effects which are presented here therefore provide only a qualitative rationale for interpreting the reaction mechanisms and it is not possible to predict exact isotope effects for a given reaction.

Reactions of CH_3^+. Fuchs[6] has previously reported $C_2H_3^+$ as a product of CH_3^+ ion reactions with methane. Wexler and Jesse[7] and Field. Franklin, and Munson[9] have reported $C_2H_4^+$ as a product, while Derwish, Galli, Giardini-Guidoni, and Volpi report that CH_4^+ is the major product ion from CH_3^+ reaction with methane[10]. With the exception cited there is general agreement that $C_2H_5^+$ is the major product ion. Our results show that this is indeed the case. In addition we observe small amounts of $C_2H_3^+$, confirming reaction 7, but no $C_2H_4^+$. When methyl ions are impacted on CH_4, no CH_4^+ is observed as a product; hence reaction 9 does not occur. When CH_3^+ is impacted on CD_4, low intensities of ions at m/e 16, 17, and 18 are observed, suggesting both hydride transfer and H-D exchange reactions to produce a methyl ion product. In these reactions the sum of products containing one carbon is about 5% of the sum of those containing two carbon atoms.

Analysis of the ethyl ion products from the reaction of CH_3^+ with CD_4 indicates that HD elimination from the $C_2H_3D_4^+$ complex is roughly twice as probable as H_2 or D_2 elimination. The only model consistent with this result is an essentially randomized complex; that is, one with all hydrogens equivalent. Randomization of an intermediate $C_2H_nD_{7-n}^+$ complex has been reported previously[10,21] from studies of CH_4-CD_4 mixtures, and this phenomenon is exhibited as well in metastable decompositions[22], radiolysis experiments[23], and in charge exchange mass spectra[24]. To test the randomization hypothesis quantitatively we prepared the $C_2H_7^+$ type intermediate complex in a number of ways using partially deuterated methanes. The results are summarized in Table IV where the spectra of ethyl ions are reported as the ions resulting from loss of isotopic hydrogens from the given intermediate ion.

In his studies of dissociative charge exchange of deuterated ethane[24] von Koch has observed isotope effects of $2;\sqrt{2}$, and 1 for the relative probability of H_2, HD, and D_2 elimination. Callear and Cvetanovic[25] have also found these numbers in the photolysis of partially substituted ethylenes. These factors may also be derived from the reduced mass effect on vibrational frequencies of X-H and X-D species. If we apply these correction factors to the statistical probabilities for the proposed randomized intermediate one obtains the calculated distributions of Table IV. Although there are some minor differences in the ratios for various reaction pairs, the generally consistent view emerges that the intermediate is completely randomized. No specific chemical structure is suggested by these data.

The effect of translational energy of the methyl ion on product distribution was investigated briefly and is indicated in Table V. The relative magnitude of the two-carbon secondary ions at two kinetic energies is shown in the table. These results clearly demonstrate that kinetic energy may be converted rather

efficiently into internal energy. The sequential breakdown of the complex

$$[C_2H_7^{+*}] \rightarrow C_2H_5^{+*} + H_2 \quad (21a)$$

$$\rightarrow C_2H_3^{+} + H_2 \quad (21b)$$

is further indicated by the absolute intensities of the product ions. At 4.2 eV the absolute intensity of $C_2H_3^+$ is more than twice the intensity at 0.3 eV, while the $C_2H_5^+$ has descreased drastically.

CH_2^+, CH^+ and C^+ Reactions. Because of the high appearance potentials of these fragments, many of their reactions have not been identified in single stage instruments. These reactions are also included in Table IV at two different reactant ion energies. Again, kinetic energy plays an important role in the reactions. Because of their low intensities and because the secondary signal diminishes at the higher energy, the data for C^+ and CH^+ at the higher energy are only qualitative.

Tertiary Ion Reactions. In a recent study, Field and Munson[15] have shown that the secondary ions CH_5^+, $C_2H_5^+$, and $C_2H_4^+$ are unreactive toward methane. Their experimental study involved a rather high source pressure of 2 Torr and it seemed desirable to confirm their results by an independent approach. Accordingly we produced the desired ions in our primary source, using methane d-4, ethane, and ethylene as the source gases for CD_5^+, $C_2H_5^+$, and $C_2H_4^+$ ions, respectively. Our findings are in accord with these workers, as no ion products could be detected, except for the resonance deuteron transfer reaction from CD_5^+ to CH_4. The reaction

$$CD_5^+ + CH_4 \rightarrow CH_4D^+ + CD_4 \quad (22)$$

was compared with the analogous reaction 1 for CD_4^+ in order to obtain information about the cross section for reaction 22. Because the two reactions are very similar, a comparison of secondary ion signals from primary beams of equivalent intensity provides a measure of relative cross sections for these reactions. We find that $(I_s/I_p)_{CD_4^+}/(I_s/I_p)_{CD_5^+} = 30$ or $k_{23} = 3.3 \times 10^{-11}$ cc./molecule-sec. This is a surprisingly small rate constant compared to

$$ND_3H^+ + ND_3 \rightarrow ND_4^+ + ND_2H \quad (23)$$

where Munson and Field[26] find a rate constant which is the order of 10^{-9} cc./molecule-sec. However, in a radiolytic system, Lawrence and Firestone[27] find a rate constant which is much less than 10^{-9} cc./molecule-sec. for reaction 24. We therefore support the observations of Lawrence and Firestone and note that there must be some significant difference in the chemical nature of hydronated methane compared to hydronated ammonia which accounts for the large difference in reactivity between the two species.

The ions $C_2H_3^+$ and $C_2H_2^+$ were also impacted on methane. The reactions

$$C_2H_2^+ + CH_4 \rightarrow C_2H_3^+ + CH_3 \quad (.47) \quad (24)$$

$$\rightarrow C_3H_3^+ + H_2 + H \quad (.03) \quad (25)$$

$$\rightarrow C_3H_4^+ + H_2 \quad (.09) \quad (26)$$

$$\rightarrow C_3H_5^+ + H\cdot \quad (.41) \quad (27)$$

$$C_2H_3^+ + CH_4 \rightarrow C_3H_5^+ + H_2 \quad (.77) \quad (28)$$

$$\rightarrow C_3H_6^+ + H\cdot \quad (.23) \quad (29)$$

were observed with percentages of the reaction paths as noted in parentheses. These percentages were the same for $C_2H_2^+$ from ethylene or acetylene and for $C_2H_3^+$ from ethylene or ethane. We further agree with the findings of Munson and Field[15] that there is a large difference in the reaction rates for $C_2H_3^+$ and $C_2H_2^+$. They find that the $C_2H_2^+$ species reacts about 5 times faster than $C_2H_3^+$ and we observe an approximately 30-fold difference in reactivity.

We attempted to follow the ionic polymerization chain one step further by impacting C_3 ions on methane. For $C_3H_3^+$, $C_3H_4^+$, and $C_3H_5^+$ we did not observe any reaction products, from which we conclude that chain-lengthening ion-molecule reactions of these ions with methane have cross sections at least two orders of magnitude smaller than those of the methane primary ions.

REFERENCES

1. V. L. Talroze and A. K. Lyubimova, Doklady Akad. Nauk. SSSR, 86, 909 (1952).

2. D. P. Stevenson and D. O. Schissler, J. Chem. Phys., 24, 926 (1956).

3. F. H. Field, J. L. Franklin, and F. W. Lampe, J. Am. Chem. Soc., 79, 2419 (1957).

4. C. D. Wagner, P. A. Wadsworth, and D. P. Stevenson, J. Chem. Phys., 28, 517 (1958).

5. V. L. Talroze and E. L. Frankevich. Zh. Fiz. Khim., 34, 2709 (1960).

6. R. Fuchs, Z. Naturforsch., 16a, 1026 (1961).

7. S. Wexler and N. Jesse, J. Am. Chem. Soc., 84, 3425 (1962).

8. A. Henglein and G. A. Muccini, Z. Naturforsch; 17a, 452 (1962), ibid., 18a, 753 (1963).

9. F. H. Field, J. L. Franklin, and M. S. B. Munson, J. Am. Chem. Soc. 85, 3575 (1963).

10. G. A. W. Derwish, A. Galli, A. Giardini-Guidoni, and G. G. Volpi, J. Chem. Phys., 40, 5 (1964).

11. C. W. Hand and H. von Weyssenhoff, Can. J. Chem., 42, 195 (1964).

12. T. W. Shannon, F. Meyer, and A. G. Harrison, Can. J. Chem. 43, 159 (1965).

13. K. R. Ryan and J. H. Futrell, J. Chem. Phys., 42, 824 (1965); ibid., 43, 2748 (1965).

14. H. von Koch, Arkiv Fysik, 28, 529 (1965).

15. F. H. Field and M. S. B. Munson, J. Am. Chem. Soc., 87, 3289 (1965).

16. J. H. Futrell and C. D. Miller, Rev. Sci. Inst. (to be published).

17. We suggest hydron as a generic term for the isotopic hydrogen nucleus (i.e., H^+, D^+, T^+).

18. F. H. Field and J. L. Franklin, "Electron Impact Phenomenon", Academic Press, New York, N. Y. (1957).

19. L. Melander, "Isotope Effects on Reaction Rates", Ronald Press, New York, N. Y., 1960.

20. D. O. Schissler, and J. Turkevich, Disc. Faraday Soc. 10, 46 (1951).

21. P. Ausloos and S. Lias, J. Chem. Phys., 38, 2207 (1963).

22. A. Kropf, E. M. Eyring, A. L. Wahrhaftig and H. Eyring; ibid., 32, 149 (1960).

23. P. Ausloos and S. Lias, ibid., 36, 3163 (1962).

24. H. von Koch, Arkiv Fysik, 28, 559 (1965).

25. A. B. Callear and R. J. Cvetanovic, J. Chem. Phys., 24, 873 (1956).

26. M. S. B. Munson and F. H. Field, J. Am. Chem. Soc., 87, 4242, (1965).

27. R. H. Lawrence Jr. and R. F. Firestone, ibid., 87, 2288, (1965).

PROTON TRANSFER REACTIONS IN ETHANOL

L. Wayne Sieck*, Fred P. Abramson+ and Jean H. Futrell

Aerospace Research Laboratories
Wright-Patterson Air Force Base, Ohio

INTRODUCTION

The ion-molecule chemistry of the lower alcohols has been the subject of several investigations[1-8]. For both methanol and ethanol proton transfer has been observed as the major reaction path. The use of isotopically labelled methanols in single stage[1,7] and tandem mass spectrometers[4] has established several of the reactions occurring in methanol. A very interesting recent article by Munson[8] has demonstrated the formation of higher order aggregates of the type $(CH_3OH)_nH^+$ at elevated pressures.

Although much is known about the methanol system, little detailed information is available concerning the ion-molecule chemistry of ethanol. The present study was undertaken with the anticipation that a correlation of data from a single stage high pressure instrument with that obtained from a tandem spectrometer with a mass-energy selection capability would provide much useful information concerning this system.

EXPERIMENTAL

During the course of this investigation three research mass spectrometer systems were utilized. A modified Consolidated 103-C[9] described previously was used to obtain data concerning the effects of varying several operational parameters including source pressure, ionizing voltage, current density, and field strength. Multiple order reactions and relative reactivities were investigated in this apparatus and concurrently in a Bendix Model 12-101 equipped with the Bendix high pressure source. As data from these two instruments were nearly identical, the 103-C was used most extensively because of its increased resolving power at elevated pressures. Ionizing currents in most experiments were maintained at levels below 0.15 microamps to avoid the ion-trapping phenomena at higher current densities reported previously[9].

The reaction modes of individual ions were determined in the ARL Tandem Mass Spectrometer also described in detail elsewhere[10]. The mass-energy selectivity of this instrument complements those data obtained from the single stage instruments. The nominal translational energies of the impacting ion beams were maintained at 0.3 ± 0.3 (these values reflect the 0.6 volt band width of the primary beam deceleration lens system with a particular optical configuration). Other experiments were performed with ions having kinetic energies up to 22 ± 0.3 volts for comparison.

RESULTS

Ethanol-Single Stage Instrument: The effect of pressure on the 50 volt mass spectrum of ethanol-C_2H_5OH at constant field strength (0.25 V/cm) is shown in Figure 1. The data are plotted as fraction of total ion intensity $I_i/\Sigma_i I_i$ for several of the most abundant ions. These data provide excellent confirmation for other observations of proton transfer involving the primary ions leading to the formation of $(C_2H_5OH)H^+$. Additional synthesis ions produced in bimolecular processes include, among others, m/e 19 (H_3O^+) and m/e 43 ($C_2H_3O^+$). Perhaps the most striking feature is the appearance of higher order ions formed by the association of protons with several solvent molecules, i.e., m/e 93, $(C_2H_5OH)_2H^+$ and m/e 139, $(C_2H_5OH)_3H^+$. Concurrently formed species of less importance which are not shown include ions corresponding to loss of H_2O from these aggregates, i.e., m/e 75 and m/e 121. No higher order solvated protons were observed at these pressures but this observation of course does not preclude the possible existence of $H^+(C_2H_5OH)_{4,5}$ etc.

---

*Visiting Research Associate of The Ohio State University Research Foundation, Columbus, Ohio.

+National Academy of Science-National Research Council Postdoctoral Research Associate.

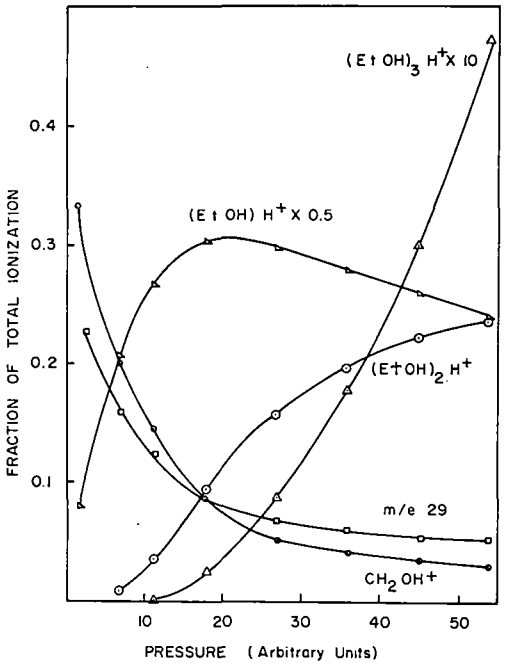

Fig. 1 Variation of 50 volt mass spectrum of C_2H_5OH with pressure.

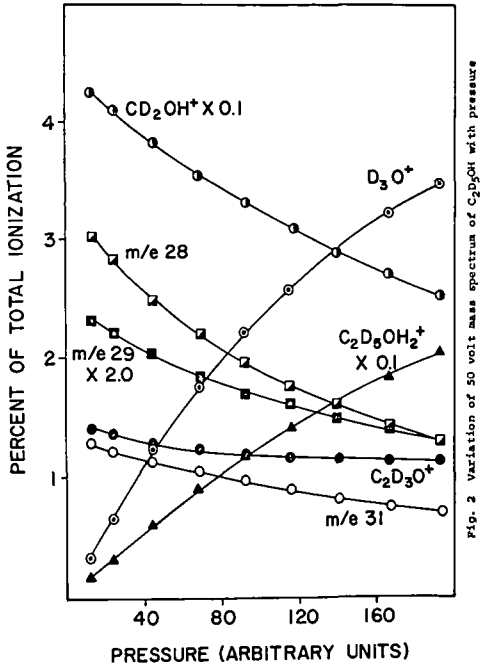

Fig. 2 Variation of 50 volt mass spectrum of C_2D_5OH with pressure for ions with m/e less than 54.

The effect of pressure on the 50 volt mass spectrum of C_2D_5OH at constant repeller is represented graphically in Figures 2 and 3. The formation of higher order species having masses greater than m/e 53 is not included because of the difficulty encountered at elevated pressures in obtaining a unique magnetic field-initial accelerating voltage combination which permitted an electrostatic scan of the complete spectrum from very low to very high mass numbers. However, a typical high pressure spectrum of C_2D_5OH is tabulated in Table I for ions having m/e > 28. The appearance of solvated species at m/e 103 $(C_2D_5OH)_2H^+$, m/e 104 $(C_2D_5OH)_2D^+$ and m/e 154 $(C_2D_5OH)_3H^+$ is particularly noteworthy. Separate experiments confirmed that m/e 85, 103, and 104 are third order and that 154 is fourth order in pressure.

The data depicted in Figure 2 and 3 may be used to derive relative cross sections for the disappearance of some primary ions using the relationship $dI_{iR}/dP\ I_i^\circ = \sigma_R$, where I_{iR} is the relative intensity of species i, σ_R is the relative cross section for disappearance, and I_i° is the relative intensity at zero pressure. The relative cross sections obtained by this method are listed in Table II and are normalized to a σ_R for m/e 28 of 1.00. Absolute values of rate constants were not derived in the present investigation.

Reference to Figures 2 and 3 indicates that secondary ions corresponding to the species $C_2D_5OHD^+$, $C_2D_5OH_2^+$, $C_2D_5^+$, D_3O^+, D_2OH^+, and H_2OD^+ are formed by the reactions of primary ions at higher pressures. It is also apparent that m/e 46 ions $(C_2D_3O^+)$ are produced and destroyed in the system. Similar behavior cannot be ruled out for m/e 34 on the basis of such data. However, the simultaneous production and disappearance of ions having the same mass numbers as primaries is easily investigated in a tandem instrument, and those results will be discussed later in the appropriate portion of the text.

The effect of field strength at various pressures on the ratio of m/e 53 $(C_2D_5OHD^+)$ to m/e 52 $(C_2D_5OH_2^+)$, henceforth referred to as the D^+/H^+ ratio, is shown in Figure 4. A related plot of D^+/H^+ as if a function of pressure (derived from the data presented in Figure 2) is presented in Figure 5. Consideration of these data leads to two descriptions of the system: (i) At low pressures (bimolecular reaction region) and higher field strengths (reduced source residence times) the D^+/H^+ ratio is 0.25. This value is indicative of the situation in which ions suffer, on the average, less than one collision in the source region, and thus reflects the interactions of primary ions only. (ii) Conversely, at elevated pressures or vanishingly small field strengths, where multiple order processes are likely, a value of approximately 0.40 is approached.

The effect of changing ionizing voltage, and concurrently, the distribution of primary ions, on the ratio of $C_2D_5OHD^+/C_2D_5OH_2^+$ at various field strengths and constant pressure (source pressure = 2.7 microns) is displayed in Figure 6. The overall shape of the D^+/H^+ curve, characterized by a minimum in the region of 14 to 16 volts, is unaffected by orders of magnitude changes in pressure and/or field strength.

Ethanol-Tandem Results: The secondary ionic species observed when C_2D_5OH is selectively bombarded with the various important ions comprising the primary spectrum are listed in Table II. Although in this tabulation the results for nominally 0.3 eV ions are presented, we feel that the relative values cited may be taken as indicative of the products one would obtain from nearly thermal species. For comparison, the products resulting from the interactions of C_2D_5OH with CD_2OH^+ ions having 22 eV translational energy are also tabulated.

Qualitatively, the results included in the Table may be summarized as follows: (i) Hydron transfer, hydron transfer followed by dissociation, or hydride transfer are the major reaction paths for the primary ions. (ii) Several ambiguities exist in any study of this system. Methide transfer to the impacting ion is indistinguishable from hydron transfer followed by the dissociation which yields CD_2OH^+. Hydron transfer followed by loss of the hydron and the alpha deuterium in indistinguishable experimentally from hydride transfer to the impacting ion from the alpha position, since both reactions yield $C_2D_4OH^+$. In addition, both OH^- transfer and hydron transfer followed by elimination of water yields ions of m/e 34 $(C_2D_5^+)$. (iii) Dissociation following hydron transfer is energetically possible by four different paths, any of which may or may not occur simultaneously depending upon the nature of the donating species. For $C_2H_5OH_2^+$ the decomposition modes would be represented as; $C_2H_5OH_2^+ \rightarrow$ (1) $H_3O^+ + C_2H_4$, (2) $CH_2OH^+ + CH_4$, (3) $C_2H_5^+ + H_2O$, and (4) $C_2H_4OH^+ + H_2$. The investigation of modes 2, 3, and 4, however, suffers from the ambiguity discussed in comment (ii) above. (iv) The interactions of primary ions not containing oxygen $(C_2D_2^+, C_2D_3^+, C_2D_4^+)$ are much more likely to result in dissociation following hydron transfer.

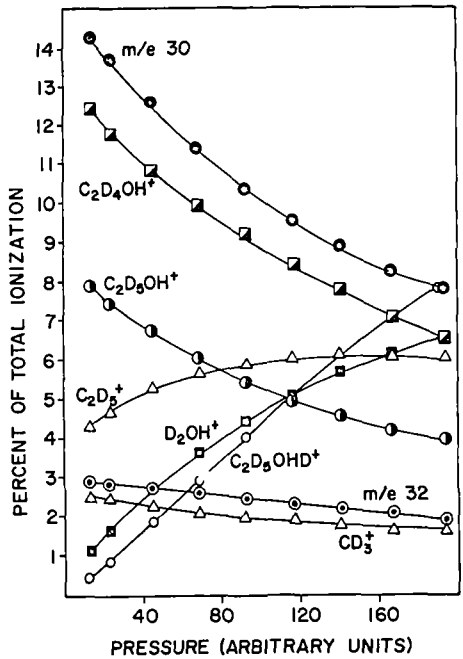

Fig. 3 Variation of 50 volt mass spectrum of C_2D_5OH with pressure for ions with m/e less than 54.

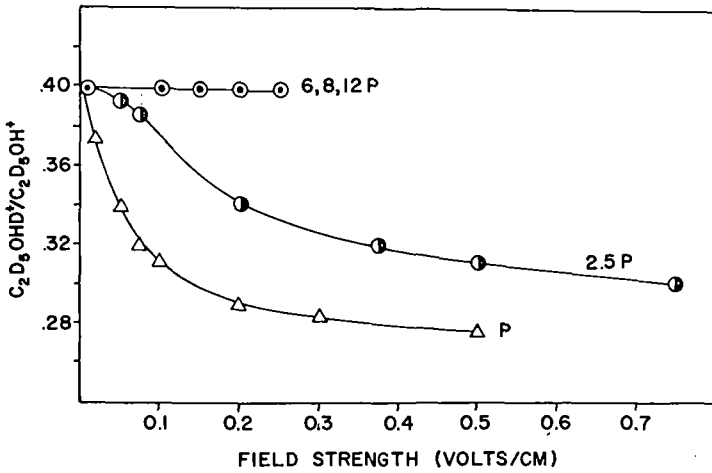

Fig. 4 Variation of $C_2D_5OHD^+/C_2D_5OH_2^+$ ratio with repeller field for various pressure of C_2D_5OH using 50 volt electrons.

In addition to the data presented in the Table, some additional observations were made. (i) When C_2H_5OH is bombarded with a beam of $C_2D_5OH_2^+$ ions produced in the first stage source at higher pressures, the H^+/D^+ transfer ratio is approximately 2.0. (ii) Similarly, when C_2H_5OH interacts with $C_2D_5OHD^+$, the ratio for H^+/D^+ transfer is approximately 0.6. (iii) The ratio of D^+/H^+ transfer from $CH_3CD_2OH^+$ to ethanol is the same as for $C_2D_5OH^+$, (1.53 ± 0.06), demonstrating that only the alpha and hydroxyl positions are involved. In addition, the relative probabilities are also independent of the translational energy of the impacting ion up to 3.0 eV. (iv) Neutral atom abstraction reactions of parent molecular ions were also investigated. When C_2D_5OH is reacted with $C_2H_5OH^+$ ions, the formation of $C_2H_5OH_2^+$ is 1.8 times more probable than the formation of $C_2H_5OHD^+$. However, the total cross section for abstraction is only 7% of that for proton transfer. (v) Resonance methide transfer was observed for reactions of CH_2OH^+ with C_2D_5OH. The exchange leads to the formation of CD_2OH^+ and presumably CD_3CH_2OH as the reaction products. This mode comprises 5.3% of the total reaction cross section for CH_2OH^+. (vi) A series of experiments was carried out in which the nominal kinetic energy of the impacting CD_2OH^+ beam was varied by 0.5 volt increments. In the low energy region (< 1 volt) the relative composition of the secondary spectrum changes by only a few percent.

DISCUSSION

Reactions of Primary Ions: In an earlier article by Ryan, et al.[7] from this laboratory it was incorrectly suggested that only $C_2H_4OH^+$ contributes significantly to the formation of $C_2H_5OH_2^+$ in ethanol-C_2H_5OH at elevated pressures. This conclusion was based on a consideration of normalized ionization efficiency curves in the region near threshold. It was found by this method that m/e 47 ($C_2H_5OH_2^+$) superimposed exactly on m/e 45 ($C_2H_4OH^+$) for at least 5 volts above the appearance potential. This observation may now be understood in terms of a fortuitious situation existing in ethanol involving simultaneous proton transfer from $C_2H_5OH^+$, $C_2H_4OH^+$, and CH_2OH^+, which are the most abundant primary species obtained at reduced ionizing voltages. Using actual relative intensities of these ions in the lower energy region and the respective partial cross sections for hydron transfer (obtained by summing the D^+ and H^+ transfer probabilities and multiplying by the σ_R's listed in Table II), it is possible to construct a composite m/e 47 curve having essentially the same slope as m/e 45 in the threshold region. Although the original conclusion was dictated by the nature of the experimental data, it is now obvious that several simultaneous processes are responsible for the observation.

Formation of $C_2D_5OH_2^+$ and $C_2D_5OHD^+$: The molecular ion, $C_2D_5OH^+$, transfers hydrons from both the alpha and hydroxyl skeletal sites. Since the D^+/H^+ transfer ratio is 0.66 is apparent that the positional probabilities per available hydron are not statistical even allowing for the classical isotope effect. This situation parallels that observed for the methanol molecular ion in a previous study. In contrast, donation occurs almost exclusively from the hydroxyl position for the species $C_2D_4OH^+$ and CD_2OH^+. Assuming a protonated aldehyde structure for these reactants, the exothermicity of the transfer process can be related to the higher proton affinity of ethanol (P ≥ 185 kcal/mole) when compared to formaldehyde (163 kcal/mole) and acetaldehyde (182 kcal/mole)[11].

Although deuteron transfer with the subsequent formation of $C_2D_5OHD^+$ is observed for the oxygen deficient ions $C_2D_5^+$, $C_2D_4^+$, $C_2D_3^+$, and $C_2D_2^+$, dissociation following transfer is favored. This situation may be contrasted with that found for the oxygenated reactants discussed above, which induce fragmentation to a much lesser degree at the same impacting energies.

Dissociation Following Hydron Transfer: The further decomposition of hydronated ethanol-d_5 appears to proceed mainly via two paths. These are the concurrent production of (i) hydronated waters and variously labelled ethylene molecules or (ii) ethyl-d_5 ions and variously labelled water molecules. As pointed out earlier, several ambiguities exist in the data. In spite of the ambiguities, however, several interesting trends manifested in the labelling of the hydronated waters produced in the dissociation involving elimination of ethylene from the solvated hydron may be discussed. (i) Although the interactions of CD_2OH^+ induce a greater degree of total fragmentation than $C_2D_4OH^+$, the relative amounts of H_2OD^+, D_2OH^+, and D_3O^+ are identical (1:2.2:1.2). (ii) When the translational energy of the impacting CD_2OH^+ beam is increased the relative amount of H_2OD^+ is increased over the thermal value. At 22 eV 61% of the solvated hydrons dissociate as compared to only 10% at 0.3 ± 0.3 eV. The observation of charge exchange to produce $C_2D_5OH^+$, which is endothermic by approximately 2.8 volts for ground state ions, is another example of the conversion of kinetic energy into internal energy of a complex available for reaction along otherwise thermodynamically unfavorable paths. (iii) Deuteron transfer from $C_2D_5^+$ or $C_2D_3^+$ enhances the formation of D_2OH^+ and D_3O^+ to

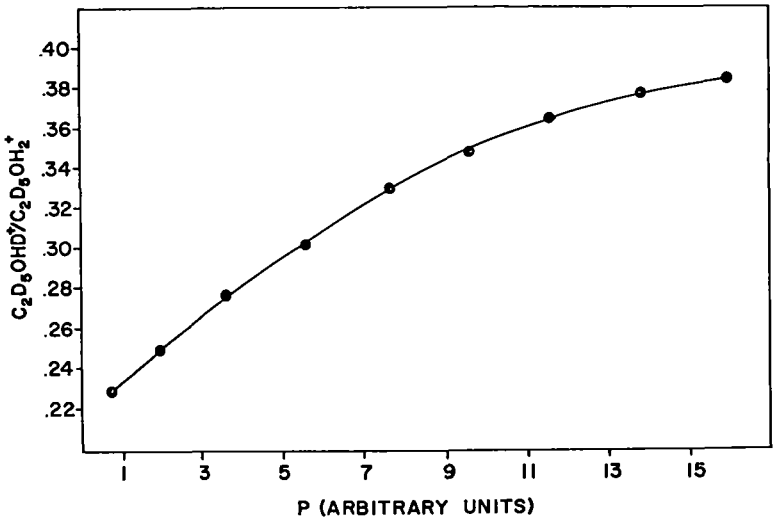

Fig. 5 Variation of $C_2D_5OHD^+/C_2D_5OH_2^+$ with pressure for 50 volt electrons.

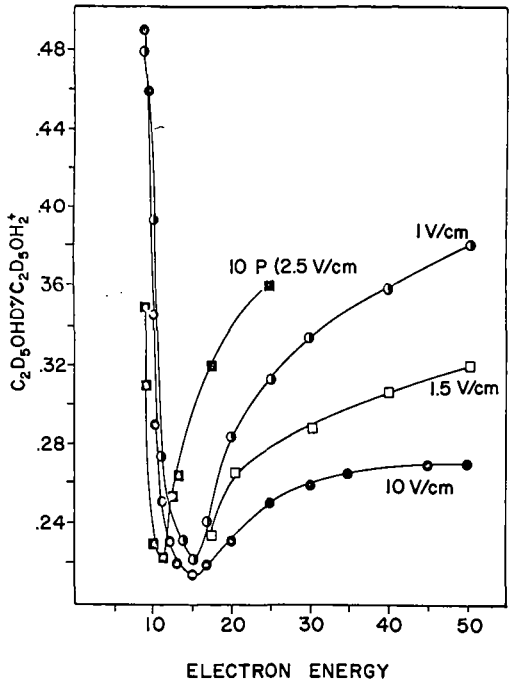

Fig. 6 Dependence of D^+/H^+ ratio on ionizing voltage at various repeller fields.

a greater extent than the analogous sequence involving the molecular ions $C_2D_4^+$ and $C_2D_2^+$. For both alkyl fragments the favored elimination mode involves incorporation of the hydroxyl hydrogen atom from the acceptor molecule (formation of D_2OH^+) in the charged product.

Other Reactions of Primary Ions: Another reaction path observed for the interactions of thermal alkane molecular ions is of interest. This mode is charge exchange to form $C_2D_6OH^+$. In the observed cases the overall process is exothermic for nearly ground state reactants based on relative ionization potentials[12].

Secondary Mass Spectrum: Using (i) the data presented in Table II, (ii) the actual relative abundance of primary ions obtained under analytical conditions, and (iii) the relative compositions of composite peaks in the primary spectrum[13] it should be possible to generate independently a distribution of secondary ions which can be compared with the data obtained from the single stage instrument operating under bimolecular conditions. Consideration of the data of Figures 2 and 3 demonstrates that $C_2D_6OHD^+$, $C_2D_6OH_2^+$, $C_2D_3O^+$ (perhaps), $C_2D_6^+$, D_3O^+, D_2OH^+, and H_2OD^+ are produced by second order kinetics. The responsible reactions may now be understood in view of the known reaction modes of the possible precursors.

Perhaps the most useful parameter characterizing the ethanol-d_6 system is the D^+/H^+ transfer ratio. In Figure 4 an extrapolated value (after correcting for C_{13} contributions) of 0.21 is suggested. An evaluation of the observed transfer probabilities for the major primary ions taking into account the σ_R values and the respective contributions of each species to the primary mass spectrum results in an independently predicted value of 0.20. In making this calculation we have recognized that the experimentally obtained m/e 52 peak (Figure 3) is in fact a composite containing a significant fraction of $C_2D_6OD^+$ in addition to $C_2D_6OH_2^+$. Because of the excellent agreement between the experimental and predicted value of the D^+/H^+ parameter it would seem that the bimolecular mechanisms leading to the formation of stable solvated hydrons in ethanol are now essentially understood.

The general shape of the ionization efficiency plot for D^+/H^+ transfer (Figure 6) may now also be interpreted in qualitative fashion. At the lowest electron energies, a value of > 0.5 is indicated which may be compared with a value of 0.66 for transfer from $C_2D_6OH^+$ according to the tandem data. A decrease with increasing ionizing voltage for a few volts above threshold certainly results from the interactions of $C_2D_4OH^+$ and CD_2OH^+. These ions have very low appearance potentials and dominate the primary spectrum for a few volts above threshold. Because these structures transfer overwhelmingly from the hydroxyl position, the D^+/H^+ parameter decreases accordingly. At approximately 14-16 volts on our scale the rapidly rising ionization efficiency curves for the various deuterated C_2 alkyl primary ions results in an increase in relative importance of deuteron transfer in this range. Thus the observed behavior of the relative hydron transfer probabilities may be understood by consideration of the individual reaction modes of the various precursor ions.

As discussed previously, the hydron transfer reactions of primary ions result in dissociation of the solvated hydron in some cases. The major decomposition path observed involves elimination of ethylene and the concurrent production of H_2OD^+, D_2OH^+, and D_3O^+. The relative total cross sections for the formation of these species can be evaluated by determining the initial relative rates of production indicated in Figure 3. Converting to a percentage scale, the distribution obtained experimentally is H_2OD^+ (19%), D_2OH^+ (53%), and D_3O^+ (29%). A method analogous to that used to predict the bimolecular D^+/H^+ ratio may be used to obtain a calculated secondary spectrum of hydronated waters. Using (i) the distributions listed in Table II resulting from the interactions of $C_2D_4OH^+$, CD_2OH^+, $C_2D_4^+$ and the composite m/e 30 peak, (ii) the respective σ_R values, and (iii) the relative contributions of these species to the primary spectrum, a predicted secondary spectrum consisting of 11% H_2OD^+, 57% D_2OH^+, and 32% D_3O^+ may be calculated. The agreement between the predicted and experimental distribution is quite good and is a further indication of the excellent complementary data which can be obtained from the concurrent usage of single stage and tandem spectrometer systems.

Higher Order Processes: Before beginning this discussion the authors would like to point out that they are well aware of the difficulties encountered in some cases at elevated pressures in differentiating between the effects of collisional stabilization and reduced kinetic energies of reactant ions, since both conditions may induce changes in the reaction mode. Although we have established experimentally in the tandem instrument that the relative importances of various reaction paths for some species are essentially independent of translational energy at very low values, we cannot of course investigate quaternary and higher order reactions in any detail in this apparatus. We recognize that absolute rate

constants for the ionic interactions occurring in systems containing molecules with permanent dipole moments are energy dependent[14] and that increased translational energy (e.g., CD_2OH^+, Table II) drastically alters the product distribution. However, the good agreement between the tandem and low-repeller single stage spectrometer data indicate that kinetic energy effects are probably of little importance in interpreting the higher order chemistry occurring in this system.

The existence of extensive solvation in ethanol is clearly demonstrated by the formation of higher order aggregates. For ethanol-C_2D_5OH, variations in the ratio of $C_2D_5OHD^+/C_2D_5OH_2^+$ at very low field strengths and elevated pressures may also be related to consecutive processes. Reference to Figure 4 indicates that a value of 0.40 for this ratio is approached at vanishingly small repeller fields. At much higher pressures, where the effects of field strength are effectively cancelled by an increased collision frequency, the value (0.40) is also obtained. Two interrelated reaction mechanisms are involved in the variation of the D^+/H^+ ratio. These are (i) generation of species of the type $C_2D_5OHD^+$ and $C_2D_5OH_2^+$ and (ii) their conversion to solvated aggregates.

It is apparent that the rate of production of the secondary species H_2OD^+, D_2OH^+ and D_3O^+ are greatly reduced at elevated pressures. We attribute this effect to a reaction of the type $H_3O^+ + C_2H_5OH \rightarrow C_2H_5OH_2^+ + H_2O$, which is quite exothermic. Although the transfer reactions of the hydronated waters have not been investigated specifically, the fact that the isotopic composition is overwhelmingly in favor of deuterium labelling suggests that transfer will serve to increase the $C_2D_5OHD^+/C_2D_5OH_2^+$ ratio from the 0.25 low pressure value. The other major fragment produced by the interactions of the primary mass spectrum is $C_2D_5^+$ (m/e 34). The subsequent reaction of this species with the solvent can also only serve to increase $C_2D_5OHD^+$ (Table II).

The subsequent reactions of the species $C_2D_5OHD^+$ and $C_2D_5OH_2^+$ have been investigated in the tandem instrument. These two secondary ions are produced in the first stage ion source by operation at low repeller and elevated pressure and these mass selected ions were impacted on ethanol (refer to Results section). Since $C_2D_5OH_2^+$ transfers both D^+ and H^+ and since a normal isotope effect in the ratio of D^+/H^+ transfer is observed, both these reactions lead to an increase in the D^+/H^+ ratio. In addition, five times as much $C_2D_5OH_2^+$ is formed following the interactions of primary ions ($D^+/H^+ \cong 0.20$) and any sequence destroying this species quickly increases the observed transfer ratio.

The exchange reaction may result from the decomposition of the higher order complexes at intermediate pressures, since the aggregates may require additional collision for stabilization. There is a significant apparent isotope effect operating in the formation of these aggregates. The data in Table I, which is representative of the isotopic composition of the complexes obtained from repeated experiments in two different high pressure instruments, clearly indicates that rate of aggregation with the form $(C_2D_5OH)_2H^+$ is favored over $(C_2D_5OH)_2D^+$ by an order of magnitude. Species corresponding to loss of water from these solvated hydrons also appear in the high pressure spectrum.

In an attempt to elucidate the sequence of reactions leading to solvated protons an additional series of experiments was performed in the tandem experiment. Various primary ions were impacted on ethanol and the pressure dependence of secondary ion signal was investigated. For deuteron transfer ions (for example, $C_2D_5^+$) the following reaction sequence was established: (5) $RD^+ + C_2H_5OH \rightarrow C_2H_5OHD^+ + R$, (6) $C_2H_5OHD^+ + C_2H_5OH \rightarrow C_2H_5OH_2^+ + C_2H_5OD$, (7) $C_2H_5OH_2^+ + C_2H_5OH \rightarrow (C_2H_5OH)_2H^+$. In a single stage instrument with the complete spectrum of primary ions to initiate this chain of events the precursor solvation ion $C_2H_5OH_2^+$ in equation (7) may be formed by second, third, or fourth order reactions. Hence the protonated dimer is the composite product of processes which are kinetically of third, fourth, and fifth order in pressure.

REFERENCES

1. L. P. Theard with W. H. Hamill, J. Am. Chem. Soc. 84, 1134 (1962).

2. H. von Koch and E. Lindholm, Arkiv. Fysik 19, 123 (1961).

3. P. Wilmenius and E. Lindholm, Arkiv. Fysik 21, 97 (1962).

4. E. Lindholm and P. Wilmenius, Arkiv. Fysik 20, 255 (1963).

5. V. L. Tal'roze, Pure Appl. Chem. 5, 455 (1962).

6. V. L. Tal'roze and E. L. Frankevich, J. Am. Chem. Soc. 80, 2344 (1958).

7. K. R. Ryan, L. Wayne Sieck and J. H. Futrell, J. Chem. Phys. 41, 111 (1964).

8. M. S. B. Munson, J. Am. Chem. Soc. 87, 5313 (1965).

9. L. W. Sieck and J. H. Futrell, J. Chem. Phys., accepted for publication.

10. J. H. Futrell and C. D. Miller, Rev. Sci. Inst., in press.

11. M. S. B. Munson, J. Am. Chem. Soc., 87, 2332 (1965).

12. M. I. Al-Joboury and D. W. Turner, J. Chem. Soc., 4434 (1964).

13. L. Friedman, F. A. Long and M. J. Wolfsberg, J. Chem. Phys. 27, 613 (1957).

14. K. R. Ryan and J. H. Futrell, J. Chem. Phys. 43, 3009 (1965).

TABLE I

High Pressure Mass Spectrum of C_2D_5OH

m/e	Probable Species	Intensity (Arbitrary Units)
155	C_{13}-$(C_2D_5OH)_3H^+$	8.7
154	$(C_2D_5OH)_3H^+$	84
136		9.2
135		2.0
104	$(C_2D_5OH)_2D^+$	61
103	$(C_2D_5OH)_2H^+$	585
85		42
84		10
53	$C_2D_5OHD^+$	330
52	$C_2D_5OH_2{}^+$	822
51	$C_2D_5OH^+$	51
49	$C_2D_4OH^+$	31
46	$C_2D_3O^+$	82
34	$C_2D_6{}^+$	77
33	CD_2OH^+	109
32	$C_2D_4{}^+$	12
31	$CDOH^+$	10
30	$C_2D_3{}^+$, CDO^+	97
29	CHO^+	14

TABLE II

Secondary Mass Spectra Produced by the Reactions of 0.3 ± 0.3 eV Ions with C_2D_5OH

Reactant Ion	Products[a]										σ_R Values[f]
	H_2OD^+	D_2OH^+	D_3O^+	CD_2OH^+	$C_2D_5^+$	$C_2D_4OH^+$	$C_2D_5O^+$	$C_2D_5OH^+$	$C_2D_5OH_2^+$	$C_2D_5OHD^+$	Relative Cross Sections for Reaction
$C_2D_5OH^+$	-	-	-	-	-	-	-	-	60.5	39.5	0.86
$C_2D_4OH^+$	1.2	2.7	1.5	-	0.4	-	1.9	-	84	4.8	0.83
CD_2OH^+	2.9	6.3	3.5	-	3.2	-	-	-	75.9	4.9	0.71
CD_2OH^+ (22 eV)[b]	10	14	5.5	-	31	-	-	20	5.2	-	-
$C_2D_5^+$	-	20	18	-	12[c]	-	-	-	-	49	-
$C_2D_2^+$[d]	-	-	-	42	3.3	27	1.4	14	-	13.4	1.00
$C_2D_3^+$[d]	-	19	11	6.7	30	4.0	-	-	-	28.5	-
$C_2D_4^+$[d]	-	3.6	3.1	11	2.5	17	2.1	17	-	43.1	0.61
CDO^+ with $C_2D_3^+$[e]	-	24	14	6.2	2.6	-	-	4.6	-	25.7	0.81

[a]Tabulated as % of total secondary signal

[b]Also produces 14% m/e 48

[c]Obtained from impacting $C_2H_5^+$ on C_2D_5OH

[d]Primary beam obtained with C_2D_4 in first stage source

[e]Composite m/e 30 beam produced from C_2D_5OH in first stage source

[f]Normalized to σ_R = 1.00 for $C_2D_2^+$

THE EVAPORATED SILVER BROMIDE FILM AS AN ION DETECTOR

by

Maynard H. Hunt
Air Force Cambridge Research Laboratories,
L.G. Hanscom Field, Bedford, Massachusetts

and

Joseph I. Masters and James P. Clune
Technical Operations Research, Burlington, Massachusetts

AS MASS SPECTROGRAPHERS, WE ARE AWARE THAT THERE ARE ONLY A LIMITED NUMBER OF PHOTOGRAPHIC EMULSIONS WHICH ARE SENSITIVE TO THE ION BEAMS PRODUCED IN MASS SPECTROGRAPHS. THESE SPECIALIZED EMULSIONS ARE ALL OF THE CLASS TERMED "GELATIN POOR". THE PLATES GENERALLY IN USE TODAY HAVE ONLY ENOUGH GELATIN TO SERVE AS A BINDER FOR THE SILVER HALIDE GRAINS. IT IS PRINCIPALLY THE SHIELDING EFFECT OF THE GELATIN TO WHICH IS ATTRIBUTED BOTH THE LACK OF SENSITIVITY OF GELATIN EMULSION, AND THE VARIATION OF SENSITIVITY WITH MASS AND ENERGY.

TECHNICAL OPERATIONS RESEARCH, BURLINGTON, MASS., HAS FOR SOME TIME BEEN ENGAGED IN RESEARCH COMPRISING THE DEVELOPMENT OF SILVER HALIDE VAPOR DEPOSITION TECHNIQUES, AS WELL AS THE EVALUATION OF SENSITIVITY TO ALL TYPES OF RADIATION AND THE STUDY OF PHYSICAL PROPERTIES OF THE THIN DEPOSITED FILMS. IN PARTICULAR, THE EVAPORATED AgBr SYSTEM HAS BEEN SUCCESSFUL AS A VERY SENSITIVE RECEPTOR FOR ELECTRON BEAM RECORDING[1] WITH NO APPRECIABLE LOSS IN SENSITIVITY AND RESOLUTION, EVEN FOR ELECTRON ENERGIES AS LOW AS 2kV. FOR EVALUATION AND STUDY, THE AIR FORCE CAMBRIDGE RESEARCH LABORATORIES HAD REQUESTED SAMPLES OF THIS MATERIAL PREPARED SPECIFICALLY FOR THE MASS SPECTROSCOPY APPLICATION IN THE FORMAT OF 2x10 INCHES GLASS PLATES. THE RESULTS OF INITIAL TESTS WERE REPORTED BY HUNT IN ANALYTICAL CHEMISTRY FOR APRIL 1966.[2] SINCE THIS PRELIMINARY WORK, SOME IMPROVEMENTS IN PLATE PERFORMANCE HAVE BEEN ACHIEVED AND MUCH KNOWLEDGE HAS BEEN GAINED ABOUT THEIR CHARACTERISTICS.

THE PLATES ARE COATED FROM A TUNGSTEN BOAT EVAPORATION SOURCE AND HAVE A THICKNESS OF ABOUT 0.5 MICRON. FIGURE 1 IS AN ELECTRON MICROGRAPH OF A POSITIVE CARBON REPLICA OF SUCH A FILM SURFACE SHADOWED WITH CHROMIUM AT APPROXIMATELY 15°. THE AREA SHOWN IS ABOUT 3.4 MICRONS AND SINCE THIS FILM IS ABOUT 0.5 MICRONS THICK, IT IS EVIDENT THAT THE LATERAL DIMENSIONS OF THE AVERAGE CRYSTALLITE IS ROUGHLY THE SAME AS ITS DEPTH.

IT IS EVIDENT FROM THE APPEARANCE OF THIS FILM, WHICH IS ESSENTIALLY A CONTINUOUS LAYER, THAT IT IS IMPOSSIBLE FOR AN ION TO STRIKE THE PLATE WITHOUT INTERACTING WITH A CRYSTAL OF SILVER BROMIDE. THERE IS NO PROTECTIVE LAYER OF GELATIN TO SHIELD THE CRYSTALS, NOR ARE THERE ANY VOIDS FOR THE ION TO TRAVERSE WITHOUT ENCOUNTERING A CRYSTAL. ALSO, THE FILM IS THICK ENOUGH ($0.1 mg/cm^2$) SO THAT ALL BUT A FEW OF THE LIGHTEST IONS MUST COME TO REST WITHIN THE FILM.

FIGURE 2 IS A PHOTOMICROGRAPH OF A TYPICAL SPECTRAL LINE ON A TECH/OPS PLATE, AND FIGURE 3 IS A SIMILAR PHOTOMICROGRAPH OF THE SAME LINE AT THE SAME EXPOSURE ON A Q-2 PLATE. THE FILAMENTARY NATURE OF THE BROMIDE PLATE IS DUE TO THE MECHANISM FOR IMAGE FORMATION INHERENT IN A CONTINUOUS FILM AND IS TREATED IN SOME DETAIL IN A PUBLICATION NOW IN PREPARATION FIGURE 4 IS A LOWER MAGNIFICATION OF THESE SAME LINES SHOWN TOGETHER FOR COMPARISON. ALTHOUGH THE Q-2 PLATE IS ONE THAT WE WOULD TERM GOOD, HAVING A UNIFORM, SLIGHTLY GREY APPEARANCE, THE COMPARISON SHOWS A STRIKING ESTHETIC AS WELL AS METRIC ADVANTAGE OF THE EVAPORATED FILM. A MICROPHOTOMETER TRACE OF THESE LINES SHOWS THAT THE Q-2 LINES ARE APPARENTLY THE WIDER DUE, IN PART, TO THE SHAPE OF THE SENSITIVITY CURVE OF THAT EMULSION.

FIGURE 5 SHOWS A SPECIFIC EXAMPLE OF THE RELATIVE SENSITIVITY OF THE SILVER BROMIDE FILM AND A Q-2 PLATE. THE MATRIX MATERIAL WAS ZIRCONIUM AND THE PLATES WERE EXPOSED IN AS NEARLY IDENTICAL FASHION AS POSSIBLE. THE TRANSMITTANCE OF EACH PLATE WAS SET TO 100% ON THE MICROPHOTOMETER IN THE CLEAREST PORTION OF EACH PLATE, AND ZERO SET BY OCCULTING THE MICROPHOTOMETER SLITS. THE ORDINATE SCALE IN T, FOLLOWS THE FUNCTIONAL FORM OF THE BAKER-SEIDEL FUNCTION, $\mathrm{Log}\left(\frac{1}{T}-1\right)$. THIS FIGURE SHOWSTHAT THE RESPONSE OF THE TECH/OPS PLATE EXCEEDS THAT OF THE Q-2 PLATE EXCEPT FOR THE THRESHOLD EXPOSURES. EVEN IN THIS REGION, HOWEVER, THERE IS AN ADVANTAGE IN THAT I HAVE BEEN ABLE TO IDENTIFY LINES HAVING TRANSMITTANCES

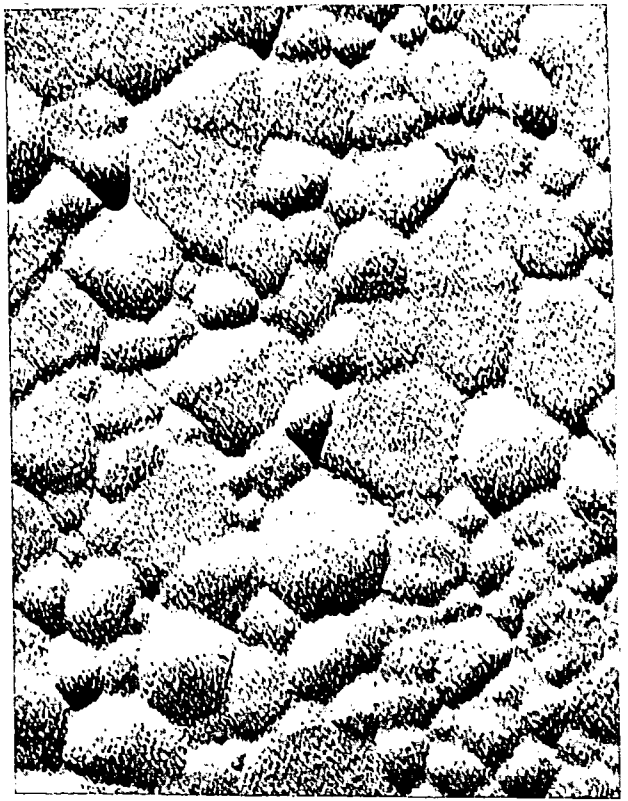

Fig. 1 - Positive carbon replica of evaporated AgBr film shadowed with chromium at 15°. Area 2μ x 3μ.

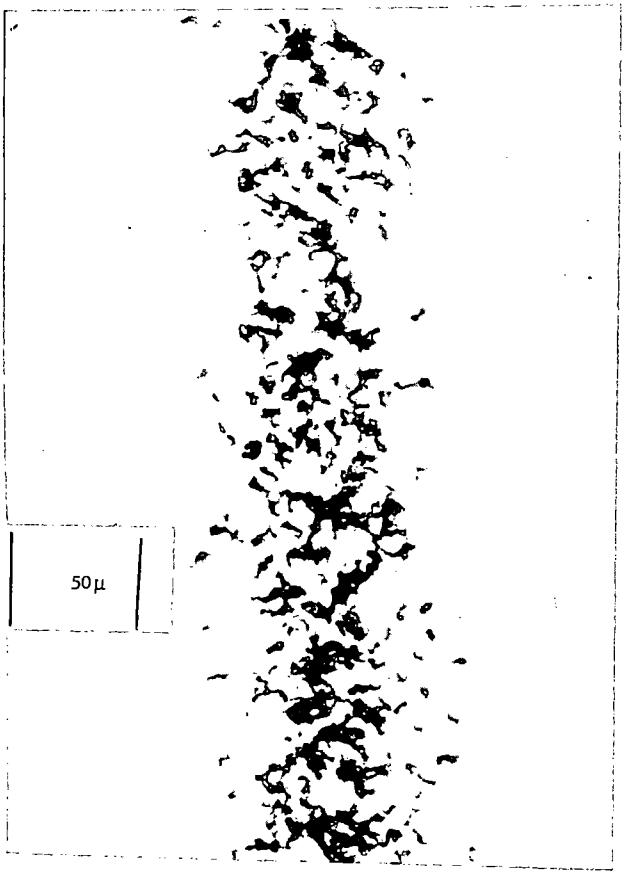

Fig. 2 - A portion of the line m/e = 29, Tech/Ops plate.

EQUAL TO 97.5% WHERE A SIMILAR LINE ON A Q-2 PLATE WAS HIDDEN BY RANDOM FLUCTUATIONS; THAT IS, NOISE WHICH WAS 2% PEAK TO PEAK.

THE SATURATION TRANSMITTANCE OF THE Q-2 PLATE WAS 2.8% WHEREAS THAT OF THE HIGHER DENSITY TECH/OPS PLATE IS CLOSE TO 0.5%. THE NEARLY STRAIGHT CHARACTERISTIC ON THE BAKER-SEIDEL PLOT SHOWS THAT THESE PLATES CAN BE USED FOR QUANTITATIVE MEASUREMENTS TO LOWER TRANSMISSION VALUES THAN THE Q-2, THUS PARTIALLY COMPENSATING FOR THE APPARENT NARROWER LATITUDE THAT OCCURS WHEN TRANSMISSION IS THE READ-OUT QUANTITY. ON THE OTHER HAND, THE STEEPER CHARACTERISTIC SHOULD MAKE POSSIBLE MORE ACCURATE CONCENTRATION DETERMINATIONS.

THE CONTINUING COOPERATIVE EFFORT BETWEEN AFCRL AND TECHNICAL OPERATIONS RESEARCH SHOULD LEAD TO A COMPREHENSIVE MASS SPECTROMETER EVALUATION OF THEIR EVAPORATED AgBr PLATE, AS WELL AS IMPROVEMENTS IN THE BASIC PROCESS. IN THE MEANTIME, THE PLATES ARE NOT AVAILABLE EXCEPT IN THE SPECIAL CASE OF MUTUAL INTEREST FOR RESEARCH PURPOSES.

WE WISH TO THANK MR. VERNON NORDSTROM OF THE AIR FORCE CAMBRIDGE RESEARCH LABORATORIES FOR PREPARING THE ELECTRON MICROGRAPHS.

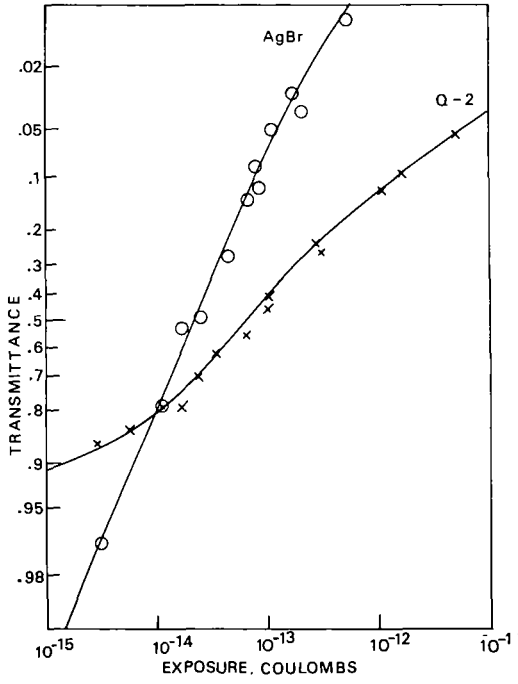

Fig. 5 - Response of Tech/Ops and Q-2 plates to Zr^+ ions.

LITERATURE CITED

1. R. Whitney, J. Masters, and A. Shepp, "Evaporated Silver Bromide as an Electron Beam Recording Material", presented at the Society of Photographic Scientists and Engineers; San Francisco, California (9-13 May 1966).

2. Maynard H. Hunt, "Vapor Deposited Silver Bromide as an Ion Detector for Mass Spectrography", Anal Chem, 38, No. 4, pp. 620-622 (April 1966).

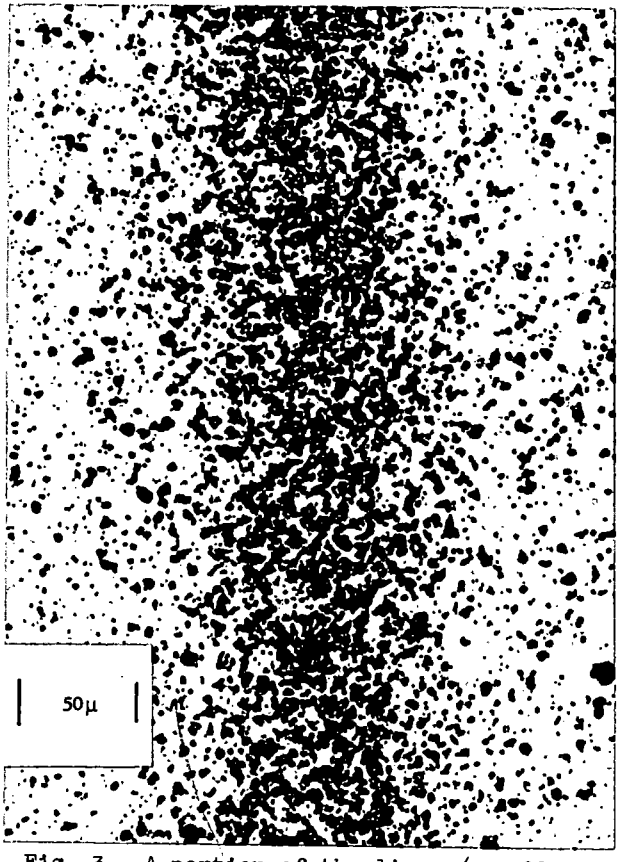

Fig. 3 - A portion of the line m/e = 29, Q-2 plate. Same exposure as Fig. 2.

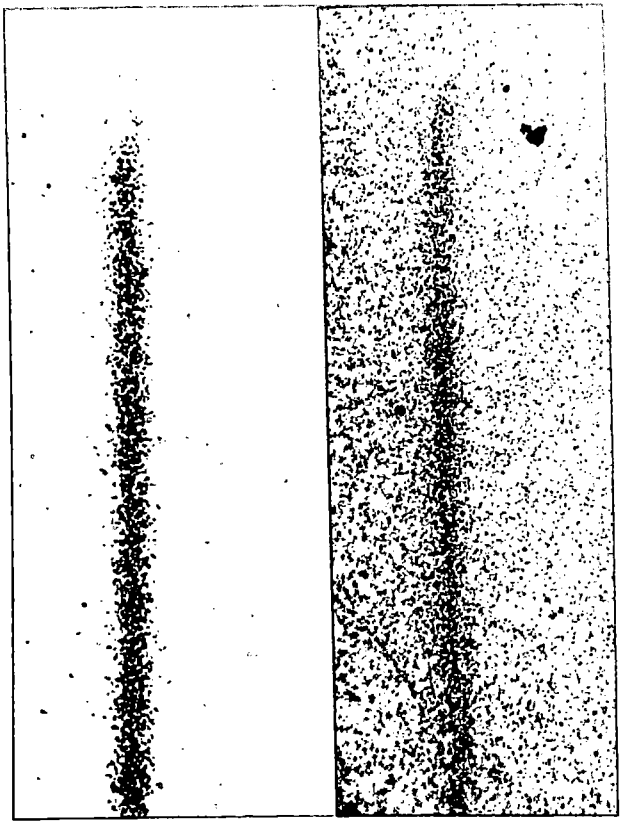

a. b.

Fig. 4 - Lines of Figs. 2 and 3 compared for background. a. - Tech/Ops, b. - Q-2.

PHOTOGRAPHIC VERSUS ELECTRIC RECORDING

K.E. Habfast and K.H. Maurer
Fried. Krupp MAT, Bremen, Germany

During last years there were used in high resolution mass spectrometry electric as well as photographic recording techniques. With both systemsit is possible to evaluate the mass spectrum automatically and to get an element map or some other kind of data presentation by the aid of a computer. This has been shown by several independant groups (1). The digitizing equipment, tape-recorders and analog-to-digital-converters on the one side and automatic plate readers on the other side, are also available and meet the requirements of the analyst, that is, neither method of data reduction introduces much error.

Under these circumstances, and probably promoted by commercial considerations, a lively discussion about technical merits and demerits of both recording methods has begun before complete understanding could be established about the fundamental differences of both methods with respect to detection sensitivity and the accuracy of mass determination. To get this understanding, we performed some calculation and experiments with a Mattauch-Herzog mass spectrometer of the type MAT - SM 1.

a) Electric Recording

The mass spectrum is scanned exponentially, to get the same measuring time for each peak, independant of mass:

$$M_t = M_o \cdot e^{\frac{\ln d}{\tau_d} \cdot t}$$

τ_d: time to scan the Mass Spectrum from Mass M_o to Mass d . M_o

Assuming, the mass spectrometer has an absolute sensitivity of E_{abs} (measured in $^{Coul}/_{\mu g}$) and the sample is evaporated with an evaporation rate of w' ($_{\mu g}/_{sec}$), then the number n_A of ions of one peak, which comes to the collector, is given by

$$n_A = \frac{1}{2} \cdot \frac{\tau_d}{\ln d} \cdot \frac{E_{abs} \cdot w'}{q_e \cdot R}$$

R: resolving power, based e.g. on 5 % - peak-width (10 % - valey definition)

q_e: elementary charge

Sensitivity E is inversly proportional to resolution R, or, the product E x R is constant

$$E_{abs} \cdot R = E_o \cdot R_o = const.$$

If we now define, that ions are sufficient, to represent a measurable peak, then the sample size w in μg is given by

$$W = B \cdot \varepsilon_a \cdot \frac{q_e}{E_o \cdot R_o} \cdot \ln d \cdot \frac{\tau_s}{\tau_d} \cdot R^2$$

B is the dynamic range (e.g. 50 : 1) of the intensity measurement. τ_s is the time, during which the sample is evaporated.

This basic relation of electric recording is shown in figure 1 for several different mass ranges.

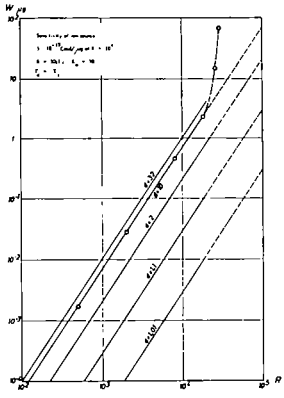

Fig. 1: Variation of usable sample size W with resolution R

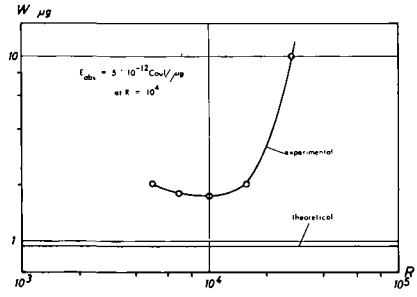

Fig. 2: Usable sample size w for σ_M = 3 ppm

We see for instance, that for a mass range of one octave and a resolution of 1 000, a sample as small as about 2 ngr is necessary to get a usefull mass spectrum. On the other side, at resolution of 15 000 we need for the same mass range a sample of at least 1 μg. The points on the decade-line indicate our experimental results, which have been the basis for constructing the other lines.

Increasing the resolution above 15 000, the sample-consumption increases very rapidly, due to ion optical abberations and decreased signal-to-noise ratio.

In high resolution mass spectrometry we are not only interested in ion current measurement, we are more interested in precise mass measurement. The standard deviation σ_M of mass determination depends on the number n_A of ions, which we get for one peak (2):

$$\sigma_M = \frac{10^6}{R \cdot \sqrt{24 n_A}} \quad ppm$$

Therefore, we need a sample size w of

$$W = B \cdot \frac{10^{12}}{12} \cdot \ln d \cdot \frac{q_e}{E_o \cdot R_o} \cdot \frac{\tau_d}{\tau_s} \cdot \frac{1}{\sigma^2}$$

to be able to measure the mass of all peaks in the intensity range B with standard deviation σ_M . This is theoretically independant of resolution, as shown in figure 2 by the lower line. Experiments however show, that the theoretical estimation is somewhat too optimistic (figure 2, upper curve). Only when we use very slow scanning speeds, say 10 minutes for one mass decade at resolution $R = 10^4$ can the signal-to-noise ratio be made high enough so that the theoretically estimated sample size is sufficient.

b) Comparison between photographic and electric recording

The number of ions which fall on a photographic plate during exposure time τ_p is

$$n_p = \frac{i_p \cdot \tau_p}{q_e} = \frac{\tau_p}{q_e} \cdot j_p \cdot h_p \cdot b_p''$$

j_p: current density of the measured line
h_p: height of line
b_p'': width of line

To compare the detection limits of photographic and electric recording, we must know the number of ions ε_p or ε_a, which is necessary to produce a detectable line or peak. If we use these numbers ε_p and ε_a to normalize the number of ions n_p and n_a, which really meet the plate or the collector, we get so called "normalized numbers" l_p or l_a

$$l_p = \frac{n_p}{\varepsilon_p} \qquad l_a = \frac{n_a}{\varepsilon_a}$$

Comparison of these numbers leads to a direct comparison of limits of detection of photographic and electric recording.

$$V_{pa} = \frac{\ell_p}{\ell_a}$$

A simple calculation gives the result

$$V_{pa} = 8 \cdot \ln d \cdot \frac{\mathcal{E}_a}{\sigma_p} \cdot \frac{\tau_p}{\tau_d} \cdot \frac{1}{h_a \cdot K_{ma}} \cdot \frac{r_{ma}}{r_{mp}} \cdot R^2$$

σ_p is the photographic sensitivity for the ions in question measured in $^{Ions}/mm^2$ for a given transparency of the blackened line. The other values are

r_{ma} : radius of mag. deflection for electric recording
r_{mp} : radius of mag. deflection for photogr. recording
K_{ma} : dispersion constant at r_{ma}
h_a : height of collector
$\mathcal{E}_a$: number of ions which represent one peak (e.g. $\mathcal{E}_a$ = 10)
d : mass range
τ_p : exposure time of photogr. plate
τ_d : scanning time for mass range d

Our first conclusion is that sensitivity is independant of time, when scanning time and exposure time are equal. The unknown quantity is the sensitivity of the photographic plate for organic ions. We have measured this sensitivity for some organic ions. The result is given in figure 3.

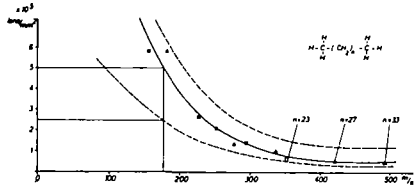

Fig. 3: Sensitivity of photogr. plate for org. ions

Two methods have been used for the determination of the sensitivity σ_p.

1) The organic ions were measured together with Krypton, which has been taken as a reference. Photographic sensitivity of Krypton is known (3).

2) We have evaporated known amounts of sample and have measured the absolute sensitivity in $^{Coul}/_{\mu g}$ of the mass spectrometer for the compounds used. In this way it was possible to get the absolute blackening curve for the ion in question.

As one can see, photographic sensitivity is strongly dependant on mass. In addition, for different ions of the same nominal mass, the sensitivity values often differ by more than a factor of 2 (as indicated by the dotted lines). But ions of the same structure typ, for instance the aliphates C_nH_{2n+2}, are on a fairly good reproducable curve. This means, that photographic sensitivity depends on the kind of ion in question.

Figure 4 shows the ratio of limits of detection, based on the measured sensitivity values for about mass 400.

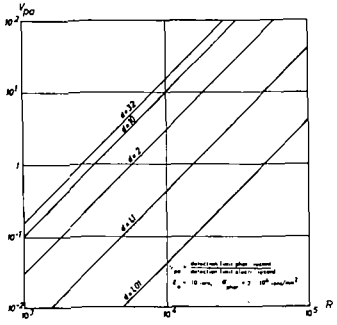

Fig. 4: Comparison of limits of detection

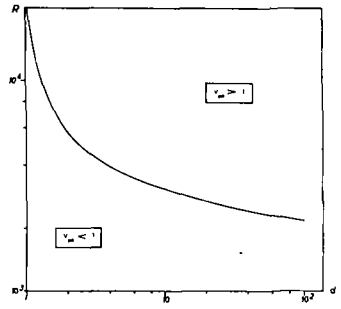

Fig. 5: Usable mass range at resolution R for photogr. and electric recording

For high resolution, photographic recording may be more sensitive by orders of magnitude, dependant on the mass range, used with electric recording. Figure 5 shows in a mass-range-resolution-diagram the line of equal sensitivity. For operating conditions which fall above this line, less sample is needed when using photographic recording. Below the line, electric recording is more sensitive.

In figure 6 a is shown the Molecular peak of Cholesterol, Mass 386, which was obtained at a resolution of about 15 000, using a sample of 0,1 µg. Figure 6 b shows the same peak, which we obtained with a sample of 0,01 µg. Exposure time in both cases was 2 sec.

Figure 6

a)

b)

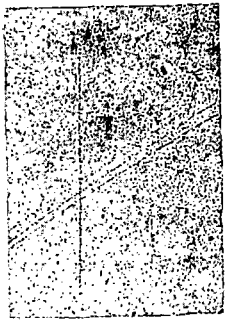

c) e/p-Spectra

In a preleminary test we have measured the mass spectrum of Pentacosan ($C_{25}H_{52}$) electrically and photographically. We have divided the ion-currents for each peak of electric and photographic recording by each other and have corrected for mass dependancy. So we got a so called e/p - Mass Spectrum, whose lines have all the same height (figure 7 a). We have done the same for some peaks of Anthracene, using also the mass correction for Pentacosan. The result is a e/p - Spectrum of quite another typ (figure 7 b). The low line at mass 89 for instance indicates high photographic sensitivity, or a doubly charged ion.

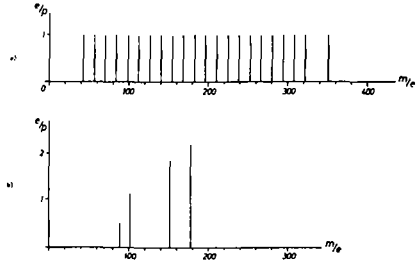

Fig. 7: e/p - Spectrum

Up to now, we don't know exactly which property of structure does make different sensitivity for the same mass. We believe that the number of Hydrogene-Atoms, the number of double-bounds and the number of light hetero-atoms play a rôle on this effect. In every case, by combination of electric and photographic recording methods we get additional information on the ion in question.

Thus, it can be said in summary that, depending on the kind of problem to be solved, fundamental merits are furnished in some cases by the electric recording method and in other cases by photographic recordings and that possibly the application of both methods for the same analysis problem might give additional information.

Automatic Evaluation of Photographically Registered Mass Spectrograms. Instrumentation, Physical and Technological Limitations

Klaus Heinecke
Ernst Leitz GMBH
Wetzlar, Germany

For automatic evaluation of spectrographic plates instruments for objective line identification (localization and density measurement) and linear measurement are required.

Two basic concepts of photo-electrically working sensor arrangements for linear scaling are described and compared with each other. The physical and technological limitations of resolution are explained and problems of photometric image accuracies are discussed. Methods for creating a signal of line localization (profile maximum finder) are reached.

The high precision spindles usually employed in longitudinal measurements are confronted with a newly developed grid measuring system with incremental, electric output. The working process and the advantages of the grid systems are explained. The necessary computers are indicated and evaluated according to their required efficiencies. A manually or automatically controlled Abbe comparator will be described in its various components and the complete function of the evaluator will be demonstrated.

A SYSTEM FOR THE QUANTITATIVE EVALUATION OF MASS SPECTROGRAPH PLATES

by
P. R. Kennicott
G.E. Research and Development Center
Schenectady, N. Y.

ABSTRACT

An ideal system for the quantitative evaluation of spark-source mass spectrograph plates would determine accurately the total charge to which a line on a plate has been exposed regardless of the width or shape of the line. In addition, it would generate its own function relating photographic density to ion exposure. A plate evaluation system is described which has these two attributes.

The system consists of equipment for recording photographic density information in computer-compatible format, together with the necessary programs for evaluating the information. Line width and shape problems are avoided by sampling line density approximately 100 times for each line and converting each sample to exposure separately. The information from the matrix data on the plate is used to obtain a preliminary characteristic curve. Information from other elements is then used to refine the initial curve. The final curve is obtained by an iterative process using information from all elements.

As an example of the use of the system, it has been possible to obtain data on impurities in copper in which the reproducibility is better than 20% without the use of an internal standard. The human effort in this analysis was reduced by more than a factor of ten.

As the spark-source mass spectrograph technique has come of age, more and more interest is being directed to obtaining quantitative data from the technique. When the technique was new, one was satisfied with data whose precision was of the order of plus or minus a factor of 3. At present, the state-of-the-art seems to be $\pm$ 40%. Obtaining quantitative data from the mass spectrograph technique implies some system for obtaining and processing data from the mass spectrograph plates.

There are two problems involved with spark source mass spectrograph plates which have strongly influenced the design of the processing system to be described here. The first is the strong variation of line width and shape through the spectrum. This variation is due in part to the theoretical variation in dispersion across the plate, but it is also due to such things as differing ionization processes for different lines. A well-known example is the extremely sharp line at mass 39 due probably to thermally ionized potassium. The second problem is the difficulty of obtaining reproducible characteristic curves from plate to plate in a given emulsion batch. Thus, an ideal system for the quantitative evaluation of spark source mass spectrograph plates would determine accurately the total charge to which a given area on a plate has been exposed, regardless of the width or the shape of the area. In addition, it would not depend upon previously prepared calibration curves.

I reported a computer program at the Montreal Conference in 1964[1] which was a preliminary attempt at meeting these requirements. The present report is a progress report in a sense, as work is still going on, but it describes an interpretation system which has been operating for two years, and which gives significantly better results than the first program.

I used the word system in the title to imply that we are now concerned with more than a simple computer program which reads data and gives results. The present system consists of equipment for obtaining data from the plate, transferring it to the computer, processing it, allowing the human to interject his judgment during the processing in the most convenient manner, and finally displaying the results in a useful manner.

Figure 1 shows a flow chart for the system. One first collects the data, taking a sample twice during a period corresponding to the time constant of the measuring equipment. This is done using a microdensitometer with a strip chart recorder to which a retransmitting slide wire has been added to produce a voltage which is proportional to the per cent transmission. This voltage is temporarily stored on an analogue tape recorder. When all data for a given run have been collected, the output of the tape recorder is digitized by an analogue to digital converter and fed into the computer memory.

The first step for the computer is to find background and line limits. The data are recorded by scanning each line individually, including sufficient information on either side of the line to establish the background. It is convenient for the computer itself to locate the beginning and the end of the line in order to calculate the background. This is done by obtaining the second derivative of the data. When the second derivative vanishes, the data are linear, and one may assume that this data corresponds to the background. Thus, the computer simply looks through the second derivative information and averages all data for which the second derivative vanishes. Where the second derivative rises above zero, it assumes that the line is beginning and uses this point for the limit of integration. A similar procedure is followed in the opposite direction to obtain the other limit.

The next step is to construct a preliminary characteristic curve. This is done using the technique based on Churchill's method which I reported at the Montreal conference. The information used to construct this curve consists of the peak heights at various exposures of two matrix lines whose relative abundances are of the order of 1.5.

Having constructed the preliminary characteristic curve, the computer uses it to correct the data point by point and integrates between the line limits established in the second previous box. The ion exposure equivalent to the background at each point is subtracted from the total exposure. The result is a single number corresponding to each line. If the preliminary characteristic curve were exactly correct, this number would be proportional to the number of ions striking the plate within the area of the line. Unfortunately, this is seldom the case. One should note, however, that by the procedure of correcting the data using the preliminary curve, the problems of varying line width and line shape are solved. In addition, much of the non-linearity of the data is removed. Thus, even if only an approximately correct curve has been used, the data at this point are in much better shape than is usually the case upon entering a program for the processing of mass spectrograph data. The remainder of the system is simply a program for processing data consisting of one number per line and obtaining element concentrations. It is similar in function to the program I described in Montreal[1] or to the one described by Woolston[2] in St. Louis, and could be run independently of this system. It operates by obtaining a characteristic curve from the data, calculating concentrations for all elements, and using the resulting data in an attempt to improve the curve. Note that the curve referred to here is different from the preliminary curve used to convert the data points prior to integration.

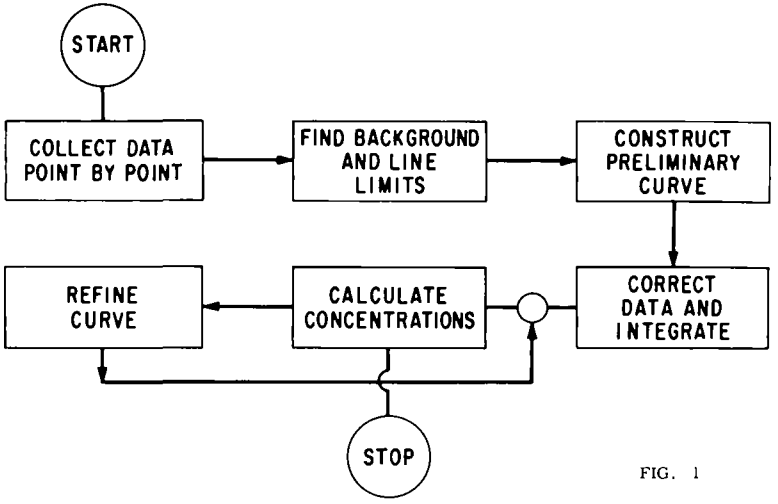
START
COLLECT DATA POINT BY POINT
FIND BACKGROUND AND LINE LIMITS
CONSTRUCT PRELIMINARY CURVE
REFINE CURVE
CALCULATE CONCENTRATIONS
CORRECT DATA AND INTEGRATE
STOP

FIG. 1

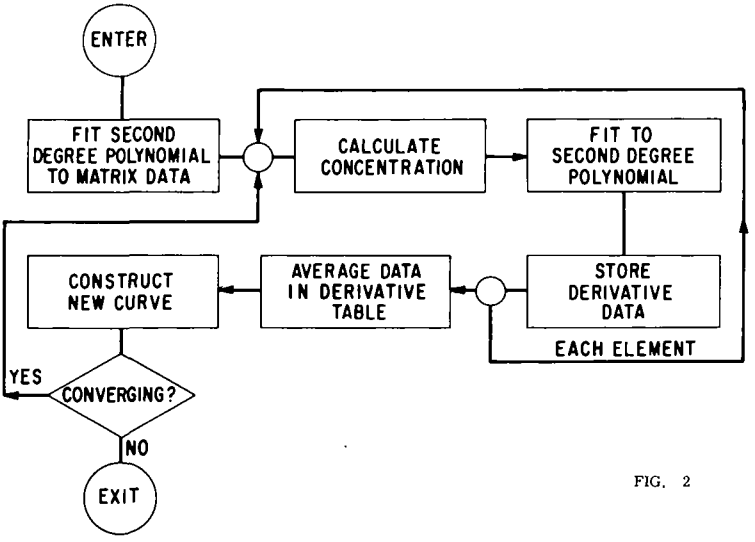
ENTER
FIT SECOND DEGREE POLYNOMIAL TO MATRIX DATA
CALCULATE CONCENTRATION
FIT TO SECOND DEGREE POLYNOMIAL
CONSTRUCT NEW CURVE
AVERAGE DATA IN DERIVATIVE TABLE
STORE DERIVATIVE DATA
EACH ELEMENT
YES
CONVERGING?
NO
EXIT

FIG. 2

The detailed manner in which the calculation is done is shown in Fig. 2. The program starts by fitting a second degree polynomial to the matrix data. Concentrations for each element are calculated using this second degree polynomial. For each element whose data consist of four or more points, the data are fitted to another second degree polynomial. The derivative, obtained from this second polynomial, is stored in a table according to the corresponding value of the characteristic curve ordinate. The process is repeated through a loop for each element. When all the elements have been processed, the data in the derivative table are averaged and used to construct a new characteristic curve. If the characteristic curve is converging, i.e., if the mean deviation of the data in the derivative table is decreasing, the program goes back and repeats the process. When the characteristic curve no longer converges, the program exits, and the calculation is complete. This process of averaging the derivatives and computing a new curve is equivalent to the process of plotting data for each element on an exposure scale with arbitrary origin and sliding the resulting plots along the exposure scale until they superimpose to form one curve.

The justification for any system is that it will help one to obtain better information or information in a form which was not possible without it, and that it will do this more quickly and conveniently. We had been spending about 16 hours on a plate to obtain the desired information using graphical techniques. The information consisted of 12 samples from the matrix element and data from 25 elements. Using the system described here, the same information is obtained from the microdensitometer in about 45 minutes. The computer time is of the order of 5 minutes using a G.E. 235 computer. Finally, about 15 minutes of the operator's attention is required to study the results and monitor the progress of the programs. The precision of the results has also been improved using this system. The state-of-the-art using graphical techniques seems to give a precision of the order of ± 40%. In a recent Round Robin of MS-7 users on impurities in copper, reproducibility using this system was ± 15%. This refers to deviation from emission spectrographic values after applying relative sensitivity coefficients. Experience on internal consistency on a large number of samples indicates that with care, one should be able to stay between ± 10% and ± 20% for all data. It should be pointed out that these results are obtained using the matrix element as the internal standard.

To conclude, the results using this system have convinced me more than ever that there is a use for some mechanized help in interpreting mass spectrograph plates. The digital computer with its accessores has proved a convenient source of this help.

References

(1) P. R. Kennicott, 12th Annual Conf. on Mass Spectrometry and Allied Topics, Montreal, June 1964.

(2) J. R. Woolston, 13th Annual Conf. on Mass Spectrometry and Allied Topics, St. Louis, May 1965.

Propagation of Error From Densitometer Data to Spectrographic Results

J. M. McCrea
Applied Research Laboratory
United States Steel Corporation
Monroeville, Pennsylvania 15146

Abstract

A treatment similar to that used by Slavin is combined with a logarithmic-logistic equation for a spectrographic emulsion response curve and used to develop conditions for minimizing the propagation of random error in transmittance data into exposure measurements and analytical results. In cases without spectral background, the optimum transmittance levels for reduced propagation depend sharply on behavior in the photometric system, but not on the slope or contrast terms in the emulsion equations. Optimum levels with spectral background involve contrast specifically and present prohibitive difficulties for direct algebraic treatment. Such cases can be studied by numerical computation and plotting techniques, and results for selected simple background situations are compared. A small effect of graininess on results obtained from Ilford Q2 plates is discussed.

Propagation of Error From Densitometer Data to Spectrographic Results

Introduction

For calculation of the exposure E that produced a spectrographic line of transmittance T, the relation between E and T for the emulsion is customarily assumed to be explicitly predetermined from calibration procedures as a graph, a table of values, or an algebraic expression. Under this assumption, statistical variation in transmittance measurements is propagated into exposure values according to the equation

$$\sigma_E = \sigma(T) \left| \frac{dE}{dT} \right| \qquad \text{(I)}$$

where σ_E and $\sigma(T)$ are respectively the standard deviations of corresponding data for E and T. Both σ_E and $\sigma(T)$ retain the conventional positive sign of a standard deviation regardless of the sign of dE/dT in Equation I.

Logarithmic-Logistic Characteristics

Evaluation of the derivative term dE/dT can be accomplished most easily if the relation between E and T is expressible through the whole range of T in a compact, readily differentiable equation. Slavin[1] studied the effect of dE/dT on error propagation and implicitly recognized the desirability of such an equation when, lacking one, he evaluated dE/dT from separate equations for the curved toe and linear central regions of the characteristic plot of log E and optical density. The response of many spectrographic emulsions can in fact be approximated by the equation

$$\log \left[\frac{1}{\left(\frac{T - T_m}{T_o - T_m} \right)} - 1 \right] = G \log E + \Delta_o \qquad \text{(II)}$$

where T varies between the limits T_o at E = 0 and T_m at saturation and where G and Δ_o are constants. Equation II is a logarithmic-logistic function representing a logistic variation of T with log E between the limits T_o and T_m and, with the simplifying assignment $T_o = 1$, is algebraically equivalent to an exponential form used by Hull[2] for the ion response of Ilford Q2 plates. Baker[3] used the symbol Δ for log (1/T - 1) and noted that plots of log E and Δ for photon response were nearly linear. Although the data used by Slavin[1] are not convincing cases for near linearity, ASTM accepts the plotting of log E and Δ as good spectrochemical practice.[4] A strict linearity requires that T between the limits of 0 and 1 be logistically related to log E.[5] In practice, Equation II is a good algebraic representation of data that yield a nearly linear plot of log E and Δ because T_o and T_m approach the limits unity and zero, respectively, for most spectrographic work with photon exposure.

Propagation in Background - Free Case

Differentiation of Equation II and substitution of the result of Equation I gives

$$\frac{\sigma_E}{E} = \frac{\sigma(T)}{G} \cdot \frac{T_o - T_m}{(T_o-T)(T-T_m)} \qquad \text{(III)}$$

a simple expression for σ_E/E, the coefficient of variation of E valid for all values of T between T_o and T_m.

Equation III shows that σ_E/E increases as G decreases and becomes very large if T is close to T_o or T_m, and $\sigma(T)$ remains nonzero. For a given G the behavior of σ_E/E can be ascertained only if $\sigma(T)$ is determined as a function of T.

Any densitometer measurement is subject to a variety of random and constant errors arising in its optical, photometric, and read-out systems. Only the random errors determine $\sigma(T)$. The author's extended experience with a single-beam densitometer (Jarrell-Ash Co. Model JA203) and Slavin's findings for his double-beam instrument[1] suggest that $\sigma(T)$ comprises just two noncorrelated components, one independent of T and the other proportional to T. The component independent of T, to be denoted by a, may be considered to arise largely from the dead band of a strip-chart recorder or from scale-reading errors with a meter. The component proportional to T, denoted by the product abT, may arise largely in electronic instabilities in the phototube and the amplifier of a densitometer. The coefficient b is determined by the relative magnitudes of the components; when the dead band component a alone is negligible, the product ab remains finite but b approaches infinity. If the proportional component is negligible, b=0. When the two noncorrelated component standard deviations are combined statistically, use of the product form abT for the proportional component permits extraction of the common factor a, giving

$$\sigma(T) = a\sqrt{1 + b^2 T^2} \qquad \text{(IV)}$$

An effect of graininess on $\sigma(T)$ is evident with Ilford Q2 plates, and will be mentioned later.

When Equations III and IV are combined, it follows that the value of T at which the σ_E/E is a minimum results from differentiating

$$\frac{\sqrt{1 + b^2 T^2}}{(T_o-T)(T-T_m)}$$

and solving for the real positive root of the cubic

$$b^2 T^3 + (2 - b^2 T_o T_m) T - (T_o + T_m) = 0 \qquad \text{(V)}$$

that remains after the derivative is equated to zero and nonzero common factors are cancelled. Equation V is already in reduced form suitable for arithmetical evaluation. Two special cases yield very simple results. If the proportional or instability component is zero, the value of T required for a minimum σ_E/E is the <u>arithmetic mean</u> of T_o and T_m. If the dead band component only is zero, the required value of T is the <u>geometric mean</u> of T_o and T_m.* These cases show that the nature of the photometric system as expressed in the coefficient b plays the key role in determining the optimum T for which σ_E/E takes a minimum value.

The role of b in the error propagation was examined further by obtaining the positive roots of Equation V for $T_o = 1$ and several sets of b and T_m with the aid of a computer program for the solution of cubics. The roots in Table I are confined to a range of values limited by the special cases of the arithmetic and geometric means of T_o and T_m. Figure 1 illustrates the variation of σ_E/E with T as plots of T and the ratio of σ_E/E to its minimum value for given b values. Because $(T_o-T)(T-T_m)$ and its reciprocal are unchanged by the substitution of (T_m+T_o-T) for T, the plot for b=0 is symmetric about the average value $\frac{1}{2}(T_m+T_o)$. The shift in the position of the minimum from $\frac{1}{2}(T_m+T_o)$ towards $\sqrt{T_o T_m}$ as b assumes larger values introduces increasing skewness in the plot. For highly skewed plots with minima near $\sqrt{T_o T_m}$, the low transmittance side is compressed and reading T data from the curve is not as easy as it is for T data above the minimum. The compression and reading difficulty are readily circumvented by preparing plots with a logarithmic scale for transmittance to complement

*Transmittance T is related to optical density D by the equation D = -log T, and therefore when b = ∞ the value of D required for the minimum σ_E/E is <u>arithmetic mean</u> of the saturation density D_m and the density D_o of the processing fog level.

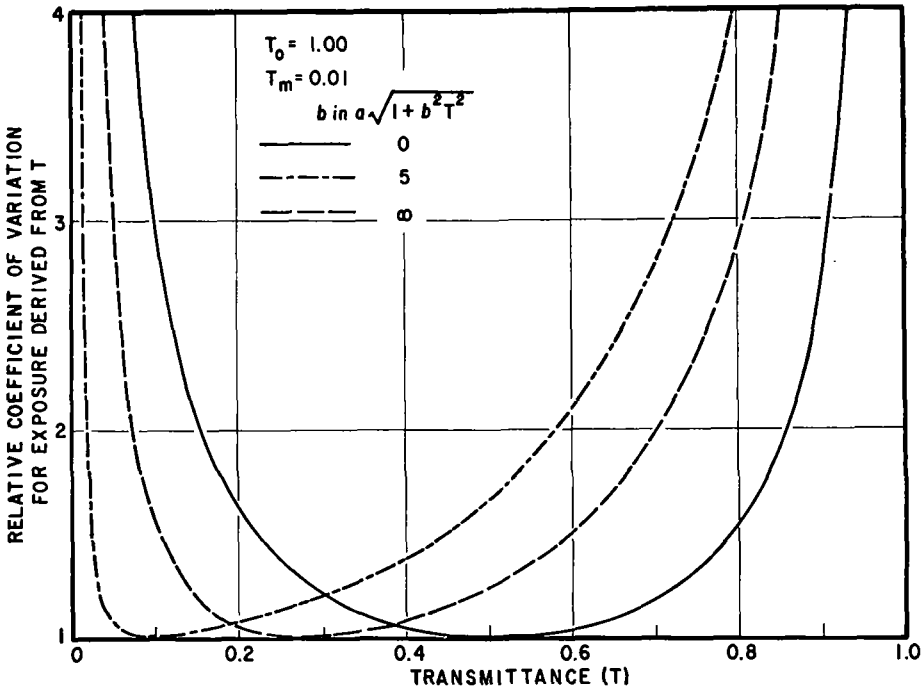

FIGURE NO. 1

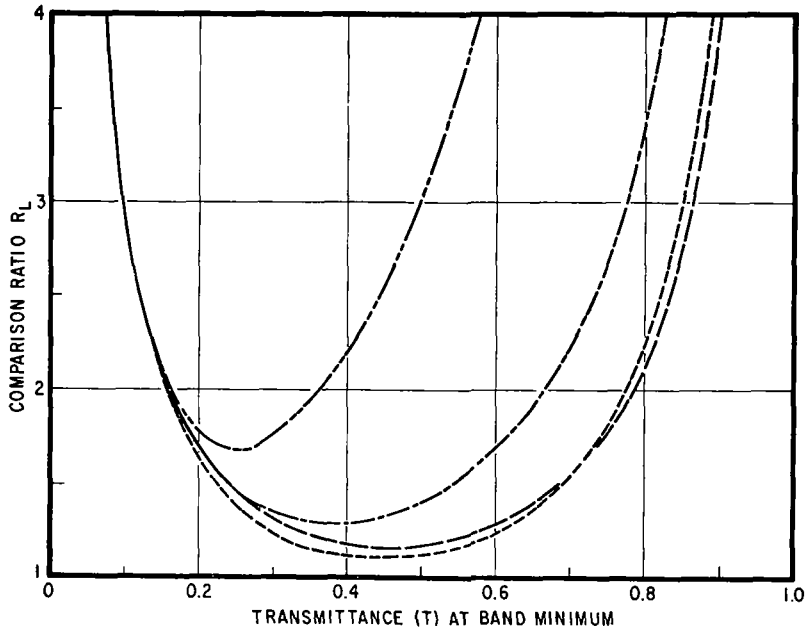

FIGURE NO. 2

the linear scale of Figure 1. The most highly skewed complementary plot is that for b=0, and the complementary plot for b = ∞ is symmetric about the geometric mean $\sqrt{T_o T_m}$ because the expression

$$\frac{T}{(T_o-T)(T-T_m)}$$

is unaltered by the substitution of $T_o T_m/T$ for T.

The ranges of T values for which the coefficient of variation σ_E/E does not exceed 1.5, 2, and 3 times its minimum value were determined graphically for listing in Table II. The width of the range is affected by the coefficient b in the analysis of the variance for T data, but not as markedly as the optimum transmittance values given before in Table I. Similar dependence of the minimum position and the range may be expected with emulsion characteristics other than Equation II, and a suitable working range for analytical spectrography cannot be properly selected without knowledge of the coefficient b for the densitometer system. This conclusion is new and surprising; possible wide departures of optimum transmittance from the normally accepted value of 0.3 are neither revealed by Slavin's studies,[1] nor expected from the spectrographic viewpoint in which the emulsion characteristic generally plays the significant role.

Instruments with both meter and strip-chart displays have two distinct dead band or a values, and although the product ab may be the same for both displays, it is only a coincidence if b has a common value for both displays. The optimum level of transmittance consequently depends on the display actually used. For the strip-chart display on the single-beam unit used by the author, a and ab approximate 0.003 and 0.005 respectively, b = 1.7 and the optimum level is about 0.4 in a low-graininess, background-free situation. Slavin reported an optimum level near 30 percent or 0.3 for a double-beam instrument with random error components corresponding to 0.002, 0.010, and 5.0 for a, ab, and b, respectively. His conclusion, based on tabulated data for the Kodak Spectrum Analysis No. 1 emulsion characteristic, is in fair agreement with the entries at low T_m in the appropriate row of Table I. As Slavin noted, random error components of these magnitudes apply to a well-designed densitometer and cause it to yield less precise final results than optimistic statements in the literature call for. The large propagation effect arises from the factor $(T_o-T_m)/(T_o-T)(T-T_m)$ in Equation III. This factor can never be less than 4, and the minimum values for various sets of T_o, T_m, and b can be readily obtained by use of the optimum T levels given by Equation V. The optimum values of Table I yield the minimum values of the factor shown in Table III. These minima apply strictly only for a logarithmic-logistic emulsion response, Equation II, but values for most spectrographic emulsions will be similar because the response equation for such emulsions generally approximates Equation II.

Effect of Spectral Background

The foregoing discussion of error propagation applies to an exposure E derived from a corresponding transmittance T. Unfortunately, useful spectrographic lines may lie in regions of background where the observed transmittance T and the corresponding exposure result from the superposed effects of the analytically important line exposure L and an interfering or background exposure B. In such cases spectrographic results for L must be obtained from the equation L = E-B, and the standard deviation σ_L for L has two independent components, σ_E for E and σ_B for B, combined statistically in accordance with the equations

$$\frac{\sigma_L}{L} = \frac{\sqrt{\sigma_E^2 + \sigma_B^2}}{L} = \frac{\sigma_E}{L}\sqrt{1+\left(\frac{\sigma_B}{\sigma_E}\right)^2} = \frac{\sigma_E}{E}\cdot\frac{E}{L}\cdot\sqrt{1+\left(\frac{B}{E}\right)^2\left(\frac{\sigma_B}{B}/\frac{\sigma_E}{E}\right)^2} \qquad \text{(VI)}$$

Both the term E/L and the square root term are greater than unity and increase the coefficient of variation σ_L/L relative to σ_E/E. Consequently the exposure component B always affects analytical precision adversely.

Equation VI summarizes in principle the propagation of random errors, but is very cumbersome algebraically when combined with expressions for B and σ_B in terms of T. The exposure B must be estimated either empirically or theoretically from measurements independent of that of exposure E. The estimating rules propagate into B both statistical variation and errors of bias. Although errors of bias have an important effect on accuracy, they result from scientific decisions and cannot be minimized

Table I

Transmittance Required to Give a Minimum Coefficient of Variation of Exposure Determined From Transmittance

Term b	Transmittance (T) Required at Indicated T_m with $T_o = 1$				
	0.100	0.030	0.010	0.003	0.001
0.0	0.5500	0.5150	0.5050	0.5015	0.5005
0.5	0.5373	0.5011	0.4908	0.4872	0.4861
1.0	0.5094	0.4701	0.4589	0.4551	0.4539
2.0	0.4538	0.4057	0.3922	0.3875	0.3861
3.0	0.4150	0.3576	0.3414	0.3357	0.3341
5.0	0.3719	0.2975	0.2762	0.2688	0.2667
10.0	0.3358	0.2329	0.2008	0.1895	0.1863
∞	0.3162	0.1732	0.1000	0.0548	0.0316

Table II

Range of Transmittance Values for Which the Coefficient of Variation of Exposure Determined From Transmittance is Less Than a Given Multiple of the Minimum Coefficient
(For $T_o = 1$, $T_m = 0.01$)

Term b	Range of Transmittance Values								
	1.5 x Min σ_E/E			2.0 x Min σ_E/E			3.0 x Min σ_E/E		
	Upper Limit	Lower Limit	Width	Upper Limit	Lower Limit	Width	Upper Limit	Lower Limit	Width
0.0	0.789	0.220	0.569	0.885	0.152	0.703	0.906	0.101	0.805
1.0	0.752	0.197	0.555	0.825	0.139	0.686	0.890	0.096	0.794
2.0	0.695	0.164	0.531	0.777	0.115	0.662	0.857	0.077	0.780
3.0	0.651	0.139	0.512	0.748	0.097	0.651	0.834	0.066	0.768
5.0	0.598	0.105	0.493	0.702	0.076	0.626	0.804	0.051	0.753
10.0	0.529	0.070	0.469	0.651	0.051	0.600	0.769	0.034	0.735
∞	0.442	0.024	0.418	0.587	0.017	0.570	0.726	0.013	0.713

Table III

Minimum Values of $(T_o-T_m)/(T_o-T)(T-T_m)$ for $T_o=1$ and Various b and Tm Values

Term b	Minimum Value for Indicated T_m				
	0.100	0.030	0.010	0.003	0.001
0.0	4.44	4.12	4.04	4.01	4.00
0.5	4.45	4.13	4.04	4.01	4.01
1.0	4.48	4.16	4.08	4.05	4.04
2.0	4.66	4.34	4.26	4.24	4.23
3.0	4.88	4.61	4.54	4.51	4.50
5.0	5.27	5.16	5.14	5.13	5.13
10.0	5.75	6.23	6.50	6.59	6.62
∞	6.09	8.19	12.2	20.4	33.7

List of Captions for Figures

Fig. 1 Propagation of Transmittance Variation to Exposure (Background Free)

Fig. 2 Propagation of Transmittance Variation to Exposure ($T_o=1$, T_m-0.01 and dead band error only)

Background cases B=L, G=1.25 — — — G=2.50 — - — -
B=0.25L, G=1.25 _ _ _ _ G=2.50 — - - — - -

Solid line where two or more curves coalesce.

Fig. 3 Propagation of Transmittance Variation to Exposure ($T_o=1$, $T_m=0.01$ and without dead band error)

Background cases B=L, G=1.25 — — — G=2.50 — - — -
B=0.25L, G=1.25 - - - - G=2.50 — -- - —

Solid line where two or more curves coalesce.

by statistical selection of optimum experimental conditions. Only the statistical variations represented by σ_E and σ_B are considered in the following discussion of precision of the results for L. The discussion is also restricted to a simple background situation and a logarithmic-logistic emulsion characteristic.

When the transmittance immediately on either side of the spectral position for L has the same value T_B and changes only slowly with distance, B may reasonably be taken from the emulsion characteristic as the exposure corresponding to T_B. Then coefficient of variation σ_B/B is equal to the right-hand side of Equation III with T_B substituted for T provided that only one measurement of T_B is used and that the statistical behavior is the same for line and background levels and depends only on transmittance.

With these simplifications and assumptions, Equation III converts Equation VI to a function of T and T_B. The concept of background presumes that B/L is primarily determined by the spectrum, spectral excitation, and resolving system, and is not dependent on exposure level. Accordingly T_B is calculable from T by Equation II at any given B/L ratio. Because attempts to derive an explicit expression for σ_L/L as a function of T alone run into prohibitive algebraic difficulties, the differentiation technique used to develop the minimization conditions for σ_E/E is not practical for σ_L/L. Numerical evaluation of σ_L/L for different T values requires supplementary calculations of the corresponding T_B data from Equation II. The supplementary calculations give G and B/L active roles in determining the T required for minimum σ_L/L, although, without background, G plays no role in minimization conditions such as Equation V. A consequence of the algebraic difficulties and of the presence of G and B/L in the minimization conditions is a difficulty in summarizing propagation effects for various background situations; statements cannot be simultaneously broadly applicable and highly quantitative.

Trends in computed σ_L/L data are compactly displayed by plots of T or log T and the ratio of the quantity $\sigma_L/L \cdot L/E$ obtained from Equation VI to the minimum value of σ_E/E obtained by substituting for T the real positive root of Equation V. This ratio will be denoted R_L and called the comparison ratio. The plots of T and R_L, Figure 2, apply for b = 0, two levels of G, and two levels of B/L. For b = ∞, plots of log T and R_L, Figure 3, give a less compressed display at low T than plots with linear T scales. The level B/L = 1 represents a strong background, and B/L = 0.25 represents a moderate case. The high G applies to exposures of Kodak SWR plates by incandescent tungsten light, and the low G is representative of the response of the newer Ilford Q2 to positive ions of 5 to 25 kv energies. The plots in Figures 2 and 3 show selected special cases representing a vast field of possible values for G, B/L, and b.

On each plot the transmittance at which the minimum in R_L occurs is both less than that required for a minimum in σ_E/E and greater than that required for the minimum in σ_B/B determined from the corresponding T_B. The plot for G = 2.50, B/L = 0.25, and b=0 is distinctive and exhibits the highest minimum value of R_L. The increase of R_L on both sides of the minimum is steep and the transmittance range for operation under a specified R_L is restricted. The plot also corresponds to the greatest difference between the optimum transmittance for R_L and the transmittance required for a minimum in σ_E/E. Sharp minima with high minimum values for R_L complicate experimental work; several exposures may be needed before one of a suitable duration finally yields a transmittance in the desirable range for determination of L. The spectrographic problem and the available apparatus generally place B/L and b beyond routine adjustment, but selection of an emulsion from an inventory of different types makes different levels of G accessible. The propagation effects for an emulsion with G = 1.25 make a useful comparison with the G = 2.50 case previously singled out. The minimum values of R_L are respectively 1.08 and 1.66. The minimum σ_E/E with G = 1.25 is twice the similar minimum with G = 2.50. The minimum σ_L/L with G = 1.25 has a value of 2 x 1.08/1.66 or 1.30 times the minimum with G = 2.50. But the broad curve for G = 1.25 in Figure 2 shows a much greater exposure range with near-minimum conditions than is present with the sharp minimum for G = 2.50. If care is taken with closely spaced graded exposures on a G = 2.50 emulsion, low propagation and a minimum σ_L/L can be attained in principle. But an emulsion with G near 1.25 will give results that are almost as precise with less difficulty, and is a desirable practical choice because precision will not be sharply influenced by deviation of exposure from optimum.

The preference for a lower contrast emulsion for quantitative measurements results from a complicated interplay of G, B/L, and b in the evaluation of R_L. If B/L is not negligible and G is high, T_B yields an imprecise B if T is near the optimum

for determination of E. Similarly if T_B is near optimum for B, T takes values giving poor precision in E. Compromise levels for T and T_B turn out to be poor but critical compromises, giving an R_L plot that has a high and narrow minimum. The transition from a high and narrow minimum in R_L to a broader minimum dipping near unity occurs in the experimentally desirable range for G.

Although Equation VI provides a framework for evaluating propagation effects when background must be considered, algebraic problems and the variety of background types and measurement techniques preclude truly general statements of preferred experimental conditions. Choices must be made by analysis of the particular situation and by examination of plotted or tabulated data. The Figure 2 plots show the practical desirability of a G of 1.25 compared to 2.50 when B/L = 0.25 and if B and T_B are obtained in the manner specified. Treatment of these cases by Equation III, neglecting background, would lead to erroneous selection of G and the transmittance levels best for use with the emulsions. The relatively simple results for background-free conditions cannot be applied to lines in background without careful consideration of the background contribution.

Emulsion Graininess Effect

The graininess of sensitive plates complicates the statistical treatment of output data from a photometric system recorder. Extensive experience with Ilford Q2 plates has shown that the noise on the trace depends on transmittance level. The noise for plates with a low processing fog is low, and tends to zero at $T_o = 1$ with very gentle processing that unfortunately is also ineffective in developing the images of weak exposures. With practical development procedures there is noticeable noise at $T = T_o$. The noise increases to a maximum near T = 0.75 and then falls more or less linearly as T decreases towards T_m. The noise component of variation in the output of the photometric system caused by graininess of Q2 plates may be approximated empirically by the expression

$$acT \cdot \left[1 - e^{\alpha(1-\frac{1}{T})}\right]$$

where α is about 4.5 and c is a constant that converts the graininess noise to the corresponding component of the standard deviation $\sigma(T)$. For $T_m < T < 0.6$, the exponential is numerically small, and if it is neglected,

$\sigma(T) = a\sqrt{1 + (b+c)^2T^2}$. Below T = 0.6, the treatment of the background-free case is therefore valid in the case of graininess upon substitution of (b+c) for b. The same optimum exposure conditions and similar working ranges apply because these are largely in ranges with T < 0.6. The term ac for the rather grainy Q2 plates is about 0.020, and the resulting b+c for the combined emulsion-densitometer system is slightly greater than 8. As a result the optimum transmittance level for the background-free case shifts down from 0.40 to about 0.25 as graininess increases from a minimal level to the level of the Q2 plate processed in Ilford ID-19 developer. The precision attainable in exposure results deteriorates substantially with the increase in graininess. Computations made for the author's data on Q2 plates show that improvement in precision from the drop in noise level above T = 0.75 is only moderate, but weak exposures are determined more precisely than if the noise did not decrease. The effect is advantageous and large enough to be considered in treatment of lines with background present.

Summary and Conclusions

Given enough patience on the part of spectrographer, the propagation-of-error situation applicable to any specified conditions can be solved numerically by use of Equations I and VI. Prerequisite to the calculations is emulsion-characteristic data for evaluation dE/dT and an analysis of precision components of the combined photometry-emulsion system. Whether the effort necessary to evaluate a given situation should be expended is determined from the importance of stiff precision requirements and from the number of analytical determinations involved.

The findings for the logarithmic-logistic emulsion characteristic without background, and for the specific background situations discussed, indicate guide lines for selection of desirable exposure conditions in other cases, where a detailed study of the propagation situation is not warranted. Exposure durations should be scheduled so that line exposures utilized do not have transmittances much greater

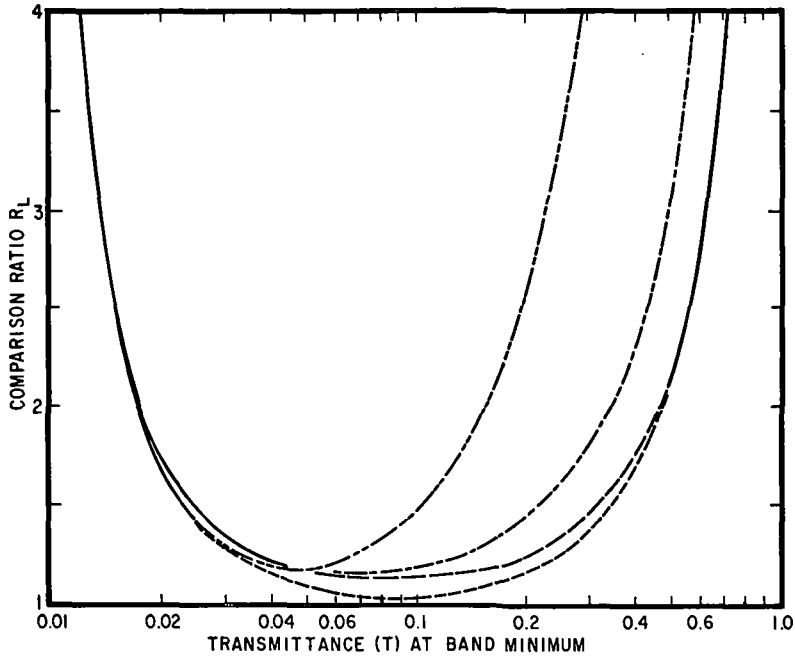

FIGURE NO. 3

than $\frac{1}{2}(T_o+T_m)$ nor much less than $\sqrt{T_oT_m}$. In the case of moderate background, transmittances less than $\sqrt{T_oT_m}$ may be preferable, but those greater than $\frac{1}{2}(T_o+T_m)$ should be avoided. If the guide lines appear suspect in a given case, their validity can be assessed from the results of a series of numerical calculations that may occasionally reveal some unexpected feature of the propagation of random variations from the photometric system into the spectrographic results.

Literature Cited

(1) M. Slavin, Appl. Spectry., 19, 28-30, (N) (1965).
(2) C. W. Hull, 10th Conference on Mass Spectrometry and Allied Topics, New Orleans, La., (June, 1962), paper No. 72.
(3) E. A. Baker, Proc. Roy. Soc. Edin., 45, 166-186 (1925).
(4) ASTM Designation E116-59T, Tentative Recommended Practices for Photographic Photometry in Spectrochemical Analysis, American Society for Testing and Materials, Philadelphia, Pa.
(5) J. M. McCrea in Developments in Applied Spectroscopy, Vol. 4, E. N. Davis, Ed. (Plenum Press, New York, 1965), pp. 514-515.

Electronic Analog Computer for Measuring Intensity Areas on Mass Spectrographic Plates

P. J. Paulsen, and P. E. Branch
Spectrochemical Analysis Section
National Bureau of Standards
Washington, D.C. 20234

The need to correct for variations in peak widths on mass spectrographic plates is a generally recognized problem. (1,2) Basically the information needed is the total number of ions which produce a given mass line. Due to variations in line widths and shapes between the matrix lines and impurity lines, plus variations of these across the photographic plate, the maximum peak intensities are not a valid measure of the number of ions producing the different peaks. In addition to line width variations with mass there will also be changes of width upon repairing and refocussing of an instrument, and there will certainly be differences in line widths between any two instruments. Because of these variations in widths, maximum peak intensity measurements cannot be used to undertake any long term study of elemental sensitivity factors in various matrices or to compare these data among laboratories. The intensity-area of a peak is a valid measure of the number of ions causing a line and would be unaffected by variations in both line width and shape. There are several ways an intensity peak area can be measured: peak width at one-half intensity multiplied by maximum intensity, a point by point replotting of the percent transmittance (% T) peak as an intensity peak followed by graphical integration, collection of many % T values for each peak combined with the digital computer computation of peak area, or the use of an analog computer system. Based upon considerations of speed, accuracy, and cost, the analog computer system was selected.

Figure 1 shows the block diagram of the computer built in our laboratories. Basically the unit is simple; a slave slide wire on the microphotometer recorder to retransmit the percent absorption (% abs.) signal, a function generator with an input of % abs. and an output of intensity, a means of subtracting the plate background signal after it has been converted to intensity (labeled offset), and an integrator to measure the area of the intensity peak. An analog computer with a similar basic block diagram was described by Socha and Willardson at a previous E-14 conference (3).

The detailed circuit wiring diagram is shown in figure 2. All components of the unit are commercially available. The cost of the parts for building the unit is approximately $500 exclusive of the digital voltmeter and recorder. The digital voltmeter is essential for inserting the plate calibration curve into the function generator; the recorder is used to measure the integrated areas. Detailed operating instructions for the analog computer plus other information will be made available upon request to anyone interested.

The most critical component of the system is the function generator which must electronically reproduce the response curve of the photographic plate. We were able to obtain the loan of a prototype transistorized function generator (now in production) from Philbrick Researches Inc.* This unit is considerably simpler and more amenable to our specific requirements than the tube-type function generators previously available. This function generator has 10 adjustments to the slope of its output current (Δ output current / Δ input voltage). The first adjustment is effective for inputs of 0.5V and up, the second is effective from 1.5V and up, the third from 2.5V, etc., at one volt intervals. These adjustable output slopes add up to give a continuously variable response which can electronically reproduce the response curve of a photographic plate.

The left hand side of figure 3 shows a plot of %abs. reading on the probability scale vs the log of the exposure for several elements in a platinum sample. The % abs. readings are based on the clear plate reading adjusted to 0% abs. and no light set at 100% abs.

*Identification of commercial equipment does not imply recommendation or endorsement by the National Bureau of Standards.

The results are straight lines which curve off to different maximum values of % abs. for each element. If the % abs. values for each element are multiplied by 100/%abs. at maximum darkening, plots such as are shown on the right of figure 3 are obtained. All the elements give a straight-line response with essentially the same slope. This correction of the data (which we have referred to as "stretching") readjusts all the % abs. data by a constant factor such that the maximum darkening for a line reads 100% abs. The variable gain on amplifier number I (fig. 2) labeled "stretch factor" allows for this correction. This "stretch" factor is analogous to the T-infinity correction used by C. W. Hull (4). Based on this and other data we are now representing the photographic plate response curve by a linear response between the log of intensity and the probability value of the "stretched" % abs. Although this system is being discussed in terms of a log-probability response curve, any method of plate calibration can be used to determine the % abs. vs intensity curve for insertion into the function generator of the analog computer.

Figure 4 illustrates the ability of the function generator to reproduce the desired photographic plate response curve. The error in the output of the function generator is plotted vs the "stretched" absorption input. The upper curve is the original curve with the triangular points being the set points used to introduce the curve into the function generator. A positive bias was thus introduced which gave an average bias of +1% at 80% abs. The set points were then readjusted low by one-half the error found previously to give the lower graph. This plot shows no net bias, with errors at any input of less than 1%. At approximately 87% abs. the function generator is no longer capable of reproducing the function, as is indicated by the upper graph, and area measurements cannot be made for peaks above this value. This limitation doesn't pose a practical problem since we would not normally collect data at 90% abs. and above for these reasons:

(1) At this % abs. level a 1% error in abs. corresponds to approximately a 6-7% error in intensity.

(2) On a typical plate the % abs. at maximum darkening is not available for most of the lines to be measured and this value must be estimated from data from other lines in order to "stretch" the % abs. data. The estimated values can be expected to be in error by several percent.

Typical peak area integrals are shown in the upper part of figure 5 along with their % abs. peaks (lower part). The vertical deflection of the recorded integrals is proportional to the peak area. All data were collected at the same sensitivity settings except for the last area measurement on the right which is 10 times as high as is recorded. The recording on the left was made with both the microphotometer and analog computer running; however, the plate was not being scanned. The perfectly straight line for this integral indicates that the noise level of the combined equipment is considerably lower than the noise level of the photographic plate.

The plate "noise", caused by emulsion graininess, is illustrated by the wanderings of the "baseline" immediately before and after the vertical deflection of the area recordings for the 10 and 45% abs. peaks. This baseline wandering (noise) is the basis of our choice of a recorder readout of the peak area instead of digital voltmeter readout, since it is obvious from the recording that the digital voltmeter reading would be highly dependent on the arbitrary timing involved in reading the voltage before and after the peak was scanned.

Area measurements were made on the isotopes of tin from a "six nines" pure sample. The results are shown in figure 6. There is a linear relationship between the area measured and the abundance of the tin isotope. In general, the deviations from the straight line response corresponded to less than a 5% error. The areas were measured from peaks ranging from 6 to 80% abs. From the consistency of these results it was concluded that the use of a linear log-probability plate response combined with data correction for the maximum darkening on the plate ("stretching") gives an adequate representation of the true response of the photographic plate to ions.

An example of how the variation of peak widths across a plate affects the results calculated from maximum peak intensities is presented

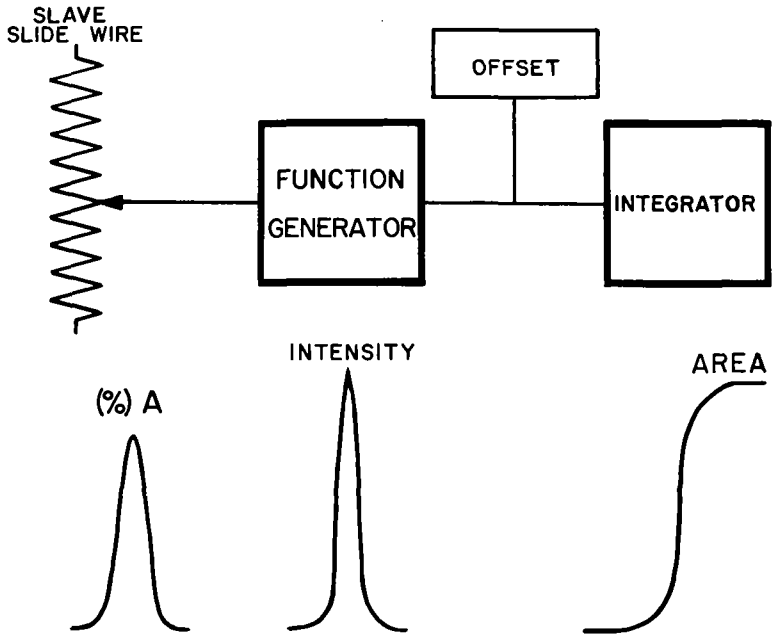

Figure 1. Block diagram of analog computer.

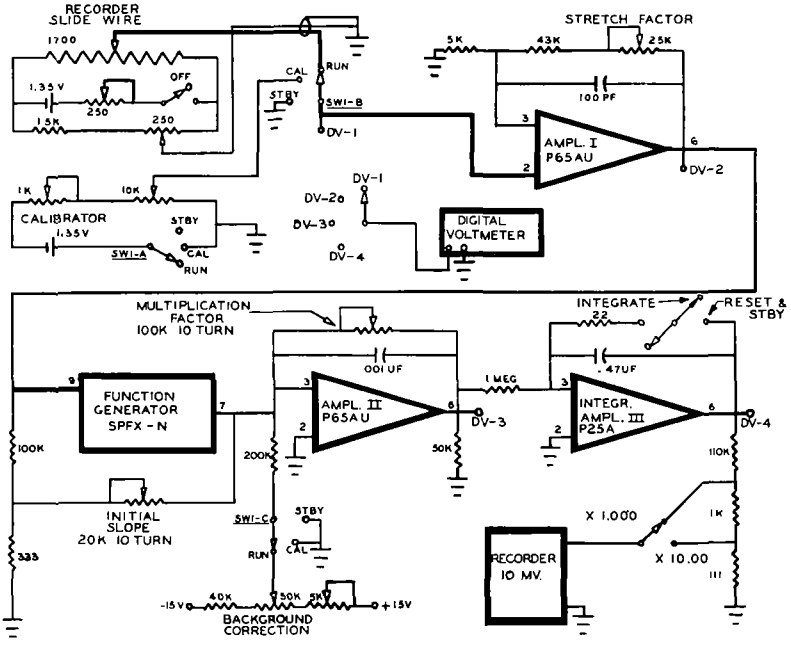

Figure 2. Detailed wiring diagram for analog computer.

in table 1. These data were compiled for a sample of doped platinum using the same plate response curve for both area and intensity measurements. The data were computed for seven equal exposures. The intensity and area measured for each line on an exposure were divided by the corresponding value for Pt 190, the Pt 190 line thus served as an internal standard. At Pb 207 which has nearly the same peak width as Pt 190 there was no significant difference between the results computed from peak intensities and peak areas. However at lower masses the difference increases until at Mg 25 the intensity measurements give a ratio of more than twice that computed from areas. The difference in values is a direct result of the decrease in line width which a decrease in mass.

COMPARISON OF RESULTS FROM AREA AND

INTENSITY MEASUREMENTS ON A DOPED PT SAMPLE

	Area of Line / Area of Pt 190	Intensity of Line / Intensity of Pt 190	Difference Between Results
Pb 207	.0834 ±14%*	.0805 ±15%*	- 3.5%
Ag 109	.0871 ±15%	.132 ±16%	+52%
Pd 106	.0756 ± 6.9%	.115 ±12%	+52%
Zr 90	.165 ±12%	.251 ±14%	+52%
Cu 63	.605 ± 9.0%	1.12 ±13%	+85%
Fe 56	.424 ± 7.8%	.794 ±11%	+87%
Al 27	.263 ± 5.9%	.569 ± 5.5%	+116%
Mg 25	.654 ± 5.6%	1.43 ± 9.1%	+119%

*%Standard Deviation

In order to prove the ability of area measurements to compensate for changes in peak widths, the instrument was deliberately defocused to change the widths. Fourteen equal exposures were made on a doped platinum sample, seven with the instrument focused, seven with it defocused. Both maximum peak intensities and area measurements were made on the focused and defocused exposures using the same photographic plate response curve. The results of these measurements are shown in the table 2. Listed in the first column are the ratios of the average peak intensity of the focused lines divided by the average peak intensity of the defocused lines. The deviations from a value of 1.00 indicate how much the changes in peak width brought about by defocusing have affected the maximum peak intensity readings. The second column was computed from the same peaks except that the peak areas were measured instead of maximum peak intensities. All of the data were within the 2 σ limits of the ratio of 1.00, indicating that the area measurements have compensated for the changes in peak widths.

AREA MEASUREMENT COMPENSATION

FOR CHANGES IN PEAK WIDTHS

(14 equal exposures - of doped Pt - 7 focused, 7 defocused)

	Ratio of focused to unfocused values	
	INTENSITY	AREA
Pb 208	1.43 ±18%*	1.00 ±16%*
Pt 190	1.40 ±10%	.91 ± 5.9%
Ag 107	1.74 ±24%	1.00 ±18%
Pd 106	1.85 ±14%	.99 ±13%
Zr 90	2.17 ±19%	1.10 ±21%
Cu 63	1.88 ±14%	1.08 ±13%
Fe 56	1.66 ±17%	1.07 ±10%
Al 27	1.64 ± 9.6%	1.16 ± 8.7%
Mg 26	1.46 ±13%	1.11 ±11%

*%Standard Deviation

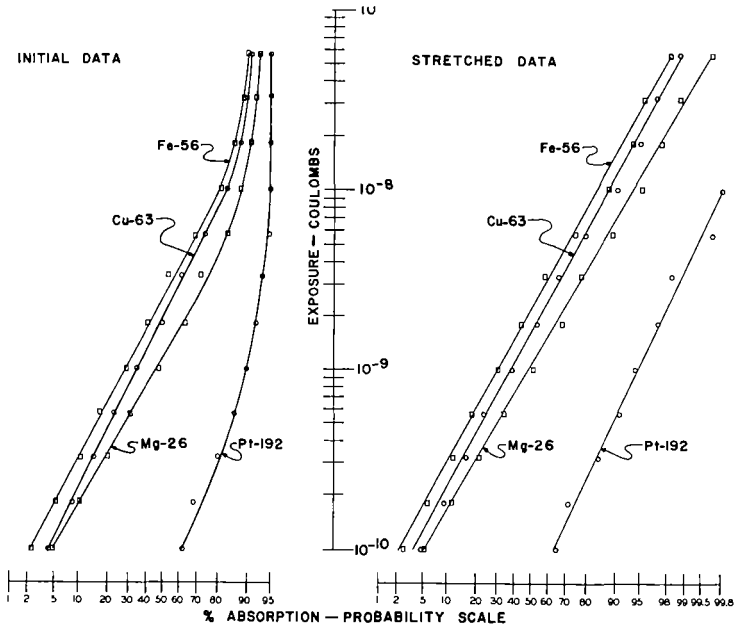

Figure 3. Photographic plate response curve, log. of exposure vs percent abs. on the probability scale.

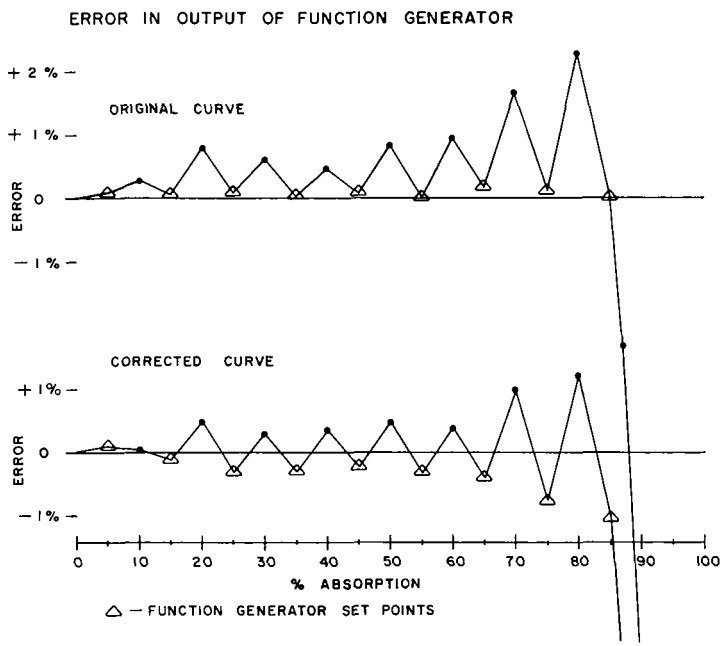

Figure 4. Error in the output of the function generator vs the percent abs. input.

REFERENCES

1. E. B. Owens, N. A. Giardino
   Anal. Chem. 35, 1172 (1963)

2. G. C. Cookson, W. Fletcher, R. Tushingham
   "The Importance of Variations in Line-Width and Emulsion Sensitivity in Spark Source Mass Spectrography"
   Mass Spectrometry Conference, St. Louis, Missouri, May 1965

3. A. J. Socha, R. K. Willardson
   "Analytical Techniques"
   Mass Spectrometry Conference, San Francisco, Calif., May 1963

4. C. M. Judson, C. W. Hull
   "Precision, Accuracy, and Sensitivity in Spark Mass Spectrometry"
   Mass Spectrometry Conference, San Francisco, Calif., May 1963

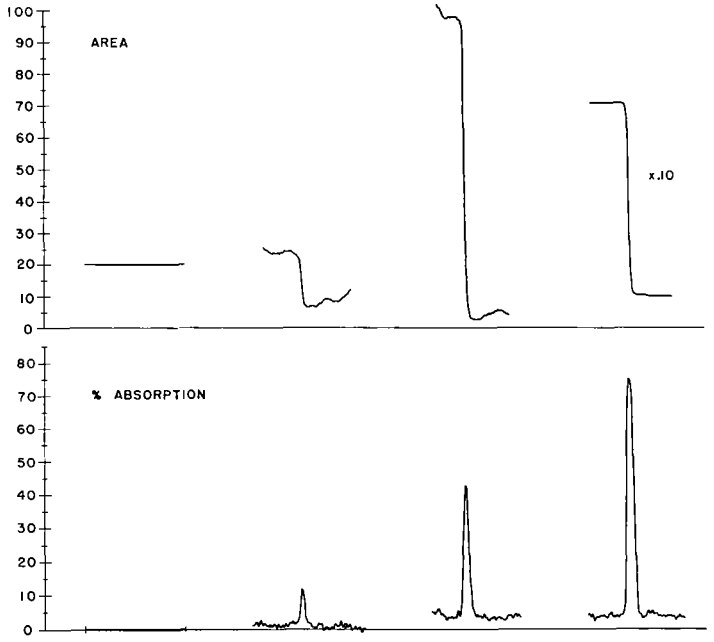

Figure 5. Percent abs. peaks and their corresponding area integrals from a typical plate.

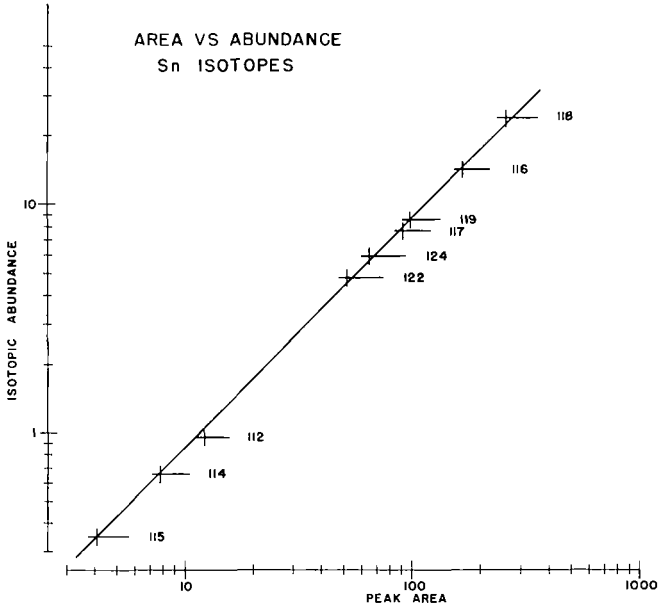

Figure 6. Area measured for the isotopes of tin vs their isotopic abundance.

Computer Techniques for Fast Scanning High Resolution Mass Spectrometers

W.J. McMurray and S.R. Lipsky
Yale University School of Medicine
New Haven, Connecticut 06510

Introduction:

Two years ago at the Montreal meeting Desiderio and Biemann (1) discussed the computer techniques for the fast and facile conversion of the line positions recorded on a photographic plate to exact masses and elemental compositions. In the ensuing period considerable interest was evolved over the possibility of recording high resolution mass spectra on magnetic tape, particularly for the case in which the entire spectrum is recorded by magnetically scanning a decade in mass in ten seconds. Papers presented here (2,3,4) and in the journals (5) indicated the feasibility of this approach to recording mass spectra and also indicated (6) the advantages of magnetic tape as a recording medium.

Instrumentation:

The mass spectra were generated by a modified Associated Electrical Industries MS-9 mass spectrometer. The spectra were recorded in analog form in FM mode on an Ampex FR1300 tape recorder. The recording speed was sixty inches per second when scanning a decade in mass in ten seconds at a resolution of ten thousand. The output of the tape recorder is processed by an IBM 1912 A/D converter capable of speeds up to 1.5 Kc per channel and with a resolution of ten bits. The slowness of the digitizer necessitated a speed reduction by a factor of thirty-two to obtain the required rate of digitization. The effective rate of digitization was 48 Kc (7).

The digital data was processed by a series of programs written in the FORTRAN 1V language on the IBM 7040-7094 direct couple system at the Yale Computer Center.

Results:

The output from the A/D converter is a digital mass spectrum i.e., it contains not only the digital values corresponding to the peak profiles but also the digital values corresponding to the baseline. The program must be capable of performing the following steps. First, it must extract the digital values corresponding to the peak profiles. Second, if necessary, it must amplify the digital values for any attenuation introduced during the recording. Third, it should contain the necessary logic to recognize a peak as a peak. Fourth, a time which is representative of the peak must be calculated, and fifth, the time must be converted to an accurate mass from which the correct elemental composition may be determined.

The digital data is read in and the average baseline for the first thousand readings is calculated and to it is added an empirical value to produce the threshold value. Any digital value which exceeds this threshold is extracted and then amplified mathematically to correct for the linear-log attenuation scheme employed in the recording. Peak recognition is based on the number of consecutive digital points which exceed the threshold and the number of consecutive digital values below the threshold between values which exceed the threshold. On the basis of these criteria, the computer identifies each peak and calculates the mean time as that time value representative of the peak.

The computer now contains in storage the mean times corresponding to all the peaks in the spectrum. The peaks represent the fragments from the sample as well as the reference compound which is introduced simultaneously with the sample.

The problem now is to locate the necessary reference masses to convert the mean times to masses. An extrapolation technique similiar to that reported (1)

but employing a different mathematical relationship is used. As input for this routine, the program requires the approximate time of three standard masses to be designated. The list of mean times in storage is searched for those times which fit within the required error range the input times. Having located these, the remainder of the mean times corresponding to the reference masses are located. A summary of such an output is shown in Table 1. The DIFF column in this table represents the error in microseconds between the predicted time of the standard mass and where it actually was located in time. The peak width in a scan of a decade in mass in ten seconds at a resolution of ten thousand is approximately four hundred microseconds. It can be seen that in general the location in time of the reference masses can be predicted to better than the width of a peak and usually to better than half the width of a peak. The observation that the mathematics allows us to predict the location of the standard masses was put to use. One wishes to avoid premature termination of the processing procedure. The reference masses have an intensity requirement which must be fulfilled. If this is not the case, the computer either uses a value found within the time range or substitutes the predicted value for the missing reference time. This is indicated by the asterisk which brackets that mass which is either absent or present in low abundance. It will be noted that this permits processing to continue.

It can be seen that the entries listed under Time Constant are not constant. The plot in Figure 1 shows however that they change smoothly with time. As a result, a modification to the exponential scan law incorporating the rate of change of the time constant with time is employed in the conversion of time to mass.

In Table 2, a portion of the masses obtained from a ten second scan at resolution ten thousand from the effluent of a gas chromatograph are shown. The elemental compositions are calculated which fit the mass to an error of ten parts per million or three millimass units, which ever is larger. The column reading LRELI indicates the number of digital points in the peak, the second column contains the area under the peak and therefore a measure of the intensity of the peak. The third column contains the time in seconds from the start of the scan and column four the error in millimass units between the mass calculated from the scan and the mass calculated for the elemental compositions shown to the right of this entry.

The versatility of the programs are shown by the fact that they are independent of scan time. This is illustrated by extrapolation summary in Table 3 for a scan of seventy-two seconds per decade in mass at a resolution of better than sixteen thousand. The plot in Figure 2 shows a similiar smooth curve for the variation of time constant with time (mass). In Table 4 is shown a small portion of the masses and elemental compositions for the alkaloid tazettine obtained employing the same scan law for the conversion of time to mass. In Table 5 is shown a portion of the element map output for the alkaloid tazettine derived from the above scan.

References

1. Desiderio, D. and Biemann, K., Twelfth Annual Conference on Mass Spectrometry and Allied Topics, Montreal, June, 1964, pp. 433.

2. Banner, A.E., Thirteenth Annual Conference on Mass Spectrometry and Allied Topics, St. Louis, May, 1965, pp. 193.

3. Campbell, A.J., and Halliday, J.S., ibid, pp. 200.

4. Green, B.N., Merren, T.O., and Murray, J.G., ibid, pp. 204.

5. Merritt, C., Jr., Issenberg, P., Bozinet, M.L., Green, B.N., Merren, T.O., Murray, J.G., Anal. Chem. 37, 1135 (1965).

6. Issenberg, P., Bazinet, M.L., Merritt, C., Jr., ibid, 37, 1073 (1965).

7. McMurray, W.J., Green, B.N., Lipsky, S.R., ibid, August (1966).

Table 1

C-16 D810

THE **TIME** IS 0 HOURS 5.15132 MINUTES.

EXTRAPOLATION SUMMARY

STANDARD MASSES		STANDARD TIMES		DIFF	TIME CONSTANT
354.97930	342.97930	4.1298350	4.2459030	0.0	3.3791122
342.97930	330.97930	4.2459030	4.3659160	0.0	3.3698026
* 330.97930	318.97930	4.3659160	4.4901654	-0.0	3.3644928
* 318.97930	304.98250	4.4901654	4.6411716	-0.0	3.3652793
304.98250	292.98250	4.6411716	4.7759563	-273.6	3.3577375
292.98250	280.98250	4.7759563	4.9162915	334.3	3.3556537
280.98250	268.98250	4.9162915	5.0625741	-228.5	3.3519609
268.98250	254.98560	5.0625741	5.2414728	87.4	3.3477015
254.98560	242.98560	5.2414728	5.4027175	-11.9	3.3449855
242.98560	230.98560	5.4027175	5.5719698	-55.4	3.3418182
230.98560	218.98560	5.5719698	5.7500553	22.8	3.3380954
218.98560	204.98880	5.7500553	5.9704692	29.6	3.3370461
204.98880	192.98880	5.9704692	6.1714914	-176.6	3.3324174
192.98880	180.98880	6.1714914	6.3853750	215.9	3.3316763
180.98880	168.98880	6.3853750	6.6139061	-249.6	3.3312264
168.98880	161.99040	6.6139061	6.7547456	-20.0	3.3299018
161.99040	149.99040	6.7547456	7.0108421	37.0	3.3274084
149.99040	142.99200	7.0108421	7.1697989	89.9	3.3266675
142.99200	130.99200	7.1697989	7.4612619	-83.7	3.3252126
130.99200	118.99200	7.4612619	7.7808557	62.6	3.3263298
* 118.99200	111.99360	7.7808557	7.9825473	-247.2	3.3274461
* 111.99360	99.99360	7.9825473	8.3597845	-0.0	3.3284984
99.99360	92.99520	8.3597845	8.6014018	7.2	3.3299757
92.99520	81.07050	8.6014018	9.0582690	-30.9	3.3292389
81.07050	69.99860	9.0582690	9.5468493	303.7	3.3272080
69.99860	61.99680	9.5468493	0.0000000	190.0	-0.0000000

STD MASS 61.99680 EXPECTED AT 0.0000000 NOT FOUND

THE **TIME** IS 0 HOURS 5.17168 MINUTES.

Table 2

C-16 D810

THE **TIME** IS 0 HOURS 5.20497 MINUTES.

REL I	INT	TIME	CORRELS	CALC	ERROR	C12/13 N Q Q	
12	1339	4.2699023	342.97927				CAL10. COMPD -0.03
13	1828	4.3659162	330.97920				CAL10. COMPD -0.03
9	380	4.5119436	316.97022				NO COMP CALC
11	675	4.6411716	304.98250				CAL10. COMPD 0.00
13	1425	4.7759563	292.98249				CAL10. COMPD -0.00
4	159	4.9196460	281.08140				NO COMP CALC
15	5153	4.9162915	280.98249				CAL10. COMPD -0.01
12	457	5.0342713	271.26048	271.25961	1.27	16/1 34 0 2	C-13 SPECIE
17	6351	5.0625741	270.25376	270.25406	1.68	17 34 0 2	
10	762	5.2427561	260.98251				CAL10. COMPD 0.01
12	564	5.2427561	260.98251				CAL10. COMPD -0.27
9	135	5.3179955	252.98213				CAL10. COMPD 0.13
10	454	5.4196728	244.98560				CAL10. COMPD -0.00
15	5071	5.4027175	242.98560				CAL10. COMPD -0.00
12	2635	5.5271944	241.21599	241.21691	-0.91	15 29 0 2	
8	272	5.5446479	240.24100	240.24100	-0.22	15/1 31 0 1	C-13 SPECIE
15	4875	5.5546891	239.23720	239.23765	-0.46	16 31 0 1	
4	226	5.5603877	235.98813				CAL10. COMPD 0.93
10	8083	5.5719698	228.98561				CAL10. COMPD 0.01
4	140	5.5970236	229.26031				NO COMP CALC
10	1700	5.6124389	228.20394	228.20460	-0.66	13/1 27 0 2	C-13 SPECIE
18	13454	5.6471703	227.19874	227.20129	-2.46	14 27 0 2	
9	124	5.6597042	226.99546				CAL10. COMPD 4.84
17	6223	5.7500553	218.98559				CAL10. COMPD -0.01
15	5672	5.8196460	213.18603	213.18559	-1.54	13 25 0 2	
5	184	5.9426897	212.98020				CAL10. COMPD -4.11
7	634	5.9596514	211.98459				CAL10. COMPD -5.11

Table 3

TA/ETIME

THE **TIME** IS 0 HOURS 0.52722 MINUTES.

EXTRAPOLATION SUMMARY

STANDARD MASSES		STANDARD TIMES		DIFF	TIME CONSTANT
604.96330	597.96330	16.7080484	19.1932970	0.0	34.2072648
597.96330	590.96330	19.1932970	20.0878330	0.0	33.9467500
590.96330	584.96330	20.0878330	20.9096611	-0.0	33.7324927
584.96330	576.96330	20.9096611	21.8267769	-947.7	33.5069553
576.96330	567.96330	21.8267769	22.3590737	185.5	33.5197002
567.96330	559.96330	22.3590737	23.0599514	-808.3	33.3499148
559.96330	550.96330	23.0599514	23.9770155	-199.8	32.9820147
550.96330	543.96330	23.9770155	24.7469909	-76.1	32.8144737
543.96330	542.96330	24.7469909	25.5334742	16.5	32.6715337
542.96330	540.96330	25.5334742	26.3555160	-401.5	32.5464113
540.96330	536.97290	26.3555160	27.2427928	-1.0	32.4130234
536.97290	535.97290	27.2427928	28.1134684	247.0	32.2937344
535.97290	532.97290	28.1134684	28.9935539	-150.5	32.1744844
532.97290	530.97290	28.9935539	29.8734154	-154.4	32.0532874
530.97290	525.97610	29.8734154	30.9500592	-344.5	31.9740179
525.97610	524.97610	30.9500592	31.6404451	-194.4	31.8464442
524.97610	522.97610	31.6404451	32.8170276	-149.8	31.7491910
522.97610	520.97610	32.8170276	33.6001468	-912.8	31.7257157
520.97610	518.97610	33.6001468	34.8170847	549.9	31.6168055
518.97610	516.97610	34.8170847	35.6118254	-293.2	31.5454215
516.97610	512.97610	35.6118254	37.1131254	-194.7	31.4421149
512.97610	510.97610	37.1131254	38.4197281	795.4	31.3807451
510.97610	506.97610	38.4197281	39.5611102	-1126.2	31.3119434
506.97610	504.97610	39.5611102	40.7767425	239.8	31.2163667
504.97610	502.97610	40.7767425	41.8149248	45.2	31.1587885
502.97610	500.97610	41.8149248	42.1821847	14.1	31.1017170
500.97610	498.97610	42.1821847	43.8947215	-484.4	31.0134572
498.97610	496.97610	43.8947215	44.5464147	158.9	30.9435645
496.97610	492.97610	44.5464147	45.8176491	-1.0	30.8127927
492.97610	490.97610	45.8176491	46.4147745	134.1	30.7454504
490.97610	488.97610	46.4147745	47.5126748	-1258.1	30.6755572
488.97610	484.98020	47.5126748	50.8745533	710.4	30.5634147
484.98020	482.98020	50.8745533	51.9333330	-718.2	30.4100711
482.98020	480.98020	51.9333330	52.4052752	-839.0	30.3442363
480.98020	478.98020	52.4052752	53.0133120	1336.7	30.2710003
478.98020	474.98020	53.0133120	60.4540740	-1260.0	30.1597117
474.98020	472.98020	60.4540740	62.2969066	-558.5	30.0336115
472.98020	470.98020	62.2969066	64.1024843	-10.0	29.9217653
470.98020	466.98020	64.1024843	66.7741491	-4.1	30.7844934
466.98020	464.98020	66.7741491	69.7824235	2434.4	30.6411274
* 464.98020	461.98020	69.7824235	71.9445204	692.1	30.5115453
* 461.98020	458.98020	71.9445204	74.4031165	-0.0	30.3740845
* 458.98020	452.98020	74.4031165	77.1962183	2549.1	30.2417242
* 452.98020	450.98020	77.1962183	81.3752652	-7316.6	30.1075972
* 450.98020	448.98020	81.3752652	85.9842315	-0.0	30.0365149
448.98020	442.98020	85.9842315	88.0000000	2413.8	-0.0000000

STD MASS 441.98020 EXPECTED AT 0.0000000 NOT FOUND

THE **TIME** IS 0 HOURS 1.98326 MINUTES.

Table 4

6	153	44.5650315	270.11124	270.11311	-1.87	16	16	1	3	
4	274	44.5676007	270.08886	270.08930	-0.44	16	14	0	4	
25	3015	44.6948819	268.98251							CALIB. COMPO 0.01
13	743	44.9259524	266.98550							CALIB. COMPO -0.10
4	314	45.3931612	262.49172							CALIB. COMPO -0.28
10	264	45.6197867	261.07449	261.07455	-0.07	16/1	10	1	2	C-13 SPECIE
				261.07191	2.58	13/1	12	0	5	C-13 SPECIE
5	209	45.7366052	260.09175	260.09237	-0.62	14	14	1	4	
20	1525	45.7493794	260.06845	260.07121	-2.76	17	10	1	2	
				260.06856	-0.11	14	12	0	5	
10	[illegible]	45.9761[illegible]	258.08805	258.08747	0.58	17/1	11	1	1	C-13 SPECIE
16	689	46.2969601	257.08242	257.08412	-1.70	18	11	1	1	
				257.08147	0.95	15	13	0	[illegible]	
3	65	46.2157493	256.09600	256.09745	0.55	15	14	1		
6	176	46.2166735	256.07215	256.07364	-1.49	15	12	0	[illegible]	
15	543	46.3386351	255.08821	255.08962	-1.41	15	13	1	3	
14	686	46.4408170	255.06528	255.06581	-0.53	15	11	0	4	
17	1113	46.3504682	254.98564							CALIB. COMPO -0.00

Table 5

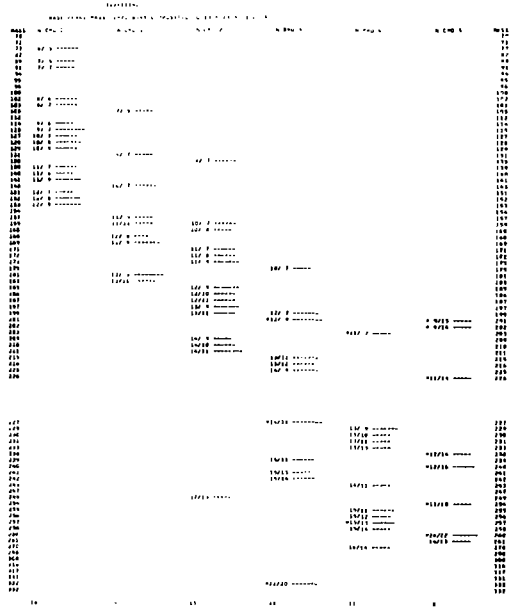

Fig. 1

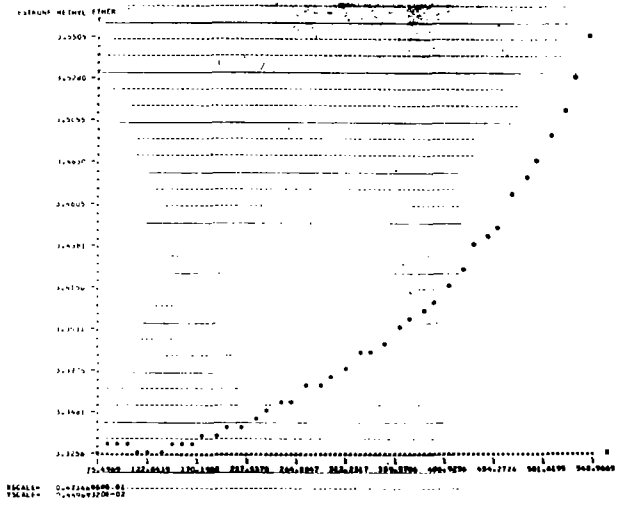

Fig. 2

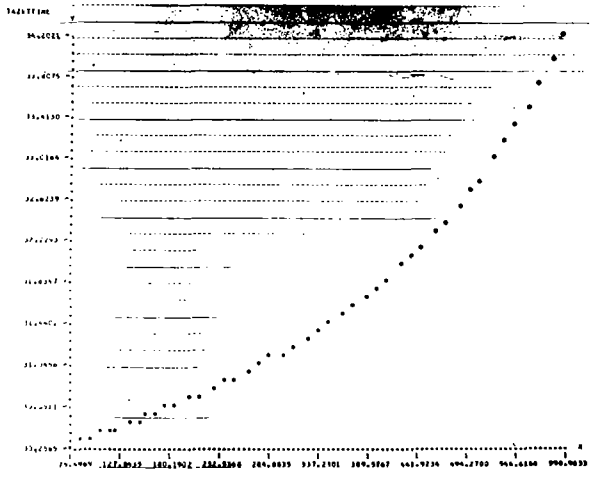

SCINTILLATION DETECTION COINCIDENCE SYSTEM

by

W. E. Duffy and C. P. Ruiz

General Electric Company
Nuclear Technology Department
Vallecitos Atomic Laboratory
Pleasanton, California

A detection system, similar to that reported by Daly[1] has been constructed. In spite of the relatively good resolution, i.e. separation between signal and noise,[2] the phototube dark current does hav e a pulse-height distribution which extends beneath that of the signal (Figure 1). This count rate is usually low but becomes significant as the signal count rate decreases and thus is one of the factors which limits abundance sensitivity. An effort has been made to reduce this background by employing two phototubes operated in coincidence to detect the scintillations arising from the interactions of the electrons with the phosphor.

The detector system, shown schematically in Figure 2, illustrates the 2 photomultiplier tubes optically coupled to the scintillator. At the present time 56 AVP tubes which have 14 stages, and a pulse rise time of 3 nsec and pulse half-width of 5 nsec are used. Magnetic shielding is provided by an annealed Armco iron block which also provides mechanical support for the tubes. The optical coupling is provided by a clear silicone potting compound (RTV-602)[3] which is poured into the internally reflective iron assembly, with the phototube and scintillator in place, and sets to a gelatin-like consistency.

To minimize the background from any stray radiation, a small circular scintillator (NE 102)[4] 0.020 in. thick by 3/8 in. diameter is cemented onto a lucite disc 1/4 in. thick by 1-1/4 in. diameter which provides the vacuum seal. The scintillator and lucite disc are flashed with aluminum to provide a conducting film for an electrical ground, as well as a reflector for the light.

In the present system, the positive ions at 10 keV enter the detector system and are accelerated to the aluminum electrode operated at a negative potential of 45 keV. The focussing of the emitted secondary electrons onto the scintillator is achieved by movement of the electrode, mounted on bellows, to optimize the pulse-height distribution and center the image by visual observation. A comparison with the monoenergetic conversion electrons from the decay of Cd-109 indicates that on the average 7 secondary electrons are emitted from the surface with U^+ ions. The electrons, detected by the scintillator, are counted with both phototubes operated with a gain of about 10^6, at approximately 1500 Volts.

The pulses from each of these tubes are amplified by a gain of 10 (Figure 3). This combined with the initial gain achieved from the conversion and detection of the 45 keV electron results in a total gain of 10^9 for the system.

The pulses from each of these amplifiers, which are really part of the Chronetics coincidence system, are fed into separate discriminators operated at a minimum threshold of 100 mV. The shaped 7 nsec wide output pulses from each of these are then fed into the coincidence circuit which is operated at a resolving time (2τ) of 9 nsec. The output pulses from this are routed to a series of 100 mc scalers.[5]

A typical singles and coincidence spectrum obtained from a single tube with a 400-channel pulse-height analyzer is shown in Figure 1. The maximum of the distribution corresponds to about 0.1 Volts from the photomultiplier tube. The portion of the coincidence spectrum shown, which is also that accepted by the coincidence system, is in excess of 95% of all events. This high counting efficiency minimizes mass discrimination effects. The background count rate under these conditions is in the range 5-15 counts per minute compared to 50-200 counts per minute in the singles mode. This system is capable of fast counting operation with dead time losses consistent with the pulse shaping of the discriminator and coincidence systems, i.e., at 50 mc operation a counting loss of $\approx 2\%$ is observed for a count rate of 10^6 counts per second.

An effort is continuing to reduce the residual background count in the system, which is from two sources: discharge from the high voltage electrode and coincidence noise between the phototubes themselves. The electrode noise count rate is dependent on the voltage on the electrode, its surface, and the pressure in the system.

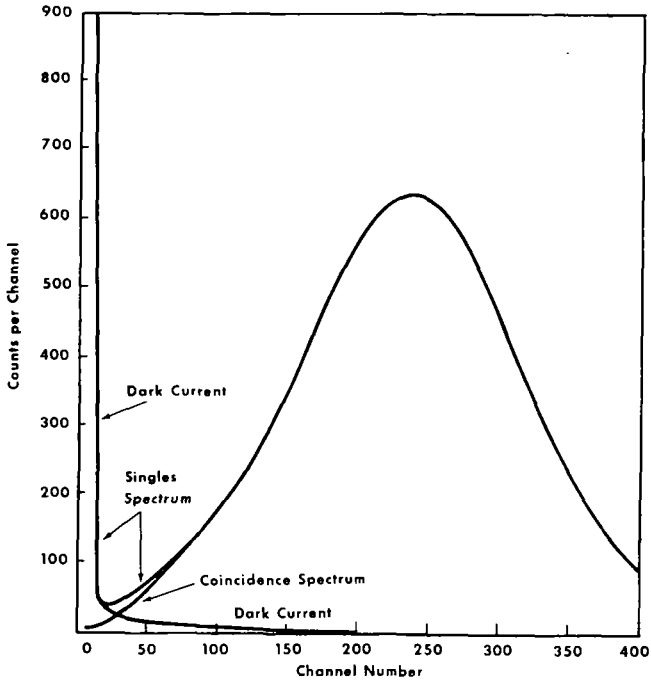

FIGURE 1. TYPICAL PULSE-HEIGHT DISTRIBUTION FROM A SINGLE PHOTOMULTIPLIER TUBE.

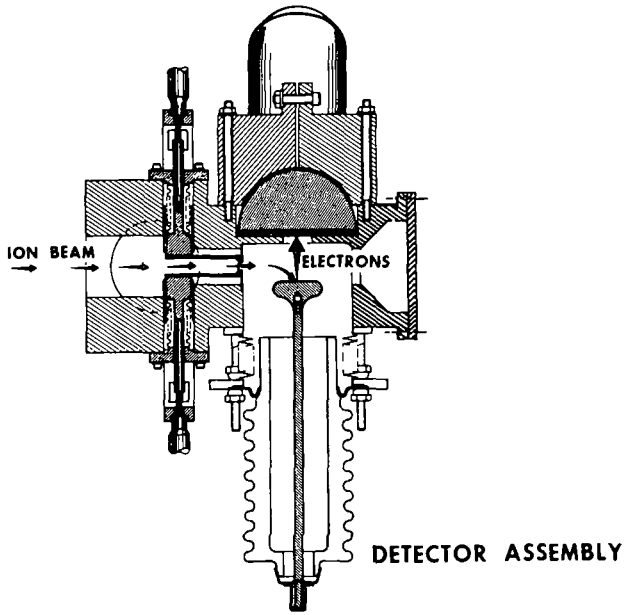

FIGURE 2. SCHEMATIC OF DETECTOR ASSEMBLY

The coincidence tube noise count rate is also a function of the high voltage on the tubes. The source of this coincidence noise appears to be a discharge within one tube which is detected optically by the other tube. In addition to this there is some noise transmitted electrically through the system. It has been found that this latter coincidence noise has a distribution in time which extends beyond the signal resolving time. Some additional reduction has been accomplished by routing all pulses through a 10 nsec delay to the anti-coincidence mode (Figure 3). This has the effect of rejecting all pulses which occur earlier than the true coincidence pulses by 2-7 nsec. Any line noise can also be filtered from the system by operating a third tube in the anti-coincidence mode. Finally, some additional reduction in noise is possible by splitting the pulses from the photomultiplier tubes and routing to each of 2 amplifiers. The pulses from one amplifier from each tube (set) are routed through the circuit shown (Figure 3). The pulses from the other set of amplifiers are summed and passed through a third discriminator in which the threshold is raised to selectively discriminate against low energy pulses. The output pulses from the discriminator are then fed to the coincidence unit which then imposes a third requirement on the system for a countable output pulse. This latter option is especially useful in cases of poor resolution.

Acknowledgement

The untiring efforts of E. W. Skoog in the development of the electronic system are gratefully acknowledged.

References

1. N. R. Daly, Rev. Sci. Instr. 31 264 (1960).

2. W. A. P. Young, R. G. Ridley and N. R. Daly, ASTM, E-14 (1965).

3. Manufactured by General Electric Company.

4. Manufactured by Nuclear Enterprises, Ltd., Winnipeg, Canada.

5. This meeting, paper 68.

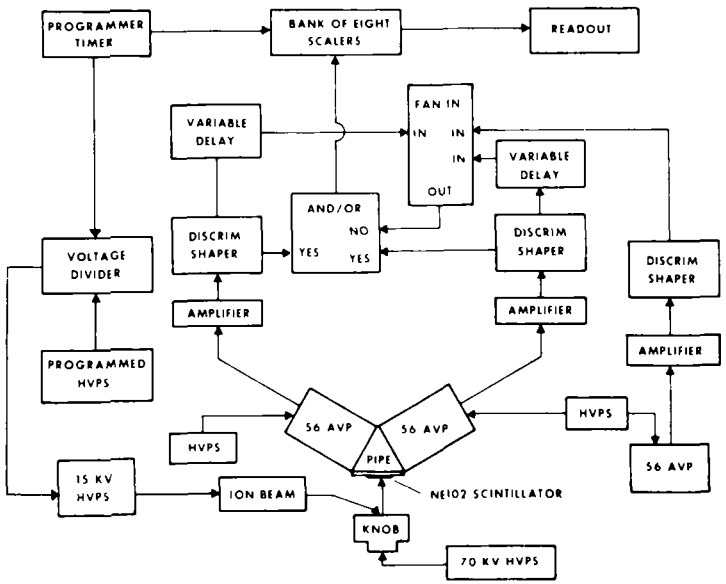

FIGURE 3. SCINTILLATION DETECTION COINCIDENCE/ANTI-COINCIDENCE PULSE COUNTING SYSTEM.

A FLEXIBLE DIGITAL DATA SYSTEM FOR SECTOR FIELD INSTRUMENTS

G. H. Riley and D. L. Bacon

Geosciences Division,
Graduate Research Center of the Southwest, Dallas, Texas

INTRODUCTION

Mass spectrometric techniques have been applied to problems of geochemistry with great success in the past. Isotopic abundance variations due to natural fractionation processes or decay of radioactive nuclides have been measured with sufficient accuracy to enable a number of definitive interpretations of particular geologic problems to be made. A better understanding of the evolution of the earth may be possible with improvements in precision and/or sensitivity in isotopic abundance studies. This paper describes a measuring system capable of determining the intensity ratio of two ion beams very precisely or determining isotopic abundances when ion beams of very low intensity must be tolerated.

GENERAL INSTRUMENT

A generalized schematic of the instrumental layout is shown in Figure 1. The spectrometer is a commercially available 12" radius, 68° deflection analyzer with a 60° magnet. A non-commercial filament supply of very high short term stability is used to generate ions in a triple filament, thermal ionization source. The high voltage supply is a solid state commercial unit modified by us to allow remote and rapid programming over a narrow but variable range. The double collector system was fabricated in our workshop.

In the analytic mode shown in Figure 1, two ion beams are collected simultaneously (under conditions of constant magnetic field and accelerating potential) and amplified with two vibrating reed electrometers connected in a "master-slave" configuration. The electrometer outputs are each converted to a frequency with converters whose maximum output is one megahertz corresponding to full scale deflection of the electrometer on any scale. The two pulse trains are counted simultaneously for a preset period and the data read into appropriate memory locations.

The other principle mode of operation allows ion pulse counting. This is accomplished by opening the rear of one Faraday cup in the collector with a linear travel magnetic feed-through in the vacuum housing. A high gain electron multiplier behind the Faraday cup provides pulses which are amplified, discriminated, and shaped before being counted.

Figure 2 shows a section of the dual collector system. This particular configuation was designed for collection of two calcium beams--either the 40-42 pair or the 42-44 pair. The two Faraday cups are placed at the focal points corresponding to mass 40 and 42. One collector is fixed; the other is transversly adjustable in the plane of the optic axis, in a direction normal to the median ion beam vector. Micrometer adjustment by bellows operation through the vacuum housing allows precise centering of two ion beams in the two collectors simultaneously. Correct position is initially monitored

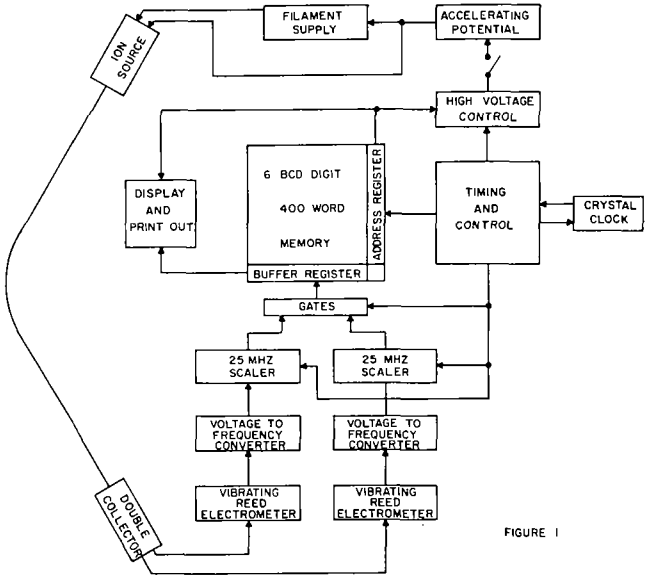

FIGURE 1

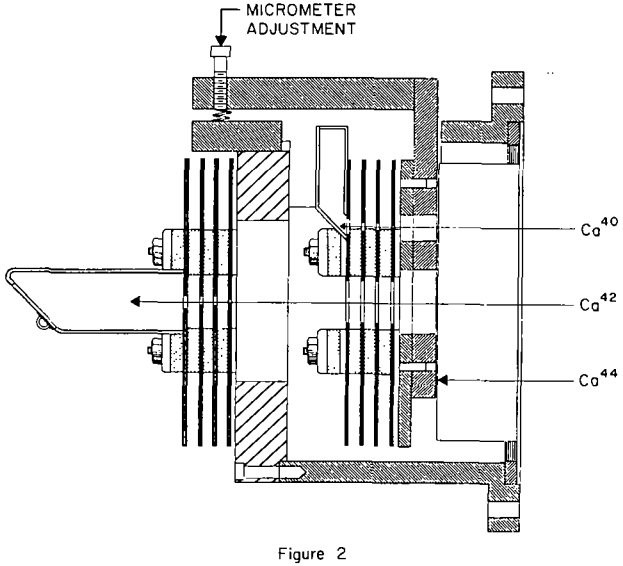

Figure 2

by drawing the two peaks simultaneously on a dual pen chart recorder. The dual spectrum is also examined to compare the beam image shape at each collector's defining slit. The longitudinal spacing of the collectors in this system was such that two calcium beams could be refocussed at their respective collector slit with an image width of .007 inches. The measurement of the ratio, Ca^{40}/Ca^{42} in natural calcium has a standard error of .025% using this collector. At the present time, Ca^{42}/Ca^{44} data are distorted by reflected ions from the high intensity, off-axial Ca^{40} beam.

BASIC DIGITAL EQUIPMENT

The digital system was developed from a commercially supplied pulse height analyzer which was purchased without an analog to digital converter. The memory assembly is a random access 1-2-4-8 BCD parallel logic, ferrite core memory. Its capacity is 400 words of 24 bits (6 BCD decades) per word. The memory cycle time is 13 usec. A core location is determined by the address register which consists of an address scaler with a scale of 100 and a two binary stage register. Address transfer gates allow parallel transfer of any address into the address register. The address register may be changed by parallel entry at the rate of 25,000 entries per second or advanced serially at about 200 KHz.

The data registers, each consisting of six 1-2-4-8 BCD decades, are zero carry-time scalers. They may be advanced serially by pulsing an advance line or loaded in parallel by the memory sense amplifiers. The serial input of each decade has its own enable line and the whole register or individual decades may be reset. The data output is either register parallel or decade serial.

All basic memory functions are controlled by a fixed program cycle. This memory programmer consists of a three stage binary scaler and an octal decoder. The memory cycle is initiated by advancing the scaler from its zero state, scanning sequentially through seven positions until it reaches zero and then stops.

Operational control is accomplished by a 32 position data transfer programmer. This consists of a five stage binary scaler and decimal decoder which is serially advanced at a 20 KC rate. The zero state of the scaler is again designated as the home position.

LOGIC OPERATION

A front panel switch allows any of six fixed programs to be selected for data acquisition. They are:

(I).	Static	-	constant ion acceleration potential
(II).	Swept	-	400 increment monotonic accelerating potential ramp controlled by the memory address
(III).	Stepped	-	up to four sequentially selected, adjustable accelerating potentials.

Single or simultaneous dual collection programs may be used with anyone of these three modes. No digital control is exercised over the magnetic field. The sequence of operations necessary to achieve the more useful programs will be described below with reference to Figure 3.

Dual Collection

When a push button accumulate signal is given, the address register is cleared, data registers disabled and the master clock enabled. A clock pulse is immediately generated and both data registers are enabled simultaneously until the next clock pulse. On this second pulse, the data transfer programmer cycle is initiated by enabling an internal 20 KHz time base generator to scan the program scaler. When the data transfer programmer leaves its home position "0", the master clock is reset and the data registers disabled. In the subsequent 32 steps, the following operations occur:

1. The information in data register #1 is written into a memory location in the first half of core.
2. Date register #1 is reset and the memory address advance 200.
3-14. Information from data register #2 is transferred decade by decade to data register #1 via a commutator.
15. Information in data register #1 is written into the memory location in the second half of core.
16. Both data registers are reset; the memory address is advanced 1.
17. Information in the new memory location is read into date register #1.
18-29. Information from data register #1 is transferred decade by decade to data register #2 via the commutator.
30. Date register #1 is reset; the memory address is decremented 200.
31. Information in the new memory location is read into data register #1.
0. Data transfer programmer stops; the master clock is enabled and immediately generates an output pulse initiating a new data collection cycle.

It should be noted that precise timing is necessary only during the period when the data registers are enabled. The crystal clock has a short term stability of better than 1 in 10^6. The count period it defines may be varied in 45 steps from 100 μsecs. to 9 secs; this period is independent of the transfer programmer's own time base (fixed at 20 KHz).

The logic allows new data to be added to data already in core. In practice, sufficient data are obtained by repeating the above cycle 199 times, so that the memory can be clear at the commencement of accumulation and memory overlay is not necessary. After 199 double collection points have been stored, the system reverts to a display mode, generating an analog representation of the memory contents on an oscilloscope. Each memory half contains data representing the time-intensity curve of a single isotope; the display enables a rapid visual assessment to be made of the quality of the data e.g. unacceptable ion beam decay, transients, etc.

The data may be read out of core by any convenient means such as a printer, magnetic tape or punched paper tape.

Single Collection

A) Swept, accumulate.

Conventionally, where single collection techniques are used in the measurement of high intensity ion beams, the magnetic field is stepped from peak-to-peak. The step magnitude is empirically adjusted by visually monitoring the large analog signal generated by an electrometer. When pulse counting low intensity ion beams however, the statistical fluctuations of ion arrivals at the multiplier do not allow an easily monitored output to be developed. Therefore,

some other scheme must be devised to ascertain that the beam is centrally located in the collector. The technique described here relates mass number to known and accessible memory locations in the following manner:

The memory is cleared and a push button accumulate signal given. This clears the address register, disables the data register and enables the master clock. A clock pulse is immediately generated enabling the data register and allowing ion counts to be accumulated for exactly one clock period. The clock pulse defining the completion of this count period initiates the internal time base of the memory programmer scaler which advances eight steps at a 300 KHz rate. When this scaler advances from its home position, the data register is disabled.

The subsequent seven steps of the memory programmer accomplish the following operations:

A memory location is cleared.

The contents of the data register are written into this address.

The address scaler is incremented 1. This also advances the digital-to-analog converter 1 and thus the accelerating potential is increased one step.

The data register is cleared.

The contents of the new memory location are read into the data register, and, since memory-read is a destructive function, this information is immediately written back into the same address.

The memory cycle is completed when the programmer returns to its home position "0". Elapsed time is 25 μsec. The cycle continues until an address overflow is detected and a display mode generated. Continuous recycling is available via a front panel switch inhibiting the display mode. When address overflow occurs, the digital-to-analog converter and therefore the accelerating potential suffers a large negative going transient, so that a 50 msec. delay is generated to allow the high voltage supply adequate recovery time.

The operation described above creates a voltage generated mass spectrum in the memory. The number of scans sufficient to develop a recognizable spectrum depends on the intensity of the ion beam. With sufficiently stable magnetic field and accelerating voltage, it is easily seen that the mass spectrum of interest is calibrated with respect to a memory address-referenced accelerating voltage.

B) Swept, display.

The memory programmer runs continuously in the same cycle as described above with the exceptions that no new data are accepted and the address digital-to-analog converter is inhibited. Its function is merely to display the memory contents on an oscilloscope. The display repetition rate is 40,000 points or 100 frames per second. It is desired to identify from this display, the precise address (or accelerating voltage) at which any mass number may be collected.

When a beam selector push button is depressed and the address overflow flip-flop is set, a new display function is generated. In this mode, the address register and data register are cleared. The address that is set up in the corresponding digital switch is transferred to the address register. The push button also enables a 300 KHz local oscillator to increment the data register and display a vertical line of points overlaying the mass spectrum display. This vertical cursor has horizontal coordinates corresponding to the number set in the digital switch and may be moved along the mass

spectrum as long as the beam selector push button is depressed. When 1000 points on the vertical line have been displayed, the oscillator is inhibited, the data register cleared, the address register cleared and the normal memory display mode enabled. The dual cycle takes about 13 msec. and is repeated as long as the beam selector push button is depressed. It should be noted that the oscilloscope horizontal linearity, gain or position are of no significance because the location of the cursor is address determined by the manually set digital switch. Figure 4 shows a representation of a rhenium spectrum with a cursor display defining the address-mass relation of Re^{187}.

The same alignment procedure is carried out for 2,3 or 4 peaks in a mass spectrum. The peak heights are examined from the display and a clock period multiplier chosen to yield the best statistical division of available measuring time. Period multiplication refers only to the duration time of data collection for each mass and bears no relation to other local timing operations in the program.

C) Stepped, accumulate.

When it is desired to determine the relative abundance of four isotopes, the necessary accelerating voltage (for a fixed magnetic field) to focus each isotope centrally in the collector slit is determined by the procedure described above.

The memory is cleared and an accumulate signal given. This resets the address register, resets the beam programmer, clears the data register and resets the master clock. The reset beam programmer in position "O" transfers the number set in its digital switch to the digital-to-analog converter. Thus the accelerating voltage is stepped to focus the first ion beam in the collector. On enabling the clock, a pulse is immediately generated to enable the data register. The count period is a function of the basic clock period and the period multiplier selected by beam programmer position "O".

At the expiration of the count period, the memory programmer time base is enabled. In the subsequent seven steps of the memory program the following operations are performed:

The information in the data register is written into memory location 0 and the date register cleared.

The beam programmer is incremented 1.

The address register is incremented 100.

The beam programmer transfers the number set up in the next digital switch to the analog-to-digital converter which steps the accelerating potential by the appropriate amount to direct the next selected isotope into the collector.

If a higher accelerating voltage has been selected a 10 msec. clock delay is initiated. If the accelerating voltage is stepped to a lower value, a 50 msec. clock delay is initiated. These delay times allow the high voltage power supply to stabilize at its new value.

When the memory programmer completes its cycle and returns to its home position (25 μsec) and the clock delay has expired, the clock is re-enabled. An immediate clock pulse starts the next data accumulation period which is defined by the period multiplier setting at this new beam programmer position. The information accumulated in this time is written into location 100 during the subsequent memory program cycle.

This basic cycle is repeated until the four step (i.e. four isotope) beam programmer cycle is completed. Isotope #1 is then remeasured, the basic address advanced 1, and this new information written into memory location 1. Isotopes 2, 3 and 4 are sequentially

collected, measured and the data written into locations 101, 201 and 301 respectively.

The process is continued until the four isotopes have been sampled 100 times each at different but very close points in time. Note that for a typical basic count period of say, 1 second, a duty cycle of 98% is achieved.

Contribution 37
Geosciences Division
Graduate Research Center of the Southwest
Dallas, Texas

Figure 3

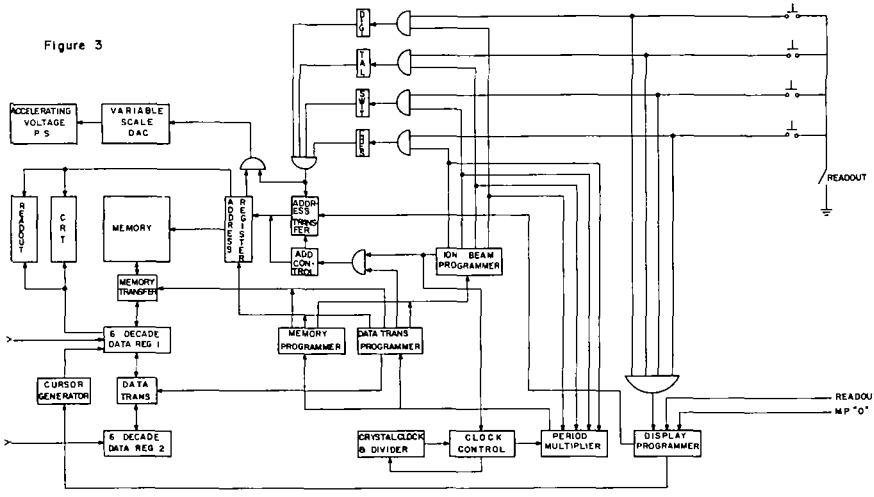

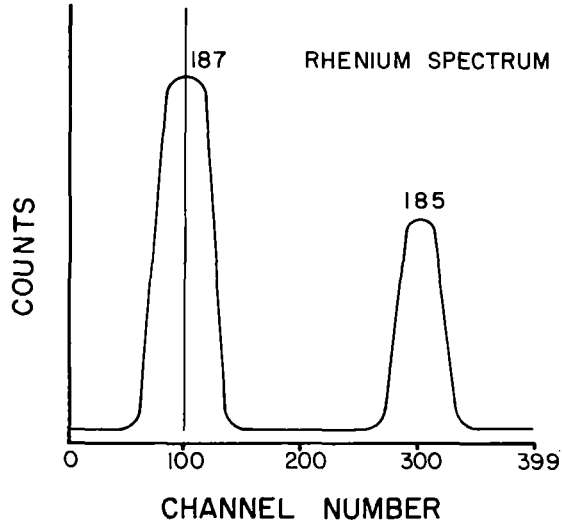

Figure 4

SEMI-AUTOMATIC DATA COLLECTION SYSTEMS FOR MASS SPECTROMETERS*

C. M. Stevens, D. B. Walling, and P. E. Moreland, Jr.

Chemistry Division, Argonne National Laboratory
Argonne, Illinois 60439

ABSTRACT

Improved data handling systems have been added to two mass spectrometers to improve the precision, speed, and efficiency of data collection and analysis. A large, high sensitivity spectrometer using pulse counting has been equipped with a programmed multiscaler to store counts for up to four masses in four sub-groups of core memory. The simpler scheme of adding a programmed integrating digital voltmeter and printer to the electrometer output of an analytical spectrometer is used where high sensitivity is not required. Both instruments use voltage switching between masses, determined simply, but precisely and directly by use of operational amplifier techniques in voltage supplies.

INTRODUCTION

The desire to reduce the time and effort required to make certain isotopic analyses of solid samples and to improve accuracy and instrument sensitivity has resulted in the development of the two data collection systems to be described. These systems are designed to record data for a limited number of isotopes of one or two elements, not for spectral abundance data over a wide mass range. The first system to be built was adapted to the Argonne 100 inch radius double focusing spectrometer[1] which had been equipped to use the ion pulse counting detection technique[2] in order to achieve very high sensitivity. In this case, signals available on the existing magnetic sweep circuit are used to trigger a solid state programmer. This unit controls the 400 channel multiscaler[3] associated with the pulse counting system and also a previously developed direct reading mass selection circuit which happens to lend itself to simple external programming. The mass peaks are recorded as stored counts in either two groups of 200 channels, or four groups of 100 channels in a manner similar to that described by McKown et al.[4]

The second system was added to a 12 inch radius single focusing instrument which employs an electron-multiplier detector and vibrating reed electrometer amplifier. The magnetic sweep of this instrument is triggered by the programmer, which also causes an integrating digital voltmeter to sample the electrometer output for a preset period three times during each sweep. The programmer also controls another direct reading mass selector circuit to sequence through preset masses, and sets amplifier attenuations for each mass. A parallel printer records the mass, attenuation setting, and digital voltmeter reading.

DIRECT READING MASS SELECTOR CIRCUIT

This circuit is used in both systems to switch the spectrometer ion source acceleration voltage from a value appropriate to a "reference" mass to values corresponding to other masses. The switching is done by mercury

*Work performed under the auspices of the U. S. Atomic Energy Commission.

contact relays controlled by the programmers. Within mass ranges determined by the circuit and magnetic field value, the reference mass can be read directly from a standard Helipot dial, and the settings for the nearby masses can also be read directly in mass units and millimass units. A range of ± 5 u from the reference mass in steps of one mass unit, with a ± 50 mu variation about these values, has been found satisfactory.

The high voltage power supplies are treated as operational amplifiers with 100% negative feedback as shown in Figure 1. It is seen that the input summing resistance of such an amplifier is inversely proportional to the output voltage and hence is proportional to mass. Figure 2 shows the form of the input resistance. The fixed resistance $(R_o + \rho + \Delta)$ and the amplifier feedback resistance are chosen to limit output voltage to the maximum available from the power supply. This resistance corresponds to the lowest mass, M_o, obtainable for a given magnetic field, while the ratio $R/(R_o + \rho + \Delta)$ determines the fractional mass range available, $(M_{max} - M_o)/M_o$. For example, if a 10-turn potentiometer is used for R and its dial interpreted as having a range of 100 mass units with a resolution better than 0.05 u, then if $(R_o + \rho + \Delta) = R$ the mass range 100–200 u is available with an appropriate magnetic field and the mass value is the dial reading plus 100. With a magnetic field $\sqrt{2}$ times larger, the mass range 200–400 u is covered by applying a factor of 2 to all dial readings. The use of a ten position switch in the ΔM circuits assures that unit mass increments can be made in the $\times 2$ dial reading mode. The programmer circuit (or a manual switch during manual control) keeps all but one of the relay contacts closed at any one time.

Calibration is achieved by setting the magnetic field to roughly the correct value of a mass range, setting the reference mass dial for a known mass peak, then tuning in this mass peak by means of the CAL. control in the amplifier feedback resistance.

The application of the mass selector circuit to an ordinary regulated H.V. (15 kV) power supply is given in Figure 3. The usual voltage divider string–difference amplifier–reference voltage control circuit is modified by grounding one side of the difference amplifier and applying the zener regulated reference voltage through the mass selector circuit, using the voltage divider string as the feedback resistor.

PROGRAMMED ION PULSE COUNTING DATA SYSTEM

This system controls the mass selector relays and multichannel scaler (M.S.) to provide sequential sweeping of up to four mass peaks. The number of sweeps/cycle can be selected for each mass over a range of 1–15. After a mass has been swept the selected number of times, the programmer advances to the next mass, setting the mass selector and the corresponding group of the multiscaler. Scanning can be automatically stopped after 1 to 15 cycles of either two or four masses each, or allowed to continue until manually stopped.

As can be seen in the block diagram of the system, Figure 4, the masses are scanned by a sawtooth magnetic field modulation and pulses derived from the flyback portion of this waveform are used to trigger the logic counting circuit and to stop and immediately restart the scan of one group of multiscaler channels. The sawtooth frequency is the basic system frequency, and its amplitude governs the apparent peak width and therefore the amount of time per sweep spent counting a mass peak.

The 16-line output of the 4-bit SWEEP COUNTER and DECODER is fed to four parallel 16 position SWEEP SELECTION switches. The correct one of these is chosen by a set of AND gates feeding an OR gate and allows the 2-bit MASS COUNTER and DECODER to be advanced after a preset number of sweeps. The decoded MASS COUNTER signal is used to drive the MASS SELECTOR circuit relays, set the previously mentioned AND gates, and cause

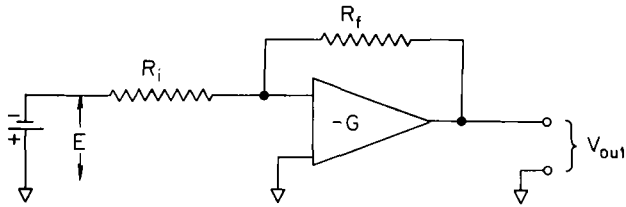

$$V_{out} = -E \frac{R_f}{R_i} \left[1 + \frac{1}{G} \left(1 + \frac{R_f}{R_i} \right) \right]^{-1}$$

$$\simeq -E \frac{R_f}{R_i} \quad , \text{ if } G \gg \frac{R_f}{R_i} .$$

$$\therefore \text{ MASS } \propto \frac{1}{V} \propto R_i .$$

FIG. 1. BASIC 100% FEEDBACK OPERATIONAL AMPLIFIER

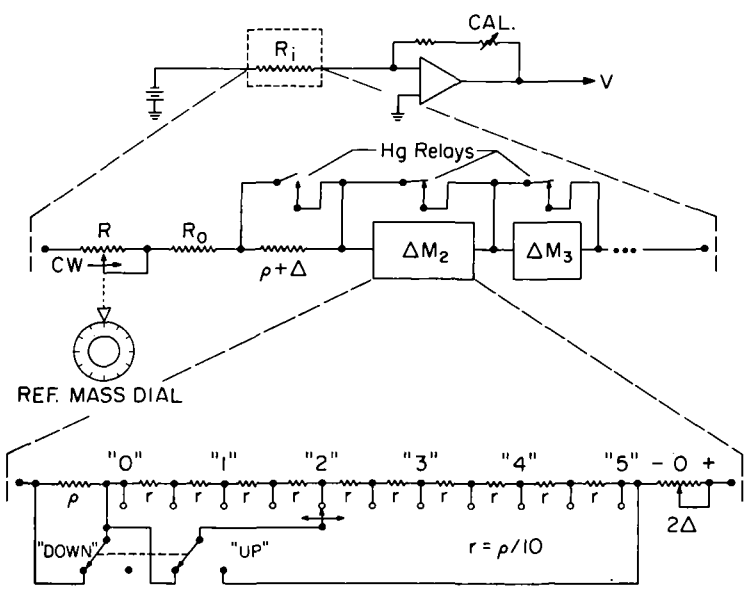

FIG. 2. DIRECT READING MASS SELECTOR

the multiscaler to shift to the group of 100 (or 200) channels corresponding to the mass being swept. After each cycle consisting of either 2 or 4 masses, a signal is fed from the MASS COUNTER to the CYCLE COUNTER and DECODER. When the decoded output of this counter reaches a selected number of complete cycles, the pulses from the sweep circuit to the multiscaler and the logic system are gated off, stopping the taking of data. This enables an accurately known number of scans of each mass to be made even at fairly rapid scan rates. Manual control of this function is also possible at the slower scan rates.

This programmed multiscaler system has been in operation for over a year. The solid state circuitry has required no maintenance during this time. Figures 5 and 6 are an example of the multiscaler CRT display, showing the results of accumulating the counts from four uranium isotopes of a NBS standard sample for less than one minute. The 235 and 238 isotopes of equal abundance were scanned once per cycle, whereas the 234 and 236 isotopes were scanned 10 times per cycle.

The relative intensity of the mass peaks is conveniently obtained by integrating the counts in each mass peak with the digital spectrum stripper[5] shown in Figure 4. The integration mode of this unit permits instantaneous summing of the counts in a preset range of channels and the typing of this value. Thus the recording of all 400 channels of memory is seldom required for well resolved peaks.

ANALOG-TO-DIGITAL DATA SYSTEM

As shown in Figure 7, the sweep of this system is divided into 16 equal intervals by the 4 bit INTERVAL COUNTER. Any three of these intervals can be selected for sampling the electrometer output with the integrating digital voltmeter (IDVM).[6] This samples the output voltage for a preset time (0.01, 0.1, 1.0 sec.) and causes a data print. After each sweep, the MASS COUNTER is advanced, which controls the MASS SELECTOR relays, the attenuation of the electrometer amplifier, and one print wheel of the parallel printer. The MASS COUNTER can be set to recycle after 2, 3, or 4 sweeps. The printed output consists of a series of three readings for each sweep, each giving the mass, attenuator setting and IDVM reading. The system continues cycling through the selected number of masses until manually stopped.

The use of an integrating digital voltmeter provides electronic averaging of the detector signal during the sample time. Two of the samples during each sweep can be taken on the flat top of a mass peak, while the third is used to measure the baseline voltage at the base of the peak. If the ion intensity variation with time is nearly linear, raw isotopic ratios corrected for this drift can be obtained very quickly by suitably summing the readings of a series of cycles using a desk calculator. More elaborate correction methods are necessary for non-linear drifts severe enough to influence ratio accuracy. This system has been in operation about one month and appears to yield isotopic ratios with a precision about an order of magnitude better than previously obtained from strip chart records, with a considerable saving in time.

REFERENCES

1. C. M. Stevens, et al., in Proceedings of the International Conference on Nuclidic Masses, H. E. Duckworth, ed., University of Toronto Press, 1960, p. 403.

2. G. W. Barton, Jr., L. E. Gibson, and L. F. Tolman, Anal. Chem. 32, 1599 (1960).

3. Radiation Counter Laboratories Model 20631.

4. H. S. McKown, A. E. Cameron, W. H. Christie, and A. S. Trundle, ASTM Comm. E-14 Thirteenth Annual Conference, paper 49.

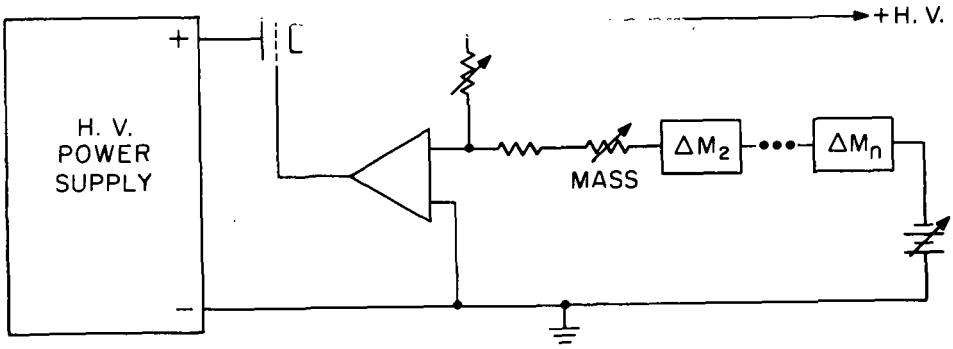

FIG. 3. ADDITION of D.R. MASS SELECTOR to H.V. SUPPLY

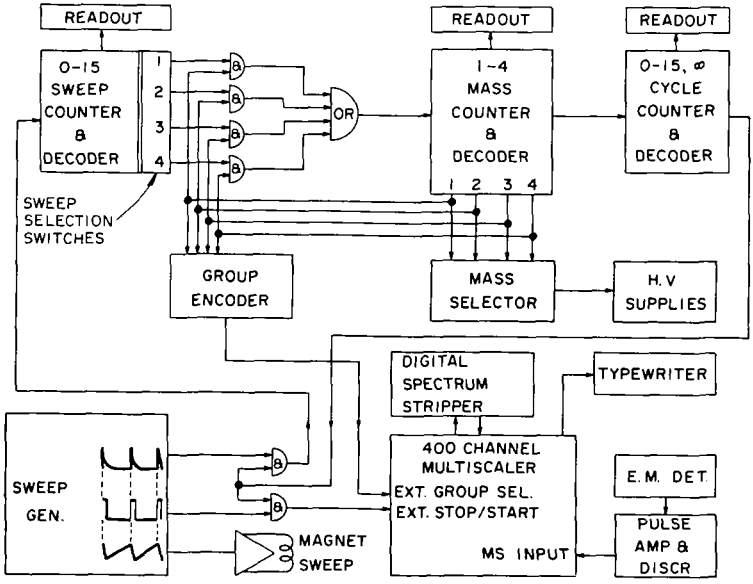

FIG. 4. PULSE COUNTING CONTROL SYSTEM LOGIC

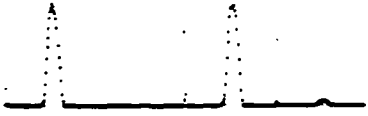

Fig. 5. Display of NBS U-500 Uranium Standard Spectrum, Masses 238, 236, 235, 234 in Four Groups of 100 Channels Each

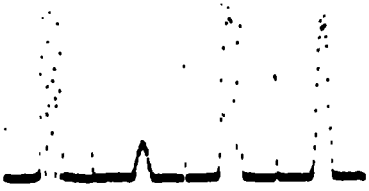

Fig. 6. Display of NBS U-500, X30 Magnification of Vertical Scale

5. Radiation Counter Laboratories Model 31047.

6. Non-Linear Systems Model 2917-S.

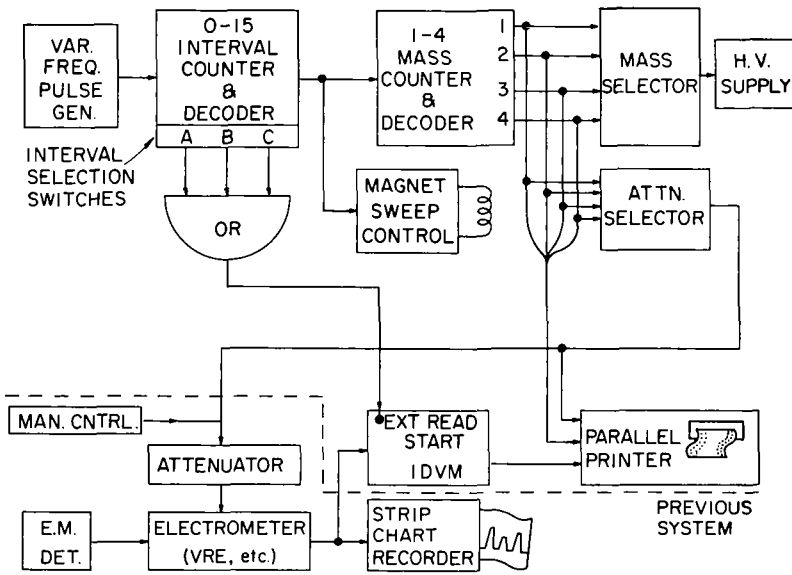

FIG. 7. ANALOG-TO-DIGITAL DATA CONTROL SYSTEM

A PROGRAMMED VOLTAGE SCANNER AND DATA COLLECTION SYSTEM FOR HIGH SPEED ION PULSE COUNTING

by

W. E. Duffy

General Electric Company
Nuclear Technology Department
Vallecitos Atomic Laboratory
Pleasanton, California

The Data Collection System described in this report was developed to meet the rather special requirements related to the isotopic analysis of heavy elements. Since such analyses are fairly common within the nuclear energy industry details of the system may be of interest.

The instrument employing this system is a thermal emission, direction focussing mass spectrometer with two successive stages of electromagnetic, ninety degree deflection on 12-inch radii. It evolved from a design first reported by F. A. White and T. L. Collins of the Knolls Atomic Power Laboratory in 1954.[1,2] The magnetic fields of the two magnets are held constant and the masses are scanned by varying the source accelerating voltage. Individual ion pulses are counted.

It is common practice when determining isotopic abundances to measure the ratio between two adjacent isotopes by sequential observance of first one and then the other until sufficient data are collected to provide the precision required. If an element contains more than two isotopes the ratios must be inter-related. This measurement requires additional time. During this time the sample is depleting itself and errors may be introduced. After all mass peaks concerned are measured an isotopic composition may be calculated.

It would be ideal if all masses of interest could be observed simultaneously; this often expressed desire has not yet been realized fully. There have, however, been many attempts, some of them quite successful, to scan across the mass peaks rapidly and collect the data rapidly, usually on magnetic or paper tape for computer processing.[3-6]

The present system being used at the Vallecitos Atomic Laboratory of General Electric Company attempts to combine high speed pulse counting capability with rapid automatic, programmed voltage scanning. This approaches nearer to the ideal of simultaneous collection of all masses, reduces analytical time and provides sufficient data for a precise and accurate determination of the isotopic composition of the element being analyzed.

A. General Description

The purpose of this system is to

1. Observe sequentially from one to eight adjacent mass positions. Each position is observed from one millisecond to ten seconds, in decade steps, depending on its intensity.

2. Enter the data for each mass into an individual scaler. Each scaler accumulates the counts for one particular position during an analysis.

3. Shift the accelerating voltage rapidly from one preselected value to the next after the completion of any individual counting period. When the voltage has been advanced through all eight steps it is returned at once to its starting value and advanced as before.

4. Be able to switch the voltage through eight mass positions from 1 to 999 times within fifteen minutes. The total switching time between two adjacent voltage settings does not exceed 100 milliseconds. This includes the OFF gating of the scaler, the switching of the voltage to the next position, and the ON gating of the next scaler.

5. Preselect the number of scans to be made (in hundreds and tens) and indicate at any time the actual number which has been made during the programmed sequence.

A schematic of this system is shown in Figure I.

B. Description of Components

1. Programmer

This device signals the scaler to start counting, counts for a selected period, and stops counting. After the counting is stopped it signals the voltage power supply to advance to the next selected value. This is done for positions 1 through 8. The order is then repeated until the analysis is complete. A manual control is available to advance through each of the 8 positions in order to select the voltage settings prior to beginning a sweep sequence. Means are provided to preselect the number of scans made (in hundreds and tens) and to indicate the number completed at any time. It is possible to stop the sequence manually but it stops only at the end of a scan. If appreciable time is required for the high voltage to stabilize after changing, an adjustable delay is available to control the start of the counting cycle. This delay may be as little as five milliseconds.

2. Variable Voltage Divider

The variable voltage divider is advanced by the programmer circuit in two to eight discrete steps. The circuit is shown in Figure II. An additional eight potentiometers and variable position switches are included to permit overlap between all positions and allow a span of two or more mass points in one step.

3. Programmed Power Supply

This 0-500 V power supply precedes the 15 kV power supply and is the unit which is stepped through the eight variable positions.

4. High Voltage Power Supply

This is a 15 kV high voltage power supply which has been designed specifically for mass spectrometer use.

5. Ion Source

This is an integral part of the mass spectrometer.

6. Ion Pulse Detector

This is a photomultiplier detector whose pulse is amplified and transmitted to the scaler bank through a 100 Mc coincidence circuit.

7. Fanout

This fanout provides 8 outputs of 300 mV peak to peak and 50 ohms impedence to the scalers.

8. Auxiliary Scaler Bank

This bank includes eight 100 Mc scalers. Each of the scalers accumulates the counts for one particular peak or position during a series of voltage steps. The scalers do not reset after each count. When the analysis is completed the counts accumulated in each scaler are recorded by hand or printed out automatically. The individual scalers are then reset manually in preparation for the next analysis.

Each of the 8 scalers has seven digit readout, 10 nanosecond pulse-pair resolution and negative polarity input.

The choice of optimum counting times for peaks and background is based upon considerations discussed in references (7) and (8).

References

1. White, F. A., and Collins, T. L., Appl. Spectroscopy 8 No. 4, 169 (1954).

2. Duffy, W. E., Proceedings Mass Spectrometry Conference, June 3-8, 1962, New Orleans, ASTM Committee E-14, pp 280-288.

3. Barton, G., Anal. Chem. 32 1599, Nov. 1960.

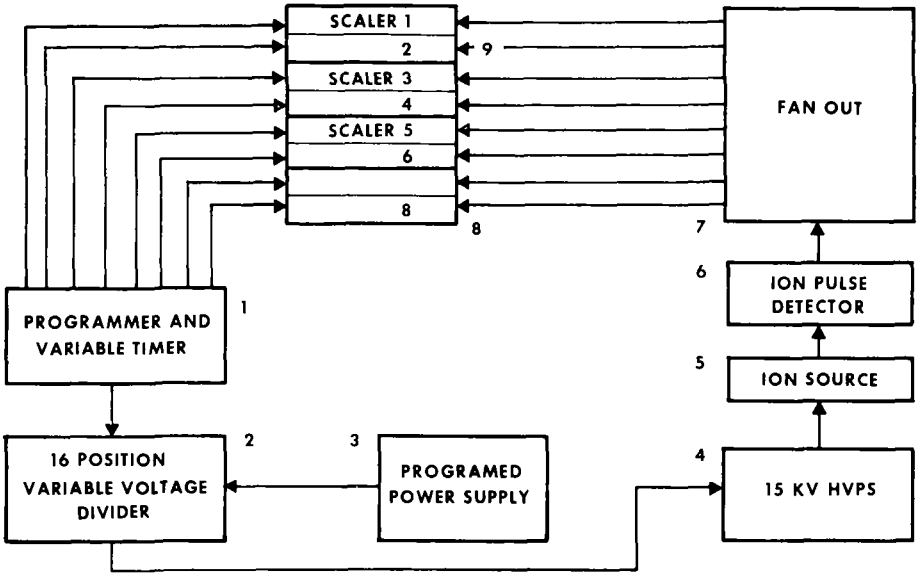

FIGURE 1.

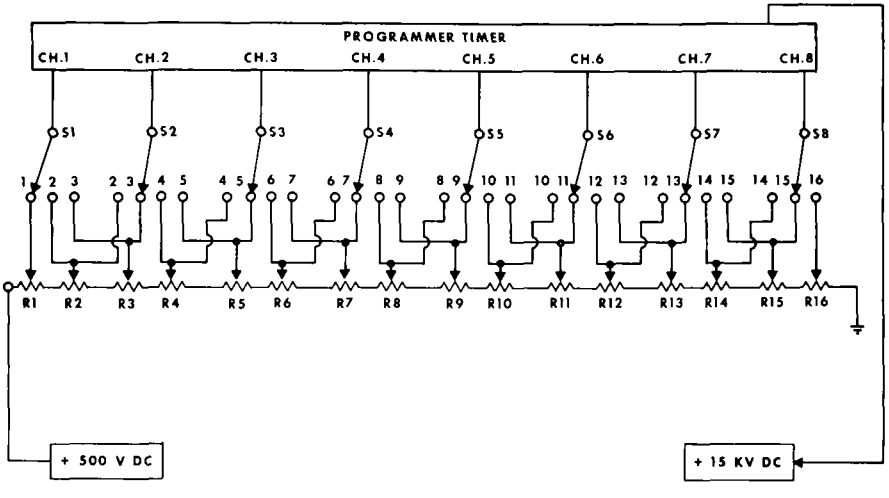

FIGURE 2.

4. Barton, G., Rev. Sci. Inst. 31 995, Sep 1960.

5. Dupzyk, R. J., et al, Proceedings Mass Spectrometry Conference, Montreal, 1965, 14th Conference, ASTM Committee E-14, pp 557-558.

6. McKown, H. S., et al, ASTM Proceedings 13th Conference E-14 Committee. 1965. pp 296-301.

7. Jaech, J. L., "Optimum Counting Times for Two Sources and Background in Mass Spectrometry," Anal. Chem. 36 1164, May 1964.

8. Jaech, J. L., "Optimum Counting Times for m Peaks and Background in Mass Spectrometry," Anal. Chem. 36 2196, Oct 1964.

Computer-Aided Interpretation of High Resolution Mass Spectra

K. Biemann and P. V. Fennessey
Department of Chemistry, Massachusetts Institute
of Technology, Cambridge, Mass.

The development (1, 2) of techniques routinely permitting the determination of complete high resolution mass spectra, i. e. the elemental composition of each ion formed has undoubtedly increased considerably both in quality and quantity, the information available by mass spectrometry. This increase in the complexity and volume of the data has, however, also increased the complexity of the necessary interpretation.

Some relief was possible merely by a more meaningful presentation of the data according to their elemental composition (rather than mass), e. g. in the form of an "element map" (1c, 3). It soon became apparent that further treatment of the data, already produced by and therefore available to the computer could be attempted, eventually leading to "automatic" interpretation of the spectra.

While this would be possible in principle, it soon became apparent that the process of interpretation of such a spectrum represents a very complex "decision tree", i. e. long series of consecutive decisions among many possibilities at each level. Such computer programs would be very complex if we would incorporate a reasonable part of what we know about the behavior of organic molecules in the mass spectrometer. While this batch-processing, i. e. the use of one single program to enable the computer to arrive at the correct answer without human intervention, is presently not possible in a generalized form, it can be used for specific compound types if their mass spectrometric behavior is well understood and rigidly defined.

An example is the determination of the amino acid sequence in small peptides of the general structure I. It is based on the fact that the spectrum of such a compound

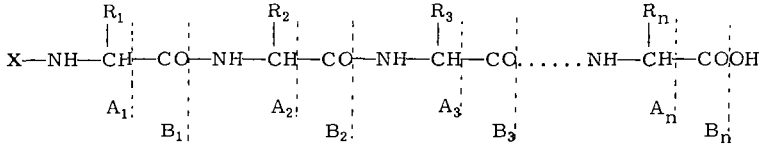

I

will exhibit ions due to cleavage of either the CH-CO bonds ($A_1 \ldots A_n$) or the CO-NH bonds ($B_1 \ldots B_n$) and on the knowledge that naturally occurring proteins contain a limited number of amino acids (thus limiting the possibilities of the nature of the substituents, R_1-R_n). The computer is asked to search for the occurrence of ions of type A ("amine fragments") and/or B ("amino acyl fragments") while varying the R-groups continuously until the value fits one of the elemental compositions (i. e. accurate masses) in the spectrum. Using a substituent X of elemental composition dissimilar to those occurring in the R-groups the N-terminal sequence is marked and can be distinguished from the various other ions arising by other, non-sequence-specific fragmentation processes.

This search for the presence of particular elemental compositions leads, in most cases, to more than one solution, particularly as one should not rely on the presence of the molecular ion (which is tested for by adding the mass of COOH, or COOR in case of esters to each amine fragment). To eliminate all but the most probable sequence, the one in which the ions of type A and B as well as the molecular ion represent the largest fraction of all ions formed is then selected. Finally, further fragmentation processes expected for each of the A and B ions on the basis of the amino acids present are checked. An actual result is illustrated in Figure 1 and more

details of the approach can be found elsewhere (4). The same basic principle was suggested simultaneously by Senn and McLafferty (5).

Once one deals with a more variable chemical system, the inability of present computers to make decisions on the basis of experience and intuition becomes a serious obstacle and limitation. It is for this reason that we have explored the possibility and potentiality of combining the computer's ability to exhaustively compare and transform with extreme speed numerical data with the human mind's capability of making intuitive decisions based on a wealth of experience. The necessary real-time interaction of a fast computer of the required large storage capacity, with the human mind is provided by so-called "time-shared" computer systems which are based on the fact that in most instances the time required for a computer to execute a set of instructions takes much less time than it takes the person to decide which instructions to issue and to do so. Thus a number of people can make use of the same computer apparently simultaneously. Usually they would work on entirely different computational problems, but it is evident that more than one of them could, in principle, be interpreting their individual mass spectra using the same master program but with different data in each case.

The operational principle of the system is very schematically depicted below.

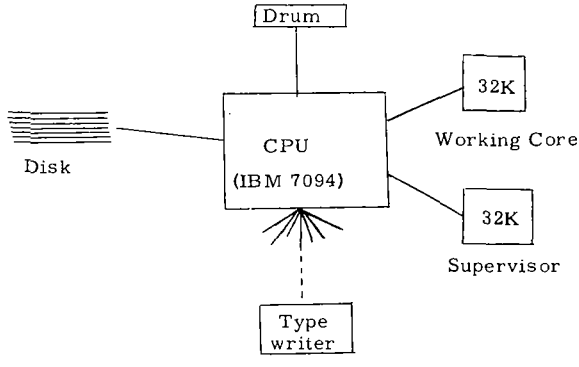

The programs and data for up to a few hundred users are stored on magnetic discs. Using one of a number of typewriter-like consoles scattered throughout the Institute and at more distant locations one can ask the central processing unit (an IBM 7094 computer) via the "supervisor program" (a core of 32K) to lead one's program and data (i. e. complete high resolution spectrum in terms of accurate masses and intensities) into the working core (also 32K) and to execute the first instruction, if the allotted time (usually a fraction of a second) permits. Otherwise, one has to wait for the next cycle, i. e. after all other programs had their fraction of a second. Under normal load this delay is not felt by the user. During that period one's program and data might not actually be in core but temporarily on a high-speed magnetic drum.

The system thus permits one to interrogate the data for information contained therein without actually ever seeing the mass spectrum itself. The questions one asks are, in principle, the same occurring in the conventional interpretation of data representing elemental compositions. The dynamic process and the question-and-answer like interaction of user and computer was illustrated using motion film (16 mm). Some of the more important steps are outlined below:

(1) In order to deduce the elements present in the compound the ions of low mass (i. e. <100) are tested for N- or O-containing ones, based on the fact that a nitrogen or oxygen containing compound will produce some small fragments retaining at least one of these atoms.

```
 SEQUENCE FOUND FOR SAMPLE 372-09-4

    CARBOBENZOXY-VAL -APG[a]-LEU -OME -

BASED ON FOLLOWING DATA

AMINE FRAGMENTS
INTENSITY[b]          666   29   49   25
ERROR[c]             -2.0  2.9  2.8  1.7
AMINO ACYL FRAGMENTS
INTENSITY[b]           66   70    3
ERROR[c]              2.2  1.0  1.4
SUM OF INTENSITIES IS-   908     TOTAL INTENSITY =  9733[d]
AVERAGE ERROR IS-  1.986

   INT       FRAGMENT LOST FROM R-VAL-
    19       VAL-H[e]

   INT       FRAGMENT LOST FROM R-VAL-APG-
     2       NH3
     2       CONH2

   INT       FRAGMENT LOST FROM R-VAL-APG-LEU-
     1       LEU-H[e]

   INT       FRAGMENT LOST FROM R-VAL-APG-CO -
    36       CONH2

   INT       FRAGMENT LOST FROM R-VAL-APG-LEU-CO -
     1       C3H6

   INT       FRAGMENT LOST FROM MOLECULAR ION
     3       H2O
     2       CBM[f]
     3       VAL-H
    27       NH3
     1       CONH2
    14       LEU-H
     3       C3H6

SUM OF INTENSITIES WITH FRAGMENTS LOST    1022
```

Figure 1

Reproduction of the result of a sequence analysis provided by the computer (explanatory footnotes added manually). (a) APG = asparaginyl; (b) in the order of A_1 through A_n, and B_1 through B_n, respectively; (c) difference between calcd. and found mass, in millimass units; (d) above mass of R (163 for carbobenzoxy); (e) side chain of valine and leucine, respectively, minus one hydrogen transferred to peptide chain; (f) benzylcarbamate.

(2) The presence of Cl, Br, S or Si is tested by checking the presence of pairs of ions differing by 1.998 ± 0.003 mass units and are of approximate intensity ratios between 1:1 and 30:1.

(3) The ions of highest mass in the data are then asked for. From these the most probable molecular ion is chosen by inspection and its elemental composition is tested using the elements found present in steps 1 and 2, in addition to C and H.

(4) Once the most probable elemental composition of the compound is thus found, the compositions of all ions in the spectrum are calculated with that restriction and summarily presented in form of "ion-types" and decreasing intensity. An ion-type refers to the ions belonging to the general series $C_nH_{2n+x}N_yO_z$..... Within each type only n varies while x, y, z..... is constant, i.e. it is a homologous series of a given degree of saturation (also expressed in number of rings and/or double bonds, e.g. 2F refering to a fragment with two rings or double bonds) and heteroatom content (6). This representation is chosen as the most compact one relating best the characteristics of an ion of interest to the chemist.

Obviously, if a considerable part of the ions (in terms of total abundance) would not agree with the assumed composition of the molecule (see above) the latter would be in error and the data would be inspected for indications of a different one.

(5) The various prominent ion-types listed under (4) convey a large amount of structural information. E.g. if the C_nH_{2n+1} type is abundant, one deals with a compound containing a saturated hydrocarbon chain of at least n carbon atoms. Similarly, ions with X = -8, N = 1 and O = 1 indicate highly unsaturated or aromatic fragment ions (with 5 double bonds or rings) containing one nitrogen and one oxygen atom.

(6) In addition to the types of ions present, the number of carbon atoms encompassed, as well as the relative abundance vs. number of carbon atoms (n), is important. Thus, if the $C_nH_{2n-8}N_1O_1$ have a minimum of seven carbon atoms and an increasing carbon number up to the maximum permitted by the molecule itself, one can conclude that there is a C_7H_6NO moiety present which is substituted by an unbranded chain of consecutive CH_2 groups.

Similar information can be deduced from other ion types and is, in fact, in some cases produced directly by the computer (e.g. the presence of C_nH_{2n+1} ions leads to the statement "ALKYL IONS WITH A MINIMUM OF ... CARBON ATOMS").

(7) It is of course also possible to test the characteristic meaning of intense peaks in the spectrum by comparison of their accurate mass (equivalent to elemental composition) with a list of masses of ions that are felt to be characteristic for a certain structural entity (e.g. $C_3H_6O_2$ for long chain methyl esters, $C_5H_5N_5$ for adenine derivatives, $C_8H_{10}N$ for aspidosperma alkaloids etc.). If present, the computer lists these suggestions upon request.

(8) Various other commands are available; for example, one can ask for the presence of a certain ion, a certain ion type, pairs of ions differing by a certain group (H_2O, CO, CH_3OH.... or any other) etc.

(9) Whenever one reaches a certain conclusion on the basis of the answers presented by the computer one types them out, thereby temporarily storing them. At any given point these conclusions can be repeated by the computer, thus forming a permanent record of the completed interpretation or the state reached when the interpretation was interrupted for one reason or another.

The above mentioned film demonstrated the use of this program on a simple compound of known structure (palmitanilide, $C_6H_5NHCO(CH_2)_{14}CH_3$), as well as a new compound isolated in the course of the work on the structure of a nucleic acid. For this compound structure II resulted. (7)

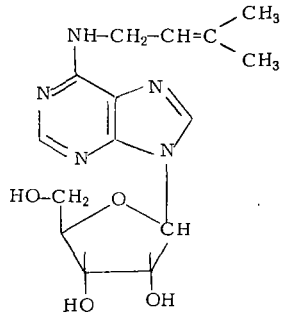

II

Acknowledgement: This work was supported in part by research grants from the National Institutes of Health (GM-90532) and from the National Science Foundation (GP-3734). It was carried out using the facilities of Project MAC at M.I.T.

References

(1) (a) P. Bommer, W. McMurray and K. Biemann, 12th Annual Conference on Mass Spectrometry, p. 428, Montreal, June 1964; (b) D. M. Desiderio and K. Biemann, ibid., p. 433; (c) K. Biemann, W. McMurray and P. Bommer, ibid., p. 442.

(2) K. Biemann, P. V. Fennessey and J. M. Hayes, Symposium on Filmed Data and Computers, Society of Photo-Optical Instrumentation Engineers, Boston, June 1966.

(3) K. Biemann, P. Bommer and D. M. Desiderio, Tetrahedron Letters, No. 26, 1725 (1964).

(4) K. Biemann, C. Cone and B. Webster, J. Am. Chem. Soc., 88, 2597 (1966).

(5) M. Senn and W. McLafferty, Biochem. Biophys. Res. Comm., 23, 381 (1966).

(6) K. Biemann, W. J. McMurray and P. V. Fennessey, Tetrahedron Letters, in press (July 1966).

(7) K. Biemann, S. Tsunakawa, J. Sonnenbichler, H. Feldmann, D. Dütting and H. G. Zachan, Angew. Chemie, 78, 600 (1966).

Current Status of Type Analysis by Mass Spectrometry

W.C. Ferguson
Union Oil Company of California
Brea, California

Abstract

Mass spectrometry has proven the most versatile technique for the analysis of the hydrocarbon and related non-hydrocarbon classes associated with petroleum and shale oil processing. Procedures have been developed for the analysis of mixtures ranging from gasolines through high boiling fractions with end points around 1000°F. Analytical data may be obtained in terms of composition by type, without regard to carbon number distribution within each class, by direct analysis of the sample; on the other hand, by appropriate chromatographic separation of the misture to prepare suitable fractions, the carbon number distribution within any class may be determined, as well as its absolute concentration.

Use of Labeled Molecules in Mass Spectral Studies of Organic Molecules

L.C. Leitch
National Research Council
Ottawa, Canada

Abstract

A critical survey of the available methods for labeling organic compounds will be presented under the following heads:

a) acid-or base-catalyzed exchange in molecules which contain labile hydrogen.

b) exchange reactions catalyzed by metals.

c) special methods.

SUPPLEMENTAL MEASUREMENTS IN PROBING ELECTRON IMPACT-INDUCED DECOMPOSITIONS VIA MASS SPECTRA OF LABELED COMPOUNDS

by

Seymour Meyerson

Research and Development Department, American Oil Company, Whiting, Indiana

ABSTRACT

The value of isotope labeling in probing the chemistry underlying mass spectra is well established. The usefulness of this approach and the reliability of conclusions reached thereby can be greatly increased by checking dependence of label retentions in fragment ions on operating conditions. For example, varying the ionizing voltage, source temperature, or repeller potential alters the relative contributions of the two competing processes by which methylcyclopentane loses a methyl radical to form isomeric $C_5H_9^+$ ions. The ions resulting from the two processes are derived from different parts of the original molecule and so can be distinguished by appropriate labeling.

INTRODUCTION

Mass spectra arise from chemical degradation of isolated molecules under electron impact. A knowledge of the reactions involved is needed for interpreting the spectra in attempts to identify unknown compounds, to determine molecular structures, to follow isotopic labels in reaction mechanism studies, and to assess the validity of thermochemical conclusions derived from electron-impact measurements. The spectra consist of data on a sampling of the ionic species among the decomposition products about a microsecond after impact. These products arise by a complex network of competing and consecutive reactions, and changes in instrument conditions--by altering reaction rates and residence time--can be expected to alter the distribution of chemical species contributing to the spectrum. Thus, the knowledge to be gained from isotope labeling, which has been the most fruitful single approach in exploring the chemistry underlying mass spectra of organic compounds, can be greatly expanded by studying the changes in spectra of labeled compounds as instrument conditions are varied.

The spectrum of a compound labeled in a specific known position may show a number of fragment ions in which label retention is 100% and others in which it is nil. Particularly if, in addition, several differently labeled species of the compound are available, one then stands a good chance of being able to define confidently what parts of the original molecule are incorporated in each of several fragment ions, and mechanistic interpretation is likely to be relatively simple and straightforward. Often, however, label retentions are less than 100% but greater than zero. One must then consider whether the observed retentions result from fragmentation by a single path or by two or more reaction paths producing ions of the same mass. A clear decision can often be reached by varying one or more of three instrumental settings--ionizing voltage, source temperature, and repeller potential. A labeling study reported some time ago,[1] which included voltage-dependence measurements, has been supplemented by further measurements of retention dependence on operating conditions. The results illustrate the usefulness of such additional tests and, conversely, the hazard incurred by omitting them.

To clarify the process by which a methyl radical is lost from methylcyclopentane, we measured label retention in the $C_5H_9^+$ ions in the spectra of this compound labeled in three different ways.[1] Forty-two and 40%, respectively, of the $C_5H_9^+$ ions derived from methylcyclopentane-α-^{13}C and -α-$\underline{d}$ retain the label, and 38% of those from the α-$\underline{d}_3$ species retain all three deuterium atoms. The three values agree well with each other, but they differ significantly from a value of about 52% previously reported by Stevenson[2] for the α-^{13}C case. The discrepancy, presumably a result of some difference in operating conditions that influenced the kinetics of the reacting system, suggested that more than one process was involved.

Our finding[1] that label retention in the $C_5H_9^+$ ion is a function of ionizing voltage advanced this suggestion to a certainty. Measurements on the α-$\underline{d}_3$ species, which are plotted in Figure 1, show intensities of the $C_5H_9^+$ ions containing 2, 1, and 0 deuterium atoms relative to that of the $\underline{d}_3$ ion at ionizing voltages (uncorrected) ranging from 7.9--slightly above the appearance potential--to 14.7 and at 70 volts. Relative intensities of the $\underline{d}_3$, $\underline{d}_2$, and $\underline{d}_1$ ions are essentially constant throughout the entire range. That of the unlabeled ion is constant for something less than a volt at the lowest energies employed, and then begins a steady climb, ultimately leveling out at a value about twice the initial one. All the deuterium-containing $C_5H_9^+$ ions and the unlabeled ones corresponding to the initial intensity thus appear to have a common origin, I--

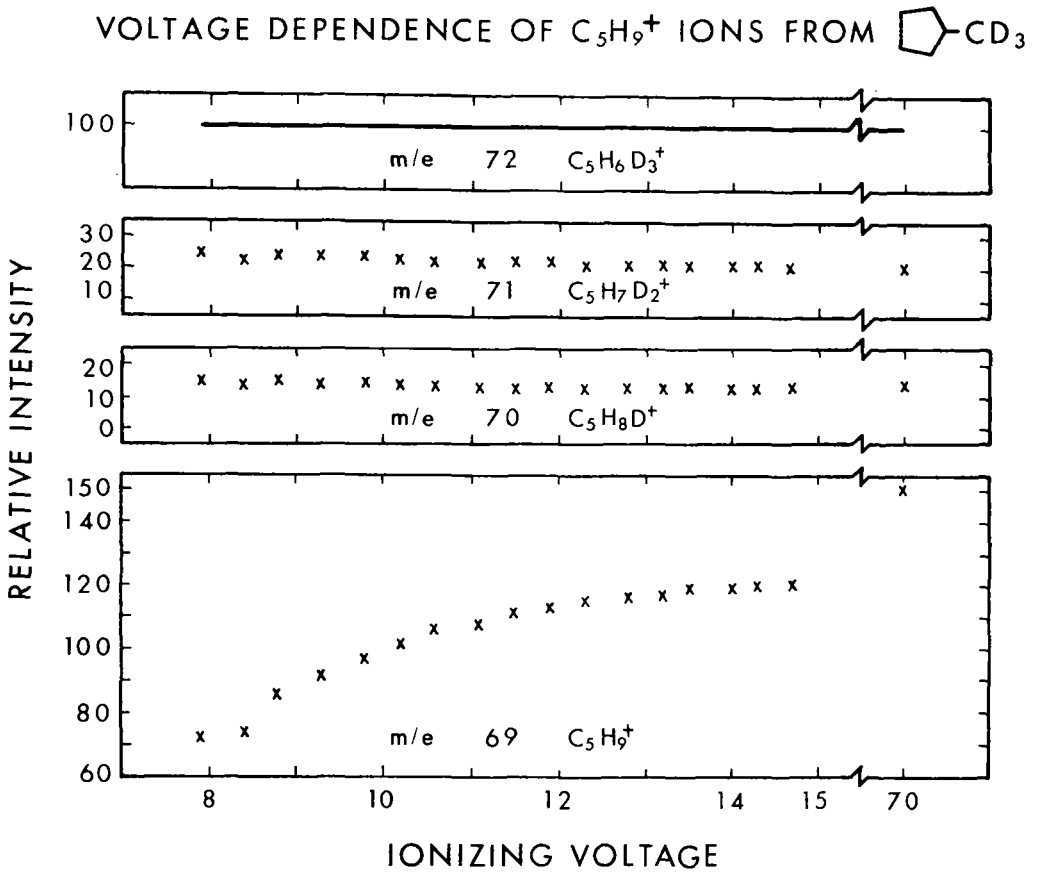
VOLTAGE DEPENDENCE OF $C_5H_9^+$ IONS FROM
CD_3
RELATIVE INTENSITY
100
m/e 72 $C_5H_6D_3^+$
30
20
10
m/e 71 $C_5H_7D_2^+$
20
10
0
m/e 70 $C_5H_8D^+$
150
140
120
100
80
60
m/e 69 $C_5H_9^+$
8
10
12
14
15
70
IONIZING VOLTAGE

FIGURE 1

opening of the ring adjacent to the substituted carbon, accompanied by some redistribution of hydrogen atoms, and followed by loss of CH_3 from either end of the resulting linear structure, as proposed by Stevenson to account for the approximately 50% retention he had found in $C_5H_9^+$ from methylcyclopentane-α-^{13}C. Departure from constancy of relative intensity of unlabeled $C_5H_9^+$ evidently signals the intervention of a second process, II, in which only the original triply labeled methyl group is lost. The data thus indicate two contributing processes leading to isomeric $C_5H_9^+$ ions--pentyl from I and cyclopentyl from II--and they permit an estimate of the relative contributions of the two processes--73% I and 27% II, based on the 70-volt spectrum measured under our normal instrument operating conditions. Similar measurements on the $C_5H_9^+$ ions from methylcyclopentane-α-^{13}C gave a similar picture, with relative contributions of 71% I and 29% II. Stevenson's published spectrum of the α-^{13}C species, coupled with the initial retention value from our voltage-dependence measurements on $C_5H_9^+$ from this same species, corresponds to relative contributions of 87% I and 13% II.

RESULTS AND DISCUSSION

To identify the operating parameters that might be responsible for the difference between Stevenson's and our results, a series of measurements were made on methylcyclopentane-α-$\underline{d}_3$ in which source temperature, repeller voltages, and operating mode--focused vs. nonfocused--were varied, as listed in Table I. Runs 1 and 2 included voltage-dependence measurements; the initial $C_5H_9^+$ isotopic distributions in the two runs were indistinguishable--$\underline{d}_3$, 100; $\underline{d}_2$, 21; $\underline{d}_1$, 14; and $\underline{d}_0$, 75--and were assumed to correspond to the products from path I in all runs. The 70-volt isotopic distributions and the derived relative contributions of paths I and II are listed in Table II. Runs 1, 2, and 3 were made with the repellers at fixed potentials, selected to give maximum sensitivity while maintaining an average value of 3 volts. Runs 4 and 5 were made under normal conditions, in which the repeller potentials are fixed fractions of ion-accelerating voltage; the values shown in the Table correspond to the ion-accelerating voltage at which $C_5H_9^+$-$\underline{d}_1$ (mass 70) is collected. All measurements were made on a modified[3] Consolidated model 21-103c instrument.

Source temperature and repeller potential--as well as ionizing voltage--affect the observed isotopic distribution and thus the relative contributions of the competing paths leading to $C_5H_9^+$ ions. The choice of focused vs. nonfocused mode has no effect except insofar as switching from nonfocused to focused in normal operation also steps up the fraction of the ion-accelerating potential applied to the repellers. Stevenson's data were obtained on an instrument of different geometry than ours, and factors that we have not explored may have contributed to the difference in results. However, a large part of the difference, at least, can be accounted for by the differing source temperatures and repeller settings. He employed a source temperature of 125° and a repeller potential of 5 volts.

The special relevance of repeller potential in this context derives from the fact that it controls the residence time of the ions in the ionization chamber--for present purposes, the reaction chamber. Residence time is directly proportional to the distance between the electron beam and the ion-exit slit and inversely proportional to the square root of the repeller potential. The approximate residence times listed in Table I were calculated for an ion of mass 70--$C_5H_8D^+$--on the admittedly oversimplified assumption that decomposition of the parent ion to the product of mass 70 is instantaneous and thus precedes any movement of the ion from the point at which electron impact occurred. The similarly calculated residence time in Stevenson's work--estimated from data reported in his paper coupled with the assumption that the electron beam is centered between the repeller plates and the exit slit, as in the Consolidated instrument[4]--is 1.5 microseconds, significantly longer than in our runs 1, 2, and 3. Likewise, Stevenson's source temperature was somewhat lower than the 140° of run 1--the approximate equilibrium temperature attained by our source with the heater turned off. Increasing the ionizing voltage or source temperature thus favors process II, which has the higher energy requirement, at the expense of I. Increasing repeller potential, by decreasing residence time, also favors II, apparently a simple bond dissociation, over I, a more complex process presumably requiring more time.

Converging reaction paths--two or more processes leading to ions of the same mass--have been demonstrated in other systems also[5] and must be presumed to occur commonly. In using isotopic labels to probe the chemistry underlying mass spectra, one or more of the supplemental measurements described here can often clearly reveal converging paths not otherwise readily recognized. In other cases, they can furnish evidence that an ion in question arises by only one path.[1,6] Failure to utilize such checks may well lead to erroneous conclusions.

One can reasonably hope that the added leverage gained by the use of such auxiliary techniques in conjunction with labeling will permit the promotion of at least

some decomposition processes from McLafferty's category of "random"[7] to the more aesthetically satisfying one of "specific" rearrangements.

POSTSCRIPT

Findings of the present study and of the earlier work[1] leading to it can perhaps help focus attention on some considerations relevant to the use of mass spectra in other contexts.

A survey of comparative spectra measured on instruments of different types, as well as on instruments of the same type but at different operating conditions, showed large differences in over-all response that varied erratically with mass and with molecular composition.[8] In addition to the multiple effects often loosely referred to as mass discrimination,[9] differences in source temperature and residence time undoubtedly contributed heavily to this state of affairs. The large number of competing and consecutive reactions underlying mass spectra and the sparsity of knowledge of the kinetics of these systems amply justify the pessimistic conclusion[8] that spectra characteristic of one type of instrument or one set of operating conditions cannot, in general, be calculated from measurements made on another type or at different conditions. Inadequate appreciation of the effects of operating conditions has led to generally incomplete reporting of the conditions used in recording mass spectra. The API[10] and MCA[11] Catalogs, for example, report source temperature but not repeller voltage or focused or nonfocused mode of operation. The problem becomes particularly acute in attempts to develop standard methods of analysis employing sets of coefficients suitable, hopefully, for all instruments operated in accord with some prescribed specifications. So long as critical operating conditions are not standardized--and, admittedly, an "optimum" standardization may not be feasible or even definable at the present state of the art--a good deal of caution is called for in using existing standard methods or in formulating new ones.

Relative contributions of the competing processes by which methylcyclopentane loses the methyl side-chain or its equivalent seem to be determined largely by ring strain and the dissociation energy of the bond to the side-chain.[1] In methylcyclohexane, in which ring strain is close to zero, 99 to 100% of the $C_6H_{11}^+$ ions evidently arise by a path analogous to II, that is, by loss of the original side-chain.[1] In ethylcyclopentane, in which the strength of the bond between the ring and side-chain is about 2 kcal. per mole less than in methylcyclopentane, relative contributions of the corresponding paths for loss of C_2H_5 are 53% I and 47% II.[1] These results furnish a striking demonstration of the sensitivity of mass spectra to structural differences corresponding to energies that are minute beside the energy of the impinging electrons, and thereby suggest that similar sensitivity may also be found in other high-energy systems. Such a suggestion is supported by recent studies of radiolytic and photolytic reactions. Thus, the radiolysis of liquid cyclopentane is characterized by a greater probability of ring opening than is that of cyclohexane.[12] Similarly, although the greater differences in ring strain make these examples somewhat less relevant, ring opening is more extensive in the photolysis of cyclobutane than in that of cyclopentane or cyclohexane,[13] and also in the radiolysis of perfluorocyclobutane than in that of perfluorocyclohexane.[14]

REFERENCES

(1) S. Meyerson, T. D. Nevitt, and P. N. Rylander, Advan. Mass Spectrometry, 2, 313 (1963).

(2) D. P. Stevenson, J Am. Chem. Soc., 80, 1571 (1958).

(3) H. M. Grubb, C. H. Ehrhardt, R. W. Vander Haar, and W. H. Moeller, 7th Annual Meeting of the American Society for Testing Materials, Committee E-14 on Mass Spectrometry, Los Angeles, Calif., May, 1959.

(4) C. E. Berry, private communication.

(5) S. Meyerson and P. N. Rylander, J. Chem. Phys., 27, 901 (1957); N. Dinh-Nguyen, R. Ryhage, S. Ställberg-Stenhagen, and E. Stenhagen, Arkiv Kemi, 18, 393 (1961); E. L. Eliel, J. D. McCollum, S. Meyerson, and P. N. Rylander, J. Am. Chem. Soc., 83, 2481 (1961); J. D. McCollum and S. Meyerson, J. Am. Chem. Soc., 85, 1739 (1963); S. Meyerson and H. Hart, J. Am. Chem. Soc., 85, 2358 (1963); S. Meyerson and L. C. Leitch, J. Am. Chem. Soc., 86, 2555 (1964); S. Meyerson, J. Chem. Phys., 42, 2181 (1965); S. Meyerson and J. L. Corbin, J. Am. Chem. Soc., 87, 3045 (1965); C. R. Enzell and R. Ryhage, Arkiv Kemi, 23, 367 (1965); S. Meyerson and L. C. Leitch, J. Am. Chem. Soc., 88, 56 (1966).

(6) S. Meyerson, J. Chem. Phys., 34, 2046 (1961); S. Meyerson, J. Am. Chem. Soc., 85, 3340 (1963); S. Meyerson, H. Drews, and E. K. Fields, J. Am. Chem. Soc., 86, 4964 (1964).

(7) F. W. McLafferty, Anal. Chem., 31, 82 (1959).

(8) V. J. Caldecourt, Appl. Spectroscopy, 12, 167 (1958).

(9) E. B. Jordan and N. D. Coggeshall, J. Appl. Phys., 13, 539 (1942); G. P. Barnard, "Modern Mass Spectrometry," Inst. of Physics, London, 1953, pp. 69-85; C. C. McMullen and H. D. Thode, in "Mass Spectrometry," C. A. McDowell, ed., McGraw-Hill Book Company, Inc., New York, New York, 1963, chap. 10; cf. W. R. Shields, E. L. Garner, and V. H. Dibeler, Advan. Mass Spectrometry, 2, 163 (1963).
(10) American Petroleum Inst., Research Project 44, "Catalog of Mass Spectral Data," Chemical Thermodynamics Properties Center, Agricultural and Mechanical College of Texas, College Station, Texas, 1947-65.
(11) Manufacturing Chemists Association, "Catalog of Mass Spectral Data," Chemical Thermodynamics Properties Center, Agricultural and Mechanical College of Texas, College Station, Texas, 1959-65.
(12) B. M. Hughes and R. J. Hanrahan, J. Phys. Chem., 69, 2707 (1965).
(13) R. D. Doepker and P. Ausloos, J. Chem. Phys., 43, 3814 (1965).
(14) M. B. Fallgatter and R. J. Hanrahan, J. Phys. Chem., 69, 2059 (1965).

Table I

OPERATING CONDITIONS FOR MEASUREMENTS ON $C_5H_9^+$ IONS DERIVED FROM METHYLCYCLOPENTANE-α-d_3

Run No.	1	2	3	4	5
Source Temperature, °C	140	250	250	250	250
Focused (F) or nonfocused (N) mode	N	N	F	N	F
Repeller Voltages					
Inner	3.55	3.55	3.55	10.2	25.0
Outer	2.45	2.45	2.45	8.7	23.0
Approximate residence time, microseconds	1.2	1.2	1.2	0.7	0.4

Table II

$C_5H_9^+$ ISOTOPIC DISTRIBUTIONS AND DERIVED RELATIVE CONTRIBUTIONS OF COMPETING REACTION PATHS

Run No.	1	2	3	4	5
Relative intensities of isotopic $C_5H_9^+$ ions,					
d_3	100	100	100	100	100
d_2	21	21	20	19	18
d_1	15	15	14	15	14
d_0	127	137	138	155	169
Relative contributions,					
path I, %	80	77	77	73	70
path II, %	20	23	23	27	30

"Mass Spectrometric Identification of Gaseous Products from Thermal Analysis"

H. G. Langer and R. S. Gohlke*
Eastern Research Laboratory
The Dow Chemical Company
Wayland, Massachusetts

The trend in modern analytical chemistry is towards miniturization and combination of techniques to save time and material, which is especially important for destructive methods.

Mass spectrometry and, as the name implies, thermal analysis use thermal energy in their analytical procedures but surprisingly little effort is being made to combine these two methods. The reason is the difference in ideal conditions under which each analysis should be carried out: while a static system (sample pressure, temperature, etc.) is employed for mass spectrometry a dynamic one is utilized for thermal analysis.

TABLE I

Method	Result	Condition: Temp. Control	Condition: Pressure Control
TGA	weight loss	yes	no
DTA	energy change temperature	yes	possible
MSA	Mass spectrum	no	no
MTA	Mass spectrum temperature	yes	no
MDTA	Mass spectrum energy change temperature	yes	no

TGA=Thermogravimetric Analysis
DTA=Differential Thermal Analysis
MSA=Mass Spectrometric Analysis
MTA=Mass Spectrometric Thermal Analysis (1)
MDTA=Mass Spectrometric Differential Thermal Analysis (2)

Considering the limitations of the methods mentioned in Table I, the following examples will show how thermal analysis and mass spectrometry can be successfully combined. The objective is not to obtain information about gases under equilibrium conditions, but to study reacting solids or liquids. *For this purpose the sample inlet system is of primary importance* as shown in Table II.

TABLE II

COMPOSITION OF SULFUR VAPOR (S_n)

Free Evaporation		Knudsen Cell		Conventional Gas Inlet		MTA	
n	*Intensity*	*n*	*Intensity*	*n*	*Intensity*	*n*	*Intensity*
8	100	8	100	2	100	2	100
2	70	2	95	1	8	1	51
4	48	4	64	6	7	4	40
5	29	5	41	4	2	8	36
3	15	6	39	8	2	3	25
6	15	3	24	5	2	5	17
1	11	1	10	3	1	6	13
7	<1	7	8	7	<1	7	2
Temp. °C. 73°		75°		sample 250° inlet 120°		50-700°	

*Present Address: Dow Corning Corporation, Midland, Michigan

The equilibrium composition of sulfur vapor is represented by the Knudsen Cell experiment although even in the "free evaporation" example (3) some equilibration seems to have taken place. At higher temperatures in a gas inlet system (4) almost all of the sulfur vapor consists of S_2 molecules. Under the conditions of MTA, however, the composition of sulfur vapor from an undefined sulfur and sulfide containing sample remains practically constant over a temperature range of nearly 700°.

For the MTA experiment a sample is heated in a miniature furnace (Figure 1) which is located beneath the ionizing electron beam of a Bendix Time-of-Flight Mass Spectrometer (5).

The technique known as Mass Spectrometric Differential Thermal Analysis (MDTA) utilizes a modified DTA cell as shown in Figure 2 (6). For this method a sample of the gas from the cell is continuously drawn into the mass spectrometer through a pressure reducing valve. In both cases the heating rate is predetermined but can be stopped or changed at any given time. The operator can choose freely between monitoring several mass peaks or recording complete mass spectra.

Triphenyltin hydroxide (Figure 3) is shown by DTA (broken line) to melt with subsequent decomposition. MTA at approximately 10^{-7}torr identifies this decomposition as diffusion controlled dehydration, which by MDTA at 10^{-3}torr is further characterized as solid state dehydration of the hydrated oxide which, in its anhydrous form, subsequently melts at 123°C.

A "true" hydroxide (Figure 4) on the other hand requires an activation energy to break the metal-oxygen bond characterized by the sharp break in the curve for $Mg(OH)_2$.

The decomposition depicted in Figure 5 for the dihydrate dihydrochloride of ethylene diamine tetraacetic acid is typical for a multi component system with both successive and simultaneous decomposition ranges.

The germanium chelate of ethylene diamine tetraacetic acid (Figure 6) shows a stepwise dehydration. Integration proves that equal amounts of water are released in each step, so that this compound might possibly be used as an internal standard for quantitative investigations.

The thermal decomposition of a dimethyl sulfoxide complex of magnesium chloride (shown in Figure 7) proceeds without hydrolysis (absence of HCl at <u>all</u> times) in contrast to hydrated magnesium chloride which always produces HCl upon heating.

Whereas hydrolysis is undesired in the case of magnesium chloride it can be utilized for decomposition of calcium carbonate as shown in Figure8 In the presence of water vapor, release of carbon dioxide begins at a much lower temperature through the intermediate formation of calcium hydroxide evidenced by the reduced vapor pressure of water between 200-600°.

Although the method described here is applicable to every field of chemistry, its most important use is in studying fast and overlapping reactions. Since existing thermo-analytical and mass spectrometric instrumentation is capable of providing all of the necessary data for these studies, a combination with a capable data handling system can easily provide a three-dimensional plot of mass versus intensity versus temperature. Thus the tedious and time consuming thermal analysis of the past can be reduced to a straight forward data handling operation.

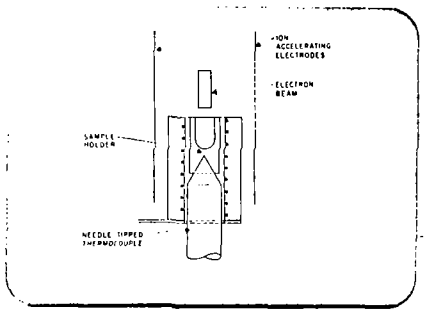
ION ACCELERATING ELECTRODES
ELECTRON BEAM
SAMPLE HOLDER
NEEDLE TIPPED THERMOCOUPLE

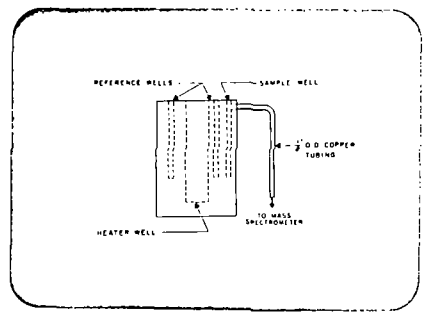
REFERENCE WELLS
SAMPLE WELL
TUBING
TO MASS SPECTROMETER
HEATER WELL

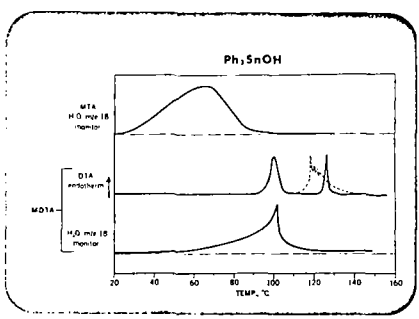
Ph₃SnOH
MTA
H₂O m/e 18 monitor
DTA endotherm
MDTA
H₂O m/e 18 monitor
20
40
60
80
100
120
140
160
TEMP. °C

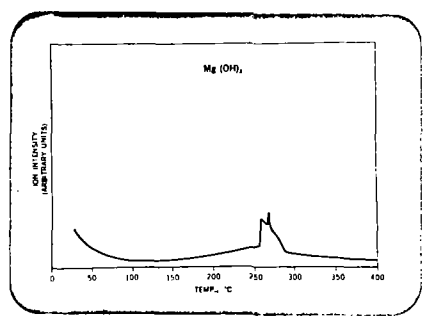
Mg (OH)₂
ION INTENSITY (ARBITRARY UNITS)
0
50
100
150
200
250
300
350
400
TEMP., °C

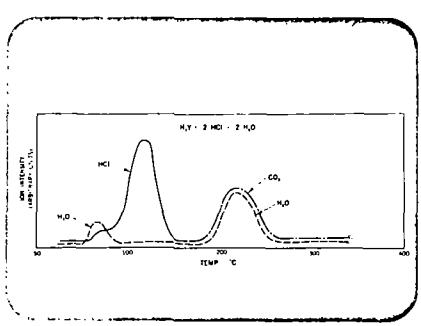
H₄Y · 2 HCl · 2 H₂O
ION INTENSITY (ARBITRARY UNITS)
HCl
H₂O
CO₂
H₂O
50
100
200
300
400
TEMP °C

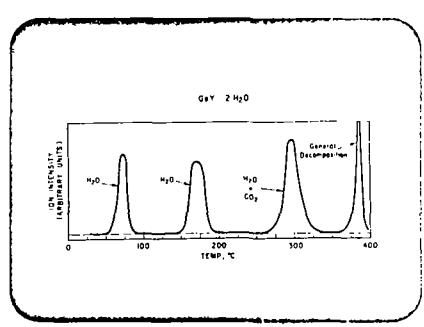
GeY · 2 H₂O
ION INTENSITY (ARBITRARY UNITS)
H₂O
H₂O
H₂O + CO₂
General Decomposition
0
100
200
300
400
TEMP. °C

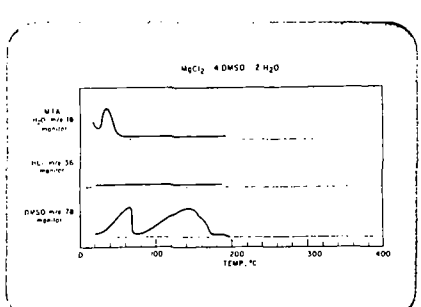
MgCl₂ · 4 DMSO · 2 H₂O
MTA
H₂O m/e 18 monitor
HCl m/e 36 monitor
DMSO m/e 78 monitor
0
100
200
300
400
TEMP. °C

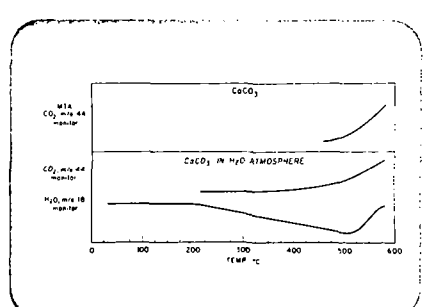
CaCO₃
MTA
CO₂ m/e 44 monitor
CaCO₃ IN H₂O ATMOSPHERE
CO₂ m/e 44 monitor
H₂O m/e 18 monitor
0
100
200
300
400
500
600
TEMP °C

REFERENCES

(1) Langer, H. G., and Gohlke, R. S., Anal. Chem., 35, 1301 (1963).

(2) Langer, H. G., Gohlke, R. S., and Smith, D. H., Anal. Chem., 37, 433 (1965).

(3) Berkowitz, J., and Chupka, W. A., J. of Chem. Phys., 40, 287, (1964).

(4) Dilling, M., The Dow Chemical Company, Chemical Physics Research Laboratory, Midland, Michigan - Private Communication (1964).

(5) Gohlke, R. S., Chem. and Ind., (London) 946 (1963).

(6) E. I. du Pont de Nemours and Company, "900 Differential Thermal Analyser".

THE USE OF PHOTO-IONIZATION IN ANALYTICAL MASS SPECTROMETRY

PART I - by C. E. BRION

INSTRUMENTATION

In analytical mass spectrometers ions are generally produced by electron impact. Such sources are simple in operation and have the important property that a high ionizing flux is easily obtained resulting in large and easily measured ion currents. However despite its general usefulness, ease of operation, and appeal for a wide variety of problems there are some disadvantages of the electron impact source for certain applications. Due to the proximity of the hot tungsten filament (∿2000°K.) the ion source usually operates at 80-200°C. above room temperature depending on the construction of the particular source.

In addition to the general field of organic chemistry, mass spectrometry is assuming an increasing importance in biochemistry. Here many delicate molecules may be subject to thermal decomposition in the mass spectrometer ion source and pyrolysis on the filament could be even more serious. In addition, in physical chemistry and allied subjects, there are many problems where thermal decomposition is an operational hazard, frequently of an unknown magnitude since it is often difficult to ascertain whether a given fragment has been produced by thermal or electron impact induced dissociation. Numerous problems immediately suggest themselves where it would be of advantage to be able to operate a mass spectrometer ion source at a series of closely controlled temperatures. All these applications are, at best, difficult using the conventional electron impact ion source.

Suitable photoionization sources overcome many of these problems. However photoionization sources have received relatively little attention probably due to the technical difficulties involved in their operation and construction. Since the cross-section for photoionization is much smaller than for electron impact the use of such sources requires high sensitivity detection.

Typical light sources utilize an electrical discharge in a capillary containing helium or a mixture of gases at relatively high pressure (∿1 mm.). Unless very efficient differential pumping is employed it is necessary to isolate the light source from the high vacuum of the mass spectrometer with a lithium fluoride window. Such an arrangement has been used by Inghram and his co-workers and also by Lossing and Tanaka. However the use of a LiF window restricts the photon beam to wavelengths about 1050 A.--i.e., energies below 11.8 e.v. A windowless differentially pumped system placed no restriction on the energy of the transmitted photon beam. This technique has been used in photoelectron spectroscopy and for UV spectroscopy. It has also been exploited by Frost et al and also by Dibeler for the study of threshold phenomena and autoionization in the mass spectrometer. However for an analytical mass spectrometer a high photon flux is required at a high energy.

A microwave discharge in helium produces a line emission spectrum and in the far ultraviolet the 584 A. (21.21 e.v.) helium resonance line accounts for the majority of the radiation. At first it might appear that 21 volts is a rather low ionizing energy in that electron impact spectra at this energy are of relatively low intensity. However the differing nature of the threshold law for photoionization should compensate for this to a large extent. Spectra at lower energy are also somewhat simpler since highly excited states of the ion are not accessible.

In view of the potential usefulness of photoionization in analytical work it was decided to construct a suitable light source for the M.S.9 mass spectrometer. A prototype light source is shown in Figure 1. A needle valve controls the flow of tank helium into the quartz tube where the discharge is produced by a Raytheon 2450 Mc/s unit coupled to a microwave cavity which is a modified form of that described by Zelikoff et al. The discharge is initiated with a tesla coil. The discharge tube is cooled with compressed air. To prevent excessive helium from entering the mass spectrometer the lower portion of the source consists of a fine quartz capillary (0.5 mm. diameter) which transmits a very narrow light beam but severely impedes the flow of helium. A 4-cm. pumping line is situated close to the mouth of the capillary and helium is pumped away as rapidly as possible by a 100 liters/sec. oil diffusion pump backed by a 400 liters/min. mechanical pump. With this arrangement and the optimum helium pressure (that giving the maximum light intensity), the mass spectrometer operating source pressure was 10^{-7} mm. Hg. Under these conditions and using 70-volt electrons only a very small peak due to He^+ was detected in the mass spectrometer. The photon beam passes into the ion source through a small hole in the ion chamber wall and passes out through a similar hole in the far side. The photon beam is perpendicular to the long axis of the ion source exit-slit. This transverse mounting allows use of an electron beam in the same source.

For some molecules it is highly probable that thermal decomposition occurs at the ion source ambient temperature (∿225°C. for the M.S.9) and also pyrolysis may occur on the filament. The following examples taken from recent work in this laboratory clearly demonstrate these effects and their subsequent elimination using photoionization.

In studying osmium tetroxide (OsO_4) a mass spectrometric analysis was required. This extremely volatile solid is stable at room temperature but is now known to decompose to a black solid (OsO_2) at high temperatures. On introducing OsO_4 into the spectrometer, high voltage breakdown rapidly ensued and it was impossible to make the analysis. Subsequent dismantling of the ion source for cleaning showed quite clearly that thermal decomposition had occurred particularly in the hotter regions of the source around the filament. No problem was encountered using photoionization and a satisfactory mass spectrum was obtained with no detectable source contamination. In this way it is now possible to study many other compounds which decompose under electron impact source conditions.

Thermal decomposition effects are rather more spectacular in the study of trans-4-tertiary butylcyclohexanol which is a stable molecule by normal standards. It was suspected that thermal decomposition was occurring when this sample was introduced via a conventional high temperature inlet system into the electron impact ion source. On the other hand, use of a direct insertion probe was undesirable since the compound was so volatile at the ion source ambient temperature that a steady vaporization was impossible. In this situation it is often the practice to switch on the filament immediately before a scan is made. For quantitative work this practice is undesirable and irreproducible spectra are often obtained. Subsequently the sample was placed in a tube outside the source and the vapor allowed to flow directly into the ion chamber. A suitable source pressure was obtained without any heating. However the mass spectrum was still dependent on the length of time the filament had been switched on and even at thermal equilibrium it was suspected that thermal decomposition had taken place. Using photoionization with the source at room temperature a satisfactory and reproducible mass spectrum was immediately obtained. A series of experiments have been carried out to ascertain the extent and nature of the thermal effects.

Figure 2 shows the appearance of the mass spectrum of trans 4-t-Bu cyclohexanol in the parent peak region as a function of ion source conditions and ionizing mode. The photoionization spectrum (a) shows the molecular ion unambiguously. Case (b) shows a spectrum obtained when a scan is made as soon as the filament is switched on with the source relatively cool. Already the parent peak has slightly decreased and the P-H_2O peak increased suggesting thermal decomposition on the filament as does the appearance of a large P-2 peak. To ensure that the differences in spectra (a) and (b) are not due to differences in ionization probability for photoionization and electron impact spectrum (c) was obtained using photoionization with the electron beam filament switched on just before the scan and at zero electron energy. All ions must be produced by the photoionization source. The new peaks which appear in (b) are also present in (c) and therefore originate from pyrolysis on the filament and not from direct ionization and dissociation of the sample. Spectrum (d) is the result of electron impact ionization with the source at thermal equilibrium (∿225°C.) Equilibrium is only attained after approximately 2 hours and it is important to note that a continuously changing mass spectrum is recorded during this time. Large changes have occurred in (d) probably due to decomposition on the hot ion chamber walls. The parent peak has almost disappeared while the P-2 peak remains the same as in (b) and (c). In an unknown compound the identity of the parent could be subject to some uncertainty. Spectrum (e) shows the photoionization mass spectrum with the source heated to 250°C. but with the filament off. The P-2 peak is no longer observed and therefore arises from filament pyrolysis as previously deduced. The parent peak has increased slightly over (d) and m/e 138 and 123 remain similar. The source was then allowed to cool to room temperature and the photoionization spectrum taken at various temperatures. The ratio P/P-H_2O increased until at room temperature spectrum (a) was re-obtained.

These experiments clearly indicate some of the possible thermal hazards associated with the use of electron impact for the study of fragmentation. It should be stressed that the normal electron impact operating conditions have been used in this study of what is by normal standards a stable molecule. It is evident that caution must be used in the interpretation of spectra and for reproducible quantitative work it is necessary that the source acquires an equilibrium temperature. The photoionization method can remove many uncertainties and ensures that the source temperature need not be in excess of that necessary for vaporization of the sample. In addition a relatively larger parent peak can be expected for those compounds subject to thermal decomposition.

The conventional electron impact source can be modified to minimize the effects of filament pyrolysis and ion chamber decomposition if the filament is placed in a separate differentially pumped box at some distance from the ion chamber. This is desirable in all analytical mass spectrometers but entails major reconstruction of the source and its housing. Photo-ionization offers a simple alternative.

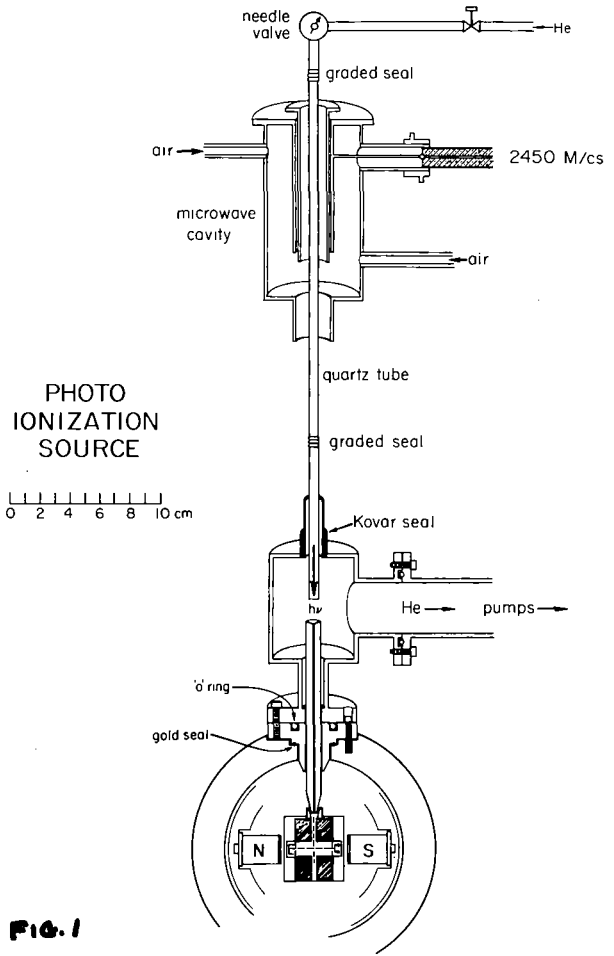
needle valve
He
graded seal
air
2450 M/cs
microwave cavity
air
quartz tube
PHOTO IONIZATION SOURCE
graded seal
0 2 4 6 8 10 cm
Kovar seal
hν
He
pumps
'o' ring
gold seal
N
S

FIG. 1

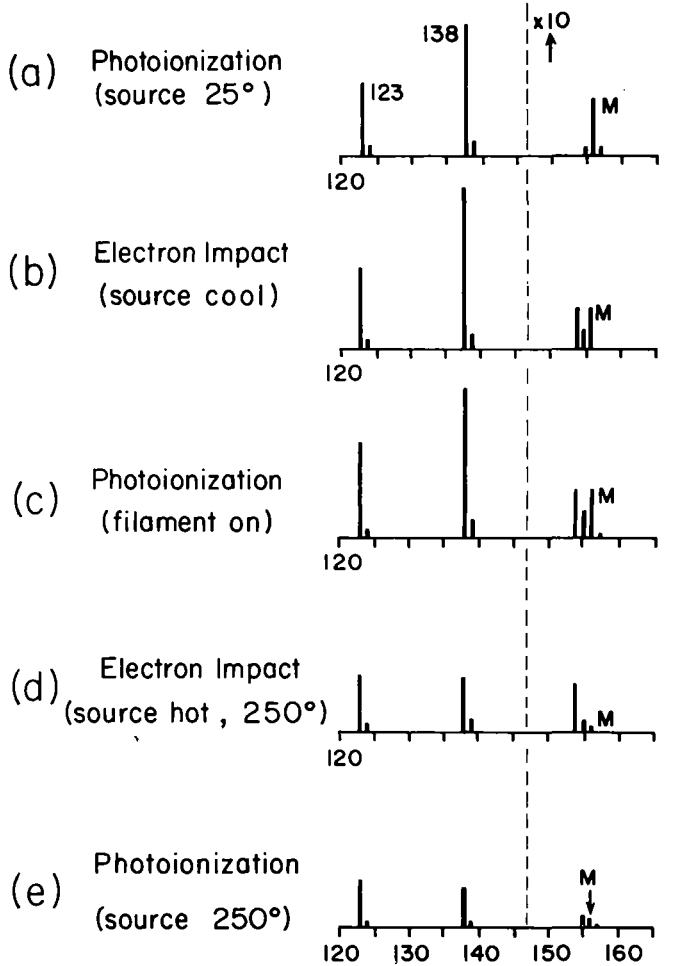
(a) Photoionization (source 25°)
138
x10
123
M
120
(b) Electron Impact (source cool)
M
120
(c) Photoionization (filament on)
M
120
(d) Electron Impact (source hot, 250°)
M
120
(e) Photoionization (source 250°)
M
120 130 140 150 160

FIG 2

Despite its usefulness the light source (I) just described was felt to be inadequate for several reasons. Firstly in the existing arrangement the light beam enters the mass spectrometer via the vacuum lock port in the source housing thus precluding the simultaneous use of a solid sample probe. Accordingly the light source (Figure 3) was mounted on the side of the source housing so that the light beam traverses the path normally taken by the electron beam. This not only permits the study of involatile solids but also provides some increase in ion intensity. The capillary has also been enlarged to further increase the ultraviolet flux. In the earlier source (I) it was suspected that some contribution from photo-electrons was present in the total ionization. Source II has been designed to minimise this effect. Figure 4 compares the mass spectra of 2 pentanone under various conditions. A small increase in ionization is obtained by using argon in the discharge tube; at the expense of a rather higher gas pressure and a certain amount of additional heat production. It can be deduced that the photo-ionization mass spectrum (I) contains a large contribution from photo-electrons. Source II produces a much higher proportion of photons. The relative increase in the size of the parent peak is noteworthy.

PART II by C. E. BRION and L. D. HALL

STUDIES OF STEREOISOMERISM BY PHOTOIONIZATION MASS SPECTROMETRY:

FRAGMENTATION OF CIS AND TRANS-4-t-BUTYLCYCLOHEXANOLS

AND RELATED COMPOUNDS

It has been suggested by Biemann that the process of water elimination from alcohols which occurs in the mass spectrometer, shows some slight stereospecific dependence insofar that for several epimeric pairs of alcohols it has been observed that the one having the most sterically hindered hydroxyl function generally exhibits the lower intensity molecular ion (M^+) and the higher intensity ($M-H_2O$) peak. However, a mass spectrometric investigation of the cis (I) and trans (II) isomers of 4-t-butylcyclohexanol (figure 5) reveals an unexpectedly large steric dependence for water elimination and which, furthermore, at first sight appears to contravenc the generalization outlined by Biemann for this process.

Our initial study of these compounds utilised a conventional electron impact ionization source and under these conditions our results were irreproducible and inconclusive. In view of studies discussed in part I it seemed highly probable that this was the result of spurious processes caused by the hot filament together with the attendant high temperature of thc ion chamber (200°). Accordingly we repeated our measurements using the improved photoionization source discussed above. This source operates at any desired temperature at or above room temperature. The spectra obtained were quantitatively reproducible and are shown in Figure 6. The higher mass peaks in the photoionization mass spectrum are much more intense than their electron impact counterparts. It has already been shown that this is due at least in part, to thermal effects. It is also clear that there is a most significant difference between the fragmentation patterns of the two isomers particularly in the high mass region of the spectrum. If we assume that the molecular ions of (I) and (II) adopt the same conformations in the gas phase as are believed to be preferred for the neutrals (I) and (II) in solution, then the cis-isomer (I) would have the hydroxyl function in the more sterically hindered position (axial) and should thus eliminate water more readily than the trans isomer (II). In fact the reverse is observed, with the relative ($M-H_2O$) peak abundances being ($M-H_2O$)TRANS/($M-H_2O$)CIS = 38/1. There is also a significant difference in the ratio of parent ion abundance with M TRANS/M CIS = 38/1. A simple rationale of these findings, together with other characteristics of the spectra, can be given if we abandon the above conformational hypothesis. Previous studies by Shannon et al and also by Djerassi and his coworkers on the fragmentation of cyclohexanol have shown that water elimination occurs preferentially (83%) via 1,4 and 1,3 elimination processes and furthermore have lead to the suggestion that 1,4 elimination will occur preferentially when the substituents to be eliminated from these positions have a trans relationship.

Shannon et al have suggested the ion resulting from the 1,4 elimination may be related to the 2,2,0-bicyclohexane system (V). If this is so, and if 1,4 elimination can occur in the 4-t-butylcyclohexanol system then the simple expedient of inverting the conformation of the ion derived from the trans isomer (II) into the boat symmetry (IV) would enable the 1,4 elimination of water to occur quite readily. This elimination would be far less likely to occur in the cis isomer (III). Further evidence supporting this hypothesis follows from the work of Srinivasan who obtained the mass spectrum of 2,2,0-bicyclohexane and found major peaks at M, M-15, M-28, M-41 and M-43. If it is correct that an ion related to 2,2,0-bicyclohexane is an intermediate in the fragmentation of the trans isomer and not in the case of the cis isomer, then we should expect to

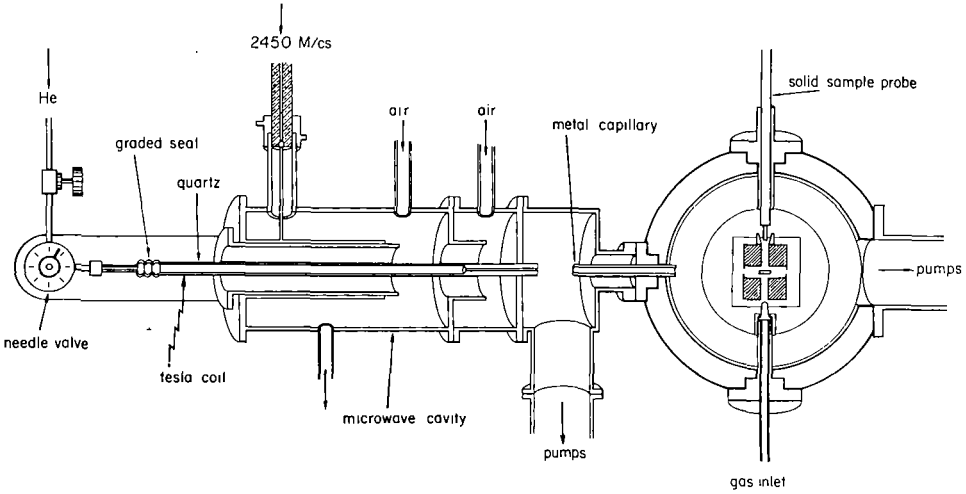

FIG. 3

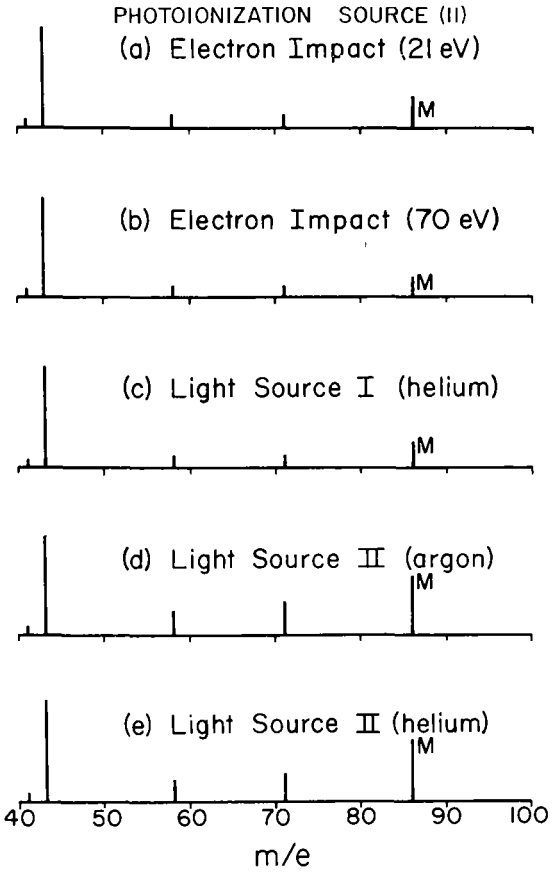

PRINCIPLE IONS IN THE MASS SPECTRUM OF 2 PENTANONE. (normalized at m/e = 43)

FIG. 4

see prominent peaks in the spectrum of the trans isomer at mass numbers 138, 123, 110, 97 and 95. These have been indicated by dotted lines in figure 6 from which it can be seen that peaks occur as required.

The methane sulfonic acid analogues have also been studied and figure 7 shows that the same general trends are observed. The toluene sulfonic acid and p-nitro benzoic acid derivatives have also been examined. Here stereospecificity is much less marked due to the fact that a high temperature (180°C) was required to volatilize these compounds.

It is a pleasure to acknowledge the technical co-operation of Associated Electrical Industries Ltd. and also the financial assistance of the National Research Council of Canada.

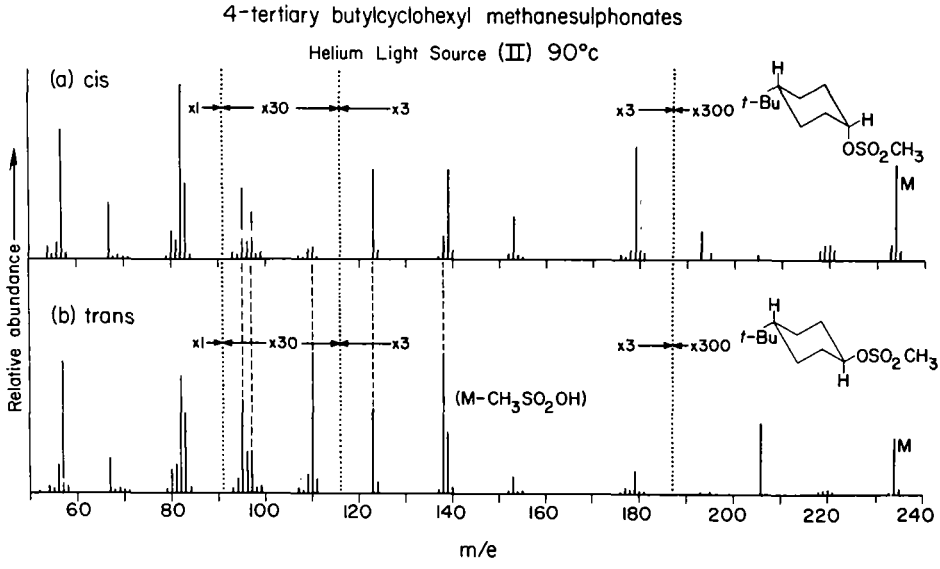

FIG. 7

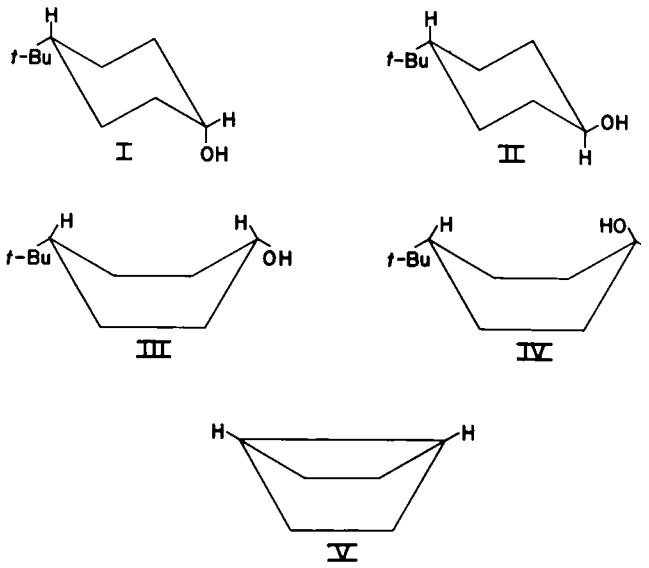
H
t-Bu
H
OH
I
H
t-Bu
OH
H
II
H
t-Bu
H
OH
III
H
t-Bu
HO
IV
H
H
V

FIG. 5

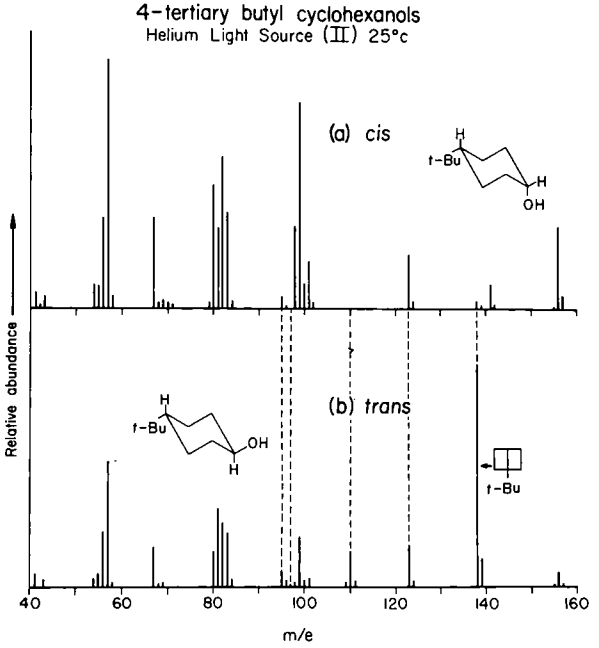
4-tertiary butyl cyclohexanols
Helium Light Source (II) 25°c
(a) cis
(b) trans
t-Bu
Relative abundance
40
60
80
100
120
140
160
m/e

FIG. 6

SIMPLIFIED MASS SPECTRA II - BY MEANS OF A DUAL FIELD IONIZATION/ELECTRON IMPACT SOURCE (1)

By: G. G. Wanless and G. A. Glock, Jr.
Analytical Research Division
Esso Research and Engineering Company
P. O. Box 121
Linden, New Jersey 07036

ABSTRACT

Simplified mass spectra, which are advantageous in analyzing mixtures are obtained with a dual field ionization/electron impact source. The degree of simplification is defined and compared with electron impact mass spectra at two levels of cracking pattern severity. Molar sensitivity data are reported for 90 compounds covering 17 classes of aliphatic compounds. Detailed considerations are presented for 3 octadecane isomers, 6 hexadecane isomers and 18 octane isomers. Greater usefulness of primary metastable ions is indicated. They provide a new "cracking pattern" which is not redundant in homologous series. The variation in abundances of these primary metastable ions correlates with simple cleavage rules for mass spectra of isomers. This provides a better means of distinguishing among isomers and in many cases may serve as proof of structure. Specific use of such metastable ions is proposed for analysis of paraffin/olefin mixtures based on conversion of olefins to alkyl thiols.

I. INTRODUCTION

Increased parent ion intensities and decreased fragmentation make possible the detection of many more compounds in unknown mixtures. This paper will show that simplified spectra can be achieved without loss of diagnostic information, by use of field ionization mass spectrometry. This is possible because the conventional electron impact fragmentation peaks are largely replaced with more specific information, contained in primary metastable ion peaks. These latter peaks do not contribute redundant fragmentation in the way that electron impact spectra do, for many organic mixtures.

In an earlier paper on this subject (2) the degree of improvement obtained with two 60° sector electron impact instruments was reported. Some comparison was given also with photoionization spectra. The improvement was demonstrated for 13 classes of aliphatic compounds. In this work, the same compounds, together with additional examples, are used to evaluate spectra obtained from a field ionization source.

The present work was done on an Atlaswerke CH4 mass spectrometer, which was fitted with a prototype dual source (Figs. 1,2). This source can deliver field ionization spectra and electron impact spectra successively, on the same sample charge. /It is appropriate to mention that the basic kinds of mass spectra (e.g., electron impact, field ionization, elektronenanladerung, and ion-molecule reaction spectra (chemical ionization) are frequently complementary. Hence, the advantage of running more than one kind of spectrum on a given sample./

Field ionization mass spectra have been discussed: (a) Based on small radius tips as anode by Inghram and Gomer (3,4,5); Müller (6,11); Beckey and Coworkers (7,8,9,10, 12,13,14,16,20,22,26,27,28); Melmed (15); and Schmidt (21); and (b) using small diameter wires and razor blades as anode by Beckey (17,18,23,25); Robertson (19,24).

Most of the literature studies of compound types are based on spectra from small radius tips. The studies reported here have been made using small diameter platinum wires as anodes. This latter type of anode has given spectra with less fragmentation, in most cases.

In all of the published work, few data have been presented on molar sensitivities of various compounds. This is understandable because the sensitivity values have been very low. Furthermore, sensitivities using wire anodes can be 100-1000 times greater than those obtained with anode tips. Much ion source development work remains to be done, particularly in enhancing the quality of the anode wires. But improvements made in operation of the present dual source now yield useful sensitivity levels. The data demonstrate what will be possible on a consistent basis when the "wire problem" is solved.

II. EXPERIMENTAL SECTION

Instrumental Parameters

(a) The Atlaswerke CH4 mass spectrometer is a versatile 60°, 20 cm.radius instrument which can accommodate several kinds of ion sources. One of these is the prototype dual electron impact/field ionization source which was used for this work. Figure 1 defines the essential dimensions and voltage parameters for it, when used in the field ionization mode.

Figure 1

DUAL ELECTRON IMPACT/FIELD IONIZATION SOURCE

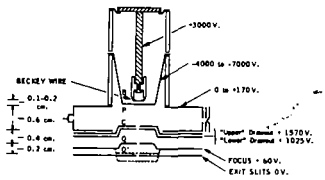

Figure 2

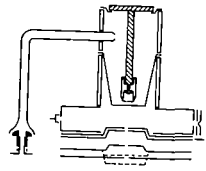

Both of the focus plates are held at the same potential. All of the compounds reported in Table I, with the exception of the octane isomers and alkyl thiols were examined with a field ion cathode potential of -7000 v. These last two series were studied at -5000 Thus, the electrostatic potential between the Beckey-Wollaston wire (anode) and the cathode varied between 8000 and 10,000 volts. If the approximation $F = \frac{V}{r \ln \frac{(R)}{(r)}}$ is accepted, an electrostatic potential V = 10,000 volts is equivalent to a field stress of 1.03×10^7 volts/cm., where $r = 1.25 \times 10^{-4}$ cm. (anode dia.) and R = distance between anode and cathode in cm. (0.3 cm.).

By working at a fixed set of conditions, one discriminates against small paraffin molecules (methane to butane), but the conditions are quite reasonable for the larger paraffins as well as other types of molecules.

Studies on ion gun parameters are incomplete but the above conditions (Fig.1) have contributed to the improved sensitivities given in this report.

(b) A second feature which increases sensitivity is the modified sample inlet line which is shown in Fig. 2. Since the field ion cathode (part P in Fig. 1) is shaped like a thimble, introduction of the sample vapor into the closed space above it increases the sample pressure near the wire. Greater sensitivities result. The combined effect of these two modifications is an increase in average sensitivity by 5- to 6-fold.

Resolving Power of Field Ionization Portion of Dual Source

Under the present conditions, and on a 1% valley basis, the approximate resolving power is:

	Source Exit Slit Width	Collector Slit Width	Resolving Power
1.	0.3 mm	0.9 mm	75
2.	0.1 mm	0.3 mm	180
3.	0.03 mm	0.07 mm	240

Beckey-Wollaston Wires

Most of our work has been done with Beckey-Wollaston platinum wires of about 2.5μ diameter as supplied by the Atlaswerke factory in Bremen, Germany. The lifetime of the wires is quite variable. Some wires have lasted for a month, but many for only half a day. It can be shown (29) that the stresses in these wires approach their breaking strength. Work is under way to obtain more uniformly reliable anode wires.

Conditioning of Beckey-Wollaston Wires

Some kind of conditioning effect does appear to exist. Wires have been observed to increase 50-75 per cent in sensitivity throughout their lifetime. This effect is cancelled out by running a daily n-hexane standard. All data reported were adjusted to a common sensitivity basis using this standard.

Source and Sample System Conditions

The ion source temperature and the one-liter sample bottle and lines were held at 185°C. The Granville-Phillips variable leak was set at "130" on their scale. With these arrangements, a sample charge of 0.00070 ml would yield an average pressure of 5.0×10^{-6} mm Hg. as measured on the Penning gauge in the analyzer tube. This is a convenient operating pressure. No linearity problems have been observed up to a Penning gauge pressure of 2.0×10^{-5} mm Hg.

The sensitivity value of 39000 chart divisions per micro mole of acetone (see Table I) corresponds to a parent ion signal of 1.6×10^{-11} amps at the first dynode of the photomultiplier.

Sensitivity Data

The field ionization sensitivity data presented in the last column of Table I are expressed as chart divisions (0.1 in.) per micromole of sample as charged to the sample system described above. The "wide" Atlas CH4 slits were used; i.e., source exit slit 0.3 mm, and collector slit 0.9 mm. The 20-stage electron multiplier was operated with 240 volts per stage. A filter imposes a series load of 2750 ohms. The Sanborn model 650 oscillograph was used at its standard sensitivity of 4 chart divisions per millivolt.

Adjustments have been made in order to attempt to present the sensitivity data of Table I on a comparable basis (i.e., a field ion cathode potential of -7000 v), even though some of the Beckey-Wollaston wires had to be used at lower field stresses.

"MS-1" Electron Impact Mass Spectra

The electron impact mass spectra reported in Table I (2) were obtained on a 6" radius 60° General Electric mass spectrometer under the following conditions:

Ion gun slit	0.008 in.	Filament to shield	
1st Collimeting slit	0.008 in.	voltage	10 ev.
2nd Collimeting slit	0.008 in.	Ion gun temp..	80°C.
Accel. voltage	1750 v.	Sample system	75°C.
Drawout voltage	1675 v.	Thoria-coated	
Repeller Field	1.5 v/cm.	iridium filament	

Silyl Derivatives

0.005 moles of compound, 0.01 moles of hexamethyl disilazane and 0.01 moles of trimethyl chlorosilane were placed in a sealed Pyrex tube. It was heated in an oil bath to 180°C. After cooling to room temperature the tube was opened and heated once again to 180°C. to remove excess reagents. The residual product was used for the mass spectral sensitivity determination.

III. RESULTS AND DISCUSSION

A. Comparison of field ionization mass spectra with electron impact spectra of aliphatic compounds.

The quality of each spectrum is defined as the ratio of (the parent ion abundance)/(abundance of largest fragment ion above m/e 43 in spectrum). The "gain" for a simpler mass spectrum is obtained by comparing this ratio to the same ratio for the reference spectrum; e.g.,

$$\text{"Gain"} = \frac{\text{Ratio Parent Ion/Fragment Peak (simplified spectrum)}}{\text{Ratio Parent Ion/Fragment Peak (reference spectrum)}}$$

It is traditional to express the parent ion as a percentage of "total ionization," where total ionization is simply the sum of all ions in the spectrum. However, it is not meaningful to do so in this case. This is because (a) fragment peaks m/e 43 and lower cause little interference in interpretation of most spectra and (b) in many cases, most of the fragmentation peaks in field ionization mass spectra are m/e 43 and 29.

Using 17 classes of aliphatic compounds, in Table I, we compare three kinds of mass spectra:

(a) 70 e.v. reference electron impact spectra as published by API Project 44.

(b) Simplified electron impact mass spectra ("MS-1") using modified conditions described in the Experimental Section (2), above.

(c) Field ionization mass spectra using the dual source under modified conditions defined in the Experimental Section, above.

The "MS-1" data in Table I probably represent the best that can be done in improving conventional electron impact spectra. These results are contrasted with a larger improvement using field ionization spectra:

(a) For 12 hydrocarbons in Table I where direct comparisons can be made, the average "gain" compared to the reference spectra was:

1. "MS-1" electron impact - 48X
2. Field ionization - 427X

An example -- n-hexadecane				"Gain"
(A)	API-44	m/e 226/57	= 0.021	
(B)	"MS-1"	m/e 226/71	= 4.0	B/A = 190x
(C)	Field ionization	m/e 226/126.38	= 25.	C/A = 1190x

(b) The "gain" varies widely from one class of compounds to another. For the normal paraffins C_5 to C_{16}, the field ionization "gain" ranges from 57- to 1821-fold.

(c) Molar sensitivities of linear paraffins and olefins generally increase with increasing molecular weight.

(d) Although the sensitivity data presented in Table I are quite useful in a practical way, they are at present about 60-fold lower than one can obtain with the electron impact portion of the dual source, at the same slit settings, and 70 e.v., using 18μ A trap current.

B. Greater usefulness of metastable ions

(1) Paraffins and isoparaffins

In Table I, it will be noticed that the largest fragment peak above m/e 43 in the field ionization spectra, is frequently that of a primary metastable ion. For example, in n-hexadecane the largest such fragment peak is m/e 126.38, which corresponds to the loss of 57 mass units from the parent ion.

Since the "regular" fragment peaks of nominally unit mass numbers above m/e 57 are usually small, the field is left relatively clear up to the parent ion, to be inhabited by the "primary" metastable ions. These abundant primary metastable ions will be most useful in identifying isomeric species.

The abundances of the metastable ions, relative to 100 chart divisions of parent ion, are given for n-hexadecane in Table II, for (a) field ionization and (b) electron impact 70 e.v., 18μ A spectra. These data were obtained using the two portions of the dual source, successively, with the same slit settings. At least 12 primary metastable peaks are obtained in a clear area of the spectrum of n-hexadecane above m/e 70 in the field ion spectrum. It will be shown by means of Table III that these primary metastables are specific for a given mass number in the paraffin series and will not be redundant in an homologous series. Furthermore, the relative abundances of these primary metastable ions will vary with the structure of the isomers, and will identify with the "cracking patterns" based on simple cleavage rules.

Thus, we obtain a new "cracking pattern" which is reflected in the relative abundances of the primary metastable ions. The advantage over electron impact spectra is that these new cracking patterns are specific and will not become additive in an homologous series of compounds.

For paraffins there are two principal series which may be defined as P-15 and P-16; i.e.,

P-15, P-29, P-34 ----- and
P-16, P-30, P-44 -----

Table III gives the exact location of these ions in a "metastable map," together with the relative abundances per 100 chart divisions of parent ions. Although the abundances apply to the normal paraffins, the location of the metastable ions will be the same for all isomers of a given molecular weight.

Briefly, the normal paraffins give a very broad distribution of primary metastable ion intensities. By comparison, the abundances of primary metastable ions in isomers vary greatly - the most predominant of such ions correlating with the "expected" modes of fragmentation.

How this new information can be used to distinguish among isomers will be seen in Table IV, which compares the field ionization spectra of three isomers of octadecane and six isomers of hexadecane. It will be observed that the location of a given set of metastable ions, e.g., P-15 (18) .... for the octadecanes and P-15 (16) .... for the hexadecanes never overlap. But for a given molecular weight (i.e., several isomers) the abundances of these primary metastable ions vary. This idea is grasped better from Fig. 3, where the data on the three octadecane isomers are presented in graphical form. It provides a new means of distinguishing among isomers, which may serve as proof of structure for many larger molecules.

(2) Olefins and Thioalkyls

The dominant processes which yield primary metastable ions in field ionization mass spectra of olefins (31) are:

P-28, P-42, P-56 ----, and
P-29, P-43, P-57 ----

The location of these metastable ions and their relative abundances for normal olefins up to 1-hexadecene, are given in Table VI.

Comparison of the positions of these metastable ions with those of metastable ions in paraffins (Table III), will show that the separation between certain ions can be as small as 0.22 atomic mass units. This would make it difficult to assay olefin isomers in the presence of paraffin isomers.

However, it turns out that the dominant metastable ion-producing processes in alkyl thiols are P-32 and P-34 (i.e., P-S and P-H_2S). Their locations and the abundances for C_1-C_{18} normal alkyl thiols are listed in Table VII. A comparison of the positions of these ions with the metastable ions of paraffins (Table III) will show the following distances of closest approach:

Major Primary Metastables		Minor Primary Metastables	
P-34 in RSH and P-29 in Par.		P-32 in RSH and P-30 in Par.	
4.83 to 2.47 a.m.μ		0.43 to 0.97 a.m.μ	
e.g., P-29 (n-pentane)	25.68	P-30 (n-octadecane)	197.54
P-34 (n-propylthiol)	23.21	P-32 (n-hexadecylthiol)	197.97
	Δ= 2.47		Δ= 0.43

These are the most unfavorable cases. The situation improves with increasing molecular weight. So also do the abundances. In the case of n-hexadecane thiol, the metastable ion at m/e 194.48 is 86% of the height of the parent ion.

This approach may be of practical use in a very common problem; i.e., the assaying of paraffin/olefin mixtures, without prior chromatographic separation.

IV. SUMMARY AND PRESENT STATUS

1. Significant improvement in sensitivity levels have been made for field ionization mass spectra obtained with Beckey-Wollaston wires.

2. A principal problem is to improve the reliability of these anode wires, and work on this problem is under way.

3. Paraffins, olefins and alkyl thiols are discussed in some detail. Attention is drawn to the usefulness of the metastable ions in distinguishing among isomers. To some extent this will be possible even in mixtures. Thus, the diagnostic information lost because of the absence of the conventional cracking patterns is replaced with more specific structural information contained in the location and abundances of the metastable ions. The new information does not become redundant in homologous series of paraffins.

In many cases the specificity of these new data will probably serve as proof of structure.

TABLE I

SIMPLIFIED MASS SPECTRA OF ALIPHATIC COMPOUNDS

A Comparison With API-44 Reference Spectra

	Compound	(A) API-44	(B) MS-1(b)	"Gain" B/A(d)	(C) Dual Field Ion Source(b) Ratio(a)		"Gain" C/A(d)	Field Ion Sensitivity(c)
(1)	Propane	1.3(a)	--	--	44/0	--	--	55.
(2)	n-Butane	5.1	--	--	58/0	--	--	55.
(3)	n-Pentane	0.70	--	--	72/43	≈40	*57x*	1100.
(4)	n-Hexane	0.14	0.90	*6.4x*	86/57	91.	*645x*	1700.
(5)	n-Heptane	0.27	1.05	*3.9x*	100/50.50	35.	*129x*	2800.
(6)	n-Octane	0.20	0.62	*3.1x*	114/63.40	8.9	*44x*	1950.
(7)	n-Nonane	0.095	--	--	128/76.50	12.	*126x*	2000.
(8)	n-Decane	0.075	1.16	*15x*	142/90.49	17.	*227x*	2050.
(9)	n-Undecane	0.045	--	--	156/103.39	26.	*578x*	2600.
(10)	n-Dodecane	0.082	--	--	170/94.88	29.	*353x*	2950.
(11)	n-Tridecane	0.053	--	--	184/108.05	33.	*623x*	3550.
(12)	n-Tetradecane	0.028	--	--	198/143.95	51.	*1821x*	4700.
(13)	n-Hexadecane	0.021	4.0	*190x*	226/126.38	25.	*1190x*	5500.
(14)	n-Octadecane	0.010			254/152.79	22.	*2200x*	3300.
(15)	Neopentane	0.0001	0.0064	*64x*	72/57	0.0063	*63x*	8.3
(16)	2,2 di me butane	0.0006	0.0073	*12x*	86/57	0.025	*42x*	82.
(17)	2,3 di me butane	0.23	0.26	*1.1x*	86/58.65	14.	*60x*	200.
(18)	3,3 di me pentane	0.0015	0.015	*100x*	100/71	0.014	*92x*	114.
(19)	2 me heptane	0.067	--	--	114/85.97	4.8	*72x*	600.
(20)	3 me heptane	0.045	--	--	114/57	2.3	*51x*	950.
(21)	4 me heptane	0.059	--	--	114/71	9.0	*152x*	1550.
(22)	3 ethyl hexane	0.057	--	--	114/61.89	7.7	*135x*	900.
(23)	2,3 di me hexane	0.027	--	--	114/71	3.2	*110x*	1700.
(24)	2 me, 3 ethyl pentane	0.025	--	--	114/71	2.6	*104x*	1450.
(25)	2,4 di me hexane	0.023	--	--	114/57	2.9	*128x*	800.
(26)	2,5 di me hexane	0.048	--	--	114/110	2.42	*50x*	800.
(27)	3,4 di me hexane	0.022	--	--	114/57	1.9	*86x*	500.
(28)	2,3,4 tri me pentane	0.0054	--	--	114/71	0.46	*85x*	65.
(29)	2,2 di me hexane	0.0003	--	--	114/57	0.03	*100x*	85.
(30)	3,3 di me hexane	0.0002	--	--	114/71	0.03	*143x*	25.
(31)	2,2,3 tri me pentane	0.0003	--	--	114/57	0.01	*33x*	70.
(32)	3 me, 3 ethyl pentane	0.0002	--	--	114/85	0.02	*100x*	35.
(33)	2,2,4 tri me pentane	0.0002	--	--	114/57	0.02	*100x*	70.
(34)	2,3,3 tri me pentane	0.0002	--	--	114/71	0.01	*50x*	90.
(35)	2,2,3,3 tetra me butane	0.0002	--	--	114/57	0.0056	*28x*	2.5
(36)	2 me pentadecane	0.006	--	--	226/148.15	1.5	*250x*	1120.
(37)	7 n propyl tridecane	0.19	--	--	226/148.40	3.6	*19x*	1140.
(38)	5,8 di ethyl dodecane	0.0014	--	--	226/70	6.0	*4286x*	2000.
(39)	5 ethyl, 5n propyl undecane	0.0	--	--	226/169	0.06	--	45.
(40)	2,2,4,4,6,8,8 heptamethyl nonane	--	--	--	226/57	0	--	--
(41)	2 me heptadecane	0.0064	--	--	254/175.28	1.0	*156x*	950.
(42)	4,9 di n propyl dodecane	0.00007	--	--	254/175.28	1.7	*24000x*	1300.
(43)	Propylene	0.69	--	--	42/41	21.3	*31x*	3600.
(44)	1-Butene	0.41	--	--	56/55	18.6	*45x*	6000.
(45)	1-Pentene	0.51	--	--	70/69	55.5	*109x*	6550.
(46)	1-Hexane	0.33	--	--	84/56	18.	*55x*	2250.
(47)	1-Heptane	0.19	--	--	98/57	6.7	*35x*	1500.
(48)	1-Octene	0.14	--	--	112/56	7.1	*51x*	1400.
(49)	1-Nonene	0.10	--	--	126/56	7.5	*75x*	1400.
(50)	1-Decene	0.083	3.10	*37x*	140/88.03	9.3	*112x*	1500.
(51)	1-Undecene	0.11	--	--	154/101.46	9.4	*85x*	1300.

TABLE I - cont'd

	Compound	(A) API-44	(B) MS-1(b)	"Gain" B/A(d)	(C) Dual Field Ion Source(b) Ratio(a)		"Gain" C/A(d)	Field Ion Sensitivity(c)
(52)	1-Dodecene	0.028	--	--	168/56	8.3	296x	1400.
(53)	1-Tetradecene	0.053	4.2	72x	196/56	11.0	208x	1800.
(54)	1-Hexadecene	0.016	--	--	224/171.50	13.8	862x	2050.
(55)	3,3 di me-1-pentene	0.09	1.06	12x	98/69.00	3.6	40x	1050.
(56)	Cyclopentene	0.43	--	--	69/68	30.	70x	450.
(57)	Cyclohexene	0.39	--	--	96/70.50	111.	285x	1750.
(58)	Cyclooctene (e)	0.31	--	--	110/55	46.	148x	4300.
(59)	1,3 Cyclo-octadiene (e)	0.40	--	--	108/80.17	71.	177x	2350.
(60)	1,5 Cyclo octadiene (e)	0.061	--	--	108/59.42	13.	213x	700.
(61)	1-Pentyne	0.17	0.34	2.0x	68/66	0.5	3.0x	150.
(62)	2-Pentyne	1.1	2.9	2.6x	68/67	21.	19.x	1600.
(63)	Acetal	1.8	--	--	44/43	53.	30x	600.
(64)	Propanal	3.5	22.1	6.3x	58/56	111.	32x	1100.
(65)	Acetone	14.	46.	3.3x	58/43	1333.	95x	39000.
(66)	Methy ethyl ketone	2.9	6.3	2.2x	72/55	455.	157x	32300.
(67)	3-Heptanone	0.08	2.0	25x	114/63.43	50.	625x	6000.
(68)	Diethyl ether	0.65	2.1	3.3x	74/73	56.	86x	250.
(69)	1-Decanol	0.00035	0.40	1140x	158/124.37	0.11	310x	4.2
(70)	Silyl ether of 1 decanol (f)(g)	2.0	22.7	11.4x	215/161.07	18.	9x	2500.
(71)	Henanoic acid	0.0004	--	--	117/99	2.7	6700x	19.
(72)	Silyl ether of 1-hexanoic acid (f)(g)	0.18	--	--	173/73	2.4	13x	74.
(73)	1-Decanoic acid (e)	0.094	0.512	5.4x	172/97	11.3	112x	280.
(74)	Silyl ether of 1-Decanoic acid (f)(g)	1.5	--	--	244/73	1.04		2350.
(75)	1-Hexane nitrile	0.011	0.43	39x	98/68	0.83	75x	3650.
(76)	Succinonitrile (e)	0.14	0.75	5.2x	81/75.5	200.	1389x	2550.
(77)	1-Bromohexane (e)	0.046	0.20	4.4x	164/85	0.61	13x	167.
(78)	2-Bromohexane (e)	0.0012	0.0051	4.3x	164/85	0.0051	4.3x	29.
(79)	3-Bromohexane (e)	0.0026	0.012	4.6x	164/85	0.0033	1.3x	16.
(80)	Ethyl thiol (f)	1.2	--	--	62/61	18.	15x	4800.
(81)	n-Propyl thiol (f)	0.70	--	--	76/75	59.	84x	3900.
(82)	n-Butyl thiol (f)	0.54	--	--	90/88.6	11.	20x	4900.
(83)	n-Pentyl thiol (f)	0.69	--	--	104/102.5	10.	14x	4900.
(85)	n-Hexyl thiol (f)	0.25	--	--	118/59.80	11.	42x	5400.
(85)	n-Heptyl thiol (f)	0.35	--	--	132/72.76	4.4	13x	4600.
(86)	n-Octyl thiol (f)	0.14	--	--	146/85.92	3.8	27x	3600.
(87)	n-Nonyl thiol (e)	0.20	--	24x	160/99.23	4.6	23x	2900.
(88)	n-Decyl thiol (f)	0.03	--	--	174/112.64	2.6	87x	1600.
(89)	n-Dodecyl thiol (f)	0.022	--	--	202/139.72	1.6	73x	900.
(90)	n-Tetradecyl thiol (f)	0.016	--	--	230/167.03	1.4	88x	1100.
(91)	n-Hexadecyl thiol (f)	0.012	--	--	258/194.48	1.2	100x	1300.
(92)	n-Decylamine (f)	0.025	--	--	158/56	16.1	640x	1180.

(a) The parameters reported are the ratios of the parent ion divided by the largest fragment ion above m/e 43.
(b) Conditions defined in Experimental Section.
(c) Sensitivities given in chart divisions per micromole. See Experimental Section for details of inlet system.
(d) "Gain" defined in detail in Results and Discussion (I).
(e) Uncertified mass spectrum. Origin will be provided by authors.
(f) Esso Research spectrum.
(g) See experimental Section for preparation.

4. A possible solution to the analysis of paraffin/olefin mixtures is proposed, based on conversion of the olefins to alkyl thiols.

5. It is probably that the relative abundances of the metastable ions can be increased by reducing their residence time in the ion source, and possibly in certain cases, their shape may be improved. Such experiments are planned.

V. ACKNOWLEDGMENTS

It is a pleasure to acknowledge communications with Prof. E. W. Müller, Prof. H. W. Beckey and Prof. L. Herzog and his staff. We are indebted to Mr. M. J. O'Neal and the Shell Oil Company for the gift of two isomers of hexadecane, and to Prof. Joseph Dixon, Director of American Petroleum Institute Project 42, Pennsylvania State University, for other pure compounds used in this work.

VI. REFERENCES

(1) Part of this work was presented at the Fourteenth Annual Conference on Mass Spectrometry and Allied Topics, Dallas, Texas, May 25, 1966.
(2) "Simplified Mass Spectra," presented at 12th Annual Conference on Mass Spectrometry and Allied Topics, McGill University, Montreal, Canada, June 12, 1964. Copy available from authors.
(3) M. G. Inghram and R. Gomer, J.Chem. Phys., 22, 1279 (1954).
(4) R. Gomer and M. G. Inghram, J.A.C.S., 77, 500, (1955)
(5) M. G. Inghram and R. Gomer, Z. Naturforschg. 10a, 863 (1956)
(6) E.E.Müller and K. Bahadur, Phys. Rev. 102, 624 (1956)
(7) H.D. Beckey, Naturwiss, 45, 259 (1958)
(8) H.D. Beckey, Z. Naturforschg. 14a, 717-21 (1959)
(9) H.D. Beckey and W. Groth, Z. Phys. Chemie (NF) 20, 307-12 (1959)
(10) H.D. Beckey, Z. Anal. Chemie, 170, 358-364 (1959)
(11) E.W. Müller, "Field Ionization and Field Ion Microscopy," in Advances in Electronics and Electron Physics, XIII (1960)
(12) H. D. Beckey and D. Schütte, Z. Instrumentenkunde 68, 302-307 (1960)
(13) H.D. Beckey, Z. Naturforschig., 16a, 505-510 (1961)
(14) H.D. Beckey, ibid, 17a, 1103-1111 (1961)
(15) A.J. Melmed, J. Chem. Phys., 38, 607-612 (1962)
(16) H.D. Beckey and G. Wagner, Z. Anal. Chemie, 197, 58-80 (1963)
(17) H.D. Beckey, Z. Anal. Chemie, 197, 80-90 (1963)
(18) H.D. Beckey, Z. Instrumentenkunde, 71, 51-54 (1963)
(19) A.J.B. Robertson, B.W. Viney, and M. Warrington, Brit. J. Appl. Phys., 14, 278-283 (1963)
(20) H.D. Beckey, Z. Naturforschg. 19a, 71-83 (1964)
(21) W.A. Schmidt, ibid, 19a, 318-327 (1964)
(22) H.D. Beckey, Bull. Soc. Chem. Belg., 73, 326-356, (1964)
(23) H.D. Beckey, H. Knöppel, G. Metzinger and P. Schulze, Advances in Mass Spectrometry III (1966) 35
(24) A.J.B. Robertson, Advances in Mass Spectrometry, III (1966) 23
(25) H.D. Beckey, Z. Anal. Chemie, 207, 99-104 (1965)
(26) H.D. Beckey and G. Wagner, Z. Naturforschg., 20a, 1329-1335 (1965)
(27) H.D. Beckey and P. Schulze, ibid, 20a, 1329-1335 (1965)
(28) H.D. Beckey and P. Schulze, ibid, 20a, 1335-1344 (1965)
(29) T. Harrett, J. Sci., Inst. 42, 584-590 (1965)
(30) A photographic representation of the excellent shape of some field ionization metastable ions will be found in the spectrum of 1-decene. See reference (28), p. 1343.

NOTE: Section III (2) The 18 Octane Isomers has been left out due to lack of space.

TABLE II

METASTABLE IONS OF n-HEXADECANE

Fragmentation Process	m/e	Electron Impact(2)	Field(1) Ionization	Fragmentation Process	m/e	Electron Impact(2)	Field(1) Ionization
	226	100.	100.				
P-29	171.22	2.1	2.5		46.68	3.5	--
-30	169.98	--	0.6		45.55	1.8	--
P-43	148.18	3.1	3.5		44.64	15.	
-44	146.57	1.1	0.97		39.73	8.	--
					39.16	17.	--
P-57	126.38	--	4.1		38.23	7.8	--
-58	124.88	--	1.4		37.25	4.1	--
					36.48	3.1	--
P-71	106.31	3.4	3.1		35.83	2.5	--
-72	104.94	2.0	0.97		34.47	1.0	--
					33.73	1.8	--
	100.93	2.0	--		32.93	18.	--
					31.17	0.88	--
P-85	87.97	5.2	1.8				
-86	86.73	1.5	0.87		29.52	7.3	--
					27.62	1.0	--
	75.64	3.4	--		26.07	15.	--
	74.82	2.0	--		25.16	1.7	--
					24.39	1.5	--
P-99	71.37	--	0.63		21.78	2.4	--
-100	70.25	--	0.29				
					16.95	2.3	--
	63.27	1.8	--		15.30	0.56	--
	61.80	2.4	--		14.77	0.31	--
	60.00	2.4	--				
	51.21	6.1	--				
	50.03	4.9	--				

(1) Conditions defined in Experimental Section
(2) Electron impact portion of dual source; 70 ev., 229°C, 18 μA Trap current.

Figure 3

FIELD IONIZATION MASS SPECTRA OF OCTADECANE ISOMERS SHOWING ABUNDANCES OF PRIMARY METASTABLE IONS

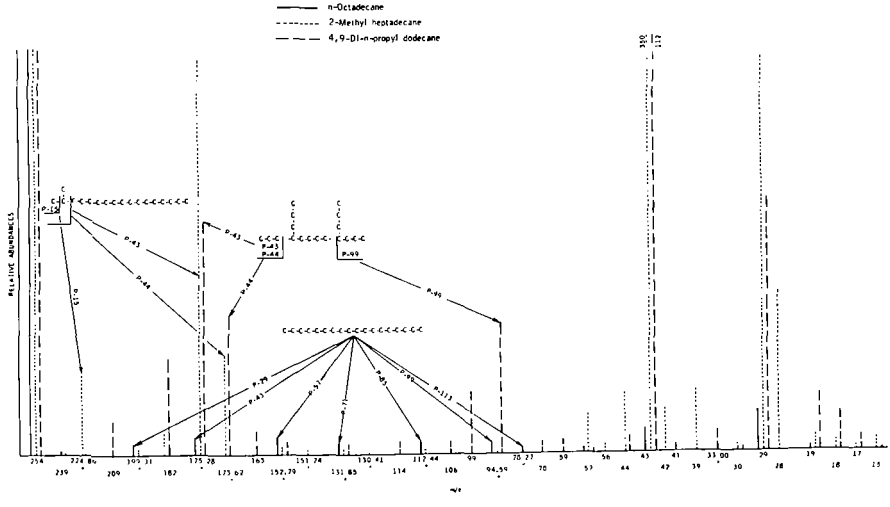

TABLE IV -- Field Ionization Mass Spectra of Isomers of Octadecane and Hexadecane - Showing Abundances of Primary Metastable Ions - as a Percentage of Parent Ion Abundance

Probable Process	m/e	n-Octadecane	2 me heptadecane	4,9 di n-pr. dodecane	n-Hexadecane	2 me pentadecane	7 n propyl tridecane	5 Ethyl 5 n propyl undecane	5,8 diethyl dodecane	2,2,4,4,6,8,8 Heptamethyl nonane
	254	100.	100.	100.		100.				
	239	1.7	0.9							
	226				100.		100.	5.8	100.	0.
P-15(18)	(3)224.89		20.	0.4						
	211					1.4				0.8
	210									
	(3)209.30			8.8					9.5	
	202					3.5				
P-29(18)	(3)199.31	2.9	1.6							
P-30(18)	(3)197.54									
P-15(16)	(3)197.00					14.		99.(2)		
	196								8.3(1)	
	195					1.4				
	183							99.		
	182		6.0	24.					14.R(1)	
P-43(18)	(3)175.28	4.2	97.	58.						
P-44(18)	(3)173.62		25.	35.						
P-29(16)	(3)171.72				2.5		2.2		60.	
P-30(16)	(3)169.98				0.6		1.9		33.	
	169							100.		
	163			6.3						
	156							3.3		
	155									5.
P-57(18)	(3)152.79	4.6	1.9	3.4						
	152					14.				
P-58(18)	(3)151.24		0.9							
P-43(16)	(3)148.18				3.5	68.	28.			
P-44(16)	(3)146.57				1.0	24.	28.			
	141							99.	4.8	
P-71(18)	(3)131.85	3.3	1.7	2.5						
P-72(18)	(3)130.41		0.7							
P-57(16)	(3)126.38				4.1	0.7	1.9		21.	
P-58(16)	(3)124.88				1.4		2.2			
	114			3.6					24.R	
	113								11.	
P-85(18)	(3)112.44	3.3	1.3							
	112					0.7				
P-71(16)	(3)106.31				3.1	0.9	0.7			
	106			3.6						
P-72(16)	(3)104.98				1.0		1.1			
	99			16.						
P-99(18)	(3) 94.59	2.9	0.8	33.						
	90					0.6				
	(3) 88.15					0.7		3.3		
P-85(16)	(3) 87.97				1.8		2.2			
P-86(16)	(3) 86.73				0.9		7.9			
	85							4.9		
P-113(18)	(3) 78.27	1.3								
	72								7.2R	
P-99(16)	(3) 71.37				0.6	0.6				
	71									6.4
P-100(16)	(3) 70.20				0.3					
	70			3.1		0.6			4.8	1.1
	(3) 69.57							3.3		
	59			3.8						
	58						4.9R			3.9
	57	1.3	4.7	0.6	4.8	2.8		25.	9.5	100.
	56		2.0			1.1				6.7
	44		15.	4.4		10.	1.2			
	43	4.6	350.	112.	8.2	333.	12.	16.	7.2	0.6
	42			11.		5.6				3.3
	41	1.7				1.4		8.2	4.8	0.6
	39	15.4				14.		82.	9.1	4.7
	(3) 33.00			3.6						
	30		2.4	1.3	0.9	1.1	1.2			

TABLE IV - continued

Probable Process	m/e	n-Octa-decane	2 me hepta-decane	4,9 di n-pr. dode-cane	n-Hexa-decane	2 me penta-decane	7 n propyl tri-decane	5 Ethyl 5 n propyl undecane	5,8 diethyl dodecane	2,2,4,4,6,8,8 Hepta-methyl nonane
	29	5.4	97.	63.	35.	32.	45.	16.	4.8	0.6
	28		40.			13.				
	(3) 23.10					2.1				
	19	1.3	4.0	14.		5.6		3.3		1.1
	18		2.7	10.		1.4				
	17		1.3	4.4						
	15		3.7	1.0		1.1				

(1) R = rearrangement ion
(2) Not a metastable ion in this case.
(3) Denotes metastable ion

TABLE III

FIELD IONIZATION METASTABLE MAP FOR PARAFFINS(1)

(Primary metastable ions only)

Probable Process	C_3	C_4	C_5	C_6	C_7	C_8	C_9	C_{10}
P-15		31.88-4.2	45.13-0.51					
-16		30.41-2.3	43.56-0.22					
-29			25.68-0.29	37.78-1.7	50.41-2.9	63.38-11.2	76.57-8.3	89.92-5.8
-30			24.50-1.5	36.47-2.8	49.00-2.4	61.89- 3.4	75.03-2.0	88.34-1.3
-43							56.45-3.7	69.02-4.5
-44							55.13-1.7	67.63-1.7
-57								50.88-1.1
-58								49.69-0.73

Probable Process	C_{11}	C_{12}	C_{13}	C_{14}	C_{15}	C_{16}	C_{18}
P-29	103.39-3.8	116.95-3.0	130.57-2.8	144.25-2.0		171.72-2.5	199.31-2.9
-30	101.77-0.83	115.29-0.85	128.89-0.6	142.55-0.51		169.98-0.6	197.54-
-43	81.85-3.8	94.88-3.4	108.05-3.0	121.34-2.7		148.18-3.5	175.28-4.2
-44	80.41-1.3	93.39-1.1	106.52-1.0	119.77-0.72		146.57-0.72	173.62-
-57	62.83-1.9	75.11-2.3	87.66-2.8	100.41-2.7		126.38-4.1	152.79-4.6
-58	61.56-0.94	73.79-1.1	86.28-1.0	98.99-0.90		124.88-1.4	151.24-
-71		57.66-0.85	69.39-1.3	81.46-1.6		106.31-3.1	131.85-3.3
-72		56.49-1.1	68.17-1.1	80.16-0.72		104.94-0.97	130.41-
-85				64.49-0.44		87.97-1.8	112.44-3.3
-86				63.35-0.18		86.73-0.87	111.12-
-99						71.37-0.63	94.59-2.9
-100						70.25-0.29	93.37-
-113							78.27-1.3
-114							77.17-

TABLE VII

FIELD IONIZATION PRIMARY METASTABLE MAP FOR ALKYL THIOLS(1)

Probable Process	C_3	C_4	C_5	C_6	C_7	C_8	C_9
P-32	-	-	-	62.86-2.0	75.76- 5.5	89.01- 5.2	102.40-
-34	23.21-0.20	34.84-0.83	47.12-1.9	59.80-9.4	72.76-22.8	85.92-26.1	99.23-21.7

Probable Process	C_{10}	C_{11}	C_{12}	C_{13}	C_{14}	C_{15}	C_{16}	C_{18}
P-32	115.89- 7.2		143.07-13.5		170.43-37.3		197.97-15.	
-34	112.64-38.6		139.72-61.5		167.03-69.5		194.48-85.7	222.04-

(1) The locations of metastables apply to all isomers of a given molecular weight. The abundances reported are for normal paraffins and 1-alkyl thiols respectively, relative to 100 chart divisions of parent ions.

A MASS SPECTROGRAPH WITH VERY LARGE DISPERSION

H. Matsuda, S. Fukumoto and Y. Kuroda
Institute of Physics, College of General Education
Osaka University, Toyonaka, Osaka, Japan
and
M. Nojiri
Japan Electron Optics Laboratory
1418 Nakagamicho, Akishimashi, Japan

I want to describe our new mass spectrograph with very large mass dispersion. At the Mainz Conference in 1956, Prof. Ogata and I described the large mass spectrograph at Osaka University. With that instrument, the maximum resolving power of about 900,000 had been obtained.[1] But, unfortunately, it was destroyed by the flooding of the laboratory in 1961. Since then, we were planning to construct a new type of mass spectrograph which has much higher resolution.

About three years ago, I proposed a new method which might provide a high resolution and a high mass dispersion without requiring very large linear dimensions.[2][3] The essential feature of this method is to use a mass dispersing field which has no lens action. I will describe the principle briefly.

Fig. 1(b) shows an ordinary sector type mass spectrometer. The uniform magnetic field has focusing and dispersive actions simultaneously. If it is divided in two at the point where ion beams become parallel, then the source and the image are located at the respective focal points of the divided sector fields. Let the focal lengths be f_1 and f_3, then the dispersion D at the image is given by:

$$D = \left(\frac{a}{f_1} + \frac{a}{f_3}\right) f_3\delta',$$

where a is the mean radius and $\delta' = \gamma + \beta$, γ and β are fractions of mass and velocity respectively.

Now, suppose we separate these two fields and insert a dispersing field in between them as shown in Fig. 1(c). This arrangement of the fields is quite analogous to the optical prismatic spectrograph shown in Fig. 1(a). Separated fields act as the focusing lenses, so we can call them the focusing fields. The dispersing field is the field which has no lens action but has the dispersive action. It is realized by the magnetic field in which the field strength varies in inverse proportion to radius. The dispersing angle of it is given by $\Phi_2\delta'$, where Φ_2 is the deflecting angle.

The total dispersion at the image is given by:

$$D = \left(\frac{a}{f_1} + \frac{a}{f_3} + \Phi_2\right) f_3\delta'$$

Accordingly, comparing with the ordinary case, the dispersion increases by $\Phi_2 f_3\delta'$. The magnification of the image is given by f_3/f_1, and is the same as before. If f_1, f_3 and Φ_2 are large, very large dispersion and resolution can be expected. For example, if the separated fields are homogeneous magnetic fields of 30°, and the inserted field is an inverse radius magnetic field of 180°, then an approximate fourfold increase in both dispersion and resolution is expected. Nevertheless, the total size of the whole apparatus will not become too large. Since the dispersive action does not depend on the radius, the dispersing field may be chosen to be much smaller than the focusing fields.

In order to get high resolving power for a mass spectrograph, the apparatus should be a double focusing one. Therefore, let the first focusing field be an electric field with opposite deflection. A toroidal

electric field is suitable because the velocity dispersing angle which must be compensated is very large. If a toroidal electric field, an inverse radius magnetic field and a homogeneous magnetic field are arranged in tandem, the first order double focusing condition is given by

$$\frac{2}{K_e} \sin K_e \Phi_e = \Phi_{m_2} + \sin \Phi_{m_3},$$

where suffices e and m indicate electric and magnetic fields respectively. When this condition is satisfied, the mass dispersion at the image point is given by

$$D_m = \frac{a_{m_3}}{2} \left(1 + \frac{\Phi_{m_2}}{\sin \Phi_{m_3}}\right) \gamma,$$

and the resolving power by

$$R = \frac{a_e}{K_e^2 s}.$$

Fig. 2 shows the ion path and the parameters of the apparatus. The mean radii of those three fields are 30cm, 22cm and 120cm respectively. The total ion path is about 6.5m. The pole boundaries of the dispersing magnet are made curved in order to get the second order focusing. The effect of the longitudinal focusing is also considered. The mass dispersion perpendicular to the ion beam is calculated to be 4.75cm for 1% mass difference and the magnification of the image to be 1.01. If the width of the source slit is taken to be 4μ, the maximum resolution of about 1.2 million may be expected. The angle between the direction of focusing beam and the image curve is calculated to be about 23° for directional focusing and 17° for velocity focusing. The inclination of the photographic plate is chosen to be 20°, so the mass dispersion on the photographic plate is expected to be about 14cm for 1% mass difference.

Fig. 3 is the schematic drawing of the apparatus constructed. All vacuum chambers are made of stainless steel, and 6 oil diffusion pumps with liquid nitrogen traps and 2 ion getter pumps are used for evacuation. The vacuum during operation was estimated to be 1 - 3 x 10^{-7}Torr measured with ionization gauges.

As a preliminary test, potassium 39 thermal ions accelerated to about 14.5kV were used. The potential between the electrodes of the toroidal condenser was supplied from the layer dry batteries grounded at the center. The total voltage of the batteries was able to be set at several different values around 1776V. The exciting current for the dispersing magnet is finely adjusted so that the ion beam passes along the calculated orbit. The beam position in the magnetic field can be traced by means of the monitor electrodes which can be inserted at three different points along the ion path.

A collector slit is placed at the top of the plate holder in the camera chamber. By setting the position of the collector slit in the beam plane, ions can be detected by means of a 15-stage electron multiplier. A small Helmholtz coil is placed between the focusing magnet and the camera in order to sweep an ion beam across the collector slit. The exciting current for the focusing magnet is adjusted so that a pattern on an oscilloscope is located at the desired position.

There are two auxiliary electrodes placed above and below the gap of the condenser electrodes as shown in Fig. 4. The potential applied to them can be varied continuously around the ground potential. By these adjustments the shape of the field between condenser electrodes may be slightly varied, so that the fine adjustment for final focusing can be easily done. This adjustment is carried out by observing the pattern on the oscilloscope.

When exposures are made, the potentials applied to the condenser electrodes and also the accelerating voltages are slightly shifted for

each succesive exposure while keeping the magnetic fields constant, so that several spectral lines are photographed in one exposure series. The shifted potential was about 1.1 volt. Fig. 5 shows the artificial multiplet thus obtained. The spectral lines in Fig. 5 may correspond to mass numbers 1774, 1775 and 1776 respectively. The distance between lines was about 9mm, and the line width was measured to be 12 microns, so that the resolving power is estimated to be about 1.2 million. Very high resolving power can be obtained by the method described here.

References

1. K. Ogata and H. Matsuda, Z. Naturforschung, 10a, 843 (1955).
2. H. Matsuda, Mass Spectroscopy (Japan), 11, 127 (1964).
3. H. Matsuda, S. Fukumoto, Y. Kuroda and M. Nojiri, Z. Naturforschung, 21a, 25 (1966).

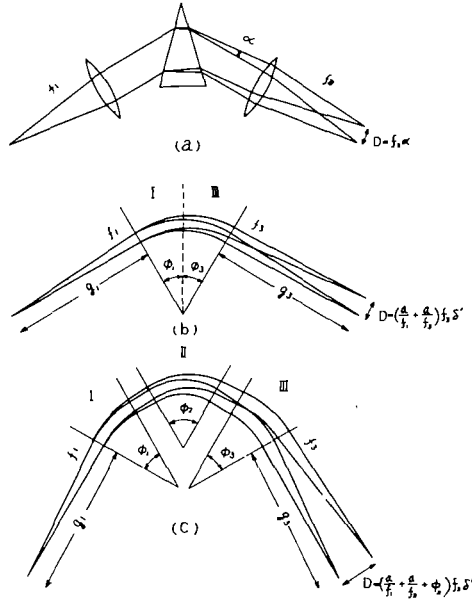

Fig. 1

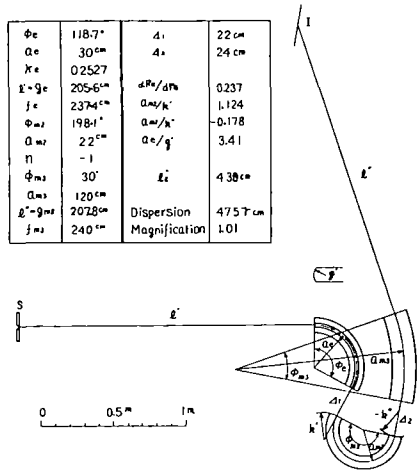
Φe 118.7°
ae 30cm
Xe 0.2527
ℓ'-ge 205.6cm
fe 237.4cm
Φm2 198.1°
am2 22cm
η -1
Φm3 30°
am3 120cm
ℓ''-gm3 207.8cm
fm3 240cm
Δ1 22cm
Δ2 24cm
dΦe/dΦm 0.237
am2/k' 1.124
am3/k'' -0.178
ae/g' 3.41
ℓ'' 438cm
Dispersion 475.7cm
Magnification 1.01
I
ℓ'
S
ℓ'
0
0.5m
1m

Fig. 2

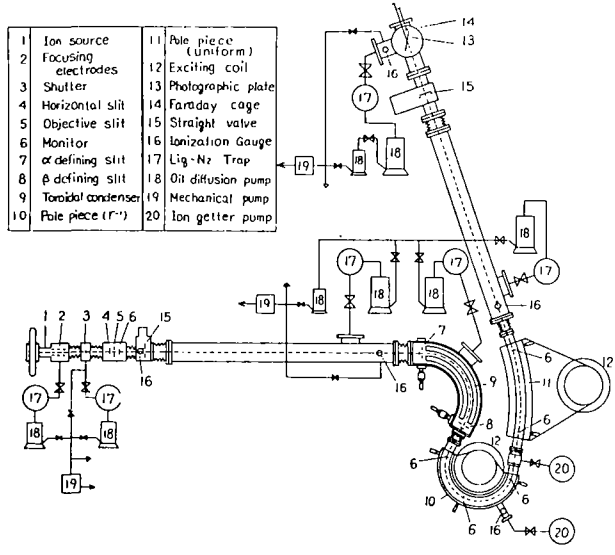
1 Ion source
2 Focusing electrodes
3 Shutter
4 Horizontal slit
5 Objective slit
6 Monitor
7 α defining slit
8 β defining slit
9 Toroidal condenser
10 Pole piece (Γ⁻¹)
11 Pole piece (uniform)
12 Exciting coil
13 Photographic plate
14 Faraday cage
15 Straight valve
16 Ionization Gauge
17 Liq.-N2 Trap
18 Oil diffusion pump
19 Mechanical pump
20 Ion getter pump

Fig. 3

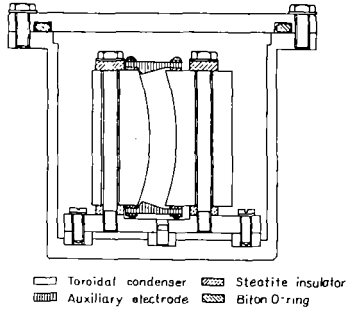
Toroidal condenser
Steatite insulator
Auxiliary electrode
Biton O-ring

Fig. 4

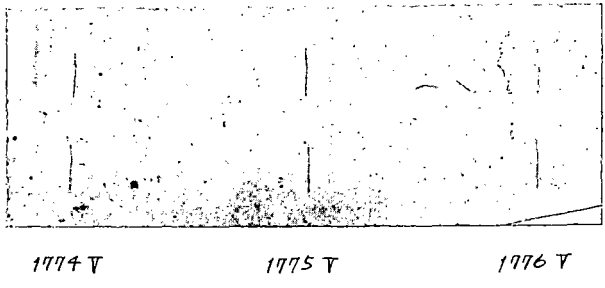
1774 V
1775 V
1776 V

Fig. 5

"A NEW COMMERCIAL DOUBLE FOCUSING MASS SPECTROMETER/SPECTROGRAPH WITH A MATTAUCH - HERZOG OPTICS DESIGN"

J. Guibourg, J-C. Merlivat, Ph. Dard and B. Swiners

COMPAGNIE FRANCAISE THOMSON HOUSTON
PARIS - FRANCE

DEVELOPMENT OF THE MASS SPECTROMETER TH. N 208 / 210

Only a few years ago, Mass Spectrometers having a high degree of resolution were considered as complex instruments necessitating specially trained personnel. Since then, the application of these instruments to new fields of industrial and university research, has led manufacturors to build an equipment which would meet the double requirements of reliability and operational facility. In the light of this evolution, THOMSON-HOUSTON decided to develop a double focusing mass spectrometer which functions equally as a mass spectrograph.

The most exciting feature of the spectrograph is its impact on the instrument's performances and standards. Thanks to the spectrograph, the inconveniences of scanning can be eliminated and total information may be obtained simultaneously on the various masses being analyzed. This guarantees that the conditions of measurement are the same for all masses, while previously, using scanning, such a stability would not be possible.

Furthermore, with the film plate, we are able to obtain very simply the equivalent of a highly complicated electronic device. This becomes obvious when one considers that first of all, the sensitivity of the plate is greater than the electron multiplier, and secondly, as the plate measures both weak and intense peaks, its mass dynamic is very high. In addition, complications arising from the necessity of changing the recorder's sensitivity in the middle of analysis because of the peak differences are now excluded.

Finally, it must be pointed out that by using a film plate, we have reduced considerably the quantity of sample required. As a result, an easy analysis of microsamples, difficultly volatile samples and short-lived samples becomes a reality.

One might be tempted to think that these improvements are obtained at the cost of accuracy. On the contrary, by eliminating the collector slit, resolution becomes doubled. Even more, the mass of a peak can be determined by this means with greater precision than ever.

As the various component systems of the universal mass spectrometer TH.N 206 have proved to be extremely reliable and capable of high quality performances, it was decided to integrate these systems, whenever possible, into the TH.N 208 / 210. Consequently, the inlet systems ion source, double effect differential pumping system and most of the various electronic chassis of the TH.N 206 are also found in the TH.N 208 / 210. In brief, this means that the versatility of the universal mass spectrometer is also a characteristic of the mass spectrometer / spectrograph and that this latter instrument can effectuate all the analyses proper to the field of Organic Chemistry.

Our choice of geometry was, therefore, guided by three basic principles :

- Maintain an open detection configuration which would permit the instrument to be used either as a spectrometer or as a spectrograph.
- Keep the ion beam loss as slight as possible in order to obtain the best conditions for fine isotopic analysis.
- Acquire a degree of resolution between 30 and 35,000 at 10 % Valley, with a light weight, minimum bulk instrument.

An evaluation of the various possibilities let us to conceive an instrument using Mattauch - Herzog geometry, particularly as this would allow an easy adaptation between electric and photographic detection due to the common point of penetration into the magnetic field of all speed and direction focusing trajectories.

As regards the minimizing of the beam loss, we have opted for a spherical electrostatic sector in accordance with the recommendations of Ewald and Stevens. Furthermore, this type of sector has the added advantage, assuming the same conditions of size and double focusing, of doubling the magnification over that obtainable with a cylindrical sector.

In the case of photographic detection, the degree of resolution, independent of any effect of aberration, is, therefore, also twice as high.

Finally, considering the necessity to minimize the aberrations along the photographic plate, we have worked out the following geometry :

1) Departing from the classical Mattauch - Herzog geometry, we have placed the focusing plane outside of the magnetic field and not at its limit. Though there is always the possibility of a leaking field affecting the particules as they leave the magnet, the position of our focusing plane results in a decrease in the number of particules due to ions and electrons coming out of the photographic plate and which bombard the polar masses. Thus in our opinion, if the plate is brought away from the influence of the field, the elimination of the halo effect becomes more feasible.

2) For the electric detecting version of the instrument, we have sought to obtain the maximum degree of resolution along the average radius which is, in this case, 12 inches. As it is most improbable that we could eliminate an existing 2nd order angular aberration, considering that the ratio, (magnetic sector radius/electrostatic sector radius) is nearly one, we preferred to give a negative curvature to the zone of admission into the magnetic sector so that by definition there would be no 2nd order angular aberration for the radius Rm = - 6.2 inches corresponding to the deflection radius of 12 inches.

For the radius, the aberration coefficients are :

$$B_{11} = 0 \qquad (\alpha^2)$$
$$B_{12} = -2{,}01 \qquad (\alpha\beta)$$
$$B_{22} = -0{,}24 \qquad (\beta^2)$$

3) In addition, as the spherical sector introduces slight aberrations due to the aperture angle in the vertical plane $\alpha\,\zeta$ and to the image height, it was decided that a negative curvature should be given to the zone of admission into the electrostatic sector so as to minimize these effects.

Therefore, taking into consideration the above mentioned refinements as well as the mechanical adjustments that we have introduced to assure the correct alinement of the different subassemblies, we have reason to believe that our instrument can attain a degree of resolution at about 30,000 with a 10 % Valley.

In conclusion, the product of this development is an instrument having a high degree of resolution through a directional and speed focusing Mattauch - Herzog geometry. It is provided with two devices so as to permit the user to choose between detection by film plate or electron miltiplier.

In terms, however, of its main specifications, the mass spectrometer TH.N 208 / 210 can be described as follows :

Analyzer :

- Geometry : Mattauch - Herzog.
- Ion accelerating voltage : continuous adjustment from 500 to 15,000 Volts.
- Electrostatic sector : type : spherical
  radius : 18" (45 cm)
  deviation : 45°
- Magnetic sector : radius : 12" (30 cm)
  average deviation : 80°

Detector System :

- Electron multiplier.
- Photographic plate.

Ion Source :

- Electron bombardment source.
- Thermoionization source.

Inlet Systems :

- Direct inlet into ionization chamber TH. N 207 - 05
- High Temperature Line (350° C) TH.N 207 - 03
- Double lines for molecular and viscous inlet TH.N 207 - 02, TH.N 207 - 01.

- Gas phase chromatography inlet TH.N 207 - 04
- Knudsen Cell.

BIBLIOGRAPHY

1) STEVENS -
Advances in Mass Spectrometry - Edited by Elliott, Pergamon Press 1963 page 199.

2) H. EWALD, G. SAUERMANN and H. LIEBL -
Advances in Mass Spectrometry - Edited by Waldron 1959 - page 10.

3) H.HINTERBERGER and L.A. KÖNIG -
Advances in Mass Spectrometry - Edited by Elliott, Pergamon Press 1963 - page 16.

4) J. MATTAUCH and HERZOG -
Z. Phys. 89, 786 (1934).

5) H. EWALD and H. LIEBL -
Z. fur Naturforschung - 10 a - 1955 - page 872.

6) H. HINTERBERGER and L.A. KÖNIG -
Z. fur Naturforschung - 12 a - 1957 - pages 140 - 147, 377 - 385, 775 - 785.

7) J.H. BEYNON -
Mass Spectrometry and its application to organic chemistry.

8) K. BICHMANN -
Mass Spectrometry Organic Chemical Applications - McGraw Hill, N.Y.1962

9) C. DJERASSI -

MASS SPECTROGRAPH WITH SPHERICAL CONDENSER

L. A. Cambey, R. J. Hessler, and L. E. Snurr
Nuclide Corporation, State College, Pennsylvania

The use of toroidal condensers with mass spectrographs has been pioneered by Ewald and his co-workers. The toroidal condenser offers the advantages of increased resolving power for a given radial radius of curvature of the electrostatic analyzer together with z focusing.

The general first order equation for the resolving power of a mass spectrograph with photoplate detection is:

$$\text{RESOLVING POWER} = \frac{a_e}{\chi^2 S_o}$$

where $\chi = \sqrt{2 - {}^{a_e}/_{R_e}}$

a_e = Radial Radius of Curvature of ESA

R_e = Axial Radius of Curvature of ESA

S_o = Object Slit Width

There are two points to notice in this equation. One, that the resolving power is dependent not only on the radial radius of curvature of the electrostatic analyzer, a_e, but also on the axial radius of curvature of the analyzer, R_e. The other point to note is that the resolving power, at least to a first order, is independent of the radius of curvature of the ions in the magnetic field. No parameters of the magnetic analyzer enter explicitly into this equation.

In a direct comparison between the case of the commonly used cylindrical electrostatic analyzer and the spherical one we have:

CYLINDRICAL CONDENSER	SPHERICAL CONDENSER
$R_e = \infty$	$R_e = a_e$
$\chi = \sqrt{2}$	$\chi = 1$
$\text{RESOLVING POWER} = \frac{a_e}{2S_o}$	$\text{RESOLVING POWER} = \frac{a_e}{S_o}$

For the cylindrical case the axial radius of curvature is infinite and the resolving power is $a_e/2S_o$. For the spherical case the two radii of curvature are equal, and the resolving power is a_e/S_o. Thus, in a direct comparison for a given value of a_e, there is a difference of a factor of 2 in the resolving power.

The spherical condenser by virtue of its axial radius of curvature also gives z-focusing. In a double focusing mass spectrograph geometry ions of the same energy that initially diverge from the ion source follow parallel paths between the electrostatic and magnetic analyzers. With a spherical condenser, because the radial and axial radii of curvatures are equal, this is also true for ions having an initial divergence in the z plane. The equivalent optical system is shown in Figure 1.

The thin lens at the entry to the magnet results from the fringing magnetic field. The focal length of the lens is dependent on the radius of curvature of the ions in the magnetic field and on the angle of entry of the ions into the magnet. For most mass spectrograph geometries, this angle of entry is positive and the lens is convergent as is the case shown in Figure 1. As the path length traversed by the ions before they strike the photoplate and the focal length of the lens are proportional to the radii of curvatures of the ions in the magnet, we see that z focusing is the same for all ions regardless of mass. This is not true for the general case of a toroidal condenser where the ion beam in the z plane is not parallel between the electrostatic and magnetic analyzers.

These considerations of resolving power and z focusing independent of ion mass led us to select a spherical electrostatic analyzer for our mass spectrograph.

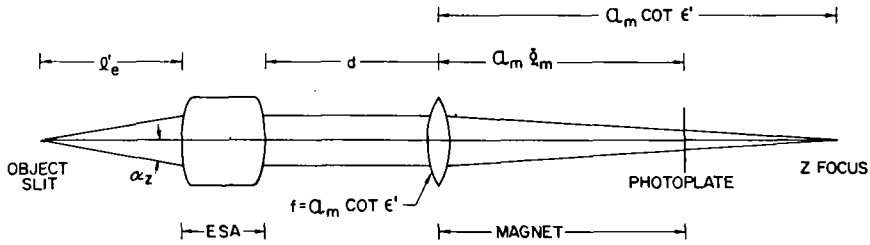

Figure 1. Z-Focusing Conditions for the Case with $l''_m = 0$

We approached the problem of the selection of design parameters for the spectrograph in the following way. To facilitate practical optimization of the instruments performance, we made the distance of the image from the magnet exit pole boundary equal to zero ($l''_m = 0$).

With a double focusing mass spectrograph with the image distance equal to zero, only one variable needs to be selected and the instrument geometry is completely determined. We chose Øm, the angle of deflection in the magnet as this variable. We plotted all the other variables as a function of Øm, and selected a range of Øm that gave reasonable physical dimensions for the other variables.

Also of concern to us was the z-focusing. It was thought that a true z-focus would be a disadvantage as line spectra are required for densitometry. A true z-focus in this type of geometry is formed when Øm is equal to 117°, thus we wanted to restrict the value of Øm substantially less than this so that we would obtain line spectra.

These considerations lead us to select a value of Øm equal to 110°. We calculated the second order aberrations for different values of the radius of curvature of the entry boundary of the magnet, and the distance between the electrostatic and magnetic analyzers. These parameters do not effect the first order focusing conditions, and thus we could vary them to obtain optimum values for the second order aberrations.

These aberrations are smaller than those in the traditional Mattauch-Herzog geometry with a cylindrical condenser and 90° deflection in the magnetic analyzer. We also calculated out those second order aberrations resulting from alpha z, the angular divergence of the ions in the z plane. However, as the alpha z transmitted is substantially smaller than the alpha transmitted in the radial plane, this additional aberration is of little consequence.

The geometry for the instrument is shown in Figure 2. The angle of the electrostatic analyzer is approximately 45°. The ions enter the magnetic analyzer 20° from normal and the angle of deflection of the ions in the magnet is 110°. The radius of curvature of the optic axis in the spherical condenser is 15". Ions with radii of curvature from 1.83" to 11" in the magnet are recorded on a photoplate 15" in length. An electrical detector slit is mounted for ions with a radius of curvature of 12". The object slit is 14.7" from the electrostatic analyzer. The separation between the analyzers is 8" and the radius of curvature of the entry boundary of the magnet is 5".

This geometry gives a double focus for all masses along the exit pole boundary, records a 36 to 1 mass range on a 15" photoplate, and allows for electrical detection for ions with a radius of curvature of 12". It also provides a partial z-focus which is constant along the length of the photoplate.

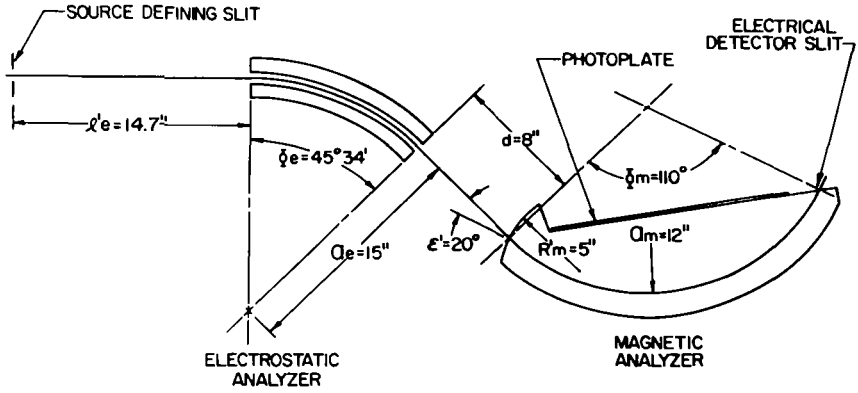

Figure 2. Geometry of the Mass Spectrograph

The ion source is the r-f spark in this particular case. The object slit is externally variable from zero to 10 mils. There is also external control on the angular orientation of the slit. The accelerating voltage is continuously variable to 30 kV.

The region between the electrostatic analyzer and the ion source is differentially pumped. There is an externally variable slit located at the entry to the electrostatic analyzer. This slit enables us to vary the angular divergence of the ion beam entering the analyzer.

The plates for the spherical condenser are made from fused silica. They are held together by three precision spacers so that the plates may be taken apart and readily reassembled. The plates have a fired on silver coating to make them conducting. A gold plating was used on top of the silver. They are fitted with Herzog terminators at both ends.

At the entry to the magnetic analyzer we have a variable width slit. This enables us to vary the energy spread of the ion beam entering the magnet. Of course, this control on energy spread also effects the angle divergence of the beam because of the cross correlation between these parameters in this region.

The pole shoes for the magnet are enclosed in their own vacuum housing. The pole shoes are made from Armco Iron and are gold plated. They are held apart with precision ground stainless steel blocks. The magnet nose cone is fitted with a two element Herzog shunt to limit the extent of the fringing field. The beam monitor that intercepts a fraction of the ion beam entering the magnet is located between the Herzog shunt and the magnet nose cone.

The photoplate racking mechanism is driven via a bellows sealed shaft. The electrical detector slit is variable in width from outside the vacuum system. Its angular orientation is also variable. An electron multiplier is mounted behind this slit.

The photoplate prepumping chamber is located adjacent to the source rather than at the far end of the magnet. We did this to decrease the overall length of the instrument. The photoplates from the prepumping chamber are pushed through a slot milled out in the nose cone of the magnet 2" below the magnet gap. The prepumping chamber has a capacity for 8 plates, and can be loaded in daylight from a casette. A pushrod is used to inject the photoplate holders into the magnet and to retract them.

The drift tube, the electrostatic analyzer, and the magnetic analyzer are individually pumped by 50 liter/second ion pumps. The prepumping chamber is pumped with a 750 liter/second oil diffusion pump with water baffle and cold trap. The ion source is evacuated with a 400 liter/second ion pump. The system is constructed from stainless steel and metal gaskets are used in all places except on the prepumping chamber and on the large 6" gate valve above the source pump. The pushrod and the cross drive on the prepumping chamber are differentially pumped through packing glands by a separate mechanical pump. The ion source and the prepumping chamber are pumped down to fore vacuum by a separate 250 liter/minute mechanical pump through 1" diameter fore lines.

The magnet may be moved by two independent motion mechanisms. One allows for movement of the magnet at right angles to the ion trajectory at the entrance to the magnet. The other allows for a simple rotation of the magnet about the point of entry of the ions into the magnetic field. This is the main focusing adjustment.

In operation of the instrument we found that the focusing adjustments we had allowed for greatly facilitated the alignment. The use of variable slits not only in the ion source but also to control the alpha and beta of the ion beam enabled us to readily vary operating conditions within the instrument.

The position of ions in the magnet proved to be very sensitive to the angular orientation of the spherical condenser. The adjustment necessary is quite critical, and we had to design the tube supports for the electrostatic analyzer so that we could make this adjustment while operating the instrument.

The most striking difference between an instrument with the cylindrical condenser and with a spherical condenser is the length of the lines on the photographic plate. With no mechanical aperture at the exit to the pole boundary the line length is approximately 1.5 millimeters. Towards the end of the lines there is a slight decrease of intensity due to the alpha z distribution from the ion source. The lines are uniform in width and intensity over a length of about 3/4 millimeters.

The plate shown in Figure 3 was obtained with a zircalloy sample. The source slit width was 3 mils. The resolving power is approximately 3000 along the plate except for the last inch where it falls off. This plate was taken with an aperture at the exit of the pole boundaries equal to 1 1/2 mm.

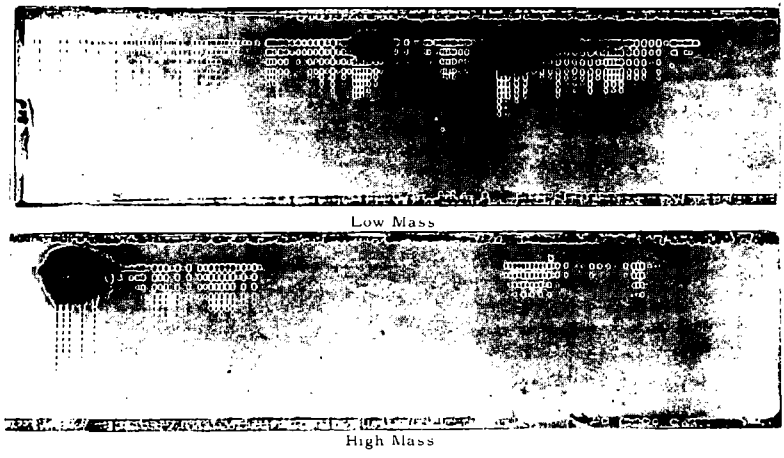

Figure 3. Mass Spectrum of Zircalloy

We experienced some difficulty with the line width being somewhat dependent upon the position of the spark in the ion source. The effect was reasonably small for variations in spark position over an area of about 1/2" in diameter. However, if the spark was outside this region there could be some changes in line shape. We were able to eliminate this effect by using a tungsten mesh over the aperture behind which the spark is made. This is similar to the technique used by Franzen and discussed at the Montreal E-14 meeting.

For very low exposures for the matrix elements we require only one spark. On these exposures we have noted that the ratio of doubly charged to singly charged ions may vary considerably.

We have also noticed that for the focusing of the instrument to be independent of magnetic field strength it is necessary to establish the operating value of the magnetic field by going through a standard procedure.

We carried out a series of experiments with the instrument and obtained resolving powers at the high mass end of the plate in excess of 7500 with a 1 mil slit. Most of the work on the instrument has been done with a 3 mil slit where the resolving power is somewhat above 3000 using a 10% valley definition. The sensitivity of the instrument is difficult to state in a direct fashion. With this particular plate there was a uranium 235 present to approximately 22 parts per billion and using that as a guide it was estimated that the limit of detection is approximately one part per billion in that region of the plate.

The exposure required to get this limit of detection was between 20 and 30 minutes. The accelerating voltage used was 26 kilovolts.

We have also used the instrument with a vacuum lock thermionic source. The vacuum lock assembly has been mounted on a separate frame which can be wheeled up to the instrument and bolted to it. We find that in doing surface ionization work the abundance sensitivity is a factor of 5 or so better than we obtain with our single focusing instruments.

Constant Momentum Mass Spectrometer for Ionospheric Investigations

by

H. M. Luther and B. R. F. Kendall

Ionosphere Research Laboratory
and
Department of Physics
The Pennsylvania State University
University Park, Pennsylvania

Abstract

A mass spectrometer is being developed in which pulsed fields give all ions the same momentum. The final ion energy is therefore mass dependent. A mass spectrum can be obtained by analyzing the energy distribution of the ions reaching the collector. The advantages of this type of spectrometer are compactness, simplicity, light weight, absence of magnets, and ability to operate at comparatively high pressures. These characteristics make the apparatus suitable for analyzing the ion composition of the lower regions of the ionosphere. Preliminary results of attempts to find operating conditions insensitive to initial ion energies are discussed.

The constant momentum mass analyzer was originally proposed by J. A. Hipple.[1] A later paper by Fiks[2] proposed the same device; but neither author reported any experimental work on the analyzer. The first successfully operating constant momentum mass analyzer was described by Bracher.[3]

The basic operating principle of the constant momentum mass analyzer is shown in Figure 1. Ions are admitted into the region between electrodes (1) and (2) and then pulses of amplitude V and duration Δt are applied to electrode (1). The time Δt is chosen such that the ions to be analyzed do not have time to leave the region between the electrodes before the pulse is over. Under these conditions all the ions, assuming them to be singly charged, gain the same momentum, and thus the final ion energy will be:

$$E = \frac{k}{m} \left(\frac{V\Delta t}{d}\right)^2$$

where E is measured in electron volts, m in a.m.u., V in volts, Δt in μ secs and d in cm. K is a constant equal to 0.483. The energy gain is therefore mass dependent and can be analyzed by sweeping a retarding field placed in front of an ion collector.

Advantages of such an analyzer include simplicity of operation and compactness. The analyzer can operate at pressures well above 10^{-3} Torr, since the dimensions of the spectrometer can be made less than the mean free path of the ions at such pressures. The instrument is therefore well-suited for positive ion analysis in the region of the ionosphere between 80 and 250 km where the pressure varies from 10^{-3} Torr to 10^{-7} Torr.

A disadvantage of this type of analyzer is the limitation of resolving power by the initial thermal energy distribution of the ions. This initial distribution is amplified is amplified in the pulsing region, since the more energetic ions fall through the greater potential difference; so that either large energy gains or some form of ion energy focusing is required to obtain adequate resolution. The advantages and disadvantages were realized experimentally in Bracher's instrument which had a resolution of

$$\left(\frac{M}{\Delta M}\right)_{50\%} = 30$$

where ΔM is the width of the mass peak at half-height. His instrument was further characterized by a very high sensitivity of 0.1 amp/Torr for neutral gases.

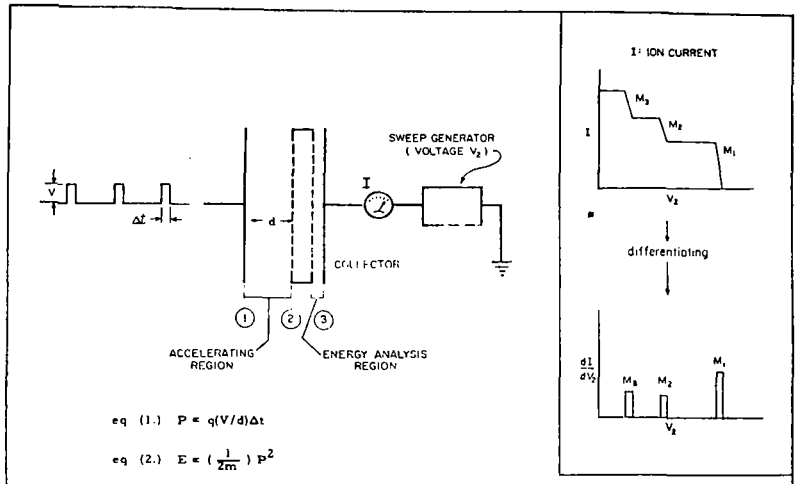

BASIC CONSTANT-MOMENTUM MASS ANALYZER
FIGURE 1

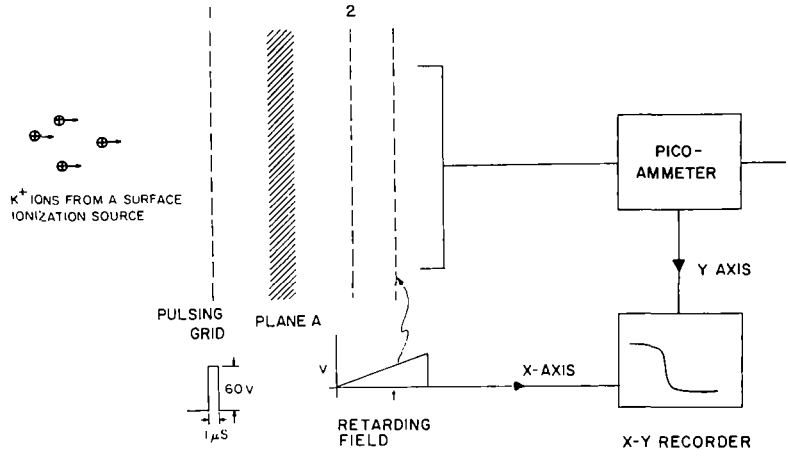

ACCELERATING MODE I OF THE CONSTANT MOMENTUM MASS ANALYZER
FIGURE 2

Bracher's mass analyzer used pulsed fields with an amplitude of 3 KV and a curved electrostatic energy analyzer. Since such pulse voltages are not obtainable in rockets, we have concentrated our attention on instruments using applied voltages of 50-200 volts.

To date three operating modes have been investigated. The simplest mode is shown in Figure 2. To simulate ions in the ionosphere K^+ ions from a surface ionization source are used. The ions are reflected in the plane A inside the pulsing region by a small D. C. bias voltage applied to the electrodes (1) and (2). A large positive pulse is then applied to electrode (1) and the final ion energies are analyzed with a sawtooth retarding field. The output of the picoammeter can be displayed as a function of the retarding voltage with an x-y recorder. The mass spectrum can then be obtained by differentiating the output of the x-y recorder. The results of this mode of operation were rather modest. The effective resolution with an analyzing system about 1 cm long was

$$\left(\frac{M}{\Delta M}\right)_{50\%} \simeq 5$$

The second mode shown in Figure 3 is somewhat more complex. As in the first mode the K^+ ions are reflected in a plane just in front of grid (1). A small negative pulse applied that grid admits a cloud of ions into the pulsing region. The gating pulse triggers the main pulse applied to grid (2). A variable delay line between the gating pulse generator and the main pulsing unit insures that the ions are all inside the pulsing region before they are accelerated. As in the first mode, the ion energies are analyzed with a sawtooth retarding voltage. The results obtained with this mode of operation together with a view of the instrument is shown in Figure 4. The effective resolution is:

$$\left(\frac{M}{\Delta M}\right)_{50\%} \simeq 16$$

The third mode shown in Figure 5 should be the most effective, since the initial energy distribution would be reduced instead of being amplified. Ions from the K^+ source are gated into the pulsing regions between grids (1), (2) with grid (a). These ions have a definite initial energy E_i. A positive pulse applied at grid (2) subtracts a fixed amount of momentum from these ions, and then the ions are collected with a Faraday cage. The ion energies may be analyzed by sweeping the pulse duration of the main pulse, keeping the initial ion energy constant. This mode of operation is still being investigated.

Acknowledgment

This project is supported by NASA Grant NGR 39-009-032.

References

1. J. A. Hipple, U.S. Patent 2,764,691. Filed August 3, 1953.

2. V. B. Fiks, Soviet Physics, 1, 89 (1956).

3. J. Bracher, Zeit. Angew, Phys. 4, 19 (1965); 347-48.

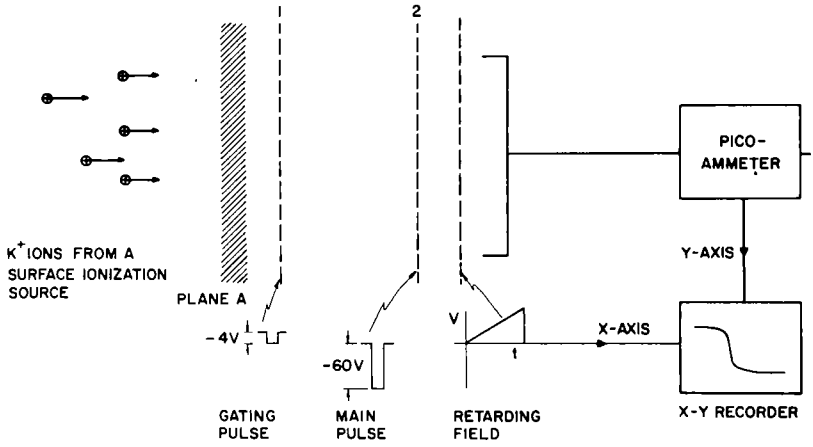

ACCELERATING MODE II OF THE CONSTANT MOMENTUM MASS ANALYZER

FIGURE 3

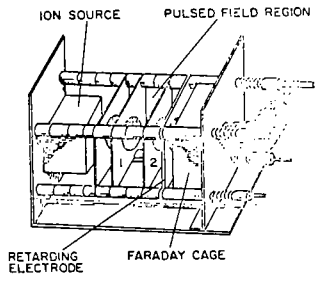

CONSTANT MOMENTUM
MASS SPECTROMETER

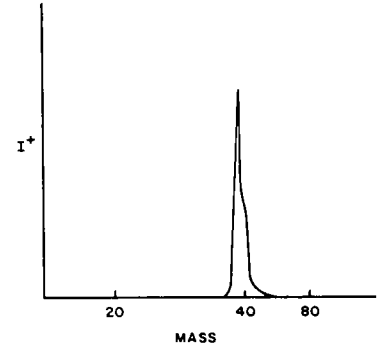

MASS SPECTRUM FOR POTASSIUM
(MASSES 39 AND 41)

FIGURE 4

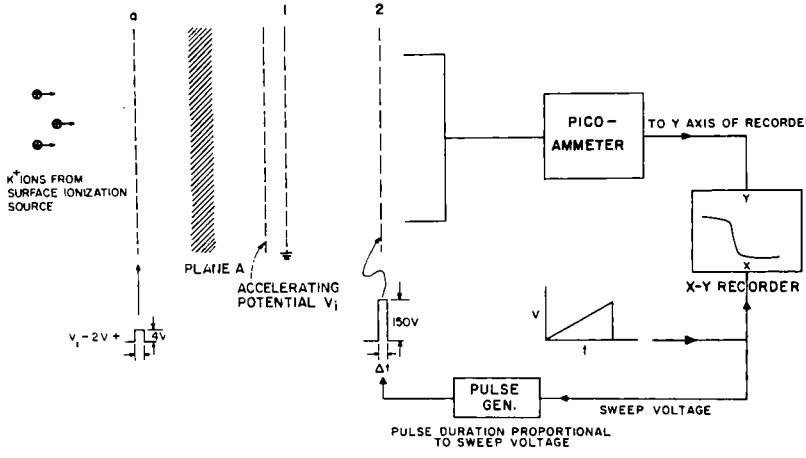

DECELERATING MODE OF THE CONSTANT MOMENTUM MASS ANALYZER

FIGURE 5

"A NEW UNIVERSAL SINGLE FOCUSING 12", 15,000 VOLTS MASS SPECTROMETER OF HIGH PERFORMANCE"

- Development of the Mass Spectrometer TH.N 206.
- An Investigation of the Performances of Mass Spectrometer TH.N 206.

J. Guibourg, J-C. Merlivat, G. Bernard, Ph. Dard, and B. Swiners

COMPAGNIE FRANCAISE THOMSON HOUSTON
PARIS - FRANCE

DEVELOPMENT OF THE MASS SPECTROMETER TH.N 206

I - INTRODUCTION -

In 1964, our Company initiated the development of a mass spectrometer capable of meeting the requirements of laboratory research and adapting for use in the fields of both Organic and Isotopic Chemistry.

After having analyzed the various factors which influence the performance of a mass spectrometer, we decided upon the following specifications as being the most appropriate instrument design for the intended applications :

Isotopic Analysis :

- An easily accessible and removable High Performance Source, characterized by a small aperture.
- A high accelerating voltage.
- An excellent operating ultra-vacuum System.
- Readily handled, high stability input stages and power supplies.

The logic of this choice is evident. The first two factors limit the importance of the aberrations and increase the degree of resolution. Taken together with the third, they permit the attaining of the abundance sensitivity limits of a single focusing instrument.

Organic and Inorganic Chemistry :

- A gas source compatible with the various inlet systems normally employed, such as : molecular inlet, direct inlet, high temperature inlet.
- The highest obtainable degree of single focusing.
- An excellent vacuum which would eliminate memory effects.
- A large choice in scan and sweep speeds and ranges.

Taking into account these and many other points, such as space requirements, we were led to the concept of an instrument operating at 15,000 V, whose configuration would be based on a 12 inch radius and a 60° deflection.

II - DESCRIPTION -

In a brief word, the TH.N 206 as worked out, can be described as an open configuration, solid and gas sampling MASS SPECTROMETER for the 2 to 3,500 mass range, with the following characteristics :

- Electron bombardment or thermoionization Source.
- 12 inch radius, 60° deflection.
- 15,000 ion accelerating voltage.
- Double acting differential vacuum system using ion pumps.

Fig. 1

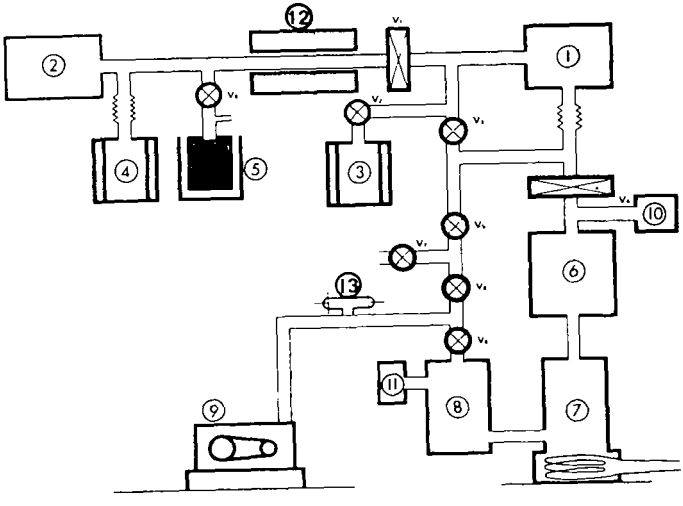

THN 206

VACUUM SYSTEM FLOW SHEET

1. Source Housing
2. Collector Housing
3. 15 L./s. Ion Pump
4. 50 L./s. Ion Pump
5. Sorption Pump
6. Liquid Nitrogen Trap
7. Diffusion Pump
8. Vacuum Reservoir
9. Primary Pump
10. Penning Gage
11. Primary Vacuum Protective Device
12. Electro-Magnet
13. Primary Vacuum Gage

V1 - Electro-pneumatic & Hand-Operated Valve
V2 - V4 Electro-pneumatic Valves
V3 - V5 - V6 - V7 - V8 Electro-pneumatic Valves
V9 - Hand-Operated Valve.

Fig. 2

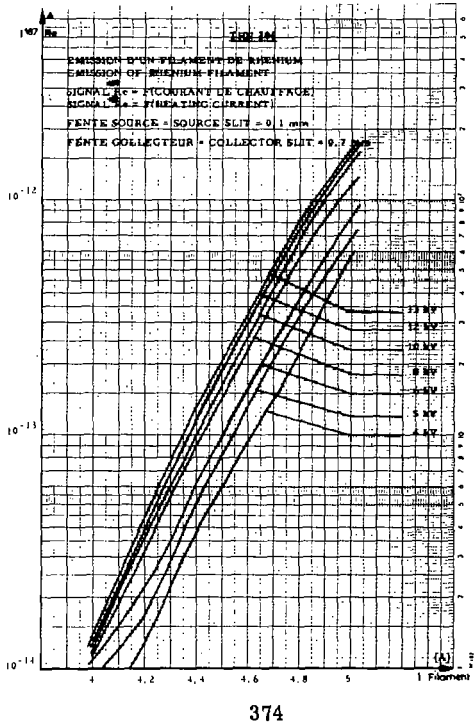

The instrument is designed so that the two sources can be interchangeably used and operated on the same filament power supply. The version having a gas source includes, therefore, in addition to what is found in the solid sampling version, inlet systems which are supplied as kits and which can be mated to the Mass Spectrometer.

According to the logic of its conception, the Mass Spectrometer TH.N 206 has been divided into two distinct units : the electronic unit placed in the control cabinet and the analyzer unit in the console. This layout and configuration have been guided by the overriding desire for easy accessibility to the various organs, high standards or performance, and facility for adaptation through the use of special devices. This last point, naturally, guarantees the instrument an extraordinary flexibility in application.

The analyzer unit is comprised of 5 component systems : analyzer, vacuum system, electro-magnet, ion source, and collector system.

Each of these component systems can be outlined as follows :

The Analyzer :

The analyzer consists of the analyzer tube and the slits defining both the source and collector. It operates under a high vacuum of 10^{-9} Torr which eliminates the importance of the gas scattering of the ion beam so as to assure the abundance sensitivity and the peak shape. An additional feature of this system is a special device which permits the orientation of the slits and the adjustment of their width. The operator thus controls the degree of resolution and the cancellation of non - parallel aberration effects.

The reliability of the system can be estimated by the care taken to assure that all metallic parts under vacuum are made from a carefully polished stainless steel except the gaskets which are of the gold wire type. Consequently, the assembly can resist thermal cycling under vacuum up to 350° C.

The Vacuum System :

The vacuum system must be considered in the light of its three principle functions and devices : pumping, protection, and control or, respectively, pumps, valves, gages. In addition to the usual rapid primary pumping stage, there is a special designed double action differential secondary pumping stage composed of a mercury diffusion pump and two ion pumps.
The security of the vacuum is obtained by various liquid nitrogen traps and baffle valves. The latter, permits the isolation of the vacuum in the analyzer tube and detection systems when the source has been returned to atmospheric pressure.

The vacuum control and measuring elements of the Mass Spectrometer are three gages : a Penning gage for the ion source and two ion pumps for the intermediary sleeve and the analyzer tube. Furthermore, different protective measures on the primary and secondary vacuum circuits prevent failure of the instrument.

Electro - Magnet :

The electro-magnet provides a stabilized but variable magnetic field which can rise to a maximum value of 10,000 Gauss before approaching saturation. The 23/32 inch gap was designed so that the beam enters and leaves normally the dihedral angle created by the magnetic field after a total deviation of 60°. This avoids a loss of focussing in the direction of the beam, increasing, therefore, both the intensity received in the collector and the sensitivity of the Mass Spectrometer. As a special feature, the position of the electro-magnet is easily adjusted in order to obtain the best peak shape.

Ion Source :

The designation, ion source, comprises the source (filament with sample and filament holder block) and the accelerating electrodes (three high voltage, four low voltage). The thermoionization source is of the Inghram Chupka triple filament type which totally separates the functioning of the three filaments and permits the reproduction of the same precise setting of the filament holder block and filaments.

The seven electrodes accelerate up to 15,000 Volts the ions which have been made available. The voltage is such that the inevitable speed aberrations due to the electric resistance of the electrodes are minimized. All electrodes are made from a non - magnetic stainless steel, carefully polished and finished. Mounted on alumina insulating supports by means of a constant pressure spring, they can be easily removed

Fig. 3

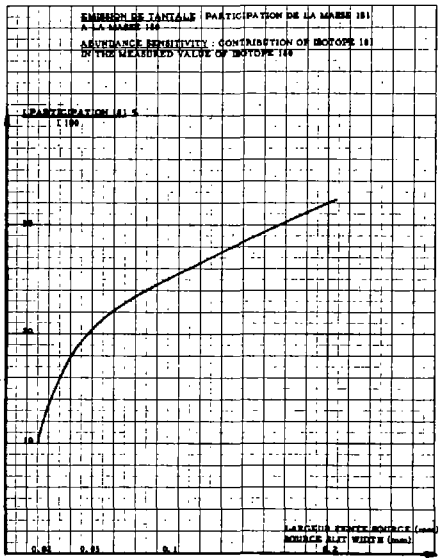

Fig. 4

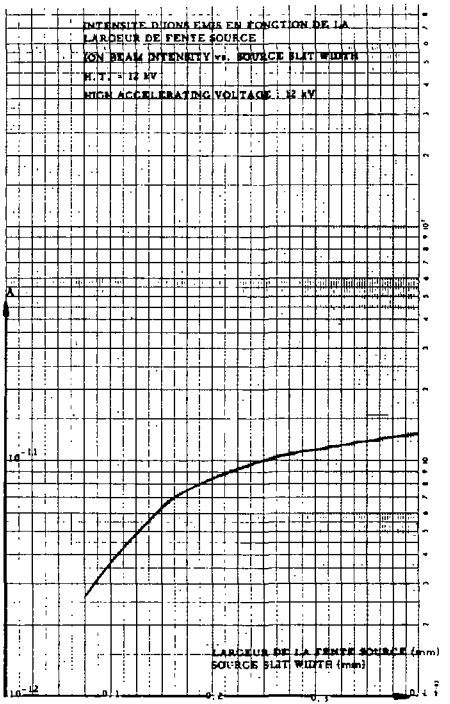

Fig. 5

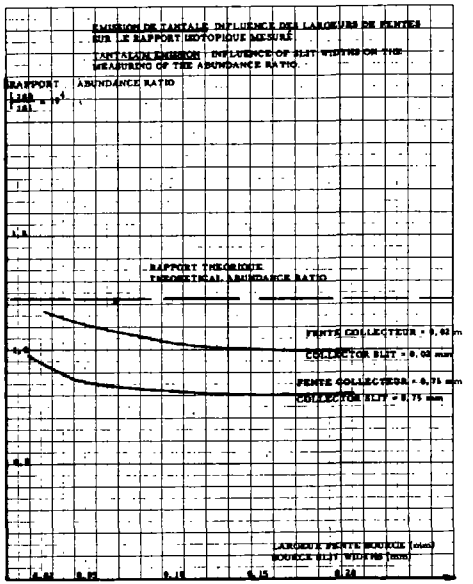

and automatically returned to their correct setting, particularly the first three electrodes. This feature was introduced to erase memory effects. It is to be noted that the open configuration of the source also permits the use of such devices as a Bayard Alpert ionization gage and a quartz pyrometer.

Collector System :

The basic collector system comprises a Faraday cup collector having a defining slit and a secondary electron suppressor. The collector system is so conceived as to catch the ion beam on the target or the first dynode of the electron multiplier without having neither to break the vacuum of the analyzer tube not to change any of the parameters concerning the functioning of the instrument.
Various and diverse collections can be envisaged thanks to the open configuration concept, particularly the Allen type electron multiplier. This permits optimizing the yield according to the problem.

Electronic Unit :

The electronic unit groups the various organs controlling the measuring and regulation of the Mass Spectrometer. This unit comprises 5 functional assemblies, each one is a complete entity. Printed circuits are systematically used and the unit has been transistorized to assure good performance and reliability.

15,000 Volts High Voltage Power Supply :

The supply, adjustable between several hundred and 15,000 Volts, provides a 1 part per 500,000 stabilized ion accelerating high voltage to the different electrodes of the ion source by means of a distribution bridge incorporated in the power supply of the source.

The value of the high voltage is continuously adjusted by multiturn potentiometers and a pure electronic sweeping device, which allows in special cases the user to scan the masses by high voltage, as magnetic scanning is generally reserved for isotopic analysis.

Electro-Magnet Power Supply :

A weak voltage, high intensity power supply whose current is stabilized to better than 1 part per 500,000, it is equipped with a scanning system similar to the one used by the high voltage supply. The operator has the possibility of effectuating all the types of recordings usually employed for the interpretation of results requiring the possibility of return positioning during up and down mass scanning.

Sweeping Systems :

The two sweeping systems incorporated in the high voltage and electro-magnet power supply differ only in the choice of scan speeds. The operator has the possibility of choosing separately the scan limits (i.e., to define exactly the scan gate), scan mode (saw tooth : symmetrical, asymmetrical), and in certain cases, the direction of scanning which he can reverse at any moment. Several scan speeds can be chosen by push-button. In addition, a special control cuts the scanning at a given moment, keeps the power at its selected value, and reintroduces the scanning when desired. Reverse scanning can also be effectuated.

Filament Power Supply :

The filament power supply for the electron bombardment ionization source and the thermoionization source, is completely transistorized. The input stability of each filament is superior to 1 part per 10,000. The output can rise beyond 7 Amperes.

The voltage distribution of the seven accelerating electrodes is regulated by multiturn potentiometers. Their correlation with the electrodes is directly assured by the conception of the source control panel.

The disposition which has been adopted permits an easy adjustment of the geometry of the ions and the emission of the ion source.

Detection Unit :

The detector, manufactured in series, comprises 2 amplifiers and the power supply of the electron multiplier. One of the amplifiers usually serves for direct detection on the collector and the other amplifier for detection by an electron multiplier. One of these two amplifiers can also be used to detect the total ion current. The amplifiers are of a d.c. type having a total counter reaction on high value resistors and 7 scales of sensitivity.

Fig. 6

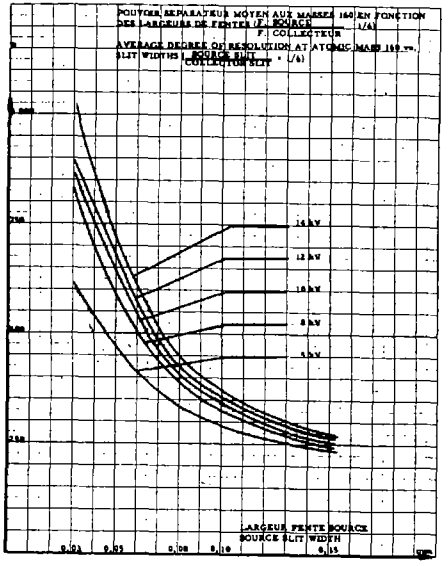
POUVOIR SEPARATEUR MOYEN AUX MASSES 160 EN FONCTION DES LARGEURS DE FENTES (F. SOURCE = 1/6)
F. COLLECTEUR
AVERAGE DEGREE OF RESOLUTION AT ATOMIC MASS 160 vs. SLIT WIDTHS (SOURCE SLIT = 1/6)
COLLECTOR SLIT
14 kV
12 kV
10 kV
8 kV
6 kV
LARGEUR FENTE SOURCE
SOURCE SLIT WIDTH
0.03
0.05
0.08
0.10
0.15

Fig. 7

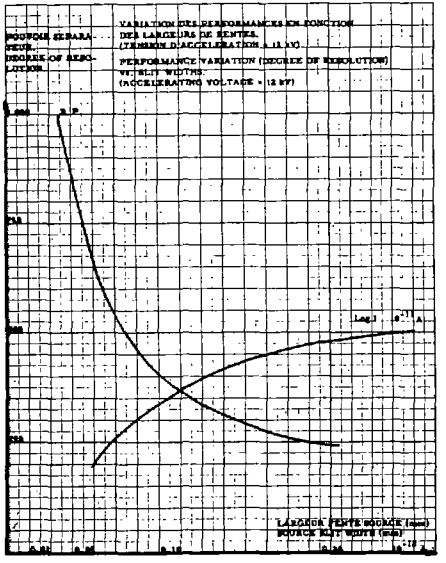
VARIATION DES PERFORMANCES EN FONCTION DES LARGEURS DE FENTES.
(TENSION D'ACCELERATION = 12 kV)
POUVOIR SEPARATEUR
DEGREE OF RESOLUTION
PERFORMANCE VARIATION (DEGREE OF RESOLUTION) vs. SLIT WIDTHS.
(ACCELERATING VOLTAGE = 12 kV)
LARGEUR FENTE SOURCE (mm)
SOURCE SLIT WIDTH (mm)

Vacuum Regulation :

The vacuum control unit allows the operator to effectuate all the operations requiring the creation of a vacuum or the return to atmospheric pressure from the control desk. As a security measure, the push-buttons used to control the valves lock into the desired position so that the operator can verify at all time if the valves are closed or open. The measuring instruments, one for the Penning gage and the other for the ion gage, control the degree of the vacuum

AN INVESTIGATION OF THE PERFORMANCES OF MASS SPECTROMETER TH.N 206

Having a greater experience with the use of solid sources than with gas sources, the scope of our explanations will be mainly limited to results obtained while using the former, particularly as our principle work in this field has been more in fundamental analytical research than in solving specific problems.

The following results from our studies on the effects of ion accelerating voltage on :

- Sensitivity
- Abundance sensitivity
- Degree of resolution
- Aberrations

I - SENSITIVITY -

The tests on the sensitivity were performed using a central Rhenium filament having a 11 × 0.75 × 0.025 mm. form. The filament was heated between 4 and 5 Amp. by increment of 200 mA. In each emission temperature, the accelerating voltage was varied between 4 and 13 KV. This produces an increase of the ion current on the collector by a factor of 4 between the lower and upper voltage limits.

According to STEVENS, the sensitivity increment per 1 KV high voltage is greatest between 4 and 9 KV, with saturation being reached in the vicinity of 15 KV. Test results indicate that our source follows this rule. For a given accelerating voltage, we have found the signal to vary according to the formula :

$$I_{Re}\ 187 = \exp.\ (I\ \text{chauffage}) = \exp.^{(KT)}\ (\text{figure } 2)$$

II - ABUNDANCE SENSITIVITY -

In general, the usually given literature values for the abundance sensitivity for a simple focusing mass spectrometer are of the order of 10^{-4}.

Our tests concerning this point are based on the emission of Tantalum which normally exists in the form of two isotopes whose relative abundance ratio is 1.23 part per 10,000 :

- Isotope 181 (99.988 %)
- Isotope 180 (0.0123 %)

The choice of this element was based on the above interesting characteristics as well as the fact that highest mass weight isotope is also the most abundant. This last reason raises the problem of the importance of the peak tail on low mass side of isotope 181 due to gas scattering.

The abundance sensitivity tests were effectuated at 12 KV and under the most favorable conditions. On one hand, the width of the source slit was varied; while, on the other hand, the collector source was adjusted as fine as possible ($\simeq$ 0.02 mm) in order to obtain the real form of the ion beam. A standardized height for peak 181 was maintained during testing by regulating the gain of the electron multiplier, to an average of 10^{-4}, thus fixing I_{181} at 2×10^{-10} A.

Figure 3 shows up clearly the dependance of the abundance sensitivity on the source slit width and the contribution of isotope 181 in the measured value of isotope 180. In brief, for source slit widths varying between 0.02 to 0.02 mm., the contribution is found to vary accordingly between 10% and 33 %, and represents for the major peak a relative loss in abundance between 10^{-5} and 3×10^{-5}. With the source slit fixed at an average width of 0.1 mm. and the collector slit at a corresponding 12 KV

width of 0.6 mm. so as to allow a degree of resolution of 350, the contribution becomes 25 % or, in terms of relative major peak loss, 1.5×10^{-5} (figure 4).

In another series of tests, the collector slit was adjusted to 0.75 mm. Under this condition, the signal corresponds to an integration of a part of the beam. Consequently, the measured ratio between the isotopes differs from the theoretical value and the measured abundance ratio 180/181 decreases due to the increase of the isotope 181 peak base (figure 5).

III - DEGREE OF RESOLUTION -

A systematic study of the degree of resolution was undertaken using isotopes of neodymium (neodymium chloride) placed on the side filament, different accelerating voltages, and different source slit widths. The ratio of collector slit width per source slit width was kept at a fixed value of 6. Indicating the degree of resolution by the symbol PR, it can be defined in terms of the following equation :

$$PR = \frac{M}{\Delta M} \times \frac{L}{\alpha}$$

where L is the distance between peaks and α the breadth of the peak at 1 % of its height.

A very important change in the degree of resolution takes place as the source slit narrows (figure 6). Moreover, it is to be noted that this change is accented considerably by the variation of accelerating voltage, so that a very fine source slit and high accelerating voltage produces a very high degree of resolution. The maximum value which we have found to date was greater than 1,000, the source slit being at 0.03 mm. and the accelerating voltage at 14 KV. For the same sized slit, an accelerating voltage of 5 KV yields a degree of resolution of 600. This means that the reduction of the accelerating voltage by 2.8 times only decreases the degree of resolution by 1.6 times.

Consequently, it becomes evident that a high accelerating voltage is an important factor on the degree of resolution at a fine slit width.

IV - ABERRATION -

The half angle of the beam aperture, α , can be considered as being $7,5 \times 10^{-3}$ radians in conformity with the real geometry of our instrument and with the configuration obtained through the use of a slit value as a limiting diaphragm. Knowing the value of the factor $R\alpha^2$, is is possible to calculate the other aberrations, in terms of energy, which take place during the measuring of the Neodymium isotopes and for which a 0.03 mm. source slit is used.

High Voltage	5 KV	8 KV	10 KV	12 KV	14 KV
Δ V	3.4	2.6	3.0	3.2	2.5

This means that the average energy aberration can be assumed to be 3 (electron) Volts.

MASS SPECTROMETER FOR ROUTINE WORKS ON RADIOACTIVE PRODUCTS.

G. NIEF, P. LOHEZ, M. LUCAS*

INTRODUCTION -

The considerable development of studies on burn-up during the last few years entails the analysis of a large number of irradiated fuels. Since the determinations most commonly in demand,i.e isotopic composition of the plutonium produced, its concentration in the fuel (measured by isotopic dilution) isotopic composition of the uranium, are performed on a thermal-ionization mass spectrometer, we have designed a type of instrument especially adapted to routine analysis of radioactive products.

GENERALITIES -

This mass spectrometer, intended for the isotopic analysis of solid samples of mass between 6 and 300, is a first order focussing instrument.

The principles of ion formation, acceleration, focussing and collection are conventional.

The main features of this instrument are listed table I.

The improvements are of a technological nature and concern especially the introduction sample system ; access to the ionization chamber is simplified to allow quick changing of the sample and easy decontamination of the ion source.

The pumping system was designed in such a way that a pressure compatible with normal working conditions is quickly re-established in the ionization chamber, while at the same time a pressure of the order of 10^{-7} torrs is maintained in the analyser tube. A focussing electrode was placed before the first dynode of the electron multiplier in order to avoid gain variations, when scanning the spectrum.

INLET SYSTEM (Fig. I) -

In most conventional mass spectrometers the ion source container is pumped continuously, except for the ionization chamber itself which can be moved to make it accessible.

Such a system involves the construction of complex and expensive control and leak-prevention devices, and radioactive contamination of the units greatly complicates the manipulations necessary in the case of accident. The ionization chamber of the instrument described is fixed and the source container is restored to atmospheric pressure for introduction of the sample.

This container is cylindrical in form and its upper part includes a plate (1) holding a movable cover (2), the seal is provided by an O-ring held in compression simply by atmospheric pressure.

Inside the container the source is connected to the analyser tube (3) by a mobile shutter (4). This latter takes the form of a flat sliding drawer which can be moved horizontally between the bottoms of two cups (5-6) fitting one inside the other and covering the upper end of the analyser tube ; it is provided with a slit (7) and a leak-tight joint.

This drawer is manipulated inside the container simply by means of a valve with a metallic bellows (8).

* Commissariat à l'Energie Atomique - Service des Isotopes Stables - B.P. N° 2
GIF S/YVETTE (91) - France.

Fig. 1

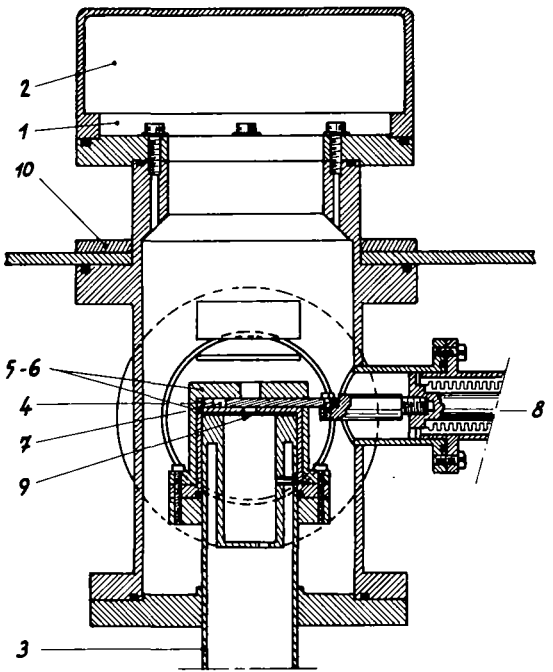

SAMPLE INTRODUCTION SYSTEM

Fig. 2

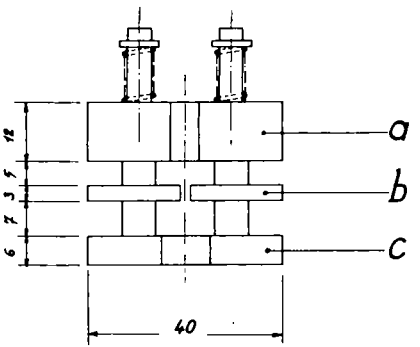

	POTENTIAL
CENTER FILAMENT	+ 5000 VOLTS
SIDE FILAMENTS	+ 5000 to + 4890 VOLTS
ELECTRODE I (a)	+ 5000 VOLTS
ELECTRODES II and II' (b)	+ 5000 to + 4500 VOLTS
ELECTRODE III (c)	EARTH
BETWEEN II and II'	0 to 50 VOLTS

ION SOURCE

In the closed position the container is isolated from the tube and can be brought to atmospheric pressure.

In the working position the slit in the drawer and those provided in the bottoms of the cups are made to coincide, and the ion beam from the ionization chamber can then pass through the definition slit (9).

On the cylindrical body of the source container is fitted one horizontal flange (10) to which a small glove box can be fixed;all the manipulations necessary for mounting radioactive samples on the ion source can be carried out in a controlled atmosphere.

The ion source (Fig. II) of this mass spectrometer consists of :

- a triple-filament assembly which is readily removed from the source for replacement of the sample; the sample is loaded on one of the side filaments and ionization takes place at the center filament.

- the ionization chamber and the focussing electrodes.

These latter, circular in form, are connected to one another by 4 insulating rods ; insulating beads hold them in position, and the whole system is held together by means of small springs and copper clips.

This source is fixed only by 2 screws to the mobile shutter and can be removed quickly from its container for decontamination and cleaning.

Immersion for a few minutes in nitric acid causes the copper clips to dissolve, and dismantling is thus very easy. The various components are rinsed, dried and checked for activity. After polishing and degreasing of the electrodes, the source is remounted, and only the springs and clips must be changed each time.

PUMPING SYSTEM (Fig. III) -

Two pumping systems linked together by the definition slit provide differential pumping between the tube and source compartments. Each includes a rotary pump (1), an oil diffusion pump (2) and a water-baffle ; the pressure is measured by an inverted triode ionization gauge (3).

A valve (4) is provided to isolate the tube from the diffusion pump when it is necessary to clean the mobile shutter ; the vacuum can then be restored rapidly in the tube.

A main line, which can be closed by a valve (5) connects the source container to the diffusion pump ; in addition this container is linked directly with the rotary pump through a by-pass (6).

Two other valves (7-8) are provided, to shut off the by-pass and to isolate the diffusion pump from the rotary pump.

To allow access to the ionization chamber the vacuum inside the container can be broken by opening a stop-cock which supplies dry gas.

After the sample is introduced into the ionization chamber, the pressure is lowered to a few 10^{-2} torrs by pumping for one minute with the rotary pump.

The diffusion pump is then branched to the circuit, and after about 10 minutes pumping, the pressure in the container is sufficiently low for the analysis to begin (a few 10^{-6} torrs)

ION COLLECTION -

Ion currents higher than $5 \cdot 10^{-15}$ A are detected by means of a Faraday cup followed by a direct current amplifier ; this collector can be slid into position without breaking the vacuum in the spectrometer.

An Allen type 10-stages electron multiplier combined with an amplifier is used to collect low ion currents (limit of detection 10^{-18} A). The dynodes are made of copper-beryllium alloy sheet containing 2% beryllium.

The gain of this multiplier is of the order 180.000 for a potential difference of 3.000 volts at the terminals ; it is effectively insensitive to air leaks. In the absence of ion currents the noise level measured on the amplifier is less than 10^{-18} A for a gain of about 10.000, corresponding to normal working conditions.

During scanning of the spectrum the impact point of the ion beam moves on the input dynode of the multiplier which can lead to variations in gain resulting in deformation of the tops of the peaks.

To avoid this disadvantage a focussing electrode was placed before the first dynode of the multiplier ; it projects on this dynode the fixed point around which the ion beam seems to relolve, and enables a constant response of the multiplier to be obtained.

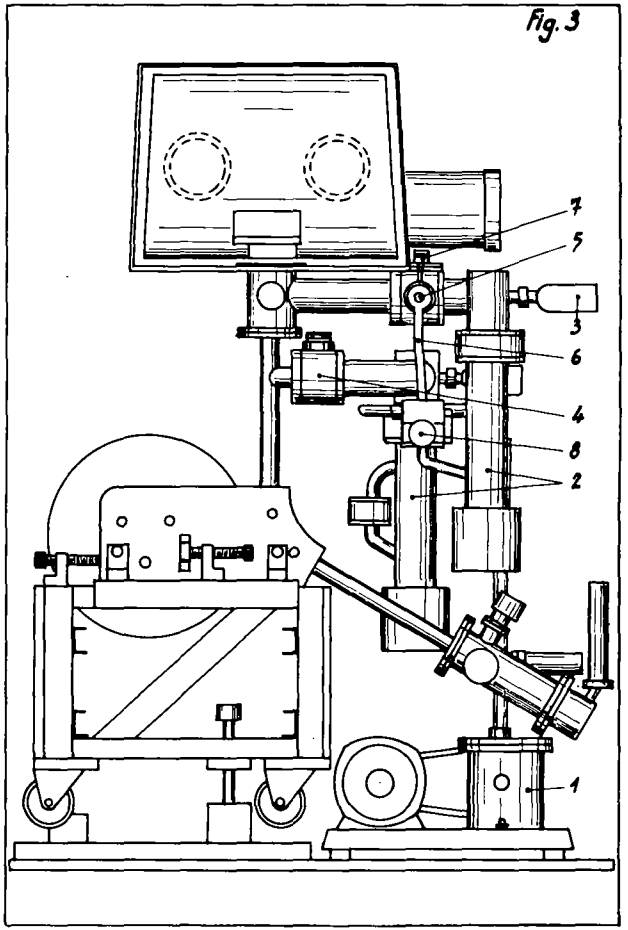
Fig. 3
7
5
3
6
4
8
2
1

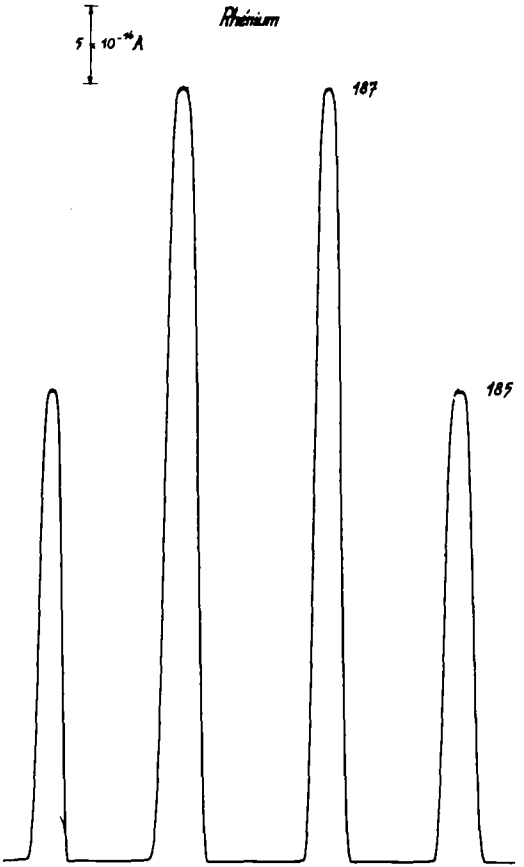
Rhénium
5 × 10⁻¹⁶ A
187
185

PERFORMANCES -

The resolution is defined by the geometry of the spectrometer : radius of curvature of the tube, width of the source and collector slits ; the collector slit width is variable.

With the parameters shown in the table I (R = 20 cm, width of source slit : 0.15 mm, width of collector slit : 0,5 mm) the resolution measured on a spectrum of natural uranium at 1% of the 238 peak height is equal to 280.

- Sensitivity tests were carried out on samples of uranium and plutonium. The ion currents obtained for the main peak are of the order of 10^{-12} A for a 10^{-7} g deposit of uranium, and reach $2 \cdot 10^{-13}$ A for a $2 \cdot 10^{-8}$ g deposit of plutonium.

- Speed of analysis. The average time for an analysis can be estimated at one hour.

It consists of :

- the return to atmospheric pressure of the source compartment.
- the mounting of the sample.
- the pumping time.
- the various adjustments of the ion source electrode potentials.
- the recording on paper of the ion currents relative to each mass.

The measurements are generally made on a series of 10 successive recordings of the spectrum in question.

- Precision. Let n be the atomic concentration of the isotope measured :
  - for $n \geqslant 1\%$, the mean value of the relative precision $\frac{dn}{n}$ is 0.5%
  - for $n < 1\%$, we can assume a constant absolute error $/dn/ = 0.005\%$

CONCLUSION -

This mass spectrometer has been in use for a year in our laboratories for routine isotopic analysis of radioactive products.

Because of its simplicity of design, maintenance and decontamination problems are easily solved while the frequency and duration of inactive periods can be reduced to a minimum.

An average analysis rate of 6 samples a day has been obtained.

TABLE I

MAIN FEATURES

- First order focussing spectrometer tube

  radius : 20 cm - deflection angle : 60°

- Ion source with multiple filament arrangement

  slit width : 0.15 mm

- Accelerating voltage : 5000 volts

- Scanning of spectra by varing magnetic field

  magnetic field strength : 8500 gauss (mass 300)

- Detector system

  Collector slit width $\simeq$ 0.5 mm

  Faraday cup + D.C. amplifier ($R = 10^{11}\ \Omega$)

  Electron multiplier + D.C. amplifier ($R = 10^{10}\ \Omega$)

  Focussing electrode

- Vacuum system

  Rotary pump : pumping speed : 3.5 m^3/h

  Oil diffusion pump : pumping speed : 100 l/seconde

  Tube pressure $< 5 \cdot 10^{-7}$

  Ion source pressure $< 10^{-6}$

BIBLIOGRAPHY

INGRAM M.G., CHUPKA W.A - Rev. Sci. Inst. 24, 518, (1953)

STEVENS C.M. and INGRAM M.G. - U.S.A.E.C., Report A.N.L. 5251 (1954)

CRAIG R.D. - J. Sci. Inst. 36, 38 (1959)

ALLEN J.S. - Rev. ScI. Instrum. (1947), 18, 739-749

INGRAM M.G. - Mass spectroscopy in physics Research - U.S. Department of commerce National Bureau of Standard Circular 522, (1953)

BARNETT C.F. - ORNL 1669, Oak Ridge National Laboratory (1954)

NIEF G., LOHEZ P. - Rapport C.E.A. N° 692 (1957)

Uranium

Sample : 10^{-7}g nitrate

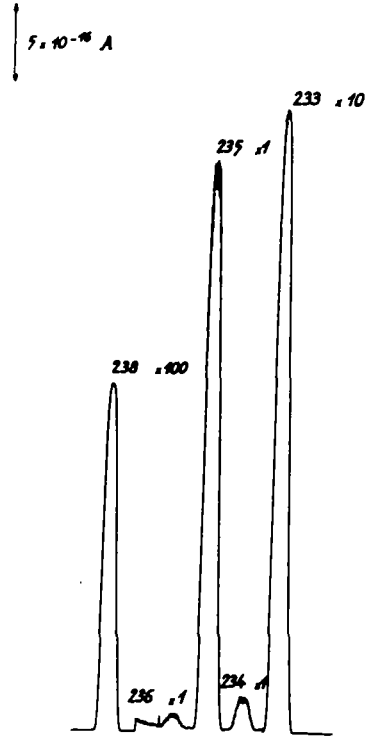

The Small Mass Spectrometer-
A New Approach to Analysis

D. Allenden
Associated Electrical Industries Limited
Manchester, England

Abstract

Mass spectrometry has been dominated since its emergence by the large analytical mass spectrometer, often costing around $100,000 and requiring the exclusive services of a skilled operator installed in a special laboratory. Many small mass spectrometers have appeared on the market, but these have, almost without exception, been conceived, marketed, and employed as residual gas analyzers. It is the object of this paper to show that a small, inexpensive mass spectrometer, if conceived as an analytical instrument rather than as an R.G.A., can be applied with complete success to many applications from which the large instrument may be excluded on grounds of economics, low utilization, bulk and inflexibility or sheer complexity, while being able to complete in fields hitherto dominated by classical chemistry or other analytical methods such as infrared spectroscopy.

The performance and design criteria for the small mass spectrometer are stated, and a description is given of the AEI MS10 series instrument in which these criteria have been applied to provide a true analytical mass spectrometer at low cost, with a mass range up to 400. The instrument design is based on a "functional module" conception which assures great versatility.

The major part of the paper deals with selected applications which emphasize the title theme. Examples described include problems in organic chemistry, food technology, metallurgy, process control, automotive engineering, biology and botany, geology and petrology. A comprehensive bibliography is included.

NEW PERFORMANCE RESULTS FOR THE

12-90 G MASS SPECTROMETER SYSTEM

By D.J. Marshall, Nuclide Corp., Medford, Mass.
T.J. Eskew, Nuclide Corp., St. College, Pa.

Abstract

Further development of the 12-90 G Mass Spectrometer System is described.

A Retarding Potential Difference source, operated in the pulsed mode, is described. This source exhibits a day-to-day reproducibility of details of the ionizing efficiency curves for krypton and argon of 30 mV.

The operational characteristics of a razor blade type Field Ionization Analytical Source are outlined.

A mass marking system with precision of 1/1000 and sufficient time response to follow a magnet scan rate of 10,000 gauss/second is described.

INTRODUCTION

The Nuclide 12-90 G is a versatile mass spectrometer system developed to fit the varied needs of the organic and physical chemist.

One of the principal uses of the instrument is for the determination of structures of complex molecules by study of their fragmentation pattern. Its performance for this type of analysis with the Direct Inlet Probe has been described previously. Gas Chromatograph effluent analyses have been made with a heated capillary connection and a dual ionizer arrangement to discriminate against carrier gas. The sampling method of Amy and Co-workers (1965) has also been used, for example, in the analysis of small samples of pesticide residues in forage crops.

In this paper we will describe the performance of a Retarding Potential Difference Source and other new accessories.

RETARDING POTENTIAL DIFFERENCE SOURCE

The Retarding Potential Difference method is a method of studying the ionization efficiencies of atoms and molecules with a low effective energy spread in the electron beam.

Retarding Potential Difference (RPD) Sources have been constructed by many workers since Fox and co-workers (1951), first published their description of this type of ionizer.

There has been a tendency to place limited confidence in the results obtained from the source because of anomalous results obtained in some instances.

We observe that there is a growing recognition of some of the factors which affect the quality of performance of the RPD type of source. We do not presume to know all of the requirements which are critical but wish to present our results as one more piece of information on this subject.

The RPD Source was developed for use on a Nuclide 12-90 G, 12" radius, 90° sector single focusing mass spectrometer. It is interchangeable with the standard electron bombardment source. More precisely, the RPD electron gun is interchangeable with the standard electron gun.

The RPD electron gun and the ionization chamber are shown in Figure I. The axial magnetic field indicated has a strength of 200 to 300 gauss.

The electron gun electrode aperture sizes increase slightly along the electron path to a maximum of 0.060". These electrodes are made of Inconel electropolished in the conventional manner.

The filament is lit with 4 volts and 5 amperes of direct current. The filament heating current is regulated to 1/20,000 or better. The electron energy measured between the filament center tap and the ionization chamber, is regulated to ± 10 mV or better under conventional operating conditions.

The entire source is heatable but was not heated during the tests to be described.

The voltages on the various electrodes are indicated in Figure I. Under these conditions, 5 microamperes of trap current was easily attained. The source magnets used were adjusted for maximum trap current which corresponds closely with maximum ion current.

The retarding grid was set at about -1.0 to -1.5 volt and was switched by an amount adjustable up to 100 mV. Zener diode regulation is provided on the retarding voltage supply.

The data was recorded with the instrument set up for a resolving power of about 350. An electron multiplier with a 10^5 gain was used with a 10^9 ohm input resistor in the electrometer.

The output of this multiplier was displayed on a conventional recorder without buckout.

Data taking consisted of letting the system warm up for about one hour under actual operation conditions with gas flowing in. The RPD curve on the peak of interest was then taken in a sequence of adjusting the electron energy in 50 or 100 mV steps, making a high and low retarding potential setting at each value, then proceeding to the next value of electron energy. Approximately 15 minutes were required to complete a run. The trap current varied by less than ± 5% over the period of a run and this variation was related reproducibly to the electron energy changes and not to random drifts.

The source operates also in the pulsed mode which is the preferable one.

Pulsing is done by switching the voltages on grids #2 and #4 in Figure I between -10 & +1 volt with respect to the filament center tap. The pulsing sequence is shown in Figure II.

The positive excursion of the turn-on pulse is limited by means of a clamping circuit referred to the filament mid-point and the stability of this voltage is 10 mV or better under conventional operation conditions.

The amplitude of the negative excursion of this pulse, which turns off the electronbeam is not particularly critical. Negative 10 volts was chosen to insure complete turn-off of the electron beam.

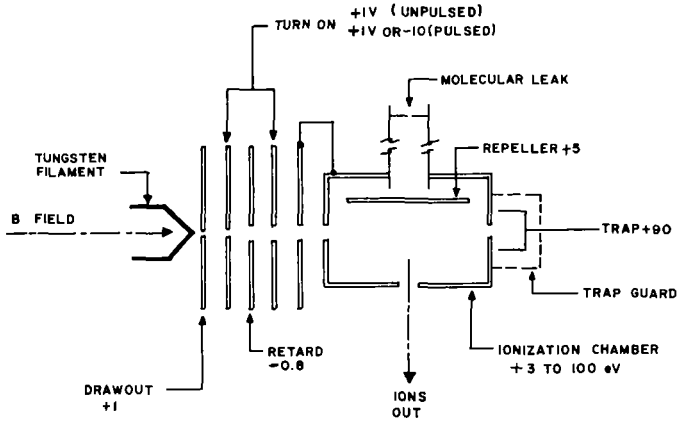

RETARDING POTENTIAL
DIFFERENCE SOURCE SCHEMATIC

Figure I

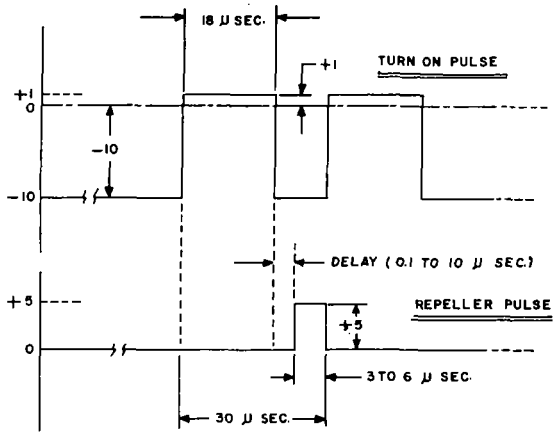

RPD PULSE RELATIONSHIPS

Figure II

It is, of course, most important to observe the pulse shapes at the electrode themselves, if possible. We observed, initially, good pulse shapes at the generator but found an appreciable amount of ringing and extraneous spikes when observations were made at the electrical lead-through.

The repeller is switched on after a selected delay.

The pulse repetition rate is variable from 20 KC to 100 KC with a maximum duty cycle of 60%. Figure II displays the general relationship of the pulses. In actual runs made, the duty cycle was usually 5%.

The inherent efficiency, defined as the number of ions reaching the collector, per gas molecule entering the source, per ionizing electron, was essentially the same for pulsed operation as for unpulsed operation.

The resolving power was essentially unchanged during pulsing and an example of high resolving power with the pulsing on is shown in Figure III.

Figure IV shows data points from several studies of Argon. The retarding potential difference was 50 or 100 mV in these runs. The average trap current was 0.5 microamperes. The delay was 1μ sec. and the duty cycle 5%.

Figure V is of the same data with linear segments drawn in. The position of the first three breaks, averaged over the three curves and measured from threshold is

0.21 eV
0.52 eV
0.94 eV

The spectroscopic value corresponding to the first observed break is 0.18 eV.

The reproducibility of the RPD results for Argon and Krypton, based on tests made to date, is of the order of ± 30 mV. This is based upon fitting the linear segments by eye and does not presume the use of any sophisticated statistics.

FIELD IONIZATION SOURCE

A Field Ionization Source which incorporates a razor blade type emitter has been designed and partially tested. It operates with a voltage variable up to 12 KV. The anode-cathode spacing is 13 mils. A cathode slit with a length to depth ratio of 1 has been found to be most effective in establishing the field at the emitter. The field ionizer is interchangeable with the Electron Bombardment ionizer and used the same ion optics. Both the direct inlet probe and the molecular or GC inlets may be used with the field ionizer.

The razor blade for the Field Ion Source was cleaned with trichloroethylene but untreated, otherwise, before use.

Preliminary results only are available. The source provides stable ion currents from background and from N-Butane. The total ion currents for a pressure of 10^{-4} torr of N-Butane and 9.5 KV of voltage are 10^{-11} to 10^{-10} amperes. Analyzed currents at a Resolving Power of 200 - 300 are of the order of 5×10^{-15} amperes and appeared to be predominately parent peak.

N_2 - CO DOUBLET

PULSED RPD
20 KC
4 KILOVOLTS
12-90-G1.6 2/2/66

Figure III

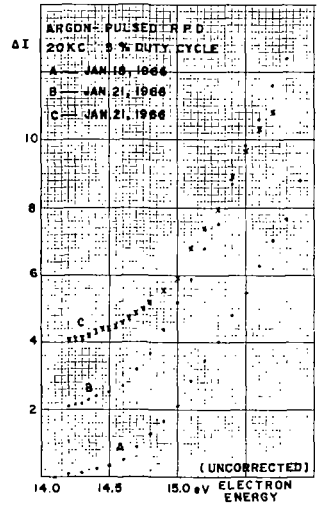

Figure IV

MASS MARKER

The Mass Marker used with the 12-90 G is designed for operation at fast scan rates while maintaining good precision. It employs a high performance Hall effect magnetic field sensing device whose output is balanced against a precision 10 turn potentiometer by means of a high speed servomechanism. The position of the servomechanism output shaft, the analog value of the mass in focus, is displayed optically on a ground glass screen window and photoelectrically on a recorder or oscillograph. The ground glass screen window display is particularly useful for making adjustments and for routine operation of the instrument at low scan rates.

A 400 gauss portion of the scale is visible in the window. At the upper end of the mass range this corresponds to about 0.1" spacing between adjacent masses.

Both the optical and photoelectric readout have precision of 0.1% at moderate scan rates and are better than 1% at fast scan rates of the order of 2000 gauss/second.

The Mass Marker output printed on the recorder or oscillograph chart consists of a mark every 5 mass units and a special mark every 50 mass units in the 1 - 1000 amu mass range.

When the system is adjusted for the 1 - 2000 amu mass range, a mass mark is made every 10 mass units and a special mark every 100.

The markers which indicate every fifth mass position are individually adjustable to compensate for non-linearities in the mass spectrometer equation and in the remainder of the system.

Two calibrations are required daily - one to set the zero and one to set the scale range. These adjustments are typically done at mass 15 and mass 200.

Figure VI shows a portion of the spectrum of para-pard DDT run in the Direct Inlet. The scan rate in this instance was such that the mass range of 10 to 400 amu was covered in 50 seconds.

ACKNOWLEDGMENTS

We wish to acknowledge the assistance of Dr. L.A. Cambey, Mr. E.G. Kerfoot, and Mr. A.J. Smith of Nuclide Corp. We also wish to acknowledge the assistance of Dr. Sydney Gordon and Dr. G.J. Krige of the Atomic Energy Board of the Union of South Africa.

BIBLIOGRAPHY

Amy, J.W., Chaint, E.M., Baitinger, W.E., McLafferty, F.W. (1965) A general technique for collecting gas chromatograpmic fraction for introduction into the mass spectrometer. Anal, Chem 37(10)1265-6.

Fox, R.E., Hickam, W.M., Kjeldaas, and Grove, D.J., (1951), Phys. Rev., 84, 859.

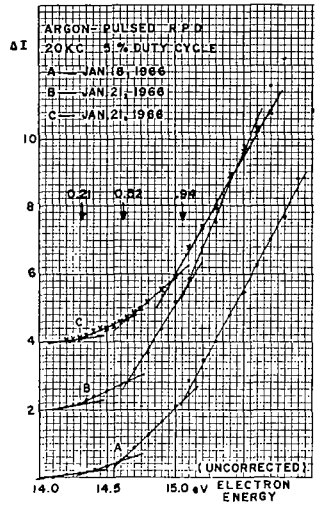

Figure V

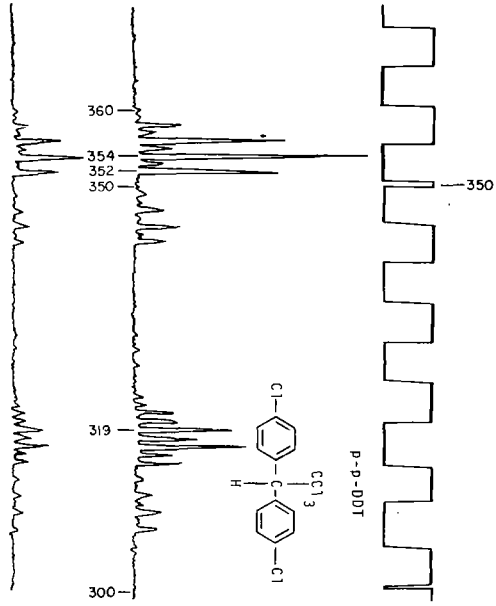

Figure VI

PERFORMANCE CHARACTERISTICS OF A NEW TIME-OF-FLIGHT MASS SPECTROMETER

by R. W. Bonham, D. C. Damoth and C. J. Moorman
The Bendix Corporation
Cincinnati Division

At the Twelvth Annual Conference on Mass Spectrometry held in Montreal in 1964, one of us (D. C. Damoth) announced the design concepts of a new mass spectrometer based on the time dispersion principle. Since that time, several generations of this instrument have evolved and the authors have compared the performance with the original design targets. This article reports on the performance of the Model 3012 Time-of-Flight Mass Spectrometer.

DESIGN

The instrument design was a joint effort of the Research Laboratories Division and the engineering department of the Cincinnati Division of The Bendix Corporation. The ion optics were the result of a computer evaluation done by the Research Laboratories Division and the vacuum and electronics consoles were developed in Cincinnati.

The pumping system supporting the drift tube, is protected against loss of vacuum, cooling water, liquid nitrogen or low temperature in the freon cooled baffle. Although this instrument has been pumped to the 10^{-9} Torr range, the background pressure normally runs in the 10^{-8} Torr range. Pressure measurements are by a thermocouple gauge in the foreline and by a nude Bayard Alpert gauge in the drift tube. Individually replaceable ceramic feed-throughs and crushable copper gasket sealed flanges yield complete high temperature bakeout capability.

The electronic console is about one third solid state. These devices are used where they offer advantages and standard tube circuits are used where tests indicated solid state circuits to be lacking. The electronic console is maintained at a positive pressure with filtered air to minimize dust collection.

The final optics design is as shown in Figure 1. The filament is heated by direct current. The trap current is controlled by regulating the filament drive with a choice of pulsed or nearly continuous electron beam generation. Maximum integrated ionizing current exceeds 2 microamps in the pulsed mode and 100 microamps in the continuous electron beam mode of operation. The five electron gun slits are used as grounded collimating slits or as components of a RPD gun for ionization potential work. The electronic circuitry for this latter application are built into the instrument offering maximum versatility in this mode. The standard repetition frequency of the spectrum is 10,000 times per second, with 10-100 kilocycles optional.

The ion gun is a series of four planar grids of 0.002 inch thick molybdenum each with a transmission efficiency of better than 85%. A practically square negative ion draw out pulse of up to 80 volts amplitude and two microseconds duration is applied to grid one. Grid two operates with a zero to 400 volt pulse or zero to 400 volts D.C. bias. The two pulse operation usually offers better resolution and reduced field peek through into the ionizing region. Grid three is held at about -900 volts D.C. and grid four at -2800 volts D.C., as is the high voltage screen extending the length of the flight tube. The deflecting plates shown in the drift tube section direct the ion bunches onto the magnetic electron multiplier cathode at the far end of the tube. An adjustable voltage may be applied to the ion lens to effect electrostatic focusing of the ion bunches. The seven anode right angle multiplier is capable of monitoring six individual ion signals or scanning six portions of the spectrum while the seventh anode carries the complete spectrum to an oscilloscope for constant visual monitoring of the mass spectrum.

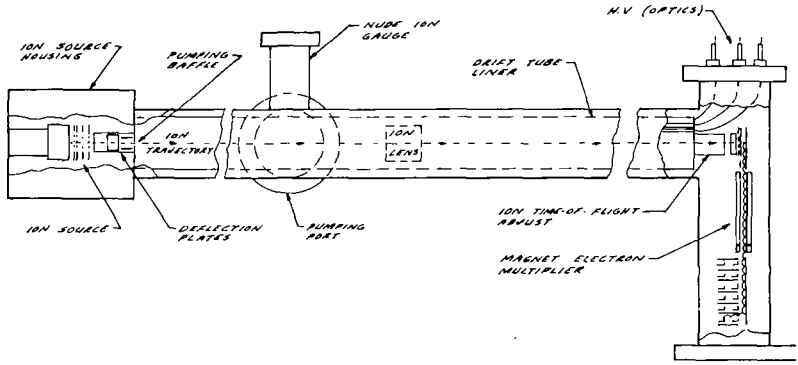

3012 / 3015 TOFMS ANALYZER TUBE
(TOP VIEW)

FIGURE ONE

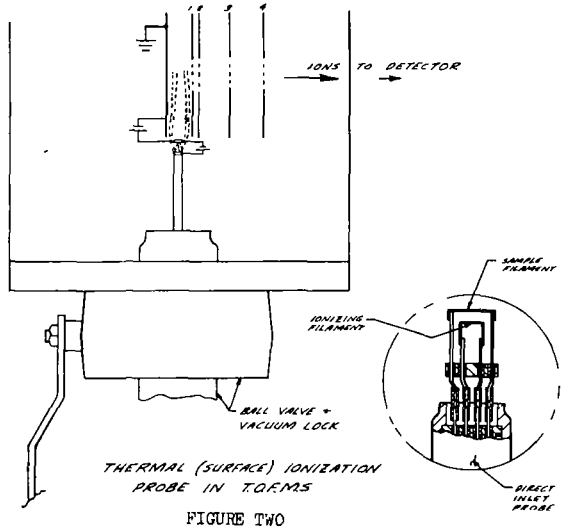

THERMAL (SURFACE) IONIZATION PROBE IN TOFMS

FIGURE TWO

As in all previous Time-of-Flight instruments, the voltage on the short "stack" on the multiplier may be made positive enough to delay the charged ion spectrum and permit study of metastables. Since these peaks occur at the same mass position as the original ion, mass identification is simple and straightforward. As the voltage on the stack is changed the relative position of metastable species changes faster than the regular ions.

PERFORMANCE

In the performance tests, our first concern was the resolution evaluation. The basis of comparison was the performance of a standard Model 12-107 with typical organic compounds. The resolution was about 20% better with the new source: the backing plate to drawout grid distance had been reduced from 0.270 inch to 0.070 inch to improve energy focusing. We suspected that the change had been too drastic, so spacers were added to extend this spacing to 0.100 inch. Measured resolution went from about 325 to nearly 375. A second set of tests were made with the spacing widened even further, to 0.130". The resolution improved again, being measured at about 425. On the third test with the spacing set at 0.160 inch, the resolution decreased to just under 400. The 0.130 inch spacing was optimum. The grounded backing plate was floated and several combination of small pulses and D.C. biases were tried, but no marked changes were seen. The backing plate was then completely removed, the 0.130 inch spacing being maintained and again no marked change observed.

Next, we examined the isotope ratio stability. The stability was such that the standard deviation of a series of ten such determinations was significantly better than $\pm$ 0.2%. The average of two such runs, made several hours apart, checked to within 0.2%.

The sensitivity of the instrument is such that a source pressure of nitrogen of 1×10^{-6} Torr results in an output current of better than 1×10^{-7} amperes in the two pulse mode. The minimum signal readable, defined as 10 times the background noise, is 1×10^{-13} amperes, indicating the basic sensitivity of 10^{-14} Torr for detection. Use of the continuous ionization mode may extend this because the duty cycle increase is a factor of several hundred but we have no data as yet.

SOURCES AND INLETS

There are several sources available with the instrument; the previous data was obtained with the new standard analytical source. Also available are the ion molecule reaction source for operation to 100 millitorr, a nude source that can be cantilevered into a vacuum system for R.G.A. work, an atmospheric sampling system and a source featuring direct line-of-sight sampling into the ionization region for flame and plasma analysis.

A new addition to the sources available with the Time-of-Flight Mass Spectrometer is the Surface Ionization Source. This technique, first used with the Time-of-Flight instrument by Dr. Martin Studier of Argonne National Laboratories, shows great promise. The device built by us is a single sample filament model as shown in Figure two. The filaments are mounted on the end of a direct inlet probe and may be easily inserted and withdrawn. The upper ribbon is the sample holder and temperature ranges from ambient to about 2000°C. The lower ribbon is the ionizing filament and suitable biases are applied to focus the ions into the ion drawout region prior to mass separation. Since the surface ionization probe does not interfere with the electron beam, one can switch rapidly from the S.I. source to the gas source.

TYPICAL BACKGROUND SPECTRUM WITH THERMAL IONIZATION PROBE IN PLACE.

FIGURE THREE

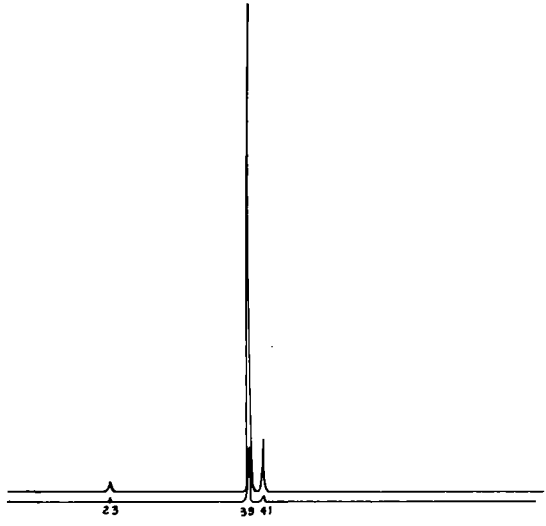

THERMAL IONIZATION SPECTRUM OF Na & K.

FIGURE FOUR

Figure three shows the spectrum obtained with the thermal source inserted and the background generated by the preliminary heat up. Pressure read on a Bayard-Alpert gauge was 3×10^{-7} Torr. The sample is a mixture of sodium and potassium chloride. Figure four shows the sample a few seconds later with the ionizing electron beam turned off and the sodium and potassium ions focussed directly on the multiplier cathode. In figure four, the vertical velocity component of the sample vapors threw them off the detector. Lithium salts and uranyl nitrate were ran successfully also.

Figure five is a graphic representation of the new Total Output Integrator for the Time-of-Flight. This device is an analog output plug-in but does not scan the mass spectrum. It gives an output signal proportional to the sum of the intensities of the mass peaks above some selected mass number; for example, by integrating above mass 40, the output is a sensitive, linear gas chromatograph ionization detector which does not see helium, water or air and is completely coincident with the mass spectrum output.

The Total Output Integrator operates on a count-down cycle of 8 mass spectra, each complete in 100 microseconds. On the first six cycles, the analog output scanning channels operate normally. On the seventh cycle, the analogs are turned off and the oscilloscope sweeps the mass spectrum. On the eighth cycle, the Total Output Integrator turns on at some selected mass position below 240 amu and integrates the spectrum. Then the eight cycle countdown repeats.

CONCLUSION

The general design and operating specifications of the new Time-of-Flight Mass Spectrometer indicate versatility and ease of operation in all applications. It is capable of nearly double the resolution of previous models and a full order of magnitude more sensitivity. The addition of surface ionization capability adds to the instrument's usefulness.

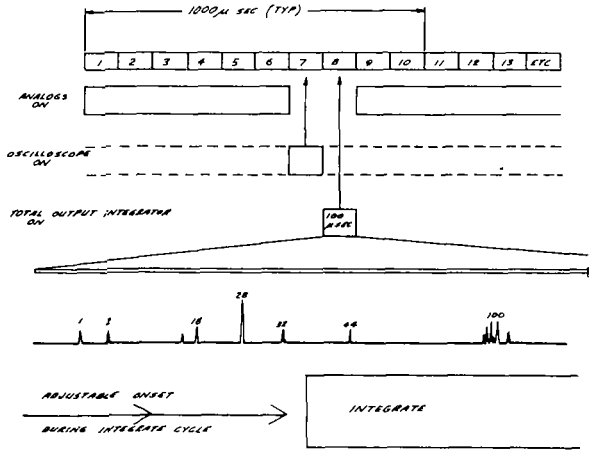

TOTAL OUTPUT INTEGRATOR TIME SEQUENCE
FIGURE FIVE

"A SOLID STATE DIGITIZER OF PEAK HEIGHT AND MASS NUMBER FOR MASS SPECTROMETERS"

J. Guibourg, J-C. Merlivat, G. Bernard, Ph. Dard, and B. Swiners

COMPAGNIE FRANCAISE THOMSON HOUSTON
PARIS - FRANCE

DIGITAL ANALYSIS OF MASS SPECTROMETRY DATA

Assigning a numerical value to the measured characteristics of a sample opens the possibility of operating a computer directly on the information obtained from a mass spectrometer. With the intermediary readings and encodings thus eliminated, the operator is freed from the tedious task of following the unfurling of the classical recorder chart. Moreover, the information is readily available in a usable form; namely, the numerical value corresponding to the maximum amplitude rise and the mass value detected for each peak, during analysis, is recorded by a printer or perforator. An additional feature of this system is that it can be linked up to a programmer or a process control computer.

The block diagram of the system, found in figure 1, may be explained in the following terms :

- With the systematic variation of the magnetic field, the mass spectrometer is made to function in automatic scanning. The digital analyzing system associated with the mass spectrometer is programmed to detect the maximum rising current values collected. This corresponds to peak positions. Whensoever a peak is located, the scanning stops and a small incorporated analog computor determines the corresponding mass. The information concerning mass and amplitude of the peak is then converted into a numerical value and recorded serially in its output form by a translator. Finally, thanks to an adapter, the electromagnets of a printer or perforator can be activated to transcribe the message.
  Physically, the system can be described as a three rack cabinet, with each rack corresponding to a specialized electronic chassis.
- The numerical encoder.
- The amplitude and mass information analyzer.
- The output stage with a printer or perforator.

The system receives three kinds of information :

- The strength of the deviating magnetic field.
- The ion accelerating voltage.
- The strength of the ion beam current.

On the basis of this information, the system calculates the mass value, detects the location of a peak point, converts into a numerical value the various analog potentials corresponding to the amplitude and mass values of a peak, and transmits the encoded information in series to the output organ.

I - MASS COMPUTATION -

This operation consists in obtaining an analog potential whose amplitude is proportional to the instantaneous scanned mass and can be expressed in terms of the following equation :

$$RB = \sqrt{\frac{2\ mU}{e}}$$

where : R is a constant equal to the trajectory curvature radius,
e is a constant equal to an electron charge,

B is the magnetic induction,
U is the accelerating voltage, and
m is the mass, after ionization, hitting the target under the condition of the above mentioned parameters.

Consolidating the various constant factors, the equation may be given in terms of :

$$m = \frac{K B^2}{U}$$

Furthermore, as the voltage is maintained constant for a given spectrometer, the equation can be simplified to $m = KB^2$. By using two Hall cells, B^2 can be measured and, consequently, the mass as well.

Once the unit has been calibrated in function of the various ion accelerating voltages, it is only necessary to know this potential in order to measure the mass as a function of the voltage output of a special circuit composed of Hall cells linked to an operational amplifier. For this reason, a hand operated switch was foreseen to fix the accelerating voltage at a definite value.

In brief, using a table of values, the operator can choose precisely the accelerating voltage to give him the term KB^2 in 10 mV units, i.e., the equivalent in absolute value to the real mass.

II - DETECTING THE LOCATION OF A PEAK -

The function of detecting the location of a peak corresponds to a detection of the moment of maximum current rise on the collectors.

The output potential of the current amplifier is injected into a five scale analog numerical convertor having a 20 millisecond rate of conversion. A circuit inhibits the conversion order, if the present value of the input potential is less or equal to the value obtained in the previous conversion. Consequently, an effective conversion only takes place if the measured signal is rising. The system provides an output signal each time there is a conversion. If, at a given moment, the signal disappears, the input potential is considered to have stopped rising and thus is passing by a maximum. The logical manipulation of conversion signals takes place in two steps :

a) detection of a continuous rise
b) detection of the highest point

This arrangement avoids detecting unimportant events such as noise or zero level. When a peak position is detected, the system switches over and orders the transcription and the stopping of the scanning.

III - TRANSCRIPTION OF OUTPUT INFORMATION -

The output of the system is a word made of 16 ciphers which can be broken down into 2 half-words of 5 numerical characters plus reading instructions. The transcribing consists in sending the 16 cipher series to the output element. The first action is to ground the input of the numerical converter whose memory stocks the last encoded value, which, in this case, is the peak amplitude.

A series-forming circuit selects the 5 decimal or binary-decimal digits, according to the case, and provides the characters indicating the reading instructions. When the numerical value of the peak amplitude has been transcribed, i.e., the first half-word, the numerical analog convertor input is switched on to the output of the mass - computor. The series-forming circuit acts a second time to transcribe the numerical value of the mass. With the end of this operation, the return to zero of the scan circuits is released. The scanning starts up again and the system begins the analysis of the next peak.

IV - PERFORMANCES -

This system even permits the detecting of peaks whose amplitude corresponds to 10 millivolts. The measuring error is less than $\pm$ 3 millivolts for low values, and $\pm$ 1 % for the others based on a dynamic range of 70 decibels, i.e., 10 millivolts at 30 volts.

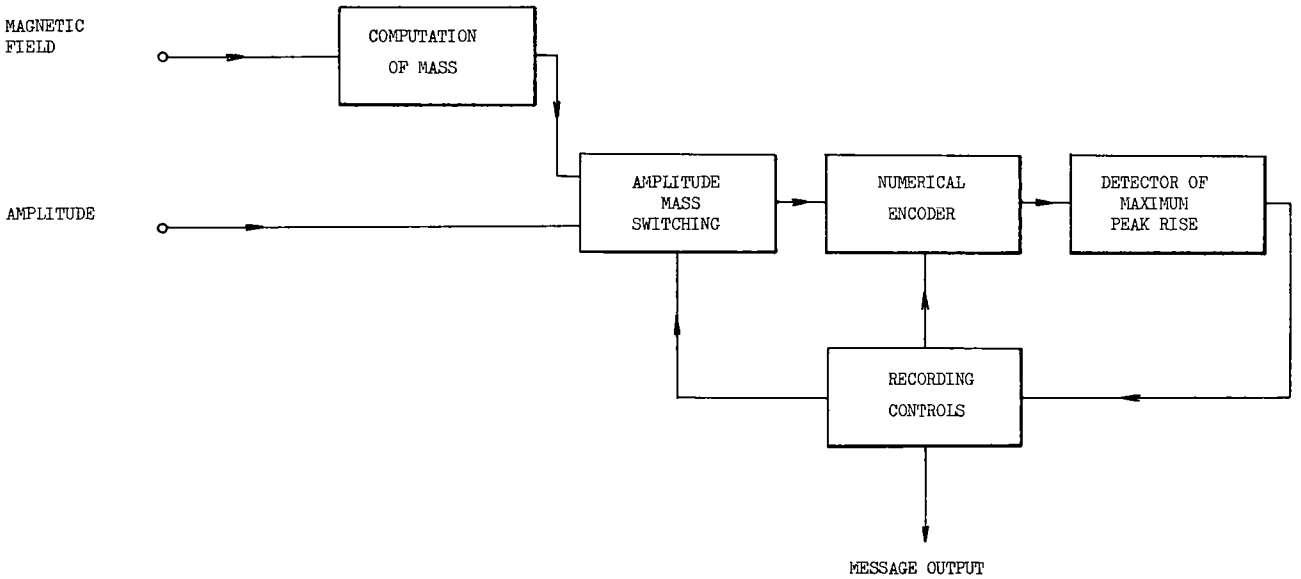

OPERATIONAL SCHEMATIC : FIGURE 1

The maximum error implicated in the measuring of the mass is 0.3 % due to a slight non linearity of the Hall cells. This can be further diminushed by adding a simple linear compensating circuit.

CONCLUSION

Complete automation in mass spectrometry has been achieved by means of the previously described system. Furthermore, this type of analysis can also be employed for continuous functioning process control.

FIGURE N° 2

RULES FOR DECODING

1) The information obtained on each detected peak is transmitted in a coded, 16 cipher word form.

2) The code is based on the position and value of each cipher, i.e. :

Position of cipher in word.	M E A N I N G
1	Signal indicating beginning of information on a particular detected peak.
2	Signal indicating beginning of half-word concerning amplitude.
3, 4, 5, 6, 7	5 grouped ciphers indicating amplitude value (peak strength).
8	Signal indicating half-word on amplitude "out".
9	Signal indicating separation of half-word.
10	Signal indicating beginning of half-word concerning mass.
11, 12, 13, 14, 15	5 grouped ciphers indicating the mass value.
16	Signal indicating word "out".

MASS SPECTRA OF ORGANIC COMPOUNDS DEMONSTRATING A NEW VACUUM LOCK DIRECT INTRODUCTION SYSTEM AND AUTOMATIC MASS MARKING

By

H. W. Major, Jr. and A. H. Struck

Perkin-Elmer Corporation
Norwalk, Connecticut

The determination of the correct mass number of the peaks in a mass spectrum is a well recognized problem. The MK-12 Automatic Mass Marking System was designed for use with the Hitachi Perkin-Elmer RMU-6 series of Mass Spectrometers. It provides an accurately located mass interval indication on the spectrum. This marking interval may be selected by the operator for each 1, 5 or 10 mass units. In addition to the chart indication, a digital display of the mass number is simultaneously exhibited via neon lights on the front of the cabinet. This feature makes it a simple matter to go to any portion of the spectrum if a more detailed examination of a peak or peaks is desired.

Figure 1 shows a block diagram of the operating principle of this system. The probe that measures the magnetic field is a rotating coil dynamometer. When the coil is rotated in the magnetic air gap with a constant velocity, an AC EMF proportional to the magnetic flux density is obtained. A sampling switch selects waves with a certain amplitude and excludes others. The difference between this sample voltage and a reference voltage is amplified as a positive or negative pulse, shaped in wave form and fed to the counter. The digitized decimal output is converted into a square root voltage (D-A converter) via a programmer arranged so as to approximate $M/e = Kx^{1/2}$. This voltage becomes the reference to be compared with the sample voltage. The counter continues to work in this fashion until the generated and reference voltage difference becomes zero.

The rotating coil is driven by a synchonous motor to which a frequency stabilized AC voltage is fed from a supply made up of a quartz oscillator and LF amplifier to assure high stability.

The coil shaft is supported in oil inclusion bearings to reduce friction and is provided with a flywheel to stabilize the rotation. On this flywheel is a slit aperture with which the sampling period is determined. The slit forms an optical system with a light source, condenser lens and photo transistor, which together play the role of the control gate of the sampling switch.

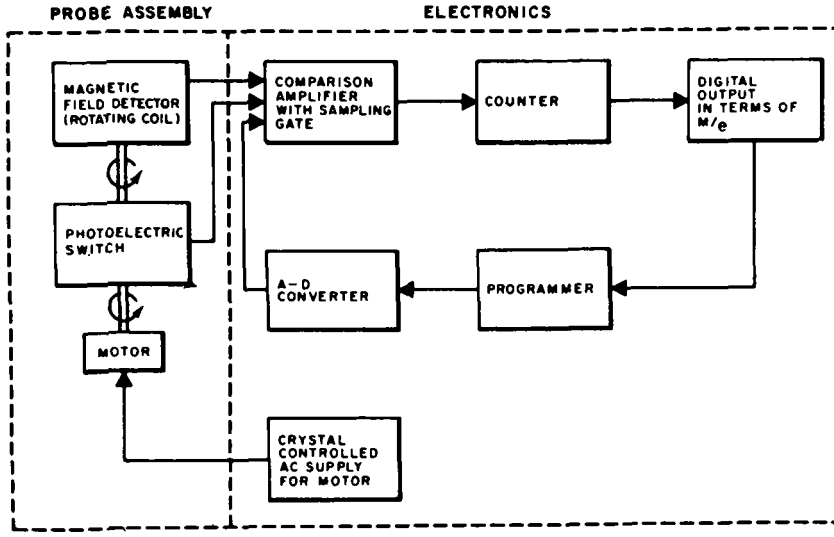

FIGURE 1

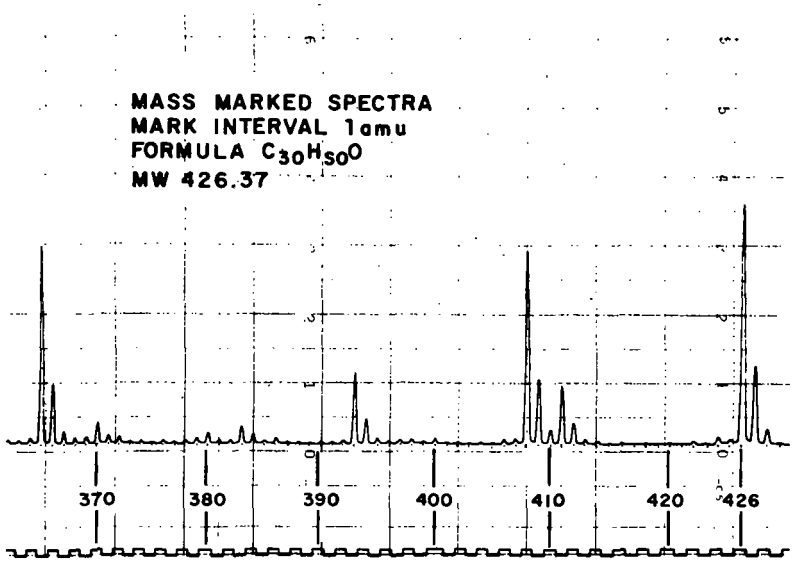

FIGURE 2

The satisfactory introduction of samples into a mass spectrometer is sometimes the most difficult and time consuming part of obtaining a meaningful spectrum. This is especially true as the sample volitility decreases and/or the sample instability increases. The MG-150 Direct Introduction System to be described has been tested and shown to be a highly satisfactory system for the introduction of such samples.

Among its distinctive features are the following:

1. Operation in front of the instrument.

2. Tilted turret design enables vertical replacement and horizontal insertion of the sample.

3. Independent source and sample heater temperature regulation in combination with a heat shield between the ion source and sample heater.

4. A new sample can be mounted, evacuated and ready for analysis during the spectrum recording for a previous sample.

5. Stabilized DC heating for sample evaporation eliminates peak height fluctuation during the run.

6. A silver ball compression seal isolating the exchanger from the analyzer vacuum results in a minimum background.

7. An additional tiny chamber for sample replacement allows break-free evacuation of the exchanger.

8. High vacuum pumping system with a cold trap prevents analyzer vacuum degradation during sample replacement.

9. Last but not least, is its simplicity of operation.

Figure 3 shows a cutaway of the MG-150. The sample is charged in the sample container after which the cap is replaced and forepump pressure is achieved through valve #2. The handle is then drawn into the exchange block where the diffusion pump reduces the pressure to that of the analyzer. The other sample holder is then drawn from the ion source into the exchanger and the two handles exchange positions by rotation through 180° on an axis of 45° with respect to both of them. The new sample is then inserted into the ion source and is ready for analysis while the old sample is removed and the next may be prepared and prepumped.

Figures 4, 5 and 6 show some samples run with this Introduction System. The cholestrol spectra shows the loss of H_2O to be less than 30%. Spectra of other samples such as curare and penicillin have been obtained with this system.

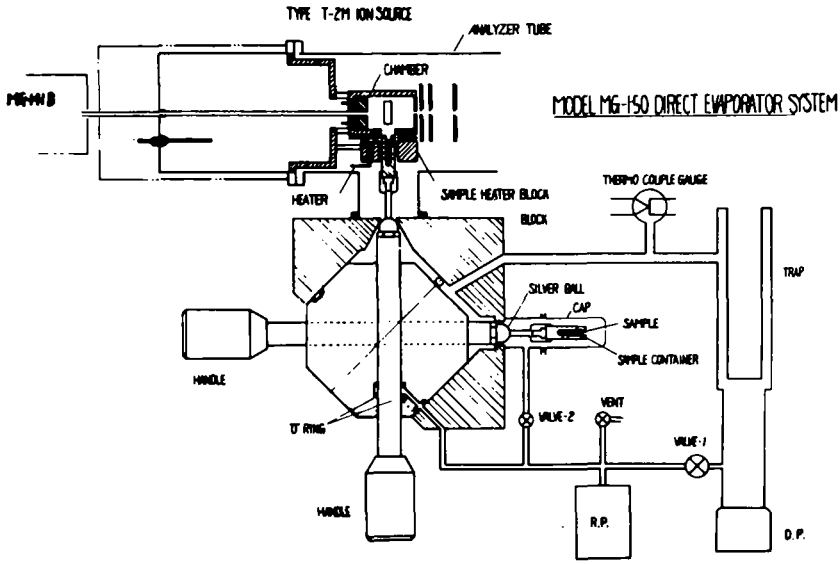

FIGURE 3

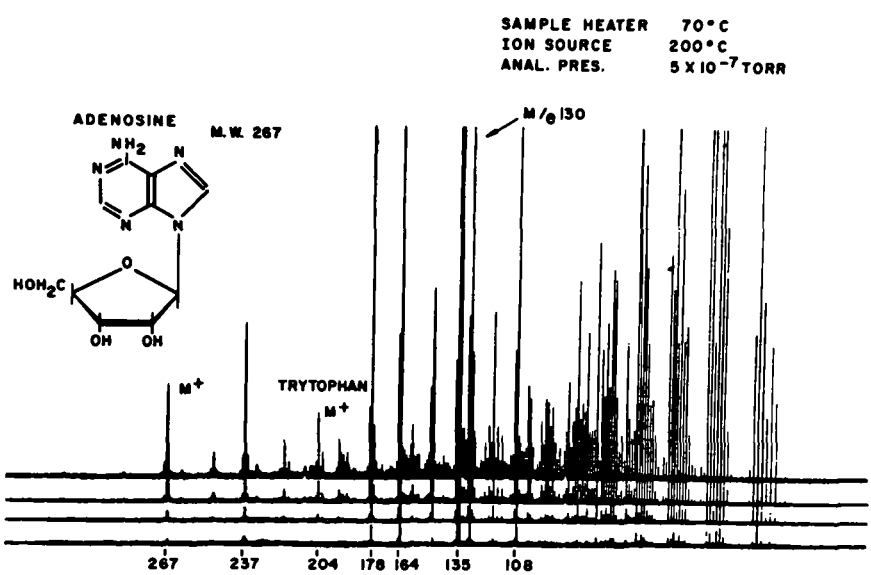

FIGURE 4

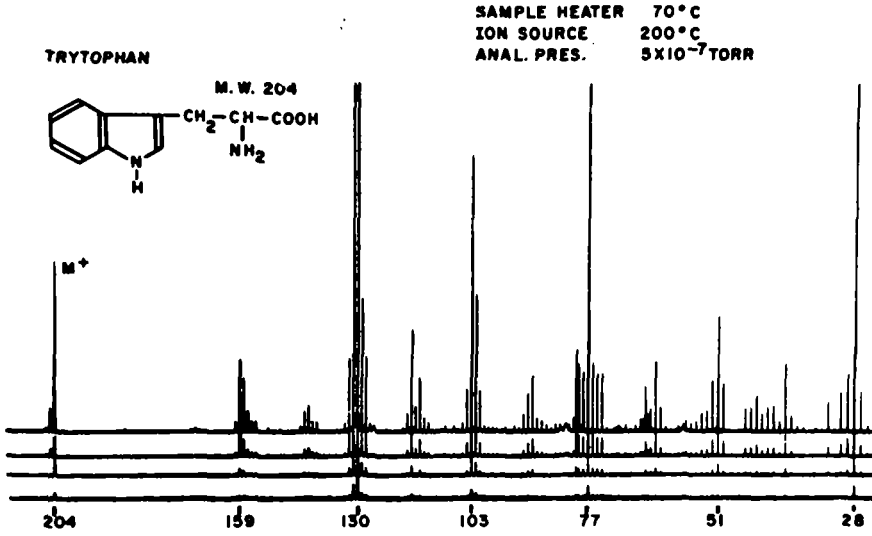

FIGURE 5

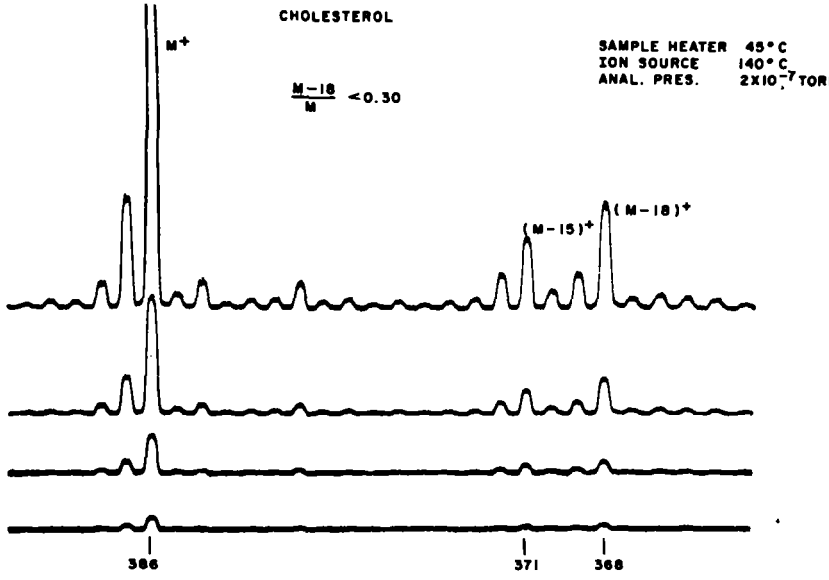

FIGURE 6

Thermal decomposition and electron impact fragmentation of some typical organic molecules

C. Brunnée, Fried. Krupp Meß- und Analysentechnik,
Bremen, Germany.

Summary: The published mass spectra of many organic substances often differ considerably. These differences are mainly due to (1) thermal excitation prior to electron impact fragmentation in the source (Spiteller 1964), (b) time dependent thermal decomposition during evaporation. Results of a study of both effects are given.

The application range of mass spectrometry for structure studies ends where the volatility of the substance becomes so low that transformation into the gaseous phase required for ionization in the vacuum is no longer possible without thermal decomposition. Thus, the problem of optimal sample introduction is of particular importance. During the last years, quite a number of devices for introduction of thermally unstable samples by direct evaporation in the ion source were described which have extended this range considerably. However, when the published spectra of one specific compound are compared considerable differences are frequently found. Such typical differences result from two effects:

1. Temperature dependent thermal decomposition of the sample in the crucible or at the hot ion source walls. Consequently, fragments which are already thermally formed prior to the electron impact are ionized by the electron beam.

2. Temperature dependent electron impact fragmentation. The higher the temperature - that means, the higher the thermal energy of the molecule - the more fragments are produced when the electron hits the molecule. This last effect is well known since the early days of mass spectrometry. However, a more detailed study in connection with structure investigations of organic molecules was recently started by Spiteller [1] .

As an example of the first effect(thermal fragmentation or thermal reactions prior to the electron impact)in fig.1, three cut-outs from the spectra of the voacamine are shown. These spectra are very noticeably different. In fig. 1 a the molecular peak is very low and the presence of a m + 14 peak indicates that an intermolecular pyrolytic reaction has happened before the ionization, namely a transfer of a methyl group. Moreover, a strong thermal fragmentation seems to occur. Fig. 1 b: the pyrolytic reaction is already considerably reduced in this case. Almost no reaction has occured when the spectrum of fig. 1 c was recorded.

An example of the second effect: Fig's 2a and b show the two main peaks of the well-known xylene spectrum recorded with an ion source temperature of 250°C and 100°C respectively. For recording the spectrum of fig. 2 c a molecular beam ion source has been used with the sample vapour having room temperature. Of course, the very noticeable decrease of the molecular peak with rising temperature is not due to a prior decomposition of the thermally very stable xylene molecule. But: the thermal energy of the molecule is so high at a temperature of 250°C that the probability of electron impact fragmentation is rather great.

The molecular beam system used to produce such spectra under very low vapour temperature is shown in fig.3. It consists of a jet system with a collimator slit for producing an intense molecular beam. The sample vapour traverses the open ion source at room temperature or even lower temperature without any wall collisions and is frozen out on the cold trap.

Another example for this thermal excitation effect: In fig. 4a the API spectrum of pentatriacontane is given showing practically no molecular peak as all other long chain paraffins in the API catalogue. But if one reduces the vapour temperature to about 70°C (fig.4b) the molecular peak is increased by a factor of thousand. This strong dependency of the paraffin spectra on the thermal energy of the molecule has been demonstrated first by Spiteller [1] .

The two just discussed effects thermal fragmentation and electron impact fragmentation due to the thermal excitation often appear simultaneously and not always is it possible to differentiate between both. In order to keep these effects under control, some requirements must be met by the evaporation system and by the ion source of an analytical mass spectrometer: Ion source temperature and sample temperature should possibly be independent of each other. One adjusts then the sample temperature only to such a high value as is required to produce sufficient vapour pressure. The ion source temperature can be higher (to avoid condensation) when care is taken that the number of wall collisions of the sample molecules in the ionization region remains small, that means, when an open ion source is used. The separation of both temperatures is also desirable in order to have a possibly small time constant for sample temperature setting: The sample has then to withstand less thermal stress and is kept under evaporation temperature only as long as absolutely required.

Furthermore, the temperature of the sample should be controllable up from room or coolant temperature, and the distance between sample surface and electron beam should be as small as possible in order to obtain high vapour pressure in the ionization region.

Fig. 5 shows an inlet system with which we have tried to realize the mentioned viewpoints to some degree. The sample is in a small gold crucible which is put into a heating coil. Connected to the heating coil is a miniature thermocouple for temperature measurement. Fitted between crucible and ion source is a water-cooled shielding. Thus, ion source temperature and sample temperature do not influence each other and can be set independently. If an initial temperature of the sample is required which lies below room temperature, then the shielding might also be connected to a suitable coolant circulation system. The sample evaporates out of the crucible directly into the ionizing electron beam. The distance between crucible and electron beam is 6 mm.

For sample change, the sliding rod is drawn back until the crucible is in the lock chamber and the gate valve between source and lock chamber is closed. After venting and opening of the glass window, the sample crucible can be exchanged and the chamber can again be evacuated. The vacuum lock is flange-mounted and self-aligning; it can be heated up to 150°C.

The voacamine and pentatriacontane spectra of fig. 1 c and 4 b respectively were taken with this inlet system. Mass spectrometer was an ATLAS CH4 - B.

It was stated that the temperature of the sample is independent of the ion source temperature because of the water-cooled heat shield between source and evaporator. One can e.g. operate the ion source at 250°C and maintain the sample at room temperature. Since the sample passes the ion source as quasi molecular beam, further sample decomposition is kept small even with higher ion source temperature, as shown in fig.6. Plotted is for cholesterol the ion current of the molecular peak and of the (M-18) peak which results from water abstraction. When the ion source temperature is increased by 120°C to 220°C, then the peak heights do practically not change, i.e. the water abstraction remains very small. The evaporation temperature was 70°C, the sample quantity 1 µg. With this sample quantity, a collector ion current of 10^{-12} amps could be maintained for the molecular peak for about 15 minutes. Thus, the total yield (collector ion current x time/sample quantity) was 10^{-9} coul/µg. The resolution of the CH 4 - B mass spectrometer was set to about 350.

It was already mentioned that the sample could also be cooled during evaporation. With a slightly modified device it was possible to analyse even some extremely unstable peroxydes. These analyses have been performed in cooperation with Dr. Lawesson, Aarhus University, Denmark. For example: with an evaporation temperature of minus 70°C we could obtain rather high molecular peaks for di-t-butylperoxyde, t-butylperbenzoate and others.

The time constant for reaching thermal equilibrium, i.e. the thermal inertia of the evaporation system, is primarily dependent on the mass of the metal parts to be heated, that means heating coil, crucible, support etc. Since the total weight of all these parts is very small in the described device, namely 300 mg, a quick temperature equilibrium is obtained. As shown in fig. 7, thermal

equilibrium is achieved in about 3 minutes after alteration of the heating output, and the ion current becomes constant. Thus, thermally unstable samples can be brought to optimum evaporation temperature within a few seconds. The spectrum is in this case recorded on tape.

For measurements of this type we have used a recently developed magnet power supply which is based on a new principle and which allows an exponential magnetic scanning of extremely high speed: one mass decade can be scanned in 40 msec. Rapid decomposition processes can be observed by using this method. Fig.8 shows as example the rise of the (M + 14) - peak as related to the M-peak, i.e. the increase with time of the above mentioned pyrolytic reaction of the voacamine. The whole spectra up to mass number 720 were recorded every sec. Temperature was changed from room temperature to 250°C within 35 sec.

Reference:
[1] Spiteller - Friedmann, M., Eggers, S. and Spiteller, G.: Mh.Chem.95, 1740 (1964).

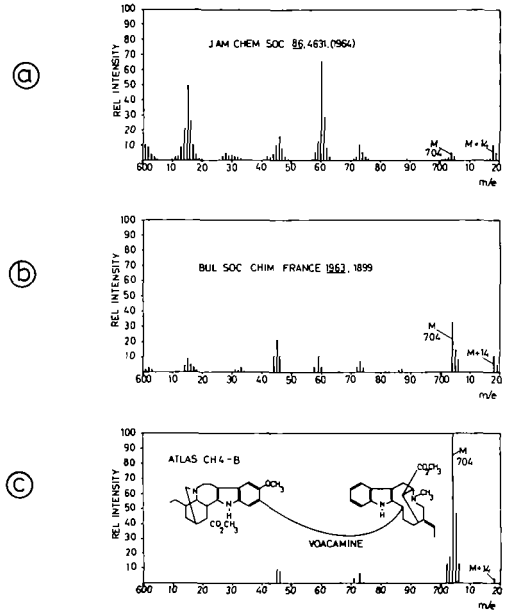

Fig. 1 High mass end of voacamine spectra recorded under different evaporation conditions

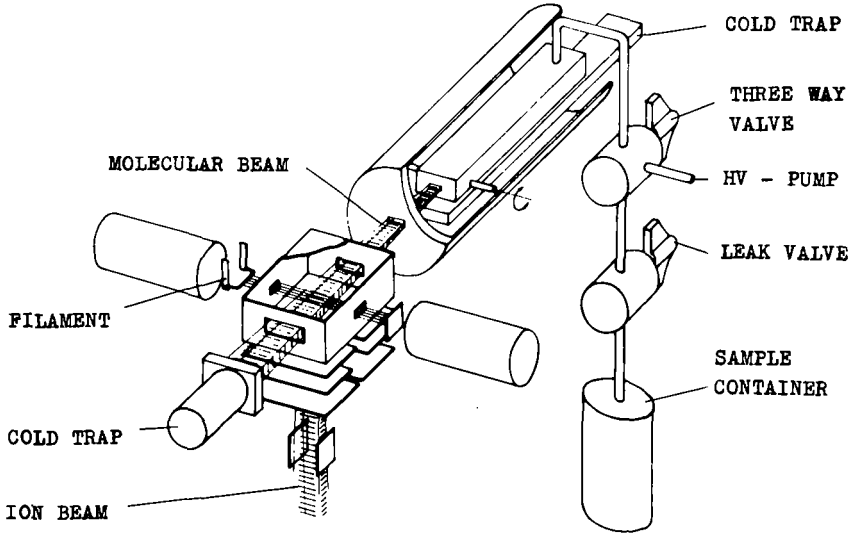

Fig. 3 Molecular beam inlet system

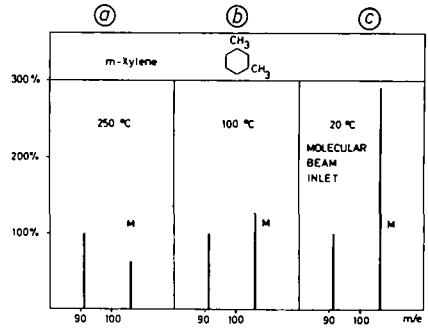

Fig. 2 The 91 and 106 peak of m-xylene for different vapour temperatures

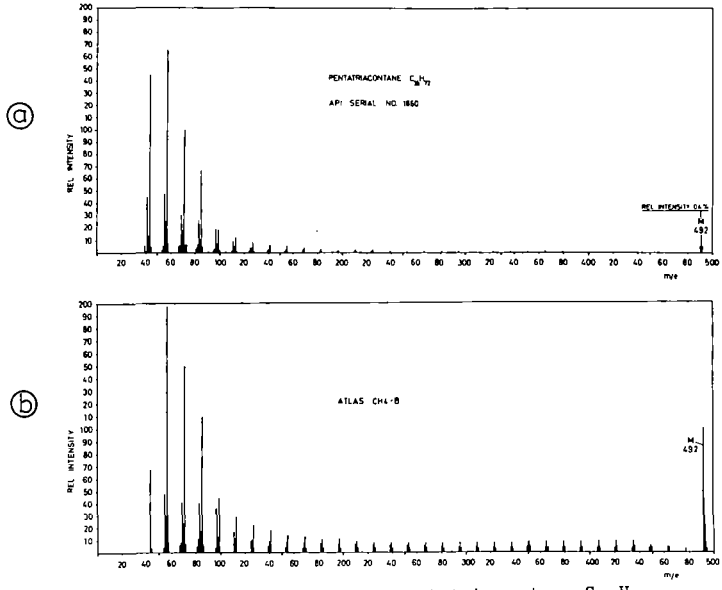

Fig. 4 Mass spectra of pentatriacontane $C_{35}H_{72}$

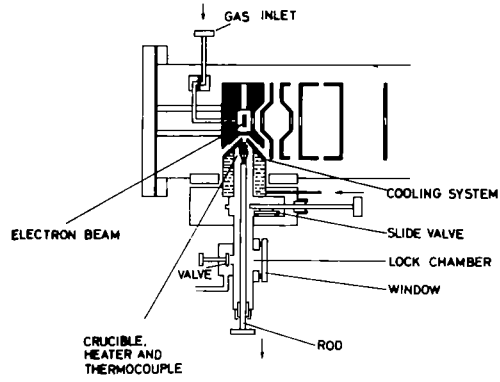

Fig. 5 Direct inlet probe of the ATLAS mass spectrometers CH4-B and SM1

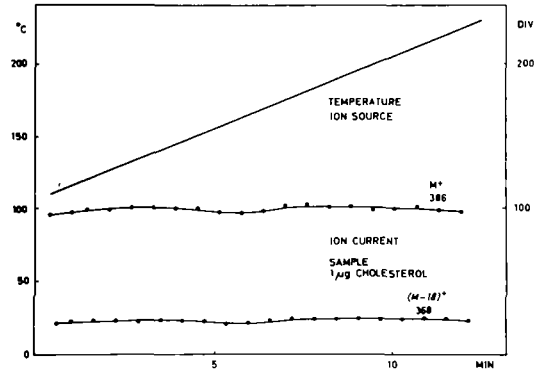

Fig. 6 M- and (M-18)-peak of cholesterol with changing ion source temperature

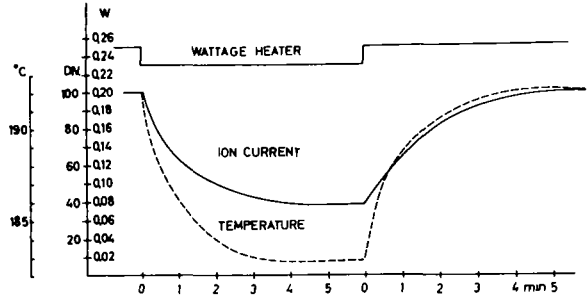

Fig. 7 Temperature equilibrium of the direct inlet probe

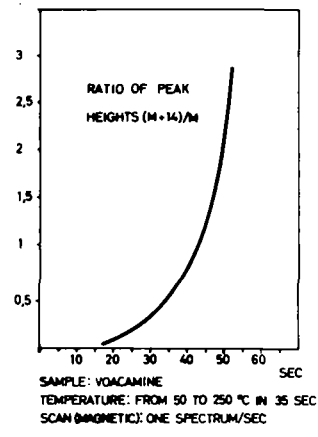

Fig. 8 Change of peak heights (M+14)/M with time and temperature. Sample: voacamine

Temperature Effect Upon Ketone Mass Spectra

R. A. Meyer and M. Cher
North American Aviation Science Center
Thousand Oaks, California

ABSTRACT

Rearrangement peaks have been observed in the mass spectra of selected ketones such as the 2, 3, and 4-heptanones. These rearrangements may be explained by a process similar to the Norrish type II rearrangement observed in photochemistry. The effect of isatron temperature upon the peaks generated by this rearrangement will be discussed and the data correlated with new photolysis work at a range of different temperatures.

In 1960 Erhardt and Osberghaus (1) showed a relation between the activation energy of a decomposition and the mass spectrometric thermal sensitivity of the fragment ion from the decomposition. Their work involved simple hydrocarbon molecules.

In 1938 Bamford and Norrish (2) studied the photochemical rearrangement of aliphatic ketones. Their work coupled with that of subsequent authors such as Srinivasan (3), Nicholson (4), and McNesby and Gordon (5) has well established the Norrish type II photochemical rearrangement shown in Fig. 1. In the first step a gamma hydrogen couples to the carbonyl oxygen followed by the β carbon-carbon bond rupture. This produces an olefin and the enol form of the R-methyl ketone. The ketone is then formed by rapid rearrangement. In the case of 3-heptanone, the products are ethyl-methyl ketone and propylene.

In 1954 Nicholson (4) suggested the Norrish rearrangement in the mass spectra of ketones and in 1956 Sharkey, Shultz, and Friedel (6) reported the mass spectra of many ketones. Conspicuous in their data was a rearrangement peak at the parent of lower mass ketones. There can be little doubt that the source of this peak is the Norrish type II rearrangement since it is present in every case of non terminal γ hydrogens and absent in the rest and is also consistent with the predicted R-methyl molecule.

It is also a well proven fact that mass spectra change with ionization temperature. In high mass work many laboratories adjust the pattern by altering the isatron temperature as other source parameters change. The rest work in spite of the variation by calibration and precise thermostating. However, it was our hope that we could use the combination of primary fragmentation and unimolecular rearrangement in selected ketones to better understand the temperature effect on mass spectra.

The 21-103 mass spectrometer (7,8) has been shown to have kinetic energy discrimination but several authors have used this type of instrument to study temperature effects. Since our mass spectrometer is a 21-103C, we also had to consider discrimination effect. Figure 2 presents data for the noble gases helium, argon, and xenon. Applying the tests suggested by Cassuto (9), the close agreement of the xenon and argon curves and even the helium data indicate a minimum of mass discrimination in our source. The further agreement of the doubly ionized xenon and argon with the singly ionized species shows a surprising lack of energy discrimination. The triply ionized xenon does show the expected discrimination. Ehrhardt and Osberghaus (1) found that if they related total ionization to an internal standard noble gas such as neon the total ionization remained nearly constant over a wide temperature range. The total ionization data for 2- and 3-heptanone is also shown on the figure and agrees well with the noble gas data. Thus, it is shown that total ionization may equally well be used as a basis for elimination of the expected gas law changes in peak height. All the heptanone data are therefore calculated as percent of total ionization and for easy comparison are normalized to the lowest temperature as 1.00.

4-Heptanone, the dipropyl ketone, is not of interest to this study. As may be seen from Fig. 3, the Norrish rearrangement to methyl-propyl ketone only accounts for 0.3% of total ionization. The fragmentation peaks resulting from bond rupture at the carbonyl group and other typical hydrocarbon fragmentations comprise the spectra.

The 3-heptanone, shown in Fig. 4, however, does not have its γ hydrogens in a terminal position and 5% of its total ionization is methyl ethyl ketone which is formed by rearrangement. As before, the rest of the spectra comes from bond rupture at the carbonyl group and other typical hydrocarbon type fragmentations.

We photolyzed 3-heptanone in the vapor phase at three temperatures corresponding to the three ionization temperatures used in our mass spectra work. The photolysis was performed in a quartz cell using a pyrex filtered mercury arc. The effective energy was between 3000 and 3400 A. The photolysis products were analyzed by gas chromatography with a two step technique. The photolyzed mixture was pumped through a 77°K trap and the non-condensables such as CO, Methane, and parts of other light hydrocarbons compressed into the sample loop for chromatographic analysis. The condensed material, predominately 3-heptanone was sealed into a small glass ampoule. The glass ampoule was then crushed at elevated temperature in the flowing carrier gas stream of a second chromatograph.

In photolysis we have a choice of products to look at since, in contrast to mass spectrometry, both products of a fragmentation or rearrangement are evident in the final analysis. For this preliminary look at the temperature dependence of photolysis reactions we chose methyl ethyl ketone and carbon monoxide. The methyl ethyl ketone is formed by the Norrish type 2 rearrangement while the fragmentation produces CO. Figure 5 shows the relation of the MEK and CO produced during photolysis at 119°C, 252°C, and 335°C. The work of Davis and Noyes (10) in 1947 showed that the production of rearrangement products was independent of temperature of photolysis. Our preliminary data are in disagreement with their findings. The work is continuing since the work of Davis and Noyes was on a methyl butyl ketone while ours was on ethyl butyl ketone. We see no reason for the rearrangement process to have a different temperature dependence in this molecule but will of course repeat the study with the other ketones.

The data show, however, that the fragmentation reactions as indicated by the production of carbon monoxide increase at a much more rapid rate than the rearrangement reaction leading to the production of methyl ethyl ketone. These data may be explained by a difference in activation energy of the competing reactions since low activation energy processes such as the rearrangement are much less temperature dependent than higher activation energy process such as the fragmentation.

Unfortunately, 2-heptanone, Figure 6, has not been photolyzed as yet. However, the mass spectra indicates a much larger amount of rearrangement, 19% as compared to the 5% for the 3-heptanone. We see no reason not to expect that the photochemical data will show the same rearrangement fragmentation ratio temperature dependence. In 2-methyl heptanone the R is a methyl group so acetone is formed as the rearrangement peak.

The effect of temperature on the mass spectra of the two heptanones is consistent with the activation energy hypothesis. In Fig. 7 the rearrangement peaks are plotted as fraction of total fragmentation. Since the molecule ion ranges between 4.7 and 1.5% of total ionization for the 3-heptanone and from 3.5 to 0.6% for the 2-heptanone its contribution to total ionization is not significant. The data show an increase in fragmentation at the expense of rearrangement as temperature is increased. Again the higher activation energy fragmentation process is the more temperature dependent. Still another point is that in photolysis only about 4-electron volts are available as an energy source and 80% of the products are formed by rearrangement. In mass spectra, the rearrangement peak is much smaller, down to 5%, due to the larger amount of energy transferred to the molecule.

A brief study of the relative appearance potentials of selected peaks in the 3-heptanone spectra also support the activation energy hypothesis. We emphasize the relative aspect of the data since no effort was made to correct the data for instrumental parameters. The three peaks showing a negative slope of the percent of total ionization vs. temperature curve in 3-heptanone were the 114 peak (the parent) whose appearance potential was 7.6 volts; the 85 peak from fragmentation at the carbonyl group, appearance potential 9.6 volts, and the 72 peak from Norrish type II rearrangement whose appearance potential was 9.3 volts. The 57 peak from fragmentation had an appearance potential of 10.6 volts and gave a positive temperature dependence as did all other higher activation energy processes.

In conclusion, we feel that differences in the activation energies of the competing processes that combine to form a mass spectrum provide a clue to the effect of temperature on mass spectra. Conversely, of course, the relative activation energies may be studied through the temperature effect on the mass spectra.

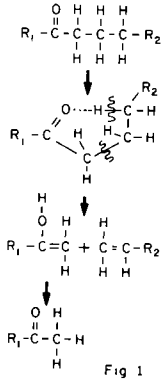

Fig 1

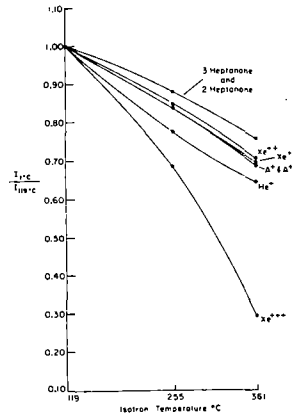

Fig 2

4 Heptanone

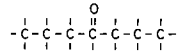

		me	%ΣI
Rearrangement	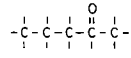	86	0.3
Fragmentation	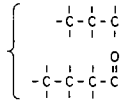	43	29.6
		71	24

Fig. 3

3 - Heptanone

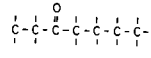

		m/e	%ΣI
Rearrangement	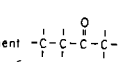	72	5.1
Fragmentation	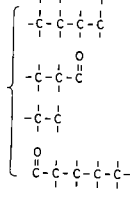	57	24.9
		29	17.6
		85	7.8

Fig 4

References

1. H. Ehrhardt and O. Osberghaus, Z. Naturforshg 15a 575-84 (1960).
2. C. H. Bamford and R. G. W. Norrish, J. Chem. Soc., 1538 (1938).
3. R. Srinivasan, J. Amer. Chem. Soc., 81, 5061 (1959).
4. A. J. C. Nicholson, Trans. Faraday Soc. 50, 1067 (1954).
5. J. R. McNesby and A. S. Gordon, J. Amer. Chem. Soc., 80, 261 (1958).
6. A. G. Shavkey, J. L. Shultz, and R. A. Friedel, Anal. Chem. 28, 934 (1956).
7. N. D. Coggeshall, J. Chem. Phys., 12, 19 (1944).
8. H. W. Washburn and C. E. Berry, Phys. Rev. 70, 559 (1946).
9. A. Cassuto, Advances in Mass Spectrometry, Vol. 2.
10. W. Davis, Jr. and W. A. Noyes, Jr., J. Amer. Chem. Soc., 69, 2153 (1947).

3- HEPTANONE

Temperature	Moles CO / Moles MEK
119°	0.18
252°	0.17
335°	0.49

Fig. 5

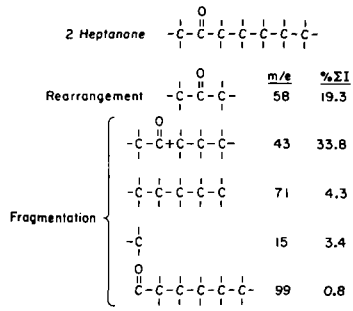

Fig. 6

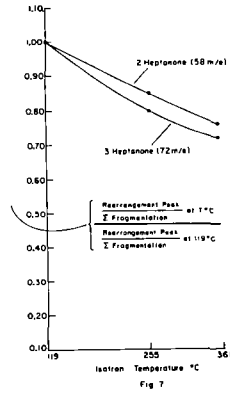

Fig. 7

MASS-SPECTROMETRY AND RADIATION CHEMISTRY OF ACETONE VAPOUR

by

B. C. deSouza* and J. H. Green**

Department of Nuclear and Radiation Chemistry
University of New South Wales, Sydney, Australia

*Now at Atomic Energy Establishment Trombay, Bombay, India

**Now at New England Institute, Ridgefield, Connecticut, USA

Introduction

Radiolysis studies of a number of ketones have been carried out by Ausloos and collaborators (1958, 1961) as well as by Pitt and Osborne (1961). In the absence of any definite evidence for ionic processes in these systems and also due to similarities with photochemical effects (which have been well studied in some ketones) these authors have minimized the contribution of ionic effects.

Mass spectrometric techniques have been used in this study to search for ionic processes, since the events occurring in the ion source of a mass spectrometer are similar to those occurring in β- or γ-irradiated gases.

Experimental

An AEI MS2SG mass spectrometer was the basic instrument which was used in two ways:

(1) With sample inlet system unchanged and the standard Nier source, but with some electrical modifications, experiments with source pressures up to about 5×10^{-4} Torr. were conducted ("low-pressure studies"). These have been previously described (deSouza and Green, 1965, 1966).

(2) With a modified Nier source and differential pumping across the mass spectrometer inlet slit source pressures up to about 0.1 Torr. could be used ("high-pressure studies"). A special thermistor pressure gauge and thermocouple were built into the source to give the best measure of pressure in the ion-molecule reaction region. Figures 1 and 2 show details of construction of the high pressure source as well as the arrangement of the mass-spectrometric system. Mass-spectrometric and gas-chromatographic techniques were used for the separation of radiation products.

Results and Discussion

Low-pressure studies revealed the occurrence of secondary ions of mass 59 with appreciable intensity, and of secondary ions of high mass numbers but much lower intensity. Reactions leading to the formation of such ions must be highly favoured. Mass 59 ions in acetone could be formed by the following three processes:

1. $CH_3COCH_3 + RH^+ \rightarrow CH_3COCH_4^+ + R$ (Proton transfer)

2. $CH_3COCH_3^+ +^* CH_3COCH_3 \rightarrow CH_3COCH_4^+ +^* CH_3COCH_2$ (Hydrogen transfer)

3. $CH_3COCH_3^+ +^* CH_3COCH_3 \rightarrow {}^*CH_3COCH_4^+ + CH_3COCH_2$ (Proton transfer, a special case of 1.)

[The asterisk denotes a carbon skeleton from the neutral molecule.]

Reactions of ketones are strongly directed by the keto group which makes the molecule very dipolar and which leads to the presence of a lone pair of electrons in the non-bonding orbital. These are the electrons most easily lost by ionization, or, if any other electron in the molecule is lost, the vacancy is transferred by a quick radiationless transfer to this orbital. In this case the ion tends to fill the vacancy either by abstracting an electron from its side chain or from another molecule. Processes 1 and 3 above are proton transfers due to the polarity of the molecule and process 2 is a hydrogen transfer arising from the filling of the electron vacancy in the ion ("ionic effect").

Thermodynamic data are not adequate to distinguish between the three cases. Mass-spectrometric data, however, support the proton transfer process by showing that ions of appreciable intensity at masses between 43 and 59 do not appear as they would otherwise. (deSouza and Green, 1965). More conclusive evidence in favour of the proton

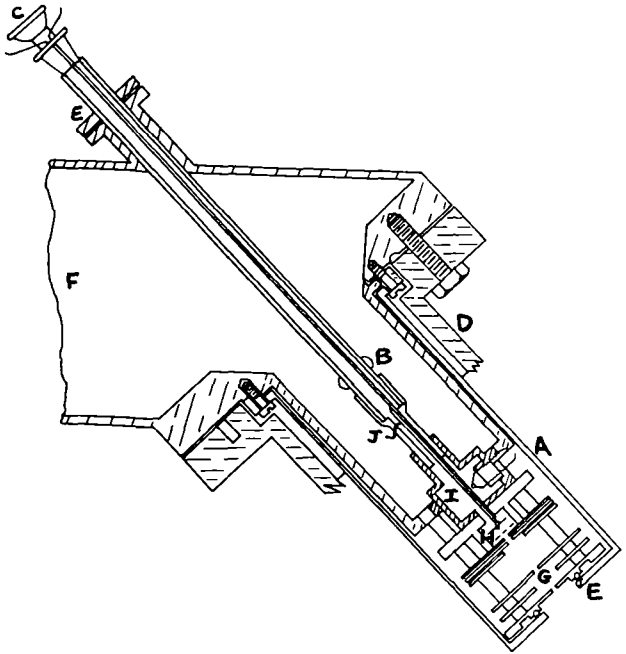

Figure 1: Diagramatic Cross-section of the High Pressure Source

A. Isolating cap.
B. Glass-to-metal tube joint.
C. Gas inlet from leak.
D. Mass spectrometer tube.
E. Neoprene O-rings.
F. To 3" oil diffusion pump.
G. Slits of accelerating system.
H. Ion chamber.
I. Thermistor chamber with thermistor.
J. Chromel-alumel thermo-couple.

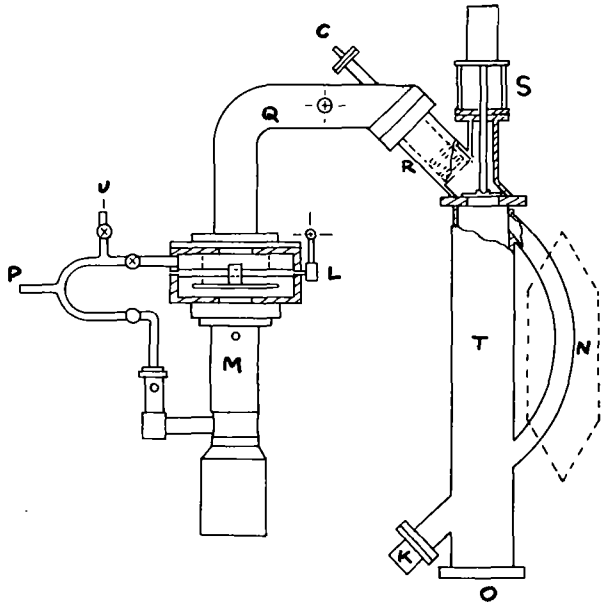

Figure 2: Differential Pumping System

C. Gas inlet. K. Ion collector.
L. Cut away view of flap valve.
M. Source evacuating diffusion pump.
N. Magnet pole pieces. O. To liquid air trap and main pumps.
P. Connection to backing pump. The pump was also used to obtain rough vacuum after opening the source to atmosphere.
Q. 3" source evacuation connection. R. Ion source end of the mass spectrometer tube partly cut away to show position of ion sources.
S. Cut away view of vacuum lock. T. Main pumping tube. U. Air inlet.

transfer mechanism was obtained in studies on acetone-water mixtures. (deSouza and Green, 1966). From these results the proton affinity of acetone was estimated as ≥142 Kcal.

Low pressure studies did not enable the determination of reaction cross-sections or rates of reaction because the precursors of mass 59 could not be identified.

High-pressure studies gave results which confirmed the conclusions reached in the low-pressure work and showed also the formation of ions of the following types: (1) Ions whose relative intensity decreased with increasing pressure (reactant ions), (2) Ions whose intensities remained almost constant (non-reactants), (3) Ions whose intensity increased rapidly at lower pressures and then more gradually at higher pressures. These included secondary ions of masses 59, 72 and 100. At the highest pressures, 0.1 Torr. their intensities were about 34.3 and 2.3% respectively of the total ions, (4) Ions whose intensities increased slowly at lower pressures and then more rapidly at high pressures. The ion of mass 115 was the only one observed of this type. This is a tertiary ion whose intensity was about 14% of the total at 0.1 Torr. Figure 3 shows the intensity-pressure behaviour of some of the ions of the types mentioned above.

The log intensity-pressure curves of a number of primary reactant ions were found to be composite curves and could be resolved into two straight lines corresponding to two processes one of which was much faster than the other. Figure 4 illustrates the behaviour of one such ion. From the intensity of the secondary ion of mass 59, it was concluded that the ions of mass 59 in acetone arose mainly from proton transfer reactions of the type 1. The contribution of parent ions to the formation of mass 59 ions (process 3) was negligible. The average rate constant for proton transfer formation of mass 59 ions was 55.6×10^{-10} cc/molecule sec. based on the rates of disappearance of the primary reactants.

On the basis of intensities, reaction rates and energetics, the formation of mass 72 and 100 secondary ions and of mass 115 tertiary ions was believed to be due to the following reactions:

$$\text{(A)}\ CH_3COCH_3^+ + CH_3COCH_3 \xrightarrow{k_1} [\text{complex}] \xrightarrow{\text{fast}} CH_3COCH_2CH_3^+ + CH_3CHO$$

$$\text{(B)}\ CH_3COCH_3^+ + CH_3COCH_3 \xrightarrow{k_2} [\text{complex}] \xrightarrow{\text{fast}} CH_3COCH_2CH_2COCH_3^+ + CH_4$$

$$\text{(C)}\ CH_4COCH_4^+ + CH_3COCH_3 \xrightarrow{k_3} [\text{complex}] \xrightarrow{\text{fast}} CH_3COCH_2CH_2COCH_3^+ + H_2$$

Reaction rates for A, B and C were found to be $k_1 = 5.8 \times 10^{-10}$, $k_2 = 10.1 \times 10^{-10}$ and $k_3 = 0.55 \times 10^{-10}$ cc. molecule^{-1} sec^{-1}. These rates are high enough for the ion-molecule reactions to complete successfully with neutralization and subsequent radical reactions in gamma-irradiated acetone vapour.

To substantiate this conclusion, calculations were made to estimate the contribution of these ion-molecule reactions to the yields of the main radiolysis products in acetone - CO, CH_4, H_2, C_2H_6 and C_2H_4.

The principal contributions arise from the following processes:

a. Primary fragmentation: To evaluate this part, the primary mass spectrum of acetone was reviewed and the various possible paths were selected with the aid of data given in Field and Franklin's book.

b. Ion-molecule reactions as discussed above.

c. Neutralization reactions arising from the neutralization of primary, secondary and tertiary ions.

d. Radical-radical and radical-molecule reactions following neutralization.

These estimated contributions are compared in Table I with experimental results obtained from mass spectrometric and vapour phase chromatographic analyses. It will be seen that, although the estimates do not account for the whole of the observed yields, nevertheless major contributions are made by ionic processes.

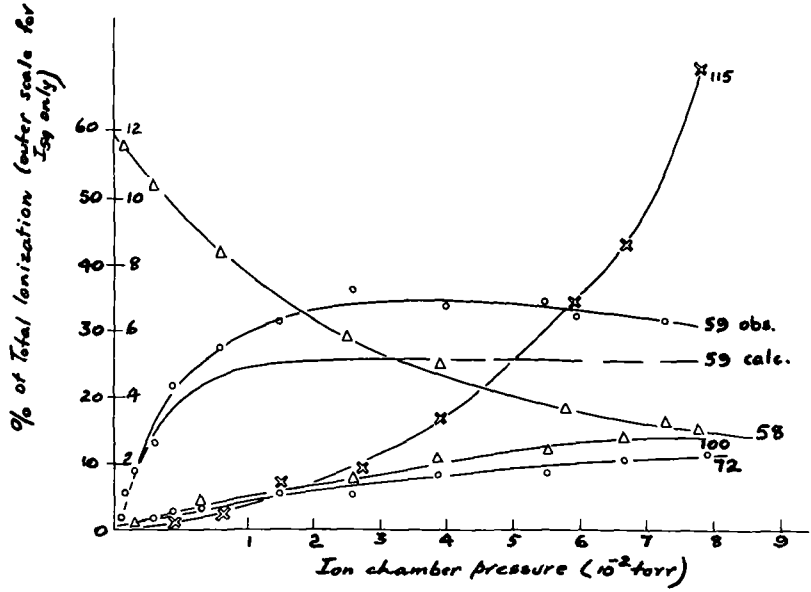

Figure 3: Intensity-Ion Chamber Pressure Curves of some Ions in Acetone

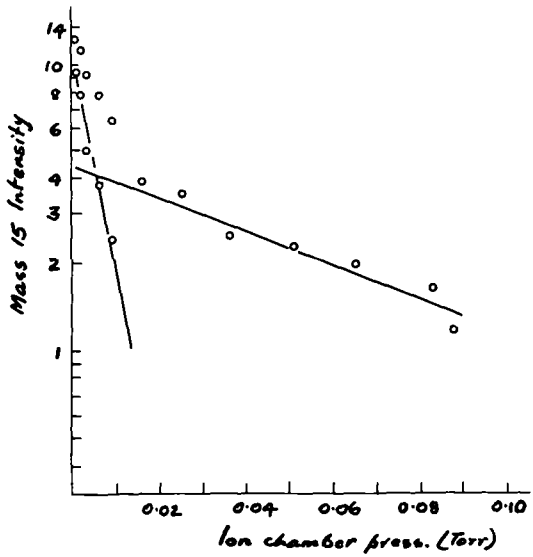

Figure 4: Graphical Resolution of a Composite Intensity-Ion Chamber Pressure Curve of Ion of Mass 15 in Acetone

References

Ausloos P. and Paulson, J. F., (1958), J. Amer. Chem. Soc. 81, 5117.

deSouza B. C. and Green J. H., (1965), Aust. J. Chem. 18, 1153.

deSouza B. C. and Green J. H., (1966), Aust. J. Chem. 19, 59.

Pitts (Jr.) J. N., and Osborne A. D., (1961), J. Amer. Chem. Soc. 83, 3011.

Stief L. J., and Ausloos P. (1961), J. Phys. Chem. 65, 1560.

TABLE XI

Experimental and Calculated Yields of Main Products per 100 ion pairs initially formed in γ-irradiated Acetone Vapour at 100 torr. and 27°C.

Product	Calculated Yields					Experimental Yields	
	From initial fragmentation	From ion-molecule reactions	From neutralization reactions	From radical-radical reaction	Total	Without scavenger	With scavenger (3% cyclohexene)
Hydrogen	14.4	40.0	52.4	0	106.8	169.3	101.3
Carbon Monoxide	22.3	8.6	43.9	0	74.8	83.4	79.8
Methane	3.1	2.3	0	62.2	67.6	116.4	6.7
Ethane	0	0	0	21.6	21.6	75.2	0
Ethylene	1.6	0	0	0	1.6	7.7	7.9

A COMPUTERIZED MASS SPECTRAL CORRELATION STUDY ON CYCLIC KETONES

Mynard C. Hamming

Continental Oil Company, Ponca City, Oklahoma

and

E. J. Eisenbraun

Oklahoma State University, Stillwater, Oklahoma

ABSTRACT

A correlation between mass spectra and molecular structures of several cyclic ketones has been developed using a computer program. A novel approach has been applied to systematically selecting peaks from spectra arranged in a rectangular array. Differences between selected peaks have been shown to be useful in relating mass spectra to structural features of the compounds. The method should be applicable to several other classes of compounds.

INTRODUCTION

Correlation studies relating mass spectra to molecular structures have proven to be one of the most effective means of identifying unknown compounds without reference standards. However, correlation studies, if applied to a large number of compounds, require a great deal of time and effort. Often after correlations are completed and even published, discrepancies exist due to the massive amount of data which had to be examined. Too often a correlation is not kept up-to-date because of the problems involved and the expense of making revisions. To aid in deriving and revising correlations while keeping the cost of such studies as low as possible we have written a number of rather simple subroutines which can be inserted into a main computer program.

Mass spectra from several cyclic ketones having a tetralin or indan structure were examined to find possible differences in fragmentation patterns which could be related to slight structural variations. In using the programs no effort was made to obtain any anticipated correlations. The newly programmed subroutines were to be tested for their capability of selecting interpretative peaks which would epitomize complete mass spectra is such a way that correlations could be more readily deduced. The compounds examined were as follows. Structures are shown in Figure 1.

2,4-dihydro-3,5,8-trimethyl-1(3H)naphthalenone (1)
3,4-dihydro-2,5,8-trimethyl-1(2H)naphthalenone (2)
3,4-dihydro-4,5,8-trimethyl-1(2H)naphthalenone (3)
3,4-dihydro-4-methyl-1(2H)naphthalenone (4)
5,6-dimethyl-1-indanone (5)
5,7-dimethyl-1-indanone (6)
4,7-dimethyl-1-indanone (7)
Indan-1-one (8)
3,3,5,6-tetramethyl-1-indanone (9)
3,3,5,7-tetramethyl-1-indanone (10)
3,3,4,7-tetramethyl-1-indanone (11)
3,3-dimethyl-1-indanone (12)

When the above spectra were subjected to examination by our subroutines, the principal fragmentation process was readily deduced. It was then possible to propose a probable mechanism of decomposition for these ketones. This understanding now makes possible the identification (from mass spectra) of compounds similar to the ones listed above even though reference standards are not available.

SOME CYCLIC KETONES

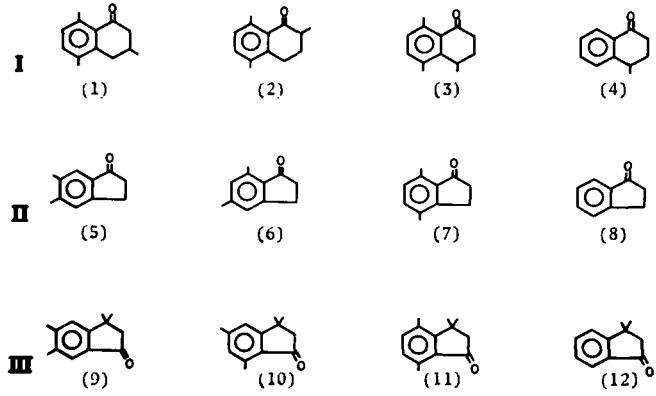

Figure 1

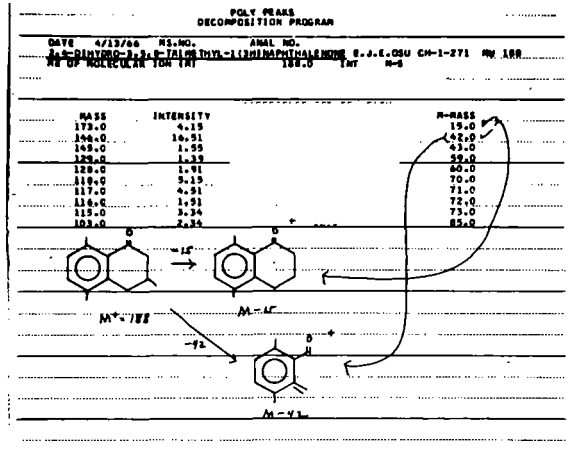

Figure 2

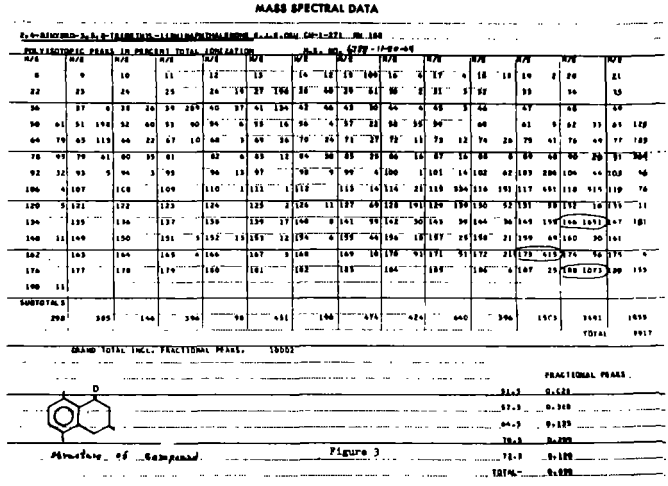

EXPERIMENTAL

All spectra were obtained on a Consolidated Electrodynamics Corporation model 21-103C mass spectrometer. Modifications to the mass spectrometer include a heated inlet system (2) and a 40-liter getter-ion exhaust vacuum system. Spectra were recorded on a CEC Mascot digitizer. Instrument performance was routinely checked by reference to n-hexadecane standard, and typical values obtained were m/e 226/57 peak ratio of 3.50 and m/e 57 sensitivity of 17.3 per cent of total ion yield.

RESULTS AND DISCUSSION

To incorporate the desired flexibility and ease of modification, our main computer program is set up to include 13 subroutines (this number can be increased if required). All possible combinations of the optional subroutines can be called upon in any single case. Subroutines can be removed as well as added or modified with relative ease.

More than one subroutine is required in correlation studies because organic compounds fragment in grossly different ways under electron bombardment in the mass spectrometer. Differences in fragmentation can be illustrated by considering a mass spectrum separated into two parts by the most intense peak of the spectrum. One part consists of peaks of mass numbers below the most intense peak and the other part consists of peaks with mass numbers higher than that of the most intense peak. Some compound types, such as paraffins, give mass spectra with the most intense peak very near the lower end of the spectrum and have the greatest per cent of the ion yield near the most intense peak. Other classes of compounds, such as naphthalenes, give their most intense peaks near the high end of the spectrum with only a few peaks in the low region of the spectrum which are useful in a correlation study. Different criteria must be used to select the interpretative peaks from these and other compound types; therefore, a number of different subroutines are required. In practice, we have found it convenient to examine a group of spectra by several subroutines and then to select the most pertinent data. For the cyclic ketones being discussed in this report, two of our subroutines were found to supply most of the information necessary to correlate fragmentation with molecular structure.

One of the subroutines is called "decomposition". This program selects interpretative peaks above the most intense peak and also below the most intense peak. However, the selection is different for each of the two parts. For those peaks above the most intense peak, the program searches a mass spectrum starting at the molecular ion (part of the input) for peaks of increasing intensities until the most intense peak is recorded. The program continues to search in the low mass region of the spectrum for those peaks greater than a given per cent (part of the input) of the total ionization until eight such peaks are selected. This selection is depicted below. Only the peaks shown in heavy black lines are selected by the "decomposition" program.

MASS SPECTRUM

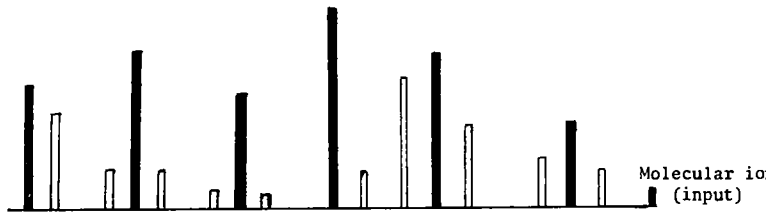

Peaks are selected which have an intensity greater than a given per cent of the most intense peak.

Most intense peak

Peaks selected of increasing intensities between the molecular ion and the most intense peak of the spectrum.

Mass differences between selected peaks were determined which readily enabled a mechanistic interpretation of the fragmentation processes involved to be made.

INTERPRETIVE PEAKS NEAREST THE MOLECULAR ION WHICH WERE >2% OF Σ

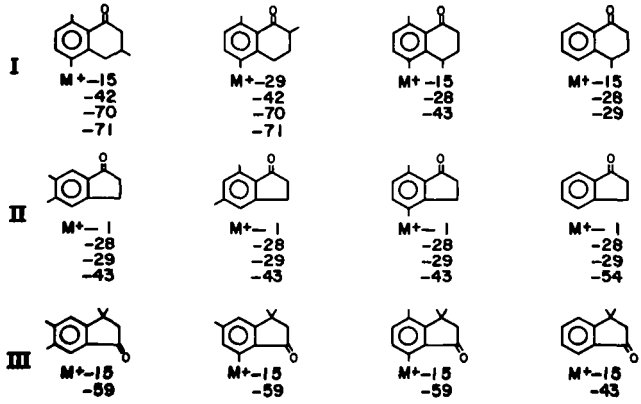

Fig. 4

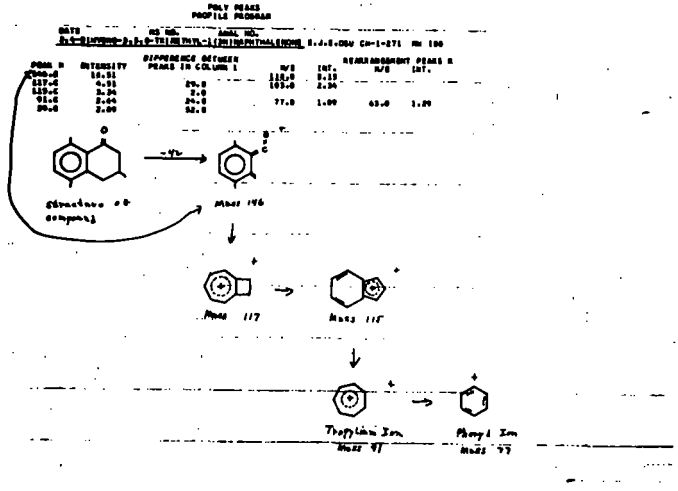

Figure 5-A

MASS SPECTRAL DATA

m/e		m/e		m/e		m/e		m/e		m/e		m/e		m/e		m/e		m/e		m/e		m/e		m/e	
8		9		10		11		12		13		14	12	15	100	16	6	17	4	18	19	19	2	20	
22		23		24		25		26	15	27	146	28	48	29	61	30	2	31	3	32		33		34	
36		37	6	38	24	39	289	40	37	41	154	42	46	43	12	44	6	45	3	46		47		48	
50	61	51	198	52	60	53	90	54	6	55	16	56	4	57	23	58	16	59		60		61	1	62	33
64	79	65	119	66	22	67	10	68	3	69	39	70	34	71	27	72	13	73	12	74	26	75	41	76	49
78	93	79	61	80	35	81		82	6	83	13	84	30	85	15	86	16	87	16	88	8	89	48	90	30
92	32	93	9	94	3	95		96	13	97		98	9	99	4	100	1	101	14	102	62	103	234	104	44
106	6	107		108		109		110	1	111	1	112		113	14	114	21	115	954	116	193	117	492	118	915
120	9	121		122		123		124		125	2	126	11	127	69	128	191	129	134	130	52	131	18	132	10
134		135		136		137		138		139	17	140	8	141	59	142	30	143	30	144	36	145	155	146	1651
148	11	149		150		151	5	152	13	153	12	154	6	155	44	156	18	157	25	158	21	159	69	160	37
162		163		164		165	4	166		167	3	168		169	18	170	41	171	51	172	21	173	419	174	54
176		177		178		179		180		181		182		183		184		185		186	6	187	25	188	1073
190	11																								
SUBTOTALS																									
	208		365		166		106		90		411		190		476		424		640		306		1903		5481
																								TOTAL	9917

GRAND TOTAL INCL. FRACTIONAL PEAKS, 10002

FRACTIONAL PEAKS

91.5	0.229
97.5	0.349
94.5	0.139
78.5	0.253
72.5	0.120
TOTAL	0.890

Structure of Compound

Figure 5-B

The output from "decomposition" is shown in Figure 2 for the compound 2,4-dihydro-3,5,8-trimethyl-1(3H)naphthalenone. The output can be compared with the complete mass spectrum which is shown in Figure 3. The molecular weight of this compound is known to be 188 and is given to the computer as input. This is shown in the output by the line reading "M/E of molecular ion (M)". The program then selects the first peak below the molecular ion which is greater than a given per cent of the total ionization. This per cent is given as input data. In the examination of these cyclic ketones a value of 0.5 per cent was put into the program and therefore the 174 peak was selected because its intensity was 0.6 per cent of total ion yield. The output shows this peak to be 14 mass numbers below the molecular ion (M - S, meaning molecular ion minus selected peak). Because of the small intensity, this peak was not considered by us to be important in the decomposition. Judgment is still required in how much of the data shown on the output is useful to any given correlation study. We will discuss here only the data which is useful in deriving a correlation between mass spectral data and molecular structures of cyclic ketones. Columns labeled "Mass", "Intensity", and "M - Mass" supplied the information necessary from the decomposition program in this correlation study. In fact, the first two peaks selected in these columns provided the key to understanding the fragmentation of these cyclic ketones. The first of these two peaks is the 173 peak and is shown to have an intensity of 4.15 per cent of the total ion yield and is 15 mass units below the molecular ion (M - Mass). Presumably this is due to loss of a methyl group. The second peak selected by the subroutine is at m/e 146 and is shown as 42 mass units below the molecular ion. We have depicted in Figure 2 this to be due to the loss of the hydrocarbon fragment, C_3H_6. (This has not been confirmed by high resolution mass spectrometry -- the loss of 42 mass units could also be due to loss of CH_2CO.)

Similar data for the other ketones included in this study are shown in Figure 4. The M^+ denotes the molecular ion. Minus figures are the number of mass units below the molecular ion at which interpretative peaks appeared on the spectrum.

The selection of interpretative peaks by our computer subroutine points to the observation that the position of methyl substitution on the saturated moiety has more effect upon the fragmentation of these cyclic ketones than similar changes in the position of the methyl groups attached to the benzene ring. For the dimethyl indan-1-ones (Group II) the same series of interpretative peaks (M-1-28-29-43) was selected for the three isomers shown. Likewise, for the tetramethyl-1-indanones (Group III) the selection of interpretative peaks was the same (M-15-59). However, for the dihydrotrimethylnaphthalenones (Group I) the selection of interpretative peaks was different for each of the isomers.

The information summarized in Figure 4 points out how the structure of a molecule controls decomposition reactions. All except two of the dihydrotrimethylnaphthalenones (Group I) and indan-1-ones (Group II) have as the second minus peak 28 or 42. For all of the compounds having a minus 28 peak no methyl groups are attached on the No. 2 or No. 3 carbons to the carbonyl group. The two dihydrotrimethylnaphthalenones (Group I), which have a second minus peak at 42, have one methyl group attached to either carbon No. 2 or 3. Cleavage of the two bonds β to the benzene ring with removal of either a C_2H_4 or C_3H_6 group appears to be the preferential cleavage of these cyclic ketones. If this observation is correct, the data from the other computer subroutine should provide additional supporting evidence.

These minus peaks can serve to elucidate the molecular structures if applied to an unknown structure. For example, had indan-1-one 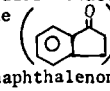 been received as an unknown, the minus peaks, -1, -28, and -29, would have classified it in Group I as an indanone and would differentiate it from the tetramethyl-1-indanones (Group III) and the dihydrotrimethylnaphthalenones (Group I).

The second subroutine which provided useful information achieves two different but related functions. This subroutine is called "profile-rearrangement". In order to understand the "profile-rearrangement" program, a mass spectrum must be visualized as arranged in the form referred to by API as the matrix form. (We prefer to call this form a rectangular array.) A mass spectrum thus arranged is shown in Figure 5-B. The rectangular array consists of rows with elements differing by one mass unit and columns with elements differing by 14 mass units (corresponding to one CH_2 group). The data are conventionally arranged in a rectangular array, but should be thought of as in a cylindrical array. For example, the 190 peak is but one mass number higher than the 189 peak but these peaks are at different ends of the spectrum as shown in the rectangular array.

The profile-rearrangement program selects the most intense peak in each of the columns. For the compound shown in Figure 5-B, the peaks 91, 146, 117, 115, and 39 were selected. (The minimum per cent was put in as 2.0%, thus peaks below 2.0% were excluded in the listing.) The output of this data is shown in Figure 5-A. Peaks selected are arranged and printed out in decreasing mass numbers in the column marked "peak H". Intensities are shown in the second column. Differences between selected peaks arranged in decreasing mass numbers are printed out in the third column. Thus, the most intense peak in the spectrum is printed out first in the column labeled "peak H". For example, for the compound shown in Figure 5-B, the most intense peak is m/e 146. (It will be recalled from the decomposition subroutine that the 146 peak was shown to be 42 mass units below the molecular ion.) The second peak selected was m/e 117 and is the most intense peak in the series in which it appears. (It should be kept in mind that this is <u>not</u> the second most intense peak in the spectrum, but is the most intense peak in the series in which it appears and is the second most intense peak selected by the profile-rearrangement program.) The program continues to select the most intense peak in each of the series differing by 14 mass units (CH_2 group). From the peaks selected a possible mechanistic interpretation of the fragmentation is symbolically shown on Figure 5-A. While decomposition routes shown cannot be rigorously defined, the selection of peaks serves to stimulate interest in decomposition.

Another important aspect of the profile-rearrangement computer program is its ability to select peaks which may be due to migration of an hydrogen atom from one part of the molecule to another. Such peaks are commonly called rearrangement peaks. In the study of methyl substituted cyclic ketones rearrangement peaks are not expected due to a lack of γ hydrogens and other structural requirements in the formation of rearrangement peaks. Therefore, when the computer program selected several peaks which could have been rearrangement peaks other explanations were investigated. The data in Figure 6 shows that for the first two structures the selected peaks were at 42 mass numbers below the molecular ion and that for the last two structures the selected peaks were at 28 mass numbers below the molecular ion. From the data presented by the computer subroutine and the structures shown, it becomes evident that elimination of a C_3H_6 group would result from cleavage of the two bonds β to the benzene ring for the first two structures and elimination of a C_2H_4 group would also result from cleavage of the two bonds β to the benzene ring. The selected peaks at $(M-42)^+$ and $(M-28)^+$ for dihydrotrimethylnaphthalenones (Group I) suggest that fragment ions are due to the mass spectrometric equivalent to a retro-Diels-Alder reaction. This reaction is shown at the bottom of Figure 6. Such retro-Diels-Alder reactions have been discussed in detail by Biemann (1). The aromatic ring provides the double bond responsible for the initiation of this decomposition reaction. Because the carbonyl group is attached α to the benzene ring it remains with the benzene ring with the charge going to that moiety of the molecule.

The profile-rearrangement subroutine continued to examine the spectral data for other possible rearrangement peaks. Thus for the dihydrotrimethylnaphthalenones (Group I) a second even-numbered peak of the general formula $C_nH_{2n-10}O$ was selected at 28 mass numbers below the previously selected peak which was at either $(M-42)^+$ or $(M-28)^+$. The data selected by the subroutine is shown in Figure 7. It is assumed that this peak is formed by loss of carbon monoxide in a manner similar to that which has been shown for bicyclic ketones (3). We noted that the main cleavage is at the bonds α and γ to the carbonyl group for these structures. The same two bonds are also β to the benzene ring.

Another test of the usefulness of these subroutines is the ease with which they enable an analytical scheme to be devised for the determination of molecular structures of unknown compounds from mass spectral data. Based upon the output data of these subroutines, an analytical scheme was devised for the structural determination of cyclic ketones (the time required was about one hour). This scheme is shown below. Since the scheme was formulated it has been applied to several reference standards and has served to confirm their molecular structures. Some minor revisions may be required later in the refinement of the scheme due to the rather small number of spectra covered by this study.

STRUCTURAL FEATURES OF CYCLIC KETONES
DEDUCED FROM MASS SPECTRAL DATA

This scheme of structural deduction calls for the mass spectra to be first displayed in the form of a rectangular array. Peaks which then appear in the molecular ion column and those in the column directly to the left of the molecular ion column are the only peaks to be considered in determining which carbons are methyl substituted.

Column containing peaks at one lower mass number than a corresponding peak in the molecular ion column of peaks	Peaks in the molecular ion (M) column
If M-15 > M-29 then a methyl group is on carbon No. 3 or No. 4 of the cyclic moiety.	If M-28 > M-42 then methyl groups are not on carbon No. 2 of the cyclic moiety.
If M-29 > M-15 then one or more methyl groups are attached to carbon No. 2 of the cyclic moiety (provided the molecular weight allows methyl substitution).	If M-42 > M-28 then methyl groups are attached to either carbons No. 2 or No. 3 of the cyclic moiety.
If M-42 > M-29 or M-15 then no methyl groups are on the cyclic moiety.	If M-14 > M-42 or M-28 then one or more methyl groups are substituted on carbon No. 3 of the cyclic moiety.

Also --

If a peak in the column to the left of the molecular ion column is more intense than any peak in the molecular ion column

then one or more methyl groups are substituted on carbon No. 3.

In summary, it has been shown for the cyclic ketones examined in this study that our subroutines, when inserted into our main computer program, have been effective in searching complete mass spectral data for those peaks having the greatest structural significance and diagnostic value. The data, once selected, is arranged in such a manner that differences between selected peaks indicate possible fragmentation paths.

For the cyclic ketones examined, it was shown that the carbonyl group did not greatly influence the fragmentation. The fragmentation was influenced mainly by the benzene moiety rather than the carbonyl group. Cleavage of the two bonds β to the benzene ring was prominent in the fragmentation. Intense peaks were formed at even mass numbers due to the retro-Diels-Alder cleavage which was initiated by the aromatic ring. Fragmentation proceeded by removal of the C=O group if it had been attached α to the benzene ring.

The selection of peaks by the computer program enabled us to devise an analytical scheme which permits deduction of structural features of cyclic ketones from mass spectral data.

ACKNOWLEDGMENTS

Mrs. Wanda Wright did most of the computer programming which was required in this correlation study. Mr. Harry Gartside aided in setting up the programs and in training Mrs. Wright.

Dr. Gerald Perkins, Jr. and Mr. Dale Leavesley gave their support to this work in the beginning stages. Without the understanding shown by Mr. Leavesley of our Central Computer Department it is quite possible that the required computer programs would not have been completed.

The technical assistance of Mr. W. K. Moore in running the samples on our mass spectrometer is greatly appreciated.

BIBLIOGRAPHY

(1) Biemann, Klaus, "Mass Spectrometry", McGraw-Hill Book Company, Inc., New York, 1962, page 102.

(2) Boyer, E. W., Hamming, M. C., and Ford, H. T., Anal. Chem., 35, 1168 (1963).

(3) Budzikiewicz, Herbert, Djerassi, Carl, and Williams, Dudley H., "Interpretation of Mass Spectra of Organic Compounds", Holden-Day, Inc., San Francisco, 1964, page 142.

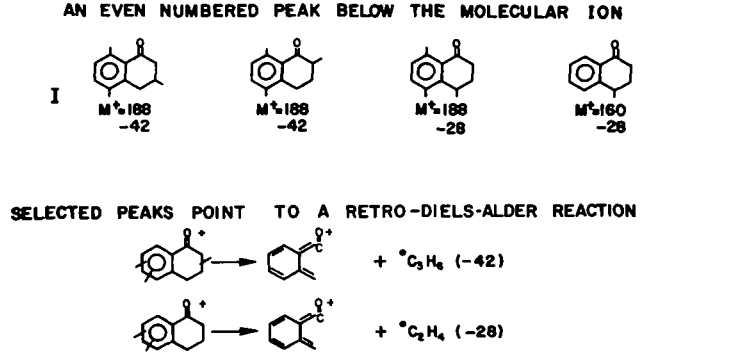

Figure 6

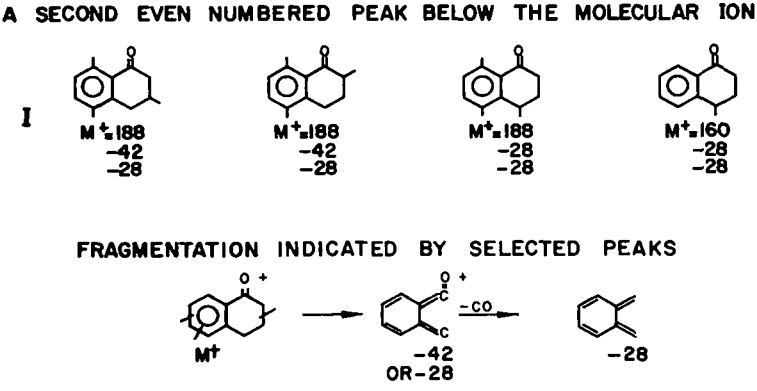

Figure 7

A Generalized Mechanism for Mass Spectral Reactions*

F. W. McLafferty
Purdue University
Lafayette, Indiana

Abstract

A recent communication from this laboratory proposes the separate consideration of the effect of the ionic and radical sites in the direction of decomposition of an ion. Identifying the most probable site for removal of an lectron in a molecule localizes both the ion and radical site. Particularly favored reactions triggered by these sites appear to include:

Radical site. Donation of the unpaired electron to form an additional bond to an adjacent atom; and abstraction of hydrogen atom from a sterically-favorable site in the molecule by the radical site.

Cation site. Transfer of an electron pair moving the site of the positive charge and transfer of another atom from an attached group to the site, thus displacing the attached group and forming a stable molecule.

Further examples will be given of the general usefulness of this approach for the rationalization of unimolecular ion decomposition reactions.

*The generous support of this research by the National Institutes of Health is gratefully acknowledged.

STRUCTURES OF GASEOUS IONS: UTILIZATION OF METASTABLE ION TRANSITIONS

T. W. Shannon* and F. W. McLafferty
Department of Chemistry,
Purdue University
Lafayette, Indiana

The unequivocal identification of a gaseous organic ion by mass spectrometry is a difficult task. The main physical and chemical properties which may be measured are the exact mass and the heat of formation of the ion. A knowledge of the molecular weight does not allow one to distinquish between isomers, and appearance potential measurements are somewhat laborious and often have insufficient accuracy to distinquish between similar structures. Thus if two mass spectra exhibitions identical, within experimental error, in mass and heat ot formation, these ions do not necessarily have the same structure.

Rosenstock et al.,[1] reported recently that a series of n-hexyl derivatives produced identical abundance ratios of the m/e 21.8 and 38.2 peaks resulting from metastable ion decompositions.[2] We now find that ions of the elemental composition $C_2H_5O^+$, found in the spectra of a wide variety of compounds, may be classified in a few distinct structural types according to the relative abundance and shape of the peaks resulting from the metastable decompositions of these ions.

Metastable peaks are usually much smaller and broader than peaks due to normal ions and their shape generally resembles a Gaussian distribution. Some metastable peaks have been observed which are much broader than normal and have a flat top. The width of such metastable peaks has been interpreted by Beynon and co-workers[3] in terms of the kinetic energy released in the decomposition of the metastable ion. This is illustrated in Figure 1. The width of the top, d, in atomic mass units, is related to the total energy T released in the decomposition by means of Eq. (1)

$$d = \frac{4m_2^2}{m_1}\left[\frac{(m_1-m_2)T}{m_2 eV}\right]^{1/2} \qquad (1)$$

V is the accelerating voltage and m_1 and m_2 are the masses of the parent and daughter ions respectively involved in the transition.

Figure 2 shows a typical flat-topped metastable observed in 2-pentanol. This metastable peak and all following data were obtained on a Hitachi RMU-6A mass spectrometer using an electron energy of 75 volts. The spectra were recorded with a wide collector slit, corresponding to a resolution of approximately 300. The centre of the peak shown in Figure 2 occurs at a mass of 18.7 and corresponds to the loss of methane from the mass 45 ion and formation of the mass 29 ion.

Figure 3 shows a metastable peak which is also observed in 2-pentanol. This occurs at a mass of approximately 8.0. The peak corresponds to the loss of acetylene from the mass 45 ion and formation of the H_3O^+ ion. This metastable has been observed previously[4] and exhibits the expected normal shape.

The other metastable peak of interest in this work is shown in Figure 4. This peak occurs in methylal at mass 18.7 and corresponds to the loss of methane from the mass 45 ion. In contrast to that observed in 2-pentanol, shown in Figure 2, this peak exhibits a normal shape.

From the spectra of the compounds we have run to data, it was noted that whenever a flat-topped metastable was observed at mass 18.7, a normal shaped metastable peak at mass 8.0 was also observed. Further, when a normal metastable at mass 18.7 appears, no metastable peak at mass 8.0 is observed.

---

*Present address: Eastern Research Laboratory, The Dow Chemical Company
Wayland, Massachusetts

The ratios of the metastable ion abundance to that of the precursor and the energies released in the transition, calculated via Eq. (1), are shown in Table I for a number of secondary alcohols. The relative abundance of the metastable peaks with respect to the mass 45 ion are reasonably consistent while the ratio of metastable peak heights is approximately two to one. The values of the energy released are in good agreement. For these compounds, the mass 45 ion is most likely to have the structure CH_3-CH=$\overset{+}{O}$H.

The data for compounds exhibiting the ethoxy moiety is given in Table II. For these molecules the mass 45 ion is formed via a rearrangement and probably has the same structure as in the secondary alcohols. The data is quantitatively similar to the secondary alcohols in all features.

Similar data for a number of primary alcohols and diols as well as for compounds containing the CH_3OCH_2- moiety are given in Tables III and IV respectively. In the case of the primary alcohols and diols, although the scatter in the data is much larger than that previously shown, the ratio of the abundance of the metastable peaks to that of the mass 45 ion is a factor of approximately five greater than for secondary alcohols. Again the relative abundance of the two metastable peaks is approximately two to one.

Compounds of the structure CH_3OCH_2-Y are qualitatively different from those previously discussed in that the mass 45 ion decomposes to HCO^+ with the release of very little excess energy. Furthermore, no metastable at mass 8.0 is observed indicating that loss of methane is not favored, at least when considering processes having rate constants such that they may be observed as metastables. The data thus indicate that these $C_2H_5O^+$ ions have a unique structure; for which CH_3-$\overset{+}{O}$=CH_2 is probably a favored canonical form.[5] Loss of CH_4 from this structure should be much more favored than loss of C_2H_2 as indicated by the metastable abundances.

The averaged data for the various types of compounds studied is given in Table V.

TABLE V

Structure	Abundance Ratio $m^* = 18.7$	$(m^*/C_2H_5O^+) \times 10^4$ $m^* = 8.0$	Energy Released (ev)
CH_3OCH_2Y	12.3 ± 1.8	<0.1	<0.1
$CH_3CH(OH)Y$	5.3 ± 1.2	10.1 ± 2.6	0.44 ± .02
$HOCH_2CH_2Y$	30 ± 14	55 ± 27	0.50 ± .04
CH_3CH_2OY	6.9 ± 2.3	13.7 ± 5.3	0.52 ± .05

For compounds other than CH_3OCH_2-Y the ion abundances at masses 8.0 and 18.7 appear to be roughly the same with respect to each other, although not with respect to the mass 45 ion. The energy released in the transitions giving rise to the metastable peaks at mass 18.7 are also in reasonable agreement. This data suggests that these metastables have a common precursor: the protonated oxirane structure. Such a structure has been previously postulated by Van Raalte and Harrison[4] to explain the energetics and isotopic label retention in the formation of the H_3O^+ ion from a number of secondary alcohols. Thus, for the cases in which a flat-topped metastable of mass 18.7 is observed, the formation of the mass 29 and 19 ions from the mass 45 ion may be written as proceeding via the following mechanism:

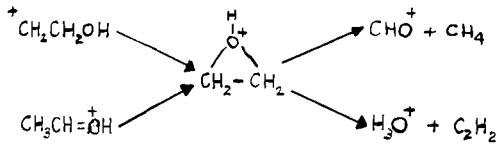

TABLE I

MOLECULAR STRUCTURE OF TYPE $(CH_3CH(OH)-Y$

-Y	Abundance Ratio $m^* = 18.7$	$(m^*/C_2H_5O^+) \times 10^4$ $m^* = 8.0$	Energy Released (ev) Calc. from 18.7 Peak
-H	5.5	10.0	0.45
$-CH_3$	4.7	9.2	0.44
$-C_2H_5$	6.6	15.2	0.43
$-C_3H_7$	3.1	6.0	0.42
$-CH_2OH$	5.5	9.0	0.49
$-C_2H_4OH$	4.9	9.1	0.41
$-COCH_3$	6.9	11.9	0.45
Average	5.3 ± 1.2	1.01 ± 2.6	0.44 ± .02

TABLE II

MOLECULAR STRUCTURE OF TYPE CH_3CH_2O-Y

-Y	Abundance Ratio $m^* = 18.7$	$(m^*/C_2H_5O^+) \times 10^4$ $m^* = 8.0$	Energy Released (ev) Calc. from 18.7 Peak
$-C_2H_5$	5.9	11.3	0.50
$-C_2H_4CN$	10.8	22.7	0.56
$-CONH_2$	4.6	9.4	0.57
-COH	6.2	11.3	0.44
Average	6.9 ± 2.3	13.7 ± 5.3	0.52 ± .05

TABLE III

MOLECULAR STRUCTURE OF TYPE $HOCH_2CH_2-Y$

-Y	Abundance Ratio $m^* = 18.7$	$(m^*/C_2H_5O^+) \times 10^4$ $m^* = 8.0$	Energy Released (ev) Calc. from 18.7 Peak
-OH	40	64	-
$-CH_2OH$	17	32	0.46
$-CH_2CH_2OH$	10	16	0.51
$-CH_3$	45	89	0.56
$-C_2H_5$	37	75	0.46
Average	30 ± 14	55 ± 27	0.50 ± .04

TABLE IV

MOLECULAR STRUCTURE OF TYPE CH_3OCH_2-Y

-Y	Abundance Ratio $(m^*/C_2H_5O^+) \times 10^4$ $m^* = 18.7$
$-OCH_3$	15.1
$-CH_2OH$	9.3
$-CH_2OCH_3$	12.3
$-CH_2CN$	12.6
Average	12.3 ± 1.8

The relatively high values of the ratio of metastable peak height to mass 45 peak height in the case of compounds of type $HOCH_2CH_2Y$ indicates that ions of the structure $^{+}CH_2CH_2OH$ isomerize more rapidly to the oxirane structure than do ions of the structure $CH_3CH{=}\overset{+}{O}H$.

It is obvious that such observations on metastable processes could be extremely useful in deciding if an unknown compound may contain an ether or alcohol moiety. Furthermore, other processes may also give rise to charactersitic flat-topped metastables. Indeed, recent results indicate that aromatic nitro compounds also lose NO with the conversion of a specific amount of internal energy into kinetic energy of the fragments.[3,6]

On further point deserves some mention. The identity of the energy released in the decomposition of the $C_2H_5\overset{+}{O}$ ion formed from a variety of sources may indicate the involvement of a common electronic state. However, processes which are observed as metastables have a relatively narrow range of rate constants and thus arise from ions will a relatively specific amount of internal energy. Thus under the experimental conditions only slight variations in the energy released would be observed. Further experiments are planned to investigate this point in greater detail.

REFERENCES

1. H. M. Rosenstock, V. H. Dibeler and F. N. Harlee, J. Chem. Phys., 40, 591 (1964)

2. J. H. Beynon, "Mass Spectrometry and Its Application to Organic Chemistry" Elsevier, New York

3. J. H. Beynon, R. A. Saunders, A. E. Williams, Z. Naturforschg., 20a, 180 (1965)

4. D. Van Raalte and A. G. Harrison, Can. J. Chem., 41, 3118 (1963)

5. F. W. McLafferty, Anal. Chem., 29, 1872 (1957)

6. T. W. Shannon, F. W. McLafferty and C. R. McKinney, Chem. Comm., (1966) to be published.

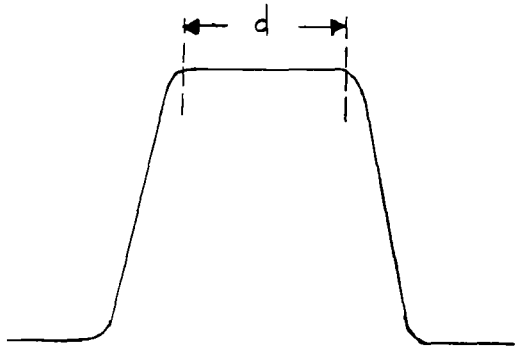

META-STABLE PEAK WITH FLAT TOP
FIGURE 1

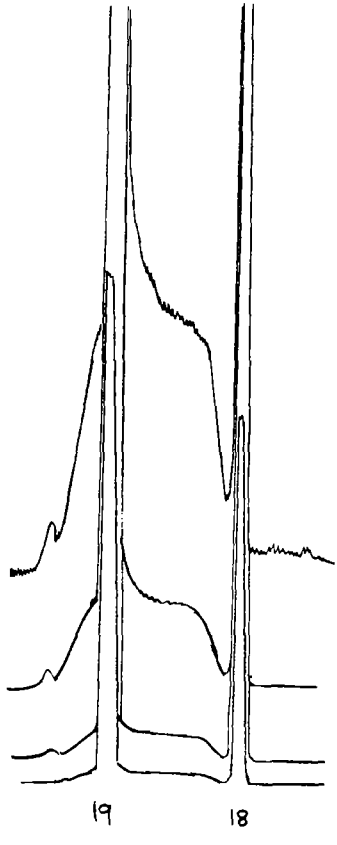

2-PENTANOL
FIGURE 2

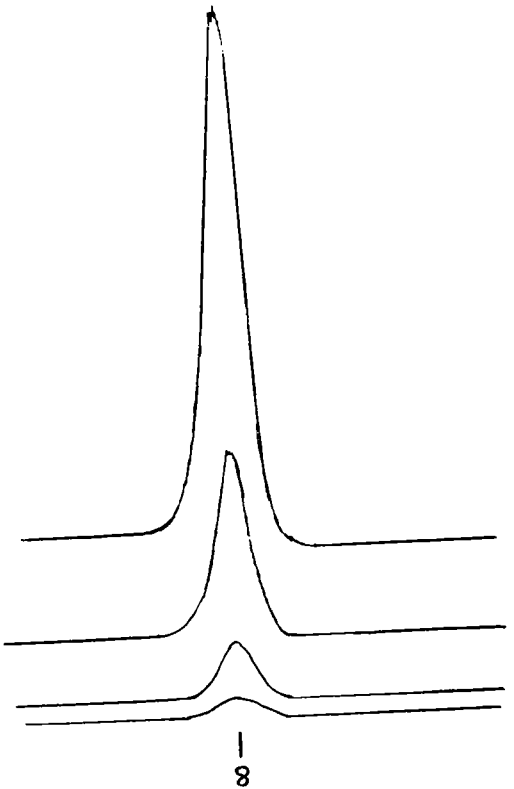

2-PENTANOL
FIGURE 3

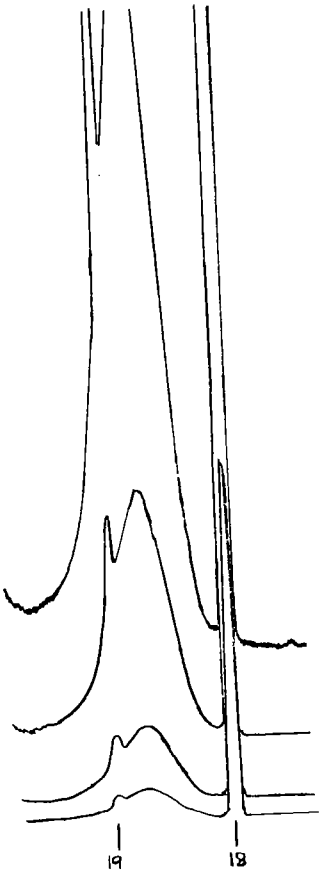

METHYLAL
FIGURE 4

Some Aspects of the Production of Metastables

by

R.I. Reed and (Miss) M.T. Robert-Lopes
The University, Glasgow, W.2, Scotland.

Recent developments suggest that the theory which underlies the origin of metastable ions is now better understood[1, 2] and that the presence of such ions in the mass-spectra is becoming increasingly important in the understanding and interpretation of cracking-patterns. It has been known for some time that many of the metastables present in a spectrum are collision-induced[3] and that the best way of producing these ions would be to increase the pressure of the compound under examination. It was apparent to us that the greatest advantage which would accrue from the study of an unknown compound by means of mass-spectrometry was the extraordinary sensitivity of the method which would allow, for example, an analysis on 0.1 mgm. of a steroid. This benefit is largely wasted if, in order to obtain the metastable ions, it is necessary to increase the pressure greatly above the minimum required to obtain the fragmentation-pattern. Accordingly attempts have been made to increase the gas pressure by means of the addition of a suitable gas. Here we record the results of some of these experiments.

i These investigations have been carried out upon camphene, limonene, and α-pinene. The metastables obtained from these compounds are reported in the following tables 1 and 2.

TABLE 1.

a^+	b^+		c	calc. value
136	121	+	15	107.65
121	105	+	16	91.11
92	91	+	1	90.01
93	91	+	2	89.04
136	107	+	29	84.18
121	93	+	28	71.48
136	95	+	41	66.36
93	77	+	16	63.75
136	92	+	44	62.23
105	79	+	26	59.43
82	67	+	15	54.74
95	69	+	26	50.11
121	77	+	44	49.
91	65	+	26	46.42
136	78	+	58	44.73
107	68	+	39	43.21
43	42	+	1	41.02
108	65	+	43	39.12
121	67	+	54	37.09
69	41	+	28	24.36

a^+ - parent ion
b^+ - daughter ion
c - neutral fragment.

TABLE 2

Camphene	Limonene	α-Pinene
107.66	107.66	107.66
-	-	-
91.1	-	91.1
89.04	89.04	89.04
84.18	84.18	84.18
-	-	-
-	-	-
71.49	71.49	71.49
-		
63.74	63.74	63.74
62.25	62.25	62.25
-	-	-
-	61.15	-
59.37	59.37	59.37
-	-	-
-	50.15	-
-	-	-
46.41	46.41	46.41
44.73	-	-
43.2	-	-
-	41.02	41.02
-	-	-
37.1	37.1	37.1
-	35.12	-
-	34.72	-
24.4	24.4	24.4

ii Small quantities of each of these compounds have been examined alone and in the presence of differing concentrations of several gases namely helium, xenon, methane, nitrogen and nitric oxide.

TABLE 3

Camphene + Y

Ionization Potential	24.6	15.6	13.1	12.2	9.2
Y	He	N_2	CH_4	Xe	NO
	107.66	107.66	107.66	107.66	107.66
	91.1	91.1	91.1	91.1	91.1
	90.01	90.01	90.01	90.01	90.01
	89.04	89.04	89.04	89.04	89.04
	84.18	84.18	84.18	84.18	84.18
	71.49	71.49	71.49	71.49	71.49
	66.33	66.33	66.33	66.33	66.33
	63.74	63.74	63.74	63.74	63.74
	62.25	62.25	62.25	62.25	62.25
	54.75	54.75	54.75	54.75	54.75
	49.11	49.11	49.11	49.11	49.11
	39.15	39.15	39.15	39.15	39.15
	37.1	37.1	37.1	37.1	37.1
	-	-	26.12	-	-
	24.4	24.4	24.4	24.4	24.4

TABLE 4

Limonene + Nitric Oxide

Limonene	Limonene + NO	Limonene	Limonene + NO
113	113	63.14	63.14
107.66	107.66	62.25	62.25
90.01	90.01	59.37	59.37
89.04	89.04	49.11	49.11
84.18	84.18	47.27	47.27
78.2	78.2	46.41	46.41
77.39	77.39	39.15	39.15
75.25	75.25	37.1	37.1
71.49	71.49	24.4	24.4
66.33	66.33	15.3	15.3
63.74	63.74	13.7	13.7

iii These gases were chosen to investigate the effects, if any, of the different properties of the various additives:

(a) nitrogen is of a much higher ionization potential (~ 15.60 eV.) than either camphene or limonene; so that, if a collision occurred between neutral camphene and an ion of the added gas, charge transfer is probable. Helium also belongs to this class (~ 24.6 eV.)

(b) methane has a much lower ionization potential (~ 13.12 eV.) which would make collisions between neutral camphene molecules and methane ions without charge transfer more likely.

(c) xenon was used for two reasons; not only is the ionization potential (~ 12.1 eV.) lower than that of the compounds used above, but it is possible that this element may combine with an ion at least under certain circumstances.[4]

(d) nitric oxide was used to examine the possibility of the attachment to the radicals formed in the fissions observed and to see if by any chance such attachment would have an observable effect upon the number or nature of the metastables produced.

As was expected the results obtained showed little if any effect which is peculiar to the nature of the added gas. It is concluded that the function of the added material is solely to impart energy to the ion which then decomposes by a unimolecular process to yield the fragment ions, and the associated metastables observed.

iv These studies have provided us with the opportunity of determining the activation energy of some of the processes. While these differ in value, depending upon the particular dissociation involved, they are always small 5Kcal. or less.

v Particular differences in the shapes of the metastable ions which appeared in any one spectrum were also noticed.

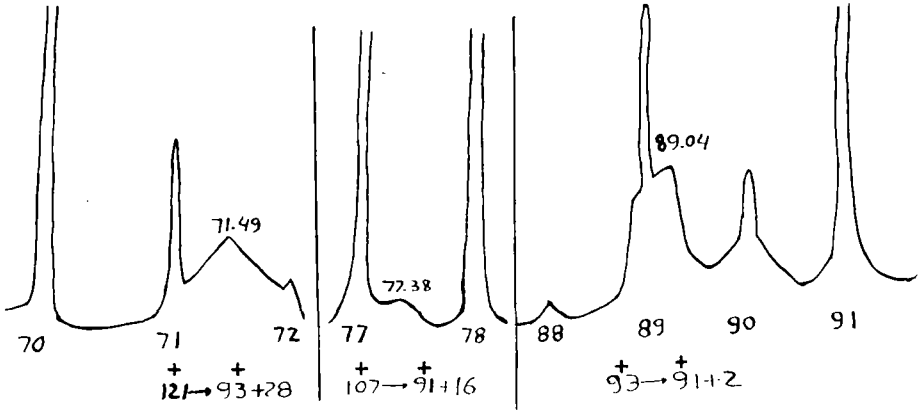

This would suggest that some metastables are of greater importance - possibly as indicating change in the shape of the ion, or as a means of estimating the release of energy - than is often realised.

vi Finally some of the peculiar variations observed may be concerned more with the shape of the molecule than has so far been considered; as distinct from the behaviour of the saturated alkanes.

It is hoped that ultimately these combined observations will be of value in the determination of organic structures from their cracking-patterns.

References

1. Franklin, J.C. and Field, F.H., "Electron Impact Phenomena", (1957), Academic Press, New York.

2. Beynon, J.H., Saunders, R.A., and Williams, A.E., Zeit. fur Nat., 20, (1965) 180.

3. Melton, C.E. and Rosenstock, H.J., J. Chem. Physics, (1957), 26, 568.

4. Rudolph, P.S., Lind, S.C. and Melton, C.E., J. Chem. Physics, (1962), 36, 1031.

APPEARANCE POTENTIAL STUDIES OF SOME POLYPHENYLS USING AN AUTOMATIC VOLTAGE SCANNER

By E. J. Gallegos and R. F. Klaver
Chevron Research Company, Richmond, California

Appearance potentials were measured for the principal positive ions in the mass spectra of several polyphenyls using an automatic voltage scanner designed for use on the AEI MS-9 high resolution mass spectrometer. The peak-matching circuitry of the MS-9 normally used for exact mass measurements is utilized in the voltage scanner. Therefore, this system also identifies the species measured by its empirical formula. This novel system is described.

Several polyphenyl compounds were studied using this system. The measured ionization potentials were m-octaphenyl, 8.28 e.v.; p-hexaphenyl, 7.67 e.v.; m- and p-quinquephenyl, 8.45 e.v., 8.18 e.v.; o-, m-, and p-quatraphenyl, 8.52 e.v., 8.51 e.v., 8.08 e.v.; o-, m-, and p-terphenyl, 8.64 e.v., 8.88 e.v., 8.78 e.v.; and diphenyl, 8.95 e.v. The parent molecule ion is the most intense peak in the spectrum for all the polyphenyls. The intensity of the doubly charged parent is second in abundance to the parent of the m- and p- polyphenyls studied. Metastable ion transitions, spectra, and energetics data are used in a discussion of ionization and dissociation processes of the polyphenyls.

Introduction

Systematic electron impact studies have recently been made on a number of polynuclear aromatic hydrocarbons;[1] however, very little is found in the literature on the mass spectra and energetics of polyphenyls other than biphenyl.[2] Bradt and Mohler[3], however, have reported the mass spectra and relative sensitivities of several meta-polyphenyls.

Unique features of the mass spectra of the higher molecular weight, highly conjugated compounds are the low abundance of fragment ions and relatively high abundance of multiply charged ions. Of interest, therefore, is the percent of total ionization of the parent single and doubly charged ions. Observed also is an expected increase in the intensity of the doubly charged parent with increased total number of - electrons with a corresponding decrease in the appearance potentials. The lack of recent and complete investigations of the higher molecular weight polyphenyls provided an incentive to undertake this study.

Experimental

The data were obtained on an AEI MS-9 high resolution mass spectrometer.

The ionization potential data were obtained using an automatic voltage scanner which decreased the electron accelerating voltage in increments of 0.05 or 0.2 volt in the range of 80 to 3 volts. This system is described in the following section. The ionizing voltage was calibrated using a suitable inert gas or bis(trifluoromethyl)benzene or certain fragment peaks from perfluorotributylamine as secondary calibrants. All were introduced simultaneous with the polyphenyl.

Reported mass spectra were obtained at 70 e.v. with 20 microamps ionizing current, using a rhenium filament.

[1]Wacks, Morton E., 13th Annual Conference on Mass Spectrometry and Allied Topics, May 16-21, 1965, St. Louis, Missouri.

[2]Natalis, P., and J. L. Franklin, Journal of Physical Chemistry, 2935, 69 (1965).

[3]Bradt, P., and F. L. Mohler, Journal of Research of the National Bureau of Standards, 143, 60 (1958).

The polyphenyls were obtained from K and K Laboratories. o-, m-, and p-terphenyls showed no impurities in the gas chromatogram, each showing unique retention times, showing negligible isomer contamination. Of the polyphenyls of higher molecular weight, p-hexaphenyl, and m-octaphenyl showed impurities. These were further purified by microsublimation under nitrogen. Ultraviolet spectra of each of the polyphenyls show only one absorption maximum. Infrared spectra were also obtained showing little impurities. Mass spectra of the polyphenyls used as purified or as received show only negligible impurities of higher molecular weight in the mass spectrometer.

Automatic Voltage Scanner

This system takes advantage of the peak switching capabilities of the MS-9. Normally, peak switching is used to compare two mass peaks for precise mass measurements.

The main feature of the system is the electron acceleration potentiometer driven by the Ledex digimotor shown in Figure 1, which is triggered from the peak switching chassis. Simultaneously, the event marker located on the recorder is activated and marks the recorder paper at the exact time that the voltage decrease takes place, which is immediately after the high mass ion is scanned. Triggering of the digimotor occurs only after both low and high mass scans are complete and intensities recorded. The potentiometer drive system is constructed to scan in increments of 0.2 e.v. This can easily be converted to increments of 0.05 e.v. by changing the gear box ratios. A wiring diagram of the system is shown in Figure 2. In operation C_1 charges to 50 VDC. A step voltage appearing at the cathode of V_7 triggers the SCR, C_1 then discharges operating the Ledex motor and recorder event marker.

The monitored ion currents of the calibrant and unknown peaks are adjusted such that the linear portion of the ionization efficiency curves, as displayed by the recorder, are parallel. This serves to normalize the ionization efficiency curves. Typical ionization efficiency curves recorded by the MS-9 are shown in Figure 3. The curves shown are for krypton and xenon.

Appearance potentials of bis(trifluoromethyl)benzene parent and selected fragments of perfluorotributylamine were determined using inert gases and subsequently used as secondary calibrant ions for ionization potential determinations of some of the higher molecular weight polyphenyls. Fragment ions from perfluorotributylamine were chosen on the basis of relatively low appearance potentials and the similarity of the ionization efficiency curves to that of a molecular ion. Both bis(trifluoromethyl)benzene and perfluorotributylamine were used as secondary calibrants for ease of introduction to the mass spectrometer and due to the fact that using the peak matching facilities of the MS-9 requires that the ratio of the low to high mass be no greater than two.

General Features of the Mass Spectra

The mass spectra of the polyphenyls clearly show that the observed ionization is due primarily to the parent and the doubly charged parent. The loss of H and H_2 becomes decreasingly significant as the molecular weight increases. The partial mass spectra of the polyphenyls studied are given in Table I.

Table I

Partial Mass Spectra of Several
Polyphenyls
Source Temperature 240°C

m/e	o-3φ*	m-3φ	p-3φ	o-4φ	m-4φ	p-4φ	m-5φ	p-5φ	p-6φ	m-8φ
29										2.7
36										2.4
39	2.2	2.9								
43										
50		2.1								3.6
51	2.8	4.7		2.0						
55										2.0
57										2.0
63	2.4	3.2								
75	2.2	2.5								
76	2.3	3.0	2.3							
77		3.1								
88	4.2	2.6	2.3					2.1		
89		2.2	2.0							
91				2.8				2.2		
189++		1.2	1.2							
99										
100	4.3	1.7								
101	12.7	5.2	5.3							
203++	3.8	1.0	1.1							
102		2.6								
213++	1.9									
215++	8.0	1.1								
112	2.6									
224++	1.9									
113	13.2	3.1	3.8							
227++	4.3		1.2							
114	14.4	1.9	2.1							
229++	4.7									
115	1.0	1.7	4.0							
230++	3.0	6.9	9.5							
231++	0.6	1.4	1.9							
239++				1.2						
125				2.3						
126		1.7		2.0						
128		3.0	2.4							
261++				1.0						
263++				3.6	1.2					
137				2.3						
138				7.3	2.4					
277++				2.3						
139				2.7						
144				2.0						
287++				3.4						
289++				10.6	2.3			2.4		
145				13.0			2.3	4.1		
291++				4.2						
150				4.9						
301++				1.7						
151		3.4	2.5	6.5	3.2	2.3				
303++				2.2						
152	2.5	6.9	4.8	3.6	3.6	3.7			1.9	
153		2.5	2.2						1.0	
306++				2.2	16.6	13.6				
307					4.2	3.3				
165	2.8	1.4		3.0						
178	2.3			2.0						
189	2.4	2.3		1.3					1.0	
381++							1.1			
382++							22.4	12.7		
383++							7.3	3.9		
200	2.7									
201	2.4									
202	10.2	6.4	4.6	4.5	2.3					

*φ represents phenyl.

Table I (Cont.)

Partial Mass Spectra of Several Polyphenyls
Source Temperature 240°C

m/e	o-3φ	m-3φ	p-3φ	o-4φ	m-4φ	p-4φ	m-5φ	p-5φ	p-6φ	m-8φ
203	3.9	2.3								
213	2.0									
215	28.7	3.8	3.3	14.5						
216	5.4			2.7						
226	14.5	6.1	5.9	8.6	3.5	3.9	2.3	4.0	2.8	
227	10.5	4.7	4.8	4.9		2.3		2.0	2.1	
228	29.9	12.4	12.2	18.3		33.9	2.1	3.2	4.0	
229	58.2	9.7	8.8	22.3						
458^{++}									21.2	
459^{++}									8.5	
230	100.0	100.0	100.0	4.1						
231	18.3	19.1	19.7							
232	1.7	1.8	1.8							
252				2.2						
265				4.0						
276				5.0					1.1	
277				3.0		2.0		2.4		
278				2.6						
289				16.5	5.5				2.1	
290				9.2	2.2	5.4				
291				10.0		2.2		2.8		
292				2.3						
300				2.9						
302				8.1	3.4	3.7			2.1	
303				7.3	2.9	3.0			1.4	
304				5.4	2.5	2.7				
305				18.2	1.6	1.5				
610^{++}										38.6
611^{++}										19.3
612^{++}										4.8
306				100.0	100.0	100.0				
307				25.1	28.8	26.1				
308				3.2	3.3	3.3				
382							100.0	100.0		
383							32.2	32.2		
384							5.3	5.2		
458									100.0	
459									38.1	
460									7.4	
610										100.0
611										46.8
612										11.5
613										2.0

Ions accounting for less than 1% of the base peak have been deleted.

Table II

MW	Molecule	% of Total Ionization of $M^{++} + M^{+}$	Ratio P^{++}/P^{+}
230	p-3φ	50.9	0.14
306	p-4φ	61.0	0.16
382	p-5φ	67.0	0.18
458	p-6φ	70.0	0.21
230	m-3φ	44.2	0.09
306	m-4φ	56.8	0.17
382	m-5φ	62.5	0.22
610	m-8φ	85.2	0.35
230	o-3φ	25.8	0.05
306	o-4φ	26.0	0.03

Table II shows the sum of the percent of total ionization of the parent singly and doubly charged species.

Significant contribution of fragment ions to the one-half parent are observed for the lower molecular weight polyphenyls. See Table III.

Table III

Contribution of Fragment Ions to One-Half Parent Mass

Cmpd	$(M+1)^{++}/M^{++}$	% M^{++}	% 1/2 M^{+}	$(M+1)^{+}/M^{+}$	Calcu. $(M+1)^{+}/M^{+}$
o-3φ	0.16	80	20	0.20	0.20
m-3φ	0.14	70	30	0.20	0.20
p-3φ	0.17	81	19	0.21	0.20
o-4φ	0.23	85	15	0.27	0.26
m-4φ	0.26	96	4	0.27	0.26
p-4φ	0.26	96	4	0.27	0.26
m-5φ	0.33	~99	~1	0.33	0.33
p-5φ	0.33	~99	~1	0.33	0.33
p-6φ	0.40	100	-	0.40	0.39
m-8φ	0.52	100	-	0.57	-

Sensitivity reproducibility approximately 3%.

As a result, all appearance potentials of the doubly charged parent ion were made from the C^{13} isotope peak.

The m-polyphenyls generally show the parent as the largest peak in the spectrum followed by the doubly charged parent. One exception is apparently the m-terphenyl where M-H and M-2H are slightly more intense than M^{++}. The percent of total ionization of the $parent^{+}$ and $parent^{++}$ is less than that for the corresponding p-polyphenyls as shown in Table II.

o-Terphenyl and o-quaterphenyl show by far the greatest fragmentation, with the parent accounting for less than one-third of total ionization. The $parent^{++}$ becomes a minor peak in the mass spectrum. M-H and M-2H for these molecules increase greatly in intensity along with the corresponding doubly charged species. The o-polyphenyls show substantial ions representing the loss of a methyl group.

Appearance Potentials

The ionization potentials of the polyphenyl molecular ions and the appearance potentials of their corresponding doubly charged parents are given in Table IV.

Table IV

Ionization Potentials of Several Polyphenyls

	This Work		IP
	IP	AP(M^{++})	Literature
m-Octaphenyl	8.28 ± 0.05	20.3 ± 0.4	-
p-Hexaphenyl	7.67 ± 0.05	19.5 ± 0.4	-
m-Quinquephenyl	8.45 ± 0.05	20.0 ± 0.4	-
p-Quinquephenyl	8.18 ± 0.05	19.6 ± 0.4	-
o-Quaterphenyl	8.52 ± 0.05	20.5 ± 0.4	-
m-Quaterphenyl	8.51 ± 0.05	20.5 ± 0.4	-
p-Quaterphenyl	8.08 ± 0.05	20.2 ± 0.4	-
o-Terphenyl	8.64 ± 0.05	21.5 ± 0.4	-
m-Terphenyl	8.88 ± 0.05	21.5 ± 0.4	-
p-Terphenyl	8.78 ± 0.05	21.5 ± 0.4	-
Diphenyl	8.95 ± 0.05	-	8.96[2]

Heats of formation of the three and higher membered polyphenyls are not available to the author's knowledge. Nevertheless, very approximate heats of formation of the molecule may be calculated using the group equivalents method due to Franklin[4] if the degree of resonance between phenyl groups is known for o-, m-, and p-polyphenyls. o-Polyphenyls, from steric considerations, are not planar and, therefore, should not exhibit interphenyl resonance.

The p-polyphenyls should exhibit the greatest resonance stability. Indeed, from ultraviolet data by Gillman and Hey[5] and work done here, the para series shows that the wave length λmax of the most intense absorption increases almost regularly with the number of benzene rings, but for the m-polyphenyls, λmax has a nearly constant value of 2530 ± 20 Å. o-, ter-, and o-quaterphenyls show a lower λmax of 2310 ± 10 Å and 2225 ± 10 Å, respectively.

A number of appearance potentials were measured and are listed in Table V.

Table V

Appearance Potentials of Selected Fragment Ions of Some Polyphenyls

m/e		A.P.	
229	o-3[illegible]	11.7	± 0.1
228	o-3[illegible]	11.7	± 0.1
215	o-3[illegible]	12.0	± 0.1
454	p-6[illegible]	15.6	± 0.2
229	p-6[illegible]	19.5	± 0.3
228	p-6[illegible]	18.5	± 0.3
228	m-4[illegible]	16.7	± 0.3
226	m-4[illegible]	18.3	± 0.3
305	o-4[illegible]	11.7	± 0.1
291	o-4[illegible]	12.7	± 0.1
289	o-4[illegible]	15.5	± 0.2
229	o-4[illegible]	12.8	± 0.1
228	o-4[illegible]	13.0	± 0.1
226	o-4[illegible]	19.0	± 0.4
215	o-4[illegible]	13.0	± 0.2

No attempts were made to calculate heats of formation of ions due to incomplete information on the heats of formation of neutral species and molecules.

Observed metastables for o-, m-, and p-terphenyl are shown in Table VI.

Table VI

o-TERPHENYL
Metastables

m^*	m_1	m_2		m_1-m_2
200.89	230^+ ——>	215^+	+	15
230.00	232^+ ——>	231^+	+	1
229.00	231^+ ——>	230^+	+	1
228.00	230^+ ——>	229^+	+	1
227.00	229^+ ——>	228^+	+	1
226.00	228^+ ——>	227^+	+	1
225.00	227^+ ——>	226^+	+	1

[4]J. L. Franklin, Industrial and Engineering Chemistry, 41 No. 5, 1070 (1949).

[5]A. E. Gillman and D. H. Hey, J. Chem. Soc. 1939, 1170.

Table VI

m-TERPHENYL
Metastables

m*	m_1		m_2		m_1-m_2
200.89	230^+	——>	215^+	+	15
230.00	232^+	——>	231^+	+	1
229.00	231^+	——>	230^+	+	1
228.00	230^+	——>	229^+	+	1
227.00	229^+	——>	228^+	+	1
226.00	228^+	——>	227^+	+	1
225.00	227^+	——>	226^+	+	1

p-TERPHENYL
Metastables

m*	m_1		m_2		m_1-m_2
200.89	230^+	——>	215^+	+	15
230.00	232^+	——>	231^+	+	1
229.00	231^+	——>	230^+	+	1
228.00	230^+	——>	229^+	+	1
227.00	229^+	——>	228^+	+	1
226.00	228^+	——>	227^+	+	1
225.00	227^+	——>	226^+	+	1

The intensity of the observed metastables decreased generally from o-, to m-, to p-terphenyl. Typical metastables of the quaterphenyl are shown in Table VII. The m- and p-terphenyl show the same metastables at decreased intensity.

Table VII

o-Quaterphenyl
Metastables

m*	m_1		m_2		m_1-m_2
305.00	307^+	——>	306^+	+	1
301.00	303^+	——>	302^+	+	1
288.00	290^+	——>	289^+	+	1
276.00	278^+	——>	277^+	+	1
274.00	278^+	——>	275^+	+	1
226.04	306^+	——>	263^+	+	43
171.38	306^+	——>	229^+	+	77
168.88	306^+	——>	228^+	+	78

:lg

FIGURE 1

MS-9 VOLTAGE SCANNER MOTOR ASSEMBLY

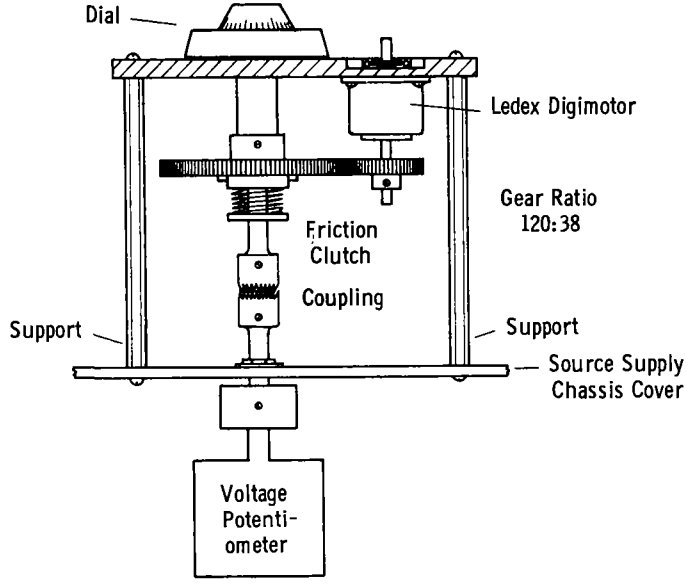

FIGURE 2

MS-9 VOLTAGE SCANNER DIAGRAM

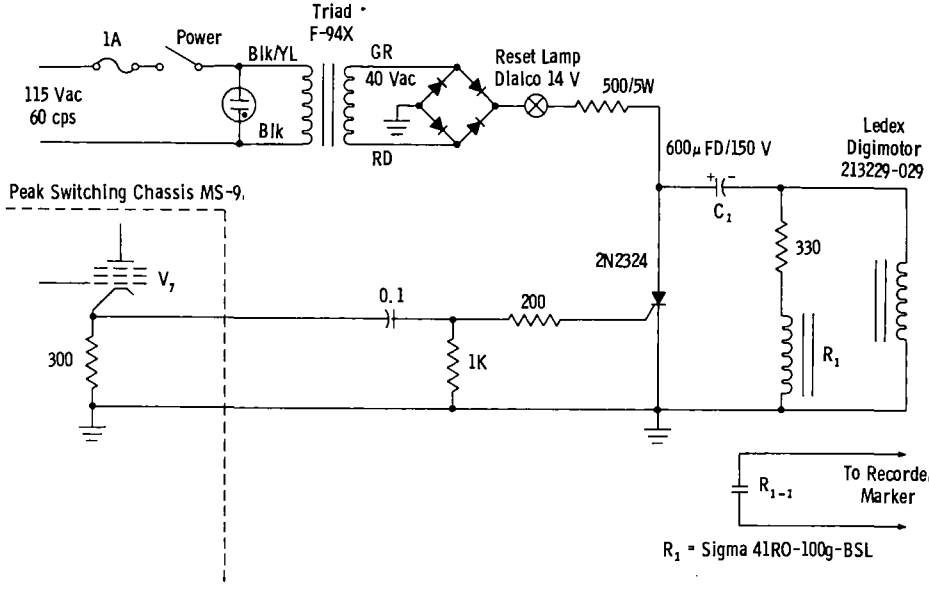

FIGURE 3

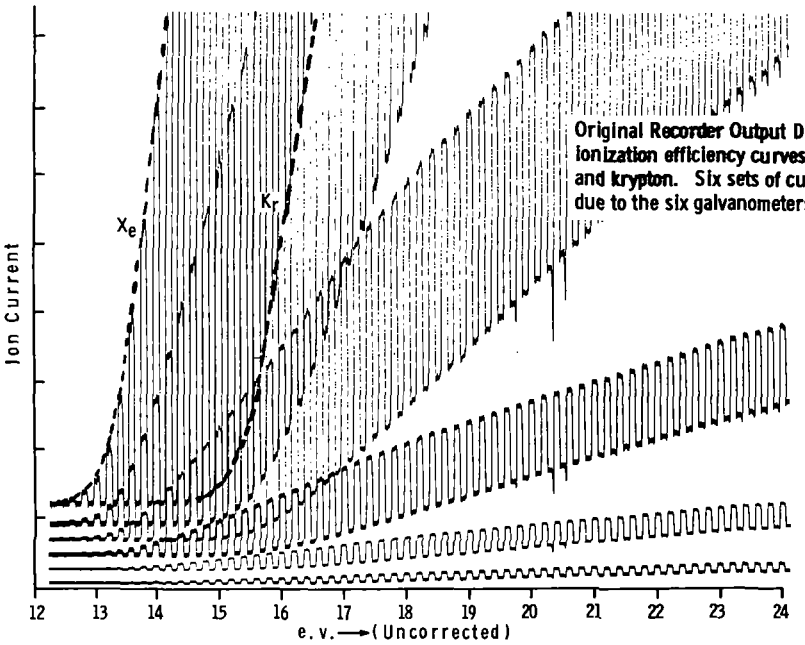

Original Recorder Output Display of the ionization efficiency curves for xenon and krypton. Six sets of curves are seen due to the six galvanometers.

DECOMPOSITION OF TROPYLIUM AND SUBSTITUTED TROPYLIUM IONS

Keith R. Jennings* and Jean H. Futrell

Aerospace Research Laboratories
Wright-Patterson Air Force Base, Ohio

ABSTRACT

Metastable transitions arising from the decomposition of tropylium ions have been investigated in a double-focusing mass spectrometer. It has been shown that the loss of an acetylene molecule is the only major decomposition process, and metastable peaks in the mass spectrum of toluene-α-d_3 have been interpreted in terms of this. The relative intensities of the metastable peak and the normal peak at m/e = 65 in the mass spectra of several compounds have been shown to correlate with the apparent heat of formation of the $C_7H_7^+$ ion. Metastable transitions in the mass spectra of several halogenated and alkylated toluene and benzyl compounds have been interpreted in terms of the decomposition of substituted tropylium ions by the elimination of C_2H_2 or C_2HX (X = F, Cl, Br). No evidence could be found for the existence of a pseudotropylium ion in which a CH group is replaced by a N atom in the mass spectra of alkyl pyridines.

INTRODUCTION

The m/e = 91 peak due to the $C_7H_7^+$ ion is very prominent in the mass spectra of benzyl compounds and many alkyl benzenes.[1] A metastable peak at m/e = 46.5 is attributed to the decomposition of this ion:

$$C_7H_7^+ \rightarrow C_6H_5^+ + C_2H_2 \qquad (1)$$

$$91^+ \rightarrow 65^+ + 26.$$

Despite differences in the apparent heat of formation of the $C_7H_7^+$ ion from hydrocarbons and benzyl halides, the above reaction appears to be the major mode of decomposition. Extensive experiments using deuterated compounds and ^{13}C-labeled compounds carried out largely by Meyerson and his co-workers provide strong evidence that the species undergoing decomposition is the symmetrical tropylium ion rather than the benzyl ion.

Label retention measurements on the $C_6H_5^+$ ion in the mass spectra of deuterated toluenes led to the suggestion that a small percentage of these ions arise by another path, and a metastable peak at m/e = 44.5 in the mass spectrum of toluene-α-d_3 has been attributed[2] to the reaction

$$C_6H_5.CD_3^+ \rightarrow C_6H_5^+ + C_2D_3 \qquad (2)$$

$$95^+ \rightarrow 65^+ + 30.$$

However, the corresponding metastable peaks have not been detected in the mass spectra of unlabeled toluene or singly labeled toluene. In each case, the peaks would be difficult to observe owing to interference by large, closely spaced normal peaks. An alternative mode of decomposition of the $C_7H_7^+$ ion has also been suggested,[3] based on the observation of a metastable peak at m/e = 43.7:

$$C_7H_7^+ \rightarrow C_5H_3^+ + C_2H_4 \qquad (3)$$

$$91^+ \rightarrow 63^+ + 28.$$

Appearance-potential measurements[4] on R-$C_7H_6^+$ ions in the mass spectra of substituted benzyl compounds suggest that for R=CH_3, F and OH, the ions are most probably substituted tropylium ions, whereas for R=CH_3O, the ion is probably best represented as CH_3O-C_6H_4-CH_2^+.

Since the double focusing mass spectrometer is a very sensitive instrument for the investigation of metastable transitions, the modes of decomposition of

*Visiting Research Associate, The Ohio State University Research Foundation, Columbus, Ohio.

TABLE I

Observed $C_7 \rightarrow C_6$ Metastable Decompositions

Transition		Intensity	Suggested Assignment
95^+	69^+	weak	$C_6H_5CD_3^+ \rightarrow C_5H_3D_3^+ + C_2H_2$[a]
94^+	68^+	v. strong	$C_7H_4D_3^+ \rightarrow C_6H_2D_3^+ + C_2H_2$
95^+	68^+	v. weak	$C_6H_5CD_3^+ \rightarrow C_5H_4D_2^+ + C_2HD$
94^+	67^+	strong	$C_7H_4D_3^+ \rightarrow C_6H_3D_2^+ + C_2HD$
93^+	67^+	strong	$C_7H_5D_2^+ \rightarrow C_6H_3D_2^+ + C_2H_2$
93^+	66^+	strong	$C_7H_5D_2^+ \rightarrow C_5H_4D^+ + C_2HD$
94^+	66^+	v. weak	$C_7H_4D_3^+ \rightarrow C_5H_4D^+ + C_2D_2$
91^+	65^+	weak	$C_7H_5D^+ \rightarrow C_5H_3D_2^+ + C_2H_2$ $C_7H_3D_2^+ \rightarrow C_6HD_2 + C_2H_2$
93^+	65^+	weak	$C_7H_5D_2^+ \rightarrow C_5H_5^+ + C_2D_2$
91^+	64^+	v. weak	Loss of C_2HD by $C_7H_5D^+$ or $C_7H_3D_2^+$
90^+	64^+	v. weak	Loss of C_2H_2 by $C_7H_7D^+$ or $C_7H_2D_2^+$
90^+	63^+	v. weak	Loss of C_2HD by $C_7H_4D^+$ or $C_7H_2D_2^+$

[a]Almost certainly contain significant contributions due to decomposition of $C_7H_4D_3^+$ ions containing a ^{13}C atom; the peak due to $95^+ \rightarrow 69^+$ transition is very weak but is approximately 8% of that due to $94^+ \rightarrow 68^+$, compared with 7.8% calculated for the isotope peak.

TABLE II

Relative Intensities of Metastably

Produced and Normal $C_6H_6^+$ Ions From Selected Molecules

Compound	I_m^*/I_m	$\Delta H_f(C_7H_7^+)$ kcal/mole
Benzyl chloride	0.14	208[1]
Benzyl bromide	0.14	208[1]
Toluene	0.11	232[1]
Benzyl alcohol	0.11	234[a]
Ethylbenzene	0.105	236[1]
p-Xylene	0.075	241.5[b]
m-Xylene	0.075	244[b]

[a]Based on appearance potentials given by S. Meyerson, P. N. Rylander, E. L. Eliel, and J. D. McCollum, J. Am. Chem. Soc. 81, 2506 (1959).

[b]Based on appearance potentials given by F. H. Field and J. L. Franklin, J. Chem. Phys. 22, 1895 (1954).

tropylium ions and what are believed to be substituted tropylium ions have been reinvestigated.

EXPERIMENTAL METHOD

Observations were made using a double-focusing mass spectrometer of Mattauch-Herzog geometry. Ions which decompose after acceleration and before entering the electric sector are usually lost. If the process

$$m_1^+ \rightarrow m_2^+ + (m_1 - m_2)$$

occurs in this region, m_2^+ ions will be transmitted by the electric sector only if the accelerating voltage V_0 is increased to m_1V_0/m_2, the voltage across the electric sector being unchanged.[5] Under these conditions, normal ions are not transmitted and they therefore do not interfere with the observation of peaks due to ions formed by decomposition between the source and electric sector.

The instrument is tuned to collect m_2^+ ions under normal conditions (V_0 = 3.78 kV), and the accelerating voltage is increased to V_1 at which voltage m_2^+ ions formed by decomposition are transmitted. The precursor m_1 is then given by m_2V_1/V_0 and the metastable transition is unequivocally identified.[6,7] The relative heights of the normal and metastable peaks correctly represent the ratio of the number of m_2^+ ions extracted from the source and the number formed by the decomposition of m_1^+ ions between the source and the electric sector since the transmittance of the instrument is the same for the m_2^+ ions in each case. In a single-focusing instrument, m_2^+ ions formed by the decomposition of m_1^+ ions between the source and the magnetic field give rise to diffuse peaks of low intensity at an apparent mass of m_2^2/m_1, but the collection efficiency for metastable ions is much less than that for normal ions, (e.g., ~ 5%).[8]

During the course of this work, weak spurious peaks were observed with V = 4050 V, which would correspond to the transition $69^+ \rightarrow 65^+$. Since this transition is most unlikely to be found in the mass spectrum of toluene, metastable transitions giving rise to intense peaks in the mass spectra of several other compounds were also investigated. In each case, a spurious peak of low intensity was observed when the accelerating voltage had been increased by about 15% of the increase needed to observe the true metastable peak. Since the spurious peaks are not given by ions which do not undergo decomposition, it is possible that the peaks arise from ions which travel part of the way through the electric sector before decomposing, after which they are reflected by collision with the inner wall of the sector.

RESULTS AND DISCUSSION

a. Toluene and Toluene-α-d_3

Metastable transitions leading to the C_5 fragment ions m/e = 61-66 in the mass spectrum of unlabeled toluene were investigated. In each case, a metastable peak was observed at an accelerating voltage which indicated that these ions are formed by the loss of C_2H_2 molecules from C_7 ions. No evidence was found for any metastable transitions in which fragments other than C_2H_2 were lost, e.g., reactions (2) and (3), nor was there any evidence of decomposition of C_6 fragment ions to give C_5 ions. By far the strongest peak was that due to the transition $91^+ \rightarrow 65^+ + 26$; the peak arising from the transition $89^+ \rightarrow 63^+ + 26$ was of moderate intensity, the remaining peaks being of low intensity. The weak peak arising from the transition $92^+ \rightarrow 66^+ + 26$ is probably largely to be ascribed to the decomposition of C_7H_7 ions containing one ^{13}C atom.

These observations suggest that the tropylium ion may lose one or more hydrogen atoms before eliminating an acetylene molecule, i.e.,

$$M^+ \rightarrow (M - 26)^+ + C_2H_2$$

is a mode of decomposition common to most of the C_7 fragment ions. Furthermore, the loss of other fragments, such as C_2H_3 or C_2H_4, appears to be unimportant, and the loss of C_2H_2 by $C_7H_7^+$ seems to be the only significant source of $C_5H_5^+$ ions.

Further fragmentation of the $C_5H_5^+$ ions was shown to occur by observing metastable peaks for m/e = 63 and 39 at accelerating voltages indicating that these

ions are formed by the loss of H_2 and C_2H_2, respectively, by $C_5H_5^+$ ions.

A similar study was made of the metastable transitions leading to the C_5 fragment ions m/e = 63-69 in the mass spectrum of toluene-α-d_3. Since the intensity of the m/e = 93 peak is about 60% that of the m/e = 94 peak, it appears that H and D atoms are lost statistically in forming $C_7H_4D_3^+$ and $C_7H_5D_2^+$ ions.[1] By analogy with the metastable transitions found in the mass spectrum of unlabeled toluene, the deuterated tropylium ions are expected to lose C_2H_2, C_2HD, and C_2D_2 on a statistical basis. The results quoted in Table I are clearly consistent with this view, with metastable transitions corresponding to the loss of 26, 27, and 28 atomic mass units by ions m/e = 94 and 93 being observed in the expected intensity sequence. In view of the observations on the unlabeled toluene, it seems very unlikely that the loss of 27 and 28 amu can be ascribed to the loss of fragments other than acetylene molecules. Metastable peaks observed at m/e = 39, 40, and 41 indicate the loss of further acetylene molecules by $C_5H_5^+$ and its deuterated analogues.

These observations suggest that the only major route of decomposition of the tropylium ion is the successive loss of acetylene molecules to give $C_5H_5^+$ and $C_3H_3^+$ ions. Recent work on the heats of formation of fragment ions from aromatic molecules[9,10] suggests that these ions are usually linear rather than cyclic, although uncertainties inherent in both the measured appearance potentials and the theoretically computed ionic heats of formation render this conclusion somewhat tentative. Unfortunately, the intensities of metastable peaks from acetylene elimination from $C_5H_5^+$ and its deuterated analogs are too low to shed any light on the probable structure of these ions.

b. Variation in Decomposition Rate of the $C_7H_7^+$ Ion

The relative intensities of the metastable peak arising from the process $91^+ \rightarrow 65^+ + 26$ and the normal peak at m/e = 65 were measured in the mass spectra of several compounds with the results given in Table II. These intensity ratios have no absolute significance since they depend on the ion-repeller-plate voltage and the cleanliness of the source. The values quoted are averages obtained over several days using 70-V electrons and zero-repeller voltage. Measurements were repeated several times in order to ensure internal consistency. Also reported in Table II are literature values for heats of formation of $C_7H_7^+$ derived from appearance-potential data for the corresponding compounds. These thermodynamic quantities for the electron-impact dissociation $e + C_7H_7X \rightarrow C_7H_7^+ + X + \Delta E + 2e$ are calculated from the expression $\Delta H_f(C_7H_7^+) = A.P.(C_7H_7^+) + \Delta H_f(C_7H_7X) - \Delta H_f(X) - \Delta E$ with the assumption that the excess energy, ΔE, is zero. If one makes the plausible assumption that the $C_7H_7^+$ ion has the same structure when it is formed from these related compounds, the differences in heats of formation may be interpreted as differences in the minimum excess energy involved in forming this ion. The manner in which the excess energy is partitioned between the ion and neutral fragments is, in general, unknown but at least a qualitative indication of the magnitude of excess energy available as excitation energy of $C_7H_7^+$ is given by the figures in Table II.

The simplest form of the quasiequilibrium theory of mass spectra[11] suggests that the rate constant k for the decomposition of an ion varies with the internal energy E according to the equation

$$k = \nu[(E - E_0)/E]^{s-1},$$

where ν may be looked upon as a frequency factor, E_0 is the activation energy for decomposition, and s is the number of effective harmonic oscillators. Hence for a given decomposition, a range of values of k will exist if the ions are formed with varying amounts of internal energy. In general, metastable peaks are observed only for those processes for which $k = 10^5 - 10^6$ sec^{-1}, and the rate constants for fragmentation processes are usually much greater than this. Consequently, it is the ions possessing relatively low excess energies which will give rise to the metastable peaks, and it can be seen that the results in Table II are consistent with this explanation in that the intensity ratio of the metastable peak to normal peak rises as the apparent heat of formation of the $C_7H_7^+$ ion falls.

Implicit in the above argument are the assumptions that the $C_5H_5^+$ ion is formed only by the decomposition of the $C_7H_7^+$ ion, and that once formed, it decomposes at a constant average rate in each case. Isotopic-retention measurements[1] together with the observations on metastable peaks reported in Sec. a support the first assumption. It seems probable that the average decomposition rate of $C_5H_5^+$ ions will vary with their source in much the same way as that of the $C_7H_7^+$ ions, but it is unlikely that the differences will be very marked.

c. Substituted Tropylium Ions

Features in the mass spectra of substituted benzyl compounds have been interpreted in terms of substituted tropylium ions, such as $C_7H_6F^+$, $C_7H_6OH^+$ and $C_7H_6CH_3^+$.[4] On the other hand, $CH_3O\text{-}C_6H_4\text{-}CH_2^+$ behaves as a substituted benzyl ion. No evidence has been reported to support the suggestion that substituted tropylium ions are formed by loss of H and retention of X in the mass spectra of compounds such as $C_6H_5CH_2X$, although the formation of $C_7H_4D_3^+$ from toluene-α-d_3 may be classed as such. Examples of metastable transitions which could be ascribed to the decomposition of substituted tropylium ions formed by either process were therefore sought.

In the mass spectra of ethylbenzene and *p*-xylene, the intense m/e = 105 peak might be formulated as a methyltropylium ion,[1] and this is supported by the observation of strong metastable peaks corresponding to $105^+ \rightarrow 79^+ + 26$ in each case, with I_m^*/I_m being approximately 0.1 and 0.2 for ethylbenzene and *p*-xylene, respectively. Loss of 26 amu by m/e = 101-104 ions gave rise to weak metastable peaks, analogous to the loss of acetylene by m/e = 87-90 ions in the mass spectrum of toluene. Very weak metastable peaks were observed at accelerating voltages which suggested that C_2H_4 could be lost by m/e = 105 and 106 ions to form m/e = 77 and 78. Examination of metastable transitions leading to m/e = 52 and 53 ions showed that the only significant processes were the loss of C_2H_2 by m/e = 78 and 79 respectively. These processes are analogous to the loss of C_2H_2 by the $C_5H_5^+$ ion in the mass spectrum of toluene. The over-all process may therefore be formulated as follows:

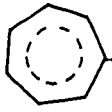

$$\text{—}CH_3^+ \xrightarrow{-C_2H_2} C_6H_7^+ \xrightarrow{-C_2H_2} C_4H_5^+$$

In the mass spectra of benzyl chloride and *p*-chlorotoluene, peaks of fairly low intensity due to the $(M - 1)^+$ ion might be considered to arise from the chlorotropylium ion. Support for this view was obtained by observing metastable transitions corresponding to the successive loss of two acetylene molecules by these ions:

$$\underset{(125,127)}{C_7H_6Cl^+} \xrightarrow{-C_2H_2} \underset{(99,101)}{C_5H_4Cl} \xrightarrow{-C_2H_2} \underset{(73,75)}{C_3H_2Cl}$$

In addition, a chlorotropylium ion might be expected to eliminate CH≡CCl giving rise to metastable transitions $127^+ \rightarrow 65^+ + 62$ and $125^+ \rightarrow 65^+ + 60$. Metastable peaks corresponding to these processes were observed in the mass spectrum of *p*-chlorotoluene, and provide additional support for the view that $C_7H_6Cl^+$ should be formulated as a chlorotropylium ion.

Although the very intense m/e = 91 peak in the mass spectrum of benzyl bromide indicates that the bromine atom is readily lost, low-intensity $(M - 1)^+$ peaks are also observed. Metastable transitions corresponding to the loss of two acetylene molecules were again observed:

$$\underset{(169,171)}{C_7H_6Br^+} \xrightarrow{-C_2H_2} \underset{(143,145)}{C_5H_4Br^+} \xrightarrow{-C_2H_2} \underset{(115,117)}{C_3H_2Br^+}$$

By analogy with the above arguments, the $C_7H_6Br^+$ ion might be formulated as a bromotropylium ion.

Since the above observations appear to suggest that halogenated tropylium ions play a role in the fragmentation of halogenated alkylbenzenes, the metastable transitions in the mass spectrum of benzotrifluoride, $C_6H_5CF_3$, were examined. The two most prominent fragment peaks are m/e = 127 and 145, corresponding to $(M - 19)^+$ and $(M - 1)^+$. It is suggested that these might be formulated as difluorotropylium and trifluorotropylium ions, respectively, analogous to the $C_7H_5D_2^+$ and $C_7H_4D_3^+$ ions in the mass spectrum of toluene-α-d_3. Carrying the analogy further, one would expect these ions to give rise to metastable peaks corresponding to the successive elimination of C_2H_2 and C_2HF molecules to form C_5 and C_3 fragment ions. In addition, since the elimination of HF is favored over the elimination of H_2 on energetic grounds, fluorotropylium ions from which HF has been eliminated are expected to lose C_2H_2 and C_2HF in a manner analogous to the loss of C_2H_2 by the $C_7H_5^+$ ion in the mass spectrum of toluene.

Following the above reasoning, the following scheme of decomposition

reactions can be drawn up for the fluorotropylium ions:

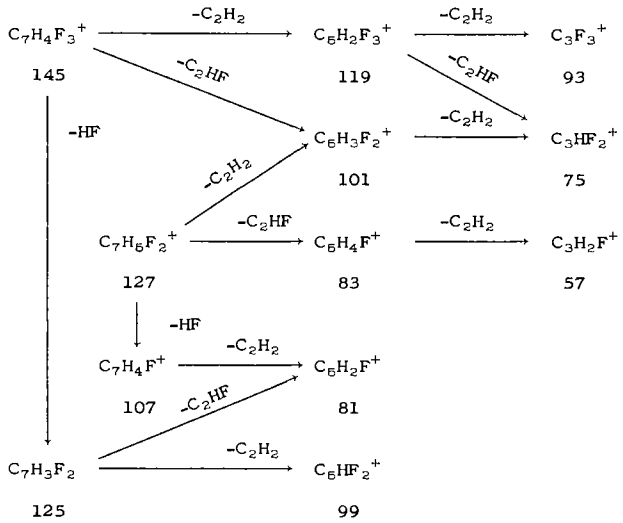

Metastable peaks corresponding to every reaction postulated were observed, although many were quite weak owing to competition from other modes of decomposition. In particular, strong metastable peaks were observed arising from the elimination of CF_2. The importance of this elimination step in the mass spectrum of benzotrifluoride has been cited by Majer.[12] Except for certain special cases,[13] the analogous elimination of CH_2 from hydrocarbons is relatively unimportant, doubtless because of the much greater stability of CF_2. The m/e = 75 ions, are formed largely by loss of HF and CF_2 from the m/e = 95 and 125 ions, respectively, and the metastable peaks corresponding to the loss of C_2H_2 and C_2HF by the m/e = 101 and 119 ions, respectively, are relatively weak. While the elimination of acetylene cannot be taken as proof of the postulated tropylium structure, it is nevertheless significant that it was possible to predict the occurrence of a large number of metastable transitions by arguing in terms of the decomposition of fluorinated tropylium ions.

d. Pseudotropylium Ions

A search was made in the mass spectra of 2-methylpyridine and 3-methylpyridine for metastable transitions arising from the decomposition of $(M - 1)^+$ ions which might be formulated as a pseudotropylium ion in which a -CH- group had been replaced by a N atom. In each case, the $(M - 1)^+$ peak was much weaker than the peak due to the molecular ion, and no metastable peaks arising from the decomposition of the $(M - 1)^+$ ion were unequivocally identified. In each case, several metastable transitions arising from the decomposition of the molecular ion were observed, and it was concluded that a pseudotropylium ion was probably not formed.

Similar observations were made on the mass spectrum of 2,6-dimethylpyridine, and in this case, strong metastable peaks were observed arising from the loss of 27 and 28 amu from $(M - 1)^+$ ions, together with a rather weak peak due to the loss of 26 amu. These transitions probably correspond to the loss of C_2H_2 (26), HCN (27) and C_2H_4 or CH_2N (28). In view of the observations on 2- and 3-methylpyridines, it seems unlikely that substituted pseudotropylium ions take part in the decomposition of 2,6-dimethylpyridine. Related studies of ionization potentials of anilino and pyridylmethyl radicals[14] and of label retention in the mass spectra of deuterated and ^{15}N labeled aniline[16] have also led to the conclusion that the azepinyl ion, $C_6NH_6^+$, clearly does not play the dominant role in mass spectra that tropylium plays in alkylbenzenes.

ACKNOWLEDGMENTS

The authors wish to express their appreciation to Seymour Meyerson of the American Oil Company for the sample of toluene-α-d_3 used in this research and to acknowledge helpful discussions of the problem with him.

REFERENCES

1. H. M. Grubb and S. Meyerson, *Mass Spectrometry of Organic Ions*, F. W. McLafferty, Ed. (Academic Press Inc., New York, 1963), Chap. 10, pp. 488-508.

2. S. Meyerson and P. N. Rylander, J. Chem. Phys. 27, 901 (1957).

3. A. P. I. Mass Spectral Data Sheet No. 251, National Bureau of Standards.

4. J. M. S. Tait, T. W. Shannon, and A. G. Harrison, J. Am. Chem. Soc. 84, 4 (1962).

5. J. H. Beynon, R. E. Saunders, and A. E. Williams, Nature 204, 67 (1964).

6. K. Ryan, L. W. Sieck and J. H. Futrell, J. Chem. Phys. 43, 1832 (1965).

7. K. R. Jennings, J. Chem. Phys. 43, 4176 (1965).

8. J. Hipple, Phys. Rev. 71, 594 (1947).

9. J. Momigny, L. Brakier, and L. D'or, Bull. Classe Sci., Acad. Roy. Belg. 48, 1002 (1962).

10. P. Natalis and J. L. Franklin, J. Phys. Chem. 69, 2935 (1965).

11. H. M. Rosenstock and M. Krauss, *Mass Spectrometry of Organic Ions*, F. W. McLafferty, Ed. (Academic Press Inc., New York, 1963), Chap. 1.

12. J. R. Majer, J. Appl. Chem. (London) 11, 141 (1961).

13. S. Meyerson, J. Am. Chem. Soc. 85, 3340 (1963).

14. T. F. Palmer and F. P. Lossing, J. Am. Chem. Soc. 85, 1733 (1963).

15. P. N. Rylander, S. Meyerson, E. L. Eliel, and J. D. McCollum, J. Am. Chem. Soc. 85, 2723 (1963).

MASS SPECTRA OF SUBSTITUTED PHENYL ESTERS

by

John G. Larson and A. Bruce King
Gulf Research & Development Company
Pittsburgh, Pennsylvania 15230

Summary

A method has been developed for the quantitative determination of mixtures of n-carboxylic acids by low voltage mass spectral analysis of their phenyl ester derivatives. It has been found that good quantitative results are obtained when constant molar sensitivities are employed. The base peak in the 70-volt spectra of all these compounds was found to correspond to the rearrangement ion, $C_6H_6O^+$. By using substituent groups (Cl, NO_2 and CH_3O) on the aromatic ring together with deuterium tracers, it has been shown that hydrogen is transferred from the alkyl side chain to the phenoxy oxygen rather than to the ring. In the case of phenyl acetate, this would seem to require a four-membered ring transition state, viz:

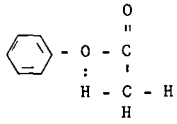

The mass spectra of paranitrophenylacetate, as observed with a high resolution instrument (CEC 21-110), show a very broad metastable corresponding to the reaction:

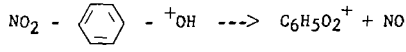

where the nitrophenol ion arises by rearrangement from the paranitrophenylacetate molecular ion. Using the equations developed by Beynon (1) for broad metastables, the internal energy release in this reaction is calculated to be about 1.8 ev. This is about 1 ev greater than that obtained from the same reaction using nitrophenol itself.

---

1. J. H. Beynon, R. A. Saunders and A. E. Williams, Z. Naturforsch 20, 180 (1965).

MASS SPECTROMETRIC STUDIES OF SELECTED IONS IN DEUTERATEDALKYLTHIOPHENES

Norman G. Foster and Robert W. Higgins
Department of Chemistry
Texas Woman's University
Denton, Texas 76204

ABSTRACT

Many fragmentation processes of ions formed by electron impact involve the apparent intramolecular rearrangement of hydrogen atoms. Specific studies on the alkylbenzenes and alkylthiophenes have shown many interesting parallels, and also some intriguing differences in fragmentation. This paper reports on continuing studies utilizing 2-n-alkylthiophenes that have been labeled with deuterium atoms in various positions. Specifically, four compounds have been prepared: the 1,1-dideutero-1-(2-thienyl)butane, 2,2-dideutero-1-(2-thienyl)butane, 3,3-dideutero-1-(2-thienyl)butane and 1-(5-deutero-2-thienyl)butane. The mass spectra of these compounds have been obtained and are partially reported. The unlabeled 1-(2-thienyl)butane has been examined and reported previously.

Base peak formation of the alkylthiophenes occurs by beta cleavage of the alkyl chain from the ring. Some alpha and gamma cleavage of considerably less importance also occurs. Hydrogen rearrangements accompanying these cleavages can be studied by an examination of the ions at m/e 97, 98, 99, etc., for beta cleavage, and ions at m/e 84, 85, 86, etc., for alpha cleavage. Using the compounds mentioned, the percentage contribution of hydrogen atoms from each carbon atom by rearrangement to form these ions has been estimated. The effects of structure of the sidechain are discussed.

The data demonstrate that some random processes are occurring during fragmentation, and at the same time some rather specific processes are also occurring. The significance of these results is discussed in terms of fragmentation theories in mass spectrometry. This work also demonstrates the value of using isotopically labeled molecules in studying fragmentation mechanisms.

INTRODUCTION

This work was begun a number of years ago at the Bureau of Mines (Bartlesville Petroleum Research Center, Bartlesville, Oklahoma) in conjunction with the American Petroleum Institute Research Project 48, "Sulfur in Petroleum". Many interesting questions have been raised and some have been answered through these studies of the mass spectra of sulfur compounds, and the resulting correlations with structure (1,2,3,4,5). Specific studies on the alkylbenzenes and alkylthiophenes have shown many interesting parallels (1), and also some intriguing differences in fragmentation (2,3,4,5). The spectra and correlations with structure of over 50 alkylthiophenes have been reported.

Kinney and Cook (1) first reported upon a group of alkylthiophenes and showed that beta fragmentation of the alkyl chain was favored thus forming the base peak for these types of compounds at mass 97. Figure 1 presents a schematic diagram which delineates some of the problems involved in studying fragmentation, and visualization of the knowledge acquired. These same authors also showed that some alpha cleavage apparently occurred to form the ions at mass 84 and 85. This requires the rearrangement of one and two hydrogen atoms respectively, with origins and destinations unknown. In 1959, Hanus and Cermak (6) using butyl and smaller alkyl substituted compounds proposed the ring expansion of the alkylthiophenes to parallel the tropylium ion formation in the mass spectrometer (7). With the availability of higher molecular weight isomers Foster et. al. (2,3,4) concurred and reported the increase in rearrangement ion intensity at mass 98 (base plus one) with increasing chain length. At this time it was also proposed that the processes involved might be the parent ion producing the mass 98 ion, and it in turn producing the mass 97 ion. A metastable ion at mass 96 substantiating that the process of 98 to yield 97 occurred has been reported (8). For the alkylbenzenes, Meyerson and McCullom (9) have reported that a substantial amount of the rearrangement ion was formed by a process involving the gamma hydrogen atom. To study the alkylthiophenes, a program of isotopically labeled molecules in specific positions was undertaken.

An alpha carbon-13, 2-hexylthiophene was first prepared and examined (10). The alpha carbon-13 atom remained with the mass 98-97 moiety as expected. Some evidence for the ring expansion was obtained in that the label showed up in the $C_5H_5^+$ ion apparently formed by subsequent fragmentation of the mass 97 species. Some randomization of the carbon atoms had apparently occurred, but the theoretical ratio was not found, indicating that the processes involved did not lend themselves to simple interpretations. Examination of the unlabeled species upon a high resolution instrument (11) showed that the $C_3H_3S^+$ ion (analog of the $C_5H_5^+$ ion from benzene) accounted for most of the mass 71 peak observed. This further established that the ring expansion occurred and that it fragmented similar to the

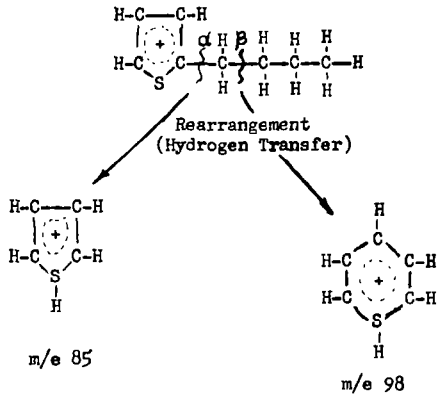

FIGURE 1

tropylium ion. Subsequently Earnshaw, Cook and Dineen (12) showed from studies of the benzenethiol molecule that the fragment ions formed could only be explained upon the basis of some molecule ions undergoing a ring expansion, while others did not.

Since the fragment ions produced by alpha and beta cleavage may yield the same ions by further fragmentation, knowledge about the approximate amounts of ions formed for each cleavage is difficult to obtain and yet is essential to understanding the processes involved. Unknown at this time and what one would like to learn are:

1) Where do the hydrogen atoms originate that are involved in these rearrangements?
2) Are the processes involved random or specific, or are combinations involved?
3) Where do the hydrogen atoms reside in the rearranged ions?
4) Although the ten electron sulfur atom may be involved in the m/e 98 cyclic structure, is it possible that a hydrogen atom is bound to a sulfur atom in any fashion other than a transitory, highly excited intermediate?
5) Does the m/e 98 (or 97) moiety fragment to yield the 85 or 84 ion as a daughter?
6) What are the main fragmentation routes of the ions formed by initial alpha, beta and gamma cleavages?

EXPERIMENTAL

The isotopically labeled species prepared for this study are listed in Table I. Details of the various syntheses are available in the literature or in theses (13). The purity of each preparation is indicated in the table. The spectra of the gamma and beta dideuterated compounds are reported without corrections, while the remainder were corrected as indicated. The unlabeled compound was run each time the labeled species were examined. The unlabeled, 1-(5-deutero-), and the beta dideutero compounds were run on the same instrument and on the same day.

TABLE 1 - ISOTOPICALLY LABELED 2-BUTYLTHIOPHENES

1-(2-Thienyl) Butanes
Mole % Composition

Deuteration	Unlabeled	1-(5-D-)-	1,1-di D-or α	2,2-di D- or β	3,3-di D- or γ
Non-	99.9+	6.4[1]	1.1[1]	-----	-----
Mono-	(Naturally	93.6	6.5[2]	1.6	-----
Di-	Occurring	-----	90.6	97.9	99.5
Tri-	Isotopes)	-----	1.8	0.5	-----
Impurity	-----	-----	-----	-----	0.5

(1) Spectra reported corrected for non-D.
(2) Spectra reported corrected for mono-D contributions to parent peak region and base peak region.

The data obtained on these compounds were taken from 1962-66 on two different Consolidated Electrodynamics Corporation mass spectrometers equivalent to their type 21-103C instrument. These were the Bartlesville U.S. Bureau of Mines and the Ponca City Continental

Oil Company instruments. Previous cooperative work (14) had shown that these two instruments produced patterns that were very similar. The CEC heated inlet systems were operated at 135°C and 150°C respectively. The temperature of the ionization chamber was controlled automatically at 250°C and the high voltage mass spectra were obtained using 70 volt electrons. The ionizing currents were 9.5 and 12 microamperes respectively. The ionizing voltage scale was calibrated using the method of Warren (15) and with benzene as the primary standard. The scale was shifted for the various instruments to make the benzene parent ion appear at 9.2 ev (16). Recognizing the problems associated with comparing data from more than one instrument as summarized at this meeting (17), the authors plan to repurify these compounds by means of GLC and rerun the mass spectra (including low voltage data) of the entire series of compounds on a single instrument, under rigorously uniform conditions.

GENERAL FEATURES OF THE MASS SPECTRA

The mass spectra presented in Table II agree well with the unlabeled spectra previously reported (3,18). The small differences in the parent peak intensities can be attributed to the differences in the inlet temperatures of 135°C for the alpha and gamma compounds, and 150°C for the remainder. The expected parent peak m/e's appear for the respective labeled species. The spectra are reported using the largest intensity ion as the base peak. The parent peak and the base peak account for slightly more than half of the total ion intensity from mass 33 up.

TABLE II - PARTIAL MASS SPECTRA - THE 2-BUTYL THIOPHENES

Relative Intensities

m/e	Unlabeled	1-(5-D-)-	α-di-D-	β-di-D-	γ-di-D-
83	.47	.54	.43	.48	.42
84	2.83	.44	2.28	2.06	1.49
85	1.73	2.86	1.40	1.11	2.32
86	.39	1.55	.80	1.13	.78
87	.24	.36	.41	.55	.21
88	----	.21	.07	.22	.07
97	100.0	.57	.74	100.0	100.0
98	15.74	100.0	3.21	18.80	10.58
99	5.33	15.63	100.0	6.00	12.29
100	.80	5.29	15.74	1.02	1.09
101	.20	.82	5.33	.25	.42
110	1.13	.85	.48	.57	1.12
111	2.98	1.13	.97	.98	3.25
112	.54	2.91	1.16	1.12	.59
113	.28	.51	2.17	2.88	.43
114	----	.27	.34	.45	.13
140	20.36	.15	.05	.20	.08
141	2.09	20.40	.43	.71	.48
142	1.10	2.09	22.27	20.94	22.42
143	.21	1.09	2.29	2.27	2.29
144	----	.21	1.20	1.15	1.08
145	----	----	.20	.24	.10

RESULTS AND DISCUSSION

Ions from gamma cleavage of the chain.

Ions from gamma cleavage of the parent molecule ion occur at mass 111 for the unlabeled and gamma labeled isomers, while the alpha, beta, and 5-deutero compounds all show the expected label retention. Loss of the label in the gamma compound proves that the cleavage consists of a sample break of the gamma bond with no transfer of hydrogen atoms. If a neutral olefin by product is formed, it retains the dideutero label as well. There is no evidence of the subsequent fragmentation routes of these ions from gamma cleavage but it is possible that further study of the fragment ions below mass 80 will eventually reveal the processes involved.

Ions from beta cleavage of the chain.

The base peak ions occur as predicted for these compounds, and are apparently formed principally by simple cleavage at this bond, the weakest in the molecule ion. Some rearrangement involving hydrogen transfer from the alkyl chain with the formation of a neutral particle containing an olefin bond also occurs. To be useful for consideration of the ions from beta and alpha cleavage, the data from these m/e's have been made monoiso-

topic with respect to naturally occurring carbon-13, sulfur-34 and hydrogen-2. The results are presented in Table III.

TABLE III - PARTIAL MASS SPECTRA - THE 2-BUTYL THIOPHENES

Monoisotopic Relative Intensities

m/e	Unlabeled	1-(5-D-)-	α-di-D-	β-di-D-	γ-di-D-
83	.47	.54	.43	.48	.42
84	2.81	.42	2.26	2.04	1.47
85	1.57	2.85	1.26	.99	2.23
86	.26	1.40	.63	.99	.71
87	.12	.14	.36	.51	.21
97	100.0	.57	.74	100.0	100.0
98	9.46	100.0	3.21	12.52	4.32
99	.13	9.37	100.0	.55	7.41
100	.11	.09	9.49	.15	.19
101	.18	.15	.12	.19	.06

The rearrangement peak at the base plus one is consistently present regardless of the labeling of the position in the compounds. Therefore it can be said that hydrogen atoms are migrating toward the ring species.

1) The alpha compound produces the m/e 99 base indicating the retention of the deuterium atoms with the moiety. Simple cleavage appears to predominate. Reasoning:

a) If randomization of the rearranged ion at m/e 100 (ring plus CHD_2) into an expanded ring system had occurred then one should find twice as much m/e 98 ion as m/e 99 ion on a purely statistical bases, and neglecting isotope effects, once the ion loses a hydrogen.

b) The m/e 98 ion cannot possible form from the alpha dideutero compound and simple cleavage unless the ring expansion to form the $C_5H_6S^+$ ion with randomization of the hydrogen atoms has occurred. I.e., $C_5H_3D_2S^+ \rightleftarrows C_5H_2D_2S^+$. If this does occur, then statistically the ratio of 98/97 should be 2/3, neglecting isotope effects. M/e 97 is a negligible peak in the alpha spectrum.

c) On the basis of the above, the percent appearing on m/e 99 from an expanded ring ion at m/e 100 would be 1.6%. Also on this basis the m/e 99 from simple cleavage without rearrangement would be 98.4%.

2) The beta compound produces the m/e 97 base peak, probably mainly from simple cleavage. The 98 peak from the rearrangement is present and is greater than in the unlabeled compound, possibly due to an isotope effect on the process involved. A small amount of deuterium is rearranged as indicated by the m/e 99 peak. On the basis of these data the rearrangement favors gamma (or delta) hydrogen transfer about 25/1 over beta transfer.

a) Making the same statistical assumptions as in the case of the alpha compound, the beta species should produce the m/e 98 peak of 0.32% and m/e 97 peak of 0.16% from the 0.55% occurring on m/e 99.

b) The species at m/e 98 containing only hydrogen would then equal 12.20%.

c) Most of the label is being lost with the neutral olefin fragment and other fragmentation processes.

d) No direct evidence for the location of the rearranged hydrogen atom is apparent from the alpha and beta labeled compounds.

3) The gamma compound also produces a base peak at m/e 97, once again indicating that simple cleavage must predominate.

a) If rearrangement and ring expansion occurs, it involves the ring plus a CH_2D group since only one deuterium atom will be shifted when the neutral olefin forms. The m/e 99 ion is the rearrangement ion if the deuterium was transferred from the gamma position. The 98 ion can be the rearrangement ion if the hydrogen was transferred from the beta or delta position. The 98 ion can also form from the 99 species by loss of a hydrogen atom. Assuming that the 99 ion is formed as the exclusive rearrangement ion, it will decompose to give a 98/97 ratio of 2/1 if simple statistics are followed. Thus if the 98 ion (4.32%) is all from this source, then the m/e 97 ion from the same source should be 2.16%. By difference, the 97 ion from simple cleavage would be 97.8% which is an excellent check with the 98.4% found from the alpha labeled compound.

b) If a 5 membered cyclic ring intermediate is formed involving the alkyl chain and the sulfur atom (or active site on the thiophene ring), then the gamma hydrogen atoms would be favored to transfer to the sulfur atom (or possibly some other active site on the pi ring system). If this occurs, the gamma labeled compound data indicates that such a hydrogen atom is not randomized in forming a cyclic $C_5H_6S^+$ ion. The hydrogen atom on the sulfur atom (or some other active site) would have to be preferentially lost so as to form the 97 ion in quantity from an m/e 99 intermediate. This possibility should not be ruled out since the site of residence of the hydrogen atom would probably not be in the plane of

the pi ring and hence the bond would not be expected to be energetically equivalent to the carbon-hydrogen bonds of the ring. The authors do not favor structures in a pi ring system that require two hydrogen atoms on a given carbon atom since this would require reversion to sp^3 bond hybridization on the part of the carbon atom with two hydrogens. Likewise, the energy of these two hydrogen bonds could not be equivalent to the remaining pi system carbon-hydrogen bonds.

4) The 1-(5-deutero) compound shows that the label is retained with the ring moiety at all times, and that it has essentially no effect (other than to raise the m/e observed by one unit) upon the mass spectrum observed. There is little or no exchange with the alkyl portion of the molecule.

Ions from alpha cleavage of the chain.

The m/e 83 ion would be produced by simple cleavage of the alpha bond in all of the labeled species (except for 84 in the 5-D-compound). From its low intensity one can see that the more important ions are the m/e 84 and 85 ions, formed by the transfer of one or two hydrogen atoms from the alkyl chain. The alpha carbon-13 labeled compound had proven that these ions involved only the four original ring carbon atoms (10). Utilizing the deuterated species one must also consider the m/e 86 and 87 ions since these could be, and are formed.

The data from the gamma compound leave little doubt that somehow the gamma hydrogen atom participates very actively in forming the m/e 84 ion. This data supports the five-membered cyclic intermediate in which the hydrogen is at least temporarily attached to the sulfur atom (or some other active site associated with the pi ring). It follows from this concept that the 5-membered cyclic must be formed, and then cleavage either alpha or beta occurs, with the beta cleavage being favored. The small amount of beta deuteration reaching this position was mentioned under the beta cleavage ions. It is likely that the delta hydrogen atoms could also reach this ion moiety through a similar 6-membered cyclic ring process.

The data from the beta compound show peak ratios of 2:1:1 for the peaks 84, 85, and 86. This also supports the favored gamma hydrogen activity in the rearrangement to the sulfur atom, but it also supports a beta hydrogen transfer, either to the sulfur atom, or by a shift to the cleavage alpha bond position. It appears that the beta position can participate in either fashion or both.

The data from the alpha compound show only that a small amount of deuterated material is moving, but hardly a statistical amount. The data from the 5-deutero-compound show little change from the unlabeled material. A small isotope effect may be operating on the sulfur atom from the adjacent deuterium atom to reduce slightly the amount of 86 ion formed.

At this point it is intriguing to consider that perhaps conformation of the molecule at the moment of ionization might be important. If hydrogen transfer occurs by the formation of a cyclic intermediate then the net processes involved seem to favor alpha cleavage over beta cleavage on the basis of the ions produced as described above. However, if the ring cannot form, then beta cleavage far outweighs alpha cleavage in importance. This can be interpreted to indicate the actual strengthening of the beta bond when the cyclic intermediate forms.

Since the 84 ion can only form by alpha cleavage and a single hydrogen transfer in the scheme developed, a calculation can be made, neglecting isotope effects, ion-molecule interaction and assuming all hydrogen movements to be intramolecular. For each deuterated molecule, the 85 peak would show, not the 84, for the deuterated position. Therefore, the intensity at 84 from that position would be zero. Hence, subtracting the alpha compound 84 intensity from the unlabeled molecule leads to the intensity shown in Table IV. Similarly for the beta and gamma positions, subtraction from the unlabeled species spectrum leads to the contribution from that position. Substituting these values in the equation shown and summing one can obtain the value of the delta contribution by subtraction. On this basis, about 48% of the hydrogen atoms are coming from the gamma position. The results obtained from the 1-(5-deutero) compound show a good check on the percentage contributions. This approach cannot be used for the 85 ion since two atoms are required to be transferred and a single valued equation cannot be set up. There is no positive proof to date that the m/e 84 peak cannot be formed from the m/e 97 moiety, however, there is also little evidence to support such a process either. If one allows for possible errors due to the small intensities of the ions involved here, it is still apparent that a rather specific process is taking place, and at the same time statistical processes are taking place. The apparently small contributions of the hydrogen atoms on the delta carbon are rather surprising, even though duplicated fairly well for the 1-(5-deutero)-compound. It should be noted that the errors are accumulated for the delta position contribution.

TABLE IV - CHAIN HYDROGEN CONTRIBUTIONS TO THE M/E 84 PEAK

Assume: $I_\alpha + I_\beta + I_\gamma + I_\delta = I_\Sigma$

For Unlabeled	α	β	γ	δ	Σ
Rel. Int.	.55	.77	1.34	.15	2.81
H % From	20	27	48	5	100
R.I./H Atom	.275	.385	.67	.05	----

For 1-(5-Deutero)-	α	β	γ	δ	Σ
Rel. Int.	.59	.81	1.38	.07	2.85
H % From	21	28	48	3	100
R.I./H Atom	.295	.405	.67	.025	----

Ions Observed at Low Ionization Potential

Low ionization data was obtained as described earlier, and the data in Figure 2 are plotted after correcting all ion intensities to equivalent parent ion intensities for the various labeled species.

The data on the left half of the figure show that the ions from the unlabeled and the 1-(5-deutero)- compound are produced in essentially the same fashion despite the label. There is a slight indication of depression of intensity for the heavier isotope as expected. Note the change in divisions scale from the upper half to the lower half of the figure. For the right hand portion of the figure matters seem to be parallel with two notable exceptions. Ion intensities of the alpha cleavage, alpha dideuterated compound are markedly suppressed. This is certainly a very large isotope effect if this is all that is involved.

The second notable item is that for the gamma dideuterated compound, the m/e 98 and m/e 99 ion intensities must be added (indicated as 98 + 99) to give an ion production curve that equals the rearrangement ion in the cases of the alpha and beta compounds. This is strong support for the importance of gamma movement of hydrogen atoms, and yet shows a rearrangement ion for this compound in which either beta or delta hydrogen atoms must be involved. The alpha base peak (99) and the beta compound base peak (97) show the slight differences that might be expected from isotopes here. The rearrangement peaks for these are: alpha (100), beta (98) and gamma (both 98 and 99). If the alpha compound produces an m/e 98 ion at low voltages, this was not detected.

In the lower right hand portion of the figure the beta compound produces the 84 ion in the same quantity as the gamma compound produces the 85 ion. This strongly supports the earlier arguments that a single hydrogen is ordinarily transferred from the gamma carbon atom to form the m/e 84 ion as a quite specific process. Similarly, the parallel production of the m/e 85 and 86 ions for the beta labeled molecule suggests that about half of the 85 ions normally formed contain a hydrogen from a beta position. The low intensities of ions found for the alpha compound is puzzling.

CONCLUSIONS

In the molecules of this study the gamma hydrogen atom is quite active in forming a rearrangement ion when beta cleavage of the alkyl chain from the thiophene ring occurs. It is also apparent that the gamma hydrogen atom participates strongly in forming the m/e 84 ion by alpha cleavage. Both of the above facts point to the formation of a five-membered cyclic ring intermediate in which a hydrogen atom is shifted (at least temporarily) to the thiophene sulfur atom (or other active ring site). Conformation of the molecules during the period of fragmentation may be important in determining the extent of rearrangement observed. The beta hydrogen atom apparently participates to the extent of about 50% in the formation of the m/e 85 ion. It is uncertain whether this last process involves a ring intermediate or a hydrogen shift along a chain. Finally, this work strongly suggest that for the ions reported in this work, some statistical processes are involved, and superimposed upon these are some very specific processes.

The authors plan to continue studies of the lower m/e ions in these spectra so as to delineate a larger portion of the fragmentation paths of these types of molecules.

ACKNOWLEDGMENTS

The authors are indebted to a number of people for their kind assistance throughout the years. These include: coworkers at the U.S. Bureau of Mines (NGF), in particular, D.E. Hirsch, R.F. Kendall and H.T. Rall. The late Roy Bolen also contributed assistance in determining NMR on some of the compounds. The authors are also indebted to the R.A. Welch Foundation for supporting the preparation of the labeled materials, to Dr. William Glaze

of North Texas State University for running two NMR spectra, and especially indebted to the Continental Oil Company Research Laboratories, Ponca City, Oklahoma, and to Messrs. E. Boyer, M. Hamming, H. Ford, Knox Moore, and their associates for obtaining mass spectra.

REFERENCES

1) Kinney, I.W., Jr., and G.L. Cook, Anal. Chem., 24, 1391-6, (1952).

2) Foster, N.G., D.E. Hirsch, R.F. Kendall, and B.H. Eccleston, Bur. Mines Rept. of Inv., 6433, (1964), 38 pp.

3) Foster, N.G., D.E. Hirsch, R.F. Kendall, and B.H. Eccleston, Bur. Mines Rept. of Inv., 6671, (1965), 31 pp.

4) Foster, N.G., Bur. Mines Rept. of Inv., 6741, (1966), 30 pp.

5) Cook, G.L. and N.G. Foster, Proc. Am. Petrol. Inst., 41 III, 199, (1961).

6) Hanus, V., and V. Čermak, Coll. Czech. Chem. Comm., 24 1602, (1959).

7) Rylander, P.N., S. Meyerson, and H.M. Grubb, J. Am. Chem. Soc., 79 842, (1957).

8) Mass Spectral Data #1896, API Proj. 44.

9) Meyerson, S., and J.D. McCullom, J. Am. Chem. Soc., 81, 4116, (1959).

10) Foster, N.G., R.F. Kendall, B.H. Eccleston and R.W. Higgins, ASTM E-14 Committee on Mass Spectrometry, Chicago, 1961.

11) Private communication, R.H. Hunt, Shell Oil Company.

12) Earnshaw, D.G., G.L. Cook, and G.U. Dineen, J. Phys. Chem., 68, 296 (1964).

13) Unpublished theses, Texas Woman's University, Department of Chemistry.

14) Boyer, Ernest, ASTM E-14 Committee on Mass Spectrometry, Special Report on Evaluation of Ion-Getter Pumps, New Orleans, 1962.

15) Warren, J. W., Nature 165, 810 (1950).

16) Field, F.H. and J.L. Franklin, "Electron Impact Phenomena and the Properties of Gaseous Ions", Academic Press, New York, N.Y., 1957, p.242.

17) Meyerson, S., ASTM E-14 Committee on Mass Spectrometry, Dallas, 1966.

18) Hartough, H.D., "Thiophene and Its Derivatives", Interscience Publishers Inc., New York, 1952, pp. 132-141.

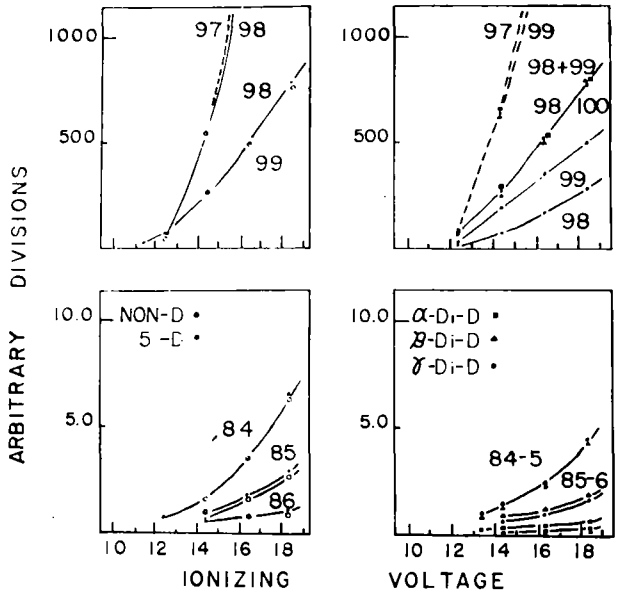
1000
500
97
98
98
99
1000
500
97
99
98+99
98
100
99
98
ARBITRARY DIVISIONS
10.0
5.0
NON-D •
5 -D •
84
85
86
10.0
5.0
α-Di-D ▪
β-Di-D ▲
γ-Di-D •
84-5
85-6
10 12 14 16 18
IONIZING
10 12 14 16 18
VOLTAGE

Fig. 2

THE RESPONSE OF ION-SENSITIVE PLATES AS A FUNCTION OF ION ENERGY*

by
J. R. Woolston
R. E. Honig
E. M. Botnick
RCA Laboratories
Princeton, New Jersey

I. INTRODUCTION

In mass spectrography, ion-sensitive plates are generally used as the ion detector. Such plates are unique in that they provide a means of simultaneously recording and integrating every separated ion beam in the instrument, but they also give rise to a serious limitation on quantitative accuracy and to a host of other problems. Both to aid in optimizing results with existing plates and to assist in the development of superior plates, a fundamental understanding of the mechanism of ion detection by such ion-sensitive plates is needed. For any given plate, the "response" is a function of various parameters and properties of the bombarding ions, such as: total number per unit area, impact energy, mass, arrival rate, angle of incidence, "chemical nature" (e.g. number of atoms in and structure of a polyatomic ion). In this context, the term response is meant to include both the "sensitivity" and the functional relationship between exposure and blackening. Furthermore, for different types of ion-sensitive plates, the relative importance of these parameters differs appreciably. The present study was directed at examining in detail the first two parameters (exposure and energy) for a variety of commercially available and experimental ion-sensitive plates.

Most prior work as reported in the literature has been limited to one of two emulsions, i.e. Ilford Q plates or AGFA-Schumann plates, and has suffered from experimental difficulties which limited the range of ion energies or has inadvertently included other parameters. In 1963, Owens and Giardino[1] presented in double-logarithmic fashion a linear dependence of "apparent yield" on ion energy, based on three points (3.75, 7.5, and 15 keV). For six elements, they found slopes that ranged from 1.0 to 1.5. By utilizing doubly- and triply-charged ions they were able to add points at 30 and 45 keV for two of these elements, again indicating a double-logarithmic linear relationship. However, the "apparent yields" at all energies were calculated from a calibration curve obtained at 15 keV, which is valid only for the 15 keV point. Furthermore, Owens and Giardino obtained all their data with one fixed exposure value which resulted in reduced accuracy at both ends of the energy range, since both extremes of the calibration curve had to be utilized. For energies ranging from 6.9 to 24 keV, Burlefinger and Ewald[2] obtained a nearly linear relationship between sensitivity and ion energy for Ar^+ ions on Ilford Q1 plates. Wagner[3] investigated the sensitivity of Ilford Q2 plates over an energy range of 2.5 to 20 keV, and found linear relationships on a double-logarithmic presentation with slopes near 1.6 for the heavier elements (Kr, Xe, and Hg) only. On AGFA-Schumann plates,[3] however, the same relationship appeared to be non-linear for these elements. In a later publication, Wagner and Mai[4] examined a lower energy range, 250 to 2500 eV, with AGFA-Schumann plates. When their data for He, Ar, and Xe are replotted in double-logarithmic fashion, straight lines with slopes near 2.0 are found. In 1964, Hintenberger[5] presented data for Ar^+ ions on Ilford Q2 plates taken from a thesis by K. I. Grais (Mainz, 1964). These data, when replotted as above, show a linear relationship with a slope of 2.0 over an energy range of 2.0 to 7.0 keV.

II. INSTRUMENTAL

Figure 1 shows schematically an overall view of the experimental setup. Only the first "half" of an AEI type MS7 double-focussing mass spectrograph was utilized, which consisted of the ion source region, electrostatic sector, and monitor-collector. A 2.5 cm by 5.0 cm (1"x2") portion of the material to be studied was positioned in a tantalum holder between the monitor-collector and the entrance boundary of the magnetic sector. The holder in turn was located in a bracket attached to the normal photoplate carriage so that it could be traversed in the z-direction. It was thus possible to expose up to 31 separate "patches" each 0.1 cm by 0.25 cm (the aperature size of the monitor-collector) on the 2.5 by 5.0 cm plate. The magnetic sector was kept energized as its fringing field prevented the secondary emission of electrons from both the monitor-collector and the ion-sensitive plate.

Cesium singly-charged ions were used exclusively for all results reported here. They were obtained from a specially designed source consisting of a closed stainless steel tube which contained at one end a supply of Cs_2CrO_4 and could be heated by an external tungsten-wire heater to a temperature of about 1000°K, sufficient to decompose the compound. The Cs atoms then migrated to the other end of the tube where they diffused through a porous tungsten plug, heated externally by a separate heater winding to a

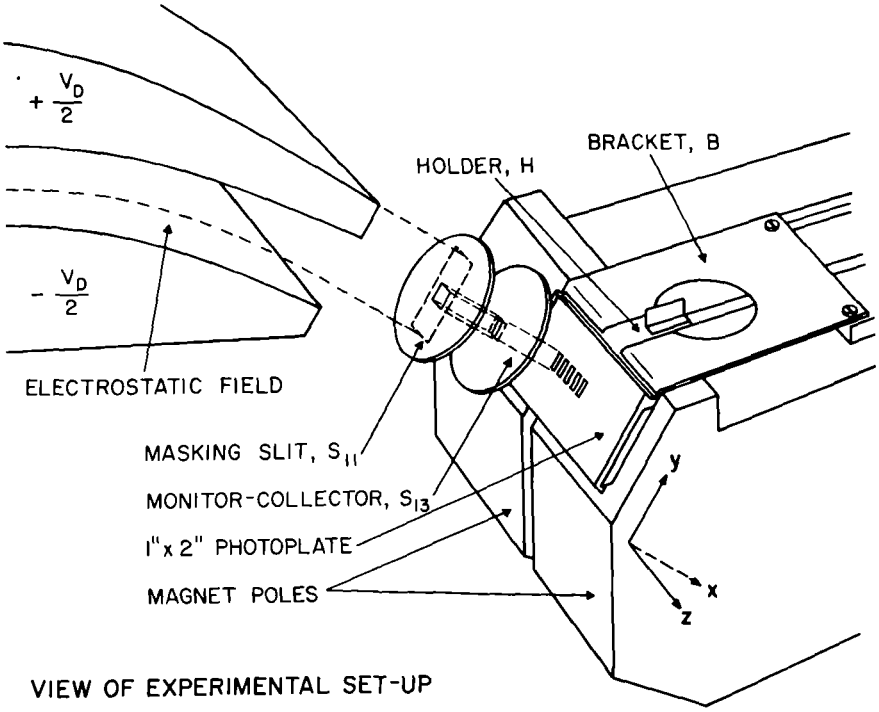

FIG. 1.

DATA REDUCTION ALGORITHM

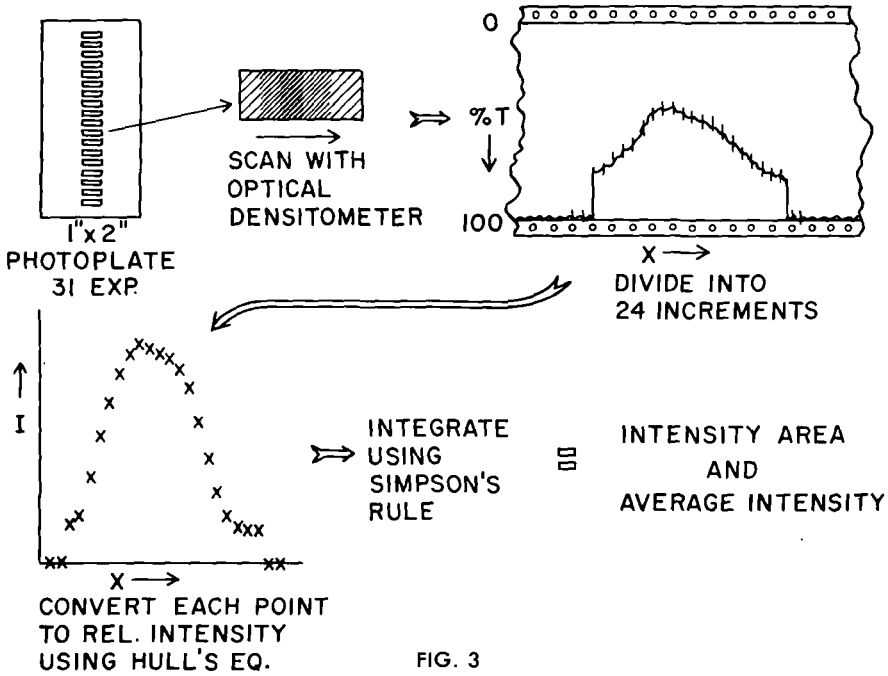

FIG. 3

temperature of about 1500°K. This source was capable of providing very stable ion currents at the monitor-collector. Even at an accelerating potential of 250V, 5.10^{-11}A could be obtained. With the MS7 operating as an analytical instrument, the spectral purity of this Cs^+ source was found to be better than 95%.

To increase ion transmission through the instrument as well as improve the uniformity of illumination by the ions at the monitor-collector, the normal rectangular beam-collimating slits in the ion source were replaced with circular aperatures 0.15 cm in diameter.

For ion energies down to 2.5 keV, the standard power supplies in the MS7 were used for both the accelerating potential and the electrostatic sector. For the lower energies external supplies were used for the accelerating potential and a special resistive divider chain was used for the electrostatic sector potential.

The ratio of the ion beam current collected by the monitor-collector to that falling on the 0.1 cm by 0.25 cm "patch" of the ion-sensitive plate was determined in a separate experiment. A Faraday cup connected to an additional amplifier was substituted for the ion-sensitive plate which made it possible to measure simultaneously both currents. The ratio was found to be 1.0 ± 0.1, and was constant over the range of energies used.

III. EXPERIMENTAL PROCEDURE

Three 2.5 x 5.0 cm portions of a standard size glass plate were scored with a glass cutter and broken off under safelight illumination for the Ilford Q2, Kodak SWR, and the RCA thin-film plates.[6] The Kodak-Pathé SC5 emulsion was supplied on unperforated 35 mm film-base and similar sized portions were cut with a common paper cutter. The first of the three portions was immediately developed to provide a reference for later comparison of the background blackening of the portion used. The second portion was inserted into the Ta holder. The third portion was maintained as a control check on possible fogging during loading into the MS7, and was developed after the second portion was loaded, but prior to pumpdown of the MS7. With the instrument vented and the room under safelight illumination, the second portion in its Ta holder was inserted into the special bracket in the MS7 through an access port. The instrument was then sealed and evacuated to a pressure in the 10^{-6} torr range.

A planned sequence of exposures was made at predetermined energies and magnitudes. A few plates were made with small increments between successive exposures, all at one energy. With 31 points distributed between threshold of detectability and saturation, these plates provided very accurately-determined "calibration curves". In so far as possible, all exposures on these plates were made at constant ion beam intensity (typically $1 \cdot 10^{-11}$A). Other plates were made with only one or a few exposures each at energies covering the whole experimental range (0.1 keV to 20.0 keV). These plates permitted sensitivity to be determined as a function of ion energy, free of plate-to-plate sensitivity and development variations. Still other plates were made at only the lower energies ($\leq$ 1.0 keV) with sequences of equal exposures at a constant energy, but with various ion beam intensities ($2 \cdot 10^{-12}$A to $4 \cdot 10^{-11}$A) to determine the effect of this parameter.

After all exposures had been made the instrument was vented and, under safelight illumination, the plate was removed and a new one inserted. The Ilford Q2 plates were developed in straight D19 for 3 minutes at 20°C, stopped for 10 seconds, fixed in Acid Fixer for 2 minutes, washed 10 minutes, and allowed to dry. The same procedure was used for the Kodak SWR plates, except that they were developed in D19 diluted 1:1 with water for 2 min. Care was taken to insure a rapid transfer from developer to short stop as this was found to appreciably reduce background chemical fogging.[7] Straight D19 for 2 minutes was used for development of the Kodak-Pathé SC5. The RCA thin-film plates were processed as described by Honig, Woolston, and Kramer.[6]

IV. DATA REDUCTION

The objectives of this study were to provide a measure of the "sensitivity" of various ion-sensitive plates as a function of ion energy, independent of all other parameters, and to determine the plate blackening as a function of ion exposure at various ion energies with all other parameters remaining constant. The data were a series of "patches" exposed fairly evenly to a known total charge. Some typical data are shown in Fig. 2. It is required to determine the charge per unit area that gives rise to a particular blackening, B, defined as:

$$B = 1 - T \tag{1}$$

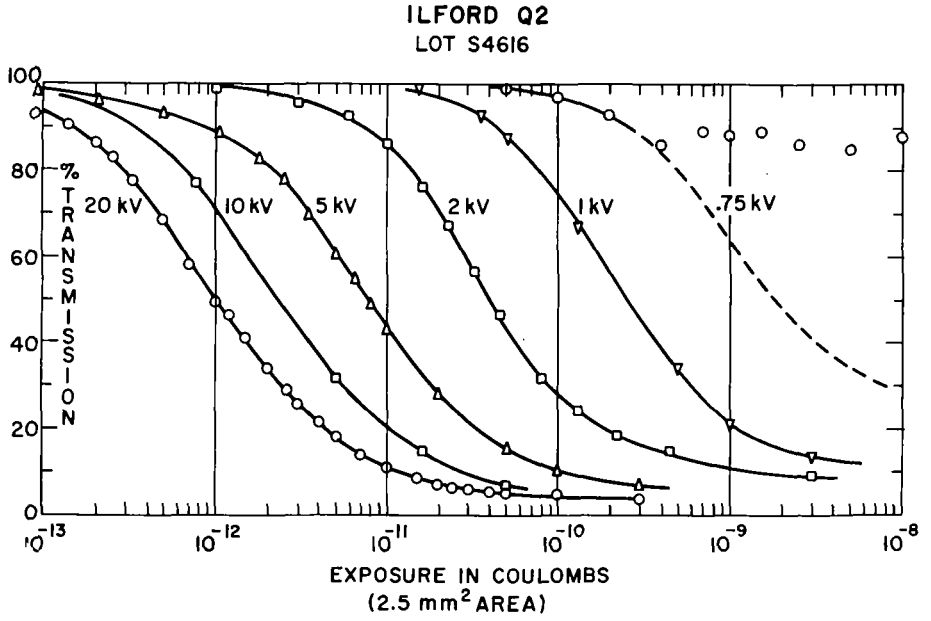

FIG. 4. TRANSMISSION VS. EXPOSURE CURVES FOR ILFORD Q2 PLATES.

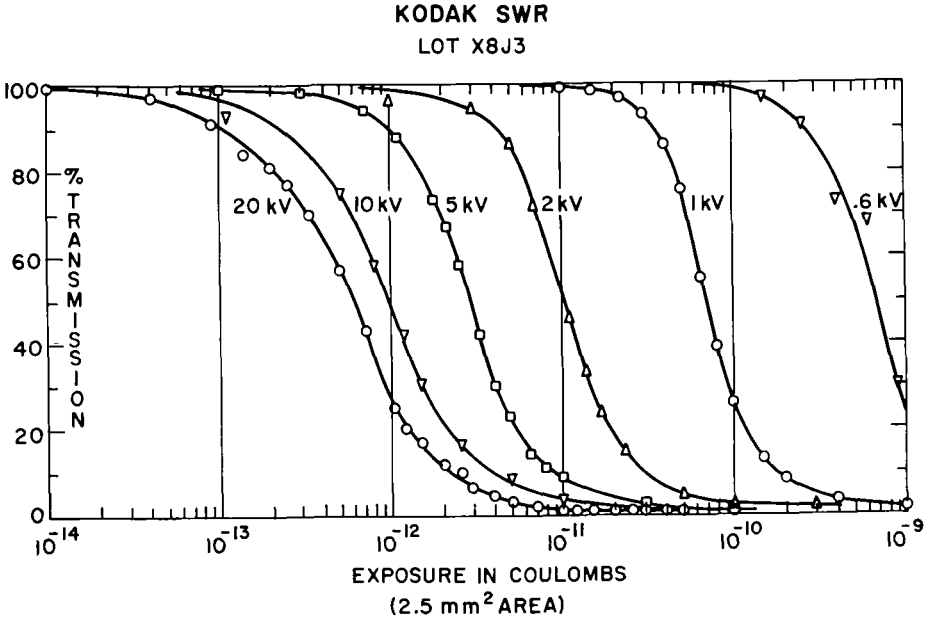

FIG. 5. TRANSMISSION VS EXPOSURE CURVES FOR KODAK SWR PLATES.

where T is the fractional transmission of the area. While optical measurements of photoplates have customarily been expressed in units of density or transmission (usually in percent), blackening, B, is particularly logical and convenient.

Sensitivity shall be defined, arbitrarily, as follows:

$$S_Q = \frac{A}{Q}\bigg|_{B = 0.5B_s} ; \quad S_N = \frac{A}{N}\bigg|_{B = 0.5B_s} = 1.6 \cdot 10^{-19} S_Q \tag{2}$$

where,

S_Q is the sensitivity expressed as the reciprocal of the charge in coulombs per cm^2 required to produce one-half saturation blackening

Q is the charge in coulombs

A is the area blackened by Q, in cm^2

B is the blackening as defined in Eq. (1)

B_s is the saturation, or maximum, blackening produced by an infinite exposure

N is the number of ions blackening area A

S_N is the sensitivity expressed as the reciprocal of number of ions per cm^2 required to produce one-half saturation blackening.

While this definition of sensitivity requires a knowledge of B_s, it avoids the uncertainties involved in definitions based on "threshold blackening" or "just-detectability". When measurements are made in transmission, one-half saturation blackening may be expressed as:

$$T_{0.5} = 1 - 0.5\ B_s = \frac{1 + T_s}{2} \tag{3}$$

If, as is the case, the experimental data do <u>not</u> consist of patches whose measured transmission is equal to $T_{0.5}$, one must resort to a "calibration curve" which shows T as a function of exposure per unit area, or else to a mathematical relationship between these quantities. Hull[8] presented in 1962 such a formula which accurately expresses E/A, the exposure in coulombs per unit area, as a function of T. In modified form, it may be written as:

$$\frac{S_Q \cdot E}{A} = \left(\frac{1 - T}{T - T_s}\right)^{1/R} = \frac{S_N \cdot N}{A} \tag{4}$$

where R is proportional to the maximum slope (at $T_{0.5}$) of T as a function of $\log_{10}E$.

If, as is also the case, the patches are not uniformly illuminated, one must convert local transmission $T_{y,z}$ over the patch area to relative intensity $I_{y,z}$ by:

$$I_{y,z} = \left(\frac{1 - T_{y,z}}{T_{y,z} - T_s}\right)^{1/R} \tag{5}$$

In order to obtain sensitivity S_Q, $I_{y,z}$ is integrated over the patch area:

$$S_Q = \frac{A}{E} \iint I_{y,z}\ d_y\ d_z \tag{6}$$

As the patch illumination was reasonably uniform in the z-direction, it was necessary only to integrate in the y-direction, which greatly simplified the data reduction.

To accomplish this integration, the patches were scanned in the y-direction with a Jarrell-Ash Model 23-100 recording optical microdensitometer which plotted T vs distance. These plots were then manually subdivided into 24 equally-spaced increments in distance and the transmission values for each increment tabulated. Each transmission value was then converted to relative intensity using Eq. (5), and the integrated intensity obtained using Simpson's Rule. Fig. 3 illustrates this data reduction algorithm.

The data conversion via Eq. (5) requires a knowledge of both R and T_s. For all but the lowest energies, T_s was determined directly by making at least one exposure adequate to blacken the plate to saturation. At the lowest energies, an estimate of T_s had to be used. The value of R may be calculated from Eq. (4) by means of a pair of

KODAK-PATHÉ SC5

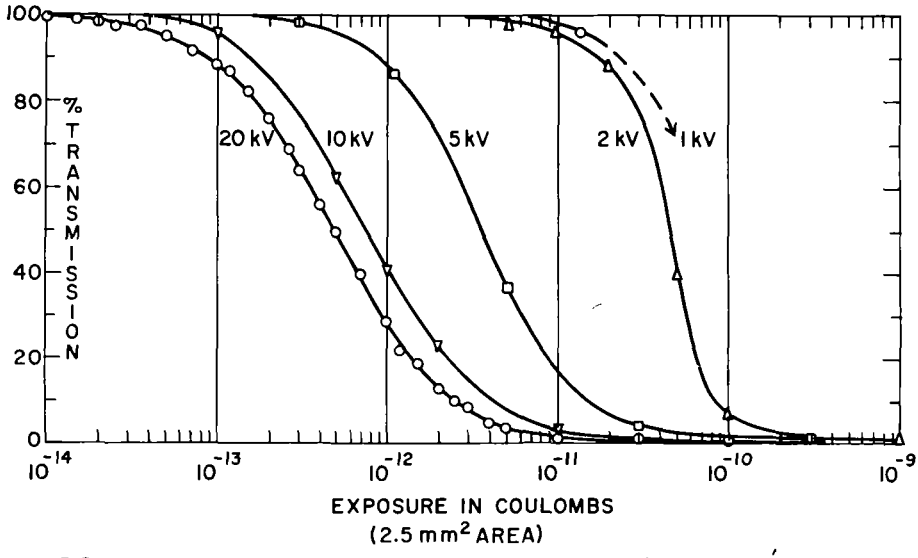

FIG. 6. TRANSMISSION VS EXPOSURE CURVES FOR KODAK-PATHÉ SC5 FILM.

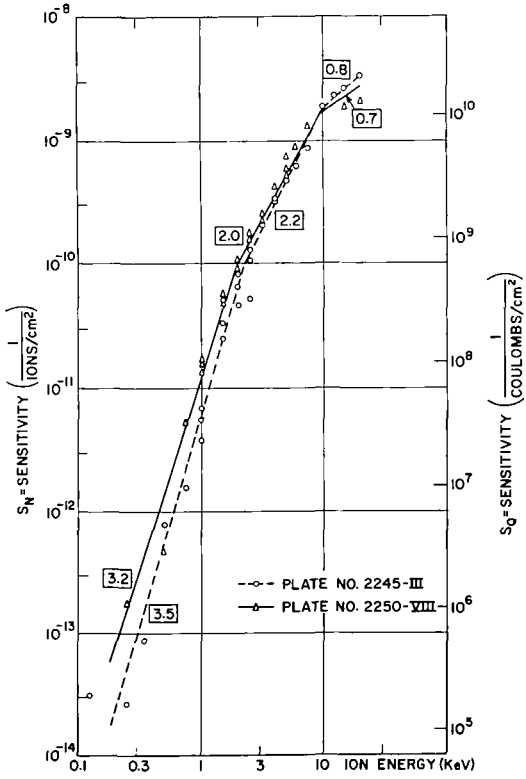

SENSITIVITY VS ION ENERGY OF ILFORD "Q2" PLATES

FIG. 7.

measurements E_1, T_1 and E_2, T_2, where the calculation is independent of S_Q and A. For a better determination of R, a FORTRAN language computer program was used in some cases to accomplish at least-squares fit of as many data points as were available to Eq. (4). For the very lowest energies, the value of R had to be estimated. A certain amount of iteration was involved in some cases whereby a preliminary data reduction with estimated R-values subsequently permitted a more accurate data reduction with calculated R-values to be made. The process converges rapidly.

Because of the volume of data involved, a FORTRAN language computer program was written to accept the tabulated transmissions and carry out the remainder of the calculation, producing S_Q for each patch. Altogether, 22 plates were evaluated, each with about 30 patches, of which each patch required 24 measurements and calculations, resulting in nearly 16,000 solutions of Eq. (5) and 660 integrations.

V. RESULTS

Figures 4,5, and 6 show the experimentally determined relation between optical transmission (in percent) and exposure (plotted logarithmically) at several discrete ion energies, for three commercial ion-sensitive materials. The points plotted in these figures are the "equivalent transmissions" of the patches versus the exposures of the patches. The equivalent transmissions, $\bar{T}$, were obtained from the average intensity, $\bar{I}$, by means of the following relation:

$$\bar{I} = \iint I_{y,z} \, dy \, dz = \frac{S_Q \cdot E}{A} = \left(\frac{1 - \bar{T}}{\bar{T} - T_s} \right)^{1/R} \tag{7}$$

In the majority of cases, $\bar{T}$ differed only slightly from the transmission measured near the center of the patch. In Figs. 4,5, and 6, curves are shown only for those energies for which sufficient exposures were made to cover the whole transmission range.

All points on a given curve were obtained from one plate to avoid discontinuities in the curves due to plate-to-plate sensitivity variations, but all curves did not necessarily come from the same plate.

In Figs. 7,8, and 9, sensitivity as defined in Eq. (2) is plotted versus ion energy in double-logarithmic fashion for Ilford Q2, Kodak SWR, and the RCA thin-film plates. There were insufficient data for such a plot for the Kodak-Pathé SC5 material. Fig. 10 shows, for convenience, a comparison of these plates by reproducing one of the curves from each of the three prior figures. Each of the points on these plots was calculated via Eq. (6). Again, for a given curve, all points were obtained from a single plate. The values shown in the boxes alongside the curves are the slopes, $\Delta \log S / \Delta \log \text{Energy}$, for the various straight-line segments indicated.

VI. DISCUSSION

The physical and chemical makeup of the four ion-sensitive materials examined in this study differs considerably. The Ilford Q2 plates appear to consist of an emulsion of AgBr grains in a small amount of gelatin coated on a glass substrate. The nearly round grains have a wide size-distribution ranging from 0.5 to 5 μm. The Kodak SWR plates contain two layers: The outermost layer is a Schumann-type emulsion with a very low gelatin content and contains irregularly-shaped AgBr grains, again ranging in size from 0.5 to 5 μm; underlying this layer is a thick coating of plain gelatin. The Kodak-Pathé SC5 film consists of a single emulsion layer of unique construction[7]: The emulsion, while liquid and coated on a temporary substrate, is centrifuged, driving the AgBr grains against the substrate in a densely-packed layer. When it has solidified, the emulsion is stripped from the temporary substrate and transferred to its permanent film-base substrate with the dense layer of AgBr grains now outermost and containing practically no gelatin at the surface. The RCA thin-film plates[6], on the other hand, contain no gelatin and cannot be considered an emulsion: They are prepared by the direct vacuum-evaporation of AgBr onto a glass substrate.

While qualitatively similar, the four materials differ in their quantitative response to ion impact. For all materials, the sensitivity increases monotonically with ion energy, but with different degrees in various energy ranges as seen in Fig. 10. The shape of the response curve as a function of exposure is seen to be a sigmoid at all energies, but becomes steeper with decreasing ion energy. This effect is more pronounced for some materials than for others (Figs. 4,5, and 6). The saturation transmission is observed to become greater with decreasing ion energy, but again to a markedly different extent for the various materials.

An additional effect was observed during this work which remains to be studied more fully in the future: On some materials, the blackening produced by low-

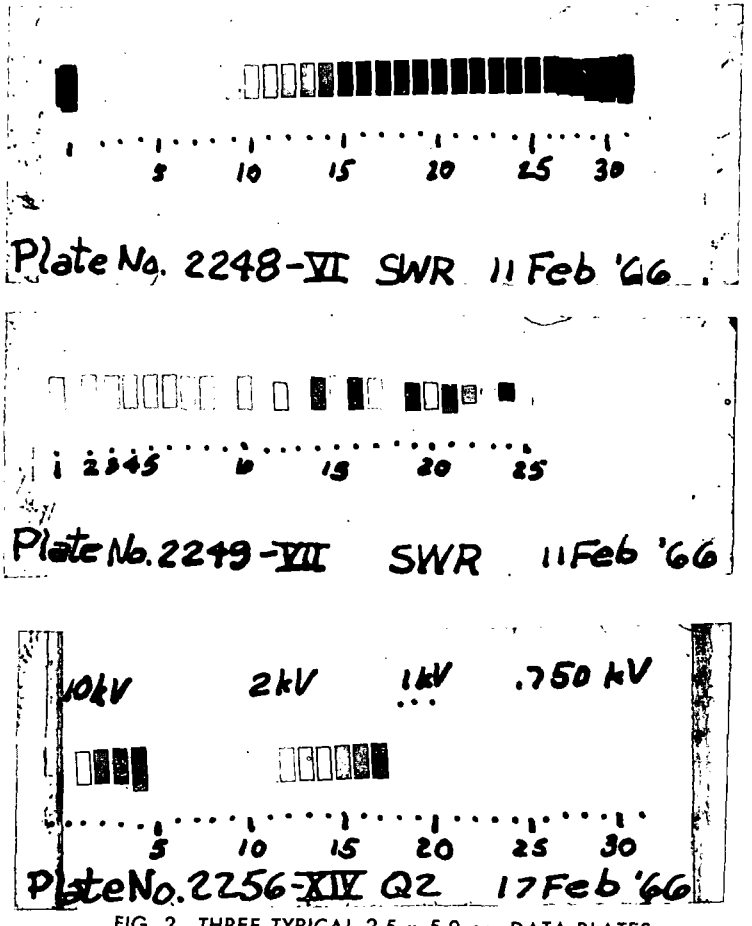

FIG. 2. THREE TYPICAL 2.5 x 5.0 cm DATA PLATES

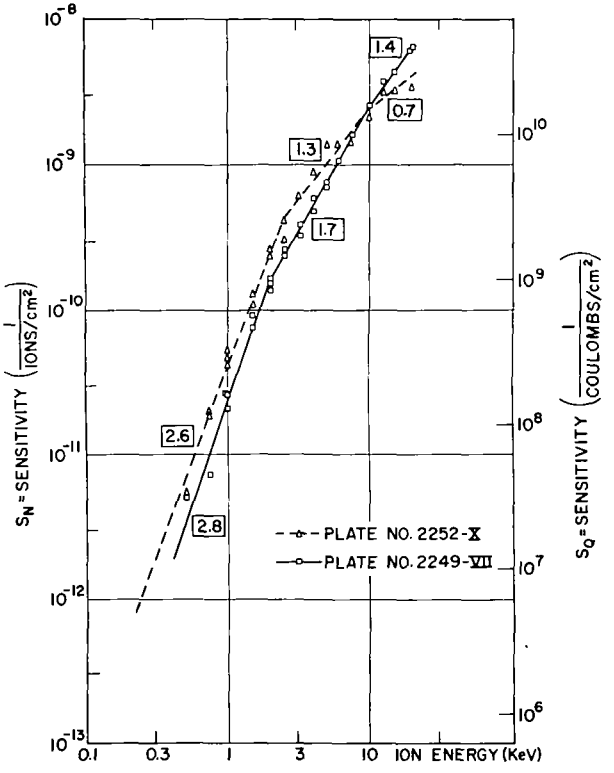

SENSITIVITY VS ION ENERGY OF KODAK "SWR" PLATES

FIG. 8.

energy ions (< 1.0 keV) is strongly dependent on the ion arrival rate. This is illustrated in Fig. 4 by the data obtained with an ion accelerating potential of 0.75 kV. The curve shown has been extrapolated from the first few points rather than drawn through the remainder of the experimental points shown. This is felt to be valid as the longer exposures clearly do not represent saturation blackening for this energy, and very likely the actual exposures are much less than indicated by the monitor-collector. The plate from which these data were obtained is reproduced at the bottom of Fig. 2. Here it can be seen that the patch size grew beyond the geometrical image of the monitor-collector. Clearly, in this case, the surface potential of the patch increased, due to surface resistivity, to the point where impinging ions were deflected, thereby enlarging the patch area. This potential may have become great enough to so reduce the net impact energy of the ions that they became ineffective to produce further blackening, and even to prevent the further landing of ions. The extrapolated curve shown in Fig. 4 may be considered to be an asymptote for the response as the ion arrival rate approaches zero. The same effect was operative to an even greater extent in the case of the Kodak-Pathe SC5 emulsion. In contrast, however, the 0.6 kV curve shown in Fig. 5 for the Kodak SWR plate is well-defined and only a slight patch-area enlargement was observed. For the RCA thin-film plates, the patch areas remained essentially constant for all ion energies down to 0.1 keV, and no charge-up effects were observed.

The curves representing sensitivity as a function of ion energy, as shown for the various materials in Figs. 7,8, and 9, have been drawn as if they consisted of three straight-line segments. This made it convenient to determine the slope of these log-log plots for various energy regions, but should not be interpreted literally: The location of the inflection points is obviously somewhat subjective. In any event, sensitivity as a function of ion energy cannot be represented by a single straight line on such a double-logarithmic plot as has been stated by previous workers. A more detailed discussion of this functional form is beyond the scope of the present work, but a number of obvious facts may be pointed out: the discrete grain-in-gelatin nature of the commercial emulsions; the depth of ion penetration into this mosaic increasing with energy; the need to form an adequate number of hole-electron pairs in a grain to render it developable; and the effect of a high-resistivity surface layer becoming charged, thereby reducing effective bombardment energy. All these considerations as well as others give rise to the observed complex functional form.

Further work is underway by the present authors to delineate the roles of some of the other parameters affecting the response of ion-sensitive plates to ion bombardment, particularly the effect of ion mass, and will be reported in the future.

REFERENCES

(1) E. B. Owens and N. A. Giardino, Anal. Chem. 35, 1172 (1963)

(2) E. Burlefinger and H. Ewald, Z. Naturforsch. 18A, 1116 (1963)

(3) H. Wagner, Ann. Physik 7, 189 (1964)

(4) H. Wagner and H. Mai, Z. Naturforsch. 19A, 1624 (1964)

(5) H. Hintenberger, Naturwissenschaften 51, 473 (1964)

(6) R. E. Honig, J. R. Woolston, and D. A. Kramer, "Gelatin-Free Thin-Film Ion Sensitive Plates", Paper No. 99, 14th Annual Conference on Mass Spectrometry and Allied Topics, 22-27 May 1966, Dallas, Texas

(7) J. M. McCrea, U. S. Steel Corp., Monrovia, Pa., private communication

---

*The research reported in this paper was sponsored, in part, by the Air Force Cambridge Research Laboratories, Office of Aerospace Research, under Contract No. AF 19(628) 5106.

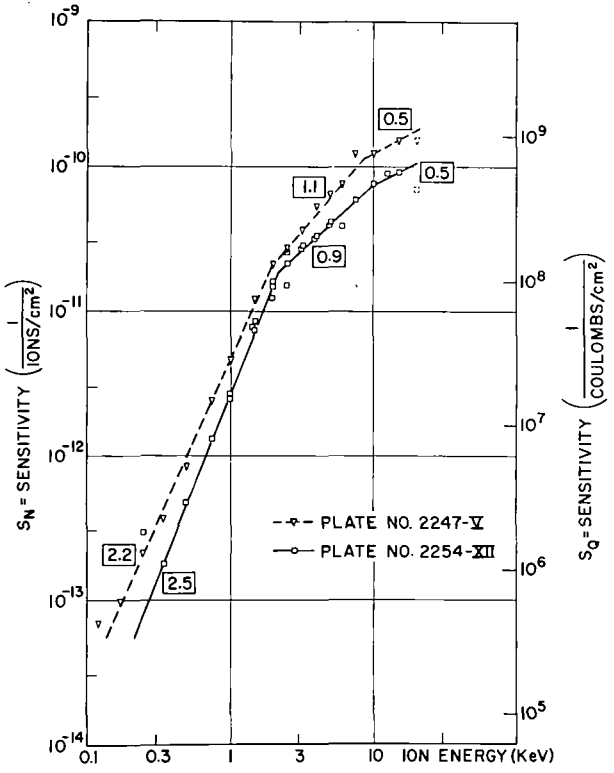

SENSITIVITY VS ION ENERGY OF RCA THIN-FILM PLATES

FIG. 9.

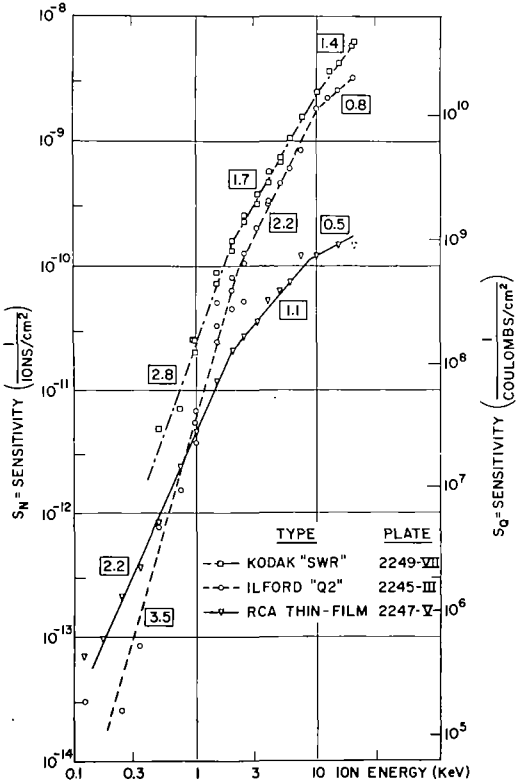

COMPARISON OF SENSITIVITY VS ION ENERGY PLOTS FOR THREE TYPES OF PLATES

FIG. 10.

GELATIN-FREE ION-SENSITIVE PLATES FOR MASS SPECTROGRAPHY*

By

R. E. Honig, J. R. Woolston, and D. A. Kramer
RCA Laboratories, Princeton, N. J.

I. INTRODUCTION

For more than 50 years, photographic emulsions consisting of AgBr crystals embedded in gelatin have been widely used in mass spectrography to detect positive ions. For this purpose, a number of thin-emulsion plates are commercially available, such as "Ilford Q2", "Kodak SWR", and "Agfa Schumann" plates, but they suffer from several shortcomings in spite of their relatively low gelatin content. Figure 1A indicates schematically that the gelatin layer surrounding the active AgBr crystals absorbs some of the initial ion energy. This leaves only a variable fraction available for AgBr activation and produces unpredictable variations in sensitivity, not only from plate to plate, but also along a given plate. Other problems resulting from the presence of the gelatin are: scattering of the ions, which produces diffuse line edges; space charge broadening of the lines due to the poor electrical conductivity of the emulsion; heavy fogging ("halo") surrounding the major lines after long exposures; poor vacuum characteristics due to a high water content; and storage problems resulting from the deterioration of the gelatin.

For these reasons, exploratory work was started in late 1963 to see if plates suitable for ion detection could be made by depositing thin films of silver halides or other materials on glass without gelatin. From the diagrammatic representation of Fig. 1B it is clear that for such a film the full initial energy of each ion is available for rendering the AgBr crystals developable. If, in addition, one can control and keep constant the size and distribution of the crystals, then both plate sensitivity and shape of response curve (as defined below) will be reproducible.

Three potential methods for producing thin AgBr films on glass substrates were investigated:

1) the chemical reaction of $AgNO_3$ with KBr and subsequent precipitation of AgBr;
2) the bromination of vacuum-deposited Ag films; and
3) the vacuum-deposition of AgBr.

Preliminary results obtained by method 1) showed the size of the resulting particles to be too small and hard to control. Method 2) produced crystals of appropriate size, but the sensitivity obtained was too low to be generally useful. Because of its flexibility, method 3) was found to be best-suited and will be described in detail below.

The present work was undertaken without any knowledge that studies to produce light-sensitive plates by thin-film evaporation were carried out by Technical Operations, Medford, Mass., for some years. More recently, they have begun to investigate, in collaboration with Air Force Cambridge Research Laboratories, the applicability of such plates to ion detection (1).

II. EXPERIMENTAL

A. General Considerations

The most important characteristics of an ion-sensitive plate are its sensitivity and the shape of its response curve. While sensitivity can be defined in a variety of ways, the simplest and

TABLE I
COMPARISON OF PLATE CHARACTERISTICS

PLATE TYPE		THIN FILM		ILFORD "Q2"	KODAK "SWR"
SUBSTRATE TEMP.		30°C	200°C		
SENSITIVITY S_Q (cm²/Coulomb)		10^7	3×10^9	10^{10}	10^{10}
SLOPE R OF RESPONSE CURVE		2-3	2-3	1	1.5
PARTICLE	SIZE (μ)	1	1	0.5-5	0.5-5
	SHAPE	ROUND	ROUND	IRREGULAR ROUND	FILAMENTARY
LINE EDGES		SHARP	SHARP	DIFFUSE	DIFFUSE
BACKGROUND NOISE		VERY LOW	LOW	HIGH	MEDIUM
BACKGROUND LEVEL		VERY LOW	LOW	HIGH	MEDIUM
HALATION		SLIGHT	SLIGHT	SEVERE	SEVERE
VACUUM PROPERTIES		GOOD	GOOD	MEDIUM	VERY POOR
SLOPE OF SENSITIVITY CURVE		MEDIUM	MEDIUM	VERY STEEP	STEEP
CONDUCTIVITY		ADEQUATE	ADEQUATE	LOW	LOW
STORAGE PROBLEMS		NONE	NONE	MEDIUM	SEVERE

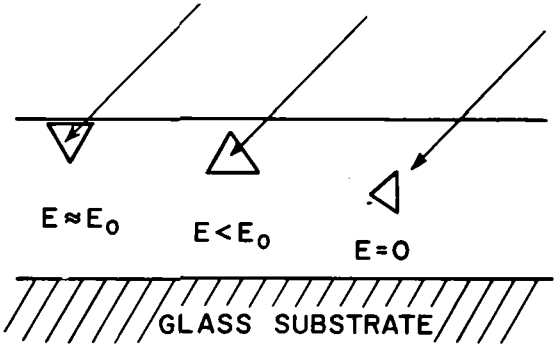

A

SCHUMANN-TYPE PLATES: GELATINE-POOR Q2, SWR, AGFA

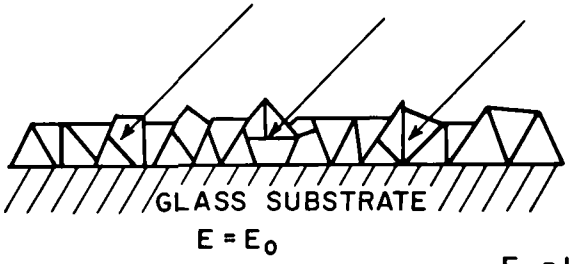

B

THIN-FILM PLATES: GELATINE-FREE

E_0 = INITIAL ENERGY
E = AVAILABLE ENERGY

FIG. 1 SCHEMATIC DRAWING OF POSITIVE IONS INTERACTING WITH AgBr CRYSTALS.

perhaps most basic expression has been presented by Burlefinger and Ewald (2). They define sensitivity as the number of blackened AgBr grains per incident ion, measured over unit area, for ion density approaching zero. This dimensionless ratio, which is always observed to be less than unity, represents an absolute sensitivity, but is of little practical value when plates are to be compared because it does not include grain size. Franzen, Maurer, and Schuy (3) have redefined sensitivity as the fractional unit area blackened per incident ion, for vanishingly small ion densities. This takes grain size into account, but still poses practical problems because barely detectable blackening is difficult to evaluate with any precision.

For the present purpose, it is convenient to define sensitivities S_N and S_Q as the inverse of the ion density required to produce one-half saturation blackening:

$$S_N = \frac{A}{N}\bigg|_{B=0.5B_S} ; \quad S_Q = \frac{A}{Q}\bigg|_{B=0.5B_S} = 6.25\times10^{18} S_N \qquad (1)$$

where A = blackened area, in cm^2
N = number of ions impinging on A
Q = ionic charge falling on A, in coulombs
B = fractional blackening, = 1 - T
B_s = saturation blackening produced by an infinite exposure
T = fractional transmission

While response curves can be represented in many ways, for the present study it was found convenient to plot transmission T vs. log E, where E is the exposure. Modifying an equation first presented by Hull (4), the response can be expressed analytically as

$$\left(\frac{S_Q E}{A}\right)^R = \frac{1-T}{T-T_S} \qquad (2)$$

where E = total expsoure, in coulombs
T_s = saturation value of T
R = proportional to the maximum slope, s_{max}, of the response curve. It is readily shown that $[dT/d(\log E)]_{max} = s_{max} = -0.576\ R\ (1 - T_s)$.

The properties of a thin-film plate depend on a multitude of experimental parameters, among them: crucible material and shape; charge material, which may include dopants; deposition rate; substrate material and temperature; and film thickness. Furthermore, the response of a plate depends on ion energy, mass, conditions of development, and other parameters. It is readily seen that sensitivity must be directly proportional to the projected area of the developed particles. Therefore, these particles should be as large as is compatible with adequate line sharpness. Typical line widths are about 50μ, which suggests an optimum particle size of about 5μ. This size is more than sufficient to produce adequate saturation (T < 0.02) with a dense single layer of particles. In a qualitative manner, it can be shown that slope R of the response curve is inversely proportional to the width of the particle size distribution function. A steep slope is desirable from the standpoint of analytical accuracy, but this seriously reduces the dynamic range of the plate and makes it mandatory to increase the number of graded exposures in an analysis.

B. Equipment

Evaporations were carried out in a 12" x 18" bell jar vacuum system which had been modified to allow a number of experimental parameters to be controlled and evaluated. Crucibles were readily exchanged

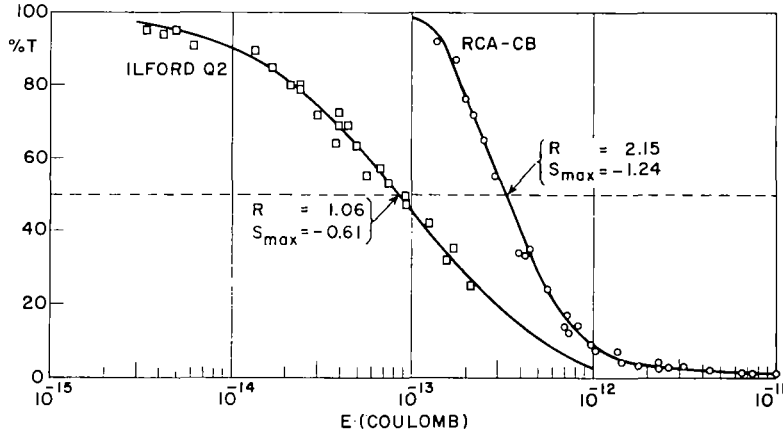

RESPONSE CURVES BASED ON Sn^+ LINES

FIG. 2.

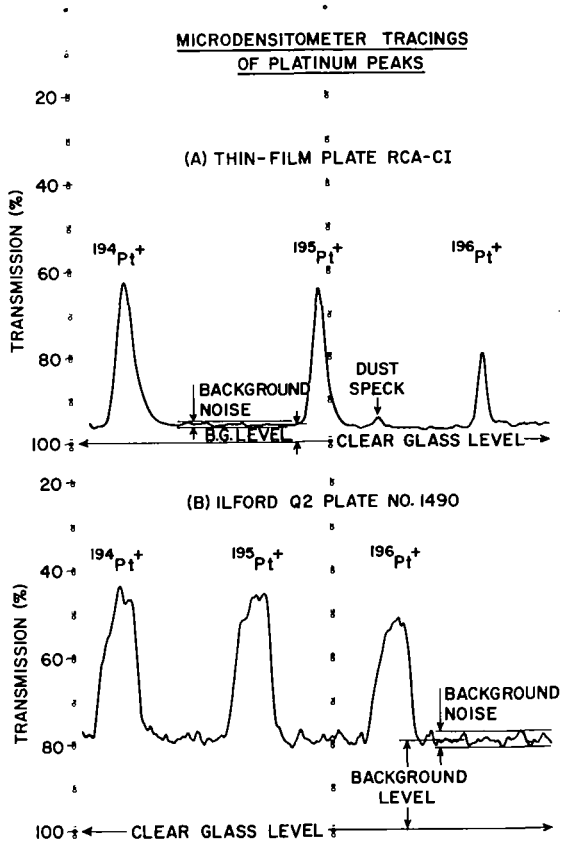

FIG. 3.

to study the effects of crucible shape and material. Crucible power could be closely adjusted to control the deposition rate, the crucible temperature being calibrated in terms of applied voltage and the melting point of AgBr (434°C). Substrate temperatures could be adjusted and measured between room temperature and 250°C with the help of substrate heaters and small thermocouples.

In general, standard microscope slides (5 cm x 7.5 cm x 1 mm thick) were used as substrates while in a few tests plates coated with a conducting layer of stannic chloride ("TIC") were employed. A mask inserted between crucible and substrates permitted three plates to be processed in sequence. Completed plates were evaluated by exposing them to ion beams in a double-focusing mass spectrograph (AEI type MS7).

C. Procedure

The blank plates to be used as substrates were thoroughly cleaned and degreased, dipped in a 0.1% gelatin solution, and dried. After a new crucible had been installed in the evaporator, it was first degassed, at a pressure of 10^{-6} torr or less, by heating it to near 1000°C. Next, the crucible was charged with about 0.3 g of high-purity AgBr powder, sometimes with dopants added, and the plates put into place. To avoid the exposure of the AgBr crystals to light, this, as well as all subsequent operations, were carried out under a yellow safelight. The evaporation was started by raising the crucible temperature in small steps up to the melting point of AgBr, allowing the charge to melt completely. The evaporation was carried out at a temperature of about 650°C. Since the material evaporating during the early stages contains many volatile impurities, it was collected on a preliminary plate. This plate could also be used to determine the deposition rate by observing interference fringes. Deposition onto the other two plates was started only after thermal equilibrium had been established and continued until an adequate film thickness (about 1.0μ) had been obtained. When desired, the substrates were preheated to an appropriate temperature, usually 200°C, before the start of the evaporation. After deposition, the plates were allowed to cool to less than 100°C, removed from the vacuum system, placed in cassettes, introduced in the mass spectrograph, and exposed to ions. After a graded set of exposures had been obtained, the plates were coated with a 1% gelatin solution (to prevent chemical fogging during development); developed in standard strength Microdol-X for about 8 minutes at 68°F; passed through a stop-bath; fixed for 30 seconds; and washed for 3 minutes.

III. RESULTS

Approximately 90 thin-film plates have been produced and evaluated to date. It was found that their sensitivity is a sharp function of substrate temperature: thin films deposited at 200°C have sensitivities about one third that of typical Q2 plates, while films deposited at room temperature are too insensitive to be generally useful. In Fig. 2 are plotted transmission values T (in percent) as a function of exposure E (plotted logarithmically) for a typical thin-film plate (RCA-CE) and for an Ilford Q2 plate. It is seen that the slope s_{max} of the response curve is considerably steeper for the thin-film plate than for the Q2 plate. This means that the intrinsic quantitative accuracy of a thin-film plate is considerably improved, but that for a given range of concentrations the exposures have to be more closely spaced and numerous.

Microdensitometer tracings of Pt peaks recorded on thin-film plate RCA-CI are reproduced in Fig. 3 A (top) and compared to an equivalent Q2 tracing (Fig. 3B, bottom). In both cases, a patch of clear glass was used to set the 100% transmission level. It is seen that the thin-film background level is near 97%, and the the peak-to-peak noise is at most 1.5 divisions wide. In contrast, the Q2 plate shows a high

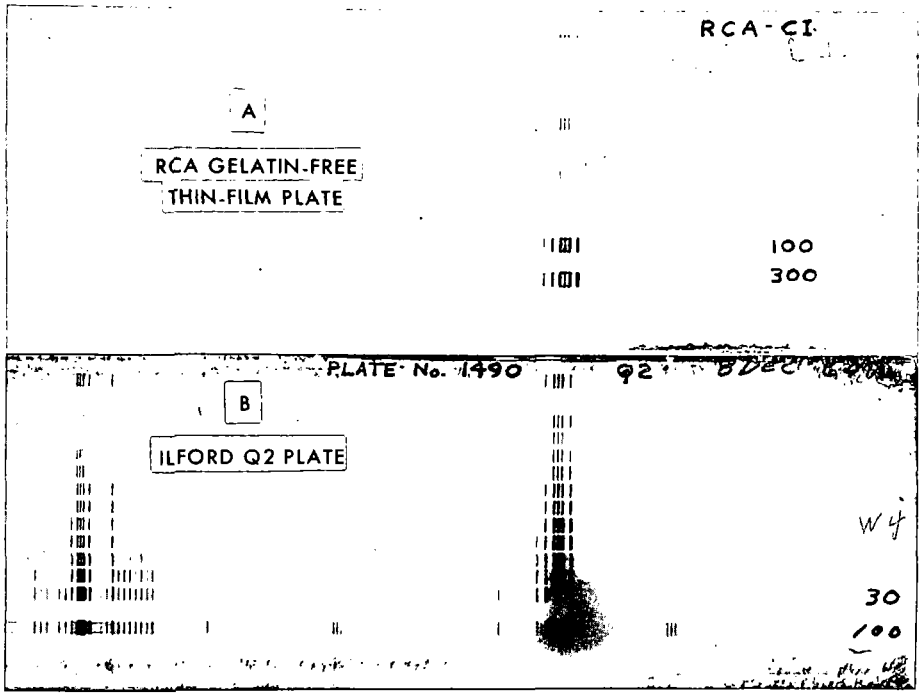

FIG. 4. COMPARISON OF HALATION EFFECTS CAUSED BY VERY LONG EXPOSURES

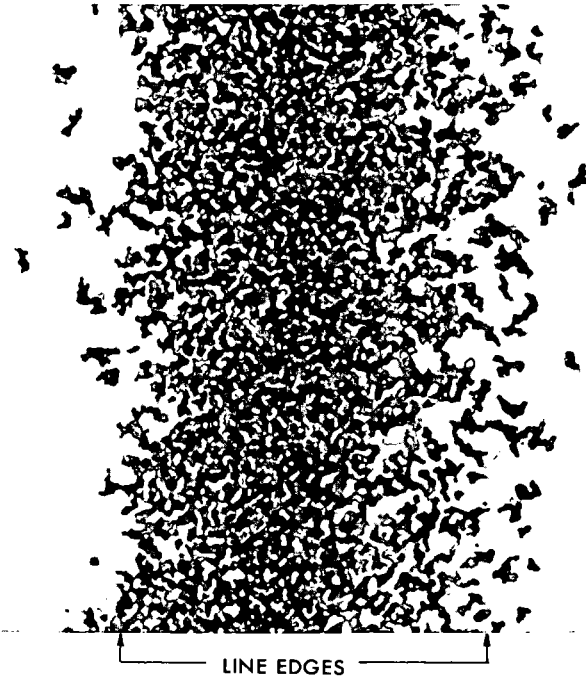

FIG 5. PHOTOMICROGRAPH OF Ge^{+} LINE (1000 × MAGNIFICATION) ON RCA - AZ

background level (near 80%) and considerable noise (about 4 divisions). While Figs. 3 A and B show a considerable difference in peak widths, this is largely due to different instrumental conditions; only in part does it reflect the fact that the thin film particles are smaller in size which produces better-defined line edges (see below).

Fig. 4 compares thin-film plate RCA-CI (top) with an Ilford Q2 plate (bottom). It shows background fogging on the two plates and brings out the fact that very little halation occurs on the thin-film plate even at long exposures (4A, bottom line: E = 300 nC) as compared to the dense black area found on the Q2 plate for equivalent blackening (4B, bottom line: E = 100 nC).

A high-power microscope has been used to compare the size and shape of the developed Ag grains. The results of this study are shown in Fig. 5 for thin-film plate RCA-AZ (substrate at room temperature); in Fig. 6 for thin-film plate RCA-BA (substrate at 200°C); in Fig. 7 for an Ilford Q2 plate; and in Fig. 8 for a Kodak SWR plate. The lines on both thin-film plates are made up of round particles, approximately 1μ in diameter. The Q2 particles are also round, but show a considerable range in size (0.5 to about 5μ), while the SWR particles are filamentary in nature. The same photographs bring out clearly the considerable differences in edge sharpness between thin-film and conventional plates.

It is of special interest to study the dependence of sensitivity on ion energy and mass, since this information should be helpful in understanding the basic mechanism of AgBr crystal activation by ion impact. The work done to date with thin-film and conventional plates on the dependence of sensitivity on ion energy is discussed elsewhere (5) in more detail and will be reviewed here only briefly. Studies of mass dependence will be carried out in the near future.

Measurements of plate sensitivity were made with ion energies ranging from 0.1 to 20 keV, employing the ion source and the electrostatic analyzer section of the MS7 double-focusing mass spectrograph. Areas of 1.0 mm x 2.5 mm were exposed evenly by a d.c. beam of Cs^+ ions. The results of this work can be summarized conveniently in log-log plots of sensitivity vs. ion energy, as shown in Fig. 9 for two thin-film plates. It is seen that the energy dependence is not a simple linear function, as previously assumed in the literature, but shows two breaks, near 2 and 10 keV, which appear to divide these curves into three separate regions with different slopes. The slopes are indicated as the boxed numbers. Fig. 10 compares sensitivity as a function of energy for three types of plates: gelatin-free thin-film, Kodak "SWR" and Ilford "Q2". It is seen that (with one exception) the slopes are smallest for the thin-film plates, intermediate for SWR and largest for Q2.

In an effort to increase the sensitivity of gelatin-free plates, a number of thin films were prepared by evaporating AgBr charges together with small amounts of various dopants, such as PbS, Ag_2S, and AgI. There has been no instance to date where such additives produced a substantial improvement in sensitivity.

A comparison of the most important characteristics of thin-film and conventional plates is presented in Table I. It is seen that the sensitivity of thin films deposited on hot substrates approaches that of conventional plates, while thin films on cold substrates are useful only in applications where high sensitivity is not essential. In all other respects, thin-film plates are clearly superior to conventional plates.

IV. DISCUSSION

The results obtained to date present a number of interesting problems, some of which should be pursued in more detail. There exists, at this time, a large volume of studies (6) which attempts to explain photon-induced latent-image formation and sensitivity in terms

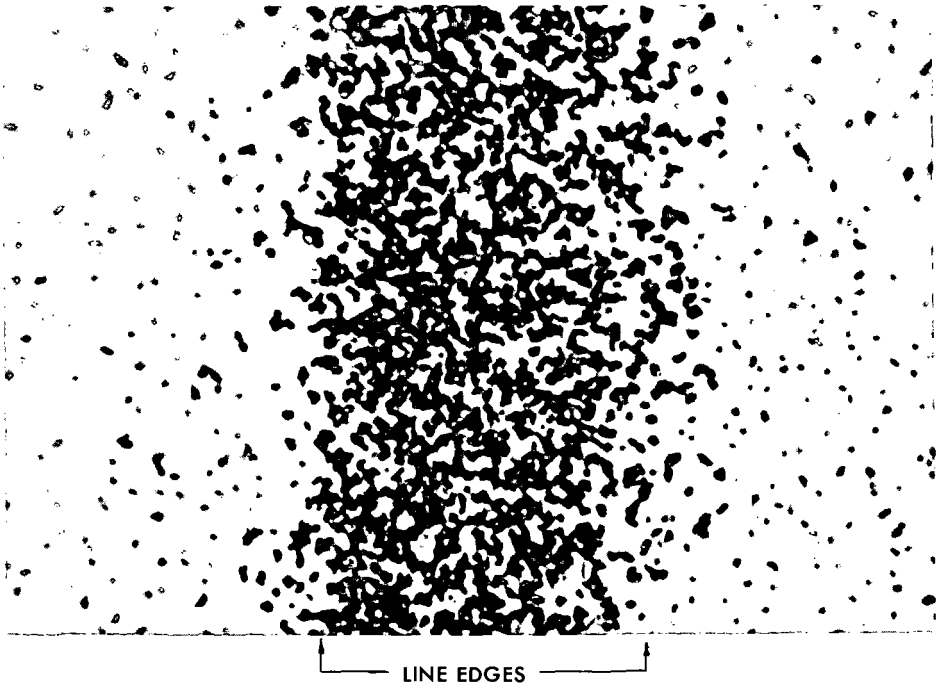

FIG 6. PHOTOMICROGRAPH OF Ge^+ LINE. (1000 × MAGNIFICATION) ON RCA - BA

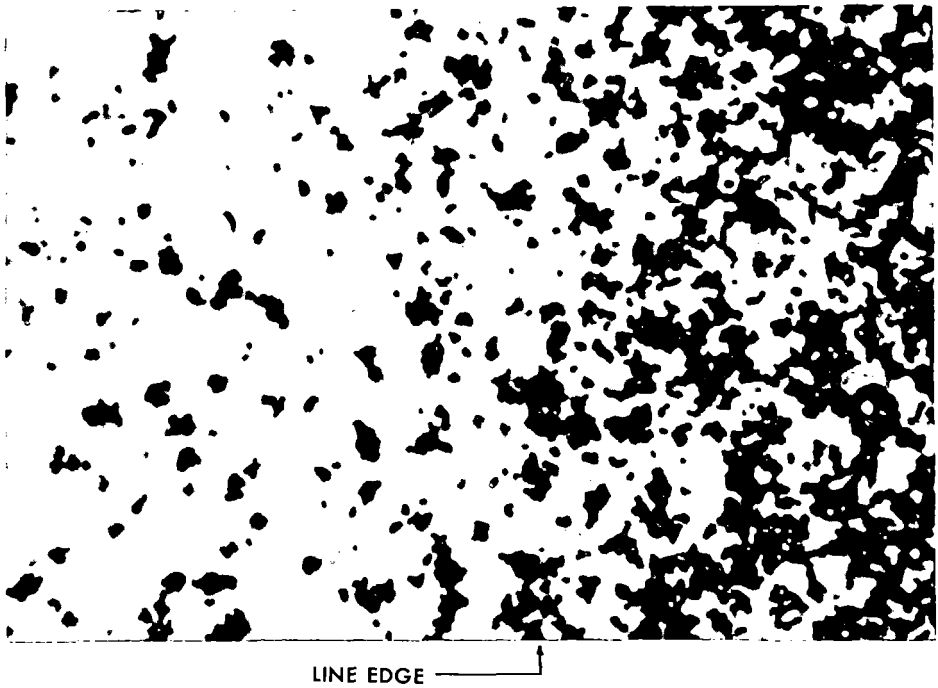

FIG. 7. PHOTOMICROGRAPH OF Sn^+ LINE (1000 × MAGNIFICATION) ON ILFORD - Q2

of the trapping of conduction electrons and of free Ag^+ ions and their subsequent neutralization at dislocation sites. Parallel reasoning, when applied to the interaction of ions with AgBr crystallites, may help explain some of the questions raised in the present study. In particular, why do hot-substrate and cold-substrate sensitivities differ by a factor of 300, when the particle size is identical for both films? It is believed at this time that heating the substrate has two effects, both of which may contribute to high sensitivity: 1) the concentration of interstitial Ag^+ ions ("Frenkel defects") goes up with temperature; and 2) stresses set up in the crystallites when the hot substrate cools down produce a high concentration of dislocation sites.

Another major problem is the shape of the sensitivity vs. ion energy curves. At this time, the mechanism of energy transfer from ion to AgBr lattice is not known in sufficient detail to explain the energy dependence shown in Fig. 9. In this connection, it would be desirable to extend these sensitivity curves to higher energies to see where the sensitivity reaches a saturation value.

REFERENCES

1) M. Hunt, private communcation (July, 1965); Anal. Chem. 38, 621 (1966).

2) E. Burlefinger and H. Ewald, Z. Naturforsch. 16A, 430 (1961).

3) J. Franzen, K. H. Maurer, and K. D. Schuy, Z. Naturforsch. 21A, 37 (1966).

4) C. W. Hull, ASTM E-14 Mass Spectrometry Conference, Paper 72 (1962).

5) J. R. Woolston, R. E. Honig, and E. M. Botnick, Paper 98, Fourteenth Annual Conference on Mass Spectrometry, Dallas (1966).

6) See for example, "The Mechanism of the Formation of the Latent Image", Ch. 5 in The Theory of the Photographic Process, Third Edition (C. E. K. Mees and T. H. James, Editors) Macmillan Company, New York (1966) pp. 87-119.

---

*The research reported in this paper was sponsored, in part, by the Air Force Cambridge Research Laboratories, Office of Aerospace Research, under Contract No. AF 19(628) 5106.

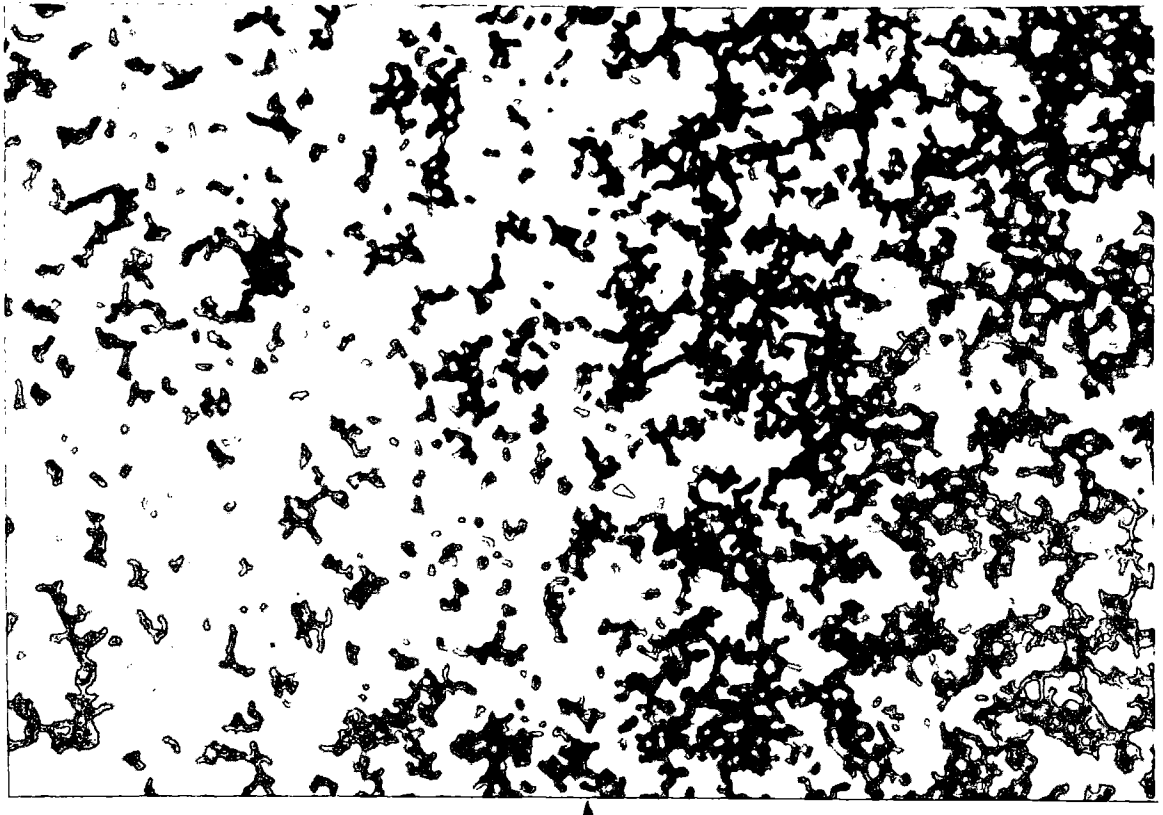

LINE EDGE

FIG. 8. PHOTOMICROGRAPH OF Sn^+ LINE (1000 × MAGNIFICATION) ON KODAK - SWR

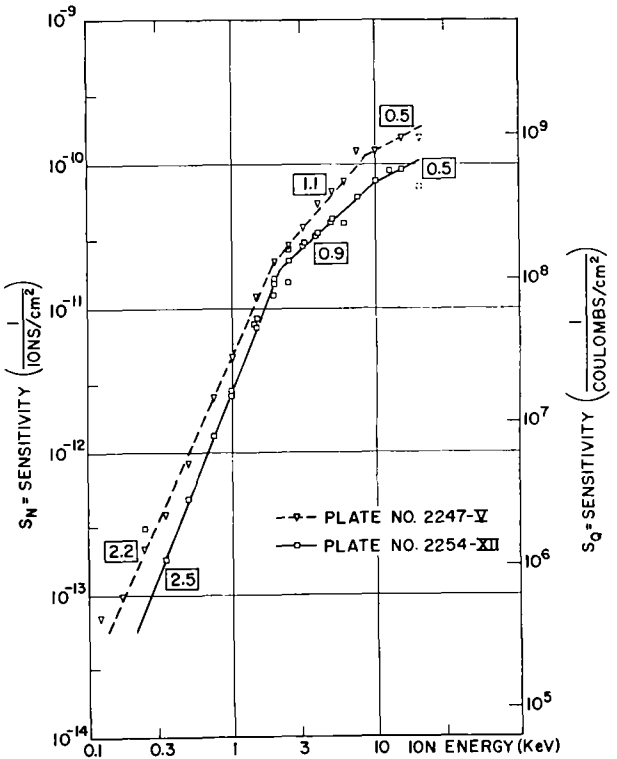

SENSITIVITY VS ION ENERGY OF RCA THIN-FILM PLATES

FIG. 9.

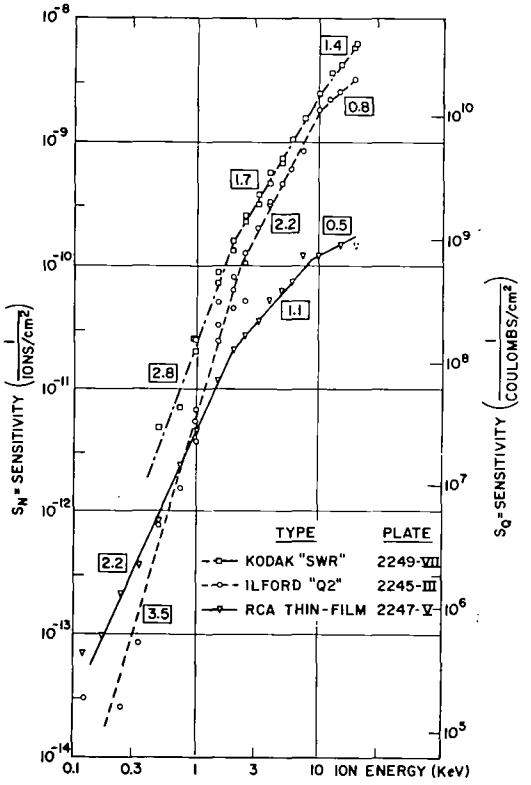

COMPARISON OF SENSITIVITY VS ION ENERGY PLOTS FOR THREE TYPES OF PLATES

FIG. 10.

The use of negative thermal ions for the determination of the isotopic composition of boron.

S. J. van Rensburg*

Introduction:

Boron is of great importance in reactor technology because of the large neutron capture cross-section of the boron-10 isotope. Boron is used both in normal composition and in the form of highly enriched boron-10 for neutron detection, neutron absorption and for control of reactor activity. With the increasing use of boron-10 enriched materials it becomes increasingly important, not only for the reactor physicist, but also for the analytical chemist to know the $^{11}B/^{10}B$ ratio in order to obtain the correct atomic weight of any boron. Further, accurate knowledge of the extent of any differences in ratio between terrestrial and extra-terrestrial materials, is important to geo- and cosmochemistry.

It was clear from a review of the literature that at the present time workers in the field of Mass Spectrometry do not feel as confident about boron measurements as they do about determining the isotopic composition of many other elements. The author, as well as others (Goris et al 1961) felt that more work on the isotopic analysis of boron should be performed. The author was of opinion that the use of negative thermal ions for the determination of the boron isotopic composition warranted investigation as an as yet untried technique.

A technique was developed whereby isotopic analyses of good quality could be obtained from microgram-size samples of boron, even without the use of an electron multiplier detector.

Previous work:

It is known to be difficult to produce by surface ionization positive ions of elements with high ionization potential. Such elements generally have a relatively high electron affinity and may therefore form in some cases thermal negative ions more readily than positive ions. Boron with an ionization potential of 10eV is one such element. The positive ion beams obtained by heating simple boron salts in a surface ionization source are very small even in terms of the sensitivity available with electron multipliers. (Palmer 1958.) An analysis of the boron isotopes has, however, been obtained when sodium tetraborate was used in a single-filament surface ionization source; in this case the $Na_2BO_2^+$ ions of mass 88 and 89 corresponding to the boron-10 and boron-11 isotopes were utilized. Boron has also been analyzed as BF_3 in an electron-bombardment gas analysis mass spectrometer, but the very troublesome memory effect encountered with this gas requires special operating procedures and instrument design (Riedel 1965, Horton 1966.) to reduce the memory effect to a level which may be acceptable.

Table 1 summarizes the results obtained by various workers on the isotopic composition of boron in nature, and clearly shows that there still is some disagreement as to the variability of this ratio in nature. Many of the discrepancies observed may be the result of incomplete chemistry rather than variations in the sample composition. (Cameron 1964.) Differences in technique may also account for a part of the variations.

An ordinary surface ionization source for positive ions can be used for the production of negative ions by merely reversing the polarity of the voltages. Such a source is based on the principle that when an atom or molecule is evaporated from a surface it has a probability of being evaporated as a negative ion given approximately by the equation (Langmuir 1925):

---

* Permanent address: Chemistry Section, South African Atomic Energy Board, Private Bag 256, Pretoria, Republic of South Africa.

$$\frac{N^-}{N_o} = \exp \frac{e\ (A - w)}{kT}$$

where, N^- = number of negative ions,
N_o = number of neutrals,
e = electronic charge = 1.6021×10^{-19} coulombs.
A = electron affinity of the atoms to be ionized, in electron volts (eV),
w = work function of surface, in eV,
k = Boltzmann constant = 1.3804×10^{-23} joule/degree,
and T = temperature of hot surface, in ^oK.

It appears from this that for the efficient production of negative ions by surface ionization one will have to fashion a filament from a material with a work function lower than the electron affinity of the atoms to be ionized. Unfortunately most elements with low work functions either have low melting points or cannot be drawn into filaments, and are therefore unsuitable for filaments. Hintenberger (1951) constructed a negative ion source where the sample to be analyzed was mixed with thorium-powder, pressed into pellets and then heated in this special source.

Although negative surface ionization has frequently been applied for the determination of electron affinities (Zandberg et al 1959), it has found to this time, however, limited application in the determination of isotopic composition. It has been used only in the isotopic analysis of halides (Shields 1962; Catanzaro 1964) and silicon (Newton et al 1960). However, complex nagative ions of the higher oxides of rhenium, tungsten, molybdenum, tantalum and thorium have been observed. (See table 2.) by the author as well as others.

A method was developed whereby boric acid was thermally ionized in either a single - or triple - filament surface ionization source. Negative ion peaks of BO_2^- at mass numbers 42 and 43 corresponding to the boron-10 and boron-11 isotopes respectively, were recorded and used to calculate the $^{11}B/^{10}B$ ratio directly.

Apparatus:

(A) A single focussing 6" radius, 60° deflection mass spectrometer equipped with an electromagnet and a high voltage supply unit of which the polarity was reversible, was employed for all experiments with the single-filament source. The ion beams were collected in a Faraday cup collector and the collector currents dropped through a 10^{12} ohm resistor. The resultant voltages were measured with a vibrating reed electrometer to which a strip chart recorder was connected. For the study of the negative ions a negative accelerating voltage of 3kV was used, the polarity of the magnetic field was reversed by changing the direction of the magnet current and the vibrating reed electrometer was switched to a negative polarity. This instrument was not equipped with an electron multiplier detector or a vacuum lock, but it was differentially pumped. During analyses the source and analyzer pressures were of the order of 1.2×10^{-6} and 3×10^{-7} torr respectively.
(b) A Nuclide 12-90-SU2 mass spectrometer was used for the experiments with a triple-filament source. This instrument was equipped with a sliding bar vacuum lock and a 16 stage electronmultiplier which was operated at a low gain. The output of the electromultiplier was connected to a vibrating reed electrometer which had an input resistor of 10^9 ohm. Recording was done with a strip chart recorder. A negative accelerating voltage of 4kV was used in these experiments.

Method:

In all experiments, the ion peaks were scanned magnetically, and after having recorded a set of peaks sweeping up-mass, the same set of peaks was recorded by sweeping down-mass. A standard method of interpolation between peaks (Stevens 1963) was used to obtain independent ratios. The $^{11}B/^{10}B$ ratio was directly calculated from

Reference.	Specimen.	Chemical form of sample.	Ion Source.	Ions Measured.	$^{11}B/^{10}B$
Inghram 1946.	———	BF_3	Gas	BF_3^+, BF_2^+, B^+	4.31
		$BO(CH_3)_3$	Gas	BF_2^+, B^+	
Thode 1948.	Minerals(9)	BF_3	Gas	BF_2^+, B^+	4.27 - 4.42
Osberghaus 1950.	Minerals(6)	BF_3	Gas	BF_2^+, B^+	4.11± 0.02
		BCl_3		BCl_2, B^+	
Shiuttse 1955.	From Italy.	BF_3, BCl_3	Gas and surface	BCl_2, BCl^+, B^+	4.10± 0.02
	From central Asia.	$B_2O_3, Na_2B_4O_7$		B^+	4.25± 0.05
Parwel 1956.	Minerals(43)	BF_3	Gas	BF_2^+	No significant variation.
	Sea-water(3)				2% heavier.
Semenov 1959.	———	B_2O_3	Single Filament	$B_2O_3^+, B^+$	4.15± 0.02
		BF_3	Gas	B^+	4.22± 0.05
Lehman 1959.	———	Diborane	Gas	———	4.00
Haas 1959.	Synthetic samples(4)	$Na_2B_4O_7$	Single Filament	$Na_2BO_2^+$	No statistically significant bias.
McMullen 1961.	Searles Lake Borax(4)	$Na_2B_4O_7$	Surface	$Na_2BO_2^+$	4.040 - 4.072
McMullen 1961.	Samples analyzed by Thode 1948.	KBF_4	Surface	$K_2BO_2^+$	Confirm previous results.
Finley 1962.	Minerals(7)	$Na_2B_4O_7$	Single filament	$Na_2BO_2^+$	3.922 - 4.141
Shima 1963.	Terrestrial Meteorite	$Na_2B_4O_7$	Single filament	$Na_2BO_2^+$	4.04± 0.05 3-6% less.
Shergina 1963.	Various deposits	$Na_2B_4O_7$	Single filament	$Na_2BO_2^+$	2.5% fractionation.

Table 1

$^{11}BO_2^-$ and $^{10}BO_2^-$ peak heights which were taken from the recorder chart by means of a linear scale. No correction was applied for the contribution (approximately one part in 1300) of the oxygen-17 isotope to the mass 43 ion peak from the $(^{10}B^{16}O^{17}O)^-$ ion, nor has any other correction for possible mass discrimination of the multiplier, instrument bias, etc. been made as yet.

A new set of filament posts and a new filament were used for each run. The sample filaments were in all cases 0.03" wide and 0.001" thick, except for the platinum filaments which had a thickness of 0.0015".

A solution of boric acid (Fisher certified reagent batch no. 724041) containing 0.60 ugm boron per uliter was made up with triply distilled water and stored in a polythene bottle. Micro-liter quantities of this solution were transferred with the aid of a micro-liter syringe onto the sample filaments through which a current of 1.5 amp was passing, in air.

Experimental results:

1. With the single-filament source:

Negative ions of BO_2^- of mass 42 and 43 corresponding to the boron-10 and boron-11 isotopes respectively were the only boron containing ions produced when a dried sample of boric acid was evaporated in a single filament source. These ions were detected at the low filament current of approximately 1.6 amp. The ion emission obtained with all the different filaments was, however, very erratic at this stage. These fluctuations in ion emission decreased with time and increased filament temperatures. At a filament current of approximately 2.2 amp stable ion currents of 5×10^{-13} amp could be obtained over a period of at least two hours with a sample containing a maximum of 3 ug boron with molybdenum or niobium as filament material. With rhenium as filament material an ion current of equal intensity could be obtained, but this required a larger sample of approximately 5.5. ug boron.

Although ion currents of 10^{-13} amp and even larger were obtained when tungsten, tantalum, platinum or thoriated-tungsten was used as filament material respectively, the ion emission decreased so rapidly that the recording of peaks was impossible. Even when larger samples were heated carefully this rapid decay in ion emission could not be prevented.

Table 3 summarizes the results obtained with the single-filament source. No fractionation effect outside these error limits could be observed over a period of three hours, in one of the runs with niobium as filament material.

2. With the triple-filament source:

In all the triple-filament experiments tungsten sample filaments were used and only different ionization filament materials were experimented with. The results obtained with the triple-filament source are summarized in table 4.

Molybdenum proved to be the most suitable ionization filament material. With 1.2 ug boron on each of the two sample filaments stable ion currents of 1.5×10^{-12} amp to the first dynode of the multiplier could be obtained for several hours by running 1.8 amp through the ionization filament and no current through the sample filaments. The fluctuations observed previously with the single filament experiments were not observed.

Over a period of three hours three sets representing at least 15 ratios each were recorded with 45 minute intervals between sets, while the filament current and ion focussing controls were left unchanged. The $^{11}B/^{10}B$ ratios obtained for these three sets were 4.00, 4.00 and 3.99 respectively, indicating no significant fractionation effect. Ion peaks corresponding to $(^{10}B^{16}O^{18}O)^-$ and $(^{11}B^{16}O^{18}O)^-$ were also recorded at mass numbers 44 and 45 respectively.

Reference.	Filament material.	Complex ions observed.
Ridley 1964.	Rhenium	ReO_4^-
Bakulina 1964.	Tungsten	WO_3^-
	Molybdenum	MoO_3^-
	Tantalum	TaO_2^-
Present study.	Rhenium	ReO_4^-
	Tungsten	WO_3^-
	Molybdenum	MoO_3^-
	Tantalum	TaO_2^-
	Niobium	-
	Thoriated-Tungsten	ThO_2^-

Table 2

Source	Sample filament material	Thermionic work function (eV).	Melting point °C	$^{11}B/^{10}B$
Single filament:	Molybdenum	4.20	2610	(a) 4.05 (b) 4.03
	Niobium	3.90	2415	4.05± 0.01
	Rhenium	5.10	3150	(a) 4.03 (b) 4.06
	Platinum	5.32	1774	---
	Tungsten	4.52	3410	---
	Tantalum	4.03	2996	---
	Thoriated-Tungsten	3.35	---	---

Table 3

Source	Ionization Filament material	Thermionic work function(eV).	Melting point °C	$^{11}B/^{10}B$
Triple filament:	Molybdenum	4.20	2610	4.10± 0.01
	Niobium	3.90	2415	---
	Rhenium	5.10	3150	4.00
	Thoriated-Tungsten	3.35	- - -	3.97

Table 4

The BO_2^- ions formed just as readily when a niobium filament was used (no results are reported for this case because instrument regulation problems were encountered), but with rhenium and thoriated-tungsten a higher current through the ionization filament as well as heating of both sample filaments were required to produce ion currents of 10^{-12} amp.

The vacuum lock of the 12-90-SU2 mass spectrometer made it possible to load a new triple-filament holder into the source and record 18 ratios in less than 30 minutes. The analyzer - and source pressures during runs were of the order of 1.7×10^{-8} and 4.9×10^{-8} torr respectively.

Discussions:

Cameron (1964) has already pointed out the advantages of measuring boron isotope abundances by positive surface ionization as opposed to the electron bombardment of a boron containing gas. To this a few additional advantages of using the negative surface ionization method may be added as a result of this study.

(i) The simplicity of the negative ion background spectrum makes any corrections for background peaks unnecessary.

(ii) Negative thermal ionization eliminates the possible interference of ^{88}Sr and ^{87}Rb ions encountered when a positive surface ionization method is employed.

(iii) Significantly smaller sample sizes may be used.

(iv) On extraction from minerals boron is usually obtained in the form of boric acid which can be directly analyzed with the negative surface ionization method. Further conversion to sodiumtetraborate or BF_3 required for positive ion mass spectrometry is thus eliminated, as well as possible fractionation effects produced by such a conversion.

Future work:

The study reported is in the nature of a reconnaissance. It has been demonstrated that stable negative ion beams of boron dioxide can be obtained for periods of hours from microgram boron samples. It also appears that fractionation during ion analysis may be smaller with this technique than with positive thermal ions. This needs to be further studied by additional experiments with different boron compounds and different substrate filaments.

The relative advantages of the multiple filament technique also require further investigation.

The absolute discrimination of the overall analytical system must be determined in order for the system to be made useful for measurements of reactor-material boron. Then, the question of the extent of natural variations of boron may be investigated.

Acknowledgements:

The author wishes to thank Dr. Leonard F. Herzog in whose laboratory in the Department of Geology and Geophysics at the Pennsylvania State University this work was performed while the author was on attachment from the South African Atomic Energy Board. He also wishes to thank Messrs. Nuclide Analysis Associates for the opportunity he had to run a few experiments on one of their 12-90-SU2 mass spectrometers. The experimental work was supported, in part, by National Science Foundation grant no. GP2759.

References:

Bakulina I.N., Zandberg E. Ya.and Ionov N.I.(1965). Zhur. Techn. Fiz.35, no. 3,562. (English translation: Sov. Physics. Techn. Phys., 10, no. 3, Sept. 1965).
Cameron A.E. (1964) Analysis of essential nuclear reactor materials. (Ed. C. J. Rodden.)
Catanzaro E.J., Murphy T.J., Garner E.L. and Shields W.R.(1964). J. of Res. NBS-A. Physics and Chemistry, 68A, no. 6, 593.
Daly N.R. and Ridley R.G. (1964) Nature, 202, 896.
Finley H.O., Eberle A.R., and Rodden C.J. (1962). Geochim, et Cosmochim Acta, 26, 911.
Goris P., Morgan T.D. and Nielsen R.A. (1961), Rep. IDO-14549.
Haas W.O., Rourke F.M., Mewherter J.L. and McDonald P.H. (1959) Rep. KAPL-2062.
Hintenberger H. (1951). Helv. Phys. Acta, 24, 307.
Horton J.C. (1966) Anal. Chem. 38, 198.
Inghram M.G. (1946). Phys. Rev. 70, 653.
Langmuir I. and Kingdon K.H. (1925). Proc. Royal Soc. (London), 107, 61.
Lehman, W.J. (1959). Nature, 183, 1324.
McMullen C.C. (1961). Geochim et Cosmochim Acta, 23, 147.
Newton D.C., Sanders J. and Tyrrell A.C. (1960) Nature, 187, 683.
Osberghaus O. (1950). Z. Phys. 128, 366.
Palmer G.H. (1958). J. Nuclear Energy, 7, 1.
Parwel A., von Ubisch H. and Wickman F.E. (1956). Geochim et Cosmochim Acta 10, 185.
Riedel J.T. (1965). Przegl. Elektron, 6, 385.
Scheer M.D. and Fine J. (1965). J. Chem. Phys. 42, 3465.
Semenov G.A. and Zonov Yu.A. (1959). Zhur. Anal. Khim. 14, 137.
Shergina Yu. P. and Kaminskaya A.B. (1963). Geokhimiya, no. 8. 725.
Shields W.R., Murphy T.J., Garner E.L. and Dibeler V.H. (1962). J. Am. Chem. Soc. 84, 1519.
Shima M. (1963). Geochim et Cosmochim Acta, 27, 911.
Shiuttse V. (1955) Zhur. Eksptl. i. Theor. Fiz., 29, 486. (English translation: Sov. Physics JETP, 2, 402, 1956).
Stevens C.M. and Harkness H.L., Slected measurement methods for plutonium and uranium in the nuclear fuel cycle. (Ed. R.J. Jones.)
Zanberg E.Ya. and Ionov N.I. (1959). Review, Usp. Fiz. Nauk. 57, 581.

A MASS SPECTROMETER WHICH SIMULTANEOUSLY COLLECTS POSITIVE AND NEGATIVE IONS*

H. J. Svec and G. D. Flesch

Institute for Atomic Research and Department of Chemistry
Iowa State University, Ames, Iowa

We have studied the positive ion mass spectra of halogen compounds of chromium, vanadium, titanium, xenon and silicon during the past few years in an attempt to obtain heats of formation and bond energies from appearance potential data. A major problem in this work has been the identification of the chemical processes taking place in the source. The strongly electronegative groups in these molecules make the role of negative ions which may be formed as the result of resonance processes, electron capture followed by dissociation, or ion-pair production, of particular importance. Furthermore the reactive nature of many of these substances makes it difficult to properly assess the electron energy due to the variable character of contact potentials, voltage drops across semi-conducting layers etc. in the ion source. These difficulties become grave problems when these materials are first studied as positive ions and then as negative ions by reversing appropriate voltage polarities in conventional mass spectrometers. A better approach is to simultaneously detect both positive and negative ions. In 1961 we reported the results of a test of a model of a mass spectrometer in which positive and negative ions were simultaneously detected. The model consisted of two 180° mass spectrometers which were arranged back-to-back and employed a single electron gun. Fig. 1 is a schematic of this model which demonstrated the feasibility of the proposition that negative and positive ions could be collected simultaneously. The next step was to expand the work and build a full scale instrument which would provide for independent scanning of the spectra observable in either half of the instrument and an ion source amenable to ionization efficiency studies. We had planned to give a progress report on the work a year ago but had to withdraw the paper because of some mysterious behaviour of the instrument when it was first set up. The mystery was solved soon after we returned from St. Louis when a wiring error was discovered which drastically altered the ion source potentials. We have tested the instrument extensively during the past year and can now report more definitively its operation. Actually, in some respects the mass spectrometer has exceeded our expectations.

In planning the instrument, several objectives were kept in mind.

1. Adequate space should be provided around the ion source and collectors to provide for possible future design modifications and developments.
2. Both ion source and collectors should be readily accessible.
3. Both analysers should be electically insulated well enough so that potentials up to 5000 volts from ground could be applied.
4. Similarly the ion source should be capable of operation to 3000 volts from ground.
5. Alignment should be readily checkable and as simple as possible to attain.
6. The mass range on each side should be 10-300 and initially all slits would be of such size as to provide resolution at mass 200 with less than a 10 percent vallye between adjacent peaks.

These moderate specifications were met with the arrangement which is shown schematically in Fig. 2 which shows a top view of the instrument. The instrument consists of two 6 inch radius, 60° sectors. The distance between collectors is about four feet and the plane of the analysers is horizontal. While the instrument is completely symmetrical and can be operated in a number of modes, we choose for the normal mode to retain the ion source at ground and the collectors and analysers at ±2500 volts with

* Work was performed in the Ames Laboratory of the U. S. Atomic Energy Commission

respect to ground. The ion source vacuum housing consists of a four inch, borosilicate, glass pipe-Tee which effectively insulates the potential difference of 5000 volts between the analysers and is structurally stable. The system is supported at or near the two ion source housing flanges and the two collector housing flanges by mounts which pivot and allow for both vertical and horizontal adjustments. The mounts are insulated from the analysers by Kel-F bushings.

The source housing is pumped with a 40 liter per second mercury pump and the analysers and collector housings are pumped with 11 liter per second ion pumps. A two inch pumping lead accomodates the source pumping system and two 1-1/2 inch pumping leads connect the ion pumps to the collector housings. The only connections between the source housing and analysers are the ion source exit slits. The ion pumps are at ground potential and are insulated from the analysers by short lengths of glass tubing sealed to Kovar pipes. Both sector magnets are also grounded. Sheets of 0.030 inch Teflon serve to insulate the portion of the analysers in the gap from the magnet pole faces.

Figure 2 also presents an insight into the difficult alignment problems. The difficulties stem from the fact that five sets of slits must be aligned and the analyser tubes must be moveable in order to allow the glass Tee to be put into place. Furthermore, the slits are on three different reference franges because of the manner in which they are mounted.

Three decisions, made early in our planning simplified the alignment problem. First, the object slit and ion collimating slits along with the beam center electrodes were mounted on the analysers and these collimating assemblies were not attached to the ion box structure. The latter was mounted on the flange closing the stem of the glass Tee. Second, the table on which the instrument was to be mounted, was designed in such a way that half of it could be displaced sideways. A V-track in which a linear rack of ball bearings roll, makes movement easy and assures precise repositioning. Third, the magnets and the supports for the analyser tubes were mounted on granite surface plates, one for each side of the instrument. This provided a good reference from which to make all alignment measurements. It also made it possible to move the magnets easily by means of an air cushion. The granite blocks were set on adjustment screws which made it possible to make both surfaces exactly parallel. Furthermore the ends of the analyser tubes on which the ion collimating systems are mounted were machined to precisely the same dimension so that interalignment of the two analysers was possible using V-blocks in conjunction with precision levels and dial indicators. Since the alignment required that the two analyser tubes be coplanar and the portions of the tubes adjacent to the ion source be coaxial, we fixed the position of the left-hand tube and made all adjustments on the right hand, moveable analyser.

A more detailed picture of the alignment design is shown in Fig. 3 which is an enlargement of the ion source region of the mass tube. The ends of the analyser tubes on which the source collimation assemblies are mounted are rotatable in their respective flanges, thus allowing for adjustment of parallelism of both sets of collimating slits. The slit assembly in turn is attached to a heavy metal disc which is held in place on positioning pins by means of screw-locakable metal clips. This makes it easy to remove the assemblies for cleaning. A calibrated angle scale and appropriate index simplifies the repositioning of the collimating assemblies. We do not have a figure showing the detail of the dual collector assembly mountings but it is very similar to the source mounting and performs the same functions.

Aligning the ion box with the ion collimating assemblies was a more difficult problem. As the figure indicates, the glass-Tee is a secondary reference frame for placement of the ion box. The left and right ends of the Tee were ground parallel and the end of the stem was ground perpendicular to the other ends. Since the glass-Tee could not be accurately keyed to either of the analysers and is indeed free to rotate on its flange closures, the end of the stem of the Tee must be perpendicular to the surface plate on which the fixed analyser is mounted, before the left hand flange is tightened. The same problem exists concerning the

flange to which the ion box is attached. However, after these two alignments are made by trial and error, the ion box slits are parallel to the collimation slits. None-the-less their position must be still adjusted by using the three dimensional movement, possible with the ion box mount. To make allowance for slight non-parallelism of the glass-Tee surfaces and small dimensional variations in glass-Tee's, a short metal bellows was inserted between the moveable analyser and its flange. The mount for the source end of this analyser is actually a little to the right and off the figure.

An additional reason for grouping the ion source electrodes as they are, is that the normal operating potentials of the electrodes in each group are similar. This resulted in much less severe insulation problems.

All electrical feed-throughs into the mass tube are demountable. Fig. 4 shows the type of multiple feed-through used on the ion box flange. The right-hand portion is a one inch internal diameter flare fitting which is welded to the flange. A Teflon or aluminum gasket is placed between the fitting and a Fusite, multilead bulkhead. These may have as many as nine electrical leads per bulkhead. This is followed by a slip ring and a tightening nut. The assemblies have been trouble free and have been vacuum tight since we first assembled them. Electrical leakage to ground is <0.1μa when 3000 volts is applied to any of the leads. Each lead is surrounded by metal at ground potential so no problems result from interelectrode leakage. An adapter attached to the tightening nut fits a standard Cannon cable plug. We are currently using two heavy current leads and six voltage leads in two such feed throughs. There is a spare lead in each assembly.

The electrical feed-throughs at the other flanges of the analyser tubes are all high impedance, single leads. Again they are demountable with sex-less nibs bearing on aluminum gaskets. Fig. 5 shows the construction detail. A BNC connector is attached to the brass tightening nut to allow for quick electrical connection to any of the feed-throughs. Six of these are on each collector flange and four on each object slit flange. Their use on the object slit flanges makes it possible to monitor the ion current to any of the ion collimating electrodes.

The inlet systems employs dual viscous leaks and is pumped with another 40 liter per second mercury pump. The design is such that samples may be prepared on the inlet system and used without transfer.

Two NJE 500-5000 volt supplies provide the ion accelerating voltages. Two home built 250 milliampere current supplies, fitted for automatic variable speed scanning, power the magnets. The transistorized emission regulator is also a home built circuit which provides for several modes of emission current control. This emission regulator and its associated electron gun is quite versatile and is the subject of a paper which appears later in this volume.

The various electrode potentials are drawn from a voltage divider across the high voltage supply. The voltage to each source electrode is independently and continuously variable between the ion box and analyser tube potentials. The design is such that we are free to experiment with any combination of electrode potentials we wish. Since we also study ion source conditions with large scale, tank or membrane models, we have an immediate opportunity to adjust and test a real ion source to any conditions dictated by the model experiments.

We are using battery operated electrometers as ion current detectors. Because of the high voltage at which the analysers operate, these electrometers float at the analyser potential. This posed a real problem for any attempt to record mass spectra with strip chart or X-Y recorders since it is impossible to safely maintain any of these at ±2500 volts. A d.c. to d.c. isolation circuit has been developed which enables an ion current to be measured at ±2500 volts but displayed by a recorder at ground potential. An important by-product of this development has been that we were able to design a system in which ionization efficiency curves may be plotted directly by using the electron accelerating voltage for the X input and the ion current as the Y input of an X-Y recorder. This system should work with any mass spectrometer and could be the subject

of another paper.

The next few figures are photographs of the instrument and its components. Fig. 6 shows the ion box assembly. The electron gun was fabricated from a 3/16 inch stainless steel block to which is attached the gas inlet, (upper center), the filament and anode (trap) assemblies, (left and right) and the draw-out and focus electrodes. Fig. 7 shows the ion box mount and the flange complete with electrical leads. The electrical insulators between the ion box and the mount are easily seen. The mount is a bulky looking mass of stainless steel which was the result of our inability to attain and maintain the required accuracy and precision of adjustment, with lighter components. Fabrication of the rugged mounting was also much simpler. You'll note the wide open electron gun exit slits in this figure which were used during the initial adjustment of the instrument.

Fig. 8 shows the partially assembled instrument. It offers an uncluttered view of several of the features. Note the spectrometer table which is open to show the track on which the right half moves. Also, note the right object slit mount and the bellows; the granite surface plates; the stainless steel mixing bowls used to cover the collector assemblies; the battery operated electrometers; the glass Tee and its associated flanges; the source housing isolation valve. Fig. 9 is a front view with the table closed. Note the mount for the source end of the right analyser. Fig. 10 shows the completed instrument with some of the safety guards removed. The electrometers are now housed in Plexiglass containers. We will be adding two more electrometers.

Fig. 11 is a side view of the instrument and illustrates the labor caused by a design error. It turns out the table was eight inches too low to accomodate the liquid-N_2 dewar of the sample vacuum system. However the tedious job of alignment was already completed and we didn't want to repeat it if things went wrong during the raising of the table. Accordingly, we ground an 8 inch I-beam parallel, cut it into pieces, and then after jacking up the entire instrument with 4 screw jacks, 0.001 inch at a time, we settled the legs of the table on the I-beam sections without any impairment of the alignment. It took the whole group the day to get the job done though.

Testing and Results

The mass tube was assembled, leak tested and evacuated to a pressure of 2×10^{-7} Torr without problems. Initial testing began with each of the halves of the instrument operating as a conventional mass spectrometer with the ion source at +2500 volts and the analysers grounded. This made it possible to make necessary mechanical adjustments and position the magnets safely. First one side of the instrument was adjusted and then the other.

During the testing period the sizes of slits and apertures in the ions source were those shown in Table 1. The 0.070 inch ion box slits were

Table 1. Aperture and Slit Sizes (inches)

Ion box exits	0.070 x 0.535
Draw-out	0.135 x 0.840
Focus	0.135 x 0.535
Object slits	0.010 x 0.325
Beam Center	0.135 x 0.840
Large Collector	0.070 x 0.535
Small Collector	0.017 x 0.535

used to obtain high sensitivity. The length of the object slit, 0.325 inches, was dictated by the inside dimension of the flattened portion of the analyser tube in the magnet gap. The defining slit in front of the first collector was only 0.070 inches. Only single beams of ions of integral mass-to-charge-ratio less than 100 fall through this slit. This simplified the evaluation of the ion beam properties during the initial adjustment period. The slit in front of the second collector is actually in the botton of the first collector. With a 0.017 inch slit in each first collector, the drop through for each side of the instrument was better than 95 percent. This was considered to indicate a satisfactorily

focussed ion beam at this stage of the development.

The next test involved accelerating positive ions simultaneously down both analyser tubes. It was found that the ion source electrode potentials required to optimize the ion currents on either side of the electron gun were nearly identical and that they did not change very much from those used during the previous test. However, the intensity of the ion currents in each analyser were highly dependent upon the position of the electron collimating magnet. This was to be expected since each side is competing for the same ions. An experiment was done in which N_2^+ ions leaving the ion box were monitored at the object slit in the ion source depending upon whether the ions were travelling in one direction or the other or simultaneously in both directions. It was found that in each case, the ion current on both sides remained equal within ±10 percent for all electron energies used. We interpret this observation to indicate that the probability of an ion leaving the ion box is independent of the force fields which extract it. Another interesting observation was that the ratio of total collector to monitor ion currents varied from one to ten percent depending upon the ion source electrode potentials. When this ratio was 10 percent, the drop-through to the second collector was better than 97 percent. When this ratio was one percent, the drop through was only 90 percent.

Chromyl fluoride was used to test the instrument because of its interesting positive and negative ion spectra. With the instrument operating in the ++ mode, and when the intensity of the parent ions on each side were equal, fragment ion currents varied as much as 30 percent between the two sides of the instrument and the total ion currents differed by about 10 percent. This indicates that there is some discrimination in the two sets of ion collimating slits and/or the mass analyser. We have not as yet made extensive studies of this problem.

When the instrument was switched to operate in the -- mode, we found the magnitude of ion source potentials for optimum ion current intensities to be essentially the same as required for positive ions although the total ion current intensity for negative ions was appreciably less. The drop-throughs at the 0.017 inch collector slits were about the same as for positive ions.

Finally the instrument was arranged to collect positive and negative ions simultaneously. We found that the magnitude of the ion source potentials for good ion beams of either form of ions remained relatively the same as in the previous tests. Furthermore it made no difference whether the spectrometer was operating in a + - mode or a - + mode.

Fig. 12 shows a copy of a recorded spectrum of the negative and positive ions from CrO_2F_2. The two spectra are not precisely aligned because it is very difficult to exactly synchronize the two magnetic scan rates. Note the difference in scale factor of 100 between the two records. The total negative ion current in this case was only one percent that of the positive ion currents under the conditions given here. We do not yet have enough experience to claim that this is generally true. In any event it pretty much indicates that there is more than a single process leading to ionization of these molecules.

Fig. 13 shows ionization efficiency curves for some positive ions from CrO_2F_2 along with A^+ from argon which was running into the instrument with the chromium compound. The anode (trap) current was maintained constant during these runs. The figure is actually a picture of the traces made by an X-Y reocrder. Even the framing and the grid marks were made by the recorder pen and only the lettering was added by the draftsman. It took about five minutes to obtain all four curves. By changing the scale factors, one can look at as much detail in an ionization efficiency measurement as is desired. These data are essentially the same as we'd obtained previously for this compound with one of our other mass spectrometers.

Fig. 14 shows ionization efficiency data for the major negative ions from CrO_2F_2 but over a smaller electron energy range. Again the data was obtained via the X-Y recorder and this slide was made on the recorder. A constant filament current was maintained during these experiments. No

regulation of the emission was employed. The two CrO_2F^- and $CrOF_2^-$ peaks indicate a single resonance process for each ion species in this energy range while the parent, $CrO_2F_2^-$ peak shows considerable structure. We offer these data today only as observations which illustrate the versatility of this positive-negative mass spectrometer. No attempt will be made to interpret these data.

It seems to us that the complete symmetrical character of this instrument may be valuable in solving other mass spectrometer problems. It may well lend itself to the study of metastable ions. With some modification of the collector system and ion readout it may be used to measure coincident events in ion-pair production. The ion source design is fluid enough so that we could add facilities for retarding potential measurements or even add an electron energy selector. We believe we'll have an interesting time working with this instrument in the future.

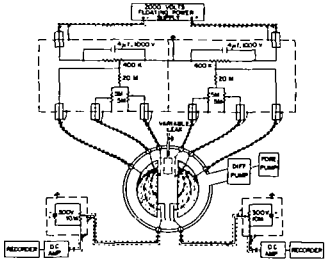

Figure 1.

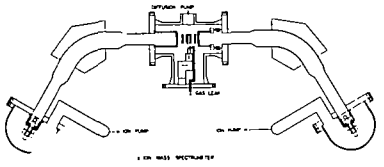

Figure 2.

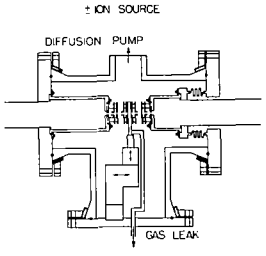

Figure 3.

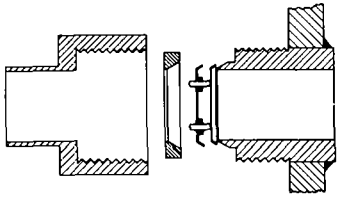

MULTIPLE LEAD FEED-THROUGH ASSEMBLY

Figure 4.

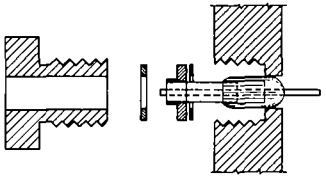

LOW LEAKAGE FEED-THROUGH ASSEMBLY

Figure 5.

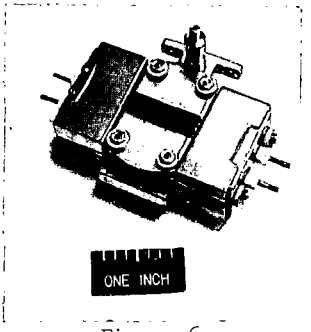

Figure 6.

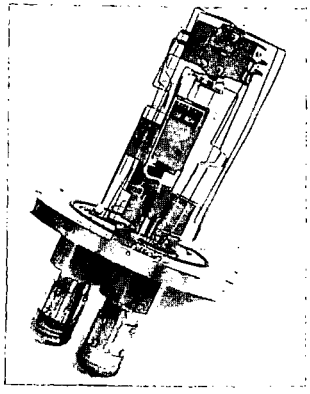

Figure 7.

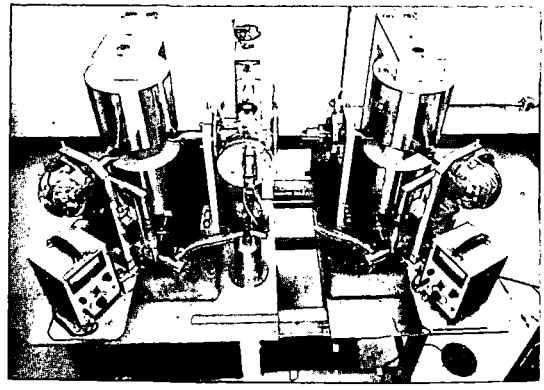

Figure 8.

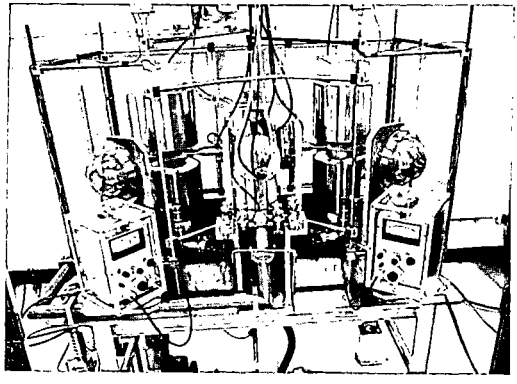

Figure 9.

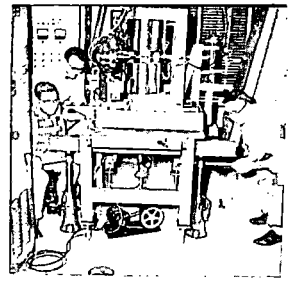

Figure 11.

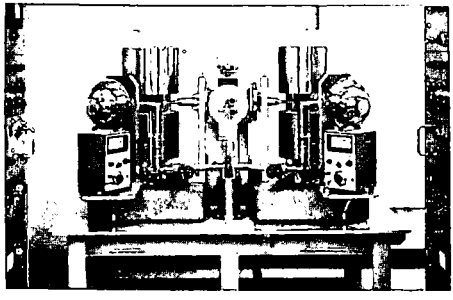

Figure 10.

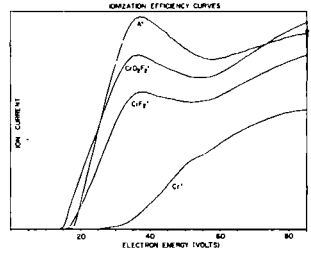

Figure 13.

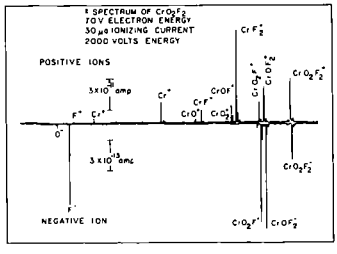

Figure 12.

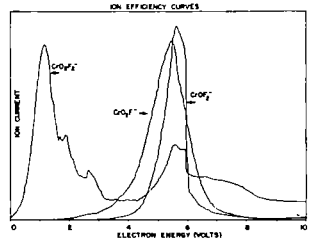

Figure 14.

PRESENT STATUS OF THE PRINCETON RF SPECTROMETER*

Lincoln G. Smith, Palmer Physical Laboratory, Princeton, N. J.

Introduction

This device for precision mass measurement was proposed in September, 1960[1]. Its construction at Princeton was begun a year later and is now nearing completion. Like the mass synchrometer[2], it is designed to measure cyclotron frequencies (and hence mass-to-charge ratios) of ions circulating in a homogenous magnetic field in terms of much higher frequencies of rf signals applied to a "modulator" located 180° from the entrance and exit slits. It differs from the synchrometer (1) in that both source and detector are located well outside the magnetic field and (2) in that ions are made to miss the injecting and ejecting electrodes by being given a small axial component of velocity so that they describe slightly helical paths in the magnetic field. Thus the dc ion beam travels from source to detector with no rf applied as it could not do in the synchrometer where ions were made to miss the source and detector by action of the rf field.

Description of Instrument

Figure 1 shows plan and elevation views of the parts of the instrument in the magnetic field and illustrates its operation. Ions are injected into and ejected from the magnetic field radially at the edge of the 2 in. gap between the 22 in. diameter pole pieces. They are turned to and from azimuthal directions at the entrance and exit slits by "internal" electrostatic deflectors of mean radius 3 9/16 in. The beam makes two turns in the gap passing twice through the modulator at different heights and once through a "phase defining slit" located midway axially between entrance and exit slits. The orbit diameter is 16 in. The gap is shown enlarged in the lower diagram for clarity.

With rf voltage applied to the central slit of the modulator, the velocity (v) of ions or their orbit diameter (D) is modulated very nearly sinusoidally on each transit. In order that an ion then reach the detector, the sum of the two velocity changes (Δv) must be very nearly zero. Thus if we plot modulation (1) and minus modulation (2) as a function of time or phase (Φ) of the rf when an ion passes the central slit, as has been done in Figure 2a, we see that ions can only reach the detector for cases where these two curves cross. By changing the frequency, we change the phase of (-2) relative to (+1). We see that, while two small groups of ions each cycle reach the detector at any frequency, all ions do so when the two curves coincide or when the applied frequency (f) in an odd half integral multiple ($n + \frac{1}{2}$) of the cyclotron frequency (f_o). To determine detector current (I) we may give each curve for ΔD a small vertical extent equal to the common width of the entrance and exit slits. On computing the overlapping areas as a function of f, we find an intensity distribution such as is shown in Figure 2b. Inspection shows that the skirts on the peaks are due to ions getting nearly maximum velocity change on the first transit. Such ions are prevented from reaching the detector and the undesirable skirts are eliminated by action of the phase-defining slit whose width is set less than twice the amplitude of ΔD. (The maximum positive and negative values of ΔD for which ions can pass the phase defining slit are indicated by the horizontal dashed lines in Figure 2a.) The resultant intensity distribution is as shown in Figure 2c where the sharp peaks are theoretically triangular, of height about 1/3 of the intensity of the dc beam. The broad "peaks" midway between successive sharp ones are flat-topped and of intensity only about one percent of the sharp peaks. They therefore should cause little error in either mass or intensity measurements. Consecutive orders for a second ion species (of different n and f_o) are shown in Figure 2c.

---

* Work supported by grants from The National Science Foundation.

1 "Proceedings of the International Conference on Nuclidic Masses" University of Toronto Press (1960), P418

2 Lincoln G. Smith and C. C. Damm, Rev. Sci. Instr., 27, 638 (1956)

A plan view of the entire spectrometer is shown in Figure 3. An image of the source slit is formed one inch outside the gap edge by two 90°, 8-inch, toroidal deflectors in series. An image of this image is formed on the entrance slit by the first "internal" deflector. An image of the exit slit is formed one inch outside the gap edge by the second "internal" deflector and an image thereof is formed on the detector slit by two identical 90°, 8-inch, toroidal deflectors. It has been found in an auxiliary experiment that the inhomogeneity of the magnetic field near the gap edge and off the median plane does not seriously deteriorate the quality of images formed by the internal deflectors. The beam height at the gap edge and at the source and detector is 1/16 inch, while, at the modulator, it is 1/8 inch.

The toroidal deflectors are made of beryllium copper very carefully stress relieved and machined. They are now being gold plated. The mean equipotential in each is an 8-inch sphere, and the vertical radii of the plates are chosen to minimize second order angular aberrations. The plates are also curved at their ends to eliminate second order aberrations in such deflectors due to Z-motion. Aside from providing good two-directional focusing from the source slit onto the entrance slit and from the exit slit onto the detector slit with source and detector well outside the field, the toroidal deflectors also provide an energy dispersion equivalent to that of a single 127° cylindrical, electrostatic deflector or a 180° magnetic deflector of 48 inch radius. This results in an increase in phase sensitivity or in resolution for given slit widths of a factor of six over what would be obtained from the energy dispersion of the last half turn in the magnetic field alone. It thus also materially reduces rf power required and distortion of velocity modulation for given resolution and slit widths. It is interesting to note that the path length from object to image of each pair of toroidal deflectors is 65.1 inches, while for a 127° cylindrical deflector of radius 48 inches, it is 106.6 inches. The total beam path length from source to detector slits is 243.8 inches.

The toroidal deflectors and the entire beam path outside the magnetic field are housed in stainless steel tubing. The internal beam, the internal deflectors, the entrance, exit and phase defining slits, the modulator and electrostatic einzel lenses on either side of the modulator for z-focusing, are housed in a toroidal chamber that was electroformed on a polished aluminum mandrel. Three mils of gold were first laid down on the mandrel, and about 80 mils of copper on the gold. The aluminum was then dissolved out leaving the copper chamber with a very smooth gold liner. Metal seals and Vacion pumps will be used and the entire vacuum system may be slid on ways so that the toroidal chamber is entirely outside the magnet gap for baking at temperatures up to 150° C if desired. A high through-put Vacion pump will exhaust the ion accelerating and focusing regions in front of the source to provide differential pumping.

The ion source is of the type used in isotope separators whence ions are drawn parallel to the electron beam at the opposite end thereof from the filament. While this source will yield a greater energy spread than one from which ions are drawn normally to the electron beam, we hope to get more ions from it even in the very narrow energy range that we can accept than from the more conventional source. Provision is being made for study of gases, liquids and solids.

A Faraday collector is being built as a detector but an electron multiplier will eventually be substituted for it for most measurements.

The magnet and associated power supply, made by Varian Associates, are stated to provide a field homogenous to one or two parts in 10^5 at 9 kg over the region of the helical orbits and to one part in 10^5 in time. While it is believed that spatial homogeneity will be satisfactory at least at high fields, better time stability will have to be provided. Circuitry has been developed to differentiate the ion peaks and thus to obtain a correction current proportional to departure of a peak from the center of the scope which will be applied to auxiliary windings to keep peaks centered and hence to lock the field to the crystal oscillator that determines the frequency.

It is expected that values of the "order" (n) near 2000 will be used for which the appropriate spacing and width of the modulator slits will be about 0.009 inches and 0.003 inches respectively. With source and detector slits 0.002 inches wide, the half width of a peak should be only about 1/500th of the separation of successive orders so that the theoretical resolution will be 2000 x 500 or 1 x 10^6. Figure 4 shows the maximum values of magnetic field (H) accelerating voltage (V) and cyclotron frequency (f_0) that may be used plotted as functions of mass number (M).

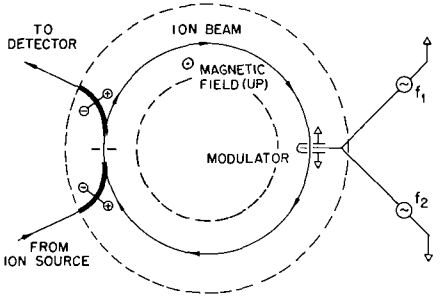

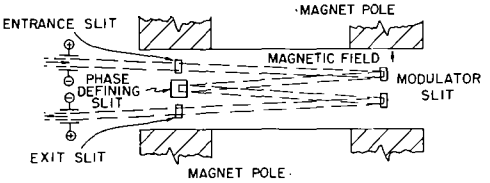

FIG. 1 16" R.F. MASS SPECTROMETER ORBIT IN MAGNETIC FIELD

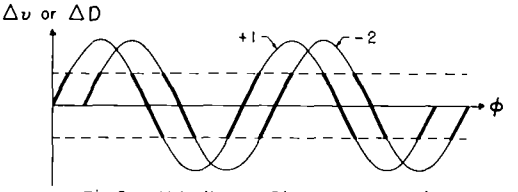

Fig. 2a Velocity or Diameter Modulations

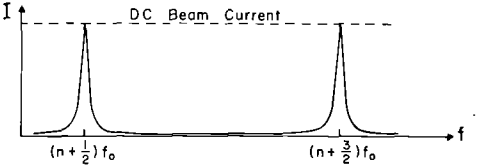

Fig. 2b Intensity Distribution Without Phase-Defining Slit

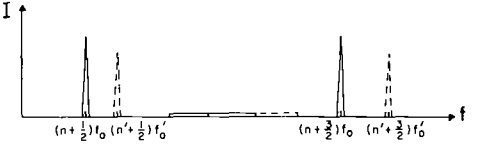

Fig. 2c Intensity Distribution With Phase-Defining Slit

Above mass 80, the limiting factor is the maximum field H_{max} = 10 kg. set (a) by the magnet power supply and (b) by homogeneity considerations. Below mass 80 it is the maximum accelerating voltage V_{max} = 25 kV obtainable from our high voltage supply. Both V and H will probably also have to be reduced below mass 3 because of inability to obtain adequate power at frequencies above 2000 mc. (f_o = 1.215 mc for a 25 kv deuteron in a 16 inch diameter orbit.) Figure 4 indicates that optimim performance should be obtained near mass 80.

High Voltage Supply

A block diagram of the high voltage supply appears in Figure 5. Two commercial, highly regulated and filtered supplies adjustable from 0 to 2 kV provide the + and - voltages for the electrostatic deflectors and beam benders, both of which voltages may be switched rapidly between two values having any ratio from 1 to 2 so that two masses in any such ratio may be alternately displayed on successive sweeps. The voltage ratio is continuously adjustable and settable to one ppm. The negative supply also provides the reference voltage for the high voltage regulator whose amplifier has an open-loop gain of 2×10^5. Thus the high voltage as well as all other voltages may be rapidly switched between two values which are accurately inversely proportional to the masses of the two ion species being compared.

The performance of the high voltage supply is illustrated in Figure 6. The upper part shows an oscilloscope display of the sawtooth sweep voltage from the scope on which peaks are displayed together with a square wave modulation of the high voltage by 1 ppm or 12.5 mv at V = 12.5 kv. The sweep period is 33 mec. The high voltage modulation is obtained with a capacitance divider so that there is some apparent droop that is not real. A delay in the vacuum relay of about 2 mec is not serious since the start of each sweep is delayed 5 mec after the end of the preceding one. It is clear that the noise (largely residual hum) is considerably less than one ppm, a level that is entirely satisfactory. The lower part of Figure 6 shows high voltage modulation by a factor of two from 12.5 kV to 6.25 kV together with the sawtooth sweep voltage. Here the sweep period is 18 mec. We note an increase in rise time of the high voltage caused by the regulator momentarily losing control. However, it recovers before the start of the next sweep.

The RF System

Figure 7 shows a block diagram of the RF system. Two frequencies between 50 and 500 mc set inversely proportional to the two masses being compared are generated by continuously running commercial oscillators O_1 and O_2. Their outputs are amplified to a level of several watts by two commercial, tunable power amplifiers whence signals are fed to the modulator either directly or via frequency doublers or quadruplers and additional (homemade) power amplifiers which cover the range from 500 to 2000 mc or more. The two signals are alternately placed on the modulator primarily by applying plate voltage to only one power amplifier (or chain of power amplifiers) at a time. Thereby is obtained the required suppression of the other frequency by at least 65 db. A system of tuned air lines with the modulator at the end of a common branch has been found feasible that may be resonated to any two frequencies in the range from 50 to 2000 mc whose ratio is anywhere between 1 and 2.

In order to stabilize the two frequencies at accurately known values, the rather complex system shown in Figure 7 has been found to be the most satisfactory. A 10 mc crystal-controlled oscillator feeds two harmonic generators and selectors from each of which any harmonic from the fifth to the fiftieth may be selected. The output of each of these, after amplification and further filtering in a tuned amplifier (not shown), is fed to a mixer along with a second output from oscillator O_1 or O_2. O_1 is set 30 mc below or above the selected harmonic and the difference frequency is amplified by a broad-band 30 mc amplifier (not shown) and fed to a phase detector. To the other coil of this phase detector is applied a signal of 3 x 10 = 30 mc exactly. The phase detector thus gives out a dc voltage proportional to the phase difference of the two 30 mc signals. This is fed through a low pass filter to a varactor coupled to the tank circuit of O_1, thereby phase locking O_1 to an exact known multiple of 10 mc.

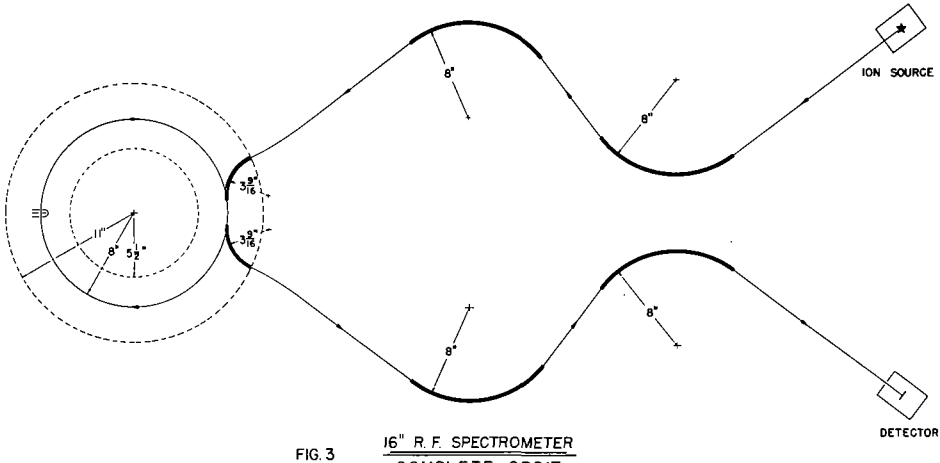

FIG. 3 16" R. F. SPECTROMETER / COMPLETE ORBIT

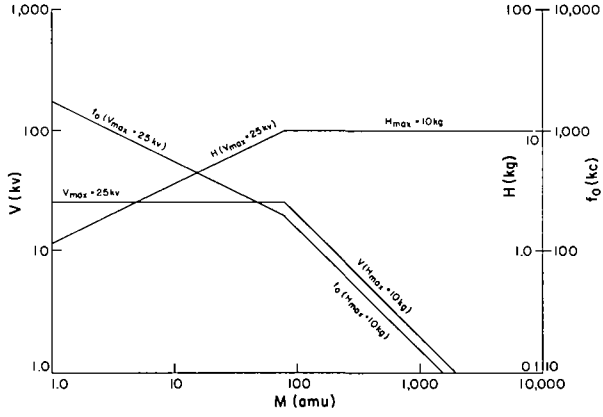

FIG. 4 MAXIMUM VALUES OF H, V AND f_0 vs. M

0_2 is similarly phase locked to another harmonic of 10 mc $\pm$ a reference frequency (S) obtained from a frequency synthesizer. This commercial device can provide any frequency from 0 to 30 mc accurately referenced to the 10 mc standard. S, which is continuously adjustable and measurable to 0.1 cycles/sec, generally lies in the range from 25 to 30 mc.

In order to display peaks, the sawtooth sweep voltage from the display scope is fed to a reactance tube in the 10 mc oscillator so that the frequencies of both 0_1 and 0_2 are swept exactly the same fractional amount (a few ppm). The procedure for accurate mass determination is then to set 0_1 to the value nearest that which will allow use of the highest magnetic field and accelerating voltage for the smaller mass. The field and voltage are then adjusted so that the desired order of this mass is centered on the scope. The voltage for the larger mass is then adjusted, as is the frequency (by adjustment of S) so as to bring the same order of that mass to the center of the scope. Final precise adjustments are made by the well-known peak-matching technique. The ratio of the two applied frequencies and hence of the masses may then be determined to an accuracy of 10^9 or better.

The performance of this rf system is indicated in Figure 8. In the upper part, we see the sawtooth voltage from the display scope along with a frequency sweep of 30 ppm which it causes in a phase-locked oscillator running at about 500 mc. This picture represents the output of a 10.5 mc frequency discriminator fed with the difference between the frequency of the phase-locked oscillator and that of a free-running bfo set 10.5 mc away. This sweep is ten times that required for presenting a peak with a half width of one ppm. The maximum that the crystal oscillator may be swept (with some nonlinearity) is 50 ppm. Much broader sweeps (also somewhat non-linear) for displaying the spectrum over a whole order or more as in Figure 2c may be obtained by unlocking an oscillator and connecting the sweep voltage directly to the varactor in its tank circuit.

In the lower parts of Figure 8, we see the output of the discriminator showing the FM noise of an oscillator locked at 470 mc in comparison with a shift of 47 cycles/sec (one part in 10^7) produced by a shift of this amount in the synthesizer frequency. The discriminator band width is 200 kc in the upper trace and 2 kc in the lower one. The switching rate is 30 per sec for a full square wave cycle. Such pictures are typical of those obtained at all frequencies from 50 to 2000 mc and show a peak-to-peak FM noise in a 200 kc bandwidth of about four parts in 10^8 corresponding to an rms noise of about one part in 10^8. Since this is only one percent of the hoped-for peak half-width, it is clear that FM noise should cause negligible peak broadening.

Conclusion and Acknowledgments

All the major mechanical parts and most of the minor ones are now either complete or nearly so. Virtually all of the electronic equipment has been assembled with many modifications and appears to function quite satisfactorily. It should thus be a matter of but a few months time before the instrument becomes operational.

The project has been most fortunate from its start in having all the details of mechanical design and construction supervision ably handled by mechanical engineer Ernest Bolze. It has also enjoyed for about half its duration the expert assistance of electrical engineer Robert Poirer in designing and constructing and proving much of the specialized electronic gear required.

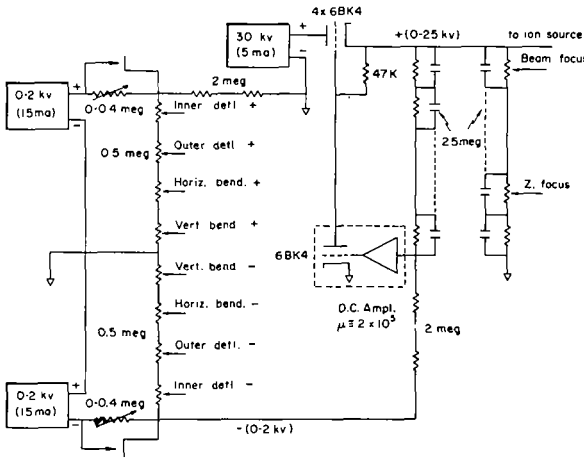

FIG. 5 HIGH VOLTAGE SUPPLY

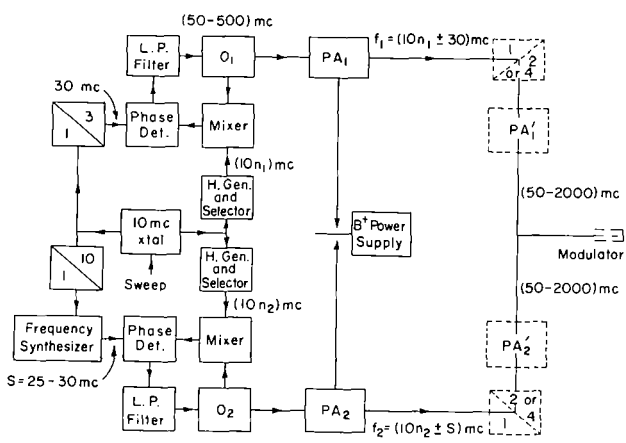

FIG. 7 MASS SPECTROMETER R.F. SYSTEM

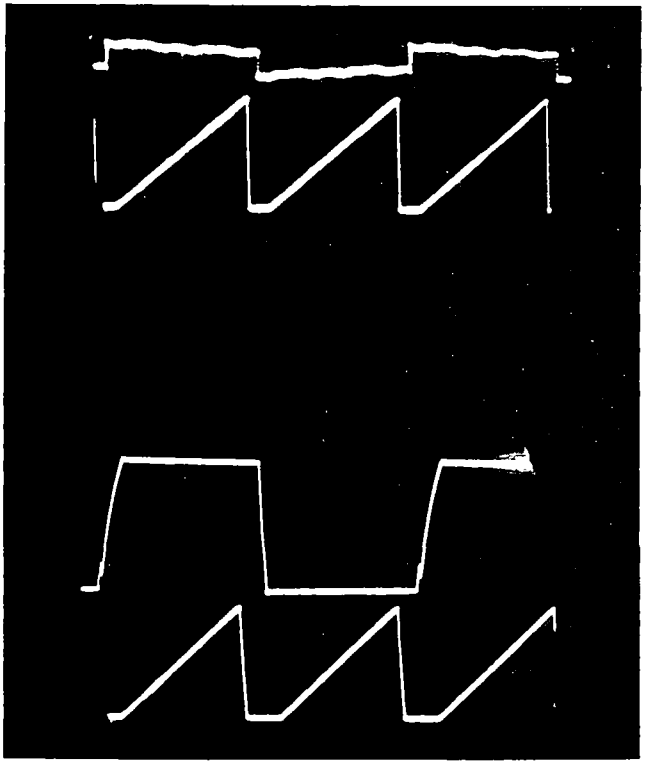

SWEEP VOLTAGE AND SHIFTS OF HIGH VOLTAGE BY 1PPM (UPPER) AND BY A FACTOR OF 2 (LOWER) AT 12.5 KV.

FIG. 6

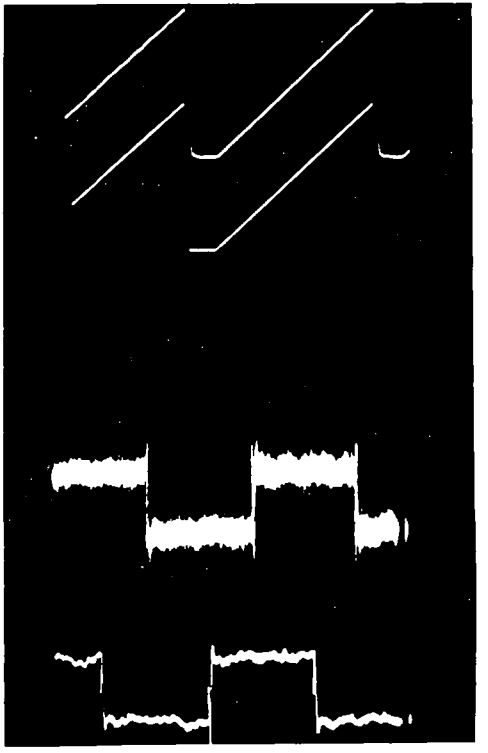

UPPER, SWEEP VOLTAGE AND FREQUENCY SWEEP BY 30 PPM (TOP).
LOWER, FREQUENCY SHIFT BY 0.1 PPM AT BAND WIDTHS OF 200 AND 2 KC.

FIG. 8

MAGNET DESIGN OF A MULTI-TRAJECTORY ION BEAM ANALYZER

F. A. White

Department of Nuclear Engineering and Science

Rensselaer Polytechnic Institute

Troy, New York

A large electromagnet has been designed for a mass spectrometer that provides for a multiplicity of ion trajectories. Some design features are patterned after the instrument previously reported by White, Sheffield and Rourke.[1]

The magnet yoke is comprised of low carbon steel plate of ten inches thickness in an arrangement indicated in Figure 1. A pair of exciting coils surround one of the yoke pieces so as to leave the total pole piece area available for a mass spectrometer chamber. Each coil consists of 6,000 turns of No. 12 copper conductor which is insulated by a heavy Formex coating. The mean length of each turn is approximately ten feet, and the weight of each coil is about 1,200 pounds. The coils have been would in four sections such that a parallel terminal connection results in a 6 ohm impedance. With two coils the net impedance is 3 ohms. The coils are thus matched to a commercially available 60 volt - 20 ampere regulated current supply.

Figure 2 indicates the multiple ion paths that can be accommodated within the 700 square-inch pole face area. The first trajectory has the source located at S_1 for a Mattauch-Herzog double focusing system. A second trajectory is the "cascade" path with the source at S_2. Primary ions can either be reflected (by an electrostatic field) or produce a secondary spectra of ions by impact on a "target" at S_4. The distance from S_2 to S_4 is twenty-four inches, thus permitting two 12"-180° magnetic analyzers in cascade. The third trajectory has its source at S_5; it is conceived as a single magnetic analyzer for mass spectrometry or for use in collecting small isotopic samples of high purity. The fourth possibility can be visualized by considering an ion gun situated at S_4. If ions are accelerated and caused to pass through a gas cell or a thin foil at this location, positive and negative ions can be simultaneously analyzed via the clockwise and counter-clockwise trajectories within the magnet.

It will be noted that an array of p-n junction detectors is indicated to replace the usual photoplate. This is a long-range technical objective which may be difficult to implement, but the feasibility of detecting single ions with junctions (via secondary electrons) has at least been demonstrated.[2] Such detectors could not only integrate the mass spectral data, but time-dependent information on the arrival of ions in a multichannel analyzer might be valuable in highly specialized situations.

Studies in which this cascade magnet may prove useful include general surface physics, sputtering, ion reflection, molecular dissociation, surface diffusion, and effects of "doping" of surfaces as these relate to semiconductor junctions, and thermionic and photoelectric emission phenomena. It should also be a valuable tool in developing improved sputter ion-type sources.

---

1. F. A. White, J. C. Sheffield, and F. M. Rourke, Applied Spectroscopy, 17, No. 2, 39 (1963).

2. F. A. White, J. C. Sheffield, and J. M. Moyer, Electronics, 34, No. 3 74 (1961).

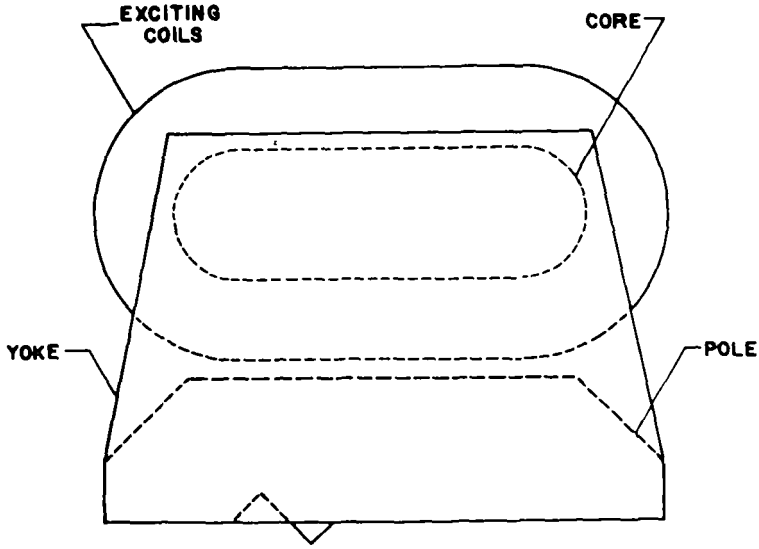

Figure 1 Top View of Magnet and Exciting Coils

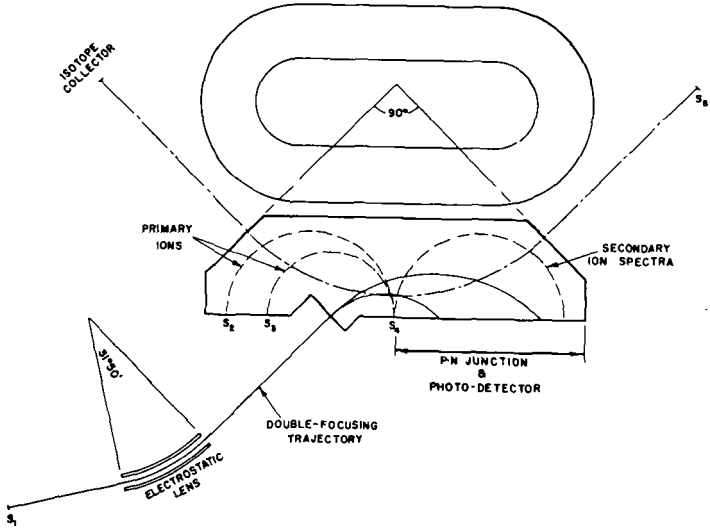

Figure 2 Schematic of Magnet Pole Piece and Multiple Ion Trajectories

USE OF A TIME-OF-FLIGHT MASS SPECTROMETER AS A MODULATED MOLECULAR BEAM DETECTOR

by

F.T. Greene and T.A. Milne
Midwest Research Institute
Kansas City, Missouri

INTRODUCTION

In molecular beam experiments which use a mass spectrometer as a detector, there is often a substantial advantage in using a chopped (pulsed) beam and incorporating phase sensitive detection in the mass spectrometer output circuitry. With this modulated beam technique, it is generally possible both to improve the signal-to-noise ratio over ordinary DC detection and to discriminate against interfering ions which have the same nominal mass but are formed from residual gases in the ion source.[1] We have been using a Bendix TOF mass spectrometer as the detector in a nozzle beam system, and have been able to obtain useful results with the modulated beam technique.[2] It is part of the purpose of this paper to point out the simplicity with which the beam modulation technique can be applied, using commercial instrumentation, to the Bendix TOF mass spectrometer or to any other mass spectrometer which has an electron multiplier. Also described are the performance of the system, effects with the "Studier"[3] continuous mode of operation, time-of-flight measurements and their application in the elucidation of complex mass spectra and, finally, a unique, direct comparison of the Bendix TOF and EAI quadrupole as molecular beam detectors.

EQUIPMENT

The molecular beam system, which has been discussed[2,4] previously, is shown in Fig. 1. This apparatus is a more or less typical "nozzle beam" system. It was set up to attempt to sample unstable species into a mass spectrometer from gases at elevated temperatures and at least atmospheric pressure. With this system we have been able to quantitatively sample free radicals and other unstable species from 1 atm. flames at temperatures of up to 3000°K.[2] With it we hope to be able to use mass spectrometry to determine the thermochemical properties of systems at pressures of 1 atm. and above. The gas, which is normally at a pressure of 1 - 10 atm., is expanded through an orifice into the first stage to form a "free jet."[5] The jet is then collimated into a molecular beam by a slit system as it passes through two stages of differential pumping. Finally, the molecular beam is crossed with an electron beam in the ion source of the Bendix TOF mass spectrometer. Beams formed from gases at atmospheric pressure have intensities of 10^{16}-10^{17} molecules/cm^2/sec in the ion source. The beam is chopped by a slotted disk mounted on a Globe Type SC subminiature motor in the intermediate pumping stage. On a similar system we have successfully used a magnetically driven vibrating reed chopper, in the third stage directly under the ion source. The usual chopping frequency is a nominal 50 cps; frequencies from 8 to 1,080 cps have been used successfully.

The Bendix TOF mass spectrometer is normally operated at 10,000 cps. When the beam is chopped, the multiplier output consists essentially of a 10 kilocycle carrier modulated at the chopping frequency of the beam. This signal is fed into one of the high-speed electrometer amplifiers which are standard components of the Bendix analog units, amplified, and rather incidentally pulse shaped by the inherent time constant of the amplifier. The output of the electrometer amplifier is then fed directly into a Princeton Applied Research "Lock-in" amplifier. The entering pulse shape is fairly noncritical and no improvement was obtained with use of external pulse shaping networks. The 12 db integration network of the PAR is used with nominal time constants from 1 to 50 sec., and the output displayed on a strip chart recorder.

PERFORMANCE

With the modulated beam and phase sensitive detection system, a discrimination ratio of background signal to the minimum detectable beam signal of greater than 1,000 for a signal-to-noise ratio of 1 is typically obtained with the longer time constants. This ratio was estimated from the observed peak-to-peak noise amplitudes from unmodulated

background peaks of varying strengths, and was verified by leaking sufficient gas into the ion source to produce ion levels 1,000 times those from the beam. The discrimination ratio of 1,000 has been obtained for background peaks estimated to have strengths of 2,000 - 10,000 ions/sec, and is therefore about what one would expect from ion statistics. The discrimination ratio will, of course, vary with the square root of the background peak strength.

The use of modulated beam techniques not only discriminates against residual gases in the ion source but also against gases scattered from the beam itself and randomized in the ion source. It cannot discriminate against molecules reflected from a surface directly back into the electron beam; however, with good geometry, this latter effect is not significant. In order to have good discrimination against background gas scattered from the beam, the time for one chopping cycle must be short compared to the time constant for the pump-out of gas from the ion source.[1] Otherwise, the scattered gas pressure will drop during the off part of the chopping cycle, and the resulting in-phase modulation of the random gas will give a positive AC signal. The effect of chopping frequency on scattered gas modulation is shown in Fig. 2. An argon beam containing substantial quantities of Ar_2,[6] which is almost 100 per cent dissociated upon collision with a wall, was chopped at frequencies ranging from 0 to 160 cps. The 80^+ signal, since it does not occur in the scattered gas, is independent of frequency. The 36^+ signal (which was used because the 40^+ signal from these very intense nozzle beams partially saturated the multiplier and overloaded the lock-in amplifier), on the other hand, decreases with increasing frequency until it reaches an asymptotic value which represents only direct signal from the beam with no detectable modulation of the scattered beam gas. The plot of $36^+/80^+$ shows the expected behavior. Note the errors involved in measuring ratios of stable-to-unstable species with manual shutter. From these data, it appears that a chopping frequency of 15 cps is adequate for the Bendix Model 12 ion source. Electronic considerations do, however, suggest the use of a somewhat higher frequency.

Electronic noise has never been the limiting factor in the signal-to-noise ratio in our work, even at the relatively "clean" masses. With the Bendix gate set between masses, the noise corresponded to 10^{-7} of the normal beam strength with a 50-sec. time constant.

OPERATION IN CONTINUOUS MODE

The above discrimination and noise levels were obtained using the normal pulsed mode of operation of the TOF mass spectrometer. It would be desirable to improve the effective sensitivity of the mass spectrometer by operation in the continuous "Studier" mode. However, when this was attempted with nozzle beams, a large AC signal was observed which was 180° out-of-phase with that from the beam. Some typical data are shown in Table I.

TABLE I

Mode	Ion	DC Signal	Modulated Signal
Pulsed	40^+		3.0×10^5
"	18^+		10 ± 5
"	56^+		0 ± 5
"	72^+		0 ± 5
Studier	40^+	2700	3.0×10^7
"	18^+	120	-2.0×10^5
"	56^+	8	-1.5×10^4
"	72^+	1.7	-1.6×10^3

Although there is a negligible component of 18^+, 43^+ and 56^+ in the beam, as evidenced by measurements made with operation in pulsed mode, enormous out-of-phase signals appear in the Studier mode which are directly proportional to the strength of the background peak. Further work has shown that if the multiplier load and gain are held constant but the ion source conditions (control grid pulse height, electron energy, pulse shape, and ion focus) varied, the per cent out-of-phase modulation could be changed considerably.

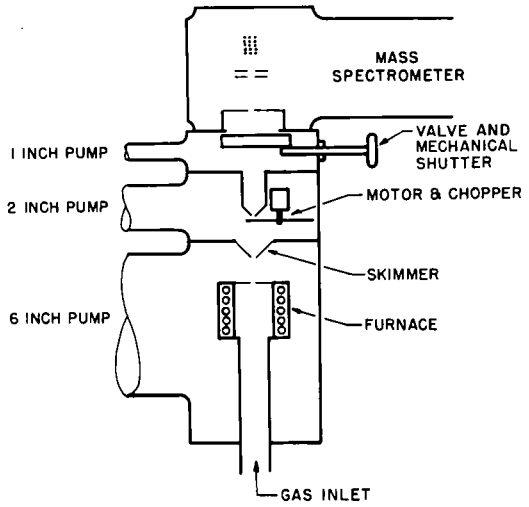

FIGURE 1

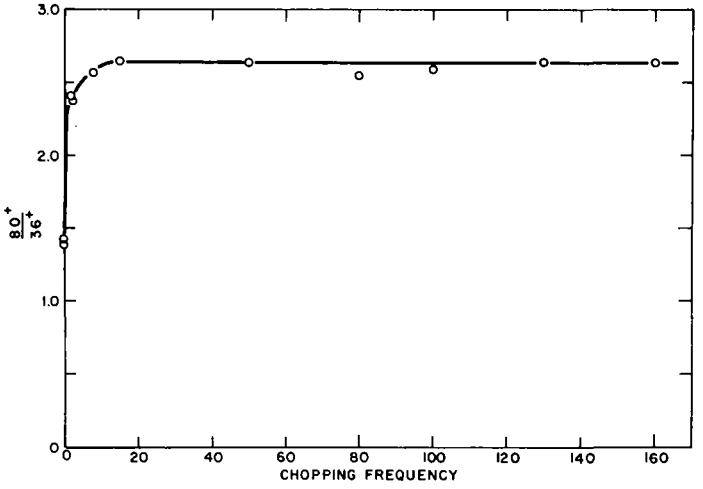

FIGURE 2

Conversely, if the ion source conditions were held constant and the multiplier load varied both by defocusing the ion beam and by changing the gain, the per cent modulation also varied. There are, then, both ion source effects and multiplier effects responsible for out-of-phase modulation. The multiplier effect is almost certainly caused by saturation while the beam is on, reducing the effective gain. With the beam off, the multiplier recovers, its gain increases, and an out-of-phase component proportional to the difference in gain is produced. The ion source effect is also easily explained. In the continuous "Studier" mode of operation, the ions are presumed to be trapped in the potential well of the electron beam.[3] During the on part of the beam cycle, a large number of ions are trapped in the beam. This reduces both the effective trapping potential and the effective ionizing energy. Both effects will reduce the apparent ionization efficiency during the part of the chopping cycle with the beam on, and an out-of-phase signal will result. The presence of these out-of-phase signals and their unpredictability at present make operation in the Studier mode of questionable value for intense molecular beam detection.

TIME-OF-FLIGHT MEASUREMENTS

In addition to discrimination against background peaks and improvements in the signal-to-noise ratio, the beam modulation technique also permits the measurement of velocities of the various species in the beam by a time-of-flight phase shift method. The velocity measured is very close to the most probable velocity and corresponds for a given beam to the maximum in the function

$$\rho_{(v)} \propto \frac{G_{(v)}}{v}$$

where $\rho_{(v)}$ is the density of molecules with a velocity v and $G_{(v)}$ is the velocity distribution in the beam. It would appear to be possible to also determine the velocity distribution with a considerable gain in sensitivity over other techniques.

A block diagram of the time-of-flight apparatus is shown in Fig. 3. The mass spectrometer signal and the reference signal are fed into a lock-in amplifier. The reference signal is phased with the mass spectrometer output by adjusting the phase of the reference signal, and the phase difference between the shifted and unshifted reference signal measured. If the phase relationship between the reference signal and the molecular beam chopper is known, either from first principles or calibration, and any incidental phase shifts in the detection circuitry determined, the absolute value of the most probable velocity can be calculated.

Figure 4 shows the results obtained when the phase shift TOF method was used to determine the velocity of a nozzle beam of argon. The beam velocity shows the expected behavior, approaching a limiting, high Mach number, terminal velocity for a monatomic gas initially at room temperature as the source pressure is increased. The TOF phase shift technique was also applied to "seeded" nozzle beams.[5] Figure 5 shows the results obtained when a series of room temperature mixtures of helium and argon were expanded through an orifice 0.002 inch in diameter. The chopping frequency was 1,080 cps, and the flight path of the beam was about 40 cm. Since the phase angle could be readily measured to within ± 1 degree, it was possible to measure velocity differences as small as 100 cm/sec. It is of interest that, although almost complete translational equilibration is achieved over most of the composition range, appreciable relaxation effects were observed when the beams consist predominantly of helium atoms.

In addition to the use of the TOF phase shift technique for high pressure molecular beam diagnostics, it should be valuable as a tool for sorting out cracking patterns in such diverse applications as organic analysis and high temperature vaporization studies. In organic analysis, a substance to be analyzed would be vaporized to form a conventional effusion beam. From the velocities of the various fragments the masses of the parent molecules can be inferred whether the parent peak appears or not. The determination of the velocities should also assist considerably in sorting out the contribution to the observed spectrum of different molecules in a mixture, particularly if some of the fragmentation patterns are unknown. An even more promising application for TOF methods in the analysis of mass spectra lies in the area of high temperature vaporization experiments. Here one is working with mixtures of vaporizing species whose fragmentation behavior is

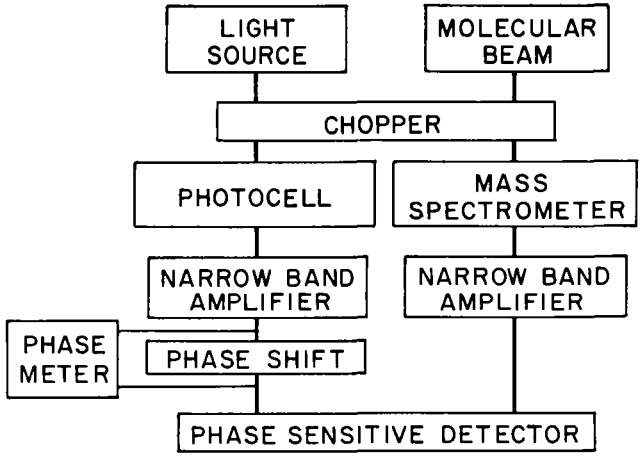

FIGURE 3

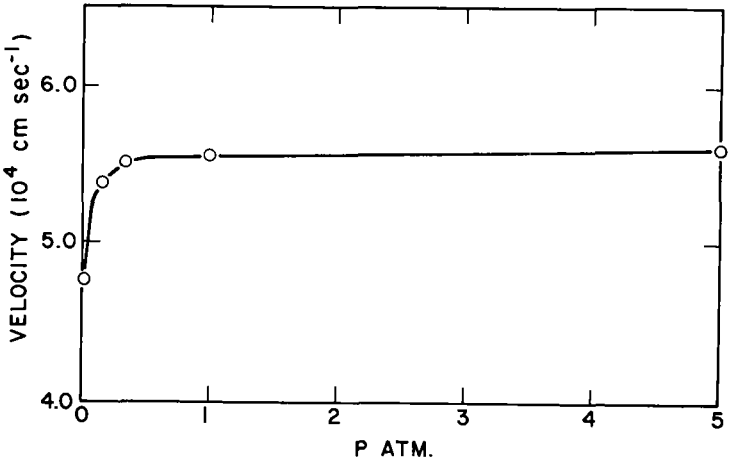

FIGURE 4

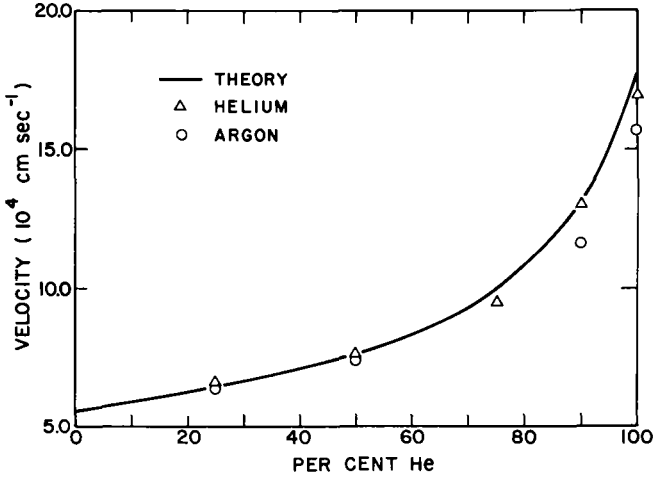

FIGURE 5

completely unknown. Frequently, these species are studied over temperature ranges in which their fragmentation patterns may change significantly. Even in the simplest cases it is often not clear from appearance potentials and thermochemical considerations whether an observed peak is a fragment or represents a second vaporizing species. This type of problem, as well as more complex problems of sorting out fragmentation effects, could often be resolved by velocity measurements.

COMPARISON OF A QUADRUPOLE MASS FILTER WITH A TOF MASS SPECTROMETER

The modulated, nozzle beam system with the Bendix TOF mass spectrometer as a detector presented an excellent opportunity for the comparison of the TOF with a quadrupole mass filter, which is an increasingly popular molecular beam detector. This comparison allows a rough determination of the variation of ion transmission of the quadrupole mass filter with mass and resolution. When an argon beam is formed from room temperature and a few atmospheres pressure in the nozzle beam system, the argon is partially condensed during the initial expansion, and numerous clusters of argon atoms are produced.[5] These can be ionized by electron impact, producing ions at 40 mass unit intervals. Consequently, this beam is a convenient, if not very portable, device for calibrating the mass scale of a spectrometer. It is also a convenient source for the calibration of the transmission of a mass spectrometer if the concentration of clusters and their ionization efficiencies are known. The modulation is a particularly significant feature since it allows the resolution of the quadrupole to be reduced until adjacent Ar clusters interfere.

We are currently undertaking such a comparison, with the axial beam ion source of an EAI quadrupole mass filter mounted in the crossed beam mode directly above the ion source of a Bendix TOF mass spectrometer. A "condensed" argon beam is passed simultaneously through the electron beams of the quadrupole and TOF mass spectrometers and ion intensities are measured simultaneously on the TOF mass spectrometer and the quadrupole mass filter. The resolution of the quadrupole is varied from about one to unit resolution or better for each peak from 40^+ to 480^+ . The Bendix TOF provides a reference spectrum of cluster concentration.

These results will be reported later after some apparent discrepancies, which have been attributed to the quadrupole rod alignment, have been resolved.

REFERENCES

1. Foner, S.N., and R.L. Hudson, J. Chem. Phys., 21, 1374 (1953).

2. Milne, T.A., and F.T. Greene, J. Chem. Phys., 44, 2444 (1966).

3. Studier, M., Rev. Sci. Instru., 34, 1367 (1963).

4. Greene, F.T., and T.A. Milne, Advances in Mass Spectrometry, Vol. 3, p. 841, The Institute of Petroleum, London (1966).

5. Anderson, J.B., R.P. Andres, and J.B. Fenn, Advances in Atomic and Molecular Physics, Vol. 1, p. 345, Academic Press, New York (1965).

6. Greene, F.T., and T.A. Milne, J. Chem. Phys., 39, 3150 (1963).

An information retrieval system for organic mass spectrometry

By Sixten Abrahamsson, Gunnar Häggström and Einar Stenhagen

Department of Medical Biochemistry
University of Göteborg, Sweden

Introduction

The large amount of mass spectral data available at present and the increased rate of production of such data require a computer storage and retrieval system for adequate use of the information. In connection with the installation of a digital computer at this Department we have undertaken to collect from different sources mass spectra of organic compounds and punch them on cards for storage on magnetic tape. So far it has been possible to include some 7000 spectra in the data file. Computer programmes have been written to allow efficient use of these data in organic mass spectrometry work.

Information stored

All m/e- and intensity values are stored for each spectrum (see Table 3) as well as the name of the sample, the molecular weight (MOLVIKT), the source and serial number of the spectrum (eg. API 512), the temperature of the ion source (TEMPJ) and inlet system (TEMPI), the electron energy (EV) and an instrument identification number. Due to limited information in our original data the molecular weight given is in many cases the mass number of the molecule-ion. It is planned, however, to add to the file exact masses (elemental composition) and a type classification for each compound. Special labels are given to peaks which arise from metastable and doubly charged ions, from impurities, and from rearrangements.

Programme system

The data file can, of course, be used in a number of ways. Any information in the spectra can be listed and sorted after various items, such as molecular weight (Table 1) and chemical name (Table 2). Several programmes for this purpose have been written but we shall describe in more detail only the routines for compound identification.

An efficient search programme must be able to handle instrument variations in the spectra and to find isotope labelled compounds. Moreover, if an identical spectrum to that under study cannot be found in the file, the programme should try to find similar ones. This flexibility has been accomplished in our system by extracting from the spectrum a key of a few lines and searching through the file considering this key alone. The search can thereby be performed at the full reading speed of the magnetic tape unit (in our case 12000 words/sec) which means that it takes about 5 minutes to sweep through 10000 spectra.

The key can be extracted from the spectrum in several ways. We have found it convenient to use the five strongest lines, but keys are also available on the tape using the five strongest weighted intensities (e.g. weighted $I = I \times m/e$) and the strongest lines in different m/e intervals of the spectrum. Keys are also provided using the five strongest weighted and unweighted intensities with $m/e > 50$. The user specifies the key he wants to use (K in Table 7). If a nonstandard key is desired the whole file must be copied.

For the search programme the user has to give two further parameters (D, N in Table 7). When comparing the key of the unknown spectrum with that of a file spectrum, lines are regarded as common to the two keys if their m/e differ by up to D units. If N such pairs are found, the spectrum is extracted from the file as a possible entry. If these parameters are given as 0 and 5 respectively only such spectra are accepted which contain the same key lines as the unknown one. The relative intensity of the key lines is immaterial. D = 1 could be specified to cover mono-deuterium labelled compounds.

The programme system now contains the major routines shown in Table 7. The user can write a short control paper tape specifying the routines he wants to use. (Standard tapes are also available). Table 6 shows the instructions on the control tape for the test illustrated in Tables 3 - 5. In this case two spectra are read (dimethyl malonate and testethane A) and printed (Table 3). If PLOT had been commanded the spectra would have been reproduced in the usual schematic form (Fig. 1). The file was then searched with D = 0 and N = 5 using the key with the 5 strongest lines. The

extracted spectra are shown in Table 4. Another search was then made with N = 4. In this case the extracted spectra were also compared in detail and sorted after the disagreement index (Table 5). In both cases there is a unique identification of dimethyl malonate. In the ethane case deuteroethene spectra are extracted as well as ethane ones. In the less rigorous search (Table 5) some other compounds have also been extracted but it is easily seen from the disagreement index and molecular weight which are the ethane analogues.

Another test is shown in Table 8. It is quite clear that the "unknown" spectrum is 2-methylnaphtalene. The list contains also several more or less related compounds. A second search was performed using the key of the 5 strongest weighted intensities. The resulting list was identical to that of Table 8 except for a few spectra.

Acknowledgements

Financial support has been obtained from the Wallenberg Foundation and the Swedish Technical Research Council. The punching of the data was made possible by generous help from the Swedish Office for Organization and Management (Kungl. Statskontoret).

Table 1

Index of spectra in the data file sorted after molecular weight.

184.000	S UNDECALACTONE	ARC	10	108
184.030	150 BUTYL IODIDE	ARC	35	28
184.030	N-BUTYL IODIDE	ARC	8	30
184.030	SEC. BUTYL IODIDE	ARC	31	28
184.030	TERT. BUTYL IODIDE	ARC	43	37
186.000	DI-N-HEXYL ETHER	MOR	72	98
186.000	1-FLUORO-2,4-DINITROBENSENE	MOR	153	108
186.000	HEPTYL ISOPUTYRATE	MOR	152	108
186.033	1-DODECANOL (GAS)	API	881	128
187.000	1,2,3,5,7-PENTAMETHYL INDOLE	ICI	22	120
187.000	1-N-BUTYL-3-METHYLINDOLE	ICI	23	119
187.880	1,2-DIBROMOETHANE(ETHYLENE BROMIDE)(GAS)	API	173	34
188.000	ETHYLENE DIBROMIDE	MOR	154	84
188.300	1-PHENYL-1-CYCLOHEXYLETHANE (GAS)	API	584	172
188.300	1-PHENYL-2-CYCLOHEXYLETHANE (GAS)	API	597	143
190.030	2-PHENYLOCTANE (GAS)	API	890	120
192.000	TETRAETHYL ORTHOCARBORATE	MOR	155	75
194.000	2-N-BUTYLDECALIN	KOP	25	132
194.000	2-T-BUTYLDECALIN	KOP	24	117
194.040	1,2-DICYCLOHEXYLETHANE (GAS)	API	754	80
194.040	1-CYCLOHEXYL-3-CYCLOPENTYLPROPANE (GAS)	API	757	83
194.040	1,1-DICYCLOHEXYLETHANE (GAS)	API	753	91
194.360	1-ETHYL-2-CYCLOHEXYLCYCLOHEXANE(LOW BOILING)	API	1673	139
194.360	1-ETHYL-2-CYCLOHEXYLCYCLOHEXANE(HIGH BOILING)	API	1674	133
194.400	1,2-DICYCLOHEXYLETHANE (GAS)	API	674	113
194.400	1,1-DICYCLOHEXYLETHANE (GAS)	API	599	108

Table 2

Index of spectra sorted in alphabetical order.

116.220	CYCLOHEXANETHIOL (GAS)	API	944	71
100.000	CYCLOHEXANOL	KOD	12	38
98.140	CYCLOHEXANONE (GAS)	API	449	73
98.000	CYCLOHEXENE OXIDE	ICI	4	69
114.000	CYCLOHEXENE SULFIDE	KOP	21	79
82.140	CYCLOHEXENE (GAS)	API	209	70
142.000	CYCLOHEXYL ACETATE	DOW	1179	92
154.000	CYCLOHEXYL ACRYLATE	DOW	2744	86
99.000	CYCLOHEXYL AMINE (AMINO HEXA HYDROBENZENE)	LRL	17	90
204.000	CYCLOHEXYL BENZOATE	DOW	2827	71
168.000	CYCLOHEXYL CROTONATE	DOW	4028	77
210.000	CYCLOHEXYL CYCLOHEXANECARBOXYLATE	DOW	2564	28
182.000	CYCLOHEXYL ETHER	DOW	1199	67
102.000	CYCLOHEXYL FLUORIDE	DOS	32	87
128.000	CYCLOHEXYL FORMATE	DOW	4130	60
176.000	CYCLOHEXYL PHENYL ETHER	DOW	1133	120
142.000	CYCLOHEXYLACETIC ACID	DOW	1763	96
160.250	CYCLOHEXYLBENZENE (GAS)	API	1294	112
166.310	CYCLOHEXYLCYCLOHEXANE (BICYCLOHEXYL)	API	1508	142
166.300	CYCLOHEXYLCYCLOHEXANE (GAS)	API	1288	70
112.210	CYCLOOCTANE (GAS)	API	842	74
104.140	CYCLOOCTATETRAENE (GAS)	API	690	83
70.130	CYCLOPENTANE(GAS)	API	116	50

Table 6

Control tape for test case illustrated by Tables 3-5.

```
READ, PRINT, KEYSEARCH (1,0,5), LIST, KEYSEARCH (1,0,4)
COMPARE, SORT (5), LIST, START.
```

Table 3

Print out after READ and PRINT for test case with two "unknown" compounds. NYCKEL is followed by the m/e values of the key lines.

```
2.UNKNOWN.SPECTRA                                        SIDA   1

MOLVIKT TITEL                                            BETECKN. ANT

132.000 DIMETYL MALONATE                                 ARC    3  84
 30.070 TESTETHANE A                                     XYZ 1234  20


DIMETYL MALONATE                                  MOLVIKT 132.000  ARC-0000  TEMPJ      TEMPI      FV       INSTR  V

                                                                   NYCKEL     15.0       59.0     101.0    29.0     42.0

   12.0   16   13.0   38   14.0  185   15.0 1000   16.0   16   17.0    5   18.0   17   19.0    1   22.0    1   24.0    2
   25.0    4   26.0   13   27.0   77   28.0   79   29.0  493   30.0   45   31.0   75   32.0   15   33.0    5   34.0    1
   35.0    1   36.0    1   37.0    1   38.0    1   39.0    3   40.0    8   41.0   68   42.0  470   43.0  248   44.0   29
   45.0  144   46.0    3   47.0    3   48.0    1   49.0    1   50.0    1   51.0    1   52.0    1   53.0    2   54.0    1
   55.0    4   56.0    3   57.0  236   58.0   52   59.0 1000   60.0   25   61.0    4   62.0    1   63.0    1   64.0    1

   65.0    1   66.0    5   69.0   92   70.0    7   71.0    2   72.0    5   73.0    5   74.0  419   75.0   15   76.0    2
   77.0    1   78.0    1   79.0    1   83.0    1   84.0    1   85.0    1   86.0    1   87.0    1   88.0    1   89.0    1
   90.0    1   91.0    3   92.0    1   99.0    2  100.0   37  101.0  919  102.0   43  103.0    7  104.0   18  105.0    3
  106.0    1  114.0    1  115.0    3  116.0    1


TESTETHANE A                                      MOLVIKT  30.070  XYZ-1234  TEMPJ 245  TEMPI      FV  70  INSTR 99

                                                                   NYCKEL     26.0       27.0     30.0     28.0     29.0

    1.0   21    2.0    2   12.0    4   13.0   10   13.5U    1   14.0   30   14.50    6   15.0   44   16.0M    1   24.0    5
   24.5M    1   25.0   35   25.5M    2   26.0  232   26.5M    3   27.0  332   28.0 1000   29.0  215   30.0M  262   31.00    6
```

Table 4

Result from KEYSEARCH. ANT gives the number of lines in the spectra. NR is the number of the unknown spectrum to which the extracted spectrum is similar. MRK shows the number of common key lines.

RESULT.AFTER.SEARCH.ALL.5.KEY.LINES.OF.UNKNOWN.PRESENT

MOLVIKT	TITEL	BETECKN.	ANT	NR	MRK
132.000	DIMETHYL MALONATE	ARC 3	84	1	5
30.070	ETHANE (GAS)	API 2	20	2	5
30.070	ETHANE(GAS)	API 111	19	2	5
30.060	1,1-DIDEUTEROETHENE (1,1-DIDEUTEROETHYLENE) (GAS)	API 1165	21	2	5
30.070	ETHANE(GAS)	API 61	13	2	5
30.060	1,CIS-2-DIDEUTEROETHENE(1,CIS-2-DIDEUTEROETHYLENE)	API 1166	17	2	5

Table 5

Result from KEYSEARCH and COMPARE. Spectra are sorted in order of increasing disagreement index (MRK).

RESULT.AFTER.COMPARE.SORTED.AFTER.DISAGREEMENT

MOLVIKT	TITEL	BETECKN.	ANT	NR	MRK
132.000	DIMETHYL MALONATE	ARC 3	84	1	0
30.070	ETHANE (GAS)	API 2	20	2	0
30.070	ETHANE(GAS)	API 111	19	2	1
58.000	TRI-METHYLENE OXIDE	ICI 1	39	2	20
30.060	1,TRANS-2-DIDEUTEROETHENE (GAS)	API 685	21	2	30
31.060	METHYLAMINE (GAS)	API 1123	8	2	32
30.060	1,1-DIDEUTEROETHENE (1,1-DIDEUTEROETHYLENE) (GAS)	API 1165	21	2	32
31.070	TRIDEUTEROETHENE (TRIDEUTEROETHYLENE) (GAS)	API 1167	22	2	36
58.080	PROPANAL (PROPIONALDEHYDE) (GAS)	API 428	26	2	36
29.060	MONODEUTEROETHENE (MONODEUTEROETHYLENE) (GAS)	API 1164	17	2	37
30.070	ETHANE(GAS)	API 61	13	2	37
30.060	1,CIS-2-DIDEUTEROETHENE(1,CIS-2-DIDEUTEROETHYLENE)	API 1166	17	2	39
58.080	PROPANAL (PROPIONALDEHYDE) (GAS)	API 374	37	2	40
75.070	NITROETHANE (GAS)	API 1138	49	2	44
58.080	1,2-EPOXYPROPANE (PROPYLENE OXIDE) (GAS)	API 768	41	2	46
28.050	ETHENE(ETHYLENE)(GAS)	API 65	11	2	50
57.000	GLYCOLONITRILE	DOT 21	48	2	55
64.000	ETHYL CHLORIDE	MOR 75	42	2	62

Table 7

Programmes (in Algol) for mass spectrometry information retrieval system.

	Programme	Function
1	READ	Reads and checks mass spectrum from punched cards or paper tape, normalizies the intensities and converts the spectrum into the correct magnetic tape format.
2	ADD	Adds spectrum to master file.
3	PRINT	Prints all information stored for any desired spectrum (see Table 3).
4	PLOT	Plots line diagram of spectrum (Fig. 1).
5	KEYSEARCH (K, D, N)	Searches through master file using key number K. For parameters D and N see text.
6	COMPARE	Compares in detail unknown spectrum with spectra extracted from master file by KEYSEARCH. A "disagreement index" (MRK in Table 5) is attached to each extracted spectrum which is proportional to the sum of the absolute values of the differences in intensities between the unknown and extracted spectrum. $\left(\sum_{m/e=1}^{M} \lvert I_1 - I_2 \rvert_{m/e}\right)$
7	LINESEARCH (P_1, R_i, P_{i+1} etc.)	Extracts from master file spectra with lines of $m/e = P_i$, P_{i+1} etc. of intensity greater than R_i, R_{i+1} etc. respectively.
8	SORT	Sorts spectra in order after item S (S can specify name, molecular weight, disagreement index etc.)
9	LIST	Lists the result of programmes 5 - 8 (see Table 4).

Table 8

Search through the data file with 2-methylnaphtalene as the unknown spectrum. The extracted spectra are sorted in order of increasing disagreement index.

```
RESULT.AFTER.COMPARE.AND.SORT

MOLVIKT TITEL                                          RETECKN. ANT  NR MRK

142.000 2-METHYLNAPTHALENE                             NOW 2579  92  1   0
142.190 2-METHYLNAPHTHALENE (GAS)                      API  891 114  1   1
142.190 2-METHYLNAPHTHALENE (GAS)                      API  855 126  1   2
142.200 2-METHYLNAPHTHALENE (GAS)                      API  894 120  1   2
142.190 2-METHYLNAPHTHALENE (GAS)                      API 1015 134  1   2
142.190 1-METHYLNAPHTHALENE (GAS)                      API  900 118  1   2
142.200 1-METHYLNAPHTHALENE (GAS)                      API  893 132  1   2
176.000 1-(CHLOROMETHYL) NAPHTALENE                    NOW 2897  58  1   5
142.000 1-METHYLINAPTHALENE                            NOW  352  52  1   8
170.000 PHENYL ETHER                                   NOW  779  82  1   9
186.000 LICORDACETIC ACID                              NOW 3399  72  1  11
142.190 1-METHYLNAPHTHALENE (GAS)                      API  487  41  1  11
158.000 4P(ROCIM,4X1,5,9-TRIOXAUNDECANE (+D)           ARC  105   7  1  12
184.270 2-N-BUTYLNAPHTHALENE (GAS)                     API 1016 163  1  13
142.000 6-CHLORO-O-CRESOL                              NOW 1049 111  1  13
154.000 1-ETHYLNAPHTHALENE                             NOW 4118 126  1  13
142.000 BROMO-1,2-DIFLUOROETHYLENE                     NOW 1211  66  1  13
184.280 2-N-BUTYLNAPHTHALENE                           API 1518 149  1  14
140.000 2-CHLORO-P-XYLENE                              NOW 2195  94  1  16
143.180 6-METHYLQUINOLINE                              API 1560 102  1  16
154.000 1-METHOXYNAPHTHALENE                           NOW 1447  98  1  16
140.000 X-CHLORO-O-XYLENE                              NOW 2764 108  1  16
184.000 6-CHLORO-O-TOLYL ACETATE                       NOW 3659  96  1  16
140.000 -DIFLUOROSTYRENE                               NOW 2203  85  1  16
140.000 4-CHLORO-P-XYLENE                              NOW 2823  92  1  17
142.000 IODOMETHANE                                    NOW  445  16  1  17
142.000 4-CHLORO-M-CRESOL                              NOW 4590 104  1  17
145.000 2,3-DIMETHYL INDOLE                            ICI   18  95  1  17
157.218 2,6-DIMETHYLQUINOLINE (GAS)                    API  831 168  1  17
140.000 O-CHLOROBENZALDEHYDE                           NOW 2855  88  1  17
124.000 1-ETHYL-4-FLUOROBENZENE                        NOW  461 118  1  17
141.950 IODOMETHANE (GAS)                              API  696  15  1  17
140.000 P-CHLOROBENZALDEHYDE                           NOW 4802  96  1  19
186.000 2-(4-CHLORO-2-METHYLPHENOXY)ETHANOL            NOW 5470 139  1  19
156.000 ((2-CHLOROPHENYL) ETHANOL                      NOW 1302 131  1  20
140.000 M-CHLOROBENZALDEHYDE                           NOW 4801 116  1  20
171.000 1,2,3,4-TETRAHYDROCARBAZOLE                    SHA   10 128  1  20
140.000 1-CHLORO-3-ETHYLBENZENE                        NOW 1792 119  1  21
142.000 4-CHLORO-O-CRESOL                              NOW 2088 123  1  21
155.000 2-(O-CHLOROPHENYL)ETHYLAMINE                   NOW  896 131  1  21
140.000 1-BROMO-P-CHLOROETHYLENE                       NOW  468   6  1  21
142.000 M-CHLOROBENZYL ALCOHOL                         NOW 3592 118  1  22
184.000 2-TERT-BUTYL-6-CHLOROPHENOL                    NOW 2327 153  1  22
142.000 1-CHLORO-2-BROMOETHANE                         NOW  464  78  1  24
176.000 4,6-DICHLORO-O-CRESOL                          NOW 3574 156  1  27
140.000 ORTHOCHLOROBENZALDEHYDE                        CCC   31 115  1  30
142.000 BROMOPENTAROMANE                               CCC   30 148  1  80
```

```
TESTETHANE A                                   MOLVIKT  30.070  XYZ-1234  TEMPJ 245  TEMPI      EV  70  INSTR 99
```

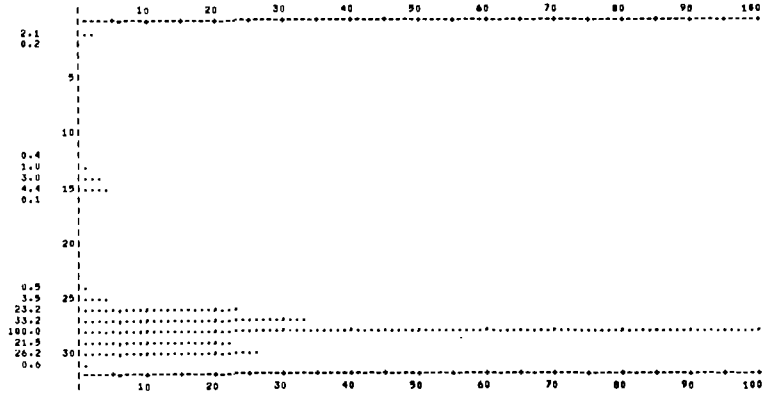

Fig. 1

Line diagram of mass spectrum produced by PLOT.

SIMPLIFIED UNITS AND EQUATIONS APPROPRIATE FOR USE WITH MASS SPECTROMETER CALCULATIONS

Wilson M. Brubaker
Bell & Howell Research Center
Pasadena, California

Abstract

Since the unit of mass used by mass spectrometrists is the atomic mass unit, it is expedient to use it as the basis for a simple, self-consistent set of familiar units to describe the motion of charged particles in electric and magnetic fields. If for mass, length, and time we use atomic mass unit, centimeter, and microsecond respectively, we can eliminate use of awkward factors and constants in the equations which describe the response of ions to accelerations. We define the electric field E in volts per centimeter, and the magnetic field B in 100 gauss units (centi-tesla). The electronic charge of 1.6×10^{-19} coulombs then becomes 0.965--which for most calculations may be considered as unity.

Using this simple set of units, equations for acceleration reduce to those of sophomore physics, without complicating conversion factors and constants. For instance, an ion which has been accelerated through a potential difference of V volts has a velocity given by the equation $V = (1/2)\ m\ v^2$, where m is in atomic mass units and v is in centimeters per microsecond. The angular frequency of an ion in an omegatron is $\omega = (B/m)$ radians per microsecond, where B is the magnetic field expressed in centi-teslas and m is the mass in atomic mass units. The number of cycles which occur while an ion traverses a quadrupole of length L centimeters, excited at a frequency of f megacycles, is $n = L \times (f/v)$, where v is the velocity of the incident ion in centimeters per microsecond. These few typical examples illustrate the simplicity of the equations of mass spectrometry when expressed in these units.

Introduction

As each branch of our technology has matured, a set of consistent, convenient units has emerged. It would seem that mass spectrometry has reached that stage of maturity which would entitle it to its own system of units. However, no self-consistent system has appeared. One of the most recent books on mass spectrometry uses ergs per esu for potentials, grams for ionic mass, and other awkward units.

This paper proposes the use of a self-consistent set of units which are of convenient size, thus eliminating the need for powers of ten in the usual calculations. Further, as an added bonus, the use of these units eliminates all constants except those of sophomore physics for the first order expressions for motion of ions in electric and magnetic fields. Most of these units are familiar ones.

In mass spectrometer theory the important quantity is acceleration. The ions are set into motion by their acceleration through potential differences. Further, mass separation is possible only because their accelerations in force fields are mass dependent. Said otherwise, their trajectories result from accelerations which are mass dependent.

In choosing the set of units for a specific application, it is desirable that the usual values of the parameters are expressed by numbers between 0.1 and 1,000. Potentials between 0.1 and 1,000 are usually expressed in volts. Millivolts is generally used for potentials less than 0.1 volts, and kilovolts is reserved for potentials in excess of 999 volts. The metric system terms deci, deka, and hekto are seldom used.

Consideration of Quantities Used in Mass Spectrometry

The usual quantities considered for a system of units are mass, length, and time. It is most obvious that mass spectroscopists don't measure ionic masses in either grams

or in kilograms. Since neither of these units is used in this field, there should be no objection to ignoring them in favor of the unit that is sometimes printed on mass scales of mass spectrometers, the atomic mass unit. Unfortunately, there is no comparable agreement on the appropriate unit to use for length. If the meter is used, many dimensions would turn out to be less than the 0.1 mentioned earlier. This is particularly true of the source and detector regions. Since the trend toward the use of metric units is so strong, the centimeter is certainly preferable to the inch!

This leaves the unit of time. In mass spectrometry, time is used to express the duration of the traversal of the instrument by the ion. Because of the very high velocity of the ions, the second is obviously an awkwardly large unit. The microsecond is more appropriate, as will be seen later.

Thus far it is established that from the standpoint of the size of the units, mass, length, and time are appropriately expressed in atomic mass units, centimeters, and microseconds, respectively. However, the results of these considerations alone are not sufficient to warrant the use of these units for mass spectrometry. Accordingly, in order to merit their serious consideration, these units must have additional advantages over others. These are found in the forms of the pertinent equations, as discussed below.

Mass Spectrometer Equations in the Proposed Units

The starting point for the development of the pertinent equations is chosen as the rationalized MKS system. All mass spectrometers work on physical principles which involve the kinematic accelerations of the ions. Thus, expressions for the mass of ions always appear as (M/e), never as M alone. M is in kilograms, e in coulombs. The atomic mass unit is defined as 1/12 the mass of carbon 12. Numerically, the ratio of M/e is equal to 1.035×10^{-8} m, where m is the mass of the ion in atomic mass units (amu).

The development of the transformation from the MKS system to the amu, cm, μsec system is readily followed by reference to Table I. Here the acceleration is expressed in three manners. First, the kinematic acceleration is given. This has the dimensions of MT^{-2}, as always. In the MKS system it is meters/second^2, as shown in line 1. Ions respond to applied forces which may be either electric or magnetic in origin. The dimensions of the acceleration are the same in each case, MT^{-2}.

In line 1 the quantities are presented in the conventional, MKS system. In line 2 mass has been changed to amu, and the appropriate numerical changes made. In line 3 meter is replaced by centimeter, and second by microsecond. Note the change this makes in the definition of the electric field. The kinematic acceleration is still in meters/second^2. In line 4 the kinematic acceleration is changed to cm/μsec^2. This removes all powers of ten from the acceleration in the electric field, but leaves 10^2 in the expression for the magnetic field acceleration. By reducing the size of the magnetic unit from tesla to centi-tesla, even this factor is eliminated. This is shown in line 5.

Application of the Proposed System of Units

The application of the proposed system of units is very direct and easy. The starting equation for the development of the equations of motion for the ions is Newton's second law: force equals mass times acceleration (F = ma).

The following steps illustrate the use of the new system:

1. Write the force equation as applicable to the specific problem in "sophomore physics" expressions.

2. Substitute 0.965 (or unity) for the electronic charge.

3. Express mass in amu.

4. Express length in cm.

TABLE I

UNITS

Line	Kinematic $\ddot{x}$	ACCELERATION in Electric Field E	ACCELERATION in Magnetic Field B	Electric Field E	Electron Charge e	Ionic Mass M, m	Magnetic Field B	Ionic Velocity v	System
1	meters/sec^2	$\frac{Ee}{M}$	$\frac{Bev}{M}$	$\frac{\text{Volts}}{\text{meter}}$	1.6×10^{-19} Coulombs	Kilo-grams	teslas $\left(\frac{\text{Webers}}{\text{meter}^2}\right)$	$\frac{\text{meters}}{\text{sec}}$	Meters, kilograms, seconds
2	meters/sec^2	$\frac{0.965\times10^8 E}{m}$	$\frac{0.965\times10^8 Bv}{m}$	$\frac{\text{Volts}}{\text{meter}}$	Unity	Atomic Mass Units	teslas	$\frac{\text{meters}}{\text{sec}}$	Meters, atomic mass units, sec
3	$10^{10}\ \frac{\text{cm}}{\mu\text{sec}^2}$	$\frac{0.965\times10^{10} E}{m}$	$\frac{0.965\times10^{12} Bv}{m}$	$\frac{\text{Volts}}{\text{cm}}$	Unity	amu	teslas	$\frac{\text{cms}}{\mu\text{sec}}$	cm, amu, μsec
4	$\frac{\text{cm}}{\mu\text{sec}^2}$	$\frac{0.965E}{m}$	$\frac{0.965\times10^2 Bv}{m}$	$\frac{\text{Volts}}{\text{cm}}$	Unity	amu	teslas	$\frac{\text{cms}}{\mu\text{sec}}$	cm, amu, μsec
5	$\frac{\text{cm}}{\mu\text{sec}^2}$	$\frac{0.965E}{m}$	$\frac{0.965Bv}{m}$	$\frac{\text{Volts}}{\text{cm}}$	Unity	amu	centi-teslas (or 100 gauss units)	$\frac{\text{cms}}{\mu\text{sec}}$	cm, amu, μsec, (B in centi-teslas or 100 gauss units)

5. Express time in microseconds.

6. Express electric field in volts/cm.

7. Express magnetic field in centi-teslas (100 gauss units).

In the above set of rules, only one new unit is introduced, centi-tesla. But as a result, the force equations all appear with no awkward powers of ten. For most calculations, the 3.5% error introduced by neglecting the 0.965 factor is of negligible importance. In these instances the equations of elementary physics are used directly, with no factors of any kind to be remembered.

Examples

To illustrate the effectiveness of the proposed units, they will be used to calculate some of the more familiar expressions used in mass spectrometry. First, consider the radius of curvature of an ion path in a magnetic field. The basic equations used to calculate the radius are the centripital force and the conservation of energy. The force equation yields:

$$mv^2/r = Bev \tag{1}$$

and the energy equation states:

$$(1/2)\ mv^2 = Ve \tag{2}$$

where V is the potential difference through which the ion has been accelerated. Eliminating v, and replacing e by 0.965,

$$r = 1.018(1/B)(2Vm)^{1/2} \tag{3}$$

In this equation, r is in cm, B in centi-teslas (100 gauss units), V in volts, and m in amu.

Contrast Equation (3) to one found in a book entitled Introduction to Mass Spectrometry and Its Applications, first published in 1965,

$$r = (c/B)(2Vm/e)^{1/2}. \tag{4}$$

At first glance these equations appear quite similar. But consider the units used in Equation (4). c is the velocity of light in cm/sec, B is in gauss, V in ergs/esu, m in grams, and e in electrostatic units! Certainly these are not quantities for which many people know the conversion factors required to convert to ordinary volts, atomic mass units, etc.!

Equation (1) applies also to the ion spinning in an omegatron. Noting simply that $\omega = v/r$, and replacing e by 0.965,

$$\omega = 0.965B/m. \tag{5}$$

Here ω is in radians per microsecond, or $2\pi f$ where f is the excitation frequency in megacycles.

Summary

Through the use of the proposed set of units the equations of motion of charged particles in electric and magnetic fields are reduced to those of elementary physics. The units for the various quantities are of appropriate and convenient size, ranging from 0.1 to 1,000 in all but a few instances. The units are all familiar ones, with the sole exception of the magnetic field strength. Even here the new unit differs from the more familiar ones by factors of ten, with no additional coefficients.

Theoretical Aspects of a Momentum Focusing Ion Optic System

W. S. Updegrove
Automatic Welding Company
Tulsa, Oklahoma

Abstract

The theoretical aspects of a first order momentum focusing ion optic system are reviewed to show the applicability of this theory in the modern design of mass spectrometers. The graphical methods and the analytical methods for determining ion optic parameters are reviewed. These calculations, and the resulting data, are compared to an actual system to show sources of error. The phenomena relating resolution and dispersion to mass spectrometer design are analyzed considering the effects of the aberrations. An effort is made to look at all the actual factors that contribute to the shape of the indicated mass spectrometer peak. Each of ten aberrations are reviewed individually. Conclusions as to the applicability of this theory to actual system construction are drawn.

MATTAUCH-HERZOG TYPE MASS SPECTROGRAPH
WITH TWO-STAGE ELECTROSTATIC FIELD

Isao Takeshita
Matsushita Electric Industrial Co., Ltd.
Kadoma, Osaka, Japan

A Mattauch-Herzog type mass spectrograph is unique in that it is double-focusing for all masses along a straight line. Today this type of instrument combined with a spark ion source is widely used for the chemical analysis of solid material. But this instrument has one disadvantage. It is difficult to find an available slit in order to control the velocity spread (β) regardless of the beam divergence (α). Even when the energy stop is infinitesimally narrow, the ion beam enters the magnetic field having a still wide energy spread.

If we can make a Mattauch-Herzog type mass spectrograph by using two cylindrical electrostatic fields followed by a homogeneous magnetic field, and in addition if we can get the real image of ion source between two electrostatic fields, the energy slit at the position of real image can control β independently of beam divergence α, in a similiar way to the Bainbridge-Jordan type instrument.

Fig. 1 shows the schematic diagram of the new optical system. E and F are the first and the second electrostatic fields and H is the homogeneous magnetic field and S_1 is the source slit and S_2 is the energy slit.

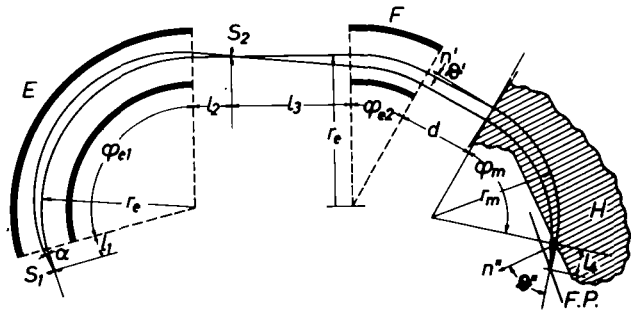

Fig. 1

From a practical view point, the electrostatic fields of this paper is the cylindrical field having an equal radius of center beam. Then we can get the following equations.

$$\frac{l_1}{r_e} = \frac{\frac{1}{\sqrt{2}} D_3 \cos\varphi_1 + \sin\varphi_2 \{1-(1\mp1)\cos\varphi_1\}}{\{D_3 - (1\mp1)\, 2\sin\varphi_2\} \sin\varphi_1} \qquad 1)$$

$$\frac{l_2}{r_e} = \frac{\frac{D_3}{2} - \frac{1}{\sqrt{2}}\sin\varphi_2 (1\mp1-\cos\varphi_1)}{\sin\varphi_1 \cdot \sin\varphi_2} \qquad 2)$$

$$\frac{l_3}{r_e} = \frac{1}{\sqrt{2}} \cot\varphi_2 \qquad 3)$$

$$l_4/r_m = \sin\varphi_m \frac{D_3 - \tan\varphi_m}{D_3} \qquad 4)$$

$$D_3 = \sin\varphi_m + (1-\cos\varphi_m)\tan\theta' \qquad 5)$$

$$\varphi_1 = \sqrt{2}\,\varphi_{e_1} \qquad \varphi_2 = \sqrt{2}\,\varphi_{e_2} \qquad 6)$$

The upper sign is for deflections in the two electrostatic fields in the same direction and the lower sign for opposite direction. D_3 is a paprameter which only depend on the geometry of magnetic field shown in equation 5.

Fig. 2 shows the possible combination of φ_1 and φ_2. The possible area is white. In this white area l_1, l_2 and l_3 are all positive. The left side of this figure shows the case where the deflections in the electrostatic fields are in the same direction and the right side of this slide shows the case where the deflections in opposite direction.

The resolving power (R) of the new Mattauch-Herzog type mass spectrograph is equal to those of the usual Mattauch type instruments when the deflections in the electrostatic fields are in the same direction. In the case of the opposite deflections, however, the resolving power is given as shown in Fig. 3. The left side of this slide shows the change in resolving power as a function of φ_2, and the regions 1, 2, 3 correspond to the regions 1, 2, 3 of the right figure. We can find from this figure that the resolving power in region 1 and region 2 possibly increases.

Now we only consider the case where the deflections in the electrostatic fields are in the same direction. For this case we will check the second-order aberration coefficients. Previous study has corrected the image defects in connection with only one mass. However the mass spectrograph for chemical analysis of solid material, needs the small image defects over a wide mass range. Therefore, we have studied the special configuration in order to correct the individual second-order aberration coefficient for all masses.

The first problem is that we make the second-order angular aberration to be zero for all masses. We can get the solution if D_3 is smaller than $6/\sqrt{34}$.

We can calculate the design parameters numerically. The table 1 shows the several favourable examples. The configuration is shown schematically on this slide. There are two type of solution, one is the case where the deflections in the magnetic field has the same direction as the two-stage electrostatic field. And the other is the case where two deflections have the opposite directions. The same direction is more preferable if we consider any other coefficients of aberration. By using these instruments we can make the correction of $\alpha\beta$ and β^2 aberration at one masses as well as the correction of the second-order angular aberration for all masses. T_{18} is a limitting value of $\alpha\beta$ aberration and T_{19} is a limitting value of β^2 aberration when r_m is infinity.

Fig. 4 shows the calculated image defects of the most preferable example. The total image defects are shown as a function of r_m/r_{mo}. In connection with the particular ion beam radius having r_{mo}, we can correct three image defects at the same time. The total image defects of the usual Mattauch-Herzog type instruments and Hintenberger's X-2* are shown in order to compare with the present data. We made the calculation under the condition $\alpha o = \beta o = 1$. The beam in this rectungular area on the α-β plane can enter the magnetic field in the present case, but with the conventional instrument the allowable area shows parallelogram. This figure shows that the image defect of the present instrument is considerably small.

****

* X-2 is the abbreviation of No.2 in Table X which appeared in Advances in Mass Spectrometry Vol.1

Especially image defect becomes smaller and smaller when the energy slit is narrowed, on the other hand the image defect of the usual instruments tends to the finite value even when the energy stop is narrowed infinitesimally.

The second problem is to make the mixed angular and velocity aberration zero for all masses. Table 2 shows the design parameters of the typical examples and the schematic diagram of configurations we are now interested in. In the some of the instruments in this table, the total image defects are considerably small and approximately constant.

The third problem is that we make the second-order velocity aberration zero for all masses. Table 3 shows the design parameters of the typical example and the schematic diagram of configuration we are now interested in. You can see in this slide that φ_1 and φ_m of these solution is small and the total ion path becomes long and the other coefficients of the second-order aberration are not small. T_{16} is a limitting value of α_2 aberration when r_m is infinity. But these instruments are useful, when the ion beam has large energy spread something like a spark ion source.

In order to improve the image defects of the double-focusing mass spectrograph, usually the curvature of entrance boundary of magnetic field is introduced. This method, however, correct the image defects only at one mass. Substituting a two-stage electrostatic field for usual single one, we can improve the image defects over a wide mass range as stated above.

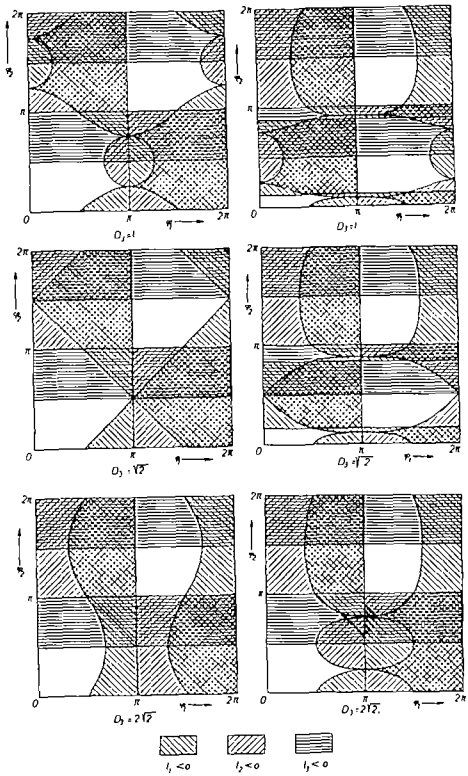

Fig. 2

Fig. 3

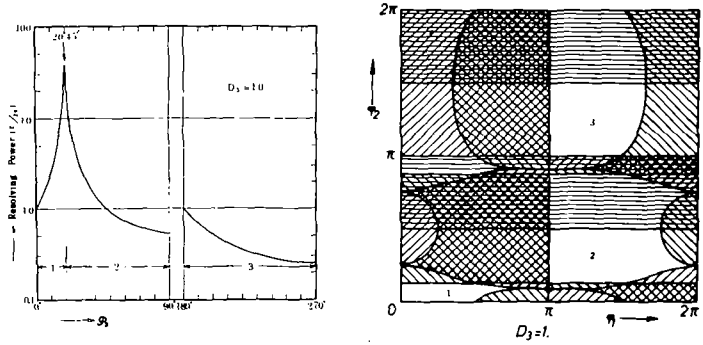

$$R=\frac{r_s}{2s}\left|\frac{D_s}{2\sqrt{2}\,\sin\Re-D_s}\right|$$

c

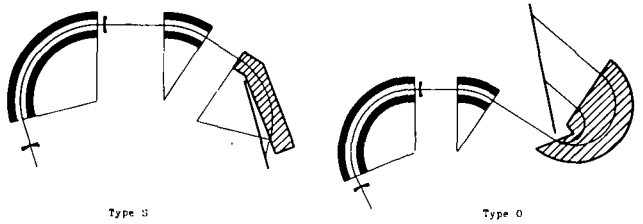

No.	D_3	φ_1	θ'	θ''	φ_2	φ_3	l_1/r_e	l_2/r_e	l_3/r_e	l_4/r_m	r_{mo}/r_e	d/r_e	T_{18}	T_{19}	Type
1	1.029	74°24'	5°09'	-52°48'	127°17'	33°01'	0	0	0.666	0.253	0.272	0.473	1.274	-1.571	S
2	1.00	73°08'	3°28'	-53°26'	112°49'	33°	0.186	0.0711	0.667	0.247	0.244	0.587	1.429	-2.229	S
3	0.943	70°32'	0	-54°44'	104°34'	33°30'	0.342	0.0787	0.772	0.236	0.252	0.527	1.402	-2.432	S
4	0.8	63°16'	-9°37'	-58°22'	94°02'	35°21'	0.650	0.0546	0.593	0.205	0.309	0.232	1.207	-2.167	S
5	0.6	51°01'	-25°33'	-64°29'	74°32'	36°	1.147	0.206	0.575	0.159	0.403	0.090	1.063	-1.616	S
6	1.00	163°05'	-34°15'	-8°27'	112°49'	33°	0.186	0.0711	0.667	2.449	0.292	1.183	3.938	-3.800	O
7	0.9	164°29'	-33°37'	-7°45'	103°43'	34°18'	0.439	0.0180	0.626	2.239	0.327	1.047	3.815	-4.648	O

Table 1 Examples of Mass Spectrographs with corrected α^2 image defect for all masses

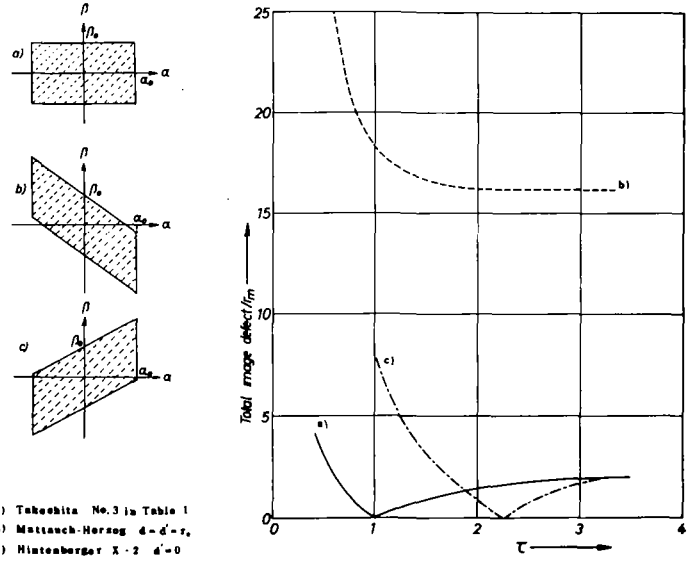

a) Takeshita No. 3 in Table 1
b) Mattauch-Herzog $d = d' = r_e$
c) Hintenberger X · 2 $d' = 0$

Fig. 4

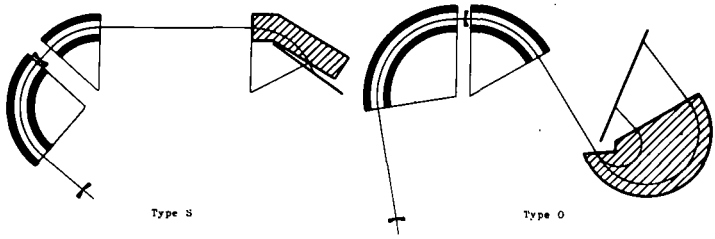

No.	D_3	$\mathcal{G}_m$	θ'	θ''	$\mathcal{G}_n$	$\mathcal{G}_s$	l_1/r_e	l_2/r_e	l_3/r_e	l_4/r_m	r_{mo}/r_e	d/r_e	$\hat{T}_{16}$	$\hat{T}_{19}$	Type
1	1.5	85°13'	28°46'	-47°23'	91°55'	62°27'	0.277	0.386	0.021	0.384		1.198	0.939	-2.472	S
2	0.9	64°14'	-3'	-57°53'	91°55'	49°14'	0.766	0.033	0.262	0.273		2.281	0.692	-1.524	S
3	0.7	53°44'	-14°35'	-63° 8'	84°51'	47° 8'	1.106	0.032	0.305	0.223		3.081	0.662	-1.137	S
4	1.2	187° 1'	-28°25'	3°30'	99° 0'	59°34'	0.447	0.095	0.071	1.538	0.288	1.443	1.945	-3.464	O
5	1.0	195°36'	-20°25'	7°48'	91°55'	50°58'	0.649	0.093	0.229	1.695	0.314	2.034	2.388	-4.283	O

Table 2 Examples of Mass Spectrographs with corrected $\alpha\beta$ image defect for all masses

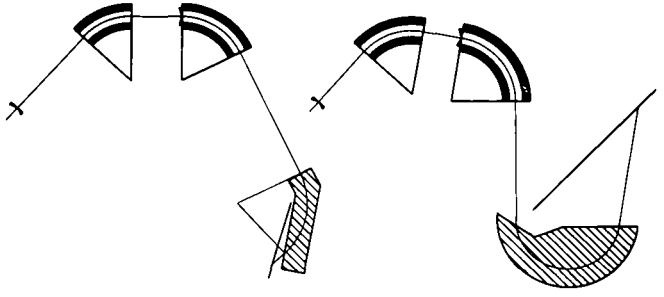

No.	D_3	$\mathcal{G}_m$	θ'	θ''	e1	e2	l_1/r_e	l_2/r_e	l_3/r_e	l_4/r_m	d/r_e	$\hat{T}_{16}$	$\hat{T}_{18}$	Type
1	0.9	64°14'	-3'	-57°53'	48°18'	63°38'	1.476	0.765	0	0.273	2.143	-4.15	4.55	S
2	0.8	59°15'	-6°56'	-60°22'	49°49'	63°38'	1.578	0.676	0	0.249	2.427	-4.01	4.09	S
3	0.7	53°44'	-14°35'	-63° 8'	51°13'	63°38'	1.721	0.591	0	0.223	2.790	-3.85	3.62	S
4	1.0	163° 5'	-34°15'	- 8°27'	57°38'	63°38'	1.116	0.611	0	2.449	1.989	-8.06	8.92	O

Table 3 Examples of Mass Spectrographs with corrected β^2 image defect for all masses.

PRECISE MASS DETERMINATIONS WITH A MEDIUM RESOLUTION MASS SPECTROMETER

Harmon W. Brown and Robert C. Jones
Analytical Instrument Division
Varian Associates, Palo Alto, California 94303

In the past few years high resolution mass spectroscopy has become an extremely powerful and important tool in the determination of organic molecular structure. The technique is even more elegant when a high resolution mass spectrometer is coupled to a large digital computer as demonstrated by Professor K. Biemann[1] and others. The cost of these instruments is so large as to be prohibitive for many laboratories, yet the chemists yearn to take advantage of the information contained in a precise mass measurement. We wish to point out that very often useful measurements of this sort can be made with an instrument with a resolving power of a few thousand. Indeed, Aston[2] made measurements to an accuracy of 1 part in 10,000 with a resolving power of about 600. Presently, measurements are being made to an accuracy of about 1 ppm on instruments having a resolving power of approximately 20,000, so it should be possible to make measurements to 10 ppm (corresponding to 5 millimass units at mass 500) at a resolving power of 2,000.

REQUIREMENTS

A number of requirements must be met if one chooses to make a precise mass determination. First, one must select mass peaks that consist only of a single species. The molecular ion peak is a logical choice, but the empirical formula of the molecular ion can often be deduced by measurement of the M + 1 peak (due to naturally abundant ^{13}C) or the M - 1 peak (due to loss of a hydrogen atom) or perhaps the M - 18 peak (due to loss of a molecule of water). Unresolved mass doublets can often be detected by an increased line width, and it is usually not possible to make precise measurements on such peaks that are meaningful. Additionally, the experiment requires that one measure the position of the mass peak to 1/50 of a line width, and it is desirable to have a signal-to-noise ratio of about 50 or more. The peak shape must be reproducible, and a triangular or gaussian peak shape facilitates location of the peak center.

It is obvious that the electronic parameters that effect the peak position must be accurately controlled. In the M-66 Cycloidal Mass Spectrometer, mass depends linearly upon the electric field strength so this must vary less than 10 ppm during the course of a measurement, and mass depends quadratically on the magnetic field strength so this must be controlled to 5 ppm or better in order to obtain the desired precision in the mass measurement.

Another important criterion is that the mass scale must be scanned in an accurately known fashion. In the M-66 the mass scale is linear which makes interpolation and extrapolation straightforward. The equation which relates the mass peaks brought to focus at the detector is:

$$\frac{M}{e} = \frac{kFH^2}{E}$$

Since the focal distance F and the electric field E remain constant, mass is simply proportional to the square of the magnetic field. A linear mass scale is accomplished by utilization of the Hall effect which is described by:

$$V_{out} = k' I_{in} H$$

A Hall crystal is basically a multiplying device that provides a voltage proportional to the product of the input current and the magnetic field strength. It is possible to use two Hall devices in series to produce a voltage proportional to the square of the magnetic field and thus also proportional to the mass (Fig. 1). This system allows an accurate, linear mass scan. However, in a precise mass determination non-linearities in recorder X-axis potentiometers are in the order of 0.1% (1/1000) so that if one wishes to make mass measurements to 1 part in 100,000, the reference peak should be within 1% of the unknown (for example, within 5 mass units at mass 500). This imposes a limit on reference compounds that is sometimes bothersome. It is often possible to use perfluorokerosene or some other fluorinated compound. Alternatively one can consult a tabulation of mass spectra to locate a suitable reference peak.

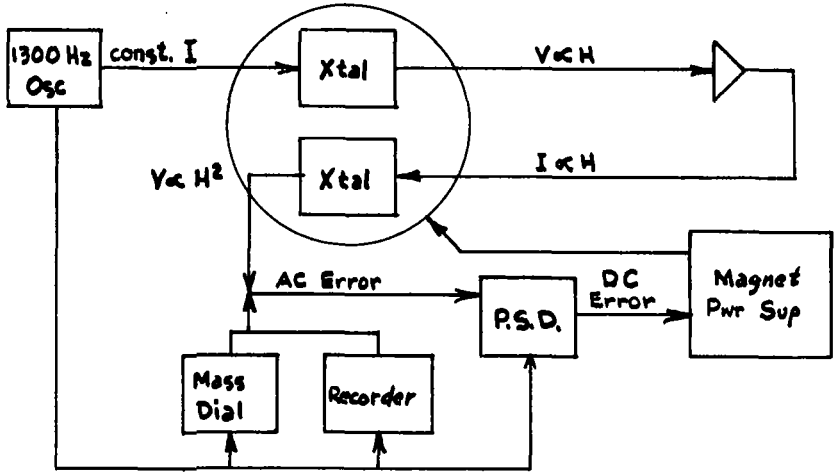

Figure 1

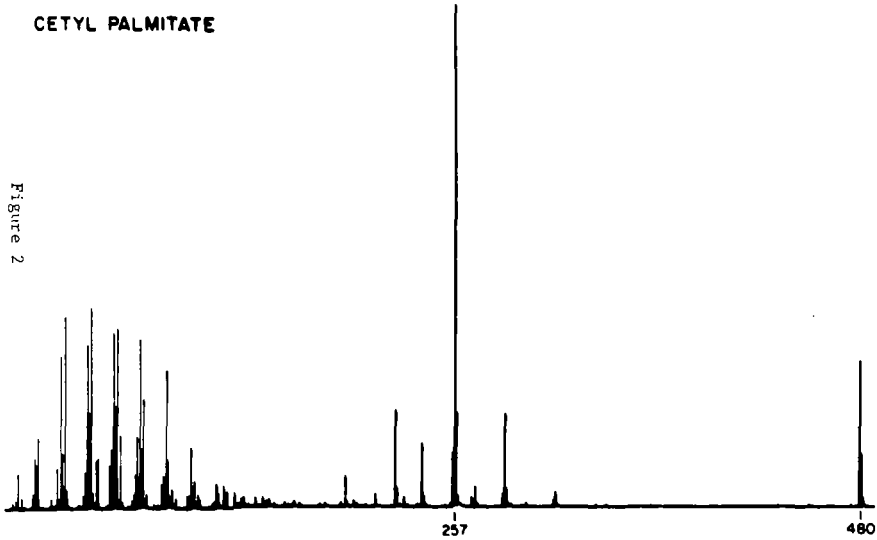

Figure 2

EXAMPLES

Figure 2 shows the spectrum of cetyl palmitate (this is not a replotted spectrum). Figure 3 shows the molecular ion region of cetyl palmitate to which perfluorokerosene was added as reference. The $C_{10}F_{19}$ peak(R) has a mass of 480.970, and the separation between the molecular ion peak(M) and the M + 1 peak is taken to be the difference between carbon 12 and carbon 13 isotopes which is 1.003 a.m.u. Then in order to determine the mass of the molecular ion, one must *locate the center of each peak and measure with a ruler the separation* between M and M + 1 and between M and R. Since the mass scale is linear, the separation in mass units is proportional to the separation in millimeters. This leads to a value of 480.493 compared to the literature value of 380.491. We have employed two methods to locate peak centers in these experiments. The first is simply the "eyeball" method which is fast and usually adequate. We have also used the method of bisecting the peak width at various amplitudes (perhaps at 40%, 60% and 80% of full height) and then connecting the bisecting points with a vertical line.

The next example is that of a compound with a molecular ion at mass 245, an M + 1 peak which we assume to be due to naturally abundant carbon 13, and an M - 1 peak which must be due to the loss of a single hydrogen. The reference compound chosen was dichlorohexafluorocyclopentene ($C_5F_6Cl_2$) which has peaks at 244, 246 and 248. We performed the precise mass determination in two ways; first, we used M, M + 1, and the 246 reference peak (Fig. 4) and second, we used M, M - 1, and the 244 reference peak (Fig. 5). From a series of measurements we obtained 245.2543 a.m.u., whereas the literature value for the compound ($C_{16}H_{23}NO$) is 245.2564.

The next example (Fig. 6) is desosamine with a molecular ion at mass 175 and isotope peak (due to carbon 13) at 176. Bromoform was used as reference which has a strong peak at mass 175 due to $CH^{81}Br_2$. Using the method described above we measured 175.1759 compared with a literature value of 175.1768 for $C_8H_{17}NO_3$.

The last example is an alkaloid with a molecular weight of 458. The upper part of Fig. 7 shows the spectrum of this compound having a rather weak molecular ion, but an intense fragment peak at mass 440 which is likely to be due to loss of a molecule of water. The bottom trace in Fig. 7 shows the region about mass 440 with perfluorokerosene added which gives a reference peak at mass 443. The trace above shows a further expanded spectrum indicating the isotope peaks at 441 and 442 (related to the fragment peak at mass 440 and referred to as F + 1 and F + 2) and the PFK peak at 443. Figure 8 illustrates a series of measurements on this peak giving the mass difference between the F + 2 and the reference. These data lead to a value of 440.276 for the M - 18 peak, and to this we must add the precise mass of H_2O to get a value for the molecular ion. We have no knowledge of the correct empirical formula and hence, the correct precise mass of this compound. However, it does serve to illustrate how one can arrive at the empirical formula for the molecular ion even though it may not be convenient to measure this peak.

We have also done some experiments using electric field sweeps at constant magnetic field. The preliminary results indicate that the same order of precision is obtainable but also it is possible to have the reference peak much further away from the unknown.

CONCLUSION

We have found that it is possible to make precise mass measurements to an accuracy of 10 ppm using a medium resolution mass spectrometer. The primary disadvantage of the method is that it requires somewhat more operator time than the high resolution mass spectrometer--digital computer combination, but the method has the decided advantage of using a much less expensive instrument.

REFERENCES

1. K. Biemann and P. V. Fennessey, ASTM Conference on Mass Spectrometry and Allied Topics, Dallas, 1966.

2. F. W. Aston, Roy. Soc. Proc. 115, 487 (1927).

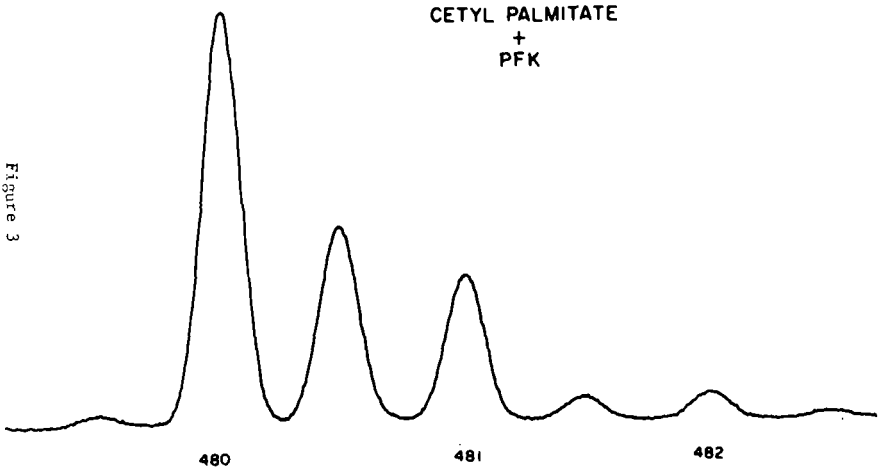

Figure 3

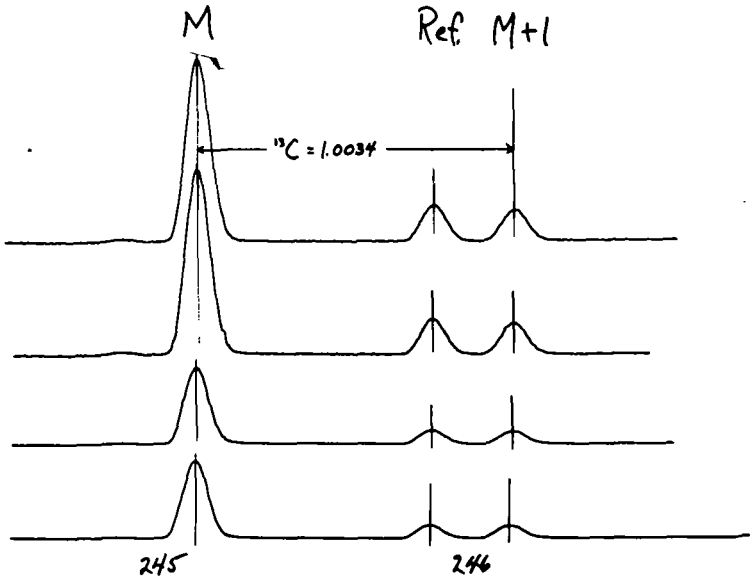

Figure 4

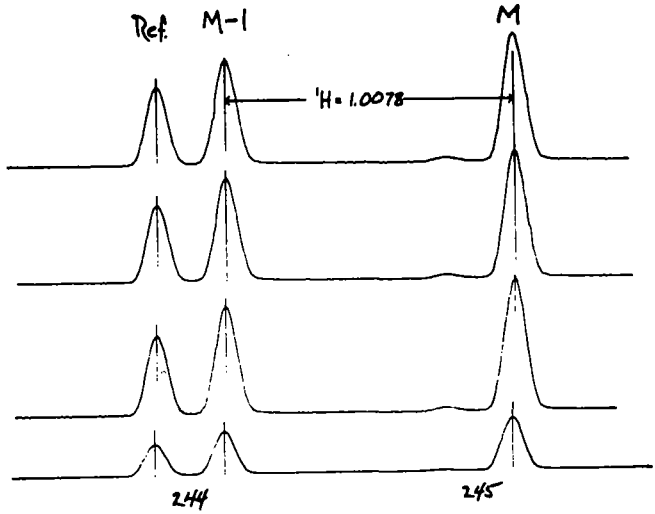

Figure 5

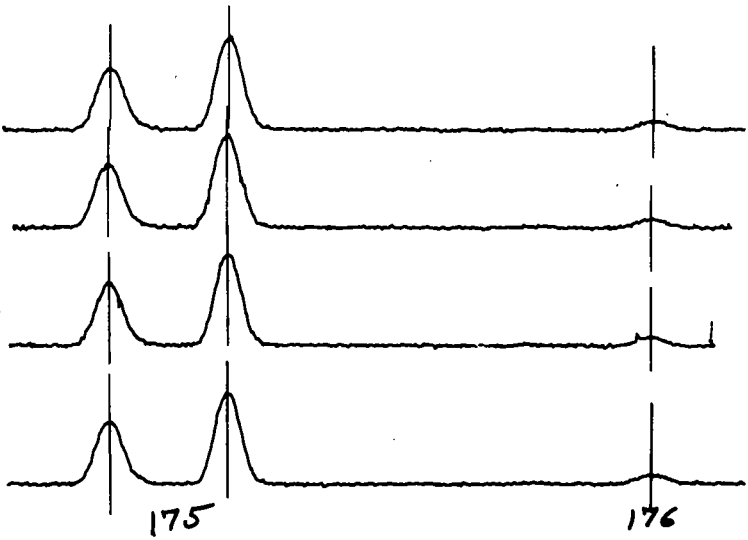

Figure 6

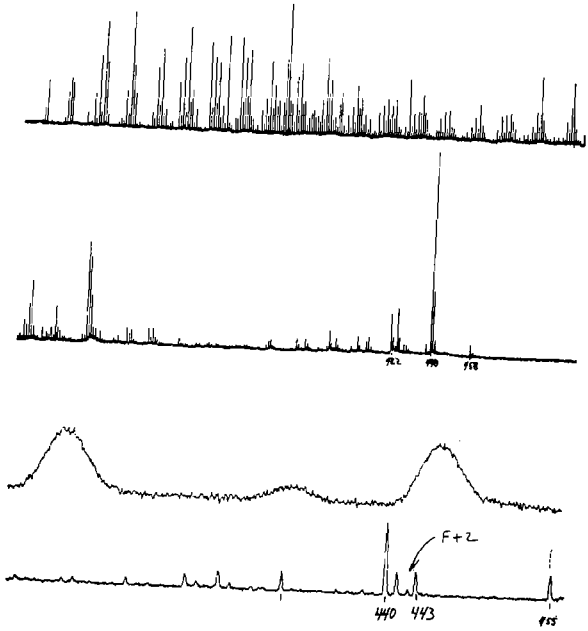

Figure 7

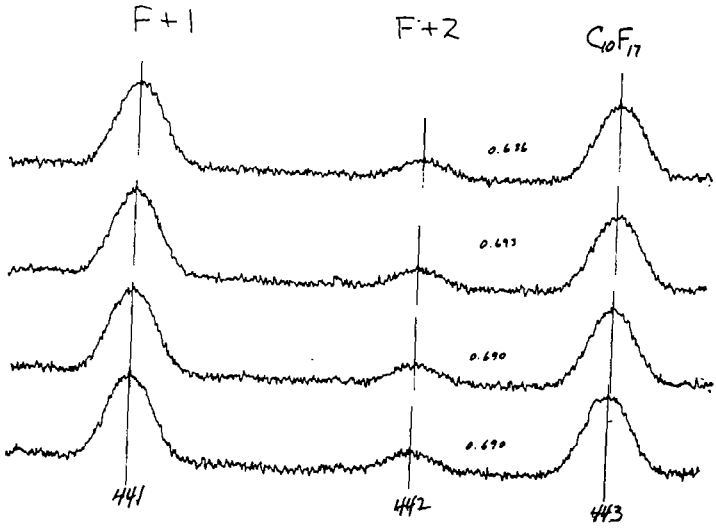

Figure 8

THE EFFECTS OF INHOMOGENEOUS FIELDS IN A CYCLOIDAL MASS SPECTROMETER

H. Benz and Harmon W. Brown
Analytical Instrument Division
Varian Associates, Palo Alto, California 94303

INTRODUCTION

The work to be described represents a general consideration of the effects of inhomogeneous fields in any cycloidal mass spectrometer.

It is well known that a cycloidal mass spectrometer is double focusing only in the case of homogeneous magnetic and electric fields. Robinson[1] has described the effects of first order gradients on focusing. He showed that linear terms in the magnetic and electric field give rise only to a shift without a significant deterioration of the focal point. We have evaluated the effects of higher order field inhomogeneities by means of a numerical calculation of the ion trajectories.

I. MAGNETIC FIELD

The magnetic field is assumed to be axially symmetric with a symmetry plane perpendicular to the axis. The magnetic potential Ω, which has to be a solution of the Laplace equation, can be expanded in spherical harmonics. Due to the assumed symmetry all even order spherical harmonics vanish. The expansion is truncated after the first three odd order terms:

$$\Omega = \sum_n C_n \cdot r^n \cdot P_n (\cos \vartheta) \qquad n = 3,5,7$$

with r = radius

P_n = spherical harmonic

C_n = constant

In order to get the magnetic field components one has to take the partial derivatives of the magnetic potential Ω. The three expansion coefficients have been evaluated by means of a comparison with an experimental field plot of a prototype Varian M-66 mass spectrometer. In Fig. 1 both the experimental field plot (solid line) and the calculated field (crosses) are represented. Three points, indicated by arrows have been used for the fit. One has to bear in mind, that according to the assumed symmetry no linear terms occur.

1. Angular Dependence

Ion trajectories have been calculated for a mass of 200 a.m.u. as a function at the injection angle. The electric field has been assumed to be homogeneous. The trajectories near the exit slit are shown in Fig. 2. It turns out that we get both a shift and a deterioration at the focal point. The new focal line is almost parallel to the line which connects entrance and exit slit. The effect of an angular spread is small for small angles ($\pm 2^o$). In order to calculate the line shape, one is forced to know the angular spread of the ion source. For the following calculations, a Gaussian angular distribution is assumed with a width in half height of $\pm 5^o$. With this angular distribution one can calculate the intensity distribution of ions which is identical with the line shape one would obtain by using an infinite small detector slit.

The line shape for a finite slit can be obtained by calculating the *convolution integral of the intensity distribution with a combined unit-step function* which represents the detector slit.

Figure 3 shows the intensity distribution of the ions in arbitrary units for three different slit positions, which are indicated in Fig. 2 by arrows. Fig. 4 is the same for a slit width of 1 mil. One can see that the place of the detector slit has a considerable influence on the resolution as well as on the sensitivity. But even with the optimum position of the slit one cannot get narrower lines than about 0.05 a.m.u. which corresponds to a resolution of 4000.

In the case of homogeneous fields no force component acts in the direction perpendicular to the cycloidal motion. This is no longer true in the presence of an inhomogeneous magnetic field. Fig. 5 shows the decrease in focal length as a function of entrace angle (-3° - $+3^o$) in the Z direction (parallel to the magnetic field).

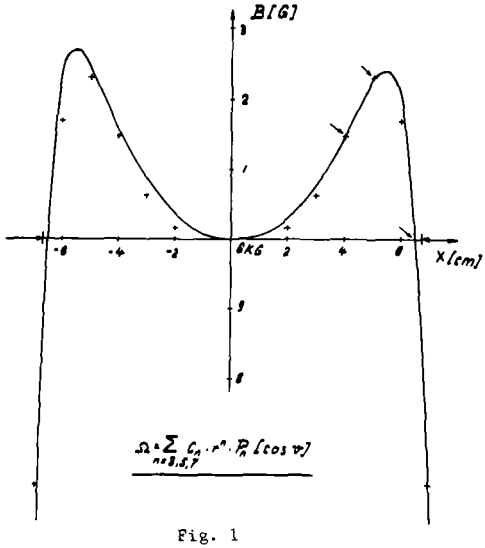

Fig. 1

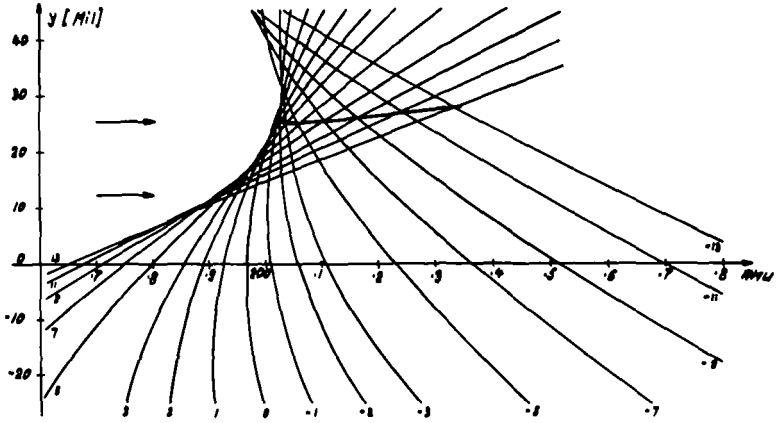

Fig. 2

It can easily be seen that a small focusing effect occurs. On the other hand, ions will intersect the focal plane no longer in a straight line. Therefore, one has to take care of the slit length in high resolution instruments.

2. Energy Dependence

For an ion beam which enters parallel to the electric field, the trajectories have been calculated as a function of the ion energy. The result is shown in Fig. 6. One can see that the effects of an inhomogeneous magnetic field on the focal property of an ion beam are in the same order of magnitude for both the angular and the energy spread.

3. Position of the Orbit in the Magnetic Field

The trajectories have been evaluated for various positions of the analyzer in the magnetic field. It turns out that small displacements (less than 1/4 inch) have negligible influence on the focal property at the ion beam.

II. ELECTRIC FIELD

The electric field is usually generated by a number of plates with different potentials. According to the experimental setup, the electric field is assumed to have a sinesoidal perturbation.

The relative amplitude of the perturbing electric field in the center plane between the plates has been figured out to be less than 0.02%. With this value the trajectories have been computed assuming a homogeneous magnetic field. The effects of this inhomogeneous electric field are at least one order of magnitude smaller than the effects due to the inhomogeneous magnetic field.

SUMMARY

The ion trajectories in a cycloidal mass spectrometer have been calculated assuming higher order magnetic and electric fields. It could be shown that mainly the magnetic field inhomogeneities have a big influence on the resolution and the sensitivity. In order to get a high resolution instrument, magnetic field corrections are unavoidable.

[1] C. F. Robinson, Rev. Sci. Instr. 27, 509 (1956).

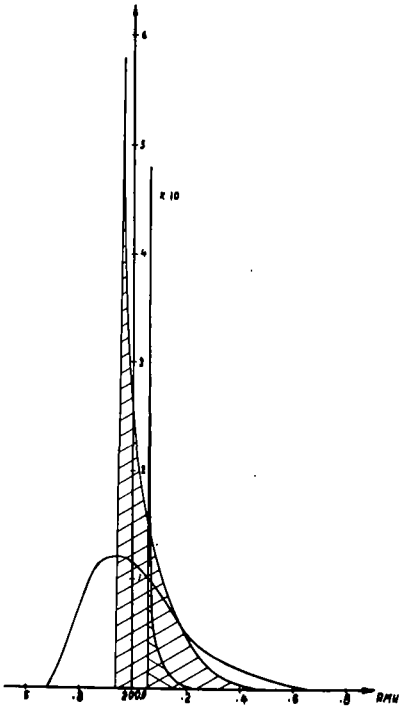

Fig. 3

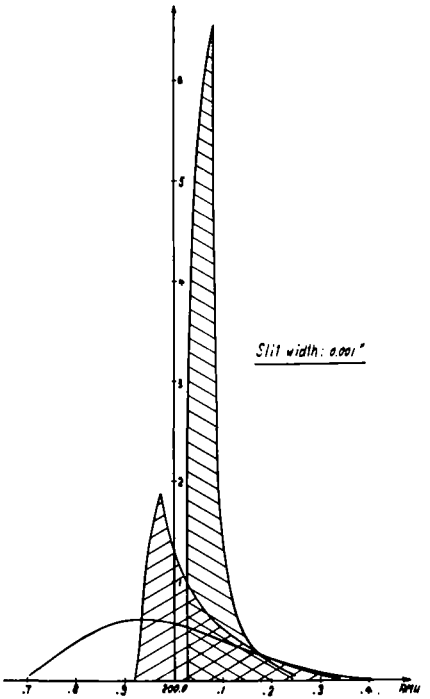

Fig. 4

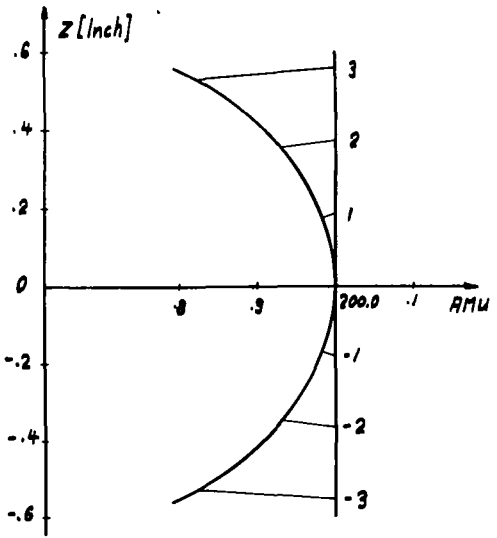
Z [Inch]
.6
.4
.2
0
-.2
-.4
-.6
.8
.9
200.0
.1
AMU
3
2
1
-1
-2
-3

Fig. 5

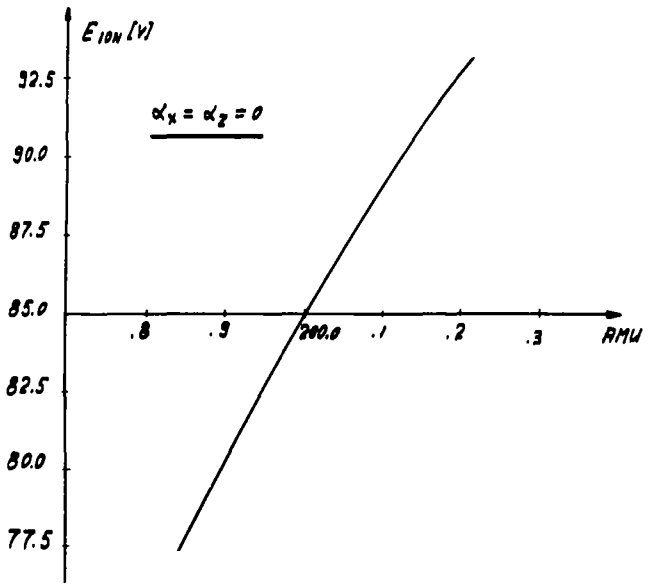
E ION [V]
92.5
90.0
87.5
85.0
82.5
80.0
77.5
αx = αz = 0
.8
.9
200.0
.1
.2
.3
AMU

Fig. 6

MEASUREMENT OF TRANSLATIONAL ENERGY IN A TIME-OF-FLIGHT MASS SPECTROMETER

J. L. Franklin, Peter M. Hierl and David A. Whan
Department of Chemistry, Rice University, Houston, Texas

ABSTRACT

A mathematical analysis of peak shapes in a Bendix time-of-flight mass spectrometer shows that ions formed with excess translational energy show considerable peak broadening. A method is developed by which this translational energy can be readily determined from the peak width. Experimental results are presented which confirm the validity of the theoretical calculations.

INTRODUCTION

Fragment ions formed with excess kinetic energy have long been observed in the mass spectra of many molecules. Accurate measurements of these excess energies are a prerequisite for all appearance potential determinations and have been undertaken by a number of investigators in the field.

The detection and measurement of initial translational energy usually involves one of two basic methods, the use of retarding potentials [1-5] or an analysis of the focusing properties of ions formed with translational energy.[6-10] Wiley and McLaren[11] have given a detailed analysis of the focusing action of a time-of-flight mass spectrometer, and it is this treatment that has been extended to permit the measurement of the initial translational energies of ions by an analysis of their peak shapes.

INSTRUMENTATION

Measurements were made on a Bendix Time-of-Flight mass spectrometer Model 12 using a S14-107 ion source and a flight tube of 180 cm. The scanning device on the mass spectrometer was modified to provide an extremely slow scan and this, in conjunction with a Honeywell chart recorder running at 8 inches per minute, enabled 10^{-8} seconds of real time to be displayed by 0.328 inches of chart paper. To ensure optimum resolution the ion lens was not used.

FLIGHT TIMES

Fig. 1 shows the major elements of a time-of-flight mass spectrometer. There are three principal regions: the ionization region, bounded by the backing plate and the ion focus grid; the acceleration region, bounded by the ion focus grid and the ion energy grid; and the drift tube, a field-free region extending from the energy grid to the collector cathode.

The pulsed electron beam is collimated by a system of slits and has a small but finite thickness, Δs. The center of the electron beam is at a distance s_o from the ion focus grid. Immediately after the electron beam is turned off, the ion focus grid receives a pulse of from 0 to -250 volts. The resulting electric field, E_s, draws the positive ions out of the ionization region into the acceleration region. The ion energy grid is maintained at -3000 volts, resulting in an electric field, E_d, in the acceleration region.

An ion of charge q, formed in the source at distance s from the ion focus grid with a component of initial translational energy U_x parallel to the axis of the flight tube, will have a total flight time given by

$$T(U_x,s) = T_s + T_d + T_D \tag{1}$$

where

$$T_s = \frac{(2m)^{1/2}}{qE_s}\left[(qsE_s + U_x)^{1/2} \pm (U_x)^{1/2}\right] \tag{2a}$$

$$T_d = \frac{(2m)^{1/2}}{qE_d}\left[(qdE_d + qsE_s + U_x)^{1/2} - (qsE_s + U_x)^{1/2}\right] \tag{2b}$$

$$T_D = (2m)^{1/2}\, D/2(qdE_d + qsE_s + U_x)^{1/2} \tag{2c}$$

The plus and minus sign in T_s correspond to initial velocities directed respectively away from and toward the collector.

RESOLUTION

If all the ions were formed at rest ($U_x = 0$) and if they were all in a plane parallel to the ion focus grid ($s = s_o$), the flight times would depend upon the ratio m/e only. Every ion of a given m/e would arrive at the collector at exactly the same instant, resulting in a mass spectrum consisting entirely of sharp lines or delta functions at the appropriate mass numbers. Any variation in initial position and/or initial energy would result in a slight variation in the flight time and a consequent broadening of the ion peak. The effects of peak broadening due to variations in initial position and in initial energy are referred to as the problems of space resolution and energy resolution, respectively.

A. Space Resolution:

Instead of being formed in a plane parallel to the ion focus grid, the ions are actually formed throughout the entire thickness of the electron beam, Δs. The effect of these variations in the initial positions of the ions is conteracted by the fact that ions farther away from the ion focus grid fall through a larger potential when accelerated by the focus pulse than do those ions formed nearer to the ion focus grid. Because of their greater energy, the former will eventually overtake and pass the latter at some distance down the flight tube. By a careful adjustment of the focus pulse, this "cross-over point" will occur just at the collector anode.

For ions that differ only in their initial positions, the variations in flight times can be calculated from a MacLaurin series expansion of $T(0,s)$ about s_o. Thus, $\Delta T_{\Delta s}$, the change in flight time corresponding to a small change Δs in the position variable s, is given by the expression

$$T(0,s_o + \Delta s) - T(0,s_o) = \Delta T_{\Delta s} = \sum_{n=1}^{\infty} \frac{1}{n!} \left[\frac{d^n T(0,s)}{ds^n} \right]_{s_o} (\Delta s)^n \qquad (3)$$

Calculation of the first three terms of the rapidly converging series shows that $\Delta T_{\Delta s}$ goes through zero at a focus pulse of -120 volts for the ion source used. Focus pulse values smaller than this do not permit the cross-over to occur before the ions reach the collector, while larger values will cause the cross-over to occur prematurely in the drift tube. A value of -120 volts, however, eliminates the effect of variations in initial position, so that the broadening of the ion packet is caused by variations in initial translational energy only.

B. Energy Resolution:

Consider the case of two identical ions formed at the same initial position, s, with equal but oppositely directed velocity components in the x direction (parallel to the axis of the flight tube).

$$-v_x \leftarrow (1)$$
$$(2) \rightarrow +v_x$$

Upon its formation ion (1) moves away from the collector, decelerating due to the electric field E_s. At time $\Delta T = mv_x/qE_s$, ion (1) comes to rest, reverses direction, and is accelerated towards the collector, returning to its original position with a velocity in the x direction equal in magnitude to its original x velocity, but this time directed toward the collector. Subsequently, its motion is identical to that of ion (2), which it continues to lag behind in time by twice the deceleration time, mv_x/qE_s. An ion formed with zero initial velocity in the x direction will have a flight time midway between those of ions (1) and (2), so that

$$T(U_x,s) = T(0,s) \pm \Delta T_U \qquad (4)$$

where

$$\Delta T_U = mv_x/qE_s = \frac{(2m)^{1/2}}{qE_s}(U_x)^{1/2} \qquad (5)$$

and the plus and minus signs refer to initial velocities directed away from and toward the collector, respectively.

The flight time is independent of velocity components perpendicular to the x axis. Moreover, because the ion beam is not collimated by a system of slits and

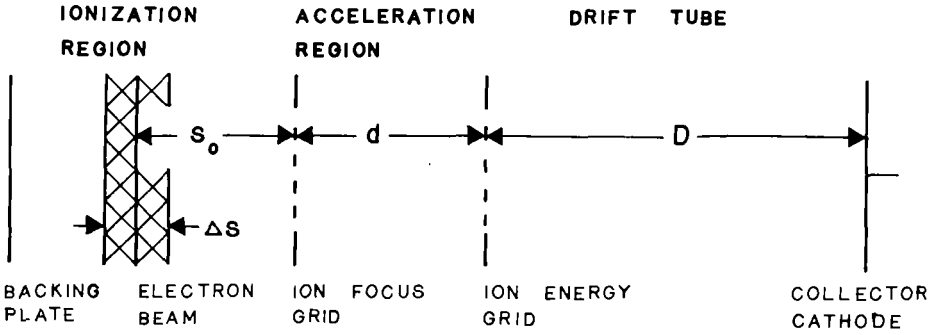

FIG. 1. SCHEMATIC REPRESENTATION OF TOF MASS SPECTROMETER

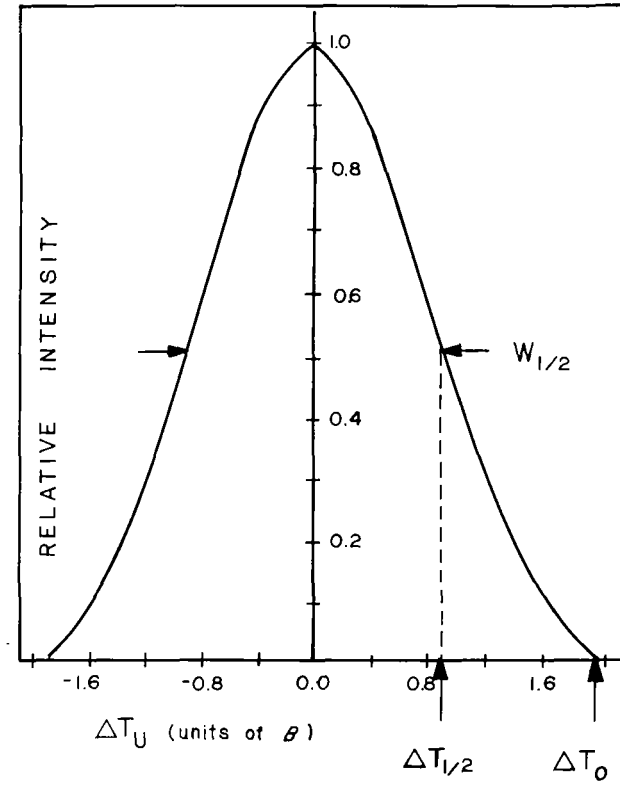

FIG. 2 PEAK SHAPE

because the area of the collector cathode is large compared to the height of the electron beam, there is no discrimination against high energy ions. That is, the collection efficiency and hence the relative intensity of the ion peak is independent of any velocity components in the y or the z direction.

If the focus condition is obeyed ($\Delta T_{\Delta s} = 0$) and the operating conditions are kept constant, then the total flight time will depend only upon the initial velocity in the x direction for an ion of given m/e. If the probability distribution for the component of initial velocity along the direction of the flight tube is known, the probability distribution for ΔT_U can be obtained. This will permit the calculation of the relative intensity of the ion signal as a function of ΔT_U and consequently a calculation of the shape of the ion peak.

If $P(v_x)$ is a known distribution function for the variable v_x, and $v_x = f(\Delta T_U)$, then the corresponding distribution function in the variable ΔT_U will be

$$Q\ (\Delta T_U) = P[f(\Delta T_U)]\ f'(\Delta T_U) \tag{6}$$

From equation (5),

$$f'(\Delta T_U) = \frac{dv}{d\Delta T_u}\left[\frac{qE}{m}\Delta T_u\right] = \frac{qE_s}{m} \tag{7}$$

The function $Q(\Delta T_U)$ represents the probability that an ion of given m/e will have a total flight time differing by a small amount, ΔT_U, from the flight time of an ion formed with zero initial translational energy, $T(0,s_o)$. It is assumed that the focus condition is obeyed so that all ions act as if they were formed at s_o. The function, $Q(\Delta T_U)$, if known, will permit the calculation of the initial translational energy of the ion from the peak shape.

1. Thermal Ions: For ions with a thermal or quasi-thermal energy distribution, the component of velocity in a given direction has a Gaussian distribution:

$$P(V_x) = \frac{1}{A\pi}1/2\ \exp(-v_x{}^2/A^2) \quad A = \left[\frac{2kT}{m}\right]^{1/2} \tag{8}$$

Where k is the Boltzmann constant and T is the absolute temperature.
The probability distribution for T_U is obtained by making the appropriate change of variables:

$$Q(\Delta T_U) = \frac{1}{B\pi}\ 1/2\ \exp\ [-(\Delta T_U)^2/B^2]\ B = \frac{m}{qE_s}\ A \tag{9}$$

For ions of a given mass and a thermal or nearly thermal distribution of energies, the intensity of the ion signal as a function of flight time will have a Gaussian distribution about the average value, $T(0,s_o)$. (See Fig. 2.)

From the known distribution it is possible to calculate the time at which the intensity has fallen to one-half of its maximum value and to express this time ($\Delta T_{1/2}$) in terms of the constant B, which in turn is a function of the parameters q, m, E_s, and k, and of the temperature of the gas, T, from which one can determine the average value of the initial translational energy, $\overline{U}_o$.

The time at which the ion peak has fallen to one-half of its maximum value is obtained from the expression

$$\exp\ [-(\Delta T_{1/2})^2/B^2\ ] = 1/2 \tag{10}$$

which yields

$$\left[\frac{\Delta T1/2}{B}\right]^2 = \ln 2 \tag{11}$$

Equivalently, the relationship can be expressed in terms of the full width at half height, $W_{1/2}$, a quantity which is more conveniently measured experimentally. Since the ion peak is symmetric,

$$W_{1/2} = 2\Delta T_{1/2} = 2(\ln 2)^{1/2}B \tag{12}$$

From equation (8) and equation (9)

$$W_{1/2} = \frac{1.664\ (2kTm)^{1/2}}{qE_s} \tag{13}$$

With $\overline{U}_o = (3/2)kT$, the average value of the initial translational energy for a thermal distribution is given by

$$\overline{U}_o = \frac{No}{3.69}\ (qE_s)^2\ \frac{(W_{1/2})^2}{M} \tag{14}$$

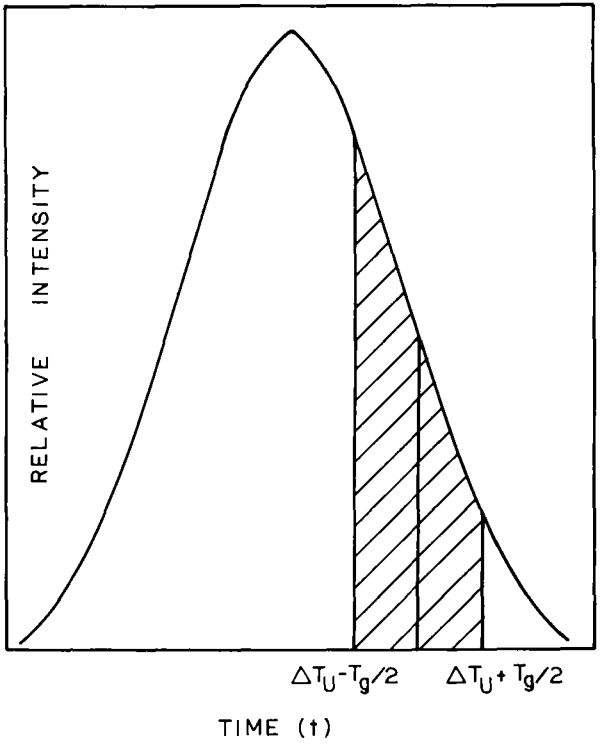

FIG. 3 EFFECT OF GATE WIDTH

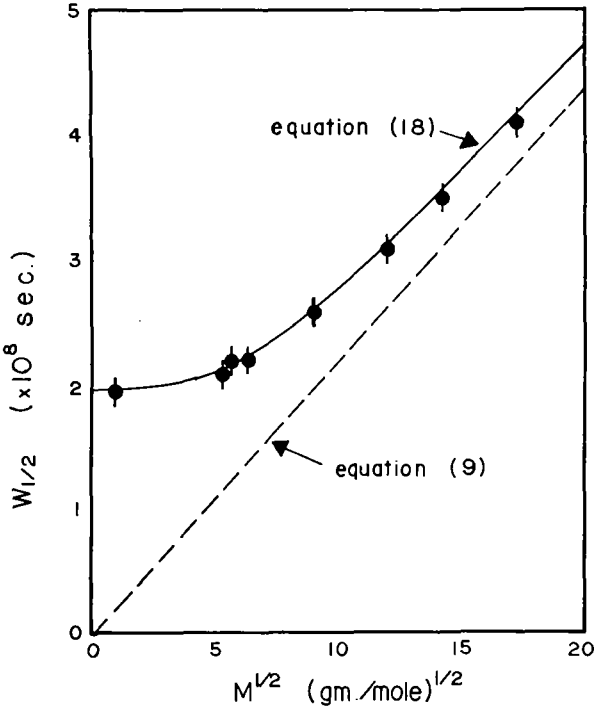

FIG. 4 CALCULATED AND EXPERIMENTAL PEAK WIDTHS

where N_o is Avogadro's number and M is the molecular weight of the ion in grams/mole.

2. Excess-Energy Ions: The distribution of initial velocities for ions formed by electron-impact induced ionization and dissociation depends upon the potential energy curves for the states involved. The most probable value for the initial energy could be anywhere from zero to several electron volts, depending upon the relative positions of the potential energy curves. Moreover, this excess energy could be distributed over a narrow or a wide range of values, depending upon the slope of the upper curve as it passes through the Franck-Condon region.

Since the present analysis of peak shapes determines the probability distribution for a given component of initial velocity rather than the distribution for the total initial speed (i.e.,energy), it is quite difficult to interpret the resulting peak shapes without prior knowledge of the potential energy curves. For example, an ion appearing at time $T(0,s_o)$ may either have been formed with zero initial energy or have been formed with considerable excess energy directed perpendicularly to the subsequent flight path. Because the ions are not collimated by slits, there is no discrimination against ions formed with non-zero components of velocity perpendicular to the flight tube.

In cases where the distribution of the excess energy is clearly not quasi-thermal, measurement of the width (W_o) at the base of the ion peak permits the calculation of a characteristic energy, U_{max}, which is taken to be the maximum initial energy possessed by a detectably significant number of ions. ΔT_o (see Fig. 2.) is the deceleration time for an ion of initial energy U_{max} whose velocity is directed entirely along the flight axis. Consequently, from equation (5) and with $W_o = 2\Delta T_o$,

$$W_o = \frac{2\ mv_x}{qE_s} = \frac{2(2m)^{1/2}}{qE_s}\ (U_{max})^{1/2} \tag{15}$$

or, upon rearrangement of terms

$$U_{max} = \frac{No}{8}\ (qE_s)^2\ \frac{(Wo)^2}{M} \tag{16}$$

3. Effect of Gate Width: An additional factor that affects the peak shape is the way in which the instrument itself detects the ion signal.

When an ion packet strikes the ion cathode, electrons are knocked from its surface and are directed onto the multiplier. The current produced in the multiplier by an individual ion packet is measured by deflecting the electron pulse for that mass from the electron pulse train (normally going to the oscilloscope anode) to one of the gated anodes of the multiplier. This is accomplished by precisely timed pulses which gate the desired mass peak to the appropriate anode.

The effect of this gate pulse is that instead of measuring the intensity of the ion signal at some particular instant in time, the instrument actually measures the sum of the ion signals for all ions of that mass that have arrived at the collector cathode over a finite period of time. (See Fig. 3.) Since the instrument measures all ions whose secondary electrons pass the gate anode during the period of time that the gate is positively pulsed, the observed ion signal has a relative intensity given by the integral

$$I(\Delta T_U) = \int_{\Delta T_U - Tg/2}^{\Delta T_U + Tg/2} Q\ (t)\ dt \tag{17}$$

where Q(t) is the distribution function defined in equation (9), which gives the intensity of the ion beam at some particular time. The duration of the gate pulse, Tg, was estimated to be 20 nano-seconds.

For thermal ions, which have the Gaussian distribution function shown in equation (9), the integral can be broken down into two well-known integrals.

$$I(\Delta T_U) = \int_{-\infty}^{\Delta T_U + Tg/2} Q\ (t)\ dt\ -\ \int_{-\infty}^{\Delta T_U - Tg/2} Q(t)dt \tag{18}$$

Values for these integrals appear in standard mathematical tables. From these tables the expected peak shapes and corresponding half-widths can be calculated.

RESULTS

1. Thermal Ions: The expected peak widths at half-height ($W_{1/2}$) for ions of thermal energy (assuming a source temperature of 300°K.) have been calculated from equation (9) and from equation (18). Fig. 4 compares the results of these calculations with a number of experimentally determined peak widths for ions over a wide mass range.

These calculations show that the gate width causes significant broadening of the narrowest ion peaks (those for ions of small mass and low energy). However, the excellent agreement between the peak widths observed and those calculated by means of equation (18) shows that the broadening effect of the gate width can be accurately calculated from equation (18).

Moreover, this instrumental factor becomes increasingly insignificant for thermal ions whose peak widths at half-height are greater than 25 nanoseconds, which is approximately the width expected for thermal ions with a m/e ratio of 28. For thermal ions of greater mass, the effect of the gate width may be neglected and the peak width may be accurately predicted from equation (13). The gate effect may likewise be neglected for any excited ions with half-width greater than 25 nanoseconds, and the peak width may be calculated from equation (15).

2. Excess-Energy Ions: In addition to the ordinary quasi-thermal methyl ion peaks, many workers (10, 12-16) have also observed "satellite peaks" in the mass spectra of many organic compounds. These satellite peaks are produced by methyl ions formed with relatively large amounts in initial translational energy (2 to 3 electron volts).

Fig. 5 shows a chart recording of the methyl ion peak obtained from the dissociation of ethyl bromide. In addition to the relatively narrow peak caused by ions with a quasi-thermal energy distribution, there is a much wider peak produced by ions with an obviously quite different energy distribution. It should be noted that the high energy group of methyl ions produce a symmetric peak whose center appears at exactly the same mass number as the center of the peak produced by the quasi-thermal group of methyl ions. That is, the most probable flight time is $T(0,s_o)$ for both types of methyl ions.

The methyl ion from ethyl bromide has been investigated previously by other workers[15] using a somewhat different method of determining initial translational energies. Table 1 compares their results with those we have obtained.

TABLE 1: Translational Energies of CH_3^+ Fragment Ions from C_2H_5Br

	This work	Olmsted, Street and Newton
Quasi-thermal ion	0.15 ev	0.21 ev
Excess energy ion	3.26 ev	3.31 ev

The methyl ion from propane is also formed with two entirely different energy distributions. Table II compares the value we obtained for the initial translational energy of the high energy fragment with the values obtained by several other workers.

TABLE II: Translational Energy of CH_3^+ Fragment Ion from C_3H_8

This Work	Mohler[5]	Stanton[16]	Bracher[10] et al
2.21 ev	2.2 ev	2.3 ev	2.2 ev

DISCUSSION

The good agreement between values obtained by this method and the values obtained by other workers confirms the usefulness of this method in accurately determining initial translational energy values up to several electron volts. Moreover, the simplicity of the calculations and the fact that the instrument need not be seriously modified permit the relatively quick and reliable determinations of excess translational energies. Consequently, this method should prove to be a useful tool in the investigation of such phenomena as the dissociation of diatomic molecules, the formation and dissociation of doubly charged polyatomic molecules, and the formation of negative ions.

ACKNOWLEDGEMENTS

The authors wish to express their thanks for the support of the Robert A. Welch Foundation. Also, one of us (PMH) would like to acknowledge the support of the National Aeronautics and Space Administration in the form of a NASA Fellowship.

REFERENCES

1. J. T. Tate and W. W. Lozier, Phys. Rev. 39, 254 (1932).
2. W. W. Lozier, Phys. Rev. 35, 1285 (1930).
3. H. D. Hagstrum, Revs. Mod. Phys. 23, 185 (1951).
4. R. E. Fox and J. A. Hipple, Rev. Sci. Instr. 19, 462 (1948).
5. F. L. Mohler, V. H. Dibeler, and R. M. Reese, J. Chem. Phys., 22, 394 (1954).
6. C. E. Berry, Phys. Rev. 78, 597 (1950).
7. N. D. Coggeshall, J. Chem. Phys. 12, 19 (1944).
8. G. Careri and G. Nencini, J. Chem. Phys. 18, 897 (1950).
9. H. W. Washburn and C. E. Berry, Phys. Rev. 70, 559 (1946).
10. J. Bracher, H. Eherhardt, R. Fuchs, O. Osbergahus, and R. Taubert, Advan. Mass Spectrometry 2, 285 (1962).
11. W. C. Wiley and I. H. McLaren, Rev. Sci. Instr. 26, 1150 (1955).
12. P. Kusch, A. Hulstrulid, and J. T. Tate, Phys. Rev. 52, 843 (1937).
13. A. Hulstrulid, P. Kusch, and J. T. Tate, Phys. Rev. 54, 1037 (1938).
14. J. A. Hipple, R. E. Foz and E. U. Condon, Phys. Rev. 69, 347 (1946).
15. J. Olmsted III, K. Street, Jr., and A. S. Newton, J. Chem. Phys. 40, 2114 (1964).
16. H. E. Stanton, J. Chem. Phys. 30, 1116 (1959).

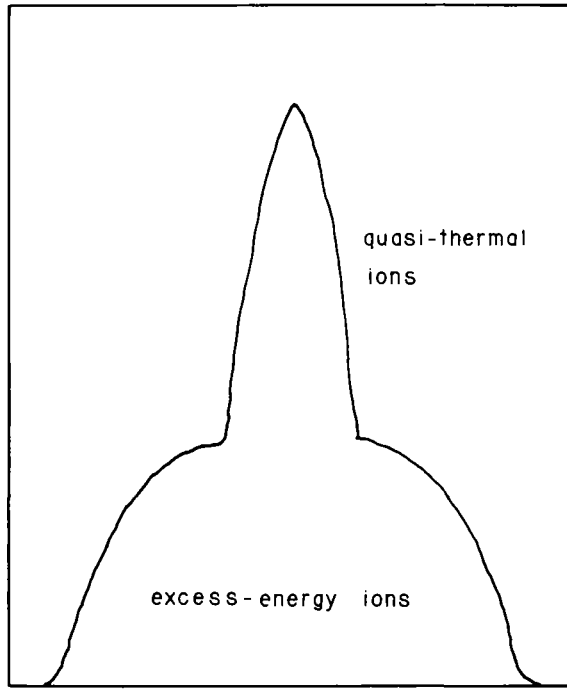

FIG. 5 CH_3^+ PEAK FROM C_2H_5Br

Structures of Gaseous Ions: Utilization of Substituent Effects

Maurice M. Bursey and F. W. McLafferty
Department of Chemistry, Purdue University, Lafayette, Indiana 47907

The significance of a correlation between the relative intensities of acyl ions in the mass spectra of substituted acylbenzenes and the sigma constants of Hammett (1) has been discussed (2,3) in terms of the strength of the bond cleaved in formation of the acyl ion from the molecular ion:

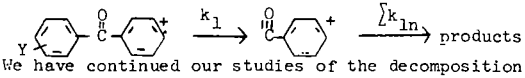

We have continued our studies of the decomposition of substituted benzophenones to include other processes which might be reasonably expected to show correlations with Hammett sigma constants.

The formation of $C_6H_5^+$ may occur by either of at least two processes:

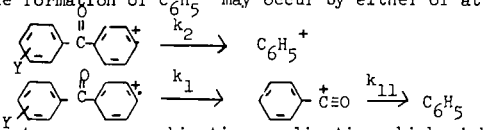

(I)

(II)

In order to remove any kinetic complication which might result from the combination of these two routes to produce $C_6H_5^+$, spectra were recorded at low ionizing voltage (19 volts). Under these conditions, as Figure 1 indicates, the substituent dependence of the relative intensity of the $C_6H_5^+$ ion is similar to that of the relative intensity of the benzoyl ion reported earlier (2,3). This similarity implies that the process of greater importance at low voltage is II, because the second step of process II is independent of substituent and does not modify the substituent dependence of the first step; as a result, the substituent dependence of the whole process (formation of $C_6H_5^+$ ion) is the same as that for the first step (formation of benzoyl ion). "Metastable" ions corresponding the formation of $C_6H_5^+$ from $C_6H_5CO^+$ are also observed at 19 volts.

At normal ionizing voltages, the substituent dependence of the intensity of the $C_6H_5^+$ ion is different (Figure 2). Instead of a simple correlation with Hammett substituent constants, a more complex correlation is observed: a curved line is obtained. This curve indicates that an additional term has been added to the correlation obtained at low voltage; in Figure 2, this new term is indicated as a second straight line of slope 0.0, to which the original line with slope 1.0 is added to produce the curved line. The significance of this new term is that it represents the contribution of the one-step process (I) at higher voltage. The negligible slope of the line (i.e., the virtual independence of the rate of this particular process on substituent) may be rationalized as follows. The bond broken in the formation of benzoyl ion, which is affected by substituents to the extent that the slope equals 1.0, is closer to the substituent than the one broken in the formation of $C_6H_5^+$; therefore, the substituent will less strongly affect the latter process than the former, in particular, the cross-conjugation of the carbonyl group intervening between the two bonds will reduce the substituent dependence of the latter process to a very small value.

Our other studies with the spectra of substituted benzophenones have been connected with the interpretation of the intensities of ions which retain the substituent: for example, $YC_6H_4^+$ and $YC_6H_4CO^+$. One difficulty arises immediately in attaching significance to intensities of ions which still contain Y: according to our treatment of mass spectral processes (2,3), ion intensities may be compared directly to obtain relative rates of decomposition only when the ion does not retain the substituent. If a substituent is retained by the ion, then the further decomposition of the ion is still dependent on the substituent; and the intensity of the ion, relative to the similar ion in the unsubstituted compound, is a function not only of the rate at which it is formed, but of the rates at which it decomposes by various routes. The relative intensities of such ions at normal ionizing voltage are thus not simply related to sigma values, and in fact no correlation is observed between such data (2). The absence of any correlation indicates that most substituents probably have a very specific influence on the decomposition of the substituted ion; the substituent itself may be involved in the major path for decomposition of the ion. Therefore, in order to obtain data from which interpretive comment may be drawn, it is necessary to remove these specific decomposition processes by using low-voltage data once again. Certain substituents have in fact been found to decompose so readily that decomposition peaks could not be removed from the spectrum without reducing the intensity of the $YC_6H_4^+$ or $YC_6H_4CO^+$ to an

unusable value, and such compounds could not be used in this study.

For many substituents, the $YC_6H_4CO^+$ ion is formed at 15.3 volts but does not have sufficient energy to decompose further. Under these conditions, therefore, the relative intensities of these ions in a set of compounds are a measure only of their relative rates of formation. Figure 3 shows a correlation of the intensities of $YC_6H_4CO^+$ ions with Hammett sigma constants. The plot has a slope of about -0.5; it is therefore easier to form $H_2NC_6H_4CO^+$ than $BrC_6H_4CO^+$. But the bond broken to form such ions is the same bond broken to form $C_6H_5^+$ directly from the molecular ion, and it was demonstrated above that this latter process has almost no substituent dependence. There must be an additional factor governing the rate of formation of substituted ions in addition to bond strength; this factor is the stabilization of the ion by the substituent. This has been postulated as a driving force before (4,5) in mass spectral decompositions, as it has been in solution chemistry (6,7); quantitative support of the hypothesis is provided by these data. As a result of the magnitude of this effect, the rho value for the formation of $YC_6H_4CO^+$ is actually opposite in sign to that for the formation of $C_6H_5CO^+$.

These data can be combined with high voltage data to yield relative values for the specific overall rates of decomposition, $\sum k_{1n}$; values for substituents examined are found in Table I. Such numbers are in the first place an empirical

Table I

Y	$Z = \frac{[YC_6H_4CO^+]}{[YC_6H_4COC_6H_5^+]}$	log (Z/Z$_0$), 75 volts	log (Z/Z$_0$), 15.3 volts	$\log \frac{\sum k_{1n}}{k^0_{1n}}$
p-CN		-0.34	-0.38	-0.04
m-Br		-0.12	-0.35	-0.23
p-Cl		0.09	0.13	0.04
H		0.00	0.00	0.00
p-CH_3		0.04	0.38	0.34
p-NH_2		0.04	0.41	0.37

device for the prediction of spectra. Positive values indicate greater overall rates of decomposition of $YC_6H_4CO^+$ relative to the parent compound; negative values, smaller rates of decomposition. Table I indicates that these rates are neither uniform nor predictable by the Hammett equation. The major decomposition pathway not directly involving cleavage of the substituent, decarbonylation of the substituted benzoyl ion, will be examined in the subsequent discussion of the abundance of the $YC_6H_4^+$ ion.

The $YC_6H_4^+$ ion may be formed, analogously to the $C_6H_5^+$ ion, via two routes from the molecular ion at normal ionizing voltages. Once again, the presence of

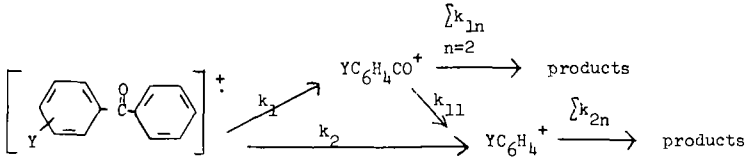

variable decomposition rate constants in the expression governing the intensity of the product ion (8) invalidates assignment of immediate significance to ion intensities without some knowledge of these relative rates of decomposition, $\sum k_{2n}$. The method for distinguishing the contribution of the rate of formation to the substituent profile is once again based on the determination of low-voltage intensity ratios; at sufficiently low energies, all decomposition pathways will be removed and all but one pathway of formation, by analogy to the results for the $C_6H_5^+$ ion. Spectra recorded for study of $YC_6H_4^+$ at 19 volts indicate that the analogy is also valid, using most Y substituents at this voltage. The spectra which were used for study contained no ion below m/e of $YC_6H_4^+$ except $C_6H_5^+$, whose formation from $YC_6H_4^+$ is either impossible or else discredited by our earlier work. Data for the same substituents examined in Table I are given in Table II; values obtained from this set of experiments include the ratio of $[YC_6H_4^+]$ to $[YC_6H_4CO^+]$

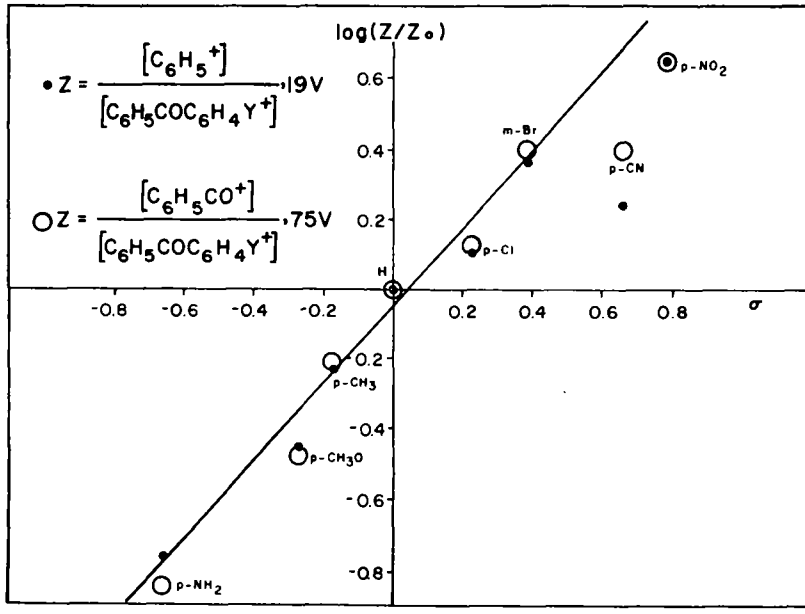
log(Z/Z₀)
• Z = [C6H5+] / [C6H5COC6H4Y+], 19V
○ Z = [C6H5CO+] / [C6H5COC6H4Y+], 75V
p-NO2
m-Br
p-CN
p-Cl
H
p-CH3
p-CH3O
p-NH2
σ

Fig. 1

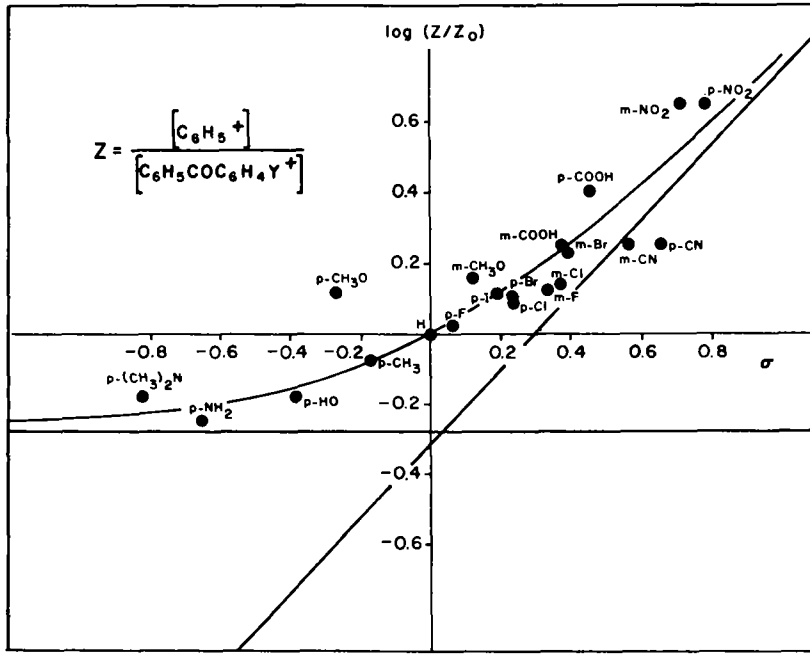
log (Z/Z0)
Z = [C6H5+] / [C6H5COC6H4Y+]
p-NO2
m-NO2
p-COOH
m-COOH
m-Br
p-CN
m-CN
m-CH3O
p-CH3O
p-Br
m-Cl
p-I
m-F
p-Cl
p-F
H
p-CH3
p-(CH3)2N
p-NH2
p-HO
σ

Fig. 2

and to $[YC_6H_4COC_6H_5^+]$.

On the basis of the assumption that all $YC_6H_4^+$ is produced from $YC_6H_4CO^+$ at 19 volts and that $YC_6H_4^+$ does not decompose further, the steady state approximation leads to eq 1 as the relation between the intensities of these species. As a result, this ratio is proportional to k_{11} in a series of compounds. This hypothesis

$$\frac{[YC_6H_4^+]}{[YC_6H_4CO^+]} = \frac{k_{11}}{\sum k'_{inst}} \qquad (1)$$

may now be tested by subtractive combination of the data in column 2 of Table I and column 2 of Table II, since the latter data represent the product of the rate constants for the two-step formation from the molecular ion; see eq 2. By subtracting

$$\frac{Z}{Z_0} = \frac{k_{11}k_1}{k_{11}^0 k_1^0} \qquad (2)$$

the values given for log Z/Z_0 in table I (which correspond to log (k_1/k_1^0), an alternate set of values for log (k_{11}/k_{11}^0) is obtained. Comparison of these data (columns 1 and 3 of Table II) indicates that the assumption of formation of $YC_6H_4^+$ solely through $YC_6H_4CO^+$ is a valid one. In further support of this mechanism, "metastable" ions corresponding to the process $YC_6H_4CO^+ \rightarrow YC_6H_4^+$ may also be detected at 19 volts, and their intensities are likewise smaller for electron-donating Y. The existence of the metastable offers no indication of the singular nature of the pathway; only the correlation of the substituent effects rules out the existence of substantial contributions from other routes.

Table II

Y	log (Z/Z_0), 19 volts $Z = \frac{[YC_6H_4^+]}{[YC_6H_4CO]}$ log (k_{11}/k_{11}^0)	log (Z/Z_0), 19 volts $Z = \frac{[YC_6H_4^+]}{[YC_6H_4COC_6H_5^+]}$	log (k_{11}/k_{11}^0) from subtractive process
p-CN	0.22	-0.21	0.17
m-Br	0.23	-0.13	0.22
p-Cl	-0.17	-0.14	-0.27
H	0.00	0.00	0.00
p-CH_3	-0.23	0.20	-0.18
p-NH_2	-0.17	0.24	-0.17

Correlation of these data with Hammett sigma constants indicates a small positive rho value (+ 0.4) for this reaction, as shown in Figure 4. This is substantially less than that (+ 1.0) for reaction I, which involves cleavage of the same bond, again probably reflecting the opposing effect of the stabilization of the product ion by the substituent Y. This reaction is therefore not analogous to the decomposition of aryldiazonium ions, which is also decelerated both by electron-withdrawing substituents capable of direct resonance donation to the reaction site (9).

Substituent effects for the decompositions of substituted benzophenones in Scheme VII have now been established. These conclude the pathways for which

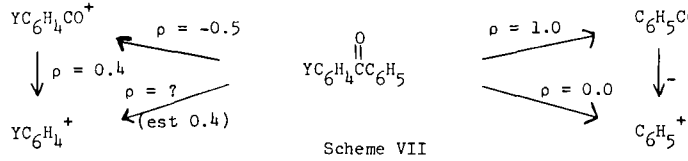

Scheme VII

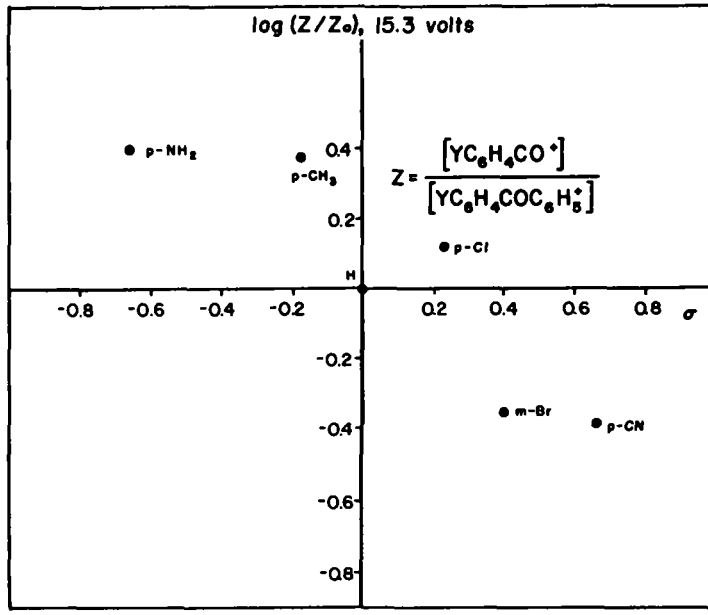
log (Z/Z₀), 15.3 volts
p-NH₂
p-CH₃
p-Cl
m-Br
p-CN
H
Z = [YC₆H₄CO⁺] / [YC₆H₄COC₆H₅⁺]
0.4
0.2
-0.2
-0.4
-0.6
-0.8
-0.8
-0.6
-0.4
-0.2
0.2
0.4
0.6
0.8
σ

Fig. 3

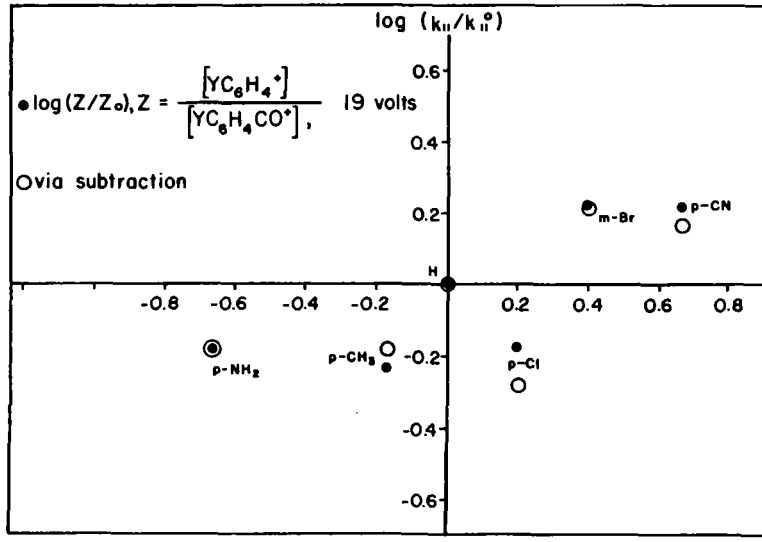
log (k_II/k_II°)
● log (Z/Z₀), Z = [YC₆H₄⁺] / [YC₆H₄CO⁺], 19 volts
○ via subtraction
m-Br
p-CN
p-NH₂
p-CH₃
p-Cl
H
0.6
0.4
0.2
-0.2
-0.4
-0.6
-0.8
-0.6
-0.4
-0.2
0.2
0.4
0.6
0.8

Fig. 4

reasonable correlation may be expected.

Acknowledgments. - The generous donation of samples by Drs. Herbert C. Brown, Saul G. Cohen, Thomas DeVries, George C. Fraenkel, J. J. Norman, and Paul J. Ricca is gratefully acknowledged. We are indebted to the National Science Foundation (GP 4335) and the National Aeronautics and Space Administration (NGR 15-005-021) for their support of this work.

Experimental. - Compounds used in this study were either gifts or commercial samples with no impurities detectable by mass spectrometry. Spectra were recorded on a Hitachi RMU-6A single-focusing instrument with inlet temperature at 185° ±5°C and source at 160°±10°C. For the high-voltage spectra, a 80-μa beam of 75-volt electrons was used; the low-voltage data were recorded at 2 μA target current. Spectra of the substituted benzoyl ions were standardized against the intensity of the molecular ion of CO_2 and recorded at the voltage at which this ion attains 2% of its value at 75 volts. This point is 1.5 volts above that where the intensity of the ion is 1%, which was assigned the appearance potential value of 13.8 volts. Data for $YC_6H_4^+$ and $C_6H_5^+$ phenyl ions were obtained at the voltage at which the intensity of Ar^+ is 10% of its value at 48 volts on this instrument. In similar fashion to the above this potential is assigned a value of 19 volts.

References

1. L. P. Hammett, "Physical Organic Chemistry", McGraw-Hill Book Company, New York, N.Y., 1940, Chapter VII.
2. M. M. Bursey and F. W. McLafferty, Abstracts, 13th Annual Conference on Mass Spectrometry and Allied Topics, St. Louis, Mo., May 1965, p. 415.
3. M. M. Bursey and F. W. McLafferty, J. Am. Chem. Soc., 88, 529 (1966).
4. F. W. McLafferty, "Mass Spectrometry of Organic Ions", Academic Press, Inc., New York, N.Y., 1963, p. 318.
5. F. W. McLafferty, "Interpretation of Mass Spectra", W. A. Benjamin, Inc., New York, N.Y., in press.
6. M. G. Evans and M. Polanyi, Trans. Faraday Soc., 34, 11 (1938).
7. G. S. Hammond, J. Am. Chem. Soc., 77, 334 (1955).
8. The data are found in Figure 5 of reference 2.
9. M. L. Crossley, R. H. Kienle, and C. H. Benbrook, J. Am. Chem. Soc., 62, 1400 (1940).
10. F. H. Field and J. L. Franklin, "Electron Impact Phenomena", Academic Press, Inc., New York, N.Y., 1957, p. 280.

A Mass-spectral Study of exo- and endo-2-Norbornyl Bromides

D. C. DeJongh and S. R. Shrader
Department of Chemistry
Wayne State University
Detroit, Michigan, 48202

The mass spectra of exo- and endo-2-norbornyl bromides are identical except forthe intensity of the molecular-ion peak, $C_7H_{11}Br^{+\cdot}$, relative to that of the base peak, $C_7H_{11}^+$. The spectrum of endo-2-norbornyl bromide is shown in Fig. 1. Both spectra are summarized in Scheme 1 and do not change from 20-70 e. v.

SCHEME 1

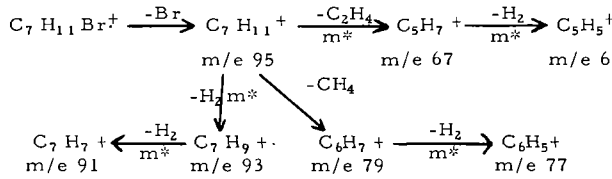

The only fragmentation of the molecular ion is cleavage of the C2-Br bond to a gaseous $C_7H_{11}^+$ ion. Since the rate-determining step in the solvolyses of 2-norbornyl derivatives is heterolytic cleavage to a solvated cation, we felt that a comparison of the solvolytic[1] and electron-impact induced formation of the $C_7H_{11}^+$ ion would be interesting.

(1) For a compilation of publications in this area see P. D. Bartlett, Nonclassical Ions: Reprints and Commentary, W. A. Benjamin, Inc., New York, 1965.

According to the kinetic approach to mass spectra developed by Bursey and McLafferty[2], the rate of formation of $C_7H_{11}^+$ from $C_7H_{11}Br^{+\cdot}$ would be proportional to the ratio of their recorded intensities. Therefore, if the molecular ions from exo and endo-2-norbornyl bromides fragment to the same $C_7H_{11}^+$ ion, the peak-intensity relationship in Scheme 2 may be derived.[2] The intensities of the two molecular-ion peaks and the two fragment-ion peaks are experimentally measurable quantities which allow calculation of the ratio of rate constants. In Table I, this ratio, determined from electron-impact studies in the gas phase, is compared to the corresponding ratio obtained from solvolytic studies by Roberts.[3]

(2) M. M. Bursey and F. W. McLafferty, J. Am. Chem. Soc., 88, 529 (1966).

SCHEME 2

$$\underline{\text{exo}}\text{-}C_7H_{11}Br^{+\cdot} \xrightarrow{k} [C_7H_{11}^+]_{\underline{\text{exo}}} + Br\cdot$$

$$\underline{\text{endo}}\text{-}C_7H_{11}Br^{+\cdot} \xrightarrow{k'} [C_7H_{11}^+]_{\underline{\text{endo}}} + Br\cdot$$

$$\frac{[C_7H_{11}^+]_{\underline{\text{exo}}} \big/ [\underline{\text{exo}}\text{-}C_7H_{11}Br^{+\cdot}]}{[C_7H_{11}^+]_{\underline{\text{endo}}} \big/ [\underline{\text{endo}}\text{-}C_7H_{11}Br^{+\cdot}]} = \frac{k}{k'}$$

(3) J. D. Roberts, W. Bennett, and R. Armstrong, ibid., 72, 3329 (1950).

TABLE I

Compound	$[C_7H_{11}^+]/[C_7H_{11}Br^{\ddot{+}}]$, rel. int. ratio	k/k' electron impact	k/k' solvolysis	$AP(C_7H_{11}^+)$, e. v.
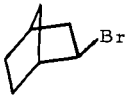	264	10	10[a]	10.27 ± 0.05
	26.4	1	1[a, b]	10.26± 0.05
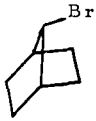	5.92	(0.22)		
	3.22	(0.12)		

a) In 80% aqueous ethanol at 55°.[3] Internal return, if any, has not been measured and compensated for in these values.

b) Twenty percent impurity of a more reactive bromide, presumable the exo-isomer.[3]

No quantitative significance can be assigned to the observation of an identical (10:1) rate from the two processes, but the fact that exo-Br is lost faster than endo-Br represents a striking correlation. Our data can be explained in terms of steric deceleration of fragmentation in the endo-isomer as well as in terms of nonclassical anchimeric assistance in the exo-isomer, as have been used to rationalize the larger rates of solvolysis of exo-2-norbornyl derivatives relative to their endo-isomers.[1,3]

Appearance-potential measurements of the intense $C_7H_{11}^+$ ions, m/e 95, by the semilog matching technique for evaluation of appearance-potential curves, are also summarized in Table I. These figures are likely reliable to ± 0.15 e.v. Due to the low abundance of the corresponding molecular ions, ionization-potential measurements were not made. The similarity of the mass spectra of the exo- and endo-isomers together with these appearance-potential data indicate that the same $C_7H_{11}^+$ ion with the same energy distribution is formed from both compounds, a requirement for the kinetic approach to be valid.[2]

We have also studied the fragmentation of the two remaining norbornyl bromides, namely the 1- and 7- isomers. A fragmentation of their molecular ions which competes with the loss of a bromine radical is elimination of the ethylene bridge. The relative-intensity ratios given in Table I indicate that these lose a bromine radical more slowly than do their 2-bromo isomers, paralleling solvolytic behavior.[1] The relative-rate ratios shown in parentheses would represent the k/k' ratios only if the

$C_7H_{11}^+$ ion is identical from all four compounds. The n.m.r. spectrum of the 2-norbornyl cation as the hexafluoroantimonate salt has been observed in SbF_5-liquid SO_2 solution;[4] it was noted that both the 1- and 7- norbornyl cations rapidly rearranged

(4) P. von R. Schleyer, W. E. Watts, R.C. Fort, Jr., M.B. Comisarow, G. A. Olah, ibid., 86, 5679 (1964).

to the more stable 2-norbornyl cation at -10°. Thus, it is probable that the gaseous $C_7H_{11}^+$ ions formed upon electron impact from the four norbornyl bromides are identical, and that the values in Table I reflect the k/k' ratios.

Additional data obtained with the isomeric 2, 3-dibromo and 2, 3-bromochloro norbornanes indicate that the more facile loss of exo-Br relative to endo-Br is general for the norbornyl system.

ACKNOWLEDGMENT

The mass spectrometer was purchased by Wayne State University with funds from a National Science Foundation Chemical Research Instrument grant.

FIGURE 1.

Mass spectrum of endo-2-norbornyl bromide. The mass spectrum of exo-2-norbornyl bromide is identical except for the relative intensity of the molecular ion peak.

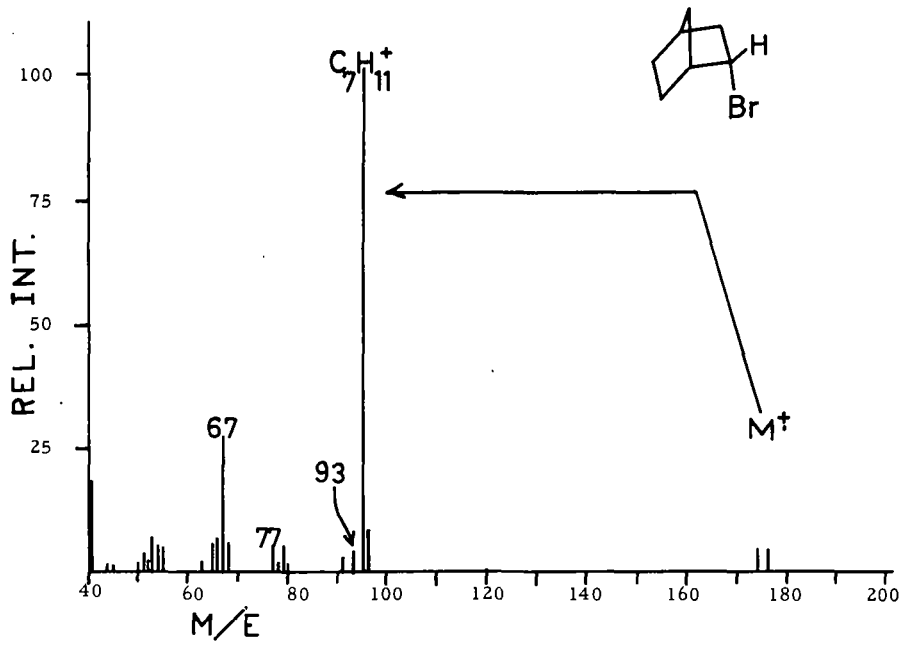

Spectra of Derivatives of Some Aromatic Compounds

Nobuhide Wasada and Toshikazu Tsuchiya

Government Chemical Industrial Research Institute, Tokyo, Japan

In order to investigate the fragmentation of aromatic compounds under electron impact, we have measured mass spectra of disubstituted aromatic compounds. The following is the relation between the spectral pattern of some of substituted anilines and their bond orders calculated by simple LCAO MO method.

Thompson[1] pointed out first a relation between electron density of n-octane and its mass spectrum. Recently, Hirota[2] investigated the relation between electron densities of a few aliphatic compounds and their mass spectra and found some interesting results.

o-, m-, and p- compounds of five aniline derivatives, aminoacetophenone, chloraniline, aminophenol, nitroaniline and anisidine, were investigated. The samples were extra pure compounds available commercially. We have numbered the atoms as are shown in Fig. 1. In the calculation of aminoacetophenone, we did not take the methyl group into account. Table 1 shows the parameters used in LCAO MO calculation.

Table 1

Coulomb Integrals and Resonance Integrals

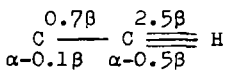

C.A.Coulson, U.A.Crawford, J. Chem. Soc., 1953, 2052.

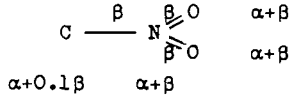

J.I.F.Alonso, Compt. Rend., 233, 403 (1951).

Substituent	a	b	l	
-Cl	1.8	0.18	0.8	H.H.Jaffé, J. Chem. Phys., 20, 279 (1952).
-OH	0.6	0	0.7	
$-NH_2$	0.4	0	0.6	
=O	2	0.2	2	L.E.Orgel, T.L.Cottrell, W. Bick, L.E.Sutton, Trans. Faraday Soc., 47, 113 (1951).
-O-	2	0.2	0.6	

Coulomb integral of substituent X: $\alpha(X)$ $\qquad \alpha(X) = \alpha + a\beta$

Coulomb integral of carbon atom adjacent to substituent: $\alpha(adj)$ $\qquad \alpha(adj) = \alpha + b\beta$

Resonance energy of C-X: $\beta(C\text{-}X)$ $\qquad \beta(C\text{-}X) = l\beta$

α and β are the Coulomb integral and exchange integral of a carbon atom, respectively.

A CEC 21-103C mass spectrometer was used. Fig. 2 shows the mean error of pattern coefficient, based on the parent peak, of m-anisidine. A sample of m-anisidine was measured once daily for 5 successive days. The mean error is 2 to 3% in larger peaks which is a little larger than that of n-butane. There was reasonable consistency of pattern coefficients with reported values, when such values were available, except for nitroanilines.

We considered the relation between bond orders and corresponding fragmentation of the bond. Investigation was confined to parent ions and to those ions which result from simple cleavages of substituents. A substituent other than NH_2 group shall be called as Y. We define ϕ' as a radical which is given by elimination from the original molecule

Fig. 1

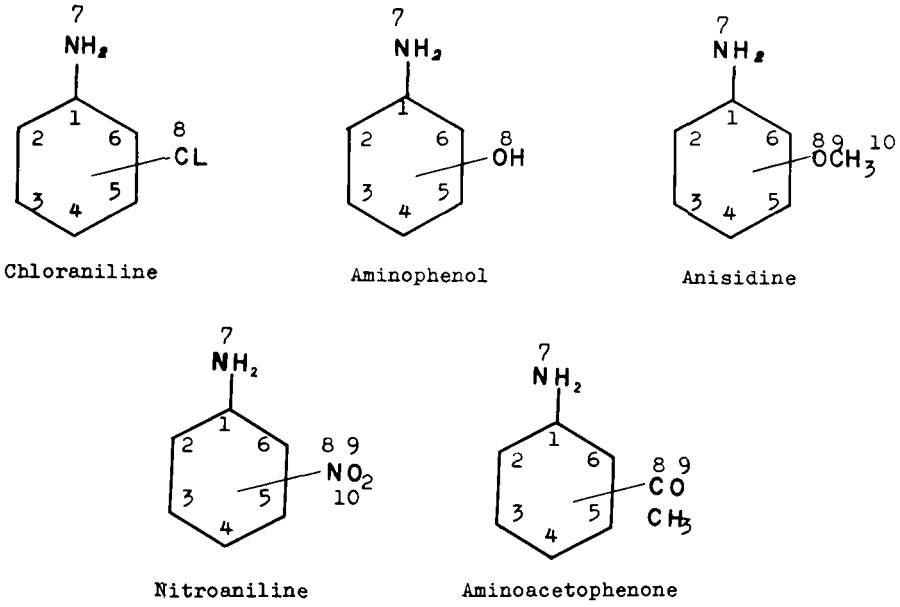

Fig. 2 Mean Error, d, versus Pattern Coefficient, C.

m-Anisidine

5 measurements

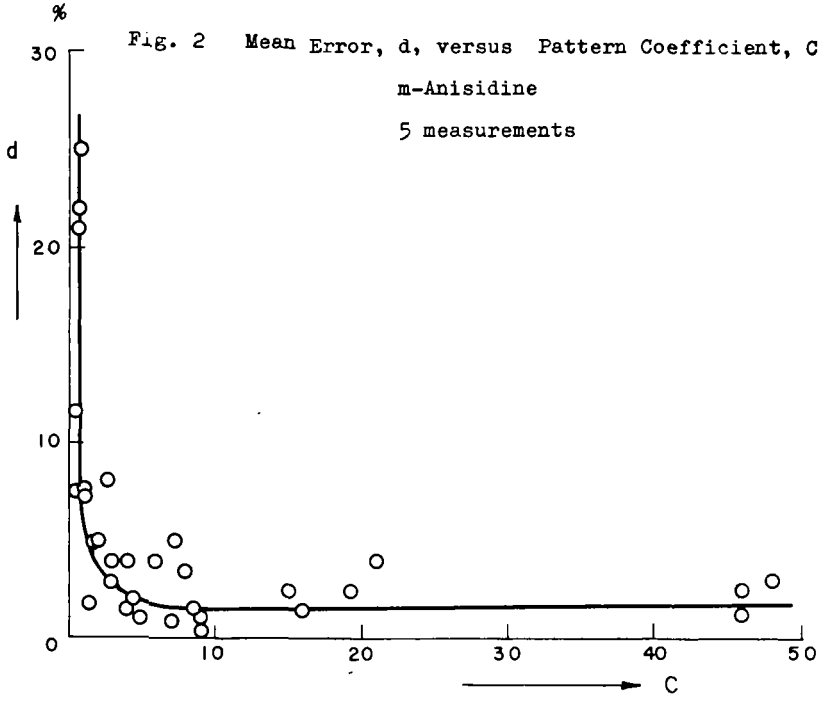

of a substituent Y. Similarly, the radical with the substituent Y and without the amino group is called ϕ'. We assume that the elimination of a frontier electron from the parent molecule results in a parent ion. By $B(\phi'-Y)$ we refer to the bond order of the bond between ϕ' and Y of the parent molecule. Similarly, by $B(I,\phi'-Y)$, we refer to the bond order of the bond between ϕ' and Y of the parent ion. The bond order between ϕ'' and NH_2 of the molecule and that of the parent ion shall be called $B(\phi''-NH_2)$ and $B(I,\phi''-NH_2)$, respectively. Finally, Δ refers to the bond order of the parent ion minus that of the parent molecule, and γ refers to this bond order difference of substituent Y, normalized by the bond order difference between ϕ'' and NH_2 of the same molecule.

Table 2 is the bond order of o-, m-, and p-aminophenol, p(12) for instance represents the bond order of 1-2 bond of the molecular state and that of the parent ion. The last column is the difference

Table 2

Bond Order, p(ij), of Aminophenols

Position of Substituents		Molecule B	Molecular Ion, B(I)	Δ
	p(12)	0.643	0.596	-0.047
	p(23)	0.660	0.700	0.039
	p(34)	0.660	0.613	-0.047
o	p(45)	0.661	0.696	0.035
	p(56)	0.639	0.599	-0.039
	p(61)	0.588	0.525	-0.063
	p(17)	0.330	0.496	0.165
	p(68)	0.349	0.475	0.126
	p(12)	0.618	0.574	-0.044
	p(23)	0.669	0.680	0.011
	p(34)	0.670	0.659	-0.011
m	p(45)	0.614	0.589	-0.024
	p(56)	0.631	0.645	0.014
	p(61)	0.636	0.609	-0.027
	p(17)	0.352	0.461	0.109
	p(58)	0.366	0.378	0.012
	p(12)	0.626	0.572	-0.054
	p(23)	0.679	0.723	0.043
	p(34)	0.622	0.571	-0.051
p	p(45)	0.622	0.571	-0.051
	p(56)	0.679	0.723	-0.043
	p(61)	0.626	0.572	-0.054
	p(17)	0.326	0.489	0.162
	p(48)	0.345	0.469	0.125

between the two bond orders, Δ . As is seen in the table, the bond order difference of amino radicals are very large in all three substances. This is a feature common to all the compounds we investigated. This will explain the fact that the $M-NH_2$ ion intensities of all the compounds are negligible. In the case of these aminophenols, the bond order difference, Δ , of the substituent OH is positive. Table 3 shows the same values for anisidines. In these substances, the bond order, p(89), and Δ value between the oxygen atom and the methyl group are very small, but there is no appreciable difference between the three isomers. Yet, the $M-CH_3$ peak in o-, and p-compounds is very intense but the same peak is very weak in the m-compound, as shall be shown later. 9-10 is a bond in the substituent Y. The bond order difference, Δ , of (9-10) bond is negative.

Table 4 shows the pattern coefficients of parent ions and the bond order differences, Δ , of substituents, Y. The pattern coef-

Fig. 3 Anisidine

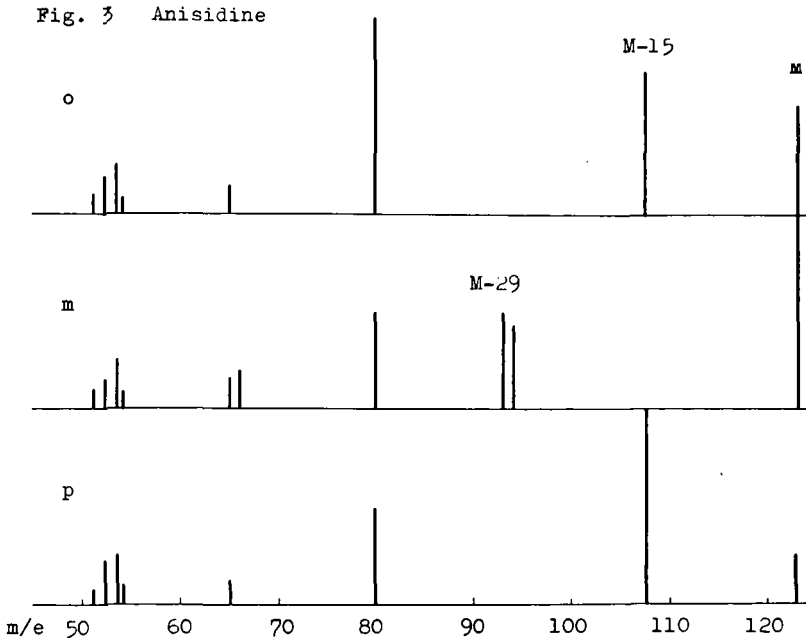

Fig. 4

$(M-CH_3)^+$ Ion from Anisidine

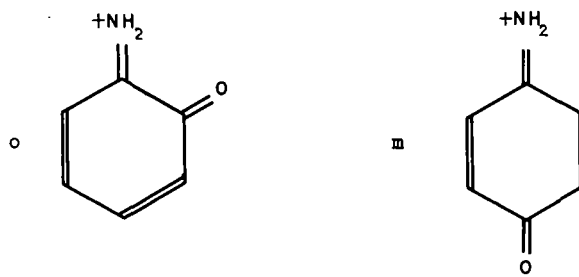

G.Spiteller, M.Spiteller-Friedmann
Mh. Chem., 93, 1395 (1962)

Table 3

Bond Order, p(ij), of Anisidines

Position of Substituents		Molecule B	Molecular Ion, B(I)	Δ
o	p(12)	0.640	0.599	-0.041
	p(23)	0.663	0.670	0.034
	p(34)	0.670	0.618	-0.042
	p(45)	0.661	0.694	0.033
	p(56)	0.645	0.607	-0.038
	p(61)	0.595	0.539	-0.056
	p(17)	0.335	0.480	0.144
	p(68)	0.314	0.451	0.137
	p(89)	0.191	0.216	0.025
	p(910)	0.979	0.972	-0.007
m	p(12)	0.619	0.574	-0.045
	p(23)	0.670	0.675	0.005
	p(34)	0.668	0.663	-0.006
	p(45)	0.622	0.586	-0.035
	p(56)	0.639	0.648	0.009
	p(61)	0.634	0.622	-0.019
	p(17)	0.352	0.440	0.088
	P(58)	0.331	0.370	0.039
	p(89)	0.191	0.207	0.016
	p(910)	0.979	0.947	-0.005
p	p(12)	0.625	0.578	-0.047
	p(23)	0.679	0.718	0.039
	p(34)	0.628	0.582	-0.046
	p(45)	0.628	0.582	-0.046
	p(56)	0.679	0.718	0.039
	p(61)	0.625	0.578	-0.047
	p(17)	0.331	0.474	0.142
	p(48)	0.310	0.445	0.135
	p(89)	0.191	0.215	0.024
	p(910)	0.979	0.972	-0.007

Table 4

Δ and Pattern Coefficient of Parent Ion

Compound	Pattern Coefficient			Δ of Substituents
	o	m	p	
Chloraniline	38	40	41	all positive
Aminophenol	32	36	32	all positive
Nitroaniline	18	16	15	one negative
Aminoaceto-phenone	18	15	14	one negative
Anisidine	15	20	18	one negative

ficient is expressed in % of summation of all peaks. Chloraniline and aminophenol, in which all the Δ values of substituents are positive, have larger parent ions than other compounds. In other compounds not all the bond order differences of substituents are positive. In this instance, there seems to be a tendency between bond order and parent ion intensity. However, as the number of atoms in the latter group of molecules, is larger than that of the former group of molecules, more extensive investigation is necessary before we definitely conclude along this line. That is, the summation of peaks is a function of the number of atoms constructing the molecule, and the value of summation affects the pattern coefficient of the parent ion.

Fig. 5 I(ϕ) versus Ratio of Bond Order, γ.

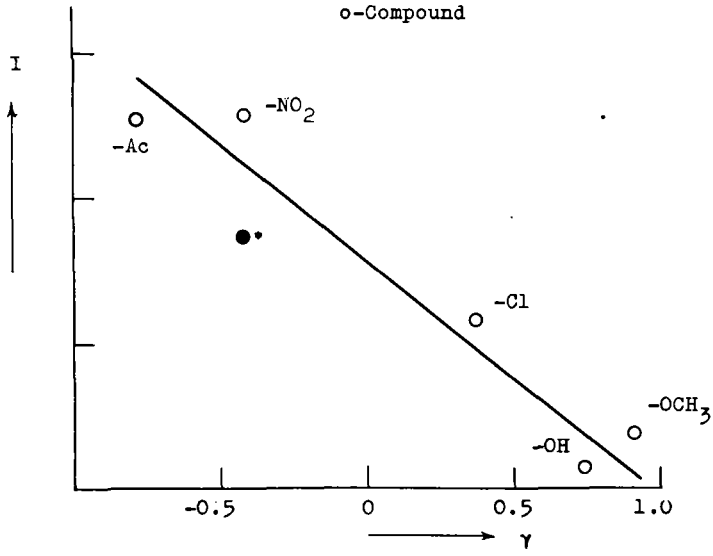

Fig. 6 I(ϕ') versus Ratio of Bond Order, γ.

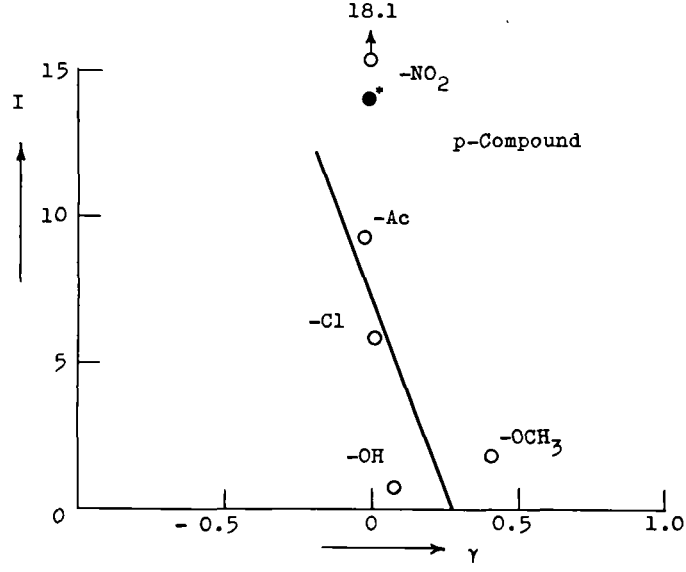

Fig. 3 shows the spectra of three anisidines. As was pointed out first by Spiteller and others[3], while o- and p- compounds show strong M-15 peaks, the m- compound has virtually no peak corresponding to it. Instead, the m-compound has a strong peak at m/e M-29. Spiteller reported that the expelled atoms are either the CHO group or the NCH_3 group. According to our results, at least an important part of the expelled group is CHO, because the M-29 group is characteristic of aromatic compounds containing a metoxy group as a substituent, regardless of the presence of an NH_2 group. As mentioned before, the bond order of molecules corresponding to the M-15 ion is remarkably small in these three isomers, so we cannot explain why the M-15 peak does not appear only in m-anisidine. Spiteller in explaining the difference of these peaks, says the M-15 ions from o- and p- compounds can assume highly stabilized structures, while the M-15 ions from a m- isomer cannot assume such a conjugated structure (Fig. 4).

In discussing the transition probability, $\int \psi(i) H \psi(f) d\tau$, from an initial molecular state, $\psi(i)$, to a final ionized state, $\psi(f)$, under an electron impact, H, we take only the first factor into account, in a sense, and leave the other factors uninvestigated in the present investigation. So, in this present instance, where the wave function for the final state $\psi(f)$ of the 3 isomers are thought to differ appreciably, we cannot explain why the M-15 peak does not appear in m-anisidine by the present approximation.

Fig. 5~7 shows the relation between peak height m/e 92, which corresponds to the M-Y ion, and γ, the bond order difference normalized by the bond order difference of $M-NH_2$. Incidentally, stared marks are where the Beynon's result[4] for nitroaniline appears. While a linear relation holds in the cases of o- and p- compounds, a larger discrepancy is seen in the case of m-compounds. In these cases, the structures of the resultant M-Y ions seem to be similar to each other.

In conclusion, as a result of these investigations, parallel relations can be found between some mass spectra of aromatic compounds and their bond orders. However, in some cases, because the stability of the resultant ions from o- and p- compounds are very different from that of the m- compound, the present consideration does not adequately explain the difference of spectra between o-, m-, and p- isomers.

1) R.Thompson, "Applied Mass Spectrometry" (Instit. of Petroleum, London, 1953) p.154.
2) M.Hatada, K.Hirota, Bull. Chem. Soc. Japan, 38, 599 (1965): Z. Phys. Chem. n.F., 44, 328 (1965).
3) G.Spiteller, M.Spiteller-Friedmann, Mh. Chem., 93, 1395 (1962).
4) J.H. Beynon, G.R.Lester, A.E.Williams, J. Chem. Phys., 63, 1861 (1959).

Fig. 7 I(ϕ') versus Ratio of Bond Order, γ.

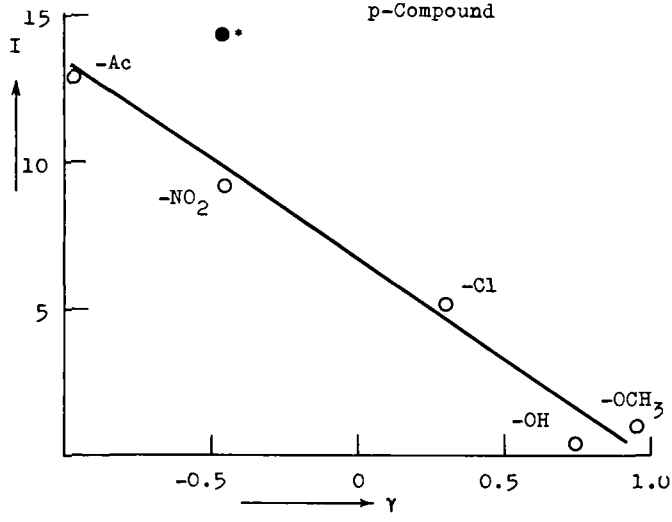

MASS SPECTROMETRIC FRAGMENTATION OF SUBSTITUTED PROPIONIC AND BUTYRIC ACIDS

R. D. Grigsby, M. C. Hamming, E. J. Eisenbraun, D. V. Hertzler, and N. Bradley, Continental Oil Co., Ponca City, Okla; Oklahoma State University, Stillwater, Okla.; and Panhandle A and M College, Goodwell, Okla.

ABSTRACT

The principal fragmentation of propionic and butyric acids substituted with methyl, benzoyl, xylyl, and xyloyl groups is discussed and compared with known fragmentation mechanisms. Several proposed mechanisms are supported by the mass spectra of compounds substituted with deuterium in specific locations. The data show that the fragmentation of the molecules is strongly dependent on the combined fragmentation-directing capabilities of all groups present.

INTRODUCTION

The mass spectra of polyfunctional compounds are known to exhibit under electron bombardment peaks which result from the combined fragmentation-directing capabilities of the various groups present. Thus, for example, if a molecule contains both an aromatic ring and a carboxyl group, its mass spectrum consists of ions characteristic of both aromatic and carboxyl-containing compounds.

In the present investigation the mass spectra of several propionic and butyric acids substituted with methyl, keto, and aromatic groups were recorded and studied in detail. The fragmentation of these acids is characterized by cleavage of the C-C bond β to either the aromatic ring or the carboxyl group. The presence of a methyl group on the alkyl chain promotes cleavage of the bond on either side of the point of branching with the tendency to retain the positive charge by the fragment containing the substituted carbon atom. Several rearrangement peaks were observed in the spectra. These could be explained by the McLafferty rearrangement involving either a keto or a carboxyl group.

The study uncovered a totally unexpected fragmentation pathway in the decomposition of at least one deuterium-containing acid. It was discovered that the D on the carboxyl group of γ-(p-xylyl-2)-α-methylbutyric acid-d was shifted to the β carbon atom during fragmentation. This phenomenon is analogous to that recently reported in the literature (1),(2) for the fragmentation of benzoic acid.

MASS SPECTRA OF BENZOYL- AND XYLOYL- CONTAINING PROPIONIC ACIDS

The fragmentation patterns of these compounds are completely dominated by cleavage of the bond β to the aromatic ring. For example, in the mass spectrum of α-methyl-β-benzoylpropionic acid, the most intense peak (34%Σ) occurs at m/e 105:

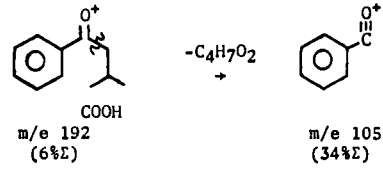

Decomposition of m/e 105 by loss of CO followed by fragmentation of the benzene ring probably leads to the formation of m/e 77 and 51:

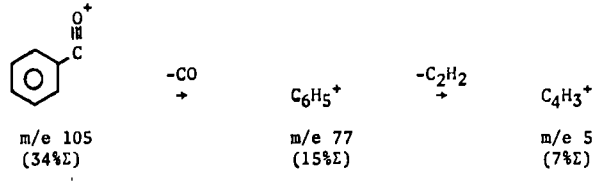

This mechanism has been proposed by Bowie et al (3) to explain the formation of the corresponding peaks in the spectra of aromatic β-keto esters.

When the benzene ring is replaced with xylene, the major fragment peaks are shifted by 28 mass units. Thus, cleavage of the bond β to the ring in β-(p-xyloyl-2)-α-methylpropionic acid produces m/e 133 and loss of CO from this fragment yields m/e 105:

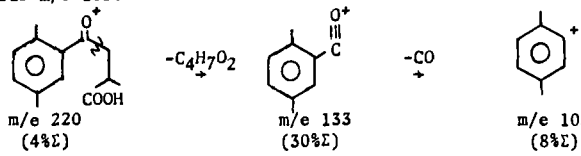

m/e 220 (4%Σ) → m/e 133 (30%Σ) → m/e 105 (8%Σ)

Two other fragment peaks of interest are those occurring at m/e 77 and 79. The corresponding ions probably originate from m/e 105 by ring cleavage to split out C_2H_2 followed by loss of molecular hydrogen:

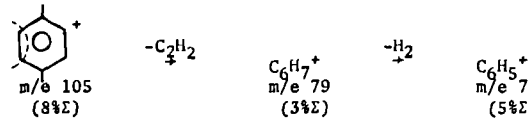

m/e 105 (8%Σ) → m/e 79 (3%Σ) → m/e 77 (5%Σ)

The process as it is shown here is analogous to that proposed by Meyerson and Rylander (4) to explain the formation of m/e 79 and 77 in the spectrum of ethylbenzene.

MASS SPECTRA OF XYLYLMETHYLBUTYRIC ACIDS

The fragmentation of these acids is also characterized by cleavage of the bond β to the aromatic ring. However, in contrast to the mass spectra of the substituted propionic acids, the spectra of the substituted butyric acids show intense peaks resulting from cleavage of the bond γ to the ring (or β to the carboxyl group).

The spectrum of γ-(p-xylyl-2)-α-methylbutyric acid is shown in Figure 1. Cleavage of the bond β to the ring produces the largest peak in the spectrum, which is located at m/e 119:

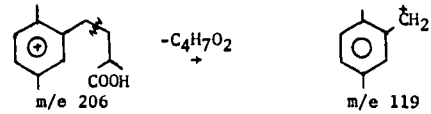

m/e 206 (3%Σ) → m/e 119 (12%Σ)

A large fragment ion also occurs at m/e 133, which arises by cleavage of the bond β to the carboxyl group without rearrangement:

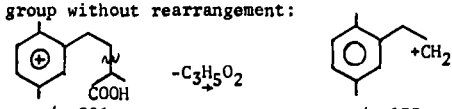

m/e 206 (3%Σ) → m/e 133 (9%Σ)

This type of cleavage is not present to an appreciable extent in the spectra of the β-methyl and γ-methyl isomers, and it apparently results from weakening of the bond β to the carboxyl group by the presence of the methyl group in the α position. The charge evidently goes with the aromatic moiety because of the relatively strong charge-attracting capability of the ring.

When the methyl group is moved to the β position (Figure 2) the fragment peak resulting from cleavage of the bond β to the carboxyl disappears, leaving only the corresponding rearrangement peak at m/e 146. On the other hand, the fragment resulting from cleavage of the bond β to the aromatic ring (m/e 119) is now much more intense than before. Evidently, location of the methyl group in the position β to the carboxyl group weakens the bond β to the aromatic ring. This factor together with the preferred fragmentation of the β bond because of the presence of the aromatic group probably accounts for the high intensity of the m/e 119 peak.

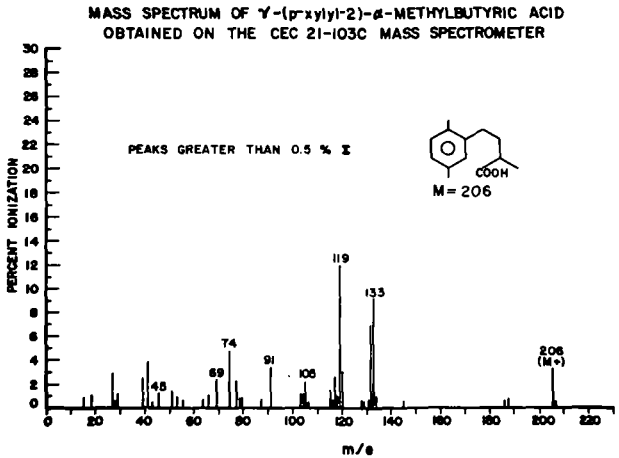

Figure 1

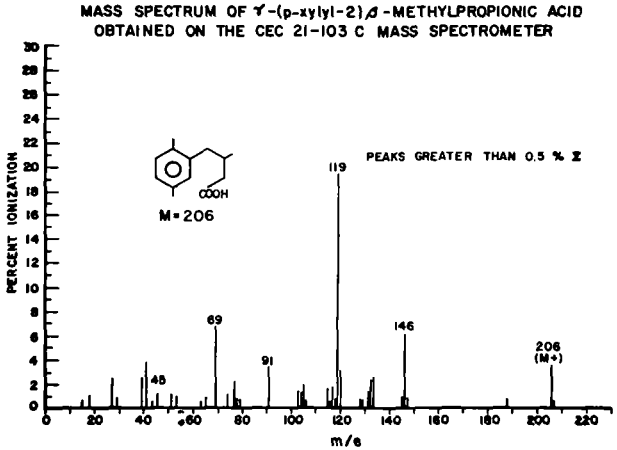

Figure 2

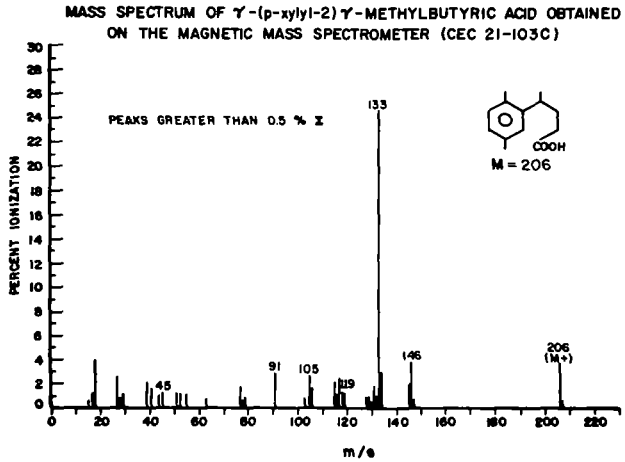

Figure 3

Another peak of interest in this spectrum is that occurring at m/e 69. In the spectrum of the α-methyl isomer it is about one-half as large as it is here, but in the spectrum of the γ-methyl isomer it disappears entirely. Although it is difficult to explain the formation of the peak, it may arise by slight thermal decomposition in the 300°C inlet of the magnetic mass spectrometer. When the compound was run at near room temperature on a time-of-flight instrument equipped with a solid-sample probe, only a very small peak was observed at m/e 69. On the other hand, the remaining peaks in the TOF spectrum were very similar to those in the spectrum obtained on the magnetic instrument.

When the methyl group is moved to the γ position (Figure 3) the intensity of the peak arising from cleavage of the bond β to the aromatic ring (m/e 133) is increased even further. The increase probably results because the presence of the CH_3 in the γ position not only weakens the bond but also tends to draw the charge toward the aromatic moiety.

Cleavage of the bond β to the carboxyl group accompanied by hydrogen transfer accounts for the formation of a number of rearrangement peaks in the spectra of the xylylmethylbutyric acids. These are summarized in Figures 4 and 5. By means of the well-known McLafferty rearrangement (5), involving the formation of a 6-membered cyclic transition state with the transfer of a γ hydrogen to the carbonyl oxygen, the moderately intense peak at m/e 74 in the spectrum of a α-methyl isomer is formed (Figures 1 and 4). In the spectra of the β-methyl and γ-methyl isomers relatively small peaks arising from the same mechanism are formed at m/e 60 (Figures 2, 3, and 4).

The intense peak for the α-methyl isomer probably arises because the location of the CH_3 in the α position tends to draw the charge toward the carboxyl-containing species. On the other hand, the location of the methyl group in the β or γ position results in the charge being drawn away from the oxygen-containing moiety (toward the aromatic ring) to produce peaks of low intensity at m/e 60. Also, the intensity of the peak for the γ-methyl isomer is probably decreased because only one γ hydrogen instead of two is available for the formation of the 6-membered cyclic transition state.

In addition to the rearrangement peaks formed by cleavage of the bond β to the carboxyl group with the charge being retained by the oxygen-containing species, intense peaks are formed upon retention of the charge by the moiety containing the aromatic ring (Figure 5). This phenomenon has been observed previously and is discussed in some detail by Spiteller and Spiteller-Friedmann (6). In the spectra of the α- and β-methyl isomers the peaks, m/e 132 and 146, respectively, both have intensities of 6 and 7%. However, in the spectrum of the γ-methyl isomer the intensity of the peak (m/e 146) is reduced to less than 4%. The reduction in intensity probably results because the γ-methyl isomer has only one γ hydrogen instead of two available to form the rearrangement peak.

The most interesting phenomenon in the mass spectra of the xylylmethylbutyric acids was observed when the H on the carboxyl group of γ-(p-xylyl-2)-α-methylbutyric acid was replaced with deuterium. Figure 6 shows the mass spectrum of the compound without deuterium. This is the same spectrum as shown in Figure 1 except that it was obtained on the time-of-flight mass spectrometer instead of the magnetic instrument to avoid the possibility of thermal decomposition. The important feature to note in Figure 6 is that the m/e 133 peak has an intensity of about 13% and the m/e 134 peak an intensity of about 2%.

In Figure 7 is shown the time-of-flight spectrum of the compound with the H of the carboxyl group replaced by D (about 50% deuteration). It should be noted that now the intensity of the m/e 133 peak has dropped from about 13 to 10% and that the intensity of m/e 134 has increased from about 2 to better than 5%. Because no significant shifts occur in the peaks of the lower mass region (excluding the oxygen-containing fragments), it can only be concluded that the deuterium is somehow transferred from the carboxyl group to the β carbon atom during initial fragmentation. This unexpected phenomenon is analogous to a transfer of D in the fragmentation of benzoic acid recently reported by Meyerson and Corbin (1) and independently by Beynon, Job, and Williams (2).

FRAGMENTATION OF METHYLXYLYLBUTYRIC ACIDS
FORMATION OF REARRANGEMENT PEAKS BY CLEAVAGE OF THE BOND β TO THE CARBOXYL GROUP WITH RETENTION OF CHARGE BY THE OXYGEN-CONTAINING MOIETY

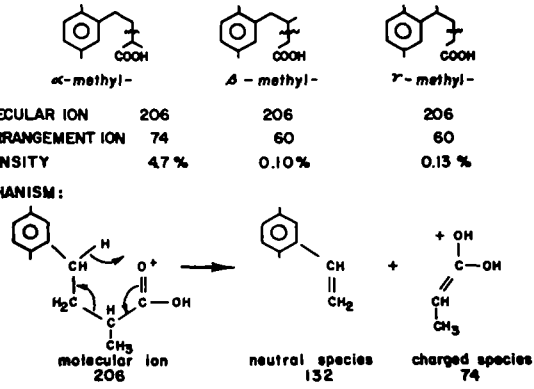

Figure 4

FRAGMENTATION OF METHYLXYLYLBUTYRIC ACIDS
FORMATION OF REARRANGEMENT PEAKS BY CLEAVAGE OF THE BOND β TO THE CARBOXYL GROUP WITH RETENTION OF CHARGE BY THE AROMATIC MOIETY

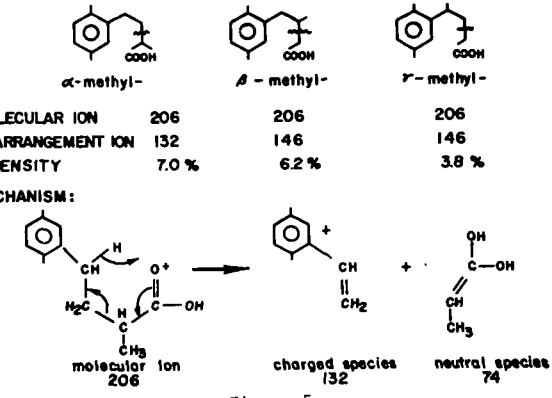

Figure 5

MASS SPECTRUM OF γ-(p-xylyl-2)-α-METHYLBUTRIC ACID OBTAINED ON THE TIME-OF-FLIGHT MASS SPECTROMETER

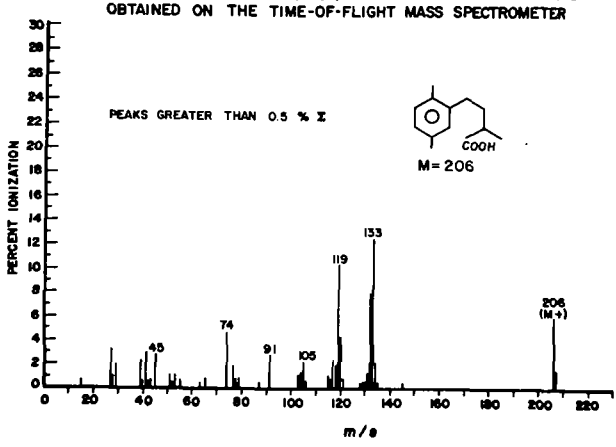

Figure 6

Obviously, sufficient evidence is not yet available to formulate a sound mechanism, but it can be proposed that the D on the carboxyl group is equilibrating with an H on the β carbon atom during initial fragmentation. This process is shown in Figure 8. Here, because of rotation of the carboxyl group, the D is pictured as being able to exchange with one of the hydrogens on the β carbon atom through the formation of a 5-membered cyclic transition state.

Although the possible transfer of deuterium in the fragmentation of the β- and γ-methyl isomers of the xylylmethylbutyric acids has not yet been tested, this is the next step in the investigation. In addition, further evidence for the transfer could be obtained from the mass spectra of the compounds in which the hydrogens on the β carbon atom were replaced with deuterium. Thus, if an equilibration is really taking place during initial fragmentation, then deuterium should appear in the carboxyl fragment, i.e., m/e 45 should shift to m/e 46.

The unexpected shift of deuterium from a carboxyl group to a β carbon atom as described above provides an example of how little is actually known about the chemistry of carbonium ions reacting in the gaseous phase. Although the reactions of these ions, either in the gaseous or the solution phase, are ordinarily described using classical organic structures, it is becoming increasingly evident that the actual structures may be entirely different than those usually pictured. These structural distinctions would, of course, lead to many unexpected results in carbonium-ion reactions. Mass spectrometric investigations have been and will continue to be a powerful tool for providing insight into this relatively new field of organic chemistry.

REFERENCES

1. Meyerson, S., and Corbin, J. L., J. Am. Chem. Soc., 87, 3045 (1965).

2. Beynon, J. H., Job, B. E., and Williams, A. E., Zeit. für Naturforschung, 20a, 883 (1965).

3. Bowie, J. H., Lawesson, S.-O., Schroll, G., and Williams, D. H., J. Am. Chem. Soc., 87, 5742 (1965).

4. Meyerson, S., and Rylander, P. N., J. Am. Chem. Soc., 79, 1058 (1957).

5. McLafferty, F. W., Anal. Chem., 31, 82 (1959).

6. Spiteller, G. and Spiteller-Friedmann, M., Monatsh. für Chemie, 95, 257 (1964).

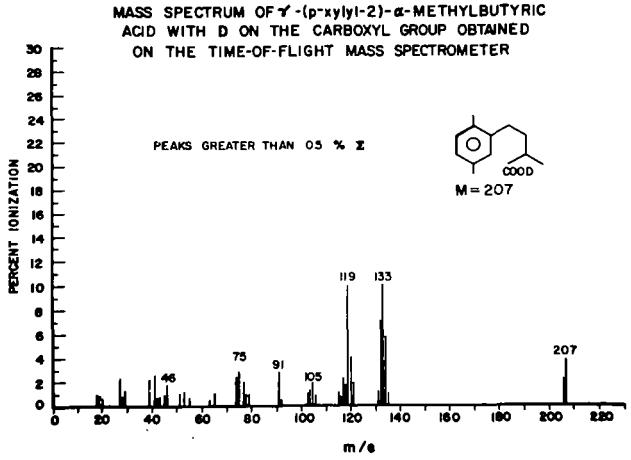

Figure 7

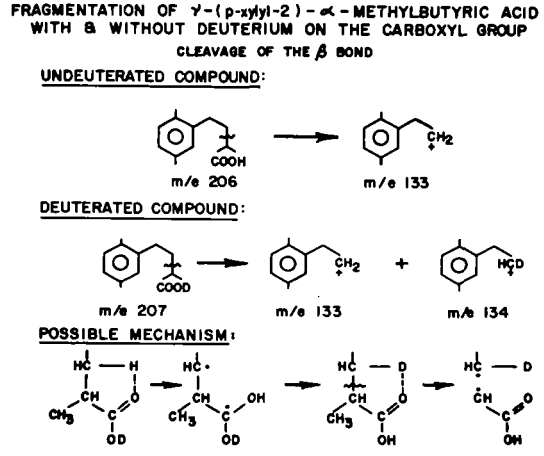

Figure 8

MASS SPECTROMETRIC ANALYSIS OF SOME 8-HYDROXYQUINOLINES*

by
Robert L. Stevenson and Morton E. Wacks
Department of Chemistry
University of Arizona
Tucson, Arizona 85721

Abstract

The mass spectra of a series of 8-hydroxyquinolines are reported. The fragmentation pathways, based upon examination of the mass spectra, isotope and metastable peaks for 8-hydroxyquinoline, 2-methyl-8-hydroxyquinoline, 8-hydroxyquinaldol, 8-hydroxyquinaldamine, 8-hydroxyquinaldal, 8-hydroxyquinaldal oxime, and 2-tertiary-butylamine-8-hydroxyquinaldolimine are discussed.

Introduction

The correlation of mass spectra with molecular structure has been demonstrated for many classes of compounds[1]. In the case of polyfunctional compounds fragmentation may occur by several competing pathways making mass spectral correlations in these compounds exceedingly difficult. This competition between different fragmentation modes can result in widely differing mass spectra from closely related compounds. In order to study the effects of varying substituents in polyfunctional compounds on their mass spectra a series of 2-substituted 8-hydroxyquinolines (8-quinolinols) was prepared. The competitive pathways for fragmentation in these compounds were evident in their mass spectra. The observed metastable transitions indicated that this competition involved fragmentation of the exocyclic constituents versus ring rupture as well as competition between fragmentation of the phenolic ring and the nitrogen containing ring.

Experimental

The mass spectra were obtained on a CEC 21-103 C mass spectrometer equipped with an all glass heated inlet system. The spectra were obtained in the laboratories of the Pittsburgh Coal Research Center, United States Department of the Interior, Bureau of Mines, Pittsburgh, Pennsylvania. The temperature of the introduction system for all samples was 120° C, except for the 2-tertiary-butylamine-8-hydroxyquinaldolimine which was run at 140° C. The sample sizes varied from one to three milligrams.

The compounds were either purified commercial product or were synthesized at the University of Arizona. A brief description of these compounds follows:

8-hydroxyquinoline; obtained from Malinkrodt Chemical Company, recrystallized from ligroin. Melting point, 73.1-73.5° C.

8-hydroxyquinaldine; purchases from Aldrich Chemical Company and recrystallized from ligroin. Melting point, 74° C.

8-hydroxyquinaldal oxime; 8-acetoxyquinaldal was condensed with hydroxylamine to give the 8-hydroxyquinaldal oxime. The oxime was sublimed before use. Melting point 166-168° C.

8-hydroxyquinaldamine; sublimed 8-hydroxyquinaldal oxine was reduced with hydrogen and 10% Pd/charcoal to give 8-hydroxyquinaldamine. The amine was sublimed before use. Melting point 142° C, dec.

8-hydroxyquinaldol; 8-acetoxyquinaldal was reduced with $NaBH_4$ in ethanol to give 8-hydroxyquinaldol. Melting point 112° C.

2-tertiarybutylamine-8-hydroxyquinaldalimine; 8-acetoxyquinaldal was condensed with excess t-butylamine to give the imine. This compound decomposes above 120° C.

8-hydroxyquinaldal was obtained as described by Buchi[2]. Melting point 99° C.

Results and Discussion

8-HYDROXYQUINOLINE. The major features of the mass spectra of 8-hydroxyquinoline are, parent ion, loss of CO followed by loss of HCN from the parent ion and the further decomposition of the resulting hydrocarbon ion. Some multiply charged ions are also observed. The peaks at m/e = 117 and 116 result from the parent ion (m/e = 145) losing CO and HCO respectively. The initial loss of HCN from the parent molecular ion is unimportant since the peak corresponding to this loss (m/e = 118) is entirely accountable as the isotopic contribution from the m/e = 117 peak, loss of CO from the parent. However, loss of a cyanide containing fragment following the loss of CO is indicated by the peaks observed at m/e = 90 and 89.

* This research was supported by a National Institutes of Health research grant.

The metastable transitions observed in this compound are shown in Table I. The metastable at m/e = 94.5 is due to the loss of CO from the parent ion. The loss of HCN from the (P-28) fragment is indicated by the metastable transition corresponding to the observed ion peak at m/e = 69.

TABLE I. 8-HYDROXYQUINOLINE

Structure

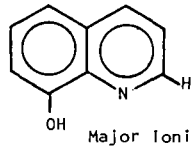

Metastable Transitions

m_i	m_f	m*	% base
145	117	94.5	0.08
$p^+ \rightarrow (p-28)^+ + CO$			
117	90	69	0.3
$(p-28)^+ \rightarrow (p-56)^+ + HCN$			

Major Ionization-Dissociation Processes

m/e	% Base Peak	Process
145	100	$p \rightarrow p^+ + e^-$
117	75.7	$p^+ \rightarrow (p-28)^+ + CO$
116	11.8	$p^+ \rightarrow (p-29)^+ + HCO$
90	21.2	$(p-28)^+ \rightarrow (p-55)^+ + HCN$
89	23.7	$\{(p-29)^+ \rightarrow (p-56)^+ + HCN$ $(p-28)^+ \rightarrow (p-56)^+ + H_2CN\}$

This preferential fragmentation of the phenolic ring which in turn is followed by fragmentation of the phenolic ring is in agreement with the calculations of Burton and Davis[3]. These calculations indicate that the carbonium ion formation is favored in the phenolic ring and thus primary decomposition should involve loss of CO from the phenoxy cation[4].

2-METHYL-8-HYDROXYQUINOLINE. The spectral features of this compound are similar to those of 8-hydroxyquinoline. The initial loss of CO is indicated by the large metastable transition observed at m/e = 108.5, as shown in Table II. The (p-27) peak can be accounted for entirely as the isotope peak of the (p-28) peak. The (p-29) peak has increased in intensity relative to the (p-28) peak in the 8-hydroxyquinoline, but it is still less than that observed with other phenols[4]. The influence of the electron donating methyl group in stabilizing the parent molecular ion with respect to ring rupture is seen by comparison with the mass spectra of 8-hydroxyquinoline.

TABLE II. 2-METHYL-8-HYDROXYQUINOLINE

Structure

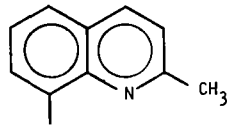

Metastable Transitions

m_i	m_f	m*	% base
159	131	108.5	0.57
$p^+ \rightarrow (p-28)^+ + CO$			
131	104	82	0.06
$(p-28)^+ \rightarrow (p-55)^+ + HCN$			
116	89	68	0.007
$(p-43)^+ \rightarrow (p-70)^+ + HCN$			

Major Ionization-Dissociation Processes

m/e	% Base Peak	Process
159	100	$p \rightarrow p^+ + e^-$
131	56.7	$p^+ \rightarrow (p-28)^+ + CO$
130	27.9	$p^+ \rightarrow (p-29)^+ + HCO$
104	4.7	$(p-28)^+ \rightarrow (p-55)^+ + HCN$
103	8.5	$\{(p-28)^+ \rightarrow (p-56)^+ + H_2CN$ $(p-29)^+ \rightarrow (p-56)^+ + HCN\}$
102	4.5	$(p-29)^+ \rightarrow (p-57)^+ + H_2CN$

The weak peaks seen in the m/e 114-117 region are due to the loss of the exocyclic methyl group and CO. The low intensity of these peaks is consistent with the low probability of losing a CH_3 as observed in monomethyl indenes[5]. The weak metastable transition observed at m/e = 68, indicating the loss of CH_3 prior to the loss of HCN is also consistent with these observations.

The peak at m/e = 104 and the metastable transition at m/e = 82 are due to the loss of HCN following the loss of CO. The mode of fragmentation of the two rings seems to

be in the order of the most basic (phenol) or electronegative substituent fragmenting first, followed by the fragmentation of the next most basic group.

8-HYDROXYQUINALDOL. The addition of a benzyl alcohol group to the 8-quinolinol system promotes the degree of fragmentation. This hydroxyl group is electron withdrawing and reduces the stability of the parent molecular ion thus promoting fragmentation. In addition, the new alcoholic group is in an especially favorable position to pick up a proton from either the 3 position or the phenolic proton. Thus the dehydration of the molecule ion is not surprising. The metastable peak at m/e = 141 verifies this dehydration of the parent molecular ion. This is shown schematically in Figure 1.

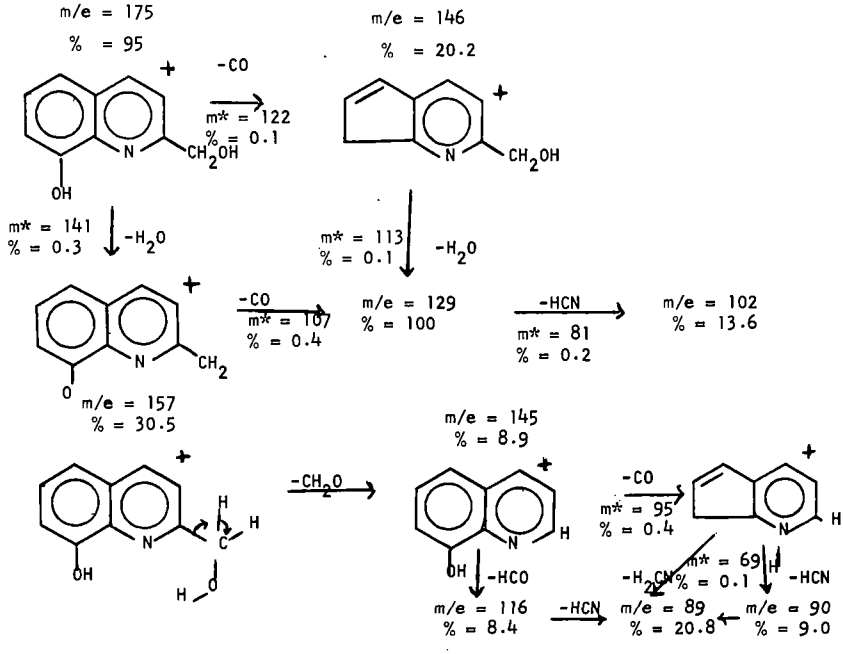

Figure 1. Ionization-dissociation processes in 8-hydroxyquinaldol.

The high intensity of the (p-29) peak relative to the (p-28) peak is explained on the basis of the geometry of the molecule. A molecular model shows that the alcoholic proton is in a much more favorable position for hydrogen bonding than the phenolic proton. Assuming that the alcoholic proton does effectively block the nitrogen to the phenolic proton, then the phenolic proton is forced to leave with the carbon monoxide as is the case for phenol.

Rupture of the exocyclic carbon-carbon bond with transfer of a hydrogen gives the 8-quinolinol molecular ion (m/e = 145). This is bond rupture β to a hetero atom, a well known fragmentation pathway. The loss of CO from the phenolic ring gives rise to the peak at m/e = 117. Further support for this mode of fragmentation is given by the metastable peak at m/e = 95, which corresponds to the loss of CO from the 8-hydroxyquinoline ion.

Further fragmentation, with the loss of HCN, explains the peak at m/e = 90 and the metastable peak at m/e = 69. The loss of an additional proton gives rise to the peak at m/e = 89. The reason for the unusually high intensity for the m/e = 89 may be due to the formation of a more stable C_7H_5 ion in which all electrons are paired.

8-HYDROXYQUINALDAMINE. The spectrum of this compound is similar to that of 8-hydroxyquinaldol. The relative importance of the competing dissociation pathways is altered by the diminished electron withdrawing ability of the NH_2 group compared to that of the hydroxyl group.

As in the methyl alcohol derivative, there are two competing modes of fragmentation

leading to the m/e = 129 peak. The metastable peaks indicate that the loss of CO can occur either before or after the loss of NH_3 (Figure 2). The NH_2 group is able to accept a proton from either the 3 position or the phenol thus enhancing the loss of NH_3, however, no metastable peak corresponding to this loss as observed. The ion resulting from loss of NH_3 from the parent molecular ion proceeds to lose a CO as indicated in figure 2. This fragmentation pathway is confirmed by the metastable transition observed at m/e = 106. The relative intensities of the ions at m/e = 146 and 157 and the metastable transitions at m/e = 123 and 106 indicate that the loss of NH_3 is a very rapid process when energetically possible.

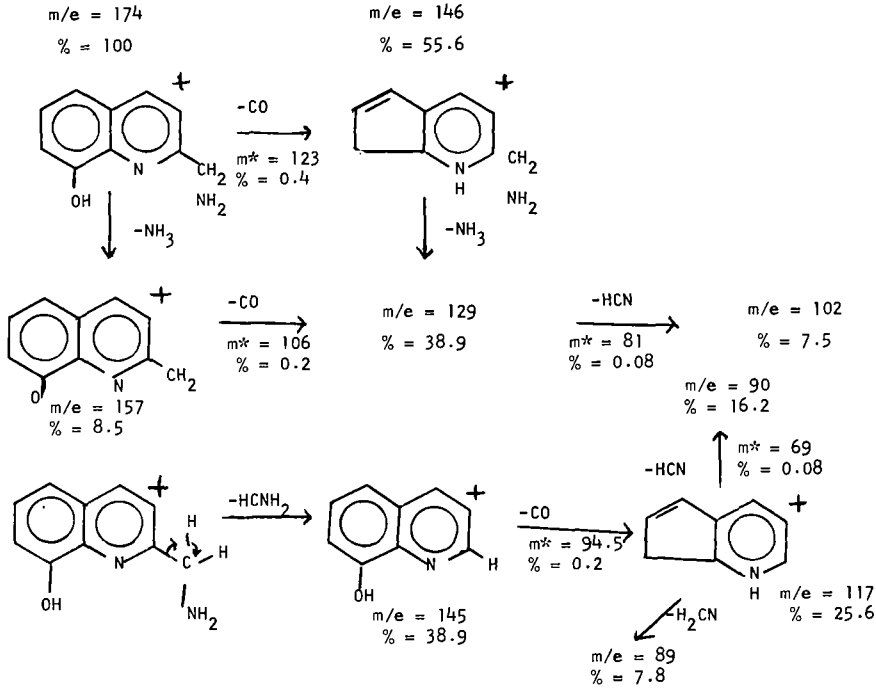

Figure 2. Ionization-dissociation processes in 8-hydroxyquinaldamine.

The large relative abundance of the m/e = 145 ion may be due to the formation of a daughter ion by the loss of H_2CN from the parent molecular ion in addition to the loss of CO as shown in fig.2. The increased intensity of the (p-29) ion peak at m/e = 145 relative to the (p-28) peak in this compound is due to the rupture of the exocyclic carbon-carbon bond. This loss of the side chain with proton transfer results in the formation of an 8-hydroxyquinoline ion. This ion then fragments, as shown previously, by loss of CO followed by loss of HCN. This pathway is confirmed by the metastable transitions corresponding to the peaks observed at m/e = 94.5 and 69.

8-HYDROXYQUINALDAL. The aldehyde group being attached to an electron deficient carbon produces a change in the mass spectral cracking pattern that which might have been expected for this compound. The (p-1) and (p-29) peaks are usually strong in aromatic aldehydes[6], however, in the case of 8-hydroxyquinaldal the (p-1) peak is weak, possibly due to the difficulty of forming an acylium ion α to the positive charge located on the 2 carbon. In this compound the loss of CO, m/e = 145, from the parent molecular ion is more important than the loss of HCO, (p-29). This may be due to the stability of the parent molecular ion of 8-hydroxyquinoline which is formed by the loss of CO from the aldehyde side chain. The metastable transition corresponding to the peak at m/e = 122, Table III, demonstrates this loss of CO from the parent ion. There is also a metastable peak at m/e = 94.5 corresponding to the loss of an additional neutral CO fragment from the m/e = 145 ion. This gives the second largest peak in the spectrum at m/e = 117. The loss of HCN from this ion is indicated by the metastable peak at m/e = 69.

In contrast to the observations of Cummings and Bleakney[7] the mass spectra of this

and the other compounds reported here which contain a single nitrogen atom show a great predominance of odd mass ions. This is due to the relative ease of losing neutral, even mass fragments in these compounds which leaves an odd mass ion in the major fragmentation pathways.

TABLE III. 8-HYDROXYQUINALDAL

Structure

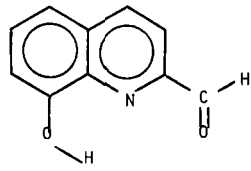

Metastable Transitions

m_i	m_f	m*	% base
173	145	122	0.6
$p^+ \rightarrow (p-28)^+ + CO$			
145	117	94.5	0.5
$(p-28)^+ \rightarrow (p-56)^+ + CO$			
117	90	69	0.2
$(p-56)^+ \rightarrow (p-83)^+ + HCN$			

Major Ionization-Dissociation Processes

m/e	% Base Peak	Process
173	100	$p \rightarrow p^+ + e^-$
145	25	$p^+ \rightarrow (p-28)^+ + CO$
144	16.8	$p^+ \rightarrow (p-29)^+ + HCO$
117	56.7	$(p-28)^+ \rightarrow (p-56)^+ + CO$
116	17.1	$(p-28)^+ \rightarrow (p-57)^+ + HCO$
115	10.7	$(p-29)^+ \rightarrow (p-58)^+ + HCO$
90	13.6	$(p-56)^+ \rightarrow (p-83)^+ + HCN$
89	32.3	$(p-56)^+ \rightarrow (p-84)^+ + H_2CN$ $(p-57)^+ \rightarrow (p-84)^+ + HCN$ $(p-58)^+ \rightarrow (p-84)^+ + CN$

It should be possible to differentiate between the initial loss of CO from the phenol and aldehyde functional groups by isotopic labelling of the aldehyde with O-18. Oxidation of 2-methyl-8-acetoxyquinolinol with O-18 enriched selenium dioxide should give the labeled aldehyde group. An increase in the relative importance of the loss of 30 mass units would show the relative importance of the loss of CO from the aldehyde group to that from the phenol.

8-HYDROXYQUINALDAL OXIME. The mass spectrum of this compound is characterized by the degradation of the exocyclic group in addition to the fragmentation pattern of the parent 8-quinolinol. As in 8-hydroxyquinaldol, the OH group of the oxime is in an especially favorable position for hydrogen bonding to the quinoline nitrogen and for picking up another hydrogen so that a neutral molecule of H_2O can be lost. This latter is the most probable process and gives rise to the base peakof the spectrum. The predicted molecular geometry indicates that the 3 position is a particularly good site for deprotonation in this process.

The fission of the phenolic ring to split our CO is the next most important process. This is also indicated by the metastable peak at m/e = 119.5. This process is followed by the loss of an HCN molecule as seen in Table IV, presumably from the side-chain, accounting for the peak at m/e = 115. The loss of an additional CN radical gives rise to the m/e = 89 peak.

As in the case of the methyl alcohol and methyl amine derivatives there are other competing pathways capable of producing the major peaks in their mass spectra. Further degradation of the side chain after loss of H_2O with the loss of HCN gives the m/e = 143 peak. In this dissociation sequence which is less important than the initial ion formed by loss of CO, the metastable peak at m/e =94 could correspond to the splitting out of CO from the m/e = 143 fragment ion. This peak is not resolved well enough to differentiate between the many probable processes involving the loss of a neutral fragment. However the intensity of this peak is greater than that at m/e = 119.5, corresponding to the loss of CO from the dehydrated fragment of mass 170 which supports the possibility that the metastable peak at m/e = 94 does not arise from a unique fragmentation step, but is a combination of two or more of the possible processes as seen in Table IV.

TERTIARYBUTYLAMINE-8-HYDROXYQUINALDALIMINE. The mass spectrum of this compound is consistent with the structure of the compound and the previous discussions. The compound is readily attacked by water or moist air, however, the isotope peaks and mass spectrum fit the molecular formula $C_{14}H_{16}N_2O$and indicate that the compound is of good purity.

The fragmentation pattern of the compound is characterized by the high probability of the loss of the side-chain from the aromatic portion of the molecule. The loss of the side chain by rupture of the exocyclic carbon-carbon bond and transfer of a hydrogen

generates the base peak of the mass spectrum at m/e = 145 corresponding to the parent molecular ion of 8-hydroxyquinoline as indicated in Table V. The loss of a C_4H_8 fragment is also a highly favored fragmentation process giving rise to the prominent peak at m/e = 172. The remainder of the observed spectrum is similar to that of 8-hydroxyquinoline with the exception of the (p-15) peak which is undoubtedly due to the not unexpected loss of a CH_3 group from the tertiarybutyl group.

TABLE IV. 8-HYDROXYQUINALDOXIME

Structure

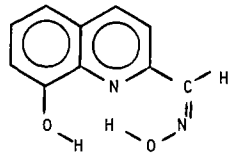

Metastable Transitions

m_i	m_f	m*	% Base
170	142	119.5	0.7
$(p-18)^+ \rightarrow$	$(p-46)^+ + CO$		
142	115	94	0.1
$(p-46)^+ \rightarrow$	$(p-73)^+ + HCN$		

Major Ionization-Dissociation Processes

m/e	% Base Peak	Process
188	88.5	Ionization
170	100	loss of water
145	21.5	loss of side chain
144	19.2	
143	28.3	loss of water, HCN from side chain
142	60	loss of water, CO
117	12.2	loss of side chain, HCN
116	14.9	
115	40.7	loss of side chain, CO
114	14.7	
90	15	
89	36.7	loss of side chain, CO and HCN
88	21.9	

TABLE V. 2-TERTIARYBUTYLAMINE-8-HYDROXYQUINALDALIMINE

Structure

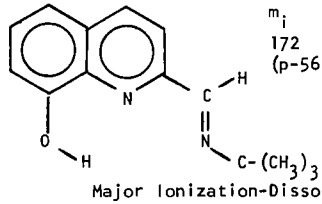

Metastable Transitions

m_i	m_f	m*	% Base
172	145	123.5	1.5
$(p-56)^+ \rightarrow$	$(p-83)^+ + HCN$		

Major Ionization-Dissociation Processes

m/e	% Base Peak	Process
228	57.2	$p \rightarrow p^+ + e^-$
213	10.7	$p^+ \rightarrow (p-15)^+ + CH_3$
172	67.8	$p^+ \rightarrow (p-56)^+ + C_4H_8$
145	100	$p^+ \rightarrow (p-83)^+ + C_5H_8N$
		$(p-56)^+ \rightarrow (p-83)^+ + HCN$
144	14.5	$p^+ \rightarrow (p-84)^+ + C_5H_{10}N$
117	16.0	$(p-83)^+ \rightarrow (p-111)^+ + CO$
116	9.0	$(p-83)^+ \rightarrow (p-112)^+ + HCO$
115	12.6	$(p-84)^+ \rightarrow (p-113)^+ + HCO$
89	13.6	$(p-111)^+ \rightarrow (p-139)^+ + H_2CN$

Conclusion

The ionization-dissociation pathways in a series of 2-substituted 8-hydroxyquinolines have been deduced from mass spectral data. Primary dissociation of the aromatic portion of the molecule was seen to be the loss of CO from the phenolic ring followed by the loss of HCN from the nitrogen containing ring. The processes associated with substituents in the 2 position were degradation of the side-chain followed by dissocia-

tion of the resulting 8-hydroxyquinoline molecular ion on the molecular ion less an ^1H.

The major dissociation processes observed were associated with loss of neutral species from the various ions. These fragmentations resulted in an unexpectedly large contribution by ions of odd mass to the mass spectra of these compounds containing one nitrogen atom. Isotopic substitution would help confirm the order of fragmentation processes as proposed on the basis of the metastable transitions observed. The structure of the relatively uncommon m/e = 89 and 90 hydrocarbon ions may be cyclic however proof of their structures based on energetic considerations would be a hopeless task.

Additional studies of isotopically substituted 8-hydroxyquinolines, their mass spectra and ionization and appearance potentials as a function of substitution position on the ring would be of extreme value in fully understanding the ionization-dissociation processes in these compounds.

References

1. K. Biemann, "Mass Spectrometry", McGraw-Hill Series in Advanced Chemistry (1962). p. 74.

2. J. Buchi, A. Aehi, A Deflovin, and H. Hurni, Helv. Chim. Acta, 39, 1676 (1956).

3. R. E. Burton and W. J. Davis, J. Chem. Soc. 344, 1766 (1964).

4. T. Aczel and H. E. Lumpkin, Anal. Chem., 32, 1819 (1960).

5. J. H. Beynon, A. E. Williams, Appl. Spectroscopy, 13, 101 (1959).

6. T. Aczel and H. E. Lumpkin, Anal. Chem., 33, 386 (1961).

7. C. S. Cummings and W. Bleakney, Phys. Rev., 58, 787 (1940).

Electron Impact Studies I : Skeletal Rearrangements
Of Semicarbazones And Thiosemicarbazones.*

K.G. Das and P.S. Kulkarni
National Chemical Laboratory, Poona 8, India.

We have recently reported on the skeletal rearrangements of various types of orgenic compounds under electron impact involving the migration of alkyl and aryl groups.[1] Evidence wes also obtained for the migration of hydroxy group induced by electron impact in various substituted acetophenones.[2]

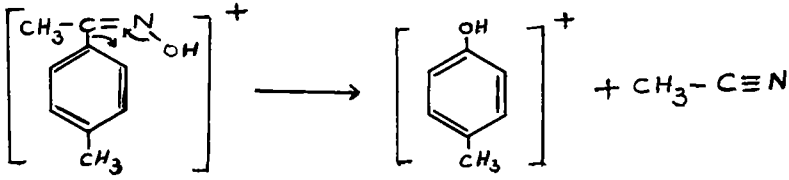

We wish to report here on skeletal rearrangements under electron impact of several semicarbazones and thiosemicarbazones of substituted acetophenones (I to V) and (VI to X).

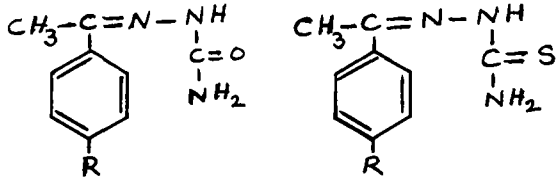

I R = H	VI R = H
II R = Br	VII R = Br
III R = CH_3	VIII R = CH_3
IV R = OCH_3	IX R = OCH_3
V R = NO_2	X R = NO_2

It was observed that in the all glass heated inlet system these compounds undergo thermal rearrangement to a very great extend. A close study of the mass spectra obtained indicate that due to pyrolysis two molecules of these compounds decompose into one molecule of the dihydrazone and one molecule of diurea or dithiourea as the case may be.

2 moles Semicarbazone ——→ 1 mole Dihydrazone + 2 moles Diurea

2 moles Thiosemicarbazone ——→ 1 mole Dihydrazone + 2 moles Dithiourea

It was possible to get satisfactory mass spectra of these compounds only by using the direct inlet system and by volatalising the compounds very slowly. It was found that pyrolysis was completely eliminated by this technique.

*N. C. L. communication number 897

The expected major fragments from the straight cleavage are observed.

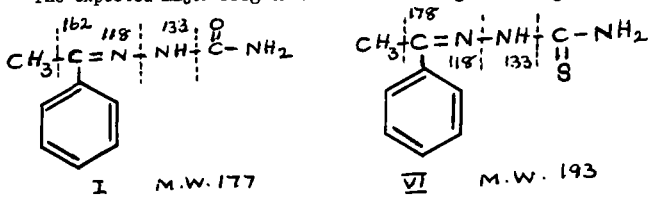

A comparison of the mass spectra of semicarbazones and thiosemicarbazones showed many similarities and a few differences in the fragmentation modes.

In our studies on the fragmentation of carbonyl derivatives under electron impact we obtained evidence for the migration of amino groups in the mass spectra of the hydrazones of several substituted acetophenones.[5]

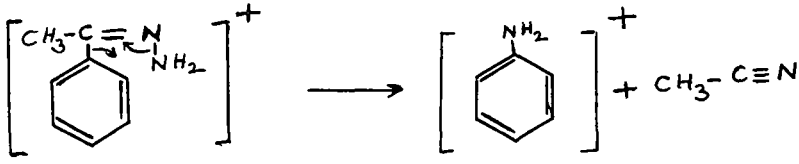

In the mass spectra of all the semicarbazones and thiosemicarbazones of the substituted acetophenones besides the fragments formed by simple cleavage there are peaks that can be explained only on the basis of skeletal rearrangement. Thus the peaks at m/e 134 and m/e 93 observed in the mass spectrum of acetophenone semicarbazone gave a clue to a rearrangement involving the migration of an amino group under electron impact.

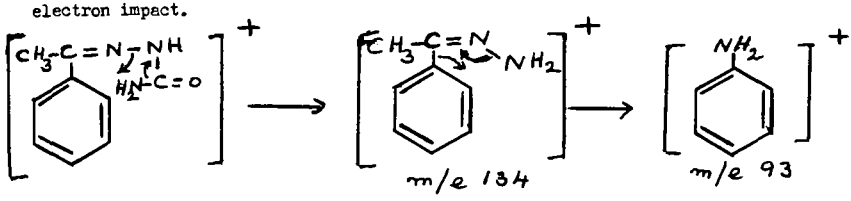

In the mass spectra of all the other substituted acetophenones II to V the expected peaks resulting from this type of rearrangement are observed. The thiosemicarbazones were also found to undergo similar type of rearrangement.

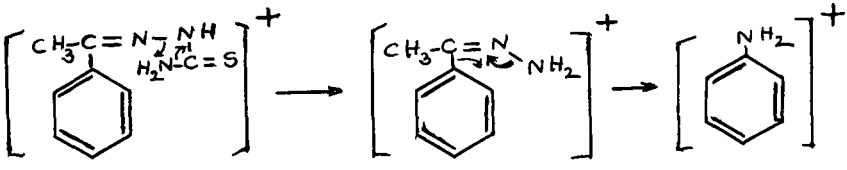

The fragments with m/e 176 and m/e 161 observed in the mass spectrum of acetophenone thiosemicarbazone can be regarded as being formed by a rearrangement involving the transfer of a proton as indicated in the following mechanism

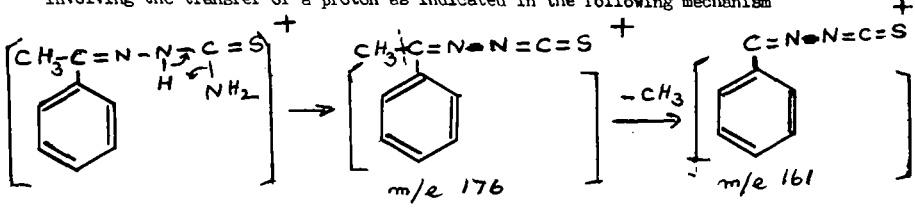

The metastable peak observed in the massspectrum of compound I at m/e 58.5 shows that the fragment A rearranges to fragment B .

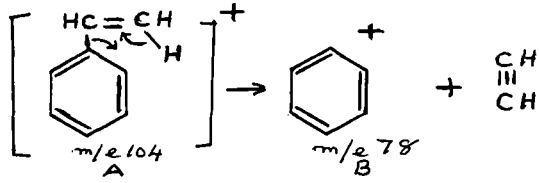

Similar type of rearrangement does not take place in the fragmentation of compound VI . This was concluded from the absence of the corresponding peaks and metastable peaks to support the rearrangement. However the metastable peak observed at m/e 57.5 in the mass spectrum of acetophenone thiosemicarbazone (VI) shows that the fragment with m/e 103 is rearranging to the fragment with m/e 77.

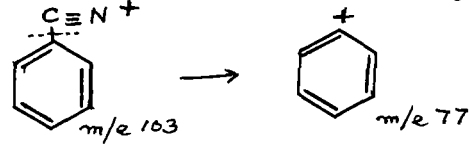

A detailed interpretation of the mass spectra of these compounds will be published elesewhere.

The mass spectra of a number of dihydrazones of substituted acetophenone were obtained using the heated inlet system and the direct inlet. An interpretation of the spectra showed all the peaks arising from straight cleavage end a few extra peaks which indicate the migration of aryl groups.

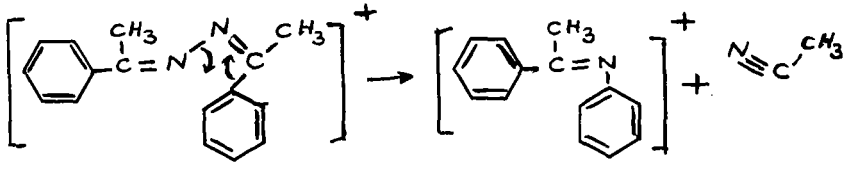

It will be seen that in all these rearrangements involving the migration of groups heavier than hydrogen atom the driving force appears to be the ease with which a stable neutral molecule is expelled and the stability of the fragment formed as a result of this migration. Probably the steric proximity of the migrating group and the receptor site also play an important part in inducing this type of rearrangements.

All the mass spectra were run on CEC 21 - 103C mass spectrometer. We are thankful to Prof. A.K.Bose, Stevens Institute of Technology, Hoboken, N.J. and Mr. J. Gurrera, International Flavours and fragrance,U.S.A. for the mass spectra.

References

1. A.K.Bose, Irene Kugajevsky, P.T.Fuke and K.G.Das, Tet. Let. 35, 3065 (1965)
2. A.K.Bose, K.G.Das, P.T.Fuke and B.F.Lee, J.Am.Chem. Soc.(in press)
3. A.K.Bose and K.G.Das (unpublished results)

Fragmentation of Some β-Lactams

M.S. Mamhas, B.N. Ghosh-Mazumdar and Ajay K. Bose
Stevens Institute of Technology
Hoboken, New Jersey

Abstract

The fragmentation under electron impact of several substituted β-lactams has been studied. Additional evidence for fragmentation modes was obtained from the spectra of some b-lactams labeled with ^{15}N or D. In the case of a few selected compounds precise molecular composition of fragments was determined by high resolution mass spectrometry.

The previously noted modes of fragmentation [W. Richter and K. Biemann, Monatsh. Chem. 95, 766 (1964)] were found to occur in all the β-lactams examined.

Evidence for aryl migration was provided by the presence of moderately strong peaks in the mass spectra of some β-lactams. These peaks have been attributed to the fluorene or substituted fluorene ions which can arise only through the migration of an aryl group. It should be noted that this migration of the phenyl ring from the nitrogen to carbon takes place across the β-lactam ring. It is quite possible, however, that this migration occurs not in the intact β-lactam but in some open chain fragment derived from it under electron impact.

Substituted β-lactam provide many pathways for fragmentation. Most of these can be rationalized in the light of our present knowledge of mass spectral fragmentation. A stable fragment that is seen in the spectra of this class of compounds can be represented as I or its equivalent. In the

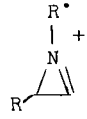

I

mass spectra of some β-lactams we have observed another set of peaks which can be rationalized on the basis of alkoxy migration. High resolution mass spectrometry was used in some cases to confirm the molecular composition of such fragments.

There is one fragment, however, for which no standard mechanism seems applicable. β-lactams of type II show intense M-44 and M-45 peaks. Appropriate metastable peaks in these spectra indicate that the molecular ion is directly converted to M-44, and the M-45 fragment is derived from M-44 through the loss of a proton. We have established by high resolution mass spectrometry that the M-44 peak corresponds to the loss of carbon dioxide. The β-lactam ring must, therefore, undergo scission and rearrangement to join two oxygen atoms in the molecule to the same carbon atom. One such possible mechanism is shown in Eq.1.

Isotope labeling work is in progress for further information on this

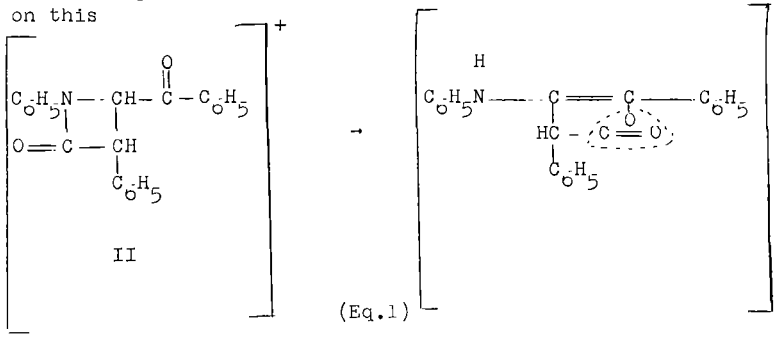

(Eq.1)

unexpected loss of carbon dioxide from β-lactams of type II.

HIGH RESOLUTION MASS SPECTROMETRY IN FRAGMENTATION STUDIES OF SESQUITERPENES AND RELATED COMPOUNDS:

THE MECHANISM OF FRAGMENTATION UNDER ELECTRON IMPACT OF WIDDROL[1, 2]

By

Catherine Fenselau,[3] W. J. Richter[4] and A. L. Burlingame
Department of Chemistry and Space Sciences Laboratory
University of California, Berkeley

ABSTRACT

The mass spectrum of the sesquiterpenol widdrol is dominated by the peak at m/e 151, corresponding to the charged species formed by loss of 71 mass units from the molecular ion. A reasonable mechanism for the genesis of the ion of mass 151 is offered by the fragmentation sequence characteristic of alicyclic alcohols. However, the mass spectra of a series of deuterium-labeled analogs of widdrol and the complete high resolution mass spectra of these compounds indicate that most of the $M-71^+$ ions arise from a rearranged "ketonic" molecular ion, rather than from the alicyclic alcoholic molecular ion. This extensive rearrangement of the molecular ion derives from the presence of the homoallylic double bond to which the hydroxyl hydrogen is transferred through a six-membered intermediate.

INTRODUCTION

The structure and absolute configuration of widdrol were established after much discussion in 1961.[5] In 1964, Dauben and Friedrich[6] demonstrated the mechanism of conversion of thujopsene to widdrol in aqueous acid. In the course of their investigation they produced 6, 6-d_2-widdrol and 8, 8-d_2-widdrol. The availability of these two isotopically-labeled analogs, coupled with the determination of complete high resolution mass spectral data,[7] has made possible a thorough study of the fragmentation under electron impact of this natural product.

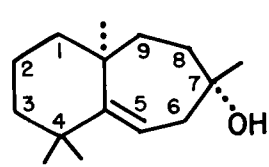

WIDDROL

EXPERIMENTAL

Widdrol-OD was obtained by exchanging a sample of widdrol on a D_2O-treated VPC column[8] and co-inserting it into the mass spectrometer with a microliter of heavy water. Its isotopic purity was calculated from the spectrum to be 83% d_1 and 17% d_0. The isotopic purity of 6, 6-widdrol is reported by Dauben[6] to be 93% d_2, and that of the 8, 8-d_2-widdrol used is reported[6] as 43% d_2 and 43% d_1.

The low resolution mass spectra of widdrol, widdrol-OD, 6, 6-d_2-widdrol and 8, 8-d_2-widdrol were measured on a modified[9] CEC-21-103C mass spectrometer with the inlet system at 100° and the source at 180°. The high resolution mass spectrum of widdrol was obtained on a CEC-21-110 mass spectrometer operating with the inlet system at 180° and the source at 200°. In the spectrum presented the masses are plotted in methylene units.[7] On the abscissa each major division marker corresponds to the saturated ion, e.g. C_nH_{2n+1}, with the number of carbon atoms given in the top row of figures and the number of hydrogen atoms indicated in the bottom row. There

LOW RESOLUTION MASS SPECTRA

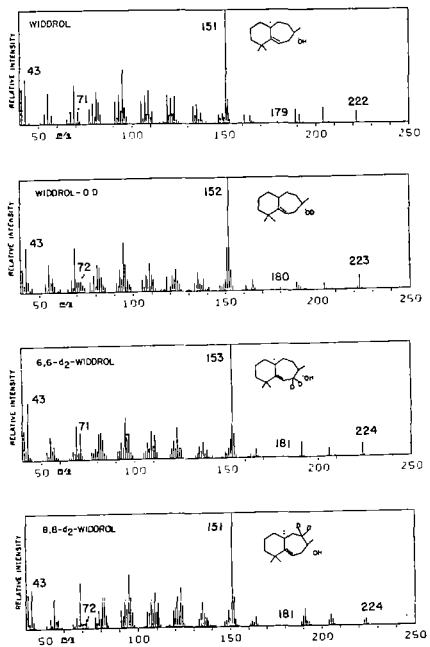

FIGURE 1

HIGH RESOLUTION MASS SPECTRA

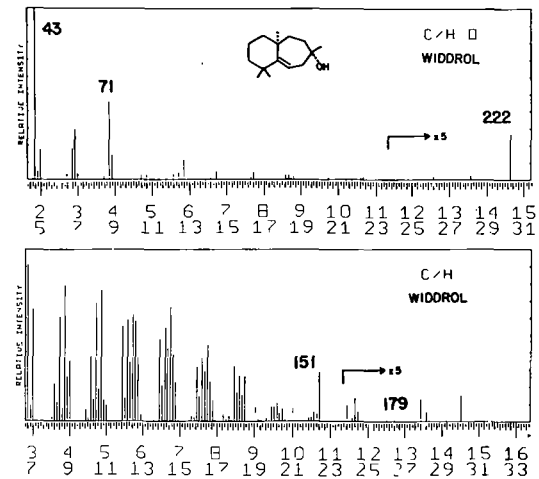

FIGURE 2

are fourteen units between each major division; to obtain the number of hydrogen atoms in an unsaturated or cyclic ion, start at the position of the saturated ion of appropriate carbon-number and count backwards.

DISCUSSION

If widdrol is viewed as a cyclic alcohol, it would be expected to undergo the characteristic fragmentation sequence outlined for alicyclic alcohols by Natalis[10] and demonstrated by use of deuterium-labeled analogs for cyclopentanol[11] and cyclohexanol.[12] Thus the molecular ion should suffer bond scission alpha to the hydroxyl group with transfer of an α-hydrogen from the other side, accompanied by cleavage of the γ-bond. This sequence occurs in the fragmentation of widdrol, (Scheme I) producing the ion of mass 71. The origin of this ion is supported by the high resolution spectrum of widdrol, which indicates that about 80% of the peak at m/e 71 arises from ions with the composition $C_4H_7O^+$ and is confirmed by the spectra of the labeled compounds. In the spectrum of 6, 6-d_2-widdrol the peak at m/e 71 remains at m/e 71, demonstrating that the ion does not contain deuterium atoms from C-6. In the spectrum of 8, 8-d_2-widdrol most of the peak at m/e 71 moves to m/e 72 after correction for the isotopic distribution[6] and contributions from $C_5H_{11}^+$ ions. Thus one of the two deuterium atoms at C-8 is retained in this fragment. Similarly in the mass spectrum of widdrol-OD about 80% of the peak at m/e 71 moves to m/e 72 (after correction for contributions from $C_5H_{11}^+$ ions and isotopic purity), confirming the retention of the hydroxyl deuterium atom in 80% of the oxygen-containing ions of mass 71. Some of the charge is retained on the hydrocarbon moiety in this cleavage, contributing about 15% of the intensity of the peak at m/e 151 in the spectrum of widdrol-OD.

There is another major cleavage sequence apparent in the mass spectrum of widdrol. This second mode of fragmentation derives from the presence of the homoallylic double bond. The hydroxyl hydrogen is transferred to the double bond through a six-membered intermediate, and the molecular ion opens into the "methyl ketone" ion (Scheme II). The "ketonic" ion then fragments exactly as one would predict. α-Cleavage produces ions of mass 43 and composition $C_2H_3O^+$, which account for about 60% of the prominent peak at m/e 43. The $C_2H_3O^+$ ions formed from the three labeled compounds contain no deuterium atoms. A minor portion of the charge is carried by an ion of mass 179. The hydrocarbon peak at m/e 179 moves to m/e 180 in the spectrum of widdrol-OD, to 181 in the spectrum of 6, 6-d_2-widdrol, and to m/e 181 in the spectrum of 8, 8-d_2-widdrol after correction for isotopic purity.

There is no γ-hydrogen in the "ketonic" ion and thus the classical McLafferty rearrangement is inoperative. The mass spectrum of another ketone, which similarly contains no γ-hydrogen, has been discussed by Arndt and Djerassi.[13] They report that the base peak in the spectrum of 2, 2, 8, 8-tetramethyl-5-nonanone results from scission of the γ-bond at the tertiary center, with retention of the major portion of the charge on the hydrocarbon moiety. This is precisely the cleavage that generates most of the base peak at m/e 151 in the widdrol spectrum (Scheme II). Eighty-five per cent of the peak at m/e 151 appears to derive from the ion formed by scission of the γ-bond at the tertiary center, as that much of the peak moves to m/e 152 (after correction for isotopic purity) in the spectrum of widdrol-OD. The peak occurs at m/e 153 in the spectrum of 6, 6-d_2-widdrol and the major portion remains at m/e 151 in the spectrum of 8, 8-d_2-widdrol. A lesser amount of the charge is carried by the complementary ion, which contributes about 20% of the $C_4H_7O^+$ ions of mass 71, calculated from the spectrum of widdrol-OD.

Thus fragmentation can be distinguished in the mass spectrum of widdrol from two different molecular ions, which both produce daughter ions of the same mass and composition in their major fragmentation processes. In one case the hydroxyl hydrogen is transferred and the charge remains primarily on the hydrocarbon moiety — in the other case a ring hydrogen is transferred and most of the charge remains on the oxygen-containing fragment.

Rearrangement of the molecular ion of a β, γ-unsaturated alcohol under electron impact is not unique to widdrol. At least three earlier papers report similar observations on 2-phenylethanol[14] and derivatives,[15] on derivatives of 4-buten-1-ol[15] and on several β-hydroxyesters[16] (see Figures).

It seemed desirable to test the rearrangement in a simple cyclic alcohol, a model compound for the functionalized ring of widdrol. 1-Methyl-cyclohept-3-enol was synthesized and the mass spectra of this alcohol and its deuterated analog were obtained. This compound undergoes the characteristic cyclic alcohol fragmentation — cleavage of the α-bond, transfer of an α-hydrogen from the other side of the

SCHEME I

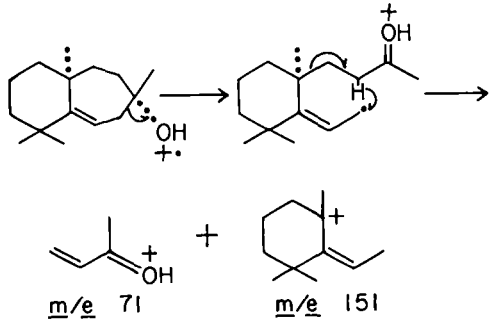

SCHEME II

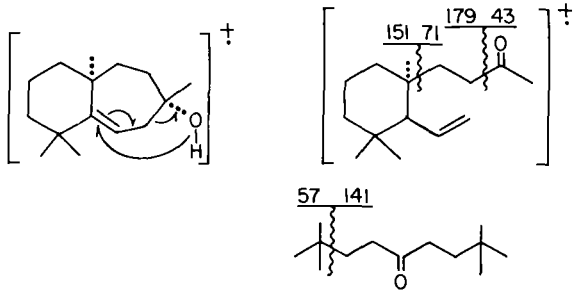

Arndt and Djerassi (1965)

MUB-10652

SCHEME III

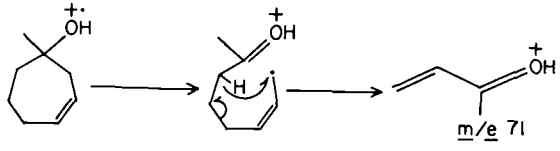

MUB-10653

hydroxyl group and scission of the γ-bond — that produces an ion of mass 71 (Scheme III). High resolution mass measurements confirm the composition of the ion as $C_4H_7O^+$. The peak at m/e 71 in the spectrum of 1-methylcyclohept-3-enol appears at m/e 72 in the spectrum of 1-methylcyclohept-3-enol-OD, indicating that the ion retains the hydroxyl deuterium. This β, γ-unsaturated cyclic alcohol also rearranges to the ketonic molecular ion (Scheme IV) as demonstrated by the appearance of an intense peak at m/e 43 in the spectra of both this compound and its OD-analog. High resolution mass measurements reveal that 95% of the ions of mass 43 have the composition $C_2H_3O^+$. Unlike the rearranged widdrol ion, this ketonic ion contains γ-hydrogen, and it can and does undergo the classical McLafferty rearrangement, which generates an ion of mass 58. This enol ion does not contain the hydroxyl deuterium when it is formed from the deuterated alcohol. The complimentary hydrocarbon ion of mass 68 is also formed. Most of the peak at m/e 68 moves to m/e 69 in the spectrum of the OD-analog, indicating that the hydroxyl deuterium is now carried in the hydrocarbon moiety. Thus fragmentation from two molecular ions is also demonstrated for 1-methyl-cyclohept-3-enol. This is one case in which the fragmentation of a model compound does approximate that of the natural product.

FOOTNOTES AND REFERENCES

1. Financial support was provided in part by the National Aeronautics and Space Administration Grant NsG 101.

2. For a more extensive report of these studies, see "High Resolution Mass Spectrometry in Molecular Structure Studies Part IV", C. Fenselau, W. J. Richter, and A. L. Burlingame, J. Am. Chem. Soc., in preparation.

3. Recipient of a Fellowship from the American Association of University Women 1965-1966.

4. Present address: Hofmann LaRoche Pharmaceutical Company, Basel, Switzerland.

5. C. Enzell, Acta Chem. Scand. 16, 1553 (1962) and references contained therein.

6. W. G. Dauben and L. E. Friedrich, Tetrahedron Letters, 2675 (1964).

7. A. L. Burlingame and D. H. Smith, Tetrahedron Letters, in preparation.

8. M. Senn, W. J. Richter, and A. L. Burlingame, J. Am. Chem. Soc., 87, 680 (1965).

9. F. C. Walls and A. L. Burlingame, Abstracts of Papers Presented at the 4th Annual Meeting of the Society for Applied Spectroscopy, Denver, Colorado, Sept. 1-5, 1965.

10. P. Natalis, Bull Soc. Roy. Sci. Liege, 31, 790 (1962).

11. P. Natalis, Bull. Soc. Chim. Belg., 69, 224 (1960).

12. H. Budzikiewicz, Z. Pelah and C. Djerassi, Monatsh. Chem., 95, 158 (1964); C. G. MacDonald, J. S. Shannon and G. Sugowdz, Tetrahedron Letters, 807 (1963).

13. R. Arndt and C. Djerassi, Chem. Commun., 578 (1965).

14. A. Gilpin, J. Chem. Phys., 28, 521 (1957).

15. H. E. Audier, H. Felkin, M. Fétizon and W. Vetter, Bull. Soc. Chim. France, 3236 (1964).

16. A. H. Etémadi, Bull. Soc. Chim. France, 1537 (1964).

SCHEME IV

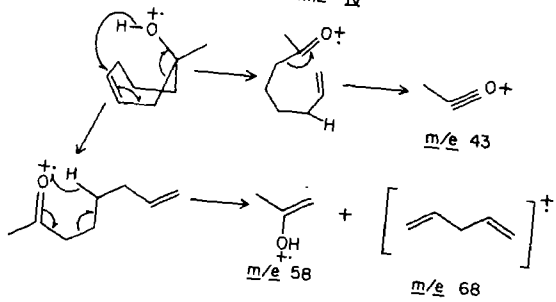

MUB-10654

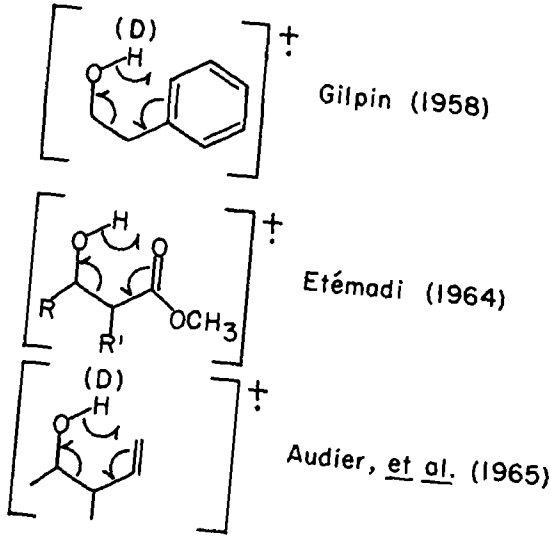

MUB-10739

High Resolution Mass Spectrometry
in Molecular Structure and Stereochemical Studies:
Effect of Stereochemistry on the Fragmentation
of Epimeric Derivatives of Azabicycloalkanes[1]

by

D. H. Smith,[2] H. K. Schnoes, and A. L. Burlingame
Department of Chemistry and Space Sciences Laboratory,
University of California, Berkeley

A recent study by A. L. Burlingame, H. O. House and co-workers[3] involved an examination of possible correlations that might be drawn between the low resolution mass spectra and the structures and stereochemistry of a series of related azabicycloalkanes, This work concluded that the stereochemistry about the bridgehead carbon atom could be determined by examining the relative intensities of molecular ion minus a hydrogen (M-1) peaks between epimeric pairs and, in some cases, namely the secondary alcohols and ethers, the relative intensities of m/e 44 and 58.

The peak at M-1 was shown to arise from loss of a hydrogen atom from a carbon atom adjacent to nitrogen. With reference to Figure 1, it may be noted that there exists considerable 1, 3-diaxial interaction between the substituent on the bridgehead carbon and the axial hydrogens (labeled H_a) on the carbons adjacent to nitrogen. Loss of one of these axial hydrogens from a molecular ion results in relief of some of this interaction plus the formation of a stable immonium ion as illustrated. Indeed, it was found that the epimer with the larger substituent oriented toward nitrogen displayed the larger M-1 peak, and thus this fragmentation proves useful in determining stereochemistry about the bridgehead.

The fragmentations of secondary alcohols or ethers mentioned above leading to m/e 44 and 58 are more complicated processes, but also proved useful in elucidating stereochemistry. These processes are summarized in Figure 2. Cleavage of an α-β carbon bond in both epimers yields an immonium ion that can be pictured as structure A. From this molecular ion it was demonstrated that two different rearrangement rpocesses take place dependent on the stereochemistry of the bridgehead. In the case of the β-epimer, with the hydroxyl group oriented toward nitrogen, a rearrangement that may be pictured as shown in structure B yields a fragment ion at m/e 44, with the composition C_2H_6N, while a similar rearrangement pictured in structure B' for the α-epimer yields a fragment ion at m/e 58, of composition C_3H_8N.

High resolution mass spectra of representative members of the series were determined employing a Mattauch-Herzog double focusing instrument (CEC type 21-110) with photoplate recording. Subsequent data acquisition and reduction employing our automatic plate scanning system and the computer facilities of the Lawrence Radiation Laboratory verified the compositions of the peaks discussed above in the initial paper, but, more importantly, proved invaluable in elucidating certain features of the fragmentation patterns of epimeric pairs. These epimers displayed fragmentation patterns that were quite different in many respects. For example, several peaks in the mass spectrum of one epimer were missing entirely in the spectrum of the other epimer, and there were, in certain regions of the spectra, marked intensity differences between the two epimers other than those mentioned above.

The first pair of epimers provides an illustrative example of the generalizations noted in the low resolution studies. The compound, as drawn, has a six-membered ring to the left and is a secondary alcohol. The distribution of peaks in the hydrocarbon and oxygen containing plots[4] is quite similar for the epimers. Figure 3 represents the nitrogen and nitrogen-oxygen containing plots for the same epimers. The molecular ion has the composition $C_9H_{17}NO$. For the β-epimer, with OH oriented toward nitrogen, the M-1 peak $C_9H_{16}NO$, is larger than that of the α-epimer, with the hydrogen (less bulky than OH) oriented toward nitrogen. Also, exactly as noted before, the peak at C_2H_6H is larger than that of C_3H_8N for the β-epimer, while the intensity ratio is effectively reversed in the C/H N plot of the α-epimer. There is one more feature of this set of spectra that has significance to the following discussion, and that is the presence of relatively intense peaks in the C/H N plot of the β-epimer at $C_9H_{15}N$ and $C_9H_{14}N$, representing loss of the elements of H_2O and H_3O respectively, from the molecular ion. These peaks are virtually absent in the C/H N plot of the corresponding epimer.

The next pair of epimers provides perhaps the most graphic examples of the dependence of the fragmentation pattern on stereochemistry. Again, the C/H and C/H O plots are quite similar with the exception of a much larger C_6H_5 fragment ion in the spectrum of the α-epimer, which has the phenyl group oriented toward nitrogen. This presumably arises from the 1, 3 diaxial interactions noted above; interactions that are considerably more pronounced for phenyl versus OH.

Figure 4, however, which contains the C/H N and C/H N O plots for the same pair, displays marked differences. In particular, one may note the larger M-1 peak for the α-epimer at $C_{15}H_{30}NO$, as expected; the presence of peaks in the lower C/H N O plot, at $C_9H_{15}N$ O (peak D') and C_6H_8NO (peak E') that are absent in the C/H N O plot of the β-epimer; the larger M-H_2O and M-H_3O peaks in the C/H N plot of the β-epimer at $C_{15}H_{19}N$ (peak D) and $C_{15}H_{18}N$; and finally the presence of an intense peak at $C_{12}H_{12}N$ (peak E) in the β-epimer that is entirely absent in the C/H N plot of the α-epimer. These differences can be explained quite readily if the fragmentation is assumed to proceed as shown in Figure 5. In both epimers the fragmentation proceeds either with loss of a hydrogen followed by loss of the group oriented toward nitrogen, or a single step elimination of the elements of H_2O or C_6H_6 in the β- and α-epimers respectively. In the case of the β-epimer this process yields the fragment ion D $C_{15}H_{19}N$, a much more favorable process than in the α-epimer, while in the case of the α-epimer, a peak at $C_9H_{15}NO$ (peak D') results. Elimination of a C_3H_7 radical as shown, to aromatize the system, from both of these fragments, yields $C_{12}H_{12}N$ (peak E) for the β-epimer, and C_6H_8NO (peak E') for the α-epimer. Thus this rather straightforward fragmentation scheme, dependent entirely on stereochemistry, is sufficient to account for the more obvious dissimilarities between the two spectra.

Also of interest are the fragmentation patterns of the β- and α-epimers of a compound similar to that discussed above, but with a seven-membered ring instead of six. The pairs of C/H and C/H O plots are virtually identical, but again as above, there exist several marked dissimilarities in the pairs of C/H N and C/H N O plots presented in Figure 6 (note peaks F, F', G, G', H, H'). These differences can be explained assuming a mechanism exactly as that discussed above. With reference to Figure 7, the more intense M-H_2O and M-H_3O peaks at $C_{16}H_{21}N$ and $C_{16}H_{20}N$ (peaks F) in the spectrum of the β-epimer are due to the more facile elimination of these elements from the molecular ion, $C_{16}H_{23}NO$, of the β-epimer. In the spectrum of the α-epimer, however, elimination of the elements of C_6H_6 or C_6H_7 initially from the molecular ion yields the peaks at $C_{10}H_{17}NO$ and $C_{10}H_{16}NO$ (peaks F'). In this case, both fragments F and F' can eliminate either a propyl or butyl radical to yield $C_{13}H_{14}N$ (peak G) or $C_{12}H_{12}N$ (peak H) in the β-epimer, or $C_7H_{10}NO$ (peak G') or C_6H_8NO (peak H') in the α-epimer. These peaks are unique for each compound with the exception of peak H and a very light elimination of H_2O and H_3O in the α-epimer. There exists a small peak at $C_{12}H_{12}N$ in the α-epimer's spectrum also, but the fragmentation process leading to this ion is obviously less favorable.

As the substituent on the bridgehead becomes less and less large compared to OH, the above processes become less clearly resolved. One can, however, still easily discern that these fragmentations are occurring, as may be seen in Figure 8. This epimeric pair has a methyl group on the bridgehead. The O/H and C/H O plots are again similar although there are several intensity differences. The C/H N and C/H N O plots as presented in Figure 8 again display a stereochemical influence on the fragmentation similar to those discussed above. The M-H_2O and M-H_3O peaks are more pronounced for the β-epimer. Loss of a propyl radical in this epimer as above yields a distinct difference in the intensity of the $C_7H_{10}N$ peak as compared to the α-epimer. Loss of a methyl group to yield a fragment ion with the composition $C_9H_{16}NO$ is more favorable for the α-epimer. It is important to note, however, that loss of a three carbon fragment in this spectrum in a mechanism analogous to those shown above to yield an ion of composition C_6H_8NO is neither a unique nor a dominant process. This may result from the fact that loss of a hydrogen radical from the molecular ion followed by loss of CH_3 or a single step process of loss of CH_4 is apparently not a favorable process.

The net results of this study may be summarized as follows:

1. M-1 is larger for the epimer with a larger substituent oriented toward nitrogen.
2. Fragmentation proceeds with loss of the substituent oriented toward nitrogen to yield a C/H N fragment ion in the β-epimers or a C/H N O fragmentation for the α-epimers.
3. Other differences in the C/H N and C/H N O plots may be explained by loss of an appropriate aliphatic radical from the ions in No. 2 above.

In summary, then, the techniques of high resolution mass spectrometry combined with heteroatomic plotting for data presentation have made possible elucidation of important fragmentation processes in the azabicycloalkane series studied; processes that are entirely dependent on stereochemical influences.

FOOTNOTES

1) This work has been supported in part by a grant from the National Aeronautics and Space Administration, NsG 101.

2) NASA Predoctoral Trainee, 1965-67.

3) W. M. Bryant, III, A. L. Burlingame, H. O. House, C. G. Pitt, and B. A. Tefertiller, J. Org. Chem., in press.

4) For detailed discussion of heteroatomic plotting presentation of high resolution mass spectral data, see A. L. Burlingame and D. H. Smith, Tetrahedron Letters, in press.

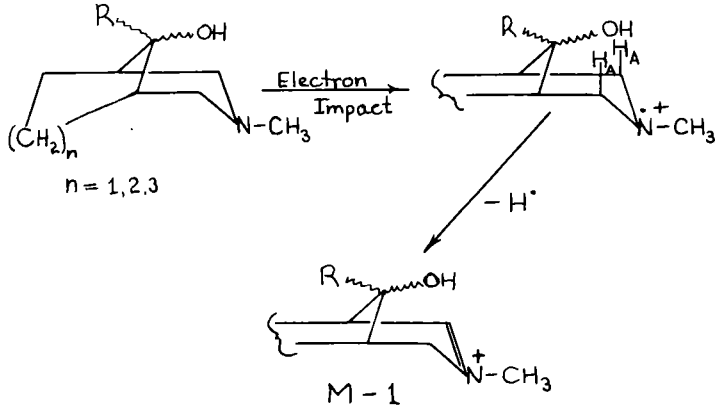

FIGURE 1

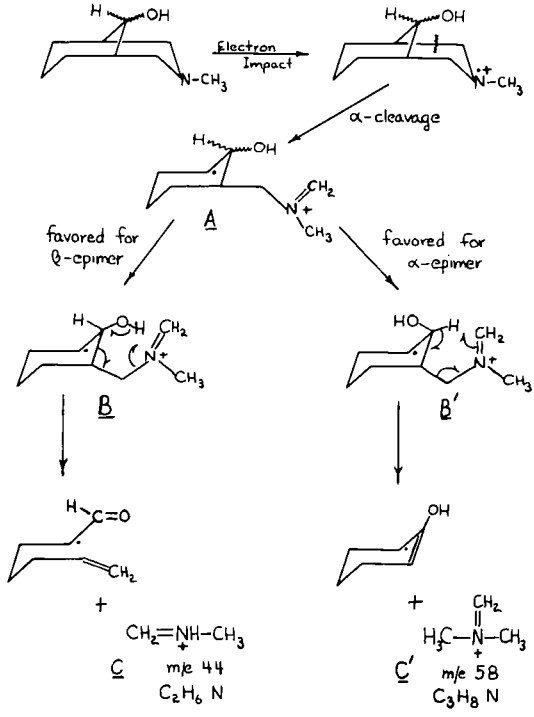

FIGURE 2

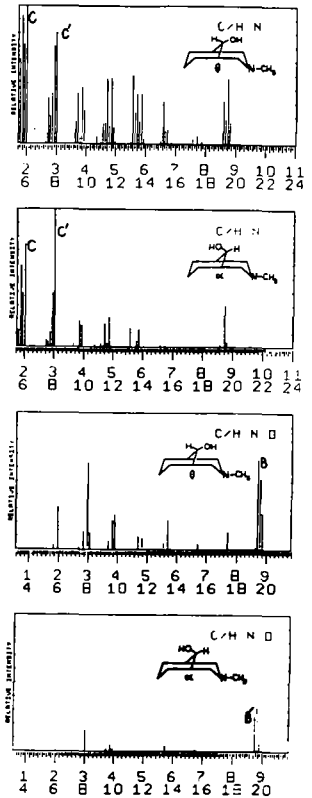

FIGURE 3

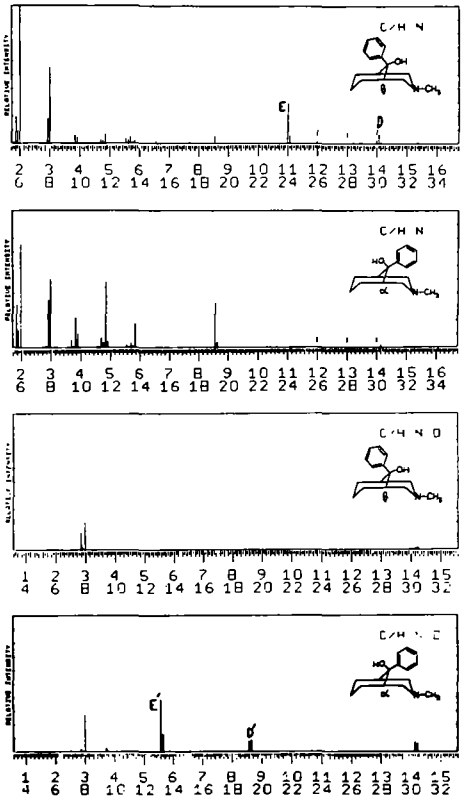

FIGURE 4

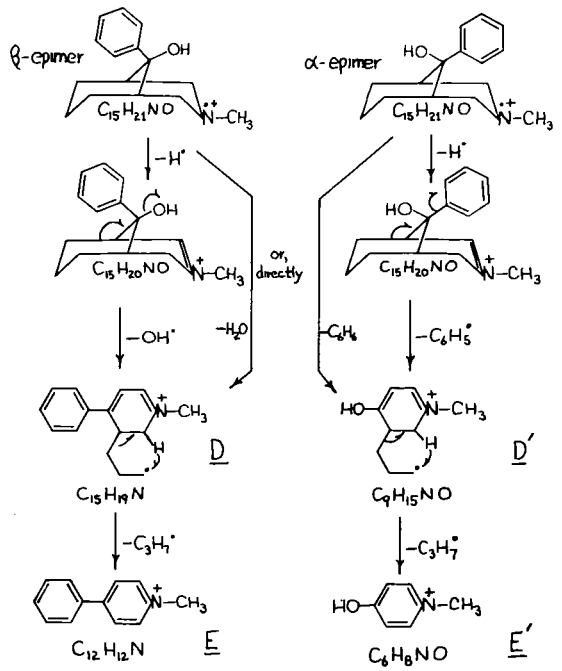

FIGURE 5

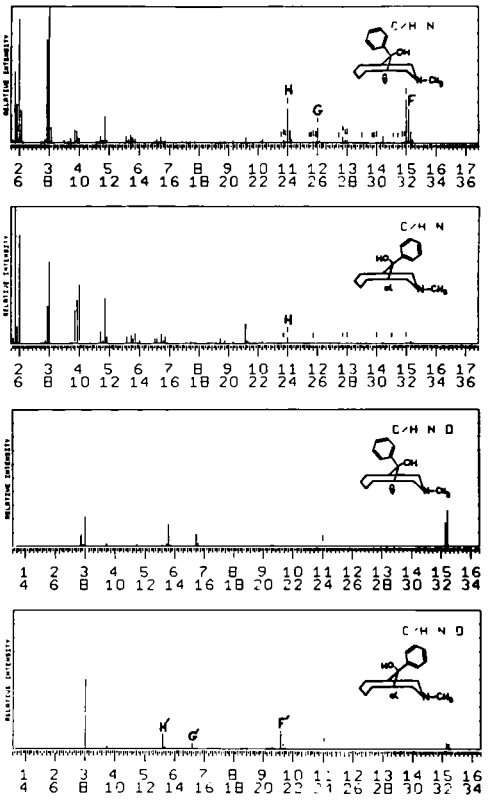

FIGURE 6

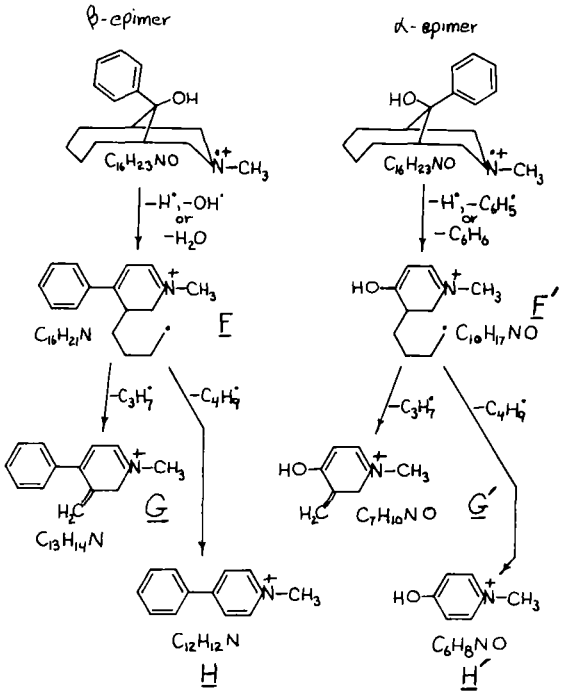

FIGURE 7

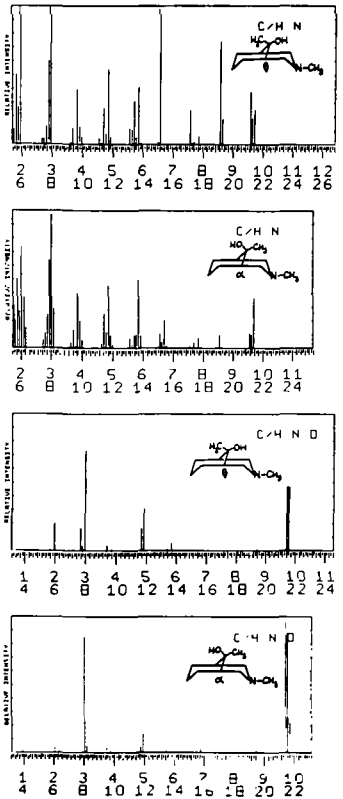

FIGURE 8

THE USE OF FRAGMENTATION PATTERNS OF 1,4 BENZODIAZEPINES FOR THE STRUCTURE DETERMINATION OF THEIR METABOLITES BY HIGH RESOLUTION MASS SPECTROMETRY

P. Bommer and F. Vane
Chemical Research Department
Hoffmann-La Roche, Inc.
Nutley, New Jersey

The study of drug metabolism is becoming increasingly important in the investigation and application of drugs. In the past, these studies have been limited because of their difficult nature and time consumption. We would like to show how mass spectrometry, and in particular, high-resolution mass spectrometry, can be an effective tool for metabolism studies. Two important reasons for the application of this type of spectroscopy are the high sensitivity of the mass spectrometer and the fact that the structure of the metabolites are similar to the starting material.

As an example, we would like to discuss the investigation of the metabolites which are formed when benzodiazepines are administered to rats. The general structure of a 1,4-benzodiazepine and two specific diazepines, Diazepam and Chlordiazepoxide, are shown in Figure I. To be able to obtain the maximum information from the metabolite spectra, we first studied the mass spectra of many different diazepines of known structures which were prepared by our chemists.

Figure 2 contains the low resolution mass spectrum of Diazepam and the postulated structures for three major fragments. There is a strong loss of hydrogen followed by the loss of HCN or CO which reduces the seven-membered ring to a five or six-membered ring. We have studied analogous compounds with different aromatic rings, with N-H instead of N-CH_3, with various 3-substituents and with N_4-oxides. In all of these compounds, the fragmentation is very similar to that of Diazepam. There is a strong tendency to loose the carbon atom in position 3 and the nitrogen atom in position 4, together with the attached substituents. This fragmentation pattern is very helpful in the interpretation of unknown diazepine derivatives. For example, with 3-methyl Diazepam there was again strong loss of hydrogen, followed by the loss of CH_3CN. The N_4 - oxide compounds show a strong loss of oxygen and the spectrum is nearly identical to the compound without the oxide.

The mass spectrum of Chlordiazepoxide (Figure 3) shows a strong loss of oxygen and oxygen plus hydrogen. As you can see from the structure of the m/e 282 fragment, the positive charge can be delocalized around the seven-membered ring. This may explain the lack of any other principal fragment. The loss of HCN from m/e 282 is present; however, the relative intensity is much less than that of the corresponding fragment in Diazepam. The compound without the N-oxide function has a mass spectrum which is very similar to this one without the molecular ion.

The pharmacological investigation of the rat metabolites of Diazepam and Chlordiazepoxide were carried out by Dr. M. Schwartz of our Research Department. A solution of 25 milligrams of Diazepam which was labeled with ^3H in the 5-phenyl ring was injected into the intestinal cavity of one rat. After four hours the rat was killed and, with the aid of the radioactivity, the largest source of metabolites was found in the intestinal tract. The tedious task of the pharmacologist consists of isolating the metabolites by extractions and repeated thin-layer chromatography. Purification of the metabolites, especially when they are only present in submilligram quantities, is very difficult. The mass spectra were run on a CEC 21-110 and recorded on a photographic plate. The ability to study these compounds by means of complete high resolution spectra has many advantages. Not only is it advantageous to have the elemental compositions of the molecular and fragment ions, but more important, the sample peaks often have elemental compositions that are different from the impurities and therefore can be distinguished. The main impurities were compounds with a high hydrogen content. Many times we had samples where the base peak of the actual metabolite spectrum was not stronger than a few per cent of the base peak of the entire spectrum. Consequently, we often had to measure hundreds of peaks to find the few masses which belonged to the metabolite. The mass spectra of blanks also helpted to identify the metabolite peaks. In very impure samples it is especially important to compare consecutive spectra to verify that all fragments of reasonable elemental composition belong to one metabolite. It is very probable that those peaks which belong to another metabolite or an impurity will increase or decrease in intensity at a different rate.

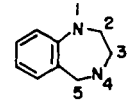

TETRAHYDRO-1,4-BENZODIAZEPINE

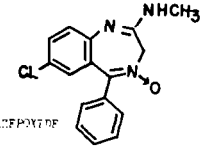

CHLORDIAZEPOXIDE

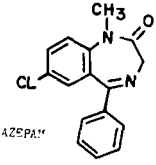

DIAZEPAM

Fig. 1

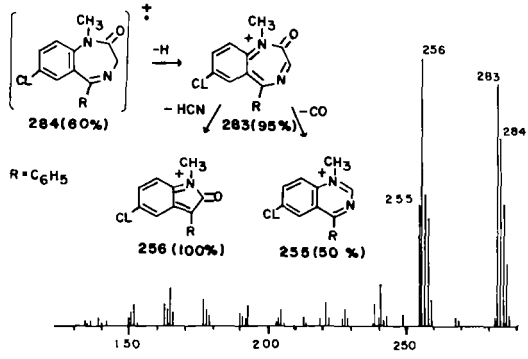

Fig. 2

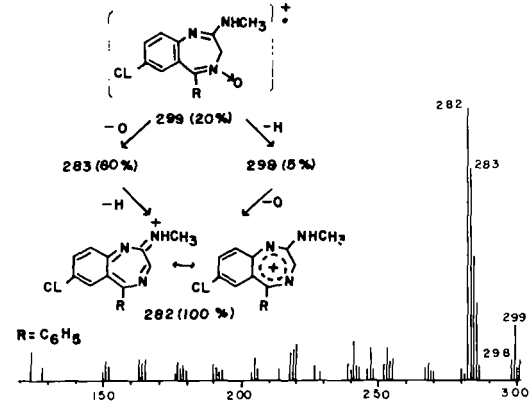

Fig. 3

Figure 4 summarizes the mass spectrometry results of the Diazepam metabolites. The first line gives the change in the molecular formula as compared to starting material All metabolites added at least one oxygen. This is expected since the body tends to convert foreign substances into a more water soluble form and thereby making it easier to excrete. From the fragment-ions, the following conclusions could be drawn. A loss of oxygen could not be detected in any of the four metabolites. This means that no N_4-oxides were formed. Loss of H,CO confirms that the 2-keto group is still present; however, in two of the metabolites (I and III), the loss of H,HCN is not present but a loss of H,HOCN appeared. This means that the oxygen was added in position 3. In metabolite III, the second oxygen was added to the phenyl ring in position 5 as in II and IV. This was confirmed partially by low mass fragments and partially by the mass spectra of the hydrolysis products. Metabolite IV also lost the methyl group in position 1. Figure 5 shows the structures of the metabolites.

Figure 6 summarizes the mass spectrometry results of the Chlordiazepoxide metabolites which were isolated from the urine of the rats. The Chlordiazepoxide was labeled in position 2 with ^{14}C and administered orally and intraveneously to two rats.

The changes in the molecular formula are shown on the first line. The loss of oxygen from the molecular ion indicates that metabolites I through IV have retained their N-oxide group. After the loss of oxygen from the molecular ion, compound I through IV lost H,HCN which shows that position 3 is unsubstituted. Metabolite V, which does not have a N-oxide, also loses H,HCN; therefore, in contrast to Diazepam, no metabolites of Chlordiazepoxide added an oxygen in position 3. The loss of carbon monoxide in IV and V indicates that the $NHCH_3$ function in position 2 has been converted into a carbonyl. The presence of the oxygen on the 5-phenyl is verified by the observance of hydroxyphenylcyanide in I, III, IV and V. The structures of the five metabolites are illustrated in Figure 7. Compound II is the only metabolite which did not add an oxygen. It is also interesting to note that metabolite V has lost its IV-oxide function and is therefore identical to a metabolite of Diazepam.

Unfortunately, studies similar to the ones reported here do not terminate when the interest and challenge of the mass spectroscopist has been satisfied. Repeated studies in different animals and in human beings, and with different analogs under different conditions make the mass spectral interpretation a routine task. Since the mass spectrometric behavior can be determined from a few model compounds and the change in the structure of a drug by the body is not drastic, this is an area where computer interpretation can be used most effectively.

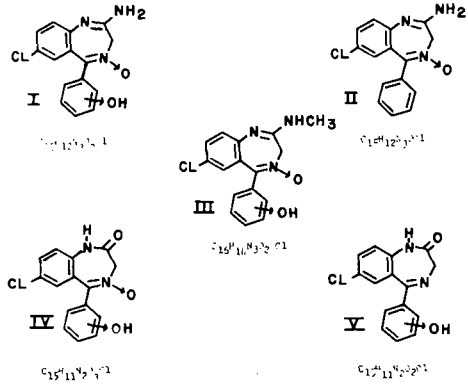

Fig. 7

DIAZEPAM METABOLITES

	I	II	III	IV
DIAZEPAM	+O	+O	+2O	+O-CH_2
M-O, M-OH	-	-	-	-
M-H,CO	YES	YES	YES	YES
M-H,HCN	-	YES	-	YES
M-H,HOCN	YES	-	YES	-
CONCLUSIONS:	NO N_4-OXIDE 2-KETO 3-OH	NO N_4-OXIDE 2-KETO 5-PHENOL	NO N_4-OXIDE 2-KETO 3-OH 5-PHENOL	NO N_4-OXIDE 2-KETO 5-PHENOL N_1-H

Fig. 4

DIAZEPAM METABOLITES

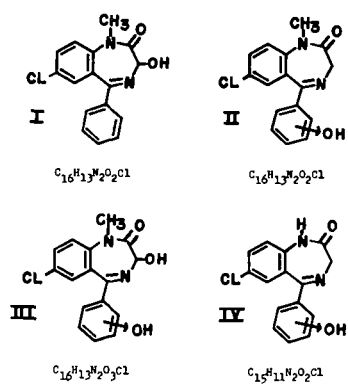

Fig. 5

CHLORDIAZEPOXIDE METABOLITES

	I	II	III	IV	V
CHLOR-DIAZEPOXIDE	+O-CH_2	-CH_2	+O	+2O-CH_3N	+O-CH_3N
M-O, M-OH	YES	YES	YES	YES	-
M-H,HCN	-	-	-	-	YES
M-O,H,HCN	YES	YES	YES	YES	-
M-H,CO	-	-	-	-	YES
M-O,H,CO	-	-	-	YES	-
HO-⟨benzene⟩-CN	YES	-	YES	YES	YES

Fig. 6

The High Resolution Mass Spectra of Primary Aliphatic Alcohols

P.A. Wadsworth
Shell Development Company
Emeryville, California

Abstract

Studies of the high resolution mass spectra of some primary aliphatic alcohols show that certain of the structural features of the alcohols can be explicitly defined. Molecular weight of the alcohol is determined by the heaviest $C_nH_{2n}^+$ corresponding to the parent minus HOH.

Configuration of the carbon skeleton of the alcohol can be deduced for some structures. Alcohols with a branch on the 2-carbon atom can be characterized and the size of this branch is indicated by the most intense ion in $C_nH_{2n}O^+$ series.

These studies have shown that, to determine the configuration of the carbon skeleton, the mass spectrum of the alcohol is preferred to that of a derivative of the alcohol. Further, in order to differentiate those ions in the mass spectrum which contain an oxygen atom and are characteristic of skeletal configuration, a high resolution mass spectrometer must be employed.

Analysis of Complex Mixtures of Aromatic Compounds by High Resolution Mass Spectrometry

By

B. H. Johnson
Thomas Aczel

Esso Research and Engineering Company
Baytown Research and Development

Introduction

The continuous expansion and progress of petroleum technology requires more and more sophisticated means to characterize the composition of complex petroleum products. Mass spectrometry has played a dominant role in this effort since the early nineteen fifties. The introduction of commercially available high resolution mass spectrometers in recent years has further extended the scope of the mass spectrometric technique.

This paper describes an analytical approach which combines the sophistication of high resolution mass spectrometry with the simplicity of low voltage techniques. Interpretation of the spectra of the aromatic portion of very complex mixtures can be accomplished in a matter of hours by using a chart reading technique which yields rapid and accurate mass measurements for up to 1000 parent peaks.

Application of this approach to petroleum fractions results in detailed compound type and carbon number characterization and in the identification of a great number of novel hydrocarbon, aromatic-sulfur, and aromatic-oxygen compounds.

The use of low ionizing voltages (1)(2)(3) restricts the mass spectra of aromatic and olefinic materials to the molecular ions. The spectra are thus greatly simplified and interferences among the components of the mixture are reduced to a minimum. This permits the accurate determination of the carbon number distribution within each compound type and, in general, makes the applicability of the method less dependent on sample origin and history than in the case of high voltage methods.

The use of high resolution instruments eliminates one major disadvantage of conventional low voltage techniques, that is, the impossibility to distinguish more than seven compound types. At a resolution of about 100 ppm C-12H and C_2H_8-S doublets can be resolved up to about m/e 950 and CH_4-O doublets up to about m/e 370. Types as alkylbenzenes and benzothiophenes, naphthobenzenes and pyrenes, naphthenonaphthalenes and dibenzofurans, etc, are resolved and can be analyzed separately.

The potential of the combination of high resolution-low voltage technique was recognized by Lumpkin (5) and Reid and coworkers(7). The peak matching mass measurement (6) technique applied by these authors was, however, extremely lengthy and could not be applied to very complex mixtures, or to the determination of minor and trace components. These difficulties are eliminated in the procedure proposed in this paper.

Discussion

Experimental Conditions

The apparatus used in this work is an Associated Electrical Industries Ltd., Manchester, England, MS-9 high resolution instrument. This is a double focusing apparatus, of the Nier-Johnson geometry. The output of the instrument is recorded with a Minneapolis-Honeywell UV visicorder.

The MS-9 is essentially a very high precision qualitative instrument, designed mainly for the identification of unknown compounds. The use of the instrument for quantitative purposes requires a very careful standardization of the operating controls.

The main variables are the position of the magnet, the electron beam and repellet voltages, and optimization of the beam focusing plates and the width of the source and collector slits. In conventional operation, these settings are optimized at the mass which is being measured. Interpretation of charts, however, requires an uniformly satisfactory and repeatable spectrum for the whole mass interval investigated, usually from m/e 500 to m/e 100. This can be accomplished by the procedures described in the following paragraphs.

The position of the magnet is optimized at the high end of the mass interval to be studied. This is necessary because the resolution decreases rapidly above the mass at which the magnet is optimized, but only very slowly below. In addition, one obviously needs the highest resolution at the high mass end of the spectrum.

The effective electron beam energy is kept constant at 12.0 electron volts. Fragments from the types of compounds likely to be present in petroleum fractions are essentially eliminated. This effective energy is due both to the electron beam voltage and the repeller voltage, according to the expression:

(1) Effective V $\cong$ Electron beam V + 1/3 repeller V

Any deviation of the repeller voltage from zero, desired sometimes for increasing sensitivity and repeatability has to be compensated by a corresponding change in the electron beam voltage.

The beam focusing plates are optimized at the effective electron beam voltage used in each experiment. Slit widths, multiplier setting, scan speed, etc, are standardized on a long range basis. Scan speed and chart speed are set in a manner to obtain a well distinguished and readable spectrum.

A set of typical instrumental conditions is shown below:

Source slit width: 0.0018 inches
Collector slit width: 0.0016 inches
Effective electron voltage: 12.0 electron volts
Multiplier gain: 4400
Scan speed: 8.7 min/octave
Chart speed: 0.4 inches/seconds
Sample size: 3-10 mg

Spectra obtained at these conditions have sufficient resolution for the separation of CH_4-O doublets ($\Delta M = 0.0364$) up to about m/e 300. The total ionization, expressed as the sum of the monoisotopic peak heights of all parent peaks is about 5 to 10 thousand millimeters. Base line noise isabout 2 to 3 mm, and thus individual components can be detected in amounts of 0.1 percent or less of the total ionization. A portion of a typical spectrum obtained under these conditions is illustrated in Figure 1.

Chart Reading Technique

Precise mass measurement from the recorded spectra are based on the correlation between the precise mass and the position of the corresponding peaks on the record. This relationship can be expressed rigorously with the following equation(5):

(2) $$\ln M_x = \frac{(\ell_b - \ell_x)\ln M_a + (\ell_x - \ell_a)\ln M_b}{(\ell_b - \ell_a)}$$ where

M_x is the unknown mass

M_a M_b are standards of known masses, bracketing M_x

$\ell_b - \ell_a$ is the distance between M_b and M_a

$\ell_a - \ell_x$ is the distance between M_a and M_x

$\ell_b - \ell_x$ is the distance between M_b and M_x

The accuracy of the measurement depends on the uniformity of the logarithmic scanning rate and of the linear chart speed. This can be assumed valid only for short mass intervals. Known standards are needed therefore at least at every four masses, and this is a very difficult requirement for low voltage work.

Fortunately, in the low voltage spectra of complex aromatic hydrocarbons, mass measurements standards are provided internally, by the presence of molecular ions and their ^{13}C containing isotopes. The distances between these easily recognizable pairs correspond to a mass difference of 1.003355 atomic mass units. In a complex hydrocarbon mixture there are generally one or more parent peaks at every even mass number, followed by the corresponding isotopes, and therefore internal standards are provided at every second integral mass number.

Within these short distances, effects of variations in chart speed, scanning speed, etc, are negligible. In addition, a simple linear relationship can be assumed between mass and distance, greatly simplifying calculations. These are illustrated by the schematic example shown in Figure 2.

This approach requires the absolute mass measurement of only one peak in the spectrum. This can be obtained by addition of one known standard. A very useful standard of this type is tetrachlorothiophene, which possesses intense low voltage peaks at m/e 219.8475, 221.8445, 223.8416, 225.8386, and 227.8357 in known isotopic abundance ratios. These peaks are well separated from naturally occurring compounds because of their high negative mass defect.

The accuracy of precise mass measurements from chart, using the above described approach, is sufficient to identify all masses which can be separated with a resolving power of about 100 ppm (Table I). In fact, it closely approaches the accuracy of manual mass measurement with the Nier peak matching technique, if an ordinary ruler and a simple magnifying glass are used.

Table I. Accuracy of Mass Measurement from Chart

Formula	Measured Mass	Theoretical Mass	Deviation, amu
$C_{13}H_{16}$	172.1277	172.1253	+ 0.003
$C_{13}H_{18}$	174.1405	174.1408	- 0.000
C_{13} 28	176.1585	176.1565	+ 0.002
$C_{11}H_{12}{}^{32}S$	176.0688	176.0660	+ 0.003
$C_{11}H_{12}{}^{34}S$	178.0611	178.0616	- 0.001

In general, due to the relatively simple low voltage mass spectra of petroleum distillates, the multiplets are separated by a few characteristic mass differences, or linear combinations of them. These can be recognized with a naked eye. Only a very few accurate mass measurements are needed for the interpretation of the spectra, and most of the peaks can be positively identfied by pattern recognition (Figure 1).

Precise mass measurements from the recorded spectra make characterization of complex mixtures practical. The time necessary for identification is reduced from weeks to hours, as the time consuming peak matching technique is eliminated. Other advantages of the technique include:

- simultaneous determination of mass and intensity (quantitative analyses)
- the possibility of identifying trace components
- independence from sample depletion in the instrument
- availability of permanent records

The simple technique described here is, however, less applicable to the interpretations of high voltage spectra due to the lack of unequivocally recognizable known mass differences as the ^{12}C-^{13}C doublets, which at these conditions are not resolved from ^{13}C-^{12}CH doublets.

Another problem is the handling of the great number of data obtained which is still more time consuming than one would wish (two to five hours). This problem can best be solved by digitization and subsequent computer analysis.

Qualitative Applications

High resolution low voltage analyses yield information only on the precise molecular weight of the components in the mixture to be analyzed. In the case of the aromatic portions of petroleum fractions, containing usually regular sequences of homologous compounds this information can be used to draw reasonable model structures. The procedure is based on a general knowledge of the nature of the sample, the qualitative use of characteristic fragment peaks, and the comparison of the molecular weight of the proposed nucleus with that of the lowest molecular weight component observed in each homologous series. This approach cannot distinguish between isomers of the same general molecular formulae, such as anthracenes and phenanthrenes. Within this limitation, the degree of characterization obtained is indeed quite high.

An example of this approach, carried out on distillation fractions of a wide boiling refinery stream, is shown in Table II. The table is limited to the identification of types of the nominal C_nH_{2n-8} series. Similar approaches can be used for the other series. It can be noted here that conventional low voltage methods would identify only one type of this series, instead of the six types identified by high resolution techniques.

Table II. Illustration of Identification Approach

Molecular Formula	Observed Integral Molecular Weight of First Homolog	Proposed Model Structures and their Integral Nuclear Molecular Weights
C_nH_{2n-8}	132	118
$C_nH_{2n-10}O$	146	118
$C_nH_{2n-12}S$	174	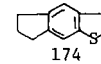 174
C_nH_{2n-22}	216	202
$C_nH_{2n-24}O$	230	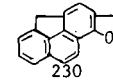 230
$C_nH_{2n-26}S$	258	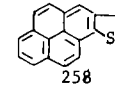 258

The number of compound types identified is necessarily limited by the resolving power of the instrument. The maximum m/e ratios, at which the most common doublets and their linear combinations can be separated with a resolving power of about 10 ppm are listed below:

Doublet	ΔM	Approximate Resolving Power Required for Separation at m/e 100	200	300	Approximate Maximum m/e at which Doublet is Resolved with 10,000 Resolving Power
C-12H	0.0939	1100	2200	3300	950
$C_2H_8-{}^{32}S$	0.0905	1100	2200	3300	950
CH_4-O	0.0364	2700	5400	8100	370
$C_3-{}^{32}SH_4$	0.0034	30,000	60,000	90,000	33
$C_3-{}^{34}SH_4$	0.0165	6,000	12,000	18,000	170
${}^{13}CH-N$	0.0081	12,000	24,000	36,000	83

In general, therefore, compounds differing by a C_3-$^{32}SH_4$ doublet, that is, types of the general formulae $C_nH_{2n-x}S$ and $C_nH_{2n-(x-10)}$ are impossible to resolve with commercial instruments presently on the market. Unfortunately, this doublet corresponds to abundant types in petroleum products, such as benzothiophenes and naphthenophenanthrenes, and in general, aromatic thiophenes and aromatic hydrocarbons with one or more condensed ring.

Occasionally, these types can be resolved, however, by using the C_3-$^{34}SH_2$ doublets. Advantage can be taken furthermore of the fact that the thiophenic types possess a nuclear molecular weight 42 or 56 lower than the interfering aromatic types. There exists thus a mass region in which the thiophenic types can be recognized unequivocally. The intensity distribution of the homologous peaks in this part of the spectrum can be used to separate semiquantitatively the unresolvable doublets in the rest of the spectrum.

In spite of this limitation, high resolution low voltage analyses resulted in the identification of a great number of novel types in petroleum fractions. The number of types identified is illustrated in Table III.

Table III. Aromatic Compound Types Identified in Petroleum

C_nH_{2n-6}	to	C_nH_{2n-40}	(18)
$C_nH_{2n-10}S$	to	$C_nH_{2n-30}S$	(11)
$C_nH_{2n-8}O$	to	$C_nH_{2n-38}O$	(16)

Quantitative Applications

The chart reading method can be adapted promptly for quantitative determinations. The spectra are reasonably reproducible if the experimental conditions are carefully standardized. The long range repeatability of the analysis of a middle distillate is illustrated in Table IV. The standard deviations obtained are acceptable, although two or three fold higher than those for low voltage analyses on a low resolution instrument, such as a Consolidated Electrodynamics Company Model 21-103C mass spectrometer.

Data on the nominal compound type distribution of the same samples from the two instruments, obtained by comparing the sums of the high resolution multiplets to the sums of the low resolution singlets, agree within the precision limits. This also indicates that pure compound calibration data obtained on the two instruments are interchangeable within certain limits. This point is corroborated by Reid(7).

Table IV. Long Range Repeatability of Quantitative Data
Partial Analysis of a Middle Distillate*

Type	Percent of Total Ionization		Average Molecular Weight	
	Avg.	SD	Avg.	SD
C_nH_{2n-8}	7.8	0.64	174.2	2.6
C_nH_{2n-12}	39.8	1.59	169.8	1.6
C_nH_{2n-16}	7.6	0.59	202.4	1.6
$C_nH_{2n-16}S$	3.0	0.33	207.7	2.3
$C_nH_{2n-16}O$	1.7	0.17	203.6	1.9

SD: Standard Deviation

*18 runs over a period of two months.

The calibration coefficients necessary for quantitative analyses thus can be obtained from published pure compound data(2)(3), and from direct calibration of pure compounds or of characteristic concentrations separated by alumina gel percolations. A third method is a theoretical approach, which assigns abritrary sensitivities to all compound types, according to the number of conjugated double bonds and heteroatoms in a model structure. This approach agrees well with experimental data on pure compounds and it is used presently in our laboratories.

Figure 1. Portion of a High Resolution-Low Voltage Spectrum of a Complex Hydrocarbon Mixture

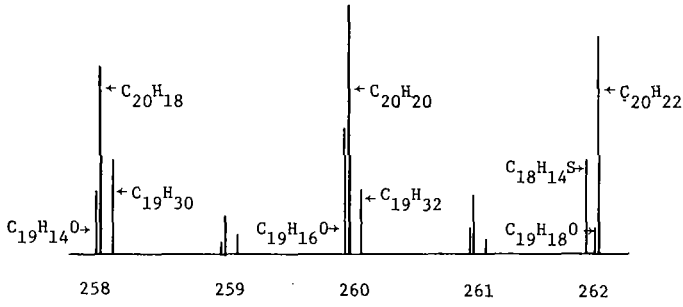

Figure 2. Principles of Mass Measurement from Chart

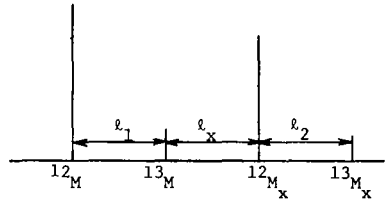

(1) $\ell_1, \ell_2 \equiv 1.003355$ amu ($^{13}C-^{12}C$)

(2) $M_x = M + 1.003355 + \frac{2\ell_x}{\ell_1 + \ell_2} \cdot 1.003355$

The validity of the quantitative data can be tested in some cases with external standards. Elemental sulfur and oxygen data, determined by both this method and by X-ray, fluorescence, and neutron activation techniques, respectively, agree within the precision of the methods used. The data reported in Table V illustrate this agreement for sulphur analyses.

Table V. Weight Percent of Sulphur in Petroleum Products

Sample	High Resolution MS	X-Ray Fluorescence
A	2.74	2.94
B	2.24	2.16
C	1.30	1.47
D	0.53	0.49
E	0.08	0.13

Conclusion

The combination of low voltage high resolution techniques together with the simple and accurate interpretation technique described in this paper results in the characterization of complex aromatic hydrocarbon mixtures heretofore unmatched in detail. The technique yields rapid analyses of mixtures containing 30 to 40 compound types, each comprised of up to 50 homologues. Both compound type and carbon number distribution data can be obtained in a matter of hours. The detectability is about 0.1 percent or less of the total ionization.

This type of work is particularly important in the oil industry. The technique described, however, could be useful for the analysis of naturally occurring mixtures in general.

Limitations of the approach are the very expensive instrumentation required, the time spent in data handling and the existence of unresolvable doublets, such as $^{32}SH_4$-C_3. The latter two problems might be resolved by the use of digitizers and computers and by the combination of fragment and parent peak methods.

Acknowledgement

The authors wish to thank Mr. H. E. Lumpkin for many helpful suggestions and Mr. G. R. Taylor and Mr. J. L. Taylor for carrying out most of the experimental work described in this paper. Thanks are due also to Mr. J. H. Harding who was responsible for the maintenance of the instrument.

References

1. Field, F. H., Hastings, S. H., Anal. Chem. 28, 1948 (1956)

2. Lumpkin, H. E., Anal. Chem. 30, 321 (1958)

3. Lumpkin, H. E., Aczel, Thomas, Anal. Chem. 36, 181 (1964)

4. Lumpkin, H. E., Anal. Chem. 36, 2399 (1964)

5. Lumpkin, H. E., personal communication

6. Quisenberry, K. S., Scolman, T. T., Nier, A. O., Phys. Rev. 102, 1071 (1956)

7. Reid, W. K., Mead, W. L., Bowen, K. M. (Miss), paper presented at the Institute of Petroleum/ASTM Spectrometry Symposium, Paris, Sept. 1964

INTERPRETATION OF HIGH RESOLUTION MASS SPECTRA

M. Barber, P. Powers and W. A. Wolstenholme
Consultant Laboratory
Associated Electrical Industries Limited
Manchester, England

Introduction

At the ASTM Committee E-14 meeting last year results were presented[1,2] showing that complete high resolution mass spectra could be recorded electrically in 10 seconds and the data then processed using computing techniques to give, if desired, an element map.[3] The sensitivity of the system is such that a useful spectrum can be obtained from 0.2 μgm.

Figure 1 shows diagrammatically the arrangement of such a system. A reference sample, usually perfluorokerosene, is admitted to the mass spectrometer together with the unknown sample which may be a single organic compound or the effluent coming directly from a GLC column.

The element map is now a well known way of tabulating in a digestable form the large amount of precise data which is obtained from a complete high resolution mass spectrum. However, for many compounds the size of such a map becomes unwieldy. For example, for a compound containing 4 nitrogen atoms and 6 oxygen atoms, the map would contain 35 columns. Also, the interpretation of such maps can become quite time consuming and tedious. The next logical step, therefore, would seem to be to program the computer to carry out at least a partial interpretation of the data.

Two possible approaches to this task are (a) to get the computer to generate all possible structures for a given molecular formula and to check each structure against the mass spectrum and (b) knowing the compound type, to program the computer to look for specific fragmentation processes for structure determination.

This paper describes some results we have obtained using the second method. For the initial study we have chosen peptides which, since they are built up from relatively simple units, lend themselves readily to this type of approach. Examples of linear, cyclic and cyclodepsipeptides have been considered. All spectra were obtained using an AEI MS9 high resolution, fast scanning mass spectrometer.

Program Logic

The basic logic and operations in the program are shown in Figure 2. The program has been written so that it can be connected directly to the element map program and so that interpretation can take place before or instead of the mapping process. The peaks in the mass spectrum are stored as atomic compositions and the first operation of the computer is to find the molecular formula of the compound. Having done this, in the case of peptides, there are several deductions the computer can make by consideration of the molecular formula alone:

(a) If mono-amino, mono-carboxyllic acids only are considered, by consideration of the numbers of nitrogen and oxygen atoms and the number of double bond equivalents in the molecular formula, the type of peptide can be determined, e.g. for a cyclic peptide the number of nitrogens is equal to the number of oxygens, and if the number of double bond equivalents is equal to the number of oxygens minus one, the peptide is linear. In this part of the program one also has to consider the presence of phenylalanine which, although mono-amino, mono-carboxyllic, does contain four "extra" double bond equivalents. The computer, therefore, is programmed during this operation to determine the number of phenylalanine units present.

(b) It is also possible for the computer to carry out an amino acid analysis, again by consideration of the number of nitrogens, oxygens and double bond equivalents in the molecular formula. The computer has been programmed to consider nineteen amino acids and to print all possible combinations of those which will give the molecular formula. This can be done directly for cyclic peptides but for linear peptides the N-acyl group and the C-terminal group, usually OCH_3, must first be subtracted. In the case of cyclodepsipeptides a knowledge of the hydroxy acids present would be necessary.

Another very important point in connection with the amino acid analysis is that the computer will accept any known chemical evidence, e.g. any qualitative and/or quantitative analysis of the amino acids present. This information, if any, can be read in and the computer will check it against the molecular formula determined by the mass spectrometer and, if necessary, correct it. An example of this type is given below.

Having performed an amino acid analysis, the computer will then only consider those acids for subsequent sequence determination.

The sequencing part of the program varies slightly depending on the type of peptide being analysed. The main features in each case are as follows:

(i) Linear Peptides

One of the main fragmentations in linear peptides is simple cleavage of the peptide bonds,[4] which results in the successive loss of amino acid units. This type of fragmentation also occurs after ring opening in cyclic and cyclodepsipeptides. The amino acids are, therefore, stored in the computer as peptide units, e.g. valine is stored as C_5H_9NO VAL.

In the case of linear peptides, the computer is programmed so that after the molecular ion has been found, the C-terminal group (OCH_3 for peptide methyl esters) is subtracted from it and the residue is stored. Each peak in the mass spectrum (stored as an atomic composition) is then subtracted from the molecular ion minus OCH_3 and the residue is compared with the amino acid units in the store. When an amino acid unit loss is found this unit is subtracted from the molecular ion minus OCH_3 and the new residue is stored. Each peak in the spectrum is then subtracted from this residue and the result compared with the amino acid units as before. Each acid unit loss found is, of course, printed out.

Since a peak in the spectrum corresponding to the acyl ion itself is not always observed, the computer is programmed to print out the residue containing the N-terminal amino acid if the acyl ion (containing no nitrogen) is not observed.

(ii) Cyclic Peptides

Two types of fragmentation, differing in the mode of initial ring opening, have been considered for cyclic peptides.[5] The first, which we have called type A occurs when the peptide ring opens via a McLafferty type re-arrangement. The simple cleavage of a peptide bond following this then involves the loss of an amino acid unit + NH_2. In this case, therefore, the computer is programmed to find the initial amino acid loss by testing each peak in the mass spectrum to see if it is deficient with respect to the molecular ion by NH_2 plus an amino acid unit. Since the peptide ring can open at more than one place all such "initial losses" are looked for and stored. These residues (M^+-NH_2-amino acid unit) are then taken in turn and used for further sequencing in the same way as for linear peptides. In this case, the completion of sequencing is recognised when the total amino acid units found equal the molecular formula. If the sequencing is incomplete using one initial loss, i.e. the computer cannot find a peak corresponding to the further loss of an amino acid unit, the residue at that stage is printed out and the next initial loss in the store is considered.

The second fragmentation (type B) we have considered for cyclic peptides is that involving ring opening by loss of an amine fragment (i.e. an amino acid unit minus CO). In this case, therefore, the initial losses are found by subtracting CO from the molecular formula and then testing every peak against the result as before. Further sequencing is carried out as for type A fragmentation.

(iii) Cyclodepsipeptides

These peptides contain hydroxy acid as well as amino acid units. There are present, therefore, ester bonds as well as the usual amide or peptide bonds. The fragmentation of these peptides has been studied in some detail,[6] and three main types are predominant. The type we have used so far for this work is that in which ring opening occurs at the ester bond involving the loss of CO_2. The resultant ion can then lose a hydrogen atom and further fragmentation proceeds by simple cleavage of the amide and ester bonds, successive units of amino and hydroxy acids thus being lost. The first step in the sequencing is for the computer to find all initial losses by looking for a peak deficient with respect to the molecular ion by an amino acid unit plus OH (the first loss after ring opening will always be an amino acid unit). Cyclodepsipeptides may contain regularly alternating units of amino acids and hydroxy acids, or the arrangement may be irregular. The computer is programmed, therefore, to look for amino acids and hydroxy acids alternately, but if a hydroxy acid can not be found, another amino acid unit is searched for. The hydroxy acid units are recognised as $C_nH_{2n-6}O_2$, since only mono-hydroxy acids have been considered at this stage. If the computer can find neither acid type unit, it will say so and try an alternative initial loss. The end of a complete sequence is recognised if the residue contains no nitrogen, i.e. after the final amino acid unit has been found, since this will be the part of the hydroxy acid involved in the initial ring opening. For completeness of print out, OH is added to this residue and the unit is then printed out as it occurs in the ring.

Results

Figure 3 shows the computer output obtained when the high resolution spectrum of $(Gly\text{-}Ala\text{-}Phe)_2$ was read into the computer. In this case an incorrect amino acid analysis was deliberately fed in. It can be seen that the computer first finds the molecular formula. The amino acid analysis was read in incorrectly as one unit of glycine, two units of alanine and three units of phenylalanine. The computer, of course, finds that this does not add up to the molecular formula and prints "amino acid analysis incorrect". It then proceeds to correct it by subtracting one unit of glycine, alanine and phenylalanine from the molecular formula and at this stage it prints the residue as "new molecular formula". All possible combinations of amino acids which could add up to this formula are then found - in this case only one, namely, one unit each of glycine, alanine and phenylalanine. This is printed and the amino acid analysis is now corrected, i.e. two units each of glycine, alanine and phenylalanine. Only these three amino acids are now used for sequencing. The initial losses found are alanine and phenylalanine. The sequencing is then completed using the initial loss of alanine - the amino acids are in this case listed vertically and "cyclo" is printed when the sequence is complete. The initial loss of phenylalanine is next taken and in this case only a partial sequence is found - Phe. Since no other initial losses are available, the sequencing using fragmentation type A is completed.

Figure 4 shows the output obtained using the complete high resolution spectrum (containing about 100 peaks) of the regular cyclohexadepsipeptide Enniatin A.[7] The first amino acid unit lost was methyl leucine (MLU) and in this case any other initial losses are stored but not printed at this stage. A C5 hydroxy acid is next found and then another methyl leucine unit, etc. The sequence is complete when the final hydroxy acid unit is found.

Figure 5 shows an example of an irregular cyclohexadepsipeptide, isariin[8,9] which contains five amino acids and one hydroxy acid. This figure shows an example of the determination of the peptide type after the molecular formula has been found. In this case no phenylalanine units are found to be present. The first amino acid unit lost is valine and the sequence is completed when the one hydroxy acid unit present at the end is found, i.e. $C_{12}H_{22}O_2$.

It should be pointed out here that in these two cases of cyclodepsipeptides, it was found that the computer could fail to complete the sequence, or even give an incorrect sequence, mainly due to peaks being present in the spectrum, particularly at low mass, which corresponded to the loss of $C_nH_{2n-2}O_2$ after the previous loss of an amino acid. An incorrect hydroxy acid was thus found. To overcome this we found it necessary, in the case of these depsipeptides only, to read into the computer a qualitative acid analysis, e.g. that which would be obtained after hydrolysis of the peptide.

Figure 6 shows an example of a linear N-acyl tetrapeptide methyl ester. In this case the acyl ion itself was present and the complete sequence together with the acyl group is printed. It is worth noting here that in our first program for linear peptides the technique we adopted was to get the computer to start with the acyl ion and work upwards in mass. When this was done the computer printed the acid sequence Ala-Val-Gly-Gly. A second unit of glycine not present in the peptide had been found by the computer because the peak in the spectrum corresponding to loss of the leucine side chain via a McLafferty re-arrangement has the atomic composition corresponding to this sequence.[4] This anomaly is avoided if our present technique of starting at high mass is adopted.

Conclusion

The results we have obtained with these peptides show great promise. Computer interpretation of the complete high resolution mass spectrum can remove completely the necessity for a quantitative amino acid analysis. Also, for linear peptides, the use of the complete high resolution scan obviates the necessity to acylate with a long chain fatty acid. An acetyl group is sufficient since the computer identifies all peaks by their atomic compositions.

This type of work will be continued with other types of compound using specific fragmentation processes where the compound type is known and also using the "structure generation" method for the more general case.

Acknowledgments

The authors would like to thank their colleague Mr. M. J. Wallington for writing the amino acid analysis part of the computer program. They also thank AEI Electronics Group for permission to publish this paper.

References

(1) Green, B.N., Merren, T.O. and Murray, J.G., Proc. Thirteenth ASTM E-14 Meeting, St. Louis, (1965).

(2) Campbell, A.J. and Halliday, J.S., ibid.

(3) Biemann, K., Bommer, P. and Desiderio, D., Tetrahedron Letters, 26, 1725, (1964).

(4) Bricas, E., van Heijenoort, J., Barber, M., Wolstenholme, W.A., Das, B.C. and Lederer, E., Biochemistry, 4, 2254, (1965).

(5) Millard, B.J., Tetrahedron Letters, 34, 3041, (1965).

(6) Wulfson et al, Tetrahedron Letters, 32, 2793, (1965).

(7) Shemyakin, M.M., Russian Chem. Rev., March, (1962).

(8) Vining, L.C. and Taber, W.A., Can. J. Chem., 40, 1579, (1962).

(9) Wolstenholme, W.A. and Vining, L.C., Tetrahedron Letters, 24, 2785, (1966).

CAPTIONS FOR FIGURES

Figure 1 Block diagram of system for recording and processing high resolution spectra

Figure 2 Basic computer operations for peptide interpretation

Figure 3 Computer output from high resolution spectrum of $(Gly\text{-}Ala\text{-}Phe)_2$

Figure 4 Computer output from a regular cyclohexadepsipeptide - Enniatin A

Figure 5 Computer output from an irregular cyclohexadepsipeptide - Isarlin

Figure 6 Computer output from an N-acyl tetrapeptide methyl ester

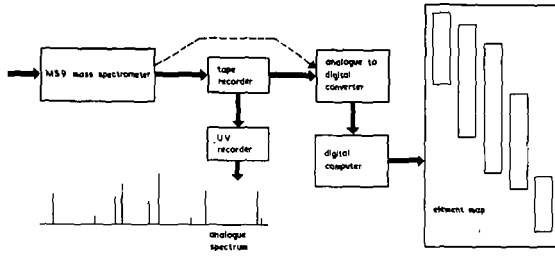

Fig. 1

```
DATE  27.4.66.
TIME  18.00

COMPUTER ANALYSIS OF MASS SPECTRA MB. A/SA/5a.7
C 28 H34 N 6 0 6
MOLECULAR  WEIGHT  =  550
KNOWN AMINO ACIDS

  1  GLY

  2  ALA

  3  PHE
AMINO ACID ANALYSIS INCORRECT
COMPLETE ANALYSIS USING KNOWN AMINO ACIDS
NEW MOLECULAR FORMULA  C 14  H 17  N 3  0 3          F  =  8

  0
  0
  0
  0
  0
  1  GLY
  1  ALA
  1  PHE

  2  GLY
  2  ALA
  2  PHE
AMINO ACID ANALYSIS NOW CORRECTED
SEQUENCING ON ABOVE BASIS
FRAGMENTATION TYPE A
INITIAL LOSS AFTER RING OPENING
ALA
PHE
END OF SPECTRA REACHED FOR INITIAL LOSSES
SEQUENCING NOW CARRIED OUT FROM INITIAL LOSSES
SEQUENCE
ALA
GLY
PHE
ALA
GLY
PHE
CYCLO
S EQUENCE
PHE
PARTIAL SEQUENCING ONLY
INTERPRETATION USING FRAGMENTATION A COMPLETED
```

Fig. 3

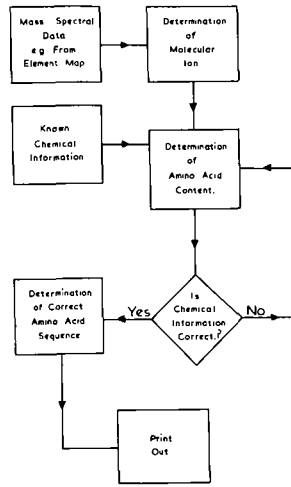

PEPTIDE ANALYSIS PROGRAM.

Fig. 2

```
DATE 12.5.66
TIME 15.33

COMPUTER ANALYSIS OF MASS SPECTRA-CYCLODEPSIPEPTIDES     A/SA/57

C 36  H 63  N  3  O  9
MOLECULAR WEIGHT =  681
FIRST AMINO ACID UNIT LOSS

MLU-C  5  H  8  O  2 -MLU-C  5  H  8  O  2 -MLU-C  5  H  8  O  2

HYDROXY ACID END NOW FOUND
SEQUENCE IS COMPLETE FOR A CYCLODEPSIPEPTIDE
```

Fig. 4

```
DATE 90.81.72
TIME 63.54

COMPUTER ANALYSIS OF MASS SPECTRA.  GENERAL          A/SA/57

C 33  H 59  N  5  O  7
MOLECULAR WEIGHT =  637

PEPTIDE IS CYCLO-DEPSI.

NO. OF PHE.=  0
FIRST AMINO ACID UNIT LOSS

VAL-ALA-LEU-VAL-GLY-C 12  H 22  O  2

HYDROXY ACID END NOW FOUND
SEQUENCE IS COMPLETE FOR A CYCLODEPSIPEPTIDE
```

Fig. 5

```
DATE 11.5.66
TIME 19.10

COMPUTER ANALYSIS OF MASS SPECTRA  1.     A/SA/51  PP.

LINEAR PEPTIDE

PARENT PEAK IS C 27  H 50  N  4  O  6

AMINO ACID ARRANGEMENT ASSUMING CH3O END GROUP IS
CH3O-LEU-GLY-VAL-ALA-C 10  H 19  N  0  O  1
```

Fig. 6

Long Range Peak-Matching Techniques Using the MS-9

H. M. Fales, R. Binks, M. Elliott and R. Freeman

National Institutes of Health, Bethesda, Maryland

The peak-matching system of Nier et al.,[1] similar to that used in the Associated Electrical Industries MS-9 mass spectrograph, was originally designed for doublet measurement in connection with accurate atomic mass determination. Beynon[2] has pioneered its application to molecular formula determination and in this application it is considered advisable to use reference masses within 10% of the unknown mass.[3] This considerably limits the utility of the system since most of the time involved in such measurements is spent in obtaining and checking the reference mass itself. In addition, for maximum accuracy, a calibration chart should be prepared relating error to mass ratio from several known masses within the 10% limit. In the MS-9 spectrometer this type of calibration curve can be extended to higher values (Fig. I). There seems to be no real reason for limiting such measurements to the 10% figure and such a curve has been used successfully for some months in this laboratory. However, the calibration curve does vary from day to day both in regard to slope and the magnitude of the individual steps, and it is necessary to apply a series of arbitrary factors to back-correct for such shifts.

We have been able to eliminate the steps in the curve by the simple expedient of replacing the precision trimmer resistors governing the 1.X00000 decade within the decade box by a series of wire-wound externally adjustable 10,000 ohm resistors. These are individually adjusted to balance known ratios near 1.10, 1,20, 1,30, etc. and effectively eliminate the steps.

The slope in the curve results from an imbalance between the observed decade setting and the actual voltage between one of the electrostatic analyzer plates and ground. It is therefore removed by inserting an adjustable potential source fashioned from a 1.5 volt battery and a 5000 ohm helipot in the electrostatic plate lead.

In this way it is possible to measure peaks within 10 ppm. using ratios from 1.0-2.0 in mass (Fig. II). In practice we find that at ratios higher than 1.70, energy and direction focussing must be carefully adjusted to preserve the shape of the high mass peak since it is being observed at a lower accelerating voltage. For the same reason, the repeller potential must be adjusted to maximize the height of the high mass peak.

In this way, the following ions have been measured on an alkaloid of unknown structure under investigation in our laboratory.

m/e	Ratio	Formula	Error
169	1.00	-	-
201	1.19	$C_{15}H_7N$	+0.7
203	1.20	$C_{15}H_9N$	-2.7
216	1.28	$C_{16}H_{10}N$	-0.8
229	1.35	$C_{17}H_{11}N$	-1.3
243	1.44	$C_{14}H_{13}NO_3$	-2.7
262	1.55	$C_{14}H_{14}O_5$	+0.1
273	1.61	$C_{15}H_{13}O_5$	-2.4

1. K. S. Quisenberry, T. T. Sealman and A. E. Nier, Phys. Rev., 102, 1071 (1956).

2. J. H. Beynon, Mass Spectrometry and its Applications to Organic Chemistry, Elsevier Pub. Co., New York, N.Y. (1960), p.39.

3. Associated Electrical Industries Operation Manual for the MS-9.

Automatic Reduction of High-Resolution Mass Spectral Data

R. Venkataraghavan, F. W. McLafferty and J. W. Amy
Department of Chemistry, Purdue University, Lafayette, Indiana 47907

Introduction

Since the demonstration by Beynon(1) of the potentialities of high-resolution mass spectrometry, various laboratories have shown the highly informative data that one can obtain using a double focusing mass spectrometer compared to a conventional single focusing instrument. It is highly desirable to use automation techniques to reduce the enormous amount of information obtained from high-resolution mass spectra into usable form. Professors Biemann and Burlingame (2,3) have shown the possibility of using a computer to calculate the exact masses and possible elemental compositions of all the fragment ions. In this approach a semi-automatic comparator densitometer is used to transfer the high-resolution mass spectral data from a photoplate onto punched cards or magnetic tape. This information is then processed in the computer to obtain the 'element map' and other desired results.

Apparatus

In this paper we would like to report about a fully automatic Grant-Datex comparator microdensitometer, designed and constructed to our specifications, which reduces considerably the amount of time required to measure a spectrum recorded on a photoplate with better accuracy and to discuss some of the results obtained.

The Grant comparator and Datex digitizer have their individual control settings which can be set to the desired values. The comparator has a viewing screen and scope display for plate alignment. The slit controlling the transmission recording photomultiplier can be adjusted both for width and height. The Datex digitizer has a series of thumb-wheel switches to control the movement of the plate both on the X and Y axes, a transmission threshold control and a spectra indexing control to record desired number of spectra. In addition, it houses an analog to digital converter, programmer, storage register and a magnetic tape recorder. The X-axis can be traversed up to a maximum of 350 mm and the Y-axis can be incremented between 0.05 mm to 4.95 mm at intervals of 0.05 mm. The threshold can be set anywhere between 0% to 99% transmission. The X- and Y-axes travel are controlled by a synchronous motor drive and an automatic incrementing device respectively. A block diagram of the apparatus is shown in Figure 1.

To begin with the photoplate is aligned manually and the settings controlling the movement of the plate on the X- and Y-axes, transmission threshold level above which recording has to be initiated and the number of spectra to be recorded are selected. When the process is initiated the comparator densitometer measures the photographic density and converts it into an electrical signal which serves as an input to a high speed digital voltmeter. A storage register accepts data from the digital voltmeter at intervals corresponding to the time required for the photoplate to move through 0.25 micron along the X-axis. A highly stable reference oscillator drives the precision screw and controls the X-axis travel of the plate as well as the magnetic tape transport. When the preset threshold limit is exceeded during the process of scanning storage and subsequent recording of data is initiated and controlled at increments representing 0.25 micron travel by the same oscillator. The accumulated position count is recorded when the density of the line drops below the threshold value. This process continues for all the bands until the limit set on the X-axis travel is reached. At this point if the number of spectra to be recorded is more than one, the plate is automatically moved along the Y-axis through a distance predetermined by the control setting, racked back to the starting point and the whole process repeated. This operation continues until the total number of recordings satisfies the number of spectra selected before hand. It requires about 12 minutes to scan a spectrum from 0 to 350 mm. As a result of the foregoing operations, transmission readings at 0.25 micron intervals across the entire band profile and the position count with respect to a starting point is recorded on a magnetic tape.

Results

The first step in the calculations is to compute the exact centers of all the lines. This is achieved by doing a curve fitting analysis in the computer using the recorded data points, assuming Gaussian distribution for peak shape. After locating all the peaks, positions are converted to masses by employing the square root relationship between distance and mass. The exact masses and line positions of perfluorokerosene serves as reference points throughout the spectrum. The lines due to the calibration compound are then separated from the lines due to the sample. Possible elemental compositions that would fit the observed masses of the sample lines within a tolerance of 3 mmu are then computed using an iterative

procedure. A portion of the computer output obtained for the spectrum of pregnanediol diacetate is shown in Figure 2. The computer output shows the relative intensity, peak position, corresponding mass, elemental composition and the difference in mmu. between the observed mass and the calculated mass. It also shows at the end the calibration lines used to compute all the relevant information. Even though a tolerance of 3 mmu. is given most of the results are well within this limit.

In order to check the reproducibility of the data, the spectrum of pregnanediol diacetate was recorded under different conditions and the data processed in the computer. The data from three different runs over the same region of the spectrum is shown in Table 1. In all the cases the computer was able to arrive at the same results well within the given tolerance of 3 mmu.

It was felt that the wide scattering in deviations might possibly result from the inhomogeneity of the magnetic field (4). One easy way to look at this would be to plot the slopes, obtained by using the line positions and masses of the calibration compound, against mass. The variation of slope with mass is shown in Figure 3. This plot shows some distinct breaks in the curve. It was found that the data is reproducible under the same instrumental operating conditions. We are investigating the possibility of adding some empirical corrections to improve the mass measuring accuracy.

Band Resolution

Most spectra recorded on photoplate show overlapping band profiles due to lack of complete resolution. Under these circumstances it is highly desirable to separate the overlapping peaks into their individual components to determine their elemental compositions. Various techniques are described in the literature for the separation of overlapping peaks (5,6) and we have adopted a damped least-squares method developed for resolving infrared absorption bands. In this approach the isolated bands are approximated by Gaussian distribution function, and its parameters are adjusted iteratively by least-squares.

The efficiency of this method was tested on the xylene-toluene, 20,000 doublet at mass 92. The spectrum of this mixture was recorded under three different front slit settings. At wider slit settings the resolution is lost. The electron multiplier output of the spectrum under these conditions are shown in Figure 4. Under narrower slit settings the doublet exhibited 33% valley. When the slit was opened there was only 80% valley and when further opened the second peak appeared as a shoulder. Figure 5 is a plot of the tape dump obtained from the photoplate recorded under the same conditions. At progressively increasing slit widths the valley diminishes and finally the second peak becomes a shoulder. The data from all the three cases were then subjected to the band resolution technique and the peak locations calculated by the computer are indicated with arrows.

The pertinent results on the doublet are shown in Table 2. Under the experimental conditions the spectrum was recorded, the two peaks should have been separated by 7.78 microns. Manual measurements on the comparator densitometer indicated a separation of only 4.5 microns. Theoretical mass difference between the two peaks is 4.47 mmu. After subjecting the data to the band resolution program the profile with 90% valley showed a separation of 7.96 microns in distance and a mass difference of 4.52 mmu. The profile with 95% valley showed a separation of 7.79 microns in distance and a mass difference of 4.43 mmu. The profile which appeared as a shoulder showed a distance separation of 8.32 microns and a mass difference of 4.73 mmu. These results show that a significant improvement in resolution of the data can be achieved by treating it with band resolution technique and at the same time eliminate the subjective errors that might be introduced in manual measurements.

Conclusions

By processing the high-resolution mass spectral data through the Grant-Datex comparator microdensitometer and the computer, one can effectively increase the speed of the calculations, obtain better mass measuring accuracy and significantly improve the resolution of the original data.

Acknowledgments

Invaluable discussions with D. D. Tunnicliff and P. A. Wadsworth of the Shell Development Company, the technical assistance of R. Board, and the generous financial support of the National Institutes of Health (GM 12755) are gratefully acknowledged.

References

1. J. H. Beynon in "Advances in Mass Spectrometry", Vol. 1, J. D. Waldron, Ed., Pergamon Press, Oxford, 1959, p. 328.

2. (a) K. Biemann, Pure and Appl. Chem., 9 : 1, 95 (1964).
(b) K. Biemann, P. Bommer and D. N. Desiderio, Tetrahedron Letters, 1725 (1964).
3. A. L. Burlingame, Thirteenth Annual Conference on Mass Spectrometry and Allied Topics, St. Louis, May, 1965.
4. W. Hargrove, Personal communication.
5. H. Stone, J. Opt. Soc. Amer., 52, 998 (1962).
6. D. Papousek and J. Pliva, Collection Czech. Chem. Commun. 30, 3007 (1965).

Table 1

Reproducibility of Mass Measurement Over a Small Region of Pregnane-Diol-Diacetate Spectrum

Elemental Composition	Calculated Mass amu.	Observed Mass amu. Run I	Run II	Run III
C_9H_9	117.07042	117.07032 -0.10	117.07037 -0.05	117.07061 0.19
C_9H_{10}	118.07825	118.07788 -0.37	118.07788 -0.37	118.07818 -0.06
C_9H_{11}	119.08607	119.08628 0.21	119.08635 0.28	119.08591 -0.16
C_9H_{12}	120.09389	120.09312 -0.78	120.09356 -0.33	120.09372 -0.18
C_9H_{13}	121.10172	121.10158 -0.14	121.10166 -0.06	121.10087 -0.85
C_9H_{14}	122.10954	122.10854 -1.00	122.10837 -1.17	122.10852 -1.02
C_9H_{15}	123.11737	123.11699 -0.38	123.11691 -0.46	123.11685 -0.52

Table 2

Results on Xylene-Toluene - 20,000 Doublet

$C_6C^{13}H_7 = 92.05813$

$C_7H_8 = 92.06260$

Calculated Distance of Separation = 7.78 Microns

Observed Distance of Separation by Manual Measurement = 4.5 microns

Theoretical Mass Difference = 4.47 mmu.

Identification	Elemental Composition	Observed Distance of Separation	Calculated Mass	Error mmu.	Calculated Mass Difference
Profile with	$C_6C^{13}H_7$		92.05940	1.27	
90% valley	C_7H_8	7.96μ	92.06392	1.33	4.52
Profile with	$C_6C^{13}H_7$		92.05907	0.95	
95% valley	C_7H_8	7.79μ	92.06350	0.91	4.43
Profile which	$C_6C^{13}H_7$		92.05898	0.86	
shows a	C_7H_8	8.32μ	92.06371	1.12	4.73
shoulder					

FIGURE NO. 1

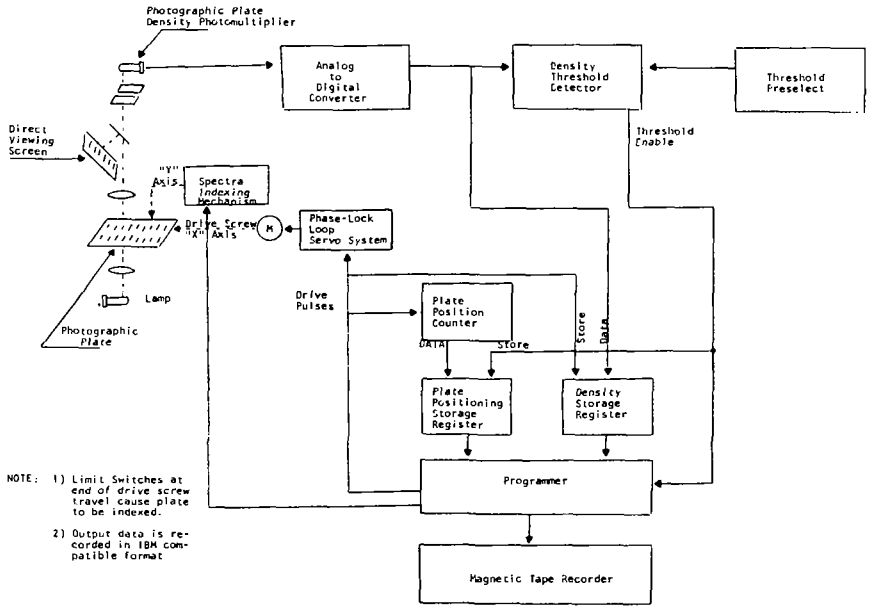

INTENSITY	DISTANCE	MASS	CALC	ERROR	C12/C13	H	O
47.5	46.C91C6	117.C7C37	117.07C42	-0.05	9/0	9	0

INTENSITY	DISTANCE	MASS	CALC	ERROR	C12/C13	H	O
25.6	46.93508	118.C7788	118.07825	-0.37	9/0	10	0

INTENSITY	DISTANCE	MASS	CALC	ERROR	C12/C13	H	O
47.1	47.77631	119.08635	119.08607	0.28	9/0	11	0

INTENSITY	DISTANCE	MASS	CALC	ERROR	C12/C13	H	O
44.9	48.61294	120.09356	120.09389	-0.33	9/0	12	0

INTENSITY	DISTANCE	MASS	CALC	ERROR	C12/C13	H	O
45.1	49.44680	121.10166	121.10172	-0.06	9/0	13	0

INTENSITY	DISTANCE	MASS	CALC	ERROR	C12/C13	H	O
36.7	50.27606	122.10837	122.10954	-1.17	9/0	14	0

INTENSITY	DISTANCE	MASS	CALC	ERROR	C12/C13	H	O
37.1	51.10340	123.11691	123.11737	-0.46	9/0	15	0

	DISTANCE1	DISTANCE2	SLOPE	CONSTANT
3				
7	46.02795	51.81985	18.16727519	-150.4771575
	46.0279498	116.9952106	CALIBRATION	
	47.6580600	118.9923620	CALIBRATION	
	48.5317202	119.9955550	CALIBRATION	

INTENSITY	DISTANCE	MASS	CALC	ERROR	C12/C13	H	O

Fig. 2

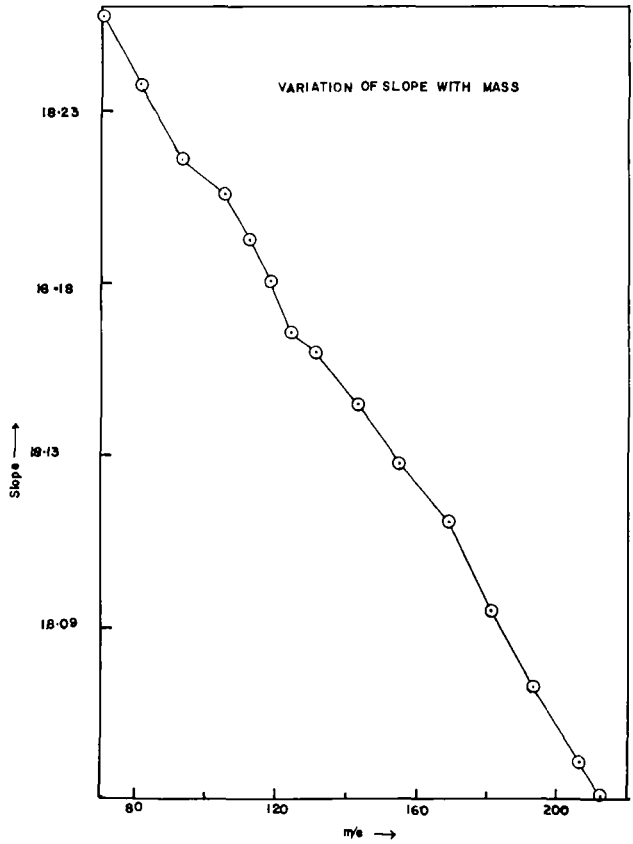
VARIATION OF SLOPE WITH MASS
18·23
18·18
18·13
18·09
Slope
80
120
160
200
m/e

Fig. 3

ELECTRON MULTIPLIER OUTPUT : 20,000 DOUBLET

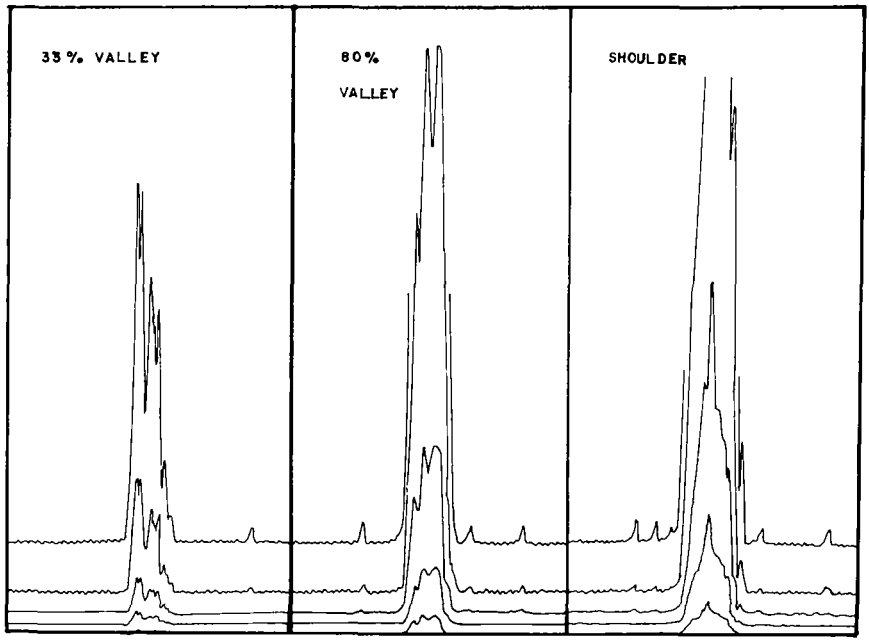

Fig. 4

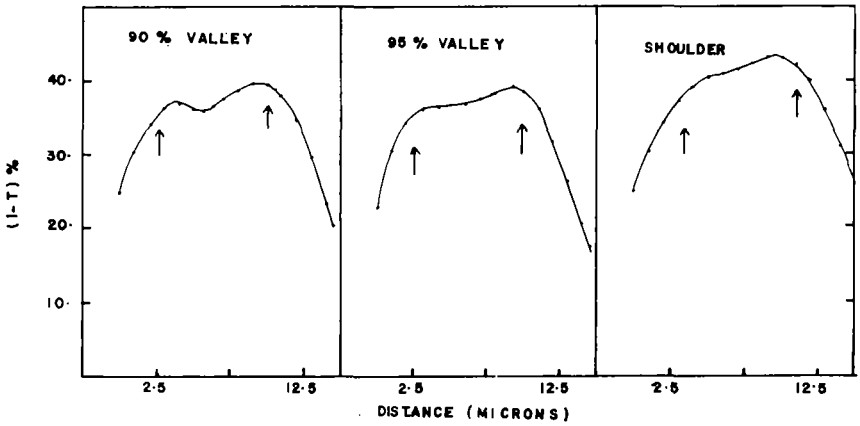

Fig. 5 PLOT OF TAPE DUMP : 20,000 DOUBLET

The Mass Spectra of Some Organophosphorus Pesticidal Compounds - By Joseph N. Damico (Division of Food Chemistry, Food and Drug Administration, U. S. Department of Health, Education, and Welfare, Washington, D. C. 20204)

The Food and Drug Administration has maintained a program to ascertain what toxic substances form under good agricultural practices when crops are field sprayed with individual organophosphorus pesticides. Ultra-sensitive techniques are necessary to identify the isolated metabolites so that they may be synthesized in large enough quantities for toxicity studies. Gas chromatography offers many desirable features and is unsurpassed in general for separation and particularly for quantitation at high sensitivity(1,2). However, identification based solely on retention time is unreliable and a more specific technique is required. Mass spectrometry in tandem with gas chromatography is one approach.

The high sensitivity and specificity of mass spectrometry make it very suitable for such a study. Accordingly, mass spectral correlations of the molecular structures of significant organophosphorus pesticides including some phosphorodithioates, $(RO)_2\text{-}\overset{S}{\overset{\|}{P}}\text{-}S\text{-}Z$; phosphorothionates, $(RO)_2\text{-}\overset{S}{\overset{\|}{P}}\text{-}O\text{-}Z$; phosphorothiolates, $(RO)_2\text{-}\overset{O}{\overset{\|}{P}}\text{-}S\text{-}Z$; and phosphates, $(RO)_2\text{-}\overset{O}{\overset{\|}{P}}\text{-}O\text{-}Z$ are necessary because calibration compounds may not be available to aid in the identification.

Thus far very few detailed mass spectrometric studies of compounds used as pesticides (3) have appeared in the literature. The mass spectra of some trivalent phosphorus esters and of some isomerically related phosphonates were studied by Occolwitz and White (4). Quayle (5) investigated some pentavalent phosphorus esters including trialkyl, aryl-alkyl, and triaryl phosphates and observed a large proportion of ions arising from hydrogen migrations as originally observed by McLafferty (6) with triethyl phosphate. Quayle reported a significant rearrangement of the trialkyl phosphates yielding the species $[(HO)_4P]^+$ (m/e 99), and was in fact the base peak (m/e 115) for the phosphorothionate compound (tri-chloropropyl) he studied. This double migration of hydrogens from the alkyl ester groups to the phosphorus-oxygen skeleton was of little significance in the present study. However, a minor rearrangement observed by Quayle (5) with an ion product configuration $[(HO)_2PO]^+$ yielded the base peak m/e 97 for two sulfur analogs, a major peak for eight other sulfur analogs, and minor peaks (m/e 81) for two phosphates in the present study. This rearrangement would be expected since it requires hydrogen migration from only two alkoxy groups. However, the intensity of the rearrangement product ion peak in this study was unexpected in view of Quayle's work (5).

Experimental - The mass spectra were obtained with a Bendix Model 14 time-of-flight mass spectrometer equipped with a vacuum lock direct inlet system. A good quality spectrum is obtained on 3-5 μg of sample. The accurate mass measurements were obtained with a C.E.C. 21-110 and an A.E.I. MS-9 mass spectrometer also using a direct inlet system.

Results and Discussions - Accurate mass measurements and elemental compositions are listed in Table 1. The mass spectra of the compounds studied are presented in Figures 1 - 23. Metastable peaks would give valuable information to confirm many of the rearrangement processes described in this paper. However, the Bendix time-of-flight mass spectrometer does not normally give definitive metastable peaks that are routinely obtained with most magnetic instruments. Accordingly, metastable peaks are not discussed in conjunction with any of the rearrangement processes postulated here.

Some observations can be made which are in general applicable for all the compounds studied. Intense peaks are produced when alpha-cleavage occurs with the charge on the phosphorus moiety. For the most part, beta-cleavage of the phosphorodithioates and phosphorothiolates produces a relatively intense peak with the charge on the Z moiety. Cleavage of this type is not observed with the phosphorothionates (except Diazinon) or phosphates (except the oxygen analog of Diazinon).

The M-45 and M-31 peaks characteristic of ethyl and methyl esters, respectively, were normally not observed with the compounds in this study. However, five of the ten ethoxy esters gave an M-28 peak which is characteristic of ethyl esters.

Group 1 (Phosphorodithioates) - Molecular ions - The only compound in this group that did not give a molecular ion was Delnav. The molecular weight of this compound is 456, but the highest mass peak observed was m/e 321.

Ions due to rearrangement - The Quayle $[(HO)_2PO]^+$ rearrangement ion type accounts for the base peak m/e 97 of Ethion and Delnav and intense peaks for Di-Syston and Trithion. The absence of m/e 97 in the spectrum of Methyl Trithion indicates that the hydrogens must rearrange from the ethoxy group which is further evidence to support Quayle's assignment of m/e 97 observed with tri(chloro-propyl)phosphorothionate as an $[(HO)_2PO]^+$ type.

The ion configuration of the base peak (m/e 87) of Dimethoate was not readily apparent; in fact an erroneous assignment would have been made without an accurate mass measurement of this ion. Methyl migration from the methoxy group to the Z moiety with the formation of N-methylpropioamide was initially postulated.

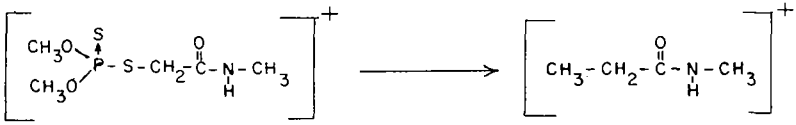

This assignment was strengthened by the favorable comparison of the mass spectrum of N-methylpropioamide (7) and Dimethoate. Furthermore, the carboxylic acid derivative of Dimethoate does not have a peak at m/e 87 (8) which indicates that the carbamyl group must be involved in the rearrangement process. However, accurate mass measurement of m/e 87 showed that it was 40 millimass units less than the mass for the elemental composition of N-methyl propioamide. Accordingly, N-methyl thioacetonitrile, $[S\text{-}CH_2\text{-}C{\equiv}N\text{-}CH_3]^+$, must be the structure of m/e 87 because it is the only structure that fits the elemental composition.

A relatively high abundance of m/e 47 for Methyl Trithion and Trithion is good evidence of hydrogen migration from the alkyl ester group to the sulfur atom attached to the Z moiety to form the stable $[HS{=}CH_2]^+$ species. Methyl Trithion is given as an example:

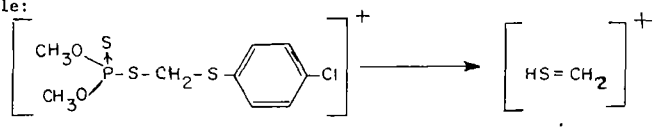

Relatively intense peaks are observed for Trithion, Methyl Trithion, Malathion, Imidan, and Guthion which suggest a similar rearrangement with the hydrogen migrating to the methylene group of the Z moiety. Methyl Trithion is given as an example:

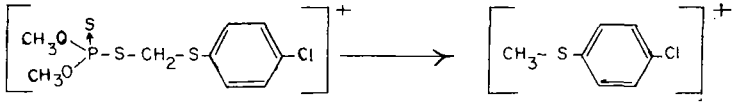

The base peak of Di-Syston could be due to rearrangement of the Z moiety to form the tetrahydrothiofuran ion (m/e 88).

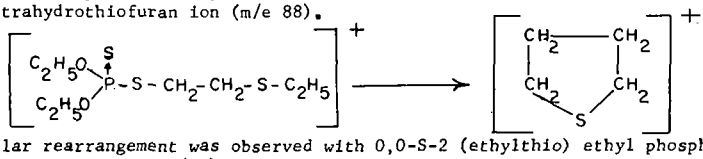

A similar rearrangement was observed with 0,0-S-2 (ethylthio) ethyl phosphate (9). The work of Levy and Sthal (10) on the mass spectra of thiols and sulfides did not show such a rearrangement with diethyl sulfide. The base peak was in fact due to alpha-cleavage (m/e 75) which was insignificant (5%) with Di-Syston.

Ions due to beta-cleavage - The base peaks of Malathion, Methyl Trithion, Imidan, Guthion, and Trithion are probably due to beta-cleavage. The presence of the chlorine isotope peak (m/e 159) and also the fact that the alkyl ester groups are different for Methyl Trithion and Trithion are good indications that the common base peak of these two compounds is due to beta-cleavage.

Loss of Chlorine - The loss of a chlorine atom from the molecular ions of Methyl Trithion and Trithion was not observed and is unusual. An intense peak at M-Cl is normally produced by the loss of chlorine attached to an aromatic ring (11).

Group 2 (Phosphorothionates) - Molecular ion intensity - A high ion-current corresponding to the molecular ion was observed for all the compounds in this group and was the base peak for Co-Ral.

Ions due to rearrangement - The Quayle $[(HO)_2PO]^+$ rearrangement was also observed with Sulfotepp, Parathion, Diazinon, and Co-Ral.

The intense peak at m/e 152 in the spectrum of Diazinon is probably due to hydrogen rearrangement from the ester group bound to phosphorus to the oxygen atom bonded to the Z moiety.

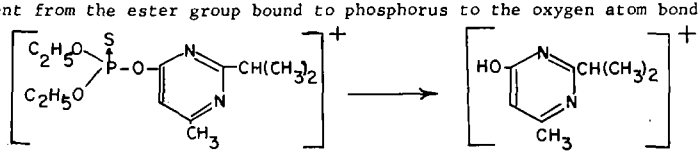

The elemental composition of the proposed ion configuration is in good agreement with the measured mass of this ion. This same type of rearrangement probably accounts for the high ion-current at m/e 210 observed for Co-Ral. The presence of an isotope peak at m/e 212 is indicative of an ion configuration containing chlorine which gives some evidence to support this rearrangement.

The fragmentation of Methyl Parathion, Sumithion, and Parathion is most interesting. All three compounds show a high ion-current at m/e 109, and give intense parent ions.

The loss of NO from the molecular ion of Methyl Parathion and Parathion to produce an intense peak at M-NO would be expected since the loss of NO from aromatic nitro compounds is well known (12) but was not observed. An intense peak at m/e 260 (M-17) was observed for Sumithion due to the loss of OH which is expected (13) because of hydrogen bonding between the methyl group and the nitro group. The base peaks of Methyl Parathion, Sumithion, and Parathion are m/e 109, 125, and 109 respectively. Hydrogen migration from the ethoxy group to the oxygen atom bonded to the Z moiety to form p-nitrophenol followed by the loss of NO was initially postulated as the rearrangement process for the formation of the base peak of Parathion. Fragmentation of p-nitrophenol (14) gives intense peaks at m/e 139 (base peak), 123, 109, 93, 81, and 65 which are also present in the spectrum of Parathion and thus support the postulated rearrangement process. However high resolution mass spectrometry shows that m/e 109 of Parathion is a quadruplet. There are two major peaks present in a ratio of 5 to 1 and consistent with elemental compositions of $C_2H_6O_3$ and $C_6H_5O_2$ respectively. Accordingly, the rearrangement postulated is only a minor process. A possible mechanism for the major rearrangement with formation of the protonated phosphenous acid ion is postulated below.

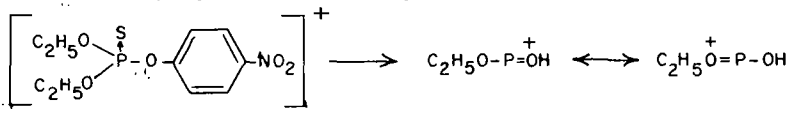

These resonance structures concur with the general structure suggested by Occolwitz and White (4) for representing ions of the type $P(OH)_2$, POH(OR), and $P(OR)_2$. This rearrangement would also account for the high ion-current observed at m/e 109 for Co-Ral.

The fragmentation of Methyl Parathion is based on the consistent fragmentation of Sumithion. If Methyl Parathion undergoes the minor rearrangement process, postulated for Parathion, then Sumithion should also undergo the same rearrangement process. Accordingly, the spectrum of Sumithion should have an intense peak at m/e 123. This is not an unreasonable assumption because the methyl group attached to the ring is the only distinction between the two compounds. However, the intensity of m/e 123 is in fact only 5%, thus one can conclude that the formation of m/e 109 in the spectrum of Methyl Parathion must be formed by a different process than was postulated for Parathion and that the 109 peak of Methyl Parathion is likely a single ion configuration. Accurate mass measurement showed this to be so. The 109 peak of Methyl Parathion and Sumithion is probably formed in the following manner.

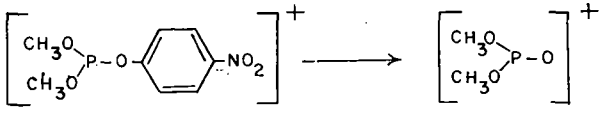

The base peak of Diazinon could be formed by migration of an ethyl group from the ethoxy group to the oxygen atom of the Z moiety with removal of a hydrogen from the isopropyl group either before or after the rearrangement.

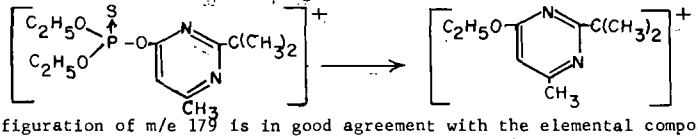

The ion configuration of m/e 179 is in good agreement with the elemental composition. The mechanism postulated involves a rearrangement of an ethyl group. Alkyl migration of esters has been reported by McLafferty (15); Daz and co-authors (16) showed evidence for phenyl migration with aromatic amides. The loss of hydrogen from the isopropyl group seems probable for the following reasons: (1) A tertiary carbonium ion could form which would stabilize the positive charge of the product ion. (2) An isopropyl group (M-43) is not lost from the molecular ion and is generally observed in similar systems. (3) The ion configuration postulated for m/e 179 could lose propylene to form the intense peak observed at m/e 137 which is also in good agreement with the elemental composition.

Ions due to simple bond fission - Diazinon was the only compound in this group that showed a high ion-current due to both alpha- and beta-cleavage with the charge on the Z moiety.

Loss of chlorine - The loss of chlorine which was not observed with Methyl Trithion and Trithion (Group 1) accounts for the base peak of Ronnel. The isotopic peaks for two chlorine atoms serve as additional evidence for the identification of the m/e 285 species.

Group 3 (Phosphorothiolates) - Molecular ion - The three compounds in this group all gave a molecular ion peak, but the intensities of the molecular ion peaks of the oxygen analog of Guthion and the oxygen analog of Malathion are small, hence a relatively large sample is required to detect them.

Ions due to rearrangement - The mass spectra of N-methylcarbamates (3) normally used as insecticides showed these compounds to give a characteristic rearrangement peak,

usually the base peak, due to the migration of the hydrogen from nitrogen to the alcohol addendum with loss of N-methyl isocyanate as the neutral species. Since the oxygen analog of Dimethoate has a portion of the molecule which is very similar to a carbamate, similar rearrangement could account for the species which shows a high current at m/e 156 in its spectrum with loss of N-methyl isocyanate as the neutral species.

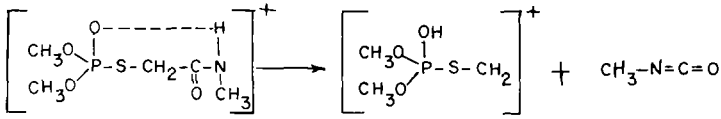

The elemental composition was confined by accurate mass measurement.

A rearrangement arising from hydrogen bonding of the hydrogens of the methylene group with the co-ordinate covalent bonded oxygen atom probably accounts for the aforementioned rearrangement and the base peak (m/e 110) of the oxygen analog of Dimethoate.

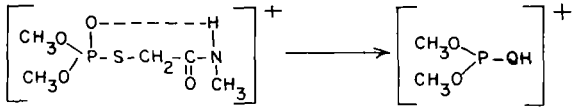

This structure is in agreement with the elemental composition. A similar rearrangement is postulated for the oxygen analog of Malathion because it has an intense peak at m/e 110 consistent with the same elemental composition. It also has an acidic methylene hydrogen. A similar rearrangement with Malathion is not observed because hydrogen bonding with sulfur does not occur which is manifested by the absence of a peak at m/e 126. Hence, lack of significant decomposition of the molecular ion of Malathion could account for the observed intensity of the Z+ moiety (m/e 173) of Malathion being greater than that of its oxygen analog. The oxygen analog of Guthion does not undergo this rearrangement because the hydrogens of its methylene group are not acidic.

Rearrangement with the formation of the ethyl oxonium ion of maleic anhydride is postulated as the base peak (m/e 127) of the oxygen analog of Malathion.

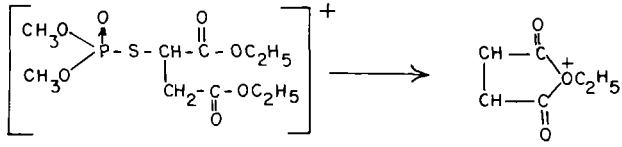

The elemental composition of this ion is in good agreement with the measured mass value. Furthermore, the ethyl oxonium ion has been shown to be an intermediate in chemical reactions (17).

The high ion-current at m/e 99 of the oxygen analog of Malathion was shown by high resolution mass spectrometry to be a doublet with peaks corresponding to elemental compositions of $C_4H_3O_3$ and $C_5H_7O_2$ respectively. The major ion, $C_4H_3O_3$, could be the protonated maleic anhydride ion.

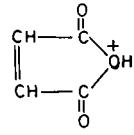

The protonated anhydride ion yields a characteristic peak for dialkylphthalates (18,19). The formation of a six-membered ring could account for the $C_5H_7O_2$ ion.

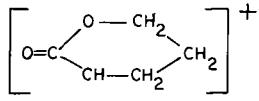

The m/e 109 peak of the oxygen analog of Malathion was shown by mass measurement of the ion to correspond to the same elemental composition as indicated previously for the like peak from Methyl Parathion. The ions m/e 127 and 99 are also observed in the spectrum of Malathion and it is reasonable to assume that they are formed by the same processes respectively as postulated for fragmentation of the oxygen analog of Malathion.

Loss of C-O - The oxygen analog of Guthion, like Guthion (Group 1) shows an intense peak at m/e 132 due to the loss of C-O from the base peak ion, m/e 160.

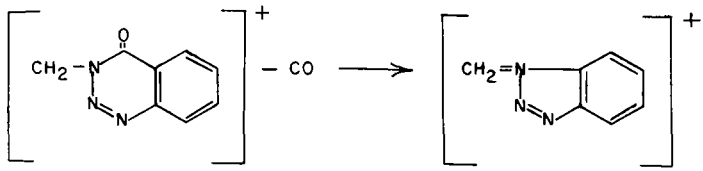

Group 4 (Phosphates) - Molecular Ions - Phosphamidon was the only compound in this group that did not give a molecular ion peak. The molecular weight can be readily determined from the M-Cl (m/e 264) fragment ion. The absence of an isotope peak (m/e 266) supports this identification; also a chlorine atom is readily lost when attached to an unsaturated carbon during fragmentation (20).

Ions due to rearrangement - Double hydrogen rearrangement from the Z moiety to the phosphorus-oxygen skeleton to give the ion configuration

$$\left[(CH_3O)_2-P-(OH)_2\right]^+$$

is postulated for the base peak ion (m/e 127) for both Phosdrin and Phosphamidon. The basis for making this assumption is two fold: (1) the structure of the Z moiety of these two compounds is markedly different, therefore, it is reasonable to assume that the same portion of each molecule must be associated with the rearrangement ion. (2) The elemental composition of m/e 127 is in good agreement with the proposed ion configuration. However, no evidence has been adduced to suggest which hydrogens are migrating from the respective Z moieties.

The spectrum of Paraoxon is very similar to that of Parathion and its base peak (m/e 109) is probably formed by the same processes. The absence of a relatively intense peak (m/e 137) due to alpha-cleavage with the charge on the diethoxy phosphoryl group is surprising. It may be that the major rearrangement process postulated for Parathion would be more favorable for Paraoxon since it could involve hydrogen migration to either the co-ordinate-covalent bonded oxygen or the covalent bonded oxygen. Furthermore, a relatively intense peak at m/e 99 indicates that Paraoxon undergoes the previously discussed rearrangement described by Quayle as characteristic of the tri-alkyl phosphates. These two processes indicate that the molecular ion can undergo such fragmentation at the expense of the diethoxy phosphoryl ion.

Absence of m/e 179 and 152 peaks from the spectrum of the oxygen analog of Diazinon indicates that it does not undergo alkyl or hydrogen migration from the alkoxy group to the Z moiety which is postulated for Diazinon. The base peak (m/e 137) is probably due to alpha-cleavage with the charge on the diethoxy phosphoryl group. It is unlikely that this peak is formed by the same process descirbed for Diazinon (m/e 137) since the other two rearrangements previously described for Diazinon to account concomitantly for the formation of peaks m/e 179 and m/e 152 do not occur. Since a relatively intense peak at m/e 109 is not observed in the spectra of either Diazinon or the oxygen analog of Diazinon the major rearrangement process postulated for Parathion must not occur with these two compounds. Possibly beta-cleavage with the charge on the Z moiety predominates which would be unfavorable to the formation of the diethoxy thiophosphoryl ion (Diazinon) or of the diethoxy phosphoryl ion (oxygen analog of Diazinon).

Conclusion - It has been demonstrated that study of the mass spectra of the organophosphorus pesticides is very helpful in the identification of metabolites of these compounds. Furthermore, without the aid of accurate mass measurements many erroneous assignments would have been made and in some cases no assignments could have been made.

However, a detailed study of labelled compounds is desirable to confirm the mechanisms postulated in this report. Such a study would be helpful in predicting the mass spectra of similar compounds and in the identification of other metabolites.

Acknowledgments - The author would like to thank Dr. Henry Fales of the National Institutes of Health, Bethesda, Maryland, and Mr. William Kuhn and the management of Philip Morris Research Laboratories, Richmond, Virginia, for their cooperation in providing the accurate mass measurements. The assistance and the apparatus for evaluating photographic plates made available by Mr. Jim Allard of the U. S. Naval Research Laboratories, Washington, D. C. are gratefully acknowledged. Special appreciation is due Mr. James Sphon of this Division for his contribution in helping to record the mass spectra and collate the data.

References
1. Guiffrida, L., JAOAC, 47, 293 (1964).
2. Giuffrida, L., Ives, N. F., Bostwick, D. C., JAOAC, 49, 8 (1966).
3. Damico, J. N., Benson, W. R., JAOAC, 48, 344 (1965).
4. Occolowitz, J. L., White, G. L., Anal. Chem., 35, 1179 (1963).
5. Quayle, A., "Advances in Mass Spectrometry," J. D. Waldron, ed., p.365, Pergamon Press, London, 1959.
6. McLafferty, F. W., Anal. Chem., 28, 313 (1956).
7. Unpublished experiments from the author's laboratory.
8. Unpublished experiments from the author's laboratory.
9. Unpublished experiments from the author's laboratory.
10. Levy, E. J., Stahl, A., Anal. Chem., 33, 707 (1961).
11. Beynon, J. H., "Mass Spectrometry and Its Application to Organic Chemistry," Elsevier, New York, 1960, p. 418.
12. Beynon, J. H., ibid, p. 269.
13. Beynon, J. H., ibid, p. 420.
14. Unpublished experiments from the author's laboratory.
15. McLafferty, F. W., "Mass Spectrometry of Organic Ions," Academic Press, New York (1963) p. 542.
16. Daz, K. G., Funke, P. T., and Bose, A. K., J. Am. Chem. Soc., 86, 3729 (1964).
17. Cram, D. J., Hammond, G. S., "Organic Chemistry," McGraw-Hill Book Co., New York, San Francisco, Toronto, London, 2nd Ed., p. 484.
18. McLafferty, F. W., Goldke, R. S., Anal. Chem., 31, 2076 (1959).
19. Emery, E. M., Anal. Chem., 32, 1495 (1960).
20. Beynon, J. H., "Mass Spectrometry and Its Application to Organic Chemistry," Elsevier, New York, 1960, p. 416.

Table 1. Mass measurements and elemental compositions of some ions observed in the mass spectra of the pesticidal compounds.

Compound	m/e	Measured mass a.m.u.	Calculated mass a.m.u.	Elemental Composition	Laboratory
Dimethoate	87	87.0139	87.0142	C_3H_5NS	Natl.Inst.of Hlth
Dimethoate	87	87.0121	87.0142	C_3H_5NS	Philip Morris
Oxygen analog of Malathion	99	99.0081	99.0082	$C_4H_3O_3$	Natl.Inst.of Hlth
Oxygen analog of Malathion	99	99.0446	99.0446	$C_5H_7O_2$	Natl.Inst.of Hlth
Dimethoate	93	93.0105	93.0105	$C_2H_6O_2P$	Natl.Inst.of Hlth
Oxygen analog of Malathion	109	109.0050	109.0054	$C_2H_6O_3P$	Natl.Inst.of Hlth
Methyl Parathion	109	109.0036	109.0054	$C_2H_6O_3P$	Philip Morris
Parathion	109	109.0004	109.0054	$C_2H_6O_3P$	Philip Morris
Parathion	109	109.0045	109.0054	$C_2H_6O_3P$	Natl.Inst.of Hlth
Parathion	109	109.0280	109.0290	$C_6H_5O_2$	Natl.Inst.of Hlth
Oxygen analog of Malathion	110	110.0130	110.0133	$C_2H_7O_3P$	Natl.Inst.of Hlth
Oxygen analog of Dimethoate	110	110.0124	110.0133	$C_2H_7O_3P$	Natl.Inst.of Hlth
Oxygen analog of Malathion	127	127.0399	127.0395	$C_6H_7O_3$	Natl.Inst.of Hlth
Phosdrin	127	127.0138	127.0160	$C_2H_8O_4P$	Philip Morris
Phosphamidon	127	126.9964	127.0160	$C_2H_8O_4P$	Philip Morris
Diazinon	137	137.0707	137.0714	$C_7H_9N_2O$	Natl.Inst.of Hlth
Diazinon	152	152.0973	152.0950	$C_8H_{12}N_2O$	Natl.Inst.of Hlth
Oxygen analog of Dimethoate	156	155.9958	156.0010	$C_3H_9O_3PS$	Natl.Inst.of Hlth
Diazinon	179	179.1152	179.1184	$C_{10}H_{15}N_2O$	Natl.Inst.of Hlth

Note: Atomic Wt. (C^{12} = 12.00000)

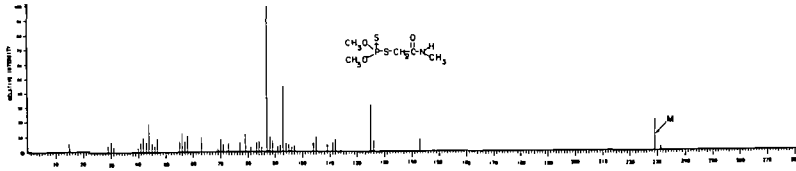

Fig. 1 Dimethoate

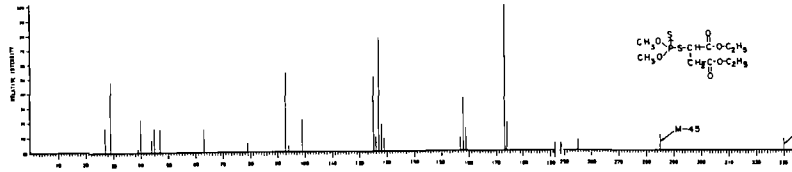

Fig 2 Malathion

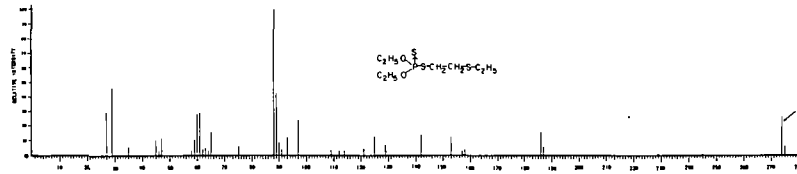

Fig 3 Di-Syston

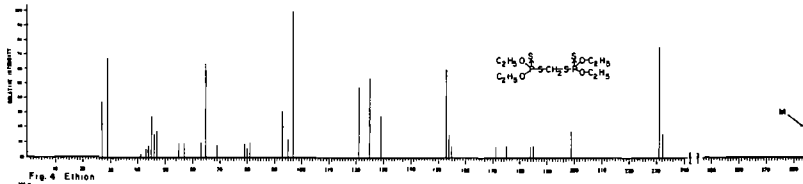

Fig. 4 Ethion

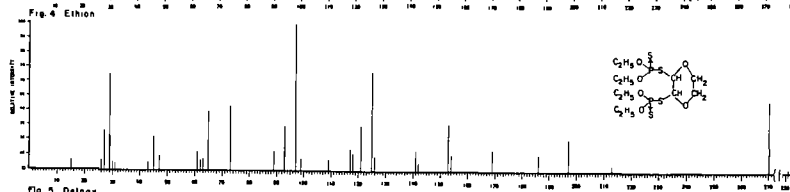

Fig 5 Delnav

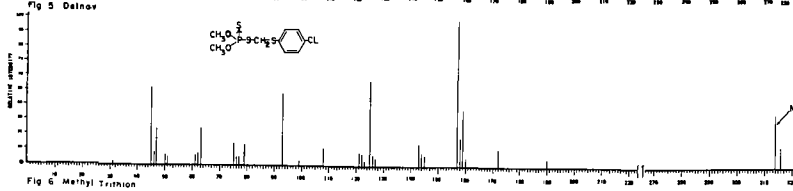

Fig 6 Methyl Trithion

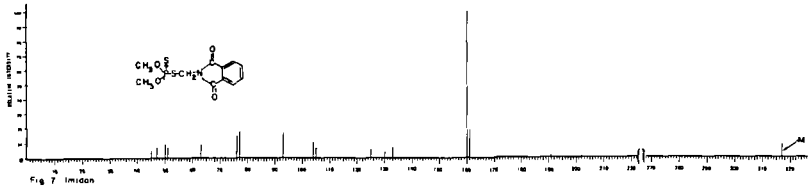

Fig 7 Imidan

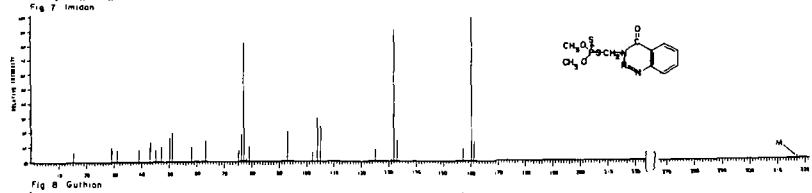

Fig 8 Guthion

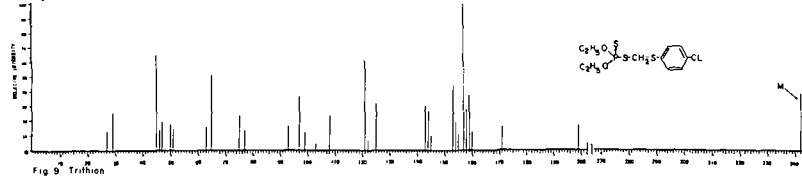

Fig 9 Trithion

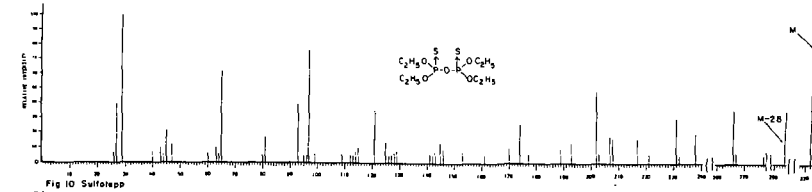

Fig 10 Sulfotepp

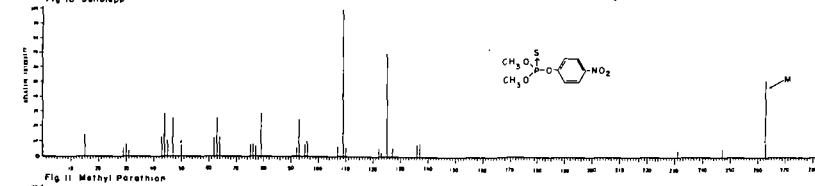

Fig 11 Methyl Parathion

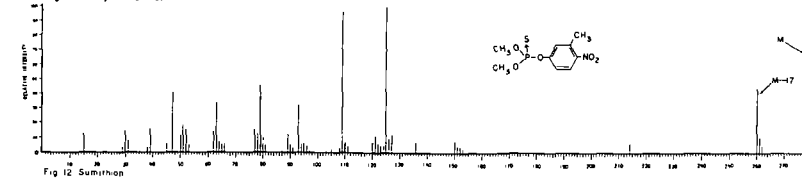

Fig 12 Sumithion

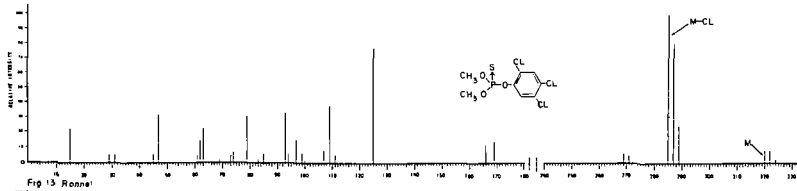

Fig 13 Ronnel

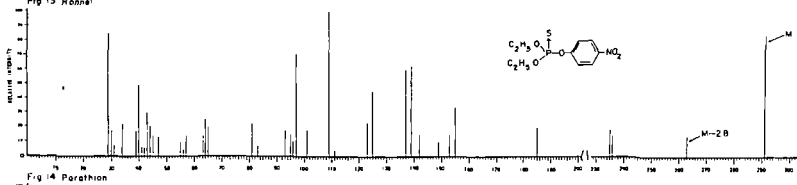

Fig 14 Parathion

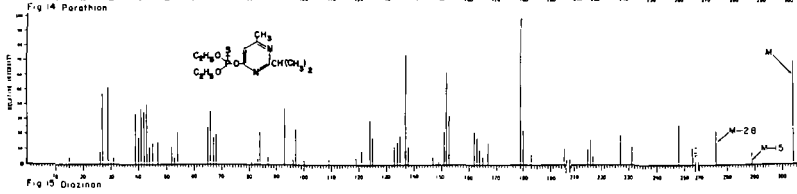

Fig 15 Diazinon

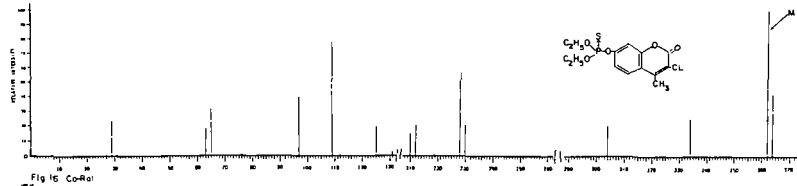

Fig 16 Co-Ral

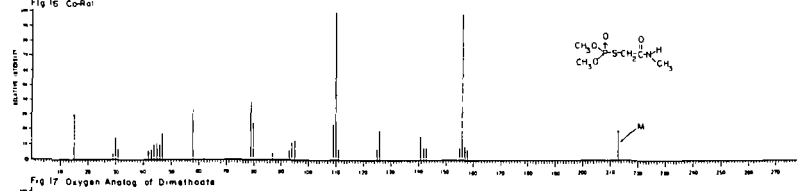

Fig 17 Oxygen Analog of Dimethoate

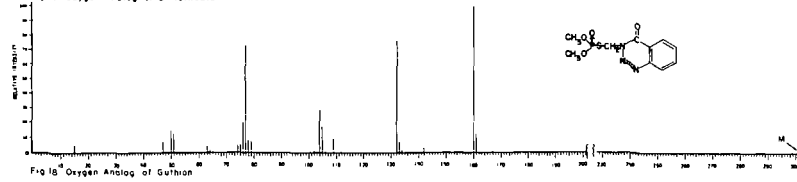

Fig 18 Oxygen Analog of Guthion

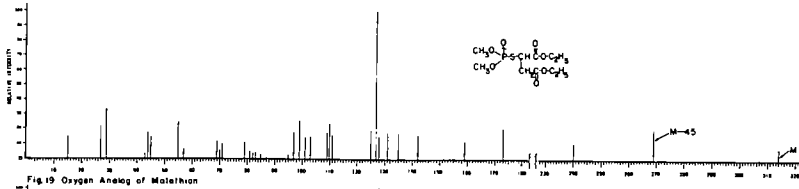

Fig. 19 Oxygen Analog of Malathion

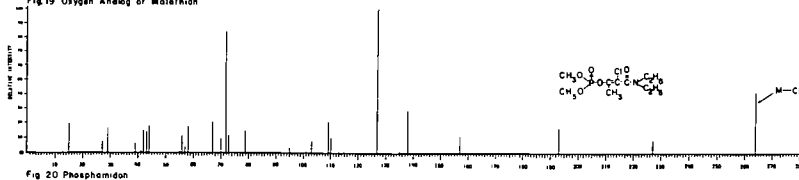

Fig 20 Phosphamidon

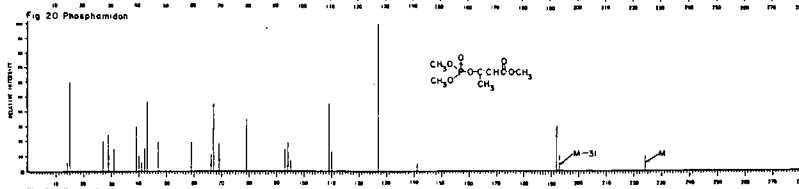

Fig. 21 Phosdrin

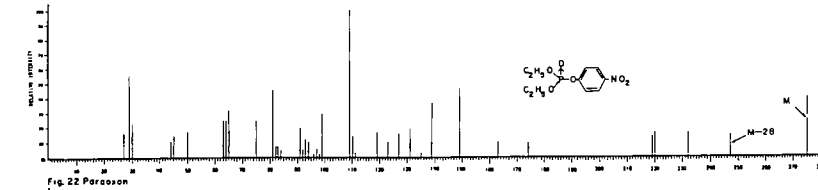

Fig. 22 Paraoxon

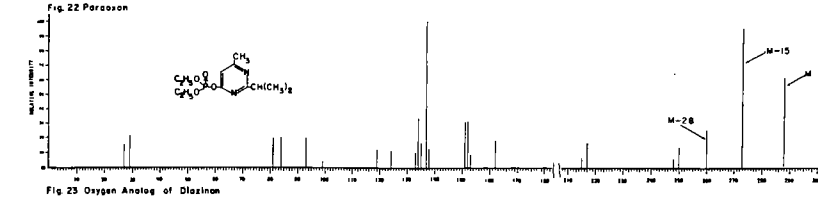

Fig 23 Oxygen Analog of Diazinon

MASS SPECTROMETRY OF BIOSYNTHETICALLY LABELED RICININE[1]

by

George R. Waller[2] and Ragnar Ryhage

Laboratory for Mass Spectrometry, Chemistry Department,
The Karolinska Institutet, Stockholm, Sweden

and

Seymour Meyerson

Research and Development Department, American Oil Company,
Whiting, Indiana

Isotope labeling has been the most fruitful single experimental approach in exploring the chemistry underlying the mass spectra of organic compounds (1,2). Confident knowledge of this chemistry, in turn, is needed if mass spectra are to be used to locate labels within isotopically enriched products resulting from reaction-mechanism studies in other contexts (2). In general, elucidation of paths of molecule-ion decompositions by labeling requires the synthesis of compounds labeled in specific known positions in high isotopic purity. In work with natural products, where these syntheses are often difficult and time-consuming, they often can be replaced by biosyntheses if the pertinent biosynthetic pathways are well enough established. Biosynthetic studies of ricinine--3-cyano-4-methoxy-N-methyl-2-pyridone--have provided labeled species that should allow the certain identification of mass-spectral fragmentation paths for this molecule. Once these paths are known, mass spectrometry can then be used to extend biosynthetic studies of ricinine to other precursors, the analysis now being used to locate the labeled precursor atoms in the ricinine structure.

Considerable knowledge about the biosynthesis of ricinine in Ricinus communis L. has become available in recent years (3-8). Figure 1 shows the positions of isotopic labels in the alkaloid formed from certain precursors labeled in specified positions: (a) ^{15}N in the amide group of nicotinamide appears solely in the nitrile group of the derived ricinine (5); (b) a tagged carbon atom in formate is distributed between the O- and N-methyl groups of ricinine (4,5); and (c) a tagged carbon atom in the 2-position of acetate ends up chiefly as carbons 2 and 3 of ricinine, with no contribution to carbons 4, 5, and 6 (3-7). The nitrile group of ricinine is derived from the carboxamide group of nicotinamide, presumably through an intramolecular dehydration, and the pyridine ring of nicotinamide becomes the pyridine ring of ricinine (5).

The chemical degradation procedure conventionally used to determine the positions of such labels (3,4,7) is time-consuming and requires at least 200 mg. of the alkaloid. This quantity is almost impossible to obtain from in vitro biosyntheses, and large amounts of expensive labeled precursors are required for in vivo experiments. Thus, substantial incentive exists for the use of mass spectrometry for isotopic analysis in such studies, provided the requisite sensitivity and accuracy can be attained. In earlier studies employing a nitrogen-15 label (5,6), enrichment was estimated directly from measured peak heights in conventionally recorded spectra. The best accuracy generally attainable by this procedure, ± 0.1%, is useful only when the samples contain at least 0.3% of labeled species. A technique was therefore needed that would allow accurate and reproducible measurements to be made at enrichment levels below 0.3%. With this end in view we employed a conventional analytical instrument equipped with a dual collector system (9), essentially similar to experimental arrangements that have been in use for many years for isotope-ratio measurements in simpler molecules (10-13). Measurements on the ricinine parent ion and on the abundant fragment ion of mass 82 are sufficiently reproducible and, apparently, accurate.

Such measurements on ricinine samples biosynthetically labeled in various positions established what parts of the ricinine molecule are retained in the fragment ion. This knowledge in turn was used to determine the position of incorporation in ricinine of nitrogen administered as formamide-^{15}N. Independent confirmation was obtained by chemically degrading the labeled ricinine to 4-methoxy-N-methyl-2-pyridone and measuring label retention in this product.

EXPERIMENTAL

Mass Spectrometry

Conventional mass spectra were measured with 70-volt electrons on a modified (14) Consolidated model 21-103 instrument with the inlet system at 250°[3] and on an Atlas model CH4 instrument with the inlet system at 225°. Isotopic analyses of labeled samples were obtained in the usual way from spectra measured at ionizing voltages low enough to eliminate interfering fragment ions in the parent-ion region (15). As an alternative procedure, especially at low enrichments, direct intensity-ratio measurements were made with 70-volt electrons on the Atlas spectrometer, which was equipped with dual collectors and associated electronics[4] for precise measurement of small spectral differences between samples differing only slightly in composition (9). Specifically, the instrument measures the ratio r of ion current at mass m + 1 to the sum of ion currents at masses m and m + 2. For example, if m = 164, the mass of the parent ion of unlabeled ricinine, and r_1 and r_0 are the corresponding ion-current ratios measured on slightly enriched--with D, ^{15}N or ^{13}C--and unlabeled samples, respectively, % enrichment is given to a close approximation by the product of $100(r_1 - r_0)/r_0$ and the (m + 1):m intensity ratio in the conventionally measured spectrum of the unlabeled species. Direct intensity-ratio measurements were found empirically to vary with sample pressure in the ionization chamber; all such measurements were therefore made at the same sample pressure, as indicated by an arbitrarily selected value of total ion current. Samples varying from 0.25 to 2.5 mg could be used satisfactorily.

Preparation of Labeled Ricinine Samples

Ricinine biosynthesis experiments used young *Ricinus communis* L. plants grown at the Stillwater, Oklahoma Agronomy Farm. A labeled precursor was injected into one of the hollow internodular spaces, and after the lapse of the appropriate time the alkaloid was isolated and purified. A complete description of this procedure has been published (7,8). Labeled presursors used were nicotinamide-^{15}N(amide N), available from previously reported work (5); formate-^{13}C and acetate-2-^{13}C, purchased from Merck, Sharp and Dohme, Montreal, Canada; and formamide-^{15}N, prepared as follows from $^{15}NH_4NO_3$ purchased from Distillation Products Industries, Rochester, New York.

Twenty-five millimoles of $^{15}NH_4NO_3$ was added to a 60% solution of KOH at -78°C. The solution was warmed and the liberated $^{15}NH_3$ was swept by a small stream of N_2 gas through 38 millimoles of methyl formate cooled to -78°C. The system was flushed with N_2 for an additional hour. The vessel containing the methyl formate and liquid $^{15}NH_3$ was sealed under vacuum, and then allowed to warm gradually to 45° and held there for 1.5 hours. The tube was opened and the unreacted methyl formate and $^{15}NH_3$ were immediately removed by a water aspirator. The formamide contained 21.0% ^{15}N excess, as measured by mass spectrometry at reduced ionizing voltage (15).

Chemical Degradation of Ricinine to 4-methoxy-N-methyl-2-pyridone

The cyano group was removed from ricinine by a modification of Winterstein's procedure (16). Ricinine was refluxed with 57.4% H_2SO_4 for two hours and neutralized with NaOH. The solution was extracted repeatedly with chloroform, the chloroform extract was evaporated to dryness, and the 4-methoxy-N-methyl-2-pyridone was purified by repeated sublimation. Yield was 60-75%. The melting point (corrected), 112-114°, agrees with the published value (16).

RESULTS AND DISCUSSION

The mass spectrum of ricinine, measured on the Atlas spectrometer, is shown in Figure 2. It is qualitatively similar to that obtained on the Consolidated instrument; differences are about what might be expected from spectrometers of different design (17). Metastable peaks and the transitions denoted by them are listed in Table 1; all those shown are clearly indicated in the spectra measured on both instruments. Decomposition reactions that can account for at least some of the prominent features could have been predicted from experience with simpler molecules containing the same functional groups: primary loss of CH_2O and the competing sequential loss of CH_3 and CO from methoxyarenes[5] (18-21); and primary loss of CO from pyridones (22-24). The metastable peaks at 135.4 and 45.1 define an origin of the ion of mass 82--the second most abundant fragment-ion in the spectrum--as the sequential loss from the parent ion of a CH_3 radical and a neutral particle of mass 67. A precise mass measurement on a high-resolution mass spectrometer[6] advanced the characterization of this process one step further by establishing the empirical formula of the ion as $C_4H_4NO^+$ and, by difference, that of the second neutral product as C_3HNO.

The "natural abundance" correction factors for ricinine and 4-methoxy-N-methyl-2-pyridone, needed to calculate enrichment from the spectra of labeled materials, were calculated from low-voltage measurements on an unlabeled control sample of ricinine isolated from castor plants and from the decyano product derived from it. The isotopic distributions so found, as shown in Table 2, differ slightly from those given by Beynon (25). Whether the discrepancies are instrumental in origin or are caused by isotope effects in the biosynthesis (26) is not known.

Table 3 shows comparative values of isotopic enrichment of six different biologically synthesized samples of ricinine, measured by the conventional low-voltage technique and by ratio recording. Especially for enrichments greater than 0.3%, the two methods agree closely. Such agreement, coupled with the high precision of ratio recording, supports the view that the accuracy of the latter technique is of the order of 0.01 to 0.02%, about equal to the precision and to the limit of detection. Similar measurements on the $C_4H_4NO^+$ ion--mass 82 when unlabeled--are also reproducible, and presumably accurate, to about ± 0.01%.

Table 4 shows enrichments, measured by direct ratio recording, in the parent and $C_4H_4NO^+$ ions of ricinine samples prepared biosynthetically from nicotinamide-^{15}N, formate-^{13}C, and acetate-2-^{13}C. None of the label from the nicotinamide or acetate, but about half that from the formate, is retained in the fragment ion. The ion thus comprises carbon atoms 4, 5, 6, and either 7 or 9 (See Figure 1 for the numbering), nitrogen atom 1, and presumably the methoxyl oxygen. One hydrogen atom from C-5, C-6, or, more likely, the remaining methyl group, has migrated to the portion of the molecule that is lost as the neutral product. The results can be represented mechanistically as:

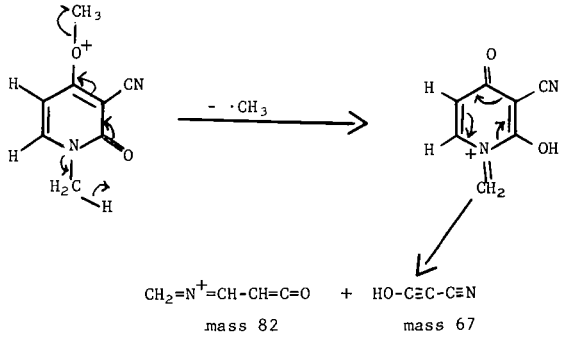

The formate-^{13}C data suggest that the formate carbon atom is distributed about equally between the two methyl groups of the resultant ricinine. This finding agrees with results of experiments using formate-^{14}C as the precursor.[7]

Table 5 shows the corresponding enrichments in ricinine formed biosynthetically from formamide-^{15}N and in the derived 4-methoxy-N-methyl-2-pyridone. Samples 1 and 2 correspond to elapsed times of 12 and 24 hours, respectively, after administration of the precursor. The essentially equal label retentions in the ricinine fragment ion and the chemical degradation product confirm the finding that the nitrogen atom in the $C_4H_4NO^+$ ion comes solely from the ring. Further, the data show ^{15}N incorporation only in position 10 in 12 hours, but in positions 10 and 1 in proportions of about 3:1 in 24 hours.

An extension of the present work has shown that nitrogen from aspartate-^{15}N becomes the ring nitrogen of ricinine (7), as pictured in Figure 1. Thus, the mass-spectral techniques described here, in combination with findings from ^{14}C-labeling studies, have demonstrated for the first time the key role of aspartic acid in the biosynthesis of pyridine compounds by plants.

SUMMARY

The high sensitivity and precision made possible by modern instrumentation enables mass spectrometry to be used effectively even at the low isotopic enrichment levels readily attainable in studies of biosynthesis. A particular virtue of mass spectrometry for studies of reaction paths in biosynthesis, as elsewhere, is the ability to locate a label within a molecule without prior wet-chemical degradation. However, the extraction of such information is contingent on prior knowledge of ionization-dissociation mechanisms induced by electron impact. Preparation of the specifically labeled compounds

needed to define these mechanisms may be greatly simplified by employing biosynthesis if the pertinent biosynthetic pathways are well enough established. Thus, findings from studies of ricinine from labeled nicotinamide, formate, and acetate furnished the necessary basis for mass-spectral interpretation to permit use of label-retention measurements on an appropriate fragment ion to determine the position in the ricinine molecule of nitrogen administered as formamide-^{15}N. Ricinine isolated 12 hours after injection of the formamide contained the label only in the ring. After 24 hours, the label was found in both the ring and the nitrile group in proportions of about 3:1.

ACKNOWLEDGEMENTS

One of us (G.R.W.) is indebted to Oklahoma State University, Stillwater, Oklahoma, for granting him a leave of absence and to the National Institutes of Health, Bethesda, Maryland, for a fellowship. The authors express their appreciation to Sten Wikstrom, Rolf Hjälm, and Sune Melkersson for technical assistance.

FOOTNOTES

1 Supported in part by Research Grant GM-08624 from the National Institutes of Health, Bethesda, Maryland.

2 Present Address: Department of Biochemistry, Oklahoma State University, Stillwater, Oklahoma.

3 At 250°, nicotinamide underwent thermal dehydration--possibly catalyzed by inadvertently exposed metal surfaces--to the nitrile, paralleling exactly the behavior of benzamide reported recently by Cotter, J. L., J. Chem. Soc. (London), 5742 (1965). The difficulty was avoided by reducing the inlet temperature to 140° for all measurements on nicotinamide, which was introduced into the spectrometer in the form of a water solution.

4 The instrument was equipped with the dual collector S, measuring bridge 4, and a device for measuring total ion current, all available as optional equipment from the manufacturer of the spectrometer. Total ion current is measured on a slit that intercepts about 10% of the ion beam in the field-free region preceding the analyzer.

5 The two-step decomposition sequence also occurs thermally. See Harrison, A. G., Honnen, L. R., Dauben, H. M., and Lossing, F. P., J. Am. Chem. Soc. 82, 5593 (1960); and Pottie, R. F., and Lossing, F. P., J. Am. Chem. Soc. 85, 269 (1963).

6 We are indebted to Dr. K. Habfast, of Atlas-Werke, Abt. Mess- und Analysentechnik, Bremen, West Germany, for this measurement, which was made on an Atlas SM-1 instrument.

7 Biosynthesis experiments using formate-^{14}C as a precursor of ricinine were conducted simultaneously with those reported here. The OCH_3 and NCH_3 groups, respectively, were found to contain 51 and 48% of the activity. The demethylations were carried out according to the method of Dubeck, M., and Kirkwood, S., J. Biol. Chem. 199, 307 (1952).

REFERENCES

1. Ryhage, R., and Stenhagen, E., in "Mass Spectrometry of Organic Ions" (F. W. McLafferty, ed.), p. 399. Academic Press Inc., New York, New York, 1963.

2. Grubb, H. M., and Meyerson, S., ibid., p. 453.

3. Juby, P. F., and Marion, L., Can. J. Chem. 41, 117 (1963).

4. Scheidt, U., and Boeckh, G., Z. Physiol. Chem. 330, 58 (1962).

5. Waller, G. R., and Henderson, L. M., J. Biol. Chem. 236, 1186 (1961).

6. Waller, G. R., and Henderson, L. M., 140th Meeting of Amer. Chem. Soc., Chicago,

Illinois, September, 1961, Abstracts, p. 30q.

7. Yang, K. S., and Waller, G. R., Phytochem. 4, 881 (1965).

8. Waller, G. R., and Henderson, L. M., Biochem. Biophys. Res. Comm. 5, 5 (1961); 6, 398 (1961).

9. Habfast, K., Zeitschrift für Instr. 68, 82 (1960).

10. Straus, H. A., Phys. Rev. 59, 430 (1941).

11. Wanless, R. K., and Thode, H. G., J. Sci. Instr. 30, 395 (1953).

12. Nier, A. O., Ney, E. P., and Inghram, M. G., Rev. Sci. Instr. 18, 294 (1947).

13. Nier, A. O., Rev. Sci. Instr. 18, 398 (1947).

14. Grubb, H. M., Ehrhardt, C. H., Vander Haar, R. W., and Moeller, W. H., 7th Meeting of Am. Soc. Testing Materials Committee E-14 on Mass Spectrometry, Los Angeles, California, May, 1959.

15. Stevenson, D. P., and Wagner, C. D., J. Am. Chem. Soc. 72, 5612 (1950).

16. Winterstein, E., Keller, J., and Weinhagen, A. B., Arch. Pharm. 255, 513 (1917).

17. Caldecourt, V. J., Appl. Spectroscopy 12, 167 (1958).

18. Barnes, C. S., and Occolowitz, J. L., Austral. J. Chem. 16, 219 (1963).

19. Pelah, Z., Wilson, J. M., Ohashi, M., Budzikiewicz, H., and Djerassi, C., Tetrahedron 19, 2233 (1963).

20. Biemann, K., "Mass Spectrometry. Organic Chemical Applications," p. 140, McGraw-Hill Book Company, Inc., New York, New York, 1962.

21. Meyerson, S., Drews, H., and Fields, E. K., Anal. Chem. 36, 1294 (1964).

22. Spiteller, G., and Spiteller-Friedmann, M., Monatsh. 93, 1395 (1962).

23. Rice, J. M., Dudek, G. O., and Barber, M., J. Am. Chem. Soc. 87, 4569 (1965).

24. Clugston, D. M., and MacLean, D. B., Can. J. Chem. 44, 781 (1966).

25. Beynon, J. H., and Williams, A. E., "Mass and Abundance Tables for Use in Mass Spectrometry." Elsevier Publishing Company, Amsterdam, 1963.

26. Bowen, H. J. M., J. Appl. Radiation Isotopes 7, 261 (1960).

Table 1

METASTABLE PEAKS IN MASS SPECTRUM OF RICININE

Apparent Mass	Transition Denoted	Probable Neutral Product
162.0	$(164^+) \rightarrow (163^+) + 1$	H
135.4	$(164^+) \rightarrow (149^+) + 15$	CH_3
112.8	$(164^+) \rightarrow (136^+) + 28$	CO
109.5	$(164^+) \rightarrow (134^+) + 30$	CH_2O
107.7	$(136^+) \rightarrow (121^+) + 15$	CH_3
104.0	$(106^+) \rightarrow (105^+) + 1$	H
86.5	$(135^+) \rightarrow (108^+) + 27$	HCN
73.0	$(121^+) \rightarrow (94^+) + 27$	HCN
46.3	$(94^+) \rightarrow (66^+) + 28$	CO
45.1	$(149^+) \rightarrow (82^+) + 67$	C_3HNO[a]

[a]See Text.

Table 2

"NATURAL ABUNDANCE" ISOTOPIC CORRECTION FACTORS

Compound	Mass	Relative Abundance Observed[a]	Relative Abundance Literature[b]
Ricinine	164	100.0	100.0
	165	9.34 ± 0.08	9.614
	166	0.83 ± 0.03	0.815
4-Methoxy-N-methyl-2-pyridone	139	100.0	100.0
	140	8.33 ± 0.03	8.168
	141	0.74 ± 0.01	0.693

[a]Averages of three measurements. The uncertainties shown are average deviations.

[b]See Ref. 25.

Table 3

ISOTOPIC ENRICHMENT OF BIOSYNTHETICALLY LABELED RICININE SAMPLES

Sample	From Low-Voltage Spectrum[a]	From Direct Ratio Recording[a]
1	1.23 ± 0.05%	1.20 ± 0.015%
2	0.86 ± 0.01	0.86 ± 0.005
3	0.23 ± 0.03	0.27 ± 0.02
4	0.14 ± 0.01	0.16 ± 0.00
5	0.06 ± 0.00	0.075 ± 0.015
6	0.00 ± 0.00	0.018 ± 0.003

[a]Averages of two or three measurements. The uncertainties shown are average deviations.

Table 4

ENRICHMENTS IN PARENT AND $C_4H_4NO^+$ IONS OF BIOSYNTHETICALLY LABELED RICININES

Precursor	Parent Ion	$C_4H_4NO^+$ Ion
Nicotinamide-^{15}N (Amide N)	0.24%	-0.01%
Formate-^{13}C	0.16	0.09
Acetate-2-^{13}C	0.09	-0.01

Table 5

ENRICHMENTS IN PARENT AND $C_4H_4NO^+$ IONS OF RICININE FORMED FROM FORMAMIDE-^{15}N AND IN THE DERIVED 4-METHOXY-N-METHYL-2-PYRIDONE

Sample	Ricinine Parent Ion From Low-voltage Spectrum	Ricinine Parent Ion From Direct Ratio Recording	Ricinine $C_4H_4NO^+$ Ion From Direct Ratio Recording	4-Methoxy-N-methyl-2-pyridone From Low-voltage Spectrum
1	0.23%	0.27%	-0.01%	-0.02%
2	0.86	0.86	0.23	0.20

Known Precursors

Figure 1

Labeling Pattern of Ricinine Formed By *Ricinus communis* L. Plants from Isotopically Labeled Precursors

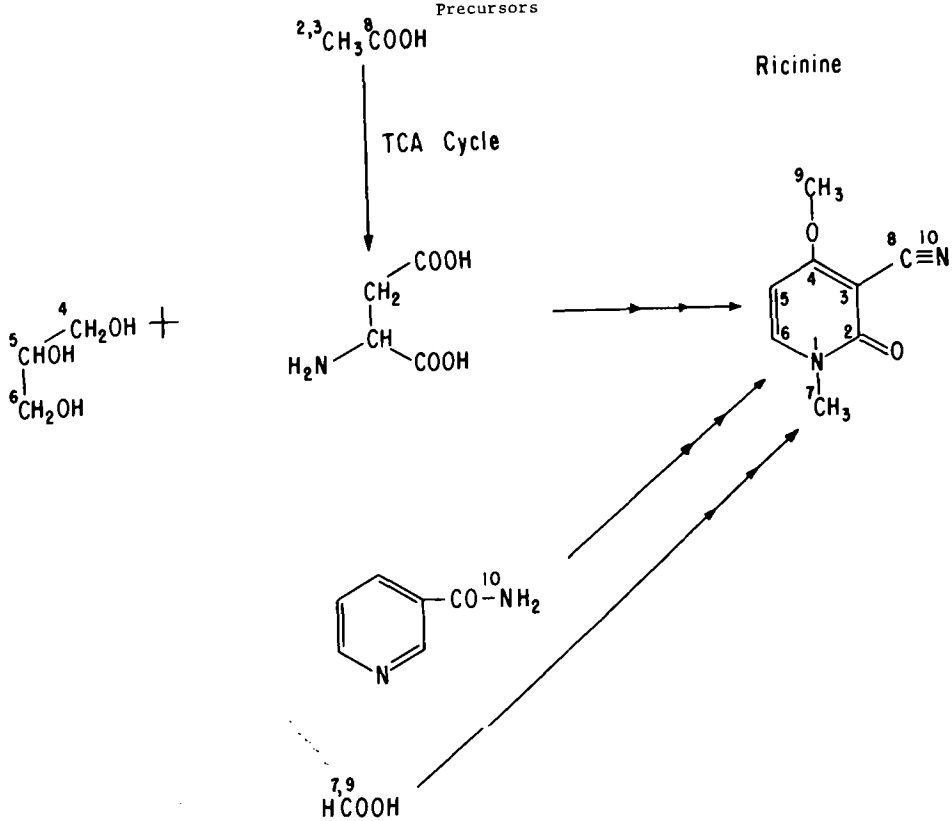

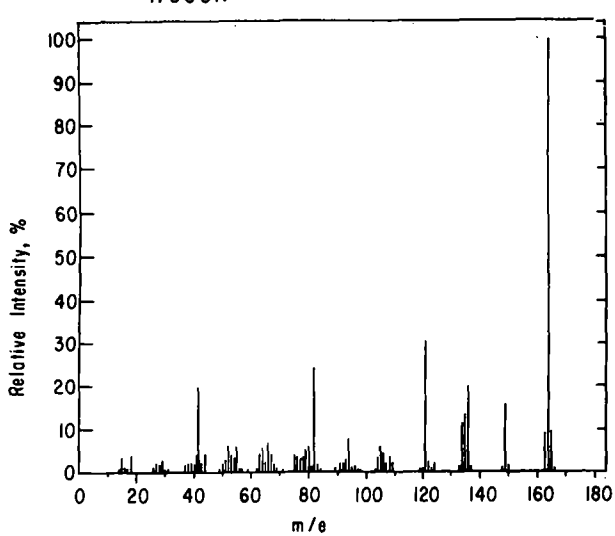

Figure 2

Mass Spectrum of Ricinine

Rearrangement in the Mass Spectrum of Methyl Isobutyrate

D.R. Black, W.H. McFadden, and L.Boggs*
Western Regional Research Laboratory
Albany, California

Abstract

The mass spectra of specifically deuterated isobutyrates have been obtained for further study of rearrangement processes of short chain esters. In the mass spectrum of methyl isobutyrate, ions occur at masses 75, 60, and 61 similar to whate is observed in other ester spectra. However, the data from the deuterated methyl isobutyrates show that the mechanism for formation of these ions differs from the mechanism known for other esters. Under electron impact, methyl isobutyrate forms a cyclic intermediate from which the carbonyl group or a $\bar{C}H\dot{C}H_3$ group can be expelled.

* A laboratory of the Western Utilization Research and Development Division, Agricultural Research Service, U.S. Department of Agriculture.

A MORE EFFICIENT ELECTRON GUN FOR MASS SPECTROMETERS *

G. D. Flesch and H. J. Svec

Institute for Atomic Research and Department of Chemistry
Iowa State University, Ames, Iowa

The control of ionizing electron currents is an important consideration in any mass spectrometer, but it is particularly important for one involved in appearance potential work. This paper describes an electron gun and its characteristics, but makes only minor mention of the electronics involved in the control circuit. The physical arrangement of the electron gun is shown in Fig. 1, where everything except the magnet pole faces is drawn to scale.

Electrons are emitted from the hot filament. They accelerate toward the ion box, pass through it and strike the anode. The gas enters the ion box through the inlet tube and is ionized by the electron beam. The ions are extracted from the electron beam by means of draw-out potentials and leave the ion box in directions perpendicular to the plane of the figure.

The usual filament-ion-box-anode arrangement has been modified by inserting an electrode between the filament and ion box. While we call this electrode a grid, it is actually a metal sheet with a circular hole in the appropriate place. This grid serves several purposes: it shields the ion box from stray electrons, it helps collimate the electron beam, and it can control the space charge about the filament and therefore the number of electrons entering the ion box.

Holes in the various electrodes help collimate the electron beam, but the principle source of collimation is the magnetic field of 112 gauss. The velocities of the accelerated electrons can be separated into components perpendicular and parallel to the lines of force of the magnetic field. The perpendicular components result in a circular motion of the electron in a plane perpendicular to the lines of force, while the parallel components move the electron toward the anode. The result is that the electrons travel in a helical path between the filament and anode.

All of the electrons which get past the grid result in either ion box or anode current. Since these are the electrons which are capable of producing ions which can be extracted through the ion collimation system, the sum of the ion box and anode currents is called total ionizing current, or TIC current.

The electrical schematic of the electron gun is shown in Fig. 2. The potentials involved are as follows: the filament potential is taken as the reference, zero volts; the grid potential is variable, -10 to +10 volts; the ion box potential is variable, 0 to +85 volts; and the anode potential is 75 volts more positive than the ion box potential. Only the anode current passes through the anode sensor while both the ion box and anode currents pass through the TIC sensor in the current path back to the filament. The grid current returns directly to the filament.

The number of electrons passing through the ion box can be controlled in several ways. In manual control, either the anode or the TIC current is regulated by the operator, who varies the heater current, the grid potential or both.

There are three modes of automatic emission control, which are called anode regulation, TIC regulation and grid regulation. In anode regulation the regulator compares the anode sensor voltage with a predetermined "reference" voltage. The difference of these voltages, the "error voltage", is amplified and applied to the filament current supply

* Work was performed in the Ames Laboratory of the U. S. Atomic Energy Commission

in such a way that the current through the filament changes. This results in a change of filament temperature and a change in the emission until the error voltage becomes a minimum. In TIC regulation the TIC sensor voltage is compared with a reference voltage, and the amplified error voltage is again applied to the filament current supply to correct the emission. In grid regulation the TIC sensor voltage is compared with a reference voltage, but the emission is corrected by applying the amplified error signal to the grid.

The emission regulation was tested in all modes of control. In the initial testing it was observed that the anode-to-TIC current ratio was not constant as the electron energy was varied from 0 - 85 volts. To observe this more readily, an X-Y recorder was used to plot the TIC and anode currents as a function of electron energy for each of the automatic modes of control. Fig. 3 shows the curves for an anode current regulation of about 15 microamperes. The range of energies was 10-85 eV and the grid potential was 0 volts. The abscissa is the ion box voltage, which is the nominal energy of the electrons as they traverse the ion box.

Peaks and valleys are apparent where the TIC current rises and falls as the regulator maintains a constant anode current. The difference between the two curves is the ion box current. Fig. 4 shows the result for TIC regulation of about 20 microamperes. Here the anode current rises and falls with changes in the ability of the electron to pass through the ion box. Fig. 5 shows the curves for grid regulation of about 50 microamperes TIC current. As expected, these curves are similar to those of the previous figure.

Fig. 6 shows the curves for a constant filament current of 4.2 amps. In this case, the energy range is 0-50 volts and the grid potential is 1.5 volts. The slide emphasizes the reproducibility of the peaks, the valleys, and a discontinuity. The various curves were obtained by changing the y-axis zero between each electron energy scan. Neither of the currents is constant since there is no regulation of the electron emission, which is apparently space charge limited.

The discontinuity at three volts is probably due to the electrostatic fringe field of the ion box suddenly dominating the potentials around the filament. These fringe fields provide gradients which accelerate the electrons more directly toward the anode. This view is supported by the observation that when the electron energy scans are repeated at varying grid potentials, the discontinuity always occurs at an ion box potential equal to twice that of the grid.

An attempt to explain the various peaks and valleys observed involves the electrons' helical paths across the ion box. Fig. 7 shows several drawings of an end view of the ion box, looking toward the anode. The circle represents the entrance hole of the ion box, the dot is the position of the electron as it passes through the entrance, and the arrow is the projection of the electron's position as it traverses the ion box. The upper left hand drawing illustrates that when the electron makes one complete revolution of its helical path as it crosses the ion box, it is refocussed on the exit hole. If the electron completes a half revolution going across the ion box, it is in least focus on the exit hole. Thus if the length of the ion box is n times the pitch of the helix, where n is an integer, the electrons which enter the ion box are refocussed on the ion box exit hole. If the ion box length is (n + 1/2) times the pitch, the electrons are in least focus and more strike the ion box. Since the pitch of the helix depends upon the electron's velocity vector which is parallel to the magnetic field, the fraction of the TIC current which is observed as anode current should be energy dependent. Thus anode current should maximize at whole-number revolutions of the helix and minimize at half revolutions. The curves shown in Fig. 8 exhibit many relative maxima and minima, and each maximum of the anode curve is matched with a minimum of the ion box curve and vice versa.

The location of the maxima and minima were determined using the constant filament current mode of operation of the regulator and zero grid potential. In measuring the maxima and minima it was assumed that if the electrons did not follow a helical path across the ion box,

all the current curves would be smooth. Thus the observed ion box and anode current curves are actually the summation of a smoothly changing current and an oscillating "delta" current. Since the delta current is relatively larger and more observable on the ion box current curve, all measurements of the maxima and minima voltages were made using ion box current curves.

The method is shown in Fig. 9. A smooth curve was drawn through the observed data such that the magnitude of the delta current had an oscillating value of increasing amplitude as the electron energy increased. Maxima and minima are said to occur at those energies where the slopes of the two curves are equal. The ion box current was plotted using several different parameters and the maxima and minima measured in the same manner. The observed values were averaged for comparison with calculated values.

Calculations of the maxima and minima were made on the basis of the measured magnetic field and the distance the electron travels while passing through the ion box. Comparison of the calculated and observed maxima and minima are shown in Table 1. The listed uncertainty is the

Table 1. Electron Energy for Maxima and Minima

n	Calc'd EAV	Observed EAV
1 1/2	61. 3 V	57.2 ± 1.1 V
2	34.5	37.9 ± 1.8
2 1/2	22.1	22.2 ± 0.6
3	15.3	15.5 ± 0.4
3 1/2	11.2	11.2 ± 0.2
4	8.6	8.1 ± 0.2
4 1/2	6.8	6.3 ± 0.2
5	5.5	4.8 ± 0.2
5 1/2	4.5	3.7 ± 0.2
6	3.8	2.9 ± 0.1

standard deviation calculated from at least seven observed values. The agreement is excellent. The discrepancies for large values of n can be explained on the basis that filament and anode fringe fields affect the energies of the electrons. For instance, the anode fringe field accelerates an electron to some degree while the electron is still in the ion box. This increases the energy of the electron, and the observed value of energy is apparently too low. The relative error is largest at low electron energies.

This is an interesting observation, but how does it affect appearance potential measurements? Because of the varying anode-to-TIC current ratio, it would appear that the choice of regulation mode might well have a bearing on the shapes of ionization efficiency curves. Indeed, this is observed and is illustrated in Fig. 10. On the left is an ionization efficiency curve obtained from data taken while in the anode regulation mode. The data were normalized by dividing the ion current observed at each electron energy by the ion current observed for 30 volt electrons. There are two linear portions which intersect at 19 volts. This might be interpreted as the onset of a higher energy process, but this conclusion is open to question, particularly when a plot of data taken with TIC regulation (curve 2) exhibits no such break. (For the purpose of clarity the second curve is displaced two volts to the right and the third 4 volts.) The only change in conditions between the taking of data for the two curves was to change the mode of emission regulation. Hence the presence of the break, (curve 1), or the absence of it, (curve 2), must be instrumental. Since the only difference between the two emission control modes is that the anode regulation mode ignores the electron current which strikes the ion box, it was decided to correct the anode regulation data on the assumption that ion box electrons are equally as efficient as anode electrons in producing ionization. A plot of the corrected data results in curve 3. The similarity of the second and third curves is too striking to be coincidental.

These curves are cited as evidence that the sum of the ion box and anode currents in an electron gun is truly a measure of the number of electrons capable of ionizing the sample gas, and that the choice of

regulation mode affects the shape of ionization efficiency curves. In particular, the intersection of the two straight line portions of the anode regulation curve at 19 volts agrees with the observed anode current minimum for n = 2 1/2. That the curve has two linear portions may be fortuitous, but it does illustrate the need to consider the mode of control of the emission regulator.

The data illustrated here may not be applicable to all sector mass spectrometers. In fact it may not be applicable under all conditions even for this mass spectrometer. For instance, at very low electron currents, 2-5 microamperes, the two modes of regulation appear to give identical ionization efficiency curves, but this may be a problem of recording sensitivity since our detection limit is 5×10^{-15} amperes.

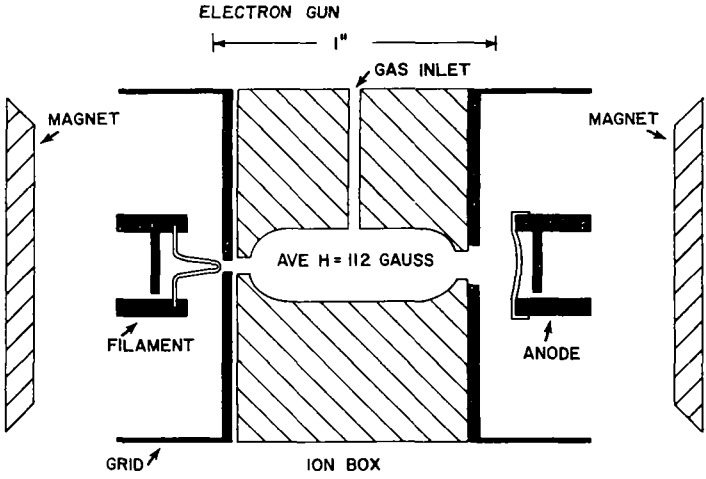

Figure 1

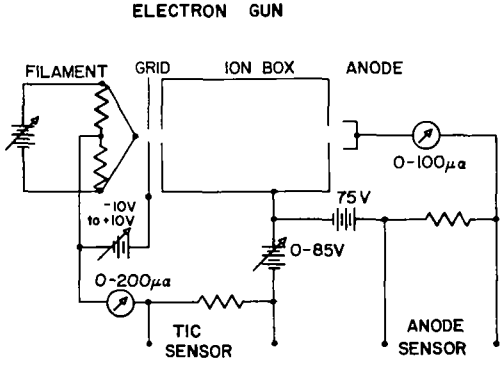

Figure 2

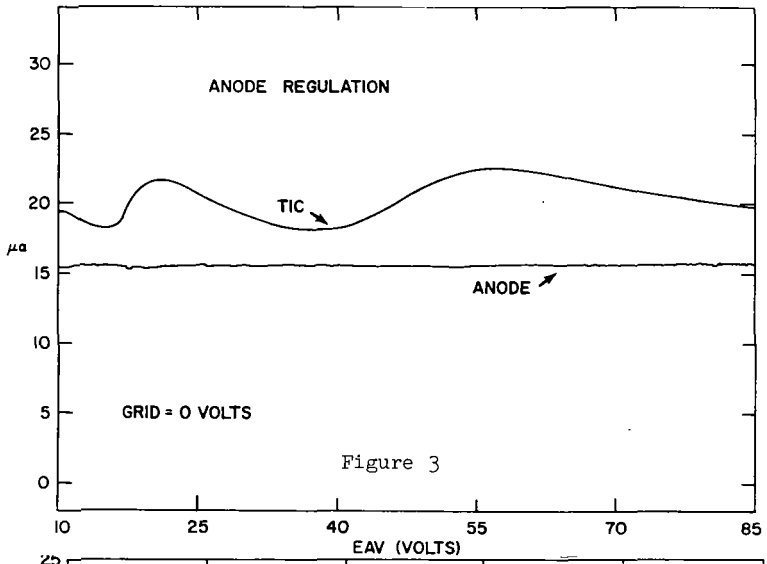

Figure 3

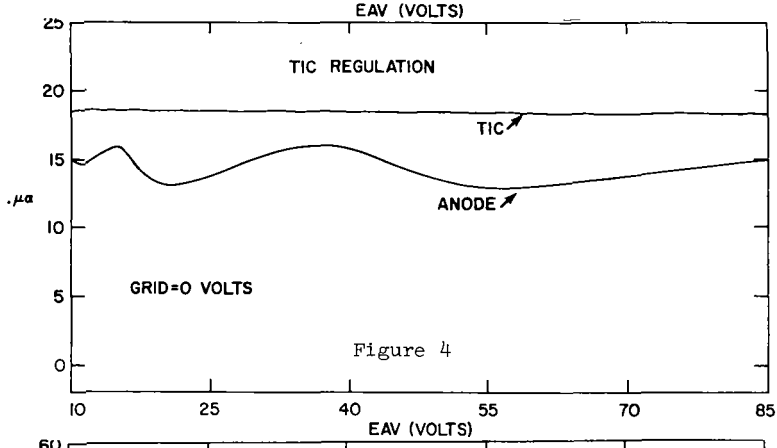

Figure 4

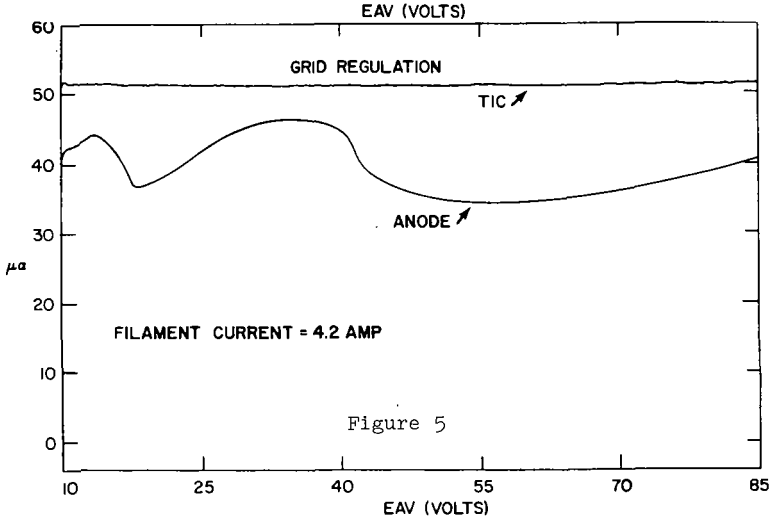

Figure 5

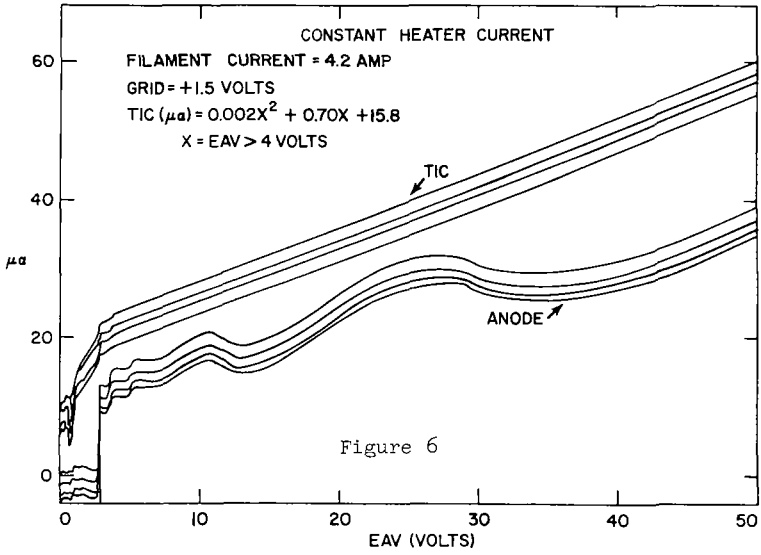

Figure 6

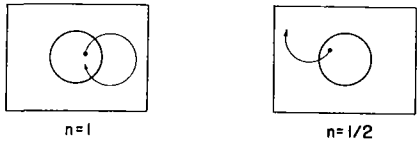

Ion box entrance and projections of electron path

Figure 7

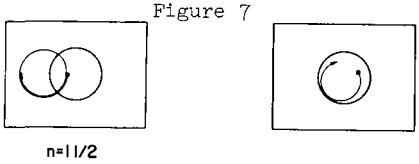

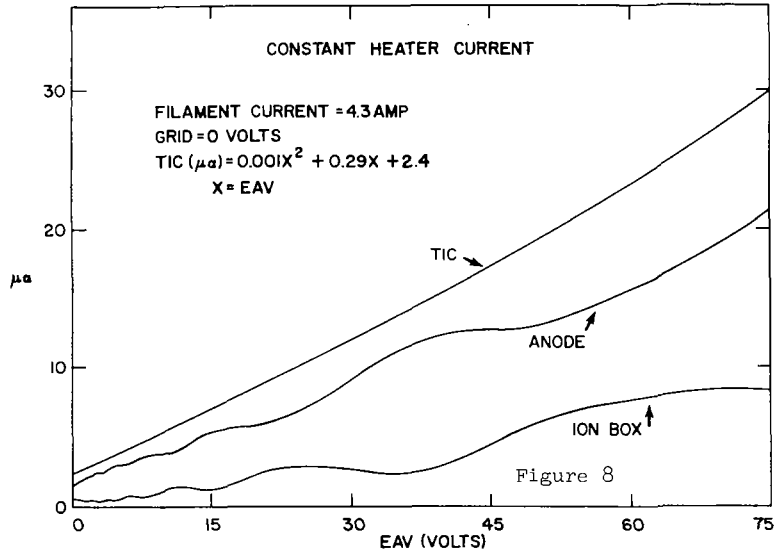

Figure 8

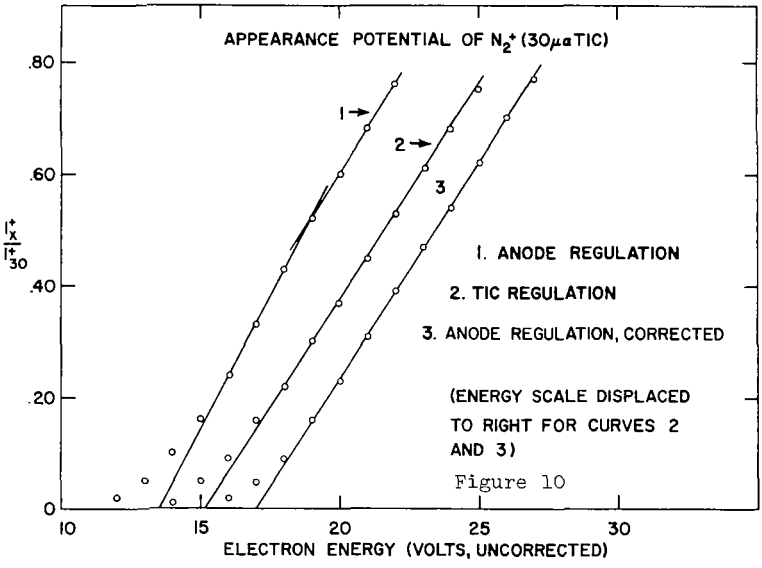

Figure 10

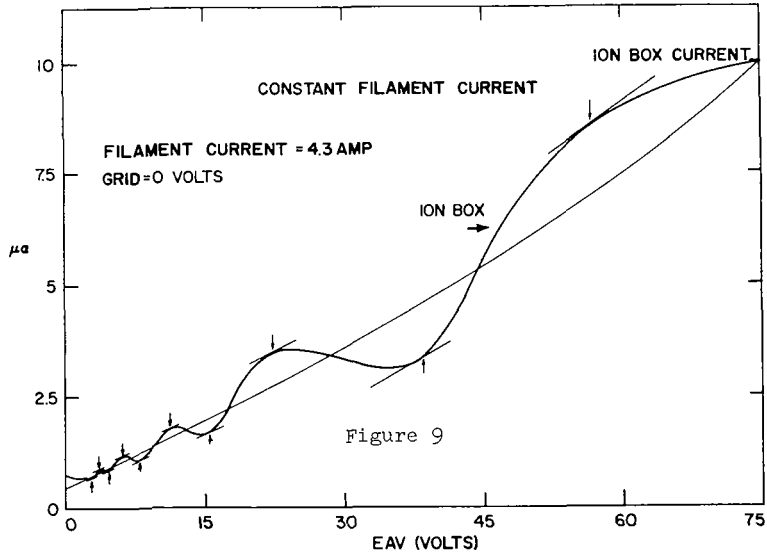

Figure 9

SOME CHARACTERISTICS OF ELECTRON-IMPACT ION SOURCES

by R. Clampitt*
Department of Physical Chemistry
The University, Bristol, England

INTRODUCTION

Many workers are using conventional ion sources of the Nier type for studies on lifetimes of metastable ions, ion-molecule reactions, the variation of ion yield with electron energy and appearance potentials. A brief discussion is given here of some instrumental effects pertaining to such sources and of one effect which is applicable to ion sources of the Fox design.

In ion sources of the Nier and Fox design, the electron beam is confined by the application of a magnetic field. It is well-known that most of the electrons describe helical paths and that the pitch of the helix, for an electron of kinetic energy eV, is given by the equation:

$$Z_0 = 2\pi\left(\frac{2mc^2}{e}\right)^{1/2} \frac{V^{1/2}\cos\theta}{H}$$

where θ is the launching angle with respect to the axis and H is the magnetic field strength. When θ and the initial kinetic energy are small most electrons will be refocussed at Z_0 and at subsequent integral values of this. Consequently there will be discrete values of electron accelerating potential for which a focus point coincides with an electron-beam defining slit. For these values the probability is high that the electrons will pass relatively cleanly through the slit. For non-integral values of Z the probability of a clean passage is low and considerable scattering may occur at the slit edges. The scattered electrons will not necessarily reach the electron trap and so there may be no indication that the effective ionising current is changing with electron accelerating potential. [1]

FIGURE 1 shows the scattered current collected at the ion repeller of the A. E. I. M. S. -2 ion source as a function of V. The spacing between peaks is proportional to $V^{1/2}$; the dependence on magnetic field strength is also evident. Numbers over the trough correspond to the estimated number of revolutions described between the filament and slit. Measurements were also made on a Consolidated Electrodynamics 180° mass spectrometer; similar characteristics were observed although the peaks and troughs of current were not so pronounced.

FIGURE 2 shows ionisation efficiency curves for the molecular ion of n-butane obtained with the A. E. I. machine and one reported many years ago by McDowell and Warren[2] for the methylene ion of methane. It is suggested that electron scattering is responsible for the sigmoidal character of these curves; these are probably the most extreme examples of such an effect. Also shown, from the recent literature, [10] is a curve obtained by the R. P. D. method; the shape of this curve might be interpreted in terms of two auto-ionising states but it is more likely that electron scattering has been neglected.

If, instead of varying only V during an appearance potential measurement, H was also varied so as to maintain the ratio $V^{1/2}/H$ at a value corresponding to, say, a minimum of scattered current, then the effective ionising current should remain reasonably constant during the measurement. However, further consideration would then have to be given to the variation of ion collection-efficiency with magnetic field strength. Better still, slits could be replaced by meshes of high transparency.

SPACE CHARGE

It would appear from the literature that little attention has been given by experimenters to the effects of electron energy, and the electron and positive-ion densities on the potential distribution in the source.

---

*Present address: Lawrence Radiation Laboratory, University of California, Berkeley, California, U. S. A.

The equations describing the potential distribution in diodes were derived many years ago by Langmuir[3] and others. More recently Brubaker[4] has applied these equations to the conditions prevailing in a mass spectrometer ion source.

FIGURE 3 shows the ion source of the A. E. I. M. S. -2. It has been found that this source can be operated in a manner that permits studies on space charge. Plate R is a beam-defining plate; this can be used to retard ions emerging from the source.[11] The retarding-potential of a thermal ion which reflects the potential at which it was formed may be studied as a function of electron energy, electron density and ion density. Penetration of the repeller and ion extraction fields can also be measured but these will not be discussed here. FIGURE 4 shows the results of measurements on the potential of the electron beam as a function of electron current for various gas pressures. At high electron currents, gas pressure (or rather ion density) affects significantly the potential of the beam. Similarly a change in electron energy will change the ion density and hence the potential of the electron beam with respect to the chamber walls. It is obvious that at high electron currents a measure of the change in applied electron accelerating potential will not be a measure of the effective change in beam potential, partly because the positive-ion density also changes. FIGURE 5 shows the potential at low electron currents; Brubaker's theoretical curves are shown inset. At low currents a five-fold change in pressure has a negligible effect on the potential.

Studies on ion-molecule reactions and metastable ions, at low repeller potentials and high electron currents, may be affected by space-charge. For example, one prediction of the statistical theory of mass spectra and of the theory proposed recently by Levine[5] is that the rate constant for decomposition of a metastable ion should vary with excitation energy. The experimental results of Momigny[6] and Schug[7] seem to support the theory in showing that indeed the relative intensity of a metastable ion changes with electron energy. However both workers used high electron currents, and since the residence time depends in part on the space-charge conditions in the source, it would seem worthwhile to confirm their findings by operating at very low currents.

There are possibly other effects which may have to be borne in mind. For example: the low energy ejected and scattered electrons will contribute a space-charge in the source[3]; in the absence of a repeller field, ions may be trapped in the potential depression across the electron beam and ions may drift along the axis of the beam[8]; a positive potential on the electron trap whilst deterring the re-entrance of reflected or secondary electrons into the ionisation region favours entrance of positive ions created near the trap; there is evidence for the existence of long-lived excited states of molecules which auto-ionise after the molecule has moved out of the electron beam.[9] It has been postulated that ions of different masses which are collected by the extraction slit originate from regions of different space potential; FIGURE 6 shows retarding-potential data of thermal ions and is evidence in support of this postulate.

REFERENCES

1. Barnard, G. P., Modern Mass Spectrometry, Institute of Physics, London, 1953.
2. McDowell, C. A., and Warren, J. W., Disc. Farad. Soc. 10, 53, 1951.
3. Langmuir, I., Phys. Rev. 33, 954, 1929.
4. Brubaker, W. M., J. App. Phys. 26, 1007, 1955.
5. Levine, R. D., J. Chem. Phys. 44, 2046 1966.
6. Momigny, J., Bull. Soc. Chim. Belg. 70, 291, 1961.
7. Schug, J. C., J. Chem. Phys. 40, 1283, 1964.
8. Hines, M. E., Hoffman, G. W., Saloom, J. A., J. App. Phys. 26, 1157 1955.
9. (a) Feldman, R. and Novick, R., Phys. Rev. Letters 11, 278, 1963.
   (b) Clampitt, R. and Dunning, W. J., Trans. Farad. Soc. (to be published).
   (c) Kieffer, L. J. and Dunn, G. H., Rev. Mod. Phys. 38, 1, 1966.
10. Kaneko, Y. and Kanomata, I., J. Phys. Soc. Jap. 18, 1822, 1963.
11. Clampitt, R. and Dunning, W. J., J. Sci. Inst. (to be published).

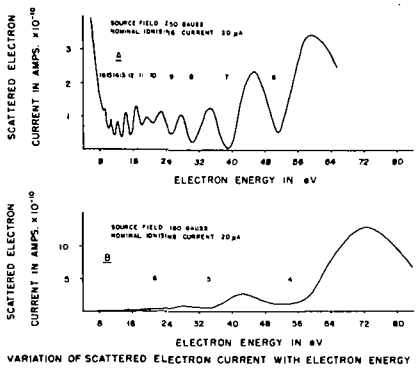

VARIATION OF SCATTERED ELECTRON CURRENT WITH ELECTRON ENERGY

Fig. 1

MUB 11272

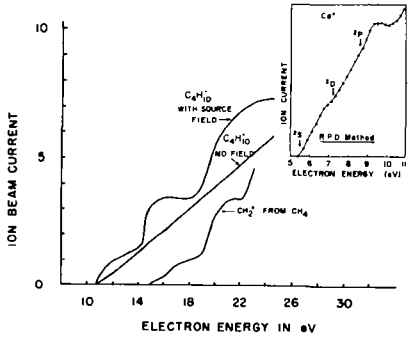

IONIZATION EFFICIENCY CURVES

Fig. 2

MUB 11268

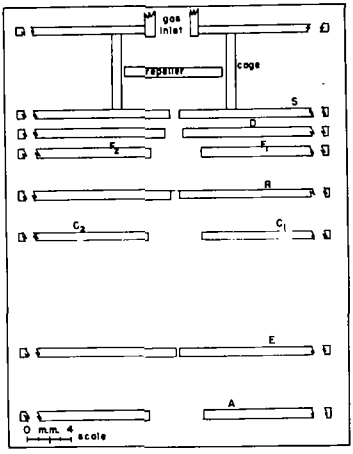

ION SOURCE - END ELEVATION

Fig. 3

MUB-11271

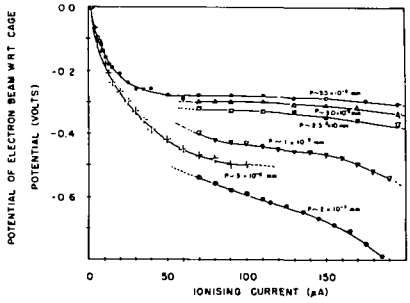

SPACE CHARGE DEPRESSION OF POTENTIAL

Fig. 4

MUB 11270

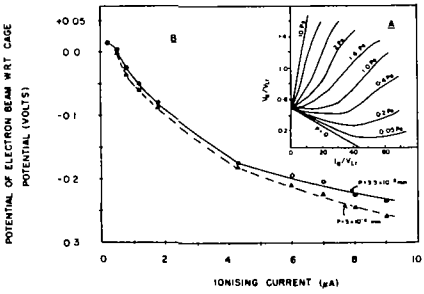

SPACE CHARGE DEPRESSION OF POTENTIAL

Fig. 5

MUB 11273

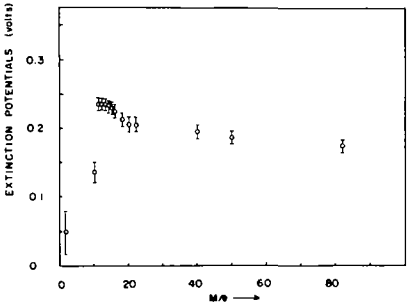

RETARDATION OF THERMAL IONS: A MASS EFFECT

Fig. 6

MUB-11269

MULTIPLE-IMPACT IONIZATION IN NEON AND ARGON USING A TRAPPED-ION SOURCE

P. A. Redhead

Radio and Electrical Engineering Division
National Research Council
Ottawa, Canada

ABSTRACT

An ion source is described in which ions can be trapped for hundreds of milliseconds at pressures below 10^{-7} Torr. Longitudinal ion trapping is achieved by potential barriers erected at either end of the ionization region and radial trapping by space-charge fields. This source has been used with a 2 cm radius, 180° mass-spectrometer. Multiply charged ions have been produced in neon up to Ne^{4+} with electron energies less than 120 eV. These ions are produced by multiple impact, stepwise ionization involving the ground state of the ions only. With argon, ions up to Ar^{6+} have been produced with electron energies less than 120 V. Stepwise ionization of argon involving metastable states of the ions is shown to occur and estimates of the energy of the metastable levels are made.

INTRODUCTION

The neutralization of electron space-charge, even at very low pressures, by means of an "ion trap" was first proposed by Heil[1] and independently by Field et al.[2] The use of an ion trap to decrease the spreading of an electron beam by space-charge has been studied by several authors.[3-6] These ion traps achieved longitudinal trapping by potential barriers raised at either end of the electron beam and radial trapping by space-charge fields.

The application of an ion trap to the ion source of a mass-spectrometer was first reported by Plumlee.[7] More recently a commercial mass-spectrometer (MS10) was used[8] and both radial and longitudinal trapping obtained by the space-charge fields produced by increasing the electron current to about 8×10^{-5} A. No attempt was made to obtain longitudinal trapping by deliberately creating potential barriers. Studies of multiple-impact ionization using similar ion trap arrangements have been made in the rare gases, CO and CH_4 (Reference 8); mixtures of H_2 and He (Reference 9); and CO (Reference 10).

The trapped-ion source used in the present work was based on the design of Field[2] and achieved longitudinal ion-trapping by applied potential barriers, permitting very high electron current density to be used ($\approx 5 \times 10^{-2}$ A cm^2). The ion-trapping times achieved with this high electron current density are such that, for example, one argon ion may suffer as many as seven collisions with electrons.

THE ION SOURCE

Figure 1 shows the trapped-ion source schematically; it differs from a conventional, magnetically immersed source only in the addition of the electrode (the grid) between the filament and the ionization box. The grid and anode are connected and operated at a potential positive w.r.t. the ionization box. The potential distribution along the axis of the electron beam, ignoring space-charge, is shown in the lower part of Fig. 1. The potential barriers, of height V_{TR}, prevent positive ions formed in the ionization region from escaping along the electron beam. Ions are restrained from escaping the electron beam radially by the radial fields caused by electron space-charge. The concentration of trapped ions in the electron beam tends to build up until the electron space-charge is almost neutralized; this process has been analysed by Linder[3] and Ginzburg.[6] With an efficient ion trap approximate neutralization of the beam can be obtained even at very low pressures (as low as 5×10^{-11} Torr in these experiments).

Performance of the ion source is summarized in Fig. 2. With $V_{TR} = 0$, i.e. no longitudinal trapping, the sensitivity increases to a maximum at $I^- = 30$ microamperes and then decreases. With $V_{TR} = 25$ V the sensitivity increases to a maximum at considerably higher electron currents ($\approx 10^{-3}$ A). In the trapped condition ($V_{TR} = 25$ V) the resolving power also increases as I^- is increased to a maximum at about 10^{-3} A. As the electron current is increased the degree of neutralization increases and the energy spread of ions emerging from the electron beam is reduced, improving the apparent resolving power in this single-focussing spectrometer.

The decrease in sensitivity and resolving power above 10^{-3} A in the trapped mode is probably associated with the maximum electron current that can be transmitted through the ionization box without instabilities occurring. Pierce[11] has shown that the maximum stable current in the presence of positive ions is of the same order as the maximum stable current with no positive ions. Using Pierce's criterion for stability we find that the maximum electron current density is

$$J^-_{max} \approx 10^{-4} \frac{V_e^{3/2}}{L^2} \quad A/cm^2 \qquad (1)$$

where L is the electron beam length. Taking $V_e = 100$ V and the dimensions of our ion source we obtain $I^-_{max} \approx 1.5 \times 10^{-3}$ A, which is in reasonable agreement with the measured value (1×10^{-3} A). *However, no instabilities or changes in the transmitted* electron current have been observed up to about 3×10^{-3} A, nor does the measured value of I^-_{max} appear to vary with V_e as predicted by Eq.(1).

RESULTS

Operating in the trapped mode with $I^- = 8 \times 10^{-4}$ A and V_e near 100 V a sensitivity of about 2×10^{-3} A/Torr and a resolving power of 80 were obtained. Multiply-charged ions of the rare gases appeared at electron energies well below their normal appearance potentials. The relationship of ion current to pressure and electron current was non-linear and will be discussed elsewhere. We are concerned here only with the ion current vs electron energy relationship which was found to be essentially unaffected by pressure.

The efficiency of this ion source in the production of multiply-charged ions of neon and argon is indicated in Table I where the relative abundances of ions produced by the trapped-ion source at $V_e < 120$ V are compared with the relative abundances observed with a conventional untrapped source at high electron energies.[12, 13]

TABLE I

Relative Abundances of Multiply Charged Ions

A. NEON

	$2+/_{1+}$ ($\times 10^2$)	$3+/_{1+}$ ($\times 10^3$)	$4+/_{1+}$ ($\times 10^5$)	Reference
Conventional Source $V_e = 1$ kV	3.67	2.04	5.3	12
Conventional Source $V_e = 15$ kV	2.42	1.47	14.3	12
Trapped Source $V_e < 120$ V	3.3	6.7	48.0	This work

B. ARGON

	$2+/_{1+}$ ($\times 10^2$)	$3+/_{1+}$ ($\times 10^3$)	$4+/_{1+}$ ($\times 10^3$)	$5+/_{1+}$ ($\times 10^4$)	$6+/_{1+}$ ($\times 10^5$)	Reference
Conventional Source $V_e \approx 1$ kV	5.22	8.67	1.72	1.99	1.6	13
Conventional Source $V_e \approx 18$ kV	5.83	15.3	2.35	3.25	6.6	13
Trapped Source $V_e < 120$ V	25.0	67.0	25.0	67.0	330.0	This work

(A). Ion Current vs Electron Energy for Neon

Figure 3 shows ion currents as a function of electron energy for charge multiplicity, n = 2, 3 and 4. The transitions indicated in rectangular boxes are the stepwise ionization potentials.[14] The electron voltages throughout are uncorrected for contact potentials. The thresholds for n = 2, 3 and 4 correspond, within the uncertainty of the experiment, with the ionization potentials from the next lower state of charge. This indicates that the ions are produced by a stepwise ionization process involving the ground state of the various ions, i.e.

$$Ne^{n+} + e \longrightarrow Ne^{(n+1)+} \tag{2}$$

Figure 4 shows the same curves over a larger range of electron energy. It can be seen that maxima occur in the n = 1, 2 and 3 curves as the next higher charged state starts up and hence reduces the ion concentration in the preceding state.

(B). Ion Current vs Electron Energy for Argon

The normalized curves for argon are shown in Fig. 5. These curves are much more complex than for neon and show that, for all values of n , the appearance potentials are below the corresponding stepwise ionization potentials indicating that metastable states of the ions are involved

$$Ar^{n+} + e \longrightarrow Ar^{n+(m)} \tag{3a}$$
$$Ar^{n+(m)} + e \longrightarrow Ar^{(n+1)+} \tag{3b}$$

The decrease in I_n^+ as I_{n+1}^+ starts to increase is once more clearly evident.

DISCUSSION

When neon is subjected to successive electron impacts at electron energies below 120 eV, stepwise ionization occurs up to n = 4 involving transitions between the ground states of the ions. Hagstrum[15] has shown that there are no metastable states of Ne^+ whereas all the other rare gases have four metastable states of the singly-charged ion.

Successive electron impacts with argon (V_e < 120 V) cause stepwise ionization up to n = 6 involving metastable levels of the ions. Table II lists approximate values of the metastable levels in argon indicated by data of the type of Fig. 5. No data could be obtained for V_e < 25 V because the space-charge is no longer fully neutralized.

TABLE II

Metastable Levels in Argon

Charge Multiplicity	Energy Levels (above ground states of ion, eV)
2	8, 14
3	23
4	19
5	13

The mean intercollision time for ions of charge multiplicity n is

$$\tau_n = \frac{\varepsilon}{J^- Q_{n,\, n+1}} , \tag{4}$$

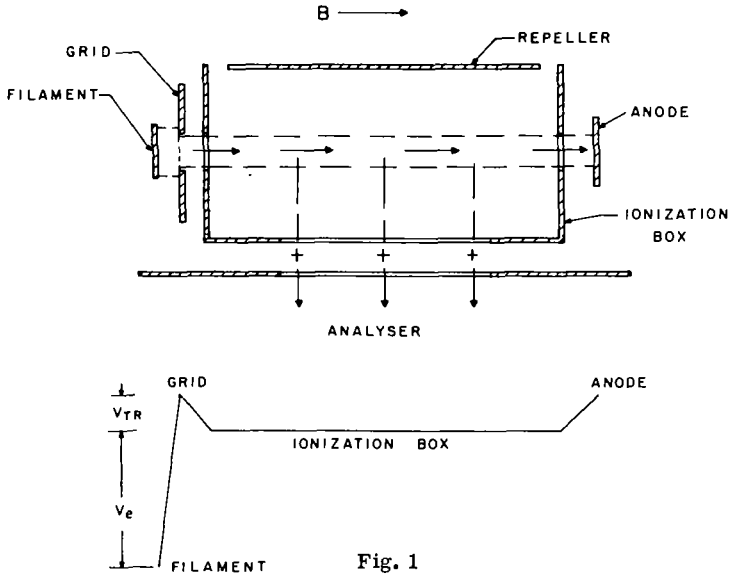
B
REPELLER
GRID
FILAMENT
ANODE
IONIZATION BOX
ANALYSER
GRID
ANODE
V_{TR}
IONIZATION BOX
V_e
FILAMENT

Fig. 1

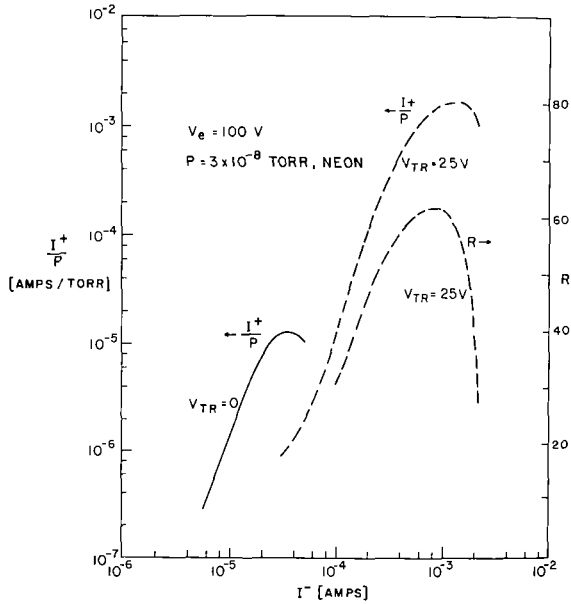
V_e = 100 V
P = 3x10^{-8} TORR, NEON
$\frac{I^+}{P}$
V_{TR}=25V
R
V_{TR}=25V
$\frac{I^+}{P}$
V_{TR}=0
$\frac{I^+}{P}$ [AMPS / TORR]
R
I^- [AMPS]

Fig. 2

where $Q_{n\,n+1}$ is the cross-section for ionization from n to (n + 1) charge multiplicity. Then the ultimate ion, of multiplicity N must have been trapped for a mean time of

$$\tau_N = \frac{\varepsilon}{J^-}\left\{\frac{1}{Q_{12}} + \frac{1}{Q_{23}} \cdots + \frac{1}{Q_{(N-1)N}}\right\} \tag{5}$$

Values of Q_{12} and Q_{23} for argon have been measured by cross-beam methods,[16] and are of the order of 10^{-16} cm^2 for V_e = 100 V. Taking all the cross-sections to be approximately 10^{-16} cm^2 for argon we obtain

$$\tau_6 = 120 \text{ milliseconds}, \tag{6}$$

with $J^- = 5.3 \times 10^{-2}$ A/cm^2, the condition used for most of the above measurements. Similar considerations for neon, taking all cross-sections to be 2×10^{-17} cm^2, [17] lead to

$$\tau_4 = 450 \text{ milliseconds}. \tag{7}$$

These estimates of trapping time are very rough and only serve to indicate that ions can be trapped in this source for sizeable fractions of a second.

Measurements of the cross-section for stepwise ionization are complicated by the fact that the transmission of ions through the ion exit slit of the source decreases with increasing charge multiplicity. It appears that this difficulty can be overcome and approximate cross-sections evaluated.

References

1. Heil, O., Electronic Industries 2, 81 (1946)
2. Field, L.M., Spangenburg, K. and Helm, R., Elec. Comm. 24, 101 (1947)
3. Linder, E.G. and Hernqvist, K.G., J.Appl.Phys. 21, 1088 (1950)
4. Ginzton, E.L. and Wadia, B.H., Proc. I.R.E. 42, 1549 (1954)
5. Hines, M.E., Hoffman, C.W. and Saloom, J.A., J.Appl.Phys. 26, 1157 (1955)
6. Ginzburg, U.E., Isvestia v.u.z. Radiotekhnika 8, 383 (1965)
7. Plumlee, R.H., R. Sci. Inst. 28, 830 (1957)
8. Baker, F.A. and Hasted, J.B., Phil. Trans. Roy.Soc. (in press)
9. Baker, F.A. and Hasted, J.B. (in press)
10. Cuthbert, J., Farren, J., Rao Prahallada, B.S., and Preece, E.R. Proc. Phys.Soc. 88, 91 (1966)
11. Pierce, J.R., J.Appl.Phys. 21, 1063 (1950)
12. Schram, B.L., Boerboom, A.J.H. and Kistemaker, J., Physica 32, 185 (1966)
13. Schram, B.L., Physica 32, 197 (1966)
14. Finkelnburg, W. and Humbach, W., Naturwiss. 42(2), 35 (1955)
15. Hagstrum, H.D., Phys.Rev. 104, 309 (1956)
16. Latypov, Z.Z., Kupriyanov, S.E. and Tunitskii, N.N., Sov.Phys. JETP 19, 570 (1964)
17. Dolder, K.T., Harrison, M.F.A. and Thonemann, P.C., Proc. Roy.Soc. A274, 546 (1963)

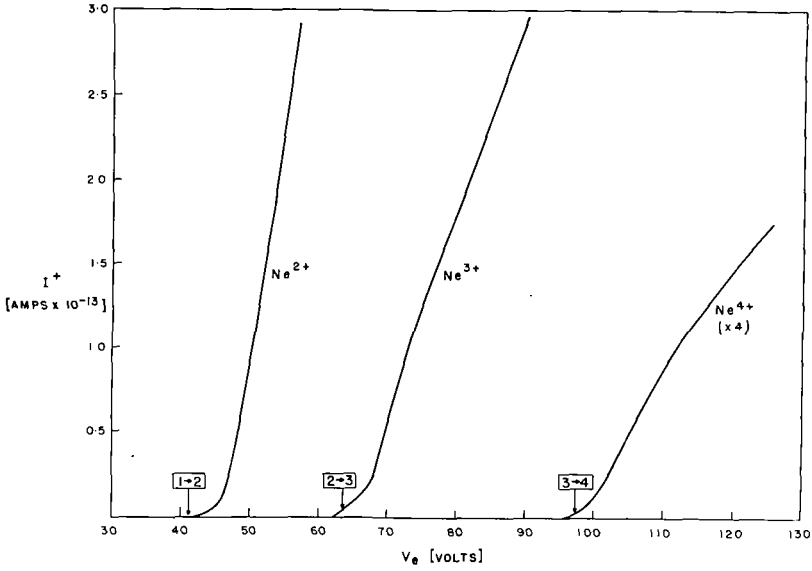
3·0
2·5
2·0
1·5
1·0
0·5
I+
[AMPS x 10-13]
Ne2+
Ne3+
Ne4+
(x 4)
1→2
2→3
3→4
30
40
50
60
70
80
90
100
110
120
130
Ve [VOLTS]

Fig. 3

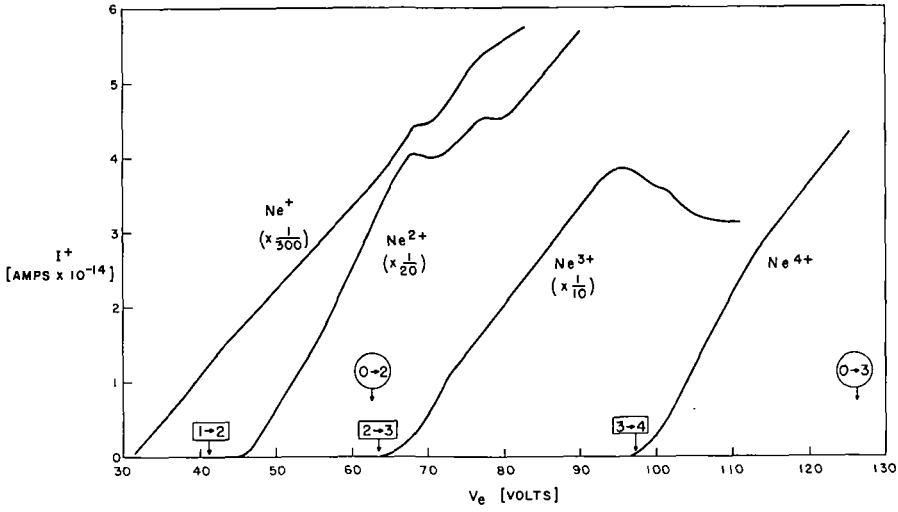
6
5
4
3
2
1
0
I+
[AMPS x 10-14]
Ne+
(x 1/300)
Ne2+
(x 1/20)
Ne3+
(x 1/10)
Ne4+
0→2
0→3
1→2
2→3
3→4
30
40
50
60
70
80
90
100
110
120
130
Ve [VOLTS]

Fig. 4

Figure Captions

Fig. 1: Schematic diagram of trapped-ion source and potential distribution along the axis.

Fig. 2: Sensitivity (I^+/P) and resolving power (R) as a function of electron current (I^-) at an electron voltage (V_e) of 100 V.

Fig. 3: Ion current from neon as function of electron voltage. $I^- = 8 \times 10^{-4}$A, V_{TR}= 25 V and $P = 6 \times 10^{-8}$ Torr.

Fig. 4: Ion currents from neon as function of electron voltage (V_e). Conditions as in Fig. 3.

Fig. 5: Normalized ion current (I^+/I^+_{max}) from argon as a function of electron voltage. $I^- = 8 \times 10^{-4}$ A, V_{TR} = 25 V, and $P = 1.5 \times 10^{-8}$ Torr.

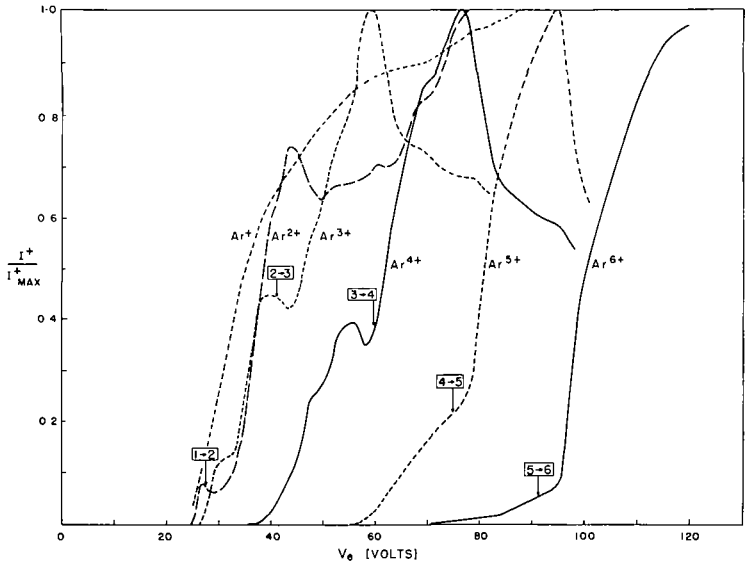

Fig. 5

Electron Monochromator Ion Source System

A.L. Yergey, D. J. Marshall, and T.J. Eskew
Nuclide Corporation
State College, Pennsylvania

Abstract

An ion source system incorporating two 127° electrostatic analyzers is described. The electron beam characteristics of the source are given. A data acquisition system for obtaining ionization efficiency curves for use with the source and a magnetic deflection mass spectrometer is described. Experimental results are given.

A TWO-STAGE DOUBLE-HEMISPHERICAL ELECTRON-ENERGY SELECTOR

Kogoro Maeda and F. P. Lossing

Division of Pure Chemistry, National Research Council,
Ottawa, Canada

Introduction

Two types of electrostatic energy selector have received attention in recent years for the production of electron beams with narrow energy distributions suitable for electron impact measurements: the 127° cylindrical selector in various modifications (1-6), and the parallel-plate selector (7,8). Although both of these types of selector have been used successfully in electron impact experiments, they suffer from two disadvantages which make their experimental application rather difficult. In order to provide a useful energy resolution, an energy half-width less than 0.1 v, the operating voltage in the selector needs to be very low - often 1 v or less. This makes the selector quite sensitive to stray magnetic fields, which has necessitated the use of extensive shielding and Helmholz coils (4). A second disadvantage is the poor collimating power of these selectors, requiring multiple-element lenses to produce a well-collimated cylindrical or rectangular electron beam which can be passed through a reaction chamber with a minimum of wall-bombardment. This latter point appears to be an important factor, in view of the secondary reactions found by Marmet and Morrison (4), and attributed to wall effects. It would appear, in the light of these results, that an improved electron selector should have two characteristics; the selector itself should operate at a voltage as high as possible while still giving an energy half-width of 0.1 v or less, and the issuing electron beam should be as well collimated as possible so that a minimum of further collimation is required before entering the reaction chamber. A consideration of these factors led Simpson (9) to design a concentric spherical selector. For this type of selector the maximum current is inversely proportional to the inverse dispersion of the selector, and this constant is one-half that of other electrostatic selectors. The present work describes the characteristics of a two-stage double hemispherical selector constructed according to Armstrong's design (10).

Constructional Details

A simplified drawing of the complete assembly of the selector is shown in Fig. 1. The two stages are overlapping and offset, so that the flight path in the second stage is at right angles to that in the first stage. In effect, the first stage produces an energy dispersion along the diameter containing the entrance aperture. In the second stage the electrons passing through the inter-stage aperture are focussed to an approximately rectangular image covering the exit aperture. The radii of the inner and outer spheres are 0.613" and 1.227" respectively, the entrance and exit apertures are 0.014" in diameter, and the inter-stage aperture is 0.250" in diameter.

The source of electrons is a standard triode gun with an uncoated tungsten filament. For best intensity and launching angle, the first electrode is held at about 0.5 v negative with respect to the center of the filament, and the second electrode is held at 40-140 v. With these values, the third electrode, which determines the operating energy of the selector can be held at 7.0 to 28 v. In typical operation, a voltage of 28 v on the third electrode requires the voltage of the inner hemispheres to be about 9.7 v, and of the outer hemispheres to be about 48.4 v. After leaving the second stage of the selector, the electron beam enters a collimator system with Einzel lens and quadrupole deflector. With suitable adjustment of the voltages the electron current issuing from the final exit aperture (0.025" diameter) can be brought to a maximum, and as will be seen below, is in the form of a well-defined cylindrical beam.

For electron impact experiments this geometry is most favorable; first, because it provides a minimum of wall-bombardment in the reaction chamber, and second, the reaction chamber is connected to the selector only through the 0.025" diam. final exit aperture, giving very favorable conditions for maintaining a high vacuum in the selector itself by differential pumping. In the present apparatus the reaction chamber and the selector were pumped separately by 60 l/sec. mercury diffusion pumps. No magnetic shielding or Helmholz coils were employed.

Operational Tests

The energy spread of the electron beam from the selector was measured by retarding potential analysis, using a gold-plated Faraday cup placed just in front of the final exit aperture. For best results the interior of the cup was covered with a fine deposit of carbon black to reduce reflection of the electrons. This method for measuring the energy half-width is not precise, in that the true half-width will always be less than the measured width.

A typical half-width measurement, with the selector operating at 11.93 v, is shown at the lower right in Fig. 2. The true half-width may be a little smaller than the 0.06 v indicated, owing to the method of measurement. The half-width obtained as a function of the selector operating energy is shown in the graph at the upper left of Fig. 2. Simple theory predicts that the half-width changes linearily with the operating energy. This was found, except at the lowest operating energy, where a minimum half width of 0.06 v was obtained. The deviation in this region from a linear relationship may result from an over-estimate of the half-width by the retarding potential method, or from disturbances by stray magnetic fields at the lower selector operating voltages or from both. The beam currents obtained at the various half-widths are indicated on the graph. These were logarithmically linear with the operating energy, as reported by Simpson (9).

The next question of interest was whether the energy of the issuing beam could be varied over a useful range (4-30 v) without disturbing the half-width or the intensity by a serious amount. This was tested using an auxiliary energy-controlling electrode, as shown at the top right of Fig. 3. The voltage of this electrode was changed over the range 4-30 v (while maintaining constant conditions in the selector) and the half-widths were measured in the same way as before. As shown in the graph in Fig. 3, no serious deformation of the half-width occurred over this energy range.

Finally, a cylindrical reaction chamber was constructed of gold-plated platinum mesh, incorporating the energy-controlling electrode, as shown in Fig. 4. Tests of the efficiency of collimation in this chamber showed that some 75-80% of the beam coming from the selector could be brought into the reaction chamber, and of this some 70-90% could be collected on the electron trap. This indicates that one of the sources of spurious breaks in ionization efficiency curves, that resulting from wall bombardment, can be overcome in the present apparatus.

Preliminary Experiments

In preliminary experiments with rare gases, it was found that a large current at the collector was obtained at energies much below the ionization threshold. This resulted from formation of metastable atoms which released electrons from the collector. A plot of collector current against electron energy is shown in Fig. 5 in the case of helium. The pressure of helium in the reaction chamber was 10^{-5} Torr, compared to a background pressure of 10^{-8} Torr. The ionization of impurities or background, therefore, is not the source of the current observed. A comparison of the upward breaks in current with the known transitions in helium (Fig. 5) shows that metastable ^3S and ^1S He atoms were being detected in abundance. This curve is essentially the same as that observed by Schulz and Fox (11).

The collector current versus electron energy curve for neon (Fig. 6) also shows breaks corresponding to formation of metastable Ne atoms below the ionization threshold. For measurements of both He and Ne a contact of potential shift of about 0.6 v was observed. A further distinct upward break, shown at the right in Fig. 6, corresponds to the onset of ionization of Ne. Resolution of the $P_{3/2}$ and $P_{1/2}$ states was probably not achieved at the electron beam half-width employed.

Fig. 7, left half, shows the formation of metastable Ar atoms, and, right half, some structure in the ionization efficiency curve for Ar. A comparison of reported structural features in the literature is shown below this graph (12,7,8, 13,5). As discussed in reference 5 there are no known spectroscopic states corresponding to the features at 1.2 - 1.3 v and 1.7 v above the ionization threshold of argon, nevertheless some evidence for structure at these points has been found by a number of investigators. The present data also show some evidence for such structure.

The curves for Kr, shown in Fig. 8, also emphasize the importance of metastable atom formation by electron impact, although detailed resolution of the structure is not possible with these preliminary data.

Further Work

The present results, although preliminary in nature, are quite encouraging for the use of this energy selector in impact experiments. The evident modifications are in progress, to permit a separation of metastable atom excitation and ionization processes, and to provide mass resolution of the ions formed.

References

1. W.B. Nottingham, Phys. Rev. 55 203 (1939)
2. E.M. Clarke, Can. J. Phys. 32 764 (1954)
3. P. Marmet and L. Kerwin, Can. J. Phys. 38 787 (1960)
4. P. Marmet and J.O. Morrison, J. Chem. Phys. 36 1238 (1962)
5. C.E. Brion, D.C. Frost, and C.A. McDowell, J. Chem. Phys. 44 1034 (1964)
6. See also several papers in the Report of the 13th Annual Conference on Mass Spectrometry and Allied Topics, May 16-21. St. Louis. Published by ASTM Committee E-14.
7. D.A. Hutchison, Advances in Mass Spectrometry 2 527 (1963)
8. S.N. Foner and B.H. Hall, Phys. Rev. 122 512 (1961)
9. J.A. Simpson, Rev. Sci. Instr. 35 1698 (1964)
10. R.A. Armstrong (to be published in Can. J. Phys.)
11. G.J. Schulz and R.E. Fox, Phys. Rev. 106 1179 (1957)
12. F.J. Comes and W. Lessman, Z. Naturforsch. 16a 1396 (1961)
13. P. Marmet, L. Kerwin and E.M. Clarke, Advances in Mass Spectrometry 2 522 (1963)

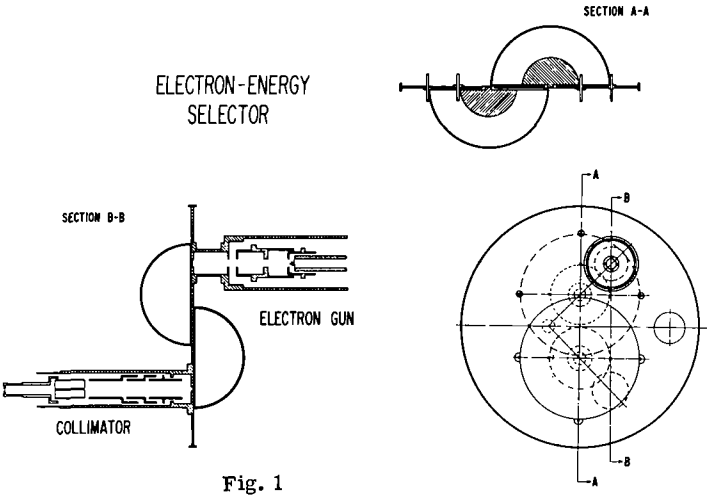
ELECTRON-ENERGY
SELECTOR
SECTION A-A
SECTION B-B
ELECTRON GUN
COLLIMATOR
A
B
B
A

Fig. 1

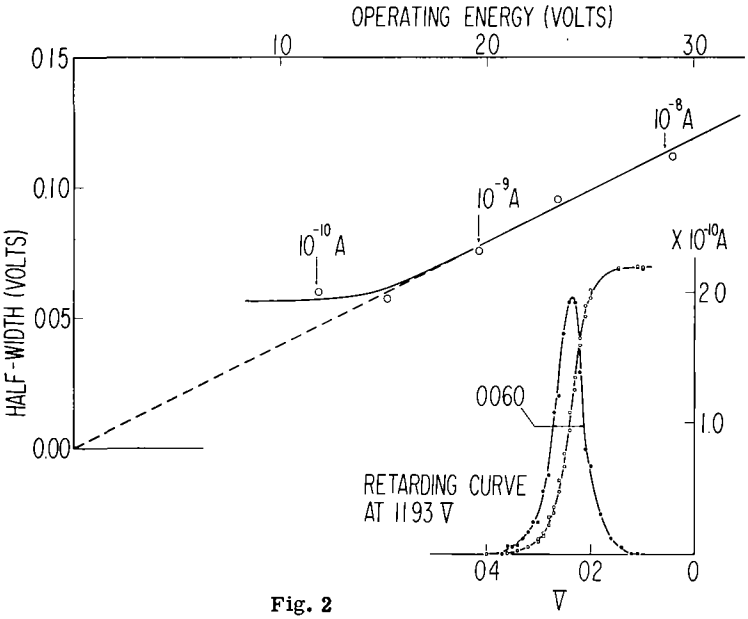
OPERATING ENERGY (VOLTS)
10
20
30
0.15
0.10
0.05
0.00
HALF-WIDTH (VOLTS)
10^{-8} A
10^{-9} A
10^{-10} A
X 10^{-10}A
2.0
1.0
0060
RETARDING CURVE
AT 11.93 V
04
02
0
V

Fig. 2

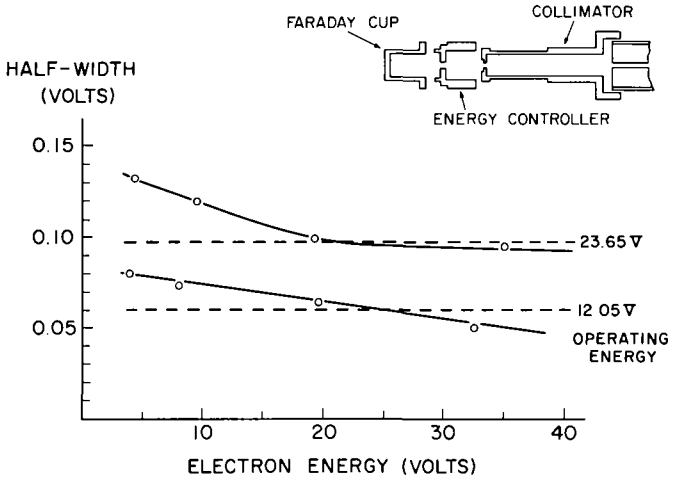

Fig. 3

REACTION CHAMBER & COLLIMATION EFFICIENCY

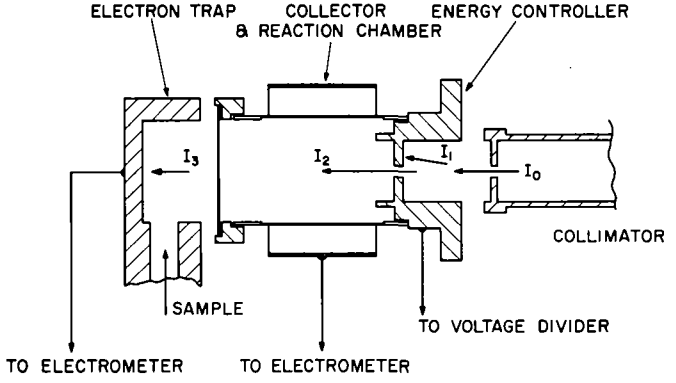

COLLIMATION EFFICIENCY : I_3/I_2 : 70 ~ 90% ; I_2/I_0 : 75 ~ 80%

Fig. 4

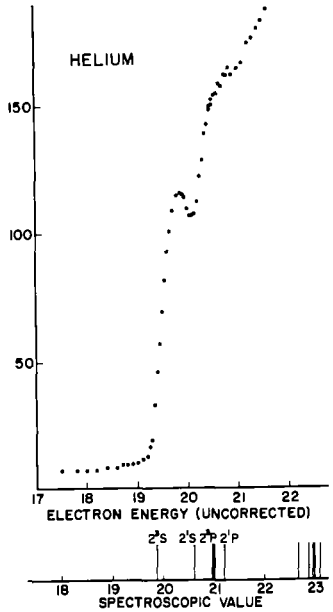

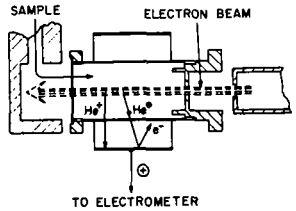

BELOW IONIZATION POTENTIAL

SAMPLE $A + e^- \longrightarrow A^* + e^-$

$A^* +$ WALL $\longrightarrow A +$ WALL $(\oplus) + e^-$

ABOVE IONIZATION POTENTIAL

$A + e^- \longrightarrow A^+ + e^- + e^-$

Fig. 5

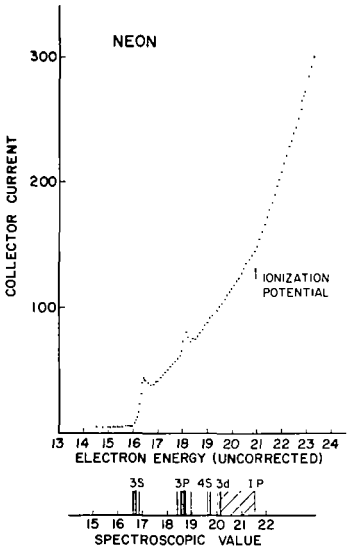

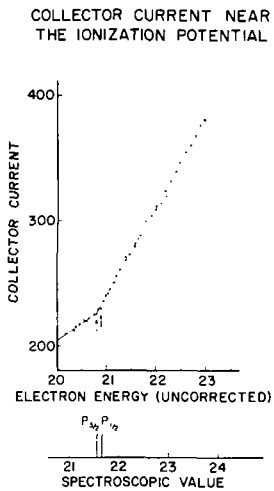

Fig. 6

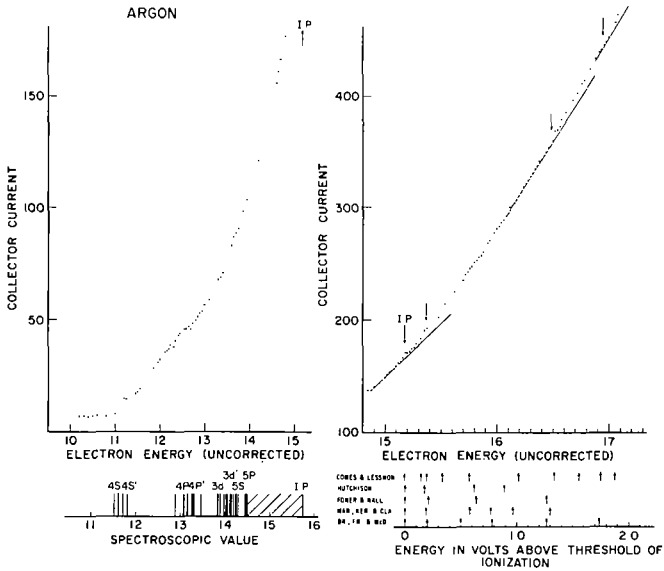
ARGON
COLLECTOR CURRENT
ELECTRON ENERGY (UNCORRECTED)
IP
4S4S'
4P4P'
3d
3d' 5P
5S
SPECTROSCOPIC VALUE
ENERGY IN VOLTS ABOVE THRESHOLD OF IONIZATION

Fig. 7

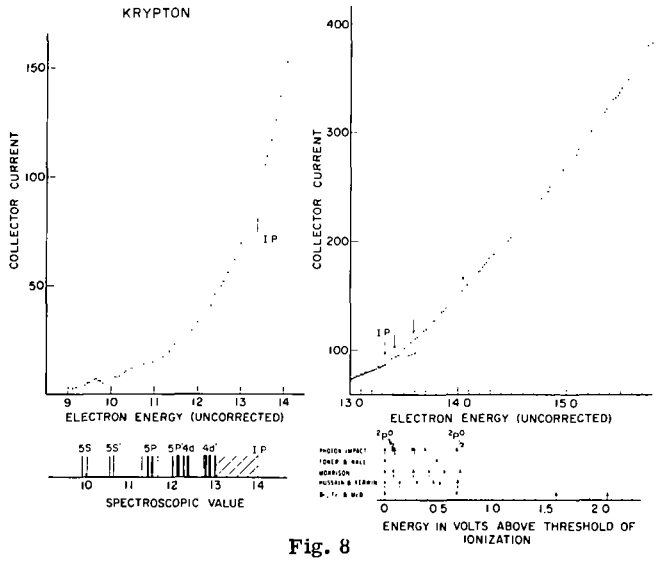
KRYPTON
COLLECTOR CURRENT
ELECTRON ENERGY (UNCORRECTED)
IP
5S
5S'
5P
5P4d
4d'
SPECTROSCOPIC VALUE
ENERGY IN VOLTS ABOVE THRESHOLD OF IONIZATION

Fig. 8

RESOLUTION OF FINE STRUCTURE IN IONIZATION EFFICIENCY CURVES

by Robert E. Winters, Jerome H. Collins and William L. Courchene

The Procter & Gamble Company, Miami Valley Laboratories

Cincinnati, Ohio 45239

ABSTRACT

An energy distribution difference method for determining ionization potentials and for detecting fine structure, i.e., breaks, in ionization efficiency curves is described which eliminates the difficulties arising from the thermal energy spread of the ionizing electrons. Although the technique gives essentially the same results as monoenergetic methods, it is much easier experimentally. Ionization efficiency curves are given for the inert gas ions Ar^+, Kr^+ and Xe^+ as well as the molecular-ions CO^+, N_2^+ and O_2^+. The "breaks" in the efficiency curves are presented and the results are compared to previously reported monoenergetic electron impact data.

INTRODUCTION

In electron impact studies the difference between the ionization efficiency (IE) curve obtained from ionization with monoenergetic electrons and the experimental curve obtained from ionization with electrons from a heated filament is generally attributed to the Maxwellian energy distribution of the thermionically emitted electrons.[1] The effect of this distribution of electron energy will be to obscure any fine structure which may occur in the IE curve, but no effect will be seen on the general shape of the curve. One solution to the problem of resolving the fine structure which may be present in these curves has been to reduce the energy spread of the ionizing electron beam.[2-5] The most successful approaches have been those in which a narrow segment of the initial electron energy distribution is used to produce ionization. However, because of experimental difficulties, the signal-to-noise ratio is low near threshold.

The retarding potential difference (R.P.D.) method developed by Fox et al.[4] will also resolve the fine structure of IE curves presumably by reduction of the effective electron energy distribution. The influence of space charge effects in the R.P.D. ion source has recently been predicted by Marmet.[6] Using the experimental observations of Hartwig and Ulmer, Marmet concluded that, once past the retarding electrode, the ionizing electrons have a symmetrical distribution whether the retarding potential is applied or not. Therefore the change in ion current observed is just the difference between two ion currents produced by two different ionizing electron distributions.

Previous attempts to remove the effect of the energy spread by analytical methods[8] have been only partially successful. The difficulties in this approach arise from the lack of knowledge of the exact form of the electron energy distribution and the inherent inaccuracy of the experimentally measured ion currents used to construct the ionization efficiency curves.

This paper describes an energy distribution difference (E.D.D.) technique by means of which the effective electron energy distribution can be reduced and thus allow the fine structure in IE curves to be observed.

THEORY

The probability (P) for excitation of a neutral molecule in its ground state to a single electronic state of the ion is given by[9]

$$P = 0 \text{ for } E < E_c$$
$$P = p(E) \text{ for } E \geq E_c$$

where E is the energy of the ionizing electron and E_c is the ionization potential. In a mass spectrometer electrons emitted from a hot filament collide with neutral atoms or molecules and cause ionization. The electrons possess a distribution of kinetic energies (U) such that the probability of finding an electron in the range U to $U + \Delta U$ in unit time is given by f(U). After emission from the filament the electrons are accelerated by a potential V and acquire an energy $E = U + V$. The ion current produced at any accelerating voltage V by the electron energy distribution $f(U) = f(E-V)$ is given by the expression[9]

$$I(V) = C \int_{E_c}^{\infty} f(E-V)\, p(E)\, dE. \qquad (1)$$

At some other voltage V' the corresponding expression is

$$I(V') = C \int_{E_c}^{\infty} f(E-V')\, p(E)\, dE. \tag{2}$$

If equation (2) is multiplied by a constant b and subtracted from equation (1) then

$$\Delta I(V) = I(V) - bI(V') = C \int_{E_c}^{\infty} \left[f(E-V) - bf(E-V')\right] p(E)\, dE. \tag{3}$$

The difference term in the brackets represents a new energy distribution $\Delta f(E-V)$. Therefore equation (3) can be rewritten as

$$\Delta I(V) = I(V) - bI(V') = C \int_{E_c}^{\infty} \Delta f(E-V)\, p(E)\, dE. \tag{4}$$

The form which this difference distribution will have can be illustrated by considering a Maxwellian distribution for electrons emitted from a heated filament[10]

$$f(E-V) = A(E-V)\, e^{-(E-V)/kT} \tag{5}$$

where A is a constant which depends on the characteristics of the filament. Figure 1 shows f(E-V) for a filament temperature of 1730° K. Values of V' and b can be found which will superimpose the lower shifted distribution bf(E-V') and the high energy portion of the original distribution. The resultant difference distribution $[\Delta f(E-V)]$ will have the high energy tail eliminated. For the distribution chosen (T = 1730° K) the parameters $\Delta V = V'-V = 0.1$ eV and b = 0.63 meet this criterion and give a difference function which is reasonably "narrow" as shown in Figure 1. The half-width of the difference distribution is approximately 0.14 eV and it has a shape comparable to an electron energy distribution obtained from some electrostatic energy selectors.[11] It is found that similar difference distributions could be obtained from Maxwellian distributions corresponding to any temperature from 1700° to 2500° K by using the appropriate value of the parameter b. For example, at a filament temperature of 2400° K; $\Delta V = 0.1$, b = 0.72 gives a difference distribution with a half-width of approximately 0.16 eV.

In order to demonstrate the difference between the ionization efficiency curves one would obtain with the f(E-V) and $\Delta f(E-V)$ distributions (Figure 1) a theoretical p(E) was selected (Figure 2) which has $E_c = 10.00$, three linear segments with relative slopes of 1.00, 1.50 and 2.00 and breaks at 10.80 and 11.60 (i.e., at 0.8 and 1.60 eV above the threshold). Using this p(E) an ionization efficiency curve [I(V) vs. V] was synthesized using the distribution f(E-V) shown in Figure 1. The I(V) values were obtained by replacing the integration of equation (1) with the summation

$$I(V) = C \sum_{E_c}^{E_{max}} \left[(E-V)\, e^{-(E-V)/kT}\right] p(E)\, \Delta E \tag{6}$$

with $\Delta E = 0.01$ eV, T = 1730° K and the summation taken only to the term where (E-V)/kT is equal to 10. The ionization efficiency curve obtained from this procedure, shown in Figure 2, is typical of experimental curves in which the fine structure has been obscured by the energy spread of the electrons. The difference curve $\Delta I(V)$ which one would find using the distribution function $\Delta f(E-V)$ is obtained from this I(V) vs. V curve by applying the simple expression

$$\Delta I(V) = I(V) - bI(V') = I(V) - 0.63\, I(V + 0.1). \tag{7}$$

This difference curve is also shown in Figure 2. It is essentially identical to p(E) with breaks at 0.80 and 1.60 and with relative slopes of 1.00, 1.50 and 2.01 for the straight line portions. Similar calculations show that even if a break occurs at 0.2 eV above E_c, the break can be resolved by this technique.

From the above example it is evident that, theoretically, one can eliminate the effect of the energy spread from curves obtained with electrons which have a Maxwellian distribution and obtain true ionization probability curves by plotting the difference ion current using the proper values of b and ΔV. The physical significance of $\Delta I(V)$ is that it is the difference in ion current one would obtain for ionization with f(E-V) containing N electrons accelerated by V and a similar distribution containing bN electrons accelerated by a slightly higher voltage $V' = V + \Delta V$. Even in the case where the Maxwellian distribution has been perturbed by space charge, relaxation and geometrical effects,[12,13] it should be possible to eliminate most of the high energy tail of this distribution by the method described here and therefore improve resolution.

If the electron energy distribution in the mass spectrometer is not known, which is almost always the case, the best set of parameters (ΔV and b) for a particular set of experimental conditions can be obtained empirically from the experimental data by choosing the values of ΔV and b which make the exponential portions[2] of the "tails" of the I(V) and bI(V') curves coincide (i.e., $\Delta I(V)$ should be essentially equal to zero

over this entire region). We have found experimentally that for a fixed value of ΔV (0.1 eV), $\Delta I(V)$ remains positive and never reaches zero if b is too small; and $\Delta I(V)$ becomes too negative if b is too large.

In order to illustrate the use of this method the ionization potentials and IE curves for Ar^+, Kr^+, Xe^+, CO^+, N_2^+, and O_2^+ obtained by this new technique are presented and the results found are compared with results obtained by other workers using mono-energetic methods.

EXPERIMENTAL

Experiments were performed using an Atlas CH-4 mass spectrometer with a normal electron impact source. The instrumental conditions used to make the ion current measurements were:

Filament current 4.6 A (approximate temperature 1730° K),
Filament emission to electron trap 10 μA,
Draw-out electrode and electron shield 0 volts with respect to ion chamber,
Ion accelerating voltage 3000 volts.

Electron energy was varied with a 10-turn potentiometer and was measured using a digital voltmeter (Hewlett-Packard Model 3440A). Ion currents were measured every 0.05 or 0.1 eV. Krypton was used as calibrating gas for the electron energy scale and the ionization potentials were determined with both the sample gas and krypton in the spectrometer at the same time. Gas pressures in the ionization region were maintained at less than 10^{-5} Torr.

The values of ΔV and b used for all curves presented in this paper were 0.1 eV and 0.65, respectively. These parameters are very close to the values predicted from the idealized Maxwellian distribution for T = 1730° K. Because of this fact and the linearity of the CO^+ data presented below, we conclude that the difference distribution $\Delta f(E-V)$ shown in Figure 1 is a reasonably good approximation to the distribution used in this work.

RESULTS AND DISCUSSION

Ionization Potential Measurements

Ionization potential measurements by electron impact are not always reliable because of difficulties associated with interpretation of the experimental data.[1] These difficulties have been removed in this work by greatly reducing the effective electron energy distribution. The results obtained for the ionization potentials of argon, xenon, carbon monoxide, nitrogen, and oxygen using the I.P. of krypton for calibration are summarized in Table 1. The uncertainties in these values represent the deviations

Table 1. Ionization potentials (eV) of Ar, Kr, Xe, CO, N_2, and O_2

Ion	This Work	R.P.D.	Photoionization	Spectroscopic
Ar^+	15.78 ± 0.03	15.75[a]	15.75[b]	15.755[c]
Kr^+	(14.00)[d]	14.00 ± 0.03[e]	13.999 ± 0.002[f]	13.996[c]
Xe^+	12.15 ± 0.03		12.129 ± 0.002 [g] 12.12[h]	12.127[c]
CO^+	14.05 ± 0.02	13.98 ± 0.02[i] 14.11 ± 0.03[k]	14.0[h]	14.009[j]
N_2^+	15.60 ± 0.03	15.60 ± 0.01[i] 15.63 ± 0.02[e] 15.63[l]	15.58[k]	15.557[j]
O_2^+	12.07 ± 0.02	12.21 ± 0.04[m]	12.065 ± 0.003[g] 12.075 ± 0.01[o]	12.0[n]

[a]reference 4, [b]reference 10, [c]reference 22, [d]Calibrant, [e]reference 20, [f]A. J. C. Nicholson, J. Chem. Phys. 43, 1171 (1965), [g]reference 27, [h]D. C. Frost, D. Mak, C. A. McDowell, and D. A. Vroom, 12th Annual Conference on Mass Spectrometry and Allied Topics, ASTM Committee E-14 on Mass Spectrometry, Montreal, Canada, 7-12 June, 1964, [i]reference 28, [j]G. Herzberg, "Molecular Spectra and Molecular Structure; I. Spectra of Diatomic Molecules" (Van Nostrand, New York, 1950), [k]G. L. Weissler, in Handbuch der Physik, edited by S. Flügge, Band XXI, (Springer-Verlag, Berlin, 1956), p. 304, [l]reference 24, [m]reference 32, [n]W. C. Price and G. Collins, Phys. Rev. 48, 714 (1935), [o]K. Watanabe, J. Chem. Phys. 26, 542 (1957).

from the mean of at least three independent determinations. The values are obviously in excellent agreement with those found by spectroscopic, photoionization and R.P.D. methods. The present method is experimentally considerably simpler since it requires no changes in the ion source of the mass spectrometer.

Fine Structure in IE Curves

The ionization efficiency curves for argon, krypton, xenon, carbon monoxide, nitrogen, and oxygen obtained from the experimental curves by the technique described are shown in Figures 3-7. These curves are for single runs but the "breaks" in the IE curves listed in Tables 2-6 are the averages of many determinations.

Argon

There is fair agreement between velocity selector data[11,14-17] and this work (Table 2), with the exception of Marmet and Kerwin[15] who detect only one break at

Table 2. Fine Structure in the Ionization Efficiency Curve for Argon

State	Spectroscopic	This Work	Velocity Selector					R.P.D.		
	(22)		(14)	(15)	(16)	(17)	(11)	(19)	(20)	(21)
$^2P_{1/2}$	0.178	0.18	0.20	0.18	0.19	0.19	0.21	0.2		0.27
		0.42	0.50		0.58	0.58	0.64			0.54
			0.78		0.77					
		1.01			0.97	0.96				
		1.36	1.27		1.30	1.25	1.27			
		1.96	1.74		1.75				1.6	

0.18 eV above onset. Several of the levels above $^2P_{1/2}$ (0.18 eV) correlate quite well with peaks in the photoionization efficiency curve.[18] Therefore it seems reasonable that some of the breaks in the curves obtained by electron impact could be attributed to autoionization.

The R.P.D. data[19-21] show little agreement with velocity selector data or this work in that only the lower breaks are definitely observed. Fox[19] detected a break at 0.2 eV and Melton and Hamill[21] detected two breaks at approximately 0.27 and 0.54 eV above onset. The R.P.D. results of Kaneko[20] show that the IE curve for argon deviates from linearity at about 1.6 eV. However, he did not examine this region of the curve in detail.

Krypton

In the present study there is a break at 0.38 eV and another at 0.96 eV (Table 3).

Table 3. Fine Structure in the Ionization Efficiency Curve for Krypton

State	Spectroscopic	This Work	Velocity Selector	R.P.D.			
	(22)		(11)	(23)	(20)	(21)	(24)
		0.38	0.48			0.35	
$^2P_{1/2}$	0.666	0.64*		0.66*	0.7*	0.67*	0.68*
		0.96	0.94			0.95	

*Obtained by extension of linear parts of IE curve.

These values are in good agreement with 0.48 and 0.94 eV determined by Foner and Nall[11] using a velocity selector. R.P.D. studies of Melton and Hamill[21] show breaks in the IE curve at 0.35 and 0.95 eV.

The $^2P_{1/2}$ state of krypton lies 0.666 eV[22] above the ground state $^2P_{3/2}$. If one extends the lower and upper linear part of the Kr^+ curve as has been done in previous R.P.D. work[20,21,23,24] the lines cross at 0.64 eV above the initial onset. This crossing has been attributed to the $^2P_{1/2}$ state by these workers.

Xenon

Two breaks at 0.33 and 1.27 eV were detected in the IE curve for Xe^+. The latter value corresponds to the spectroscopic value 1.31 eV[22] for the $^2P_{1/2}$ state of the ion. Also, our value for this break in the IE curve is in good agreement with velocity selector data[3,11] and R.P.D. data[23,25,26] as shown in Table 4. However, reports on

Table 4. Fine Structure in the Ionization Efficiency Curve for Xenon

State	Spectroscopic	This Work	Velocity Selector		R.P.D.		
	(22)		(11)	(3)	(25)	(26)	(23)
		0.33			0.35		
			0.70		0.75		
$^2P_{1/2}$	1.31	1.27	1.33	1.20	1.3*	1.31	1.27
			2.05		1.9		

*Obtained by extension of linear parts of IE curve.

other structural features in the Xe^+ IE curve are not consistent. Fox et al.,[23] Cloutier and Schiff,[26] and Clarke[3] observe only one break due to the $^2P_{1/2}$ ionization. Melton and Hamill[25] detect additional breaks at 0.75 and 1.9 eV above onset. These workers attribute the 0.35 and 0.75 eV processes to autoionization.[27]

Carbon Monoxide

In agreement with R.P.D. data,[20,28] the ionization efficiency curve for CO^+ (Figure 6) was found to be linear for 1.5 eV above onset. Since a substantial tail on the low energy side of the electron distribution would give upwards curvature, we conclude our distribution has a fairly sharp low energy cut-off.

Nitrogen

Evidence of autoionization has been detected in the ionization efficiency curve for nitrogen obtained by velocity selector studies[3,29] and by R.P.D. studies.[20] We also observe an abnormality in the IE curve which could be attributed to autoionization. The points measured deviate (Figure 5) from the linear curve at about 0.68 eV above threshold (Table 5). The autoionization portion of the IE curve for N_2^+ has a shape

Table 5. Fine Structure in the Ionization Efficiency Curve for Nitrogen

State	Spectroscopic	This Work	Velocity Selector		R.P.D.				Photoelectron
	(24)		(29)	(3)	(20)	(24)	(28)	(26)	(30)
		0.30							0.29
		0.68	0.67		0.6				0.58
$A^2\pi_u$	1.13	1.11*		1.0*	1.37	1.21	1.33	1.35	1.15
		1.44							
$B^2\Sigma_u^-$	3.17	3.00			3.31	3.13	3.24		3.15

*Obtained by extension of linear parts of IE curve.

similar to that obtained by Clarke[3] using an electron energy selector and by Kaneko[20] using the R.P.D. technique. Structure in the IE curve corresponding to this process in nitrogen was not found by Fox et al.,[28] Frost et al.,[24] and Cloutier et al.[26]

According to Clarke's explanation,[3] the shape of the curve for N_2^+ is due to excitation to vibrational states of N_2^+, and the second ionization potential ($A^2\pi_u$) is defined as a crossing point of the extensions of linear parts of the curve. Indeed, the breaks we observe at 0.30 and 0.68 eV correspond quite well with the vibrational levels found by photoelectron spectroscopy[30] and the intersection of the extensions of the linear portions of the curve (1.11 eV) corresponds quite well with the spectroscopic value 1.13 eV for the $A^2\pi_u$ state. However, the break we find at 1.44 eV is not greatly different from the spectroscopic value and is in good agreement with the value obtained by other workers.[20,24,26,28]

Oxygen

One of the first examples of an excited state of a molecular-ion being correctly identified by electron impact is provided by the work of Tate and Smith[31] on O_2^+. They detected a break in the IE curve at approximately 4.1 eV above threshold ($^4\pi_u$ state). By use of the R.P.D. technique Frost and McDowell[32] also observed this state, as well as the $^2\pi_u$ and $^4\Sigma_g^-$ states. The "tailing" near the threshold of the R.P.D. IE curve of O_2^+ has been attributed[33] to the excitation of vibrational levels. Brion[33] detected breaks at 0.26, 0.51 and 0.75 eV above the onset of the $^2\pi_g$ ground state of O_2^+. The data shown in Table 6 are in good agreement with these values.

Table 6. Fine Structure in the Ionization Efficiency Curve for Oxygen

State	Spectroscopic	This Work	Velocity Selector	R.P.D.	
	(32)		(33)	(32)	(25)
		0.29	0.26		
		0.63	0.51		
		0.92	0.75		0.90
					1.40
$^4\pi_u$	3.95	3.75	4.04	4.09	4.00
$^2\pi_u$	4.81	4.80	4.92	4.97	4.90
$^4\Sigma_g^-$	6.00	5.98	6.02	6.21	5.90

Experimental data for three inert gases and three molecule-ions are thus found to be in good agreement with data obtained using monoenergetic methods when ordinary IE curves are treated in the manner we have described. As with any such method, it is obvious that improvement in the determination of fine structure in the IE curve is limited by the precision of the data which one can obtain. The Atlas CH-4 has been found to give excellent data. We have obtained some IE curves using a Bendix TOF mass spectrometer[34] and, while results similar to those found with the Atlas are obtained, the precision of the data is less and therefore fine structure is more difficult to resolve.

It is of interest to note the possible relationship between the method described above and the experimental techniques, such as R.P.D. and the Schiff method, which

require the application of a retarding voltage to the electrons at some point in the source. It has already been mentioned that Marmet[6] has discussed the R.P.D. technique and concluded that the ionizing electrons, once past the retarding grid in the source, have a symmetrical distribution. There will therefore be a difference between the two distributions (with and without the retarding potential applied). After the retarding potential is applied the total number of electrons will be less and the average energy will be slightly shifted with respect to the original distribution. If this interpretation of the R.P.D. method by Marmet is correct, it is not surprising that the effective energy distribution (difference distribution) will lead to R.P.D. ionization efficiency curves which consist of straight line segments. In the Schiff method, a retarding potential is applied on the first grid of the electron gun. In the analysis of this method, Cloutier and Schiff[26] state that the electron energy distribution entering the ionization region of the source will be Maxwellian whether or not the potential is applied. Therefore the change in ion current measured should also be due to the difference in ionization caused by two Maxwellian distributions. As we have shown, the use of such a difference function does indeed narrow the effective distribution and allow fine structure in the IE curves to be resolved.

Studies are now in progress on more complex organic molecular-ions as well as application of the technique to appearance potential measurements on fragmentation ions.

REFERENCES

1. F. H. Field and J. L. Franklin, "Electron Impact Phenomena and the Properties of Gaseous Ions" (Academic Press Inc., New York, N. Y., 1957), p. 14.
2. W. B. Nottingham, Phys. Rev. 55, 203 (1939).
3. E. M. Clarke, Can. J. Phys. 32, 764 (1954).
4. R. E. Fox, W. M. Hickam, T. Kjeldaas, Jr., and D. J. Grove, Phys. Rev. 84, 859 (1951); Rev. Sci. Instr. 26, 1101 (1955).
5. P. Marmet and L. Kerwin, Can. J. Phys. 38, 787 (1960).
6. P. Marmet, 12th Annual Conference on Mass Spectrometry and Allied Topics, ASTM Committee E-14 on Mass Spectrometry, Montreal, Canada, 7-12 June, 1964; Can. J. Phys. 42, 2102 (1964).
7. D. Hartwig and K. Ulmer, Z. Physik. 173, 294 (1963).
8. J. D. Morrison, J. Chem. Phys. 19, 1305 (1951); 39, 200 (1963).
9. J. D. Morrison, J. Chem. Phys. 21, 1767 (1953).
10. R. E. Honig, J. Chem. Phys. 16, 105 (1948).
11. S. N. Foner and B. H. Nall, Phys. Rev. 122, 512 (1961).
12. See Reference 7.
13. See Reference 6.
14. C. E. Brion, D. C. Frost, and C. A. McDowell, 12th Annual Conference on Mass Spectrometry and Allied Topics, ASTM Committee E-14 on Mass Spectrometry, Montreal, Canada, 7-12, June 1964, J. Chem. Phys. 44, 1034 (1966).
15. See Reference 5.
16. L. Kerwin, P. Marmet, and E. M. Clarke, "Advances in Mass Spectrometry," Vol. 2, edited by R. M. Elliott, (Pergamon Press, Inc., New York, 1959), p. 522.
17. M. Hussain and L. Kerwin, Can. J. Phys. 44, 57 (1966).
18. Von F. J. Comes and W. Lessman, Z. Naturforsch. 16a, 1396 (1961).
19. R. E. Fox, Westinghouse Res. Lab. Rept. 60, 94439-4-R2 (1956).
20. Y. Kaneko, J. Phys. Soc. Japan 16, 1587 (1961).
21. C. E. Melton and W. H. Hamill, Notre Dame Report (1963).
22. C. E. Moore, "Atomic Energy Levels," Bureau of Standards Circular No. 467, U. S. Gov't. Printing Office, Washington, D. C., 1949.
23. R. E. Fox, W. M. Hickam, and R. Kjeldaas, Jr., Phys. Rev. 89, 555 (1953).
24. D. C. Frost and C. A. McDowell, Proc. Roy. Soc. (London) A232, 227 (1955).
25. C. E. Melton and W. H. Hamill, J. Chem. Phys. 41, 546 (1964).
26. G. G. Cloutier and H. I. Schiff, J. Chem. Phys. 31, 793 (1959).
27. A. J. C. Nicholson, J. Chem. Phys. 39, 954 (1963).
28. R. E. Fox and W. M. Hickam, J. Chem. Phys. 22, 2059 (1954).
29. J. D. Morrison, 12th Annual Conference on Mass Spectrometry and Allied Topics, ASTM Committee E-14 on Mass Spectrometry, Montreal, Canada, 7-12 June, 1964.
30. M. I. Al-Joboury and D. W. Turner, J. Chem. Soc. 1963, 5141.
31. J. T. Tate and P. T. Smith, Phys. Rev. 39, 270 (1932).
32. D. C. Frost and C. A. McDowell, J. Am. Chem. Soc. 80, 6183 (1958).
33. C. E. Brion, J. Chem. Phys. 40, 2995 (1964).
34. Modified Model 12-100 with a 12-107 ion source used in a conventional manner.

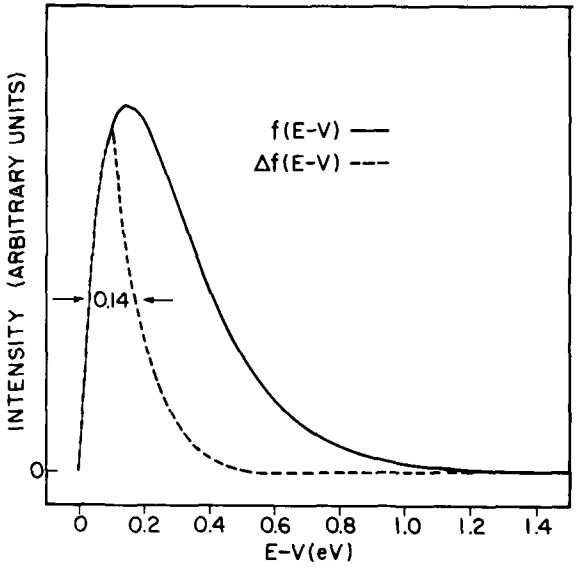

Figure I

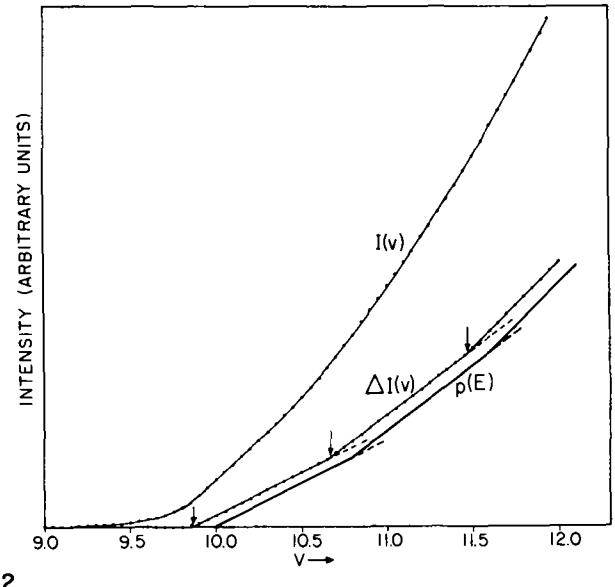

Figure 2

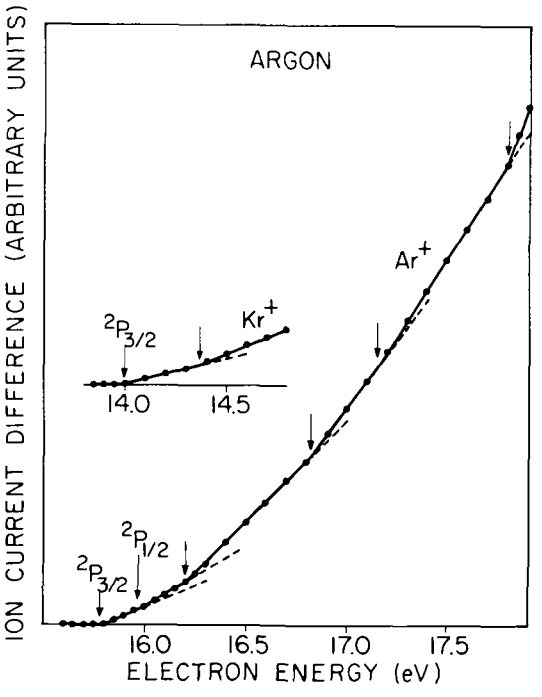

Figure 3

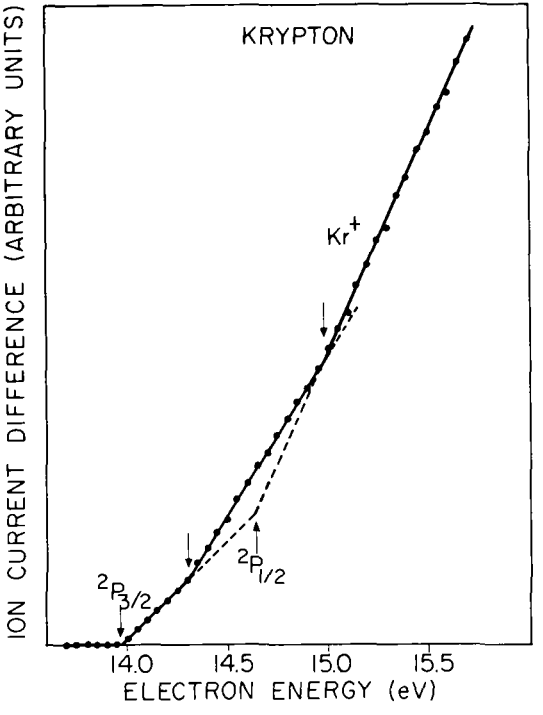

Figure 4

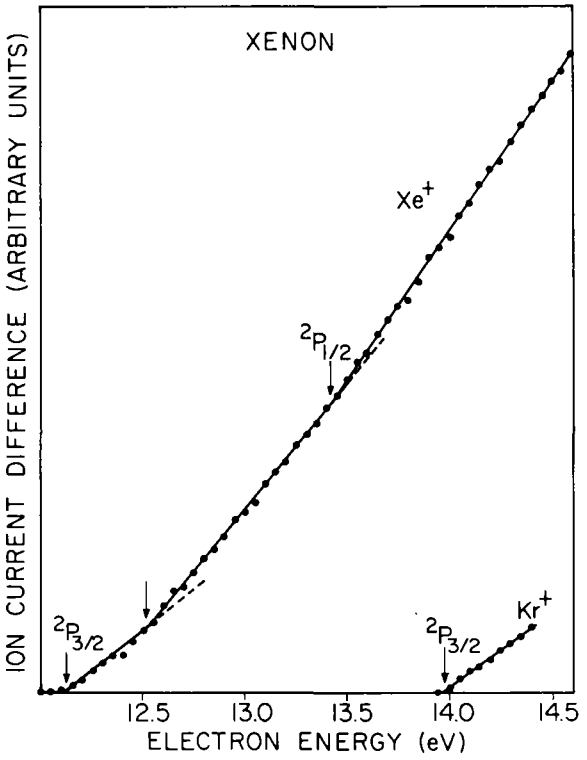

Figure 5

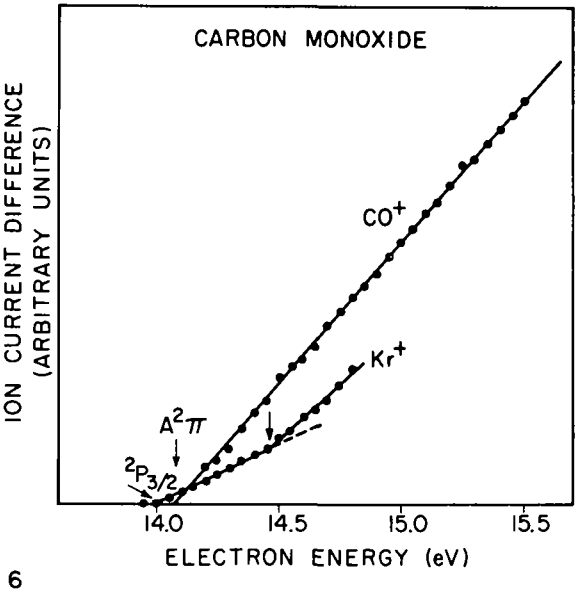

Figure 6

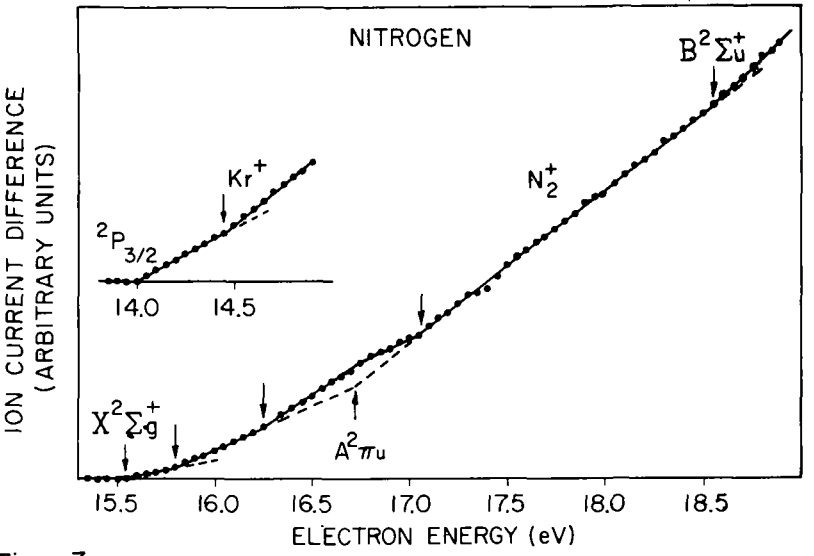

Figure 7

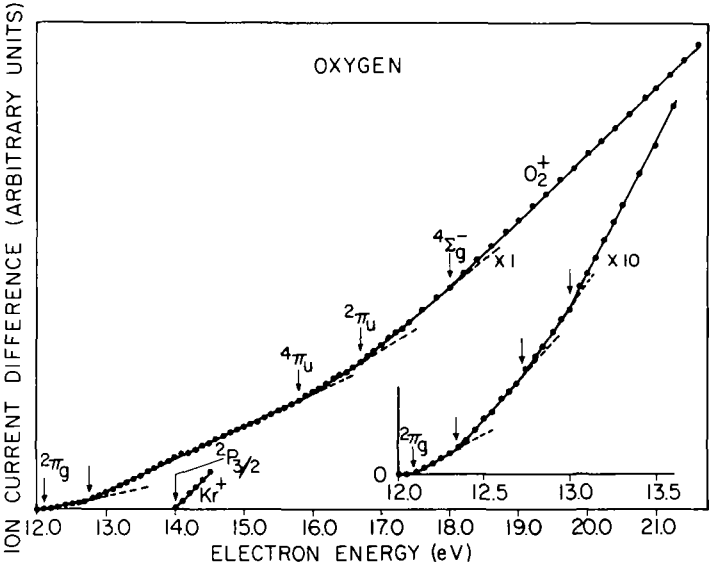

Figure 8

Fine Structure in Appearance Potential Curves by Instrumental and Analytical Techniques*

Dwight A. Hutchison

Argonne National Laboratory, Argonne, Illinois

Many workers have by various techniques made reduction of the energy spread in electron beams used for the production of ionization. As the energy spread is reduced (to 0.1-0.05 ev width at half maximum) so is the electron beam intensity ($< 10^{-8}$) with consequent reduction of collected ion current ($< 10^{-16}$ amps) near threshold for ionization. Difficult experimental problems arise in the detection of these small currents due to inherent noise.

Our method of selecting a known electron-energy distribution consists of an electrostatic parallel plate device. The energy distribution is measured by another parallel plate energy analyzer. Ions formed by the electron beam are magnetically analyzed in a 12" radius 60° sector field and collected by a 17-stage Cu-Be electron multiplier. The output pulses go to a preamplifier, a discriminator, and from there to a 400-channel multiscaler analyzer equipped with CRO, paper punch, typewriter, and plotter read-out devices. A count-rate meter in parallel with the multichannel analyzer measures the counts at a given electron energy. A recording of counts is used to monitor changes in the many voltages governing the operation of the electron and ion lenses in our system. Data to be presented consist of 20 sec ion-count scans over 0.5-3.0 volt intervals near ionization threshold. Random noise associated with the ion signals is averaged out as the square root of the number of scans which amount to 50-250 scans in present experiments. Computer smoothing of the data by binomial and Fourier methods is performed before taking a first derivative of an appearance potential curve. Smoothing is performed until certain statistical conditions are met for the removal of random variations in the data. We have investigated the fine structure in the ionization near threshold due to impact by energy selected electron beams in the gases He, Ne, Ar, and Kr. The smoothed first derivative curves are compared with photoionization and electron-scattering data. Evidence for direct ionization, autoionization, and compound formation are considered.

*Based on work performed under the auspices of the U. S. Atomic Energy Comission.

TECHNIQUES FOR IMPROVING THE CRT DISPLAY OF RAPID SCANNING MAGNETIC DEFLECTION MASS SPECTROMETERS

by George E. Salser
New York University, School of Engineering and Science
Bronx, New York 10453

When displaying mass spectra, one of the common problems is legibility. We will consider two of the many reasons for this. The first being the fact that the mass units appear as an inverse function of the acceleration voltage. Thus if we have a sweep which is linear with respect to time, as one obtains from an oscilloscope, we end up with a spectra packed at one end of the display. A second problem arises with oscilloscope display of spectra. The spot velocity is not uniform with time, being many times greater when traversing a peak as when traversing the base line. The result, with photographic recording of the oscilloscope trace is normally a badly overexposed base line with peaks barely visible. We have developed methods for solving these problems.

In our case we sweep a 60° sector mass spectrometer electrostatically at speeds of from 4 seconds to 20 milliseconds per sweep (6000-1000 volts). The rapid scan speed is used for studying transient phenomena while the slower scan is used for steady state studies. The electrostatic sweep is controlled by the sweep signal of the control oscilloscopel. The spectra are photographed from an ITT 17" oscilloscope which is slaved off of the control oscilloscope, a Tektronix.

The first device makes the mass peaks appear in a more or less linear fashion on the oscilloscope screen. We refer to this device as a "Curve Shaper" since it shapes the linear sawtooth into a hyperbolic function.

The first slide shows the spectra of n-butane. The lower spectra is without the curve shaper and the upper is with the curve shaper in operation. Not only is the trace more legible, but the frequency response requirements of the equipment are reduced. The 17" scope has a frequency limitation of 10 kc and thus frequency requirements are important. When we slow the spectra down for steady state experiments we use a visicorder to read out and here we only have a response of 1 kc and it is again important to spread the peaks in a uniform manner.

The basic element in the curve shaper is the varistor. Slide 2 illustrates a simplified version of the circuit using this device. The resistance of the varistor is a function of the applied voltage, the resistance decreases as the voltage increases. The equivalent ohmic expression for the action of the varistor is

$$I = KE^{\eta}.$$

If we feed the sweep input as shown in slide 2 we obtain a varistor output as shown. If this feeds the accelerator we obtain the desired sweep curve. The ganged potentiometer enables us to obtain a variation in the shape of the curve without affecting the endpoints.

Unfortunately, the desired degree of shaping cannot be obtained in one varistor stage. The actual circuit is shown in slide 3. Here we have 3 stages of varistor shaping, each is fed with its own cathode follower to give us the required impedance match. Unfortunately varistor shaping is a degenerative process and reduces the voltage level of the signal. Therefore we must amplify the signal and adjust the zero level after shaping. This is done by the 12AU7 following the last varistor stage. The zero level is controlled by the 500 K potentiometer in the output of this stage. Control D is a simple gain control feeding the cathode follower output to the accelerator. The ganged controls A, B, and C control the degree of shaping. It has been found that each varistor tends to affect one portion of the curve more than other portions and consequently, a certain amount of adjustment is required for the best display.

The range of shaping which may be obtained is demonstrated in Slide 4. The upper curve is the sweep with no shaping, the lower with maximum shaping and the middle is the shaping we normally use. The unit is frequency insensitive from DC to 2000 Hz. The upper frequency limit is determined by the capacitance of the varistors. The stability is excellent.

The second device is a Z-axis modulator which brightens the peaks of spectra so that they may be readily photographed. Slide 5 shows two spectra. The lower spectra was taken with no Z-axis modulation. In our work on transient phenomena we may read as many as 1000 frames per run. One can hardly blame the reader for mistakes when reading spectra such as this. The upper spectra is, of course, that taken with the Z-axis modulator.

The circuit of the modulator is shown in slide 6. The gate signal from the Techtronix scope is normally fed to the Z-axis of the ITT scope to blank the return trace. Instead we feed it to the Z-axis modulator. The vertical input is fed to T_1. T_1 and T_2 are used to preserve phase relationships and obtain proper impedance matching. T_2 also gives us a good deal of gain. Only when the vertical input is changing rapidly will the capacitor in the input signal path of T_1 pass a signal. The signal from T_1 is taken from the emitter and coupled to the emitter of T_2. Thus as the input to T_1 rises the current through T_2 decreases and the voltage at the collector of T_2 rises, brightening the trace. The point at which brightening begins is controlled by potentiometer (b) and the brightness by potentiometer (a). The ITT scope has two grids in its CRT, one for Z-axis control and one for brightness. We have found that the brightness control of the oscilloscope can be used for controlling the base line and the Z-axis modulator for the peaks.

Another improvement related to the detector or readout of mass spectrometers is a method for regenerating electron multipliers. We work a great deal with fluorine and have found that with time the gain of the electron multiplier deteriorates. By treating them with hydrogen in the presence of a glow discharge, we have been able to return them to substantially their original gain. The method of regeneration was to establish a glow discharge between two adjacent dynodes in a hydrogen atmosphere at from 1-5 torr, and with continuous flow of hydrogen. Each dynode was treated in this way, being used as both a positive and a negative electrode in relation to its neighbors. The discharge was initiated with a Tesla coil. After reduction with hydrogen, the dynodes were oxidized with oxygen using the same procedure.

It would appear that the method has general application in regeneration of electron multipliers. The rule would appear to be that if the contaminating element will form a gaseous compound which can be purged, regeneration will be successful. Treatment with a Tesla coil alone (a procedure sometimes recommended) gave only small improvement. The type of multiplier used was an RCA C-7187K with Cu-Be dynodes and external resistor network. After treatment the gain was returned to nearly that of the new multiplier.

Acknowledgement

We would like to thank the sponsors whose support made this work possible, namely the Air Force Office of Scientific Research under contract AF 49(638)-173 and the National Aeronautics and Space Administration under grant NASR-183. I would also like to thank my colleague Dr. L. Dauerman for his help and assistance.

Slide 1

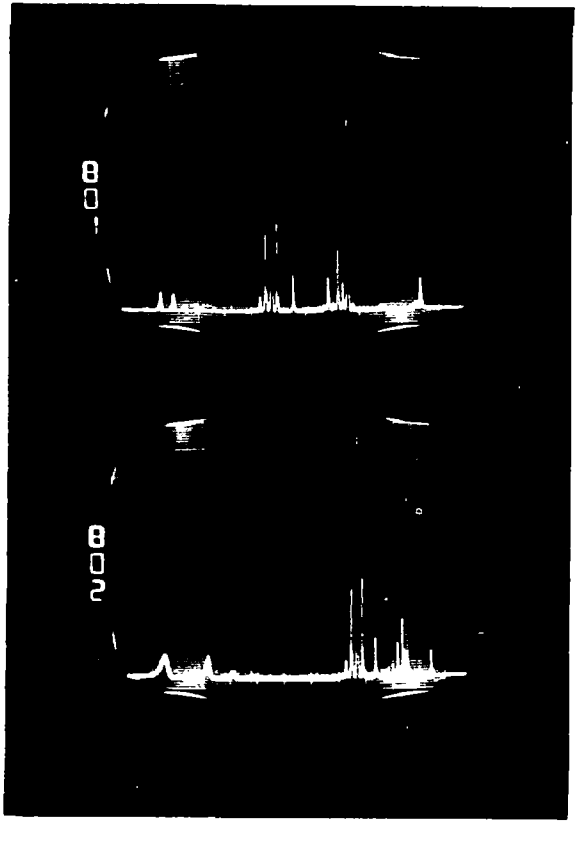

Slide 4

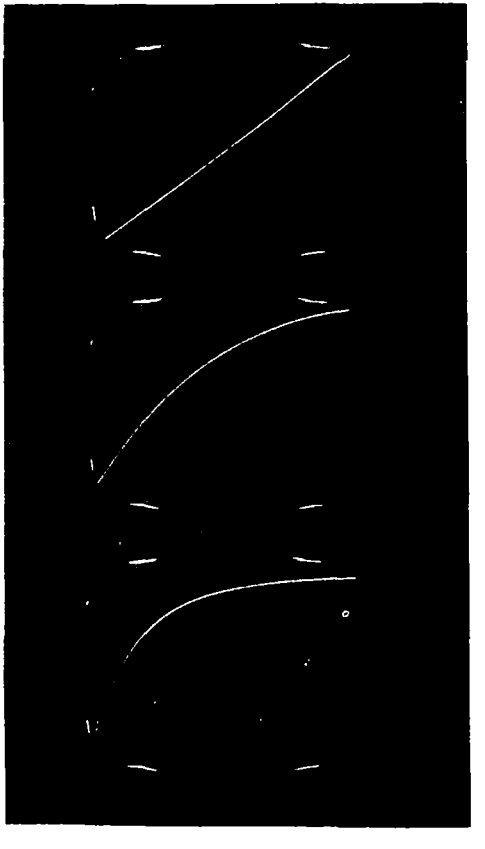

Simplified Curve Shaper · Slide 2

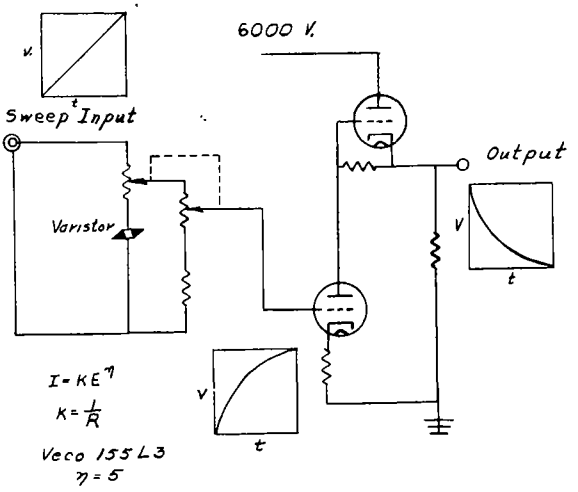

Curve Shaper Slide 3

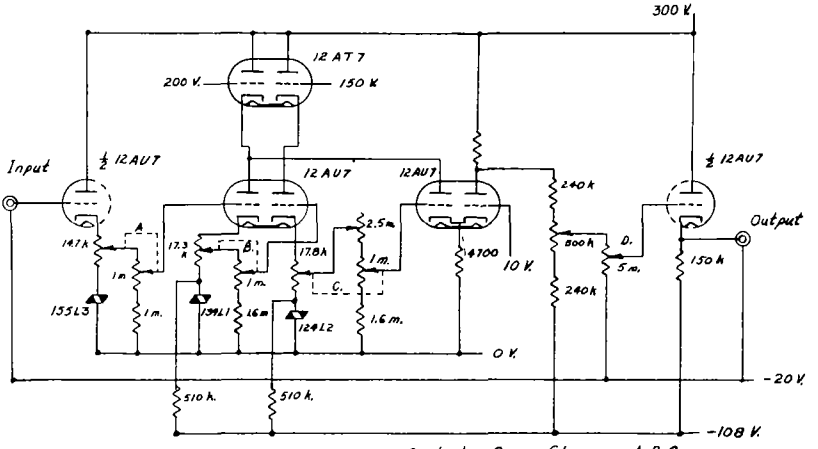

Varistors - Victory Engineering Corp. Springfield, N.J.

Controls - Curve Shaping A, B, C
Gain D.

Slide 5

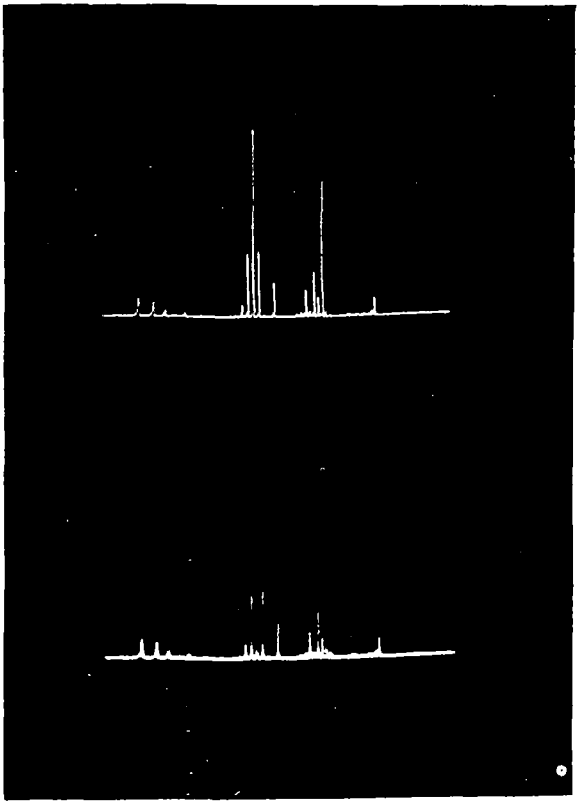

Z-Axis Modulator Slide 6

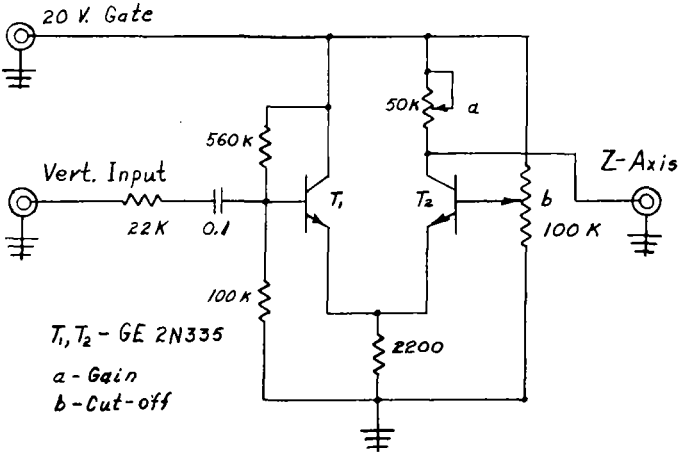

Computer Data Processing for Time Resolved Mass Spectrometry*

R. T. MEYER, C. E. OLSON and R. R. BERLINT
Sandia Laboratory, Albuquerque, New Mexico

ABSTRACT

Time resolved mass spectrometry is a potentially powerful tool for the study of rapid chemical processes. It provides a simultaneous record of mass number and ion intensity as a function of time. The number of datum points which can be generated is large; for example, a few thousand measurements are obtained in a single flash photolysis experiment. Data refinement, which incorporates corrections for systematic instrumental variation, impurity contribution and dissociative ionization, is often necessary before even simple kinetic interpretations can be attempted. A CDC 3600 Fortran program has been written to provide this data processing. Input consists of punched cards containing mass number, time reference and peak amplitude. The program can accommodate 50 masses, 250 equally-spaced time points and amplitudes ranging from 0 to 9999 (arbitrary units). Ion intensities are referenced point-by-point in time to an internal, inert standard substance to achieve correction for systematic variations. Background ion and desorbed impurity ion contributions to each mass, obtained from control experiments, are subtracted. Pre-flash data are averaged and mass-designated ion intensity ratios are calculated to provide fragment ion to parent ion ratios. An optional input scheme allows dissociative ionization factors to be supplied where several parent molecules, with overlapping mass spectral patterns, are present in the reaction mixture. A similar scheme is available for final product analyses. A plotting subroutine permits automatic oscilloscope plotting of ion intensity versus time for each mass. The ion intensity scale range can be fixed or variable. The time scale is absolute with zero time determined by experimental parameters.

INTRODUCTION

Time resolved mass spectrometry has been adapted to reflected shock tube gaseous decompositions,[1,2] flash pyrolysis of plastics[3] and celluloses,[4] gaseous desorption from heated filaments[5] and flash photolysis.[6] The flash photolysis technique is being applied by one of the authors of this paper (RTM) to gas phase chemical kinetic studies.[7-10] All of these studies have in common an enormous and complicated data reduction requirement.

Time resolved mass spectrometry provides a simultaneous record of mass number and ion intensity as a function of time. The number of datum points which can be generated in a single flash photolysis experiment, for example, is 2000 if 20 masses are observed for 100 successive points in time. By the time several experiments have been performed, the number of data amount to 10^4 or more. In addition, several corrections must be applied to the data before even simple kinetic interpretations can be attempted. The present paper describes a CDC 3600 Fortran program which has been written to provide this data processing. Although the general features of the program are applicable to the several types of studies mentioned above, the discussion will be in terms of typical flash photolysis experiments involving gaseous species.

EXPERIMENTAL DESCRIPTION

Consider a mixture of gases in a reaction chamber which is connected to the ion source of a time-of-flight mass spectrometer by a sampling orifice. If one of the component gases is strongly ultraviolet absorbing, a pulse of light from a flash lamp will produce photodecomposition and the initiation of a chemical reaction. The mass spectrometer, when operated at a 20 kc pulse frequency, then provides a complete mass spectral analysis every 50 μsec. If an oscilloscope display of these successive spectra is recorded with a revolving drum camera, the flash time can be adjusted so that a number of spectra of the reactant mixture are recorded prior to the flash. Thus, both pre-flash and post-flash data are obtained. The ion intensities for several masses will be changing after the flash as a result of the chemical reaction. The resolution of these changes is desired to elucidate the chemical mechanism. However, electromagnetic

*This work was supported by the United States Atomic Energy Commission.

interference from the flash lamp discharge frequently leads to a perturbation of the spectrometer response. In addition, the flash heating of the gases in an open-ended vessel manifests itself in a density decrease. Systematic variations of this type are accounted for by the incorporation of an inert reference gas such as argon in the reaction mixture.

Contributions to mass peaks from the spectrometer background or from non-reactive impurities in the gaseous mixture may be corrected for by performing a control experiment. In this experiment, the reactant mixture is reproduced except that an inert gas is substituted for the substance which is ultraviolet absorbing. It is essential to operate at the same total sample pressure since the spectrometer background ionization is sensitive to the rate of sample inflow. Flash desorption of surfaces exposed jointly to the flash lamp and the ionization zone leads to a transient background. This is also recorded quantitatively in the control experiment.

When a single reactant gas is utilized or when several gases not having ion fragments of the same mass/charge ratio are used, the fragment ion to parent ion ratios can be computed from the pre-flash data. This same principle applies to product molecules, once the reaction has gone to completion. For mixtures of molecules whose spectral patterns overlap, blank experiments can be performed on the pure gases or on simulated mixtures to obtain these ratios.

PROGRAM DESCRIPTION

MASPCTRO is the 3600 FORTRAN program which provides the computations and corrections. It includes a subroutine program PLOTSPCT, which generates a magnetic tape required for the data plotting operation. The program can accommodate 50 masses, 250 equally-spaced time points and amplitudes ranging from 0 to 9999 (arbitrary units). The data deck consists of a single card for each mass, ion intensity and time set of information. This deck may be punched by hand or, as in the present work, may be obtained directly from the card punch of a Telereader film reading instrument. A summary flow chart of the calculational program is given in Fig. 1. The details of the mathematical procedures and the program structure

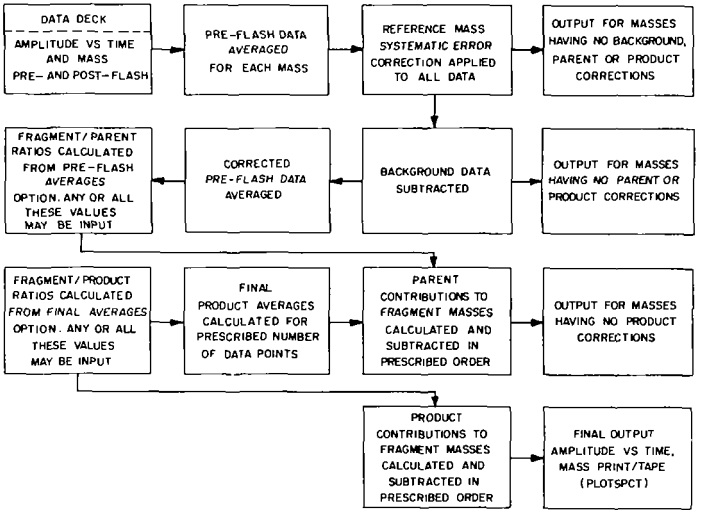

Fig. 1 Simplified flow chart of MASPCTRO computer program.

will not be discussed here.

The pre-flash and post-flash data from each experiment are initially lumped together. An instruction parameter defines the break between the data and permits the pre-flash data to be averaged for each mass. Averaging is necessary since the statistical fluctuation in the number of ions from cycle to cycle of spectrometer operation is significant. Systematic data variations are then smoothed out by multiplying the ion intensities point-by-point in time by the ratio of the reference gas pre-flash average to its actual value at each point in time.

Background data from the control experiment are supplied as a second data deck immediately behind the primary experiment deck. These data are treated similarly up to the point of subtraction from the primary data. The background-corrected pre-flash data are averaged again and from these averages are calculated the fragment ion intensity ratios.

The parent mass and its fragment masses are declared in the input instruction deck. The program will accommodate 20 parent and 20 product molecules, each having as many as 30 fragments. (The total number of masses cannot exceed 50, however.) If a fragment ion is the fragment of more than one parent molecule, the ratios can not be calculated from the pre-flash data of that experiment. Therefore, an option allows these ratios to be declared as input data. In this case, the order of the parents must be designated to allow for a stepwise calculation and subtraction of the fragment contributions from a given parent before pro-

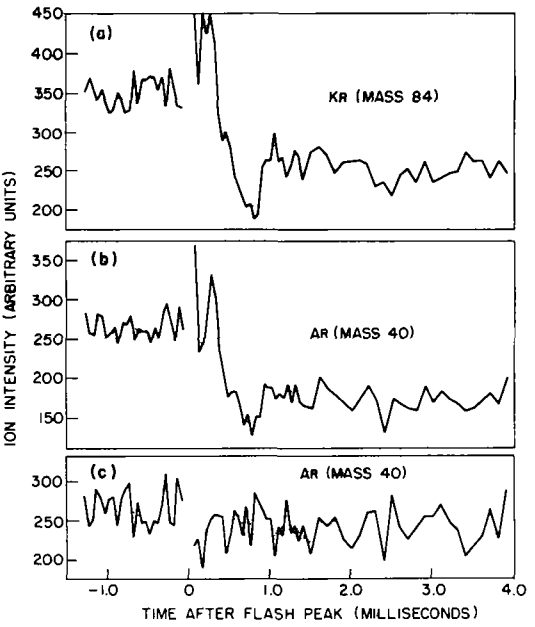

Fig. 2 Systematic error correction to argon ion intensities using spectrometer response to krypton as an internal reference: (a) and (b) show electromagnetic interference and flash heating effects upon krypton and argon ion intensities in flash photolysis experiments; (c) corrected argon ion intensity versus time.

ceeding to the next parent. This is necessary since a parent mass may overlap with a fragment mass. The fragment contributions to the several masses are subtracted for all the data points, both pre-flash and post-flash. With this done, the final product averages can be computed.

These final averages are used to compute fragment ion to product ion ratios in the same manner as done for the reactant parents. The fragment contributions are calculated and subtracted. The final result is an output of ion intensity (amplitude) versus time for each mass with corrections for systematic error, background contributions and parent and product dissociative ionization. Output consists of both a printed listing and the PLOTSPCT magnetic tape.

In addition to the final data print-out, the values of the several averages and ratios are printed. A print option allows any or all intermediate values in the computation to be recorded. A plotting option provides for either a computer determination of the optimum ion intensity scale for each mass or an operator selection of the same scale for every mass. Seven scales are available which cover at one extreme the range -1000 to +4500 and at the other extreme -10 to +45 (arbitrary units). The time scale for plotting is absolute and is determined by experimental parameters which are included as input in the instruction deck. The time

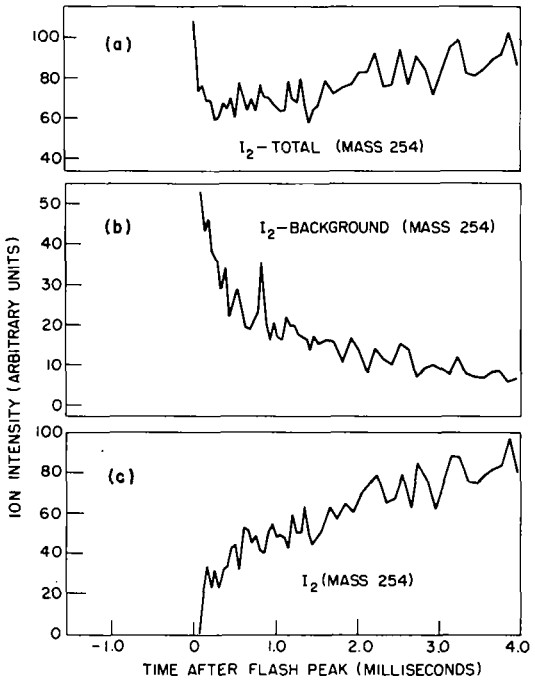

Fig. 3 Background contaminant correction to time resolved formation of molecular iodine in the flash photolysis of methyl iodide: (a) total ion intensity at mass 254, representing sum of I_2 formed during reaction and I_2 desorbed from external walls of reaction vessel; (b) ion intensity of flash desorbed I_2 recorded from a control experiment; (c) corrected I_2 ion intensity versus time.

between data points is established by specifying the number of spectra recorded within a total period of time. Zero time, in the flash photolysis experiments, is taken at the peak of the flash pulse. This is measured with respect to the last spectra recorded before the flash.

The plotting is done by a S-C 4020 High-Speed Microfilm Recorder in an off-line operation. A 9.5 inch camera records the ion intensity versus time data display for each mass as a 7.5 inch square on sensitized vellum paper.

APPLICATIONS

The features provided by this data processing and plotting program are, perhaps, best illustrated by several examples from flash photolysis experiments. Figures 2a and 2b show the spectrometer response to Kr^{84} and Ar^{40} in an experiment in which both flash heating and flash interference occurred. The reactant mixture consisted of CH_3NO_2 + 0.5 Ar + Kr at a total pressure of 3.9 torr. The nitromethane absorbs ultraviolet radiation, decomposes and releases excess energy to the system as heat.[9] The ringing response which occurs during the first millisecond after the flash results from a pulsed electromagnetic field interacting with the spectrometer output. The signal depression which persists out to four milliseconds reflects a gas density decrease due to flash heating and gas expansion. When the Kr^{84} is used as an internal reference to correct for these systematic errors, the Ar^{40} data transform to that shown in Fig. 2c. The ringing has been fully eliminated and the signal decrease has been

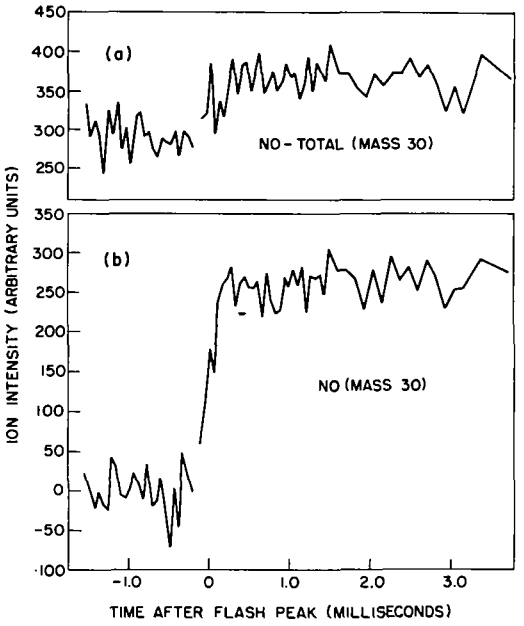

Fig. 4 Correction to mass 30 ion intensity due to NO_2 fragment ion (NO^+) contribution in the flash photolysis of NO_2: pre-flash amplitudes in (b) show that mass 30 ion intensity is completely corrected; indication of NO formation from flash decomposition of NO_2 in (a) is verified in post-flash data of (b).

almost completely normalized. Thus, there is no net change in the argon, which is what is expected.

In some recent work on the flash photodecomposition of methyl iodide (CH_3I + 0.5 Kr + 25 He, 11.7 torr), the formation of molecular iodine as a product has been time resolved, Fig. 3a. Some iodine gets trapped on surfaces between the reaction vessel and ionization chamber and is not readily pumped away under vacuum. Thus, it is subject to flash desorption in a subsequent experiment. Figure 3b shows the appearance of flash desorbed iodine in a control experiment (0.5 Kr + 26 He, 12.7 torr). The iodine persists for several hundred microseconds while it is being reabsorbed. When this background is subtracted from the primary data of Fig. 3a, the resultant data of Fig. 3c are obtained. Now the time dependence of the iodine growth can be analyzed for its kinetic significance.

The usefulness of applying corrections for reactant molecule fragments to the data is illustrated by the results from a study of the nitrogen dioxide sensitized reaction between hydrogen and oxygen.[8] Nitric oxide (mass 30) is both a product of nitrogen dioxide photodecomposition and an ionization fragment of nitrogen dioxide. To obtain a measure of the amount of NO formed in the reaction, therefore, requires that the NO_2 contribution to mass 30 be subtracted. The fragment (mass 30) to parent (mass 46) ion intensity ratio is obtained from the pre-flash data of Fig. 4a and a similar plot for NO_2. Multiplication of this ratio times the post-flash data for NO_2 gives the fragment correction to be subtracted

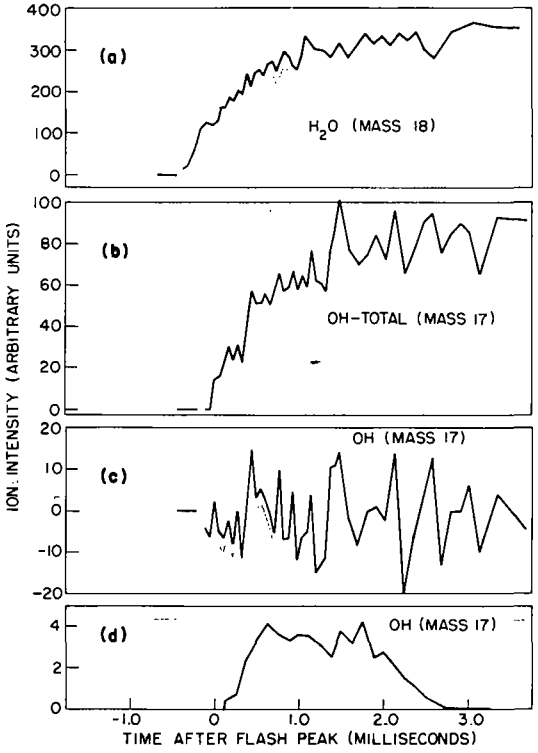

Fig. 5 Correction for OH^+ fragment ion arising from H_2O as a reaction product in the flash photolysis of NO_2, H_2 and O_2: (a) time resolved formation of H_2O; (b) total mass 17 ion intensity, representing sum of ions from OH radicals and dissociative ionized H_2O; (c) corrected mass 17 ion intensity computed from actual data points in (a) and (b); (d) OH radical ion intensity versus time obtained from statistically smoothed curves of data in (a) and (b).

from the post-flash data of Fig. 4a. Figure 4b shows the net result of this correction to the mass 30 ion intensity and represents, therefore, the time resolved formation of NO in the reaction.

The importance of considering fragment contributions from product molecules must also be stressed. H_2O (mass 18) is another final product of the aforementioned reaction of NO_2, H_2 and O_2. The ionization of H_2O gives a fragment of mass 17, corresponding to the OH^+ ion. Figures 5a and 5b show the mass 18 and mass 17 responses, respectively, after the flash irradiation of the sample. When the final data points, after reaction termination, are used to obtain the fragment to product ratio, the mass 17 data can be corrected to resolve any other contribution to this mass. The result is shown in Fig. 5c. It certainly appears, from the scatter of points above zero, that there are no free hydroxyl radicals present in the reacting gas. However, one has to be careful when dealing with transient species of low relative concentration. Since the fluctuations in the data are largely statistical, successive manipulations of the data lead to a magnification of the scatter. If smooth curves are drawn through the raw data of Fig. 5a and 5b and if new points are taken from these curves for computation, then Fig. 5d is obtained as a result. The presence of the hydroxyl radical is now clearly established.[8] For this particular example, the smooth curves were drawn by hand. It is planned that a polynomial least squares curve fitting routine will be incorporated into the MASPCTRO program in the future to provide a more accurate representation of the data.

ACKNOWLEDGMENT

The authors express appreciation to Mr. James M. Freese for valuable assistance in performing the experiments and in processing the data and to Mrs. Alexandria Alexander for film reading services.

REFERENCES

1. J. N. Bradley and G. B. Kistiakowsky, J. Chem. Phys. 35, 256 (1961).
2. R. W. Diesen and W. J. Felmlee, J. Chem. Phys. 39, 2115 (1963).
3. H. L. Friedman, Proceedings of the Eleventh Annual Conference on Mass Spectrometry and Allied Topics, San Francisco, California, May 1963, p. 518.
4. K. A. Lincoln, Rev. Sci. Instr. 35, 1688 (1964).
5. B. R. F. Kendall, Proceedings of the Tenth Annual Meeting of ASTM Committee E-14 on Mass Spectrometry, New Orleans, Louisiana, June 1962, p. 306.
6. G. B. Kistiakowsky and P. H. Kydd, J. Amer. Chem. Soc. 79, 4825 (1957).
7. R. T. Meyer and J. M. Freese, Proceedings of the Thirteenth Annual Conference on Mass Spectrometry and Allied Topics, St. Louis, Missouri, May 1965, p. 122; to be published.
8. R. T. Meyer, Paper presented at the Division of Physical Chemistry, 151st National Meeting of the American Chemical Society, Pittsburgh, Pennsylvania, March 1966; to be published.
9. R. T. Meyer, Paper presented at the Fourth National Meeting of the Society for Applied Spectroscopy, Denver, Colorado, August 1965.
10. R. T. Meyer, to be published.

SEARCH OF THE MASS SPECTROSCOPY LITERATURE BY MEANS OF A COMPUTER SYSTEM*

J. Capellen, H. J. Svec and C. R. Sage

Institute for Atomic Research and Department of Chemistry
Iowa State University, Ames, Iowa

Since mass spectroscopy is being currently used in all of the physical and in many of the biological sciences, publications describing results are found in widely diverse journals. This diversity coupled with the present day proliferation of the general scientific literature has made manual searching of the literature an increasingly burdensome task. For many years the members of the mass spectroscopy group at the Ames Laboratory of the Atomic Energy Commission have tried to keep up with the literature dealing with mass spectroscopy by the usual manual searching methods, aided by what bibliographies were available. The computer system[1-7] designed by Sage, Anderson and Fitzwater for the selective dissemination of information, SDI, offered hope of lightening the burden associated with literature searching. Therefore, we set up a "profile" and a three month test was made, during which the efficacy of parallel manual and computer searches were compared. The test showed that at least 98 percent of the documents located manually were in the notifications generated by the computer system. Of greater significance, however, the test showed that the manual method was locating only about one-fourth of the documents of interest to us when compared with the notifications generated by the computer system. These test results convincingly showed that full scale use of the computer system was warranted. The profile used during the test has been subsequently improved and if the test was rerun now, the results would be even more convincing.

Fig. 1 shows the general flow diagram of the Ames Laboratory SDI computer system. There are three vital parts in this flow diagram, the source of documents, the computer and the user. Later in the text we will further define the other terms that appear in this figure.

The document input can be in any machine-readable form, however, the format and sequencing must follow the same restrictions required for KWIC (Key Word in Context) indexing. It is only necessary to feed titles and authors' names into the computer but one can also add the source, abstracts, complete texts or key words of the abstract or text. Two sources of documents are beingly routinely used at present. One is the tapes from the weekly Magnetic Tape Service of U. S. Patents and Scientific Journals as indexed in the Science Citation Index and supplied by the Institute for Scientific Information, ISI, or Philadelphia, Pennsylvania. The other is tapes of Nuclear Science Abstracts (NSA) supplied by the Division of Technical Information Extension Service, Oak Ridge, Tennessee.

The computer system has fifteen programs which are used to scan the input documents, match profiles with input, generate notifications, update significance factors and perform other associated functions. The notifications are printed on cards and sent to the user.

The user has to fulfill two obligations in order to use the system. First, he must assemble a "profile" which represents his interests, and second, he must express judgment of the notification cards which are sent to him. The benefits the user receives from the system are proportional to the effort he spends in setting up an effective profile and his diligence in marking and returning his notification cards to the computer center. His properly marked cards are used to adjust the significance values of the entries in his profile and thus are very important in upgrading the efficiency of the system in his case.

The profile we have currently in use contains 11 uniterms, 117 word clusters of key words, 829 word clusters involving authors and their

* Work was performed in the Ames Laboratory of the U. S. Atomic Energy Commission

initials and 75 entries with a negative designation. If an entry with a negative designation is contained in the title, author list, source or abstract of a document it negates all positive matches and no notification will be generated. Fig. 2 shows sample entries from our profile. The profile may contain uniterms, that is, one term per entry, such as doublet, silicide and photoionization or word clusters such as metastable transition or J Q Public. A word cluster may contain up to six terms. The conjunction "and" is assumed when needed between the terms in a word cluster. All the terms in a word cluster must appear some where on the tape describing the document or the match is not completed. The use of authors' names and initials as word clusters does create some mismatches. For instance if J Q Doe and A B Public were co-authors on a paper, the computer would pair J Q from one author with Public from the other and consider it a match. We thought initially that this would be rare but it turns out that it occurs much more frequently than was considered possible.

Each profile may contain up to ten thousand uniterms or word clusters, and each user may have more than one profile. Thus, the user has virtually no limitations in setting up his profile. Each entry in the profile is initially assigned a significance value which can range from 0.0001 to 0.9999 and is used to determine when a notification should be generated. This value is automatically adjusted up or down by the computer on the basis of the responses on the notification cards that are returned and the number of matches that have occurred. If a match between any entry in the profile and the input occurs, but for some reason no notification is generated, the significance value of the matched entry is still increased but very slightly.

Each term is assigned a character count. If the character count is equal to the number of letters in the term, the term will match with itself and all longer words which start with the same sequence of letters. If the character count is larger than the number of letters in the term, the term will match only with itself.

Fig. 3 shows a use of this character count to cover several terms. The word clusters MASS SPECTR, with MASS having a character count of 15 and SPECTR having a character count of 6 will match with the word MASS and any other word starting with SPECTR such as spectra, spectral, spectrum, spectrometry, spectrograph, etc. It does not cover massenspectr because this is a single word or Masse spectr because the MASSE does not match MASS exactly. In this case the German and French terms would have to be included in the profile. All words containing four letters or less are automatically given character counts of 15 in the SDI system so we cannot assign a character count of 4 to MASS.

Fig. 4 shows a notification card generated by the computer while using ISI tapes as input. The left section of the card, shown above, will list the first five authors, if there are that many. If more than five authors are associated with the document they are all checked against the profile but only the first five are listed on the card. ISI tapes give only the initials of the authors with their last names. If an author uses three initials, ISI gives only the first seven letters of his last name. If an author uses one or two initials, only the first eight letters are used. Last names that are truncated are denoted by a period after the truncated name. Note that this card also contains the title, the source, a description of the document and any uniterm or last term of any word cluster that was matched. There may be as high as nine such matches listed on the card. The significance value of the matched entry is listed beside it. If only one match is listed the significance value of the entry becomes the total significance value and must exceed a threshold for the entry before a notification is generated. The threshold value is set initially by the computer group. It will be 0.3000 for ISI runs and 0.5000 for NSA runs.

The right half of the card, shown below, is the response card. It contains the user's name and location, the date of the computer run, the user's profile number, the selection number and five responses associated with Port-A-Punch boxes. The user selects the appropriate response and punches the corresponding box.

Fig. 5 shows the notification card generated by the computer when NSA tapes are used as input. The right hand sides are identical but there are several differences between the left hand section of this card and that from ISI. One difference in the left section is in the author listing. Only two authors are printed on the notification card. They appear just as they did on the original publication including first names if they were used. If more than two are associated with the document, all names are checked against the profile but only the first two are subsequently listed on the card. Another difference is that the month of the journal is given instead of the volume number. The cards do give the volume of Nuclear Science Abstracts in which the document is abstracted and the abstract number. The main difference between the two inputs are that key words from the abstracts are included on NSA tapes and as many of these key words for which there is room are listed on the card.

The notification cards are returned to our document library where they are torn in half. The right halves are sent to the computer center where the significance values of the entries are adjusted according to the type of user response. The value is increased for the first two positive responses, "Of Interest, Document Requested" and "Of Interest, Document Not Requested". The value is decreased for the single negative response, "Of No Interest". If the "Impartial, Don't Adjust Profile" or "The User Above is Absent" boxes are punched the value remains as it was. When the cards are not returned within a specific time, the computer adjusts the significance values as if all the responses were negative. If this is allowed to continue the number of your notifications decreases rapidly.

The word clusters ISOTOPIC COMPOSITION and ISOTOPIC ABUNDANCE are in our profile. These key words were matched against the profile as can be seen by the entries on the card. The word isotopic was used twice, once with COMPOSITION from the title and once with ABUNDANCE from the list of key words in the abstract. When more than one match occurs, a total significance value is calculated according to a regular formula which I will not give here for lack of time. If the total significance value exceeds the threshold, a notification is generated.

Since the authors' names on the NSA tapes are the same as they appeared on the publication, and the authors' names on ISI tapes have only initials, we have some problems with our author profile. In order to cover all possibilities we should include all possible combinations in our profile. At the present time however we are using the last name of the author , with as many combinations of initials as he is known to use in his publications. We therefore match with the authors on NSA tapes only when they use initials. We must rely upon our topic profile to pick up the documents in cases where the authors use a first or second name. This works fairly well because the NSA tapes have the key words on them. We are attempting to have NSA change to a uniform system for designating authors' names. It would simplify matters if authors were consistent.

The left hand side of any notification card in which we have expressed an interest is returned to us by the document library. If the first box is punched and the journal is available in our library, the card is stamped "Journal Available". If the journal is not available, or if the card pertains to a patent or report, a memo is sent to us asking for further instructions. The cards returned to us are placed in our reference file by subject. Last year we used 101 subject categories.

At the end of the year we decided to incorporate the 1965 list of documents into a bibliography using another computer system that was available to us. There were 1591 documents in our reference file and we included the 108 papers presented last year at the 13th Annual Conference on Mass Spectrometry and Allied Topics. The bibliography was published as the Ames Laboratory report, IS-1335.

Fig. 6 shows two entries from the bibliography section of the report. The numerical code number which is on the left, is divided into three sections. The first three numbers refer to the subject category into which the document was placed. The 65 refer to the year in which the reference was collected. The last three numbers show its placement within a subject category. The bibliography contains the code number,

the title, the authors and the source.

Fig. 7 is a section taken from the author index. It lists the authors and the numerical code number or numbers of the documents with which he is connected. The names with periods are from ISI tapes and denote truncated names.

Fig. 8 shows a section from the KWIC Index. In this example the key word is ELECTRON and the titles are "wrapped around" this key word. The numerical code number for each title is listed at the right.

In our reading we still occasionally pick up documents of interest which were missed by the computer. To overcome this we are trying to improve our profile and the computer group is continuing to improve the computer system so that we hope to be able to do an even better job in the future. One program that is presently being designed will insert a semi-colon between the authors last name and his initials. The computer would then treat this as a uniterm and do away with mismatches between one author's last name and another's initials. It would help greatly if authors would use one of our key words in their titles so we wouldn't have to wait for the NSA abstract of their papers.

At the present time the SDI system at the Ames Laboratory takes about 3 1/2 hours of computer time each week. This involves 83 profiles that are currently being used by the various people taking advantage of the system. Between 6500 and 7500 documents are scanned weekly by the computer. Each week our group receives about 180 notification cards or one card for every 40 documents scanned. About one-sixth of the notifications are of interest to us.

We have been very pleased with the results of literature searching by the computer system. In 1965 we picked up 1591 documents of interst from 341,041 scanned by the computer. The time involved was much less than was used for manual searching and even if we did no more than read only the titles, we are somewhat up-to-date on what is going on in the mass spectroscopy field.

References

1. C. R. Sage and D. R. Fitzwater, "Ames Laboratory Selective Dissemination of Information Computer System", USAEC Report IS-751, (1963).
2. R. R. Anderson, D. R. Fitzwater and C. R. Sage, "The Stability of Dynamic Feedback in an SDI System", Proceedings of the 19th International GUIDE Meeting, Toronto, October, 1964.
3. C. R. Sage and D. R. Fitzwater, "Operational Results of an Adaptive SDI System", Proceedings of the 19th International GUIDE Meeting, Toronto, October, 1964.
4. C. R. Sage, R. R. Anderson and C. H. Cameron, "Ames Laboratory SDI Reference Manual", USAEC Report IS-940 (1964).
5. C. R. Sage, R. R. Anderson and D. R. Fitzwater, "Adaptive Information Dissemination", Am. Doc. 16 No. 3, (1965).
6. C. R. Sage, "Comprehensive Dissemination of Current Literature", submitted for Publication in Am. Doc., April, 1966.
7. C. R. Sage and R. R. Anderson, "Ames Laboratory Selective Dissemination of Information Computer System - A Survey of User Evaluation", submitted for publication in J. of Chem. Doc., May, 1966.

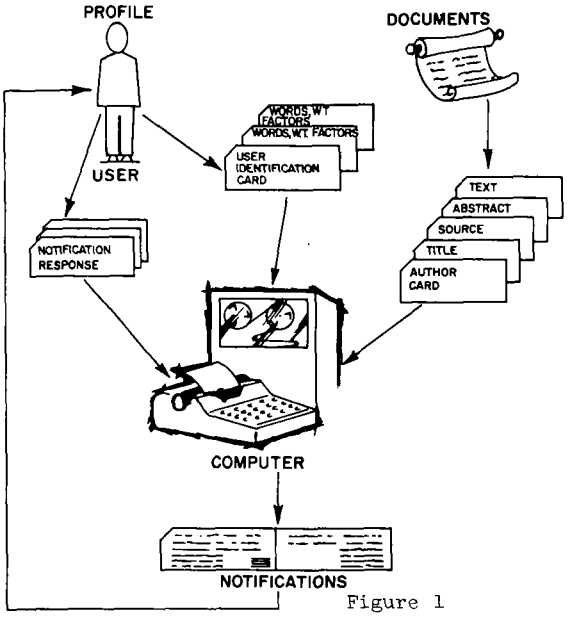

Figure 1

PROFILE SAMPLES

Uniterms

Doublet	09	0.XXXX
Silicide	08	0.XXXX
Photoionization	15	0.XXXX

Clusters

Metastable	10	
Transition	10	0.XXXX
JQ	15	
Public	06	0.XXXX

Figure 2.
TRUNCATED PROFILE TERMS

Mass	15	
Spectr	06	0.XXXX

Terms covered

mass spectra	mass spectrometry
" spectral	" spectrograph
" spectrum	" spectr.....

Terms not covered

massenspektro....
masse spectrometr

Figure 3.

DELAETER JR JEFFERY PM
ISOTOPIC COMPOSITION OF TERRESTERIAL AND
METEORITIC TIN

J-GEOPH-RES VOL- 70 PP-2895 1965 ARTICLE NO.437267
ISI ACCS.NO.65748 ARTICLE,REPORT,TECHNICAL PAPER,ETC.

TH. = .3000
TOT.S.V.=.9926

COMPOSITIO.9926

**NOTE....SPECIAL SYMBOL CONVERSIONS.....
@ = LEFT SQ.BRAC/S,ARROW OR LESS THAN
* = RIGHT SQ.BRAC/S,ARROW OR GREATER THAN
$ = APOSTROPHE

INSTITUTE FOR SCIENTIFIC INFORMATION,PHILA.,PA.

*SVEC, HARRY J. 11 CHEM 0001410 00058851
4/15/66 DATE NAME AND LOCATION SELECTION NO
PROFILE NO.0002501
OF INTEREST,DOC. REQUESTED..... ☐
OF INTEREST,DOC. NOT REQUESTED ☐
IMPARTIAL,DON/T ADJUST PROFILE ☐
OF NO INTEREST..... ☐
INSTRUCTIONS THE USER ABOVE IS ABSENT..... ☐

1 Read the Abstract
2 Push OUT the Appropriate Port-
A Punch Box with a sharp pencil
3 If you care to comment push out the comment box and write your comments on this card
4 Return this card to
THE DOCUMENT LIBRARY

COMMENTS ☐

Figure 4.

EBERHARDT, P. EUGSTER, O.
A REDETERMINATION OF THE ISOTOPIC COMPOSITION OF
ATMOSPHERIC NEON.

Z. NATURFORSCH. APR 65,VOL.19,NO.- 16,PP- 623 624, JRNL
CHEM-NSA-APR N-S-A ,USAEC.DIV.OF TECH.INFO.-

ATMOSPHERE NEON ABUNDANCE NEON 20 NEON 21 N
EON 22 TOMS WEIGH
DENSITY GASES

TH. = .5000
TOT.S.V.=.9998

ABUNDANCE .9972
COMPOSITIO.9636

*SVEC, HARRY J. 11 CHEM 000140 00058852
4/15/66 DATE NAME AND LOCATION SELECTION NO
PROFILE NO.0002501
OF INTEREST,DOC. REQUESTED..... ☐
OF INTEREST,DOC.NOT REQUESTED. ☐
IMPARTIAL,DON/T ADJUST PROFILE ☐
OF NO INTEREST..... ☐
INSTRUCTIONS THE USER ABOVE IS ABSENT..... ☐

1 Read the Abstract
2 Push OUT the Appropriate Port-
A Punch Box with a sharp pencil
3 If you care to comment push out the comment box and write your comments on this card
4 Return this card to
THE DOCUMENT LIBRARY

COMMENTS ☐

Figure 5.

SECTION OF BIBLIOGRAPHY

400 65 016 HAMILTON EI
ISOTOPIC COMPOSITION OF STRONTIUM IN A VARIETY OF ROCKS
FROM REUNION ISLAND.
NATURE, 207. 1188, 1965

520 65 001 KENNICOT. PR
SURFACE DEVELOPER FOR MASS SPECTROGRAPH PLATES.
ANALYT. CHEM., 37. 313, 1965

Figure 6.

SECTION OF AUTHOR INDEX

SCHRAM BL	350 65 016
	205 65 010
	480 65 092
SCHREIBE. K	570 65 091
SCHREINE. F	280 65 007
	280 65 017
SCHROEER JM	575 65 024
SCHROETE. SH	570 65 024
SCHROLL G	570 65 020
	545 65 002
	545 65 006
	445 65 001

Figure 7.

SECTION OF KWIC INDEX

PARAMETERS OF SECONDARY ELECTRON EMISSION.= EFFECT OF WORK F	255 65 002
COEFFICIENT ALPHA, MEAN ELECTRON ENERGIES, AND THE MOBILITY	350 65 036
FUNCTION OF BOMBARDING ELECTRON ENERGY.= RELATIVE IONIZATIO	350 65 040
ON OF ATOMIC HYDROGEN.= ELECTRON EXCHANGE IN IMPACT IONIZATI	350 65 030
CT PARAMETER METHOD FOR ELECTRON EXCITATION OF ELECTRIC QUAD	270 65 026
SOURCE WITH ADJUSTABLE ELECTRON GUN.= MAGNETIC FIELD FREE I	370 65 020
ED ETHYLENE PRODUCED BY ELECTRON IMPACT AND ARGON SENSITIZAT	245 65 010
TE OF ATOMIC HYDROGEN.= ELECTRON IMPACT EXCITATION OF 2P STA	270 65 003
C MASS SPECTROMETRY. 2. ELECTRON IMPACT FRAGMENTATION OF DIM	445 65 010
2-PYRONE.= STRUCTURE OF ELECTRON IMPACT FRAGMENTS. C4H4O CAT	490 65 030
AGMENT IONS PRODUCED BY ELECTRON IMPACT IN A MASS SPECTROMET	420 65 007

Figure 8.

The NBS Mass Spectrometry Data Center

F.N. Harllee, J. T. Herron and H.M. Rosenstock
National Bureau of Standards
Washington, D.C. 20234

Three years ago the President's Office of Science and Technology assigned to the National Bureau of Standards the responsibility for a program called the National Standards Reference Data System[1]. This program, administered by the NBS office of Standard Reference Data, has the objective of supporting and coordinating various efforts leading to compilations of critically evaluated reference data and critical review monographs.

As part of this effort, the NBS mass spectrometry section undertook to see what could be done to make more readily available the body of quantitative information on energetics of ionization processes which has been scattered in the literature. This effort culminated in the establishment of the NBS Mass Spectrometry Data Center, which is today prepared to provide rapid up-to-date answers to the questions "What is the ionization potential of molecule A?", "What is the appearance potential of ion B?", "What are the methods by which these specific numbers were obtained?", "What are the relevant references?", "What information is available on the following specific ion-molecule reactions?" In this report we shall briefly describe the workings of this data center. We feel that it has successfully met our requirements and can serve as a prototype for the processing of other moderate sized bodies of information (See fig. 1). We shall discuss in turn

1. Literature search and control
2. Data abstracting
3. Information storage
4. Retrieval and printout
5. Miscellaneous shortcuts
6. Dissemination
7. Some statistics and general comments

1. Literature search - It was decided to restrict coverage to the years since 1955, because of the availability of the Field and Franklin compilation[2]. Up to 1964, the literature references were initially obtained by using the various bibliographies of E-14 Subcommittee II, the compilations of Kiser[3], the bibliography in Advances in Mass Spectrometry[4] and in various review articles. In addition, all citations in these papers were checked. Since 1964, the primary search has been based on Currents Contents and Physics Abstracts. Document control is maintained by a simple first author indexed card file and accession number. Reprints of all articles are filed by accession number.

2. Data abstracting - Each document is read completely and all numerical and related information extracted and recorded. This includes limits of error, method, and detailed information on electronic or vibronic state where indicated. Document citations are checked against the document file to insure completeness.

3. Information storage - All information is transferred to punched cards. This includes one or more lines of numberical information and the complete reference including title (See fig. 2). The punched cards are verified and filed in the complete reference, brief reference and data files. In addition to the information described just above, additional columns are punched to permit a certain amount of subclassification and, <u>most important</u>, to permit orderly resequencing of the punched card files at any time by a few automatic card sorting operations.

The complete and brief reference files are maintained in order of accession number. The complete reference cards (several cards per reference) are maintained in complete continuation card order and can be so sorted by use of additional column punches. In addition, columns are punched which permit sorting according to year of reference.

The data file is arranged according to the empirical formula of the ion. Ions containing deuterium are stored separately, while all other isotopic species are stored together with their normal counterparts. These cards are punched to permit resequencing by sorting according to atomic numbers and number of atoms (up to four elements). Isomeric species are ignored for sorting purposes, although that information is so printed out. The data cards may also be sorted according to year of reference and by certain categories of methods used to obtain the numbers. The categories presently are:

a. Photoionization
b. Electron impact
c. Derived value
d. Photoelectron spectroscopy
e. Ultraviolet spectroscopy
f. Theoretical calculation
g. Photodetachment

Further, the entire data deck may be sorted according to

h. Positive ion
i. Ion pair formation
j. Electron affinity
k. Negative ion
l. Ion heat of formation

Thus, enough safeguards are built in to maintain classification by sorting procedures and to permit a certain amount of broad interrogation of the file.

4. Retrieval and Printout - The above filing and automatic sorting schemes permit ready retrieval of all data cards pertaining to particular ions, process categories or method categories for any or all years. Appropriate literature references are obtained by noting the document accession number which also is contained on each data card. The information is converted to usable form by a punched-card-controlled typewriter which produces the output shown in fig. 2.

5. Miscellaneous shortcuts - The use of punched cards for information to be typed out as well as for providing sorting categories has forced a number of compromises. This system cannot be sorted according to isomers, although the appropriate information is typed out. This presents no major problem since the amount of information on isomers is still rather small and, at worst can be readily distinguished on the typed output. The basic chemical sorting criterion adopted was based on the ion and not on the parent molecule. Ideally, one would like sometimes to ask for all information on ions from a particular molecule. Because of the limitations of the punched card it was decided to ignore this form of interrogation. Our experience to date indicates that the correct choice was made. This problem will have to be carefully considered for every such system. The use of a typewriter as an output medium limits the number of type symbols. Thus electronic state designations must be sometimes made in pidgin English (e.g. 2 PI g, 3/2 STATE) and there is not enough flexibility even for all semistructural formulas so that names must be used such as C_6H_6, Butadienylacetylene or C_6H_6, 1,3-Hexadiyne. However, the required information can be adequately conveyed, even if at the expense of some typographical elegance. Note also in fig. 2, the + instead of ± to indicate the limit of error.

6. Dissemination - The system was designed to rapidly provide numerical and literature information for specific ions. This has been accomplished. A mail or telephone request for specific information is frequently answered the same day with one or more type pages mailed to the requestor. There is no charge for this service other than the request to inform us of errors and omissions.

7. Some Approximate Statistics and General Comments -
The number of documents and data cards in this file is currently about 1000 and 10,000, respectively. This is a measure of the size of the body of information deveopled since 1955. The corresponding figures for the Field and Franklin compilation are roughly 400 and 2000, respectively. Currently some 20-30 new documents are acquired each month, and each may contain as many as ten new numbers. Clearly, the major problem was processing the information from 1955-1966. This is now completed. The problem of keeping up to date is much less severe, and the center is now in a position to cover other problems of interest. Recently, a bibliography on ion-molecule reaction from 1900 to March 1966 was completed[5] and the detailed information on these processes is being sorted out in a manner very similar to the ionization and appearance potential information. A bibliography on photoionization will be published shortly, and other problems are under study. Last, it should be mentioned that the effort described here is only a partial answer to the problem of standard reference data. The critical evaluation of this information is a separate effort, and is in progress. However, up to this point, the methods used here appear to have a wide range of application.

1. Status Report. National Standards Reference Data System. Ed. E.L. Brady, NBS Tech. Note 289, June 1, 1966.

2. F.H. Field and J.L. Franklin, Electron Impact Phenomena" (Academic Press, New York 1957).

3. R.W. Kiser, "Tables of Ionization Potentials", U.S. Atomic Energy Commission, Office of Technical Information, Report No. TID-6142, June 30, 1960 and Supplement June 20, 1962.

4. For the most recent see "Advances in Mass Spectrometry", Vol. 3 (The Institute of Petroleum, London, 1966).

5. F.N. Harllee, H.M. Rosenstock, and J.T.Herron, "A Bibliography on Ion-Molecule Reactions. January 1900 to March 1966", NBS Tech. Note 291, June 28, 1966.

MASS SPECTROMETRY DATA CENTRE - ALDERMASTON

R. G. Ridley
A.W.R.E., Aldermaston, Berkshire

An Advisory Committee (Fig. 1) was appointed by the U.K. Office for Scientific and Technical Information, Department of Education and Science, to assess the needs for a Data Centre for Mass Spectrometry, and to make recommendations as a result of which O.S.T.I. are supporting a Mass Spectrometry Data Centre at Aldermaston.

The particular projects at present receiving attention are as follows:

(1) Mass Spectrometry Bulletin

There is a real need for a regular information service to the whole field of Mass Spectrometry. It was felt by the committee that a classified guide to the current literature appearing monthly would best meet the requirement. A sample edition of such a Bulletin has been prepared at the Data Centre and it is hoped to go into monthly production in October this year. The field of relevant literature has been roughly divided into eight groups:

1. Instrument design and techniques;
2. Applications to isotopic analysis, precision mass measurement, isotope separation and ageing etc.;
3. Chemical analysis;
4. Application to organic chemistry;
5. Atomic and molecular processes;
6. Surface phenomena and solid state studies;
7. Thermodynamics and reaction kinetics;
8. Other applications.

In addition, the individual articles are being classified using approximately 200 descriptors, the aim being, not necessarily to retrieve a particular article but rather to indicate a series of articles likely to contain some relevant material. Organic chemical compounds are being listed separately and an index based on the structure of the compounds is being included.

It is planned to publish the Bulletin monthly with the final volume of the year containing full indexes to the year's literature. Information on the terms etc. can be obtained from the Data Centre or the distributors, the U.K. Stationery Office (H.M.S.O.).

(2) Survey of the Literature referring to Mass Spectra

A complete survey of the literature referring to mass spectra has been started with the object of providing a useful reference and retrieval service.

We would like to receive at the Centre copies of your past and future publications relevant to this topic as an aid to this survey. (Here we must thank those who have already responded to our appeal). We would also like to have information on compounds that have been partly or completely mass analysed in your laboratory but not yet published in the generally available literature.

It is planned to get up to date later this year when questions referring to the spectra of particular compounds will be answered. Indexes to the main file will then be made available.

Consideration is also being given to a retrieval system involving particular chemical groupings.

(3) Compound Identification

A study is being made, with the cooperation of Dr. W. Kelly, Unilever, of possible methods of using low resolution mass spectra for compound identification.

Attempts will be made to assess the matching efficiency of several different methods using the complete spectrum in the computer file with particular attention being

paid to instrumental effects.

(4) Low Resolution Mass Spectra

We aim to provide a central organization for collecting and distributing low resolution mass spectra that are not at present reaching established systems. Where necessary the Centre is providing assistance in the measurement of spectra.

(5) Other Topics

Other topics will be notified through the Bulletin as they arise.

Advisory Committee to
U.K. Office for Scientific and Technical Information

Chairman:	Mr. A. Quayle	(Shell Research)
	Dr. J. H. Beynon	(ICI)
	Dr. J. Cuthbert	(UKAEA)
	Dr. N. R. Daly	(UKAEA)
	Dr. C. J. Danby	(Oxford Univ.)
	Mr. R. M. Elliott	(A.E.I.)
	Dr. W. Kelly	(Unilever)
	Dr. I. Reed	(Glasgow Univ.)

FIG. 1

A combined electron impact/field ion source for high molecular weight samples of low volatility

C. Brunnée, Fried. Krupp Mess- und Analysentechnik, Bremen, Germany

Summary

A new combined electron impact/field ion source is described which can be used in connection with a direct inlet probe. The distance between the electron beam and the wire emitter is only one mm, so that the vapor of the sample reaches both ionizing zones. The vapor passes the ion source as a quasi molecular beam. Results obtained with this source will be given.

1. Construction of the source

At the ASTM meeting 1965 we reported about a combined field emission/electron impact ion source which is shown in fig. 1. During the last two years a considerable number of analyses has been carried out with ion sources of this type in various laboratories: i.e. semi-quantitative analyses of multicomponent hydrocarbon mixtures, molecular weight determinations, isomere studies, purity tests and others.

This ion source has a conventional gas inlet with an inlet line. However such inlet is suitable only for samples of not too low volatility. For the qualitative analysis of organic compounds of very low volatility evaporation out of an oven (direct inlet) in the immediate neighborhood of the ionization region is required. On principle, there are two possibilities to solve this problem for a combined field emission/electron impact ion source:

a) One uses the arrangement with two separate ionization regions as shown in fig. 1. Then one must have two separate direct inlet systems, or one must make the direct inlet probe with the vacuum lock or the ion source movable. b) The second possibility is to make the ionization region for field ionization to coincide with the one for electron impact ionization. Then one direct inlet only will suffice. This second possibility

is the more elegant and more efficient. But some ion optical problems have to be solved.

We have realized this second possibility. The respective ion source is shown in fig. 2. Electron beam and wire emitter are nearly at the same spot so that the vapor beam out of the oven can be ionized in both operating modes. The first plate in the ion source functions in case of electron impact ionization as draw-out plate for the ions. In case of field ionization, a voltage of 6 to 10 kV is applied for generation of the required high electrical field.

2. Measuring results

The stability of the ion current can be seen from fig. 3: recorded is the ion current of the molecular peak of the cholesterol. The constancy is of the order of 1 %. The maximum obtainable current is about 10^{-11} amps at the ion collector with field ionization.

A new direct inlet probe has been used for this measurements about which has been reported elsewhere [1]. The mass spectrometer used was an ATLAS CH 4.

Fig. 4 a shows a spectrum of the d-ribose with a predominant molecular and m + 1 peak. It is well known that the electron impact spectrum (fig 4 b) shows virtually no molecular peak, even at very low evaporation temperatures. The spectrum of fig. 4 a is very similar to the one published by Beckey [2] .

Another typical example is tetradecanol (fig. 5). The molecular ion is very unstable: a very small excess energy suffices to cause fragmentation. With electron impact ionization practically no molecular peak can be observed. Field ionization where no energy transfer to the molecule occurs again produces a very high molecular peak.

This example demonstrates also the possibility of differentiating between thermal decomposition of the sample and electron impact fragmentation if one uses exactly the same evaporation conditions in both ionizing modes: when there is a molecular peak in the field ionization

spectrum, then thermal decomposition has necessarily not occurred,and the eventual absence of the molecular ion in the electron impact spectrum can only be due to unimolecular fragmentation as in the case of tetradecanol.

d-ribose and tetradecanol both represent compounds with very unstable molecular ions. In fig. 6 the electron impact and field ionization spectra of the morphine molecule are shown. Because the molecular ion is rather stable in this case, both spectra differ not too much.

The spectra of an unstable high molecular weight compound, the cardenolid glycoside somalin are given in fig. 7. The sample was again evaporated out of the oven in the immediate vicinity of the wire emitter. For field ionization (fig. 7 a) the molecular peak is by far the highest. The isotope peaks are not plotted because the resolution did not suffice for separation with field ionization. ++) Fig. 7 b shows a spectrum recorded with the same ion source but using electron impact ionization: the molecular peak is very small. Fig. 7 c shows a negative ion spectrum taken recently by Ardenne, Steinfelder and Tümmler [3] with an electron attachment ion source. Here, also, the molecular peak dominates but not as strongly as in the case of field ionization.

In summery, one can say: The technique of field ionization is so far developed today that this method can be applied nearly as routinely as the method of electron impact ionization.

The advantage of field ionization - no energy transfer to the molecule and consequently only minor fragmentation (but often predominant metastables) - makes this method of ionization, especially when combined with electron impact technique, useful for applications such as: Analysis of multicomponent hydrocarbon mixtures [4] , molecular weight determinations, identification of isomeres [5] , structure studies of unstable molecules and free radical studies [2] .

++) There is a larger initial energy spread for field ionization than for electron impact ionization, so that with single focusing instruments the resolution is limited to about 300. Double focusing instruments will show no reduction of resolution.

References

[1] Brunnée, C.: Z. anal. Chem. 5, 333 (1966)

and

"Thermal decomposition and electron impact fragmentation of some typical organic molecules", this conference.

[2] Beckey, H.D., Knöppel, H., Metzinger, G. and Schulze, P.: In "Advances in Mass Spectrometry" Vol. 3, p. 35 (W.L. Mead ed.)

[3] v. Ardenne, M., Steinfelder, K. and Tümmler, R.: Z. Chem. 5, 287 (1965)

[4] Beckey, H.D. and Wagner, G.Z.: Z. anal. Chem. 197, 58 (1963)

[5] Wanless, G.G. and Glock, Jr., G.A.: "Simplified mass spectra II - by means of a dual field ionization/ electron bombardment source", this conference

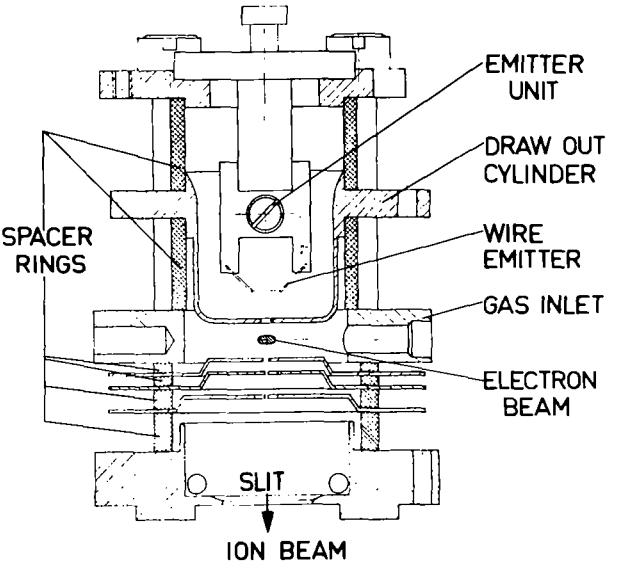

Fig. 1 *Combined field emission/electron impact ion source of the ATLAS mass spectrometer CH 4*

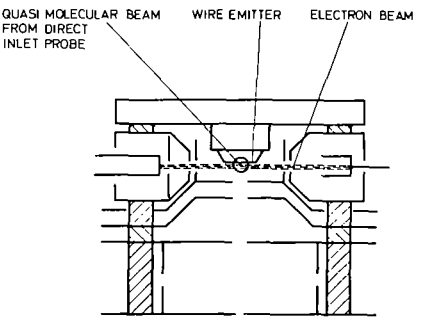

Fig. 2 Combined field emission/electron impact ion source which can be used in connection with a direct inlet probe

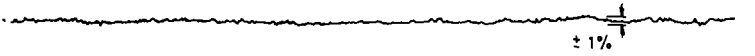

SAMPLE: CHOLESTEROL
MOLEKULAR PEAK
(EXPANDED SCALE)

Fig. 3 Constancy of the ion current

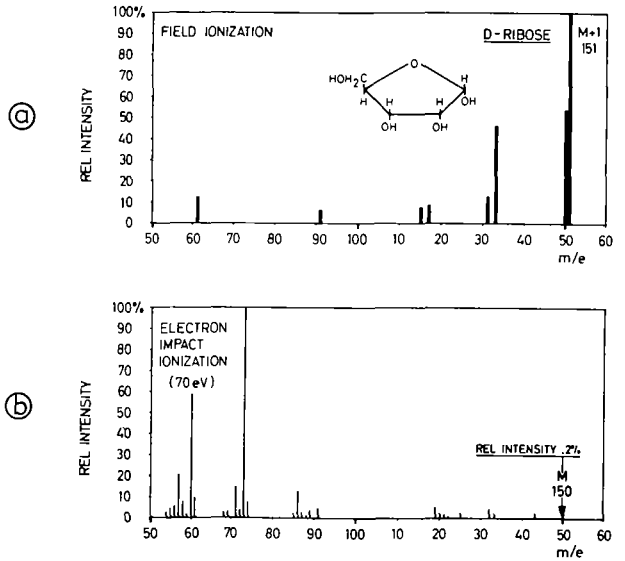

Fig. 4 Mass spectra of d - ribose: ⓐ field ionization ⓑ electron impact ionization (spectrum ⓑ from [2])

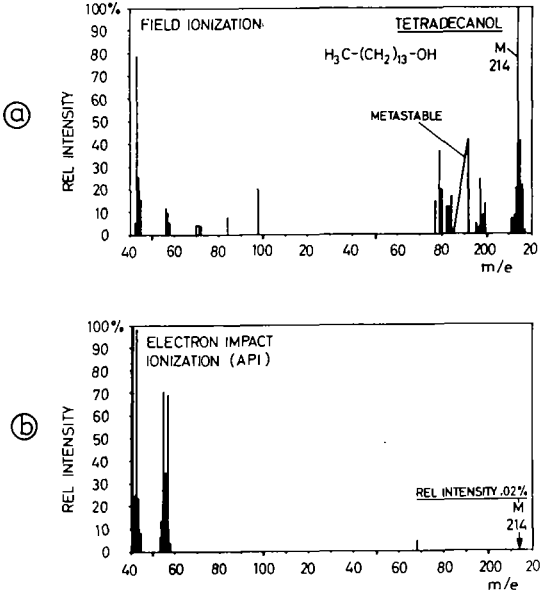

Fig. 5 Mass spectra of tetradecanol: ⓐ field ionization ⓑ electron impact ionization (70 eV)

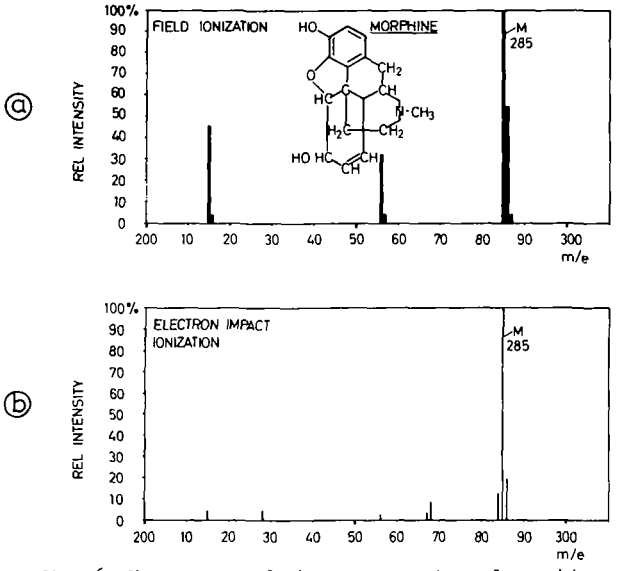

Fig. 6 Upper part of the mass spectra of morphine: ⓐ field ionization, ⓑ electron impact ionization (70 eV)

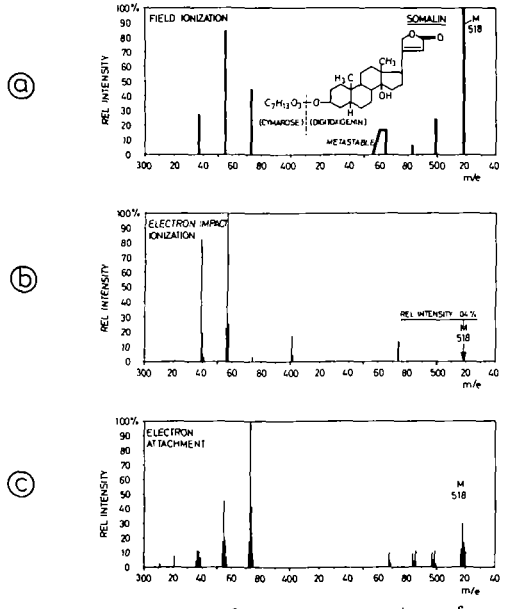

Fig. 7 Upper part of the mass spectra of somalin: ⓐ field ionization, ⓑ electron impact ionization (70 ev), ⓒ electron attachment ionization

A General Method for Collection and Mass Spectrometer Analysis of Submicrogram Samples*

E. M. Chait, J. W. Amy and F. W. McLafferty

Department of Chemistry, Purdue University, Lafayette, Indiana 47907

A recent communication from our laboratory describes collection of separated components eluted from a gas chromatograph for introduction into a mass spectrometer (1). This system depends on trapping the chromatographic peak in a small extention of the chromatographic column. The trap is fashioned from a capillary melting point tube containing a few milligrams of the column packing used in the main column, sealed at both ends and eventually the collected cut is analyzed in the mass spectrometer via a direct sample introduction probe. Since this technique depends on the chromatographic process itself for its mode of action, the trapping of a given gas chromatographic peak is as efficient as the separation with the same column packing. These collection efficiencies are quantitative for submicrogram samples in contrast to general experience with present condensation techniques.

Further studies now show the method to be of general applicability for a wide range of samples including those from thin layer and liquid chromatography.

The spectra of submicrogram quantities of endrin and malathion were obtained by direct introduction into the CEC 21-110B mass spectrometer of thin layer chromatographic coating on which the pesticides were adsorbed.

The gas chromatographic collection techniques described were particularly useful in a study of yeast lipids (2). A 1 μg. cut collected from the chromatogram of yeast lipids was identified as monofluoropalmitic acid, while an impurity which was 3.5% of the main component was identified as monofluorostearic acid. In this case the sensitivity of the mass spectrometer to amounts on the order of 10^{-2} μg. gave researchers the identity of the unexpected impurity as well as that of the expected major component. Figure 1 shows the key peaks observed in the high mass end of the spectrum giving identification of the compounds.

A new technique has been developed for the handling of volatile samples. The volatization of a trapped sample is controlled by cooling the sample in a nitrogen-cooled cold finger used as a direct introduction probe on the CEC 21-110B mass spectrometer. The low temperature direct introduction probe is shown schematically in Figure 2. The probe is capable of temperatures from ambient to - 140° C by controlling the flow of cooled nitrogen, and thus controlling the rate of volatization of the collected sample into the mass spectrometer ion source. Temperature measurement is achieved by measuring the resistance of a silicon diode located in the tip of the probe. Volatile samples such as 0.1 μg. of acetone from tomato volatiles have been analyzed by this method.

Since the method described is successful in handling submicrogram amounts of a variety of compounds, the next consideration is the sensitivity limit of mass spectrometer equipment. Evaluating the sensitivity of Ilford Q-2 photoplates in the CEC 21-110B mass spectrometer, it was found that for complete evaporation of a sample of pregnanediol diacetate from the direct introduction probe the sensitivity at a resolution of 2000 was 0.4 nanograms based on a signal-to-noise ratio of 2 for the m/e 345 line. The high sensitivity of photoplate detection at high resolution makes the use of automated data handling as well as element mapping practical for dealing with the high rate of information output.

1. Amy, J. W., Chait, E. M., Baitinger, W. E., McLafferty, F. W., Anal. Chem., 37, 1265 (1965).
2. Powell, G., Corley, R. C., personal communication, September 1965, Department of Chemistry, Purdue University, Lafayette, Indiana

* The financial support of the National Institutes of Health is gratefully acknowledged.

Fig. 1

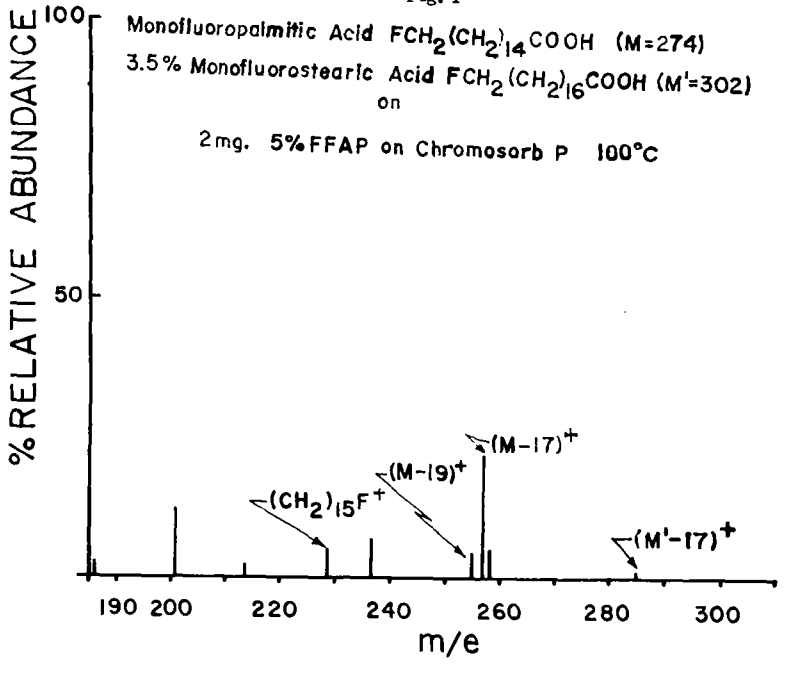
Monofluoropalmitic Acid $FCH_2(CH_2)_{14}COOH$ (M=274)
3.5% Monofluorostearic Acid $FCH_2(CH_2)_{16}COOH$ (M'=302)
on
2mg. 5% FFAP on Chromosorb P 100°C
% RELATIVE ABUNDANCE
100
50
$(CH_2)_{15}F^+$
$(M-19)^+$
$(M-17)^+$
$(M'-17)^+$
190 200 220 240 260 280 300
m/e

Fig. 2

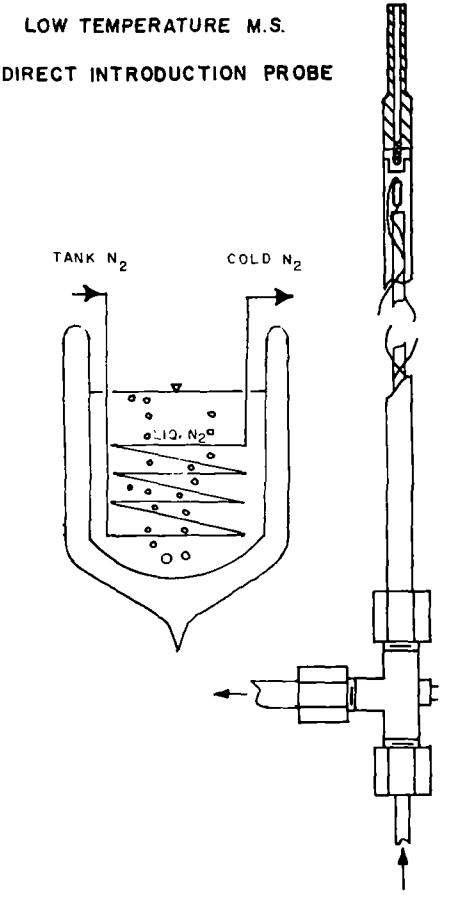
LOW TEMPERATURE M.S.
DIRECT INTRODUCTION PROBE
TANK N_2
COLD N_2
LIQ. N_2

ANALYSIS OF NATURAL PRODUCTS BY THE DIRECT COMBINATION OF GAS CHROMATOGRAPHY AND MASS SPECTROMETRY

By

A. H. Struck and W. Averill

Perkin-Elmer Corporation
Norwalk, Connecticut

In the last few years there has been a greatly increased recognition and use of the ability of Mass Spectrometry to assist in the identification of unknown samples. When identification of and individual component or components in a mixture is required, the direct addition of the gas chromatograph's highly efficient separating ability to the mass spectrometer's qualitative analytical ability makes a very powerful technique. Because of the compatibility of sample size, volatility and time requirements, this addition makes a very efficient combination. It allows spectra to be obtained on individual components in mixtures and provides more information with a considerable smaller expenditure of sample and time than any other technique currently available. Within the limits of sensitivity of the mass spectrometer any sample that can be successfully chromatographed should be capable of being run on the mass spectrometer.

The system to be described consists of a Perkin-Elmer Model 801 Gas Chromatograph connected to a Hitachi Perkin-Elmer Model RMU-6E Mass Spectrometer. The connection between the chromatograph and the spectrometer includes a sample enrichment device (Helium Separator) described by Watson and Biemann in the May 1964 edition of Analytical Chemistry.

The Model 801 Chromatograph is a dual column, linear temperature programmed instrument with flame ionization detection. It will accept open tubular columns, support coated open tubular columns as well as packed columns. When used in combination with the mass spectrometer it is used in single column operation. The Model RMU-6E Mass Spectrometer is a versatile single focusing instrument. It has a maximum resolution greater than 2,500 and a mass range of 1,800. It utilizes magnetic scanning and can cover the mass range 12 to 500 in 3 seconds. It has high sensitivity due to electron multiplier detection. The combined system can be operated to 300°C. It is possible to convert from standard inlet operation to combined gas chromatography operation or vice versa in about five minutes

The system is shown schematically in Figure 1. The effluent from the chromatographic column or a portion of it is fed to the Helium Separator which is mounted in the oven connecting the standard inlet system to the ion source of the mass spectrometer. The line connecting the chromatograph to the separator is a heated capillary line with a 0.01 inch internal diameter. The separator used in this work was designed to accept up to 10 cc/min. flow and deliver 0.1 cc/min. to the mass spectrometer. The gas not fed to the spectrometer is removed by pumping on the outer jacket of the separator with a mechanical vacuum pump. That portion of the effluent supplied to the spectrometer is considerably enriched in sample component due to the faster effusion of the lighter Helium through the fritted glass tube of the separator.

The actual enrichment is dependent on the molecular weight of the sample component. The enrichment factor for Freon 11 ($CF\ Cl_3$) was measured and found to be 20.

A portion of the total ions formed in the ion source is intercepted by a collector located after the source and before the magnetic analyzer. This provides for continuous monitoring of the chromatographic effluent and produces a chromatographic record. In all runs made in this investigation a split of the chromatographic effluent was made prior to the separator and part (10-20%) was fed to the flame ionization detector of the chromatograph providing a second chromatographic record. This made it possible to measure the transport line of the connecting system and to determine if any gas chromatographic resolution was being lost in the connecting system. The transport time for the system was of the order of 1 or 2 seconds and the chromatographic resolution was substantially the same on both records. Since the point of detection for the total ion monitor and the mass spectrum are the same in time, it is possible to scan a chromatographic peak at any point and know exactly which portion was scanned.

All the work reported in this paper was done using open tubular support coated columns. These columns retain a high degree of the separation ability of open tubular columns and the sample capacity of packed columns, with relatively short retention times. Therefore, they are an excellent choice for the combined gas chromatography/mass spectrometry technique.

Figure 2 is the spectrum obtained from 0.01 μg of tertiary butyl benzene injected into the gas chromatograph and demonstrates the sensitivity of the combined system. The spectrum was scanned at a rate of M/e 12 to 300 in three seconds. Two galvanometer traces at relative sensitivities of 1 and 30 are shown.

Figure 3 shows the chromatograms obtained simultaneously on the FID recorder and the TIM recorder from a single injection of 0.1 μl of peppermint oil. A comparison of the two records shows that there is little, if any, loss of chromatographic resolution due to the connecting system.

When a spectrum is scanned, the total ion monitor record is deflected for the duration of the scan. In obtaining the total ion record shown in Figure 3, no spectra were scanned so that a better comparison could be made with the flame ionization record. The deflections show the position and duration of the spectral scan for each peak scanned.

The early peaks in the chromatogram were mostly monoterpenes ($C_{10}H_{16}$) with a molecular weight of 136. It could be seen that they are all compounds having a molecular weight of 136 butthe pattern coefficients for the fragment peaks were quite different. A comparison with standard spectra identified peaks 1 and 2 as Alpha and Beta pinene. GLC peak number 6 was also a monoterpene and Figure 4 shows a comparison of the spectrum of this peak with a spectrum of pure limonene. Examination of the two spectra shows that they are essentially identical.

Spectra for GLC peaks number 11 and 12 are shown in Figures 5 and 6. Peak number 11 is menthone and has a large molecular ion peak at M/e 154. The spectrum for peak number 12, identified as menthofuran, has a large molecular ion peak at M/e = 150. Although the two peaks are not completely separated chromatographically, there is only a

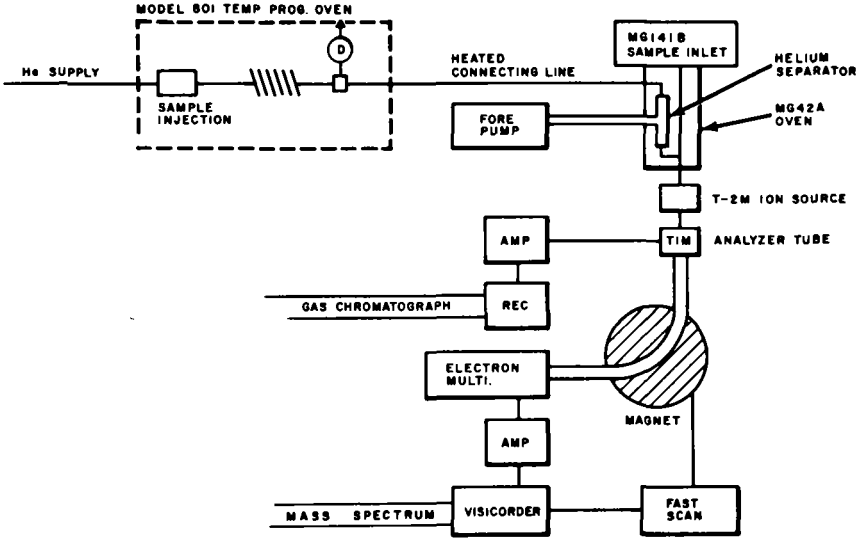

Figure 1

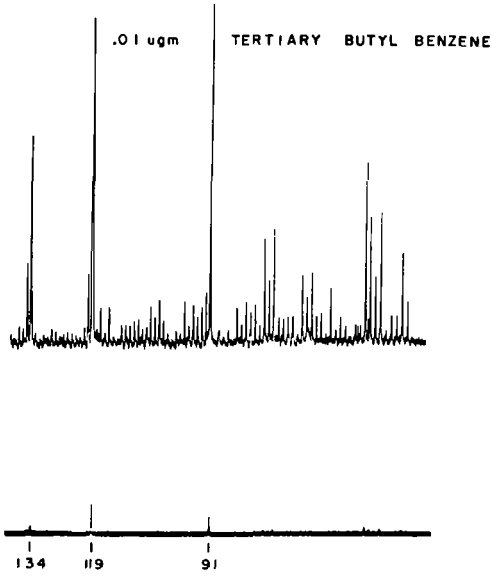

Figure 2

small peak present at M/e 154 in this spectrum from the menthone. This demonstrates that the total ion monitor record is a true indication of the composition of the sample in the ion source and the system does not have a memory or background problem from previous peaks in the chromatogram.

Figure 7 is a chromatogram obtained on the total ion monitor detector for a Synthetic Peach Flavor. The components which were identified from their mass spectra are listed. Figure 8 is the spectrum of Cinnamaldehyde. This component was known to be present to less than 0.1% concentration and since the sample size was 0.1 μl the total amount of this component injected into the chromatograph was less than 0.1 μgm.

The above chromatograms and spectra demonstrate the large amount of information that can be obtained from the combined gas chromatography/mass spectrometry technique with a relatively small expenditure of time and sample.

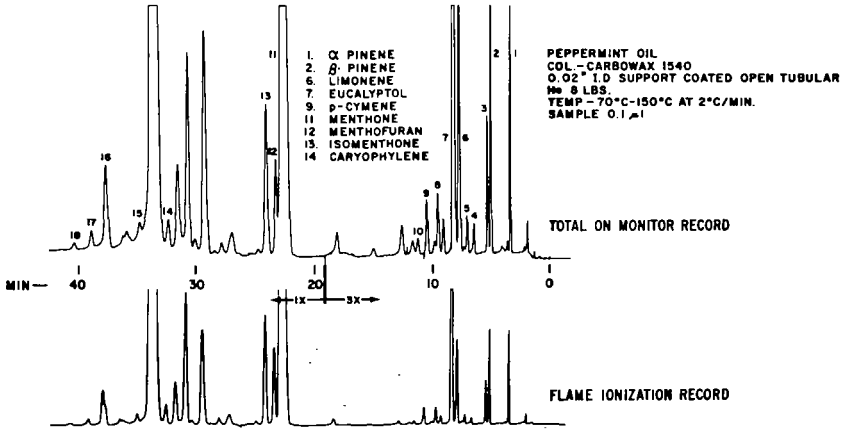

Figure 3

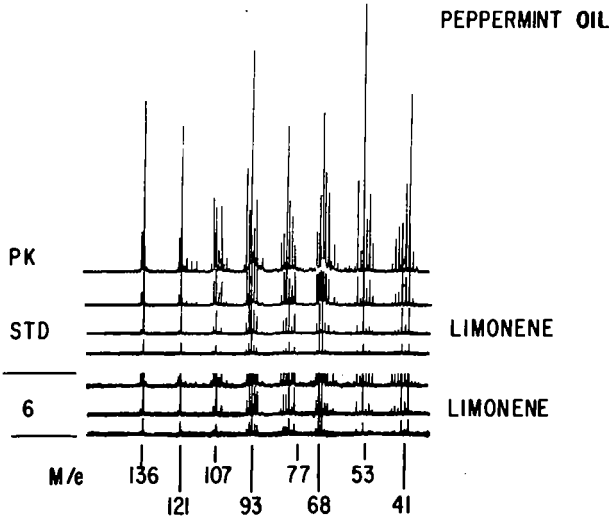

Figure 4

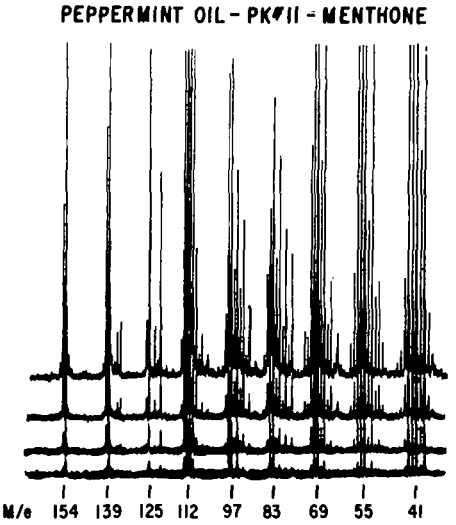

Figure 5

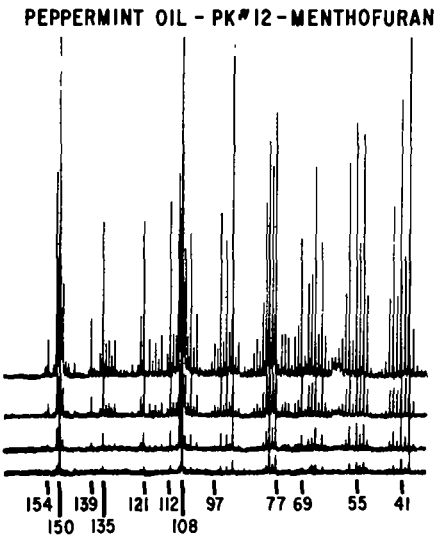

Figure 6

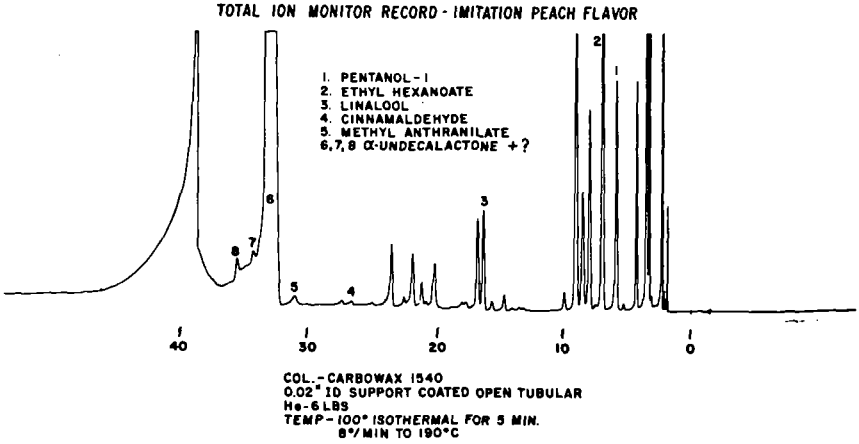

Figure 7

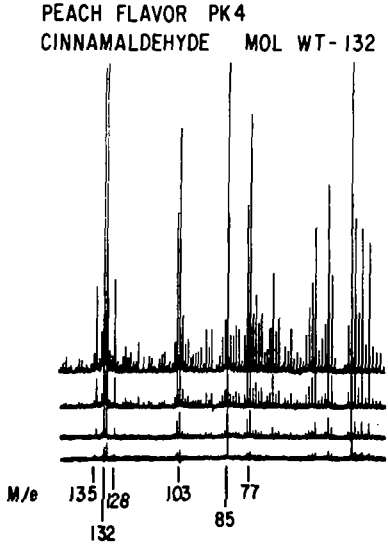

Figure 8

MASS SPECTROMETRIC DETERMINATION OF TRACE IMPURITIES IN OXYGEN

by

John Roboz

Air Reduction Company, Inc.
Central Research Laboratories
Murray Hill, New Jersey

ABSTRACT

A simple separation and preconcentration technique has been developed in which a) oxygen matrix is quantitatively removed with NaK alloy thereby eliminating adverse effects in the ion source, b) impurities are retained with 100% recovery with enrichment factor of 10^6 achieved. The method, which is adoptable for any mass spectrometer, is applicable to nitrogen, argon, and the rare gases. Threshold limits are of the order of 0.1 ppm and can be further reduced into the ppb region.

As the demand for ultrapure oxygen rapidly increases in industrial, space, and research applications, great efforts are being made to improve purification techniques in manufacturing. Simultaneously, new methods of low level impurity analysis must be developed since the conventional techniques lack the required sensitivity. The objective of this work was to develop a mass spectrometric technique for the determination of specific inorganic impurities in oxygen at the fractional parts per million level. In gas chromatography nitrogen and argon cannot be analyzed in oxygen at low levels due to insufficient resolution; present thresholds are about 4 parts per million for nitrogen and 10 parts per million for argon. Although it would be desirable to have a method for all impurities in a single analysis, the requirement for matrix removal necessitates the method to be restricted for specific impurities. Our efforts have been concentrated to nitrogen, argon, and the rare gases, so that in conjunction with gas chromatography complete coverage of all important impurities could be provided.

Mass spectrometric techniques cannot be routinely applied to the determination of trace impurities in oxygen for two reasons: First, oxygen markedly shortens the life of the filament, although we have found that rhenium can take a good deal of abuse. The second adverse effect of oxygen, a lethal one in trace analysis, is the formation of carbon monoxide in the ion source. For parts per million analysis without matrix removal, sample pressure of several hundred microns would be needed, and the carbon monoxide interference makes it impossible to accurately determine nitrogen content. Three methods have been developed to eliminate this problem. All three are preconcentration techniques: the oxygen matrix is quantitatively removed, impurities are retained with 100% recovery. In addition, an impurity enrichment factor of at least one thousand is achieved, resulting in greatly increased concentrational sensitivity and also increased reliability of the analyses. Since the third technique is far superior than the other two, these will be described only briefly to show what they will and will not do.

In all experiments a CEC Model 21-130 mass spectrometer was employed. This is a cyloidal instrument with unit resolution of about 200. Overall sensitivity was increased by installing a second input resistor which is about 10 times that of the standard 5×10^{10} ohm resistor. A one millivolt recorder is used, the amplifier system being properly modified to accommodate these changes.

In the first technique, impurity preconcentration is achieved by removing the matrix oxygen through a silver leak. The leak is used in a reverse manner: if only oxygen can penetrate silver, all other impurities must remain on the other side of the membrane and the inert

impurities can be analyzed free of oxygen intereference. A commercial silver leak from GE was connected to the mass spectrometer inlet system. The inside of the leak tube is filled with the sample gas and oxygen is removed by pumping the other side of the membrane at an operating temperature of 750°C. After removing about 90% of the matrix, the remaining gases are expanded into the mass spectrometer reservoir and analyzed routinely. The pumping speed of the leak is about 0.1 micron-liter per second and it takes about one hour to pump out enough oxygen for parts per million analysis. This slow pumping is one of the disadvantages. A second problem is a high carbon dioxide blank. The origin of this blank is not known but its contribution to the 28 peak necessitates the use of correction factors for nitrogen analysis. The silver leak technique is linear with concentration, is quite reproducible, and has thresholds for nitrogen, argon, and the rare gases at the 1 ppm level - but there are experimental difficulties with pumping speed, cooling, etc.

The second method is based on the well-known fact that copper reacts with oxygen at elevated temperatures. A 6 to 8 inch long glass tube is filled with some 10 grams of copper filings and heating is accomplished with an ordinary wire wound around the tube. Copper is conditioned first by complete oxidation, followed by reduction with hydrogen. Oxygen removal with hot copper is very fast, it takes only about 5 minutes to remove enough oxygen for a 1 ppm argon or nitrogen analysis. Sample size is not limited and practically any desired enrichment factor can be obtained. The only drawback is the presence of an unexplained carbon dioxide blank and, although it is small, it reduces the accuracy of low level nitrogen analysis; attempts to eliminate the blank were unsuccessful.

The third method, the one we are recommending, is called the NaK technique. It is based on two facts: First, oxygen matrix can be quantitatively removed from the gas phase by employing a sodium-potassium alloy - Second, there is no evidence for reaction between sodium-potassium alloy and nitrogen, argon, and the rare gases, even when the alloy is exposed to a full atmosphere pressure. The experimental technique, as will be shown momentarily, is simple, and can be adopted to any mass spectrometer.

Potassium and sodium are miscible in all portions and the alloy which is called NaK is liquid at room temperature. The eutectic contains 78% potassium. Almost any mixture is adequate for oxygen removal, but our best results were obtained with 44% potassium. The oxide formation in the alloy is a complex process and, in general, Na_2O formation is preferential. As far as the present technique is concerned, detailed knowledge of the oxide formation process is not needed. The important facts are that oxygen is quantitatively removed from the gas phase and that there is no reaction with the impurities (1, 2).

The exceptional simplicity of the experimental procedure is illustrated in Figure 1. The sample system consists of a small glass bulb of about 80 cc volume with reinforced bottom, and it is connected to the standard mass spectrometer inlet system as shown in the figure The sodium-potassium alloy, the NaK, is purchased in small glass ampoules which contain about 1 g of alloy under protective argon filling. Incidentally, one ampoule costs about one dollar, and some 15-20 analyses can be made with one ampoule. The set-up shown in Figure 1 has three advantages: First, installation takes only a few minutes, second, no outside pumping is necessary, and third, samples can be directly expanded for analysis.

Analytical procedure is straightforward: A NaK ampoule is placed into the glass bulb and with S_1 closed the assembly is removed from the inlet line and is vigorously shaken until the ampoule breaks. The ampoules are opened in air and no splashing of the alloy occurs. Next, the alloy is evenly distributed around the walls by slowly rotating the whole assembly, and a shiny film is formed. The system is re-connected to the inlet line and everything is evacuated by opening R_2 and V_2. The NaK is now ready for use.

The sample to be analyzed is introduced into the volume enclosed by R_2 and S_1. This is a constant volume and the quantity of sample is determined by measuring its pressure. Sample pressure of 80 mm is

TABLE 1

SENSITIVITIES, NaK TECHNIQUE (DIV/PPM)		
INPUT RES.	NORMAL	HIGH
NITROGEN	13.0	104
ARGON	17.0	136
KRYPTON	6.6	53
XENON	2.7	22
SAMPLE QUANTITY: 8.5 CC-ATM IONIZATION CURRENT: 80 μA		

TABLE 2

THRESHOLDS, NaK TECHNIQUE (PPM)		
INPUT RES.	NORMAL	HIGH
NITROGEN	0.24	0.03
ARGON	0.18	0.02
KRYPTON	0.48	0.06
XENON	1.10	0.14
BASED ON: 3 DIV. PEAK ABOVE NOISE LEVEL		

TABLE 3

IMPURITIES IN OXYGEN BY NaK TECHNIQUE

PRECISION DATA

IMPURITY	N_2	Ar	Kr
NUMBER OF RUNS	12	12	12
ARITHMETIC MEAN, ppm	10.7	28.9	15.8
RANGE, ppm	9.9-11.7	27.7-30.1	15.1-16.0
STANDARD DEV., ppm	0.74	0.84	0.09
REL. STAND. DEV., %	6-8	2.9	1.9

TABLE 4

TYPICAL ANALYSIS, ULTRAPURE OXYGEN		
IMPURITY	PEAK (DIV)	PPM
NITROGEN	68	5.5
ARGON	11	0.7
KRYPTON	54	8.2
XENON	3	1
INPUT RESISTOR: NORMAL IONIZATION CURRENT: 80 μA		

used normally, but this is an arbitrary number and for higher sensitivity pressure may be as high as 1 atmosphere; also the sample volume may be increased. In the next step, valve S_1 is opened and the sample gas is expanded into the previously evacuated bulb which contains the NaK. Reaction starts immediately as evidenced by a dark flushing of the film. There is no visible sign of the completed reaction and the time needed for oxygen removal must be determined experimentally. In our procedure it takes only five minutes to reduce the original 80 mm oxygen pressure to below 0.01 micron. The oxygen is thus removed with practically 100% efficiency and the oxygen peak is only some 20 divisions higher than instrument background. Thus oxygen interference is completely eliminated.

After the five minute reaction time, the remaining gas sample is expanded into the instrument reservoir and is analyzed routinely after closing valve V_6. During analysis the whole system can be pumped out via V_5 and a new sample may be taken. After about 15-20 analyses oxygen absorbing capacity ceases rather abruptly. The NaK bulb is removed and exposed to moist air for a while after which it can be simply washed out with water. Small fireworks are often observed as minute particles of remaining alloy react with water but the force is not enough to break the glass.

A fundamental way of calibration is suggested by the known and constant argon content of ordinary room air. Another method of calibration, one which eliminates the presence of large amounts of nitrogen, is as follows. Commercial cylinder oxygen contains about 3000 ppm argon. This much argon can be analyzed directly in the mass spectrometer at low sample pressure without any interference. Thus, when analyses are made using both the normal and the NaK method a concentration factor is obtained. Values for nitrogen and the rare gases are obtained by measuring basic mass spectrometer sensitivities. Calibration values were also cross-checked with specifically prepared krypton in oxygen standards and by samples analyzed gas chromatographically.

Table 1 summarizes sensitivity values; it is seen that the number of divisions per ppm is large. The div/ppm values can be used directly to determine impurity content by simply dividing measured peak heights. There is no blank apart from the basic mass spectrometer background. Threshold values are shown in Table 2. It is assumed that a minimum of 3 div. peak height is required for impurity recognition; this is a conservative measure.

It is seen that fractional ppm levels can easily be attained. Turning to the high sensitivity input resistor requires only the flipping of a switch. Sensitivity can, of course, be further increased by orders of magnitude if a larger sample size is used. Either sample volume or sample pressure may be increased. If necessary, two or more ampoules may be used at the same time. Ionization current can also be increased, up to 160 microamperes, so another factor of two is gained. For very small samples, the large reservoir of the standard sample inlet system can completely be closed off. This increases sensitivity by a factor of one thousand but, due to fast pumpout, accuracy is poorer when this technique is employed.

Table 3 shows precision data for nitrogen, argon and krypton in an oxygen sample of "medium" purity. It is seen that precision is very good.

Table 4 shows a typical ultrapure oxygen analysis. It is interesting that Kr appears to be the largest impurity. Methods have been developed to ultra purify oxygen on commercial scale and the availability of this NaK technique is an important help at Air Reduction Company to assure high purity through a product control program.

Precision at the fractional ppm level is not easy to determine. The limiting factor appears to be set by the ability to read small peak heights. It is conservatively estimated that our values are reliable within plus-minus 30% of the value quoted. At the fractional ppm level this, I believe, is adequate for most purposes.

In Table 5 a summary is given on oxygen analysis showing various methods. It is seen that the present method fills the gaps for nitrogen and argon,

TABLE 5

IMPURITY THRESHOLDS IN O_2 (PPM)							
	N_2	Ar	Kr	Xe	CO_2	N_2O	TOTAL HYDROC.
GC/TC	4	10	0.05	0.02	0.1	0.05	-
MS	0.03	0.02	0.05	0.15	-	-	-
IR	-	-	-	-	0.2	-	0.2
GC/FLAME	-	-	-	-	-	-	0.3

INDIV. HYDROC. 0.001 BY GC/TC AND GC/FLAME

CHEM. DETECTOR TUBES: 1 PPM CO AND 0.1 PPM OXIDES OF N_2

so that a complete analysis for high purity oxygen can now be performed.

In summarizing, the oxygen matrix is quantitatively removed from the gas phase by sodium-potassium alloy. Since there are no reactions with nitrogen, argon, and the rare gases, these elements can be determined in a highly concentrated form without any oxygen intereference. Threshold limits are at the fractional ppm level and overall reproducibility is better than 10% at the low parts per million range, and better than 30% at the fractional ppm range. The method is fast, simple, does not require any hardware, and can be adopted to any mass spectrometer.

It was demonstrated in the course of this work that traces of hydrocarbons, water, carbon monoxide, etc. are quantitatively and permanently removed together with oxygen by the sodium-potassium alloy. Chemical pumping by NaK may thus be used as a final pumping stage to remove residual gases from ion sources, etc. Possible applications include the ion source and analyzer sections of spark source mass spectrographs, etc. Experimental work is currently in progress for several applications.

References:

1) J. W. Mellor, "Comprehensive Treatise on Inorganic and Theoretical Chemistry, Wiley & Sons, N.Y., 1963, Vol. II, Suppl. II and III.

2) Technical Bulletin, MSAR 64 MDI
MSA Research Corporation, Callery, Pa.

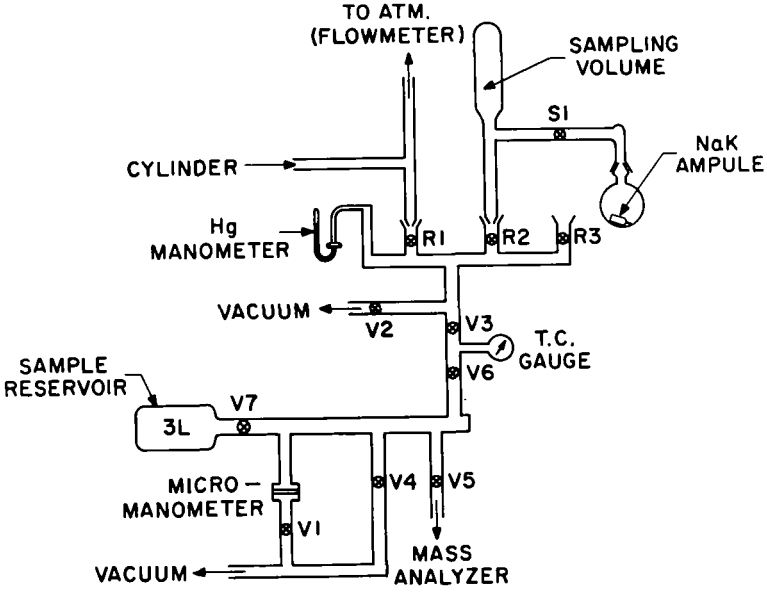

NaK ASSEMBLY AND MS SAMPLE INLET SYSTEM

Fig. 1

A COLD CATHODE QUADRUPOLE MASS SPECTROMETER

By

F.L. Torney and P. Blum
National Research Corp., 70 Memorial Dr., Cambridge, Mass.

I INTRODUCTION

Mass spectrometers commonly use a hot filament to supply electrons for molecular ionization. An important characteristic of these sources is that they produce low energy ions which are easily focused into a collimated beam for spectroscopic analysis. However, the hot filament causes certain gases to decompose and in ultrahigh vacuum analysis, this confusion is compounded by evolution of gases from the source itself due to the heat generated. In total pressure measurement, these difficulties have been overcome by the Readhead cold cathode magnetron gauges[1,2]; in addition to being clean, their sensitivities exceed that of the common hot filament type by a factor of approximately 50. They are therefore useful for pressure measurements down to the 10^{-13} Torr range. The work reported here, based on studies related in earlier reports[3,4], is the result of transformation of the magnetron cold cathode gauge into a cold cathode ion source (CCIS) for ultrahigh vacuum residual gas analysis. The source has been coupled to a quadrupole mass filter, where requirements have been found most tolerant of the relatively large ion energies and beam width of the source. The results of optimizing and characterizing a CCIS - quadrupole are discussed herein.*

II APPARATUS

A. Vacuum System

The vacuum system used is shown schematically in Fig. 1. It is divided into upper and lower manifold units, which allows the upper portion to be oven baked while being pumped from below. Subsequent to bakeout, the upper manifold, thus cleaned is valved off and pumped by the upper ion pump.

The upper manifold consists of the quadrupole spectrometer, a modulated Bayard-Alpert gauge, an 11 liter per second Ultek Model 10-252 ion pump, a bakeable Varian ultrahigh vacuum valve for isolating the upper manifold from the lower and a bakeable Varian valve for isolating the upper ion pump. A thermostatically controlled oven is used for baking the upper manifold system.

The lower manifold consists of a 20 liter/second Ultek Model 10-354 ion pump, a 2400 liter/second mechanical pump, a Varian Zeolite VacSorb pump, a port for feeding gas to the system and associated valves for closing off the pumps and gas supply inlet.

B. Quadrupole Spectrometer

On the basis of a feasibility study of the cold cathode ion source[7], it was concluded that a quadrupole mass spectrometer would be most suitable for analysis of the source's higher ion energies and larger beam cross section. An Ultek model 210 quadrupole was selected, equipped with a standard hot filament ionizer. The latter permitted spectrometer performance comparisons between both types of sources.

None of the commercially available analyzers had the optimum characteristics desired for operation with the CCIS for reasons to be discussed in section IV. However, the Ultek unit was chosen because it had the best resolution available and because it was capable of scanning

---

* Böhm and Günther[5,6] also have reported results of combining a quadrupole analyzer with a cold cathode ion source, of the Penning type. This combination is found useful for pressures above about 10^{-6} Torr; the source does not operate in the ultrahigh vacuum region.

automatically in a mode in which peak width remains constant with mass; this is desirable for the CCIS because ion energy restrictions are less stringent and because sensitivity vs. ion energy is constant with mass. The spectrometer was used with a Faraday cup ion collector rather than with an electron multiplier to allow determination of basic spectrometer characteristics, such as sensitivity, free of amplification variations and with a minimum of spectral perturbations.

Quadrupole specifications pertinent to a theoretical analysis of results are as follows: operating frequencies (ν) are 5.3 mc and 3.3 mc respectively on the low and medium mass ranges utilized, maximum available rf potential (V) is 1000 volts, the radius (r_o) of the circle inscribed by the quadrupole rods is 2.7 mm, the entrance aperture diameter is also 2.7 mm, rod lengths are 11.3 mm.

C. Cold Cathode Ion Source

The cold cathode ion source (CCIS) is a modification of the Redhead[8] magnetron gauge. An assembly drawing of the source attached to the quadrupole is shown in Fig. 2. To allow ion extraction, the single spool shaped cathode design used in the gauge is separated into two cathodes, one with a remnant stub (K_1) which is .38" long and .12" in diameter and the other with an aperture (K_2) which is .12" in diameter. All remaining electrode dimensions remain as in the gauge. However, the horseshoe magnet ordinarily used has been replaced by hollow cylindrical ceramic magnets. Dimensions and field strengths of the magnets used are given in section III H.

Source electrodes are supported on a steel cylindrical housing maintained at ground potential. Auxiliary cathodes are welded to it directly. The anode is attached and insulated by sapphire spheres. Cathodes K_1 and K_2 are supported and insulated by glass studs. This arrangement provides independent electronic access to the anode and each cathode; it also provides a guard ring design which, by preventing leakage between electrodes, prevents interference with low level current detection.

The source housing is perforated and attached to the quadrupole with heavy refractory wire and a slotted sleeve; distance was maintained at .094" between the faces of K_2 and the quadrupole aperture plate (as close as possible without causing arcing between electrodes). Rigidity and an open design for pumping facility was thus provided.

Tungsten screens were used over the K_2 aperture and the quadrupole entrance aperture for the following reasons: (a) to allow testing of the effect of potential differences between these components without causing beam defocusing, (b) to isolate magnetron and quadrupole electric fields and (c) to flatten the magnetron potential distribution at K_2 which otherwise bulges through the K_2 aperture; this is to reduce ion defocusing and resultant sensitivity losses.

III PROCEDURES AND RESULTS

A. Introduction

CCIS quadrupole performance was investigated as a function of the parameters discussed below, first to determine optimum source operating conditions and second to note the resultant spectrometer response to mass and to pressure variations. At each stage of the former investigation, values were selected which gave the best resolution and sensitivity; unless otherwise stated, nitrogen was used as the standard gas and pressure was maintained in the vicinity of 5.4×10^{-9} Torr.

B. Performance vs. Quadrupole Resolution Setting

A family of nitrogen spectra were recorded as a function of electronic quadrupole resolution settings. The latter correspond to ratios of dc and rf rod potentials, U and V respectively, in Paul's[9] equation for quadrupole spectrometer resolution

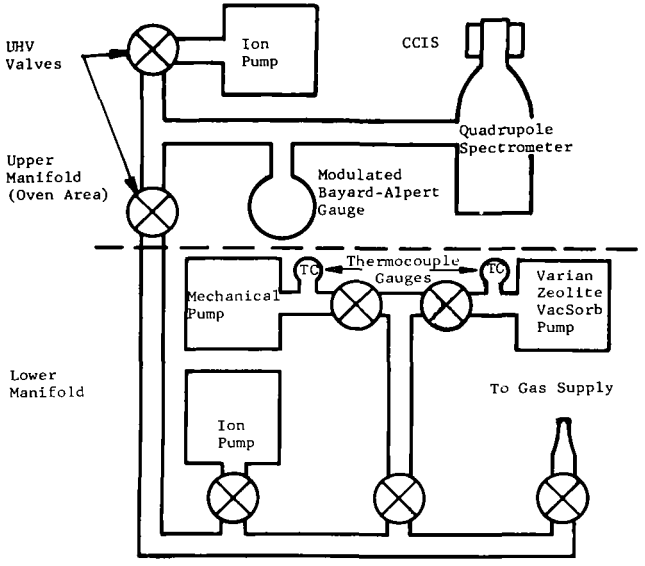

FIG. 1 VACUUM SYSTEM SCHEMATIC

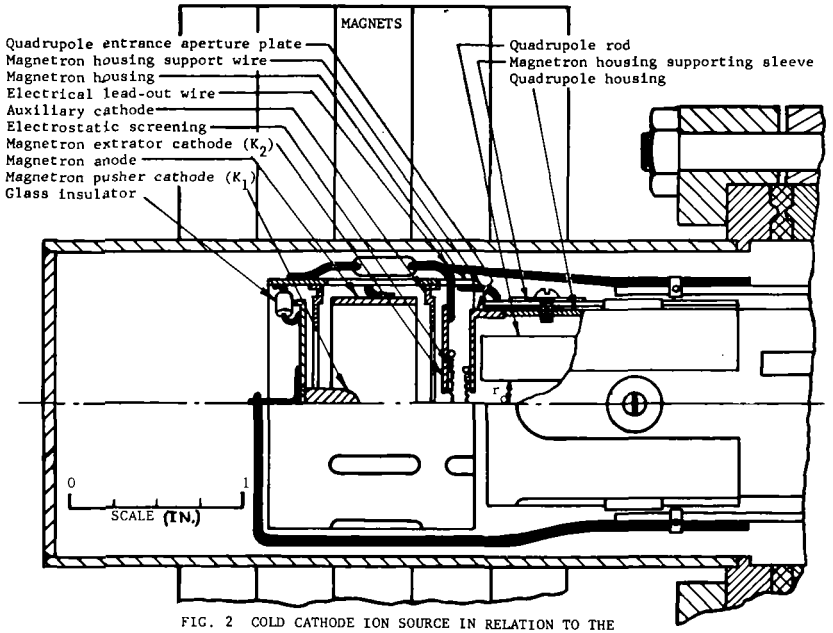

FIG. 2 COLD CATHODE ION SOURCE IN RELATION TO THE ENTRANCE OF THE QUADRUPOLE SPECTROMETER

$$\frac{M}{\Delta M} = \frac{0.126}{0.16784 - U/V} \quad (1)$$

where M is the atomic mass and ΔM the peak width at its base. Spectral resolution changes were determined by comparing the full width at half maximum (FWHM) of the nitrogen peaks. Experimental resolution improved as electronic settings proceeded toward higher theoretical resolution; sensitivity correspondingly decreased (as predicted by theory) until a setting was reached (4.95) beyond which sensitivity continued to decrease with no further resolution improvement. This setting was then selected as optimum and used in subsequent experiments.

C. Performance vs. CCIS Anode Potential

As with resolution setting experiments, FWHM measurements were made vs. anode potential (V_A) on a family of nitrogen spectra. This was done both on the low and medium mass ranges (1-50 amu and 10-150 amu, respectively). Optimum V_A for both ranges was in the vicinity of 2.0 KV (compared with 5.0 KV normally used in magnetron total pressure gauges). Fig. 3 illustrates, for the medium mass range, the resolution improvement and accompanying sensitivity reduction existent as a function of V_A. (It is evident that the discharge was unstable at 5.0 KV).

D. Performance vs. CCIS Magnet Position

Using the optimum resolution setting and optimum anode potential, discussed above, spectra were recorded against magnet position; first axially and then rotationally. Positions giving optimum resolution, as determined by FWHM, were selected. Unlike spectral variations with resolution setting and with anode potential, no sensitivity loss accompanied the positionally improved resolution. Resolution was found optimum when the magnet's center coincided with the midplane between cathodes K_1 and K_2. A $\pm$ 1/8 inch axial magnet movement caused about a 20% broadening of the peak's FWHM. A 10% FWHM maximum variation occured with rotational positioning.

E. Performance vs. CCIS Ion Retarding Potential

Acceleration and retardation of ions prior to their entrance to the quadrupole was effected by equal alteration of cathode potentials V_{K1} and V_{K2} while the quadrupole entrance aperture was maintained grounded. Acceleration was found to degrade quadrupole resolution while retardation improved it. This improvement coupled with that obtained by lowering the anode potential, discussed above, points to high ion energy as an important resolution limiting factor.

Nitrogen peak narrowing, produced by increasing retardation potentials, is shown in Fig. 4 for some of the values investigated. A 300 volt retardation potential was found optimum, when accompanying a 2.0KV (later 2.2 KV) anode potential. For this determination, the 10% valley criterion* was used, the FWHM criterion being abandoned in its favor due to improved resolution.

F. Performance vs. Potential Between CCIS Cathodes

When making cathode potential $V_{K1} > V_{K2}$ resolution deteriorated obviously. For $V_{K1} < V_{K2}$, two conditions were tested: (1) with V_{K2} at -300 volts, resolution remained constant and sensitivity declined, (2) with V_{K2} at zero volts, resolution improved but not to the extent achieved by equal variation of cathode potentials, as in E above. The investigation was therefore abandoned.

*Peak separation which allows a valley less than 10% the height of either adjacent peak. With one peak, an equivalent criterion was used; the separation between 5% of the peak height on either side of the peak's center line.

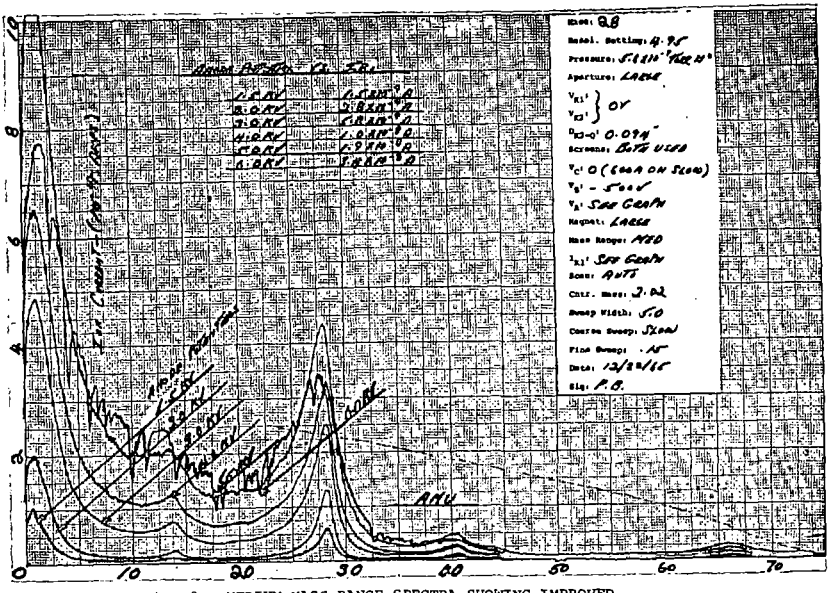

Fig. 3 MEDIUM MASS RANGE SPECTRA SHOWING IMPROVED RESOLUTION AND DECREASED SENSITIVITY AS CCIS ANODE POTENTIAL IS DECREASED

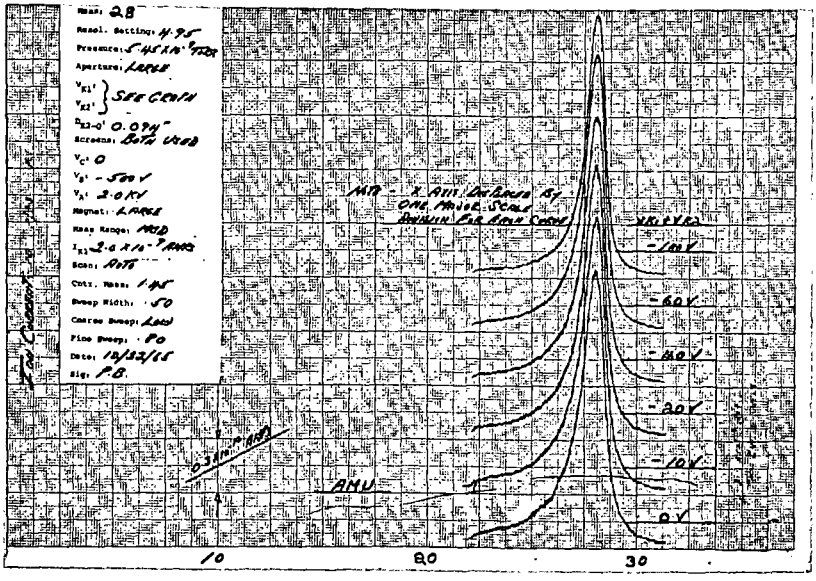

Fig. 4 MEDIUM MASS RANGE SPECTRA SHOWING NARROWING OF THE NITROGEN PEAK WITH INCREASED ION RETARDING POTENTIAL

G. Performance vs. Quadrupole Mass Range (Frequency)

Fig. 5 shows nitrogen spectra obtained on the low and medium mass ranges using optimum conditions, as discussed above. Only a portion of the spectra are shown and scales are normalized to the same amu. The superior resolution and sensitivity of the low mass range is obvious. (The noise on the medium mass spectrum is in the X-Y recorder.) Resolution at this stage of investigation using the 10% valley criterion, allowed peak separations of 2.5 amu and 1.5 amu for the medium and low mass ranges, respectively. These values were reproducible. The implications of the spectral differences as a function of mass scanning range will be discussed in part IV.

H. Performance vs. Magnet Size

Experiments heretofore described, were performed with a hollow, cylindrical, ceramic magnet stack with a 4.5" o.d., a 1.9" i.d. and a 2.25" length. Most of these experiments were repeated using a smaller magnet stack with a 3.5" o.d., 1.9" i.d. and 1.48" length. Axial magnetic flux densities, in gauss, for the large and small magnets, respectively, were as follows: (a) on axis at the magnet's center, 1220 and 838; (b) on axis at the magnet's edge, 397 and 368; (c) on the inside wall of the magnet at the magnet's center, 1426 and 957.

The small magnet spectra were very similar to those of the large magnet. Resolution at this stage of investigation, allowed peak separations of 3.0 amu and 1.5 amu (using the 10% valley criterion) on the medium and low mass ranges, respectively. This compares with 2.5 amu and 1.5 amu, respectively, for the large magnet. Sensitivity was slightly better than half that obtained with the large magnet. Most significantly, the small magnet had a comparatively high operating mode instability; during one mode change the entire nitrogen peak temporarily disappeared.

Further development might establish reliable operation with little or no loss of resolution or sensitivity, perhaps for still smaller magnets. At present, however, the larger magnet gives the more stable and sensitive performance.

I. Performance vs. Spectrometer Cleanliness

The CCIS, quadrupole and upper manifold were baked at 425°C for two days subsequent to tests heretofore described. This was in preparation for testing collector current linearity with pressure and for determining absolute sensitivity.

The baking resulted in an unexpected resolution improvement. Peak separations of 1 amu and .7 amu in the medium and low mass ranges, respectively, were obtained where 2.5 amu and 1.5 amu existed previously. The poorer resolution in the dirtier system is believed produced by increased secondary ion emmission, caused by ions or electrons from the source bombarding the quadrupole rods. Secondary ions thus produced part way down the rods would not be fully resolved and could cause the observed resolutions deterioration.

J. Performance vs. Pressure

1. Resolution

Resolution improved slightly with increased pressure but ion retarding potential had to be reduced to prevent spectral extinction; ion energy apparently decreases with increasing pressure. In accordance, a retarding potential just under that causing spectral extinction appeared optimum; the values noted at several pressures were as follows: 300 volts at 5.4×10^{-9} Torr, 200 volts at 3.8×10^{-8} Torr, 75 volts at 1.2×10^{-7} Torr, 54 volts at 2.3×10^{-6} Torr.

Fig. 6 shows a medium mass range spectrum of an inert gas mixture, obtained at 2.3×10^{-6} Torr subsequent to a 425°C bakeout. It is evident from the Xe^{131} and Xe^{132} peaks that a 1 amu separation has been obtained using the 10% valley criterion. On the low mass range resolution

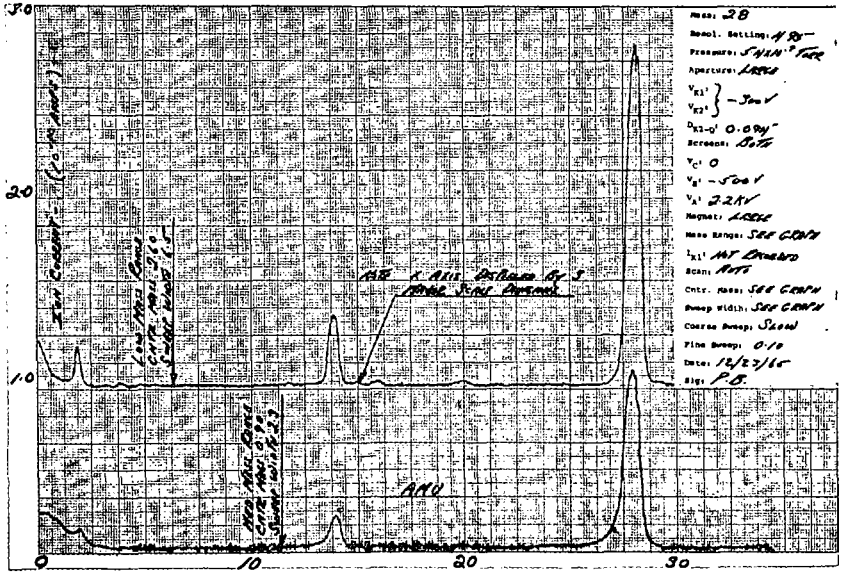

Fig. 5 COMPARISON OF OPTIMIZED SPECTRA ON THE LOW AND MEDIUM MASS RANGE. CURVES ARE NORMALIZED TO THE SAME AMU

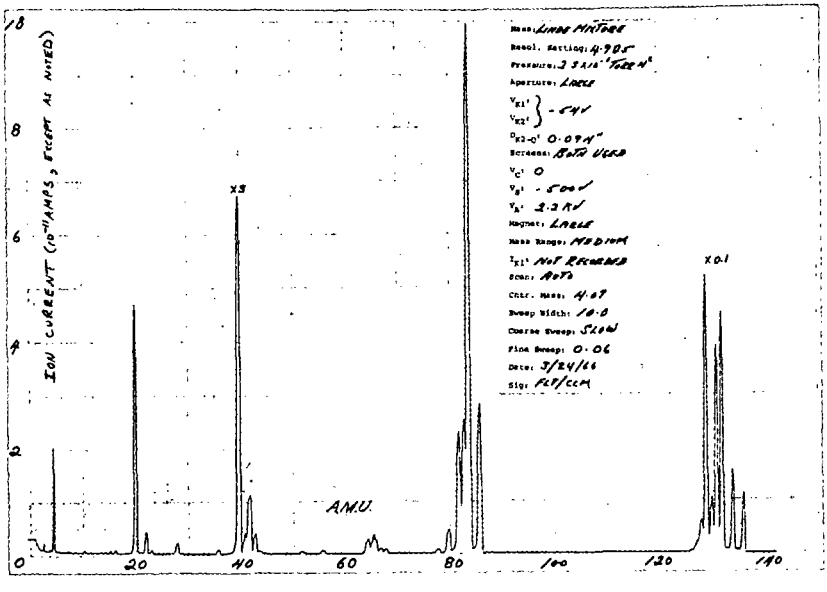

Fig. 6 MEDIUM MASS RANGE SPECTRUM OF INERT GASES ILLUSTRATING 10% VALLEY RESOLUTION OF PEAKS 1 AMU APART (Xe^{131} AND Xe^{132})

better than .7 amu was obtained. A low mass range methane spectrum at 2.5×10^{-8} Torr is shown in Fig. 7; although not optimum, the same retarding potential was used as at 2.3×10^{-6} Torr. A .7 amu peak separation can be deduced at mass 16 using the single peak 10% valley criterion. This resolution is equal or better than obtained by the authors using the quadrupole manufacturer's accompanying hot filament source at the same pressure; it appears therefore that resolution, at this point, may be limited by the quadrupole itself.

2. Ion Current

Ion current at the quadrupole collector was investigated as a function of pressure from approximately 3×10^{-9} Torr to 1×10^{-7} Torr for He^2, Ne^{20}, N^{28} and A^{40} on the low mass range and for A^{40} and Kr^{84} on the medium mass range. A constant 100 volt ion retarding potential was used and the following procedure adopted: (a) Bayard-Alpert gauge emmission current was adjusted for each gas, according to relative sensitivities tabulated for Dushman and Young in Dushman[10], to give a constant pressure sensitivity of .01 amps/Torr. (b) The quadrupole was set manually at the peak of the mass under investigation. (c) The ion pumps were valved off and the gas under investigation admitted slowly to maintain pressure equilibrium between gauge and ion source. (d) Quadrupole collector current was then continuously plotted against modulated Bayard-Alpert gauge current.

Ion current at the quadrupole collector (i_c) vs. pressure (p) was found to obey the relationship

$$i_c = kp^n \qquad (2)$$

(where k is a constant) for N^{28}, A^{40}, and Kr^{84}, while He^2 and Ne^{20} obeyed eq. (2) only in the 10^{-8} Torr range. A decrease in the exponent occured for the latter gases with decreasing pressure in the 10^{-9} Torr range and was believed due to a leak in the system or to other residual gases of higher atomic number; the low ionization efficiency of these two gases makes them more susceptible to these problems. The exponent n was between 1.15 and 1.20 for nitrogen, argon, and krypton; for neon and helium, it was .927 and .950, respectively.

A more thorough investigation of ion current over a wider pressure range is necessary more precisely to establish the value of n; this is due to the oscillations and discontinuities existent in cold cathode discharges over wide pressure ranges. The exponent may then more closely approximate unity, as it does in the magnetron gauge.

K. Performance vs. Atomic Mass

1. Sensitivity

Sensitivity vs. atomic mass for the gases investigated are given in Table I. Values are tabulated at 1×10^{-7} Torr and 3×10^{-9} Torr, which are the mean pressure extremes investigated. Sensitivities are derived from representative curves drawn from the data, which follow the relationship given by eq. (2). The lower pressure values for helium and neon are extrapolated due to leak difficulties discussed in J-2, above. Sensitivities obtained at 1×10^{-7} Torr with the hot filament source operated at a 3 ma emmission current is also tabulated for comparison; this source was a standard accessory of the spectrometer. Resolution for both hot filament and cold cathode sources was approximately 1 amu for all values shown. Sensitivities have been corrected for relative atomic abundances and for Bayard-Alpert gauge sensitivity variation with gas. The tabulated sensitivities were obtained with a Faraday cup collector and are therefore unamplified.

It is seen that CCIS sensitivities exceed those of the hot cathode source over the range of parameters investigated, even though the hot cathode source was operated at a relatively high emmission current. This sensitivity advantage increases with atomic number; under low mass range operating conditions, the CCIS/Hot Filament sensitivity ratio increases from 1.5 to 4.6 over the mass range 4 amu to 40 amu. Absolute sensitivities

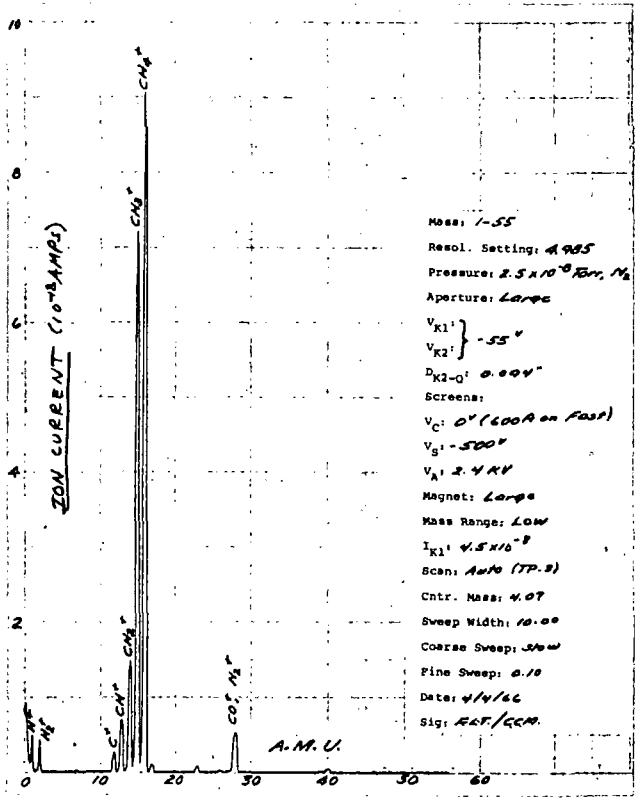

Fig. 7 LOW MASS RANGE METHANE SPECTRUM. A 10% VALLEY RESOLUTION OF PEAKS .7 AMU APART CAN BE DEDUCED

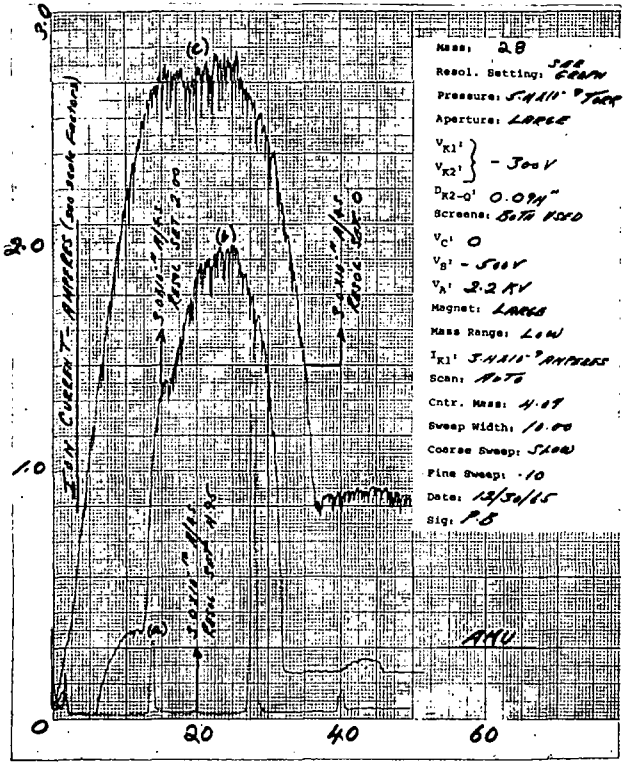

Fig. 8 LOW MASS RANGE SPECTRAL VARIATION WITH RESOLUTION SETTING SUBSEQUENT TO OPTIMIZATION

range from a low of .064 ma/Torr for helium to a high of 1.2 ma/Torr for krypton and argon. The maximum sensitivity variation with pressure for any particular gas is a factor of two over the approximately two decades investigated.

Gas.	Sensitivity (ma/Torr)		
	CCIS		Hot Fil.
	3×10^{-9} Torr	1×10^{-7} Torr	1×10^{-7} Torr
He^4	.077*(L)	.064 (L)	.042 (L)
Ne^{20}	.13* (L)	.10 (L)	.068 (L)
N^{28}	.40 (L)	.82 (L)	.25 (L)
A^{40}	.73 (L)	1.2 (L)	.26 (L)
	.38 (M)	.78 (M)	.29 (M)
Kr^{84}	.74 (M)	1.2 (M)	.35 (M)

*Extrapolated

TABLE I. Spectrometer Sensitivity vs. Atomic Mass for Hot Filament and Cold Cathode Ion Sources. L and M Indicate Low and Medium Mass Range Results, Respectively.

The sensitivity variation with mass is caused by variations both in the ion transmission of the quadrupole and in the ionization efficiency of the source. The quadrupole manufacturer supplied electronic means for adjusting relative mass sensitivities, but these controls were not investigated.

2. Resolution

Some variation in resolution as a function of mass is observable (See Fig.'s 6 and 7). This is attributed primarily to arbitrary settings of the manufacturers electronic sensitivity control noted above, since sensitivity can be increased only at the expense of resolution.

IV DISCUSSION

The above results demonstrate the capability of a quadrupole spectrometer to produce spectra with high sensitivity and resolution when coupled to a CCIS. However, the quadrupole used was selected for its commercial availability and does not represent an optimum design for a CCIS. An optimum design is discussed in two previous reports[11,12]; a larger rf potential and larger physical dimensions, primarily r_o, are required to accomodate the larger ion energy spread and larger ion beam diameter emergent from the CCIS.

An illustration of the benefits of a larger rf operating potential is the improvement resultant from a switch to the low mass range from the medium mass range, described in III G; it was noted, using Fig. 5, that sensitivity increased almost a factor of two and that resolution improved from a 10% valley peak separation of 2.5 amu to 1.5 amu (later 1.0 amu and .7 amu, respectively).

One reason for this improvement can be seen from relationships derived by Paul[13]. The rf potential V, mass M, rf frequency ν and the radius of the circle inscribed by the quadrupole rods r_o are related by

$$V = \frac{M\nu^2 r_o^2}{2.3 \times 10^{-20}} \qquad (3)$$

(the constant derives from the use of MKS units). Low mass range resolution and sensitivity improvement exists because the Ultek quadrupole employs higher frequency (5.3 mc) on the low mass range than on the medium mass range (3.3 mc). It can be seen from eq. (3) that as a result, the rf potential V on the low mass range must be increased to scan the same mass numbers common to both ranges (10-50 amu). However, the larger V

required for each mass M increases the transverse ion energy, U_{Tmax}, allowable for 100% transmission, according to:

$$U_{Tmax} = \frac{V}{15} \frac{\Delta M}{M} \tag{4}$$

where ΔM is the peak width at its base. More ions are therefore acceptable and sensitivity and/or resolution is improved.

Sensitivity and/or resolution improvement reasonably can be expected to continue by designing further increases in the required rf operating potential, until the ions with the largest U_{Tmax} are accommodated.

Indicative of higher sensitivity capabilities with larger rf potentials are results obtained with a family of nitrogen spectra recorded as a function of resolution. Here $\Delta M/M$ was varied, instead of V, to reduce the restrictions on U_{Tmax}, according to eq. (4). Spectra were recorded as in III B, but subsequent to achievement of otherwise optimum conditions (except for the 425°C bake). Results for the low mass range are shown in Fig. 8. It can be seen that when resolution is degraded just short of appreciable peak overlap, N^{28} sensitivity increased a factor of more than 10. On the medium mass range it increased a factor of 15. The .82 ma/Torr sensitivity for nitrogen at .7 amu peak separation (with 10% valley) therefore might reasonably be expected to approach 10 ma/Torr with an increased spectrometer rf potential; increasing quadrupole dimensions, primarily r_o, would also assist sensitivity improvement.

If improved quadrupole design allows enlarging the source exit apertures, a still greater fraction of the source's internal sensitivity could be realized; the ion current at the source cathodes K_1 and K_2 give sensitivities in the amps/Torr range.

V SUMMARY

A cold cathode ion source (CCIS) of the magnetron type has been developed for use in ultrahigh vacuum residual gas analysis. The purpose is to eliminate the spurious spectra produced by the conventional, hot filament, ion source and to produce increased sensitivity.

Studies were conducted using a commercial quadrupole spectrometer; the quadrupole is suitable because of its relative tolerance for a broad ion beam and large ion energies. The commercial unit was not optimally designed for the CCIS but allowed both its performance and potential to be evaluated.

Cold cathode quadrupole performance was studied against numerous parameters to determine optimum operating conditions. Resolution of mass peaks .7 amu apart was ultimately achieved, with the valley between peaks less than 10% the height of either adjacent peak. This resolution was identical to that obtained with the commercial hot filament source accompanying the spectrometer and appeared limited by the quadrupole itself. Sensitivity exceeded that obtained with the hot filament source, which was run with a 3 ma emmission current. Increased sensitivity factors of 1.5 to 4.5 were obtained depending on pressure and atomic mass; the corresponding absolute sensitivities at optimum resolution were .40 ma/Torr for N^{28} at 3×10^{-9} Torr and 1.2 ma/Torr for A^{40} at 1×10^{-7} Torr. Over the 10^{-8} and 10^{-9}Torr pressure (p) decades investigated, quadrupole collector current (i_c) obeyed the relationship $i_c = kp^{1.2}$, where k is a constant; an exponent closer to unity is expected over a larger pressure range.

The above results were obtained utilizing a 2.2 KV anode potential accompanied by an ion retarding field between source and quadrupole; hollow cylindrical magnets provided 1220 gauss at the center of the source. Smaller magnets providing 840 gauss, and having a third of the volumne of the larger magnets were also used; they gave comparable resolution but only half the sensitivity and they caused greater operating mode instability.

Following investigation of source operating parameters, sensitivity and resolution were investigated against quadrupole operating frequency

and rf and dc operating potentials; this was to determine the extent of benefits obtainable with an improved quadrupole design. Results indicated a potential sensitivity improvement factor of 10 with the same source configuration; resolution would be equal or better than that obtained thus far. If an improved quadrupole would allow enlarging the source exit apertures, a still greater fraction of the source's internal sensitivity, which is in the amps/Torr region, could be realized.

ACKNOWLEDGEMENTS

This work has been supported under Tasks 2, 6 and 8 of NASA Contract NAS1-2691. The writers wish to acknowledge the assistance of Peter Fowler for contributions to quadrupole theory analysis during the feasibility study stage.

REFERENCES

1. Hobson, J.P. and Redhead, P.A., Can. J. Phys. Vol. 36, 271 (1958).
2. Redhead, P.A., Can. J. Phys. Vol. 37, 1260 (1959).
3. Torney, F.L., and Fowler, P., NASA Contract NAS1-2691 Task 2 Final Report (1964).
4. Blum, P. and Torney, F.L., NASA Contract NAS1-2691 Task 6 Final Report (1965).
5. Böhm, H. und Gunther, K.G., Zeitsch. F. Angew. Physik 17, Band 7, Heft 16, 553 (1964).
6. Böhm, H. und Gunther, K.G., Vakuum-Technik, 14 Jhrg. Heft 7, 192 (1965).
7. Torney, op. cit.
8. Redhead, op. cit., Vol. 37, 1260.
9. Paul, W., Reinhard, H.P. and von Zahn, V., Zeitschrift für Physik, Bd. 152, 152 (1958).
10. Dushman, S., Scientific Foundations of Vacuum Technique, 2nd ed., Wiley, 324 (1962).
11. Torney, op. cit.
12. Blum, op. cit.
13. Paul, op. cit., Bd 152, 144 and 153.

A STUDY OF THE ISOTOPIC DISPROPORTIONATION REACTION BETWEEN LIGHT AND HEAVY WATER USING A PULSED-MOLECULAR-BEAM MASS SPECTROMETER*

J. W. Pyper, R. S. Newbury and G. W. Barton, Jr.
Department of Chemistry, Lawrence Radiation Laboratory, University of California, Livermore, California

INTRODUCTION

The value of the equilibrium constant for the isotopic disproportionation

$$H_2O + D_2O = 2HDO \qquad K = \frac{(HDO)^2}{(H_2O)(D_2O)}$$

reaction has come into question in the past several years.[1,2] The accepted value was 3.96[3] at 25.0°, which is virtually identical to the classical or "geometric mean" value of 4.0. This value of K was obtained from statistical mechanical calculations using measured and theoretical vibrational data obtained from infra-red spectroscopy. Recent calculations of K based on more extensive and supposedly more accurate spectroscopic data[4] lead to a value of 3.41[1,2] at 25.0°, which implies a large, unexpected quantum correction (due to anharmonicity) to the value of K. To complicate matters even more, Wolfsberg[5] has recently calculated a value for K of 3.85 using the harmonic approximation. The correct value of K is important, not only to resolve the discrepancy in the theory, but because this equilibrium is basic to many of the deuterium isotope effect studies done in aqueous media.

Until recently[6] there had not been a precise determination of K by direct experiment. This was due, in part, to the difficulty of analyzing HDO in the presence of H_2O and D_2O. Mass Spectroscopy was not used because of the "memory effect". One might hope, however, to overcome this memory effect by bleeding a mixture of the three water species into a mass spectrometer until equilibrium was reached. Preliminary experiments in this laboratory using this method were discouraging. The measured K was low and the precision of measurement poor. Thinking that it was the memory effect that was preventing the measurement of K, we devised a method that minimized this effect, e.g., the pulsed-molecular-beam mass spectrometer. Subsequent experiments indicated that extraneous water vapor was not the only problem. A background of deuterated ammonia species was present at mass numbers 18, 19 and 20. The pulsed-molecular-beam mass spectrometer minimized these interferring background species.

EXPERIMENTAL

A diagram of the apparatus used is given in Figure I. The water mixture was attached as shown and degassed by freezing the mixture, evacuating the tube and thawing the mixture several times. The water vapor species diffused through a leak valve directly into the mass spectrometer. The resulting molecular beam was pulsed by allowing it to pass through an American Time Products Type 42 Tuning Fork Chopper operating at 200 hz. The pulsed beam was then ionized by electron bombardment, magnetically analyzed and then measured with an electron multiplier. The energy of the ionizing electrons was held at a value below the appearance potentials of the fragment ions so that only parent ions were produced. The multiplier signal and the 200 hz sine wave from the tuning fork oscillator were fed into the Princeton Applied Research Model JB-6 Two-Phase Lock-In Amplifier in which all of the signal except that due to the pulsed molecular beam was filtered out. The output was converted to a single ended signal and passed through the Vidar 241 Voltage-to-Frequency Converter

*Work performed under the auspices of the U. S. Atomic Energy Commission.

1. J. W. Pyper and F. A. Long, J. Chem. Phys., 41, 2213 (1964)
2. R. E. Weston, Jr., J. Chem. Phys., 42, 2635 (1965)
3. H. C. Urey, J. Chem. Soc., 1947, 562
4. W. S. Benedict, N. Gailar and E. K. Plyler, J. Chem. Phys., 24, 1139 (1956)
5. As quoted in reference 6.
6. When the present study was being completed, we discovered that L. Friedman and V. J. Shiner at Brookhaven National Laboratory had made a parallel and independent study of K. A preliminary discussion of their results is soon to be published in J. Chem. Phys. Their data will be compared with ours in the discussion section of this paper.

into the Nuclear Data 180M Pulse Analyzer. Since only the pulsed molecular beam is ultimately analyzed, any water in the background or other interfering ions are discriminated against - minimizing the memory effect. The only place where adsorbed water might affect the analysis is in the inlet system and this difficulty can be minimized by baking the inlet system between sample analyses.

RESULTS AND DISCUSSION

Figure II shows the mass 20 beam (D_2O^+) with (upper trace) and without (lower trace) pulsing. As is seen, approximately 40% of the beam is modulated. The effect of modulation in the mass spectrum of a typical water mixture is shown in Figure III. The lower trace shows the mass spectrum of a 55 atom percent H mixture and the upper trace shows the corresponding pulsed beam spectrum. It is evident that the pulsed beam does not contain mass 17 (NH_3^+ only, since the electron energy is too low to produce OH^+) and the background water contribution to mass 18 has been eliminated. The appearance of NH_3^+ shows why we could not determine K by equilibrating the memory effect. To further illustrate this point, mass 18 has been resolved into its components in Figure IV (Resolution: 2800 - full width at half maximum). The main contribution to the peak is from H_2O^+, however there is a small but significant contribution from NDH_2^+. Similar ammonia contributions appear at mass 19 (ND_2H^+) and at mass 20 (ND_3^+). Figure V again illustrates the effectiveness of the pulsed beam system by showing that the NDH_2^+ contribution is removed from the mass 18 doublet. It is apparent, therefore, that K could only be determined in our instrument by using the pulsed molecular beam method or by working at high resolution and equilibrating the memory effect. Because of rapidity and convenience, we prefer the pulsed molecular beam method.

Experimental determinations of K were made at several deuterium compositions and at two temperatures. It was assumed in the calculations that the sensitivity of the mass spectrometer was the same for each of the three species. The results are shown in Table I. As is seen, there is no trend with hydrogen atom percent and no apparent trend with temperature. One would expect a temperature coefficient, but apparently it is so slight that our data do not detect it. It is of interest to compare our results with those of Friedman and Shiner (see reference 6). Their results are shown in the last column at three different temperatures. As is seen, the results from the two different studies confirm each other very well. Friedman and Shiner do detect a slight temperature coefficient which is of the same order of magnitude as their errors. It is interesting to note that Friedman and Shiner equilibrated the memory effect. They did not have the ammonia background problem since their instrument uses mercury diffusion pumps to attain high vacuum, while our instrument uses ion pumps. The ammonia background presumably comes from the reaction of N_2 and H_2 in the ion pumps.

Table I

SUMMARY OF EXPERIMENTAL RESULTS

T (°C)	% H (g)	Number of Experiments	K	K (Av)	Friedman[6] and Shiner
0°	32.4	7	3.80 ± 0.09		
	55.0	8	3.72 ± 0.03	3.75 ± 0.07	3.74 ± 0.02
	77.3	6	3.73 ± 0.04		
24.8 ± 0.5°	29.6	11	3.75 ± 0.07		
	54.8	38	3.75 ± 0.07	3.74 ± 0.07	3.76 ± 0.02
	77.0	13	3.71 ± 0.06		
75°					3.80 ± 0.04

This pulsed molecular beam method might well be used routinely to measure the composition of water-heavy water mixtures. Table II shows some pertinent data. Column one is the isotopic assay in atom percent given by the suppliers of the mixture - Bio-Rad Laboratories. They do not claim high accuracy. Column two is the atom % H measured in the gas phase. Column three is the measured % H in the liquid phase calculated using the known vapor pressures of H_2O, HDO and D_2O.[7] Column four

7. I. Kirshenbaum, "Physical Properties and Analysis of Heavy Water" (McGraw-Hill Book Company, Inc., New York, 1951) p. 24-5.

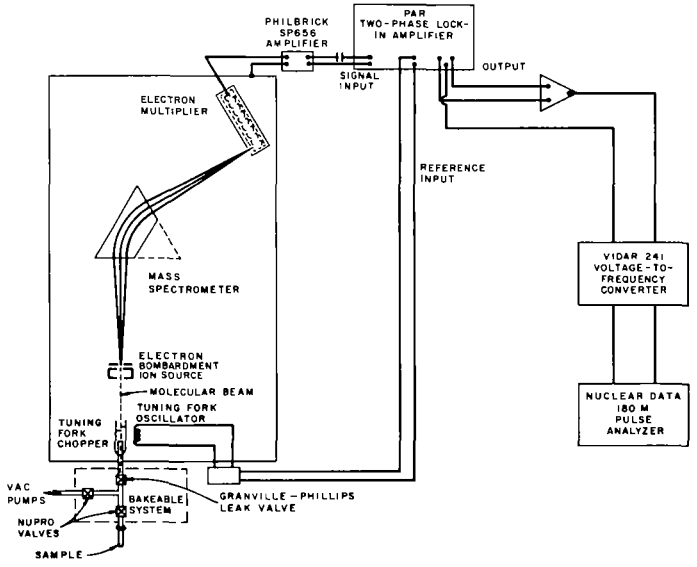

Figure I APPARATUS

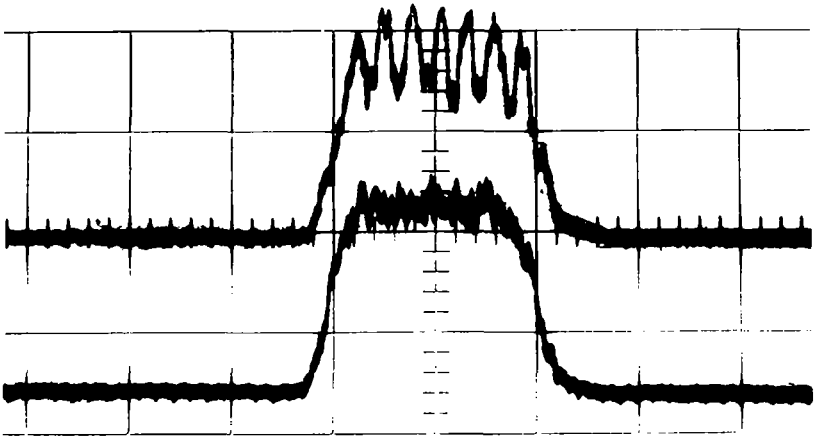

Figure II EFFECT OF MODULATION ON MASS 20 PEAK

is the atom % H in the liquid phase as measured by NMR. The agreement between our data and that of NMR is good except at 75.7 % H. The NMR data are just preliminary, however, and we are waiting for more precise analyses. The precision of the mass spectrometric method is good and we believe that this method could be developed into a useful analytical procedure. As would be expected, the equilibration time for change of sample was reduced to several hours by bakeout of the inlet system. Bakeout between samples also leads to more precise results.

Table II

RESULTS OF COMPOSITION DETERMINATIONS

% H(l) Bio-Rad	% H(g) Measured	% H(l) Calculated	% H(l) NMR
27	29.6 ± 0.7	28.3	28.0
53	54.8 ± 0.7	53.0	53.3
77	77.0 ± 0.3	75.7	74.1

Table III compares the result from the present study with equilibrium constants for similar isotopic disproportionation reactions. It is expected that as the mass difference between hydrogen and deuterium becomes small relative to the total mass of the parent molecule, the disproportionation equilibrium constant should approach the geometric mean value of 4.0. This is indeed the trend observed.

Table III

COMPARISON WITH OTHER SYSTEMS

25°C

Reaction	Exp. K	Statistical K
$H_2 + T_2 = 2HT$	2.87[8]	2.56[9]
$H_2 + D_2 = 2HD$	3.28[10]	3.24[11]
$H_2O + D_2O = 2HDO$	3.74	3.85[5]
$C_2H_2 + C_2D_2 = 2C_2HD$	3.95[12]	-----

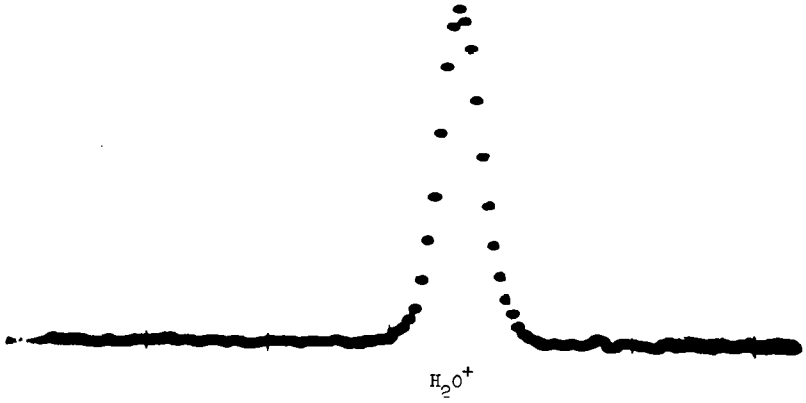

Figure V EFFECT OF MODULATION ON MASS 18 DOUBLET

8. H. C. Mattraw, C. F. Pachucki, and L. N. Dorfman, J. Chem. Phys., 20 926 (1952).
9. W. M. Jones, J. Chem. Phys., 16, 1077 (1948).
10. D. Rittenberg, W. Bleakney and H. C. Urey, J. Chem. Phys., 2, 48 (1934).
11. W. M. Jones, J. Chem. Phys., 17, 1062 (1949).
12. J. W. Pyper and F. A. Long, J. Chem. Phys., 41, 1890 (1964).

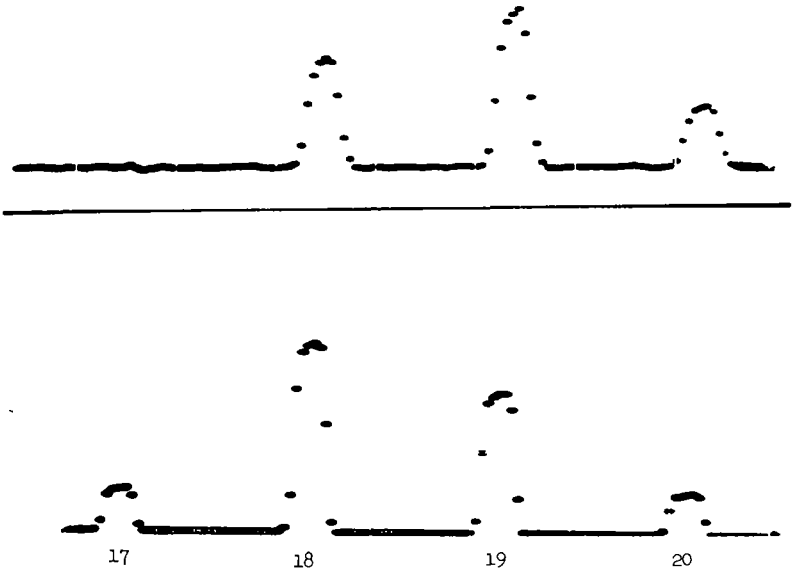

Figure III EFFECT OF MODULATION ON WATER SPECTRUM

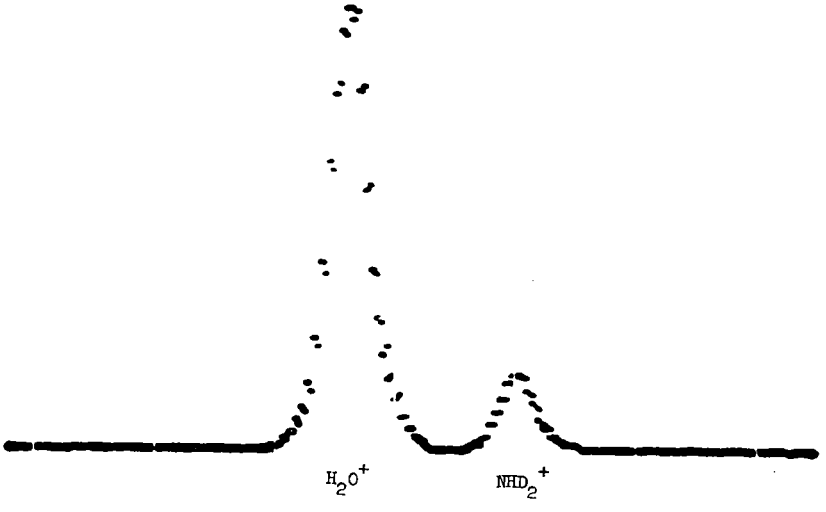

Figure IV RESOLVED DOUBLET AT MASS 18

EVOLUTION OF SAMPLING TECHNIQUES FOR MASS SPECTROMETRIC ANALYSIS OF SEALED DEVICES

B. I. Grady, Jr.

Tube Department, General Electric Company, Owensboro, Kentucky

ABSTRACT

Probably the most difficult problem encountered in mass spectrometry is to devise methods of opening sealed devices so that gases contained therein may be introduced into the analyzer without contamination. It is often necessary to analyze evacuated, or partially evacuated, production samples so that the composition and/or the pressure of the gases contained in the final product may be determined. Due to the various sizes and shapes of Tube Department products, a number of sampling techniques have been devised. This paper will discuss the evolution of several of these techniques as applied to thermionic tubes, photocells, reed switches, and other sealed devices.

* *

We have had a problem in our laboratory that some of you may have experienced. How often, in the course of mass spectrometric analysis, have you needed to analyze the final product of the assembly line, but found that it was not possible to do so with your available opening devices? As industries grow through new product lines and expand existing ones, this final product may not be of a convenient size or shape to permit a routine analysis with the existing opening devices and you must design new ones.

This has been the situation at the General Electric Company Tube Department. After the consolidation of the Power Tube and Receiving Tube Departments, the thermionic tubes submitted for analysis began to vary widely both in size and shape. Figure 1 illustrates some of the products that are presently analyzed in our laboratory. Large industrial thyratrons (back) and small ceramic-metal tubes (right) took their place on the analytical shelf, alongside with the conventional glass receiving tubes (left front). The product line was expanded with the addition of photocells (front center) of various sizes and shapes and with magnetic reed switches (right front). As each of the different products was first submitted for analysis, this required the construction of new and varied devices for opening and analyzing them.

These finished products are analyzed for various reasons:

1. To determine outgassing of parts during operation, e.g., the gases evolved during operation of receiving tubes.

2. To determine pressure in gas-filled products, e.g., the pressure in a thyratron determines the starting voltage.

3. To determine gaseous compositions, including contaminants, e.g., certain proportions of nitrogen and oxygen in a photocell are critical for its best operation.

Two analyzers are used in our laboratories: a CEC 21-620 mass spectrometer with a metal inlet system, and a General Electric Partial Pressure Analyzer. The former, of course, is used to analyze gas-filled products and the latter is for our evacuated product.

One of our first sampling devices was very simple, as shown in Figure 2. It consisted of a 12/30 glass taper joint with a quick-connect on the opposite end, and a sidearm containing a magnetic stainless steel slug. The stainless steel slug is moved with an external magnet so that it strikes the tubulation which seals the tube being analyzed. This tubulation breaks off where it has been previously scored, and the piece of tubulation is caught by a small screen in the taper joint.

This device is used primarily for opening evacuated processed tubes, without flashed getters, in order that they may be operated on the mass spectrometer without having been exposed to the atmosphere. This allows the comparison of outgassing characteristics of tube components made from different materials.

A thermionic tube with a flashed getter could not be opened and analyzed on the CEC 21-620 because the getter would tend to pump down the inlet system from 10^{-3} torr, to the range of 10^{-7} torr, which is the pressure in a good operating tube. Tubes with getters must, therefore, be operated for analysis on the Partial Pressure Analyzer, which we will discuss shortly.

This device has the advantage of easy electrical connections for tube operation. Its primary disadvantage is that no regular production tubes can be analyzed because a special elongated tip-off is necessary.

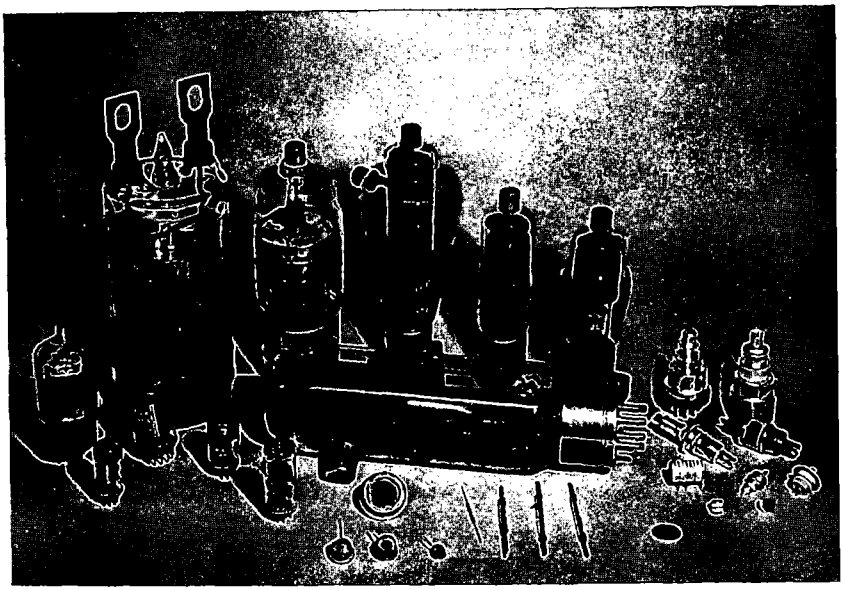

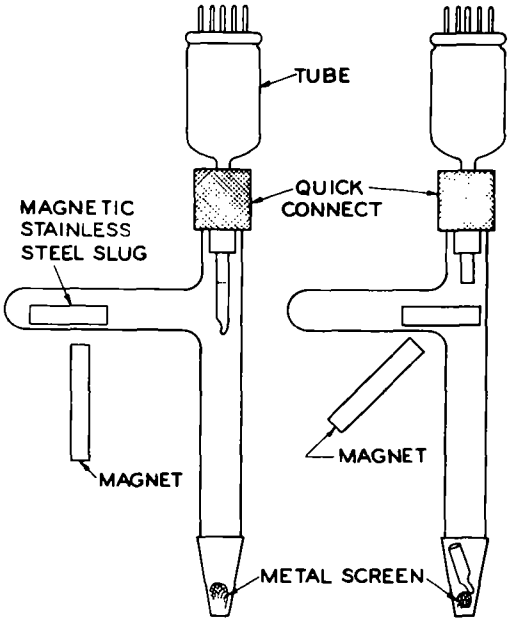
TUBE
QUICK CONNECT
MAGNETIC STAINLESS STEEL SLUG
MAGNET
MAGNET
METAL SCREEN

Figure 2

The second basic opening technique is called the hammer and anvil technique. As shown in Figure 3, it consists of a two-part Pyrex container which is sealed with Apiezon grease. The anvil is a non-magnetic stainless steel slug which rests on a wire screen in the bottom of the Pyrex container. The hammer is a magnetic stainless steel slug. A file is used to scratch the glass around the tip-off of the tube being analyzed, to facilitate breakage. The sample is then placed on the anvil and the hammer is raised with two external magnets and dropped.

This device was designed primarily for opening small xenon-filled thyratrons, in T6 1/2 bulbs, from production.

Since this tube type employs a getter, the main interest was in the pressure of the xenon filling gas, rather than contaminating gases which might be present.

This same technique was also used on photocells which were sealed into the same size bulb. These photocells were filled with dry air at pressures of about 670 torr. We were interested both in the pressure and the composition of the filling gas and any contaminants which might be present. The characteristics of photocells were related to the filling gases that were used, and the levels of contaminants also affected the operating life of the photocell.

Photocells were next made smaller and put into glass-metal packages as shown here. To open these, some means had to be found of holding the photocell and cracking its glass top. The solution was a non-magnetic holder with a point in the center that was fitted around the photocell. The magnetic hammer was used to pound the holder and drive the point through the glass cover of the photocell. This glass was 30 mils thick and in high compression, so of course, the glass had to be scratched to weaken it.

The next opening problem was encountered with the introduction of magnetic reed switches into the product line. Since the reed is magnetic, it is not possible to just place it into the Pyrex container and magnetically raise the hammer to drop on the switch. The switch will also be raised and tends to assume a vertical position in the container.

The solution was a small sidearm at the bottom of the Pyrex tube, as shown in Figure 4. The reed switch can be inserted through the sidearm and laid on the anvil. Thus, when the magnetic hammer is raised, the reed switch will remain on the anvil to be broken, since it is too long to turn the corner and move up the Pyrex tube. Regular reed switches are nitrogen-filled to a pressure of about half an atmosphere.

Figure 5. A vacuum reed switch was introduced next. This switch had a small tip-off which would not allow it to fit into the sidearm of the conventional breaker. This problem was overcome by slipping a non-magnetic stainless steel ring over the reed switch down to the tip-off. This held the switch in position in the breaker, allowing for easy opening.

It is important that all the glass-enclosed products be scratched so as to weaken the glass. If this is not done, then more than likely, the analytical container will break before the sample does.

The third basic technique is the bellow-sealed point method, of which there are two variations.

The first variation of this technique utilizes an evacuated bottle similar to one described by George Schacher of the General Electric Engineering Laboratory in Analytical Chemistry[1]. Mr. Schacher's device is operated by turning a knurled knob to apply pressure through a threaded rod to the steel point. This would have worked fine for many of our samples, but there were some tubes which could not be opened by this method. In place of the threaded rod, we designed a device that is activated by air pressure, as shown in Figure 6.

The basic components are:

1. The bottle, which is a commercial glass metal seal with a flange attached to the metal end, and a stopcock sealed to the glass end. This is a double stopcock to allow air inlet to the bottle. The other opening is attached to the mass spectrometer.

2. The bellows sealed, movable head, which is mounted on a flanged base. This head is threaded to accept a variety of points and odd-shaped slugs.

(1) Analytical Chemistry, Volume 31, p. 161, January 1959

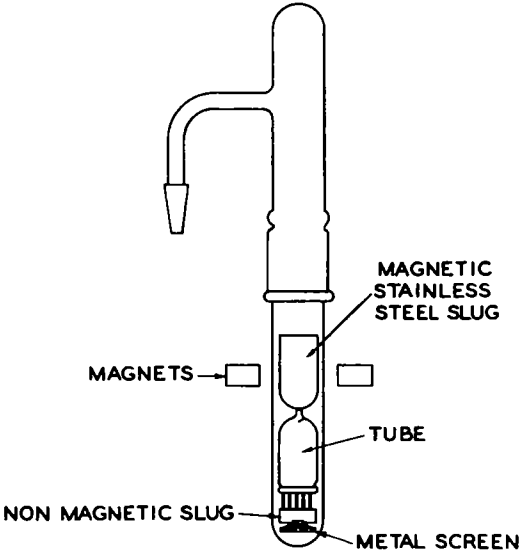

Figure 3

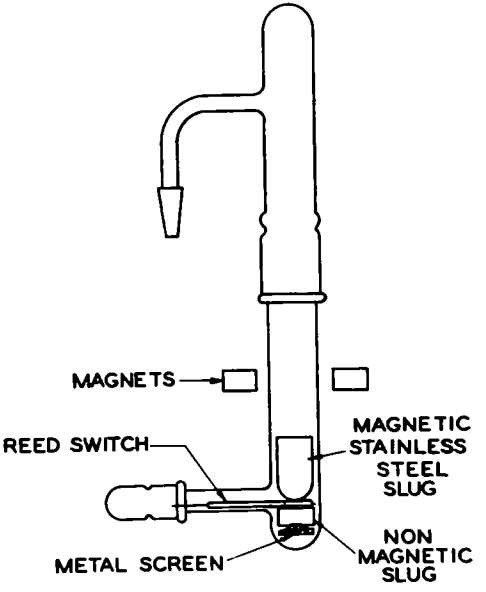

Figure 4

3. An electrically operated solenoid for releasing a burst of air pressure.

4. An airmite device which is an air-operated piston, and

5. A movable steel slug which activates the bellows sealed head.

The sample is mounted above the head. Each type tube that is analyzed requires a different holder and four stainless steel rods allow a variety of sample holders to be used. Some tubes are held completely rigid and punctured with the point, while others are mounted so that only one part of the tube is rigid, allowing the tube to fly apart when hit with a blunt head. A screen is placed over the holder to keep the tube parts from breaking the glass.

The sample is adjusted so that the point or blunt head, as the case may be, is set rigid against the sample. This is necessary to prevent premature movement of the head by atmospheric pressure, and possibly opening the tube prior to analysis.

The vacuum bottle is positioned over the flanged base and the two are bolted together with an O-ring between them. The device is then evacuated through the mass spectrometer inlet system.

After recording a background, the solenoid is activated, releasing a burst of high pressure air to the airmite device, which in turn, forces the movable slug up against the bellows sealed head, opening the tube. Samples may require air pressures varying from 25 to 75 pounds per square inch.

This device is used primarily for the tubes shown on the right in Figure 1. As previously mentioned, some tubes are shattered and some are punctured.

The second variation, which does employ the threaded rod technique, is used with the Partial Pressure Analyzer. As shown in Figure 7, the sample is placed in a stainless steel cross that is attached to the analyzer. The bellows sealed point is attached to one arm of the cross. The point is then activated by the knurled knob applying pressure through a threaded rod, as mentioned previously. With this device, we can open and operate receiving tubes with getters in the vacuum environment at which they normally operate, while observing the gases that may be evolved.

The back row of Figure 1 shows our large gas-filled thyratrons. Notice the non-uniformity of these tubes, both in shape and size. We decided that the best approach was to evacuate a portion of the tube surface rather than the whole tube. The resulting device is shown in Figure 8, and used a pointed steel rod to pierce the glass.

This device consists of a small, vacuum-tight enclosure with a large flat surface. The enclosure has three openings: (1) a quick-connect in the front, which accepts a glass tubulation for admission of gases to the mass spectrometer; (2) a quick-connect in the center of the bottom, which holds and seals a movable, pointed stainless steel rod; (3) a hole in the top, which is aligned with the bottom hole. The sample is placed over this top hole, which is surrounded by a flat neoprene gasket.

Prior to analysis, a tube must have a small pit sandblasted into the surface at that point on the tube surface that will be set over the hole in the opening device. There are two reasons for this:

First, to keep the pointed rod from slipping on the glass and forcing the tube out of position. Setting the point in this pit assures alignment of the hole with the pit, thus assuring that the weakest point in the tube surface will be directly over the sampling hole.

Secondly, this pit assures a proper opening of the sample, and the depth of this pit is very critical. If the pit is too deep, atmospheric pressure may force the point through the thin glass prematurely, or in positioning the tube, one may push the rod through the thin glass. If the pit is too shallow, the tube may crack around the periphery as the rod is struck. The ideal thickness of glass in the bottom of the pit is from 10-15 mils. This is not always easy to judge, since glass thickness varies with tube size. Some tube types use a bulb that is 30-35 mils thick, while another type uses a glass thickness that can vary from 90-120 mils.

After initial preparation, the sample is placed on the opening device with the neoprene gasket around the top hole. The point is set in the pit and the tube is strapped down to hold it in position. After pumpdown, opening is accomplished by hammering the pointed rod into the sample. The rod is then pulled back slightly to allow free movement of the gas into the mass spectrometer.

The devices which I have discussed here were designed and constructed in our laboratory as the need for them arose. They have been described here in hope that you can obtain some useful ideas that may be applied to your work.

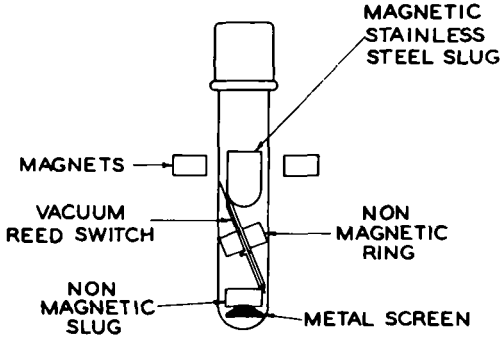

Figure 5

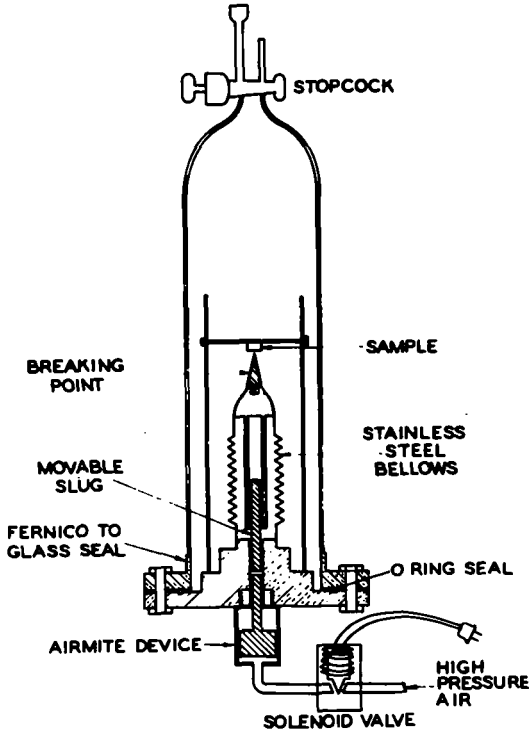

Figure 6

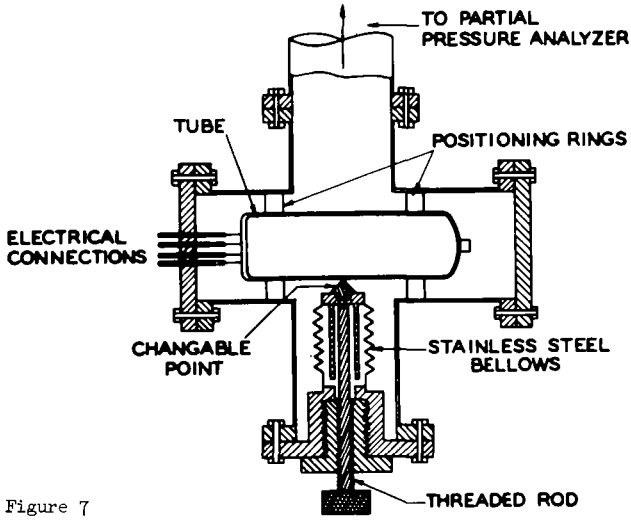

Figure 7

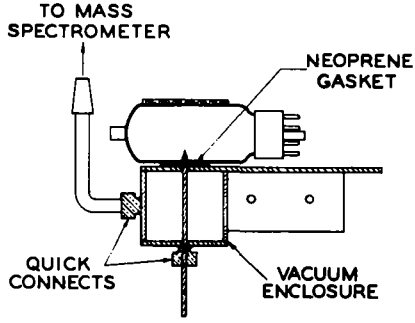

SIDE SECTION

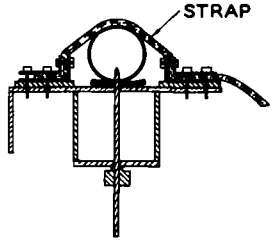

END SECTION

Figure 8

EVALUATION OF INCANDESCENT LAMPS WITH THE MASS SPECTROMETER

H. R. Schoenfeldt, General Electric Co., Cleveland, Ohio

Introduction

There are two principle measurements for evaluating lamp quality with the mass spectrometer:

1. The level of contaminants in the filling gas.
2. The contaminants that are evolved from a heated (evacuated) lamp.

In item number 1, a 500-micron sample is taken and analyzed for various gaseous impurities and for the composition of the major components. These can be reported in percentages and are accurate to about 40 ppm using a model 130 CEC mass spectrometer. In our system we use a mercury pump with a liquid N_2 trap and maintain a vacuum of 2×10^{-7} Torr.

After analysis of the filling gas is obtained, it is evacuated and the filament is heated to observe the evolution of contaminants. In a vacuum lamp, the residual gas can be measured, and after it is evacuated, the lamp can be operated at 120 volts. After the filling gas is removed from a gas filled lamp, the filament is burned at 70 volts.

For our evaluation we have found it desirable to use lamps that were manufactured without getter and without flashing of the filament.

Equipment

The incandescent lamp is inserted in a socket and held in a base up position with a slight vertical pressure to maintain a high vacuum seal between the O rings and the end of the bulb. Fig. 1 illustrates the experimental setup. The hole that is pierced through the bulb by the plunger is shown in Fig. 2. This is accomplished by the acceleration of the plunger (inside of a vacuum-tight tube) by an external coil (Figs. 1 and 3 - item 7). The position of the inner and outer O rings with respect to the bulb are illustrated in Fig. 2. Their location in the head (Fig. 3) shows the opening of the vacuum guard between them (item 4) and its extension (item 6) to the rough vacuum pump.

During the interval that the filament is lighted, the evolution of impurities can be monitored with a peak selector. We generally establish a time interval (e.g., 10 minutes) of heating and measure the total accumulation of contaminants.

We are primarily interested in the gaseous contaminants such as CO_2, CH_4, CO, N_2, H_2, H_2O and O_2. Since we do not have a heated inlet system, the H_2O values are usually disregarded.

Experimental Results

The measurement of the filling gas (or residual gas of vacuum lamps) showed only slight traces of contaminants, so they will not be reported. In Table I the results of evolved contaminants for 25W lamps when the filament is held at 120 volts for 10 minutes are listed in ascending order for the amount of H_2. The two major contaminants are H_2 and CO, with only small amounts of CH_4 and no CO_2 or O_2. These lamps had been gettered and flashed similar to our normal product.

The most significant feature of these results is the degree of variability between lamps. The H_2 ranged between 0.2-6.55 and the CO between 0.2-4.4 micron liters per lamp. This variability encouraged us to continue our investigation by obtaining some 25W, 60W and 100W lamps, with and without getter, but not flashed.

Table II compares the 25W ungettered and unflashed lamps with those that have been gettered but not flashed. Heating of the filament shows higher levels of CO than H_2, except for lamp no. 3 where the filament burned out after 9½ minutes. The gettered, but unflashed, lamps have lower levels of CO and H_2 after heating.

The filaments of the 60W and 100W lamps in Tables III and IV were held at 70 volts for 10 minutes after the filling gas was evacuated. The 60W lamps in Table III show a definite reduction in contaminants when the getter is present and is evaporated. The 100W lamps (Table IV) do not show the same degree of reduction in contaminants from the gettering action, and, in fact, they show an increase in CO.

It is our belief that most of these contaminants are evolved from the coil. In order to prove this, we compared the results of poorly washed coils with some that were rewashed, with the following results:

	25W			60W			100W		
	CH_4	CO	H_2	CH_4	CO	H_2	CH_4	CO	H_2
Inadequately Washed Coils	0.8	9.8	7.1	1.3	27.5	14.7	1.3	25.1	18.6
Rewashed	0.4	8.1	1.7	1.3	21.2	13.7	1.0	18.3	11.2

The rewashed coils showed lower levels of contaminants when the filaments were heated to incandescence in the evacuated lamp.

Conclusions

The examination of incandescent lamps with the mass spectrometer shows a wide variation of evolved contaminants when the filament is heated. This method should be useful in evaluating lamp quality. Plans are being formulated to see if there is a correlation between lamp performance and the level of contaminants.

Table I

25-Watt Lamps

Gettered and Flashed

Lamp No.	1	2	3	4	5	6	7
	After evacuation, filament is held at 120V for 10 minutes						
CO_2	0	0	0	.1	0	0	0
CH_4	0	0	.1	.1	.1	.1	.7
CO	.2	.7	1.4	2.0	.6	4.4	1.21
H_2	.2	.9	1.0	1.3	3.5	4.7	6.55

Value in Micron-liters

Table II
Evaluation of 25-Watt Lamps

After evacuation, filament held at 120V for 10 minutes

Lamp No.	1	2	3	4	5	1	2
	No getter or flashing					Gettered but not flashed	
CO_2	.1	.1	0*	.1	-	.1	.1
CH_4	0	.2	.2	0	-	0	0
CO	3.1	5.2	3.1	8.1	-	2.1	2.1
H_2	.3	1.2	12.7	1.8	-	.6	.2

* - Lamp no. 3 - filament burned out after 9½ minutes.

All values in micron-liters

Table III
Evaluation of 60-Watt Lamps

After evacuation, filament is held at 70V for 10 minutes

Lamp No.	1	2	3	4	1	2	3	4
	No getter or flashing				Gettered-not flashed			
CO_2	.3	.1	0	.1	.1	0	0	0
CH_4	2.3	2.7	1.6	.6	.4	.2	1.2	.8
CO	20.4	10.5	31.7	5.2	4.0	9.9	26.8	6.6
H_2	78.6	14.7	31.2	14.8	8.2	7.1	30.0	14.4

All values in micron-liters

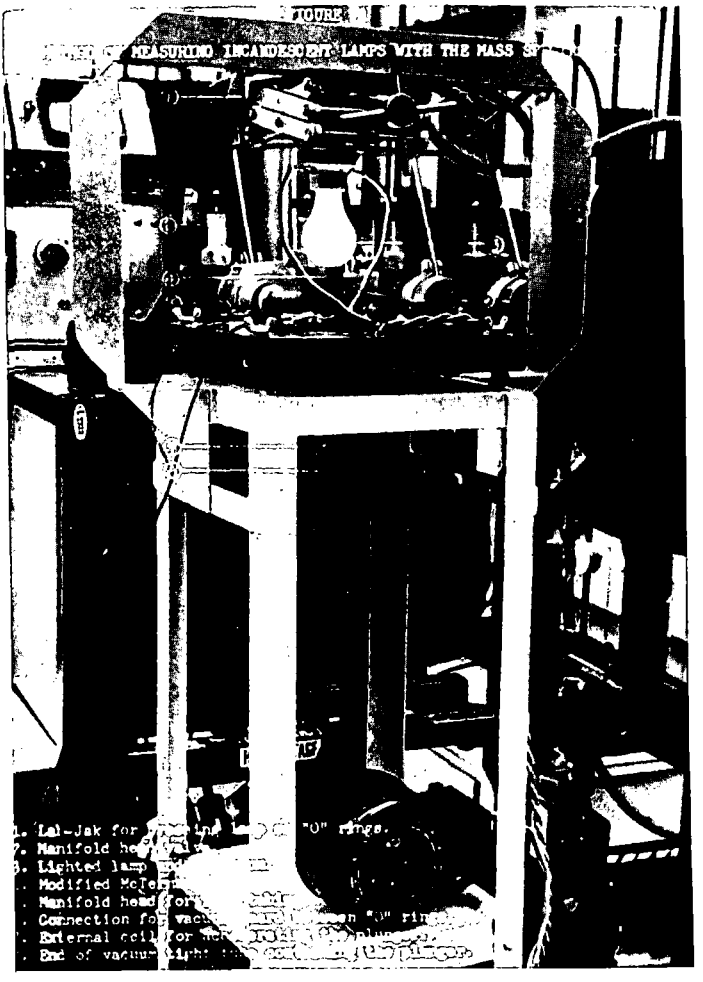

Table IV
Evaluation of 100-Watt Lamps

After evacuation, filament is held at 70V for 10 minutes

Lamp No.	1	2	3	4	1	2	3	4
	No getter or flashing				Gettered-not flashed			
CO_2	0.1	0.1	0.1	0.1	0.1	0.1	0	0.1
CH_4	1.1	0.8	1.8	1.6	0.4	0.6	0	1.8
CO	11.5	8.5	9.9	13.5	11.8	13.9	8.0	29.6
H_2	22.5	12.2	17.5	37.6	13.1	19.7	4.5	39.4

All values in micron-liters

FIGURE 4

POSITION OF "O" RINGS TO MAKE A VACUUM TIGHT SEAL

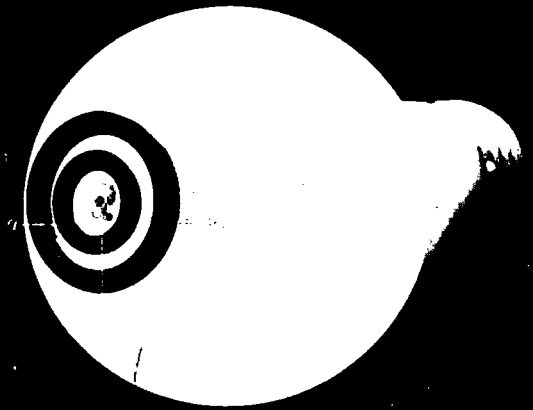

1. Inner "O" ring.
2. Outer "O" ring.
Space between "O" rings serves as a vacuum guard and is connected to a separate vacuum pump.
3. This hole is punctured by the plunger after inner "O" ring is fully evacuated.

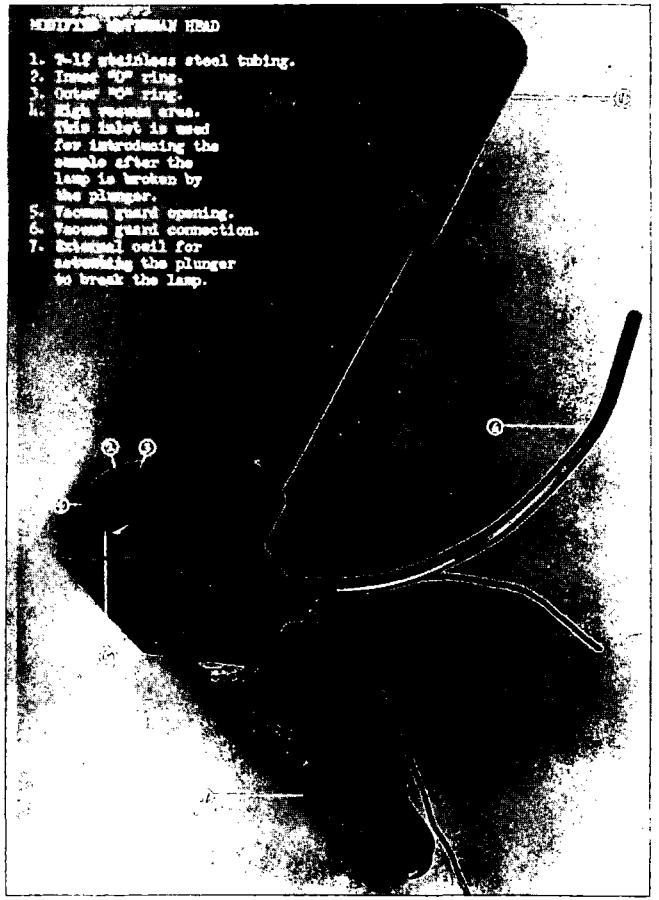

Ghost Peaks From Quadrupole Field Mass Spectrometers

N.E. Hamilton
Kennecott Copper Corporation
Lexington, Massachusetts

Abstract

A prevalant type of ghost peaks from quadrupole field mass spectrometers has been identified. Understanding of the phenomena has progressed to the point where their magnitude can be manipulated, at will, over more than three orders of magnitude.

A mechanism is proposed for their formation, involving accommodation coefficients at grazing incidents. A series of corroboratory experiments are described and discussed. Attention is called to some remaining anomalies and the benefits and limitations of correcting spectra.

1965 (and early 1966) Bibliography

Fundamental and Theoretical Aspects of Mass Spectrometry

Prepared by Subcommittee II

Ionization and Appearance Potentials . . . . . B. G. Hobrock

Gaseous Negative Ions . . . . . B. Steiner and N. Wells

Photoionization and Related Studies . . . . . F. N. Harllee

Free Radicals and Chemical Kinetics . . . . . J. T. Herron

Isotopic Abundance . . . . . E. J. Catanzaro

IONIZATION AND APPEARANCE POTENTIALS

Brice G. Hobrock

1. Al-Joboury, M. I. and Turner, D. W., J. Chem. Soc., 1964, 4434. MOLECULAR PHOTOELECTRON SPECTROSCOPY. II. A SUMMARY OF IONIZATION POTENTIALS.

2. Al-Joboury, M. I. May, D. P. and Turner, D. W., J. Chem. Soc., 1965, 612. MOLECULAR PHOTOELECTRON SPECTROSCOPY. III. THE IONIZATION POTENTIALS OF OXYGEN, CARBON MONOXIDE, NITRIC OXIDE AND ACETYLENE. 11.36, 16.27, 18.33

3. Akopyan, M. E. and Vilesov, F. I., Zh. Fiz. Khim., 40, 125 (1966). MASS SPECTROSCOPIC STUDY OF BENZENE DERIVATIVES. PHOTOIONIZATION UP TO 885 A OF THE SPECTRAL REGION.

4. Amme, R. C. and Hayden, H. C., J. Chem. Phys., 42, 2011 (1965). ION-BEAM EXCITATION EFFECTS ON THE SINGLE CHARGE TRANSFER BETWEEN ARGON AND NITROGEN.

5. Aplin, R. T., Budzikiewicz, H. and Djerassi, C., J. Am. Chem. Soc., 87, 3180 (1965). MASS SPECTROMETRY IN STRUCTURAL AND STEREOCHEMICAL PROBLEMS. LXXIII. THE NEGATIVE ION MASS SPECTRA OF SOME SIMPLE ORGANIC COMPOUNDS.

6. Aquilanti, V., Galli, A., Giardini-Guidoni, A. and Volpi, G. G., J. Chem. Phys., 43, 1969 (1965). ION-MOLECULE REACTIONS IN HYDROGEN-RARE GAS MIXTURES.

7. Balducci, G., Capallii, A., De Maria, G. and Guido, M., J. Chem. Phys., 43, 2136 (1965). TETRACARBIDE MOLECULES IN THE VAPOR PHASE OVER RARE EARTH-GRAPHITE SYSTEMS.

8. Bates, D. R., Boyd, A. H. and Prasad, S. S., Proc. Phys. Soc. (London), 85, 1121 (1965). IMPACT IONIZATION OF SODIUM.

9. Baughan, E. C., Trans. Faraday Soc., 61, 2337 (1965). ELECTRON AFFINITIES AND SCREENING CONSTANTS.

10. Baylis, A. B., Pressley, G. A., Gordon, M. E. and Stafford, F. E., J. Am. Chem. Soc., 88, 929 (1966). MASS SPECTROMETRIC INVESTIGATION OF THE PYROLYSIS OF BORANES. TETRABORANE (10).

11. Becker, P. M. and Lampe, F. W., J. Chem. Phys., 42, 3857 (1965). MASS SPECTROMETRIC STUDY OF THE BIMOLECULAR FORMATION OF DIATOMIC ARGON ION.

12. Bernal, E., Ready, J. F., and Levine, L. P., Phys. Letters, 19, 645 (1966). ABSORBED ION EMISSION FROM LASER-IRRADIATED TUNGSTEN.

13. Berry, B. S., Compt. Rend. Conf. Intern. Phenomenes Ionisation Gaz., 6e, Paris, 1, 13 (1963). DIABATIC EFFECT IN MOLECULAR IONIZATION BY ELECTRON IMPACT.

14. Beynon, J. H., Saunders, R. A. and Williams, A. E., Z. Naturforsch., 20A, 180 (1965). FORMATION OF METASTABLE IONS IN MASS SPECTROMETERS WITH RELEASE OF INTERNAL ENERGY.

15. Bibby, M. M., Toubelis, B. J. and Carter, G., Electron. Letters, 1, 50 (1965). IONIZATION AND DISSOCIATION IN CF_4.

16. Blackburn, P. E. and Buchler, A., J. Phys. Chem., 69, 4250 (1965). THE THERMODYNAMICS OF VAPORIZATION IN THE BERYLLIUM OXIDE-BORON OXIDE SYSTEM.

17. Blauer, J. A., Greenbaum, M. A. and Farber, M. J. Phys. Chem., 69, 1069 (1965). THE THERMODYNAMIC AND PHYSICAL PROPERTIES OF BERYLLIUM COMPOUNDS. VII. ENTHALPY AND ENTROPY OF SUBLIMATION OF BERYLLIUM FLUORIDE.

18. Borisov, Y. A., Gusarov, A. V. and Gorokhov, L. N., Teplofiz. Vysokikh Temperatur. Akad. Nauk S. S. S. R., 2, 487 (1964). MASS SPECTROMETRIC INVESTIGATION OF THE EVAPORATION OF CESIUM PEROXIDE.

19. Botter, R., Dibeler, V. H., Walker, J. H. and Rosenstock, H. M., J. Chem. Phys., 44, 1271 (1966). EXPERIMENTAL AND THEORETICAL STUDIES OF PHOTOIONIZATION EFFICIENCY CURVES FOR C_2H_2 AND C_2D_2.

20. Briglia, D. D. and Rapp, D., Phys. Rev. Letters, 14, 245 (1965). IONIZATION OF THE HYDROGEN MOLECULE BY ELECTRON IMPACT NEAR THRESHOLD.

21. Briglia, D. D. and Rapp, D., J. Chem. Phys., 42, 3201 (1965). IONIZATION OF H_2 BY ELECTRON IMPACT NEAR THRESHOLD.

22. Brion, C. E., Frost, D. C. and McDowell, C. A., J. Chem. Phys., 44, 1034 (1966). MASS SPECTROMETRIC STUDIES OF THE RARE GASES USING AN ELECTRON VELOCITY SELECTOR.

23. Browne, J. C., J. Chem. Phys., 41, 3495 (1964). BINDING ENERGY OF LiH AND THE IONIZATION POTENTIAL (I.P.) OF LiH^+. MIXED BASIS SET CALCULATION.

24. Brunnee, C. and Voshage, H., MASSENSPEKTROMETRIE, Verlag Karl Thiemig KG, Munich, 1964. 316 pp.

25. Burgess, A., Proc. Intern. Conf. Phys. Electron. At. Collisions, 3rd, Univ. Coll., London, 1963, 237. SEMICLASSICAL TREATMENT OF THE EXCITATION AND IONIZATION OF ATOMS AND POSITIVE IONS BY ELECTRON IMPACT.

26. Cantone, B., Grasso, F. and Pignataro, S., J. Chem. Phys., 44, 3115 (1966). DECOMPOSITION PROCESSES AND FRAGMENTATION PROBABILITIES OF $W(CO)_6$ BY ELECTRON IMPACT.

27. Cater, E. D., Lee, T. E., Johnson, E. W., Rauh, E. G. and Eick, H. A., J. Phys. Chem., 69, 2684 (1965). VAPORIZATION THERMODYNAMICS AND DISSOCIATION ENERGY OF LANTHANUM MONOSULFIDE.

28. Cermak, V., J. Chem. Phys., 43, 4527 (1965). ON THE EVIDENCE OF THE N_2NO^+ ION.

29. Cermak, V. and Herman, Z., Collection Czech. Chem. Commun., 30, 169 (1965). IONIZING REACTIONS OF NOBLE GAS ATOMS IN METASTABLE STATES WITH POLYATOMIC MOLECULES.

30. Chen, C. T., U. S. At. Energy Comm., TID-21648 (1965). STUDY OF LABELED NITROUS OXIDE. $^{15}N^{14}NO$.

31. Chupka, W. A., Argonne Natl. Lab. Rev., 1, 15 (1964). IONIZATION AND DISSOCIATION OF POLYATOMIC MOLECULES.

32. Colin, R., Drowart, J. and Verhaegen, G., Trans. Faraday Soc., 61, 1364 (1965). MASS SPECTROMETRIC STUDY OF THE VAPORIZATION OF TIN OXIDES. DISSOCIATION ENERGY OF SnO.

33. Colin, R. and Drowart, J., AD-607792. VAPORIZATION OF COMPOUNDS AND ALLOYS AT HIGH TEMPERATURES. XVII. THERMODYNAMIC STUDY OF TIN SELENIDE AND TIN TELLURIDE USING A MASS SPECTROMETER.

34. Colin, R., Drowart, J. and Verhaegen, G., AD-611365. VAPORIZATION OF COMPOUNDS AND ALLOYS AT HIGH TEMPERATURES. XXV. MASS SPECTROMETRIC STUDY OF THE VAPORIZATION OF THE TIN OXIDES. THE DISSOCIATION ENERGY OF SnO.

35. Collin, J. E., Delwiche, J. and D'Or, L., Bull. Classe Sci., Acad. Roy. Belg., 49, 1244 (1963). MASS DISCRIMINATION IN A 180° MASS SPECTROMETER: ITS APPLICATION TO THE EVALUATION OF THE INITIAL KINETIC ENERGY OF THE IONS.

36. Conway, D. C. and Yang, J., J. Chem. Phys., 43, 2900 (1965). BONDING IN HOMO-MOLECULAR ION CLUSTERS, O_{2n+2}.

37. Cook, G. L. and Dinneen, G. U., U. S. Bur. Mines, Rept. Invest. 6698 (1965). MASS SPECTRA OF ORGANIC SULFUR COMPOUNDS.

38. Cotter, J. L., J. Chem. Soc., 1964, 5477. FRAGMENTATION PATTERNS OF ACETANILIDE AND BENZAMIDE.

39. Cotter, J. L., J. Chem. Soc., 1964, 5491. FRAGMENTATION PATTERNS OF 3,5-DIPHENYL-1,2,4-OXADIAZOLE AND 2,5-DIPHENYL-1,3,4-OXADIAZOLE.

40. Cotter, J. L., J. Chem. Soc., 1965, 1520. ELECTRON IMPACT STUDIES OF SOME AROMATIC FLUOROCARBONS.

41. Cotter, J. L., J. Chem. Soc., 1965, 5742. ELECTRON IMPACT FRAGMENTATION OF PENTAFLUOROBENZAMIDE.

42. Cotter, J. L., J. Chem. Soc., 1965, 6842. THE MASS SPECTRA OF SOME FLUORINE-CONTAINING 1,3,4-OXADIAZOLES.

43. Couchet, G. and Zvenigorosky, A., Bull. Union Physiciens, 59, 681 (1965). DETERMINATION OF IONIZATION POTENTIALS BY ELECTRIC METHODS.

44. Cress, M. C., Becker, P. M. and Lampe, F. W., J. Chem. Phys., 44, 2212 (1966). PULSED MASS SPECTROMETRIC STUDY OF THE BIMOLECULAR FORMATION OF N_3.

45. De Maria, G., Gingerich, K. A., Malaspina, L. and Piacente, V., J. Chem. Phys., 44, 2531 (1966). DISSOCIATION ENERGY OF THE GASEOUS AlP MOLECULE.

46. De Maria, G., Goldfinger, P., Malaspina, L. and Piacente, V., Trans. Faraday Soc., 61, 2146 (1965). MASS SPECTROMETRIC STUDY OF GASEOUS MOLECULES, ZnS, ZeSe, AND ZnTe.

47. De Maria, G., Guido, M., Malaspina, L. and Pesce, B., J. Chem. Phys., 43, 4449 (1965). MASS SPECTROMETRIC STUDY OF THE YTTRIUM-CARBON SYSTEM.

48. Derwish, G. A. W., Galli, A., Giardini-Guidoni, A. and Volpi, G. G., J. Am. Chem. Soc., 87, 1159 (1965). ION-MOLECULE REACTIONS IN ACETYLENE.

49. Dewar, J. J. S. and Rona, P., J. Am. Chem. Soc., 87, 5510 (1965). DOUBLY CHARGED IONS IN THE MASS SPECTRA OF SOME ORGANOBORON DERIVATIVES.

50. Dibeler, V. H., Krauss, M., Reese, R. M. and Harllee, F. N., J. Chem. Phys., 42, 3791 (1965). MASS SPECTROMETRIC STUDY OF PHOTOIONIZATION. III. METHANE AND METHANE-d_4.

51. Dibeler, V. H., Reese, R. M. and Krauss, M., J. Chem. Phys., 42, 2046 (1965). MASS SPECTROMETRIC STUDY OF PHOTOIONIZATION. II. H_2, HD AND D_2.

52. Dibeler, V. H. and Walker, J. A., J. Chem. Phys., 43, 1842 (1965). ION PAIR PROCESSES IN CH_3Cl BY PHOTOIONIZATION.

53. Dillard, J. G. and Kiser, R. W., J. Phys. Chem., 69, 3893 (1965). IONIZATION AND DISSOCIATION OF RUTHENIUM AND OSMIUM TETROXIDES.

54. Doepker, R. D. and Ausloos, P., J. Chem. Phys., 44, 1641 (1966). GAS PHASE RADIOLYSIS OF CYCLOBUTANE.

55. Dorman, F. H., J. Chem. Phys., 43, 3507 (1965). IONIZATION EFFICIENCY CURVES FOR FRAGMENT IONS BY ELECTRON IMPACT.

56. Dorman, F. H., J. Chem. Phys., 44, 35 (1966). IONIZATION EFFICIENCY CURVES FOR FRAGMENT IONS BY ELECTRON IMPACT.

57. Drowart, J., Condensation Evaporation Solids Proc. Intern. Symp., Dayton, Ohio, 1962, 255. STUDIES OF THE VAPORIZATION OF INORGANIC SUBSTANCES AT HIGH TEMPERATURES.

58. Drowart, J., Colin, R. and Exsteen, G., Trans. Faraday Soc., 61, 1376 (1965). MASS SPECTROMETRIC STUDY OF THE VAPORIZATION OF LEAD MONOXIDE. DISSOCIATION ENERGY OF PbO.

59. Drowart, J., Colin, R. and Exsteen, G., AD-612780. VAPORIZATION OF COMPOUNDS AND ALLOYS AT HIGH TEMPERATURES. XXVI. MASS SPECTROMETRIC STUDY OF THE VAPORIZATION OF LEAD MONOXIDE.

60. Drowart, J., Degreve, F., Verhaegen, G. and Colin, R., AD-607511. VAPORIZATION OF COMPOUNDS AND ALLOYS AT HIGH TEMPERATURES. XXIII. THERMOCHEMICAL STUDY OF THE GERMANIUM OXIDES USING A MASS SPECTROMETER.

61. Drowart, J., Degreve, D., Verhaegen, G. and Colin, R., Trans. Faraday Soc., 61, 1072 (1965). VAPORIZATION OF COMPOUNDS AND ALLOYS AT HIGH TEMPERATURES. XXIII. THERMOCHEMICAL STUDY OF THE GERMANIUM OXIDES USING A MASS SPECTROMETER. THE DISSOCIATION ENERGY OF THE MOLECULE GeO.

62. Elder, F. A., Villarejo, D. and Inghram, M. G., J. Chem. Phys., 43, 758 (1965). ELECTRON AFFINITY OF OXYGEN.

63. Erhardt, E. and Tekaat, T., Z. Naturforsch., 19A, 1382 (1964). DETERMINATION OF THE APPEARANCE POTENTIALS OF IONIZED MOLECULE FRAGMENTS HAVING INITIAL KINETIC ENERGY.

64. Farrell, P. G. and Newton, J., J. Phys. Chem., 69, 3506 (1965). IONIZATION POTENTIALS OF AROMATIC AMINES.

65. Fehlner, T. P., J. Am. Chem. Soc., 88, 1819 (1966). THE IDENTIFICATION OF THE P_2H_2 MOLECULE IN THE PYROLYSIS OF DIPHOSPHINE.

66. Field, F. H. and Munson, M. S. B., J. Am. Chem. Soc., 87, 3289 (1965). REACTIONS OF GASEOUS IONS. XIV. MASS SPECTROMETRIC STUDIES OF METHANE AT PRESSURES TO 2 TORR.

67. Foffani, A., Pignataro, S., Cantone, B. and Grasso, F., Z. physik. Chem. (Frankfurt), 42, 236 (1964). CALCULATION OF IONIZATION POTENTIALS FOR AROMATIC COMPOUNDS.

68. Foffani, A., Pignataro, S., Cantone, B. and Grasso, F., Z. physik. Chem. (Frankfurt), 42, 221 (1964). IONIZATION POTENTIALS AND SUBSTITUENT EFFECTS FOR AROMATIC CARBONYL COMPOUNDS.

69. Foffani, A., Pignataro, S., Cantone, B. and Grasso, F., Z. physik. Chem. (Frankfurt), 45, 79 (1965). MASS SPECTRA OF METAL HEXACARBONYLS.

70. Friedman, L. and Moran, T. F., J. Chem. Phys., 42, 2624 (1965). CROSS-SECTIONS OF EXOTHERMIC ION-MOLECULE REACTIONS. He^+-H_2.

71. Fuchs, R. and Taubert, R., Z. Naturforsch., 20A, 823 (1965). THE KINETIC ENERGY OF IONIZED MOLECULE FRAGMENTS. V. CHARGE SEPARATION PROCESS IN THE CO_2 MASS SPECTRUM.

72. Garstang, R. H., J. Chem. Phys., 44, 1308 (1966). TRANSITIONS IN EXCITATION BY ELECTRON IMPACT.

73. Gingerich, K. A., J. Am. Chem. Soc., 87, 1660 (1965). APPLICATION OF HIGH-TEMPERATURE MASS SPECTROMETRY TO THE DETERMINATION OF THE ENTHALPY-COMPOSITION FUNCTION OF NONSTOICHIOMETRIC BINARY COMPOUNDS.

74. Gingerich, K. A., J. Chem. Phys., 44, 1717 (1966). MASS SPECTROMETRIC STUDY OF THE EQUILIBRIUM BETWEEN DIATOMIC AND MONATOMIC PHOSPHORUS AND DISSOCIATION ENERGY OF P_2.

75. Green, J. H. and Ryan, K. R., Proc. Roy. Soc. (London), A286, 178 (1965). KINETIC ENERGY OF FRAGMENT IONS IN A RADIO-FREQUENCY MASS SPECTROMETER.

76. Harrison, A. G., Haynes, P., McLean, S. and Meyer, F., J. Am. Chem. Soc., 87, 5099 (1965). THE MASS SPECTRA OF METHYL-SUBSTITUTED CYCLOPENTADIENES.

77. Hashizume, A., Wasada, N. and Tsuchiya, T., Bull. Chem. Soc. Japan, 39, 150 (1966). MASS SPECTROMETRIC STUDY OF PHOSPHORUS OXIDE.

78. Heddle, D. W. O. and Seaton, M. J., Proc. Intern. Conf. Phys. Electron. At. Collisions, 3rd, Uni. Coll., London, 1965, 137. THE EXCITATION AND IONIZATION OF ATOMS BY ELECTRON IMPACT.

79. Henchman, J. J., Otwinowska, H. T. and Field, F. H., AD-603314. A HIGH PRESSURE MASS SPECTROMETRIC STUDY OF NEOPENTANE.

80. Herman, Z. and Cermak, V., Collection Czech. Chem. Commun., 30, 2114 (1965). ION-MOLECULE REACTIONS IN MIXTURES OF GASES WITH ALKALI METAL AND MERCURY VAPORS.

81. Herman, Z. and Cermak, V., Collection Czech. Chem. Commun., 31, 649 (1966). ASSOCIATIVE IONIZATION IN MIXTURES OF CARBON MONOXIDE WITH SODIUM AND POTASSIUM AND THE MECHANISM OF ASSOCIATIVE IONIZATION REACTIONS.

82. Hertel, G. R. and Koski, W. S., J. Am. Chem. Soc., 87, 1686 (1965). ION-MOLECULE REACTIONS BETWEEN RARE GAS IONS AND METHANE.

83. Hess, G. G. and Lampe, F. W., J. Chem. Phys., 44, 2257 (1966). REACTIONS IN GASEOUS MONOSILANE.

84. Hess, G. G., Lampe, F. W. and Sommer, L. H., J. Am. Chem. Soc., 87, 5327 (1965). AN ELECTRON IMPACT STUDY OF IONIZATION AND DISSOCIATION OF TRIMETHYLSILANES.

85. Higgins, W. and Jennings, K. R., Trans. Faraday Soc., 60, 97 (1966). DOUBLY-CHARGED METASTABLE IONS OF AROMATIC HYDROCARBONS.

86. Hildenbrand, D. L. and Murad, E., J. Chem. Ohys., 43, 1400 (1965). DISSOCIATION ENERGY OF BORON MONOFLUORIDE FROM MASS SPECTROMETRIC STUDIES.

87. Hildenbrand, D. L. and Murad, E., J. Chem. Phys., 44, 1524 (1966). MASS SPECTROMETRIC DETERMINATION OF THE DISSOCIATION ENERGY OF BERYLLIUM MONO-FLUORIDE.

88. Hildenbrand, D. L. and Theard, L. P., J. Chem. Phys., 42, 3230 (1965). EFFUSION STUDIES, MASS SPECTRA AND THERMODYNAMICS OF BERYLLIUM FLUORIDE VAPOR.

89. Hogg, A. M., Haynes, R. M. and Kebarle, P., J. Am. Chem. Soc., 88, 28 (1966). ION-SOLVENT MOLECULE INTERACTIONS STUDIED IN THE GAS PHASE. HEATS AND ENTROPIES OF INDIVIDUAL STEPS. $NH_4^+\cdot(n-1)NH_3 + NH_3 = NH_4^+\cdot nNH_3$.

90. Hogg, A. M. and Kebarle, P., J. Chem. Phys., 43, 449 (1965). STUDY OF IONS AT NEAR-ATMOSPHERIC PRESSURE. II. AMMONIUM IONS PRODUCED BY THE ALPHA RADIOLYSIS OF AMMONIA AND THEIR SOLVATION IN THE GAS PHASE BY AMMONIA AND WATER MOLECULES.

91. Hughes, R. H. and Hendrickson, C. G., J. Opt. Soc. Am., 54, 1494 (1964). EXCITATION OF THE ^2P LEVEL IN LITHIUM BY ELECTRON IMPACT.

92. Jason, A. J., Burns, R. P. and Inghram, M. G., J. Chem. Phys., 43, 3762 (1965). STRUCTURE IN FIELD-IONIZATION ENERGY DISTRIBUTIONS.

93. Johnson, E. W., Doctoral Dissertation, State University of Iowa, Iowa City (1965). MASS SPECTROMETRIC STUDIES OF THE VAPORIZATION OF STRONTIUM SULFIDE, LANTHANUM MONOSULFIDE AND SOME LANTHANUM-SILVER ALLOYS.

94. Katsuura, K., J. Chem. Phys., 42, 3771 (1965). IONIZATION OF ATOMS BY COLLISION WITH EXCITED ATOMS.

95. Keneshea, F. J. and Cubicciotti, D., J. Phys. Chem., 69, 3910 (1965). THE THERMODYNAMICS OF VAPORIZATION OF THALLOUS FLUORIDE AND ITS GASEOUS DIMER-IZATION.

96. Kent, R. A. and Margrave, J. L., Chem. Eng. Data, 10, 296 (1965). VAPORIZATION AND SUBLIMATION OF $SrCl_2$.

97. Kent, R. A. and Margrave, J. L., J. Am. Chem. Soc., 87, 4754 (1965). MASS SPECTROMETRIC STUDIES AT HIGH TEMPERATURES. VIII. THE SUBLIMATION PRESSURE OF IRON(II) FLUORIDE.

98. Kent, R. A., McDonald, J. D. and Margrave, J. L., J. Phys. Chem., 70, 874 (1966). MASS SPECTROMETRIC STUDIES AT HIG TEMPERATURES. IX. THE SUBLIMATION PRESSURE OF COPPER(II) FLUORIDE.

99. Khvostenko, V. I. and Sultanov, A. S., Zh. Fiz. Khim., 39, 475 (1965). IONIZATION OF MOLECULES OF THALLIUM CHLORIDE, BROMIDE AND IODIDE BY ELECTRON IMPACT.

100. King, A. B., J. Chem. Phys., 42, 3526 (1965). MASS SPECTRAL FRAGMENTATION OF PHENYL-n-ALKANES.

101. Kiser, R. W., INTRODUCTION TO MASS SPECTROMETRY AND ITS APPLICATIONS, Prentice-Hall, Inc., Englewood Cliffs, New Jersey, 1965. 356 pp.

102. Koch, H. V., Arkiv Fysik, 28, 559 (1965). DISSOCIATION OF ETHANE MOLECULE IONS FORMED IN CHARGE EXCHANGE COLLISIONS WITH POSITIVE IONS. ION-MOLECULE REACTIONS OF ETHANE.

103. Krebs, K. H. and Zilinski, E., Kernenergie, 5, 98 (1962). THE DISSOCIATION OF H_2^+ AND H_3^+ IN AN ACCELERATOR TUBE.

104. Kupriyanov, S. E., Zh. Eksperim. i Teor. Fiz., 47, 2001 (1964). FORMATION OF EXCITED O_2^+ AND N_2^+ IONS DURING IONIZATION OF AIR BY ELECTRONS.

105. Kupriyanov, S. E., Dokl. Akad. Nauk S. S. S. R., 162, 865 (1965). DETECTION OF REACTIONS BETWEEN HIGHLY EXCITED HYDROGEN ATOMS AND ETHYLENE MOLECULES.

106. Kupriyanov, S. E., Kinetika i Katiliz, 6, 725 (1965). EFFECT OF ELECTRON ENERGIES AND CONDITIONS OF IONIZATION IN AN ION SOURCE ON THE MASS SPECTRA OF CARBON TETRACHLORIDE AND METHANE.

107. Kuriakose, A. K. and Margrave, J. L., Inorg. Chem., 4, 1639 (1965). MASS SPECTROMETRIC STUDIES OF THE THERMAL DECOMPOSITION OF POLY(CARBON MONOFLUORIDE).

108. Kuroda, H., Nature, 210, 1214 (1964). IONIZATION POTENTIALS OF POLYCYCLIC AROMATIC HYDROCARBONS.

109. Kybett, B. D., Carroll, Natalis, P., Bonnell, D. W., Margrave, J. L. and Franklin, J. L., J. Am. Chem. Soc., 88, 626 (1966). THERMODYNAMIC PROPERTIES OF CUBANE.

110. Lassettre, E. N., J. Chem. Phys., 43, 2046 (1965). SELECTION RULES IN EXCITATION BY ELECTRON IMPACT.

111. Latypov, Z. Z. and Kupriyanov, S. E., Zh. Fiz. Khim., 39, 1572 (1965). MASS SPECTRA AND ENERGY OF EXCITED IONS.

112. Levine, R. D., J. Chem. Phys., 44, 2046 (1966). KINETICS OF UNIMOLECULAR BREAKDOWN. V. MASS SPECTRAL PATTERNS.

113. Lifshitz, C. and Long, F. A., J. Phys. Chem., 69, 3731 (1965). APPEARANCE POTENTIALS AND MASS SPECTRA OF FLUORINATED ETHYLENES. II. HEATS OF FORMATION OF FLUORINATED SPECIES AND THEIR POSITIVE IONS.

114. Lifshitz, C. and Long, F. A., J. Phys. Chem., 69, 3737 (1965). APPEARANCE POTENTIALS AND MASS SPECTRA OF FLUORINATED ETHYLENES. III. CALCULATIONS BASED ON THE STATISTICAL THEORY OF MASS SPECTRA.

115. Lifshitz, C. and Long, F. A., J. Phys. Chem., 69, 3741 (1965). APPEARANCE POTENTIALS AND MASS SPECTRA OF C_3F_6, C_3F_5Cl AND c-C_3F_6.

116. Lifshitz, C. and Long, F. A., J. Phys. Chem., 69, 3746 (1965). SOME OBSERVATIONS CONCERNING THE POSITIVE ION DECOMPOSITION OF C_2F_6 AND C_3F_8 IN THE MASS SPECTROMETER.

117. Lyast, I. T., Zh. Strukt. Khim., 6, 271 (1965). QUANTUM MECHANICAL CALCULATION OF THE MOLECULAR IONIZATION POTENTIAL.

118. McCulloh, K. E., Sharp, T. E. and Rosenstock, H. M., J. Chem. Phys., 42, 3501 (1965). DIRECT OBSERVATION OF THE DECOMPOSITION OF MULTIPLY CHARGED IONS INTO SINGLY CHARGED FRAGMENTS.

119. McGowan, J. W., Clarke, E. M., Hanson, H. P. and Stebbings, R. F., Phys. Rev. Letters, 13, 620 (1964). ELECTRON- AND PHOTON-IMPACT IONIZATION OF O_2.

120. McGowan, J. W. and Fineman, M. A., Phys. Rev. Letters, 15, 179 (1965). ROTATIONAL STRUCTURE AT THRESHOLD IN THE H_2^+ ELECTRON IMPACT IONIZATION SPECTRUM.

121. McKinley, J. D., J. Chem. Phys., 42, 2245 (1965). MASS SPECTRUM OF YTTRIUM CHLORIDE VAPOR.

122. McLafferty, F. W. and Pinzelik, J., Anal. Chem., 38, 350R (1966). MASS SPECTROMETRY.

123. Maier, W. B., J. Chem. Phys., 42, 1790 (1965). DISSOCIATIVE IONIZATION OF MOLECULES BY RARE GAS ION IMPACT.

124. Malone, T. J. and McGee, H. A., J. Phys. Chem., 69, 4338 (1965). MASS SPECTROMETRIC INVESTIGATIONS OF THE SYNTHESIS, STABILITY, AND ENERGETICS OF THE LOW-TEMPERATURE OXYGEN FLUORIDES. I. DIOXYGEN DIFLUORIDE.

125. Malone, T. J. and McGee, H. A., J. Phys. Chem., 70, 316 (1966). IONIZATION POTENTIALS OF THE DIOXYGEN FLUORIDE FREE RADICAL AND THE DIOXYGEN DIFLUORIDE MOLECULE.

126. Marmet, P., Can. J. Phys., 42, 2102 (1964). EFFECT OF ELECTRONIC SPACE CHARGE ON THE IONIZATION PROBABILITY CURVES OF A GAS.

127. Martin, R. H., Lampe, F. W. and Taft, R. W., J. Am. Chem. Soc., 88, 1353 (1966). AN ELECTRON IMPACT STUDY OF IONIZATION AND DISSOCIATION IN METHOXY- AND HALOGEN-SUBSTITUTED METHANES.

128. Makhiev, S. D., Rizaev, R. G., Kasimov, R. and Kambarov, Y. G., Azerb. Khim. Zh., 1965, 70. MASS SPECTROSCOPY OF SOME AROMATIC NITRILES.

129. Melton, C. E. and Joy, H. W., J. Chem. Phys., 42, 1986 (1965). IONIZATION POTENTIALS AND AUTOIONIZATION LEVELS OF METHYL, ETHYL, n-PROPYL AND n-BUTYL FREE RADICALS BY AN ENERGY CALIBRATED MOLECULAR ORBITAL METHOD.

130. Melton, C. E. and Joy, H. W., J. Chem. Phys., 42, 2982 (1965). CALCULATED IONIZATION POTENTIALS OF CHLORO- AND FLUORO-METHANES. TETRAFLUOROMETHANE, XENON TETRAFLUORIDE AND XENON TETRACHLORIDE.

131. Meyer, F. and Harrison, A. G., J. Chem. Phys., 43, 1778 (1965). UNIMOLECULAR FRAGMENTATION OF THE TOLUENE MOLECULE-ION.

132. Meyer, F., Haynes, P., McLean, S. and Harrison, A. G., Can. J. Chem., 43, 211 (1965). AN ELECTRON IMPACT STUDY OF SOME C_8H_{10} ISOMERS.

133. Meyer, V. D. and Lassettre, E. N., J. Chem. Phys., 44, 2535 (1966). WEAK TRANSITIONS IN EXCITATION OF N_2 BY ELECTRON IMPACT AND COMPARISON WITH EXCITATION BY ABSORPTION OF RADIATION.

134. Meyerson, S., J. Chem. Phys., 42, 2181 (1965). ORGANIC IONS IN THE GAS PHASE. XV. DECOMPOSITION OF n-ALKANES UNDER ELECTRON IMPACT.

135. Meyerson, S., Record Chem. Progr. (Kresge-Hooker Sci. Lib.), 26, 257 (1965). ORIGINS OF MASS SPECTRA - CHEMISTRY INDUCED BY ELECTRON IMPACT OF ISOLATED MOLECULES. I.

136. Meyerson, S. and Leitch, L. C., J. Am. Chem. Soc., 88, 56 (1966). ORGANIC IONS IN THE GAS PHASE. XVII. A BICYCLIC DOUBLY HYDROGEN-BRIDGED TRANSITION STATE IN DECOMPOSITION OF 6-SUBSTITUTED ALKANOIC ACIDS AND ESTERS.

137. Miller, A. R. and Searcy, A. W., J. Phys. Chem., 69, 3826 (1965). THERMODYNAMIC STABILITIES AS A FUNCTION OF COMPOSITION FOR INDIUM SULFIDE PHASES FROM MASS SPECTROMETER INTENSITY vs TIME DATA.

138. Milne, T. A. and Greene, F. T., J. Chem. Phys., 44, 2444 (1966). MASS SPECTROMETRIC STUDIES OF REACTIONS IN FLAMES. II. QUANTITATIVE SAMPLING OF FREE RADICALS FROM ONE-ATMOSPHERE FLAMES.

139. Moore, E. B., AD-602673, THE ELECTRONIC STRUCTURE OF $B_{10}H_{12}I_2$.

140. Moran, T. F. and Friedman, L., J. Chem. Phys., 42, 2391 (1965). CROSS SECTIONS AND INTRAMOLECULAR ISOTOPE EFFECTS IN AB-HD ONE-MOLECULE REACTIONS.

141. Munson, M. S. B., J. Am. Chem. Soc., 87, 5313 (1965). REACTIONS OF GASEOUS BRONSTED ACIDS.

142. Munson, M. S. B. and Field, F. H., Virginia Univ., Project Squid, 1964, 43. REACTIONS OF IONS AND ELECTRONICALLY EXCITED SPECIES WITH ATOMS AND MOLECULES IN THE GAS PHASE.

143. Munson, M. S. B. and Field, F. H., J. Am. Chem. Soc., 87, 3294 (1965). REACTIONS OF GASEOUS IONS. XV. METHANE + 1% ETHANE AND METHANE + 1% PROPANE.

144. Munson, M. S. B. and Field, F. H., J. Am. Chem. Soc., 87, 4242 (1965). REACTIONS OF GASEOUS IONS. XVI. EFFECTS OF ADDITIVES ON IONIC REACTIONS IN METHANE.

145. Natalis, P. and Franklin, J. L., J. Phys. Chem., 69, 2935 (1965). IONIZATION AND DISSOCIATION OD DIPHENYL AND CONDENSED RING AROMATICS BY ELECTRON IMPACT. I. BIPHENYL, DIPHENYLACETYLENE AND PHENANTHRENE.

146. Natalis, P. and Franklin, J. L., J. Phys. Chem., 69, 2943 (1965). IONIZATION AND DISSOCIATION OF DIPHENYL AND CONDENSED RING AROMATICS BY ELECTRON IMPACT. II. DIPHENYLCARBONYLS AND ETHERS.

147. Natalis, P. and Laune, J., Bull. Soc. Chim. Belges, 73, 944 (1964). THE EFFECT OF ELECTRON IMPACT ON THE BEHAVIOR OF GEOMETRICAL ISOMERS. IV. CYCLOPROPANE, METHYLCYCLOPROPANE AND GEM-, CIS- AND TRANS-DIMETHYLCYCLOPROPANE.

148. Neikam, W. C., Dimeler, G. R. and Desmond, M. M., J. Electrochem. Soc., 111, 1190 (1964). CORRELATION OF ELECTROCHEMICAL OXIDATION POTENTIAL OF ORGANIC COMPOUNDS WITH PHOTOIONIZATION POTENTIAL.

149. Nicholson, A. J. C., J. Chem. Phys., 43, 1171 (1965). PHOTOIONIZATION EFFICIENCY CURVES. II. FALSE AND GENUINE STRUCTURE.

150. Nikitin, E. E., Teor. i Eksperim. Khim., Akad. Nauk Ukr. S. S. S. R., 1, 428 (1965). STATISTICAL THEORY OF EXOTHERMIC ION-MOLECULE REACTIONS.

151. Niles, F. E. and Robertson, W. W., J. Chem. Phys., 43, 1076 (1965). CONVERSION OF ATOMIC IONS TO MOLECULAR IONS FOR THE NOBLE GASES.

152. Norman, J. H. and Staley, H. G., J. Chem. Phys., 43, 3804 (1965). THERMODYNAMICS OF THE DIMERIZATION AND TRIMERIZATION OF GASEOUS TUNGSTEN TRIOXIDE AND MOLYBDENUM TRIOXIDE.

153. Olmsted, J., Newton, A. S. and Street, K., J. Chem. Phys., 42, 2321 (1965). DETERMINATION OF THE EXCITATION FUNCTIONS FOR FORMATION OF METASTABLE STATES OF SOME RARE GASES AND DIATOMIC MOLECULES BY ELECTRON IMPACT.

154. Osberghaus, O. and Ottinger, C., Phys. Letters, 16, 121 (1965). SHORT-LIVED METASTABLE MOLECULAR IONS.

155. Ostroborodova, V. V. and Ivanova, S. B., Fiz. Tverd. Tela, 6, 3481 (1964). IONIZATION ENERGY AND DEGENERATION FACTOR OF LOW LEVEL OF Ni IN Ge.

156. Ottinger, C., Phys. Letters, 17, 269 (1965). FRAGMENTATION ENERGIES OF METASTABLE ORGANIC IONS.

157. Ottinger, C., Z. Naturforsch., 20A, 1229 (1965). METASTABLE ION INTENSITIES AND FRAGMENTATION ENERGIES IN BENZENE.

158. Palmer, T. F. and Lossing, F. P., Can. J. Chem., 43, 565 (1965). FREE RADICALS BY MASS SPECTROMETRY. XXXII. THERMAL DECOMPOSITION OF CYCLOPENTYL RADICALS.

159. Pasquale, M., Morgan, R. L. and Cason, C., Rev. Sci. Instr., 36, 1783 (1965). RAPID DETERMINATION OF ELECTRON IMPACT IONIZATION AND APPEARANCE POTENTIALS.

160. Pignataro, S., Foffani, A., Grasso, F. and Cantone, B., Z. physik. Chem. (Frankfurt), 47, 106 (1965). NEGATIVE IONS FROM METAL CARBONYLS BY ELECTRON IMPACT.

161. Pirkle, W. H., J. Am. Chem. Soc., 87, 3022 (1965). STRUCTURE OF ELECTRON IMPACT FRAGMENTS. THE C_4H_4O CATION FROM 2-PYRONE.

162. Pottie, R. F., J. Chem. Phys., 42, 2607 (1965). IONIZATION POTENTIAL AND HEAT OF FORMATION OF THE DIFLUOROMETHYLENE RADICAL.

163. Pottie, R. F., J. Chem. Phys., 44, 916 (1966). CROSS SECTIONS FOR IONIZATION BY ELECTRONS. I. ABSOLUTE IONIZATION CROSS SECTIONS OF Zn, Cd, Te_2. II. COMPARISONS OF THEORETICAL WITH EXPERIMENTAL VALUES FOR ATOMS AND MOLECULES.

164. Price, W. C., Passmore, T. R. and Roessler, D. M., Discussions Faraday Soc., 35, 201 (1963). IONIZATION AND DISSOCIATION ENERGIES OF THE HYDRIDES AND FLUORIDES OF THE FIRST ROW ELEMENTS IN RELATION TO THEIR ELECTRONIC STRUCTURES.

165. Rapp, D. and Briglia, D. D., J. Chem. Phys., 43, 1480 (1965). TOTAL CROSS SECTIONS FOR IONIZATION AND ATTACHMENT IN GASES BY ELECTRON IMPACT. II. NEGATIVE ION FORMATION.

166. Rapp, D. and Englander-Golden, P., J. Chem. Phys., 43, 1464 (1965). TOTAL CROSS SECTIONS FOR IONIZATION AND ATTACHMENT IN GASES BY ELECTRON IMPACT. I. POSITIVE IONIZATION.

167. Rapp, D., Englander-Golden, P. and Briglia, D.D., J. Chem. Phys., 42, 4081 (1965). CROSS SECTIONS FOR DISSOCIATIVE IONIZATION OF MOLECULES BY ELECTRON IMPACT.

168. Resse, R. M. and Rosenstock, H. M., J. Chem. Phys., 44, 2007 (1966). PHOTOIONIZATION MASS SPECTROMETRY OF NO.

169. Refaey, K. M. and Chupka, W. A., J. Chem. Phys., 43, 2544 (1965). ENERGY DEPENDENCE OF CROSS SECTIONS FOR COLLISION-INDUCED DISSOCIATION AND ENDOTHERMIC ION-MOLECULE REACTIONS.

170. Rudge, M. R. H. and Seaton, M. J., Proc. Roy. Soc. (London), A283, 262 (1965). IONIZATION OF ATOMIC HYDROGEN BY ELECTRON IMPACT.

171. Ryan, K. R. and Futrell, J. H., J. Chem. Phys., 43, 766 (1965). ERRATUM: EFFECT OF TRANSLATIONAL ENERGY ON ION-MOLECULE REACTION RATES. I.

172. Ryan, K. R. and Futrell, J. H., J. Chem. Phys., 43, 3009 (1965). EFFECT OF TRANSLATIONAL ENERGY ON ION-MOLECULE REACTION RATES. II.

173. Ryan, K. R. and Green, J. H., J. Sci. Instr., 2, 461 (1965). KINETIC ENERGY OF FRAGMENT IONS USING A RADIO-FREQUENCY MASS SPECTROMETER.

174. Saporoschenko, M., J. Chem. Phys., 42, 2760 (1965). FORMATION OF H_3^+ AND H_5^+ IONS.

175. Schaefer, H. and Rinke, K., Z. Naturforsch., 20B, 702 (1965). GASEOUS CHROMIUM (VI) OXIDE BY MASS SPECTROMETRY.

176. Schiske, R., Abhandl. Fritz-Haber Inst. Max Planck Ges. Berlin-Kahlem, 39, 701 (1962). STATISTICS OF THE ENERGY SPREAD (BOERSCH EFFECT) IN ELECTRON BEAMS.

177. Schissel, P. O. and Trulson, O. C., J. Chem. Phys., 43, 737 (1965). MASS SPECTROMETRIC STUDY OF THE OXIDATION OF TUNGSTEN.

178. Schoen, R. R., AD-612806. ELECTRON RETARDING POTENTIAL MEASUREMENTS ON CO_2, N_2O AND NO_2.

179. Schram, B. L., Van Der Viel, M. J., De Heer, F. J. and Moustafe, H. R., J. Chem. Phys., 44, 49 (1966). ABSOLUTE GROSS IONIZATION CROSS SECTIONS FOR ELECTRONS (0.6 - 12 keV) IN HYDROCARBONS.

180. Schug, J. C., J. Chem. Phys., 43, 1426 (1965). MOLECULAR IONIZATION CROSS SECTIONS FROM THE CLASSICAL IMPULSE APPROXIMATION.

181. Schulz, G. J. and Koons, H. C., J. Chem. Phys., 44, 1292 (1966). ENERGY LEVELS OF THE COMPOUND STATE OF N_2 NEAR 2.3 eV.

182. Semenov, G. A., Zh. Neorgan. Khim., 10, 2390 (1965). MASS SPECTROMETRIC STUDY OF THE EVAPORATION OF SCANDIUM OXIDE.

183. Shahin, M. M., J. Chem. Phys., 43, 1798 (1965). ION-MOLECULE INTERACTION IN THE CATHODE REGION OF A GLOW DISCHARGE.

184. Shannon, T. W. and Harrison, A. G., J. Chem. Phys., 43, 4201 (1965). CONCURRENT ION-MOLECULE REACTIONS. I. REACTIONS IN X-CD_4 MIXTURES.

185. Shannon, T. W. and Harrison, A. G., J. Chem. Phys., 43, 4206 (1965). CONCURRENT ION-MOLECULE REACTIONS. II. REACTIONS IN X-D_2 MIXTURES.

186. Shigorin, D. N. and Potapov, V. K., Dokl. Akad. Nauk S. S. S. R., 161, 406 (1965). ROLE OF $n-\pi^*$ TRANSITIONS IN IONIZATION AND FRAGMENTATION PROCESSES.

187. Silverman, S. M. and Lassettre, E. N., J. Chem. Phys., 43, 194 (1965). ELECTRON-IMPACT ENERGY SPECTRA OF ACETONE AND 2-BUTANONE.

188. Singer, S., Kim, N. G., Merkl, A. W. and Farber, M., J. Phys. Chem., 69, 799 (1965). CHEMICAL SYNTHESIS WITH ION BEAMS.

189. Sjogren, H., Proc. Intern. Conf. Phys. Electron. At. Collisions, 3rd, Uni. Coll., London, 1963, 474. HIGHER IONIZATION POTENTIALS MEASURED BY ELECTRON IMPACT.

190. Smoes, S., Drowart, J. and Verhaegen, G., J. Chem. Phys., 43, 732 (1965). MASS SPECTROMETRIC STUDY OF GASEOUS OXIDES AND SUBOXIDES OF SCANDIUM, YTTRIUM, AND LANTHANUM.

191. Spilners, I. J. and Pellegrini, J. P., J. Org. Chem., 30, 3800 (1965). SYNTHESIS OF POLYFERROCENYLENE.

192. Spiteller, G., and Spiteller-Friedmann, M., Ann. Chem., 690, 1 (1965). THEORETICAL INTERPRETATION OF THE MASS SPECTRA OF ORGANIC COMPOUNDS.

193. Stan, I. and Weissman, A., Studia Univ. "Bases-Bolyai," Ser. Math. Phys., 1, 141 (1965). FINE STRUCTURE OF THE EFFECTIVE MASS SPECTRUM.

194. Steele, W. C., Jennings, B. H., Botyos, G. L. and Dudek, G. O., J. Org. Chem., 30, 2886 (1965). AN ELECTRON IMPACT STUDY OF NORNORNENYL AND NORTRICYCLYL CHLORIDES.

195. Storms, E. K., U. S. At. Energy Comm., LA-DA-6953 (1965). A MASS SPECTROMETRIC STUDY OF THE VAPOR PRESSURE OF U(g) AND UC_2(g) OVER VARIOUS COMPOSITIONS IN THE URANIUM-CARBON SYSTEM.

196. Streitwieser, A., Heller, A. and Feldman, M., J. Phys. Chem., 68, 1224 (1964). ON KUHN'S ω-MOLECULAR ORBITAL METHOD.

197. Stuber, F. A., J. Chem. Phys., 42, 2639 (1965). MULTIPLE IONIZATION IN NEON, ARGON, KRYPTON AND XENON.

198. Sumin, L. V. and Gur'ev, M. V., Dokl. Akad. Nauk S. S. S. R., 159, 1134 (1964). DISSOCIATION OF MOLECULAR IONS.

199. Thorburn, R., Brit. J. Appl. Phys., 16, 1397 (1965). IONIZATION AND DISSOCIATION BY ELECTRON IMPACT IN CARBON TETRABROMIDE.

200. Van Tiggelen, A., Peeters, J. and Burke, R., Chem. Eng. Sci., 20, 529 (1965). AN EMPIRICAL METHOD FOR THE ESTIMATION OF BOND DISSOCIATION ENERGIES.

201. Torshina, V. V., Smolina, G. N. and Dobychin, S. Y., Zh. Neorgan. Khim., 10, 1275 (1965). MASS SPECTROMETRIC STUDY OF THE EVAPORATION OF LANTHANUM HEXABORIDE.

202. Trulson, O. C. and Goldstein, H. W., J. Phys. Chem., 69, 2531 (1965). MASS SPECTROMETRIC STUDY OF ZIRCONIUM DIBORIDE.

203. Trulson, O. C. and Schissel, P. O., J. Less-Common Metals, 8, 262 (1965). MASS SPECTROMETRIC STUDY OF THE VAPORIZATION OF PALLADIUM.

204. Tsong, T. T. and Mueller, E. W., J. Chem. Phys., 41, 3279 (1964). MEASUREMENT OF THE ENERGY DISTRIBUTION IN FIELD IONIZATION.

205. Tsuchiya, T., Bull. Chem. Soc. Japan, 37, 1308 (1964). HIGH KINETIC ENERGY (KE) FRAGMENT IONS FROM ORGANIC COMPOUNDS UNDER ELECTRON IMPACT. IV. METHANOL.

206. Turro, N. J., Neckers, D.C., Leermakers, P. A., Seldner, D. and D'Angelo, P., J. Am. Chem. Soc., 87, 4097 (1965). INTERRELATIONS BETWEEN THE MASS SPECTROMETRY AND PHOTOCHEMISTRY OF ORGANIC MOLECULES. I. KETENE DIMERS AND OTHER SMALL RING COMPOUNDS.

207. Utterback, N. G., J. Chem. Phys., 44, 2540 (1966). CROSS SECTIONS FOR ATOM EXCHANGE WITH CHARGE TRANSFER IN A MOLECULAR COLLISION.

208. Verhaegen, G., Colin, R. and Drowart, J., AD-607680. VAPORIZATION OF COMPOUNDS AND ALLOYS AT HIGH TEMPERATURES. XXIV. MASS SPECTROMETRIC DETERMINATION OF THE STABILITY OF GASEOUS MOLYBDATES, TUNGSTATES, MOLYBDITES AND TUNGSTITES OF MAGNESIUM, CALCIUM, STRONTIUM AND TIN.

209. Verhaegen, G., Colin, R., Exsteen, G. and Drowart, J., Trans. Faraday Soc., 61, 1372 (1965). MASS SPECTROMETRIC DETERMINATION OF THE STABILITY OF GASEOUS MOLYBDITES, TUNGSTITES, MOLYBDATES AND TUNGSTATES OF MAGNESIUM, CALCIUM, STRONTIUM AND TIN.

210. Vestal, M. L., J. Chem. Phys., 43, 1356 (1965). THEORETICAL STUDIES ON THE UNIMOLECULAR REACTIONS OF POLYATOMIC MOLECULE IONS. I. PROPANE.

211. Wacks, M. E., J. Chem. Phys., 41, 1661 (1964). ELECTRON IMPACT STUDIES OF AROMATIC HYDROCARBONS. II. NAPHTHACENE, NAPHTHAPHENE, CHRYSENE, TRIPHENYLENE AND PYRENE.

212. Wada, Y., Doctoral Dissertation, Kansas State University, Manhattan, 1964. MASS SPECTROMETRIC INVESTIGATION OF SOME INORGANIC AND ORGANIC PHOSPHORUS COMPOUNDS.

213. White, R. C. and Parcell, L. J., J. Phys. Chem., 69, 4409 (1965). THE PHOTOLYSIS OF TRIFLUORONITROSOMETHANE.

214. Winchell, P., Nature, 206, 1252 (1965). MASS SPECTROMETRIC INVESTIGATION OF BARIUM IODIDE AND CESIUM IODIDE VAPORIZATIONS.

215. Winters, H. F., J. Chem. Phys., 44, 1472 (1966). IONIC ADSORPTION AND DISSOCIATION CROSS SECTION FOR NITROGEN.

216. Winters, R. E., Doctoral Dissertation, Kansas State University, Manhattan, 1965. A MASS SPECTROMETRIC STUDY OF SOME ORGANOMETALLIC COMPOUNDS.

217. Winters, R. E. and Kiser, R. W., J. Phys. Chem., 69, 1618 (1965). IONS PRODUCED BY ELECTRON IMPACT WITH THE DIMETALLIC CARBONYLS OF COBALT AND MANGANESE.

218. Winters, R. E. and Kiser, R. W., J. Phys. Chem., 69, 3198 (1965). IONIZATION POTENTIALS AND MASS SPECTRA OF CYCLOPENTADIENYLMOLYBDENUM DICARBONYL NITROSYL AND 1,3-CYCLOHEXADIENEIRON TRICARBONYL.

219. Winters, R.E. and Kiser, R. W., J. Organometal. Chem. (Amsterdam), 4, 190 (1965). IONS PRODUCED IN THE MASS SPECTROMETER FROM CYCLOPENTADIENYL-METAL CARBONYL COMPOUNDS OF COBALT, MANGANESE AND VANADIUM.

220. Winters, R. E. and Kiser, R. W., J. Chem. Phys., 44, 1964 (1966). UNIMOLECULAR DECOMPOSITION OF NEGATIVE IONS FORMED FROM THE TRANSITION-METAL CARBONYLS OF Ni, Fe, Cr, Mo and W.

221. Winters, R. E. and Kiser, R. W., J. Phys. Chem., 70, 1680 (1966). DOUBLY CHARGED TRANSITION METAL CARBONYL IONS.

222. Wolf, F. A., J. Chem. Phys., 44, 1619 (1966). COMPUTER CALCULATIONS OF ION-MOLECULE REACTIONS.

223. Woolston, J. R. and Honig, R. E., Rev. Sci. Instr., 35, 69 (1964). ENERGY DISTRIBUTION OF IONS FORMED IN THE RF (RADIO-FREQUENCY) SPARK SOURCE.

224. Wiedemeier, H. and Gilles, P. W., J. Chem. Phys., 42, 2765 (1965). MASS SPECTROMETRIC STUDY OF THE SUBLIMATION OF MnS(s) AND THE DISSOCIATION ENERGY OF MnS(g).

225. Ziesel, J. P., J. Chim. Phys., 62, 328 (1965). FORMATION OF MULTIPLY-CHARGED IONS OF NEON, SODIUM AND MAGNESIUM BY 250-2000 eV ELECTRON IMPACTS.

GASEOUS NEGATIVE IONS

Bruce Steiner and Nikita Wells

1. Adams, G. W. and Masley, A. J., J. Atmospheric Terrest. Phys., 27, 289 (1965). PRODUCTION RATES AND ELECTRON DENSITIES IN THE LOWER IONOSPHERE DUE TO SOLAR COSMIC RAYS.

2. Aplin, R. T., Budzikiewicz, H. and Djerassi, C., J. Am. Chem. Soc., 87, 3180 (1965). MASS SPECTROMETRY IN STRUCTURAL AND STEREOCHEMICAL PROBLEMS. LXXIII. THE NEGATIVE ION MASS SPECTRA OF SOME SIMPLE ORGANIC COMPOUNDS.

3. Ardenne, M. V., Steinfelder, K. and Tümmler, R., Z. Chemie, 5, 287 (1965). BEITRAG ZUR MOLEKÜL-MASSENSPEKTROGRAPHIE VON NATURSTOFFEN.

4. Bakuline, I. N. and Ionov, N. I., Zh. Fiz. Khim., 39, 157 (1965); Engl. transl.: Russ. J. Phys. Chem., 39, 78 (1965). ABSOLUTE ELECTRON AFFINITIES OF HALOGEN AND SULFUR ATOMS.

5. Bakulina, I. N., Zandberg, E. Ya. and Ionov, N. I., Zh. Tekhn. Fiz., 35, 562 (1965); Engl. transl.: Soviet Phys. - Tech. Phys., 10, 437 (1965). EMISSION OF POSITIVE AND NEGATIVE MOLECULAR IONS FROM HEATED SURFACES.

6. Banyard, K. E. and Hake, R. B., J. Chem. Phys., 43, 2684 (1965). UNITED-ATOM APPROXIMATION APPLIED TO ARGON-LIKE MOLECULES. II. PH_2^-, PH_3, AND PH_4^+.

7. Bastide, R. P., Brooks, N. B., Wittkower, A. B., Rose, P. H. and Purser, K. H., IEEE Trans. Nucl. Sci., NS-12, 775 (1965). ION SOURCES FOR HIGH CURRENT TANDEM ACCELERATORS.

8. Bates, D. R. and Moffett, R. J., Nature, 205, 272 (1965). THREE-BODY ION RECOMBINATION.

9. Baughan, E. C., Trans. Faraday Soc., 61, 2337 (1965). IONIZATION POTENTIALS, ELECTRON AFFINITIES AND SCREENING CONSTANTS. V. WAVE MECHANICAL DERIVATIONS.

10. Berry, R. S., David, C. W. and Mackle, J. C., J. Chem. Phys., 42, 1541 (1965). THRESHOLD SHAPES AND RESONANCES IN THE PHOTODETACHMENT CROSS SECTIONS OF CHLORIDE, BROMIDE AND IODIDE.

11. Chibisov, M. I., Zh. Eksperim. i Teor. Fiz., 49, 852 (1965). ATTACHMENT OF ELECTRONS TO ATOMS IN TRIPLE COLLISIONS.

12. Berry, R. S., Mackie, J. C., Taylor, R. L. and Lynch, R., J. Chem. Phys., 43, 3067 (1965). SPIN-ORBIT COUPLING AND ELECTRON AFFINITY DETERMINATIONS FROM RADIATIVE CAPTURE OF ELECTRONS BY OXYGEN ATOMS.

13. Biondi, M. A., Endeavour, 24, 40 (1965). RECOMBINATION OF IONS AND ELECTRONS.

14. Bouby, L., Fiquet-Fayard, F. and Abgrall, H., Compt. Rend., 261, 4059 (1965). ATTACHEMENT D'ELECTRONS THERMIQUES SUR QUELQUES VAPEURS ORGANIQUES.

15. Branscomb, L. M., Smith, S. J. and Tisone, G., J. Chem. Phys., 43, 2906 (1965). OXYGEN METASTABLE ATOM PRODUCTION THROUGH PHOTODETACHMENT.

16. Breene, R. G., Jr., J. Quant. Spectry. Radiative Transfer, 5, 449 (1965). BOUND-FREE CONTINUUM OF O^-.

17. Burke, P. G., Advan. Phys., 14, 521 (1965). RESONANCES IN ELECTRON SCATTERING AND PHOTON ABSORPTION.

18. Bydin, Yu. F., Zh. Eksperim. i Teor. Fiz., 49, 1094 (1965). DETACHMENT OF ELECTRONS FROM H^- IONS IN COLLISIONS WITH INERT GAS ATOMS.

19. Campbell, I. D. and Coogan, C. K., J. Chem. Phys., 42, 2738 (1965). ON THE CHARGE DISTRIBUTION AND ELECTRON AFFINITY OF THE OH^- ION IN LiOH.

20. Chamberlain, G. E., Phys. Rev. Letters, 14, 581 (1965). MULTICHANNEL RESONANCES IN THE FORWARD SCATTERING OF ELECTRONS BY HELIUM.

21. Chamberlain, G. E. and Heideman, H. G. M., Phys. Rev. Letters, 15, 337 (1965). INELASTIC SCATTERING OF ELECTRONS BY HELIUM.

22. Charkin, O. P. and Siatkina, M. E., Zh. Strukt. Khim., 6, 422 (1965). CALCULATION OF THE ELECTRON AFFINITY OF TRANSITION ELEMENTS BY THE MTHOD OF GLOCKLER.

23. Chatterton, P. A. and J. D. Craggs, Proc. Phys. Soc. (London), 85, 355 (1965). ATTACHMENT COEFFICIENT MEASUREMENTS IN CARBON DIOXIDE, CARBON MONOXIDE, AIR AND HELIUM-OXYGEN MIXTURES.

24. Christophorou, L. G., Compton, R. N., Hurst, G. S. and Reinhardt, P. W., J. Chem. Phys., 43, 4273 (1965). DETERMINATION OF ELECTRON CAPTURE CROSS SECTIONS WITH SWARM-BEAM TECHNIQUES.

25. Cole, R. K. Jr., and Pierce, E. T., J. Geophys. Res., 70, 2735 (1965). ELECTRIFICATION IN THE EARTH'S ATMOSPHERE FOR ALTITUDES BETWEEN 0 AND 100 KILOMETERS.

26. Collins, L. E. and Gobbett, R. H., Nucl. Instr. Methods, 35, 277 (1965). EXTRACTION OF NEGATIVE HYDROGEN IONS FROM A DUOPLASMATRON ION SOURCE.

27. Corinaldesi, E., Phys. Rev. Letters, 15, 335 (1965). THEORETICAL ESTIMATE OF DOUBLE QUANTUM PHOTODETACHMENT OF IODINE IONS.

28. Cox, A. N., Stewart, J. N. and Eilers, D. D., Astrophys. J., Suppl. 11, 1 (1965). EFFECTS OF BOUND-BOUND ABSORPTION ON STELLAR OPACITIES.

29. Cox, A. N. and Stewart, J. N., Astrophys. J., Suppl. 11, 22 (1965). RADIATIVE AND CONDUCTIVE OPACITIES FOR ELEVEN ASTROPHYSICAL MIXTURES.

30. Crompton, R. W., Rees, J. A. and Jory, R. L., Australian J. Phys., 18, 541 (1965). THE DIFFUSION AND ATTACHMENT OF ELECTRONS IN WATER VAPOUR.

31. Curl, R. F. Jr. and Coulson, C. A., Proc. Phys. Soc. (London), 85, 647 (1965). COULOMB HOLE IN THE GROUND STATE OF TWO-ELECTRON ATOMS.

32. Dalgarno, A. and Henry, R. J. W., Proc. Roy. Soc. (London), A288, 521 (1965). ELECTRON TEMPERATURES IN THE D REGION.

33. Davis, K. M. C., Hammond, P. R. and Peover, M. E., Trans. Faraday Soc., 61, 1516 (1965). ELECTRON AFFINITIES OF MONOSUBSTITUTED BENZOQUINONES.

34. Demkov, Yu. N., Zh. Eksperim. i Teor Fiz., 49, 885 (1965). ELECTRON DETACHMENT IN SLOW COLLISIONS BETWEEN NEGATIVE IONS AND ATOMS.

35. Demkov, Yu. N., Phys. Letters, 15, 235 (1965). ISOTOPIC EFFECT IN THE RESONANCE DISSOCIATIVE CAPTURE OF AN ELECTRON AND QUASISTATIONARY STATES OF MOLECULES.

36. Dibeler, V. H. and Walker, J. A., J. Chem. Phys., 43, 1842 (1965). ION-PAIR PROCESS IN CH_3Cl BY PHOTOIONIZATION.

37. Dillard, J. G. and Kiser, R. W., J. Phys. Chem., 69, 3893 (1965). IONIZATION AND DISSOCIATION OF RUTHENIUM AND OSMIUM TETROXIDES.

38. Dmitriev, M. T., Izv. Akad. Nauk S. S. S. R., Ser. Geofiz., 1965, 302; Engl. transl. Atmos. Oceanic Phys., 1, 179 (1965). SOME PHYSICAL AND CHEMICAL PROCESSES IN AIR CAUSED BY IONIZING RADIATION.

39. Dolan, J. F., Astrophys. J., 142, 1621 (1965). STELLAR MOLECULAR ABUNDANCES. I. POLYATOMIC MOLECULES.

40. Donnally, B. L. and Sawyer, W., Phys. Rev. Letters, 15, 439 (1965). PROPOSAL FOR A SOURCE OF POLARIZED NEGATIVE HYDROGEN IONS.

41. Drost, H., Klotz, H.-D., Behlke, H. and Pupke, H., Ann. Physik, 15, 303 (1965). DAS VERHALTEN DER ELEKTRONEN IN EINER GESCHICHTETEN NIEDERDRUCKENTLADUNG.

42. Drost, H., Klotz, H.-D., Timm, U. and Pupke, H., Exptl. Tech. Physik, 13, 170 (1965). DER ZUSAMMENHANG VON SAULENSCHICHTUNG UND GEHALT AN NEGATIVEN IONEN IN EINER VERUNREINIGTEN Ar-ENTLADUNG.

43. Drost, H., Timm, U., Behlke, H. and Pupke, H., Ann. Physik, 15, 294 (1965). DAS ANODENGEBIET EINER BEHINDERTEN GLIMMENTLADUNG IN SAUERSTOFF.

44. Ehlers, K. W., Nucl. Instr. Methods, 32, 309 (1965). DESIGN CONSIDERATIONS FOR HIGH-INTENSITY NEGATIVE ION SOURCES.

45. Ehlers, K. W., IEEE Trans. Nucl. Sci., NS-12, 811 (1965). DESIGN CONSIDERATIONS FOR HIGH-INTENSITY NEGATIVE ION SOURCES.

46. Ehrhardt, H. and Meister, G., Phys. Letters, 14, 200 (1965). DIE WINKELABHÄNGIGKEIT DER RESONANZSTREUUNG NIEDERENERGETISCHER ELECTRONEN AN HELIUM.

47. Elder, F. A., Villarejo, D. and Inghram, M. G., J. Chem. Phys., 43, 758 (1965). ELECTRON AFFINITY OF OXYGEN.

48. Fano, U. and Cooper, J. W., Phys. Rev., 138, A400 (1965). IDENTIFICATION OF ENERGY LEVELS OF NEGATIVE IONS.

49. Feibelman, P. J., J. Chem. Phys., 42, 2462 (1965). NUMERICAL STUDY OF THE THREE-BODY ION-ION RECOMBINATION RATE.

50. Foffani, A., Pignataro, S., Cantone, B. and Grasso, F., Z. physik. Chem. (Frankfurt), 45, 79 (1965). MASS SPECTRA OF METAL HEXACARBONYLS.

51. Franzen, W. and Gupta, R., Phys. Rev. Letters, 15, 819 (1965). SPIN POLARIZATION OF SLOW ELECTRONS BY ELASTIC RESONANCE SCATTERING FROM NEON.

52. Geltman, S., Astrophys. J., 141, 376 (1965). CONTINUUM STATES OF H^- AND THE FREE-FREE ABSORPTION COEFFICIENT.

53. Gilmore, F. R., J. Quant. Spectry. Radiative Transfer, 5, 369 (1965). POTENTIAL ENERGY CURVES FOR N_2, NO, O_2 AND CORRESPONDING IONS.

54. Gordon, S. L., J. Chem. Phys., 42, 4184 (1965). HYPERVIRIAL FUNCTIONS AND THE POSITIVE POWERS OF THE RADIAL COORDINATE OPERATOR IN He AND H^-.

55. Grahn, R., Acta Chem. Scand., 19, 153 (1965). NMR CHEMICAL SHIFT OF THE HYDROXYL ION.

56. Grahn, R., Arkiv Fysik, 28, 85 (1965). A QUANTUM-MECHANICAL INVESTIGATION OF THE OH^- ION.

57. Gunton, R. C. and Shaw, T. M., Phys. Rev., 140, A748 (1965). AMBIPOLAR DIFFUSION AND ELECTRON ATTACHMENT IN NITRIC OXIDE IN THE TEMPERATURE RANGE 196 TO 358°K.

58. Gunton, R. C. and Shaw, T. M., Phys. Rev., 140, A756 (1965). ELECTRON-ION RECOMBINATION IN NITRIC OXIDE IN THE TEMPERATURE RANGE 196 - 358°K.

59. Hall, J. L., Robinson, E. J. and Branscomb, L. M., Phys. Rev. Letters, 14, 1013 (1965). LASER DOUBLE-QUANTUM PHOTODETACHMENT OF I^-.

60. Harteck, P., Dondes, S. and Thompson, B., Science, 147, 393 (1965). OZONE: DECOMPOSITION BY IONIZING RADIATION.

61. Hasted, J. B. and Beg, S., Brit. J. Appl. Phys., 16, 1779 (1965). ATTACHMENT OF ELECTRONS TO NITROGEN DIOXIDE AND SULPHUR HEXAFLUORIDE.

62. Herman, K. and Giguere, P. A., Can. J. Chem., 43, 1746 (1965). LA SPECTRE INFRAROUGE DE L'OZONIDE D'AMMONIUM ET LA STRUCTURE DE L'ION O_3^-.

63. Herron, J. T., Rosenstock, H. M. and Shields, W. R., Nature, 206, 611 (1965). NEGATIVE SURFACE IONIZATION OF COMPLEX MOLECULES.

64. Hill, D. W. and Newell, H. A., Nature, 205, 593 (1965). EFFECT OF WATER VAPOR ON THE SENSITIVITY OF A MACRO-ARGON IONIZATION DETECTOR.

65. Hirst, D. M. and Linnett, J. W., J. Chem. Phys., 43, 574 (1965). ELECTRONIC STRUCTURE OF THE NITRITE ION AND RELATED SPECIES.

66. Hodges, R. R., Jr., J. Geophys. Res., 70, 185 (1965). ELECTRON ATTACHMENT RATE MEASUREMENTS IN THE LOWER IONOSPHERE.

67. Hoult, D. P., J. Geophys. Res., 70, 3183 (1965). D-REGION PROBE THEORY.

68. Indreas, G., Chein, K. C., Passyuk, A. S. and Tretyakov, I. P., Rev. Roumaine Phys., 10, 101 (1965). PRODUCTION OF NEGATIVE H IONS FROM THE ARC ION SOURCE ON A STAND.

69. Indreas, G. and Tauth, T., Rev. Roumaine Phys., 10, 877 (1965). NEGATIVE H ION ACCELERATION IN THE U-120 CYCLOTRON.

70. Ionov, S. P. and Porai-Koshits, M. A., Zh. Strukt. Khim., 6, 479 (1965). THE ENERGY AND THE EQUILIBRIUM INTERNUCLEAR SPACING OF THE BINDING OF OXYGEN AND SULFUR.

71. Jorgensen, T., Jr., Kuyatt, C. E., Lang, W. W., Lorents, D. C. and Sautter, C. A., Phys. Rev., 140, A1481 (1965). MEASUREMENTS ON CHARGE-CHANGING COLLISIONS INVOLVING NEGATIVE HYDROGEN, HELIUM, AND OXYGEN IONS.

72. Karmohapatro, S. B., J. Phys. Soc. Japan, 20, 839 (1965). CHARGE EXCHANGE OF Cl^- IONS WITH ATOMIC CHLORINE.

73. Kato, H., Yamaguchi, K., Yonezawa, T. and Fukui, K., Bull. Chem. Soc. Japan, 38, 2144 (1965). THE ELECTRONIC STRUCTURE OF SOME HYDRIDES, HALIDES AND ALKYL COMPOUNDS OF BORON AND ALUMINUM. I. MONOMERS AND IONS.

74. Khare, S. P. and Rudge, M. R. H., Proc. Phys. Spc. (London), 86, 355 (1965). AN APPLICATION OF A VARIATIONAL PRINCIPLE TO THE CALCULATION OF FREE-FREE MATRIX ELEMENTS FOR H^-.

75. Khvostenko, V. I. and Sultanov, A. Sh., Zh. Fiz. Khim., 39, 475 (1965); Engl. transl.: Russ. J. Phys. Chem., 39, 252 (1965). IONISATION OF THALLIUM (I) CHLORIDE, BROMIDE AND IODIDE MOLECULES BY ELECTRON BOMBARDMENT.

76. Kimura, K. and Nagakura, S., Mol. Phys., 9, 117 (1965). VACUUM ULTRAVIOLET ABSORPTION SPECTRA OF VARIOUS MONO-SUBSTITUTED BENZENES.

77. Kirchoff, W. H., Farren, J. and Linnett, J. W., J. Chem. Phys., 42, 1410 (1965). CALCULATION OF ELECTRONIC ENERGIES IN HCO_2^+, HCO_2, AND HCO_2^-.

78. Kleinpoppen, H. and Raible, V., Phys. Letters, 18, 24 (1965). ON THE NARROW RESONANCE IN THE SCATTERING OF ELECTRONS BY ATOMIC HYDROGEN.

79. Krugers, J., Phillips Res. Repts., Suppl. 1, (1965). IONIZATION DETECTORS IN GAS CHROMATOGRAPHY.

80. Kuyatt, C. E., Simpson, J. A. and Mielczarek, S. R., Phys. Rev., 138, A385 (1965). ELASTIC RESONANCES IN ELECTRON SCATTERING FROM He, Ne, Ar, Kr, Xe, AND Hg.

81. Kwok, K. L. and Mandl, F., Proc. Phys. Soc. (London), 86, 501 (1965). A NARROW RESONANCE IN THE ELASTIC SCATTERING OF ELECTRONS BY HELIUM.

82. Langhoff, P. W. and Hurst, R. P., Phys. Rev., 139, A1415 (1965). MULTIPOLE POLARIZABILITIES AND SHIELDING FACTORS FROM HARTREE-FOCK WAVE FUNCTIONS.

83. Lawrence, G. P., Beauchamp, R. K. and McKibben, J. L., Nucl. Instr. Methods, 32, 357 (1965). DIRECT EXTRACTION OF NEGATIVE ION BEAMS OF GOOD INTENSITY FROM A DUOPLASMATRON.

84. Lee, Y.-T. and Mahan, B. H., J. Chem. Phys., 42, 2893 (1965). PHOTOSENSITIZED IONIZATION OF ALKALI-METAL VAPORS.

85. Lichten, W., Phys. Rev., 139, A27 (1965). RESONANT CHARGE EXCHANGE IN ATOMIC COLLISIONS. II. FURTHER APPLICATIONS AND EXTENSIONS TO THE QUASI-RESONANT CASE.

86. Magill, L. R. and Hasted, J. B., Planetary Space Sci., 13, 339 (1965). FREE ELECTRON BALANCE DURING POLAR CAP ABSORPTION EVENTS.

87. Mahadevan, P., Magnuson, G. D., Layton, J. K. and Carlston, C. E., Phys. Rev., 140, A1407 (1965). SECONDARY-ELECTRON EMISSION FROM MOLYBDENUM DUE TO POSITIVE AND NEGATIVE IONS OF ATMOSPHERIC GASES.

88. Mahan, B. H., J. Chem. Phys., 43, 1853 (1965). COMMENT ON THE FAR-ULTRAVIOLET PHOTOLYSIS OF NITRIC OXIDE.

89. Mapleton, R. A., Proc. Phys. Soc. (London), 85, 841 (1965). PRODUCTION OF H^- ($1s^2$) BY HYDROGEN ATOM COLLISIONS.

90. McHugh, J. A. and Sheffield, J. C., Anal. Chem., 37, 1099 (1965). MASS ANALYSIS OF SUBNANOGRAM QUANTITIES OF IODINE.

91. Midtdal, J., Phys. Rev., 138, A1010 (1965). PERTURBATION-THEORY EXPANSIONS THROUGH 21st ORDER OF THE NONRELATIVISTIC ENERGIES OF THE TWO-ELECTRON SYSTEMS $(2p)^2$ ^3P and $(1s)^2$ ^1S.

92. Mittleman, M. H., Phys. Rev., 137, A1 (1965). CALCULATION OF THE $p + H_2 = H^- + 2p$ REACTION CROSS SECTION.

93. Miyamoto, T. and Kamatani, A., Mitsubishi Denki Lab. Rept., 6, 45 (1965). DYNAMIC BEHAVIOR OF SF_6 GAS BLAST TYPE CIRCUIT BREAKERS AROUND CURRENT SERO (1).

94. Miyamoto, T. and Kamatani, A., Mitsubishi Denki Lab. Rept., 6, 175 (1965). MASS SPECTROMETRIC STUDIES OF ARC QUENCHING REACTIONS IN SF_6 GAS (2) (WITH SPECIAL REFERENCE TO THE FORMATION OF NEGATIVE IONS IN ARCED SF_6 GAS.)

95. Moskowitz, J. W. and Harrison, M. C., J. Chem. Phys., 43, 3550 (1965). GAUSSIAN WAVEFUNCTIONS FOR THE 10-ELECTRON SYSTEMS. III. OH^-, H_2O, H_3O^+.

96. Moskvin, Yu. V., Teplofiz. Vysokikh Temperatur Akad. Nauk S. S. S. R., 3, 821 (1965). PHOTOIONIZATION CROSS SECTIONS OF ALKALI METALS AND HALOGEN NEGATIVE IONS.

97. Myerscough, V. P., Proc. Phys. Soc. (London), 85, 33 (1965). CONTINUUM CORRELATION IN C^-.

98. Nieuwpoort, W. C., Phillips Res. Repts., Suppl. 6,(1965). CHARGE DISTRIBUTION AND CHEMICAL BONDING IN THE METAL CARBONYLS $Ni(CO)_4$, $[Co(CO)_4]^-$, AND $[Fe(CO)_4]^=$.

99. O'Malley, T. F., Phys. Rev., 137, A1668 (1965). EFFECT OF LONG-RANGE FINAL-STATE FORCES ON THE NEGATIVE-ION PHOTODETACHMENT CROSS SECTION NEAR THRESHOLD.

100. O'Malley, T. F. and Geltman, S., Phys. Rev., 137, A1344 (1965). COMPOUND-ATOM STATES FOR TWO-ELECTRON SYSTEMS.

101. Paltridge, G. W., J. Geophys. Res., 70, 2751 (1965). EXPERIMENTAL MEASUREMENTS OF THE SMALL-ION DENSITY AND ELECTRICAL CONDUCTIVITY OF THE STRATOSPHERE.

102. Patel, G., J. Chim. Phys., 62, 1176 (1965). MESURES DES POTENTIELS D'APPARITION DES IONS OBTENUS PAR IMPACT ELECTRONIQUE DANS LA PHASE VAPEUR DES IODURES ALCALINS ET DES MELANGES LiI-MI.

103. Pederson, A., Tellus, 17, 1 (1965). MEASUREMENTS OF ION CONCENTRATIONS IN THE D-REGION OF THE IONOSPHERE WITH A GERDIEN CONDENSER ROCKET PROBE.

104. Pignataro, S., Foffani, A., Grasso, F. and Cantone, B., Z. physik. Chem. (Frankfurt), 47, 106 (1965). NEGATIVE IONS FROM METAL CARBONYLS BY ELECTRON IMPACT.

105. Pilipenko, D. V. and Fogel, Ya. M., Zh. Eksperim. i Teor. Fiz., 48, 404 (1965); Engl. transl.: Soviet Phys. JETP, 21, 266 (1965). COMPOSITION OF SLOW IONS FORMED ON PASSAGE OF FAST HYDROGEN ATOMS THROUGH MOLECULAR GASES.

106. Filipenko, D. V., Gusev, V. A. and Fogel, Ya. M., Zh. Eksperim. i Teor. Fiz., 49, 1402 (1965). ELECTRON LOSS AND THE FORMATION OF SLOW NEGATIVE IONS IN COLLISIONS OF HYDROGEN ATOMS AND H^- IONS WITH GAS MOLECULES.

107. Popp, H.-P., Z. Naturforsch., 20A, 642 (1965). NACHWEIS DES FLUOR-AFFINITÄTS-KONTINUUMS IN EMISSION.

108. Pritchard, H. O. and Wallis, A., J. Chem. Phys., 42, 3548 (1965). CORRELATED ORBITALS FOR EXCITED STATES OF He AND H^-.

109. Pyatigorskii, G. M., Zh. Tekhn. Fiz., 35, 1127 (1965); Engl. transl.: Soviet Phys. - Tech. Phys., 10, 867 (1965). SURFACE IONIZATION OF MOLECULES OF ALKALI HALIDE SALTS.

110. Raju, G. R. G., Brit. J. Appl. Phys., 16, 279 (1965). CALCULATION OF IONIZATION AND ATTACHMENT COEFFICIENTS FROM PRE-BREAKDOWN CURRENT MEASUREMENTS.

111. Rapp, D. and Briglia, D. D., J. Chem. Phys., 43, 1480 (1965). TOTAL CROSS SECTIONS FOR IONIZATION AND ATTACHMENT IN GASES BY ELECTRON IMPACT. II. NEGATIVE-ION FORMATION.

112. Rapp, D., Sharp, T. E. and Briglia, D. D., Phys. Rev. Letters, 14, 533 (1965). LARGE ISOTOPE EFFECT IN THE FORMATION OF H^- OR D^- BY ELECTRON IMPACT ON H_2, HD AND D_2.

113. Rees, J. A., Australian J. Phys., 18, 41 (1965). THE BEHAVIOUR OF FREE AND ATTACHED ELECTRONS IN OXYGEN.

114. Robinson, B. B., Phys. Rev., 140, A764 (1965). MODIFICATIONS OF THE IMPULSE APPROXIMATION FOR IONIZATION AND DETACHMENT CROSS SECTIONS.

115. Rutledge, R. M. and Saturno, A. F., J. Chem. Phys., 43, 597 (1965). ONE-CENTER EXPANSION WAVE FUNCTIONS FOR CH_3^-, CH_4, and CH_5^+.

116. Scheer, M. D. and Fine, J., J. Chem. Phys., 42, 3645 (1965). SURFACE IONIZATION OF NIOBIUM.

117. Schulz, G. J. and Asundi, R. K., Phys. Rev. Letters, 15, 946 (1965). FORMATION OF H^- BY ELECTRON IMPACT ON H_2 AT LOW ENERGY.

118. Smirnov, B. M., Dokl. Akad. Nauk S. S. S. R., 161, 92 (1965); Engl. transl.: Soviet Phys. - Doklady, 10, 218 (1965). FORMATION AND DECAY OF NEGATIVE IONS.

119. Smirnov, B. M., Teplofiz. Vysokikh Temperatur Akad. Nauk S. S. S. R., 3, 775 (1965). NEGATIVE IONS OF ATOMS.

120. Smirnov, B. M. and Chibisov, M. I., Zh. Eksperim. i Teor. Fiz., 49, 841 (1965). DESTRUCTION OF ATOMIC PARTICLES BY AN ELECTRIC FIELD AND BY ELECTRON IMPACT.

121. Smith, J., J. Geophys. Res., 70, 53 (1965). NEGATIVE ION EFFECTS ON WHISTLER MODE PROPAGATION.

122. Smith, L. G., Accardo, C. A., Weeks, L. H. and McKinnon, P. J., J. Atmospheric Terrest. Phys., 27, 803 (1965). MEASUREMENTS IN THE IONOSPHERE DURING THE SOLAR ECLIPSE OF 20 JULY 1963.

123. Smythe, R. and Toevs, J. W., Phys. Rev., 139, A15 (1965). COLLISIONAL ELECTRON DETACHMENT FROM HYDROGEN ATOMS AND NEGATIVE HYDROGEN IONS BETWEEN 4 AND 18 MeV.

124. Takayanagi, K., J. Phys. Soc. Japan, 20, 562 (1965). VIBRATIONAL EXCITATION OF HYDROGEN MOLECULE BY SLOW ELECTRONS.

125. Taylor, H. S. and Williams, J. K., J. Chem. Phys., 42, 4063 (1965). PROPOSED THEORY OF CALCULATING THE ENERGY OF NEGATIVE-ION RESONANT ELASTIC SCATTERING STATES AND OF THE PRE-IONIZATION STATES OF ELECTRONIC SPECTROSCOPY.

126. Temkin, A. and Walker, J. F., Phys. Rev., 140, A1520 (1965). AUTOIONIZATION STATES OF H^- BELOW THE $n = 2$ LEVEL OF H.

127. Thorburn, R., Brit. J. Appl. Phys., 16, 1397 (1965). IONIZATION AND DISSOCIATION BY ELECTRON IMPACT IN CARBON TETRABROMIDE.

128. Tietz, T., Acta Phys. Acad. Sci. Hung., 18, 141 (1965). ELECTRON SCATTERING BY ATOMS AND THE EXISTENCE OF NEGATIVE IONS.

129. Tümmler, R., Z. physik. Chem. (Leipzig), 229, 58 (1965). DIE ANWENDUNG DER MOLEKÜL-MASSENSPEKTROGRAPHIE IN DER ORGANISCHEN CHEMIE.

130. Voshall, R. E., Pack, J. L. and Phelps, A. V., J. Chem. Phys., 43, 1990 (1965). MOBILITY OF NEGATIVE IONS IN O_2 AT LOW E/N.

131. Whitten, R. C., Poppoff, I. G., Edmonds, R. S. and Berning, W. W., J. Geophys. Res., 70, 1737 (1965). EFFECTIVE RECOMBINATION COEFFICIENTS IN THE LOWER IONOSPHERE.

132. Wilson, K. R. and Herschbach, D. R., Nature, 208, 182 (1965). CORRELATION OF SODIUM ATOM REACTION RATES WITH ELECTRON CAPTURE CROSS SECTIONS.

133. Winters, R. E., Doctoral Dissertation, Kansas State University, Manhattan, 1965. A MASS SPECTROMETRIC STUDY OF SOME ORGANOMETALLIC COMPOUNDS.

134. Winters, R. E. and Kiser, R. W., J. Phys. Chem., 69, 1618 (1965). IONS PRODUCED BY ELECTRON IMPACT WITH THE DIMETALLIC CARBONYLS OF COBALT AND MANGANESE.

135. Winters, R. E. and Kiser, R. W., J. Phys. Chem., 69, 3198 (1965). IONIZATION POTENTIALS AND MASS SPECTRA OF CYCLOPENTADIENYLMOLYBDENUM DICARBONYL NITROSYL AND 1,3-CYCLOHEXADIENEIRON TRICARBONYL.

136. Winters, R. E. and Kiser, R. W., J. Organometal. Chem. (Amsterdam), 4, 190 (1965). IONS PRODUCED IN THE MASS SPECTROMETER FROM CYCLOPENTADIENYL-METAL CARBONYL COMPOUNDS OF COBALT, MANGANESE AND VANADIUM.

137. Winters, R. E. and Kiser, R. W., J. Chem. Phys., 44, 1964 (1966). UNIMOLECULAR DECOMPOSITION OF NEGATIVE IONS FORMED FROM THE TRANSITION-METAL CARBONYLS OF Ni, Fe, Cr, Mo AND W.

138. Wittkower, A. B., Bastide, R. P., Brooks, N. B., Rose, P. H. and Hopwood, L., Can. J. Phys., 43, 96 (1965). EQUILIBRIUM FRACTIONS FOR A HYDROGEN-ION BEAM (10-50 KeV) IN 17 GASES AND VAPORS.

139. Witthower, A. B., Rose, P. H., Bastide, R. P., Brooks, N. B. and Hopwood, L., Can J. Phys., 43, 404 (1965). EQUILIBRIUM FRACTIONS FOR AN OXYGEN BEAM (15-50 KeV) IN 17 GASES AND VAPORS.

140. Wobschall, D., Graham, J. R. and Malone, D. P., J. Chem. Phys., 42, 3955 (1965). OBSERVATIONS OF NEGATIVE IONS IN OXYGEN AND WATER VAPOR BY ION CYCLOTRON RESONANCE.

141. Zhikhareva, T. V., Opt. i Spektroskopiya, 19, 851 (1965); Engl. transl.: Opt. Spectry. (U.S.S.R.), 19, 474 (1965). RESONANCE PHENOMENA IN THE ELASTIC SCATTERING OF ELECTRONS BY HELIUM ATOMS.

PHOTOIONIZATION AND RELATED STUDIES

F. N. Harllee

1. Akopyan, M. E. , Vilesov, F. I. and Terenin, A. N., Bull. Acad. Sci. U.S.S.R., Phys. Ser., 27, 1054 (1964). MASS SPECTROMETRIC INVESTIGATION OF PHOTOIONIZATION OF MOLECULES AND DISSOCIATION OF EXCITED MOLECULAR IONS.

2. Aleksandrov, O. V., Gofren, M. V., Keilina, T. A. and Tveryankina, R. I., Zh. Prikl. Spektroskopii, Akad. Nauk Belorussk. S. S. R., 2, 473 (1965). MONOCHROMATORS FOR ULTRAVIOLET AND VISIBLE SPECTRUM DETERMINATIONS.

3. Alexander, R. W., Jr., U. S. Govt. Res. Develop. Rept., 40, 105 (1965). PHOTOIONIZATION OF KRYPTON AND ARGON IN THE 100-300 A RANGE.

4. Al-Joboury, M. I., May, D. P. and Turner, D. W., J. Chem. Soc., 1965, 616. MOLECULAR PHOTOELECTRON SPECTROSCOPY. III. THE IONIZATION POTENTIALS OF OXYGEN, CARBON MONOXIDE, NITRIC OXIDE, AND ACETYLENE.

5. Al-Joboury, M. I., May, D. P. and Turner, D. W., J. Chem. Soc., 1965, 6350. MOLECULAR PHOTOELECTRON SPECTROSCOPY. IV. THE IONIZATION POTENTIALS AND CONFIGURATIONS OF CARBON DIOXIDE, CARBON OXYSULPHIDE, CARBON DISULPHIDE AND NITROUS OXIDE.

6. Ando, K., Sci. Light (Japan), 13, 45 (1964). WAVELENGTH ACCURACY OF GRATING MONOCHROMATORS WITH SINE DRIVE MECHANISM.

7. Axelrod, N. N., J. Opt. Soc. Am., 55, 208 (1965). OUT-OF-FOCUS GRAZING VACUUM MONOCHROMATOR DESIGN.

8. Basu, S., Theoret. chim. Acta, 3, 238 (1965). FREE ELECTRON MODEL AND PHOTOIONIZATION OF π-ELECTRONS FROM AROMATIC HYDROCARBONS.

9. Bath, K. L. and Brehm, B., Z. Angew. Phys., 19, 39 (1965). A SEYA-GRATING SPECTROMETER WITH 0.2 A RESOLUTION.

10. Batrakov, R. I., Belozerova, V. P. and Tataurov, V. S., Tr. Komis. po Spektroskopii Akad. Nauk S. S. S. R., 2, 656 (1964). MONOCHROMATOR WITH HIGH RESOLVING POWER.

11. Beaglehole, D., Proc. Phys. Soc. (London), 85, 1007 (1965). OPTICAL PROPERTIES OF COPPER AND GOLD IN THE VACUUM ULTRA-VIOLET.

12. Bell, S., J. Mol.Spectry., 16, 205 (1965). THE SPECTRA OF H_2O AND D_2O IN THE VACUUM ULTRAVIOLET.

13. Benesch, W., Vanderslice, J. T., Tilford, S. G. and Wilkinson, P. G., Astrophys. J., 143, 236 (1966). FRANCK-CONDON FACTORS FOR OBSERVED TRANSITIONS IN N_2 ABOVE 6 eV.

14. Beynon, J. D. E., Nature, 207, 405 (1965). AN EXPERIMENTAL DETERMINATION OF THE PHOTOIONIZATION CROSS-SECTION OF ATOMIC HYDROGEN.

15. Blake, A. J. and Carver, J. H., Phys. Letters, 19, 387 (1965). PARTIAL PHOTOIONIZATION CROSS SECTION FOR MOLECULAR OXYGEN.

16. Boldt, G., J. Quant. Spectry. Radiative Transfer, 5, 91 (1965). MEASUREMENTS OF ABSORPTION OSCILLATOR STRENGTHS AND LINE BROADENING IN THE REGION FROM 1000 TO 2000 A.

17. Botter, R., Dibeler, V. H., Walker, J. A. and Rosenstock, H. M., J. Chem. Phys., 44, 1271 (1966). EXPERIMENTAL AND THEORETICAL STUDIES OF PHOTOIONIZATION EFFICIENCY CURVES FOR C_2H_2 AND C_2D_2.

18. Branscomb, L. M., Smith, S. J. and Tisone, G., J. Chem. Phys., 43, 2906 (1965). OXYGEN METASTABLE ATOM PRODUCTION THROUGH PHOTODETACHMENT.

19. Breene, R. G., Jr., Proc. Phys. Soc. (London), 86, 1369 (1965). PHOTOIONIZATION CALCULATIONS FOR ATOMS AND IONS WITH 1s, 2s AND 2p ELECTRONS.

20. Brehm, B. and Siegert, H., Z. Angew. Phys., 19, 244 (1965). AN INTENSE HYDROGEN DISCHARGE LAMP FOR THE FAR VACUUM ULTRAVIOLET.

21. Brewer, L., Bralison, G. D. and Meyer, B., J. Chem. Phys., 42, 1385 (1965). U. V. ABSORPTION SPECTRUM OF TRAPPED S_2.

22. Brion, C. E., Anal. Chem., 37, 1706 (1965). A WINDOWLESS PHOTOIONIZATION SOURCE FOR HIGH RESOLUTION ANALYTICAL MASS SPECTROMETERS.

23. Brith, M. and Schnepp, O., Mol. Phys., 9, 473 (1965). ABSORPTION SPECTRA OF SOLID CO AND N_2.

24. Burke, P. G. and McVicar, D. D., Proc. Phys. Soc. (London), 86, 989 (1965). RESONANCES IN $e^- — He^+$ SCATTERING AND THE PHOTOIONIZATION OF He.

25. Cairns, R. B. and Samson, J. A. R., J. Geophys. Res., 70, 99 (1965). ABSORPTION AND PHOTOIONIZATION CROSS SECTIONS OF CO_2, CO, Ar, AND He AT INTENSE SOLAR EMISSION LINES.

26. Cairns, R. B. and Samson, J. A. R., Phys. Rev., 139, A1403 (1965). TOTAL ABSORPTION CROSS SECTION OF ATOMIC OXYGEN BELOW 910 A.

27. Callear, A. B. and Smith, I. W. M., Trans. Faraday Soc., 61, 1303 (1965). THE (0,0), (2,0) AND (3,0) BANDS OF THE β-SYSTEM OF NO.

28. Canfield, L. R. and Hass, G., J. Opt. Soc. Am., 55, 61 (1965). REFLECTANCE AND OPTICAL CONSTANTS OF EVAPORATED COPPER AND SILVER IN THE VACUUM ULTRAVIOLET FROM 1000 to 2000 A.

29. Canfield, L. R., Hass, G. and Waylonis, J. E., Appl. Opt., 5, 45 (1966). FURTHER STUDIES ON MgF_2-OVERCOATED ALUMINUM MIRRORS WITH HIGHEST REFLECTANCE IN VACUUM ULTRAVIOLET.

30. Carlson, T. A. and Krause, M. O., Phys. Rev., 140, A1057 (1965). ELECTRON SHAKE OFF RESULTING FROM K-SHELL IONIZATION IN NEON MEASURED AS A FUNCTION OF PHOTOELECTRON VELOCITY.

31. Clark, L. B., J. Chem. Phys., 43, 2566 (1965). IONIZATION POTENTIAL OF AZULENE.

32. Clark, L. B. and Simpson, W. T., J. Chem. Phys., 43, 3666 (1965). VACUUM-ULTRAVIOLET STUDIES OF SULFIDES. I. SPECTRAL CORRELATION AND ASSIGNMENT OF THE NV TRANSITIONS.

33. Codling, K. and Madden, R. P., Appl. Opt., 4, 1431 (1965). NEWLY OBSERVED STRUCTURE IN THE PHOTOIONIZATION CONTINUA OF Kr AND Xe BELOW 160 A.

34. Codling, K. and Madden, R. P., J. Chem. Phys., 42, 3935 (1965). NEW RYDBERG SERIES IN MOLECULAR OXYGEN.

35. Cohen, I. M., Phys. Fluids, 8, 2097 (1965). ASYMPTOTIC THEORY OF A PHOTOIONIZATION CHAMBER.

36. Cook, G. R. and Ching, B. K., Aerospace Corporation Report #TDR-469(9260-01)-4, El Segundo, California (1965). ABSORPTION, PHOTOIONIZATION, AND FLUORESCENCE OF SOME GASES OF IMPORTANCE IN THE STUDY OF THE UPPER ATMOSPHERE.

37. Cook, G. R. and Ching, B. K., J. Chem. Phys., 43, 1794 (1965). PHOTOIONIZATION AND ABSORPTION CROSS SECTIONS AND FLUORESCENCE OF CF_4.

38. Cook, G. R., Metzger, P. H. and Ogawa, M., Can. J. Phys., 43, 1706 (1965). PHOTOIONIZATION AND ABSORPTION COEFFICIENTS OF CO IN THE 600 TO 1000 A REGION.

39. Cook, G. R. and Ogawa, M., Can. J. Phys., 43, 256 (1965). PHOTO-IONIZATION OF N_2 IN THE 734-805 A REGION.

40. Daley, W. W., Phys. Letters, 19, 321 (1965). VACUUM-ULTRAVIOLET ABSORPTION SPECTRA OF MERCURY IONS TRAPPED IN INERT-GAS MATRICES AT LOW TEMPERATURE.

41. Daly, N. R., Proc. Phys. Soc. (London), 85, 897 (1965). HIGHER AUTOIONIZATION PROCESSES IN ARGON AND XENON.

42. Damany-Astoin, N., Compt. Rend., 259, 1493 (1964). NEW ABSORPTION SPECTRUM OF XENON IN THE EXTREME ULTRAVIOLET.

43. Dibeler, V. H., Krauss, M., Reese, R. M. and Harllee, F. N., J. Chem. Phys., 42, 3791 (1965). MASS SPECTROMETRIC STUDY OF PHOTOIONIZATION. III. METHANE AND METHANE-d_4.

44. Dibeler, V. H. and Walker, J. A., J. Chem. Phys., 43, 1842 (1965). ION-PAIR PROCESS IN CH_3Cl BY PHOTOIONIZATION.

45. Doolittle, P. H. and Schoen, R. I., Phys. Rev. Letters, 14, 348 (1965). AUTO-IONIZATION AND THE VIBRATIONAL EXCITATION OF H_2^+.

46. Dressler, K. and Miescher, E., Astrophys. J., 141, 1266 (1965). ABSORPTION SPECTRUM OF THE NO MOLECULE. V. SURVEY OF EXCITED STATES AND THEIR INTER-ACTION.

47. Duncan, A. B. F., J. Chem. Phys., 42, 2453 (1965). THEORY OF RYDBERG TERMS OF THE NITROGEN MOLECULE.

48. Ederer, D. L., Phys. Rev. Letters, 13, 760 (1964). PHOTOIONIZATION OF THE 4d ELECTRONS IN XENON.

49. Ermisch, R. and Schonheit, E., Z. Naturforsch., 20A, 611 (1965). LIGHT SOURCE WITH LATERAL EMISSION FOR THE VACUUM U.V.

50. Fano, U. and Cooper, J. W., Phys. Rev., 137, A1364 (1965). LINE PROFILES IN THE FAR - U.V. ABSORPTION SPECTRA OF THE RARE GASES.

51. Fano, U. and Cooper, J. W., Phys. Rev., 138, A400 (1965). IDENTIFICATION OF ENERGY LEVELS OF NEGATIVE IONS.

52. Felenbok, P., Proc. Roy. Soc. (London), 86, 676 (1965). FRANCK-CONDON FACTORS AND r CENTROIDS FOR A $^1\Pi$ — $X\,^1\Sigma^+$ SYSTEMS OF CS.

53. Flannery, M. R. and Öpik, U., Proc. Phys. Soc. (London), 86, 491 (1965). THE PHOTOIONIZATION OF THE HYDROGEN MOLECULE FROM THE GROUND ELECTRONIC AND VIBRATIONAL STATE.

54. Freeman, G. H. C., Proc. Phys. Soc. (London), 86, 117 (1965). THE FAR ULTRA-VIOLET SPECTRA FROM THE VACUUM SLIDING SPARK.

55. Frost, D. C., McDowell, C. A. and Vroom, D. A., Phys. Rev. Letters, 15, 612 (1965). PHOTOELECTRON SPECTROSCOPY WITH A SPHERICAL ANALYZER. THE VIBRATIONAL ENERGY LEVELS OF H_2^+.

56. Guccione, R. and Van Kronendonk, J., Phys. Rev. Letters, 14, 583 (1965). THEORY OF HIGHER MULTIPOLE CONTRIBUTIONS TO TWO-PHOTON ABSORPTION PROCESSES.

57. Hall, J. L., Robinson, E. J. and Branscomb, L. M., Phys. Rev. Letters, 14, 1013 (1965). LASER DOUBLE-QUANTUM PHOTODETACHMENT OF I^-.

58. Hall, L. A., Schweizer, W. and Hinteregger, H. E., J. Geophys. Res., 70, 105 (1965). IMPROVED EXTREME ULTRAVIOLET ABSORPTION MEASUREMENTS IN THE UPPER ATMOSPHERE.

59. Heroux, L., Manson, J. E., Hinteregger, H. E. and McMahon, W. J., J. Opt. Soc. Am., 55, 103 (1965). PHOTOELECTRIC YIELDS FOR OBLIQUE INCIDENCE OF EXTREME ULTRAVIOLET RADIATION.

60. Herzberg, G., J. Opt. Soc. Am., 55, 229 (1965). MOLECULAR SPECTROSCOPY AND ASTRO-PHYSICAL PROBLEMS.

61. Hesser, J. E. and Dressler, K., Astrophys. J., 142, 389 (1965). ABSOLUTE TRANSITION PROBABILITIES IN THE ULTRAVIOLET SPECTRUM OF CO.

62. Hinteregger, H. E., Space Sci. Rev., 4, 461 (1965). ABSOLUTE MEASUREMENTS IN THE EXTREME ULTRAVIOLET SPECTRUM OF SOLAR RADIATION.

63. Hisdal, E., J. Opt. Soc. Am., 55, 1446 (1965). INFORMATION CONTENT OF A BEAM OF PHOTONS.

64. Hudson, R. D., J. Chem. Phys., 43, 1790 (1965). MEASUREMENTS OF THE MOLECULAR ABSORPTION CROSS SECTION AND THE PHOTOIONIZATION OF SODIUM VAPOR BETWEEN 1600 AND 3700 A.

65. Hudson, R. D. and Carter, V. L., Phys. Rev., 137, A1648 (1965). ATOMIC ABSORPTION CROSS SECTION OF LITHIUM VAPOR BETWEEN 2300 AND 1150 A.

66. Hudson, R. D. and Carter, V. L., Phys. Rev., 139, A1426 (1965). ABSORPTION OF LIGHT BY POTASSIUM VAPOR BETWEEN 2856 AND 1150 A.

67. Huffman, R. E., Larrabee, J. C. and Chambers, D., Appl. Opt., 4, 1145 (1965). NEW EXCITATION UNIT FOR RARE GAS CONTINUA IN THE VACUUM ULTRAVIOLET.

68. Huffman, R. E., Larrabee, J. C. and Chambers, D., AFCRL-65-381, 1 (1965). VACUUM ULTRAVIOLET LIGHT SOURCES: NEW EXCITATION UNIT FOR THE RARE GAS CONTINUA.

69. Huffman, R. E., Larrabee, J. C. and Tanaka, Y., Appl. Opt., 4, 1581 (1965). RARE GAS CONTINUUM LIGHT SOURCES FOR PHOTOELECTRIC SCANNING THE VACUUM ULTRAVIOLET.

70. Huffman, R. E., Larrabee, J. C., Tanaka, Y. and Chambers, D., J. Opt. Soc. Am., 55, 101 (1965). HELIUM CONTINUUM AFTERGLOW IN THE VACUUM ULTRAVIOLET.

71. Huffman, R. E., Tanaka, Y. and Larrabee, J. C., Japan. J. Appl. Phys., 4, Suupl. 1, 494 (1965). ARGON, KRYPTON AND XENON CONTINUUM LIGHT SOURCES FOR THE VACUUM ULTRAVIOLET.

72. Ivanov-Khalodny, G. S., Proc. XIII Intern. Astronaut. Congr., 1, 133 (1964). IONIZATION OF THE UPPER ATMOSPHERE BY SOLAR EXTREME ULTRAVIOLET.

73. Jaegle, P., Compt. Rend., 259, 4556 (1964). ORDER SEPARATION IN A DOUBLE GRATING SPECTROGRAPH FOR THE MEDIUM AND FAR ULTRAVIOLET.

74. Jelinek, R., Hamm, N. and Arakawa, E. T., U. S. At. Energy Comm., ORNL-TM-1164, 55 (1965). OPTICAL PROPERTIES OF VACUUM-EVAPORATED FILMS OF CADMIUM, THALLIUM, AND ZINC IN THE VACUUM ULTRAVIOLET.

75. Joshi, K. C., Proc. Phys. Soc. (London), 87, 285 (1966). THE SPECTRUM OF THE C - X SYSTEM OF N_2^+.

76. Joussot-Dubien, J. and Leschaux, R., J. chim. Phys., 61, 1631 (1964). A MAGNETIC STUDY OF THE PHOTOIONIZATION OF AROMATIC MOLECULES IN BORIC ACID.

77. Jungen, C. and Miescher, E., Astrophys. J., 142, 1660 (1965). THE EMISSION SPECTRUM OF THE NO MOLECULE IN THE VACUUM ULTRAVIOLET, 1600 - 1400 A.

78. Kamiya, K., Japan. J. Appl. Phys., 3, 167 (1964). A SIMPLE METHOD FOR MASKING THE VACUUM ULTRAVIOLET SPECTRA WITH THE INTENSITY SCALE.

79. Kasinskaya, I. V. and Startsev, G. P., Opt. Spectry. (U.S.S.R.)(Engl. transl.), 18, 416 (1965). ABSORPTION CROSS SECTION OF OXYGEN IN THE VACUUM REGION OF THE SPECTRUM.

80. Kieffer, J. and Damany-Astoin, N., Ann. Astrophys. Suppl. (France), 28, 158 (1964). RECENT DEVELOPMENTS IN THE SPECTROSCOPY OF ATOMIC AND AUTOIONIZATION CONTINUA.

81. Kim, H. H. and Roebber, J. L., J. Chem. Phys., 44, 1709 (1966). VACUUM ULTRAVIOLET ABSORPTION SPECTRUM OF CARBON SUBOXIDE.

82. Kimura, K. and Nagakura, S., Mol. Phys., 9, 117 (1965). VACUUM ULTRAVIOLET ABSORPTION SPECTRA OF VARIOUS MONO-SUBSTITUTED BENZENES.

83. Kitagawa, T., Harada, Y., Inokuchi, H. and Kodera, K., J. Mol. Spectry., 19, 1 (1966). ABSORPTION SPECTRUM OF VAPOR-PHASE AZULENE IN VACUUM-ULTRAVIOLET REGION.

84. Kokin, V. V., Zh. Prikl. Spektroskopii, Akad. Nauk Belorussk. S. S. R., 2, 561 (1965). VACUUM MONOCHROMATOR VM-I.

85. Krasavin, V. V., Kulikov, S. A., Mischenko, E. D. and Startsev, G. P., Zh. Prikl. Spektroskopii, Akad. Nauk Belorussk. S. S. R., 2, 546 (1965). MEASUREMENT OF THE INTENSITY OF THE SPECTRUM FROM A PULSE SOURCE IN THE FAR ULTRAVIOLET REGION.

86. Krasnov, K. S. and Karaseva, N. V., Opt. Spectry. (U.S.S.R., Engl. transl.), 19, 14 (1965). REEVALUATION OF THE SPECTROSCOPIC DISSOCIATION ENERGIES OF SUBHALIDES OF THE IIa GROUP.

87. Krause, M. O., Phys. Rev., 140, A1845 (1965). DETERMINATION OF L BINDING ENERGIES BY THE PHOTOELECTRON METHOD.

88. Krupenie, P. H. and Weissman, S., J. Chem. Phys., 43, 1529 (1965). POTENTIAL ENERGY CURVES FOR CO AND CO^+.

89. Kudo, K., J. Opt. Soc. Am., 55, 150 (1965). OPTICAL PROPERTIES OF PLANE-GRATING MONOCHROMATOR.

90. Kummler, R. H. and McCarty, M., Jr., J. Chem. Phys., 42, 2587 (1965). COLLISION FREQUENCY OF MOLECULES EXCITED BY MONOCHROMATIC LIGHT.

91. Lee, Y.-T. and Mahan, B. H., J. Chem. Phys., 42, 2893 (1965). PHOTOSENSITIZED IONIZATION OF ALKALI METAL VAPORS.

92. Lefebvre-Brion, H. and Moser, C. M., J. Mol. Spectry., 15, 211 (1965). CALCULATION OF RYDBERG LEVELS IN NO AND BF.

93. Leiga, A. G. and Taylor, H. A., J. Chem. Phys., 42, 2107 (1965). FAR-ULTRAVIOLET PHOTOLYSIS OF NITRIC OXIDE.

94. Lowry, J. F., Tomboulian, D. H. and Ederer, D. L., Phys. Rev., 137, A1054 (1965). PHOTOIONIZATION CROSS SECTION OF HELIUM IN THE 100- TO 250- A REGION.

95. Lukirskii, A. B., Brytov, I. A. and Zimkins, T. M., Opt. Spectry. (U.S.S.R.) (Engl. transl.), 17, 234 (1964). PHOTOIONIZATION ABSORPTION OF He, Kr, Xe, CH_4 AND METHYLAL IN THE 23.6 - 250 A REGION.

96. Matsumoto, A., Sugiura, T. and Hayakawa, T., Mass Spectry. (Tokyo), 12, 137 (1964). A MASS SPECTROMETER FOR PHOTOIONIZATION AND MICROANALYSIS. II. GAINS OF VARIOUS POSITIVE IONS BY Cu-Be SECONDARY ELECTRON MULTIPLIER.

97. Matsunaga, F. M., Jackson, R. S. and Watanabe, K., J. Quant. Spectry. Radiative Transfer, 5, 329 (1965). PHOTOIONIZATION YIELD IN THE ABSORPTION COEFFICIENT OF XENON IN THE REGION OF 860-1022 A.

98. Metzger, P. H. and Cook, G. R., J. Opt. Soc. Am., 55, 516 (1965). FLUX DISTRIBUTION OF THE HOFFIELD HELIUM CONTINUUM FROM THE PHOTOIONIZATION OF Ar, Kr, AND Xe.

99. Mikawa, Y., J. Opt. Soc. Am., 55, 569 (1965). VACUUM-ULTRAVIOLET RADIATION FROM RARE GASES IRRADIATED BY GAMMA RAYS.

100. Miller, K. and Murrell, J. N., Theoret. chim. Acta, 3, 231 (1965). THE CALCULATION OF FRANCK-CONDON FACTORS FOR THE ELECTRONIC TRANSITIONS OF POLYACENES.

101. Morse, F. A. and Kaufman, F., J. Chem. Phys., 42, 1785 (1965). DETERMINATION OF GROUND-STATE O, N, AND H BY LIGHT ABSORPTION AND MEASUREMENT OF OSCILLATOR STRENGTH.

102. Moskvin, Yu. V., Opt. i Spektrosk. U. S. S. R., 17, 499 (1964). ANALYTICAL WAVE FUNCTIONS AND PHOTOIONIZATION CROSS SECTION OF NEGATIVE IONS HAVING AN OUTER 2p ELECTRON SHELL.

103. Murakawa, K., J. Phys. Soc. Japan, 20, 1733 (1965). THE IONIZATION POTENTIAL OF Tm I.

104. Namioka, T., J. Chem. Phys., 43, 1636 (1965). ABSORPTION SPECTRA OF H_2 IN THE VACUUM ULTRAVIOLET REGION. III. POTENTIAL-ENERGY CURVES FOR THE $B\,^1\Sigma_u^+$, $C\,^1\Pi_u$, $B'\,^1\Sigma_u^+$ AND $D\,^1\Pi_u$ STATES.

105. Nicholls, R. W., Can. J. Phys., 43, 1390 (1965). FRANCK-CONDON FACTORS FOR THE O_2^+ FIRST AND SECOND NEGATIVE BAND SYSTEMS.

106. Nicholls, R. W., J. Chem. Phys., 42, 804 (1965). FRANCK-CONDON FACTORS FOR THE GAYDON-GREEN BAND SYSTEM OF N_2.

107. Nicholls, R. W., Astrophys. J., 141, 814 (1965). FRANCK-CONDON FACTORS FOR THE H_2 LYMAN-BAND SYSTEM.

108. Nicholson, A. J. C., J. Chem. Phys., 43, 1171 (1965). PHOTOIONIZATION-EFFICIENCY CURVES. II. FALSE AND GENUINE STRUCTURE.

109. Ogawa, M., J. Chem. Phys., 43, 2142 (1965). RYDBERG SERIES CONVERGING TO THE B $^2\Sigma^+$ STATE OF CO^+.

110. Ogawa, M., Tanaka, Y. and Jursa, A. S., J. Chem. Phys., 41, 3351 (1964). ABSORPTION SPECTRUM OF ELECTRONICALLY EXCITED NITROGEN MOLECULES IN THE VACUUM - UV REGION.

111. O'Malley, T. F., Phys. Rev., 137, A1668 (1965). EFFECT OF LON-RANGE FINAL-STATE FORCES ON THE NEGATIVE - ION PHOTODETACHMENT CROSS SECTION NEAR THRESHOLD.

112. Peach, G., Proc. Phys. Soc. (London), 85, 709 (1965). IONIZATION OF HYDROGEN, HELIUM, LITHIUM AND BERYLLIUM BY ELECTRON AND PHOTON IMPACT.

113. Person, J. C., J. Chem. Phys., 43, 2553 (1965). ISOTOPE EFFECT IN THE PHOTO-IONIZATION EFFICIENCY FOR BENZENE.

114. Petersson, B., Arkiv Fysik, 27, 317 (1964). REMEASURED NeI, ArI, KrI AND XeI LINES IN THE VACUUM ULTRAVIOLET.

115. Propin, P. Kh., Opt. Spectry. (U.S.S.R.), (Engl. transl.), 17, 332 (1964). THE AUTOIONIZATION OF He ATOMS, Li ATOMS AND Be^+ IONS.

116. Radwan, T. N. and Turner, D. W., J. Chem. Soc., 1966, A85. MOLECULAR PHOTO-ELECTRON SPECTROSCOPY. V. OZONE.

117. Reese, R. M. and Rosenstock, H. M., J. Chem. Phys., 44, 2007 (1966). PHOTO-IONIZATION MASS SPECTROMETRY OF NO.

118. Rosenthal, L. A., Rev. Sci. Instr., 36, 1329 (1965). REGULATED LIGHT SOURCE.

119. Ross, K. J. and Marr, G. V., Proc. Phys. Soc. (London), 85, 193 (1965). THE CONTINUOUS ABSORPTION OF LIGHT IN CADMIUM VAPOR.

120. Rudd, M. E., Phys. Rev. Letters, 15, 580 (1965). NEW AUTOIONIZING LEVELS IN HELIUM.

121. Rustgi, O. P., J. Opt. Soc. Am., 55, 630 (1965). TRANSMITTANCE OF THIN FILMS IN THE VACUUM-ULTRAVIOLET REGION BELOW 1000 A.

122. Rustgi, O. P. and Weissler, G. L., J. Opt. Soc. Am., 55, 456 (1965). OPTICAL AND PHOTOELECTRIC PROPERTIES OF THIN METALLIC FILMS IN THE VACUUM ULTRAVIOLET.

123. Samson, J. A. R., J. Opt. Soc. Am., 55, 935 (1965). PHOTOIONIZATION CROSS SECTIONS OF NEON FROM THRESHOLD TO 200 A.

124. Samson, J. A. R. and Cairns, R. B., J. Geophys. Res., 69, 4583 (1964). ABSORPTION AND PHOTOIONIZATION CROSS SECTIONS OF O_2 AND N_2 AT INTENSE SOLAR EMISSION LINES.

125. Samson, J. A. R. and Cairns, R. B., J. Opt. Soc. Am., 55, 1035 (1965). TOTAL ABSORPTION CROSS SECTIONS OF H_2, N_2, AND O_2 IN THE REGION 550-200 A.

126. Samson, J. A. R. and Cairns, R. B., Appl. Optics, 4, 915 (1965). A CARBON FILM-SCINTILLATOR COMBINATION SUITABLE FOR THE SELECTIVE DETECTION OF RADIATION IN THE EXTREME ULTRAVIOLET.

127. Samson, J. A. R. and Cairns, R. B., G. C. A. Tech. Rept. 65-30-N, Bedford, Mass. (1965). PHYSICS OF PLANETARY ATMOSPHERES. V. THE IONIZATION POTENTIAL OF O_2.

128. Schiek, O. and Winter, E., Appl. Optics, 4, 195 (1965). TWO NEW MIRROR MONO-CHROMATORS.

129. Schwenker, R. P., J. Chem. Phys., 42, 2618 (1965). TRANSITION PROBABILITY OF $^2\Pi_u \rightarrow X\ ^2\Pi_g$ SYSTEMS OF CO_2^+.

130. Seaton, M. J., Proc. Phys. Soc. (London), 87, 337 (1966). THE IONIZATION ENERGY OF THE HELIUM ATOMS.

131. Sewell, K. G., Phys. Rev., 138, A418 (1965). PHOTOIONIZATION CROSS SECTION OF NEON.

132. Soltysik, E. A., Phys. Rev., 142, 72 (1966). REORIENTATION OF HYDROGEN ATOMS BY PHOTON IMPACT.

133. Somerville, W. B., Astrophys. J., 141, 811 (1965). THE CONTINUOUS ABSORPTION COEFFICIENT OF He^-.

134. Sparapany, J . J., Appl. Optics, 4, 303 (1965). A STABLE, HIGH-INTENSITY VACUUM ULTRAVIOLET SOURCE.

135. Sroka, W., Phys. Letters, 14, 301 (1965). VACUUM ULTRAVIOLET EMISSION OF OXYGEN (GAS IONIZING RADIATION OF A CORONA DISCHARGE).

136. Tanaka, Y., Innes, F. R. and Jursa, A. S., J. Chem. Phys., 42, 1183 (1965). ABSORPTION SPECTRA OF THE PINK AND LEWIS-RAYLEIGH AFTERGLOWS OF NITROGEN IN THE VACUUM - UV REGION.

137. Taylor, R. G., Chubb, T. A. and Kreplin, R. W., J. Opt. Soc. Am., 55, 1078 (1965). TRANSMISSION DIMUNITION OF VACUUM-ULTRAVIOLET LAMP WINDOWS.

138. Temkin, A. and Walker, J. F., Phys. Rev., 140, A1520 (1965). AUTOIONIZATION STATES OF H^- BELOW THE n = 2 LEVEL OF H.

139. Tilford, S. G., Vanderslice, J. T. and Wilkinson, P. G., Astrophys. J., 141, 1226 (1965). THE HIGH RESOLUTION ABSORPTION SPECTRUM OF NITROGEN FROM 1060 TO 1520 A. III. THE B' $^3\Sigma_u^- \longleftarrow X\ ^1\Sigma_g^+$.

140. Tilford, S. G., Vanderslice, J. T. and Wilkinson, P. G., Can. J. Phys., 43, 450 (1965). HIGH-RESOLUTION VACUUM ULTRAVIOLET ABSORPTION SPECTRUM OF THE E $^1\Pi \longleftarrow X\ ^1\Sigma^+$ TRANSITION IN CO.

141. Tilford, S. G., Wilkinson, P. G. and Vanderslice, J. T., Astrophys. J., 141, 427 (1965). THE HIGH-RESOLUTION ABSORPTION SPECTRUM OF NITROGEN FROM 1060 TO 1520 A. II. THE A' $^1\Sigma_u^- \longleftarrow X\ ^1\Sigma_g^+$ SYSTEM.

142. Tomlinson, R. G., Phys. Rev. Letters, 14, 489 (1965). MULTIPHOTON IONIZATION AND THE BREAKDOWN OF NOBLE GASES.

143. Tozer, B. A., Phys. Rev., 137, A1665 (1965). THEORY OF THE IONIZATION OF GASES BY LASER BEAMS.

144. Udvarhazi, A. and El-Sayed, M. A., J. Chem. Phys., 42, 3335 (1965). VACUUM-ULTRAVIOLET SPECTRA OF CYCLIC KETONES.

145. Vanderslice, J. T., Tilford, S. G. and Wilkinson, P. G., Astrophys. J., 142, 84 (1965). THE HIGH-RESOLUTION ABSORPTION SPECTRUM OF NITROGEN FROM 1060 TO 1520 A. IV. THE A $^1\Pi_g \longleftarrow X\ ^1\Sigma_g^+$ SYSTEM OF $N^{14}N^{15}$.

146. Vanderslice, J. T., Tilford, S. G. and Wilkinson, P. G., Astrophys. J., 141, 395 (1965). THE HIGH-RESOLUTION ABSORPTION SPECTRUM OF NITROGEN FROM 1060 TO 1520 A. I. THE A $^1\Pi_g \longleftarrow X\ ^1\Sigma_g^+$ SYSTEM.

147. Vishnevskii, V. N., Vus, Ya. M., Kulik, L. N., Marchuk, E. P. and Romanyuk, N. A., Pribory i Tekhn. Eksperim., 10, 242 (1965). AN ULTRAVIOLET RADIATION GENERATOR.

148. Voronov, G. S., Delone, G. A., Delone, N. B. and Kudrevatova, O. V., Zh. Eksperim. i Teor. Fiz., Pis'ma V Redakstiyr, 2, 377 (1965). MULTIPHOTON IONIZATION OF A HYDROGEN MOLECULE BY RUBY-LASER IRRADIATION IN A STRONG ELECTRIC FIELD.

149. Wilkinson, P. G. and Byram, L. T., Appl. Opt., 4, 581 (1965). RARE GAS LIGHT SOURCES FOR THE VACUUM ULTRAVIOLET.

150. Yoshida, M. and Tanaka, I., J. Chem. Phys., 44, 494 (1966). PHOTOIONIZATION BY ARGON RESONANCE LINES.

151. Zaitsev, V. S., Fuhol', I. Ya. and Khrushch, B. I., Ukrayin Fiz. Zh. (U.S.S.R.), 10, 187 (1965). SPECTRAL RESEARCH ON CONDENSED GASES IN THE VACUUM ULTRA-VIOLET.

152. Zare, R. N. and Herschbach, D. R., Appl. Opt., Suppl. 2: Chemical Lasers, 193 (1965). ATOMIC AND MOLECULAR FLUORESCENCE EXCITED BY PHOTODISSOCIATION.

153. Zel'dovich, Ya. B. and Raizer, Yu. P., Zh. Eksperim. i Teor. Fiz., 47, 1150 (1964). CASCADE IONIZATION OF A GAS BY A LIGHT PULSE.

154. Zernik, W. and Klopfenstein, R. W., J. Math. Phys., 6, 262 (1965). TWO-PHOTON IONIZATION OF ATOMIC HYDROGEN.

155. Zweig, H. J., J. Opt. Soc. Am., 55, 525 (1965). DETECTIVE QUANTUM EFFICIENCY IN PHOTODETECTORS WITH SOME AMPLIFICATION MECHANISMS.

FREE RADICALS AND CHEMICAL KINETICS

John T. Herron

1. Ageev, V. N., Ionov, N. I. and Ustinov, Yu. K., Zh. Tekhn. Fiz., 34, 2056 (1964). CHEMISORPTION OF HYDROGEN ON POLYCRYSTALLINE TUNGSTEN FILAMENTS AS INVESTIGATED BY THE FLASH METHOD, USING A PULSED MASS SPECTROMETER.

2. Agnew, W. G. and Agnew, J. T., Tenth Sym. (Intern.) Combustion, p. 123, The Combustion Institute, 1965. COMBUSTION PROFILES OF THE DIETHYL ETHER-AIR TWO-STAGE REACTION STABILIZED IN A FLAT-FLAME BURNER.

3. Arrington, C. A., Brennen, W., Glass, G. P., Michael, J. V. and Niki, H., J. Chem. Phys., 43, 732 (1965). REACTIONS OF ATOMIC OXYGEN WITH ACETYLENE.I. KINETICS AND MECHANISMS.

4. Arrington, C. A., Brennen, W., Glass, G. P., Michael, J.V., and Niki, H., J. Chem. Phys., 43, 1489 (1965). REACTION OF ATOMIC OXYGEN WITH ACETYLENE. II. CHEMI-IONIZATION AND CHEMILUMINESCENCE.

5. Bayles, A. B., Pressley, G. A., Jr., Gordon, M. E. and Stafford, F. E., J. Am. Chem. Soc., 88, 929 (1966). MASS SPECTROMETRIC INVESTUGATION OF THE PYROLYSIS OF BORANES. TETRABORANE(10).

6. Botter, R., Hagemann, R., Nief, G. and Roth, E., Advan. Mass Spectry., 3, 951 (1966). The Institute of Petroleum, London. ETUDE THERMODYNAMIQUE DE L'HEMIOXYDE DE SOUFRE PAR SPECTROMETRIC DE MASSE.

7. Bradley, J. N., Jones, G. A., Skirrow, G. and Tipper, C. F. H., Tenth Sym. (Intern.) Combustion, p. 139, The Combustion Institute, 1965. A MASS SPECTROMETRIC STUDY OF STABILIZED LOW-TEMPERATURE FLAMES OF ALDEHYDES.

8. Brennen, W. and Niki, H., J. Chem. Phys., 42, 3725 (1965). ON THE EXCHANGE REACTION $^{16}O + {}^{18}O_2$.

9. Calcote, H. F., Kurzius, S. C. and Miller, W. J., Tenth Sym. (Intern.) Combustion, p. 605, The Combustion Institute, 1965. NEGATIVE AND SECONDARY ION FORMATION IN LOW-PRESSURE FLAMES.

10. Collin, J. C., Advan. Mass Spectry., 3, 981 (1966). The Institute of Petroleum, London. PYROLYSIS STUDIES BY MASS SPECTROMETRY.

11. Cuthbert, J., Preece, E. R. and Turnbull, A. H., Appl. Spectry., 19, 18 (1965). MASS SPECTROMETRIC OBSERVATION OF POLYMERS OF CARBON DIOXIDE IN A MOLECULAR BEAM SYSTEM.

12. Dove, J. E. and Moulton, D. McL., Proc. Roy. Soc. (London), A283, 216 (1965). SHOCK WAVE STUDIES BY MASS SPECTROMETRY. III. DESCRIPTION OF APPARATUS; DATA ON THE OXIDATION OF ACETYLENE AND OF METHANE.

13. Fehlner, T. P. and Koski, W. S., J. Am. Chem. Soc., 87, 409 (1965). THE DISSOCIATION OF BH_3CO INTO BH_3 AND CO.

14. Feugier, A. and van Tiggelen, A., Tenth Sym. (Intern.) Combustion, p. 621, The Combustion Institute, 1965. IDENTIFICATION OF NEGATIVE FLAME-IONS.

15. Fisher, I. P., Homer, J. B. and Lossing, F. P., J. Am. Chem. Soc., 87, 957 (1965). FREE RADICALS BY MASS SPECTROMETRY. XXXIII. IONIZATION POTENTIALS OF CF_2, CF_3CF_2, CF_3CH_2, n-C_3F_7, AND i-C_3F_7 RADICALS.

16. Fisher, I. P., Homer, J. B., Roberts, B. and Lossing, F. P., Advan. Mass Spectry., 3, 973 (1966). The Institute of Petroleum, London. A NEW TYPE OF FLOW REACTOR FOR MEASUREMENTS OF FAST THERMAL REACTIONS.

17. Fontijn, A., Miller, W. J. and Hogan, J. M., Tenth Sym. (Intern.) Combustion, p. 545, The Combustion Institute, 1965. CHEMI-IONIZATION AND CHEMILUMINESCENCE IN THE REACTION OF ATOMIC OXYGEN WITH C_2H_2, C_2D_2, AND C_2H_4.

18. Gay, I. D., Glass, G. P., Kistiakowsky, G. B. and Niki, H., J. Chem. Phys., 43, 4017 (1965). PYROLYSIS AND OXIDATION OF FORMALDEHYDE IN SHOCK WAVES.

19. Gay, I. D., Kistiakowsky, G. B., Michael, J. V. and Niki, H., J. Chem. Phys., 43, 1720 (1965). THERMAL DECOMPOSITION OF ACETYLENE IN SHOCK WAVES.

20. Gil'burd, M. M., Moin, F. B. and Sherchuk, V. U., Kinetika Kataliz, 7, 157 (1966). MASS SPECTROMETRIC INVESTIGATIONS ON THE KINETICS OF HIGH TEMPERATURE REACTIONS. I. THERMAL ACETONE DECOMPOSITION.

21. Glass, G. P., Kistiakowsky, G. B., Michael, J. V. and Niki, H., J. Chem. Phys., 42, 608 (1965). MECHANISM OF THE ACETYLENE-OXYGEN REACTION IN SHOCK WAVES.

22. Glass, G. P., Kistiakowsky, G. B., Michael, J. V. and Niki, H., Tenth Sym. (Intern.) Combustion, p. 513, The Combustion Institute, 1965. THE OXIDATION REACTIONS OF ACETYLENE AND METHANE.

23. Herron, J. T., J. Phys. Chem., 69, 2736 (1965). MASS SPECTROMETRIC STUDY OF THE REACTION OF NITROGEN ATOMS WITH ETHYLENE.

24. Kohout, F. C. and Lampe, F. W., J. Am. Chem. Soc., 87, 5795 (1965). ON THE ROLE OF THE NITROXYL MOLECULE IN THE REACTION OF HYDROGEN ATOMS WITH NITRIC OXIDE.

25. Kuprianov, S. E., Dokl. Akad. Nauk. S. S. S. R., 162, 865 (1965). MASS SPECTROMETRIC DETECTION OF REACTIONS BETWEEN HIGHLY EXCITED HYDROGEN ATOMS AND ETHYLENE MOLECULES.

26. Kuriakose, A. K. and Margrave, J. L., Inorg. Chem., 4, 1639 (1965). MASS SPECTROMETRIC STUDIES OF THE THERMAL DECOMPOSITION OF POLY(CARBON MONOFLUORIDE).

27. LeGoff, P., Cassuto, A. and Pentenero, A., Advan. Mass Spectry., 3, 853 (1966). The Institute of Petroleum, London, 1966. APPLUCATION DE LA SPECTROMETRIE DE MASSE A LA CINETIQUE CHIMIQUE.

28. Lichtman, D. and Kirst, T. R., Phys. Letters, 20, 7 (1966). ELECTRON PROBE SURFACE MASS SPECTROMETRY STUDY OF OXYGEN ON MOLYBDENUM.

29. Martin, T. W., J. Chem. Phys., 43, 1422 (1965). ROOM-TEMPERATURE EMISSION OF CATALYTIC IONS FROM AMMONIA AND WATER.

30. Malone, T. J. and McGee, H. A., Jr., J. Phys. Chem., 69, 4338 (1965). MASS SPECTROMETRIC INVESTIGATIONS OF THE SYNTHESIS, STABILITY, AND ENERGETICS OF THE LOW-TEMPERATURE OXYGEN FLUORIDES. I. DIOXYGEN DIFLUORIDE.

31. Malone, T. J. and McGee, H. A., Jr., J. Phys. Chem., 70, 316 (1966). IONIZATION POTENTIALS OF THE DIOXYGEN FLUORIDE FREE RADICALS AND THE DIOXYGEN DIFLUORIDE MOLECULE.

32. Miller, W. J. and Calcote, H. F., J. Chem. Phys., 41, 4001 (1964). NEGATIVE-ION FORMATION IN HYDROCARBON FLAMES.

33. Milne, T. A. and Greene, F. T., Tenth Sym. (Intern.) Combustion, p. 153, The Combustion Institute, 1965. MASS SPECTROMETRIC SAMPLING OF 1-ATM FLAMES.

34. Modica, A. P., J. Phys. Chem., 69, 2111 (1965). KINETICS OF THE NITROUS OXIDE DECOMPOSITION BY MASS SPECTROMETRY. A STUDY TO EVALUATE GAS-SAMPLING METHODS BEHIND REFLECTED SHOCK WAVES.

35. Modica, A. P. and LaGraff, J. E., J. Chem. Phys., 43, 3383 (1965). DECOMPOSITION AND OXIDATION OF C_2F_4 BEHIND SHOCK WAVES.

36. Palmer, T. F. and Lossing, F. P., Can. J. Chem., 43, 565 (1965). FREE RADICALS BY MASS SPECTROMETRY. XXXII. THERMAL DECOMPOSITION OF CYCLOPENTYL RADICALS.

37. Phillips, L. F. and Schiff, H. I., J. Chem. Phys., 42, 3171 (1965). MASS SPECTROMETRIC STUDIES OF ATOMIC REACTIONS. V. THE REACTION OF NITROHEN ATOMS WITH NO_2.

38. Pottie, R. F., J. Chem. Phys., 42, 2607 (1965). IONIZATION POTENTIAL AND HEAT OF FORMATION OF THE DIFLUOROMETHYLENE RADICAL.

39. Robbins, E. J. and Leckenby, R. E., Nature, 206, 1253 (1965). DOUBLE MOLECULES IN GASES.

40. Schissel, P. O. and Trulson, O. C., J. Chem. Phys., 43, 737 (1965). MASS SPECTROMETRIC STUDY OF THE OXIDATION OF TUNGSTEN.

41. Schofield, K. and Sugden, T. M., Tenth Sym. (Intern.) Combustion, p. 589, The Combustion Institute, 1965. SOME OBSERVATIONS ON THE IONIZATION OF ALKALI AND ALKALINE-EARTH ELEMENTS IN HYDROGEN FLAMES.

42. Sharvit, J. and Mandelbaum, A., Israel J. Chem., 3, 54 (1965). THE MASS SPECTROMETRIC DETECTION OF TETRAPHENYLCYCLOBUTADIENE.

43. Smith, J. N., Jr., J. Chem. Phys., 40, 2520 (1964). SCATTERING OF ATOMIC BEAMS BY POLYCRYSTALLINE NICKEL.

44. Spokes, G. N. and Evans, B. E., Tenth Sym. (Intern.) Combustion, p. 639, The Combustion Institute, 1965. ION SAMPLING FROM CHEMICAL PLASMAS.

45. Streng, A. G. and Grosse, A. V., J. Am. Chem. Soc., 88, 169 (1966). TWO NEW FLUORIDES OF OXYGEN: O_5F_2 AND O_6F_2.

46. Sullivan, J. O. and Warneck, P., J. Phys. Chem., 69, 1749 (1965). RATE CONSTANT FOR THE REACTION OF OXYGEN ATOMS WITH ACETYLENE.

47. Sullivan, J. O. and Warneck, P., Ber. Bunsen phys. Chem., 69, 7 (1965). MASS SPECTROMETRIC INVESTIGATION OF THE REACTION BETWEEN OXYGEN ATOMS AND CARBONYL SULFIDE.

48. Tal'rose, V. L., Strunin, V. P., Dodonov, A. F. and Lavrovskaya, G. K., Advan. Mass Spectry., 3, 993 (1966). The Institute of Petroleum, London. MASS SPECTROMETRIC INVESTIGATIONS OF REACTIONS INVOLVING FREE RADICALS.

49. Topor, D. C., J. Chim. Phys. and Phys.-Chim. Biol., 63, 347 (1966). ETUDE DE LA PYROLYSE DU DIMETHYL-ZINC PAR SPECTROMETRIE DE MASSE.

50. Vriens, L., Boers, A. L. and Smit, J. A., Appl. Sci. Research, B12, 65 (1965). MEASUREMENTS ON A MOLECULAR BEAM APPARATUS FOR MASS SPECTROMETRIC STUDY OF REACTIONS IN FLAMES.

51. Wong, E. L. and Potter, A. E., J. Chem. Phys., 43, 3371 (1965). MASS SPECTROMETRIC INVESTIGATIONS OF THE REACTIONS OF O ATOMS WITH H_2 AND NH_3.

ISOTOPIC ABUNDANCE

E. J. Catanzaro

1. Aldrich, L. T., Davis, G. L. and James, H. L., J. Petrol., 6, 445 (1965). AGES OF MINERALS FROM METAMORPHIC AND IGNEOUS ROCKS NEAR IRON MOUNTAIN, MICHIGAN.

2. Allen, P. and Keith, M. L., Nature, 208, 1278 (1965). CARBON ISOTOPE RATIOS AND PALAEOSALINITIES OF PURBECK-WEALDEN CARBONATES.

3. Allsopp, H. L., J. Geophys. Res., 70, 977 (1965). Rb-Sr AND K-Ar AGE MEASUREMENTS ON THE GREAT DYKE OF SOUTHERN RHODESIA.

4. Allsopp, H. L. and Kolbe, P., Geochim. Cosmochim. Acta, 29, 1115 (1965). ISOTOPE AGE DETERMINATIONS ON THE CAPE GRANITE AND INTRUDED MALMESBURY SEDIMENTS, CAPE PENISULA, SOUTH AFRICA.

5. Brookins, D. C. and Hurley, P. M., Am. J. Sci., 263, 1 (1965). Rb-Sr GEOCHRONOLOGICAL INVESTIGATIONS IN THE MIDDLE HADDAN AND GLASTONBURY QUADRANGLES, EASTERN CONNECTICUT.

6. Brooks, C. and Compston, W., J. Geophys. Res., 70, 6249 (1965). THE AGE AND INITIAL Sr^{87}/Sr^{86} OF THE HEEMSKIRK GRANITE, WESTERN TASMANIA.

7. Brown, J. S., Econ. Geol., 60, 47 (1965). OCEANIC LEAD ISOTOPES AND ORE GENESIS.

8. Brown, J. S., Econ. Geol., 60, 1167 (1965). LEAD ISOTOPES OF PEGMATITES, GRANITES, AND ORES.

9. Brown, P. E., Miller, J. A., Grasty, R. L. and Fraser, W. E., Nature, 207, 1287 (1965). POTASSIUM-ARGON AGES OF SOME ABERDEENSHIRE GRANITES AND GABBROS.

10. Brown, P. E., Miller, J. A., Soper, N. J. and York, D., Proc. Yorkshire Geol Soc., 35, (1) 103 (1965). POTASSIUM-ARGON AGE PATTERN OF THE BRITISH CALENDONIDES.

11. Catanzaro, E. J., Murphy, T. J., Garner, E. L. and Shields, W. R., J. Res. Nat. Bur. Std., 68A, 593 (1964). ABSOLUTE ISOTOPIC ABUNDANCE RATIO AND THE ATOMIC WEIGHT OF BROMINE.

12. Cheney, E. S. and Jensen, M. L., Geochim. Cosmochim. Acta, 29, 1331 (1965). STABLE CARBON ISOTOPIC COMPOSITION OF BIOGENIC CARBONATES.

13. Chow, T. J. and Johnstone, M. S., Science, 147, 502 (1965). LEAD ISOTOPES IN GASOLINES AND AEROSOLS OF LOS ANGELES BASIN, CALIFORNIA.

14. Colombo, U., Gazzarrini, F., Sironi, G. Gonfiantini, R. and Tongiorgi, E., Nature, 205, 1303 (1965). CARBON ISOTOPE COMPOSITION OF INDIVIDUAL HYDROCARBONS FROM ITALIAN NATURAL GASES.

15. Compston, W., Lovering, J. F. and Vernon, M. J., Geochim. Cosmochim. Acta, 29, 1085 (1965). THE RUBIDIUM-STRONTIUM AGE OF THE BISHOPVILLE AUBRITE AND ITS COMPONENT ENSTATITE AND FELDSPAR.

16. Crouch, E. A. C. and Tuplin, T. A., Nature, 202, 1282 (1964). ISOTOPIC COMPOSITION AND THE ATOMIC WEIGHT OF NATURALLY OCCURRING MOLYBDENUM: A POSSIBLE REFLECTION OF THE CREATION PROCESS.

17. Dalrymple, G. B., Cox, A. and Doell, R. R., Bull. Geol. Soc. Am., 76, 665 (1965). POTASSIUM-ARGON AGE AND PALEOMAGNETISM OF THE BISHOP TUFF, CALIFORNIA.

18. Dalrymple, G. B. and Hirooka, K., J. Geophys. Res., 70, 5291 (1965). VARIATION OF POTASSIUM, ARGON, AND CALCULATED AGE IN A LATE CENOZOIC BASALT.

19. Darnley, A. G., English, T. H., Sprake, O., Preece, E. R. and Avery, D., Mineral. Mag., 34, 159 (1965). AGES OF URANINITE AND COFFINITE FROM SOUTH-WEST ENGLAND.

20. Dechow, E. and Jensen, M. L., Econ. Geol., 60, 894 (1965). SULFUR ISOTOPES OF SOME CENTRAL AFRICAN SULFIDE DEPOSITS.

21. Doe, B. R. and Newell, M. F., Am. Mineralogist, 50, 613 (1965). ISOTOPIC COMPOSITION OF URANIUM IN ZIRCON.

22. Doe, B. R., Tilton, G. R. and Hopson, C. A., J. Geophys. Res., 70, 1947 (1965). LEAD ISOTOPES IN FELDSPARS FROM SELECTED GRANITIC ROCKS ASSOCIATED WITH REGIONAL METAMORPHISM.

23. Eberhardt, P., Engster, O. and Marti, K., Z. Naturforsch., 20A, 623 (1965). A REDETERMINATION OF THE ISOTOPIC COMPOSITION OF ATMOSPHERIC NEON.

24. Edwards, G. and McLaughlin, W. A., Nature, 206, 814 (1965). AGE OF GRANITES FROM THE TIN PROVINCE OF INDONESIA.

25. Epstein, S., Sharp, R. P. and Gow, A. J., J. Geophys. Res., 70, 1809 (1965). SIX-YEAR RECORD OF OXYGEN AND HYDROGEN ISOTOPE VARIATIONS IN SOUTH POLE FIRN.

26. Evans, C. R., Nature, 207, 56 (1965). GEOCHRONOLOGY OF THE LEWISIAN BASEMENT NEAR LOCHINVER, SUTHERLAND.

27. Evans, C. R. and Park, R. G., Nature, 205, 350 (1965). POTASSIUM-ARGON AGE DETERMINATIONS FROM THE LEWISIAN OF GAIRLOCH, ROSS-SHIRE, SCOTLAND.

28. Fairbairn, H. W., Hurley, P. M. and Pinson, W. H., Proc. Geol. Assoc. Can., 16, 95 (1965). RE-EXAMINATION OF Rb-Sr WHOLE ROCK AGES AT SUDBURY, ONTARIO.

29. Fanale, F. P. and Schaeffer, O. A., Science, 149, 312 (1965). HELIUM-URANIUM RATIOS FOR PLEISTOCENE AND TERTIARY FOSSIL ARAGONITES.

30. Faure, G., Hurley, P. M. and Powell, J. L., Geochim. Cosmochim. Acta, 29, 209 (1965). THE ISOTOPIC COMPOSITION OF STRONTIUM IN SURFACE WATER FROM THE NORTH ATLANTIC OCEAN.

31. Fitch, F. J., Grasty, R. I. and Miller, J. A., Nature, 207, 1349 (1965). POTASSIUM-ARGON AGES OF ROCKS FROM JAN MAYEN AND AN OUTLINE OF ITS VOLCANIC HISTORY.

32. Fitch, F. J. and Miller, J. A., Nature, 208, 743 (1965). AGE OF THE WEARDALE GRANITE.

33. Gorokhov, I. M. and Lobach-Zhuchenko, S. B., Geochim. Intern., 5, 944 (1964). DETERMINATION OF THE AGE OF THE KARELID GRANITES OF SOUTHWESTERN KARELIA BY THE Rb-Sr ISOCHRON METHOD (Abs.).

34. Grasty, R. L. and Leelanandam, C., Mineral. Mag., 35, 529 (1965). ISOTOPIC AGES OF THE BASIC CHARNOCKITE AND KHONDALITE FROM KONDAPALLI, ANDHRA PRADESH, INDIA.

35. Hamilton, E. I., Nature, 206, 251 (1965). DISTRIBUTION OF SOME TRACE ELEMENTS AND THE ISOTOPIC COMPOSITION OF STRONTIUM IN HAWAIIAN LAVAS.

36. Hamilton, E. I., Nature, 207, 1188 (1965). ISOTOPIC COMPOSITION OF STRONTIUM IN A VARIETY OF ROCKS FROM REUNION ISLAND.

37. Harris, P. M., Farrar, E., MacIntyre, R. M., York, D. and Miller, J. A., Nature, 205, 352 (1965). POTASSIUM-ARGON AGE MEASUREMENTS OF TWO IGNEOUS ROCKS FROM THE ORDOVICIAN SYSTEM OF SCOTLAND.

38. Hayatsu, A., York, D., Farquhar, R. M., Grittins, J., Nature, 207, 625 (1965). SIGNIFICANCE OF STRONTIUM ISOTOPE RATIOS IN THEORIES OF CARBONATITE GENESIS.

39. Heier, K. S., Compston, W. and McDougall, I., Geochim. Cosmochim. Acta, 29, 643 (1965). THORIUM AND URANIUM CONCENTRATIONS AND THE ISOTOPIC COMPOSITION OF STRONTIUM IN THE DIFFERENTIATED TASMANIAN DOLERITES.

40. Heymann, D., Geochim. Cosmochim. Acta, 29, 1203 (1965). RARE GAS EVIDENCE FOR TWO PAIRED METEORITE FALLS.

41. Hulston, J. R. and Thode, H. G., J. Geophys. Res., 70, 3475 (1965). VARIATIONS IN THE S^{33}, S^{34}, AND S^{36} CONTENTS OF METEORITES AND THEIR RELATION TO CHEMICAL AND NUCLEAR EFFECTS.

42. Hurley, P. M., Bateman, P. C., Fairbairn, H. W. and Pinson, W. H., Jr., Bull. Geol. Soc. Am., 76, 165 (1965). INVESTIGATION OF INITIAL Sr^{87}/Sr^{86} RATIOS IN THE SIERRA NEVADA PLUTONIC PROVINCE.

43. Kazachevskii, I. V., Cherdyntsev, V. V., Kua'mina, E. A., Sulerzhitskii, L. D., Mochalova, V. F. and Kyuregyan, T. N., Geochem. Intern. (Geokhimiya No. 11, Nov., 1964), 6, 1068 (1965). ISOTOPIC COMPOSITION OF URANIUM AND THORIUM IN THE SUPERGENE ZONE AND IN VOLCANIC PRODUCTS-NATURAL WATERS AND VOLCANIC DEPOSITS.

44. Kinkel, A. R., Jr., Thomas, H. H., Marvin, R. F. and Walthall, F. G., Geochim. Cosmochim. Acta, 29, 717 (1965). AGE AND METAMORPHISM OF SOME MASSIVE SULFUR DEPOSITS IN VIRGINIA, NORTH CAROLINA, AND TENNESSEE.

45. Kirilyuk, V. P., Leyfman, Ye. M., Sivoronov, A. A., Chedzhemov, G. Kh., Mamchur, G, P. and Ts'on, O. V., Geochem. Intern. (Geokhimiya No. 12, 1964), 6, 1149 (1964). NEW DATA ON THE ABSOLUTE AGE OF SOME GEOLOGICAL FORMATIONS OF THE AMAZAR-SHIKA WATERSHED (EASTERN TRANSBAYKAL). (Abs.).

46. Kistler, R. W., Bateman, P. C. and Brannock, W. W., Bull. Geol. Soc. Am., 76, 155 (1965). ISOTOPIC AGES OF MINERALS FROM GRANITIC ROCKS OF THE CENTRAL SIERRA NEVADA AND INYO MOUNTAINS, CALIFORNIA.

47. Klyarovskii, V. M., Geochem. Intern. (Geokhimiya No. 11), 1964), 6, 1125 (1964). AGE OF INTRUSIVE ROCKS OF WESTERN TRANSBAIKALLYA CONTAINING FLUORITE DEPOSITS.

48. Komlev, L. V., Ivanova, K. S. and Sayonenkov, V. G., Geochem. Intern. (Geokhimiya No. 12, 1964), 6, 1137 (1964). THE DIFFERENTIAL MOBILITY OF LEAD ISOTOPES AND THE CHARACTER OF ADMIXED LEAD IN MONAZITES.

49. de Laeter, J. R. and Jeffery, P. M., J. Geophys. Res., 70, 2895 (1965). THE ISOTOPIC COMPOSITION OF TERRESTRIAL AND METEORITIC TIN.

50. Letolle, R., Fontes, A. and Marce, J.-C., Bull. Soc. Franc. Miner. Crist., 88, 417 (1965). UN SPECTROMETRIE DE MASSE POUR MEASURE DE PRECISION DES ABONDANCES ISOTOPIQUES DE L'OXYGENE ET DU CARBONE.

51. Longinelli, A., Nature, 207, 716 (1965). OXYGEN ISOTOPIC COMPOSITION OF ORTHO-PHOSPHATE FROM SHELLS OF LIVING MARINE ORGANISMS.

52. McDougall, I. and Compston, W., Nature, 207, 252 (1965). STRONTIUM ISOTOPE COMPOSITION AND POTASSIUM-RUBIDIUM RATIOS IN SOME ROCKS FROM RUNION AND RODRIGUEZ, INDIAN OCEAN.

53. McDougall, I., Dunn, P. R., Compston, W., Webb, A. W., Richards, J. R. and Bofinger, V. M., J. Geol. Soc. Australia, 12, 67 (1965). ISOTOPIC AGE DETERMINATIONS ON PRECAMBRIAN ROCKS OF THE CARPENTARIA REGION, NORTHERN TERRITORY, AUSTRALIA.

54. McDougall, I. and Gringley, G. W., New Zealand J. Geol. Geophys., 8, 304 (1965). POTASSIUM-ARGON DATES ON MICAS FROM THE NIMROD-BEARDMORE-AXEL HEIBERG REGION, ROSS DEPENDENCY, ANTARCTICA.

55. Merchant, A. E., Bodenheimer, P. and Wallerstein, G., Astrophys. J., 142, 790 (1965). THE LITHIUM ISOTOPE RATIO IN TWO HYADES F STARS.

56. Merrihue, C. and Turner, G., Z. Naturforsch., 20A, 961 (1965). THE ORIGIN OF ANOMALOUS Xe^{129} IN METEORITES.

57. Minshew, V. H., Science, 150, 741 (1965). POTASSIUM-ARGON AGE FROM A GRANITE AT MOUNT WILBUR, QUEEN MAUD RANGE, ANTARCTICA.

58. Monster, J., Anders, E. and Thode, H. G., Geochim. Cosmochim. Acta, 29, 773 (1965). S^{34}/S^{32} RATIO FOR THE DIFFERENT FORMS OF SULPHUR IN THE ORGUEIL METEORITE AND THEIR MODE OF FORMATION.

59. Moorbath, S. and Walker, G. P. L., Nature, 207, 837 (1965). STRONTIUM ISOTOPE INVESTIGATION OF IGNEOUS ROCKS FROM ICELAND.

60. Murthy, V. R. and Compston, W., J. Geophys. Res., 70, 5297 (1965). Rb-Sr AGES OF CHONDRULES AND CARBONACEOUS CHONDRITES.

61. Murthy, V. R. and Sandoval, P., J. Geophys. Res., 70, 4379 (1965). CHROMIUM ISOTOPES IN METEORITES.

62. Nikolaev, B. S., Lazarev, K. F., Korn, O. P., Iakunin, M. I., Krozhzhin, V. M. and A. G. Samartseva, Dokl. Akad. Nauk S. S. S. R., 165, 187 (1965). ON THE ISOTOPIC COMPOSITION OF THE URANIUM CONTAINED IN THE WATERS AND SEDIMENTS OF THE BLACK AND AZOV SEAS.

63. Pankina, R. G. and Mektiyeva, V. L., Geochem. Intern., 5, 853 (1964). THE ISOTOPIC COMPOSITION OF SULFUR IN THE HYDROGEN SULFIDE OF THE NATURAL GAS OF THE BOBRIKOVO ZONE IN THE VOLGA-URALS REGION (Abs.).

64. Pepin, R. O. and Signer, P., Science, 149, 253 (1965). PRIMORDIAL RARE GASES IN METEORITES.

65. Pidgeon, R. T. and Compston, W., J. Petrol., 6, 193 (1965). THE AGE AND ORIGIN OF THE COOMA GRANITE AND ITS ASSOCIATED METAMORPHIC ZONES, NEW SOUTH WALES.

66. Pinson, W. H., Jr., Schnetzler, C. C., Beiser, E., Fairbairn, H. W. and Hurley, P. M., Geochim. Cosmochim. Acta, 29, 455 (1965). Rb-Sr. AGE OF STONY METEORITES.

67. Poschenrieder, W. P., Herzog, R. F. and Barrington, A. E., Geochim. Cosmochim. Acta, 29, 1193 (1965). THE RELATIVE ABUNDANCE OF THE LITHIUM ISOTOPES IN THE HOLBROOK METEORITE.

68. Powell, J. L., Nature, 206, 288 (1965). ISOTOPIC COMPOSITION OF STRONTIUM IN CARBONATE ROCKS FROM KESHYA AND MKWISI, ZAMBIA.

69. Powell, J. L., Am. Mineralogist, 50, 1921 (1965). ISOTOPIC COMPOSITION OF STRONTIUM IN FOUR CARBONATE VEIN-DIKES.

70. Powell, J. L., Am. Mineralogist, 50, 1075 (1965). LOW ABUNDANCE OF Sr^{87} IN ONTARIO CARBONATITES.

71. Powell, J. L., Faure, G. and Hurley, P. M., J. Geophys. Res., 70, 1509 (1965). STRONTIUM-87 ABUNDANCE IN A SUITE OF HAWAIIAN VOLCANIC ROCKS OF VARYING SILICA CONTENT.

72. Pu, L., Scientia Sinica, 14, 1663 (1965). GEOCHRONOLOGICAL DATA BY THE K-Ar DATING METHOD.

73. Rama, S. N. I. and Hart, S. R., Science, 147, 737 (1965). NEON ISOTOPE FRACTIONATION DURING TRANSIENT PERMEATION.

74. Rama, S. N. I., Hart, S. R. and Roedder, E., J. Geophys. Res., 70, 509 (1965). EXCESS RADIOGENIC ARGON IN FLUID INCLUSIONS.

75. Reuter, J. H., Epstein, S. and Taylor, H. P., Jr., Geochim. Cosmochim. Acta, 29, 481 (1965). O^{18}/O^{16} RATIOS OF SOME CHONDRITIC METEORITES AND TERRESTRIAL ULTRAMAFIC ROCKS.

76. Rosholt, J. N., Butler, A. P., Garner, E. L. and Shields, W. R., Econ. Geol., 60, 199 (1965). ISOTOPIC FRACTIONATION OF URANIUM IN SANDSTONE, POWDER RIVER BASIN, WYOMING AND SLICK ROCK DISTRICT, COLORADO.

77. Rowe, M. W. and Bogard, D. D., Brothers, C.E., and Kuroda, P. K., Phys. Rev. Letters, 15, 843 (1965). COSMIC-RAY-PRODUCED XENON IN METEORITES.

78. Rowe, M. W., Bogard, D. D. and Manuel, O. K., Geochim. Cosmochim. Acta, 29, 1199 (1965). NOBLE GASES FROM THE PEACE RIVER LaLANDE AND ACHILLES METEORITES.

79. Rutland, R. W. R., Guest, J. E. and Grasty, R. L., Nature, 208, 677 (1965). ISOTOPIC AGES AND ANDEAN UPLIFT.

80. Schaeffer, O. A. and Heymann, D., J. Geophys. Res., 70, 215 (1965). COMPARISON OF Cl^{36}-Ar^{36} AND Ar^{39}-Ar^{38} COSMIC RAY EXPOSURE AGES OF DATED FALL IRON METEORITES.

81. Schaeffer, O. A., Stoenner, R. W., and Fireman, E. L., J. Geophys. Res., 70, 209 (1965). RARE GAS ISOTOPE CONTENT AND K-Ar AGES OF MINERAL CONCENTRATES FROM THE INDARCH METEORITE.

82. Schnetzler, C. C. and Pinson, W. H., Jr., Geochim. Cosmochim. Acta, 28, 953 (1964). VARIATION OF STRONTIUM ISOTOPES IN TEKTITES.

83. Schreiner, G. D. L. and Verbeek, A. A., Proc. Roy. Soc. (London), A285, 423 (1965). VARIATIONS IN $^{39}K/^{41}K$ RATIO AND MOVEMENT OF POTASSIUM IN A GRANITE-SHALE CONTACT REGION.

84. Sharma, T. and Clayton, R. N., Geochim. Cosmochim. Acta, 29, 1347 (1965). MEASUREMENT OF O^{18}/O^{16} RATIOS OF TOTAL OXYGEN OF CARBONATES.

85. Shields, W. R., Goldich, S. S., Garner, E. L. and Murphy, T. J., J. Geophys. Res., 70, 479 (1965). NATURAL VARIATIONS IN THE ABUNDANCE RATIO AND THE ATOMIC WEIGHT OF COPPER.

86. Shields, W. R., Murphy, T. J. and Garner, E. L., J. Res. Nat. Bur. Std., 68A, 589 (1964). ABSOLUTE ISOTOPIC ABUNDANCE RATIO AND THE ATOMIC WEIGHT OF A REFERENCE SAMPLE OF COPPER.

87. Shukolyukov, Yu. A., Geochem. Intern., 5, 843 (1964). INTERPRETATION OF DISCORDANT AGES CALCULATED FROM THE ISOTOPIC RATIOS: Pb^{206}/U^{238} AND Pb^{207}/U^{235}.

88. Sinclair, A. J., Econ. Geol., 60, 1533 (1965). OCEANIC LEAD ISOTOPES AND ORE GENESIS.

89. Snelling, N. J., Nature, 205, 491 (1965). AGE DETERMINATIONS ON THREE AFRICAN CARBONATITES.

90. Stern, T. W., Nowell, M. F., Kistler, R. W. and Shawe, D. R., J. Geophys. Res., 70, 1503 (1965). ZIRCON URANIUM-LEAD AND THORIUM-LEAD AGES AND MINERAL POTASSIUM-ARGON AGES OF LA SAL MOUNTAINS ROCKS, UTAH.

91. Svec, H. J. and Anderson, A. R., Jr., Geochim. Cosmochim. Acta, 29, 633 (1965). THE ABSOLUTE ABUNDANCE OF THE LITHIUM ISOTOPES IN NATURAL SOURCES.

92. Tatsumoto, M., Hedge, C. E. and Engel, A. E. J., Science, 150, 886 (1965). POTASSIUM, RUBIDIUM, STRONTIUM, THORIUM, URANIUM, AND THE RATIO OF STRONTIUM-87 TO STRONTIUM-86 IN OCEANIC THOLEIITIC BASALT.

93. Taylor, H. P., Jr., Duke, M. B., Silver, L. T., and Epstein, S., Geochim. Cosmochim. Acta, 29, 489 (1965). OXYGEN ISOTOPE STUDIES OF MINERALS IN STONY METEORITES.

94. Tilton, G. R. and Steiger, R. H., Science, 150, 1805 (1965). LEAD ISOTOPES AND THE AGE OF THE EARTH.

95. Tugarinov, A. I., Bibikova, E. V. and Zykov, S. I., Geochem. Intern., 5, 945 (1964) AGES OF ROCKS OF THE KURSK MAGNETIC ANOMALY.

96. Turnbull, W. D., Lundelius, E. L., Jr., and McDougall, I., Nature, 206, 816 (1965). A POTASSIUM/ARGON DATED PLIOCENE MARSUPIAL FAUNA FROM VICTORIA, AUSTRALIA.

97. Umemoto, S., J. Geophys. Res., 70, 5326 (1965). U^{234}/U^{238} IN SEAWATER FROM THE KUROSHIO REGION.

98. Vdovykin, G. P., Kropotova, O. I. and Zhurov, Uy. A., Geochem. Intern., 5, 922 (1964). ON THE ISOTOPIC COMPOSITION OF CARBON IN NATURAL GASES.

99. Vinogradov, A. P., Brinenko, V. A. and Ustinov, V. I., Geochem. Intern. (Geokhimiya No. 11, No., 1964), 6, 1055 (1964). ISOTOPIC COMPOSITION OF SULFUR AND CARBON IN THE ORES OF THE SHOR-SU DEPOSIT (UZBEKISTAN).(Abs.).

100. Wasserburg, G. J., Burnett, D.S. and Frondel, C., Science, 150, 1814 (1965). STRONTIUM-RUBIDIUM AGE OF AN IRON METEORITE.

101. Weber, J. N., Nature, 207, 972 (1965). OXYGEN ISOTOPE FRACTIONATION BETWEEN CO-EXISTING CALCITE AND DOLOMITE IN THE FRESHWATER UPPER CARBONIFEROUS FREEPORT FORMATION.

102. Wetherill, G. W. and Bickford, M. E., J. Geophys. Res., 70, 4669 (1965). PRIMARY AND METAMORPHIC Rb-Sr CHRONOLOGY IN CENTRAL COLORADO.

103. Whittles, A. B. L. and Slawson, W. F., Geochim. Cosmochim. Acta, 29, 142 (1965). A MODIFIED TECHNIQUE FOR TRACE LEAD GAS SOURCE MASS SPECTROMETRY.

104. Zartman, R. E., J. Petrol., 5, 359 (1964). A GEOCHRONOLOGICAL STUDY OF THE LONE GROVE PLUTON FROM THE LLANO UPLIFT, TEXAS.

105. Zartman, R. E., J. Geophys. Res., 70, 965 (1965). THE ISOTOPIC COMPOSITION OF LEAD IN MICROCLINES FROM THE LLANO UPLIFT, TEXAS.

1965 Bibliography

High Mass Spectrometry Literature

Prepared by Subcommittee III

Members:

E. M. Emery

M. C. Hamming

C. Lifshitz

W. E. McKinstry

W. Wright

Achenbach, H. and K. Biemann, J. Amer. Chem. Soc. 87, 4177 (1965). ISOTUBOFLAVINE AND NORISOTUBOFLAVINE. TWO NEW ALKALOIDS ISOLATED FROM PLEIOCARPA MUTICA BENTH.

Achenbach, H. and K. Biemann, J. Amer. Chem. Soc. 87, 4944 (1965). 10,22-DIOXOKOPSANE, NA-METHYL-10,22-DIOXOKOPSANE. THREE NEW ALKALOIDS OF PLEIOCARPA MUTICA BENTH.

Akopian, M. E. and F. I. Vilesov, Dokl. Akad. Nauk SSSR 161, 1110 (1965). MASS SPECTROMETER STUDY OF THE PHOTOIONIZATION OF SCARCELY VOLATILE ORGANIC COMPOUNDS.

Alam, S. N., K. A. H. Adams and D. B. Mac Lean, Can. J. Chem. 42, 2456 (1964). LYCOPODIUM ALKALOIDS. XV. STRUCTURE AND MASS SPECTRA OF SOME MINOR ALKALOIDS OF L. FLABELLAFORME.

Albin, M. S., L. A. Horrocks and H. E. Kretchmer, Anesthesiology 25, 672 (1964). HALOTHANE IMPURITIES AND THE COPPER KETTLE.

Aleksankin, M. M., B. V. Chizhov, I. V. Goldenfeld and I. P. Gragerov, Zh. Organ. Khim. 1, 1909 (1965). STUDY OF MECHANISM OF HOMOLYTIC REACTIONS IN SOLUTION BY ISOTOPE AND MS METHOD. REACTIONS OF I-BENZ., A-I-NAPH., P-I-BIPHEN., AND BENZ-CL TO MG.

Amy, J. W., E. M. Chait, W. E. Baitinger and F. W. Mc Lafferty, Anal. Chem. 37, 1265 (1965). GENERAL TECHNIQUE FOR COLLECTING GAS CHROMATOGRAPHIC FRACTIONS FOR INTRODUCTION INTO THE MASS SPECTROMETER.

Anderson, J. and E. von Sydow, Acta. Chem. Scand. 18, 1105 (1964). THE AROMA OF BLACK CURRANTS. HIGHER BOILING COMPOUNDS.

Aplin, R. T., et. al., J. Amer. Chem. Soc. 87, 4888 (1965). MASS SPECTROMETRY IN STRUCTURAL AND STEREOCHEMICAL PROBLEMS. ALIPHATIC AND ALICYCLIC NITRO COMPOUNDS.

Aplin, R. T., H. Budzikiewicz and C. Djerassi, J. Amer. Chem. Soc. 87, 3180 (1965). MASS SPECTROMETRY IN STRUCTURAL AND STEREOCHEMICAL PROBLEMS. THE NEGATIVE ION MASS SPECTRA OF SOME SIMPLE ORGANIC COMPOUNDS.

Ardenne, M., K. Steinfelder and R. Tuemmler, Z. Chem. 5, 287 (1965). MOLECULAR MASS SPECTROGRAPHY OF NATURAL PRODUCTS.

Arndt, R. R. and C. Djerassi, Chem. Commun. 22, 578 (1965). MASS SPECTROMETRY IN STRUCTURAL AND STEREOCHEMICAL PROBLEMS. ABSENCE OF ELECTRON IMPACT INDUCED METHYL MIGRATION IN 2,2,8,8-TETRAME,-NONAN-5-ONE.

Audier, H. E., et. al., Bull. Soc. Chim. (France) 3236, 1965. EFFECT OF STEREOISOMERISM ON THE FRAGMENTATION IN MASS SPECTROMETRY. THREO- AND ERYTHRO- BETA- ETHYLENIC ALCOHOLS.

Audier, H. E., et. al., Tetrahedron Letters 1965, 13. MASS SPECTROMETRY OF THE MORPHINE ALKALOIDS.

Audier, H. E., M. Fetizon and J. C. Gramain, Bull. Soc. Chim. (France) 1965, 3088. ORIENTATION OF THE FRAGMENTATION IN MASS SPECTROMETRY BY INTRODUCTION OF FUNCTIONAL GROUPS. ETHYLENE KETALS OF 2-KETOSTEROIDS.

Ayer, W. A., W. R. Bowman, P. Kebarle, and R. H. Burnell, Can. J. Chem. 43, 328 (1965). STRUCTURE STUDIES BY MASS SPECTROMETRY. DETERMINATION OF THE STRUCTURE OF LYCOFAWCINE.

Ayer, W. A., T. E. Habgood, V. Deulofen and H. R. Juliani, Tetrahedron 1965, 2169. LYCOPODIUM ALKALOIDS. IX. SAUROXINE.

Bach, E., A. Kjaer, R. H. Shapiro and C. Djerassi, Acta. Chem. Scand. 19, 10, (1965). MASS SPECTRA OF TWO DEUTERATED ISO-THIOCYANATES.

Banks, R. E., R. N. Haszeldine and D. R. Taylor, J. Chem. Soc. 1965, 978. POLYHALOGENO-ALLENES. TETRAFLUOROALLENE, ITS DIMER, AND REACTION OF THE DIMER WITH TRIFLUORONITROSOMETHANE.

Barber, M., J. A. Weisbach, B. Douglas, and G. O. Dudek, Chem. Ind. (London) 1965, 1072. HIGH RESOLUTION MASS SPECTROSCOPY OF THE CLAVINE AND ERGOT PEPTIDE ALKALOIDS.

Barber, M., P. Jolles, E. Vilkas and E. Lederer, Biochem. Biophys. Res. Commun. 18, 469 (1965). DETERMINATION OF AMINO ACID SEQUENCES IN OLIGO PEPTIDES BY MASS SPECTROMETRY. STRUCTURE OF FORTUITINE. AN ACYL NONA PEPTIDE METHYL ESTER.

Barber, M., et. al., Tetrahedron Letters, 1965, 1331. DETERMINATION OF AMINO ACID SEQUENCES IN OLIGO PEPTIDES BY MASS SPECTROMETRY. STRUCTURE OF PEPTIDOLIPIN SODIUM.

Beckey, H. D. and G. Wagner, Z. Naturforsch. 20, 169 (1965). FIELD ION MASS SPECTRA OF ORGANIC MOLECULES. AMINES.

Beckey, H. D., Z. Anal. Chem. 207, 99 (1965). ANALYSIS OF SOLID ORGANIC NATURAL PRODUCTS BY THE FIELD-IONIZATION MASS SPECTROMETER.

Beckey, H. D. and P. Schulze, Z. Naturforsch 20, 1335 (1965). FIELD ION MASS SPECTRA OF ORGANIC MOLECULES. OLEFINS.

Beckey, H. D. and P. Schulze, Z. Naturforsch 20, 1329 (1965). FIELD ION MASS SPECTRA OF ORGANIC MOLECULES. N-PARAFFINS UP TO CARBON (16) AND BRANCHED PARAFFINS.

Bergman, J., B. O. Lindgren and C. M. Svahn, Acta. Chem. Scand. 19, 1661 (1965). TRITERPENES AND 4-ALPHA-METHYLSTEROLS IN BIRCH WOOD.

Bertaud, W. S., M. C. Probine, J. S. Shannon and A. Taylor, Tetrahedron 21, 677 (1965). ISOLATION OF A NEW DEPSIPEPTIDE FROM PITHOMYCES CHARTARUM.

Beynon, J. H., B. E. Job and A. E. Williams, Z. Naturforsch 20, 883 (1965). SOME DECOMPOSITION ROUTES IN THE MASS SPECTRA OF AROMATIC CARBOXYLIC ACIDS.

Beynon, J. H., R. A. Saunders and A. E. Williams, Z. Naturforsch. 20, 180 (1965). FORMATION OF METASTABLE IONS IN MASS SPECTROMETERS WITH RELEASE OF INTERNAL ENERGY.

Beynon, J. H., R. A. Saunders, A. Topham and A. E. Williams, J. Chem. Soc. 1965, 6403. THE DISSOCIATION OF O-NITROTOLUENE UNDER ELECTRON IMPACT.

Bianchi, E., C. Djerassi, H. Budzikiewicz and Y. Sato, J. Org. Chem. 30, 754 (1965). STRUCTURE OF TOMATILLIDINE.

Biemann, K. and J. Throck-Watson, Monatsh. Chemie. 96, 305 (1965). HIGH RESOLUTION SPECTRA OF CERTAIN NATURAL PRODUCTS DURING THEIR SEPARATION BY GAS CHROMATOGRAPHY.

Biemann, K. and W. Mc Murray, Tetrahedron Letters, 1965, 647. COMPUTER AIDED INTERPRETATION OF HIGH RESOLUTION MASS SPECTRA.

Bochkarev, V. N., et. al., Khim. Prirodn. Soedin., Akad. Nauk Uz SSR. 1965, (1), 52. DEPSIPEPTIDES. MASS SPECTROMETRIC STUDY OF CYCLO TETRADEPSIPEPTIDES WITH REGULAR STRUCTURE.

Bose, A. K., I. Kugajevsky, P. T. Funke and K. G. Das, Tetrahedron Letters 1965, 3065. MASS SPECTRAL STUDIES. FRAGMENTATION OF AMIDINES.

Bowie, J. H., S. O. Lawesson, G. Schroll and D. H. Williams, J. Amer. Chem. Soc. 87, 5742 (1965). MASS SPECTROSCOPY. MASS SPECTRA OF BETA-KETO-ESTERS.

Bowie, J. H., D. W. Cameron and D. H. Williams, J. Amer. Chem. Soc. 87, 5094 (1965). MASS SPECTROMETRY. MASS SPECTRA OF SUBSTITUTED NAPHTHOQUINONES.

Bricas, E., et. al., Biochemistry 4, 2254 (1965). DETERMINATION OF AMINO ACID SEQUENCES IN OLIGO PEPTIDES BY MASS SPECTROMETRY. SYNTHETIC N-ACYL OLIGO PEPTIDE METHYL ESTERS.

Brockmann, H., H. Buczikiewicz, C. Djerassi and J. Niemeyer, Chem. Ber. 98, 4, 1260 (1965). MS AND ITS USE IN STRUCTURAL AND STEREOCHEMICAL PROBLEMS. ANTIBIOTICS OF ACTINOMYCETES L. MS FRAGMENTATION BEHAVIOR OF ANTHRA CYCLINONES.

Brown, P., et. al., J. Amer. Chem. Soc. 87, 4559 (1965). MASS SPECTROMETRY IN STRUCTURAL AND STEREOCHEMICAL PROBLEMS. OCCURRENCE OF ALKYL REARRANGEMENTS IN THE FRAGMENTATION OF SOME FORMALDEHYDE ACETALS.

Brunn, T., D. P. Hollis and R. Ryhage, Acta. Chem. Scand. 19, 839 (1965). THE CONSTITUTION OF FRAGILIN.

Brunnee, C. and H. Voshage, Verlag Karl Thiemig K. G., Munchen, Germany 1964, 316. PP MASS SPECTROMETRY.

Bryce, T. A. and J. R. Maxwell, Chem. Commun. (London) 1965, 206. IDENTIFICATION OF THE N-OXIDE GROUP BY MASS SPECTROMETRY.

Budzikiewicz, H., et. al., Tetrahedron 21, 1881 (1965). MASS SPECTROMETRY AND ITS USE IN STRUCTURAL AND STEREOCHEMICAL PROBLEMS. MASS SPECTROSCOPIC INVESTIGATION OF THE HASHISH CONSTITUENTS.

Budzikiewicz, H. and Z. Pelah, Monatsh. Chemie. 96, 1739 (1965). MASS SPECTROMETRIC FRAGMENTATION BEHAVIOR OF ARYL ALKYL PHOSPHONATES.

Budzikiewicz, H., J. I. Brauman and C. Djerassi, Tetrahedron 21, 1855 (1965). MASS SPECTROMETRY AND ITS USE IN STRUCTURAL AND STEREOCHEMICAL PROBLEMS. RETRO-DIELS-ALDER REACTION OF ORGANIC MOLECULES BY ELECTRON IMPACT.

Butler, P. E., J. Org. Chem. 29, 3024 (1964). THE MASS SPECTRA OF ORGANIC MOLECULES. THE REARRANGEMENT OF ACETYLENIC ETHERS UNDER ELECTRON IMPACT.

Buttery, R. G., D. R. Black and M. P. Kealy, J. Chromatog. 18, 399 (1965). VOLATILE OXYGENATED CONSTITUENTS OF HOPS. IDENTIFICATION BY COMBINED GAS CHROMATOGRAPHY AND MASS SPECTROMETRY.

Buu-hoi, N. P., C. Orley, M. Mangane and P. Jacquignon, J. Heterocyclic Chem. 2, 236 (1965). MASS SPECTROMETRY OF BENZO(A)-AND BENZO(C)-ACRIDINES.

Bycroft, B. W., M. Hesse and H. Schmid,Helv. Chim. Acta. 48, 1598 (1965). THE STRUCTURE OF ERININ AND ERINICIN FROM HUNTERIA UMBELLATA.

Carlin, R. B., A. J. Magistro and G. J. Mains, J. Amer. Chem. Soc. 86, 5300 (1964). AN N-15 TRACER STUDY OF THE TRANSFORMATIONS OF ACETOPHENONE 2,6-XYLYLHYDRAZONE UNDER THE CONDITIONS OF THE FISCHER INDOLE SYNTHESIS.

Cascon, S. C., et. al, J. Amer. Chem. Soc. 87, 5237 (1965). ICHTHYOTHEREOL AND ITS ACETATE, THE ACTIVE POLYACETYLENE CONSTITUENTS OF ICHTHYOTHERE TERMINALA MALME, A FISH POISON FROM THE LOWER AMAZON.

Cason, J. and D. W. Graham, Tetrahedron 21, 471 (1965). ISOLATION OF ISOPRENOID ACIDS FROM A CALIFORNIA PETROLEUM.

Chaigneau, M., Chim. Anal. (Paris) 47, 619 (1965). PRESENT STATE OF MASS SPECTROMETRY.

Chaigneau, M., G. Valdener and J. Seyden-Penne, Compt. Rend. 260, 3965 (1965). STUDY OF THE MASS SPECTRA OF THIO-THEOPHILLINE.

Chaston, S. H. H., et. al., Australian J. Chem. 18, 673 (1965). THIO DERIVATIVES OF B-DIKETONES AND THEIR METAL CHELATES. SOME MONOTHIO-B-KETONES AND THEIR NICKEL(II) CHELATES.

Chaston, S. H. H., S. E. Livingstone, T. H. Lockyer and J. S. Shannon, Australian J. Chem. 18, 1539 (1965). DETERMINATION BY MASS SPECTROMETRY OF THE STRUCTURE OF BIS-BENZOYLACETONE ETHYLENE NIIMINE AND ITS METAL CHELATES.

Clugston, D. M. and D. B. Mac Lean, Can. J. Chem. 43, 2516 (1965). MASS SPECTRA OF SOME FURO-QUINOLINE ALKALOIDS.

Collin, P. J., H. Silberman, S. Sternhell and G. Sugowdz, Tetrahedron Letters 1965, 2063. INCORPORATION OF ONE OR TWO R-C-C- FRAGMENTS IN THE COURSE OF PHOTOLYSIS OF SOME SCHIFFS BASES IN PRIMARY ALCOHOLS RCH_2CH_2OH.

Cope, A. C., et. al., J. Amer. Chem. Soc. 87, 5452 (1965). RIMOCIDIN. CARBON SKELETON, PARTIAL STRUCTURE, AND ABSOLUTE CONFIGURATION AT C-27.

Costopanagiotis, A. and H. Budzikiewicz, Monatsh. Chemie. 96, 1800 (1965). APPLICATION OF MASS SPECTROMETRY TO THE ANALYSIS OF BARBITURIC ACID DERIVATIVES.

Cotter, J. L., J. Chem. Soc. 1965, 1520. ELECTRON IMPACT STUDIES OF SOME AROMATIC FLUOROCARBONS.

Cotter, J. L., J. Chem. Soc. 1964, 5491. ELECTRON IMPACT FRAGMENTATION PATTERNS OF 3,5-DIPHENYL-1,2,4-OXADIAZOLE, AND 2,5-DIPHENYL-1,3,4-OXADIAZOLE.

Cotter, J. L., J. Chem. Soc. 1965, 6842. MASS SPECTRA OF SOME FLUORINE CONTAINING 1,3,4-OXADIAZOLES.

Cross, A. D., et. al., Coll. Czech. Chem. Commun. 30, 1335 (1965). STUDIES ON THE STRUCTURE OF THE ALKALOID MORAMINE.

Crow, W. D., J. H. Hodgkin and J. S. Shannon, Australian J. Chem. 18, 1433 (1965). ALKALOIDS OF THE AUSTRALIAN RUTACEAE. HALFORDIA SCLEROXYLA. MASS SPECTROMETRY OF HALFORDINOL AND RELATED OXAZOLES.

Cupas, C., P. R. Schleyer and D. J. Trecker, J. Amer. Chem. Soc. 87, 917 (1965). CONGRESSANE.

Cuthbert, J., E. R. Preece and A. R. Turnbull, Appl. Spectry. 19, 18 (1965). MASS SPECTROMETRIC OBSERVATION OF POLYMERS OF CARBON DIOXIDE IN A MOLECULAR BEAM SYSTEM.

Damico, J. N. and W. R. Benson, J. Assoc. Offic. Agr. Chemist 48, 344 (1965). MASS SPECTRA OF SOME CARBAMATE PESTICIDES.

Das, B. C., J. Garnier-Gosset, J. Le Men and M-M Janot, Bull. Soc. Chim. (France) 1965, 1903. THE STRUCTURE OF VINCADIFFINE. ALKALOIDS OF PERIWINKLE.

Das, B. C., M. Lounasmaa, C. Tendille and E. Lederer, Biochem. Biophys. Res. Commun. 21, 318 (1965). MASS SPECTROMETRY OF PLASTOQUINONES. STRUCTURE OF THE PLASTOQUINONES B, C, AND D.

Davis, M. E. and W. E. Browning, Jr., U.S. At. Energy Comm. Ornl-TM-1009 (1964). SEPARATION AND IDENTIFICATION OF VOLATILE IODINE COMPOUNDS BY FRACTIONAL SUBLIMATION AND MASS SPECTROMETRIC ANALYSIS.

Day, E. A. and D. F. Anderson, J. Agr. Food Chem. 13, 2 (1965). CHEESE FLAVOR, GAS CHROMATOGRAPHIC AND MASS SPECTRAL IDENTIFICATION OF NEUTRA COMPONENTS OF AROMA FRACTION OF BLUE CHEESE.

De Jongh, D. C. and S. Hanessian, J. Amer. Chem. Soc. 87, 1408 (1965). ASSIGNMENT OF THE POSITION OF AMINO GROUPS IN AMINO SUGARS BY MASS SPECTROMETRY.

De Jongh, D. C. and S. Hanessian, J. Amer. Chem. Soc. 87, 3744 (1965). CHARACTERIZATION OF AMINO SUGARS BY MASS SPECTROMETRY.

De Jongh, D. C., J. Org. Chem. 30, 453 (1965). MASS SPECTROMETRY IN CARBOHYDRATE CHEMISTRY. A-CYCLIC PERACETATES OF PENTOSES AND HEXOSES.

De Jongh, D. C., J. Org. Chem. 30, 1563 (1965). MASS SPECTROMETRY IN CARBOHYDRATE CHEMISTRY. DITHIOACETALS OF COMMON MONOSACCHARIDES.

Djerassi, C. and S. D. Sample, Nature 208, 1314 (1965). MASS SPECTROMETRIC FRAGMENTATION OF NITROPHENYLHYDRAZONES.

Djerassi, C. and C. Fenselau, J. Amer. Chem. Soc. 87, 5747 (1965). MASS SPECTROMETRY IN STRUCTURAL AND STEREOCHEMICAL PROBLEMS. NATURE OF THE CYCLIC TRANSITION STATE IN HYDROGEN REARRANGEMENTS IN ALIPH. ETHER.

Djerassi, C. and C. Fenselau, J. Amer. Chem. Soc. 87, 5752 (1965). MASS SPECTROMETRY IN STRUCTURAL AND STEREOCHEMICAL PROBLEMS. NATURE OF THE CYCLIC TRANSITION STATE IN HYDROGEN REARRANGEMENTS OF ALIPH. AMINE.

Djerassi, C. and C. Fenselau, J. Amer. Chem. Soc. 87, 5756 (1965). MASS SPECTROMETRY IN STRUCTURAL AND STEREOCHEMICAL PROBLEMS. HYDROGEN TRANSER REACTIONS IN BUTYL PROPIONATE, BENZOATE, AND PHTHALATE.

Djerassi, C., J. Karliner and R. T. Aplin, Steroids 6, 1 (1965). MASS SPECTROMETRY IN STRUCTURAL AND STEREOCHEMICAL PROBLEMS. STEROIDAL DELTA(4)-3,6-DIKETONES.

Djerassi, C., et. al., J. Amer. Chem. Soc. 87, 817 (1965). MASS SPECTROMETRY IN STRUCTURAL AND STEREOCHEMICAL PROBLEMS. SYN. AND FRAG. BEHAVIOR OF 15-KETO STEROIDS. INTER-ATOM DISTANCE-MC LAFFERTY REARR.

Djerassi, C., R. H. Shapiro and M. Vandewalle, J. Amer. Chem. Soc. 87, 4892 (1965). MASS SPECTROMETRY IN STRUCTURAL AND STEREOCHEMICAL PROBLEMS. STEROSPECIFICITY IN A HYDROGEN TRANSFER REACTION CHARACTERISTICS 6-KETOSTEROIDS.

Dolejs, L., V. Hanus, Z. Voticky and J. Tomko, Coll. Czech. Chem. Commun. 30, 2869 (1965). ALKALOIDS FROM BUXUS SEMPERVIRENS L. MASS SPECTRAL FRAGMENTATION.

Dubov, S. S. and A. M. Khokholova, J. Gen. Chem. USSR. 34, 1974 (1964). MASS SPECTRA OF SOME POLYFLUORINATED ORGANIC COMPOUNDS CONTAINING THE NITROGEN-OXYGEN BOND.

Duffield, A. M., et. al., J. Amer. Chem. Soc. 87, 4902 (1965). MASS SPECTROMETRY IN STRUCTURAL AND STEREOCHEMICAL PROBLEMS. FRAGMENTATION OF SOME AMARYLIDACEAE ALKALOIDS.

Duffield, A. M., H. Budzikiewicz and C. Djerassi, J. Amer. Chem. Soc. 87, 2926 (1965). MASS SPECTROMETRY IN STRUCTURAL AND STEREOCHEMICAL PROBLEMS. FRAGMENTATION PROCESSES OF SOME TOBACCO ALKALOIDS.

Duffield, A. M., H. Budzikiewicz, D. H. Williams and C. Djerassi, J. Amer. Chem. Soc. 87, 810 (1965). MASS SPECTROMETRY IN STRUCTURAL AND STEREOCHEMICAL PROBLEMS. STUDY OF THE FRAGMENTATION PROCESSES OF SOME CYCLIC AMINES.

Duffield, A. M., H. Budzikiewicz and C. Djerassi, J. Amer. Chem. Soc. 87, 2920, (1965). MASS SPECTROMETRY IN STRUCTURAL PROBLEMS. INFLUENCE OF DIFFERENT HETERO ATOMS ON THE MASS SPECTROMETRIC FRAGMENTATION OF 5 MEMB. HETEROCYCLES.

Duffield, A. M., H. Budzikiewicz and C. Djerassi, J. Amer. Chem. Soc. 87, 2913 (1965). MASS SPECTROMETRY IN STRUCTURAL AND STEREOCHEMICAL PROBLEMS. FRAGMENTATION PROCESSES OF SOME 5-MEMBERED N-ALKYL LACTAMS AND N-ALK. SUCCINIMIDES.

Duffield, A. M. and C. Djerassi, J. Amer. Chem. Soc. 87, 4554 (1965). MASS SPECTROMETRY IN STRUCTURAL AND STEREOCHEMICAL PROBLEMS. FRAGMENTATION OF N-ACYL PYRROLIDINES.

Duffield, A. M., et. al., J. Amer. Chem. Soc. 87, 805 (1965). MASS SPECTROMETRY IN STRUCTURAL AND STEREOCHEMICAL PROBLEMS. HYDROGEN REARRANGEMENTS INDUCED BY ELECTRON IMPACT ON N,N-BU. AND N,N-PENT. PYRROLE.

Eland, J. H. D. and C. J. Danby, J. Chem. Soc. 1965, 5935, MASS SPECTRA OF DIPHENYL AND DIBENZYL COMPOUNDS.

Elgamal, M. H. A., M. B. E. Fayez and G. Snatske, Tetrahedron 21, 2109 (1965). CONSTITUENTS OF LOCAL PLANTS. LIQUORIC ACID, A NEW TRITERPENOID FROM THE ROOTS OF GLYCYRRHIZA GLABRA L.

Enzell, C. R. and R. Ryhage, Arkiv. Kemi. 23, 367 (1965). MASS SPECTROMETRY OF DITERPENES. 1-CARBO-DI-CYCLIC DITERPENES.

Eustache, H., C. L. Guillemin and F. Auricourt, Bull. Soc. Chim. (France) 1965, 1386. JOINT GAS CHROMATOGRAPHIC AND MASS SPECTROPHOTOMETRIC ANALYSIS. APPLICATION TO THE DETECTION OF TRACES OF IMPURITIES.

Facchetti, S., Chim. Ind. (Milan) 47, 966 (1965). MASS SPECTROMETRY IN THE STUDY OF POLYPHENYLS.

Fales, H. M. and T. Luukkainen, Anal. Chem. 37, 955 (1965). O-METHYL OXIMES AS CARBONYL DERIVATIVES IN GAS CHROMATOGRAPHY, MASS SPECTROMETRY, AND NUCLEAR MAGNETIC RESONANCE.

Fallgatter, M. B. and R. J. Hanrahan, J. Phys. Chem. 4, 2059 (1965). RADIATION CHEMISTRY OF PERFLUOROCYCLOHEXANE AND PERFLUOROCYCLOBUTANE. MASS SPECTROSCOPIC IDENTIFICATION OF PRODUCTS.

Fields, E. K. and S. Meyerson, Chem. Commun. 1965, 474. BENZENE BY PYROLYSIS OF PHTHALIC ANHYDRIDE.

Fisher, I. P., J. B. Homer and F. P. Lossing, J. Amer. Chem. Soc. 87, 957 (1965). FREE RADICALS BY MASS SPECTROMETRY. IONIZATION POTENTIALS OF FLUOROMETHYLENE,1,1,1,2,2-PENTAFLUOROETHYL,CF_3CH_2,F-PROPYL AND F-1-PROPYL RAD.

Flannery, J. B. and G. J. Janz, J. Chem. Eng. Data 10, 387 (1965). FLUORINATED ALIPHATIC NITRILES. MASS SPECTRA AND FRAGMENTATION.

Foffani, A., S. Pignataro, B. Cantone and F. Grasso, Z. Physik. Chem. (Frankfurt) 45, 79 (1965). MASS SPECTRA OF METAL HEXA CARBONYLS.

Foster, N. G., D. E. Hirsch, R. F. Kendall and B. H. Eccleston, U.S. Bur. Mines Rept. Invest. 1965, 6671. THE MASS SPECTRA AND CORRELATIONS WITH STRUCTURE FOR FOURTEEN ALKYLTHIOPHENES.

Franck, B., G. Blaschke and K. Lewejohann, Ann. Chemie (Liebig) 685, 207 (1965). SYNTHESIS OF ISOPILOCEREIN AND PILOCEREIN.

Friedman, H. L., J. Appl. Polymer Sci. 9, 651 (1965). PRODUCTS OF FLASH PYROLYSIS OF PHENOL-FORMALDEHYDE BY TIME OF FLIGHT MASS SPECTROSCOPY.

Fujii, K. and S. Oshima, Mass Spectroscopy (Japan) 13, 229 (1965). MASS SPECTROMETRIC INVESTIGATION OF PETROLEUM. MASS SPECTROMETRIC ANALYSIS OF NAPHTHENIC ACID.

Galimov, E. M., V. A. Grinenko and V. I. Ustinov, Pribory. I. Tekhn. Eksperim. 10, 159 (1965). PRECISE LOADING OF A MASS SPECTROMETER.

Gilbert B., et. al., Tetrahedron 21, 1141 (1965). ALKALOIDS STUDIES. THE ALKALOIDS OF 12 ASPIDOSPERMA SPECIES.

Glover, G. I., R. B. Smith and H. Rapoport, J. Amer. Chem. Soc. 87, 2003 (1965). AMIDE-AMIDE REACTION VIA CYCLOLS.

Goldup, A., A. B. Morrison and G. W. Smith, J. Chem. Soc. 1965, 3864. THE STRUCTURE OF CYCLOVERATRIL.

Gorman, M., N. Neuss and N. J. Cone, J. Amer. Chem. Soc. 87, 93 (1965). VINCA ALKALOIDS XVII. CHEMISTRY OF CATHARANTHINE.

Gorokhov, L. N., Zh. Strukt. Khim. 6, 766 (1965). MASS SPECTRUM OF 1,1-DICHLOROGERMIRENE.

Goto, T., A. Tatematsu, Y. Nakajima and H. Tsuyama, Tetrahedron Letters 1965, 757. ORGANIC MASS SPECTROMETRY. ELECTRON IMPACT FRAGMENTATION OF DIMEDONE AND 2-ETHYL-DIMEDONE.

Goto, T., A. Tatematsu and S. Matsuura, J. Org. Chem. 30, 1844 (1965). ORGANIC MASS SPECTROMETRY. MASS SPECTRA OF PTERIDINE, METHYL PTERIDINES AND HYDROXY PTERIDINES.

Govindachari, T. R., N. Viswanathan, B. R. Pai and T. S. Savitri, Tetrahedron 21, 2951 (1965). CHEMICAL CONSTITUENTS OF ALSTONIA VENENATA R.BR.

Gragerov, I. P. and B. V. Chizov, Zh. Organ. Khim. 1, 838 (1965). STUDY OF MECHANISM OF BROMOLYTIC REACTIONS IN SOLUTIONS BY ISOTOPE AND MASS SPECTROSCOPIC METHOD. PROPERTIES OF BENZYL AND C-HEXYL RADICAL.

Gragerov, I. P. and B. V. Chizov, Zh. Organ. Khim. 1, 1264 (1965). MECHANISM OF THE HOMOLYTIC REACTIONS IN A SOLN BY ISOTOPE AND MS METHODS. REACTIONS OF A-NAPHTHYL DIAZONIUM AND P-DIPHENYL DIAZONIUM CHLORIDE.

Greene, F. T. and T. A. Milne, Res./Dev. 1965, 16. DIRECT HIGH-PRESSURE MASS SPECTROMETRIC SAMPLING.

Grigg, R., M. V. Sargent and D. H. Williams, Tetrahedron 21, 3441 (1965). MASS SPECTROSCOPY. MASS SPECTRA OF SUBSTITUTED FURANS.

Gronowitz, S. and A. Bugge, Acta. Chem. Scand. 19, 1271 (1965). NEW HETEROAROMATIC SYSTEMS DERIVED FROM O-FORMYL THIOPHENEBORONIC ACIDS.

Grutzmacher, et. al., Inst. Petrol. Astm MS Symp. Paris. MASS SPECTROMETRIC INVESTIGATION OF ACETYLATED PEPTIDES CONTAINING TRIFUNCTIONAL AMINO ACIDS.

Haenni, A. L., et. al., Helv. Chim. Acta. 48, 729 (1965). THE STRUCTURAL CHEMISTRY OF ASPERGILLOMARASMINES A AND B.

Halpern, B., J. W. Westley, I. Wredenhagen and J. Lederberg, Biochem. Biophys. Res. Commun. 20, 710 (1965). OPTICAL RESOLUTION OF D,L-AMINO ACIDS BY GAS CHROMATOGRAPHY AND MASS SPECTROMETRY.

Han, I. and G. J. Fritz, Anal. Chem. 37, 1442 (1965). MASS SPECTROMETRIC MEASUREMENT OF OXYGEN-18 IN SMALL CARBON DIOXIDE SAMPLES.

Harrison, A. G. and E. G. Jones, Can. J. Chem. 43, 960 (1965). REARRANGEMENT REACTIONS FOLLOWING ELECTRON IMPACT ON ETHYL AND ISOPROPYL ESTERS.

Harrison, A. G., P. Haynes. S. Mc Lean and F. Meyer, J. Amer. Chem. Soc. 87, 5099 (1965). MASS SPECTRA OF METHYL SUBSTITUTED CYCLOPENTADIENES.

Harrison, S. A., L. E. Peterson and D. H. Wheeler, J. Amer. Oil Chemists Soc. 42, 2 (1965). DIMER ACID STRUCTURES. THE DEHYDRO-DIMER FROM METHYL STEARATE AND DI-TERTIARY-BUTYL PEROXIDE.

Hendrick, C. A. and P. R. Jefferies, Tetrahedron 21, 1175 (1965). THE CHEMISTRY OF EUPHORBIACEAE. THE DITERPENES OF RICINOCARPUS MURICATUS AND THE STEREOCHEMISTRY OF EPERUIC ACID.

Herlan, A., Brennstoff. Chem. 46, 264 (1965). MASS SPECTRA OF CARBON (10) TO CARBON(24) PARAFFINS. 3-METHYL PARAFFINS.

Hesse, M. et. al., Helv. Chim. Acta. 48, 689 (1965). THE STRUCTURE OF THE ALKALOID VILLALSTONIN FROM ALSTONIA.

Hesse, M., W. Vetter and H. Schmid, Helv. Chim. Acta. 48, 674 (1965). THE MASS SPECTROMETRIC STUDY OF QUATERNARY NITROGEN COMPOUNDS.

Heymann, D. and E. Keur, J. Sci. Instr. 42, 121 (1965). ALL-METAL GAS PIPETTE FOR USE IN MASS SPECTROMETRY.

Heyns, K. and D. Mueller, Tetrahedron 21, 3151 (1965). MASS SPECTROSCOPIC INVESTIGATIONS MASS SPECTRA OF PER METHYL N-ACETYL AMINO SUGARS.

Heyns, K. and H. Scharmann, Tetrahedron 21, 507 (1965). MASS SPECTROSCOPIC INVESTIGATIONS. EFFECT OF RING SIZE AND STEREOCHEMISTRY ON THE MASS SPECTRA OF PERMETHYLATED PENTOSES.

Heyns, K. and D. Mueller, Tetrahedron 21, 55 (1965). MASS SPECTROMETRIC INVESTIGATIONS. MASS SPECTROMETRIC INVESTIGATION OF THE DEUTERIUM-LABELLED METHYL-2,3,4-TRI-O-METHYL ARABOPYRANOSIDE.

Hirsjaervi, P., Suomen. Kemistilehti, B, 38, 119 (1965). APPLICATION OF MASS SPECTROMETRY IN ORGANIC CHEMISTRY.

Hoffman, D. R., J. Org. Chem. 30, 3512 (1965). MASS SPECTRA OF PORPHYRINS AND CHLORINS.

Honkanen, E. and A. I. Virtanen, Acta. Chem. Scand. 19, 1010 (1965). THE FIRST NATURALLY OCCURRING AMINO TRICARBOXYLIC ACID, ISOLATED FROM THE MUSHROOM LACTARIUS HELVUS.

Honkanen, E., T. Moisio and P. Karvonen, Acta. Chem. Scand. 19, 370 (1965). MASS SPECTRA OF SOME ALIPHATIC LACTONES.

Horvat, R. J., et. al., J. Amer. Oil Chemists Soc. 42, 1112 (1965). VOLATILE PRODUCTS FROM MILD OXIDATION OF METHYL LINOLEATE. ANALYSIS BY COMBINED MASS SPECTROMETRY-GAS CHROMATOGRAPHY.

Huneck, S. and R. Tuemmler, Ann. Chemie. (Liebig) 685, 128 (1965). THE STRUCTURE OF PELTIGERIN.

Ishibashi, K., J. Katsuhara, K. Hashimoto and M. Kobayashi, Kogyo. Kagaku Zasshi. 68, 1224 (1965). TERPENES AND TERPENOIDS IN THE NEUTRAL FRACTION OF THE ESSENTIAL OIL OF ARTEMISIA MARITIMA.

Issenberg, P., M. L. Bazinet and C. Merritt, Jr., Anal. Chem. 37, 1074 (1965). MAGNETIC TAPE RECORDING OF ANALYTICAL DATA.

Itagaki Y., et. al, Chem. Ind. (London) 1965, 1654. MASS SPECTRA OF ALICYCLIC COMPOUNDS CONTAINING ALKYL OXIRANE AS PARTIAL STRUCTURE.

Jackson, A. H., et. al, Tetrahedron 21, 2913 (1965). PYRROLES AND RELATED COMPOUNDS. MASS SPECTROMETRY IN STRUCTURAL AND STEREOCHEMICAL PROBLEMS. MASS SPECTRA OF PORPHYRINS.

Jennings, A. L., Jr., and J. E. Boggs, J. Org. Chem. 29, 2065 (1964). MASS SPECTROMETRY FOR STRUCTURE DETERMINATION. SIMPLE NITROGEN HETEROCYCLES.

Jones, D. S., G. W. Kenner, J. Preston and R. C. Sheppard, Tetrahedron 21, 3209 (1965). PEPTIDES. XIX. THE ISOMERIZATION OF SOME OXAZOLONES DERIVED FROM TRIPEPTIDES.

Jordan W. and P. J. Scheuer, Tetrahedron 21, 3731 (1965). HAWAIIAN PLANT STUDIES. ALKALOIDS OF OCHROSIA SANDWIENSIS A. GRAY.

Joule, J. A., M. Ohasi, B. Gilbert and C. Djerassi, Tetrahedron 1965, 1717. ALKALOID STUDIES. LIII. THE STRUCTURES OF NINE NEW ALKALOIDS FROM ASPIDOSPERMA DASYCARPON A DC.

Junk, G. A. and H. J. Svec, Anal. Chem. 37, 1629 (1965). VACUUM LOCK FOR DIRECT INSERTION OF SAMPLES INTO MASS SPECTROMETER.

Karabatsos, G. J., C. E. Orzech, Jr., and S. Meyerson, J. Amer. Chem. Soc. 87, 4394 (1965). CARBONIUM ION REARRANGEMENTS. PROTONATED CYCLOPROPANES IN THE NITROUS ACID DEAMINATION OF N-PROPYLAMINE.

Karliner, J., H. Budzikiewicz and C. Djerassi, J. Amer. Chem. Soc. 87, 580 (1965). MASS SPECTROMETRY IN STRUCTURAL AND STEREOCHEMICAL PROBLEMS. FRAGMENTATION AND H-TRANSFER REACTIONS OF B-HYDRINDANONES. SYNTHESIS OF DEUTERO.

Karlsson, K. A., Acta. Chem. Scand. 19, 2425 (1965). SPHINGOSINES. USE OF TRIMETHYL SILYL ETHERS FOR THE GAS CHROMATOGRAPHY AND MASS SPECTROMETRY OF SPHINGOSINES.

Kaschnita, R. and G. Spiteller, Monatsh. Chemie 96, 909 (1965). APPLICATIONS OF MASS SPECTROMETRY TO THE STRUCTURAL ELUCIDATION OF ALKALOIDS. ALKALOIDS FROM GONIMA KAMASSI E MEY.

Kebarle, P. and A. M. Hogg, J. Chem. Phys. 42, 668 (1965). MASS SPECTROMETRIC STUDY OF IONS AT NEAR ATMOSPHERIC PRESSURES. THE IONIC POLYMERIZATION OF ETHYLENE.

Kebarle, P. and A. M. Hogg, J. Chem. Physics 42, 798 (1965). HEATS OF HYDRATION AND SOLVATION BY MASS SPECTROMETRY.

Khan, Z. M., M. Hesse and H. Schmid, Helv. Chim. Acta. 48, 1957 (1965). QUATERNARY ALKALOIDS FROM PLEIOCARPA MUTICA BENTH.

Khmel/Nitskii, R. A., et. al., Zh. Obshch. Khim. 35, 773 (1965). MASS SPECTRA AND STRUCTURE OF ORGANIC COMPOUNDS. MASS SPECTRA OF THE 1,3-ENYNE GERMANIUM HYDROCARBONS.

Khmel/Nitskii, A. G., V. N. Kobrina and V. A. Koptyug, Coke Chem. USSR. 1965, 43. IMPURITIES IN THE NAPHTHALENE PRODUCED AT THE KEMEROVO WORKS.

King, A. B., J. Chem. Phys. 42, 3526 (1965). MASS SPECTRAL FRAGMENTATION OF PHENYL-N-ALKANES.

King, A. B. and M. R. Basila, Anal. Chem. 37, 734 (1965). MASS SPECTROMETRIC DETERMINATION OF THE ISOMER DISTRIBUTION OF CARBON-16 TO CARBON-22 PHENYL-N-ALKANES.

Kiser, R. W., Prentice-Hall, 1965. INTRODUCTION TO MASS SPECTROMETRY AND ITS APPLICATIONS.

Kishi, T., et. al., Helv. Chim. Acta. 48, 1349 (1965). ALSTOPHYLLIN, A NEW INDOL-ALKALOID FROM ALSTONIA MACROPHYLLA WALL.

Kochetkov, N. K., N. S. Wulfson, O. S. Chizhov, and B. M. Zolotarev, Izv. Akad. Nauk SSR, Ser. Khim. 1965, 776. MASS SPECTROMETRIC INVESTIGATION OF CARBOHYDRATES. FRAGMENTATION PATTERN OF 2,3,4,6-TETRAMETHYL-A-METHYL-D-GLUCOSIDE.

Kochetkov, N. K. and O. S. Chizhov, Tetrahedron 21, 2029 (1965). MASS SPECTROMETRY OF METHYLATED METHYL GLYCOSIDES. PRINCIPLES AND ANALYTICAL APPLICATION.

Kochetkov, N. K., O. S. Chizhov and B. M. Zolotarev, Dokl. Akad. Nauk SSSR 165, 569 (1965). MASS SPECTROMETER STUDY OF HYDROCARBONS. METHYL ETHERS OF CERTAIN METHYL DEOXY HEXOSIDES.

Komitsky, F., J. E. Gurst and C. Djerassi, J. Amer. Chem. Soc. 87, 1398 (1965). MASS SPECTROMETRY IN STRUCTURAL AND STEREOCHEMICAL PROBLEMS. METHYL MIGRATION IN AN ELECTRON IMPACT INDUCED FRAGMENTATION.

Kresze, G., Z. Anal. Chem. 205, 165 (1964). CONSTITUTION OF ORGANIC COMPOUNDS AND MOLECULAR SPECTROSCOPY. SPECTROSCOPIC METHODS OF CONSTITUTION ANALYSIS.

Laneelle, G., J. Asselineau, W. A. Wolstenholme and E. Lederer, Bull. Soc. Chim. (France) 1965, 2133. DETERMINATION OF AMINO ACID SEQUENCES IN OLIGO PEPTIDES BY MASS SPECTROMETRY. STRUCTURE OF A PEPTIDOLIPID FROM MYCOBACTERIUM JOHNEI.

Langer, H. G., R. S. Gohlke and D. H. Smith, Anal. Chem. 37, 433 (1965). MASS SPECTROMETRIC DIFFERENTIAL THERMAL ANALYSIS.

Lederer, E., Biochem. J. 93, 449 (1964). THE ORIGIN AND FUNCTION OF SOME METHYL GROUPS IN BRANCHED-CHAIN FATTY ACIDS, PLANT STEROLS AND QUINONES.

Lifshitz, C. and F. A. Long, J. Phys. Chem. 69, 3731 (1965). APPEARANCE POTENTIALS AND MASS SPECTRA OF FLUORINATED ETHYLENES. HEATS OF FORMATION OF FLUORINATED SPECIES AND THEIR POSITIVE IONS.

Lifshitz, C. and F. A. Long, J. Phys. Chem. 69, 3737 (1965). APPEARANCE POTENTIALS AND MASS SPECTRA OF FLUORINATED ETHYLENES. CALCULATIONS BASED ON THE STATISTICAL THEORY OF MASS SPECTRA.

Lifshitz, C. and F. A. Long, J. Phys. Chem. 69, 3741 (1965). APPEARANCE POTENTIALS AND MASS SPECTRA OF HEXAFLUOROPROPENE, PENTAFLUORO-CHLORO-PROPENE AND C-HEXAFLUORO-PROPENE.

Lifshitz, C. and F. A. Long, J. Phys. Chem. 69, 3746 (1965). OBSERVATIONS CONCERNING THE POSITIVE ION DECOMPOSITION OF HEXAFLUOROETHANE AND OCTAFLUOROPROPANE IN THE MASS SPECTROMETER.

Lincoln, K. A., Anal. Chem. 37, 541 (1965). FLASH VAPORIZATION OF SOLID MATERIALS FOR MASS SPECTROMETRY BY INTENSE RADIATION.

Linde, H. H. A., Helv. Chim. Acta. 48, 1822 (1965). THE ALKALOIDS FROM MELODINUS AUSTRALIS (F. MUELLER) PIERRE.

Lorquet, A. J., Bull. Classe. Sci., Acad. Roy. Belg. 49, 1225 (1964). BEHAVIOR OF IODOCYCLOPENTANE AND CYCLOPENTYLAMINE UNDER THE IMPACT OF ELECTRONS.

Lorquet, J. C., Mol. Phys. 9, 101 (1965). THE ELECTRONIC STRUCTURE OF IONIZED MOLECULES. ALKANES.

Luning, B. and K. Leander, Acta. Chem. Scand. 19, 1607 (1965). STUDIES ON ORCHIDACEAE ALKALOIDS.

Mahoney, L. R., J. Amer. Chem. Soc. 87, 1089 (1965). REACTIONS OF PEROXY RADICALS WITH POLYNUCLEAR AROMATIC COMPOUNDS. ANTHRACENE IN CHLOROBENZENE.

Maman, M. et. al., Compt. Rend. 260, 5795 (1965). MASS SPECTROMETRY INVESTIGATION OF SOLID ORGANIC COMPOUNDS ORIGINATING FROM ABNORMAL COMBUSTION.

Mandelbaum, A. and D. Ginsburg, Tetrahedron Letters, 1965, 2479. MASS SPECTROMETRY. STERIC DIRECTION OF FRAGMENTATION IN CIS- AND TRANS-B.C RING FUSED MORPHINE DERIVATIVES.

Mandelbaum, A. and M. Cais, Tetrahedron Letters 1964, 3847. FRAGMENTATION OF SOME SUBSTITUTED FERROCENES UNDER ELECTRON IMPACT.

Manusudzhyan, V. G., Izv. Akad. Nauk SSSR, Biol. Nauki 18, 69 (1965). APPLICATION OF MASS SPECTROSCOPY IN BIOLOGY AND BIOCHEMISTRY.

Maoz, N., A. Mandelbaum and M. Cais, Tetrahedron Letters 1965, 2087. MASS SPECTRA OF PI-BONDED COMPOUNDS.

Mason, M. E., B. Johnson and M. C. Hamming, Anal. Chem. 37, 760 (1965). MASS SPECTRAL ANALYSIS OF CARBONYLS REGENERATED FROM THEIR 2,4-DINITROPHENYLHYDRAZONES. AN EXTENSION OF THE PROCEDURE OF RALLS.

Massey, A. G. and D. S. Urch, Chem. And Ind. 1965, 607. MASS SPECTRAL STUDIES ON THE BORON SUBCHLORIDES.

Mc Closkey, J. A. and M. J. Mc Clelland, J. Amer. Chem. Soc, 87, 5090 (1965). MASS SPECTRA OF O-ISOPROPYLIDENE DERIVATIVES OF UNSATURATED FATTY ESTERS.

Mc Fadden. W. H., R. M. Seifert and J. Wasserman, Anal. Chem. 37, 560 (1965). CORRELATIONS AND ANOMALIES IN MASS SPECTRA. THIO ESTERS.

Mc Fadden, W. H., et. al., J. Chromatog. 18, 10 (1965). VOLATILES FROM STRAWBERRIES. COMBINED MASS SPECTROMETRY AND GAS CHROMATOGRAPHY ON COMPLEX MIXTURES.

Mc Fadden, W. H., E. A. Day and M. J. Diamond, Anal. Chem. 37, 89 (1965). CORRELATIONS AND ANOMALIES IN MASS SPECTRA. LACTONES.

Mc Fadden, W. H., et. al., J. Phys. Chem. 69, 1742 (1965). SPECIFIC REARRANGEMENTS IN THE MASS SPECTRA OF NEOPENTYL ESTERS.

Mc Kenna, J., J. M. Mc Kenna and P. B. Smith, Tetrahedron 21, 2983 (1965). 6-BETA- AND 6-ALPHA-NITROCHOLEST-4-ENE AND 5-ALPHA-CYANO-6-ALPHA-NITROCHOLESTANE.

Mc Kinney, R. W. and J. F. Light, Applied Spectry. 19, 193 (1965). IDENTIFICATION OF ALDEHYDES AND KETONES FROM TOF MASS SPECTRA OF THEIR 2,4-DINITROPHENYLHYDRAZONE.

Mc Whorter, E. J. and M. Anchel, J. Org. Chem. 30, 2359 (1965). PATTERN OF POLY-ACETYLENE PRODUCTION. STRUCTURAL STUDIES WITH SOME CARBON(10) POLYACETYLENES FROM CLITOCYBE SPECIES, USING NMR AND MASS SPECTRA.

Mekhtier, S. D., R. G. Rizaev, R. Kasimov and U. G. Kambarov, Azerb. Khim. Zh. 1965 70. MASS SPECTROSCOPY OF SOME AROMATIC NITRILES.

Merritt, C., Jr., et. al., Anal. Chem. 37, 1037 (1965). FAST SCANNING OF HIGH RESO-LUTION MASS SPECTRA.

Meyerson, S. and J. L. Corbin, J. Amer. Chem. Soc. 87, 3045 (1965). ORGANIC IONS IN THE GAS PHASE XVI. ISOMERIC C_7H_5O IONS FROM BENZOIC ACID.

Meyerson, S., Record. Chem. Progr. 26, 257 (1965). ORIGINS OF MASS SPECTRA. CHEMISTRY INDUCED BY ELECTRON IMPACT ON ISOLATED MOLECULES.

Meyerson, S., J. Chem. Phys. 42, 2181 (1965). ORGANIC IONS IN THE GAS PHASE. XV. DECOMPOSITION OF N-ALKANES UNDER ELECTRON IMPACT.

Milder, N. L., NASA Access. No. N65-15288, Rept. No. NASA-TN-D-2592 (1965). FRAGMEN-TATION OF ANTHRACENE IN AN ELECTRON BOMBARDMENT ION SOURCE.

Millard, B. J., Tetrahedron Letters 1965, 3041. PEPTIDES. HIGH RESOLUTION MASS SPECTROMETRY OF CYCLIC PEPTIDES.

Moshonas, M. G. and G. L. K. Hunter, Appl. Spectry. 18, 193 (1964). MASS SPECTROMETRIC SAMPLING FROM MICRO INFRARED PLATES AND RECOLLECTION OF SAMPLE FOR FURTHER ANALYSIS.

Mueller, H., et. al., Helv. Chim. Acta. 48, 320 (1965). ALKALOIDS FROM STRYCHNOS CHLORANTHA PROG.

Nakanishi, K., M. Ohashi, M. Tada and Y. Yamada, Tetrahedron 21, 1231 (1965). ILLUDINS. (LAMPTEROL).

Nakanishi, K., Y. Takahashi and H. Budzikiewicz, J. Org. Chem. 30, 1729 (1965). PRISTIMERIN. SPECTROSCOPIC PROPERTIES OF THE DIENONE-PHENOL-TYPE REARRANGEMENT PRODUCTS AND OTHER DERIVATIVES.

Nakata, H., et. al., Tetrahedron Letters, 1965, 829. MASS SPECTROMETRY OF MORPHINE ALKALOIDS. FRAGMENTATION OF MORPHINAN AND RELATED COMPOUNDS.

Nakata, H., Y. Y. Hirata and A. Tatematsu, Tetrahedron Letters 1965, 123. MASS SPECTRAL FRAGMENTATION OF MONOCYCLIC 2-PYRONES.

Nann, B., H. Wehrli, K. Schaffner and O. Jeger, Helv. Chim. Acta. 48, 1680 (1965). PHOTOCHEMICAL REACTIONS. THE PHOTOCHEMICAL ISOMERIZATION OF C-10-DIASTEREOISOMERS OF 3-OXODELTA-1,5-STEROIDS.

Natalis, P., Bull. Soc. Chim. Belges 73, 569 (1964). POSITION ISOMERY AND MASS SPECTRA. C(3), C(5) AND C(6) CYCLIC TRIMETHYL CYCLOALKANES AND METHYL ETHYL CYCLO-ALKANES.

Natalis, P. and J. L. Franklin, J. Phys. Chem. 69, 2935 (1965). IONIZATION AND DIS-SOCIATION OF DIPHENYL AND CONDENSED RING AROMATICS BY ELECTRON IMPACT. BIPHENYL, DIPHENYLACETYLENE, AND PHENANTHRENE.

Natalis, P. and J. L. Franklin, J. Phys. Chem. 69, 2943 (1965). IONIZATION AND DIS-SOCIATION OF DIPHENYL AND CONDENSED RING AROMATICS BY ELECTRON IMPACT. DIPHENYLCAR-BONYLS AND ETHERS.

Nencini, G., G. Giuliani and T. Salvatori, J. Polymer Sci. 3, 483 (1965). PYROLYSIS-MASS SPECTROMETRY METHOD FOR BLOCKINESS DETERMINATION OF ETHYLENE-PROPYLENE COPOLYMERS.

Nesmeyanov, A. N., V. A. Dubovitskii, O. V. Nogina and V. N. Bochkarev, Dokl. Akad. Nauk SSSR 165, 125 (1965). MASS SPECTRA OF SOME MONOCYCLOPENTADIENYL DERIVATIVES OF TITANIUM.

Neuer-Jehle, N., H. Nesvadba and G. Spiteller, Monatsh Chemie 96, 321 (1965). STRUCTURE ELUCIDATION OF ALKALOIDS BY MASS SPECTROMETRY. PYRROLIZIDINEALKALOIDS OF LABURUM.

Nibbering, N. M. M., T. J. De Boer and H. J. Hofman, Rev. Trav. Chim. 84, 481 (1965). MASS SPECTROMETRY OF NITRO COMPOUNDS. MASS SPECTRA OF A-, B- AND GAMMA-DEUTERATED 1-NITROPROPANE.

Nozaki, H., M. Yamabe and R. Noyori, Tetrahedron 1965, 1657. THE REACTIONS OF PHENYL-CARBENE WITH POLYNUCLEAR AROMATIC COMPOUNDS.

Nozaki, H., K. Kondo and M. Takaku, Tetrahedron Letters 1965, 251. A STABLE SULPHONIUM YLIDE.

Oae, S. and S. Kozuka, Tetrahedron 21, 1971 (1965). REARRANGEMENT OF TERTIARY AMINE N-OXIDES. THE MECHANISM OF THE REACTION OF PYRIDINE-N-OXIDE WITH ACETIC ANHYDRIDE.

Ohloff, G. and G. Uhde, Helv. Chim. Acta. 48, 10,(1965). ABSOLUTE CONFIGURATION OF TERPINENOL-4.

Osske, G. and K. Schreiber, Tetrahedron 21, 1559 (1965). STEROIDS AND TRITERPENOIDS. 24-METHYLENE-LO-PHENOL, A NEW 4-ALPHA-METHYLSTEROID FROM SACCHARUM OFFICINARUM L AND SOLANUM TUBEROSUM L.

Pailer, M., P. Bergthaller and G. Schaden, Monatsh. Chemie. 96, 863 (1965). THE ISOLATION AND CHARACTERIZATION OF FOUR NEW ARISTOLOCHIA ACIDS (FROM ARISTOLOCHIA CLEMATITA).

Pailer, M., G. Schaden, G. Spiteller and W. Fenzl, Monatsh. Chemie. 96, 1324 (1965). THE CONSTITUTION OF FRAXINELLONS FROM DICTAMNUS ALBUS L.

Pailer, M., W. Oesterreicher and E. Simonitsch, Monatsh. Chemie. 96, 1377 (1965). INVESTIGATION OF THE ODOR BODIES OF SEEFELD SHALE OIL.

Pailer, M., G. Schaden and R. Haensel, Monatsh. Chemie. 96, 1842 (1965). MASS SPECTRA OF KAWALACTONE TYPE-A-PYRONES.

Pandit, U. K., W. N. Speckamp and H. O. Huisman, Tetrahedron 21, 1767 (1965). HETEROCYCLIC STEROIDS. MASS SPECTRA OF 6-AZASTEROIDS WITH TWO AROMATIC RINGS.

Paulett, G. S. and M. Lustig, J. Amer. Chem. Soc. 87, 1020 (1965). SULFUR-NITROGEN AND OXYGEN-NITROGEN BOND DISSOCIATION ENERGIES OF SOME N-FLUORINATED AMINES.

Paulsen, H., Ann Chemie 683, 187 (1965). AMADORI REARRANGEMENT OF 5-AMINO-5-DESOXY-D-XYLOPIPERIDINOSE TO 1,5-DIDESOXY-1,5-IMINO-D-THREOPENTULOSE.

Pelah, Z., D. H. Williams, H. Budzikiewicz and C. Djerassi, J. Amer. Chem. Soc. 87, 574 (1965). MASS SPECTROMETRY IN STRUCTURAL AND STEREOCHEMICAL PROBLEMS. ELECTRON IMPACT INDUCED FRAGMENTATION OF STEROIDAL DIMETHYL AMINES.

Pelter, A., P. Stainton and M. Barber, J. Heterocyclic Chem. 2, 262 (1965). MASS SPECTRA OF OXYGEN HETEROCYCLES. MASS SPECTRA OF FLAVANOIDS.

Pelter, A., P. Stainton, A. P. Johnson and M. Barber, J. Heterocyclic Chem. 2, 256 (1965). MASS SPECTRA OF OXYGEN HETEROCYCLES. 4-HYDROXY-3-PHENYLCOUMARINS (ISOFLAVANOIDS).

Pfeifer, S., S. K. Banerjee, L. Dolejs and V. Hanus, Pharmazie 20, 45 (1965). RED PAPAVER ALKALOIDS. MASS SPECTROMETRY OF RHOEADINE ALKALOIDS. STRUCTURE OF PAPAVERRUBINE.

Pfeifer, S., I. Mann, L. Dolejs and V. Hanus, Pharmazie 20, 585 (1965). STRUCTURE OF OREODINE AND OREOGENINE. MASS SPECTROMETRY OF RHOEADINE ALKALOIDS.

Phares, E. R., M. V. Long and S. F. Carson, Ann. NY Acad. Sci. 112, 660 (1964). NEGATIVE AND POSITIVE ION MASS ANALYSIS OF DICARBOXYLIC ACIDS IN STUDIES OF THE MECHANISM OF THE METHYL MALONYL ISOMERASE REACTION.

Pirkle, W. H., J. Amer. Chem. Soc. 87, 3022 (1965). STRUCTURE OF ELECTRON IMPACT FRAGMENTS. FURYLIDENE CATION FROM 2-PYRONE.

Polaczek, A. and E. Baranowska, J. Inorg. Nucl. Chem. 27, 1649 (1965). MS INVESTIGATION OF COMPLEX COMPOUND EQUILIBRIA IN ORGANIC SOLUTIONS. COMPLEXES OF AL-TRIIODIDE WITH DIETHYL ETHER IN ETHYL IODIDE SOLUTION.

Polyakova, A. A., T. I. Popova and A. A. Petrov, Zh. Organ. Khim. 1, 822 (1965). MASS SPECTRA AND STRUCTURE OF ORGANIC COMPOUNDS. MASS SPECTRA OF VINYL ACETYLENIC ALCOHOLS.

Polyakova, A. A., R. A. Khmel/Nitskii and A. A. Petrov, Zh. Organ. Khim. 1, 818 (1965). MASS SPECTRA AND STRUCTURE OF ORGANIC COMPOUNDS. MASS SPECTRA AND STRUCTURE OF DISUBSTITUTED HYDROCARBONS.

Polyakova, A. A., R. A. Khmel/Nitskii and F. A. Medvedev, Neftekhimiya 5, 1, 153 (1965). MASS SPECTROMETRIC ANALYSIS OF PETROLEUM PARAFFINS WITH USE OF UNIFIED CHARACTERISTICS.

Polyakova, A. A., R. A. Khmel/Nitskii and F. A. Medvedev, Khim. I. Teknol. Topliv. I. Masel 10, 56 (1965). MASS SPECTROSCOPIC ANALYSIS OF THE SATURATED PARTS OF DISTILLATE OILS.

Popova, T. I., A. A. Polyakova and M. I. Khotimaskaya, Neftekhimiya 5, 1, 149 (1965). MASS SPECTROMETRIC ANALYSIS OF HEPTANOLS.

Popova, T. I., A. A. Polyakova and K. I. Zimina, Khim. I. Tekhnol. Topliv. I. Masel 10, 48 (1965). MASS SPECTROMETRIC ANALYSIS OF A COMPLEX MIXTURE OF ALCOHOLS.

Pritchard, G. O. and R. L. Thommarson, J. Phys. Chem. 69, 1001 (1965). PHOTOCHEMISTRY OF THE FLUOROKETONES. HEPTAFLUORO PROPYL ETHYL KETONE.

Puchkov, V. A., et. al., Tetrahedron Letters 1965, 543. THERMAL EFFECT IN THE MASS SPECTROMETRY OF ORGANIC COMPOUNDS.

Ralls, J. W., et. al., J. Food Sci. 30, 228 (1965). VOLATILES FROM A COMMERCIAL PEA BLANCHER. MASS SPECTRAL IDENTIFICATION.

Razuvaev, G. A., O. N. Druzhkov, S. F. Zhil/Tsov and G. G. Petukhov, Dokl. Akad. Nauk SSSR 163, 119 (1965). INTERACTION OF DIPHENYL MERCURY WITH ALCOHOLS, AS STUDIED BY THE ISOTOPIC AND MASS SPECTROMETRIC METHOD.

Redman, J. D., U.S. Atomic Energy Comm. Ornl-TM-989, 1964. A LITERATURE REVIEW OF MASS SPECTROMETRIC-THERM-OCHEMICAL TECHNIQUE APPLICABLE TO THE ANALYSIS OF VAPOR SPECIES OVER SOLID INORGANIC MATERIALS.

Reed, R. I., J. Inst. Petrol. 51, 340 (1965). APPLICATIONS OF THE MASS SPECTROMETER.

Rice, J. M., G. O. Dudek and M. Barber, J. Amer. Chem. Soc. 87, 4569 (1965). MASS SPECTRA OF NUCLEIC ACID DERIVATIVES. PYRIMIDINES.

Richter, W. J. and K. Biemann, Monatsh. Chemie. 96, 484 (1965). APPLICATION OF MASS SPECTROSCOPY TO STRUCTURAL PROBLEMS. HIGH RESOLUTION MASS SPECTRA OF CEPHALOSPORIN C DERIVATIVES.

Richter, W. J., M. Senn and A. L. Burlingame, Tetrahedron Letters 1965, 1235. CONVENIENT LABELLING TECHNIQUES FOR MASS SPECTROMETRY. ACID CATALYZED DEUTERIUM AND OXYGEN-18 EXCHANGE VIA GAS-LIQUID CHROMATOGRAPHY.

Rodin, J. O., et al. J. Food Sci. 30, 280 (1965). VOLATILE FLAVOR AND AROMA COMPONENTS OF PINEAPPLE. ISOLATION AND TENTATIVE IDENTIFICATION OF 2,5-DIMETHYL-4-HYDROXY-3(2H)-FURANONE.

Rohwedder, W. K., E. D. Bitner, H. M. Peters and H. J. Dutton, J. Amer. Oil Chemists Soc. 41, 33 (1964). DEUTERIUM-HYDROGEN EXCHANGE DURING CATALYTIC DEUTERATION OF METHYL OLEATE.

Rohwedder, W. K., A. F. Mabrouk and E. Selke, J. Phys. Chem. 69, 1711 (1965). MASS SPECTROMETRIC STUDIES OF UNSATURATED METHYL ESTERS.

Rol, N. C., Rec. Trav. Chim. 84, 413 (1965). CORRELATIONS BETWEEN MOLECULAR STRUCTURE AND MASS SPECTRA. ANOMALOUS TYPE OF REARRANGEMENT IONS FOUND IN THE MASS SPECTRA OF ACIDS; NITRILES.

Ryhage, R. and E. Stenhagen, Arkiv. Kemi. 23, 167 (1964). MASS SPECTROMETRIC STUDIES. NATURE OF THE IONS OF M/E 84+NX14 (N=0,1,2...) PRESENT IN MASS SPECTRA OF ESTERS OF DIBASIC ACIDS.

Ryhage, R., S. Wikstrom and G. R. Waller, Anal. Chem. 37, 435 (1965). MASS SPECTROMETER USED AS DETECTOR AND ANALYZER FOR EFFLUENT EMERGING FROM A CAPILLARY GAS LIQUID CHROMATOGRAPHY COLUMN.

Saalfeld, F. E., NASA Accession No. N65-14825, Rept. No. AD608977 (1964). MASS SPECTROMETRIC DETERMINATION OF THE ALIPHATIC AND AROMATIC CONTENT OF A HYDROCARBON MIXTURE.

Santavy, F., et al., Coll. Czech. Chem. Commun. 30, 335 (1965). CONSTITUTION OF RHOEADINE AND ISORHOEADINE.

Sanz, H. G. and R. Parellada, Anales. Real. Soc. Espan. Fis. Quim. (Madrid) 61, 729 (1965). MASS SPECTROMETRIC ANALYSIS OF PYROLYTIC PRODUCTS FROM POLYPHENYL COMPOUNDS. GAS FRACTION AND LIQUID FRACTION.

Sauer, H. H., E. K. Weiss and T. Reichstein, Helv. Chim. Acta. 48, 857 (1965). THE STRUCTURE OF DREVOGENIN.

Schaeffer, R. and L. J. Todd, J. Amer. Chem. Soc. 87, 488 (1965). STUDIES ON BORON-NITROGEN COMPOUNDS. SYNTHESIS AND PROPERTIES OF SOME SUBSTITUTED TRIMETHYLBORANES.

Schnoes, H. K. and K. Biemann, J. Amer. Chem. Soc. 86, 5693 (1964). APPLICATION OF MASS SPECTROMETRY TO STRUCTURAL PROBLEMS. INTERCONVERSION OF THE ASPIDOSPERMINE SKELETON TO THE REFRACTINE TYPE.

Schroepfer, G. J., Jr., J. Amer. Chem. Soc. 87, 1411 (1965). ENZYMATIC STEREOSPECIFICITY IN THE CONVERSION OF OLEIC ACID TO 10-HYDROXYSTEARIC ACID.

Scott, A. I., et al., Tetrahedron 21, 3605 (1965). TOTAL SYNTHESIS OF COLCHICINE MODELLED ON A BIOGENETIC THEORY.

Senn, M., W. J Richter and A. L. Burlingame, J. Amer. Chem. Soc. 87, 680 (1965). CONVENIENT DEUTERIUM LABELING FOR MASS SPEC. VIA EXCHANGE OF ENOLIZABLE HYDROGEN ON A GAS-LIQUID CHROMATOGRAPHY COLUMN.

Senning, A., Chem. Commun. 1965, 21, 551. MASS SPECTRUM OF 5-PHENYL-1,3,4-OXATHIAZOL-2 ONE.

Shannon, J. S. and J. M. Swan, Chem. Commun. (London) 1965, 33. METAL VALENCY EFFECTS IN THE MASS SPECTRA OF COORDINATION COMPOUNDS.

Shapiro, R. H. and C. Djerassi, J. Org. Chem. 30, 955 (1965). MASS SPECTROMETRY IN STRUCTURAL AND STEREOCHEMICAL PROBLEMS. MASS SPECTRAL FRAGMENTATION OF 6,7-DIMETHOXY COUMARIN.

Shulman, G. P., J. Polymer Sci. 3, 911 (1965). THERMAL DEGRADATION OF POLYMERS. MASS SPECTROMETRIC THERMAL ANALYSIS.

Shultz, J. L., R. A. Friedel and A. G. Sharkey, Fuel 44, 55 (1965). ANALYSIS OF COAL TAR PITCH BY MASS SPECTROMETRY.

Sih, C. J., K. C. Wang, D. T. Gibson and H. W. Whitlock, Jr., J. Amer. Chem. Soc. 87, 1386 (1965). ON THE MECHANISM OF RING A CLEAVAGE IN THE DEGRADATION OF 9,10-SECO STEROIDS BY MICROORGANISMS.

Slavik, J., L. Dolejs, K. Vokac and V. Hanus, Coll. Czech. Chem. Commun. 30, 2864 (1965). STRUCTURE OF GLAUCAMINE. AN ALKALOID FROM PAPAVER GLAUCUM BOISS ET HAUSKN. MASS SPECTROMETRIC STUDY OF FRAGMENTATION OF RHOEADINE ALKALOIDS.

Slavik, J., V. Hanus, K. Vokac, and L. Dolejs, Coll. Czech. Chem. Commun. 30, 2464 (1965). MASS SPECTROMETRIC STUDY OF HOMOLOGS OF RHOEADINE AND STRUCTURE OF DUBIRHEINE.

Snatzke, G. and G. Zanati, Ann. Chemie 684, 62 (1965). TRICYCLO(4.4.3.0)TRIDECANONE-11, TRICYCLO(4.4.-4.0) TETRADECANONE-2 AND DIONE-2,3.

Snyder, L., Anal. Chem. 37, 713 (1965). ROUTINE COMPOUND CLASS SEPARATION AND ANALYSIS OF HEAVY PETROLEUM FRACTIONS BY ADSORPTION CHROMATOGRAPHY.

Sonneveld, W., Rev. Trav. Chim. 84, 45 (1965). METASTABLE TRANSITIONS IN THE MASS SPECTRA OF FIVE SATURATED FATTY ACID METHYL ESTERS.

Speckamp, W. N., H. De Koning, U. K. Pandit and H. O. Huisman, Tetrahedron 21, 2517 (1965). HETEROCYCLIC STEROIDS. TOTAL SYNTHESIS OF SOME 6-AZAESTROGENS.

Spiteller, G. and Spiteller-Friedman, Angew. Chem. (Int. Ed) 4, 383 (1965). RELATIONSHIPS BETWEEN STRUCTURE AND MASS SPECTRA OF ORGANIC COMPOUNDS.

Spiteller, G. and Spiteller-Friedman, Angew. Chem. 77, 393 (1965). RELATION BETWEEN STRUCTURE AND MASS SPECTRUM OF ORGANIC COMPOUNDS.

Spiteller, G. and Spiteller-Friedman, Ann. Chem. 690, 1 (1965). THEORETICAL INTERPRETATION OF THE MASS SPECTRA OF ORGANIC COMPOUNDS.

Spiteller-Friedman and G. Spiteller, Monatsh. Chemie 96, 104 (1965). PIPERIDINE ALKALOIDS. KEY FRAGMENTS IN THE MASS SPECTRA OF ALKALOIDS.

Staab, H. A. and C. Wuensche, Chem. Ber. 98, 3479 (1965). SCHIFF BASES. MASS SPECTROSCOPIC INVESTIGATION OF THE DOUBLE ALDIMINES OF 1,2-DIAMINO CYCLOPROPANE DERIVATIVES AND THE IR STRUCTURAL ISOMERS.

Steele, W. C., B. H. Jennings, G. L. Botyos and G. O. Dudek, J. Org. Chem. 30, 2886 (1965). AN ELECTRON IMPACT STUDY OF NORBORNENYL AND NORTRICYCLYL CHLORIDES.

Stiefel, L. and E. F. Van Artsdalen, Ind. Eng. Chem. 57, 109 (1965). PREDICTION AND DETERMINATION OF TOXIC GASES IN PROPELLENT COMBUSTION PRODUCTS.

Szepesvary, P., Magy. Tud. Akad., Kem. Tud. Oszt., Kozlemeny 23, 19 (1965). ANALYTICAL METHODS OF MASS SPECTROMETRY AND NUCLEAR RESONANCE. (SUMMARY OF VI WORLD PETROLEUM CONGRESS, 1965).

Talroze, V. L., G. D. Tautsyrev and V. I Gorshkov, Zh. Analit. Khim. 20, 103 (1965). CHROMATO MASS SPECTROMETRY. PROBLEMS ARISING IN COMBINING OF CHROMATOGRAPHY COLUMNS WITH A MASS SPECTROMETRIC DETECTOR.

Tamas, J. and I. Opauszky, Magy. Kem. Folyoirat. 71, 352 (1965). MASS SPECTROMETRIC DETERMINATIONS OF THE O-18 CONTENT OF SMALL WATER SAMPLES, BY REACTION OF EQUILIBRIUM BETWEEN WATER AND CARBON DIOXIDE.

Tatematsu, A. and T. Goto, Yakugaku Zasshi 85, 152 (1965). ANALYSIS OF MIXED DRUGS BY MASS SPECTROMETRY. ANALYSIS OF OPIUM ALKALOIDS. MASS SPECTRA OF OPIUM ALKALOIDS AND THE ALLIED COMPOUNDS.

Tatematsu, A. and T. Goto, Yakugaku Zasshi 85, 778 (1965). ANALYSIS OF MIXED DRUGS BY MASS SPECTROMETRY. ANALYSIS OF OPIUM ALKALOIDS. INFLUENCE OF I.P. ON THE MASS SPECTRA OF CODEINES AND PAPAVERINE.

Tatematsu, A. and T. Goto, Yakugaku Zasshi 85, 786 (1965). ANALYSIS OF MIXED DRUGS BY MASS SPECTROMETRY. ANALYSIS OF OPIUM ALKALOIDS. ASSAY OF CODEINE PHOSPHATE AND DIHYDROCODEINE PHOSPHATE BY MS.

Tatematsu, A. and T. Goto, Yakugaku Zasshi 85, 624 (1965). ANALYSIS OF MIXED DRUGS BY MASS SPEC. ANALYSIS OF ANTIFEBRILE. FRAGMENTATION OF A.P.C. ETC., AND MASS SPECTRA OF THEIR MIXED SAMPLES.

Tatematsu, A. and T. Goto, Yakugaku Zasshi 85, 631 (1965). ANALYSIS OF MIXED DRUGS BY MASS SPEC. ANALYSIS OF ANTIFEBRILE. MASS SPECTRA OF MIXED ANTI-FEBRILES IN VARIOUS PHARMACEUTICAL PREPARATIONS.

Taylor-Smith, R.E., Tetrahedron 21, 3721 (1965). INVESTIGATIONS ON PLANTS OF WEST AFRICA. ISOLATION OF ANTHOCLEISTIN FROM ANTHOCLEISTA PROCERA.

Thomas, A.F., Helv. Chim. Acta. 48, 1057 (1965). METHYL-2-ISOPROPENYL-5-ANISOLE. A CONSTITUENT OF HINOKI OIL.

Thomas, D.W. and K. Biemann, J. Amer. Chem. Soc. 87, 5447 (1965). THERMAL METHYL TRANSFER. MASS SPECTRUM OF VOACAMINE-D(3).

Toekes, L. and C. Djerassi, Steroids 6, 493 (1965). MASS SPECTROMETRY IN STRUCTURAL AND STEREOCHEMICAL PROBLEMS. STEROIDAL DELTA(16)-20-KETONES AND DELTA(9(11))-12-KETONES.

Tomita, M., A. Kato and T. Ibuka, Tetrahedron Letters 1965, 1019. MASS SPECTRA OF HASUBANONINE, METAPHANINE AND THEIR DERIVATIVES.

Tomita, M., et al., Tetrahedron Letters 1965, 2825. MASS SPECTRA OF PRONUCIFERINE AND STEPHARINE.

Torssell, K. and R. Ryhage, Arkiv. Kemi. 23, 525 (1965). POSITIVE HALOGEN COMPOUNDS. THERMAL DECOMPOSITION OF ALIPHATIC NITRO SALTS. INFRARED SPECTRA OF ALIPHATIC NITRO SALTS.

Tscheshe, R., P. Welzel and H. W. Fehlhaber, Tetrahedron 21, 1797 (1965). DIGITANOL GLYCOSIDES. MASS SPECTROMETRIC INVESTIGATION OF KONDURANGOGENIN A.

Tsuchiya, M., S. Matsuhira and H. Kamada, Bunseki Kagaku 14, 465 (1965). STRUCTURE DETERMINATION OF ORGANIC COMPOUNDS BY MASS SPECTROMETRY. OXYGENATED COMPOUNDS.

Tsuda, M., Mass Spectroscopy (Japan) 12, 151 (1964). ANALYSIS OF MASS SPECTRA WITH DIGITAL COMPUTING METHODS.

Tuemmler, R., Z. Physik. Chem. (Leipzig) 229, 58 (1965). APPLICATION OF MOLECULAR SPECTROGRAPHY IN ORGANIC CHEMISTRY.

Tunnicliff, D. D., P. A. Wadsworth and D. O. Schissler, Anal. Chem. 37, 543 (1965). ORDERED EXACT MASS AND ABUNDANCE TABLES FOR MASS SPECTROMETRY.

Tunnicliff, D. D. and P. A. Wadsworth, Anal. Chem. 37, 1082 (1965). STEPWISE REGRESSION PROGRAM FOR QUANTITATIVE INTERPRETATION OF MASS SPECTRA.

Turro, N. J. et al., J. Amer. Chem. Soc. 87, 4097 (1965). INTERRELATIONS BETWEEN THE MASS SPECTROMETRY AND PHOTOCHEMISTRY OF ORGANIC MOLECULES. KETENE DIMERS AND OTHER SMALL RING COMPOUNDS.

Vandermerke, K. J., P. S. Steyn and S. H. Eggers, Tetrahedron Letters 1964, 3923. SIMPLE PREPARATION OF DEUTERIUM LABELLED O-METHYL GROUPS FOR MASS SPECTROMETRY.

Venugopalan, M. and C. B. Anderson, Indian J. Chem. 3, 20 (1965). MASS SPECTRA OF ACETOXY DERIVATIVES OF TETRAHYDROPYRAN AND CYCLOHEXANES.

Vinogradova, E. I. and M. U. Feigina, Tetrahedron Letters 1965, 2085. MASS SPECTROMETRIC DETERMINATION OF THE AMINO (HYDROXY) ACID SEQUENCE IN PEPTIDES AND DEPSIPEPTIDES.

Virin, L. I., U. A. Safin, U. A. Treger and B. V. Dzhagatspanyan, Zh. Fiz. Khim. 39, 2824 (1965). MASS SPECTRA AND STRUCTURE OF SOME ALLYL DERIVATIVES.

Von Sydow, E., Acta. Chem. Scand. 19, 2083 (1965). MASS SPECTRA OF TERPENES. ESTERS OF MONO-TERPENE ALCOHOLS.

Voticky, Z., J. Tomko, L. Dolejs and V. Hanus, Coll. Czech. Chem. Commun. 30, 3705 (1965). ALKALOIDS FROM BUXUS SEMPERVIRENS L. THE STRUCTURE OF BUXTAUINE.

Wagner, G. and H. Lahr, Pharmazie 20, (1965). THE SYNTHESIS OF GENTISIC ACID METHYL ESTER-BIS-B-D-GLUCOPYRANOSIDE.

Walser, A. and C. Djerassi, Helv. Chim. Acta. 48, 391 (1965). ALKALOID STUDIES. THE ALKALOIDS FROM VELLESIA DICHOTOMA RUIZ ET PAV.

Watson, J. T. and K. Biemann, Anal. Chem. 37, 844 (1965). DIRECT RECORDING OF HIGH RESOLUTION MASS SPECTRA OF GAS CHROMATOGRAPHIC EFFLUENTS.

Weiss, F., A. Isard and G. Bonnard, Bull. Soc. Chim. France 1965, 2332. ACETALS. FORMATION OF ALLYL BENZENE DERIVATIVES DURING THE PYROLYSIS OF ALLYL ALCOHOL BENZOATES AND 5-METHYLENE-2-PHENYL-1,3-DIOXANE.

Weiss, F., et al., Bull. Soc. Chim. France 1965, 3677. ACETALS. MECHANISM OF FRAGMENTATION IN MASS SPECTROMETRY. 2,4-DIVINYL-1,3-DIOXOLANE AND 2,4,5-TRIVINYL-1,3-DIOXOLANE.

Wendlandt, W. W., and T. M. Southern, Anal. Chim. Acta. 32, 405 (1965). AN APPARATUS FOR SIMULTANEOUS GAS EVOLUTION ANALYSIS AND MASS SPECTROMETRIC ANALYSIS.

Weygand, F., A. Prox, H. H. Fessel and K. S. K/Uo, Z. Naturforsch. 20, 1169 (1965). MASS SPECTROMETRIC SEQUENCE ANALYSIS OF PEPTIDES AS N-TRIFLUOROACETYL PEPTIDE ESTERS.

Whittles, A. B. L. and W. F. Slawson, Geochim. Cosmochim. Acta. 29, 142 (1965). MODIFIED TECHNIQUE FOR TRACE LEAD GAS SOURCE MASS SPECTROMETRY.

Widmer, E., J. W. Meyer, A. Walser and E. Haidegger, Helv. Chim. Acta. 48, 538 (1965). WELKSTOFFE UND ANTIBIOTIKA. SYNTHESIS OF ISOJAVANICINE AND VERY SIMPLIFIED SYSTHESIS OF JAVANICINE.

Wiebe, H. A., A. R. Knight, O. P. Strausz and H. E. Gunning, J. Amer. Chem. Soc. 87, 1444 (1965). THE REACTION OF SULFUR ATOMS. V. FURTHER STUDIES ON THE REACTIONS WITH OLEFINS.

Willhalm, B. and A. F. Thomas, J. Chem. Soc. 1965, 6478. MASS SPECTRA AND ORGANIC ANALYSIS. MASS SPECTRA OF MENTHONE, ISOMENTHONE AND CARVOMENTHONE.

Williams, R. E. and F. J. Gerhart, J. Amer. Chem. Soc. 87, 3513 (1965). A SIX-BORON CARBORANE FROM HEXABORANE.

Winkler, J. and W. Jenny, Helv. Chim. Acta. 48, 190 (1965). FACTS ON THE BOHN-SCHMIDT REACTION. REACTIONS OF BIS-SULFURYLDIOXY-(1,9:4,10)-ANTHRACENE-QUINONES-(5,8).

Winters, R. E. and R. W. Kiser, J. Organometal. Chem. 4, 190 (1965). IONS PRODUCED IN THE MASS SPECTROMETER FROM CYCLOPENTADIENYL METAL CARBONYL COMPOUNDS OF COBALT, MANGANESE AND VANADIUM.

Winters, R. E. and R. W. Kiser, J. Phys. Chem. 69, 1618 (1965). IONS PRODUCED BY ELECTRON IMPACT WITH THE DIMETALLIC CARBONYLS OF COBALT AND MANGANESE.

Winters, R. E. and R. W. Kiser, J. Phys. Chem. 69, 3198 (1965). IONIZATION POTENTIALS AND MASS SPECTRA OF CYCLOPENTADIENYL MOLYBDENIUM DICARBONYL NITROSYL AND 1,3-CYCLO-HEXADIENE IRON TRION TRICARBONYL.

Wulfson, N. S., et al., Tetrahedron Letters 1965, 4209. MASS SPECTROMETRY OF GIB-BERELLINS.

Wulfson, N. S., et al., Tetrahedron Letters 1965, 2805. MASS SPECTROMETRIC DETER-MINATION OF THE AMINO (HYDROXY) ACID SEQUENCE IN PEPTIDES AND DEPSIPEPTIDES.

Wulfson, N. S., et al., Tetrahedron Letters 1965, 2793. MASS SPECTROMETRIC STUDY OF CYCLODEPSIPEPTIDES. FRAGMENTATION TYPES OF REGULAR AND IRREGULAR CYCLO HEXA-DEPSIPEPTIDES.

Wulfson, N. S., et al., Bull. Acad. Aci. (USSR) Div. Chem. Sci. 1964, 1, 169. MASS SPECTROMETRIC DETERMINATION OF THE CONFIGURATION OF EPIMERIC TERTIARY ALCOHOLS IN THE D-HOMOSTEROID SERIES.

Yee, D. Y. and R. Ehrlich, J. Inorg. Nucl. Chem. 27, 2681 (1965). CHEMISTRY OF ALANE. MASS SPECTRUM OF DIMETHYLAMINO ALANE.

Zaretskii, V. I., et al., Tetrahedron 21, 2469 (1965). MASS SPECTROMETRY OF STEROID SYSTEMS. APPROACH TO CONFIGURATION OF TERT-STEROID ALCOHOLS BY MASS SPECTROMETRY.

Zbiral, E., E. L. Menard and J. M. Muller, Helv. Chim. Acta. 48, 404 (1965). THE CONSTITUTION OF ZIZYPHINS.

MASS SPECTROMETRY OF SOLIDS
A BIBLIOGRAPHY FOR 1965
SUBCOMMITTEE VII

Richard E. Honig, Chairman

This bibliography derives from three major sources: 1) titles selected by R. N. Stover and R. E. Honig from a computer-assembled bibliography covering the entire field of mass spectrometry, which was done in the Department of Chemistry, Iowa State University, under the direction of H. J. Svec; 2) a library search made by A. J. Ahearn for all items connected with the heading "Spark Source Mass Spectrometry"; and 3) a library search made by J. Drowart for all titles in the field of High Temperature Vaporization Studies.

The purpose of this triple approach was to check the completeness of the computer program, which was largely based on "Current Contents" and "Nuclear Science Abstracts", by "hand-made" surveys in limited fields, but based on the widest possible collection of journals, proceedings, and also books. It comes as no surprise that if a qualified research worker is willing to devote considerable time to scanning not only abstracts, but also current journals, proceedings, and books, he can turn up a fair number of entries not readily accessible to the computer.

The nearly four hundred items selected were classified, in alphabetical order, under the following headings:

1) Instrumentation, General
2) Sources, General
3) Thermal Ionization
4) RF Spark Source
5) Sputtering and Arc Sources
6) Ion Recording and Photometry
7) Data Processing and Quantization
8) Analytical Applications
9) Atomic Weights and Isotopic Abundances
10) High Temperature Vaporization Studies

It is a pleasure to thank Messrs. Svec, Ahearn, Drowart, and Stover for their generous cooperation in this project. The competent assistance of D. A. Kramer in compiling and sorting the entries is gratefully acknowledged.

1) INSTRUMENTATION, GENERAL

Argyle, A. and Bingham, R. A.
Direct Recording of Isotope Beams in Spark-Source Mass Spectroscopy.
12th Colloquium Spectroscopicum Internationale, p. 641-50, Exeter, July 11-17, 1965; Hilger and Watts, London (1965)

Barber, R. C.
Effect of Magnetic-Field Nonuniformities on Focusing of a Second-Order Double-Focusing Mass Spectrometer.
Can. J. Phys. 43, 716 (1965)

Barrington, A. E. Herzog, R. K. F. Poschenrieder, W. P.
Vacuum System of Ion-Microprobe Mass Spectrometer for Trace Analysis of Solids.
J. Vac. Sci. Technol. 2, 281 (1965)

Behrisch, R. Blauth, E. W. Melzner, F.
Meyer, E. H.
Mass Spectrometer.
U. S. Patent 3174034

Bister, M.
New Types of Magnetic Broad-Range Heavy-Particle Spectrographs.
Ann. Acad. Sci. Fennicae, Ser. A VI, No. 154, p. 1 (1964)

Brunnée, C. Habfast, K. Kronenberger, K.
New Instrumental Details and Measuring Results in the Development of Mass Spectrometers.
Presented at 13th Annual Conf. on Mass Spectrometry, St. Louis (1965)

Brunnée, C.
Sample Insertion Vacuum Lock for Mass Spectrometer.
U. S. Patent 3117223

Conzemius, R. J. Svec, H. J.
A High Resolution Mass Spectrometric Measurement System for a Vacuum Fusion Apparatus.
Anal. Chim. Acta 33, 145 (1965)

Craig, R. D.
Electrode Means to Electrostatically Focus Ions Separated by a Mass Spectrometer on a Detector.
U. S. Patent 3217161

Dauerman, L. Salser, G. Tajima, Y. A.
Kinetic Studies on Gases and Solids Using a Fast-Scanning 60 Degree Mass Spectrometer.
Presented at 13th Annual Conf. on Mass Spectrometry, St. Louis (1965)

Delgmann, L. Wagner, H. Walcher, W.
The Influence of the Spherical Aberration on the Imaging of the Electromagnetic Isotope Separator and the Realization of an Optimal Lens System.
Conference on the Physics of Electromagnetic Separation Methods July 1962 Conf-578-3

Demyanov, A. V. Tarantin, N. I. Dyachikhin, Y. A.
Kabachenko, A. P.
An Electromagnetic Mass-Separator of the Laboratory of Nuclear Reactions (Joint Institute for Nuclear Research).
II. A Description of Mass Separator and its Characteristics.
USAEC, Div. of Tech. Info. Jinr-P-1949

Dymnikov, A. D. Yavor, S. Y.
System of Sequentially Placed Electrostatic and Magnetic Quadrupole Lenses with Zero and Negative Chromatic Abberation.
Soviet Phys. Tech. Phys. (Engl. Trans.) 9, 1544 (1965)

Erwin, R. L. Jarosz, D. Yinger, R. J.
Design Considerations and Performance Results for a Versatile Mass Spectrometer System.
Presented at 13th Annual Conf. on Mass Spectrometry, St. Louis (1965)

Ewald, H.
The Fission Particle Mass Spectrograph.
Presented at 13th Annual Conf. on Mass Spectrometry, St. Louis (1965)

Ewald, H. Neumann, S.
Double Deflection System for Focusing Ions of Selected Mass and Charge at a Predetermined Point.
U. S. Patent 3194961

Freeman, J. H.
The Electromagnetic Isotope Separator as a Research Tool.
Atomic Energy Research Establishment, Harwell, England Aere-M-1374, May 1964

Freeman, N. J. Pagden, I. M. H.
Initial Measurements with A.W.R.E. Isotope Separator.
Conference on the Physics of Electromagnetic Separation Methods, Conf-578-7 July 1962

Green, B. N. Merren, T. O. Murray, J. G.
Fast Scanning of Mass Spectra at High Resolution.
Presented at 13th Annual Conf. on Mass Spectrometry, St. Louis (1965)

Hickam, W. M. Sweeney, G. G.
Spatially Variable Slit for Mass Spectrometer Apparatus.
U. S. Patent 3209143

Johnson, W. H. Benson, J. L.
Improvements in Mass Doublet Measurement with the Minnesota 16-Inch Mass Spectrometer.
Presented at 13th Annual Conf. on Mass Spectrometry, St. Louis (1965)

Junk, G. A. Svec, H. J.
A Vacuum Lock for Direct Insertion of Samples into a Mass Spectrometer.
Analy. Chem. 37, 1629 (1965)

Karmohapatro, S. B.
A Two-Directional Focussing, High-Intensity Mass-Spectrometer for Preparation of Isotopic Targets.
Conf. on the Physics of Electromagnetic Separation Methods Orsay, France, 1962 Conf-578-6

Kelman, V. M. Knyazkov, L. G. Krasnova, E. K.
Large Dispersion Mass Spectrometer with Double Magnetic System.
Soviet Phys. Tech. Phys. (Engl. Trans.) 9, 1303 (1965)

Kendall, B. R. F. McGinnis, P. F.
Analog Method for Simulating Effects of Spectrometer Aberrations.
Presented at 13th Annual Conf. on Mass Spectrometry, St. Louis (1965)

Kessler, T. Hickam, W. M. Sweeney, G. G.
Sharkey, A. G.
Spark Source Spectra of Several Aromatic Hydrocarbons Using a Spinning Electrode.
Presented at 13th Annual Conf. on Mass Spectrometry, St. Louis (1965)

Knyazkov, L. G. Krasnova, E. K.
Large Dispersion Mass Spectrometer with Electrostatic Prisms.
Soviet Phys. Tech. Phys. (Engl. Trans.) 9, 1307 (1965)

Lilly, A. C. Weismann, T. J.
Electrostatic Fields Associated with Mass Spectrometer, Electron and Ion Optical Systems.
Presented at 13th Annual Conf. on Mass Spectrometry, St. Louis (1965)

Love, L. O.
Electromagnetic Isotope Separations.
USAEC, Div. of Tech. Info. ORNL-TM-1047 p. 2

Matsuda, H. Nakabushi, H. Ogata, K.
Image Contractor.
Mass Spectry. (Tokyo) 11, No. 22, p. 16 (June 1963)

Miller, V. V.
Calculation of Focus of Particles by a Doublet of Quadrupole Lenses.
Instr. Exp. Tech. USSR (Engl. Trans.) p. 743, 1965

Mostovsk, A. A. Sakseev, D. A.
Use of a Pulsed Time-of-Flight Mass Spectroscope for Investigating Evaporation of Compounds.
Soviet Phys. Tech. Phys. (Engl. Trans.) 9, 1022 (1965)

Munro, R. Ridley, R. G.
Mass Spectrometer Source Loading Lock and Isolation Valve.
Rev. Sci. Instr. 36, 1538 (1965)

Perkins, G. D.
A Small Tandem Mass Spectrometer with Reduced Aberrations.
Presented at 13th Annual Conf. on Mass Spectrometry, St. Louis (1965)

Rautenbach, W. L.
Ion Beam Formation in the Pretoria Isotope Separator.
Conference on the Physics of Electromagnetic Separation Methods. July 1962 Conf-578-2

Ruby, L. Kramasz, J. H. Pon, W. G. Vuletich, T.
A Multichannel Spectrometer for Analysis of Pulsed Ion Sources.
Nucl. Instr. Methods 37, 293 (1965)

Saalfeld, F. E. McDowell, M. V.
Analytical Mass Spectrometer.
Report Naval Research Lab. Proc., p. 20, 1965

Smith, L. G.
Modulating Structure for Mass Spectrometers.
U. S. Patent 3210540

Stoffels, J. J. Lagergren, C. R.
A Sliding-Shaft Vacuum Lock for a Mass Spectrometer.
Battelle-Northwest, Richland, Wash., Pacific Northwest Lab. BNWL-SA-62 or Conf-650519-1

Strashke, A. M.
Third-Order Geometrical Aberrations of Electrostatic 2-Dimensional Quadrupole Lenses.
Soviet Phys. Tech. Phys. (Engl. Trans.) 9, 1082 (1965)

Takeshita, I.
Matrices in Ion Optics and Their Application to Mass Spectroscopy.
Natl. Tech. Rept. (Japan) 9, 99 (1963)

Takeshita. I.
Mattauch-Herzog Type Mass Spectrograph with 2-Stage Electrostatic Field.
Z. Naturforsch. 20A, 624 (1965)

Takibaev, Z. S.
Spark Spectrometer for High Energy Particles
Vestn. Akad. Nauk. Kaz. SSR 21 (8), 3-9 (1965) (in Russian)
Chem. Titles No. 20 (1965)

Tarantin, N. I. Demyanov, A. V.
An Electromagnetic Mass-Separator of the Laboratory of Nuclear Reaction (Joint Institute for Nuclear Research).
I. A Calculation of the Magnetic Analyzer for the Mass-Separator.
USAEC, Div. of Tech. Info, JINR-P-1948

Turnbull, A. H. Hart, F. Drew, D. J. M.
Improvements in or Relating to Vacuum Locks for Mass Spectrometers.
British Patent 987217

Viehboeck, F. P. Buschbeck, F.
Some Characteristics of the S.G.A.E. Electromagnetic Isotope Separators.
Conference on the Physics of Electromagnetic Separation Methods. July 1962 Conf-578-5

Viehboeck, F. P. Wotke, H. Ruedenauer, F.
Determination of the Image Curve in an Electromagnetic Isotope Separator with Inhomogeneous Magnetic Sector Field.
Z. Naturforsch. 19A, 1333 (1964)

Viehboeck, F. P.
Performance and Application of the S.G.A.E. Electromagnetic Isotope Separator.
Presented at 13th Annual Conf. on Mass Spectrometry, St. Louis (1965)

White, F. A. Forman, L.
A Tandem Double-Focusing Mass Analyzer of Large Radius.
Presented at 13th Annual Conf. on Mass Spectrometry, St. Louis (1965)

Whitehead, T. W.
Focal Properties of Isotope Separators Using Azimuthally Invariant Magnetic Fields.
J. Appl. Phys. 36, 3693 (1965)

Willdig, E.
Mass Spectrometer Assemblies.
U. S. Patent 3187180

Willdig, E.
Mass Spectrometer Electrostatic Analyzers.
U. S. Patent 3192384

Wollnik, H. Ewald, H.
Influence of Magnetic and Electric Fringing Fields on Trajectories of Charged Particles.
Nucl. Instr. Methods 36, 93 (1965)

Yagi, K.
A New Broad Range Spectrometer with a Uniform-Field Sectorial Magnet and a Preceding Quadrupole-Magnet Doublet.
Nucl. Instr. Methods 31, 173 (1964)

Yagi, K.
3rd-Order Aberrations in a Broad Range Spectrometer with a Uniform-Field Sectorial Magnet and a Preceding Quadrupole Magnet.
Nucl. Instr. Methods 34, 146 (1965)

Zashkvar, V. V. Korsunsk, M. I. Kosmache, O. S.
Correction of Angular Aberrations in 2-Sector Electrostatic Analyzer.
Soviet Phys. Tech. Phys. (Engl. Trans.) 10, 818 (1965)

Zashkvar, V. V. Korsunsk, M. I.
Experimental Study of Ion-Optical Properties of an Electrostatic Analyzer with a Linear Potential Distribution on Deflecting Electrodes.
Sov. Phys. Tech. Phys. (Engl. Trans.) 9, 993 (1964)

Zuk, W. Maczke, D. Pomorski, J.
Electromagnetic Isotope Separator at Lublin.
Nucl. Instr. Methods 37, 249 (1965)

2) SOURCES, GENERAL

Adyasevich, B. P. Antonenko. V. G. Polynin, Y. P.
Fomenko, D. E.
A Polarized Ion Source.
J. Nucl. Energy C. 7, 187 (1965)

Almazov, S. V. Myntsov, F. F.
High-Frequency Ion Source with Automatic Focusing.
Instr. Exp. Tech. USSR (Engl. Trans.) p. 967 (1965)

Aubecq, M. Brabers, M. Henuset, M.
Meuleman, M.
Evaporation Par Bombardement Electronique de Métaux à Hauts Points de Fusion.
Mem. Sci. Rev. Met. 62, 373 (1965)

Boehm, H. Guenther, K. G.
A Penning Ion Source for Mass Spectrometers.
Z. Angew. Phys. 17, 553 (1964)

Craig, R. D. Willdig, E. Bancroft, F. E.
Variable Slit Systems for Mass Spectrometer Ion Sources.
U. S. Patent 3187179

Craig, R. D. Willdig, E.
Ion Source for Mass Spectrometers with Means to Separately Mount Electrodes of Different Potentials.
U. S. Patent 3217160

Crawford, C. K.
Contamination-Proof Mass Spectrometer Ion Source.
J. Vac. Sci. Technol. 2, 280 (1965)

Dickson, J. M.
Polarized Ion Sources and the Acceleration of Polarized Beams.
Progress in Nuclear Techniques and Instrumentation Amsterdam, North-Holland Publishing Co., 1965,Vol. 1

Elkholy, S. B.
On Stabilization of an Electron Bombardment Ion Source for a Mass Spectrograph Applying Power Transistors.
Intern. J. Electron 19, 233 (1965)

Gabor, D.
Multiply-Neutralized Ion Source.
U. S. Patent 3182220

Gunther, K. G.
Ion Source for Mass Filter Wherein Electron and Ion Beam Axes are Same.
U. S. Patent 3221164

Hanlein, W. Gunther, K. G.
Mass Spectrometer with Particular Ion Source for Analysis of Solid Bodies.
U. S. Patent 3223836

Herzog, L. F. Marshall, D. J. Kendall, B. R. F.
Cambey, L. A.
Ion Sources and Detectors for the Mass Spectroscopic Study of Solids
Presented at Fourth National Meeting, Society for Applied Spectroscopy, Denver, Col., Aug. 30 - Sept. 3, 1965

Ianovici, M. Ionescu, T.
An Experimental Installation for Studying and Testing Ion Sources and Electron Injectors.
Acad. Rep. Populare Romine, Studii Cercetari Fiz 15, 355 (1964)

Imamura, G. Fujita, H.
Study on the Development of Ion Source.
Mitsubishi Denki Giho 38, No. 12, p. 27 (1964)

Lincoln, K. A.
Flash-Vaporization of Solid Materials for Mass Spectrometry by Intense Thermal Radiation.
Analy. Chem. 37, 541 (1965)

Magari, S. Kubo, K.
Improved Filament Mount for Mass Spectrometer.
Rev. Sci. Instr. 36, 403 (1965)

Magnuson, G. D. Carlston, C. E. Mahadevan, P.
Comeau, A. R.
High Efficiency Source for Metal Ions.
Rev. Sci. Instr. 36, 136 (1965)

Mavrogen, G. S. Rahler, W. J. Turner, C. B.
A Source for Multiply-Charged Ions.
IEEE Tr. Nucl. Sci. NS12, 769 (1965)

Mirianashvili, G. M. Kaviladze, M. S. Abashicze, I. V.
Ion Sources for Accurate Measurement of Isotope Ratios in Solids.
Soobshch. Akad. Nauk Gruz. SSR. 32, 311 (1964)

Mirianashvili, G. M. Kaviladze, M. S. Abashidze, I. V.
Mass Spectrometer Ion Source for Simultaneous Analysis of Three Solid-Phase Specimens.
Pribory I Tekhn. Eksp. No. 1, p. 215, (Jan-Feb, 1965)
Instr. Exp. Tech. USSR (Engl. Trans.) p. 223 (1965)

Morozova, I. G.
Characteristics of Ion Source with Electrons Oscillating in a Magnetic Field.
Uskoriteli. No. 6, p. 105 (1965)

Nagy, J. L.
Energy Spectrum of Ion Beam Emitted by a Penning-Type Ion Source.
Nucl. Instr. Methods 32, 229 (1965)

Oleinik, V. K. Rutgaize, Y. S. Shereshe, A. M.
A Unified Series of Ion Sources for Mass Spectrometers.
Instr. Exp. Tech. USSR (Engl. Trans.) p. 140 (1965)

Potapova, L. I. Taganov, K. I.
Impact-Spark Sampler for Spectral Analysis of Metals and Alloys (Exchange of Experience).
Ind. Lab. USSR (Engl. Trans.) 31, 158 (1965)

Tsuchimo, T.
Low Energy Ion Source in a Magnetic Field.
Nucl. Instr. Methods 37, 135 (1965)

Tyrrell, A. C. Roberts, J. W. Ridley, R. G.
Electron Bombardment Ion Source for Isotopic Analysis of Solids.
J. Sci. Instr. 42, 806 (1965)

3) THERMAL IONIZATION

Alekseev, N. I. Kaminski, D. L.
Ionization of Some Rare Earth Elements on Surfaces of Tungsten, Rhenium and Iridium.
Soviet Phys. Tech. Phys. (Engl. Trans.) 9, 1177 (1964)

Andresen, S. G. Shipley, C. A.
Time-Dependent Behavior of Surface Ionization Efficiencies of Li and LiF on W.
Rev. Sci. Instr. 36, 858 (1965)

Bakulina, I. N. Zandberg, E. Y. Ionov, N. I.
Emission of Positive and Negative Molecular Ions from Heated Surfaces.
Zh. Tekhn. Fiz. 35, 562 (1965)
Sov. Phys. Tech. Phys. (Engl. Trans.) 10, 437 (1965)

Chaikovskii, E. F. Pyatigorskii, G. M.
Determination of Heat of Vaporizations of Positive Ions in Surface Ionization of Atoms of Alkali Metals.
Soviet Phys. Tech. Phys. (Engl. Trans.) 9, 847 (1964)

Chaikovskii, E. F. Ptitsyn, G. V.
Positive Surface Ionization of Potassium of Texturized Ribbons of Platinum.
Zh. Tekhn. Fiz. 35, 528 (1965)
Soviet Phys. Tech. Phys. (Engl. Trans.) 10, 410 (1965)

Chaikovskii, E. F. Pyatigorskii, G. M. Ptitsyn, G. V.
Temperature Hysteresis in Positive Surface Ionization and Work Function of a Homogeneous Emitter.
Soviet Phys. Tech. Phys. (Engl. Trans.) 10, 871 (1965)

Chaikovskii, E. F. Ptitsyn, G. V.
Positive Surface Ionization of Na on Textured Platinum Ribbons.
Soviet Phys. Tech. Phys. (Engl. Trans.) 10, 893 (1965)

Dobretsov, L. N.
Effect of Electric Field on Surface Ionization on Metals.
Zh. Tekhn. Fiz. 35, 535 (1965)
Soviet Phys. Tech. Phys. (Engl. Trans.) 10, 416 (1965)

Dresser, N. J. Hudson, D. E.
Surface Ionization of Some Rare Earths on Tungsten.
Phys. Rev. A 137, A673 (1965)

Dresser, N. J.
An Experimental Investigation of Surface Ionization.
Thesis, Iowa State University, Ames, Iowa 1964

Herron, J. T.
Negative Surface Ionization of Complex Molecules.
Presented at 13th Annual Conf. on Mass Spectrometry, St. Louis (1965)

Herron, J. T. Rosenstock, H. M. Shields, W. R.
Negative Surface Ionization of Complex Molecules.
Nature 206, 611 (1965)

Husmann, O. K.
Alkali-Ion Desorption Energies on Polycrystalline Refractory Metals at Low Surface Coverage.
Phys. Rev. A 140, A546 (1965)

Katalnik, S. G. Pisarev, V. E. Kapustin, I. A.
Preparation of Trimethyl Borine Samples for Isotopic ANalysis of Boron.
Ind. Lab. USSR (Engl. Trans.) 31, 567 (1965)

Lichtman, D.
Ion Emission from Heated Metal Surfaces.
J. Vac. Sci. Technol. 2, 91 (1965)

Lorik, S. J.
A Flip-Flop Source Filament Loading Assembly.
New Brunswick Lab., AEC, New Jersey, Report No. NBL-210, p. 35

Potekhina, N. D.
On Theory of Surface Ionization.
Soviet Phys. Tech. Phys. (Engl. Trans.) 9, 842 (1964)

Potekhina, N. D.
Surface Ionization as Affected by Migration of Adatoms Along an Irregular Surface.
Zh. Tekhn. Fiz. 35, 317 (1965)
Soviet Phys. Tech. Phys. (Engl. Trans.) 10, 254 (1965)

Pyatigorskii, G. M.
Surface Ionization of Metals in an Electric Field.
Soviet Phys. Tech. Phys. (Engl. Trans.) 9, 1117 (1964)

Pyatigorskii, G. M.
Surface Ionization of Molecules of Alkali Halide Salts.
Soviet Phys. Tech. Phys. (Engl. Trans.) 10, 867 (1965)

Scheer, M. D. Fine, J.
Surface Ionization of Niobium.
J. Chem. Phys. 42, 3645 (1965)

Wilson, K. R. Ivanetich, R. J.
Surface Ionization of Na, Rb, LiI, and NaI on Tungsten, Rhenium, and Platinum - Tungsten.
Lawrence Radiation Lab., Univ. of Calif., Berkeley UCRL-11606, August 25, 1964

Zandberg, E. Y. Paleev, V. I.
Surface Ionization on Electrographite with Formation of Positive Ions of Atoms of In, K, Rb and Cs and of Molecules of CsCl, RbCl and KCl.
Soviet Phys. Tech. Phys. (Engl. Trans.) 9, 1575 (1964)

Zandberg, E. Y. Tontegod, A. Y.
Surface Ionization of Li, Na, K and Cs Atoms and LiCl, KCl and CsCl Molecules on Polycrystalline Rhenium.
Soviet Phys. Tech. Phys. (Engl. Trans.) 10, 858 (1965)

4) RF SPARK SOURCE

Cookson, G. G. Fletcher, W. Tushingham, R.
A Commentary on the Spark Source Mass Spectrograph.
8th Conference on Analytical Chemistry in Nuclear Technology, Gatlinburg, Tenn., October 1964 Conf-721-9

Faust, R. C. Fontaine, E. A. Job, B. E.
Saunders, R. A.
Spark Source Mass Spectra of Organic Solids.
Z. Naturforsch. 20A, 1128 (1965)

Semenescu, G. Ionescu, D. R.
Some Considerations of High-Frequency Ion Sources.
Rev. Roumaine Phys. 9, 939 (1964)

Tsuchimo, T.
Electron Current Release Characteristics of a High Frequency Ion Source with Mesh Grid.
Jap. J. Appl. Phys. 4, 458 (1965)

5) SPUTTERING AND ARC SOURCES

Behrisch, R.
Sputtering of Solids by Ion Bombardment.
Ergeb. Exakt. Naturw. 35, 295 (1964)

Brunnée, C.
Ion Reflection and Secondary Electron Emission During Impact of Alkali Ions on Pure Molybdenum Surfaces.
Z. Physik 147, 161, (1957); Trans. ORNL-TR-467

Chaikovskii, E. F. Ptitsyn, G. V.
Use of the Effect of Positive Surface Ionization for Investigating Cathode Sputtering of Metals.
Zh. Tekhn. Fiz. 34, 2194 (1964)

Chaudhri, R. M. Khan, M. Y. Chaudhri, M. M.
Single Bi-Particle Elastic Collisions of Fast Protons with Metals.
Nature 205, 997 (1965)

Chiplonkar, V. T. Rane, S. R.
The Angular Distribution of Sputtered Particles from Polycrystalline Plane Gold Target by Impact with Positive Ions of Argon.
Proc. Indian Acad. Sci., Sect. A, 61, 10 (Feb. 1965)

Chiplonkar, V. T. Rane, S. R.
Dependence of Angular Distribution of Sputtering by Positive Ions from Metal Targets on the Impact Angle.
Indian J. Pure Appl. Phys. 3, 131 (April 1965)

Cobic, B. Perovic, B. Tosic, C.
New Mass Spectrometer Ion Source for Solids.
Rev. Sci. Instr. 36, 1844 (1965)

Conzemius, R. J. Svec, H. J.
A Piezoelectric Vacuum Vibrator as a Source of Ions in a Mass Spectrometer.
J. Sci. Instr. 42, 136 (1965)

Davis, W. D.
Performance Characteristics of Some Mass Spectrometer Ion Sources.
J. Vac. Sci. Technol. 2, 280 (1965)

Dawson, P. H. Knewstubb, P. F. Tickner, A. W.
The Mass Spectrometry of Ions in Glow Discharges.
12th Annual Conference on Mass Spectrometry and Allied Topics, Montreal, June 1964 Conf-649-7

Dawson, P. H. Tickner, A. W.
The Mass Spectrometry of Ions in Glow Discharge Applied to the Hydrogen-Deuterium Exchange Reactions.
Presented at 13th Annual Conf. on Mass Spectrometry, St. Louis (1965)

Derek, R. Green, B. N.
Mass Spectrometer Arc-Type Ion Source Having Electrode Cooling Means.
U. S. Patent 3226542

Franzen, J. Schuy, K. D.
Time- and Energy-Resolved Mass Spectroscopy. The Condensed Vacuum Discharge Between Solid Electrodes.
Z. Naturforsch. 20A, 176-80 (1965) (in German)
Chem. Titles No. 7 (1965)

Hovick, T. J. Cambey, L. A. Deines, P.
Studies of the Vacuum Vibrator Source for the Analysis of Conductors and Insulators.
Presented at 13th Annual Conf. on Mass Spectrometry, St. Louis (1965)

Kaminsky, M.
Atomic and Ionic Impact Phenomena on Metal Surfaces.
Academic Press Inc., New York, Book (1965)

Kirchner, F. Benninghoven, A.
Mass Spectrometric Investigation of the Energy Distribution of Sputtered Particles.
Phys. Letters 8, 193 (1964)

Maskrey, J. T.
Vacuum Spark Erosion at Cathodic Inclusions
Brit. J. Appl. Phys. 16, 1583-4 (1965)

Mesyats, G. A.
Spark Pulse Peaking Devices with Low Sensitivity to Pulse Height.
Soviet Phys.-Tech. Phys. 10, 400-2 (1965)

Navinsek, B.
Sputtering Yields of Alkali Halide Single Crystals Bombarded by 2- to 10-Kev Ions.
J. Appl. Phys. 36, 1678 (1965)

Pasyuk, A. S. Tretyakov, Y. P. Stanku, V.
Sputtering of a Cathode in Arc Ion Source.
Pribory I Tekhn. Exp. No. 3, p. 42 (May 1965)

Pasyuk, A. S. Tretyako, Y. P. Stanku, V.
Cathode Sputtering in Ion Arc Sources.
Pribory I Tekhn. Exp. No 3, p. 42 (May 1965)
Instr. Exp. Tech. USSR (Engl. Trans.) p. 505 (1965)

Schroeer, J. M.
Surface Ionization of Sputtered Atoms.
Thesis, Cornell Univ., Ithaca, New York (1964)

Southern, A. L.
Ar^+ Ion Bombardment of Metal Surfaces.
Solid State Division Annual Report for Period Ending. May 31, 1964 ORNL-3676

Suladze, K. V. Plyutto, A. A.
Emission Properties of a Vacuum Spark Plasma. Part-I. Ion Beams
Zh. Tekhn. Fiz. 35, 1298-1307 (1965) (in Russian)
Abstract in Nucl. Sci. Abstr. 19 (24) 47147

Tawara, H.
Pulse Shortening in Duoplasmatron Type Ion Source.
Jap. J. Appl. Phys. 4, 687 (1965)

Van Itterbeek, A. Forrez, G. Witters, J.
Van Audekercke, R. Van Itterbeek, W.
Bombardment of Copper and Germanium Surfaces by Low Energy Argon Ions.
Appl. Sci. Res., Sec. B, 11, 286 (1964)

Zdanuk, F. J. Wolsky, S. P.
Sputtering of Single-Crystal Copper and Aluminum with 20-600 Ev Argon Ions.
J. Appl. Phys., 36, 1683 (1965)

Zorin, E. I. Tetelbaum, D. I. Popov, Y. S.
Granitsy, Z. K.
Changes in Properties of Surface Layers of N-Germanium Resulting from Bombardment with 40-Kev Nitrogen Ions.
Soviet Phys. Solid State (Engl. Trans.) 6, 1592 (1965)

6) ION RECORDING AND PHOTOMETRY

Adams, J. Manley, B. W.
Channel Electron Multiplier.
Electr. Eng. 37, 180 (1965)

Ainbund, M. R. Vildgrube, G. S. Dunaevskaya, N. V.
Louvered Electron Multiplier Tubes for Recording Charged Particles.
Pribory I Tekhn. Eksp., No. 3, p. 228 (May 1965)

Banner, A. E.
Distortion of Peak Shape in Fast Scanning of Mass Spectra.
Presented at the 13th Annual Conf. on Mass Spectrometry and Allied Topics, St. Louis, Missouri, May 1965

Capellen, J. Conzemius, R. J. Svec, H. J.
A Comparison of Electrical and Photographic Detectors in the Assay of Trace Impurities with the Spark Source Mass Spectrograph.
Presented at 13th Annual Conf. on Mass Spectrometry, St. Louis (1965)

Carver, R. D. Thomas, R. A. Dupzyk, R. J.
Barton, G. W.
Logarithmic Scaling of Exposure for a Mass Spectrograph.
Presented at 13th Annual Conf. on Mass Spectrometry, St. Louis (1965)

Cookson, G. C. Fletcher, W. Tushingham, R.
The Importance of Variations in Line-Width and Emulsion Sensitivity in Spark Source Mass Spectrography.
Presented at 13th Annual Conf. on Mass Spectrometry, St. Louis (1965)

Cornu, A.
Analysis Application of Line Width Studies in a Spark Source Mass Spectrometer.
Presented at 13th Annual Conf. on Mass Spectrometry, St. Louis (1965)

Daly, N. R. Powell, R. E. Ridley, R. G.
A Detector for Neutral and Charged Particles.
Nucl. Instr. Methods 36, 226 (1965)

Dietz, L. A.
Basic Properties of Electron Multiplier Ion Detection and Pulse Counting Methods in Mass Spectrometry.
Rev. Sci. Instr. 36, 1763 (1965)

Erickson, M. L.
Signal Amplifier of Electron Multiplier Type.
U. S. Patent 3212021

Evans, D. S.
Low Energy Charged Particle Detection Using the Continuous Channel Electron Multiplier.
IEEE Trans. Nucl. Sci., NS12, 34 (February 1965)

Evans, D. S.
Low Energy Charged-Particle Detection Using Continuous-Channel Electron Multiplier.
Rev. Sci. Instr. 36, 375 (1965)

Goodrich, G. W. Ignatowski, J. R. Norman, J. E.
Funneled Electron Multiplier
U. S. Patent 3176178

Hung, W. W. McGee, K. E. Kennedy, M. J.
Operating Characteristics of a Commercial Resistance-Strip Magnetic Electron Multiplier.
Rev. Sci. Instr. 36, 110 (1965)

Kendall, B. R. F.
Current-Induced Gas Evolution from Electron Multipliers.
J. Vac. Sci. Technol. 2, 1 (1965)

Kennicott, P. R.
An Internal-Image Developer for Mass Spectrograph Plates.
Presented at 13th Annual Conf. on Mass Spectrometry, St. Louis (1965)

Kennicott, P. R.
Surface Developer for Mass Spectrograph Plates.
Anal. Chem. 37, 313 (1965)

Kraus, D. E. White, F. A.
Secondary-Emission Coincidence Scheme for the Detection of Single Electrons and Ions.
Presented at 13th Annual Conf. on Mass Spectrometry, St. Louis (1965)

Krupnik, L. I. Shulika, N. G.
Studies of the Positive Ion Beam Effects on the Blackening of Photoplates.
Physics of Plasma and Problems of Controlled Thermonuclear Fusion (Report of the Third Conference on Physics of Plasma and Problems of Controlled Thermonuclear Fusion) Issue 3. K. D. Sinel-Nikov Ed. Kiev Publishing House of Ukranian Academy of Sciences, 1963

La Lau, C.
On the Mass Discrimination Caused by Electron Multiplier Detectors.
Presented at 13th Annual Conf. on Mass Spectrometry, St. Louis (1965)

Mai, H.
A Modified Recording Technique for Improvement of Detection Limits in Spark Source Mass Spectrography.
J. Sci. Instr. 42, 339 (1965)

McCrea, J. M.
Characteristics of Ion-Sensitive Emulsions for Mass Spectrography-II.
Presented at 13th Annual Conf. on Mass Spectrometry, St. Louis (1965)

McCrea, J. M.
A Processor for Spectrographic Plates.
Appl. Spectr. 19, 61 (1965)

McCrea, J. M.
Photographic Response and Cumulative Law of Error.
Spectrochim. Acta 21, 1014 (1965)

McKinney, C. R. Boettger, H. G.
A Comparison of Electrical and Photographic Recording of High-Resolution Spectra for Structural Analysis of Organic Compounds.
Presented at 13th Annual Conf. on Mass Spectrometry, St. Louis (1965)

Norman, J. Smith, H. Thompson, R. R.
Electron Multiplier Gate.
U. S. Patent 3197663

Picard, E. Sala, A.
Improvements in or Relating to Electron Multipliers.
British Patent 977,827

Reuter, W. Webber, J. C.
The Application of a Dual Emulsion Technique in Spark Source Mass Spectrography.
Presented at Fourth National Meeting, Society for Applied Spectroscopy, Denver, Col., Aug. 30-Sept. 3, 1965

Ridley, R. G. Young, W. A. P. Daly, N. R.
Fast Counting with the Scintillation Detector.
Presented at 13th Annual Conf. on Mass Spectrometry, St. Louis (1965)

Spindt, C. A. Shoulder, K. R.
Stable Distributed-Dynode Electron Multiplier.
Rev. Sci. Instr. 36, 775 (1965)

Thompson, R. R.
Electron Multiplier.
U. S. Patent 322539

Wagner, H. Mai, H.
Absolute Schwarzungskurven von Ionen in Energiebereich von 250-2500 ev auf Agfa-Schumann-Platten.
Z. Naturforsch. 19A, 1624 (1964)

White, F. A. Davis, W. D.
Semiconductive Electron Multiplier.
U. S. Patent 3184633

Zubkov, V. I.
Device for Automatic Shifting of a Mass Spectrometer Range.
Pribory I Tekhn. Eksp. No. 2, p. 127 (March 1964)

7) DATA PROCESSING AND QUANTIZATION

No Authors
Analysis by Spark Source Mass Spectrometry: Atlas of Lines.
Appl. Spectr. 19, 139 (1965)

Biemann, K.
Recent Developments in the Interpretation of High Resolution Mass Spectra.
Presented at 13th Annual Conf. on Mass Spectrometry, St. Louis (1965)

Biemann, K. McMurray, W.
Computer-Aided Interpretation of High-Resolution Mass Spectra.
Tetrahedron Letters, p. 647 (1965)

Desjardins, M.
Test of Absolute Analysis by Spark Source Mass Spectrometry.
Commissariat a'l Energie Atomique, Grenoble, France
CEA-R-2721 Thesis, Grenoble Univ., France

Cameron, A. E. Chistie, W. H. McKown, H. S. Trundle, A. S.
A Programmable High-Speed Data Acquisition System for Mass Spectrometric Application.
Presented at 13th Annual Conf. on Mass Spectrometry, St. Louis (1965)

Cook, H. D. Barker, F. B. Hudgens, J. E.
Computer Control and Data Processing for Isotopic Mass Spectrometers.
Presented at 13th Annual Conf. on Mass Spectrometry, St. Louis (1965)

Elliott, R. M. Swift, P.
Techniques for Estimation of Detection Limits in Spark Source Mass Spectrometry.
Presented at 13th Annual Conf. on Mass Spectrometry, St. Louis (1965)

Hull, C. W. Blanchard, C. G.
Spark Source Mass Spectrograph Sensitivity Measurement, Experiment and Improvement.
Presented at 13th Annual Conf. on Mass Spectrometry, St. Louis (1965)

Light, J. F.
Programming the CEC Mascot Mass Spectrum Digitizer.
Presented at 13th Annual Conf. on Mass Spectrometry, St. Louis (1965)

Light, J. F.
Programming a Mass Spectrum Digitizer.
Anal. Chem. 37, 1627 (1965)

Marsden, D. G. H. Forst, W. Feng, K. K.
Simple Data-Display System for Fast-Scanning Mass Spectrometer.
Rev. Sci. Instr. 36, 1109 (1965)

McCullough, H. Krouse, H. R.
Application of Digital Recording to Simultaneous Collection in Mass Spectrometry.
Rev. Sci. Instr. 36, 1132 (1965)

Olsen, E. W. Burlingame, A. L.
Entire High-Resolution Mass Spectra Via Direct Digitization of Multiplier Output on a C.E.C. 21-110 Mass Spectrometer.
Presented at 13th Annual Conf. on Mass Spectrometry, St. Louis (1965)

Olsen, R. W.
Completely Automatic Data-Reduction System for High Resolution Mass Spectrograms.
Presented at 13th Annual Conf. on Mass Spectrometry, St. Louis (1965)

Ridley, R. G. Young, W. A. P.
Data Processing for Isotopic Analysis by Mass Spectrometry.
Atomic Weapons Research Establishment, Aldermaston, Berkshire, England, Report No. AWRE 0-37/65

Socha, A. J. Willardson, R. K.
Ionization Probabilities in a Spark Source Mass Spectrometer
Presented at Fourth National Meeting, Society for Applied Spectroscopy, Denver, Col., Aug. 30-Sept. 3, 1965

Stefani, R. Desjardins, M. Bourguillot, R. Cornu, A.
Amélioration des Méthodes d'Analyse par Spectrométrie de Masse à Etincelles.
Chim. Anal. Paris 47, 3 (1965)

Woolston, J. R.
Data Processing for the Mass Spectrographic Analysis of Solids.
Presented at 13th Annual Conf. on Mass Spectrometry, St. Louis (1965)
RCA Review 26, 539 (1965)

8) ANALYTICAL APPLICATIONS

Addink, N. W. H. Werner, H. W. Witmer, A. W.
Some Remarks Concerning Inorganic Spark-Source Mass Spectrometric Analysis.
12th Colloquium Spectroscopicum Internationale, p. 651-6, Exeter July 11-17, 1965; Hilger and Watts, London, 1965

Ahearn, A. J.
The Analysis of Semiconductors by Spark Source Mass Spectrometry.
Presented at Fourth National Meeting of Society for Applied Spectroscopy, Denver, Colorado, Aug. 30-Sept. 3, 1965

Beckey, H. D.
Massenspektrometrie.
Z. Instrumen. 73, 171 (1965)

Beynon, J. H.
Introduction to Mass Spectroscopy and its Applications.
Science 150, 1802 (1965)

Beynon, J. H.
Massenspektrometrie,Physikalische und Apparative Grundlagen, Anwendungen
J. Am. Chem. Soc. 87, 2303 (1965)

Beynon, J. H.
Advances in Mass Spectrometry. Proceedings of Mass Spectrometry Conference, Oxford
Endeavour 23, 48 (1964)

Bommer, P. Biemann, K.
Mass Spectrometry.
Annual Review of Physical Chem. 16, 481 (1965)

Briggs, Thomas H.
Analysis of Surface Layers by Spark Source Mass Spectrometry.
Presented at Fourth National Meeting of Society for Applied Spectroscopy, Denver, Colorado, Aug. 30-Sept. 3, 1965

Brown, R. Wolstenholme, W. A.
Analysis of Insulating Powders by Mass Spectrometry with a Spark Source.
Publ. Group Avan. Methodes Spectrog. 1964 (3), p. 231-43 (in French)

Cabell, M. J. Wilkins, M.
Mass Spectrometric Measurements of Ratio of Thermal Neutron Capture to Fission for 241 Pu.
J. Inorg. Nucl. Chem. 27, 2481 (1965)

Cameron, A. E. Stevens, C. M.
Mass Spectrometry.
Analysis of Essential Nuclear Reactor Materials. Book Government Printing Office

Chastagner, P. J.
Determination of Trace Elemental Impurities in Organic Materials by Spark Source Mass Spectrometry.
Appl. Spectr. 19, 33 (1965)

Chemla, M.
Advances in Mass Spectrometry.
Ann. Chim. Paris 9, 542 (1964)

Chupakhin, M. S. Glavin, G. G. Karlov, Y. A.
Kormilitsyn, D. V.
A Mass Spectroscopic Method of Analyzing Oxygen in Titanium.
Dokl. Akad. Nauk SSSR, 158, 689, September 21, 1964

Chupakhin, M. S.
Polyatomic Ions in the Spark Mass Spectra of Some Solids
Sovrem. Metody Analiza, Metody Issled.
Khim. Sostava: Stroeniya Veshchestv Akad Nauk SSSR, Trist.
Geokhim: Analit. Khim. 1965, 33-43 (in Russian) CA 64
(5). 5900h

Chupakhin, M. S. Kormilitsyn, D. V.
Mass Spectrographic Analysis of Solid Substances.
Zh. Anal. Khim. 20(6), 709-18 (1965)
Chem. Titles No. 15 (1965)

Chupakhin, M. S. Glavin, G. G. Fistul, V. I.
Clusters in Semiconducting Materials.
Khim. Svyaz v Poluprov. i Tverd. Telakh, Inst. Fiz. Tverd.
Tela i Poluprov. Akad Nauk Belorussk SSR 1965, 130-4 (in Russian)

Cluley, H. J.
Trace Analysis of Semiconductor Materials. (Book Review)
Nature 205, 639 (1965)

Cook, H. D. Kessler, T. Beeles, L. T.
Spark Source Mass Spectrographic Analysis of Some Nickel and
and Iron Base Alloys.
Bettis Atomic Power Lab., June, 1964, 20 p. WAPD-T-1662
Abstract in Nucl. Sci. Abstr. 19 (18) 34114

Cookson, G. G. Fletcher, W. Tushingham, R.
Commentary on the Spark-Source Mass Spectrograph
12th Colloquium Spectroscopicum Internationale, p. 636-40
Exeter, 11-17 July 1965: Hilger and Watts, London, 1965

Cornu, A. Massot, R. Terrier, J.
Analysis by Spark Source Mass Spectrometry, Atlas of Lines
Paris, Les presses Universitaires de France, 570 p.

Elliott, R. M. Swift, P.
Quantitative Impurity Analysis of Solids by Mass Spectrometry.
12th Colloquium Spectroscopicum Internationale Exeter, 11-17
July 1965; p. 623-6, Hilger and Watts, London, 1965

Elwell, W. T.
Trace Analysis of Semiconductor Materials. Book Review
Analyt. Chim. Acta 32, 97 (1965)

Franklin, J. C. Griffin, E. B.
Spark Source Mass Spectrometric Analysis of Common and
Radiogenic Lead.
Union Carbide Corp., Oak Ridge, Tenn., Y-1481, Feb. 1965

Franklin, J. C. Griffin, E. B.
Some Applications of Spark Source Mass Spectrography to the Analysis of Alloys and Pure Elements.
Union Carbide Corp., Oak Ridge, Tenn., Y-12 Plant
9th Conference on Analytical Chemistry in Nuclear Technology, Gatlinburg, Tenn., Sept. 10, 1965 Y-KG-28

Gilmour, A. S. Giori, F. A.
The Use of the Quadrupole Mass Spectrometer for Laser-Surface Studies.
Presented at 13th Annual Conf. on Mass Spectrometry

Harrington, W. L. Skogerboe, R. K. Morrison, G. H.
Quantitative Spark Source Mass Spectrometry Using Cryosorption Pumping.
Anal. Chem. 37, 1480 (1965)

Henry, W. M.
Development of Analytical Techniques for the Determination of Minute Quantities of Selected Elements in Beryllium.
Battele Memorial Inst., Columbus, Ohio, Interim Report No. 3 May 20 to July 20, 1964, AD-607585

Hickam, W. M. Sandler, Y. L.
Mass-Spectrographic Methods for Studying Surfaces and Reactions at Surfaces
Conf. Surface Effects Detection, Washington, D. C. 1964 p. 189-96 (1965)

Hintenberger, H.
Mass Spectroscopy of the Smallest Quantitities of Matter in Nuclear Physics and Isotope Cosmology.
Naturwissenschaften 51, 497 (1964)

Hintenberger, H.
Detection of Non-Metals in Metals by Mass Spectroscopy.
Angew. Chem. 4, 255, 1965

Hintenberger, H.
Mass Spectrometry.
Naturwissenschaften 52, 462 (1965)

Hintenberger, H.
Massenspektroskopischer Nachweis von Nichtmetallen in Metallen.
Z. Anal. Chem. 209, 176 (1965)

Honig, R. E.
Mass Spectroscopy as an Analytical Tool.
Annals, N. Y. Academy of Sciences 137 Art. 1, Pg. 262 (1965)

Honig, R. E.
Mass Spectrometric Methods.
Cali. JP (Ed) Chapt. 3, p. 169-205 of "Trace A alysis of Semiconductor Materials", Macmillan, New York 19

Irsa, A. P. Friedman, L.
Trace Analysis on Limited Size Samples with a Spark Source Mass Spectrometer.
Presented at 13th Annual Conf. on Mass Spectrometry, St. Louis (1965)

Kai, J. Miki, M.
Quantitative Analysis by Means of Double-Focusing Mass Spectrograph for Solids. Part II
Mitsubishi Denki Lab. Rept. 5, 411 (1964)

Kiser, R. W.
Introduction to Mass Spectroscopy and its Applications. Book
Prentice-Hall, Englewood Cliffs, N. J., 1965

Lardy, B. C. Schindle, A. I.
Basic Studies of Metallic State (A Method of Purity Determination for Ferromagnetic Metals).
Report Naval Research Lab. Proc., p. 30, 1965

Leipziger, F. D.
Isotope Dilution Analyses by Spark-Source Mass Spectrography.
Analy. Chem. 37, 171 (1965)

Makita, T. Kai, J.
Spark Mass Spectroscopy of Solids
Bunseki Kagaku 13 (11) 1155-60 (1964) (in Japanese)
Chem. Titles H2 (1965)

Makita, T. Nishiyama, S.
Mass Spectrography for the Analysis of Solids. II
Determination of Isotopic Ratios of Lead, Thorium, and Uranium in Minerals.
Shitsuryo Bunseki, 12, 223, March 1965

McHugh, J. A. Sheffield, J. C.
Mass Analysis of Subnanogram Quantities of Iodine.
Anal. Chem. 37, 1099 (1965)

Memelova, L. Y. Kukavadz, G. M. Ershler, B. V.
Mass Spectroscopic Determination of Micro-Quantities of Boron in Some Materials.
J. Nucl. Energy AB, 19, 132 (1965)

Nalbantoğlu, M.
Analysis of Beryllium by Spark Mass Spectrometer.
Bull. Soc. Chim. Franc, No. 2, p. 539 (February 1965)

Neuert, H.
Massenspektrometrie.
Nukleonik 7, 51, 1965

Nicholls, G. D.
Analysis of Geological Materials by Spark Source Mass Spectroscopy.
Presented at Fourth National Meeting, Society for Applied Spectroscopy, Denver, Col., Aug. 30-Sept. 3, 1965

Reuter, W. Kuptsis, J. D.
On the Problem of Selective Vaporization in Spark Source Mass Spectrography.
Presented at Fourth National Meeting, Society for Applied Spectroscopy, Denver, Col., Aug. 30-Sept. 3, 1965

Saski, N. Watanabe, E.
The Application of Spark Source Mass Spectrometry to the Trace Element Analysis of Some Biological Materials.
Presented at 13th Annual Conf. on Mass Spectrometry, St. Louis (1965)

Shankar, J.
Mass Spectrometry.
J. Sci. Ind. Res. India 24, 44 (1965)

Socha, A. J.
Spark Source Analysis of High Resistivity Powders by Probe Technique.
Presented at 13th Annual Conf. on Mass Spectrometry, St. Louis (1965)

Socha, A. J. Leipolo, M. H.
Mass Spectrographic Analyses of Nonconducting Ceramics.
J. Am. Ceram. Soc. 48, 463 (1965)

Stefani, R. Desjardins, M. Grun, J. C. Cornu, A. Bourguillot, R.
Analysis of Solids by Spark Source Mass Spectrometry
Comm. Energie At. (France), Rappt. CEA-R-2757, 16 p. (1965) (in Franch)

Stefani, R. Bourguillot, R. Cornu, A.
Determination of Traces of Non-metals in Metals by Spark-Source Mass Spectrometry.
12th Colloquium Spectroscopicum Internationale p. 627-35 (in French) Exeter, 11-17, July, 1965; Hilger and Watts, London 1965

Taylor, S. R.
Geochemical Analysis by Spark Source Mass Spectrography.
Geochim Cosmochim. Acta 29, 1243-62 (1965)
Chem. Titles No. 25 (1965)

Thomas, D. W.
Advances in Mass Spectrometry. Book Review
Anal. Chim. Acta 32, 99 (1965)

Viehboeck, F. P.
Burn-Up Determination of Nuclear Fuels Using the Mass Spectrometric Methods.
Report SGAE-PH-11/1964 20 Ps. USAEC, Div. of Tech. Info.

9) ATOMIC WEIGHTS AND ISOTOPIC ABUNDANCES

Campbell, A. J. Halliday, J. S.
Mass Measurement from Low Intensity Ion Beams.
Presented at 13th Annual Conf. on Mass Spectrometry, St. Louis (1965)

Crouch, E. A. C. Tuplin, T. A.
On the Variation of the Isotopic Composition of Naturally Occurring Molybdenum.
Presented at 13th Annual Conf. on Mass Spectrometry, St. Louis (1965)

Debievre, P. J. Debus, G. H.
Precision Mass Spectrometric Isotope Dilution Analysis.
Nucl. Instr. Methods 32, 224 (1965)

Debievre, P. J. Debus, G. H.
Optimal Conditions for Mass Spectrometric Quantitative Determinations by Isotope Dilution.
USAEC, Div. of Tech. Info., EUR-2219.E

Fairbairn, H. W. Hurley, P. M. Pinson, W. H.
Re-Examination of Rb-Sr Whole-Rock Ages at Sudbury Ontario.
Proc. Geol. Assoc. Can. 16, 95 (1965)

Faure, G. Hurley, P. M. Powell, J. L.
The Isotopic Composition of Strontium in Surface Water from the North Atlantic Ocean.
Geochim. Cosmochim. Acta 29, 209 (1965)

Freegarde, M.
Mass Spectrometry - Applications of Isotope Dilution to the Analysis of Metals.
From Society for Applied Spectroscopy 3rd National Meeting Cleveland, Sept.-Oct. 1964, Report No. Conf-812-2

Fukai, R.
Analysis of Trace Amounts of Chromium in Marine Organisms by the Isotope Dilution of Chromium-51.
Symposium on Radiochemical Methods for Analysis, Salzburg, Austria, Vienna Internal Atomic Energy Agency (1964) Book

Hess, W. B. Holcomb, H. P.
Determination of Lanthanum in Actinide-Lanthanide Mixtures by Isotopic Dilution and Mass Spectrometry.
Analyt. Chem. 37, 169 (1965)

Hurley, P. M. Bateman, P. C. Fairbairn, H. W.
Pinson, W. H.
Investigation of Initial 87Sr/86Sr Ratios in Sierra Nevada Plutonic Province.
Geol. Soc. Am. Bull. 76, 165 (1965)

Kaviladze, M. S. Abashidze, I. V.
Variations in the Isotope Ratio 39K/41K in Natural Potassium.
Soobshch. Akad. Nauk Gruz. SSR 35, 67 (1964)

Nikolaev, D. S. Lazarev, K. F. Korn, O. P.
Yakunin, M. I. Drozhzhi, V. M.
On Isotopic Composition of Uranium Contained in Waters and Sediments of Black and Azov Seas.
Dokl. Akad. Nauk SSSR 165, 187 (1965)

Pinson, W. H. Schnetzler, C. C. Beiser, E.
Fairbairn, H. W.
Rb-Sr Age of Stony Meteorites.
Geochim. Cosmochim. Acta 29, 455 (1965)

Ridley, R. G. Daly, N. R. Dean, M. H.
Isotopic Analysis of Uranium Using an Internal Standard.
Nucl. Instr. Methods 34, 163 (1965)

Sakanoue, M. Hashimoto, T.
A Study of 234U/238U Ratio in Natural Samples.
Nippon Kagaku Zasshi 85, 622 (October 1964)

Shields, W. R.
Absolute Isotopic Abundance Ratios of ... by Surface or Thermal Ionization.
Presented at 13th Annual Conf. on Mass Spectrometry, St. Louis (1965)

Shields, W. R. Goldich, S. S. Garner, E. L.
Murphy, T. J.
Natural Variations in Abundance Ratio and Atomic Weight of Copper.
J. Geoph. Res. 70, 479 (1965)

Shukolyukov, Y. A.
Interpretation of Discordant Ages Calculated from Isotopic Ratios 206Pb/238U and 207Pb/235U.
Geochem. Intern., p. 843, 1964

Svec, H. J. Anderson, A. R.
The Absolute Abundance of the Lithium Isotopes in Natural Sources.
Geochim. Cosmochim. Acta 29, 633 (June 1965)

Svec, H. J.
Absolute Isotope Abundance Measurements.
Presented at 13th Annual Conf. on Mass Spectrometry, St. Louis (1965)

Taylor, S. R.
Geochemical Application of Spark Source Mass Spectrography.
Nature 205, 34 (1965)

Tunnicliff, D. D. Wadsworth, P. A. Schissler, D. O.
Ordered Exact Mass and Abundance Tables for Mass Spectrometry.
Anal. Chem., 37, 543 (1965)

Ustinov, V. I. Grinenko, V. A.
Analysis of Compensation Method for Precision Measurement of Isotopic Abundances.
Ind. Lab. USSR (Engl. Trans.) 30, 722 (1964)

Vallee, R. E.
238U, 234U, and Naturally Occurring Radioisotopes.
USAEC, Div. of Tech. Info., ORNL-TM-1047, p. 40

Wagner, H.
The Electromagnetic Separation of Isotopes.
Kerntechnik 6, 566 (December 1964)

Wagner, H.
Electromagnetic Separation of Radioactive Isotopes.
Chem. Ing. Tech. 37, 458 (1965)

10) HIGH TEMPERATURE VAPORIZATION STUDIES

Ackermann, R. J. Rauh, E. G. Thorn, R. J.
Comments on Pressure of Uranium Over Uranium - Uranium Dioxide System.
J. Chem. Phys. 42, 2630 (1965)

Ackermann, R. J. Thorn, R. J.
The Evaporation Behavior, Thermodynamic Properties and Systematic Trends of Actinide Metals - Oxygen Systems.
Symposium on Thermodynamics with Emphasis on Nuclear Materials and Atomic Transport in Solids, I.A.E.A., Vienna, July 1965

Argent, B. B. Lee, K. T.
Thermodynamic Properties of Solid Solutions. 5. Copper + Zinc + Gold and Copper + Zinc + Silver Alloys.
Trans. Faraday Soc. 61, 826 (1965)

Azizov, S.
Mass Spectroscopical Analysis of the Decomposition Products of Rochelle Salt.
Izv. Akad. Nauk. SSR, Ser. Fiz-Mat. Nauk. 8, 90 (1964)

Balducci, G. Capalbi, A. De Maria, G. Guido, M.
Tetra Carbide Molecules in the Vapor Phase Over Rare Earth - Graphite Systems.
J. Chem. Phys. 43, 2136 (1965)

Battles, J. E.
Mass Spectrometric Investigation of WO_2 and WO_3.
Dissertation Abstr. 25, 6509 (1964-65)

Bautista, R. G. Margrave, J. L.
Langmuir Studies of Sublimation of Strontium Fluoride and Barium Fluoride Single Crystals.
J. Phys. Chem. 69, 1770 (1965)

Bear, I. J. Turnbull, A. G.
Heats of Formation of Beryllium Compounds. I. Beryllium Hydroxides.
J. Phys. Chem. 69, 2828 (1965)

Belyakov, U. I. Zvigdin, U. I.
Mass Spectrometric Study of Hydrogen Penetration of Refractory Molecules.
Zavodsk. Lab. 31, 1107 (1965)

Berg, R. A. Wharton, L. Klemperer, W. Buchler, A. Stauffer
Determination of Electronic Symmetry by Electric Deflection of LiO and LaO.
J. Chem. Phys. 43, 2416 (1965)

Berkowitz, J. Chupka, W. A.
Vaporization Processes Involving Sulfur.
J. Chem. Phys. 40, 287 (1964)

Bernstein, H. Kaufman, L.
Vaporization Kinetics of Refractory Compound Phases.
J. Metals 17, 1058 (1965)

Besenbrun, G. Kanaan, A. S. Margrave, J. L.
Knudsen and Langmuir Measurements of Sublimation Pressure of Cadmium (2) Fluoride.
J. Phys. Chem. 69, 3174 (1965)

Blackburn, P. E. Buchler, A.
Thermodynamics of Vaporization in the Beryllium Oxide-Boron Oxide System.
J. Phys. Chem. 69, 4250 (1965)

Blair, G. R. Levin, H. O'Brien, R. E.
Evaporation of Silicon from Molybdenum Silicides at High Temperature and in Hard Vacuum.
J. Am. Ceram. Soc. 48, 430 (1965)

Blue, G. D. Searcy, A. W.
Mass Spectrometric Studies of the Sublimation of Alkaline Earth Suflides and the Dissociation Energy of Gaseous S_2.
Presented at 13th Annual Conf. on Mass Spectrometry, St. Louis (1965)

Boerboom, A. J. Reyn, H. W. Kistemaker, J.
Vugts, H. F.
Thermochemistry of Antimony.
Physica 30, 2137 (1964)

Boerboom, A. J. H. Reyn, H. W. Vuyts, H. F.
Kistemaker, J.
Thermochemistry of Antimony and Antimony Trioxide.
Advances in Mass Spectrometry, Vol. 3, W. L. Mead Ed., The Institute of Petroleum 1966, p. 945

Borisov, Y. A. Gusarov, A. V. Gorokhcv, L. N.
Mass Spectrometer Investigation of Evaporation of Cesium Peroxide.
High Temp. USSR (Engl. Trans.) 2, 440 (1964)

Botter, R. Hagemann, R. Nief, G. Roth, E.
Etude Thermodynamique de l'Hemioxyde de Soufre par Spectrometrie de Masse.
Advances in Mass Spectrometry, Vol. 3, W. L. Mead Ed., The Institute of Petroleum 1966, p. 931

Buchler, A. Stauffer, J. L.
Vaporization in the Lithium Fluoride-Beryllium Fluoride System.
Symposium on Thermodynamics with Emphasis on Nuclear Materials and Atomic Transport in Solids, I.A.E.A., Vienna, July 1965

Buchler, A. Stauffer, J. L. Klemperer, W.
Geometry of Transition Metal Dihalides: the Fluorides of Manganese, Cobalt, Nickel, Copper and Zinc.
J. Chem. Phys. 40, 3471 (1964)

Cater, E. O. Lee, T. E. Johnson, E. W. Rauh, E. G.
Eick, H A.
Vaporization, Thermodynamics and Dissociation Energy of Lanthanum Monosulfide.
J. Phys. Chem. 69, 2684 (1965)

Chupakin, M. S. Kormilitsyn, D. V.
Mass Spectrographic Analysis of Solid Substances.
Zh. Analit. Khim. 20, 709 (1965)

Colin, R. Drowart, J. Verhaegen, G.
Mass-Spectrometric Study of Vaporization of Tin Oxides. Dissociation Energy of SnO.
Trans. Faraday Soc. 61, 1364 (1965)

Cubicciotti, D.
Thermodynamics of Vaporization of Liquid Thallous Bromide and its Gaseous Dimerization.
J. Phys. Chem., 68, 3835 (1965)

Cubicciotti, D.
Thermodynamics of Vaporization of Liquid Thallous Iodide.
J. Phys. Chem. 69, 1410 (1965)

De Maria, G. Goldfinger, P. Malaspina, L.
Piacente, V.
Mass-Spectrometric Study of Gaseous Molecules ZnS, ZnSe and ZnTe.
Trans. Faraday Soc. 61, 2146 (1965)

De Maria, G. Guido, M. Malaspina, L. Pesce, B.
Mass Spectrometric Study of Yttrium-Carbon System.
J. Chem. Phys. 43, 4449 (1965)

Diamond, J. J.
Bibliography on the High Temperature Chemistry and Physics of Materials in the Condensed State.
Jan. - March 1965, National Bureau of Standards, Washington D.C., NP-15045

Drowart, J.
Etude en Chimie des Hautes Temperatures.
Ind. Chim. Belge, 29, 1294, 1965

Drowart, J.
Mass Spectrometric Studies of the Vaporization of Inorganic Substances at High Temperature.
"Condensation and Evaporation of Solids", Gordon and Breach Inc., New York 1964, p. 255

Drowart, J. Pattoret, A. Smoes, S.
The Heat of Sublimation of Uranium and the Consistency of the Thermodynamic Data for Uranium Compounds.
J. Nucl. Mater. 12, 319 (1964)

Drowart, J. Degreve, F. Verhaegen, G.
Colin, R.
Thermochemical Study of Germanium Oxides Uding a Mass Spectrometer - Dissociation Energy of Molecule GeO.
Trans. Faraday Soc. 61, 1072 (1965)

Drowart, J. Colin, R. Exsteen, G.
Mass-Spectrometric Study of Vaporization of Lead Monoxide-Dissociation Energy of PbO.
Trans. Faraday Soc. 61, 1376 (1965)

Drowart, J. Pattoret, A. Smoes, S.
Concerning the Influence of Oxygen on the Vapor Pressure of Uranium.
J. Chem. Phys. 42, 2629 (1965)

Drowart, J. Goldfinger, P.
The Role of Mass Spectrometry in High Temperature Chemistry.
Advances in Mass Spectrometry, Vol. 3, W. L. Mead Ed., The Institute of Petroleum 1966, p. 923

Drowart, J. Pattoret, A. Smoes, S. Degreve, F.
Detry, D.
Etudes thermodynamiques et cinétiques en chimie des hautes temperatures.
Advances in Mass Spectrometry, Vol. 3, W. L. Mead Ed., The Institute of Petroleum 1966, p. 931

Ehlert, T. C. Kent, R. A. Margrave, J. L.
Mass Spectrometric Studies at High Temperature-Sublimation Pressure of NiF_2.
J. Am. Chem. Soc. 86, 5093 (1964)

Fomin. O. K. Tikhomir
Mass Spectrum of Organic Ions Formed in an Atmosphere of Mass-Spectrometer Residual Gases on Heated Oxidized Molybdenum.
Soviet Phys. Tech. Phys. (Engl. Trans.) 9, 1114 (1965)

Franzen, H. F. Gilles, P. W.
High-Temperature Vaporization and Thermodynamic Properties of Titanium Monosulfide.
J. Chem. Phys. 42, 1033 (1965)

Gebelt, R. E. Eick, H. A.
The Preparation and Thermodynamics of Europium Dicarbide.
Symposium on Thermodynamics with Emphasis on Nuclear Materials and Atomic Transport of Solids, I.A.E.A., Vienna, July 1965

Gingerich, K. A.
Application of High-Temperature Mass Spectrometry to the Determination of the Enthalpy-Composition Function of Nonstoichiometric Binary Compounds.
J. Am. Chem. Soc. 87, 1660 (1965)

Gingerich, K. A. Wilson, D. W.
Preparation and Properties of Thorium Phosphide ThP_{1-x} and Phase Studies of the Partial System Th-ThP.
Inorg. Chem. 4, 987 (1965)

Gingerich, K. A.
The Application of High Temperature Mass Spectrometry to the Study of the Composition Function of Thermodynamic Properties in Nonstoichiometric Compounds.
Advances in Mass Spectrometry, Vol. 3, W. L. Mead Ed., The Institute of Petroleum 1966, p. 1009

Gordienko, S. P. Samasosonov, G. V. Fesenko, U. V.
Composition of Vapor of GaN.
Zh. Fiz. Khim. 38, 2974 (1964)

Gorokhov, L. N.
Mass Spectrometry of 1, 1-dichloro Germinene.
Zh. Strukt. Khim. 6, 766 (1965)

Gupta, S. K.
Thermodynamic Study of High Temperature Species in the Boron-Oxygen-Hydrogen and Halogen System.
Diss. Abs. 25, 4969 (1965)

Gusarov, A. V. Gorkhov, L. N.
Determination of Mass Spectra and Amounts of Molecular Associates in Vapor over Refractory Substances.
High Temp. USSR (Engl. Trans.) 2, 482 (1964)

Hildenbrand, D. L. Hall, W. F. Yu, F. Potter, N. D.
Vapor Pressures and Vapor Thermodynamic Properties of Some Lithium and Mangesium Halides.
J. Chem. Phys. 40, 2882 (1964)

Hildenbrand, D. L. Murad, E.
Dissociation Energy of BF from Mass Spectrometric Studies.
J. Chem. Phys. 43, 1400 (1965)

Hildenbrand, D. L. Theard, L. P.
Effusion Studies, Mass Spectra and Thermodynamics of Beryllium Fluoride Vapor.
J. Chem. Phys. 42, 3230 (1965)

Hoenig, C. L. Searcy, A. W.
Knudsen and Langmuir Evaporation Studies of Stannic Oxide.
Am. Ceram. Soc. Bull 44, 313 (1965)

Hulbert, S. F. Gray, T. J.
Use of a Mass Spectrometer to Study High-Temperature Kinetics of Vaporization of Non-Stoichiometric TiO_2.
Am. Ceram. Soc. Bull. 44, 313 (1965)

Johnson, E. W.
Mass Spectrometric Studies of the Vaporization of SrS, LaS and Some La-Ag Alloys.
Dissertation Abstr., 26, 114 (1965-1966)

Kant, A. Strauss, B.
Dissociation Energies of Diatomic Molecules of the Transition Elements (Ti, Cr, Mn and Co).
J. Chem. Phys. 41, 3806 (1964)

Kaufman, M. Wharton, L. Klemperer, W.
Electronic Structure of SrO.
J. Chem. Phys. 43, 943 (1965)

Keneshea, F. J. Cubicciotti, P.
Thermodynamics of Vaporization of Thallous Fluoride and its Gaseous Dimerization.
J. Phys. Chem. 69, 3910 (1965)

Kent, R. A. Ehlert, T. C. Margrave, J. L.
Mass Spectrometric Studies at High Temperature-Sublimation Pressure of MgF_2 and the Dissociation Energy of MgF.
J. Am. Chem. Soc. 86, 5090 (1964)

Kent, R. A. Margrave, J. L.
Mass Spectrometric Studies at High Temperatures. 7. Sublimation Pressure of Chromium(2) Fluoride and Dissociation Energy of Chromium(1) Fluoride.
J. Am. Chem. Soc. 87, 3582 (1965)

Kent, R. A. Margrave, J. L.
Mass Spectrometric Studies at High Temperature-Sublimation of FeO.
J. Am. Chem. Soc. 87, 4754 (1966)

Krikorian, O. H. Carpenter, J. H.
Enthalpies of Formation of TaO(g) and TaO_2(g).
J. Phys. Chem. 69, 4399 (1965)

Kuriakose, A. K. Margrave, J. L.
Mass Spectrometric Studies of the Thermal Decomposition of Poly(Carbon Mono Fluoride).
Inorg. Chem. 4, 1639 (1965)

Kusmenko, Al. Novikov, G. I.
Vapor Composition in the Chloride Systems of Some Alkali Metals.
Vestn. Lening, Univ., 19, n°22, Ser. Fiz. i. Khim., 102 (1964)

Lincoln, K. A.
Flash Vaporization of Solid Materials for Mass Spectrometric by Intense Thermal Radiation.
Anal. Chem. 37, 541 (1965)

Lisachenko, A. A. Vilesov, F. I. Terenin, A. N.
Mass Spectrometric Investigation of the Photosorption Processes in the O/ZnO System.
Dokl, Akad, Nauk, SSR, 160, 864 (1965)

Massey, A. G. Urch, D. S.
Mass Spectral Studies on the Boron Sub Chlorides.
Chem. Ind. (Lond) 1965, 607 (1965)

McKinley, J. D.
Mass Spectrometric Investigation of the Yttrium-Chlorine Surface Reaction.
J. Chem. Phys. 41, 2814 (1964)

McKinley, J. D.
Mass Spectrum of Yttrium Chloride Vapor.
J. Chem. Phys. 42, 2245 (1965)

Miller, A. R. Searcy, A. W.
Thermodynamic Stabilities as a Function of Composition for Indium Sulfide Phases from Mass Spectrometer Intensity vs. Time Data.
J. Phys. Chem. 69, 3826 (1965)

Mostovskii, A. A. Sakseav, D. A.
Possibility of Use of Pulsed Time-of-Flight Mass Spectrometer for Investigation of the Evaporation of Complex Materials.
Zh. Tekhn. Fiz. 34, 1321 (1964)

Mueller, C. R. Cahill, R. W.
Mass Spectrometric Measurement of Diffusion Coefficients.
J. Chem. Phys. 40, 651 (1964)

Munir, Z. A. Searcy, A. W.
The Activation Energy for the Sublimation of Gallium Nitride.
Lawrence Radiation Lab., Univ. of Calif., Berkeley,
UCRL-10702 Rev. December 31, 1964

Munir, Z. A. Searcy, A. W.
Activation Energy for Sublimation of Gallium Nitride.
J. Chem. Phys. 42, 4223 (1965)

Newbury, R. S.
Vapor Species of the Barium - Oxygen - Hydrogen System.
Thesis Calif. Univ., Berkely, Dept. of Mineral Technology
and Calif. Univ., Livermore, Lawrence Radiation Lab.,
UCRL-12225-T, December 16, 1964

Norman, J. H. Staley, H. G.
Vaporization Studies on the Mixed Trioxides of Antimony and
Arsenic.
J. Chem. Phys. 41, 1503 (1964)

Norman, J. H. Windell, P.
Mass Spectrometric Knudsen Cell Studies of the Vaporization
of Uranium Dicarbide.
J. Phys. Chem. 68, 3802 (1964)

Norman, J. H. Staley, H. G. Bell, W. E.
Mass-Spectrometric Study of Gaseous Oxides of Iridium.
J. Chem. Phys. 42, 1123 (1965)

Norman, J. H. Staley, H. G.
Thermodynamics of Dimerization and Trimerization of Gaseous
Tungsten Trioxide and Molybdenum Trioxide.
J. Chem. Phys. 43, 3804 (1965)

Norman, J. H. Staley, H. G. Bell, W. E.
Mass Spectrometric Knudsen Cell Measurements of Vapor Pressure
of Palladium and Partial Pressure of Palladium Oxide.
J. Phys. Chem. 69, 1373 (1965)

Onchi, M. Kusunoki, I.
Omegatron Mass-Spectrometric Investigation of Thermal
Decomposition of Molybdenum Trioxide and Tungsten Trioxide.
Nippon Kagaku Zasshi 85, 612 (October 1964)

Platel, G.
Determination of the Formation Potentials of Ions Obtained from
Alkali Iodides and Li-Metal Iodide Mixture in Vapor Phase by
Electron Impact.
J. Chim. Phys. 62, 1176 (1965)

Redman, J. D.
A Literature Review of Mass Spectrometric-Thermochemical
Technique Applicable to the Analysis of Vapor Species Over
Solid Inorganic Materials.
Oak Ridge National Lab., ORNL-TM-989, 1964

Rinke, K. Schaefer, H.
Mass Spectrometric Investigation of Rhenium Trichloride.
Angew. Chem. 77, 131 (1965)

Ryabachykov, L. M.
Mass Spectrometric Investigation of Degasification of Molybdenum, Tunsgten and Niobium on Heating them in a Vacuum.
Ukr. Fiz. Zh. 9, 293 (March 1964)

Schaefer, H. Rinke, K.
Gaseous Chromium (VI) Oxide by Mass Spectrometry.
Z. Naturforsch. 20, 702 (1965)

Schissel, P. O. Trulson, O. C.
Mass Spectrometry Study of the Oxidation of Tungsten.
J. Chem. Phys. 43, 737 (1965)

Schoonmaker, R. C. Buhl, A. Lemley, J.
Vaporization Catalysis Decomposition of Gallium Nitride.
J. Phys. Chem. 69, 3455 (1965)

Semenov, G. A.
Mass Spectrometric Study of the Evaporation of Sc_2O_3.
Zh. Neorg. Khim. 10, 2390 (1965)

Semenov, G. A. Ovchinnikov, K. V.
Composition of Vapors Above Rhenium Oxides.
Zh. Obshch. Khim. 35, 1517 (1965)

Siderov, L. N. Akishin, P. A. Sholts, U. B. Korenev, U. M.
Mass Spectrometric Study of Thermodynamic Properties of the Sodium Fluoride - Zirconium Tetra Fluoride System. Temperature Dependence of Partial Pressures and the Thermodynamic Properties of the Condensed Phases.
Zh. Fiz. Khim. 39, 2150 (1965)

Smoes, S. Drowart, J. Verhaegen, G.
Mass-Spectrometric Study of Gaseous Oxides and Suboxides of Scandium, Yttrium, and Lanthanum.
J. Chem. Phys. 43, 732 (1965)

Somorjai, G. A. Lester, J. E.
Composition Change of Binary Compounds under Conditions of Equilibrium and Vacuum Vaporization.
J. Chem. Phys. 42, 4140 (1965)

Storms, E. K.
A Mass Spectrometric Study of the Vapor Pressure of U(g) and UC_2(g) over Various Compositions in the U-C System.
Symposium on Thermodynamics with Emphasis on Nuclear Materials and Atomic Transport in Solids. I.A.E.A., Vienna, July 1965.

Theard, L. P. Hildenbrand, D. L.
Heat of Formation of Be_2O(g) by Mass Spectrometer.
J. Chem. Phys. 41, 3416 (1964)

Torshina, V. V. Smolina, G. N. Dobychin, S. Y.
Mass Spectrometric Study of the Sublimation of LaB_6.
Zh. Neorg. Khim. 10, 1275 (1965)

Trulson, O. C. Schissel, P. O.
A Mass Spectrometric Study of Vaporization of Palladium.
J. Less-Common Metals 8, 262 (1965)

Trulson, O. C. Goldstein, H. W.
Mass Spectrometric Study of Zirconium Diboride.
J. Phys. Chem. 69, 2531 (1965)

Velkov, L. V. Gorokhov, L. N. Mastryukov, V. S. Rusin, A. D.
Molecular Mass and Mass Spectrum of 1,1-dimethyl Germinene Vapors.
Zh. Fiz. Khim., 38, 2674 (1964)

Verhaegen, G. Colin, R. Exsteen, G. Drowart, J.
Mass Spectrometric Determination of Stability of Gaseous Molubdites, Tungstites, Molybdates and Tungstates of Magnesium, Calcium, Strontium and Tin.
Trans. Faraday Soc. 61, 1372 (1965)

Wiedemeier, H. Gilles, P. W.
Mass Spectrometric Study of Sublimination of MnS(S) and Dissociation Energy of MnS(G)
J. Chem. Phys. 42, 2765 (1965)

Winchell, P.
Mass Spectrometric Investigation of Barium Iodide and Caesium Iodide Vaporizations.
Nature 206, 1252 (1965)

Zandberg, E. Y. Ionov, N. I.
Mass Spectrometric Study of the Heats of Sublimation of Polycrystalline Re, W, Ta and Mo.
Zh. Tekhn. Fiz. 35, 1504 (1965)

Zubkov, V. I. Tikhomirov, M. V. Andrianov, K. A. Golubtsov, S. A.
Mass Spectrometric Investigation of Intermediate Products Resulting from the Interaction between Si and CuCl.
Dokl. Akad. Nauk. SSR, 159, 599 (1964)